University of Southampton

Faculty of Engineering and Physical Sciences

School of Chemistry and Chemical Engineering

The Hitchhiker's Guide to Mechanical Stereochemistry

DOI 10.5258/SOTON/D3254

by

Peter Robert Gallagher

ORCID ID 0000-0002-5501-523X

Thesis for the degree of Doctor of Philosophy

June 2025

University of Southampton

Abstract

Faculty of Engineering and Physical Sciences

School of Chemistry and Chemical Engineering

Thesis for the degree of Doctor of Philosophy

The Hitchhiker's Guide to Mechanical Stereochemistry

by

Peter Robert Gallagher

Since the earliest report of their discussion over a century ago, interlocked molecular structures have developed from theoretical oddities to readily accessible structures. While the apparent synthetic challenge they originally presented has since been overcome thanks to the development of template approaches, the understanding of stereochemistry that can arise in such systems remained vague until recently.

The first chapter of this thesis introduces the concept and consequences of mechanical bonding, followed by discussion of both how language to describe, and strategies to prepare mechanically interlocked molecules have developed. The stereochemistry that can arise in interlocked molecules is then discussed in detail, as well as advances in the selective synthesis of mechanically stereogenic molecules. The second chapter describes the synthesis of mechanically axially chiral catenanes by a co-conformational auxiliary strategy and also the identification and synthesis of a rotaxane bearing the analogous stereogenic unit. The third chapter describes the investigation into how facial selectivity can arise in mechanical bond formation towards mechanically axially chiral rotaxanes and mechanical geometric isomers. Their diastereoselective synthesis was optimised and was able to be extended to the direct enantioselective synthesis of a mechanically axially chiral rotaxane. Finally, the fourth chapter describes the diastereoselective synthesis of rotaxanes containing a previously overlooked form of mechanical geometric isomerism and also analyses stereochemistry in rotaxanes and catenanes to establish that this is the final mechanical stereogenic unit to be identified.

Table of Contents

Abstract ii

Table of Contents iii

List of Accompanying Material vi

Research Thesis: Declaration of Authorship vii

Acknowledgements viii

Definitions and Abbreviations ix

Chapter 1: Introduction 1

1.1. Mechanically Interlocked Molecules 2

1.1.1. What is a mechanical bond? 2

1.1.2. The consequence of molecular topology 3

1.1.3. Vernacular nomenclature in MIMs 4

1.1.4. Why nomenclature matters 5

1.2. Synthetic approaches towards interlocked molecules 6

1.2.1. Statistical syntheses 6

1.2.2. Covalent template syntheses 6

1.2.3. Non-covalent interaction templates 7

1.2.4. Active template approaches for the synthesis of MIMs 8

1.3. Stereochemistry arising from the mechanical bond 9

1.3.1. Conditional mechanical stereogenic units 9

1.3.1.1. Canonical conditional mechanical stereogenic units 10

1.3.1.2. The complete set of mechanical stereogenic units 11

1.3.2. Mechanical planar stereoisomerism 12

1.3.2.1. Assigning the mechanical planar chiral stereogenic unit 12

1.3.2.2. Synthesis of mechanical planar chiral molecules 12

1.3.3. Mechanical axial stereoisomerism 16

1.3.3.1. Assigning the mechanical axially chiral stereogenic unit 16

1.3.3.2. Synthesis of mechanical axially chiral molecules 17

1.3.4. Mechanical geometric isomerism 18

1.3.4.1. Assigning the mechanical geometric stereogenic unit 18

1.3.4.2. Synthesis of mechanically geometric molecules 18

1.3.5. Co-conformational stereogenic units 23

1.3.5.1. Co-conformational covalent stereochemistry 23

1.3.5.2. Co-conformational mechanical planar chirality 24

1.3.5.3. Co-conformational mechanical axial chirality 24

1.3.5.4. Co-conformational mechanical geometric isomerism 25
1.3.5.5. Co-conformational mechanical helical chirality 26
1.4. Conclusions 27
1.5. Bibliography 28

Chapter 2: Mechanically Axially Chiral Catenanes and Noncanonical Mechanically Axially Chiral Rotaxanes 33
2.1. Introduction 34
2.2. Results and Discussion 36
2.2.1. Insights from semi-structural schematic representations 36
2.2.2. A co-conformational auxiliary approach to axially chiral catenanes and rotaxanes 36
2.2.3. Stereochemical assignment and properties of the mechanically axially chiral stereogenic unit 40
2.3. Conclusions 42
2.4. Experimental and Supplementary Information 43
2.4.1. Characterisation of compounds 46
2.4.2. Effect of conditions in the synthesis of catenane **3** and rotaxane **9** 167
2.4.3. Single crystal X-ray diffraction analysis 172
2.4.4. Discussion of the structural features of mechanically axially chiral molecules 177
2.4.5. Assigning the absolute stereochemistry of mechanically axially chiral molecules 180
2.4.6. Mechanical stereochemistry in molecules containing prochiral and stereogenic centres 183
2.4.7. Other manifestations of mechanical axial stereochemistry 185
2.5. Bibliography 190

Chapter 3: Facial Selectivity in Mechanical Bond Formation: Axially Chiral Enantiomers and Geometric Isomers from a Simple Prochiral Macrocycle 195
3.1. Introduction 196
3.3. Results and Discussion 198
3.3.1. Effect of conditions and substrate structure in the synthesis of MAC rotaxanes **4** 198
3.3.2. Stereoselective synthesis of MGI-1 rotaxanes 200
3.3.3. Stereoselective synthesis of an MGI catenane 202
3.3.4. Direct enantioselective synthesis of MAC rotaxanes 203
3.4. Conclusions 206
3.5. Experimental and Supplementary Information 207
3.5.1. Characterisation of compounds 209

3.5.2. Absolute stereochemical assignment of interlocked compounds 352
3.5.3. Effect of conditions on the diastereoselective synthesis of rotaxanes **6** 362
3.5.4. Effect of conditions on the enantioselectivity of the AT-CuAAC reaction 363
3.5.5. Variable temperature NMR analysis 367
3.5.6. Single crystal X-ray diffraction analysis 370
3.6. Bibliography **376**

Chapter 4: The Final Stereogenic Unit of [2]Rotaxanes: Type 2 Geometric Isomers 383
4.1. Introduction **384**
4.2. Results and discussion **385**
4.2.1. Examining the achiral building blocks of [2]catenanes confirms the set of stereogenic units is complete 385
4.2.2. Analysing the achiral building blocks of rotaxanes reveals the final mechanical stereogenic unit 387
4.2.3. Catenane and rotaxane stereochemistry – conclusions 387
4.2.4. Retrosynthetic analysis of the "new" MGI-2 stereogenic unit 388
4.2.5. Attempted direct synthesis of MGI-2 rotaxanes **5** 389
4.2.6. Stereoselective synthesis of MGI-2 rotaxanes **11** using an interlocking auxiliary approach 390
4.2.7. Analysis of rotaxanes **10** and **11** 392
4.3. Conclusions **393**
4.4. Experimental and Supplementary Information **394**
4.4.1. Stereochemical analysis to identify the fundamental catenane stereogenic units 394
4.4.2. Stereochemical analysis to identify the fundamental rotaxane stereogenic units 400
4.4.3. Characterisation of compounds 408
4.4.4. Absolute stereochemistry of type 2 mechanical geometric isomers 469
4.4.5. Rotaxanes **4**, **5**, **10** and **11** – three possible sets of stereodescriptors 471
4.5. Bibliography **472**

Chapter 5: Thesis Conclusions and Outlook 477

Appendix A: Published Research Article **483**
Appendix B: Published Research Article **492**
Appendix C: Published Research Article **503**

List of Accompanying Material

1. Research data corresponding to Chapters 2, 3, and 4 is available through the University of Southampton data repository (10.5258/SOTON/D3254).

2. **Appendix A** contains the published research article reproduced in Chapter 2: Mechanically Axially Chiral Catenanes and Noncanonical Mechanically Axially Chiral Rotaxanes

3. **Appendix B** contains the published research article reproduced in Chapter 3: Facial Selectivity in Mechanical Bond Formation: Axially Chiral Enantiomers and Geometric Isomers from a Simple Prochiral Macrocycle

4. **Appendix C** contains the published research article reproduced in Chapter 4: The Final Stereogenic Unit of [2]Rotaxanes: Type 2 Geometric Isomers

Research Thesis: Declaration of Authorship

Print name: PETER ROBERT GALLAGHER

Title of thesis: THE HITCHHIKER'S GUIDE TO MECHANICAL STEREOCHEMISTRY

I declare that this thesis and the work presented in it are my own and has been generated by me as the result of my own original research.

I confirm that:

1. This work was done wholly or mainly while in candidature for a research degree at this University;
2. Where any part of this thesis has previously been submitted for a degree or any other qualification at this University or any other institution, this has been clearly stated;
3. Where I have consulted the published work of others, this is always clearly attributed;
4. Where I have quoted from the work of others, the source is always given. With the exception of such quotations, this thesis is entirely my own work;
5. I have acknowledged all main sources of help;
6. Where the thesis is based on work done by myself jointly with others, I have made clear exactly what was done by others and what I have contributed myself;
7. Parts of this work have been published as:-

   J. R. J. Maynard, P. Gallagher, D. Lozano, P. Butler, S. M. Goldup, *Nat. Chem.* **2022**, *14*, 1038–1044.

   A. Savoini, P. R. Gallagher, A. Saady, S. M. Goldup, *J. Am. Chem. Soc.* **2024**, *146*, 8472–8479.

   P. R. Gallagher, A. Savoini, A. Saady, J. R. J. Maynard, P. W. V. Butler, G. J. Tizzard, S. M. Goldup, *J. Am. Chem. Soc.* **2024**, *146*, 9134–9141.

Signature: _____ Date:_____

Acknowledgements

I would like to start by thanking Steve for giving me the opportunity to do a summer project in his group during the second year of my undergraduate and giving me a glimpse into the wonderful world of interlocked molecules. Steve, thank you for being an encouraging mentor, an exceptional role model as a scientist, and for surrounding me with such an incredible group of people – who all in their individual ways shaped me into the chemist and person I am today. Most importantly, in the face of many challenges, thank you for your encouragement, empathy and support personally that has enabled me to achieve so much during my PhD.

It would take pages to individually acknowledge everyone I've worked with over my PhD, but I will try to keep it short… Mike, thank you for taking me under your wing and supervising me during my summer and Masters projects. Thanks to Jack, Fede, and Poom for company on COVID weekend shifts in 4005, and Ellen for being my first PhD fumehood neighbour despite not being allowed to work at the same time as each other. Thanks to Georgia for letting me take over 4005, Jorge for being fabulous and Martin for always making the lab a happier place. Thanks to Mandeep for being the boss, Matt for always being great craic, and although I wish I worked closer with him, Andrew for being an amazing synthetic chemist. Cal, thank you for coffee breaks and showing me that the North isn't all bad. Grazie a Chiara e Ilario, who brought me so much joy and taught me so much despite being in the group for short periods of time. Thanks to the breakfast club for Eggs Royale and being an incredible group of friends. Thanks to Noël for teaching me that Les Lacs Du Connemara is a song of celebration and that the best chemistry happens after 5PM. Thanks to David and Arnau for Catalonian music and being some of the most infectiously happy and kind people I have ever met. Thanks to Alex for NMR basketball and always being able to make me laugh. Patrick, thank you for solving my first crystal structure and sending me down the rabbit hole of wanting to 3D print all of them. Thanks to Abed for teaching me so much in being both a great chemist and a great father, I am so grateful that I was able to work so closely with you and hope to keep in contact for years to come. Andrea, I will never be able to thank you enough for everything in and out of the lab. Thank you for all your hard work, chaotic influence, cat videos, and being my second favourite French lab mate.

Thank you to my family for their unconditional love and support. Finally, I would like to thank Lauren for being the most amazing wife, her unending support and motivation, and for our amazing family – Shane, Maisie and William. Thank you, William, for being more than we could ever imagine and for keeping me company on late nights while writing this thesis. I am proud of what I have achieved during my PhD, but nothing makes me prouder than being your father.

Definitions and Abbreviations

δ _____ Chemical shift

Ac _____ Acetyl

AMT _____ Active metal template

Aq. _____ Aqueous

Ar _____ Aromatic

AT-CuAAC_____ Active template copper-mediated alkyne-azide cycloaddition

Boc _____ *t*-butyloxycarbonyl

CD _____ Circular dichroism

CEATS _____ Crown ether active template synthesis

CIP _____ Cahn-Ingold-Prelog

co-c _____ Co-conformational covalent isomer

co-ma _____ Co-conformational mechanical axial isomer

co-mp _____ Co-conformational mechanical planar isomer

COSY _____ Correlation spectroscopy

CSP-HPLC _____ Chiral stationary phase high-performance liquid chromatography

D _____ Dextrorotatory isomer

de _____ Diastereomeric excess

DMF _____ N,N-Dimethylformamide

DMSO _____ Dimethylsulfoxide

dr _____ Diastereomeric ratio

EDTA _____ N,N,N',N'-ethylenediamine tetraacetate

E _____ *E* isomer (geometric)

ee _____ Enantiomeric excess

EI _____ Electron Ionisation

equiv. _____ Equivalent

ESI _____ Electrospray ionisation

Et _____ Ethyl

h _____ Hours

HMBC _____ Heteronuclear multiple-bond correlation

HPLC _____ High performance liquid chromatography

HR-MS _____ High resolution mass spectrometry

HSQC _____ Heteronuclear single quantum correlation

Hz _____ Hertz

IBX _____ 2-iodoxybenzoic acid

IR _____ Infrared

J _____ Coupling constant

JMOD _____ J-modulation spin-echo

LR-MS _____ Low resolution mass spectrometry

m _____ Mechanical isomer

M _____ M isomer (helical)

M _____ Molar

ma _____ Mechanical axial isomer

MAC _____ Mechanically axially chiral

Me _____ Methyl

MGI _____ Mechanical geometric isomerism

MGI-1 _____ Type 1 mechanical geometric isomer

MGI-2 _____ Type 2 mechanical geometric isomer

min _____ Minute

MIM _____ Mechanically interlocked molecule

mp _____ Mechanical planar isomer

m.p. _____ Melting point

MPC _____ Mechanically planar chiral

MS _____ Mass spectrometry

Ms_____ Methanesulfonyl

NMR _____Nuclear magnetic resonance

P _____*P* isomer (helical)

PCSP-HPLC _____Preparative chiral stationary phase high performance liquid chromatography

ppm _____Parts per million

q-GSD _____ Quantitative global spectral deconvolution

q-NMR _____ Qualitative nuclear magnetic resonance

quant. _____ Quantitative

R _____*R* isomer

rt _____ Room temperature

S _____*S* isomer

SCXRD_____ Single crystal x-ray diffraction

TBAF_____Tetrabutyl Ammonium Fluoride

TFA _____Trifluoroacetic acid

THF _____Tetrahydrofuran

TLC_____ Thin layer chromatography

TOF_____ Time of flight

Ts _____ 4-Toluenesulfonyl

UV_____ Ultraviolet

Z _____*Z* isomer (geometric)

Chapter 1: Introduction

Abstract: Interlocked molecular structures have intrigued chemists for over a century. This chapter introduces the concept of the *mechanical bond*, its consequences and also the consequences of the language that has developed to describe interlocked systems. It then overviews key advances in the synthesis of mechanically interlocked molecules and a detailed discussion of the interesting stereochemistry that can arise as a result of the confinement of interlocked molecules and advances in their stereoselective synthesis.

Prior publication: None of this work has been previously published.

1.1. Mechanically Interlocked Molecules

Mechanically interlocked molecules (MIMs) can no longer be described as 'new' or 'relatively unresearched' – since the earliest reports of their discussion over a century ago by Willstätter, MIMs have developed from theoretical oddities to an expansive field boasting a Nobel prize for their use as molecular machines.[1,2] Despite the maturity of the field, many concepts such as classification, nomenclature and understanding of stereochemistry remain vague. While issues surrounding mechanical stereochemistry are largely due to a lack of focussed, holistic analysis, issues around nomenclature ultimately stem from the organic growth of the field and adoption of terminology over time. While linguistic drift is usually innocent, in science where words have precise technical meaning, it often leads to confusion and imprecision. This is especially problematic in a field that intersects many others and is contributed to by a wide array of specialities. One fundamental concept that has fallen foul to this is the 'mechanical bond'.

1.1.1. What is a mechanical bond?

The archetypal mechanically bonded structures are catenanes, in which rings are interlinked like links in a chain, and rotaxanes, in which a ring is threaded onto an axle with bulky end groups to prevent de-threading (Figure 1.1).[3] Whereas Pauling defined chemical bonding as two species which are bound by interacting forces, the term 'mechanical bond' was first used by Frisch *et al.* in 1953 to describe the inseparability of the constituent rings of a catenane rather than any attraction between them.[4,5] Frisch and Wasserman later described catenanes to be 'topologically bonded'.[1] Stoddart and Bruns later wrote a clear definition of the mechanical bond to be, "*An entanglement in space between two or more molecular entities (component parts) such that they cannot be separated without breaking or distorting chemical bonds between atoms*".[6]

This leads on to the question of what structures should be regarded to be MIMs. Knots are self-intertwined single component molecules so are therefore not mechanically bonded (Figure 1.1). However, they are regarded as MIMs as their topology is maintained by the same mechanical requirement that holds the components of rotaxanes and catenanes together. Conversely, pseudorotaxanes are akin to rotaxanes but do not possess bulky end groups and are therefore not held together mechanically, any more than any other simple host-guest complex (Figure 1.1).

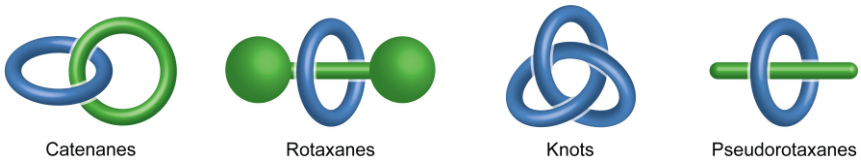

Figure 1.1 - Cartoon representations of catenanes, rotaxanes, knots and pseudorotaxanes.

1.1.2. The consequence of molecular topology

The concepts of topology and topological isomerism are fundamental to the field of MIMs but is a term often misapplied in chemistry to mean 'shape' when the term topography would be more fitting (concerning geometry, size, and shape).[7] Formally, topology concerns the properties of networks, surfaces and objects that are unchanged through continuous deformations and is an exceedingly complex subject whose rules do not always make intuitive sense in chemistry.[8] To consider the topological properties of a molecule, we must first reduce it to a molecular graph, where every atom becomes a 'vertex' and each bond becomes an 'edge' which can be freely manipulated, disregarding bond angles and lengths.[7,9] In a chemical context, topological isomers are distinct molecular entities that cannot be exchanged without breaking, making or allowing bonds to pass through each other. Topological properties are expressed even in small molecules, for example, isomers of butanol (Figure 1.2a). The stereoisomers of 2-butanol, distinguished by different spatial arrangements, are topologically identical – representable by the same molecular graph (isotopic) with the same connectivity of vertices (homeomorphic) by relaxation of Euclidean properties. In contrast, constitutional isomers 1- and 2-butanol are topologically distinct, being neither isotopic nor homeomorphic. Appropriately, Frisch and Wasserman defined catenanes to be 'topologically bonded' as catenated rings cannot be interconverted though continuous deformation to the unlinked rings and are therefore isomers that are homeomorphic (same connectivity) but not isotopic (different topology) – as a result, two-dimensional projections of such structures must have edges that cross one another (Figure 1.2b).[1] Considering a hypothetical rotaxane composed of a cyclohexane ring and stoppered n-hexane axle, when reduced to its molecular graph, they can be disassembled to the component ring and axle – allowing the structure to be drawn on a flat plane – without lines passing through each other or being broken and rotaxanes are therefore topologically trivial objects (Figure 1.2c).

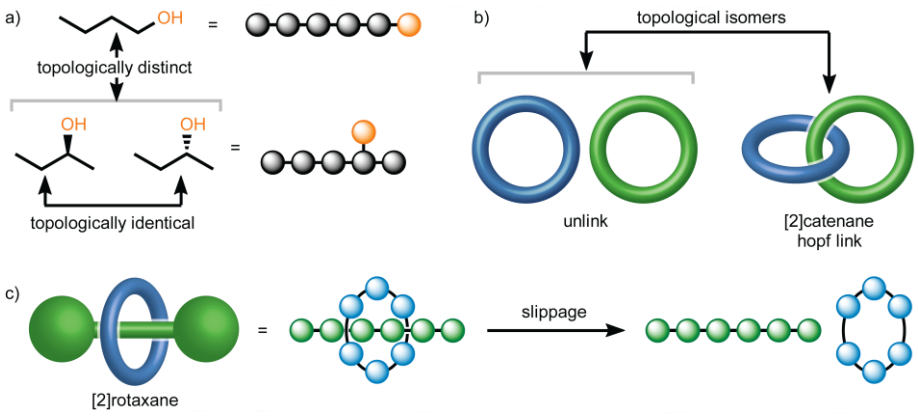

Figure 1.2 - Cartoon and schematic representations illustrating topological isomerism in a) constitutional and stereo isomers of butanol, b) unlinked rings and catenanes, and c) rotaxanes illustrating their topological triviality.

While the interlocked nature of catenanes is indisputable from topological standpoint, rotaxanes – owing to their topological triviality – open a metaphorical can-of-worms into whether they are, or the extent to which they are 'interlocked'. While it may seem simple to say that the term rotaxane should only apply to systems that can only be disassembled through breaking *covalent bonds*, as bonding is appreciated to lie on a spectrum between covalent and ionic, we quickly encounter another problem. Unfortunately, there are many examples of systems in literature which are kinetically stable due to strong intercomponent interactions or displaying very slow de-threading either being described as rotaxanes, or through omitting the use of pseudo in their vernacular name, have aided in blurring the lines between rotaxanes and pseudorotaxanes.

1.1.3. Vernacular nomenclature in MIMs

Many simple molecules have widely adopted trivial names in place of their scientifically unambiguous IUPAC name such as caffeine – which is far more approachable than 1,3,7-trimethyl-3,7-dihydro-1*H*-purine-2,6-dione.[10] Vernacular nomenclature in MIMs has been built upon as new structures were developed and, in ideal cases, balances brevity and clarity, while remaining consistent and memorable. Stoddart has previously offered suggestions for the continued growth of vernacular nomenclature in MIMs in that further additions should be pragmatic, systematic and that the first person(s) who synthesise a new class of interlocked compound having the right to name it.[6] At the most basic level, MIMs are typically described using a generic name prefixed by [n] to denote the number, n, of mechanically bonded covalent subcomponents they contain. Using this approach, catenanes and rotaxanes with different numbers of interlocked components are described as [n]catenanes or [n]rotaxanes. However, this is vague because the same value of [n] can describe many different structures (Figure 1.3a,b).

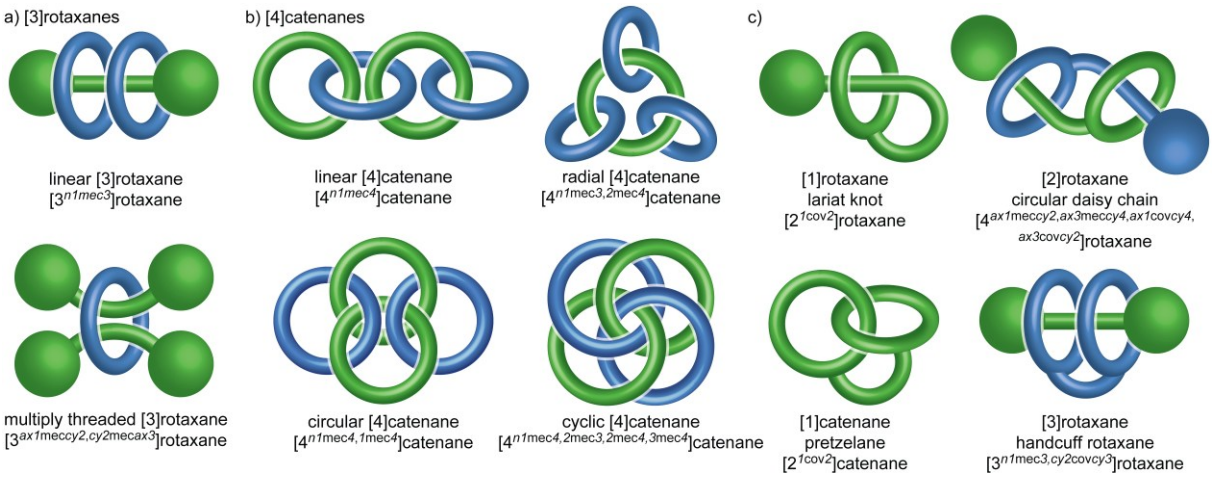

Figure 1.3 - MIMs described by generic, vernacular and unambiguous identifiers. a) [3]rotaxane isomers. b) [4]catenane isomers. c) selected MIMs with popularised vernacular nomenclature.

At the opposite extreme, attempts have been made to impose a systematic nomenclature for MIMs starting with Schill (since approved by IUPAC),[3,11,12] and later extended by Vögtle to allow structures to be defined unambiguously (Figure 1.3).[13] Under these systems, simple structures are first named according to their mechanical connectivity followed by any covalent links between them. For example, pretzelanes (covalently linked [2]catenanes) have an approachable formal definition – [2^{1cov2}]catenane (where '*1*cov*2*' indicates the covalent link between macrocycles 1 and 2, which are the only macrocycles present). Next, the systematic names of the subcomponents are included, and it is at this point that the names quickly become unwieldy as structural complexity increases. For this reason, such systematic names are not widely used because they go far beyond the point of convenience and brevity.[10]

While the majority of MIM vernacular is useful, some present problems. [2]Rotaxanes are easily visualised and [1]rotaxanes are intuitively rotaxane-like structures with a link between the macrocycle and axle (therefore becoming a single component).[6] As with knots, these are typically described as MIMs despite not containing a mechanical bond - according to Stoddart's definition - as they only contain a single component. [1]Rotaxanes are also known as *lariat knots* despite technically being neither rotaxanes, nor knots! A more correct description of the relationship between the threaded and unthreaded isomers of [1]rotaxanes is that they are atropisomers as they can be interconverted by rotation about single bonds which is prevented by steric hindrance.

1.1.4. Why nomenclature matters

To end this section, I would like to focus on why nomenclature actually matters and the impact of its imprecise and incorrect usage. One such example was reported by Puddephat and co-workers and their synthesis of what they reported to be a 'topologically chiral' catenane (see Section 1.3.3.2).[14] At the time of publication, chiral catenanes in literature exclusively displayed topological chirality, but their catenanes were actually topologically achiral. In fact, they had prepared the first example of a mechanically axially chiral catenane, a relatively under-investigated form of mechanical stereochemistry, despite being identified at the same time as topologically chiral catenanes.[1] Their misidentification allowed this paper to go unnoticed for what it truly was at the time, and is a prime example of why nomenclature should be carefully considered. Moreover, nomenclature must be precise in both usage and definition. One of the oldest paradigms in mechanical stereochemistry stated that catenanes composed of oriented rings were 'topologically chiral' with stereochemistry that is inherently topological. This was recently disputed, with the report of a catenane that is topologically achiral despite being composed of oriented rings, leading to the unification of mechanical planar stereochemistry in catenanes and rotaxanes.[15]

1.2. Synthetic approaches towards interlocked molecules

1.2.1. Statistical syntheses

Despite many attempts to synthesise MIMs in the middle and late 1950s *via* covalent or inclusion templates, they were first prepared by relying on the chance encounter and arrangement of precursor molecules – statistical syntheses.[7,16,17] This was achieved by Wasserman in 1960 by interlocking two 34-membered rings *via* acyloin condensation of di-ester premacrocycle **1** inside the cavity of macrocycle **2** (Scheme 1.1a).[18] The success of this approach was solely supported by infrared (IR) analysis at the time and only recently confirmed by modern spectroscopic methods to reproducibly prepare [2]catenane **3** in a 0.03% yield.[19] Rotaxanes were later statistically synthesised by Harrison and Harrison through iterative treatments of a solution of chloride **5** and diol **6** to resin-bound macrocycle **4** in a 6% yield of [2]rotaxane **7** (Scheme 1.1b).[20]

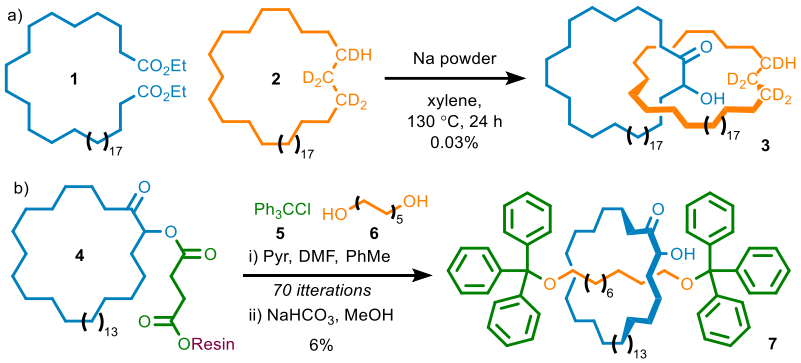

Scheme 1.1 - Early syntheses of MIMs. a) Wasserman's statistical synthesis of hetero[2]catenane **3**. b) Harrison and Harrison's statistical synthesis of [2]rotaxane **7**.

1.2.2. Covalent template syntheses

Initial efforts to increase the reliability of mechanical bond formation began by 'directing' their formation *via* pre-arrangement with intercomponent covalent linkages that would then be cleaved to liberate the independent components and afford interlocked products. Directed syntheses were first employed by Schill, initially in 1964 with Lüttringhaus to prepare [2]catenane **11** from covalently linked precursors arranged around cyclic catechol **8** (Scheme 1.2)[21] Using this methodology, Schill then successfully prepared higher order catenanes, rotaxanes, and also attempted the synthesis of knots. However, by this point, other synthetic approaches had already surpassed the efficiency of the covalent template approach.[6,22,23]

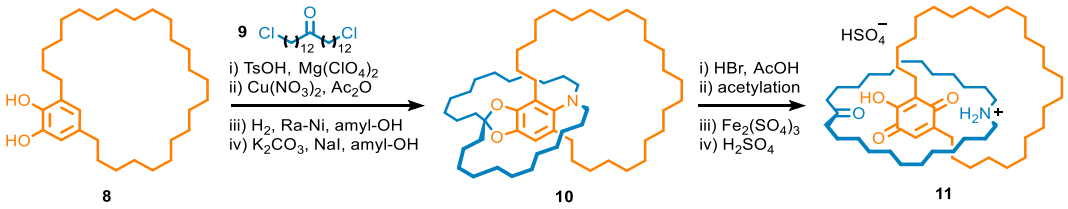

Scheme 1.2 - Schill and Lüttringhaus' covalent templated synthesis of hetero[2]catenane **11**.

1.2.3. Non-covalent interaction templates

Many strategies have been used to preorganise molecules through non-covalent interactions to favour mechanical bond formation between them. The first synthesis to utilise non-covalent interactions was reported by Ogino relying on the solvophobic effect to form an enthalpically and entropically favoured inclusion complex, followed by stoppering (Scheme 1.3a).[24] This strategy was first reported with cyclodextrin (CD) macrocycles but cucurbit[n]urils, pillar[n]arenes and other routinely available macrocyclic hosts have now been used in high yielding syntheses that rely on the solvophobic effect.[6] Donor-acceptor interactions have also been exploited, such as Stoddart's π-donor-π-acceptor inclusion complex syntheses of [n]rotaxanes and [n]catenanes (Scheme 1.3b).[25] Stoddart also employed hydrogen bonding to form ammonium-crown ether inclusion complexes (Scheme 1.3c).[26] Hydrogen bonding has since been used to template both the formation of pseudorotaxane intermediates and macrocycle formation around a preformed axle, such as reported by Leigh *via* the formation of a tetralactam macrocycle around a fumaramide axle (Scheme 1.3d).[27] Metal coordination has also been used to preorganise rotaxane and catenane precursors as pioneered by Sauvage *via* complexation of a phenanthroline based macrocycle and premacrocycle to Cu(I) prior to cyclisation (Scheme 1.3e).[28]

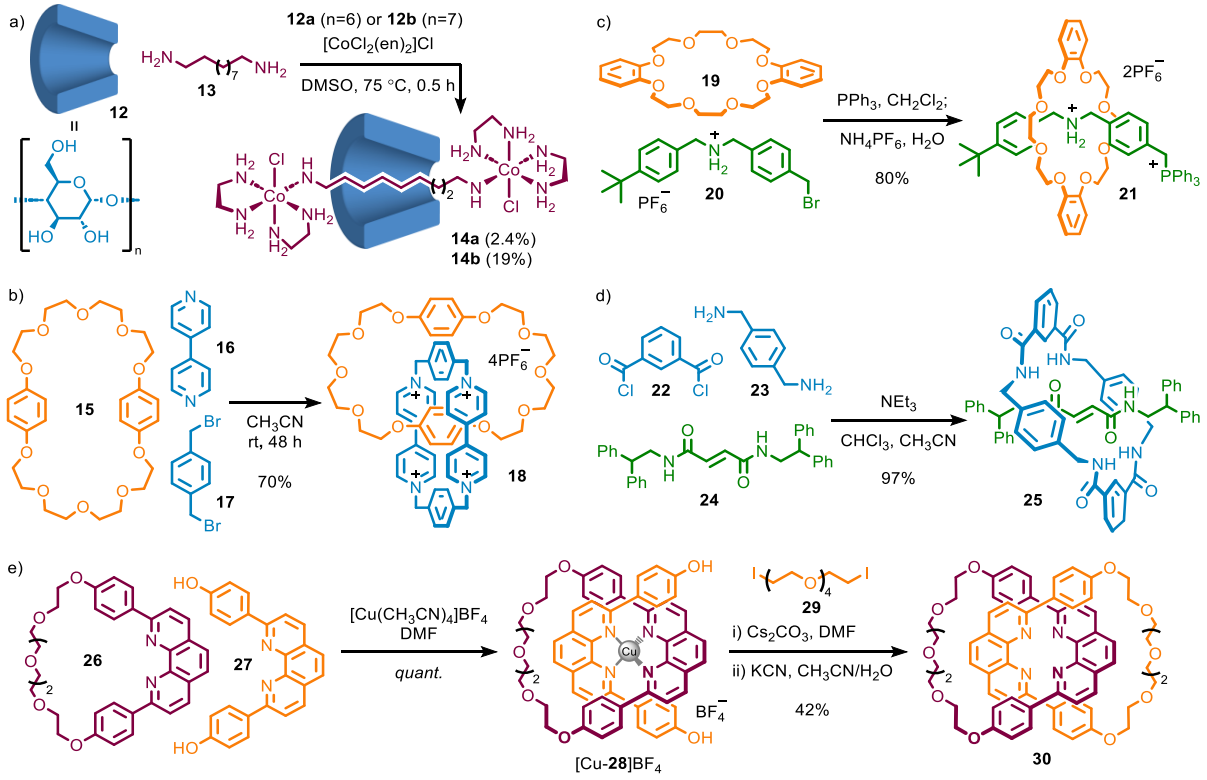

Scheme 1.3 - Non-covalent template syntheses of MIMs. a) Ogino's cyclodextrin based rotaxane **14** *via* solvophobic interactions. b) Stoddart's π-donor-π-acceptor based catenane **18** and c) ammonium-crown hydrogen bond templated rotaxane **21**. d) Leigh's tetralactamisation synthesis of rotaxane **25**. e) Sauvage's passive-metal templated approach toward catenane **30**.

1.2.4. Active template approaches for the synthesis of MIMs

In 2006 Leigh introduced the 'active metal template' (AMT) approach to MIMs.[29] Leigh and co-workers used an active template copper-mediated alkyne-azide cycloaddition (AT-CuAAC) reaction in which a macrocycle-bound copper ion catalysed axle formation selectively through the cavity of pyridine macrocycle **31** (Scheme 1.4a).[30,31] Later the same year, Saito and co-workers employed a Glaser homocoupling AMT reaction between alkyne **36** mediated by phenanthroline-based macrocyclic complex **35**-CuI to give rotaxane **37** (Scheme 1.4b).[32] Saito and co-workers also achieved the first AMT synthesis of a [2]catenane in 2009, by AT-Glaser coupling of bis-alkyne premacrocycle **38** (Scheme 1.4b).[33] AMT methodologies paved the way for the development of functional interlocked molecules and many different transition metal catalysed reactions have been utilised to synthesise interlocked molecules since these first reports.[34]

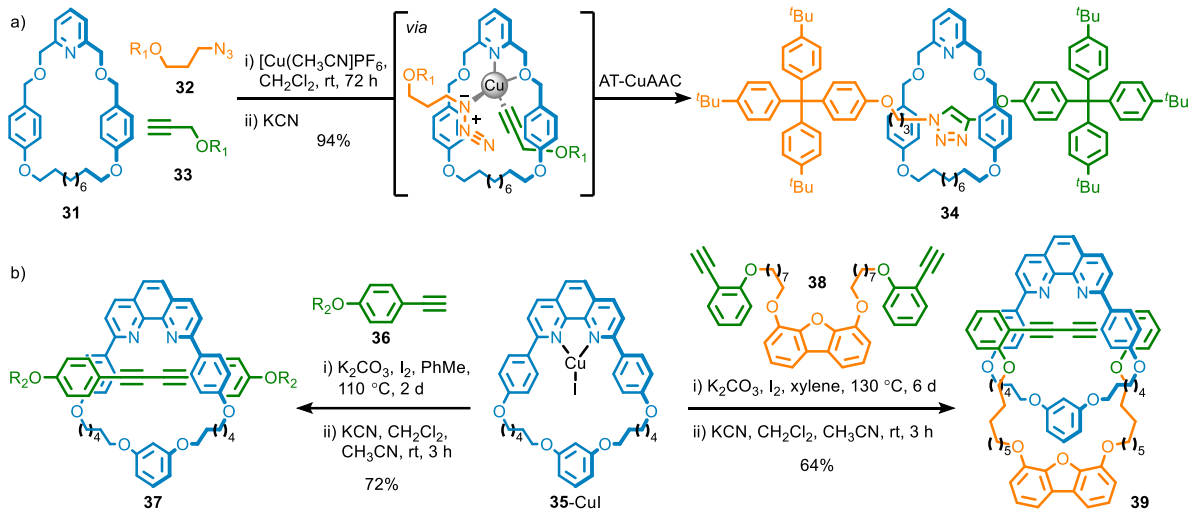

Scheme 1.4 - Seminal AMT syntheses. a) Leigh's AT-CuAAC synthesis of rotaxane **34**. b) Saito's AMT Glaser coupling approach to rotaxane **37** and catenane **39**. R_1 = -(4-C_6H_4)-C(4-^{t}BuC_6H_4)$_3$ R_2 = -$(CH_2)_6$-C(1,1'-biphenyl)$_3$.

More recently, Leigh and co-workers devised a metal-free active template methodology for the synthesis of crown-ether based rotaxanes in which they propose that the transition state leading to axle formation is stabilised inside the macrocycle cavity (Scheme 1.5).[35,36] Crown ether active template synthesis (CEATS) is an emerging and promising methodology that has demonstrated a wide substrate scope and good yields from commercially available starting materials.[37]

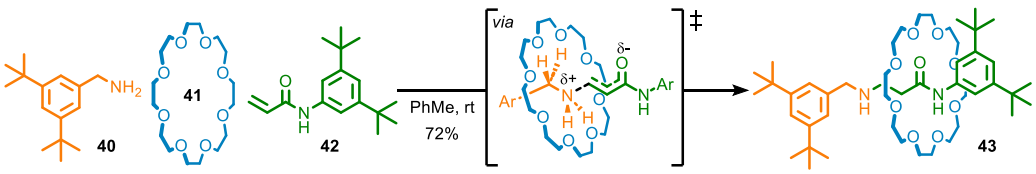

Scheme 1.5 - Leigh's metal free CEATS of rotaxane **43**.

1.3. Stereochemistry arising from the mechanical bond

Covalent stereogenic units can be defined by the way in which specific spatial relationships of atoms and groups arise and are maintained in a molecule's highest symmetry representation due to the fixed bond lengths and angles of covalent structures. Similarly, the mechanical bond can give rise to well-defined, distinguishable isomers that differ in the spatial arrangements of atoms and groups, even in the absence of covalent stereochemistry, thereby giving rise to mechanical stereogenic units.[6,38] Similar to classical covalent stereogenic units (such as centres, axes, planes and helices), mechanical stereogenic units can also be chirotopic leading to mechanically chiral structures that possess no improper symmetry operations such as mirror planes, points of inversion and/or improper rotation axes.[39,40] Some are unconditionally chiral, regardless of their chemical composition, meaning the molecule possesses a structure that is non-superimposable on its mirror image due to the pattern of crossing points (Figure 1.4). For example, a [2]catenane formed from two fully symmetrical macrocycles with two crossing points – a Hopf link – is achiral (Figure 1.4a), but if two more crossing points are added, the resulting catenane – colloquially known as a Solomon link – is topologically chiral with its topology and 'handedness' maintained through continuous deformation (Figure 1.4b). Conditional mechanical stereogenic units can also arise when the mechanical bond reduces the symmetry of the interlocked components.

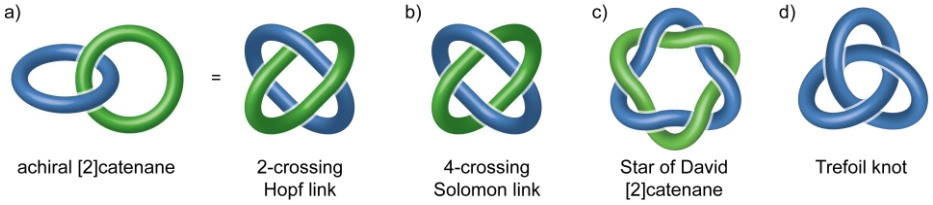

Figure 1.4 - Unconditional mechanical chirality: a) an achiral 2-crossing [2]catenane b) a chiral 4-crossing Solomon link, c) a chiral 6-crossing Star of David [2]catenane, and d) the Trefoil knot.

1.3.1. Conditional mechanical stereogenic units

The concept of conditional mechanical stereochemistry in catenanes was first discussed in 1961 by Wasserman and Frisch and later in rotaxanes by Schill in 1971. The mechanical stereogenic units which they identified have since been described by Goldup as 'canonical mechanical stereogenic units'.[1,3] A further mechanical stereogenic unit was identified in 1995 and this thesis describes the identification and synthesis of further 'non-canonical mechanical stereogenic units' previously overlooked in early reports.[41,42,43]

1.3.1.1. Canonical conditional mechanical stereogenic units

Prior to Wasserman and Frisch seminal report entitled 'Molecular Topology', Clossen had identified that interlocking oriented rings **I** (with a defined sequence of segments or atoms) results in catenanes **II** with enantiomers that cannot be converted through continuous deformation and therefore 'topologically chiral'.[1] However, it has since been proven by Goldup, that catenanes **III** composed of oriented rings can be topologically achiral (with stereochemistry that is Euclidean, arising from the rigid geometry of an exocyclic double bond) and that they are more accurately described as mechanical planar chiral (MPC) (*vide infra*). This terminology unifies catenane stereochemistry with the analogous rotaxane stereogenic unit (Figure 1.5a).[15] Wasserman and Frisch also identified that interlocking facially dissymmetric rings **IV** (with substituents projecting out of the ring plane) results in catenanes **V** which are stereochemical related to allenes, later described as mechanical axially chiral (MAC) by Stoddart and Bruns (**Figure 1.5**b).[6] In 1971, Schill also identified that enantioisomerism in rotaxanes occurs when an oriented ring encircles an oriented axle **VI** and – owing to a previous definition of enantioisomerism due to ring segment sequences and distribution of stereogenic centres in cyclic peptides – described them as 'cyclochiral' (**Figure 1.5**c).[3,44] Later, Takata described them as a form of planar chirality and Goldup proposed the term 'mechanically planar' to distinguish it from covalent planar chirality.[45,46] Schill also identified that rotaxanes **VIII** can display geometric stereochemistry related to alkenes when a facially dissymmetric ring encircles an oriented axle, which was later described by Kaifer and others as orientational isomerism, but which we prefer to refer to as mechanical geometric isomerism (MGI) (**Figure 1.5**c).[47,43]

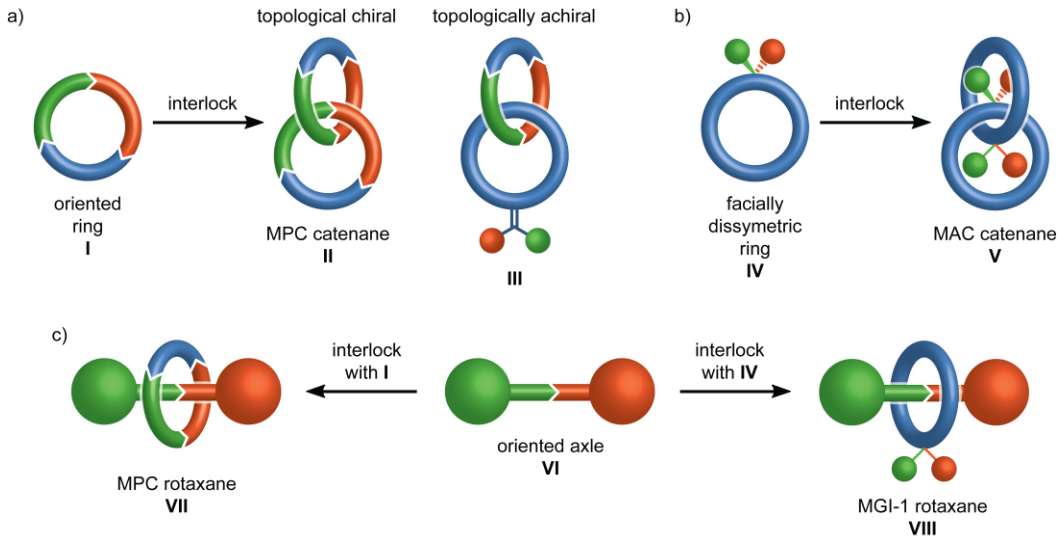

Figure 1.5 - Canonical conditional mechanical stereogenic units identified by Frisch, Wasserman and Schill. a) Topologically chiral and achiral MPC catenanes composed of oriented rings. b) MPC catenanes composed of facially dissymmetric rings. c) MPC and MGI-1 rotaxanes composed of oriented axles encircled by either an oriented or facially dissymmetric ring.

1.3.1.2. The complete set of mechanical stereogenic units

A thorough stereochemical analysis by group theory can be used to establish the complete set of mechanical stereogenic units.[48] Beginning from first-principles, C_{nv}, C_{nh}, and S_{2n} are the only ring and axle point groups that can give rise to conditional mechanical stereochemistry – of which $C_{\infty v}$, C_{1h}, and C_i (equivalent to S_2) are chemically relevant axle point groups (Figure 1.6a). Combining two oriented (C_{nh}) or facially dissymmetric (C_{nv}) rings gives rise to the chiral catenanes originally identified by Wasserman and Frisch (MPC and MAC catenanes respectively), whereas interlocking one oriented and one facially dissymetric rings produces the geometric stereogenic unit identified by Stoddart.[1,41] The same approach can be taken to define the mechanical stereogenic units in rotaxanes, but this can be achieved more elegantly through the notional ring-opening-and-stoppering of the previously defined mechanically stereogenic catenanes. Cleavage of a MPC catenane affords the analogous stereogenic rotaxane (Figure 1.6b), as does a MAC catenane as identified by Maynard and Gallagher *et al.* (Figure 1.6c).[42] Cleavage of either the oriented or the facially dissymmetric ring of an MGI catenane affords type 1 MGI or type 2 MGI rotaxanes respectively (Figure 1.6d).[43] In all cases, the absolute stereochemistry of the mechanical stereogenic units can be assigned by viewing vectors associated with each component at their mutual crossing point within the structure (Figure 1.6b inset). Chirotopic mechanical stereochemistry arises when these vectors cannot be made co-planar whereas mechanical geometric stereochemistry arises when these vectors can be made coplanar within the confines of the mechanic bond.

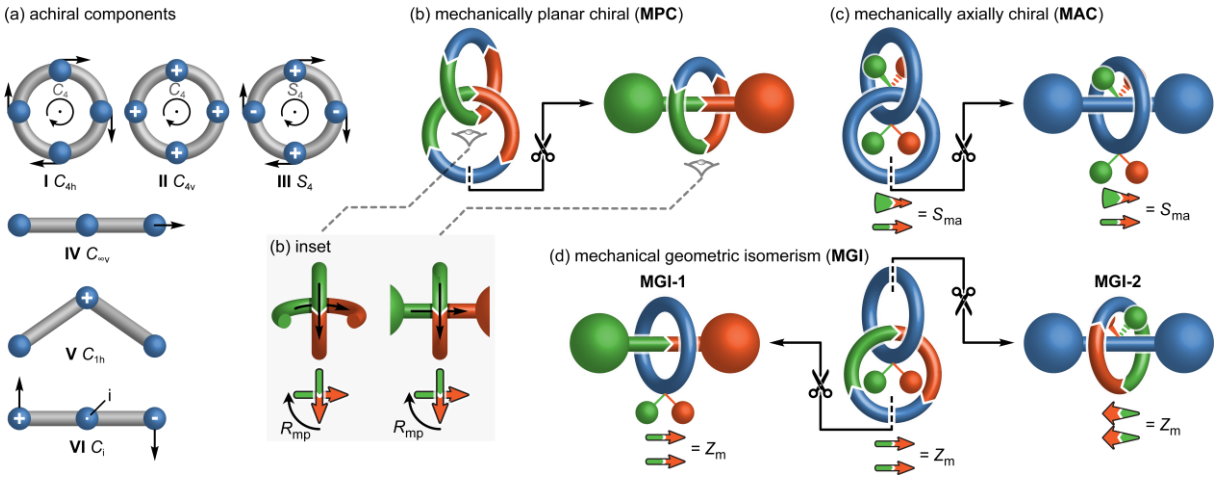

Figure 1.6 - The complete set of mechanical stereogenic units. a) achiral ring (**I-III**) and axle (**IV-VI**) components that give rise to b) MPC, c) MAC, and c) MGI stereochemistry with relevant vectors to assign their absolute stereochemistry. Priority is such that vectors run from green to orange.

1.3.2. Mechanical planar stereoisomerism

1.3.2.1. Assigning the mechanical planar chiral stereogenic unit

A method to assign the absolute stereochemistry of the MPC catenanes and rotaxanes was proposed by Vögtle based on the Cahn-Ingold-Prelog (CIP) priority rules to define component orientation.[49,50] This was refined by Goldup, who proposed that an "mp" subscript be included to indicate that the stereodescriptor refers to a mechanical planar stereogenic unit (Scheme 1.6).[48]

1) Following the CIP rules, identify the highest priority atom on one ring and label it as "**A**"
2) Moving outward from **A** in spheres, as per the CIP method for assigning covalent stereogenic centres, determine the highest priority atom (CIP) that can be used to define an orientation of the ring (typically a ligand of **A**) and label it as "**B**". If **A** does not lie within the ring structure, the same method is used but atom **B** is the atom in the earliest sphere that allows direction to be defined. The orientation of the ring is defined by the vector **A** → **B**, which, where relevant, passes through the intervening atoms (i.e., follows the bonds).

3,4) Repeat steps (1) and (2) on the second subcomponent to identity its orientation.

5) Reduce the assembly to the corresponding vectors and observe their relative orientation at the crossing point within the rings (catenanes) or from the macrocycle to the axle (rotaxanes).
6) If the path from the head of the front vector to the tail of the rear vector corresponds to a clockwise path the stereolabel is assigned as R_{mp}, counterclockwise = S_{mp}.

1.3.2.2. Synthesis of mechanical planar chiral molecules

Employing a passive-metal template, Sauvage reported in 1988 the first synthesis of racemic MPC catenates [Cu**46**]BF_4 with macrocycle orientation arising from phenyl substitution in the phenanthroline moiety of diphenol premacrocycle **44** (Scheme 1.6a).[51] Five years later in collaboration with Okamoto *et al.*, they were able to achieve partial resolution of enantiomeric catenates (R_{mp})-[Cu**46**]BF_4 and (S_{mp})-[Cu**46**]BF_4 by preparative chiral stationary phase high performance liquid chromatography (PCSP-HPLC).[52] Following this success, Vögtle in 1996 prepared the first example of racemic MPC rotaxanes **50** and later reported their enantioseparation PCSP-HPLC.[53,54]

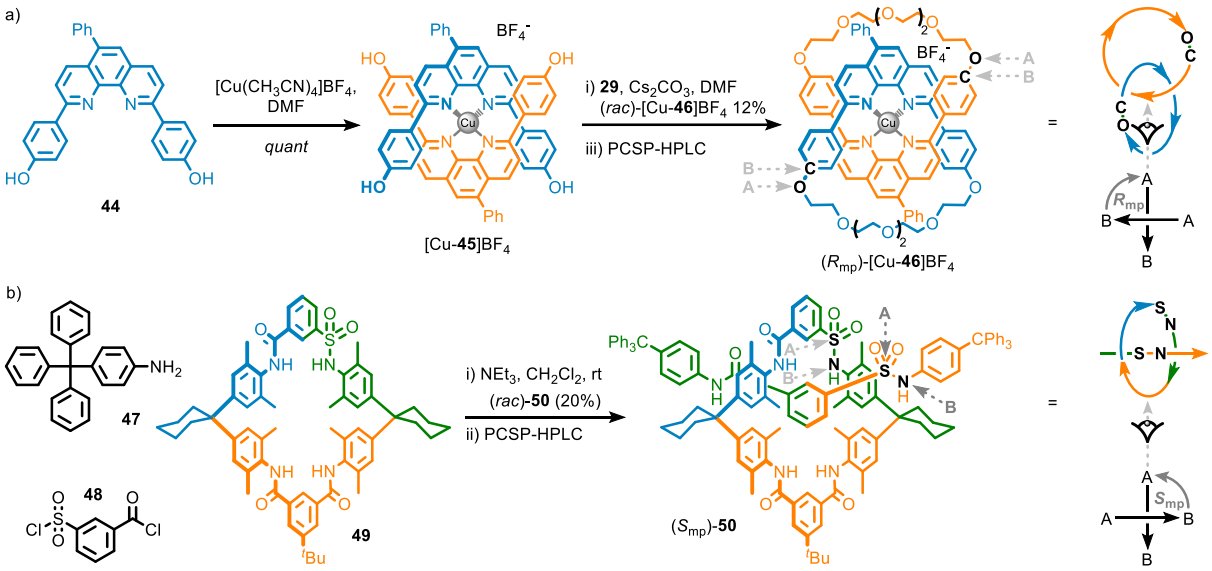

Scheme 1.6 - Synthesis and resolution of enantiomerically enriched MPC a) Cu^{I} [2]catenates by Sauvage, and b) [2]rotaxanes by Vögtle. CIP priority atoms are indicated that allow the assignment of absolute stereochemistry.

Owing to their structural similarities, the selective synthesis of MPC rotaxanes and catenanes without resolution have developed very similarly. Goldup and Bordoli reported the first successful chiral auxiliary synthesis of an MPC rotaxane by using sacrificial covalent stereochemistry that could be removed after the separation of mechanical epimers to afford enantiopure MPC rotaxanes.[46] Use of chiral azide D-**53** in the AT-CuAAC reaction afforded mechanical epimers (D,*R*/*S*$_{mp}$)-**54**. Following separation of these diastereomers by silica gel chromatography, the chiral sugar auxiliary was displaced by a simple achiral amine to afford enantiopure rotaxanes (*S*$_{mp}$)-**56** and (*R*$_{mp}$)-**56** (Scheme 1.7a). MPC catenanes have also yielded to chiral auxiliary strategies (Scheme 1.7b).[55] Goldup then found that remarkable stereocontrol can be achieved in the AT-CuAAC reaction when a phenylalanine derived α-chiral azide (*S*)-**60** is used as a coupling partner.[56] This was later developed into an 'interlocking-chiral auxiliary' strategy, inspired by works from Leigh and Coutrot,[57,58] in which azide (*S*)-**60** could be used to reliably set the orientation of macrocycle **51c** when coupled with an *o*-methyl substituted alkyne (Scheme 1.7).[59] The o-Me substituent in the product also disfavours co-conformations in which the ring encircles the auxiliary triazole unit and so the macrocycle was found to preferentially reside around almost any desired receiving unit. Suzuki cross-coupling could then be used to trap the mixture of co-conformations as the substituent introduced is too bulky to allow the ring to pass. Finally, methanolysis of the mixture of co-conformational isomers, was used to cleave the chiral auxiliary with retention of stereopurity.

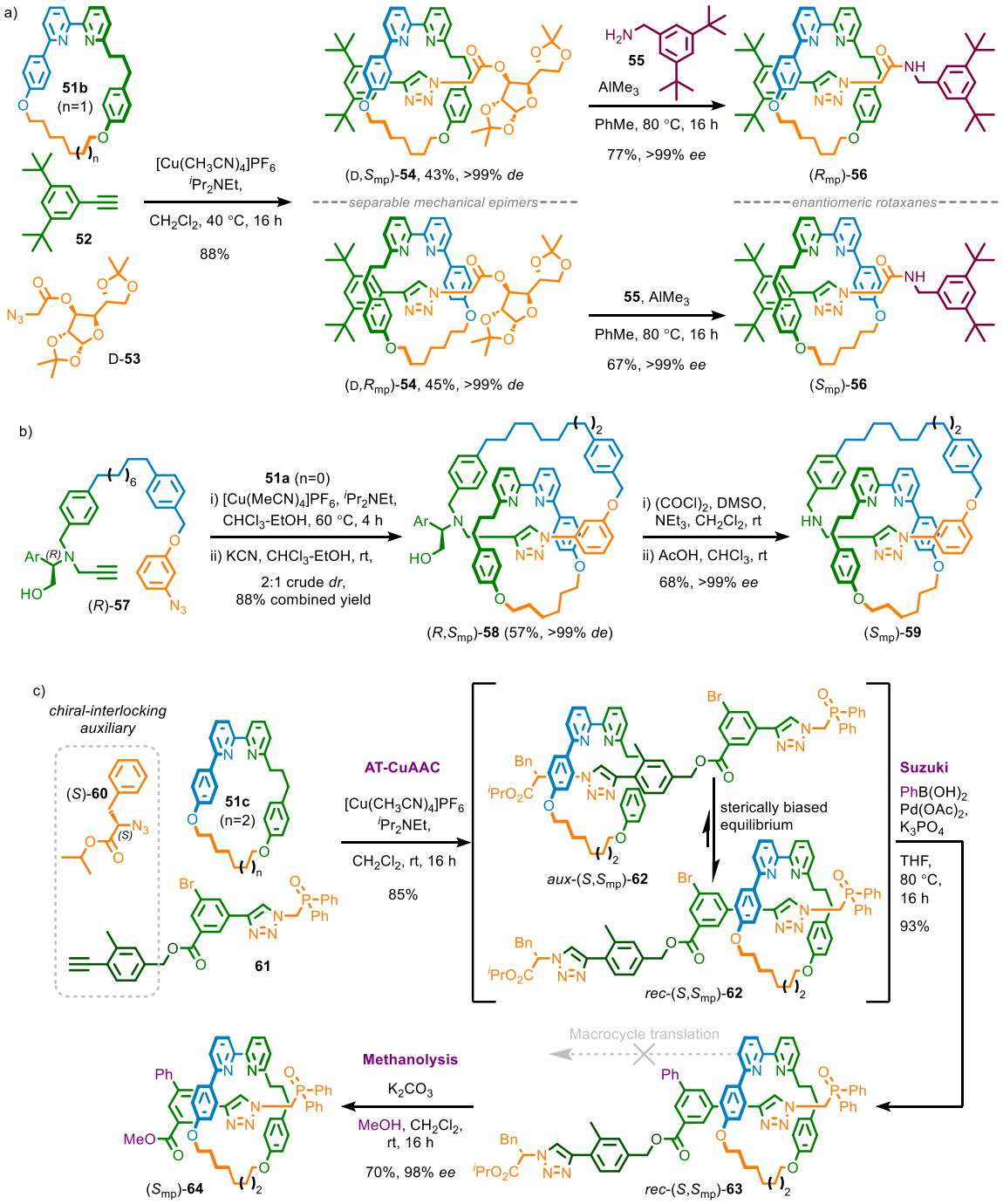

Scheme 1.7 - Goldup and co-workers' developments towards highly enantioenriched MPC molecules *via* chiral auxiliary approaches. Diastereoselective syntheses of a) rotaxanes and b) catenanes followed by removal of covalent stereochemistry. c) Chiral-interlocking auxiliary synthesis.

Catalytic enantioselective syntheses of MPC rotaxanes began with resolution strategies such as Takata's dynamic kinetic resolution of racemic crown-ether based pseudorotaxane **65** *via* acylation, affording rotaxanes **68** in 4% *ee* (Scheme 1.8a).[60,] Similar strategies have since reported selectivities of up to 40% *ee* and more recently, Zhu has published the synthesis MPC rotaxanes in up to 93% *ee via* a catalytic enantioselective desymmetrisation strategy (Scheme 1.8b).[61,62]

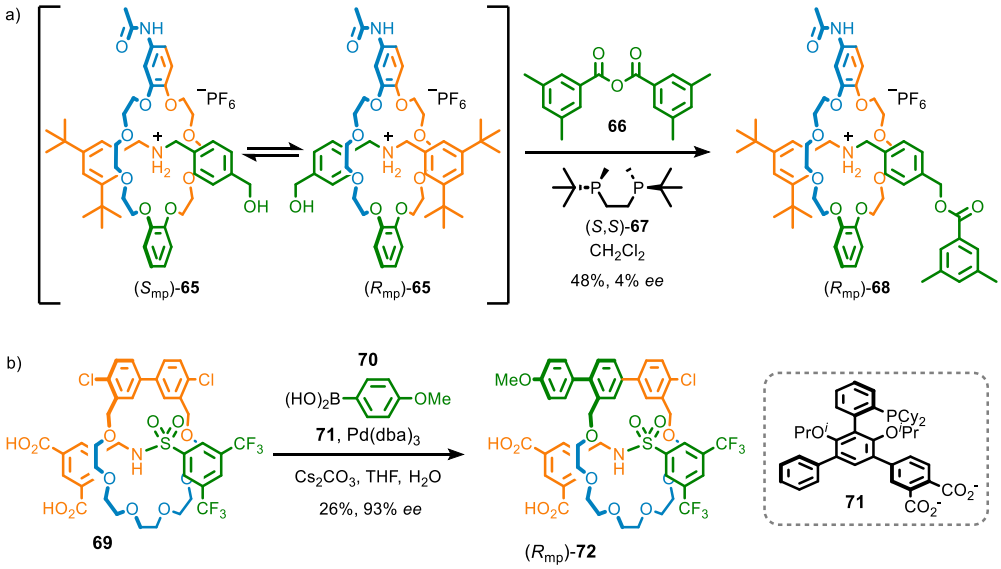

Scheme 1.8 - Advances in enantioselective syntheses of MPC rotaxanes. a) Takata's kinetic resolution strategy towards enantioenriched rotaxanes **68**. b) Zhu's enantioselective desymmetrisation of achiral rotaxane **69**.

1.3.3. Mechanical axial stereoisomerism

It is interesting to note that the notional ring-opening-and-stoppering process on a minimal schematic representation of an MAC catenane affords an achiral object (Figure 1.7a). However, when considering how this facially dissymmetry arises, the analogous rotaxane becomes clear; if both rings of the catenane contain a single prochiral unit, ring opening and stoppering gives a chiral rotaxane in which the axle is C_{1v} symmetric (Figure 1.7b). See section 2.4.7 for a more elaborated discussion on the types of structures that conform to the required symmetries.

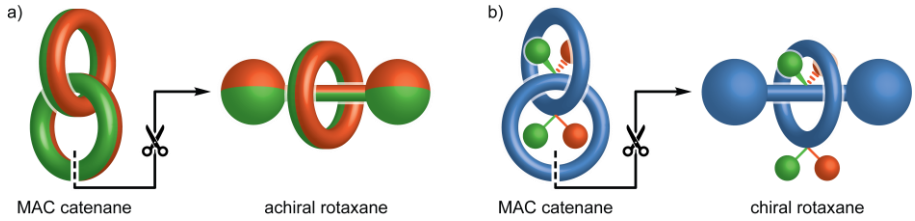

Figure 1.7 - Notional ring-opening-and-stoppering of MAC catenanes. a) a minimal schematic representation to afford an achiral object and b) a semi-structural representation to afford a chiral rotaxane.

1.3.3.1. Assigning the mechanical axially chiral stereogenic unit

To assign the absolute stereochemistry of an MAC catenane composed of prochiral macrocycles, it must be represented such that the prochiral substituents adopt an allene-like relative geometry (Figure 1.8a).[40] Tauber first acknowledged that this is achievable in two co-conformations which result in opposite stereodescriptors using the same method of assignment; one where the substituents project outward from the catenane **I**, and another where they are embedded in the cavity of the other ring **II** (Figure 1.8b).[63] Counter to Tauber's original proposal, for consistency with the assignment of MPC stereochemistry, **II** is the desired co-conformation, where the cross-vector can be viewed at the mutual crossing point of the two rings.[64] By extension, the same relative geometry must be adopted in the assignment of the MAC stereogenic unit as used in MPC rotaxanes (Figure 1.8c).

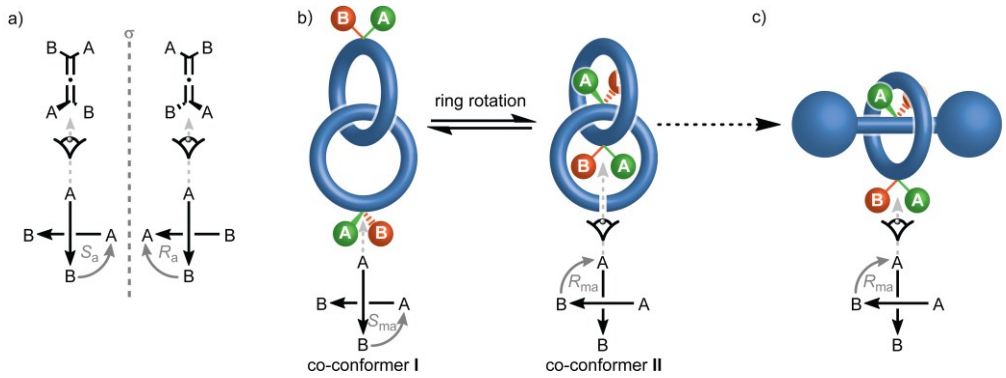

Figure 1.8 - a) Assignment of stereochemistry in axially chiral allenes, b) The consequence of co-conformation in the assignment of the MAC stereogenic unit. c) The required co-conformation for the assignment of the MAC stereogenic unit in rotaxanes.

Similarly to the MPC stereogenic unit (*vide supra*) and based on the CIP approach, Goldup has proposed a unified method for assignment of the MAC stereogenic unit where "ma" subscript is included to indicate that the stereodescriptor refers to a mechanically axial stereogenic unit (Scheme 1.9).[50,48]

1) Identify the highest priority prochiral group (or stereogenic unit in *meso* structures) in the macrocycle using the CIP priority of the central atom. Redraw the ring such that the substituents of the prochiral group in the plane of the macrocycle point into its centre.
2) Identify the highest priority ligand of the selected centre that lies outside of the macrocycle plane, again using CIP priority, and label it as "**A**"; label the lower priority group "**B**".

3,4) Repeat steps 1 and 2 for the second component. If the second component is an axle (i.e. a rotaxane), orient the selected centre such that in-axle substituents are projected towards the observer.

5) Reduce the assembly to the corresponding vectors and observe their relative orientation at the crossing point within the rings (catenanes) or from the macrocycle to the axle (rotaxanes).
6) If the path from the head of the front vector to the tail of the rear vector corresponds to a clockwise path the stereolabel is assigned as R_{ma}, counterclockwise = S_{ma}.

1.3.3.2. Synthesis of mechanical axially chiral molecules

Despite first being identified in 1961, there are very few reports of MAC catenanes. The first successful synthesis of a MAC catenane was reported by Puddephatt and co-workers from an oligomeric digold(I) diacetylide precursor complex **73** and terminal bisphosphine **74** affording racemic homo[2]catenane **75** (Scheme 1.9a).[14] Facial dissymmetry arose by the projection of *p*-bromophenyl and a hydrogen substituent above and below the plane of the macrocycle. Marinetti and co-workers later reported the synthesis of diastereomerically pure MAC phosphine oxide catenanes **79** with facial dissymmetry arising from the relative projection of the out-of-plane (oxo or phenyl) phosphorus substituents (Scheme 1.9c).[65] They were able to separate the resulting mixture by preparative HPLC to yield pure mechanically epimeric samples homo[2]catenanes (*S,S,S,S,*R_{ma})-**79** and (*S,S,S,S,*S_{ma})-**79**. This thesis later describes the synthesis of enantiopure MAC catenanes and previously overlooked analogous rotaxanes *via* a co-conformational auxiliary strategy (Chapter 2) followed by an investigation into factors leading to diastereo- and enantioselective syntheses of MAC rotaxanes (Chapter 3).

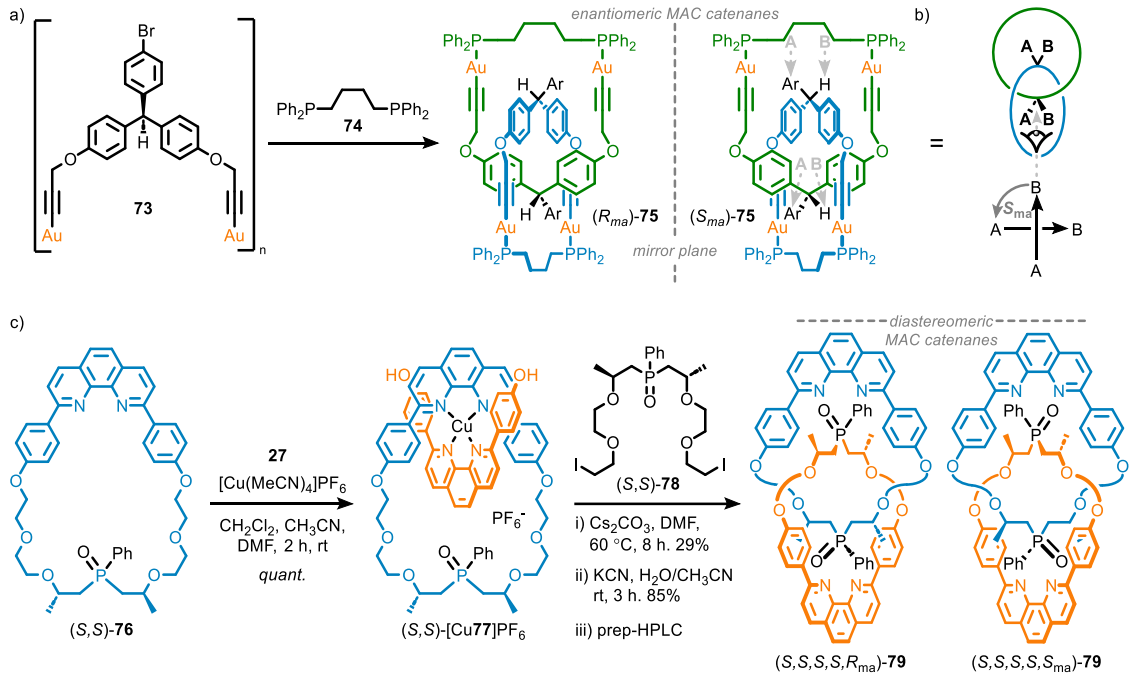

Scheme 1.9 - Syntheses of mechanically axially chiral catenanes. a) Puddephat's synthesis of racemic homo[2]catenanes **75** b) minimal schematic representation of **75** for the assignment of its absolute mechanical stereochemistry c) Marinetti and co-workers' passive template synthesis of diastereopure phosphine oxide homo[2]catenanes **79**. Ar = *p*-Br-C_6H_4

1.3.4. Mechanical geometric isomerism

1.3.4.1. Assigning the mechanical geometric stereogenic unit

The method of assignment for the mechanical geometric isomers is derived from the methods used to assign the MPC and MAC stereogenic units (see section 1.3.2.1 and 1.3.3.1); the same approach is used to determine the orientation/facial dissymmetry and the same relative orientation of axle and macrocycles are used. Thus, for each of the geometric stereogenic units, the vectors associated with each component are viewed at the mutual crossing point. If the vectors are syn to one another, the stereogenic unit is defined as Z_m, whereas anti gives rise to E_m. See section 3.5.2 for a more elaborated discussion on the method of assignment regarding facial dissymmetry in prochiral and rim-differentiated macrocycles.

1.3.4.2. Synthesis of mechanically geometric molecules

Several stereoselective syntheses of mechanical geometric isomers have been reported. Although Schill envisaged MGI molecules to rely on prochiral rings, the vast majority of reports rely on macrocycles that adopt a cone-shaped conformation – most commonly cyclodextrins (CD) and calixarenes.[3] Kaifer reported the first examples of epimeric MGI rotaxanes, utilising CD inclusion complexes followed by stoppering to prepare **82** in 20% *de* of which isomer (D,E_m)-**82** was interestingly found to slowly unthreaded in various solvents, whereas (D,Z_m)-**82** was found to be completely stable to unthreading (Scheme 1.10b).[47] Stodart later utilised CDs in the synthesis

of MGI catenanes although no selectivity was observed between the two isomers (Scheme 1.10c).[41] It should also be noted that aside from the defined facial orientation of CDs, due to their cone-shaped conformation, they are also oriented due to their covalent stereochemistry. As a result, the stereochemistry of MGI molecules based on CD macrocycles can be fully described by either mechanical planar or geometric stereodescriptors.[48]

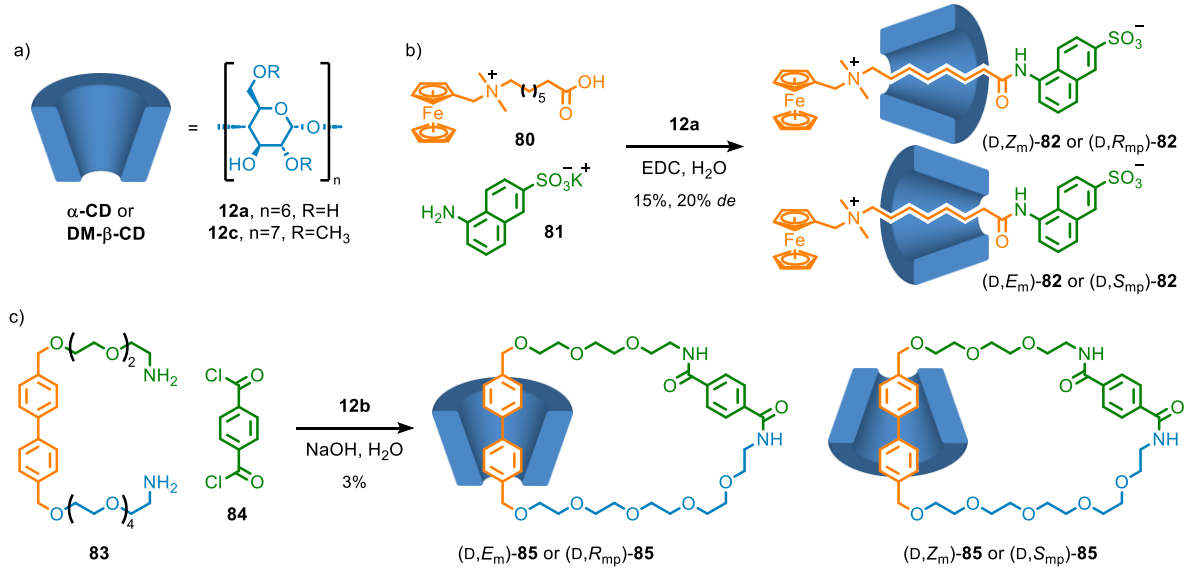

Scheme 1.10 - Syntheses of cyclodextrin-based MGI catenanes and rotaxanes. a) Structure and simplification of cyclodextrins b) Kaifer's ammonium-CD MGI [2]rotaxanes c) Stoddart's CD-based MGI [2]catenanes.

Molecules have been prepared whose stereochemistry is solely defined by the mechanically geometric stereogenic unit. Macrocycles such as calixarenes have been extensively used both due to their cone-shaped conformation imparting clear directionality, and also their impressive binding affinities for a wide range of hosts. Arduini employed rim-differentiated calix[6]arene **86** to prepare type 1 MGI [2]rotaxanes (E_m)-**92** and (Z_m)-**92** (Scheme 1.11a).[66] They found that encapsulation of viologen unit **87** afforded a single pseudorotaxane geometric isomer that was reactive towards the incoming acid chloride due to the steric preferences of macrocycle **86**. Therefore, each isomer could be selectively synthesised by choice of which stopper was already installed on the viologen unit, and which would subsequently be used to stopper the resulting pseudorotaxane. Credi later employed a similar approach in the synthesis of type 1 MGI [3]rotaxanes, being able to synthesise all three possible mechanical stereoisomers selectively by iterative active template reactions and choice of substrate (Scheme 1.11b).[67]

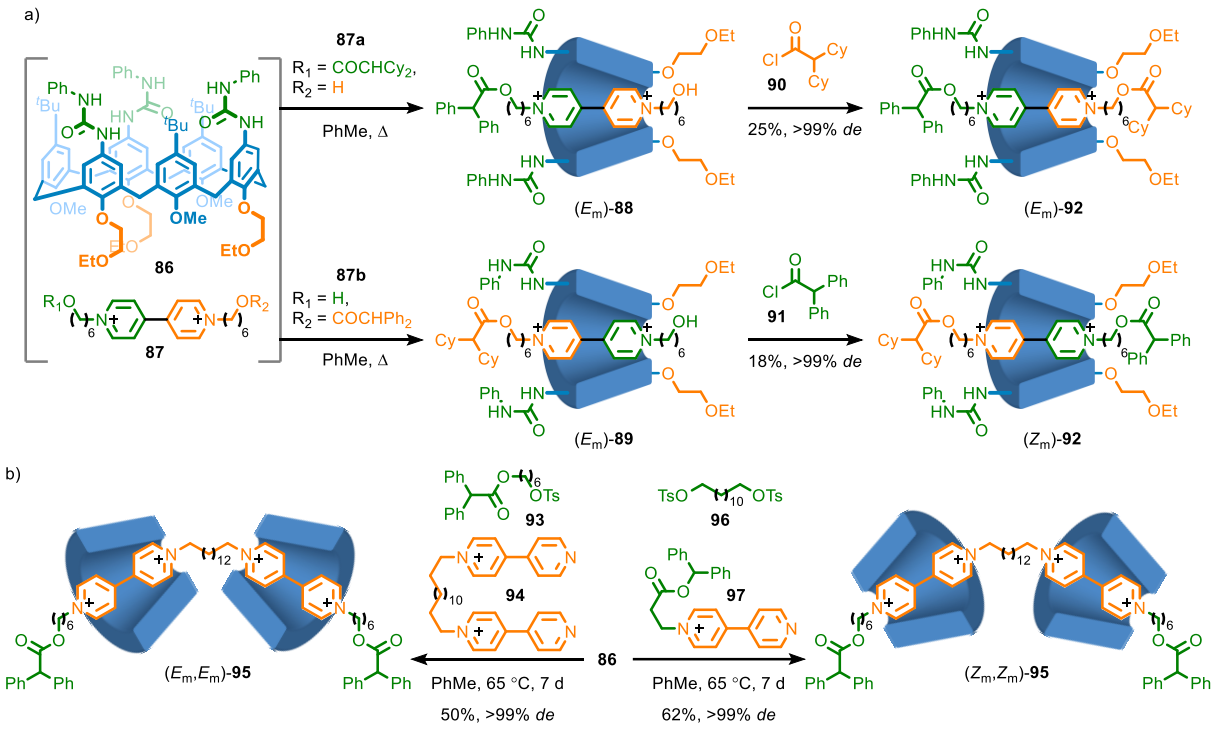

Scheme 1.11 - a) Arduini and b) Credi's stereoselective syntheses of MGI rotaxanes based on calixarene **86**. Macrocycle rim substituents in b) are omitted for clarity.

There are much fewer examples of catenanes whose stereochemistry relies solely on the MGI stereogenic unit. Neri and co-workers utilised calix[6]arene macrocycle **99** to selectively form pseudorotaxane (Z_m)-**100** that, following reaction with bis-isocyanate **101**, gave MGI [2]catenane (Z_m)-**102** in 23% yield (Scheme 1.12a).[68] Credi has also utilised the stereoselective encapsulation of viologen-based premacrocycle **103** to prepare MGI catenane (E_m)-**105** in a stereoselective manner by ring closing metathesis (Scheme 1.12b).[69]

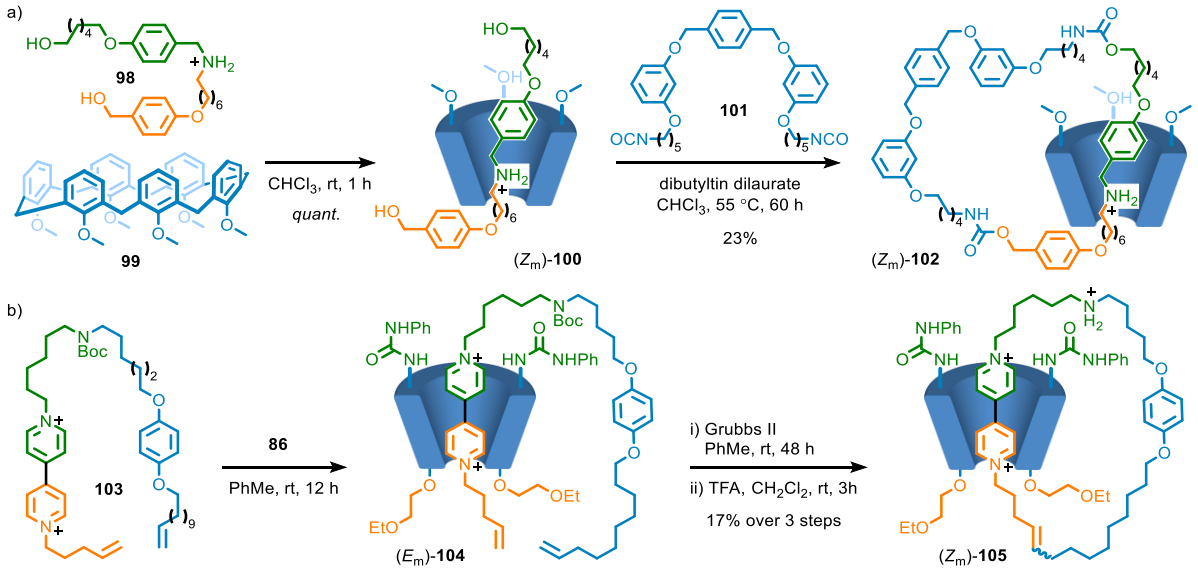

Scheme 1.12 - Stereoselective syntheses of calixarene-based MGI catenanes reported by a) Neri and b) Credi.

Macrocycles that display permanent facial disymmetry invariant of conformation have also been used to prepare mechanical geometric isomers. Chen and co-workers have demonstrated the selective synthesis of head-to-head and tail-to-tail [3]pseudorotaxane isomers and investigated the effect of temperature on the selectivity of type 1 MGI [2]rotaxanes based on triptycene macrocycle **107** (Scheme 1.13a).[70,71] Selectivity between [2]rotaxane mechanical geometric isomers (E_m)-**109** and (Z_m)-**109** was shown to decrease at higher temperatures, with the greatest selectivity of 60% *de* at 298 K. Jiang and co-workers similarly have prepared permanent mechanical geometric isomers using naphthotube macrocycle **110** (Scheme 1.13b).[72] Complexation with bisammonium alkyne **111** followed by CuAAC stoppering afforded a mixture of isomers (E_m)-**113** and (Z_m)-**113** and found that the inversion of major isomer with variation of solvent mixture polarity from +33% *de* to –50% *de*.

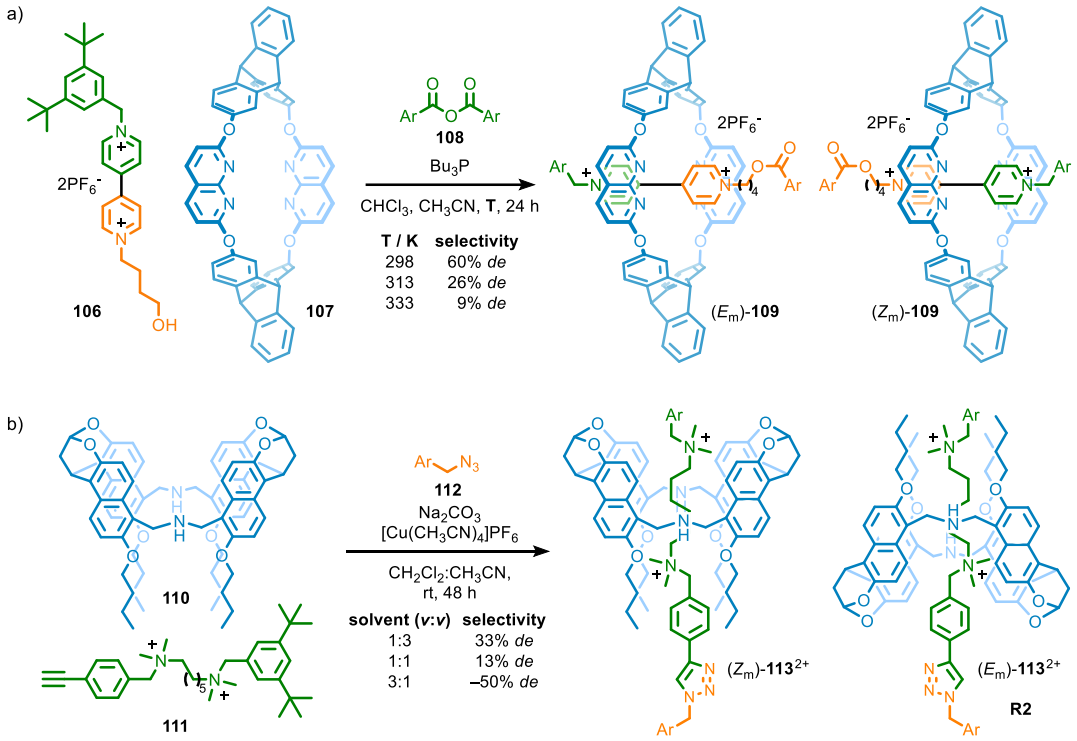

Scheme 1.13 - Type 1 MGI rotaxanes based on macrocycles displaying permanent facial dissymmetry. a) Chen's triptycene based [2]rotaxanes **109**. b) Jiang's naphthotube based [2]rotaxanes **113**. Ar = 3,5-di-^{t}Bu-C_6H_3

Type 1 MGI rotaxanes based on prochiral macrocycles have recieved very little attention. In their synthesis of synthesis of non-natural lasso peptides, Bode reported a type 1 MGI rotaxane based on prochiral crown ether macrocycle **115** (Scheme 1.14a).[73] The selectivity of this reaction was unfortunately not reported and rotaxanes **117** were characterised as a mixture of isomers. Takata also claimed a synthesis of rotaxanes displaying 'directional isomerism' with chiral crown ether macrocycle (*S*)-**119** (Scheme 1.14b).[74] However, similaly to CDs, (*S*)-**119** can be described as

both facially dissymetric and oriented due to the stereogenic centre. As a result, the stereochemistry of rotaxanes **121** can be fully described by either covalent and MGI, or covalent and MPC stereodescriptors. This thesis later investigates the factors leading to stereoselective syntheses of MGI catenanes and rotaxanes based on a prochiral macrocycle (Chapter 3) and also the identification and stereoselective synthesis of previously overlooked 'type 2' MGI rotaxanes composed of an oriented macrocycle and a prochiral axle (Chapter 4).

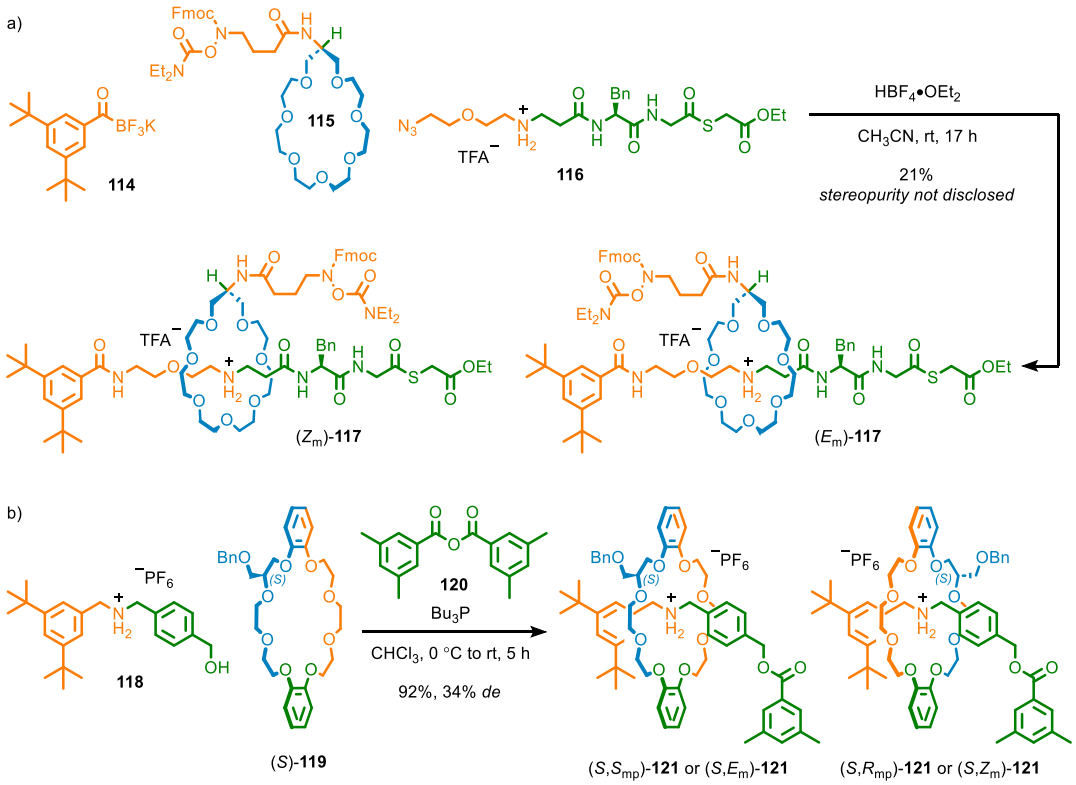

Scheme 1.14 - Rotaxanes displaying 'mechanical geometric isomerism'. a) Bode's type 1 MGI [2]rotaxane based on a prochiral crown ether macrocycle. b) Takata's crown ether rotaxanes which can be described by either MPC or MGI stereochemistry.

1.3.5. Co-conformational stereogenic units

Even in the absence of conditional mechanical stereochemistry, mechanical motion can give rise to co-conformations which can be stereogenic if the molecule is desymmetrised.[38] Therefore, covalent or mechanical stereochemistry can arise in otherwise achirotopic interlocked molecules due to the relative positions and/or orientations of their components. In unhindered dynamic systems, these stereogenic co-conformations can interconvert but if co-conformational exchange is sterically blocked, static stereoisomers can arise. Co-conformational stereochemistry is assigned in analogy to their classical stereogenic unit and subscript (co-) is added to the stereodescriptor to indicate the co-conformational nature of the stereogenic unit. [38]

1.3.5.1. Co-conformational covalent stereochemistry

Prochiral units in catenanes and rotaxanes can become desymmetrised by the relative position of a macrocycle.[38] When the prochiral unit is encircled such that the structure contains an internal mirror plane, the molecule is achiral, but displacement of the macrocycle towards either enantiotopic substituent results in co-conformational covalent enantiomers (Figure 1.9a). Co-conformational covalent stereochemistry is assigned similarly to covalent stereochemistry, by the macrocycle being considered a pseudo-substituent of the enantiotopic unit that it encircles.[38] Through symmetrisation of covalently chiral rotaxane (*R*)-**122**, Leigh and co-workers prepared co-conformationally point chiral rotaxane ($S_{co\text{-}c}$)-**124** in excellent enantiopurity where the interconversion of co-conformational covalent enantiomers is prevented due to the size of the prochiral unit (Figure 1.9b). Similarly, co-conformational analogues of any covalent stereogenic unit can also arise including geometric isomers. Credi and co-workers have reported the exchange of geometric isomers by shuttling of the macrocycle either side of the amide bond as well as by single bond rotation (Figure 1.9c).[75]

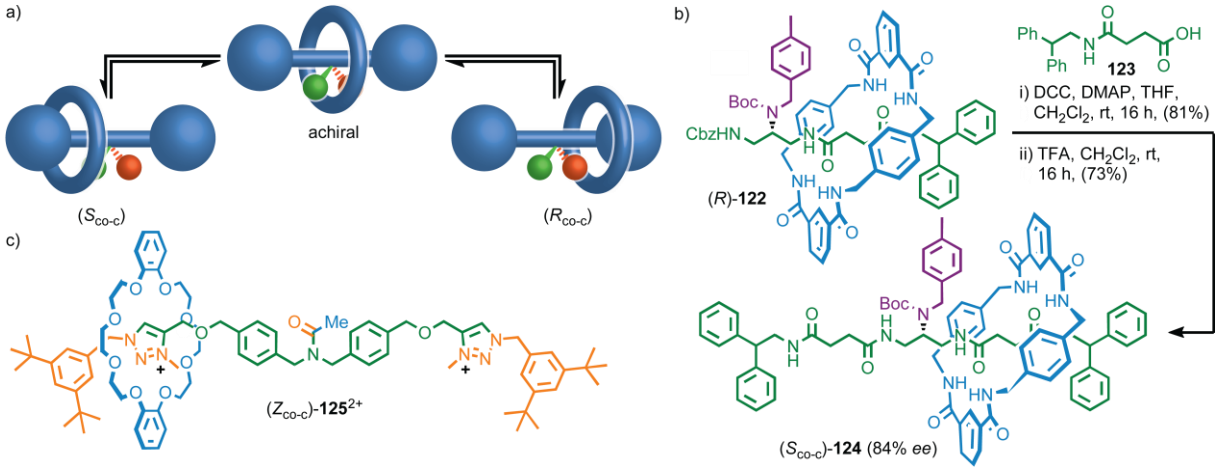

Figure 1.9 - Co-conformational covalent chirality. a) illustration of dynamic co-conformational covalent chirality in rotaxanes. b) Leigh's symmetrisation strategy towards rotaxane ($S_{co\text{-}c}$)-**124**. c) Credi's dynamic co-conformationally covalent geometric rotaxane **125**.

1.3.5.2. Co-conformational mechanical planar chirality

Co-conformational mechanical chirality can arise if the molecule as a whole becomes desymmetrised in a specific co-conformation.[38] For example, co-conformational mechanical planar chirality can arise due to displacement of an oriented macrocycle from the mirror plane of a centro-symmetric axle, thus inducing directionality (Figure 1.10a). Similar stereoisomerism can arise in [n]rotaxanes where at least one of the macrocycles is oriented and unable to exchange positions with other macrocycles as (Figure 1.10b,d).[76] When a C_{2v} symmetric macrocycle is interlocked with an oriented ring and displaced from its vertical mirror plane, catenanes can also display co-conformational mechanical planar chirality, which can be resolved by inhibiting the rotation of the rings, as reported by Goldup (Figure 1.10c,e).[77]

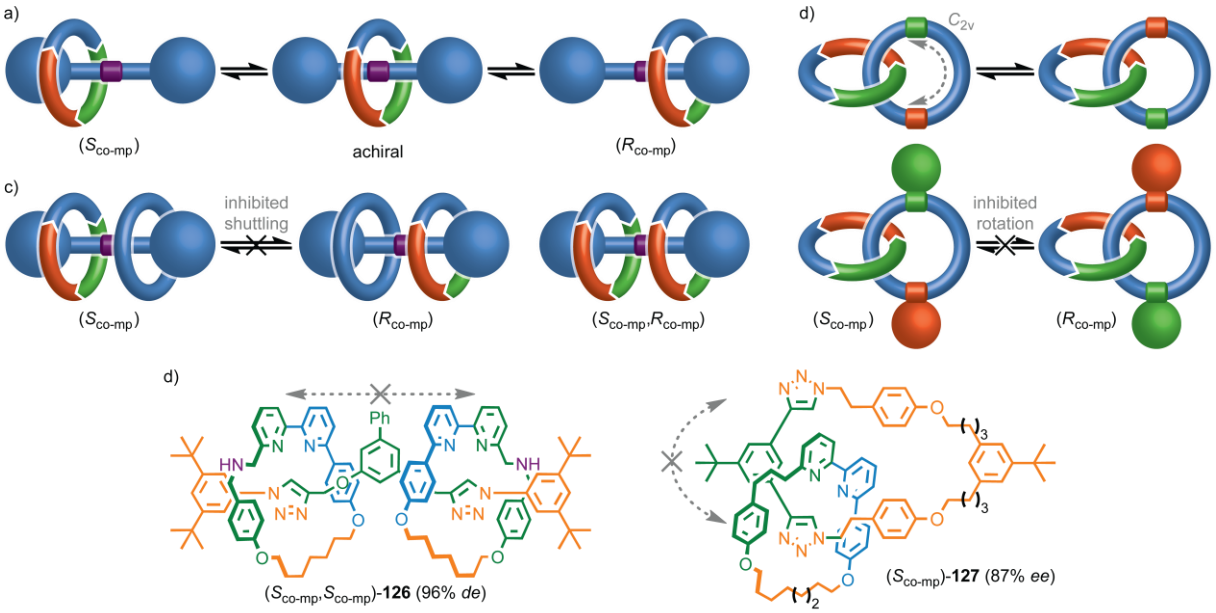

Figure 1.10 - Co-conformational mechanical planar chirality expressed in a) [2]rotaxanes, b) [3]rotaxanes where at least one ring is oriented, c) [2]catenanes based on a C_{2v} symmetric macrocycle with arbitrary stereolabels, and d) examples reported by Goldup.

1.3.5.3. Co-conformational mechanical axial chirality

Catenanes have also been shown to adopt conformations that are enantiomeric due to the facial symmetry properties of the component macrocycles, giving rise to a co-conformational mechanical axial chirality.[38] Hetero[2]catenanes composed of a C_{2h} and one C_{nv} macrocycle (Figure 1.11a) can adopt such conformations and similarly, [2]catenanes composed of C_{2h}, or D_{nd} rings, or in combination with a C_{nv} macrocycle (Figure 1.11b). Puddephat and co-workers have reported a catenane which conforms to these symmetry properties (Figure 1.11c).[78] Catenane **129** was found to self-assemble from racemic binaphthyl derivative **128** in the presence of Pd^{II} which was found to adopt mechanically axially chiral co-conformations. In the solid-state, catenane **129** is composed exclusively of C_{2h} symmetric macrocycles *meso*-**130**.

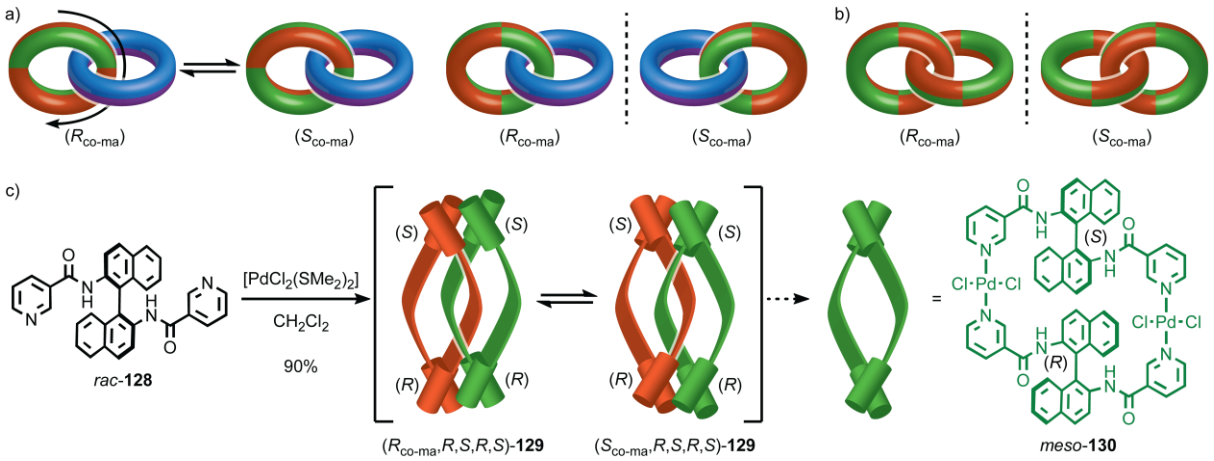

Figure 1.11 - Co-conformational mechanical axial chirality expressed in a) hetero[2]catenanes based on C_{2h} and C_{nv} macrocycles, b) homo[2]catenanes based on two C_{2h} macrocycles with arbitrary stereolabels and c) Puddephat and co-workers catenane **129** composed of *meso* macrocycles.

1.3.5.4. Co-conformational mechanical geometric isomerism

Similarly to how conformations can result in chirotopic mechanical stereogenic units, displacement of facially dissymmetric macrocycles can render molecules co-conformationally mechanically geometrically isomeric. Sollogoub and co-workers have recently reported a cyclodextrin based molecular information ratchet **131** in which different co-conformations react at different rates with Fmoc-Cl (Scheme 1.15a).[79] Jiang and co-workers studied the shuttling motion of napthotube rotaxane **133** and found it to display stable co-conformational mechanical geometric isomerism upon protonation (Scheme 1.15b).[72] They found that this motion was unidirectional and reversible, affording a single co-conformational isomer.

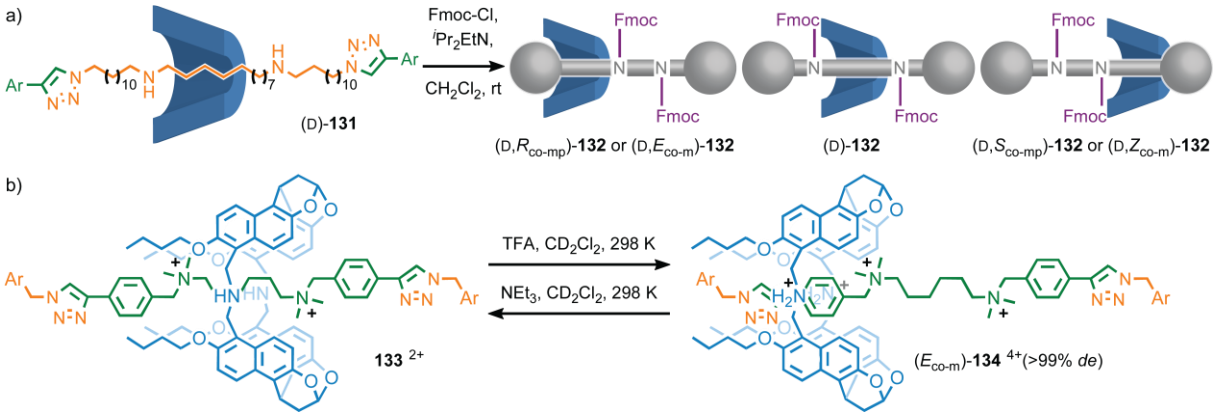

Scheme 1.15 - Co-conformational mechanical geometric isomers. a) Sollogoub's CD based information ratchet **131**. b) Jiang's naphthotube based rotaxane **133**.

1.3.5.5. Co-conformational mechanical helical chirality

Achiral catenanes can display co-conformational mechanical helical chirality due to the rocking motion of their constituent rings, similar to conformational rocking of an otherwise achiral biaryl unit (Figure 1.12a). These are assigned by viewing the assembly along the axis of chirality (a line perpendicular to the crossing point of the rings) and identifying the shortest path from the front ring to the rear ring – assigned *P* if the path is clockwise, and *M* if anticlockwise.[38] It should be noted that all catenanes will display this phenomenon due to it arising from the simple rocking motion, but there are many reports into the stabilisation of helically chiral conformations. Stoddart and co-workers have reported that these helical conformations can be biased by anion exchange between chiral shift reagent Δ-**135** and donor-acceptor [2]catenane [**18**]$4PF_6$ resulting in a 2:1 ratio of diastereomeric pairs at low temperature from an otherwise achiral catenane (Figure 1.12b).[80]

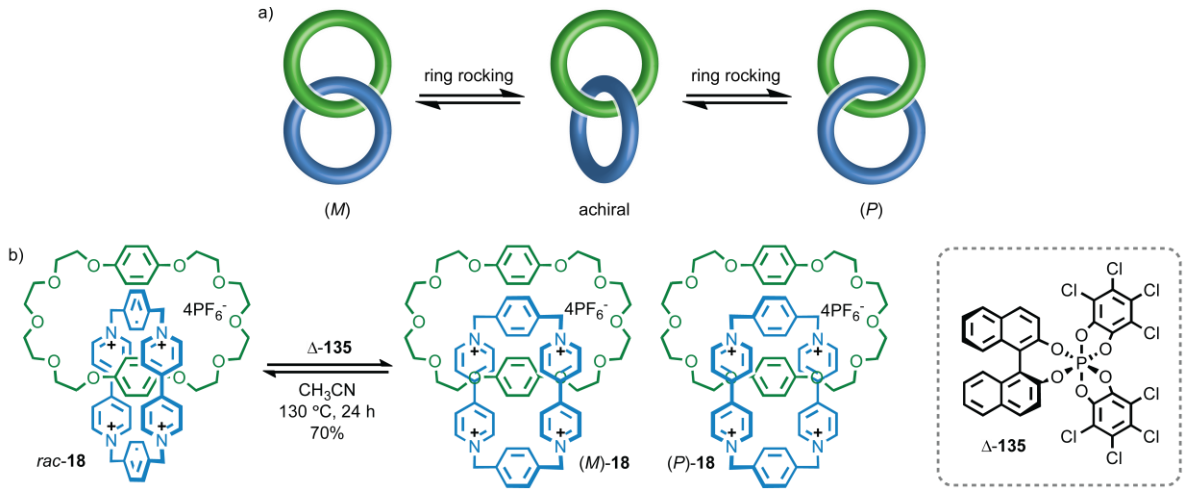

Figure 1.12 - Co-conformational mechanical helical chirality expressed in a) [2]catenanes and b) Stoddart's biasing of the mechanically helical co-conformations using a chiral anion.

1.4. Conclusions

The understanding of mechanically interlocked molecules and stereochemistry that can arise in such systems has made huge progress, built on the foundations laid by seminal works from Frish, Wasserman and Schill. This thesis will explore the synthesis of molecules expressing mechanical stereochemistry, including non-canonical mechanical stereogenic units; **Chapter 2** presents the first semi-structural analysis of the mechanically axially chiral stereogenic unit to identify a previously overlooked stereogenic unit in rotaxanes. This analysis also led to the identification of a suitable methodology for an auxiliary synthesis of MAC catenanes and rotaxanes to afford enantiopure samples. **Chapter 3** serves to build upon the discovery of MAC rotaxanes described in **Chapter 2** and efforts towards their stereoselective synthesis. Optimisation of their synthesis with respect to substrate and reaction conditions led to enantioselective syntheses of MAC rotaxanes, the first stereoselective synthesis of type 1 MGI rotaxanes and catenanes *via* intercomponent hydrogen bonding interactions to pre-organise to AT-CuAAC reaction. Finally, **Chapter 4** identifies another previously overlooked mechanical stereogenic unit through from first principles analysis such that all forms of simple mechanical stereochemistry in rotaxanes and catenanes are known. An interlocking auxiliary strategy is then employed to synthesise geometrically pure rotaxanes such that not only all stereogenic units are known, but that molecules containing them can be prepared stereoselectively.

1.5. Bibliography

1 H. Frisch, E. Wasserman, *J. Am. Chem. Soc.*, **1961**, *83*, 3789–3795.

2 J. F. Stoddart, *Angew. Chem., Int. Ed.*, **2017**, *56*, 11094–11125; J. P. Sauvage, *Angew. Chem., Int. Ed.*, **2017**, *56*, 11080–11093; B. L. Feringa, *Angew. Chem., Int. Ed.*, **2017**, *56*, 11060–11078.

3 G. Schill, *Catenanes, Rotaxanes and Knots*, Academic Press, New York, 1971.

4 L. Pauling, *The Nature of the Chemical Bond: An Introduction to Modern Structural Chemistry*, Cornell University Press, Ithaca, 1939.

5 H. Frisch, I. Martin, H. Mark, *Monatsh.*, **1953**, *84*, 250–256.

6 C. Bruns, J. Stoddart, *The Nature of the Mechanical Bond*, John Wiley & Sons, Inc., Hoboken, 1st edn., 2017.

7 D. M. Walba, *Tetrahedron* **1985**, *41*, 3161–3212.

8 E. Flapan, *When Topology Meets Chemistry: A Topological Look at Molecular Chirality*, Cambridge Univ. Press, Cambridge, 2020.

9 K. Mislow, *Bull. Soc. Chim. Belg.* **2010**, *86*, 595–601.

10 L. C. Cross, W. Klyne, *Pure Appl. Chem.* **1976**, *45*, 11–30.

11 A. Yerin, E. S. Wilks, G. P. Moss, A. Harada, *Pure Appl. Chem.* **2008**, *80*, 2041–2068.

12 J. Vohlídal, E. S. Wilks, A. Yerin, A. Fradet, K.-H. Hellwich, P. Hodge, J. Kahovec, W. Mormann, R. F. T. Stepto, *Pure Appl. Chem.* **2012**, *84*, 2135–2165.

13 O. Safarowsky, B. Windisch, A. Mohry and F. Vögtle, *Journal für praktische Chemie*, **2000**, *342*, 437–444.

14 C. P. McArdle, S. Van, M. C. Jennings, R. J. Puddephatt, *J. Am. Chem. Soc.* **2002**, *124*, 3959–3965.

15 N. Pairault, F. Rizzi, D. Lozano, E. M. G. Jamieson, G. J. Tizzard, S. M. Goldup, *Nat. Chem.* **2023**, *15*, 781–786.

16 A. Lüttringhaus, F. Cramer, H. Prinzbach, F. M. Henglein, *Liebigs Ann. Chem.* **1958**, *613*, 185–198.

17 G. A. Breault, C. A. Hunter, P. C. Mayers, *Tetrahedron*, **1999**, *55*, 5265–5293.

18 E. Wasserman, *J. Am. Chem. Soc.*, **1960**, *82*, 4433-4434.

19 A. S. Baluna, A. Galan, D. A. Leigh, G. D. Smith, J. T. J. Spence, D. J. Tetlow, I. J. Vitorica-Yrezabal, M. Zhang, *J. Am. Chem. Soc.* **2023**, *145*, 9825–9833.

20 I. Harrison and S. Harrison, *J. Am. Chem. Soc.*, **1967**, *89*, 5723–5724.

21 G. Schill and A. Lüttringhaus, *Angew. Chem., Int. Ed. Engl.*, **1964**, *3*, 546–547.

22 G. Schill and H. Zollenkopf, *Liebigs Ann. Chem*, **1969**, *721*, 53–74.

23 G. Schill and C. Zürcher, *Angew. Chem., Int. Ed. Engl.*, **1969**, *8*, 988.

24 H. Ogino, *J. Am. Chem. Soc.* **1981**, *103*, 1303–1304.

25 B. P. R. Ashton, T. T. Goodnow, A. E. Kaijer, M. I. Reddington, A. M. Z. Slawin, N. Spencer, J. F. Stoddart, C. Vicent, D. J. Williams, *Angew. Chem. Int. Ed.* **1989**, *28*, 1396–1399.

26 S. J. Rowan, S. J. Cantrill, J. F. Stoddart, *Org. Lett.* **1999**, *1*, 129–132.

27 D. A. Leigh, A. Venturini, A. J. Wilson, J. K. Y. Wong, F. Zerbetto, *Chem. Eur. J.* **2004**, *10*, 4960–4969.

28 C. Dietrich-Buchecker, J. Sauvage and J. Kintzinger, *Tetrahedron Lett.*, **1983**, *24*, 5095–5098.

29 V. Aucagne, K. D. Hänni, D. A. Leigh, P. J. Lusby and D. B. Walker, *J. Am. Chem. Soc.*, **2006**, *128*, 2186–2187.

30 V. V. Rostovstev, L. G. Green, V. V. Fokin, K. B. Sharpless, *Angew. Chem. Int. Ed.*, **2002**, *41*, 2596–2599.

31 R. Huisgen, *Proc. Chem. Soc.*, **1961**, 357–396.

32 S. Saito, E. Takahashi, K. Nakazono, *Org. Lett.* **2006**, *8*, 5133–5136.

33 Y. Sato, R. Yamasaki, S. Saito, *Angew. Chem. Int. Ed.* **2009**, *48*, 504–507.

34 R. Jamagne, M. J. Power, Z-H. Zhang, G. Zango, B. Gibber, D. A. Leigh, *Chem. Soc. Rev.* **2024**, Advance Article, DOI: 10.1039/d4cs00430b

35 G. De Bo, G. Dolphijn, C. T. McTernan, D. A. Leigh, *J. Am. Chem. Soc.* **2017**, *139*, 8455–8457.

36 D. P. Fielden, D. A. Leigh, C. T. McTernan, B. Pérez-Saavedra, I. J. Vitorica-Yrezabal, *J. Am. Chem. Soc.* **2018**, *140*, 6049–6052.

37 L. Binks, C. Tian, S. D. P. Fielden, I. J. Vitorica-Yrezabal, D. A. Leigh, *J. Am. Chem. Soc.* **2022**, *144*, 15838–15844.

38 E. M. G. Jamieson, F. Modicom, S. M. Goldup, *Chem. Soc. Rev.* **2018**, *47*, 5266–5311.

39 E. Eliel, S. Wilen, L. Mander, *Stereochemistry of Organic Compounds*, Wiley, 1994.

40 M. Robinson, *Organic stereochemistry*, Oxford University Press, New York, 2000.

41 D. Armspach, P. R. Ashton, R. Ballardini, V. Balzani, A. Godi, C. P. Moore, L. Prodi, N. Spencer, J. F. Stoddart, M. S. Tolley, T. J. Wear, D. J. Williams, *Chem. Eur. J.,* **1995**, *1*, 33–55.

42 J. R. J. Maynard, P. Gallagher, D. Lozano, P. Butler, S. M. Goldup, *Nat. Chem.* **2022**, *14*, 1038–1044.

43 A. Savoini, P. R. Gallagher, A. Saady, S. M. Goldup, *J. Am. Chem. Soc.* **2024**, *146*, 8472–8479.

44 V. Prelog, H. Gerlach, *Helv. Chim. Acta*, **1964**, *47*, 2288–2294.

45 Y. Makita, N. Kihara, N. Nakakoji, T. Takata, S. Inagaki, C. Yamamoto, Y. Okamoto, *Chem. Lett.* **2007**, *36*, 162–163.

46 R. Bordoli and S. Goldup, *J. Am. Chem. Soc.* **2014**, ***136***, 4817–4820.

47 R. Isnin, A. E. Kaifer, *Pure Appl. Chem.* **1993**, *65*, 495–498.

48 S. Goldup, *Acc. Chem. Res.* **2024**, *57*, 1696–1708.

49 C. Reuter, A. Mohry, A. Sobanski and F. Vögtle, *Chem. Eur. J.,* **2000**, *6*, 1674–1682.

50 R. Cahn, C. Ingold and V. Prelog, *Angew. Chem. Int. Ed.*, **1966**, *5*, 385–415.

51 D. K. Mitchell, J. P. Sauvage, *Angew. Chem., Int. Ed. Engl.***1988**, *27*, 930–931.

52 Y. Kaida, Y. Okamoto, J. C. Chambron, D. K. Mitchell, J. P. Sauvage, *Tetrahedron Lett.* **1993**, *34*, 1019–1022.

53 R. Jäger, M. Händel, J. Harren, F. Vögtle, K. Rissanen, *Liebigs Ann. Chem*, **1996**, *7*, 1201–1207.

54 C. Yamamoto, Y. Okamoto, T. Schmidt, R. Jäger, F. Vögtle, D. M. *J. Am. Chem. Soc.* **1997**, *43*, 10547–10548.

55 M. Denis, J. E. M. Lewis, F. Modicom, S. M. Goldup, *Chem* **2019**, *5*, 1512–1520.

56 M. A. Jinks, A. de Juan, M. Denis, C. J. Fletcher, M. Galli, E. M. G. Jamieson, F. Modicom, Z. Zhang, S. M. Goldup, *Angew. Chem. Int. Ed.* **2018**, *130*, 15022–15026.

57 J. S. Hannam, S. M. Lacy, D. A. Leigh, C. G. Saiz, A. M. Z. Slawin, S. G. Stitchell, *Angew. Chem. Int. Ed.* **2004**, *43*, 3260–3264.

58 S. Chao, C. Romuald, K. Fournel-Marotte, C. Clavel, F. Coutrot, *Angew. Chem. Int. Ed.* **2014**, *53*, 6914–6919.

59 A. de Juan, D. Lozano, A. W. Heard, M. A. Jinks, J. M. Suarez, G. J. Tizzard, S. M. Goldup, *Nat. Chem.* **2022**, *14*, 179–187.

60 Y. Makita, N. Kihara, N. Nakakoji, T. Takata, S. Inagaki, C. Yamamoto, Y. Okamoto, *Chem. Lett.* **2007**, *36*, 162–163.

61 A. Imayoshi, B. V. Lakshmi, Y. Ueda, T. Yoshimura, A. Matayoshi, T. Furuta, T. Kawabata, *Nat. Commun.* **2021**, *12*, 404.

62 M. Li, X. L. Chia, C. Tian, Y. Zhu, *Chem*. **2022**, *8*, 2843–2855.

63 S. J. Tauber, *J. Res. Natl. Bur. Stand. A. Phys. Chem.* **1963**, 67, 591–599.

64 P. R. Gallagher, A. Savoini, A. Saady, J. R. J. Maynard, P. W. V. Butler, G. J. Tizzard, S. M. Goldup, *J. Am. Chem. Soc.* **2024**, *146*, 9134–9141.

65 A. Theil, C. Mauve, M.-T. Adeline, A. Marinetti, J.-P. Sauvage, *Angew. Chem. Int. Ed.* **2006**, *45*, 2104–2107.

66 A. Arduini, F. Ciesa, M. Fragassi, A. Pochini, A. Secchi, *Angew. Chem. Int. Ed.* **2004**, *44*, 278–281.

67 M. Bazzoni, L. Andreoni, S. Silvi, A. Credi, G. Cera, A. Secchi, A. Arduini, *Chem. Sci.* **2021**, *12*, 6419–6428.

68 C. Gaeta, C. Talotta, S. Mirra, L. Margarucci, A. Casapullo and P. Neri, *Org. Lett.*, **2013**, *15*, 116–119.

69 V. Zanichelli, L. Dallacasagrande, A. Arduini, A. Secchi, G. Ragazzon, S. Silvi, A. Credi, *Molecules* **2018**, *23*, 1156.

70 H.-X. Wang, S.-Z. Hu, Q. Shia, C.-F. Chen, *Org. Biomol. Chem.*, **2016**, *14*, 10481–10488.

71 H.-X. Wang, Z. Meng, J. F. Xiang, Y.-X. Xia, Y. Sun, S.-Z. Hu, H. Chen, J. Yao, C.-F. Chen, *Chem. Sci.* **2016**, *7*, 469–474.

72 J.-S. Cui, Q.-K. Ba, H. Ke, A. Valkonen, K. Rissanen, W. Jiang, *Angew. Chem. Int. Ed.* **2018**, *130*, 7935–7940.

73 F. Saito, J. W. Bode, *Chem. Sci.* **2017**, *8*, 2878–2884.

74 Y. Makita, N. Kihara, T. Takata, *Supramol. Chem.* **2021**, *33*, 1–7.

75 S. Corra, C. de Vet, M. Baroncini, A. Credi, S. Silvi, *Chem* **2021**, *7*, 2137–2150.

76 R. Schmieder, G. Hübner, C. Seel and F. Vögtle, *Angew. Chem. Int. Ed.*, **1999**, *38*, 3528–3530.

77 A. Rodríguez-Rubio, A. Savoini, F. Modicom, P. Butler, S. M. Goldup, *J. Am. Chem. Soc.* **2022**, *144*, 11927−11932.

78 T. J. Burchell, D. J. Eisler, R. J. Puddephat, *Dalton. Trans.*, **2005**, 286–272.

79 E. Liu, S. Cherraben, L. Boulo, C. Troufflard, B. Hasenknopf, G. Vives, M. Sollogoub, *Chem* **2023**, *9*, 1147–1163.

80 S. A. Vignon, J. Wong, H. R. Tseng, J. F. Stoddart, *Org. Lett.* **2004**, *6*, 1095–1098.

Chapter 2: Mechanically Axially Chiral Catenanes and Noncanonical Mechanically Axially Chiral Rotaxanes

Abstract: Chirality typically arises in molecules due to a rigidly chiral arrangement of covalently bonded atoms. Less generally appreciated is that chirality can arise when molecules are threaded through one another to create a mechanical bond. For example, when two macrocycles with chemically distinct faces are joined to form a catenane, the structure is chiral although the rings themselves are not. However, enantiopure mechanically axially chiral catenanes in which the mechanical bond provides the sole source of stereochemistry have not been reported. We re-examined the symmetry properties of these molecules and in doing so identified a straightforward route to access them from simple chiral building blocks. Our analysis also led us to identify an analogous but previously unremarked upon rotaxane stereogenic unit, which also yielded to our co-conformational auxiliary approach. With methods to access mechanically axially chiral molecules in hand, their properties and applications can now be explored.

Acknowledgements: John R. J. Maynard and Stephen M. Goldup developed the co-conformational auxiliary concept. JRJM synthesized **3** and **5** and collected SCXRD diffraction data for a reduced product of catenane **5**. David Lozano optimized the synthesis and purification of **3**, **5**, synthesized **6** and determined the stereochemistry of catenanes **3** and assisted in managing the preparation of Supporting Information. Patrick Butler collected the X-ray diffraction data of **3**, **6** and **9** and fully refined all SCXRD data. I synthesized **9** and **10**, determined the stereochemistry of rotaxanes **9** and managed the preparation of manuscript graphics and Supporting Information.

JRJM, DL, PB, SMG and I all contributed to the analysis of the results and writing of the manuscript.

Prior publication: This chapter was previously published as:

J. R. J. Maynard, P. Gallagher D. Lozano, P. Butler, S. M. Goldup, *Nat. Chem.* **2022**, *14*, 1038–1044.

2.1. Introduction

The term chiral was introduced by Lord Kelvin over a century ago to describe objects that are distinct from their own mirror image[1]. Chirality is relevant in many scientific areas[2,3,4,5] but particularly chemistry because different mirror image forms of a molecule famously have different biological properties. Indeed, the shape of a molecule is a major determinant of its function[6]. Thus, chemists have invested significant effort to develop methods that produce molecules with control over their stereochemistry[7]. A major part of this effort, which has led to two Nobel prizes[8,9], has focused on methods to selectively make molecules in one mirror image form because these are hard to separate using standard techniques. Although chirality is a whole-molecule property[10], chemists often trace the appearance of molecular chirality back to one or more rigidly chiral arrangements of atoms in the structure. The most famous of these is the 'stereogenic centre' embodied by a tetrahedral carbon atom bonded to four different substituents, although stereogenic planes and axes are also found in important natural and synthetic structures. Chiral molecules containing such classical covalent stereogenic units have been studied extensively. Less explored are chiral molecules whose stereochemistry arises absent any covalent stereogenic unit, such as Möbius ladders[11], molecular knots[12], and mechanically interlocked molecules[13,14].

In 1961 Wasserman and Frisch identified that interlocked molecules called catenanes (two molecular rings joined like links in a chain) can display non-classical “mechanical” stereochemistry[15]; when both rings are 'oriented' (C_{nh} symmetry) a catenane exists in two mirror image forms (Figure 2.1a). A decade later, Schill proposed that rotaxanes composed of an oriented ring encircling an axle whose ends are distinct are also chiral (Figure 2.1a)[16]. In both cases, the sub-components that make up the interlocked structure are not themselves chiral, which is readily emphasized using commonly employed schematic representations that focus on the symmetry properties of the components (Figure 2.1a). These representations also make clear that such topologically chiral catenanes and mechanically planar chiral rotaxanes are related notionally through ring opening. Although such molecules were initially challenging to make as single enantiomers[17,18,19,20,21], recent efforts have allowed them to be accessed in good enantiopurity using standard synthetic approaches[22,23,24,25,26,27].

Wasserman and Frisch also hinted at, but did not explicitly depict, a second form of catenane stereochemistry that arises when achiral rings with distinct faces (C_{nv}) are combined (Figure 2.1b)[15]. In 2002, Puddephat and co-workers reported the first synthesis of such a mechanically axially chiral catenane as a racemate[28,29]. However, no enantiopure examples where the

mechanical bond provides the sole source of stereochemistry have been disclosed to date[30]. To address this challenge, we re-examined the mechanical axial stereogenic unit of catenanes with a focus on not just the symmetry of the components but how this arises structurally. This led us not only to an efficient approach to enantiopure mechanically axially chiral catenanes but also to recognize and synthesize a noncanonical class of mechanically chiral rotaxanes that had previously been overlooked.

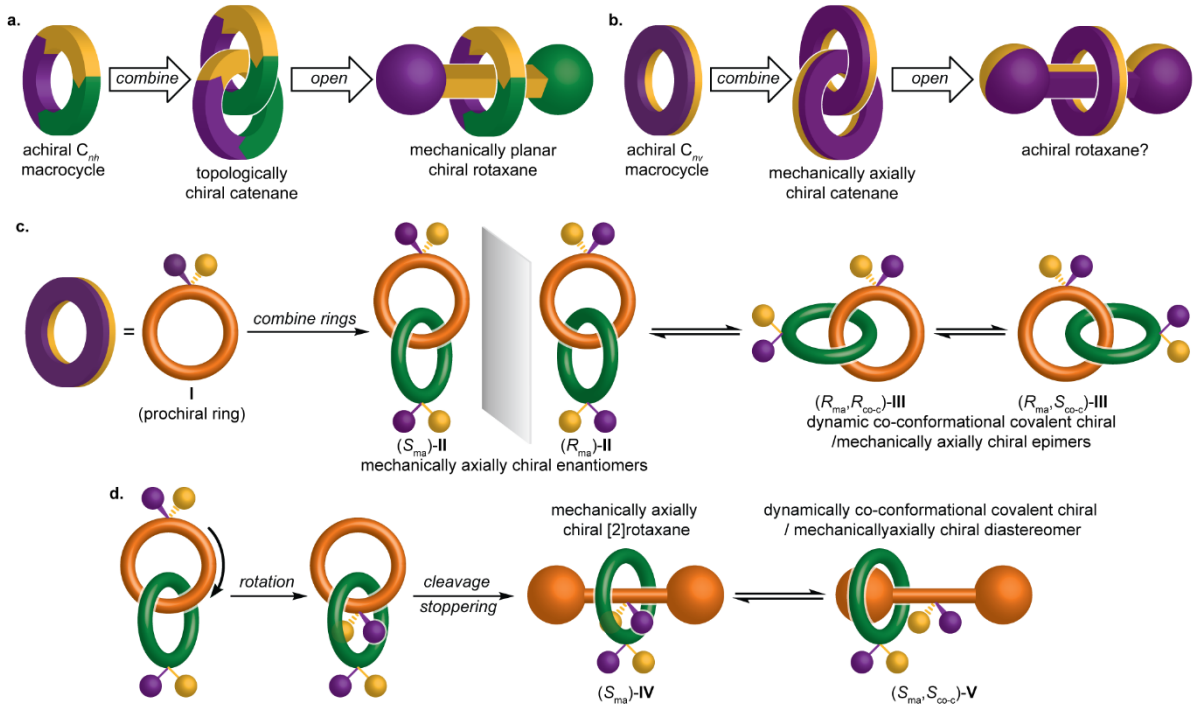

Figure 2.1 - Schematic depictions of the mechanical stereogenic units of chiral catenanes and rotaxanes (stereolabels are arbitrary). **a**, The mechanical topological and planar chiral stereogenic units of catenanes and rotaxanes are related by a notional ring-opening process. **b**, The minimal schematic representation of a mechanically axially chiral catenane suggests that there is no analogous axially chiral rotaxane. **c**, Semi-structural representations of axially chiral catenanes reveal that such molecules can display co-conformational covalent chirality alongside the fixed mechanical stereogenic unit. **d**, The semi-structural representation reveals that rotaxanes display a related but previously unrecognized form of stereochemistry

2.2. Results and Discussion

2.2.1. Insights from semi-structural schematic representations

The minimal schematic representation of a mechanically axially chiral catenane (Figure 2.1b) does not specify how the facial dissymmetry of the macrocycles arises. The most obvious way this can be achieved chemically is by including a prochiral unit in both rings (**I**, Figure 2.1c)[28,30,]. Strikingly, whereas the minimal schematic representation of a mechanically axially chiral catenane suggests there can be no rotaxane equivalent of this stereogenic unit (Figure 2.1b), the semi-structural representation reveals that the notional ring opening process gives rise to a chiral rotaxane (Figure 2.1d); even when the ring encircles the prochiral unit of the axle (**IV**) there is no representation that is achiral. Thus, we see that rotaxanes can display a previously unremarked upon noncanonical mechanically axially chiral stereogenic unit.

Building on the semi-structural analysis above, we returned to the general symmetry properties of mechanically axially chiral molecules. Whereas the components of catenane **II** and rotaxane **IV** have C_{1v} point group symmetry, more generally mechanical axial stereochemistry will arise in catenanes whose rings have C_{nv} symmetry and rotaxanes whose axle has C_{1v} symmetry (for an extended discussion see Supplementary section 2.4.4). Such structures will tend to exhibit prochirality[31] – any single structural modification that does not lie on a symmetry plane will result in a chiral object (for an extended discussion see Supplementary section 2.4.4). As a direct consequence, although mechanically axially chiral molecules can always, in theory, adopt a highly symmetrical co-conformation (e.g. **II** and **IV**) that only expresses mechanical axial stereochemistry, if either ring is displaced from this arrangement the resulting structure contains both a mechanically axially chiral stereogenic unit and a co-conformational covalent stereogenic unit (e.g., **III** and **V**). These lower symmetry arrangements exist as pairs of co-conformational diastereomers and are an inherent property of mechanically axial chiral molecules (for an extended discussion see Supplementary section 2.4.4).

2.2.2. A co-conformational auxiliary approach to axially chiral catenanes and rotaxanes

Having recognized that co-conformational diastereoisomerism is a fundamental property of mechanically axially chiral molecules, it became obvious that a co-conformational stereogenic unit could act as a temporary source of chiral information in their synthesis (Figure 2.2). By forming a mechanical bond selectively on one side of a prochiral unit (route A and designing the structure such that co-conformational exchange is initially blocked, the mechanically axially chiral catenane product would be formed as a pair of separable diastereomers with identical co-conformational configuration (here $R_{co\text{-}c}$) but opposite mechanical axial configuration (R_{ma} or S_{ma}).

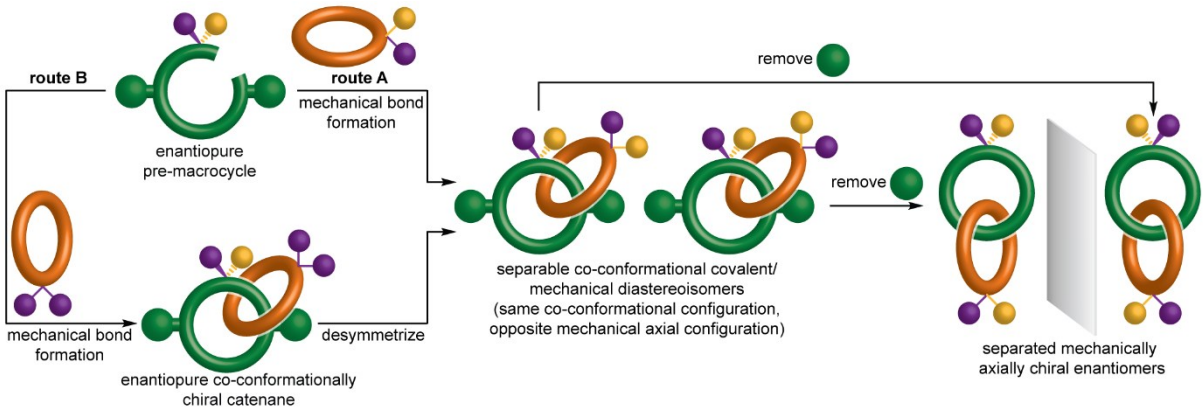

Figure 2.2 - Proposed co-conformational auxiliary approach for the synthesis of axially chiral catenanes. If the prochiral substituents and blocking groups are large enough to prevent co-conformational isomerism, the diastereomers can be separated and then converted into enantiomeric axially chiral catenanes.

Alternatively, installing a facially symmetrical ring on one side of a prochiral centre would give rise to a single co-conformational enantiomer (route B). Subsequent desymmetrization of the faces of the ring would give rise to the same pair of diastereomers. Removal of the groups preventing co-conformational motion would give mechanically axially chiral enantiomers in which the mechanical bond provides the sole fixed source of stereochemistry. An advantage of this co-conformational chiral auxiliary approach is that co-conformational enantiomers can be made using chiral pool starting materials by choosing where the mechanical bond is formed[17,32,33,34].

To demonstrate our co-conformational auxiliary approach, (*R*)-serine was elaborated to pre-macrocycle (*R*)-**1** (Figure 2.3a). Macrocycle **2**, which contains a prochiral sulfoxide, was readily synthesized using a Ni-mediated macrocyclization protocol[35]. Catenane formation was achieved by reacting (*R*)-**1** with macrocycle **2** under active template[36] Cu-mediated alkyne–azide cycloaddition (AT-CuAAC)[37] conditions[38]; slow addition of (*R*)-**1** to a solution of **2**, $[Cu(CH_3CN)_4]$ and N^iPr_2Et in a mixture of $CHCl_3$–EtOH gave catenanes **3**, in which co-conformational motion is prevented by the bulky ester and *N*-Boc groups, as a separable mixture of diastereomers (d.r. = 71:29). A brief screen of reaction solvent did not allow us to identify conditions that enhanced the stereoselectivity of the reaction (Supplementary section 2.4.2). Catenanes **3** were also synthesised by reaction of (*R*)-**1** with macrocycle **4** to give ($R_{co\text{-}c}$)-**5** followed oxidation to give catenanes **3** (route B). The diastereoselectivity obtained depended strongly on the oxidant used (see Supplementary section 2.4.2). The maximum selectivity (39:61 d.r.) without significant over-oxidation was achieved when 2-iodoxybenzoic acid[39] (IBX) was employed. Thus, under our optimal conditions, routes a and b proceeded with appreciable but opposite stereoselectivity. Single crystal x-ray diffraction (SCXRD) analysis of the major product of *rac*-**1** and **2** allowed the different major stereoisomers formed in routes A and B to be assigned (Figure 2.3c, section 2.4.3).

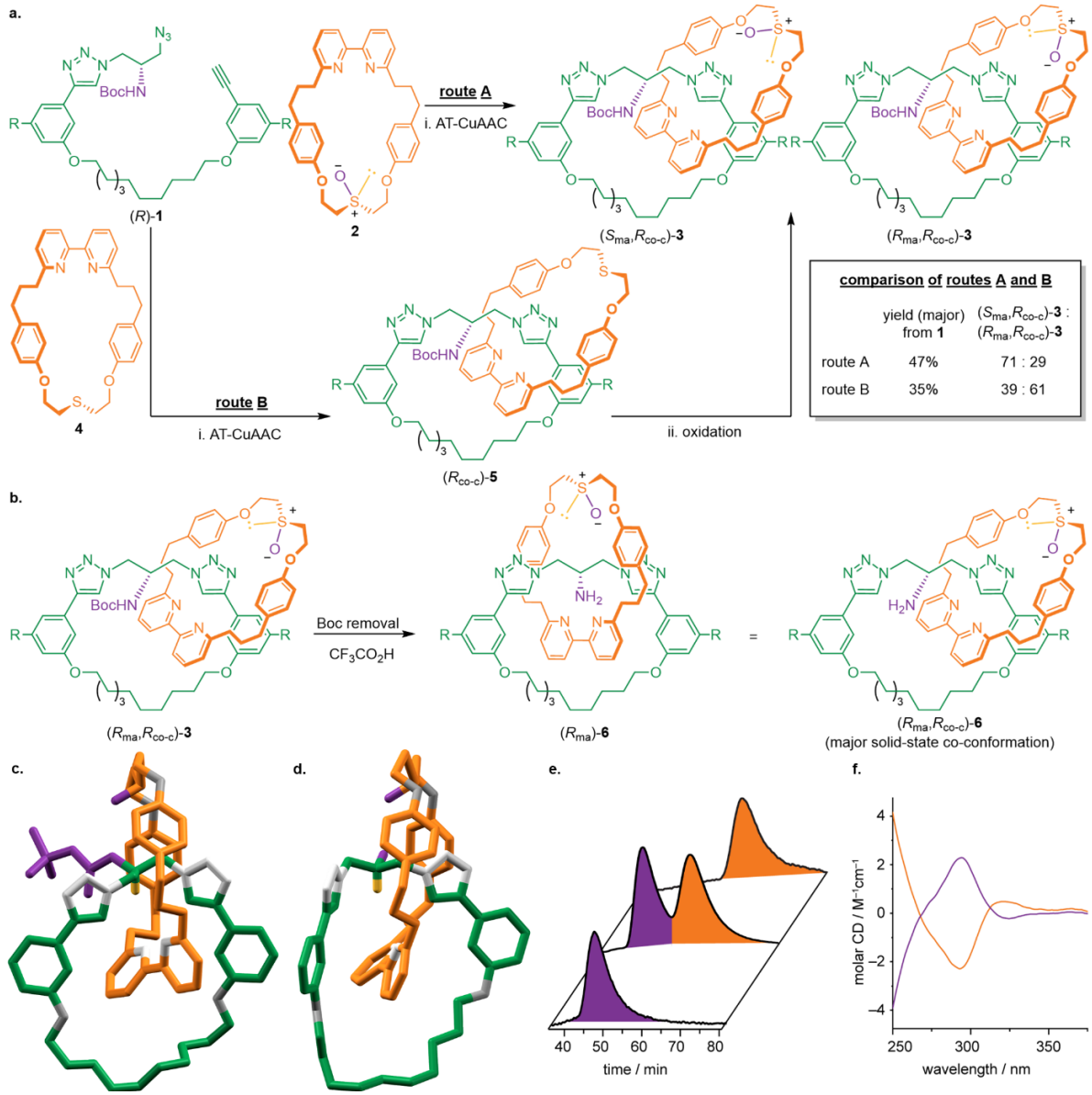

Figure 2.3 - Synthesis and analysis of enantiopure axially chiral catenane **6**. **a**, Synthesis and separation of catenane diastereomers **3** from (*R*)-**1** by route A or route B (Figure 2.2) with opposite diastereoselectivity. Reagents and conditions: i. $[Cu(CH_3CN)_4]PF_6$, N^iPr_2Et, CH_2Cl_2, rt, 16 h; ii. IBX, NEt_4Br, $CHCl_3$-H_2O (99 : 1), rt, 16 h. **b**, Conversion of catenane **3** to enantiomeric catenanes **6**. Reagents and conditions: CF_3CO_2H, CH_2Cl_2, 0 °C, 1 h. **c**, The solid-state structure (R groups and majority of H omitted for clarity) of *rac*-(S_{ma},$R_{co\text{-}c}$)-**3** allowed the major products of routes a and b to be assigned. **d**, The solid-state structure (R groups and majority of H omitted for clarity) of *rac*-**6** contains *rac*-(S_{ma},$R_{co\text{-}c}$)-**6** as the major co-conformational diastereomer. Analysis of (R_{ma})-**6** (purple) and (S_{ma})-**6** (orange) by **e**, chiral-stationary-phase high-performance liquid chromatography and **f**, circular dichroism spectroscopy respectively confirmed their enantiopurity and their chiral nature. IBX = 2-iodoxybenzoic acid. R = CO_2Me.

Conversion of diastereomers **3** to structures in which the mechanically axially chiral stereogenic unit is the only fixed source of stereochemistry can be achieved by removing the Boc group (Figure 2.3b) or reducing the esters. Accordingly, removal of the Boc group from (R_{ma},$R_{co\text{-}c}$)-**3** or (S_{ma},$R_{co\text{-}c}$)-**3** gave (R_{ma})-**6** (>99% e.e.) and (S_{ma})-**6** (>99% e.e.) respectively (Figure 2.3e). The enantiomeric nature of these structures is supported by circular dichroism (CD) analysis (Figure

2.3f). The solid-state structure of *rac*-**6** (Figure 2.3d) contains both co-conformational diastereomers with the *rac*-(S_{ma}-$R_{co\text{-}c}$) co-conformation observed to dominate (~80:20, Supplementary section 2.4.3). The same strategy was used to synthesize mechanically axially chiral rotaxane **10** (Figure 2.4). Serine-derived azide (*R*)-**7**, alkyne **8** and macrocycle **2** were reacted under AT-CuAAC conditions[40] to give a separable mixture (75:25 d.r.) of rotaxane diastereomers **9** (route A). Rotaxanes **9** could also be accessed by reaction of (*R*)-**7**, **8** and macrocycle **4** followed by oxidation (route B). As with catenanes **3**, the diastereoselectivity of route B varied depending on the oxidant used (see Supplementary section 2.4.2) and the highest diastereoselectivity was obtained with IBX (40:60). SCXRD analysis (Supplementary section 2.4.3) of the major isomer obtained using route B with (*R*)-**7** (Figure 2.4b) allowed the major products of routes A and B to be assigned. Removal of the Boc group from separated samples of (R_{ma},$R_{co\text{-}c}$)-**9** and (S_{ma},$R_{co\text{-}c}$)-**9** gave (R_{ma})-**10** and (S_{ma})-**10** respectively in excellent enantiopurity (>99% e.e., Figure 2.4c). (R_{ma})-**10** and (S_{ma})-**10** produce mirror-image CD spectra (Figure 2.4d) emphasizing the chiral nature of the new rotaxane mechanical axial stereogenic unit.

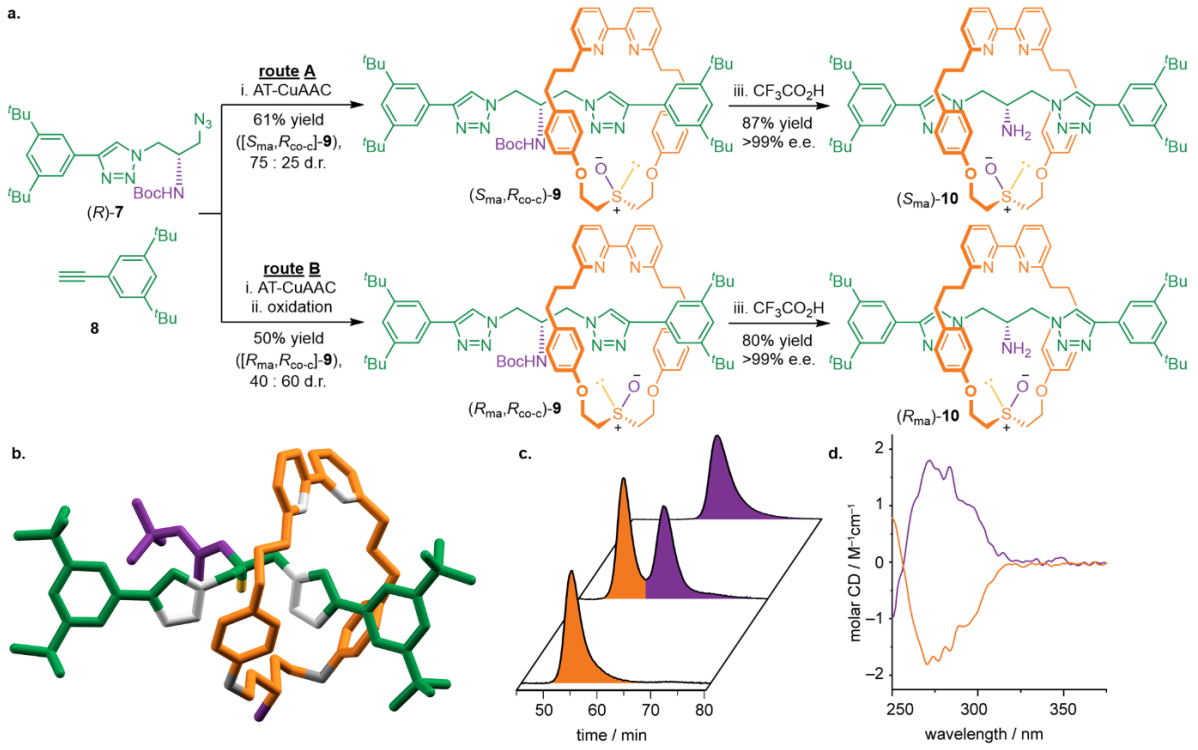

Figure 2.4 - Synthesis of mechanically axially chiral rotaxane **10**. **a**, Synthesis of diastereomeric mechanically axially chiral rotaxanes **9** by route A or B gives separable rotaxanes **9** that are converted to **10** by removal of the Boc group. Reagents and conditions: i. macrocycle **2** (route A) or macrocycle **4** (route B), $[Cu(CH_3CN)_4]PF_6$, N^iPr_2Et, CH_2Cl_2, rt, 16 h; ii. IBX, NEt_4Br, $CHCl_3$-H_2O (99 : 1), rt, 16 h; iii. CF_3CO_2H, CH_2Cl_2, rt, 16 h. **b**, SCXRD analysis of (R_{ma},$R_{co\text{-}c}$)-**9** allowed the major products of routes a and b to assigned. Analysis of (R_{ma})-**10** (purple) and (S_{ma})-**10** (orange) by **c**, chiral-stationary-phase high-performance liquid chromatography and **d**, circular dichroism spectroscopy respectively confirmed their enantiopurity and their chiral nature. IBX = 2-iodoxybenzoic acid.

2.2.3. Stereochemical assignment and properties of the mechanically axially chiral stereogenic unit

The assignment of the mechanically axially chiral stereogenic unit relies on identifying the highest priority faces of each ring, as proposed by Stoddart and Bruns[13]. However, because this rule had not been applied in a real system, we immediately encountered difficulties; to unambiguously assign the highest priority face of each ring the relative orientations of the prochiral units must be specified (for an extended discussion see Supplementary section 2.4.5). On reflection, we suggest that in the case of catenanes the in-plane substituents of the prochiral moieties be positioned at the extremities of the structure and oriented so they 'point' towards one another (Figure 2.5a). Conversely, in the equivalent rotaxane, we suggest they be oriented to point in the same direction (Figure 2.5b). The latter, somewhat counterintuitive, proposal is designed to ensure that a mechanically axially chiral rotaxane derived from the notional ring opening of an axially chiral catenane would retain the same stereolabel. The absolute stereochemistry of both mechanically axially chiral catenanes and rotaxanes can then be assigned by viewing the ensemble along the axis connecting the prochiral units and observing the relative orientation of the vectors from the out of plane substituent with the highest priority to the lowest priority as shown; a clockwise direction of rotation from the head of the front vector to the tail of the rear vector is assigned as R_{ma} and an anticlockwise path assigned as S_{ma}. This approach can be readily extended to molecules where facial dissymmetry arises due to prochiral stereogenic axes or planes (Supplementary section 2.4.5).

Finally, we considered the stereochemical nature of catenanes in which one or both prochiral units are replaced with covalent stereocentres. Such structures represent logical alternative precursors to axially chiral catenanes if they could be prepared diastereoselectively and the in-plane substituents subsequently symmetrized. Furthermore, there has been a suggestion that the latter class might contain both mechanical axial and mechanical topological stereogenic units[41]. In the case of catenanes containing one stereogenic and one prochiral centre (Figure 2.5c), ligand permutation analysis reveals two diastereomers (shown) and their enantiomers (i.e. four stereoisomers total), consistent with one covalent centre and one mechanical axial stereogenic unit (for an extended discussion see Supplementary section 2.4.6).

In the case of catenanes containing a stereogenic centre in each ring, ligand permutation reveals four diastereomers (Figure 2.5d) and their enantiomers (eight stereoisomers total), consistent with two covalent and one mechanical stereogenic unit (for an extended discussion see Supplementary section 2.4.6). However, the nature of the mechanical stereochemistry is ambiguous; each structure can be assigned both a mechanical axial or a mechanical topological

stereodescriptor, but only one of these is required to fully specify the structure. This analysis suggests that it would be incorrect to describe such catenanes as simultaneously topologically and mechanically axially chiral – one of the stereolabels would be redundant – but that it is unclear which description should take priority. Our preference would be to apply the mechanical topological stereodescriptor as this captures one of the interesting features of the system, that one of component of its stereochemistry is topologically invariant[42]. This analysis may appear philosophical in nature but has implications for the synthesis of chiral catenanes. If a single diastereomer of such a catenane could be isolated, it could be converted to an axially chiral catenane by selective symmetrization of the in-plane substituents, or a topologically chiral catenane by symmetrization of the out-of-plane substituents (Figure 2.5e). This analysis further highlights that how a stereogenic unit is conceptualized can guide the development of new methodologies.

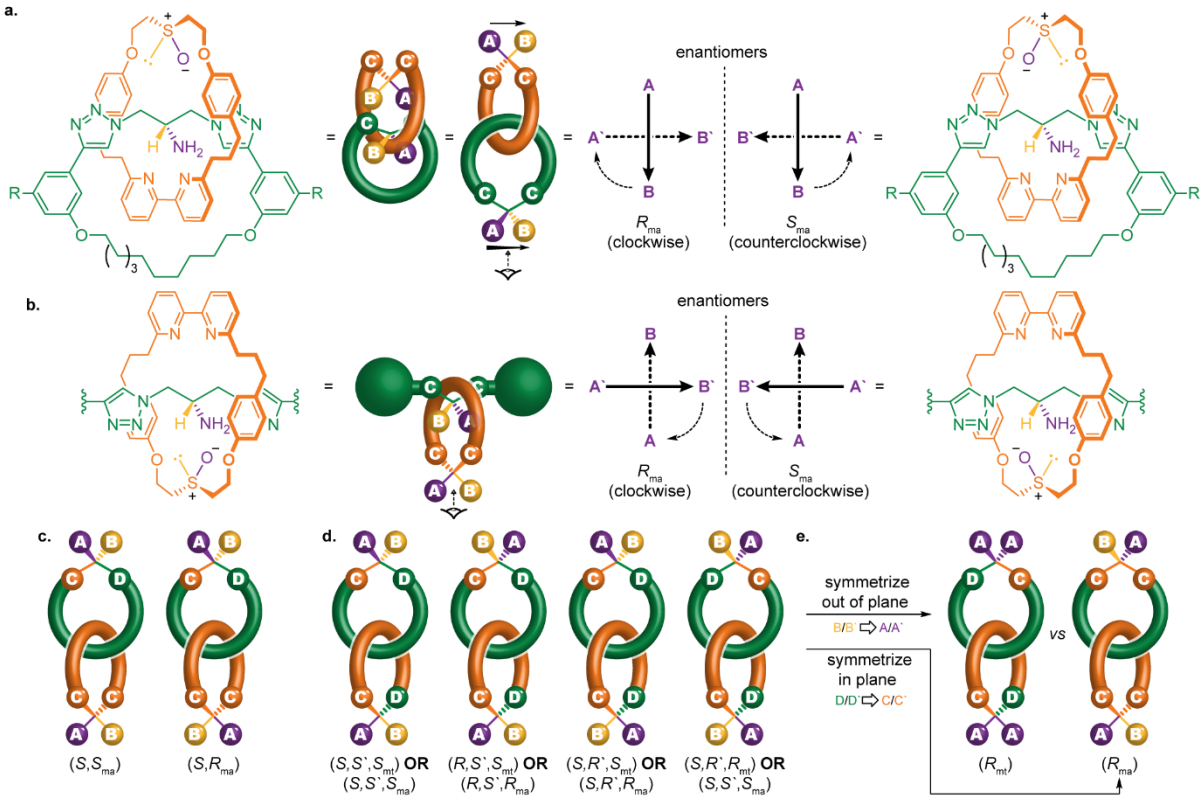

Figure 2.5 - Assignment and further analysis of the mechanical axial stereogenic unit. Methods to assign the stereogenic units of mechanically axially chiral **a**, catenanes and **b**, rotaxanes by specifying the relative orientation of prochiral moieties. **c**, The two diastereomers identified in catenanes containing one prochiral and one fixed covalent stereogenic centre. **d**, The four diastereomers identified in catenanes containing a covalent stereogenic centre in both rings whose structures can be specified using either a mechanical topological or axial stereodescriptor. **e**, Selective symmetrization of the in-plane or out of plane substituents of one diastereomers of **d** gives a topologically or axially chiral catenane respectively. R = CO_2Me.

2.3. Conclusions

Detailed analysis of the symmetry properties of the mechanically axially chiral stereogenic unit of catenanes, and in particular the use of semi-structural representations, allowed us to identify an efficient co-conformational auxiliary approach to mechanically axially chiral catenanes and revealed a previously overlooked noncanonical axially chiral stereogenic unit in rotaxanes. The latter is a rare example of a 'new' source of stereoisomerism, as opposed to an overlooked pathway of isomer exchange[43] or an overlooked opportunity for atropisomerism[44], as have recently been reported. The rotaxane mechanical axial stereogenic is so closely related to that of catenanes it is surprising that it was overlooked for so long, which may in part be due to the use of schematic structures (Figure 2.1b) that focus on symmetry without reference to underlying chemical structure; although these are useful, they can also obscure important chemical information. Indeed, given that the fixed mechanical stereogenic units of catenanes (topological and axial) now both have an equivalent in rotaxane structures (planar and axial), it appears sensible to suggest that the stereochemistry of rotaxanes and catenanes be unified rather than treated as separate as they are typically[45].

Our analysis also led to the surprising conclusion that catenanes based on two rings each containing a single stereogenic centre can be described as either mechanically topologically or axially chiral but that only one mechanical stereodescriptor is required to specify their structure, an observation with implications for future studies. Given the increasing interest in applications of chiral interlocked molecules[46,47,48,49,50,34] including examples based on mechanical and co-conformationally chiral systems[21,51,52], as well as other exotic or hard to access mechanical stereogenic units[53,54,55,56,57,58], we anticipate these results will spur progress in the development of functional chiral interlocked systems[59]. Finally, it should be noted that dynamic stereochemistry related to that of mechanically axially chiral catenanes and rotaxanes can also arise due to conformational and co-conformational processes[54,60], both of which have been observed but are poorly understood (for an extended discussion see Supplementary section 2.4.7). Such systems have potential applications as stereodynamic probes.

2.4. Experimental and Supplementary Information

General Experimental Information

Unless otherwise stated, all reagents were purchased from commercial sources (Acros Organics, Alfa Aesar, Fisher Scientific, FluoroChem, Sigma Aldrich and VWR) and used without further purification. $[Cu(CH_3CN)_4]PF_6$ was prepared as described by Pigorsch and Köckerling.[61] Anhydrous solvents were purchased from Acros Organics. Petrol refers to the fraction of petroleum ether boiling in the range 40-60 °C. IPA refers to isopropanol. THF refers to tetrahydrofuran. EDTA-NH_3 solution refers to an aqueous solution of NH_3 (17% w/w) saturated with sodium-ethylenediaminetetraacetate. IBX = 2-iodoxybenzoic acid. $CDCl_3$ (without stabilising agent) was distilled over $CaCl_2$ and K_2CO_3 prior to use. Unless otherwise stated, all reaction mixtures were performed in oven dried glassware under an inert N_2 atmosphere with purchased anhydrous solvents. Unless otherwise stated experiments carried out in sealed vessels were performed in CEM microwave vials, with crimped aluminium caps, with PTFE septa. Young's tap vessels and Schlenk techniques were used where specified.

Flash column chromatography was performed using Biotage Isolera-4 or Isolera-1 automated chromatography system. SiO_2 cartridges were purchased commercially Biotage (SNAP or ZIP (50 μm), or Sfär (60 μm) irregular silica, default flow rates). Neutralised SiO_2 refers to ZIP cartridges which were eluted with petrol-NEt_3 (99 : 1, 5 column volumes), followed by petrol (5 column volumes). Analytical TLC was performed on pre-coated silica gel plates on aluminum (0.25 mm thick, 60F254, Merck, Germany) and observed under UV light (254 nm) or visualised with $KMnO_4$ stain.

All melting points were determined using a Griffin apparatus. NMR spectra were recorded on Bruker AV400 or AV500 instrument, at a constant temperature of 298 K. Chemical shifts are reported in parts per million from low to high field and referenced to residual solvent. Coupling constants (*J*) are reported in Hertz (Hz). Standard abbreviations indicating multiplicity were used as follows: m = multiplet, quint = quintet, q = quartet, t = triplet, d = doublet, s = singlet, app. = apparent, br = broad, sept = septet. Signal assignment was carried out using 2D NMR methods (COSY, NOESY, HSQC or HMBC) where necessary. In some cases, complex multiplets with multiple contributing proton signals, exact assignment was not possible. In interlocked compounds, all proton signals corresponding to axle components are in lower case, and all proton signals corresponding to the macrocycle components are in upper case.

Low resolution mass spectrometry was carried out by the mass spectrometry services at University of Southampton (Waters TQD mass spectrometer equipped with a triple quadrupole analyser with UHPLC injection [BEH C18 column; CH_3CN -H_2O gradient (0.2% formic acid)]). High resolution mass spectrometry was carried out by the mass spectrometry services at the University of Southampton (MaXis, Bruker Daltonics, with a Time of Flight (TOF) analyser; samples were introduced to the mass spectrometer via a Dionex Ultimate 3000 autosampler and uHPLC pump in a gradient of 20% CH_3CN in hexane to 100% acetonitrile (0.2% formic acid) over 5-10 min at 0.6 mL/min; column: Acquity UPLC BEH C18 (Waters) 1.7 micron 50 × 2.1mm).

Circular dichroism spectra were acquired on an Applied Photo-physics Chirascan spectropolarimeter, recorded using Applied Photophysics software Ver. 4.2.0 in dried spectroscopic grade $CHCl_3$, following overnight desiccation of the sample, at a concentration range of <50 μM, in a quartz cell of 1 cm path length, at a temperature of 293 K.

Stereochemical purity was determined by Chiral Stationary Phase HPLC on a Waters Acquity Arc Instrument at 303 K, with *n*-hexane-^{i}PrOH or *n*-hexane-EtOH isocratic eluents. Regis Technologies (S,S)-Whelk-O1 (1-(3,5-dinitrobenzamido)-1,2,3,4-tetrahydrophenanthrene stationary phase), RegisPack (tris-(3,5-dimethylphenyl) carbamoyl amylose stationary phase), RegisPackCLA-1 (tris-(5-chloro-2-methylphenyl)carbamoyl amylose), and RegisCell (tris-(3,5-dimethylphenyl) carbamoyl cellulose stationary phase) columns were used throughout (5 micron, column dimensions 25 cm x 4.6 mm). Unless otherwise shown, racemic samples were prepared employing the same synthetic procedures and auxiliary strategy but starting from racemic **S1**.

The following compounds were synthetized according to literature procedures: (*R*)-**S1**,[62] **S3**,[63] **S11**,[35] **8**.[64]

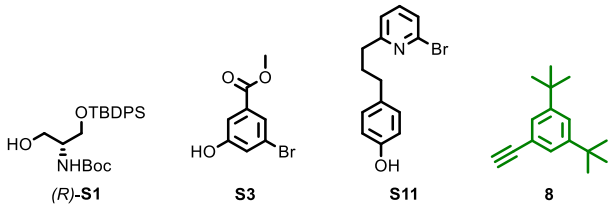

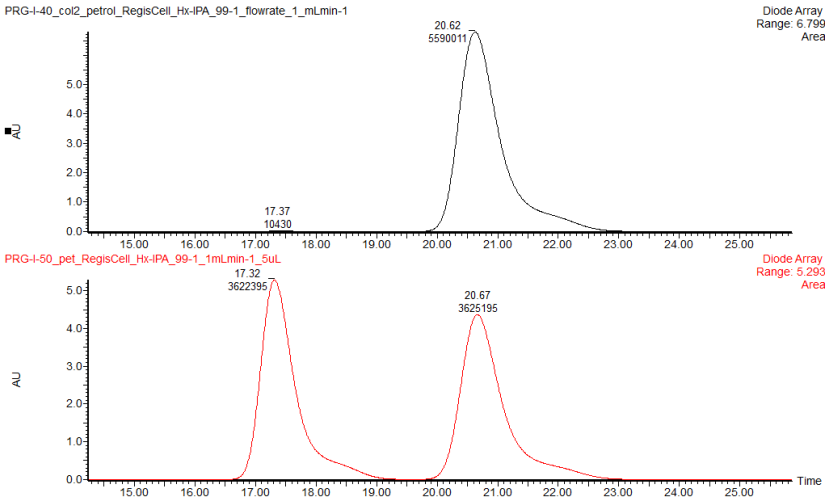

Figure 2.6 - CSP-HPLC of (*R*)-**S1** (loaded in petrol). RegisCell, *n*-hexane-IPA 99 : 1, flowrate 1 $mLmin^{-1}$. (Top) (*R*)-**S1**, (*S*)-**S1** (17.37 min, 10430, 0.2%), (*R*)-**S1** (20.62 min, 5590011, 99.8%), (Bottom) *rac*-**S1**, (*S*)-**S1** (17.32 min, 3622395, 50.0%), (*R*)-**S1** (20.67 min, 3625195, 50.0%).

2.4.1. Characterisation of compounds

Compounds leading to catenane pre-macrocycle 1

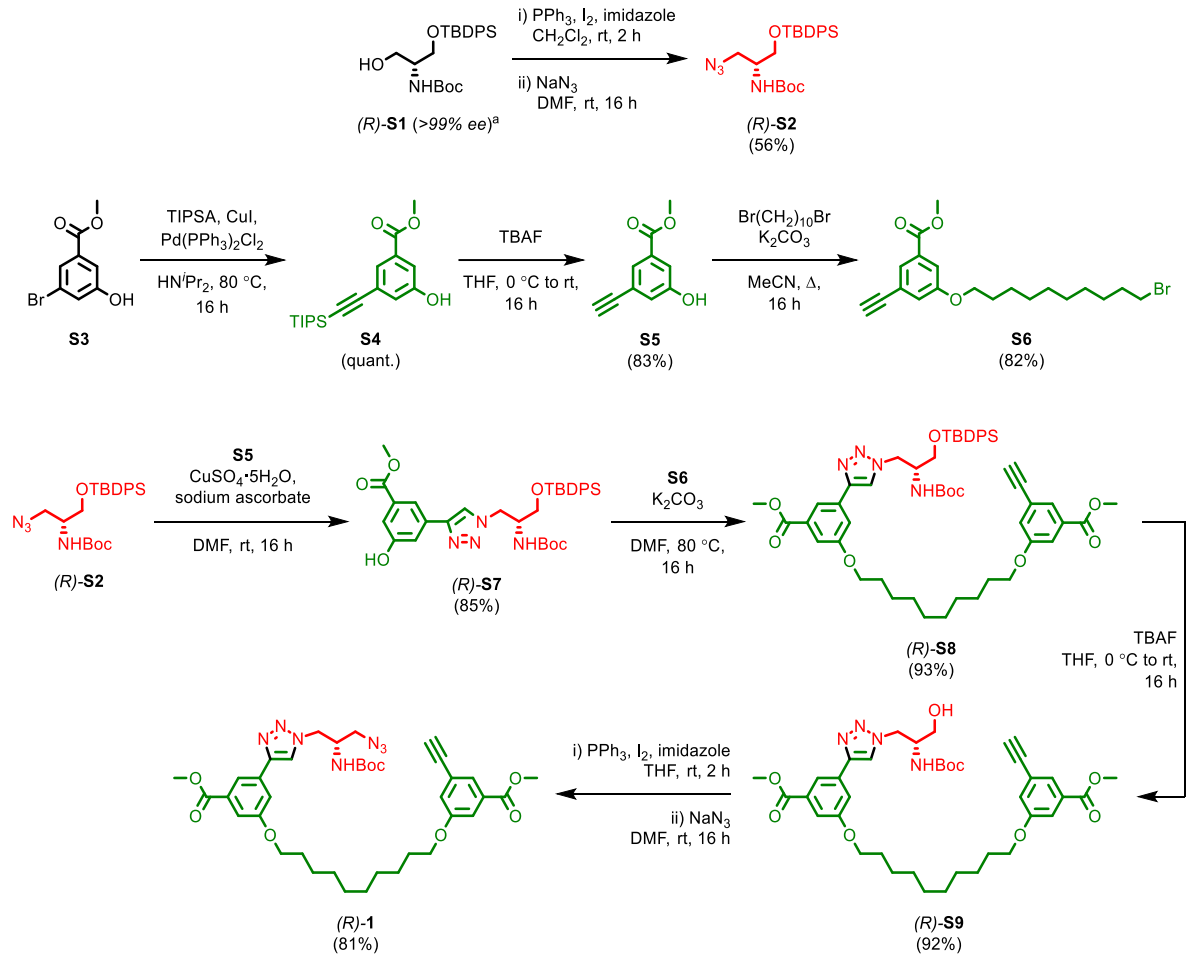

Scheme 2.1 - Synthetic route to catenane pre-macrocycle (*R*)-**1**. [a]stereochemical purity was assessed by CSP-HPLC, Figure 2.6.

Compound (*R*)-S2

To a solution of PPh_3 (2.50 g, 9.53 mmol, 3.0 eq.) and imidazole (1.08 g, 15.86 mmol, 5.0 eq.) in CH_2Cl_2 (27 mL) was added I_2 (2.42 g, 9.53 mmol, 3.0 eq.) in 1 portion at 0 °C. After stirring for 10 min, a solution of (*R*)-**S1** (1.37 g, 3.19 mmol, 1.0 eq.) in CH_2Cl_2 (7 mL) was added dropwise. The reaction mixture was allowed to warm to ambient temperature and stirred for 2 h. The crude mixture was filtered through Celite®, washing with CH_2Cl_2, and concentrated *in vacuo*. The residue was purified by column chromatography (SiO_2, petrol-EtOAc 0→10%). The resultant oil

was immediately dissolved in DMF (16 mL) and NaN_3 (1.04 g, 16.00 mmol, 5.0 eq.) was added. After stirring for 16 h at ambient temperature, the reaction mixture was diluted with EtOAc (10 mL), washed with H_2O (10 mL) and 1 M $Na_2S_2O_3{\cdot}5H_2O$ (5 mL). The aqueous layer was extracted with EtOAc (3 x 10 mL). The combined organic fractions were washed with 5% LiCl (3 x 10 mL), and brine (10 mL) then dried over $MgSO_4$, filtered, and concentrated *in vacuo*. The residue was purified by column chromatography (SiO_2, petrol-Et_2O 0→20%) to yield (*R*)-**S2** (808.6 mg, 1.78 mmol, 56% over two steps) as a colourless oil.

δ_H ($CDCl_3$, 400 MHz) 7.68 – 7.60 (m, 4H, H_b), 7.47 – 7.37 (m, 6H, H_c, H_d), 4.75 (d, *J* = 8.8, 1H, H_{NHBoc}), 3.85 (br s, 1H, H_f), 3.73 (dd, *J* = 10.3, 4.0, 1H, H_e), 3.64 (dd, *J* = 10.3, 5.5, 1H, H_e), 3.57 (dd, *J* = 12.1, 5.0, 1H, H_g), 3.47 (dd, *J* = 12.0, 6.2, 1H, H_g), 1.44 (s, 9H, H_h), 1.07 (s, 9H, H_a); δ_C ($CDCl_3$, 101 MHz) 135.7, 133.0, 130.1, 128.0, 79.8 (HMBC), 63.1, 51.6, 51.3, 28.5, 27.1, 19.5, peak corresponding to carbonyl not observed; HR-ESI-MS (+ve) m/z = 477.2290 $[M+Na]^+$ (calc. m/z for $C_{24}H_{34}N_4NaO_3Si$ 477.2292).

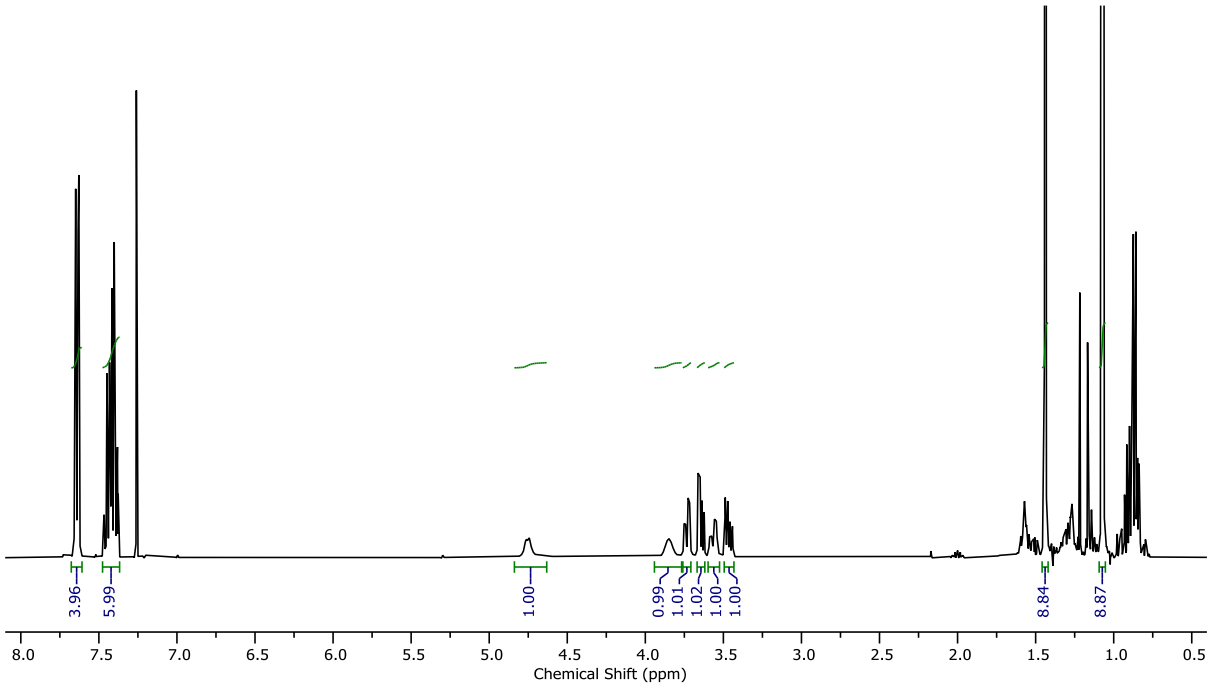

Figure 2.7 - ^1H NMR ($CDCl_3$, 400 MHz) of **S2**.

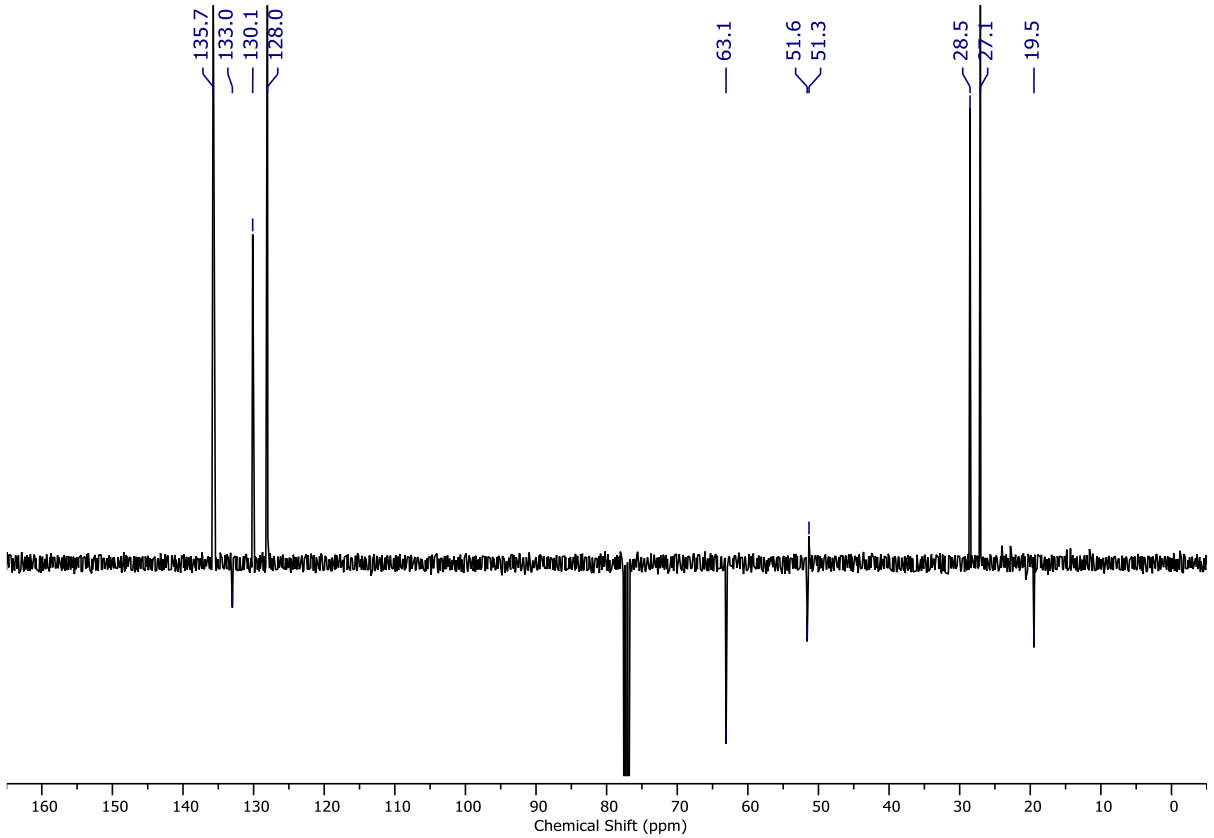

Figure 2.8 - JMOD NMR ($CDCl_3$, 101 MHz) of **S2**.

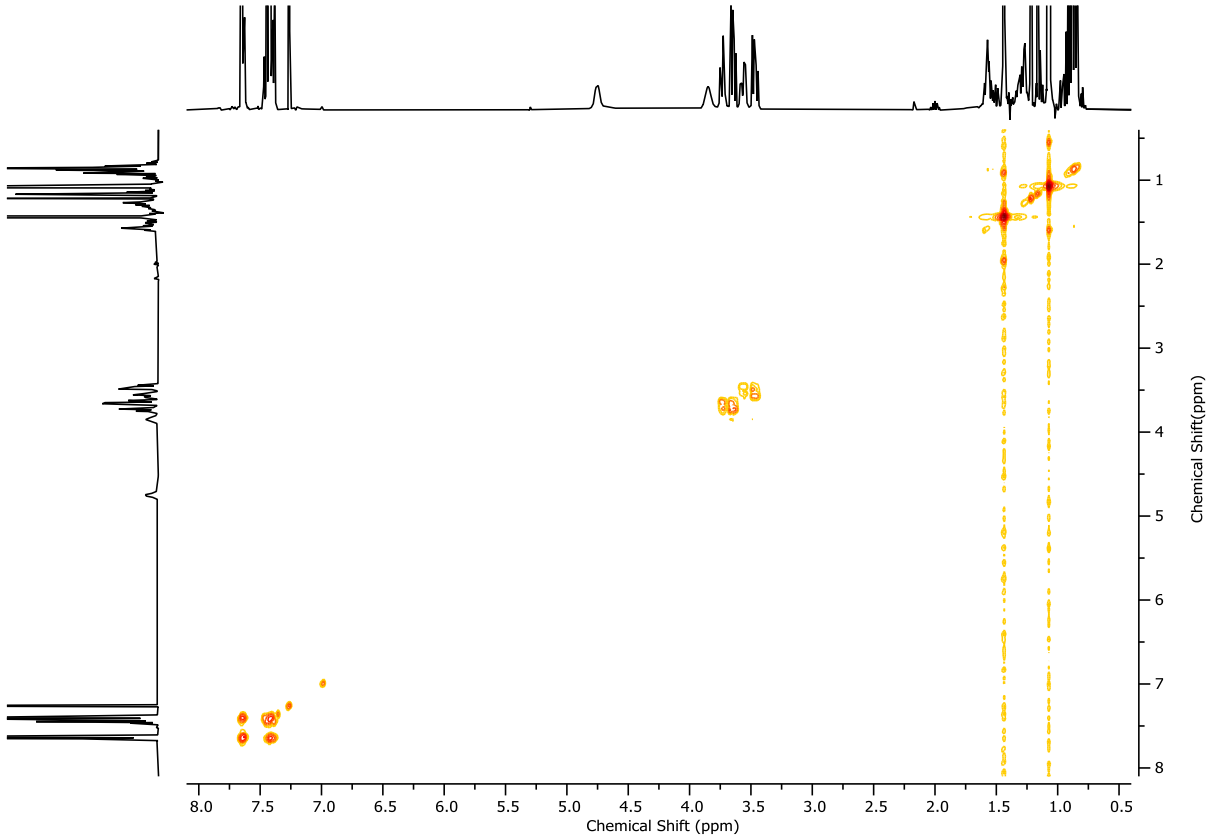

Figure 2.9 - ^1H COSY NMR ($CDCl_3$, 400 MHz) of **S2**.

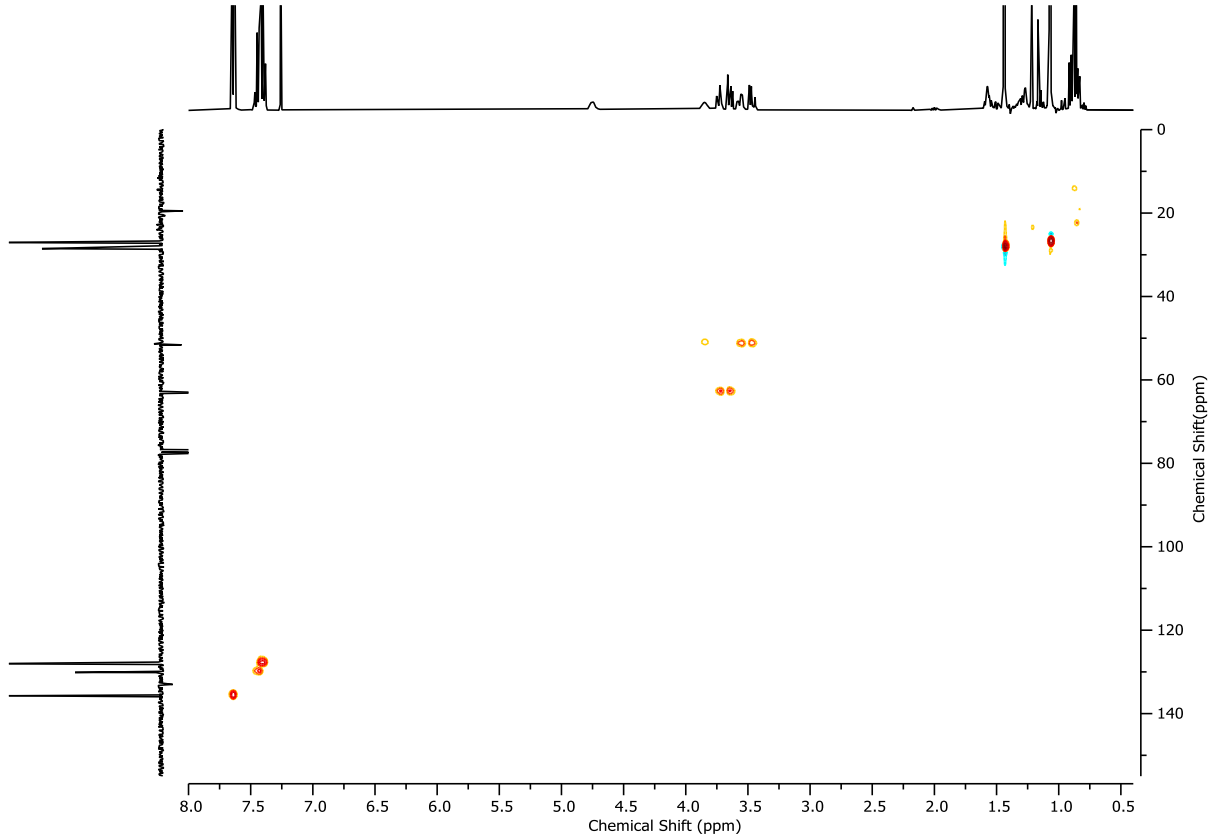

Figure 2.10 - HSQC NMR ($CDCl_3$, 400 MHz) of **S2**.

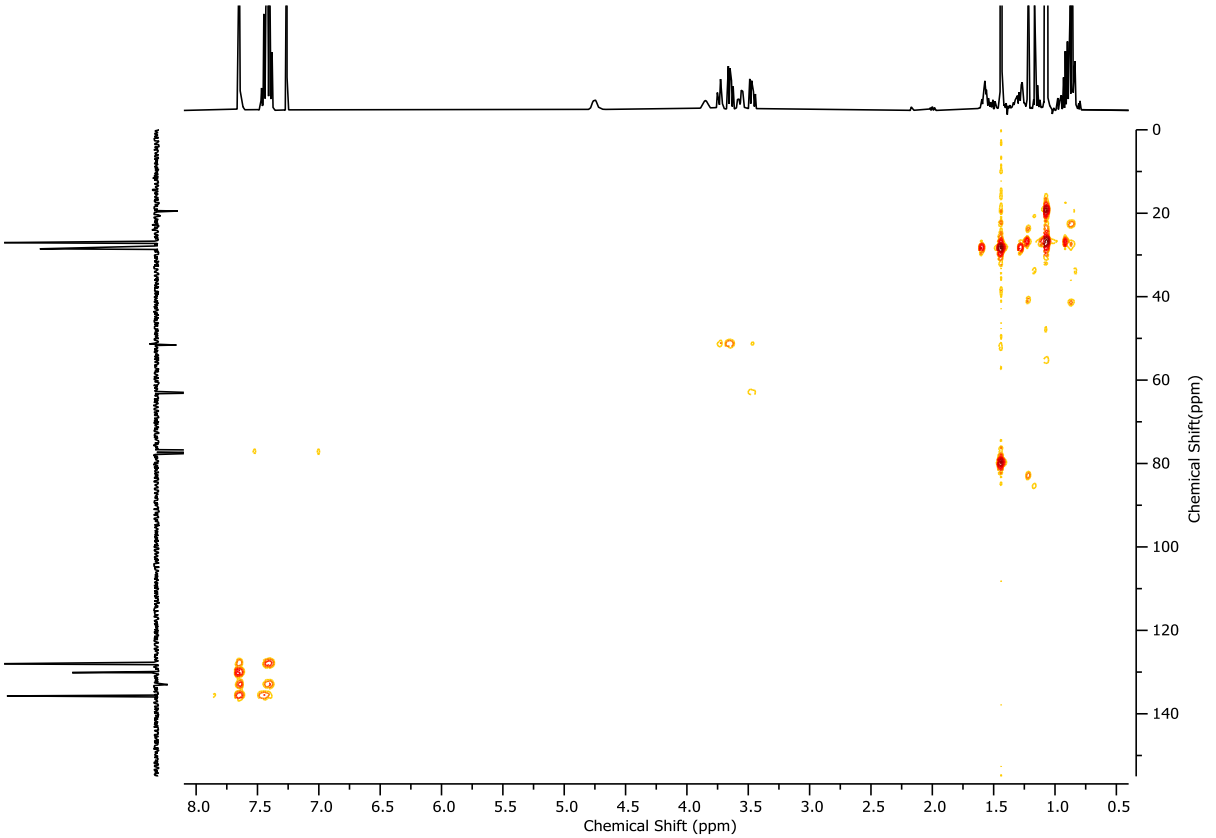

Figure 2.11 - HMBC NMR ($CDCl_3$, 400 MHz) of **S2**.

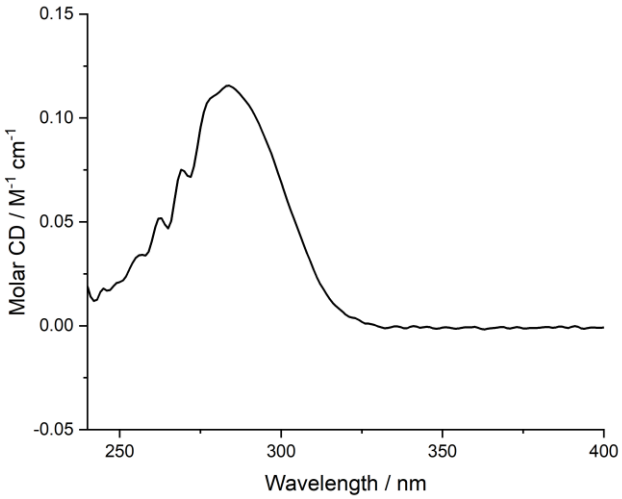

Figure 2.12 - Circular Dichroism Spectra of (*R*)-**S2** (1.3 mM) at 293 K in $CHCl_3$.

Compound S4

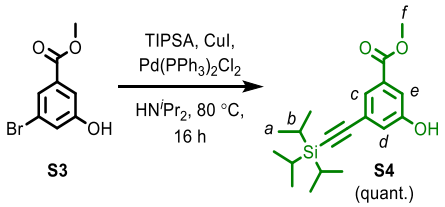

To a solution of **S3** (668 mg, 2.89 mmol, 1.0 eq.), $PdCl_2(PPh_3)_2$ (42.2 mg, 0.06 mmol, 0.02 eq.), CuI (23 mg, 0.12 mmol, 0.04 eq.) in degassed HN^iPr_2 (11.6 mL) was added (triisopropylsilyl)acetylene (1.30 mL, 5.78 mmol, 2.0 eq.), and the reaction mixture was heated at 80 °C for 16 h. After cooling to ambient temperature, and concentration *in vacuo*, the residue was purified by column chromatography (SiO_2, petrol-Et_2O 0→40%) to yield **S4** (970 mg, 2.92 mmol, quant.) as a yellow oil.

δ_H ($CDCl_3$, 400 MHz) 7.69 (t, *J* = 1.4, 1H, H_c), 7.51 (dd, *J* = 2.6, 1.4, 1H, H_e), 7.15 (dd, *J* = 2.6, 1.4, 1H, H_d), 5.99 (s, 1H, H_{OH}), 3.92 (s, 3H, H_f), 1.16 – 1.04 (m, 21H, H_a, H_b); δ_C ($CDCl_3$, 101 MHz) 167.3, 159.9, 131.7, 125.8, 125.3, 123.5, 116.8, 105.7, 92.0, 52.6, 18.8, 11.4; HR-ESI-MS (+ve) m/z = 333.1883 $[M+H]^+$ (calc. m/z for $C_{19}H_{29}O_3Si$ 333.1880).

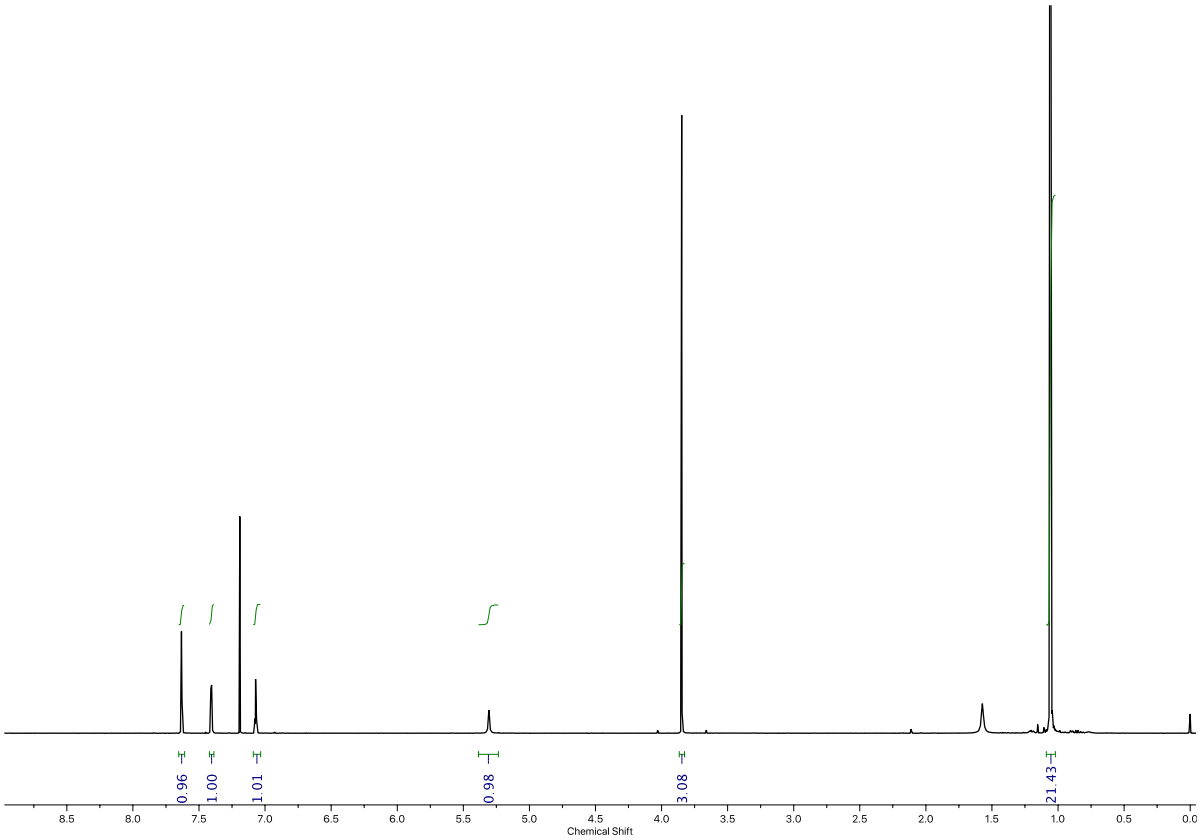

Figure 2.13 - ^{1}H NMR ($CDCl_3$, 400 MHz) of **S4**.

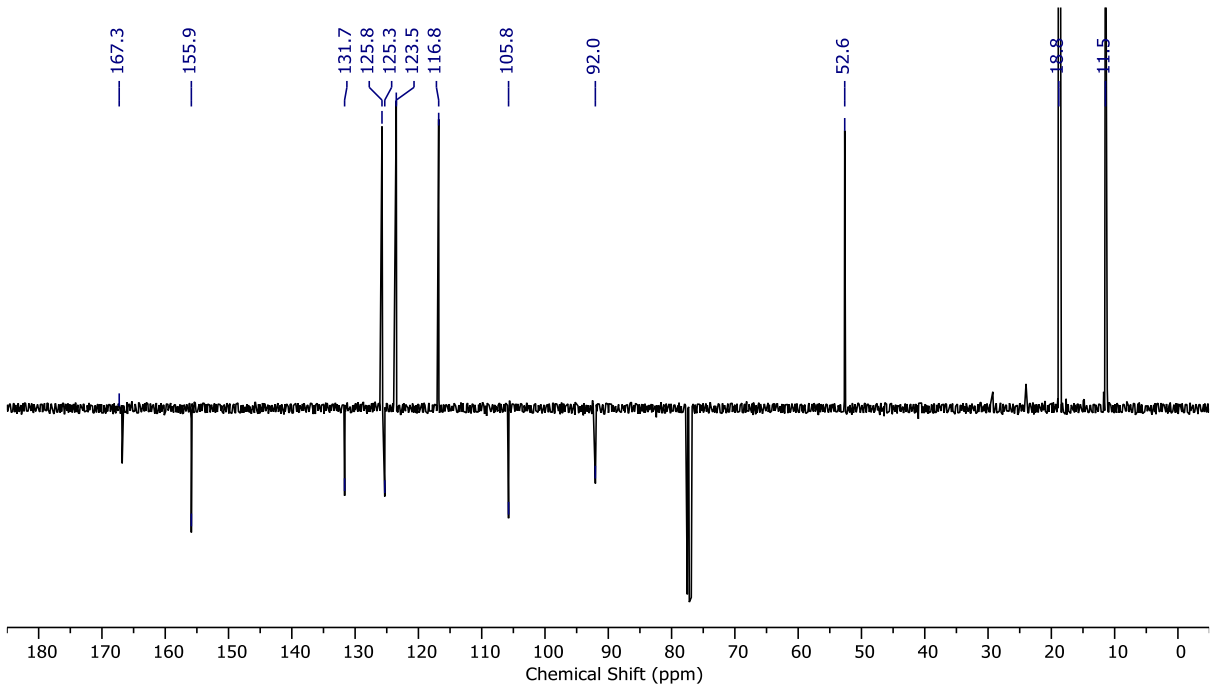

Figure 2.14 - JMOD NMR ($CDCl_3$, 101 MHz) of **S4**.

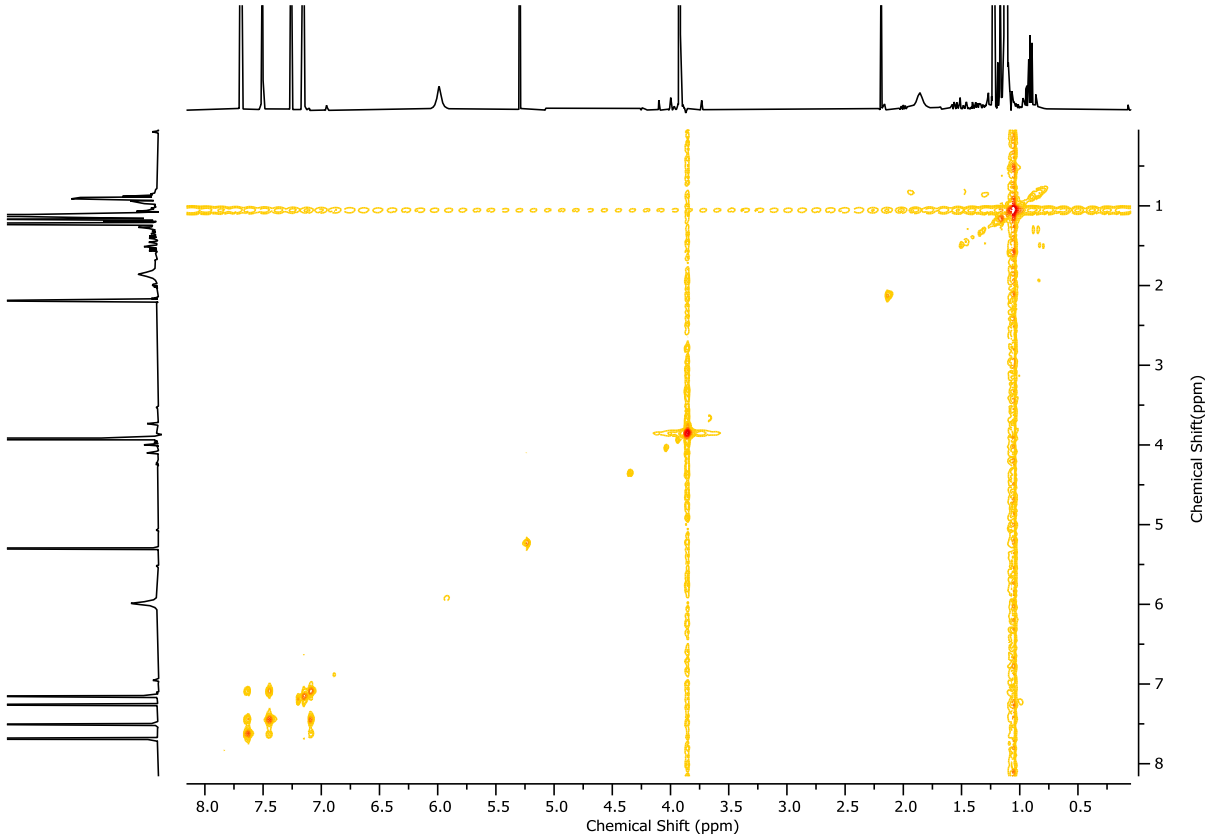

Figure 2.15 - ^{1}H COSY NMR ($CDCl_3$, 400 MHz) of **S4**.

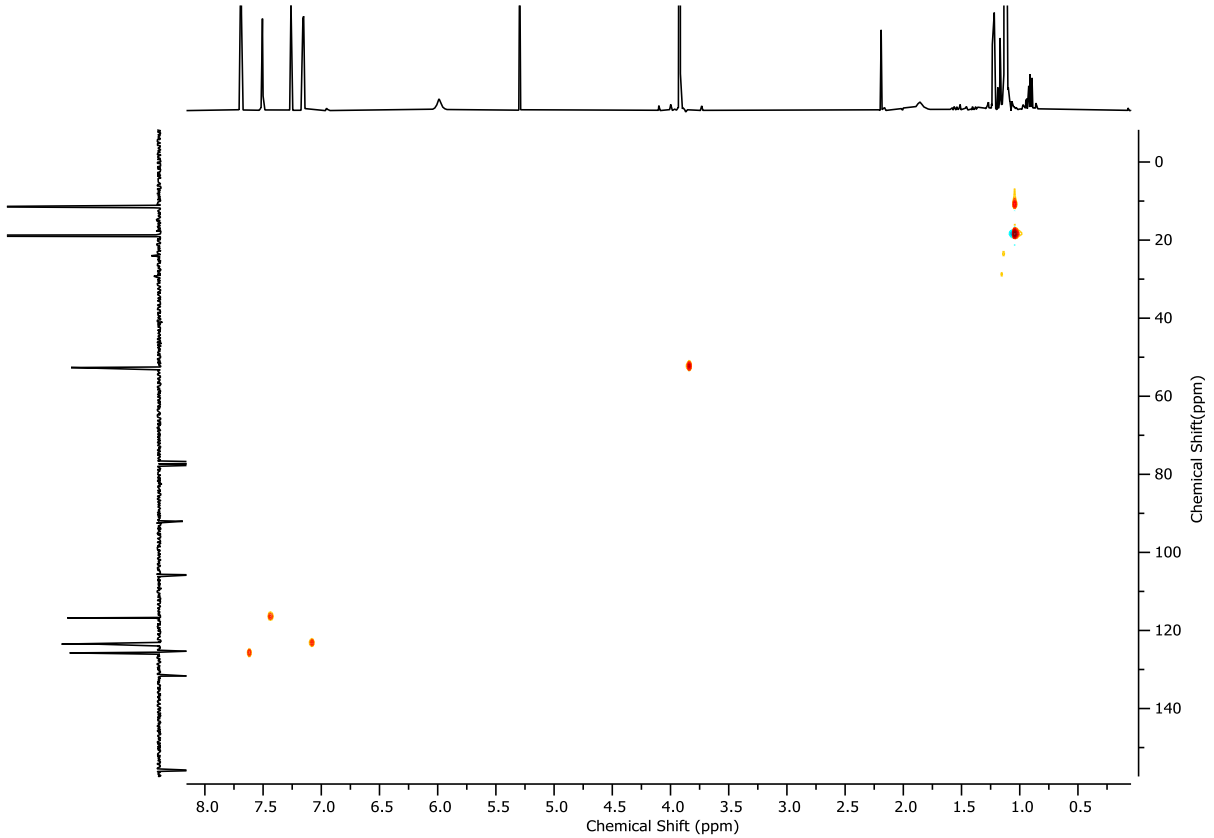

Figure 2.16 - HSQC NMR ($CDCl_3$, 400 MHz) of **S4**.

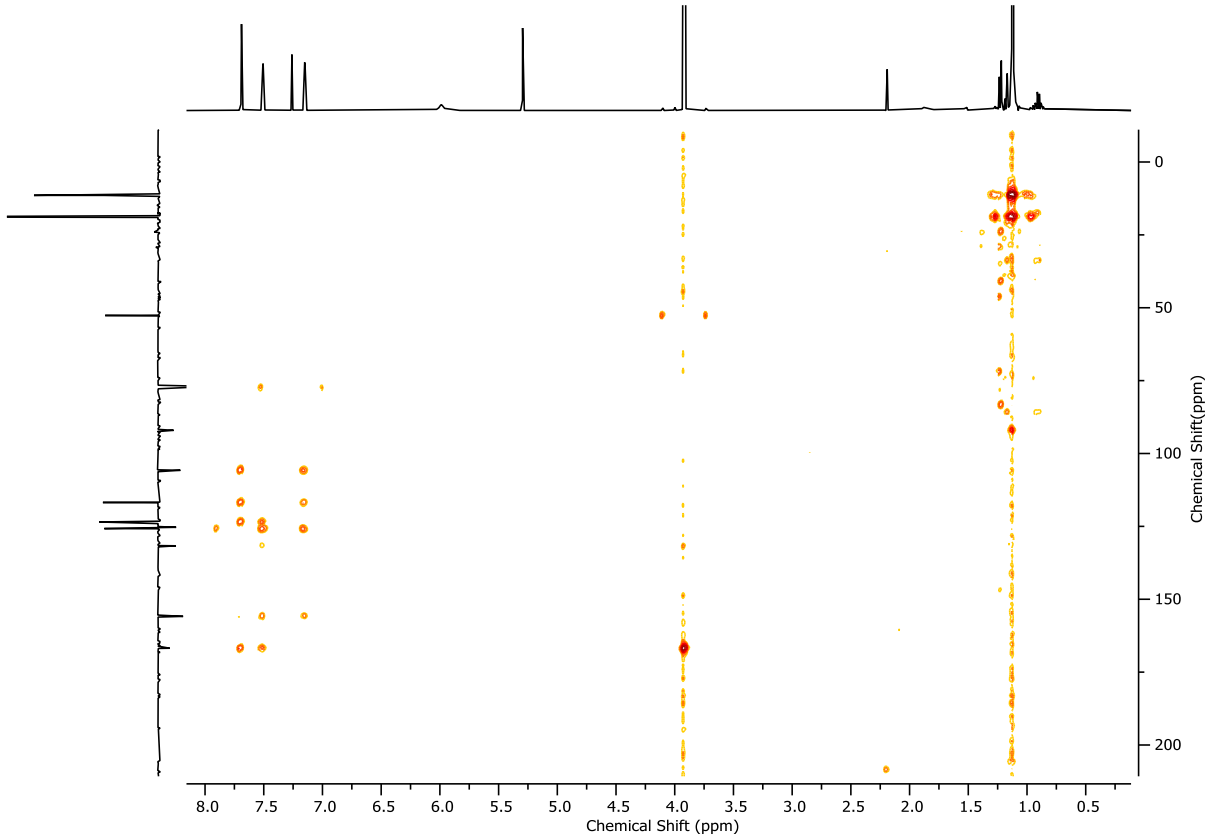

Figure 2.17 - HMBC NMR ($CDCl_3$, 400 MHz) of **S4**.

Compound S5

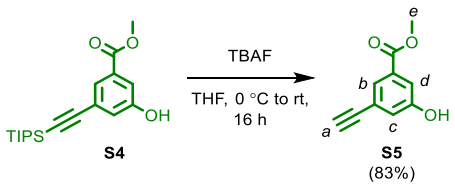

A solution of **S4** (703 mg, 2.11 mmol, 1.0 eq.) in THF (10.5 mL) was cooled to 0 °C, and a 1.0 M THF solution of TBAF (2.33 mL, 2.33 mmol, 1.1 eq.) was added dropwise. After warming to ambient temperature, the reaction mixture was stirred for 16 h before concentrating *in vacuo*. The crude material was dissolved in EtOAc (10 mL) and washed with H_2O (5 mL). The aqueous phase was extracted with EtOAc (2 x 5 mL), and the combined organics were washed with brine (5 mL), dried over $MgSO_4$, filtered and concentrated *in vacuo*. The residue was purified by column chromatography (SiO_2, petrol-EtOAc 0→20%) to yield **S5** (310 mg, 1.76 mmol, 83%) as a yellow solid.

δ_H ($CDCl_3$, 400 MHz) 7.71 (t, J = 1.4, 1H, H_b), 7.58 (dd, J = 2.5, 1.5, 1H, H_d), 7.18 (dd, J = 2.5, 1.4, 1H, H_c), 6.45 (s, 1H, H_{OH}), 3.92 (s, 3H, H_e), 3.10 (s, 1H, H_a); δ_C ($CDCl_3$, 101 MHz) 166.2, 156.8, 132.7, 125.0, 123.5, 123.0, 115.6, 52.8; HR-ESI-MS (-ve) m/z = 175.0403 $[M-H]^-$ (calc. m/z for $C_{10}H_7O_3$ 175.0401); Melting point 102-104 °C.

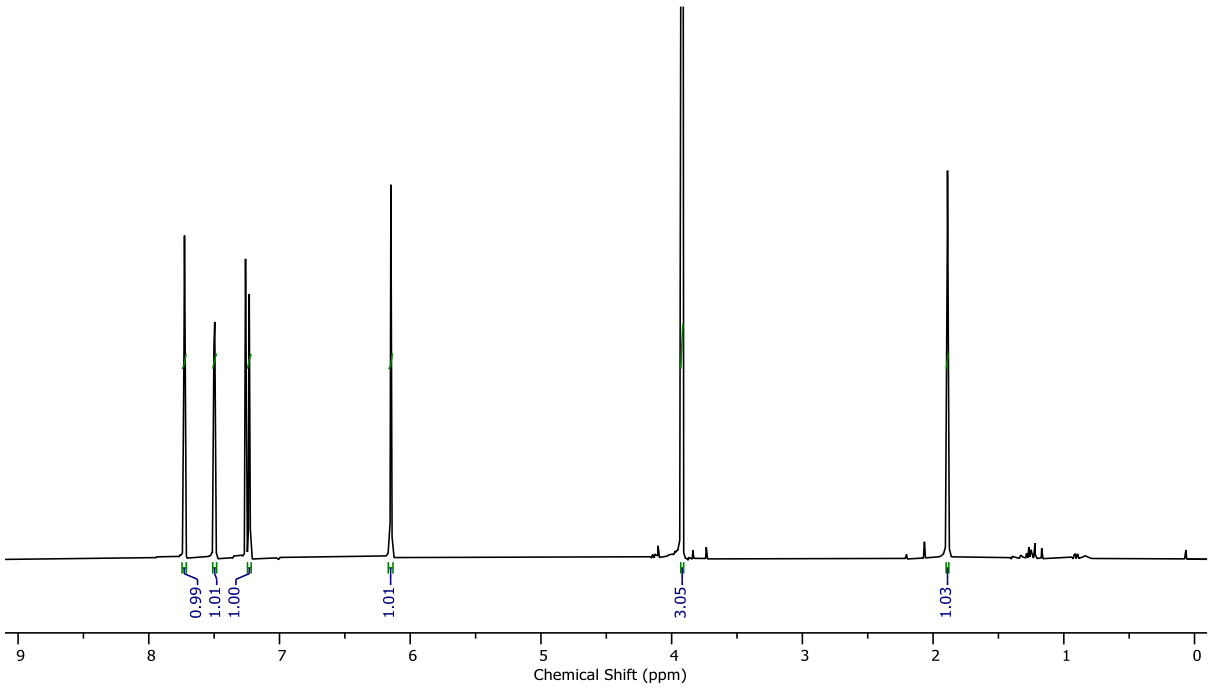

Figure 2.18 - ^{1}H NMR ($CDCl_3$, 400 MHz) of **S5**.

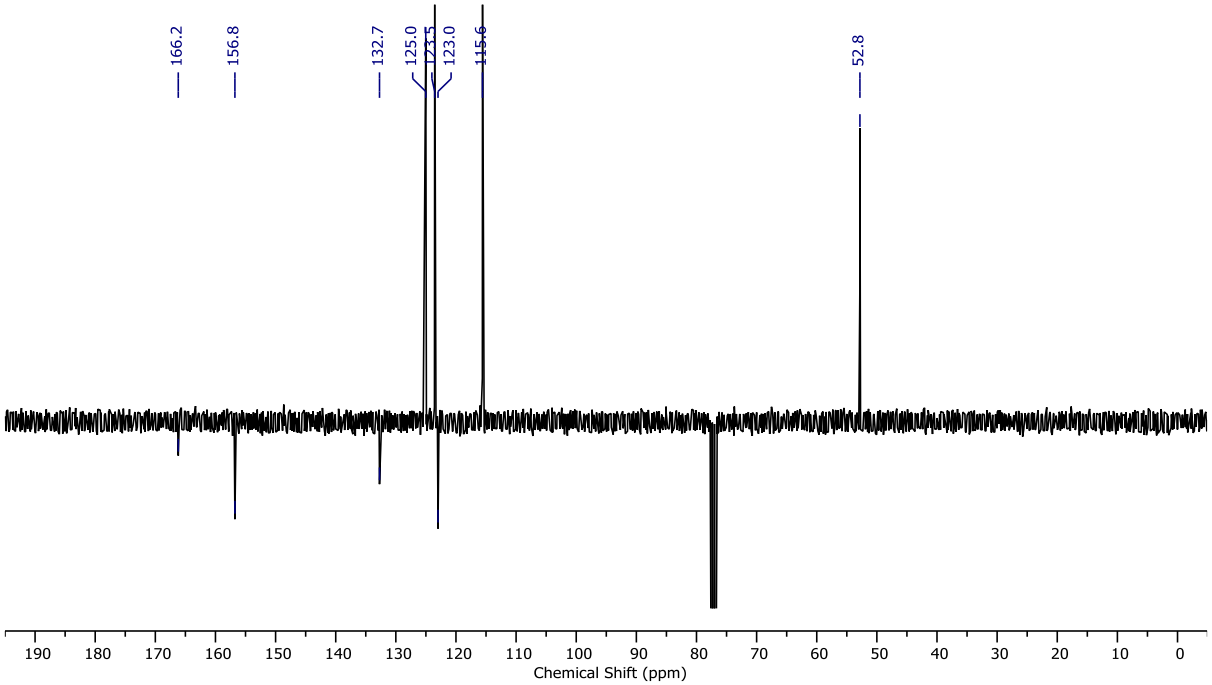

Figure 2.19 - JMOD NMR ($CDCl_3$, 101 MHz) of **S5**.

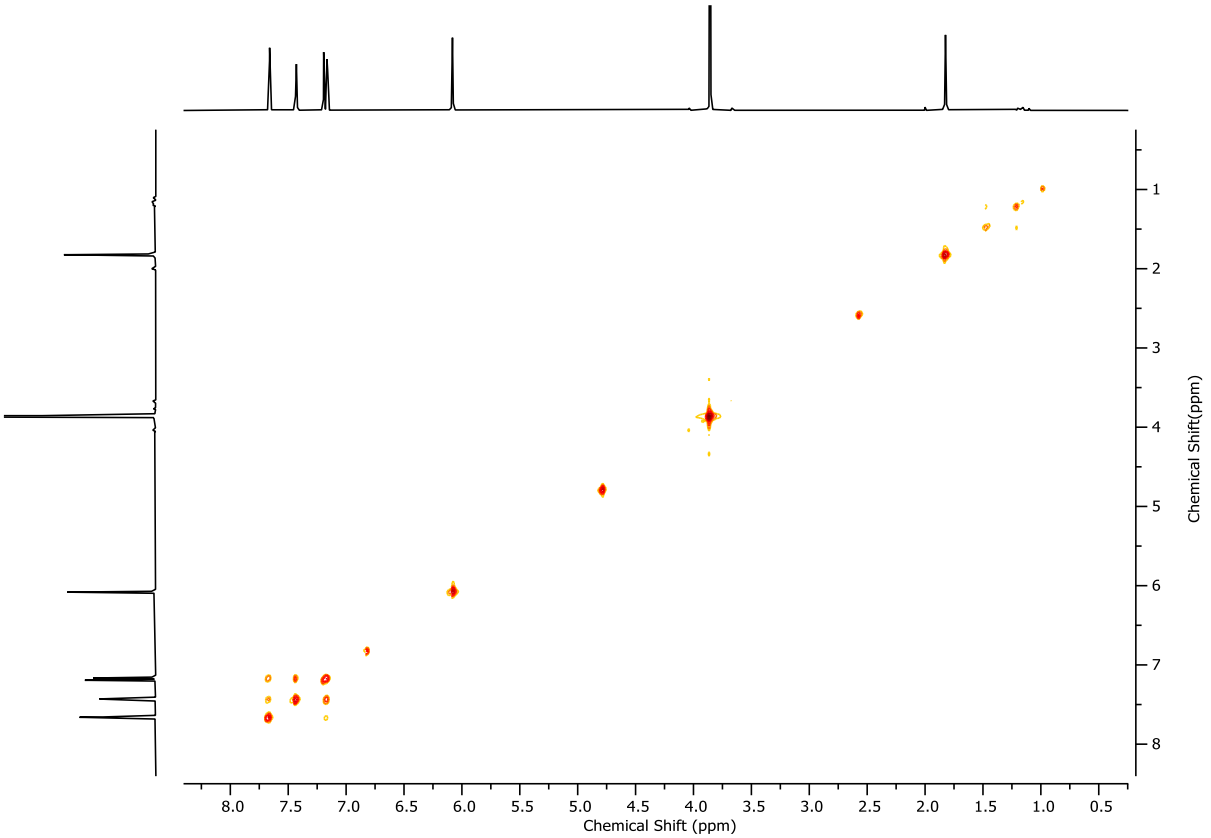

Figure 2.20 - ^{1}H COSY NMR ($CDCl_3$, 400 MHz) of **S5**.

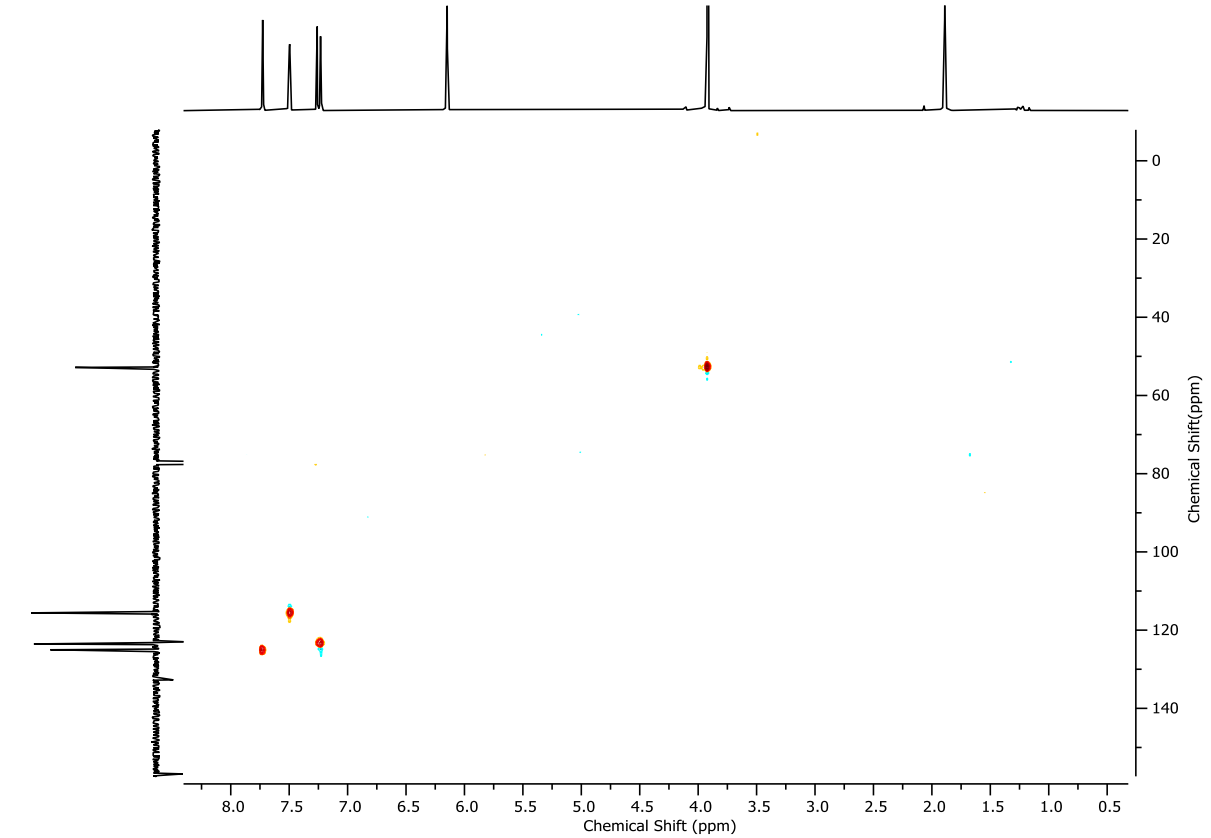

Figure 2.21 - HSQC NMR ($CDCl_3$, 400 MHz) of **S5**.

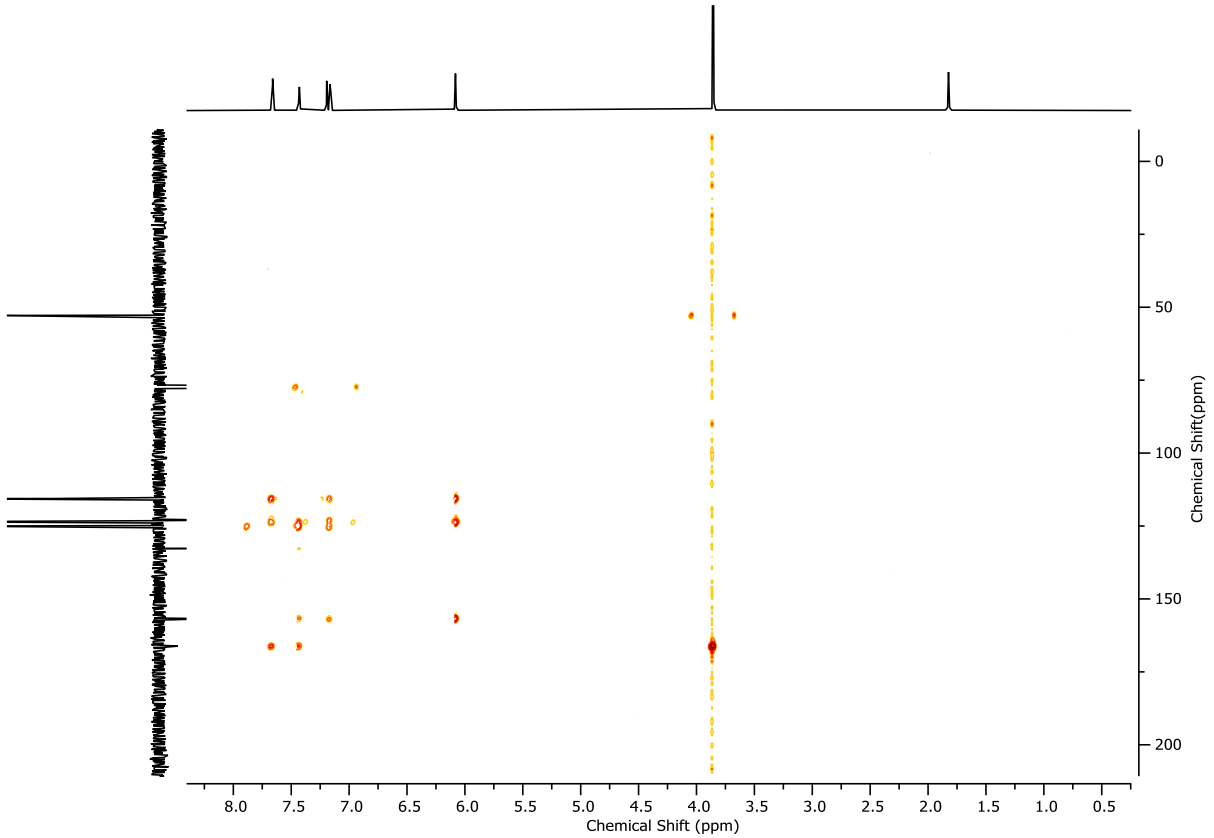

Figure 2.22 - HMBC NMR ($CDCl_3$, 400 MHz) of **S5**.

Compound S6

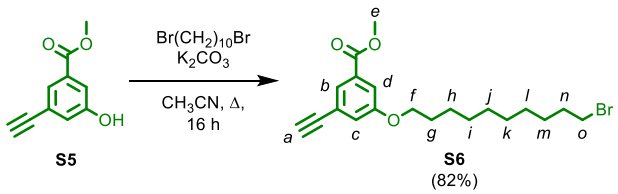

To a solution of **S5** (499 mg, 2.83 mmol, 1.0 eq.) in CH_3CN (28.3 mL) were added K_2CO_3 (1.17 g, 8.49 mmol, 3.0 eq.) and 1,10-dibromodecane (1.17 g, 14.2 mmol, 5.0 eq.), and the reaction mixture was stirred at reflux for 16 h. After cooling to ambient temperature, the reaction mixture was filtered through Celite®, washing with CH_2Cl_2, and concentrated *in vacuo*. The residue was purified by column chromatography (SiO_2, petrol-EtOAc 0→5%) to yield **S6** (960 mg, 2.43 mmol, 86%) as a white solid.

δ_H ($CDCl_3$, 400 MHz) 7.73 (t, J = 1.5, 1H, H_b), 7.53 (dd, J = 2.6, 1.5, 1H, H_d), 7.17 (dd, J = 2.6, 1.5, 1H, H_c), 3.97 (t, J = 6.5, 2H, H_f), 3.90 (s, 3H, H_e), 3.40 (t, J = 6.8, 2H, H_o), 3.08 (s, 1H, H_a), 1.90 – 1.71 (m, 4H, H_g, H_n), 1.49 – 1.26 (m, 12H, H_h, H_i, H_j, H_k, H_l, H_m); δ_C ($CDCl_3$, 101 MHz) 166.4, 159.1, 131.8, 125.7, 123.5, 122.7, 116.1, 82.8, 77.9, 68.6, 52.5, 34.2, 33.0, 29.6, 29.5, 29.4, 29.2, 28.9, 28.3, 26.1; HR-ESI-MS (+ve) m/z = 395.1211 $[M+H]^+$ (calc. m/z for $C_{20}H_{28}BrO_3$ 395.1216); Melting point 65-67 °C.

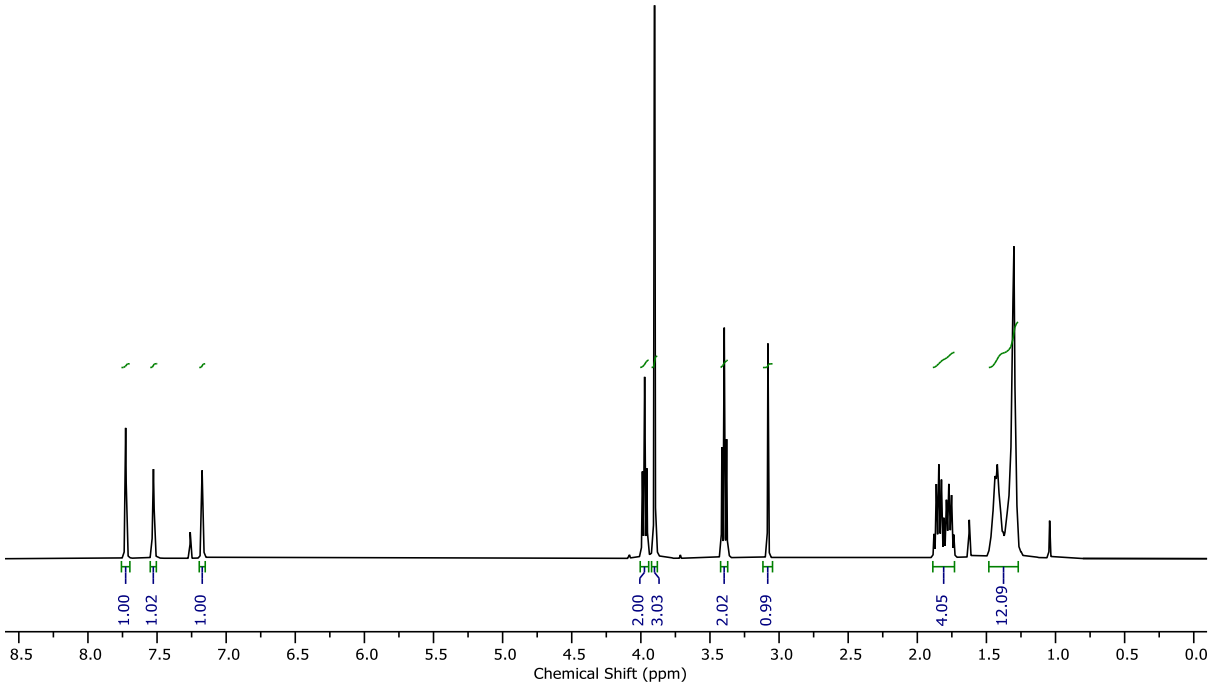

Figure 2.23 - ^{1}H NMR ($CDCl_3$, 400 MHz) of **S6**.

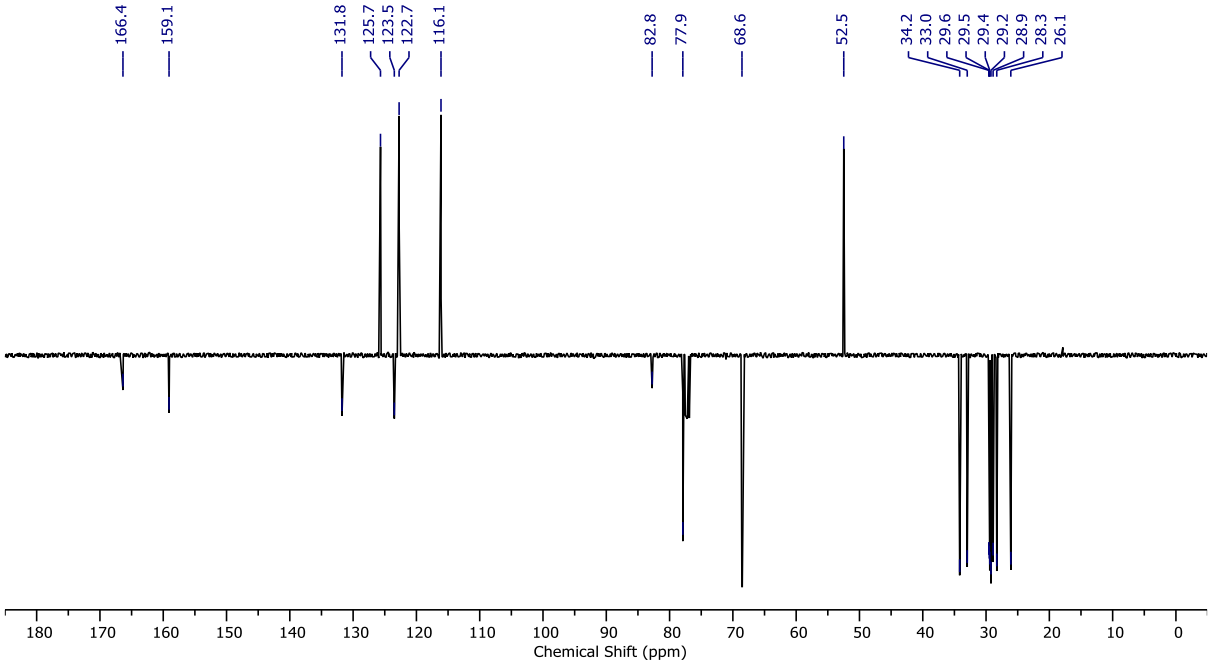

Figure 2.24 - JMOD NMR ($CDCl_3$, 101 MHz) of **S6**.

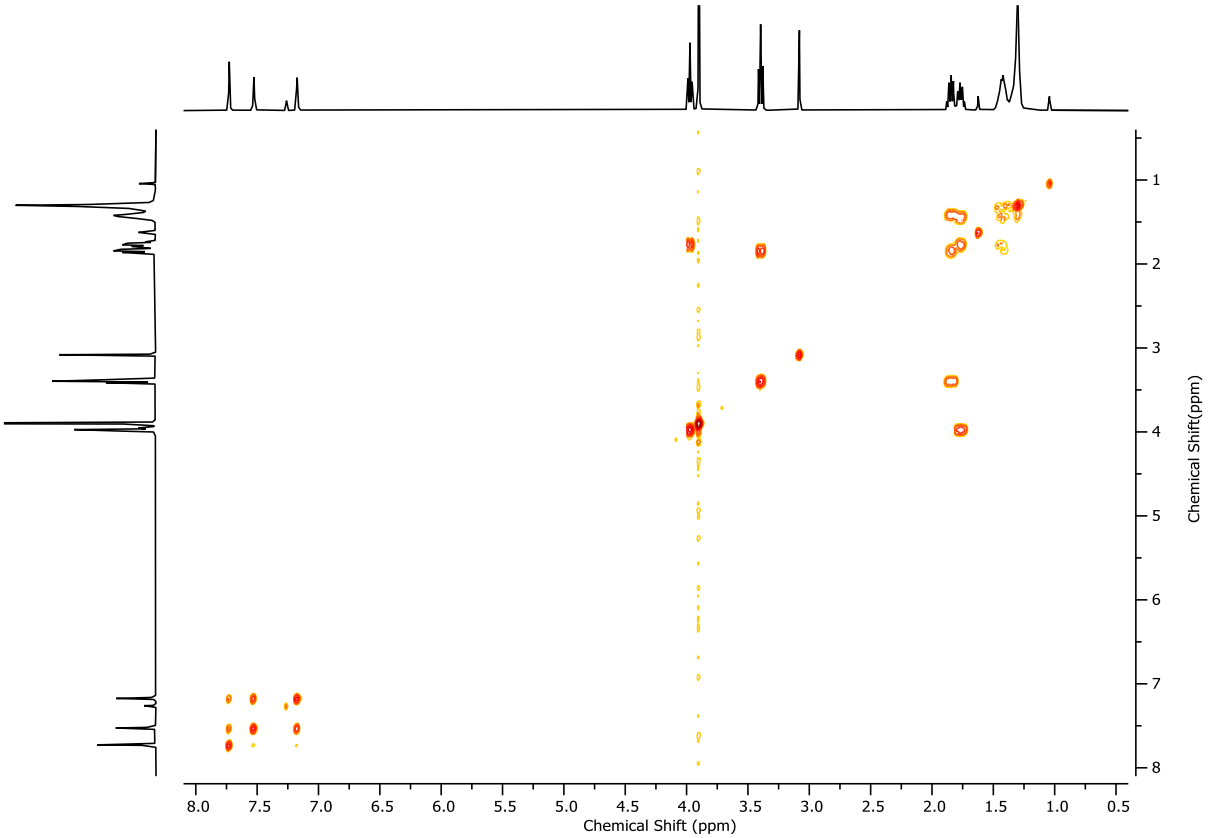

Figure 2.25 - ^{1}H COSY NMR ($CDCl_3$, 400 MHz) of **S6**.

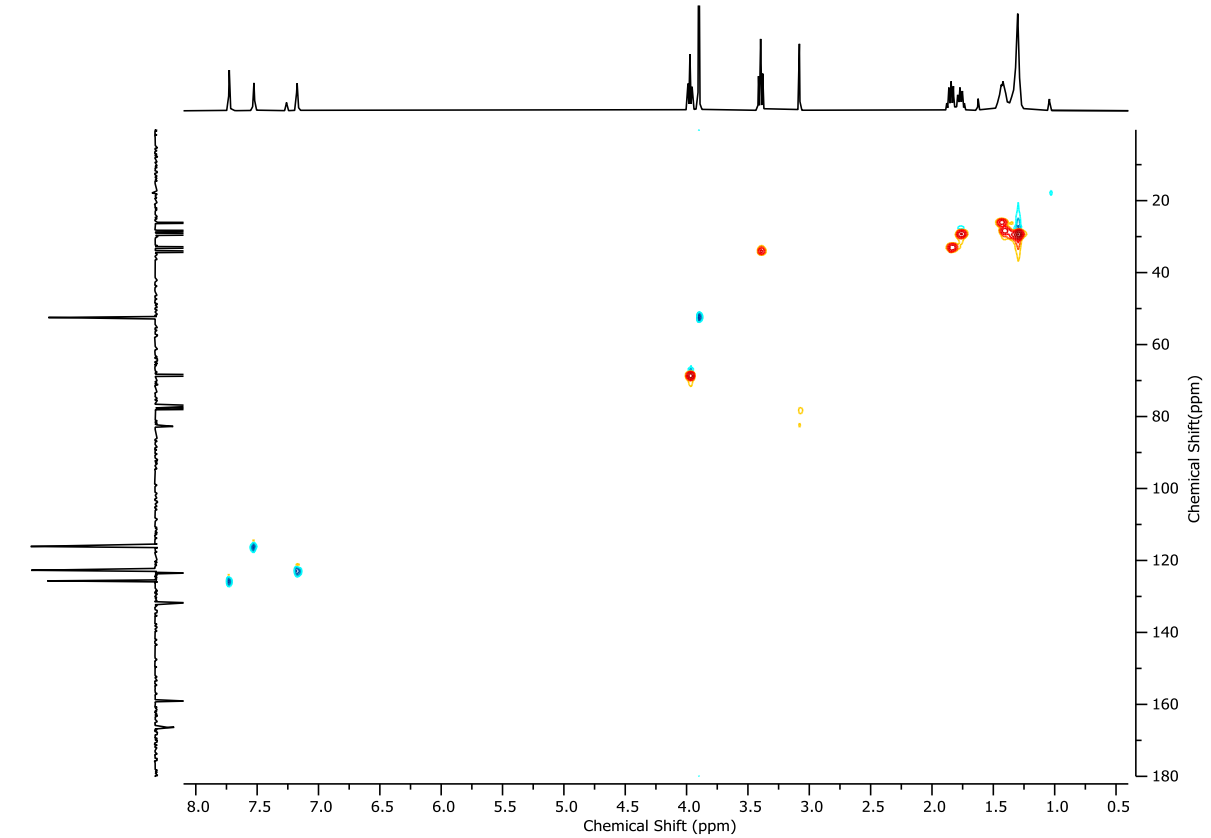

Figure 2.26 - HSQC NMR ($CDCl_3$, 400 MHz) of **S6**.

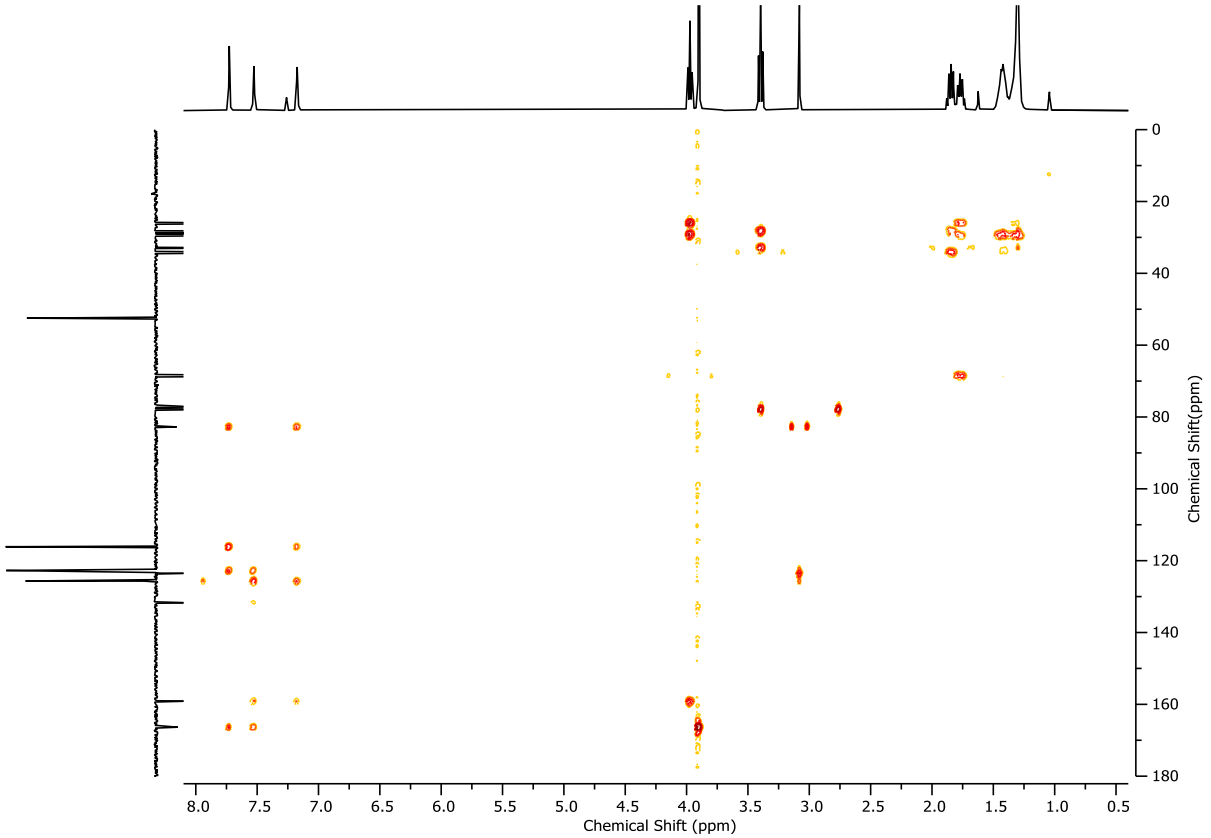

Figure 2.27 - HMBC NMR ($CDCl_3$, 400 MHz) of **S6**.

Compound (*R*)-S7

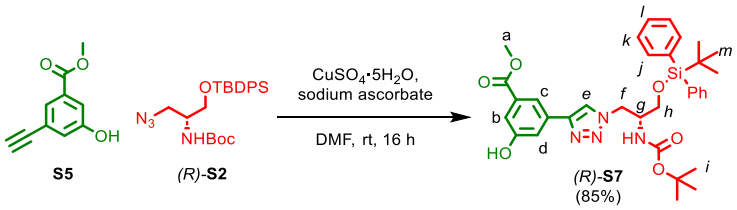

To a solution of (*R*)-**S1** (640.0 mg, 1.41 mmol, 1.0 eq.), alkyne **S5** (298.8 mg, 1.70 mmol, 1.2 eq.) and sodium ascorbate (336.4 mg, 1.70 mmol, 1.2 eq.) in DMF (7.0 mL) was added copper(II) sulfate pentahydrate (353.4 mg, 1.41 mmol, 1.0 eq.) .), and the reaction mixture was stirred at ambient temperature for 16 h. The reaction mixture was diluted with EtOAc (20 mL) and washed with a saturated EDTA/NH_3 solution (25 mL). The aqueous layer was extracted with EtOAc (3 x 15 mL). The combined organic fractions were washed with 5% LiCl (3 x 15 mL), and brine (15 mL) then dried over $MgSO_4$, filtered, and concentrated *in vacuo*. The residue was purified by column chromatography (SiO_2, petrol-EtOAc 0→20%) to yield (*R*)-**S7** (755.2 mg, 1.20 mmol, 85%) as a white foam.

δ_H ($CDCl_3$, 400 MHz) 8.73 (s, 1H, H_{OH}), 7.95 – 7.87 (m, 2H, H_d, H_e), 7.69 (s, 1H, H_c), 7.66 – 7.60 (m, 4H, H_j), 7.59 – 7.55 (m, 1H, H_b), 7.44 – 7.33 (m, 6H, H_k, H_l), 5.26 (br s, 1H, H_{NHBoc}), 4.73 – 4.55 (m, 2H, H_f), 4.28 – 4.14 (m, 1H, H_g), 3.86 (s, 3H, H_a), 3.80 – 3.63 (m, 2H, H_h), 1.39 (s, 9H, H_i), 1.10 (s, 9H, H_m); δ_C ($CDCl_3$, 101 MHz) 167.0, 157.5, 155.8, 147.1, 135.6, 135.6, 132.8, 132.5, 132.0, 131.8, 130.2, 130.2, 128.1, 128.1, 121.6, 118.6, 117.4, 116.6, 80.6, 63.0, 52.3, 52.2, 50.9, 28.4, 27.0, 19.4; HR-ESI-MS (+ve) m/z = 631.2953 $[M+H]^+$ (calc. m/z for $C_{34}H_{43}N_4O_6Si$ 631.2946).

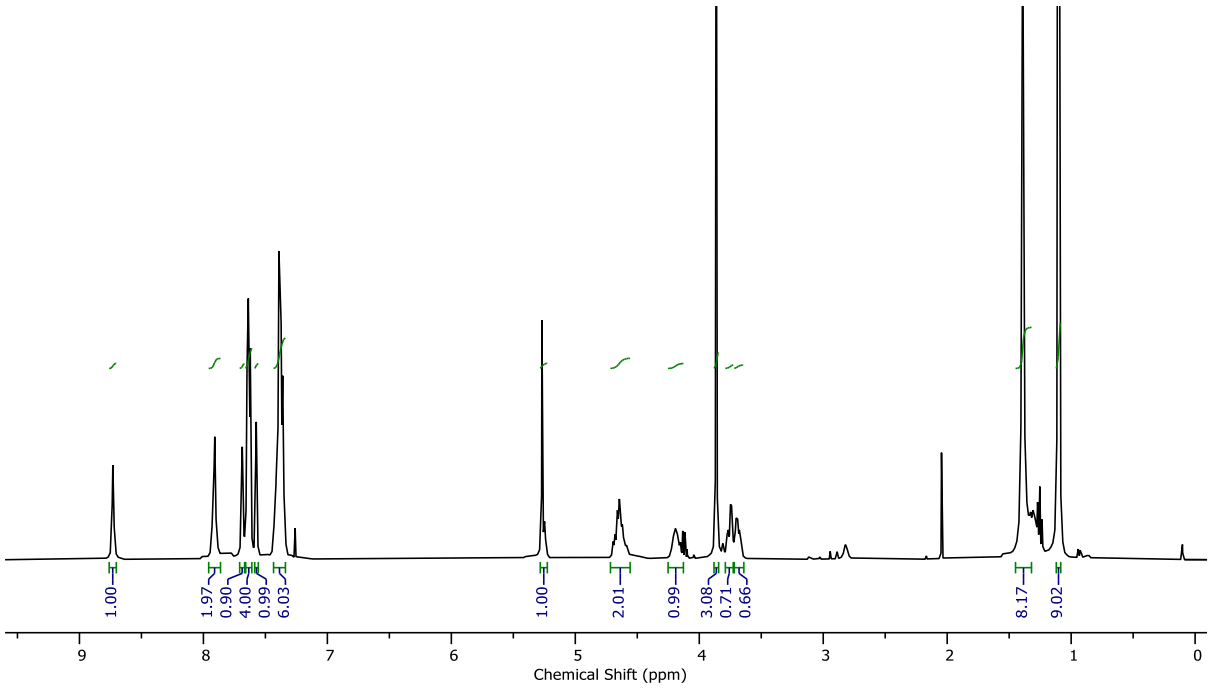

Figure 2.28 - ^1H NMR ($CDCl_3$, 400 MHz) of (*R*)-**S7**.

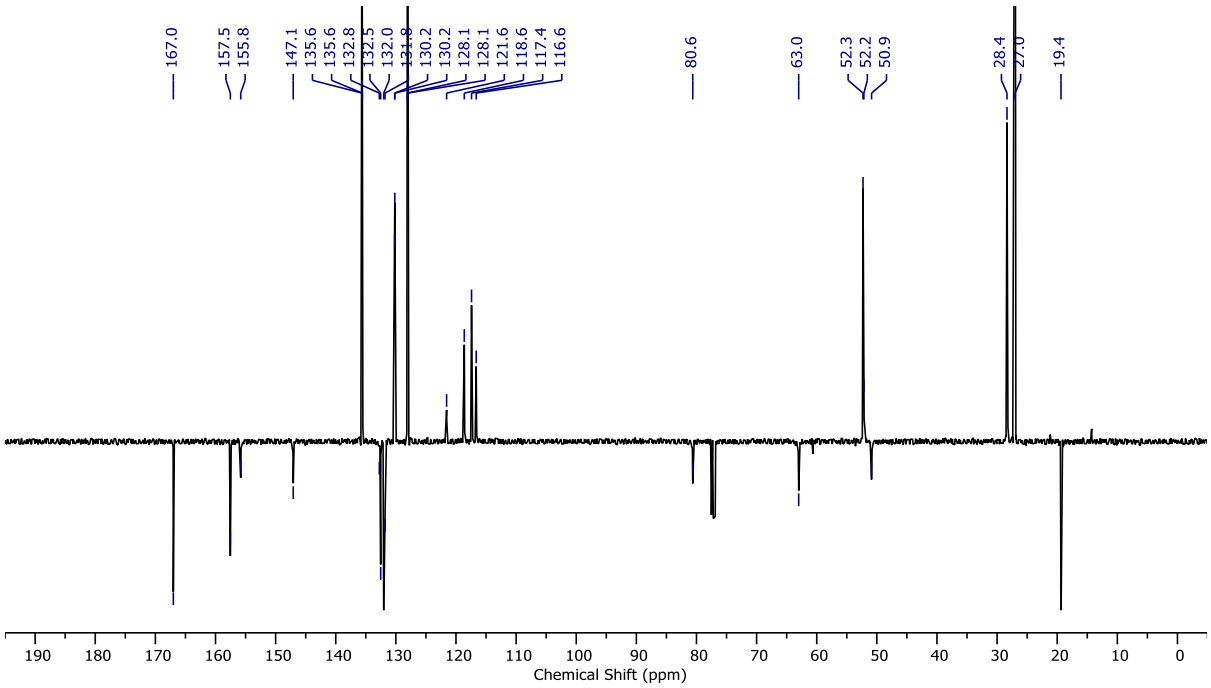

Figure 2.29 - JMOD NMR ($CDCl_3$, 101 MHz) (*R*)-**S7**

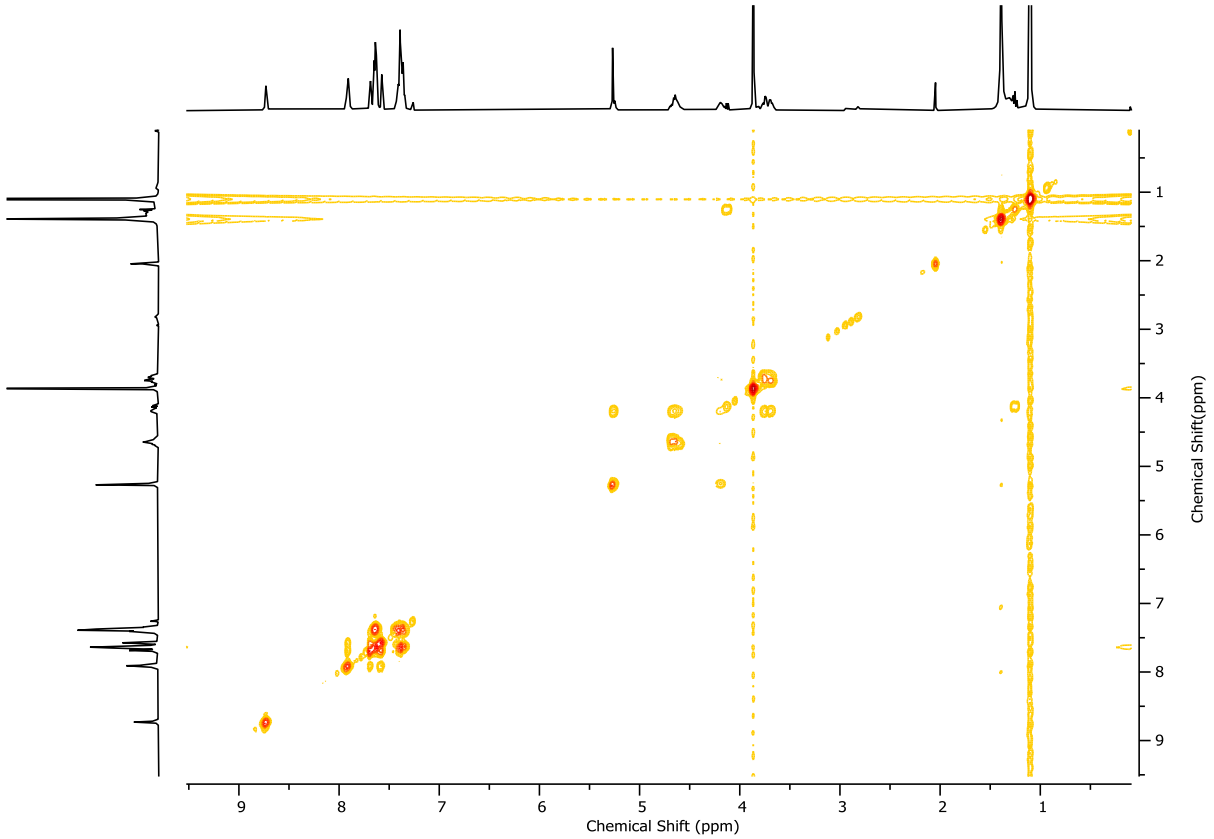

Figure 2.30 - ^{1}H COSY NMR ($CDCl_3$, 400 MHz) (*R*)-**S7**.

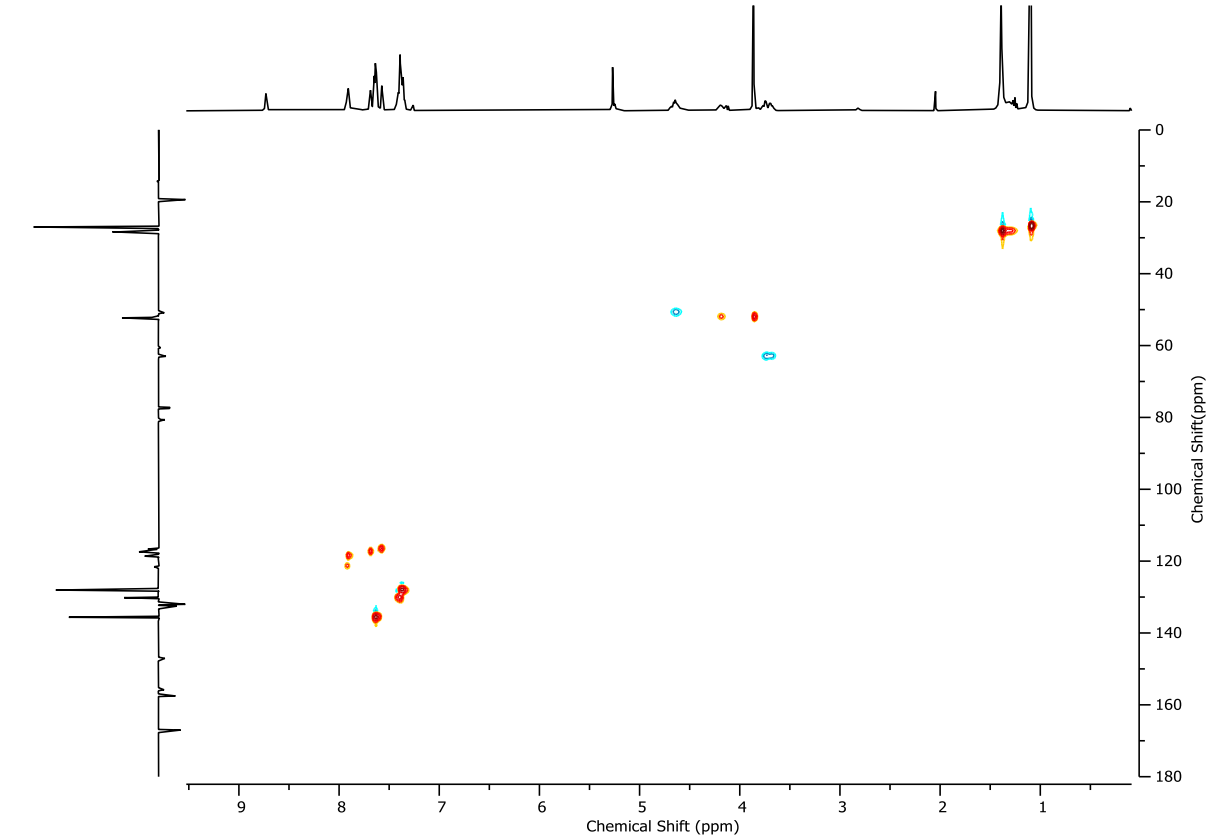

Figure 2.31 - HSQC NMR ($CDCl_3$, 400 MHz) of (*R*)-**S7**.

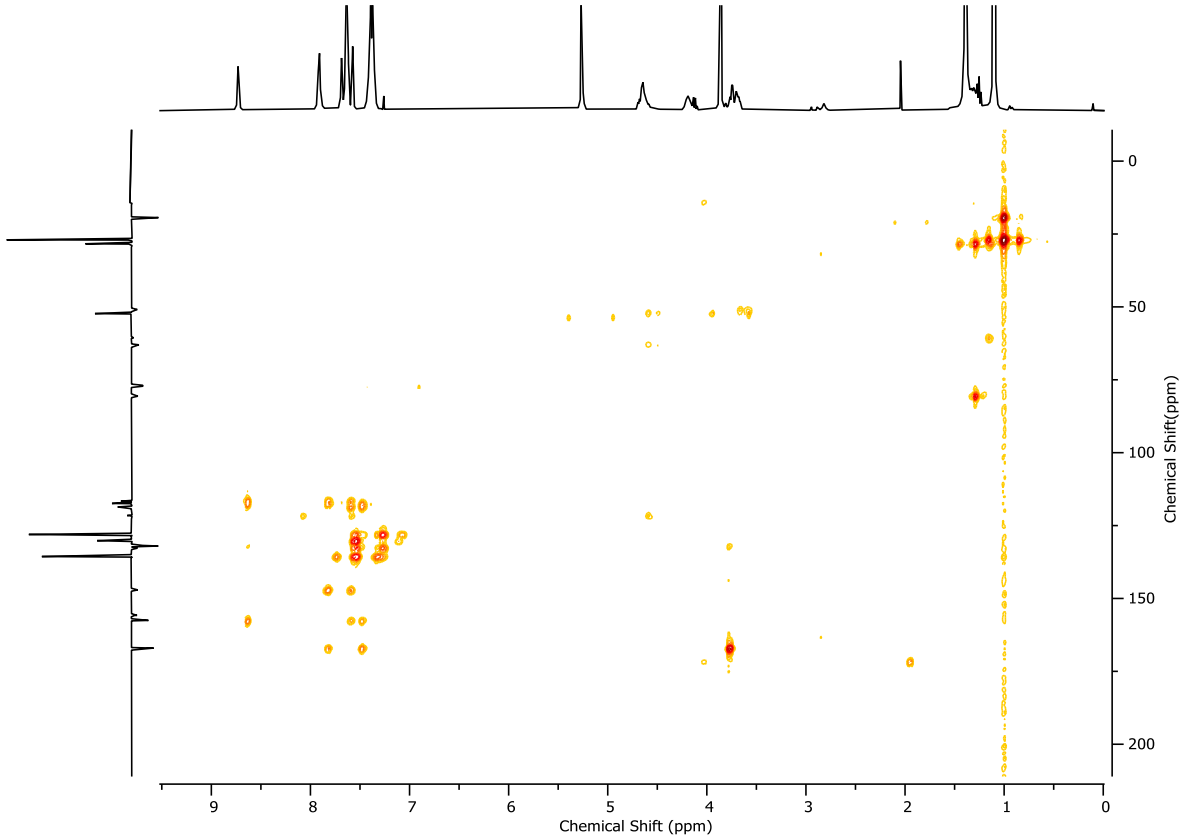

Figure 2.32 - HMBC NMR ($CDCl_3$, 400 MHz) of (*R*)-**S7**.

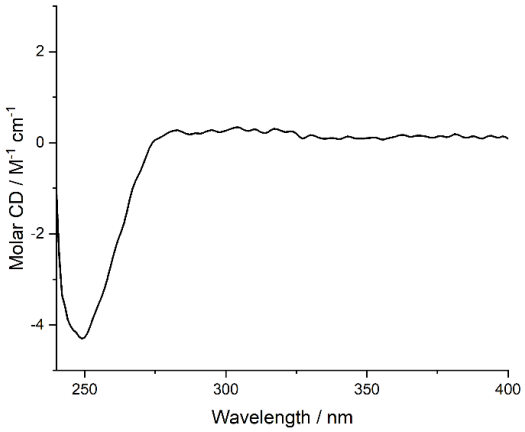

Figure 2.33 - Circular Dichroism Spectra of (*R*)-**S7** (16 µM) at 293 K in $CHCl_3$.

Compound (*R*)-S8

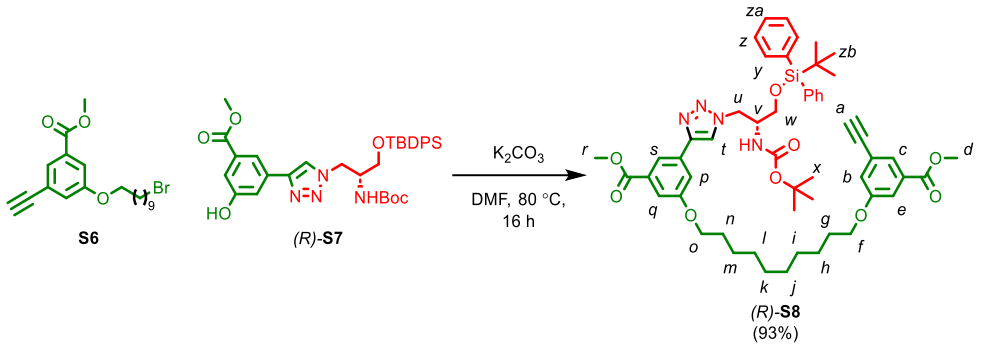

(*R*)-**S7** (425 mg, 0.67 mmol, 1.0 eq.), **S6** (399 mg, 1.01 mmol, 1.5 eq.), and K_2CO_3 (276 mg, 2.01 mmol, 3.0 eq.) were suspended in DMF (1.34 mL), and heated at 80 °C for 2 h. After cooling to ambient temperature, the crude mixture was diluted with EtOAc (10 mL) and washed with H_2O (5 mL), 5% LiCl (2 x 5 mL), and brine (5 mL). All aqueous phases were extracted with EtOAc (5 mL), and the combined organics were dried over $MgSO_4$, filtered, and concentrated *in vacuo*. The residue was purified by column chromatography (SiO_2, petrol-EtOAc 0→20%) to yield (*R*)-**S8** (591.1 mg, 0.63 mmol, 93%) as a yellow oil.

δ_H ($CDCl_3$, 400 MHz) 7.93 (t, *J* = 1.5, 1H, H_s), 7.79 – 7.76 (m, 1H, H_t), 7.73 (t, *J* = 1.4, 1H, H_c), 7.66 – 7.59 (m, 6H, H_p, H_y), 7.55 – 7.52 (m, 2H, H_e, H_q), 7.46 – 7.33 (m, 6H, H_z, H_{za}), 7.18 (dd, *J* = 2.6, 1.4, 1H, H_b), 5.00 (d, *J* = 8.6, 1H, H_{NHBoc}), 4.62 (d, *J* = 5.8, 2H, H_u), 4.23 – 4.12 (m, 1H, H_v), 4.06 (t, *J* = 6.5, 2H, H_o), 3.98 (t, *J* = 6.5, 2H, H_f), 3.93 (s, 3H, H_r), 3.90 (s, 3H, H_d), 3.72 (dd, *J* = 10.8, 4.0, 1H, H_w), 3.61 (m, 1H, H_w), 3.08 (s, 1H, H_a), 1.87 – 1.74 (m, 4H, H_g, H_n), 1.53 – 1.30 (m, 21H, H_h, H_i, H_j, H_k, H_l, H_m, H_x), 1.11 (s, 9H, H_{zb}); δ_C ($CDCl_3$, 101 MHz) 166.9, 166.4, 159.8, 159.1, 155.4, 147.0, 135.7, 135.6, 132.6, 132.2, 132.0, 131.8, 130.3, 130.3, 128.1, 125.7, 123.5, 122.8, 121.3, 119.2, 116.4, 116.2, 115.3, 82.8, 77.9, 68.6, 63.0, 52.5, 52.4, 52.0, 50.8, 29.6, 29.6, 29.5, 29.5, 29.4, 29.3, 28.4, 27.1, 26.2, 26.1, 19.5; HR-ESI-MS (+ve) m/z = 945.4830 $[M+H]^+$ (calc. m/z for $C_{54}H_{69}N_4O_9Si$ 945.4828).

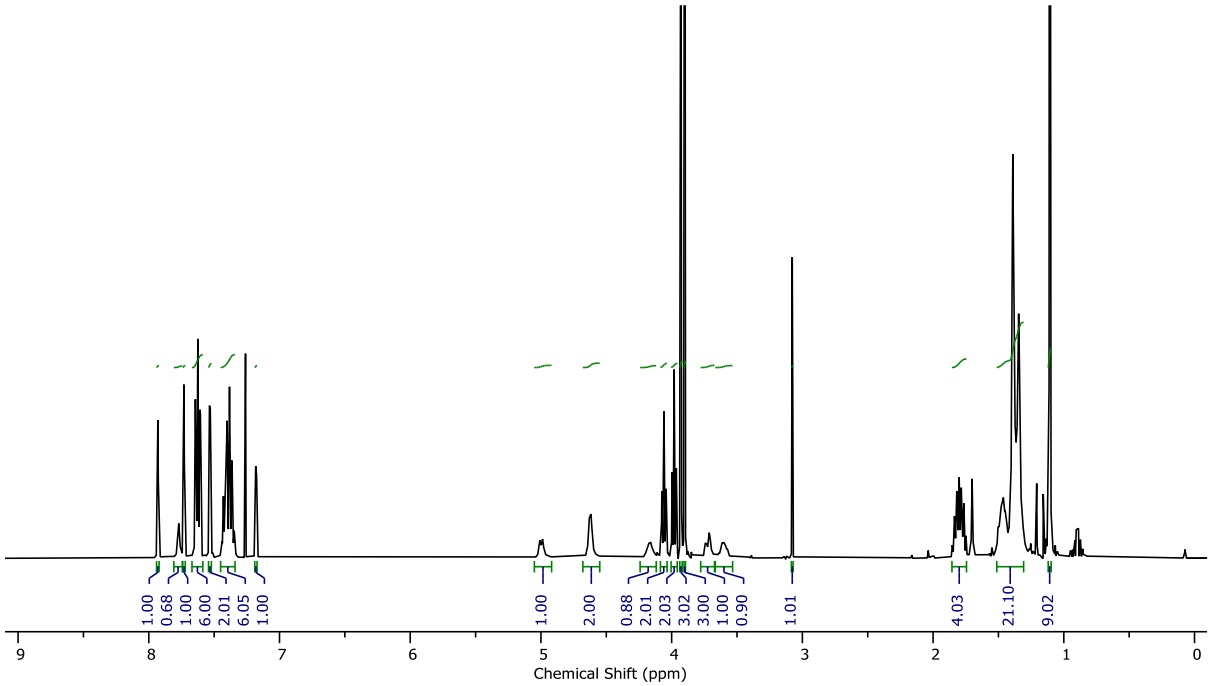

Figure 2.34 - ^{1}H NMR ($CDCl_3$, 400 MHz) of (*R*)-**S8**.

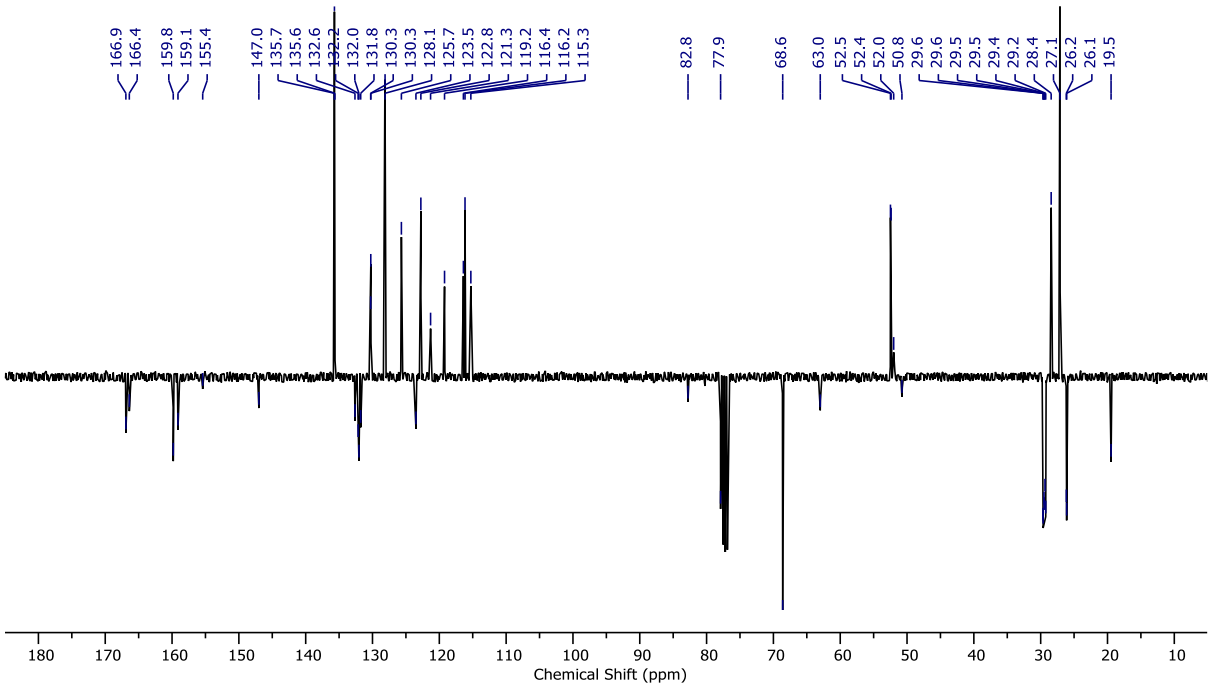

Figure 2.35 - JMOD NMR ($CDCl_3$, 101 MHz) (*R*)-**S8**.

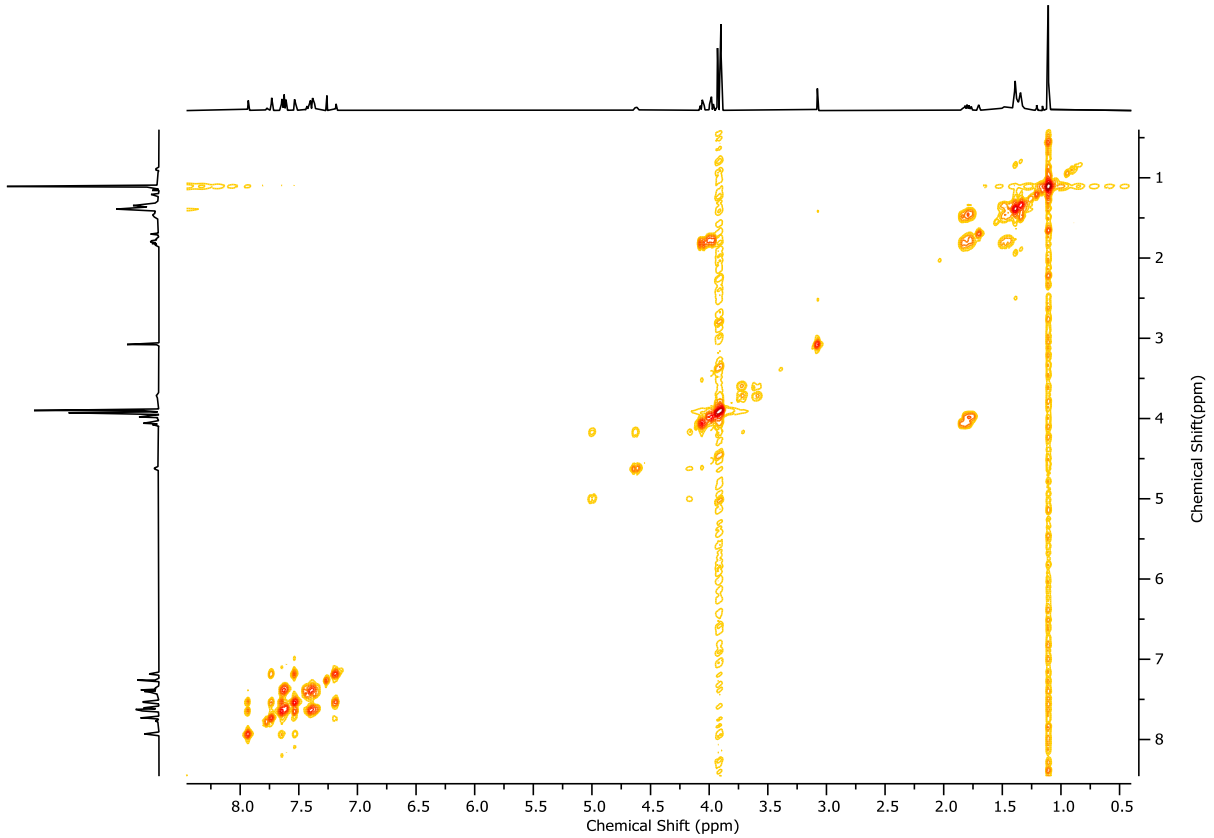

Figure 2.36 - ^{1}H COSY NMR ($CDCl_3$, 400 MHz) (*R*)-**S8**.

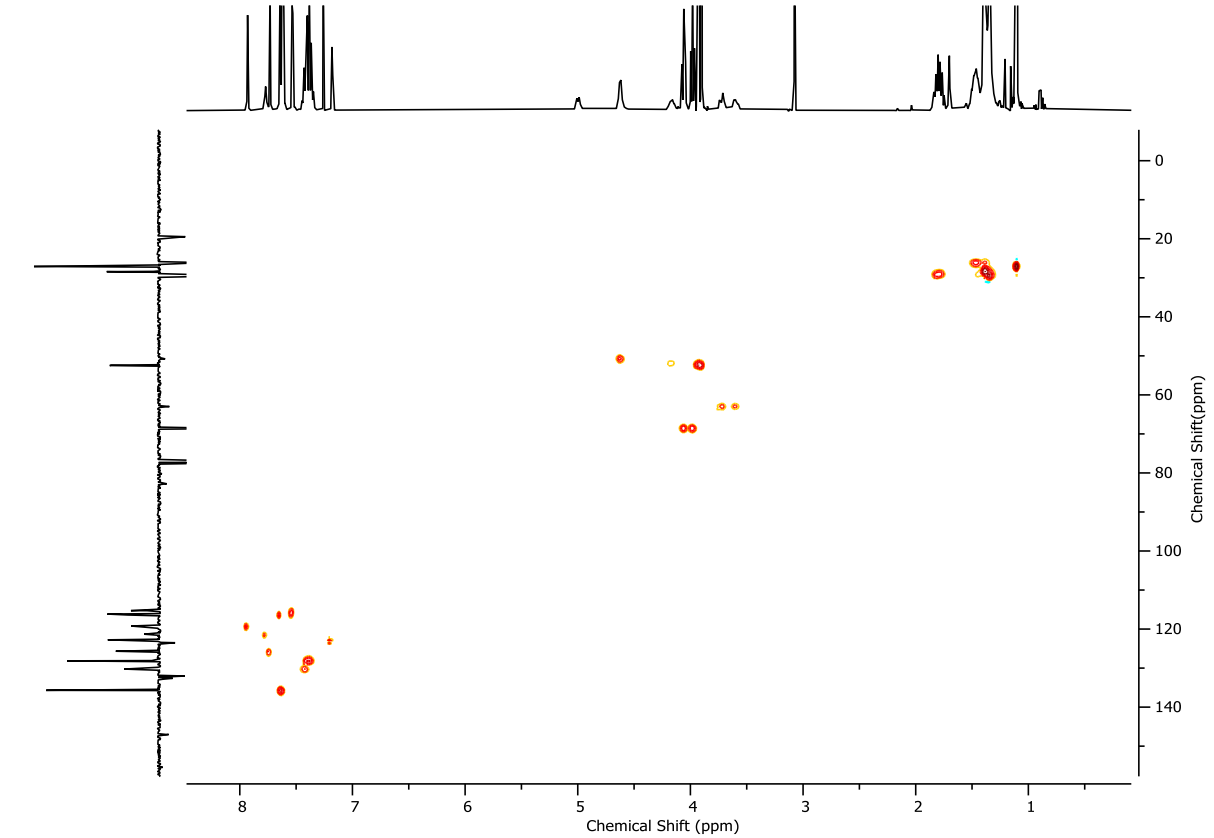

Figure 2.37 - HSQC NMR ($CDCl_3$, 400 MHz) of (*R*)-**S8**.

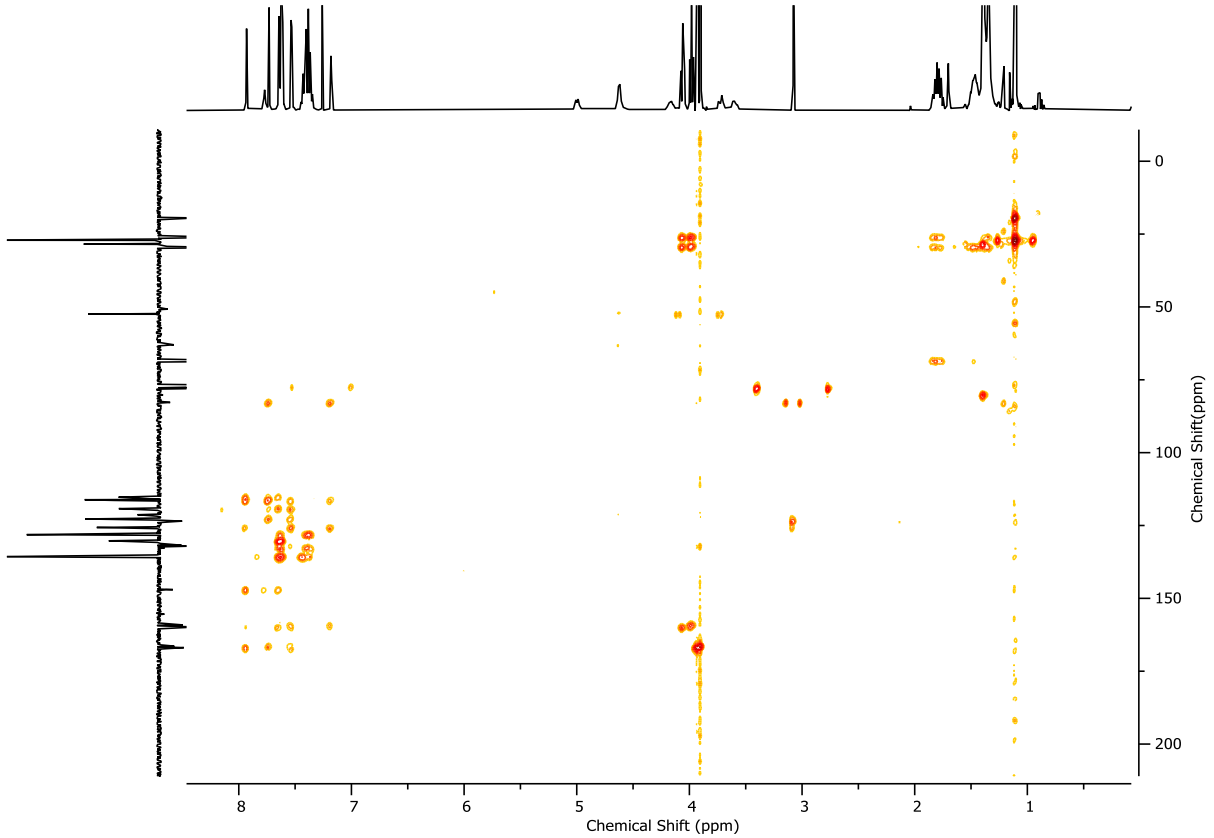

Figure 2.38 - HMBC NMR ($CDCl_3$, 400 MHz) of (*R*)-**S8**.

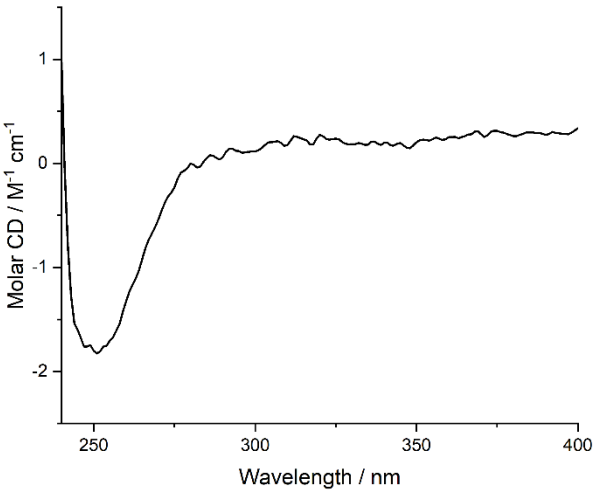

Figure 2.39 - Circular Dichroism Spectra of (*R*)-**S8** (20 µM) at 293 K in $CHCl_3$.

Compound (*R*)-S9

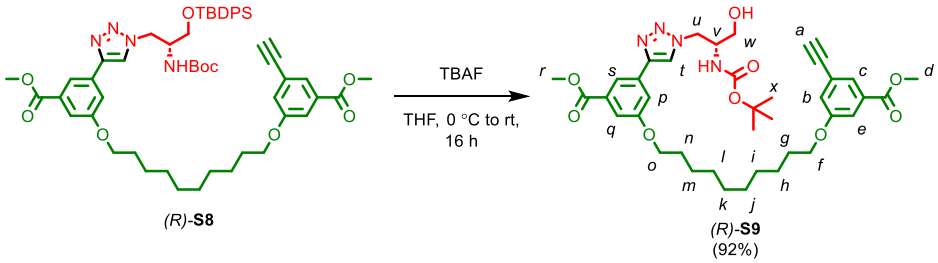

To a stirred solution of (*R*)-**S8** (591 mg, 0.63 mmol, 1.0 eq.) in THF (6.3 mL) at 0 °C was added dropwise a 1.0 M solution of TBAF in THF (690 µL, 0.69 mmol, 1.1 eq.), and the mixture was allowed to warm to ambient temperature. After 16 h, the crude mixture was concentrated *in vacuo*, the resulting residue dissolved in EtOAc (20 mL), and washed with H_2O (10 mL), and brine (10 mL). The combined aqueous layers were extracted with EtOAc (10 mL), and the combined organics were dried over $MgSO_4$, filtered and concentrated *in vacuo*. The residue was purified by column chromatography (SiO_2, CH_2Cl_2- CH_3CN 0→40%) to yield (*R*)-**S9** (409 mg, 0.579 mmol, 92%) as a white foam.

δ_H ($CDCl_3$, 400 MHz) 7.97 – 7.92 (m, 2H, H_s, H_t), 7.72 (t, *J* = 1.4, 1H, H_c), 7.65 (t, *J* = 2.0, 1H, H_p), 7.53 – 7.51 (m, 2H, H_q, H_e), 7.17 (dd, *J* = 2.6, 1.4, 1H, H_b), 5.28 (d, *J* = 8.4, 1H, H_{NHBoc}), 4.73 – 4.59 (m, 2H, H_u), 4.12 – 4.01 (m, 3H, H_v, H_o), 3.97 (t, *J* = 6.5, 2H, H_f), 3.92 (s, 3H, H_r), 3.90 (s, 3H, H_d), 3.73 (dd, *J* = 11.5, 3.9, 1H, H_w), 3.64 – 3.55 (m, 1H, H_w), 3.08 (s, 1H, H_a), 1.85 – 1.73 (m, 4H, H_g, H_n), 1.51 – 1.30 (m, 21H, H_h, H_i, H_j, H_k, H_l, H_m, H_x); δ_C ($CDCl_3$, 101 MHz) 166.9, 166.4, 159.9, 159.1, 147.3, 132.1, 131.8, 131.8, 125.7, 123.5, 122.8, 121.5, 119.2, 116.4, 116.2, 115.3, 82.8, 80.8, 77.9, 68.6, 52.5, 52.4, 51.4, 50.7, 50.2, 29.6, 29.6, 29.5, 29.5, 29.3, 29.2, 28.4, 26.2, 26.1; HR-ESI-MS (+ve) m/z = 707.3651 (calc. m/z for $C_{38}H_{51}N_4O_9$ 707.3651).

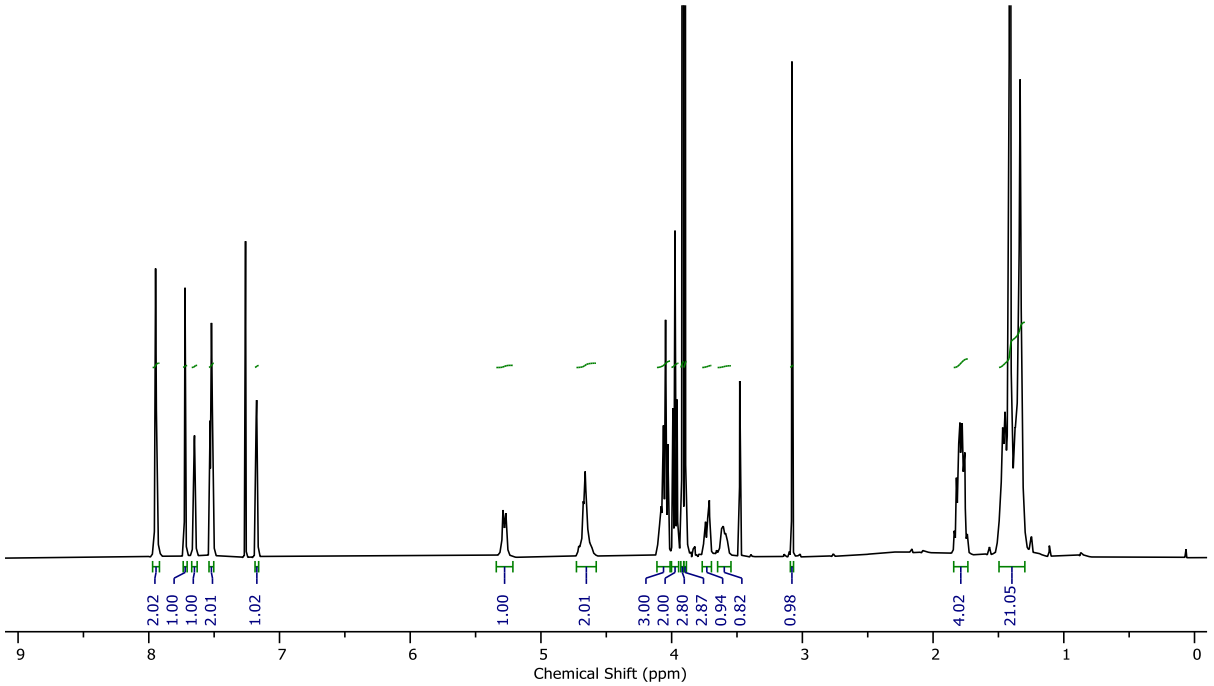

Figure 2.40 - ^{1}H NMR ($CDCl_3$, 400 MHz) of (*R*)-**S9**.

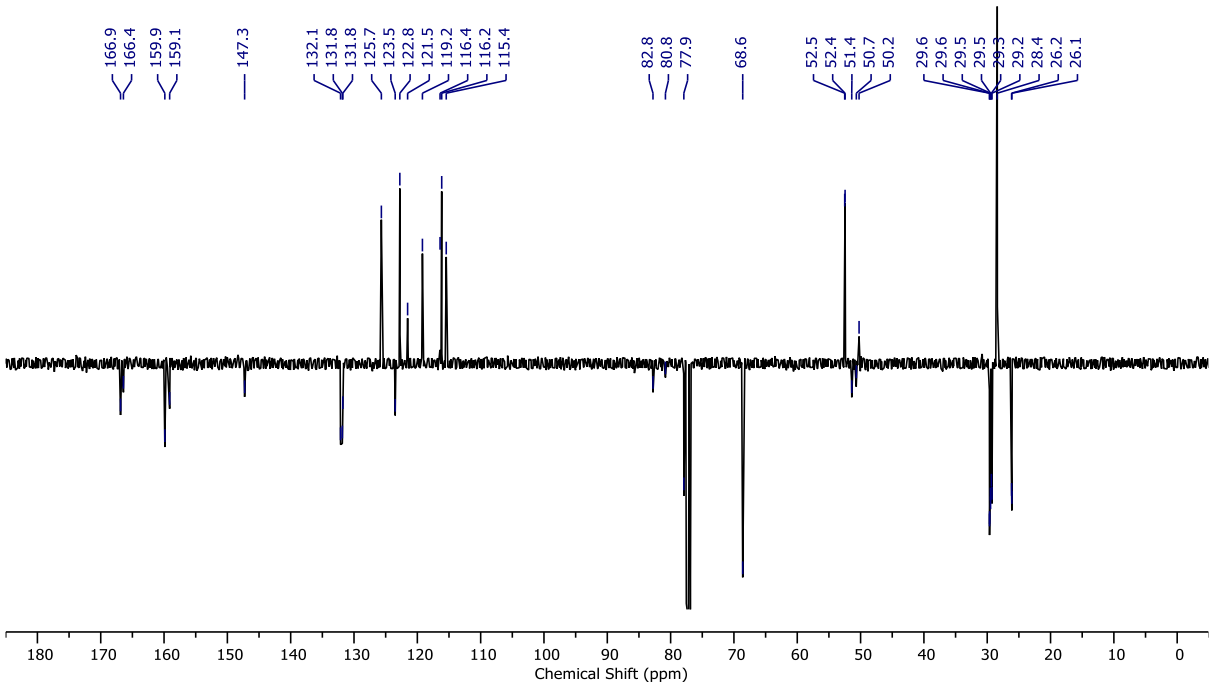

Figure 2.41 - JMOD NMR ($CDCl_3$, 101 MHz) (*R*)-**S9**.

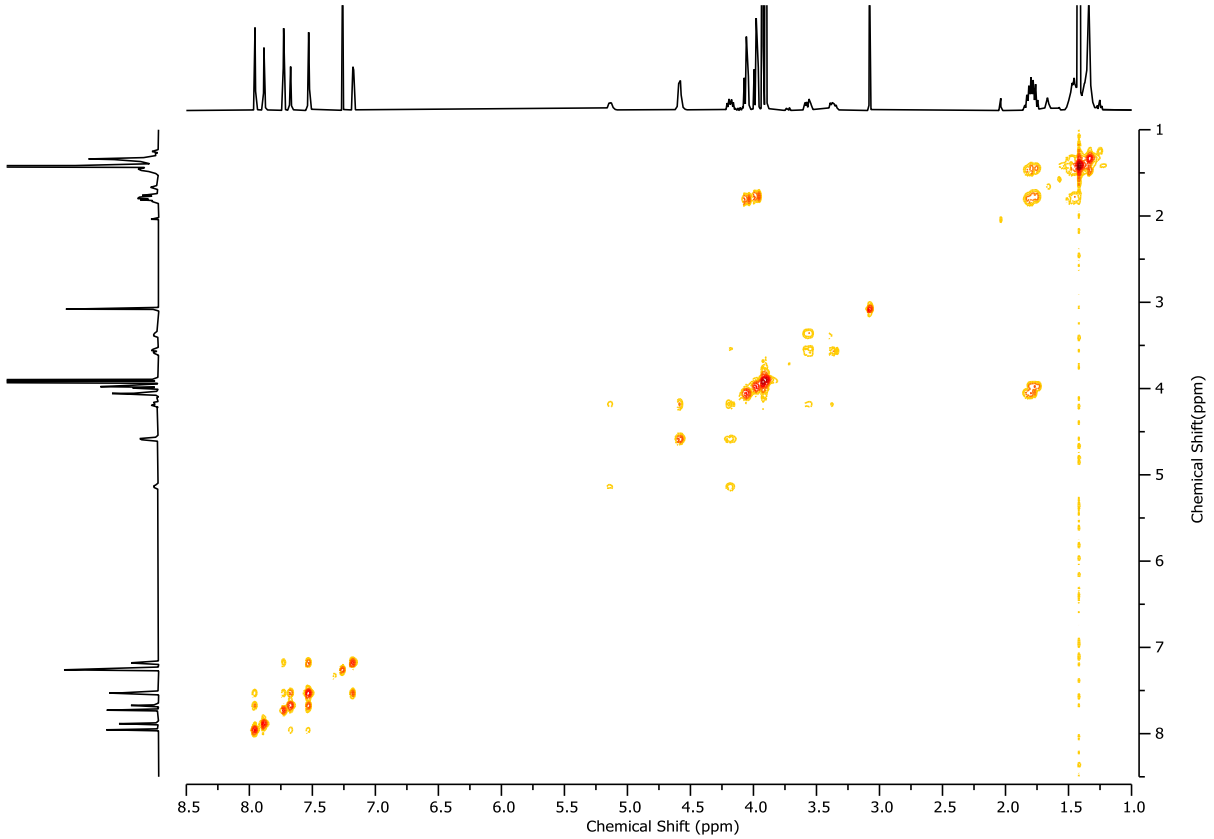

Figure 2.42 - ^{1}H COSY NMR ($CDCl_3$, 400 MHz) (*R*)-**S9**.

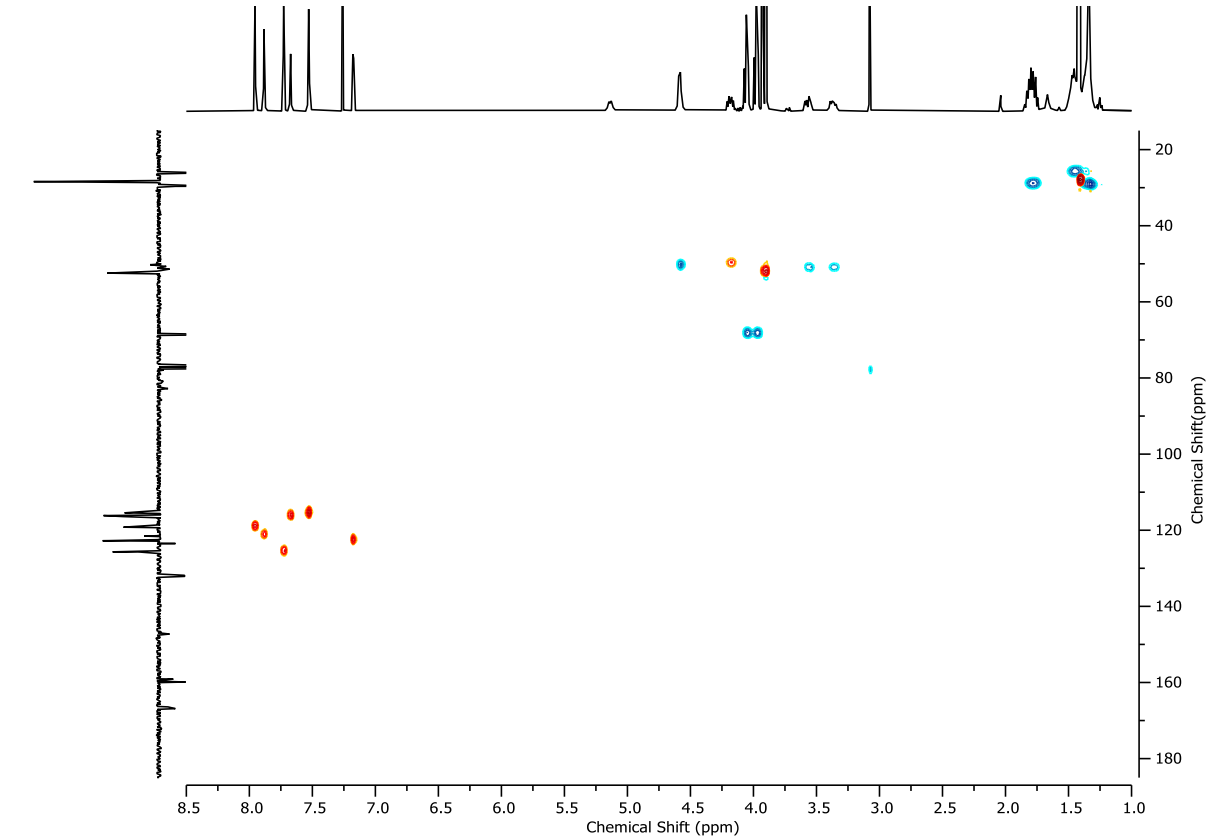

Figure 2.43 - HSQC NMR ($CDCl_3$, 400 MHz) of (*R*)-**S9**.

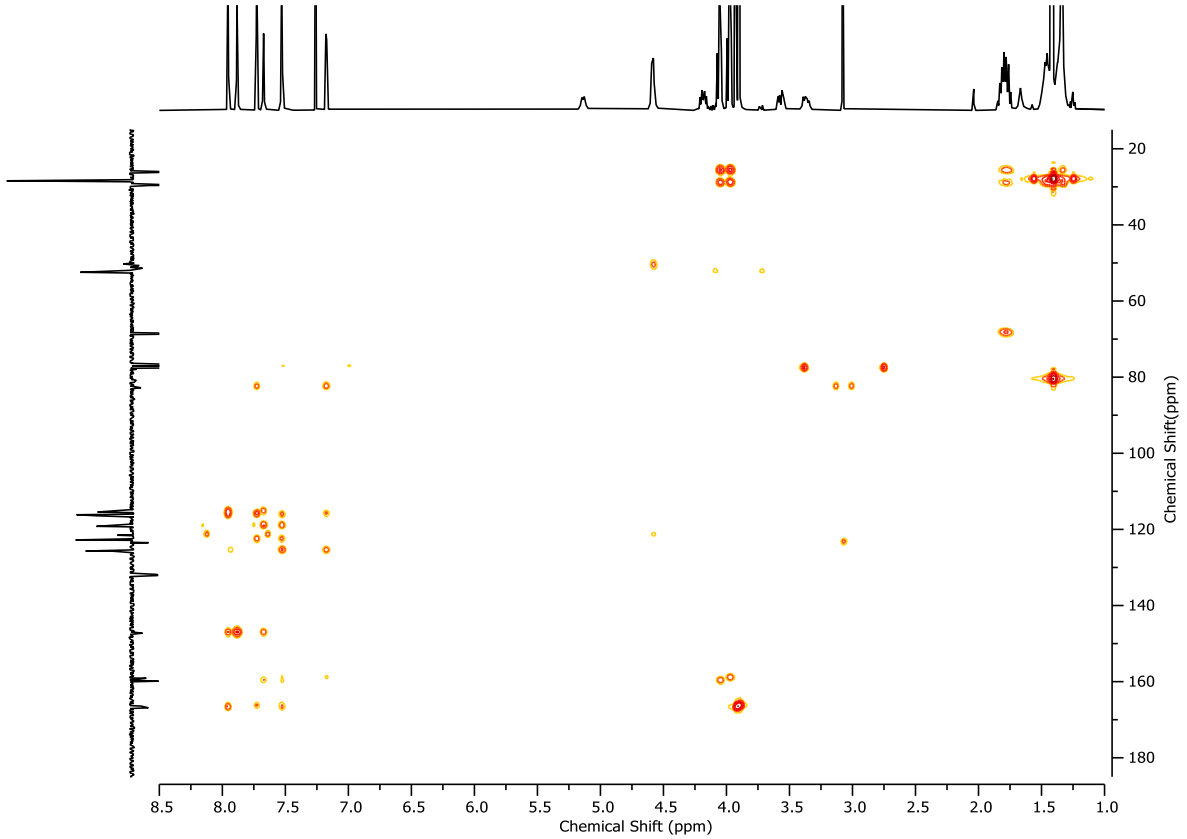

Figure 2.44 - HMBC NMR ($CDCl_3$, 400 MHz) of (*R*)-**S9**.

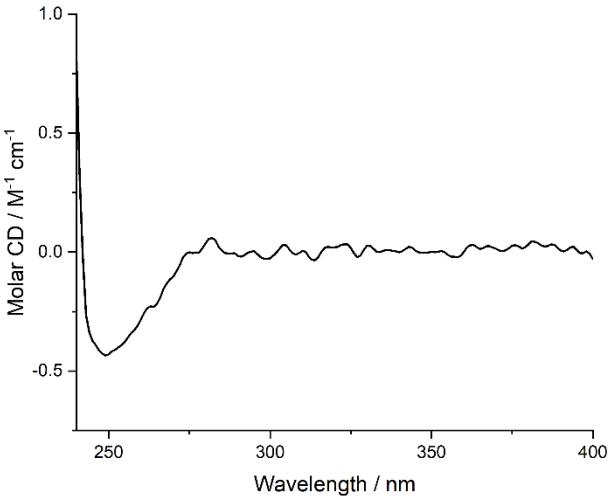

Figure 2.45 - Circular Dichroism Spectra of (*R*)-**S9** (30 µM) at 293 K in $CHCl_3$.

Pre-macrocycle (*R*)-1

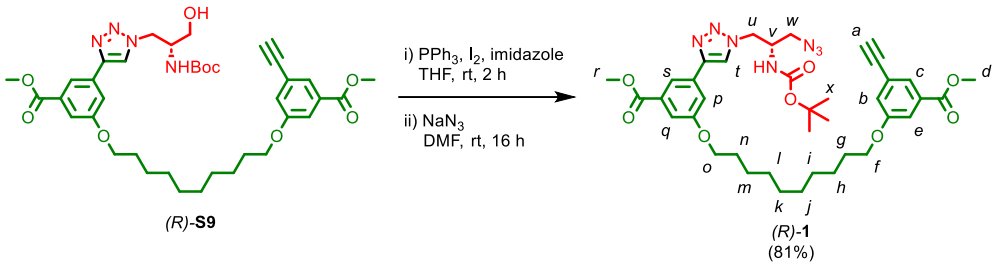

To a stirred solution of PPh_3 (467.7 mg, 0.59 mmol, 3.0 eq.) and imidazole (207.3 mg, 3.04 mmol, 5.0 eq.) in THF (4.5 mL) at 0 °C was added I_2 (451.9 mg, 1.78 mmol, 3.0 eq.) in 1 portion. After stirring for 10 min, a concentrated solution of (*R*)-**S9** (416.7 mg, 0.59 mmol, 1.0 eq.) in THF (1.4 mL) was added dropwise, the reaction mixture was allowed to warm to ambient temperature and stirred for 2 h. The crude mixture was filtered through Celite®, washing with CH_2Cl_2, and concentrated *in vacuo*. The residue was purified by column chromatography (SiO_2, petrol-EtOAc 0→40%). The resultant oil was immediately dissolved in DMF (2.9 mL) and NaN_3 (192.4 mg, 2.96 mmol, 5.0 eq.) was added. After stirring for 16 h at ambient temperature, the reaction mixture was diluted with EtOAc (10 mL), washed with H_2O (10 mL). The aqueous layer was extracted with EtOAc (3 x 10 mL). The combined organic fractions were washed with 5% LiCl (3 x 10 mL), and brine (10 mL) then dried over $MgSO_4$, filtered, and concentrated *in vacuo*. The residue was purified by column chromatography (SiO_2, CH_2Cl_2-EtOAc 0→20%) to yield (*R*)-**1** (353.1 mg, 0.48 mmol, 81%) as a white foam.

δ_H ($CDCl_3$, 400 MHz) 7.96 (t, *J* = 1.5, 1H, H_s), 7.88 (s, 1H, H_t), 7.73 (t, *J* = 1.4, 1H, H_c), 7.67 (dd, *J* = 2.6, 1.5, 1H, H_p), 7.56 – 7.50 (m, 2H, H_e, H_q), 7.18 (dd, *J* = 2.6, 1.4, 1H, H_b), 5.14 (d, *J* = 8.3, 1H, H_{NHBoc}), 4.59 (d, *J* = 5.7, 2H, H_u), 4.25 – 4.12 (m, 1H, H_v), 4.06 (t, *J* = 6.5, 2H, H_o), 3.98 (t, *J* = 6.5, 2H, H_f), 3.93 (s, 3H, H_r), 3.90 (s, 3H, H_d), 3.57 (dd, *J* = 12.4, 5.0, 1H, H_w), 3.37 (dd, *J* = 12.6, 6.4, 1H, H_w), 3.08 (s, 1H, H_a), 1.87 – 1.72 (m, 4H, H_g, H_n), 1.51 – 1.30 (m, 21H, H_h, H_i, H_j, H_k, H_l, H_m, H_x); δ_C ($CDCl_3$, 101 MHz) 166.8, 166.4, 159.9, 159.1, 147.3, 132.1, 131.8, 131.7, 125.7, 123.5, 122.7, 121.5, 119.2, 116.4, 116.1, 115.4, 82.8, 80.8, 77.9, 68.6, 52.5, 52.4, 51.4, 50.7, 50.2, 29.6, 29.6, 29.5, 29.4, 29.3, 29.2, 28.4, 26.1, 26.1; HR-ESI-MS (+ve) m/z = 732.3706 $[M+H]^+$ (calc. m/a for $C_{38}H_{50}N_7O_8$ 732.3715)

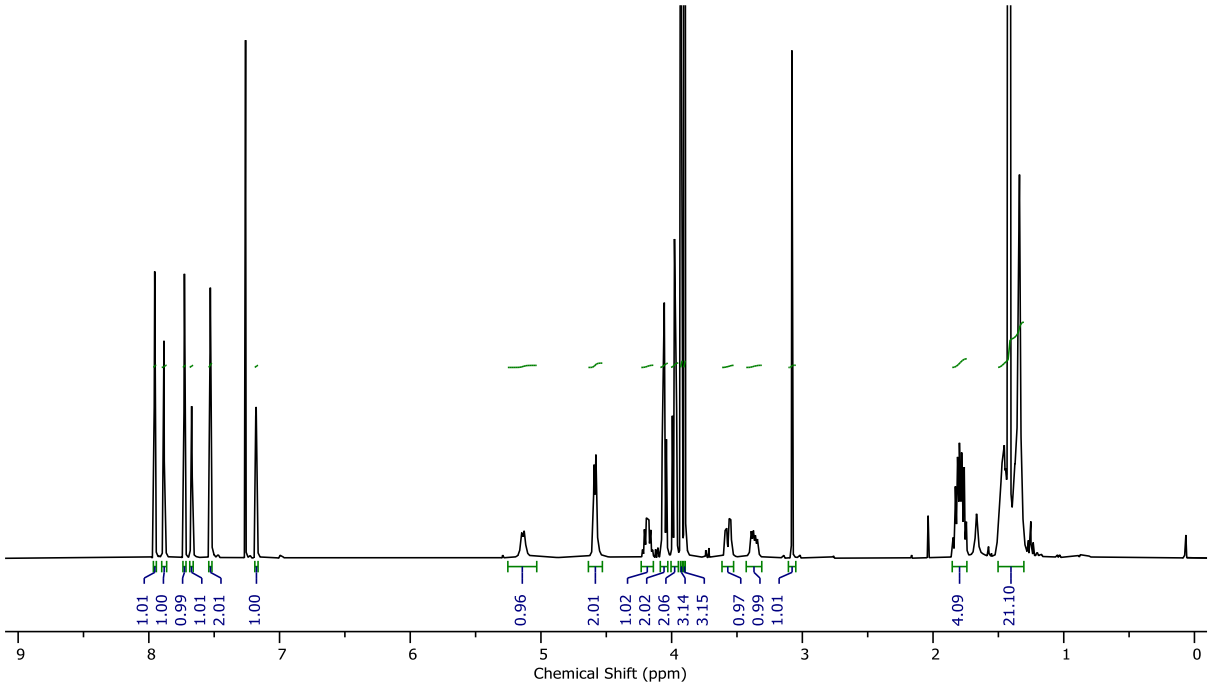

Figure 2.46 - ^{1}H NMR ($CDCl_3$, 400 MHz) of (*R*)-**1**.

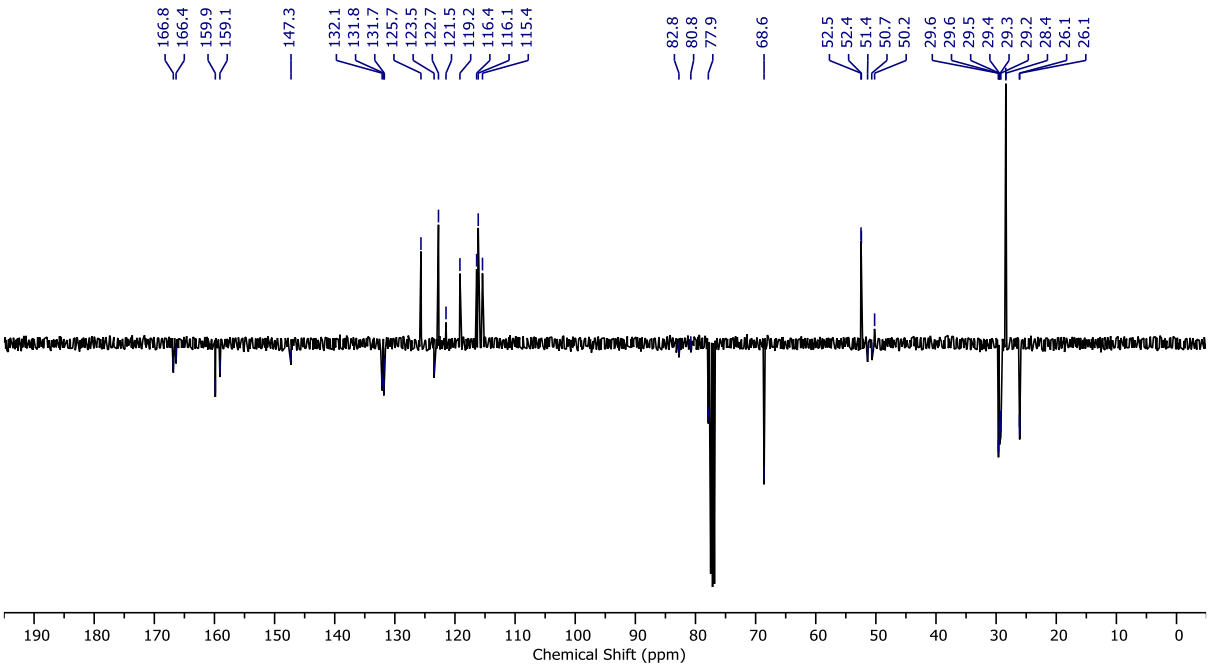

Figure 2.47 - JMOD NMR ($CDCl_3$, 101 MHz) (*R*)-**1**.

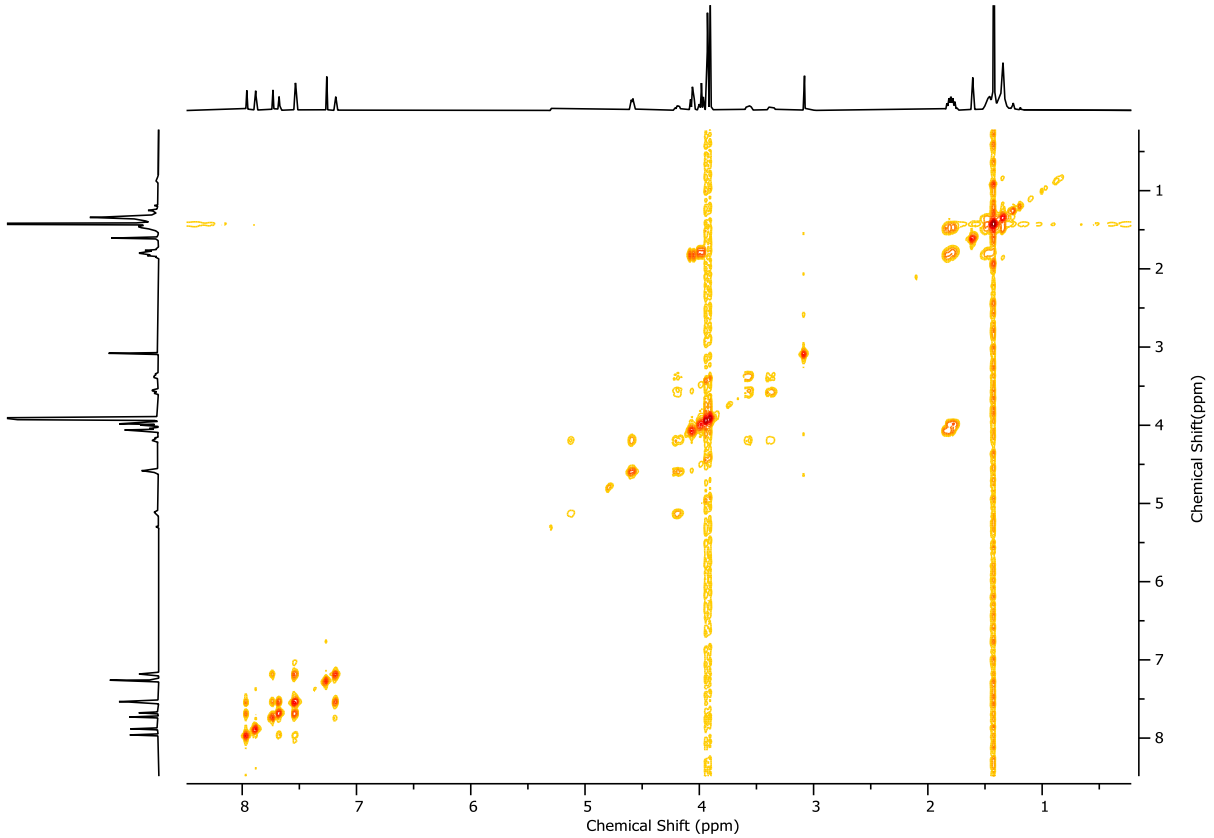

Figure 2.48 - ^{1}H COSY NMR ($CDCl_3$, 400 MHz) (*R*)-**1**.

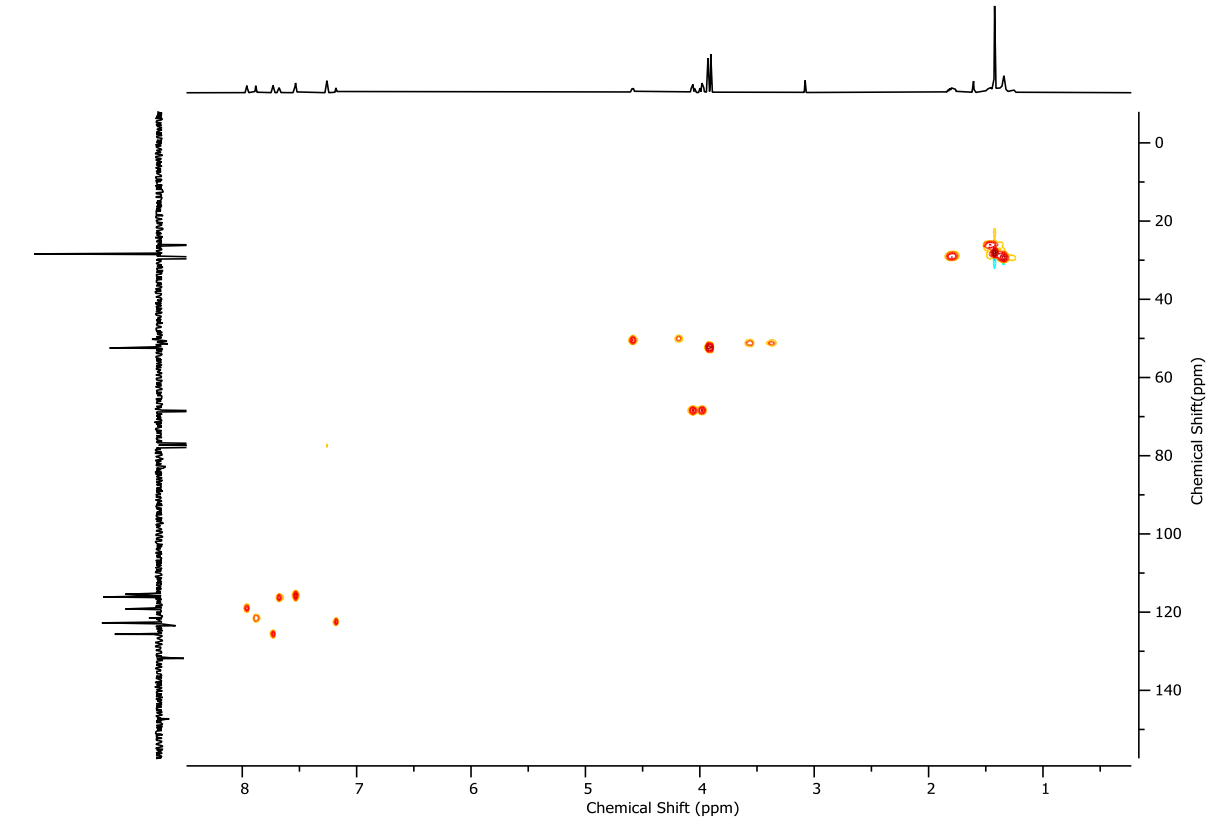

Figure 2.49 - HSQC NMR ($CDCl_3$, 400 MHz) of (*R*)-**1**.

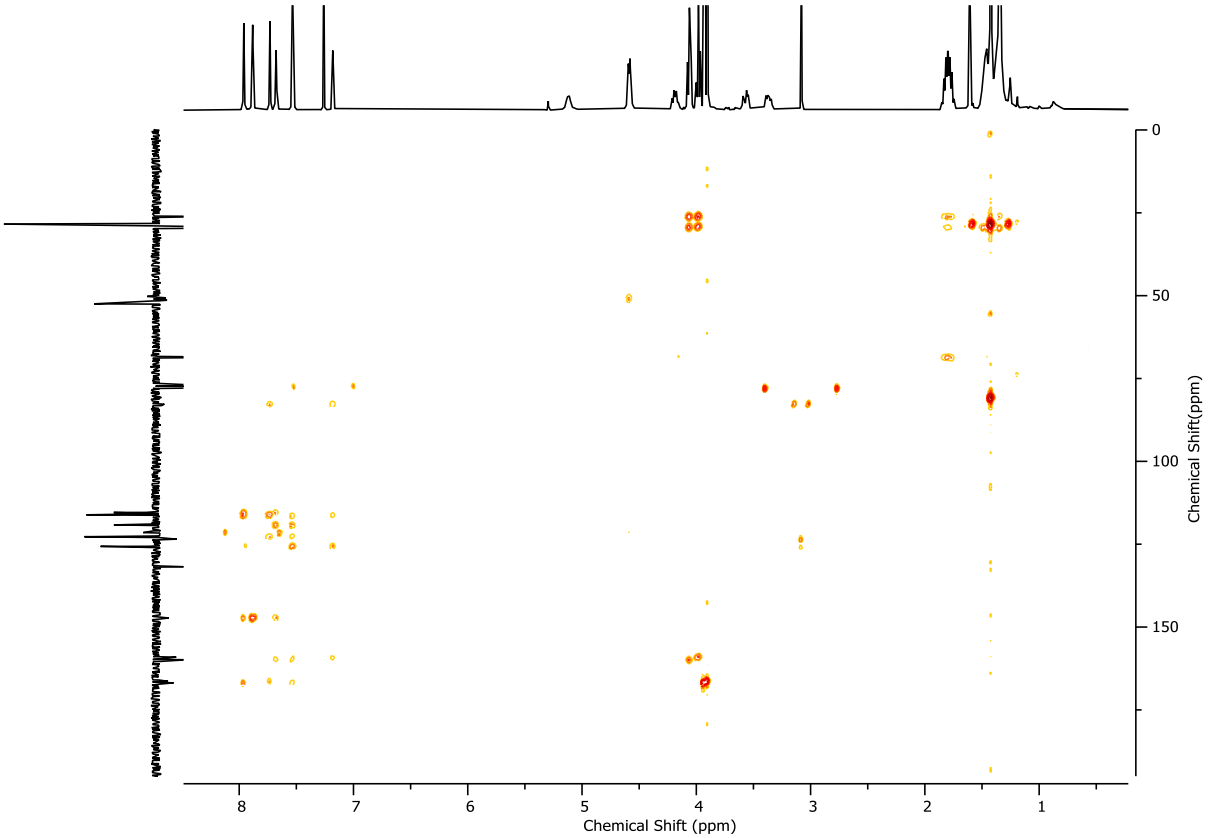

Figure 2.50 - HMBC NMR ($CDCl_3$, 400 MHz) of (*R*)-**1**.

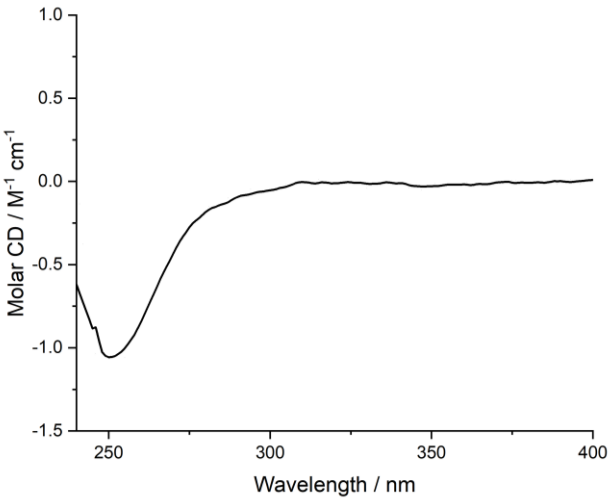

Figure 2.51 - Circular Dichroism Spectra of (*R*)-**1** (27 μM) at 293 K in $CHCl_3$.

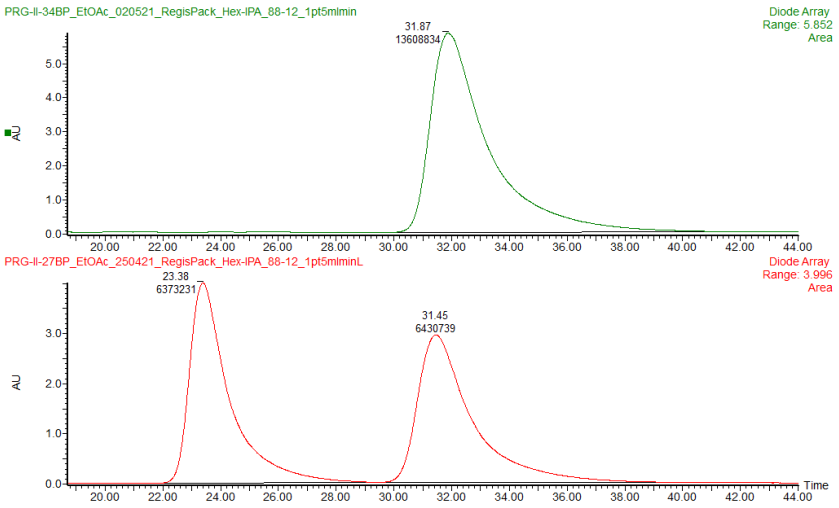

Figure 2.52 - CSP-HPLC of (*R*)-**1** (loaded in EtOAc). RegisPack, *n*-hexane-IPA 88 : 12, flowrate 1.5 mLmin^{-1}. (top) (*S*)-**1** (not observed), (*R*)-**1** (31.87 min, 13608834, >99.9%). (bottom) *rac*-**1**, (*S*)-**1** (23,38 min, 6373231, 49.8%), (*R*)-**1** (31.45 min, 6430739, 50.2%).

Compounds leading to macrocycles 2 and 3

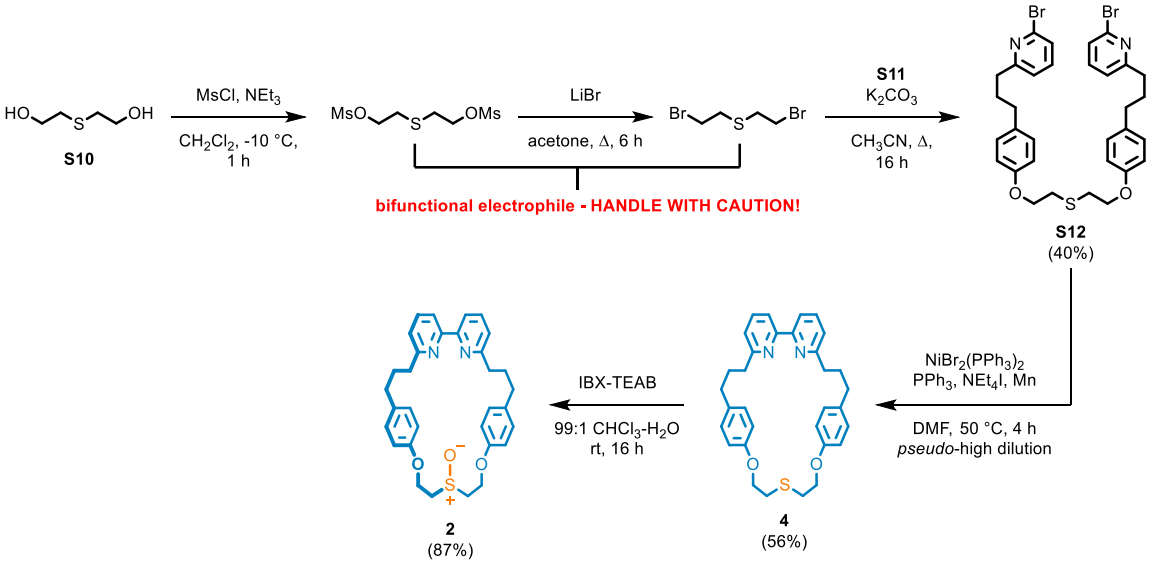

Scheme 2.2 - Synthetic route to macrocycles **2** and **4**.

Pre-macrocycle S12

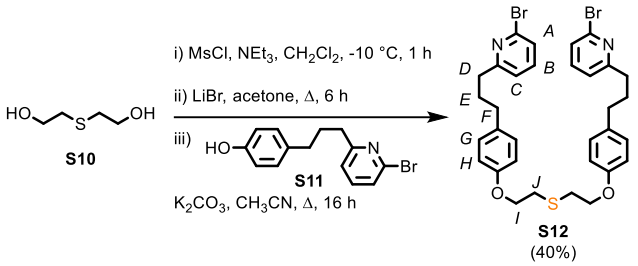

NOTE: the dimesylate and dibromo derivatives of S10 are bifunctional electrophiles, which should be handled with caution. To a stirred solution of **S10** (400 µL, 4.0 mmol, 1.0 eq.) in CH_2Cl_2 (20 mL), was added NEt_3 (3.9 mL, 27.7 mmol, 7.0 eq.), and the solution was cooled to -10°C. MsCl (950 µL, 12.3 mmol, 3.1 eq.) was added over 5 min, and the reaction mixture was stirred for 1 h. H_2O (5 mL) was added, the mixture was allowed to warm to ambient temperature, and the aqueous and organic layers separated. The aqueous was extracted with CH_2Cl_2 (2 x 5 mL), and the combined organics were washed with brine, dried over $MgSO_4$, filtered and concentrated *in vacuo*. The crude materials were dissolved in acetone (40 mL), and LiBr (3.55 g, 40.9 mmol, 10.2 eq.) was added. The reaction mixture was refluxed under an inert atmosphere for 6 h. After cooling to ambient temperature, the insoluble materials were filtered off, and the filtrate concentrated *in vacuo*. The crude materials were dissolved in CH_3CN (20 mL), and **S11** (2.39 g, 8.2 mmol, 2.1 eq.) and K_2CO_3 (2.81 g, 20.4 mmol, 5.1 eq.) were added. The reaction mixture was heated at reflux under an inert atmosphere for 16 h. After cooling to ambient temperatures, the crude mixture was filtered through Celite®, washing with CH_2Cl_2, and concentrated *in vacuo*. The residue was purified by column chromatography (SiO_2, 1:1 petrol/CH_2Cl_2-Et_2O 5→10%) to yield **S12** as a white solid (1.08 g, 1.61 mmol, 40% over 3 steps).

δ_H ($CDCl_3$, 400 MHz) 7.42 (t, *J* = 7.7, 2H, H_B), 7.28 (d, *J* = 7.8, 2H, H_A), 7.14 – 7.03 (m, 6H, H_C, H_G), 6.88 – 6.78 (m, 4H, H_H), 4.16 (t, *J* = 6.6, 4H, H_I), 3.00 (t, *J* = 6.6, 4H, H_J), 2.81 – 2.73 (m, 4H, H_D), 2.65 – 2.57 (m, 4H, H_F), 2.07 – 1.94 (m, 4H, H_E); δ_C ($CDCl_3$, 101 MHz) 163.8, 156.8, 141.6, 138.7, 134.4, 129.5, 125.4, 121.6, 114.6, 114.6, 68.1, 37.5, 34.6, 31.8, 31.6. HR-ESI-MS (+ve) m/z = 669.0774 $[M+H]^+$ (calc. m/z for $C_{32}H_{35}Br_2N_2O_2S$ 669.0781); Melting point 63-65 °C.

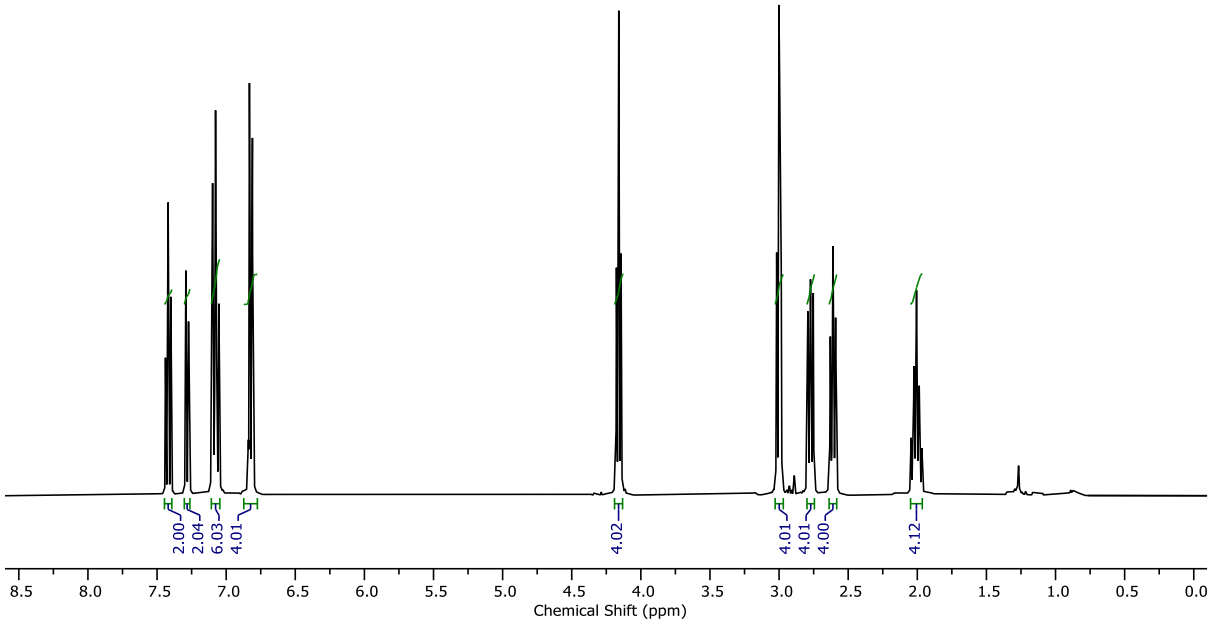

Figure 2.53 - ^{1}H NMR ($CDCl_3$, 400 MHz) of **S12**.

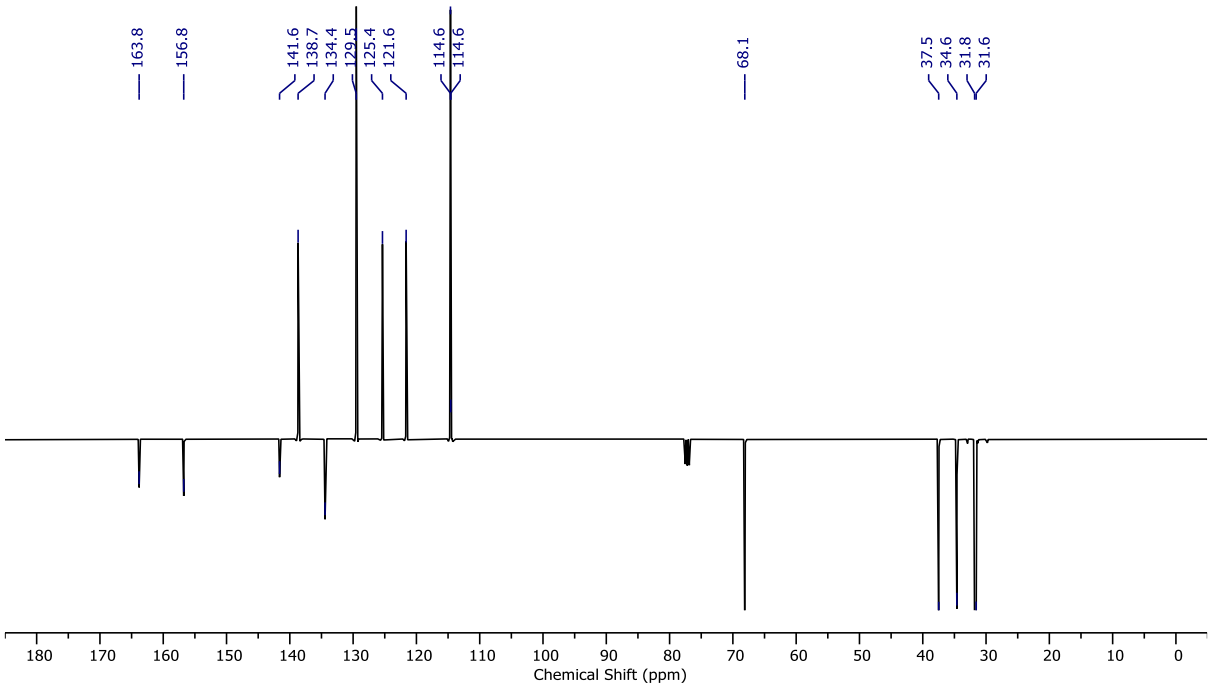

Figure 2.54 - JMOD NMR ($CDCl_3$, 101 MHz) of **S12**.

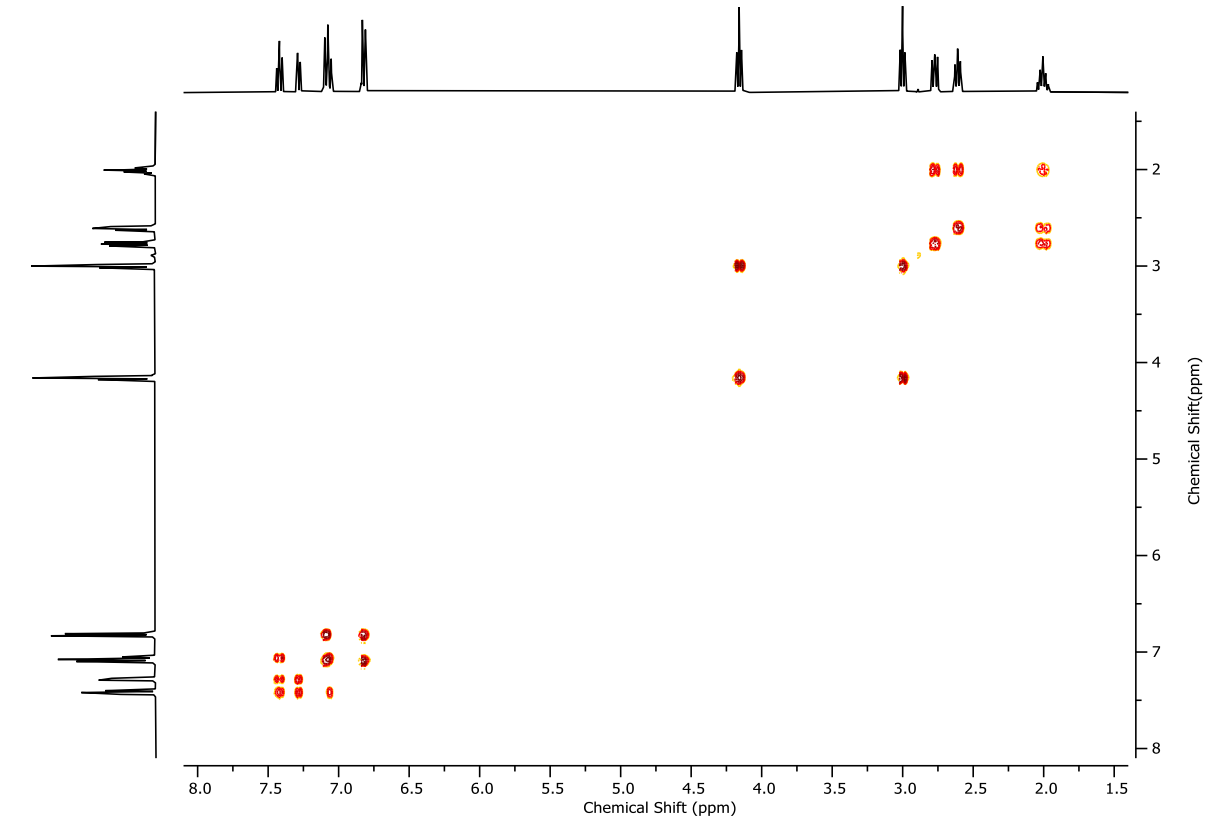

Figure 2.55 - ^{1}H COSY NMR ($CDCl_3$, 400 MHz) of **S12**.

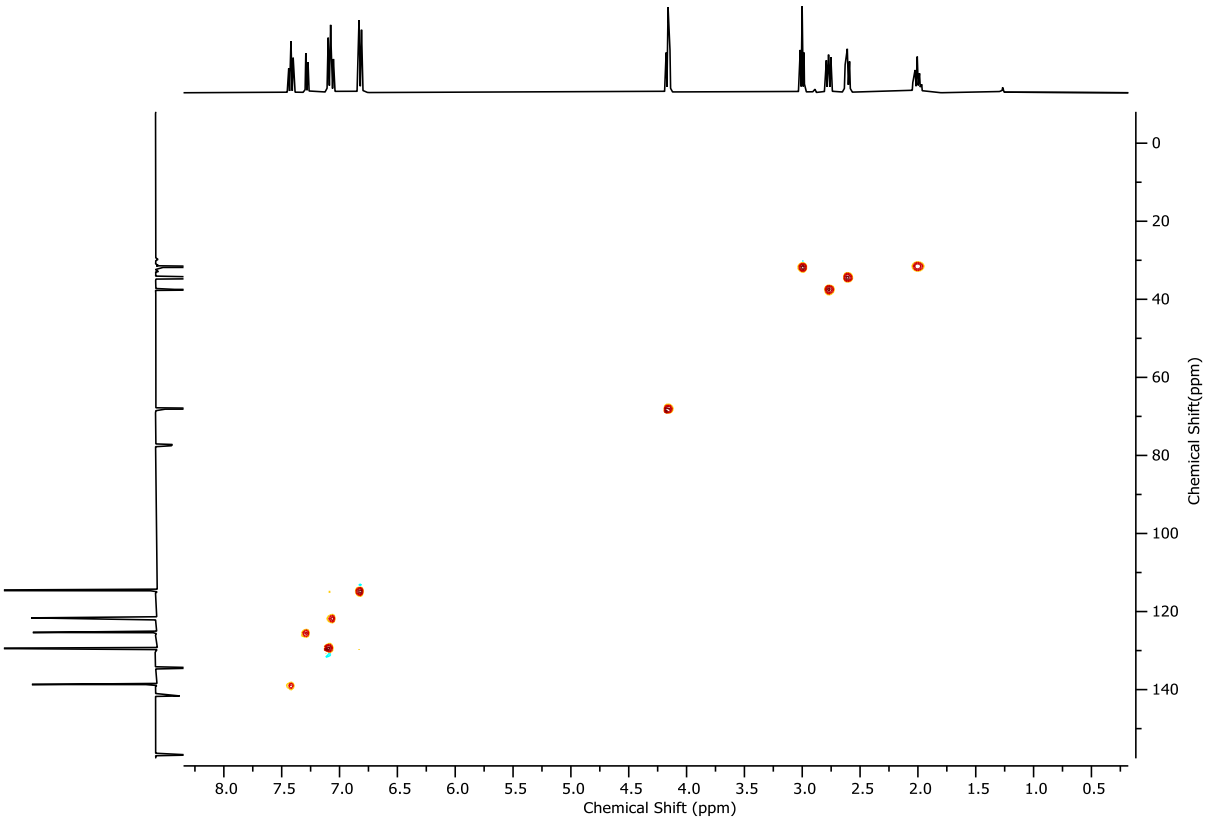

Figure 2.56 - HSQC NMR ($CDCl_3$, 400 MHz) of **S12**.

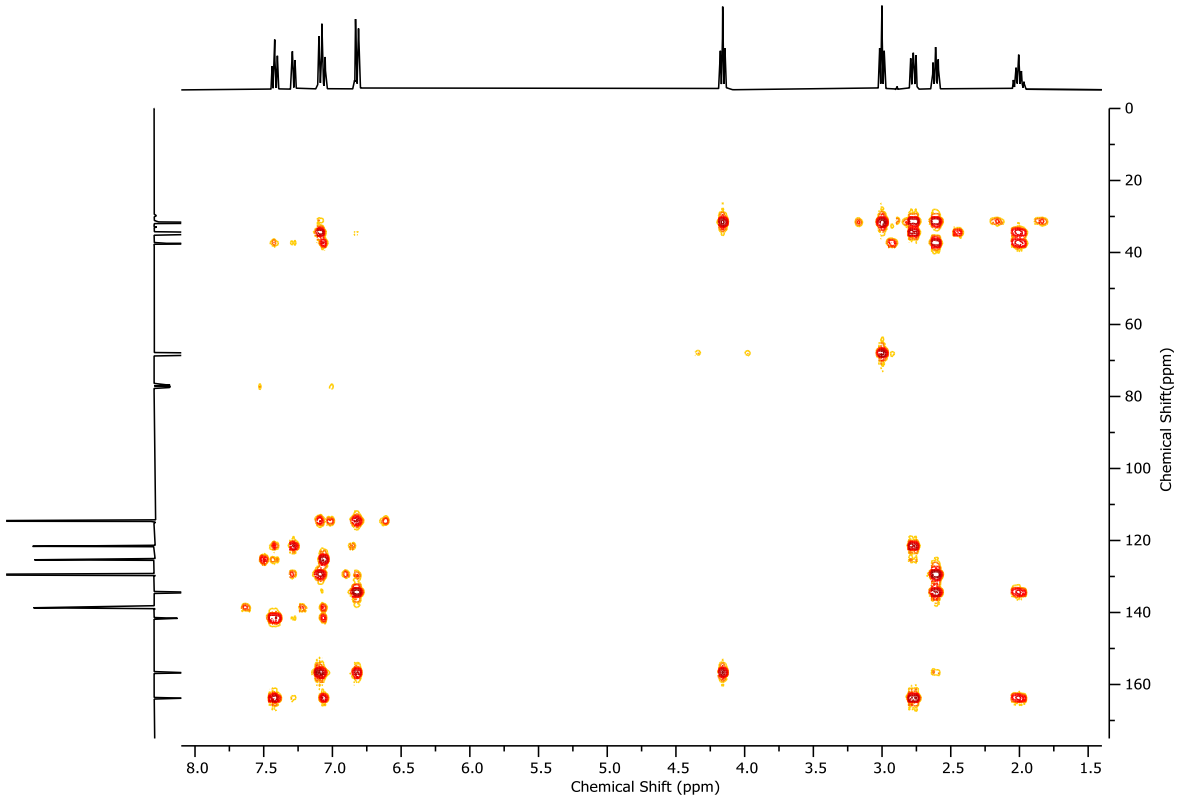

Figure 2.57 - HMBC NMR ($CDCl_3$, 400 MHz) of **S12**.

Sulfide macrocycle 4

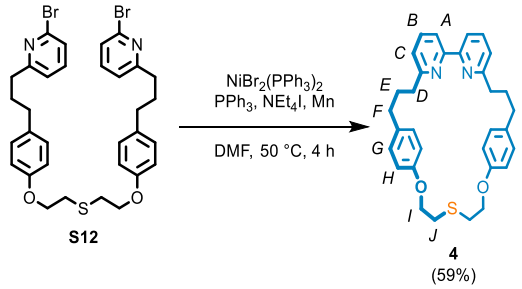

$NiBr_2(PPh_3)_2$ (1.09 g, 1.47 mmol, 1.0 eq.), PPh_3 (766.5 mg, 2.92 mmol, 2.0 eq.), Mn (802.1 g, 14.6 mmol, 10.0 eq.), and NEt_4I (376.5 mg, 1.46 mmol, 1.0 eq.) dissolved in DMF (15 mL) and sonicated for 15 min, until a deep red colour developed. The activated catalyst mixture was then stirred at 50 °C for 10 min, before a solution of **S12** (979.6g, 1.46 mmol, 1.0 eq.) in DMF (15 mL) was added *via* syringe pump over a 4 h period. After the addition was completed, the crude mixture was stirred at 50 °C for an additional 30 min, before cooling to ambient temperature. The reaction mixture was diluted with EtOAc (100 mL), and washed with a sat. EDTA/0.1 M NH_3 solution (30 mL), 5% LiCl (3 x 20 mL), and brine (30 mL). All aqueous phases were extracted with EtOAc (20 mL), and the combined organics were dried over $MgSO_4$, filtered and concentrated *in vacuo*. The residue was purified by column chromatography (SiO_2, CH_2Cl_2-petrol (1:1) with EtOAc 0→5%) to yield **4** (438.9 mg, 0.86 mmol, 59%) as a beige solid.

δ_H ($CDCl_3$, 400 MHz) 7.70 – 7.60 (m, 4H, H_A, H_B), 7.13 (p, J = 4.2, 2H, H_C), 7.06 – 6.99 (m, 4H, H_G), 6.74 – 6.66 (m, 4H, H_H), 4.15 (t, J = 6.6, 4H, H_I), 3.02 – 2.90 (m, 8H, H_J, H_D), 2.68 – 2.60 (m, 4H, H_F), 2.15 (t, 4H, H_E); δ_C ($CDCl_3$, 101 MHz) 162.3, 157.1, 156.5, 136.9, 135.1, 129.7, 122.6, 119.7, 114.7, 69.0, 37.9, 34.6, 32.1, 31.4; HR-ESI-MS (+ve) m/z = 511.2425 $[M+H]^+$ (calc. m/z for $C_{32}H_{35}N_2O_2S$ 511.2414); Melting point 79-81 °C.

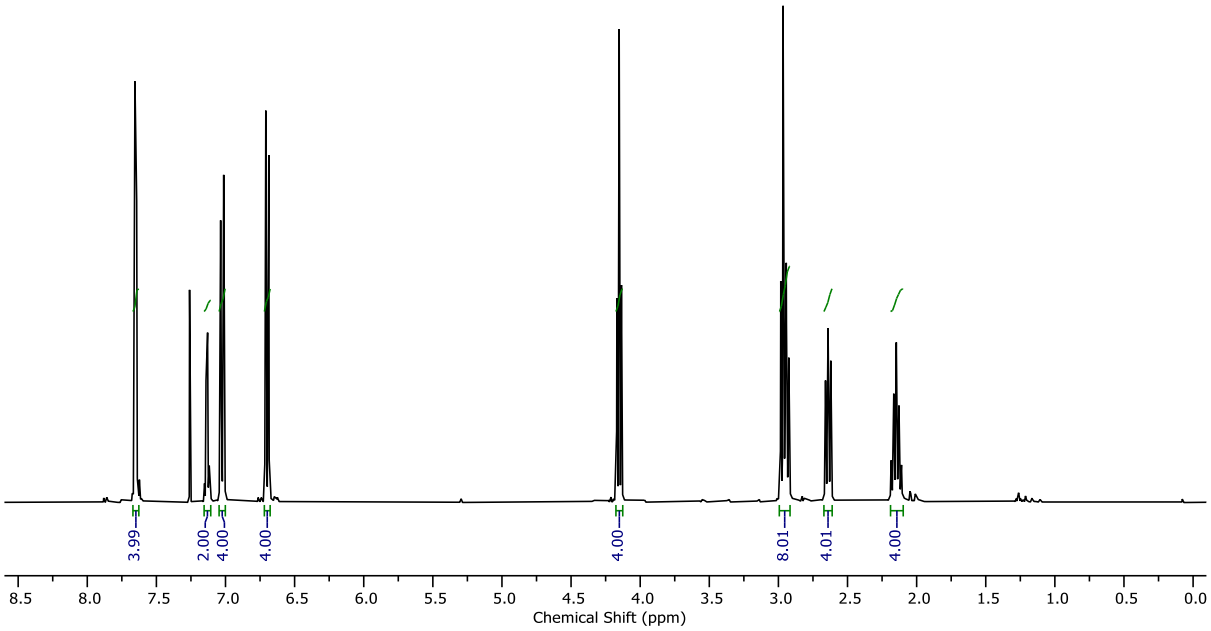

Figure 2.58 - ^1H NMR ($CDCl_3$, 400 MHz) of **4**.

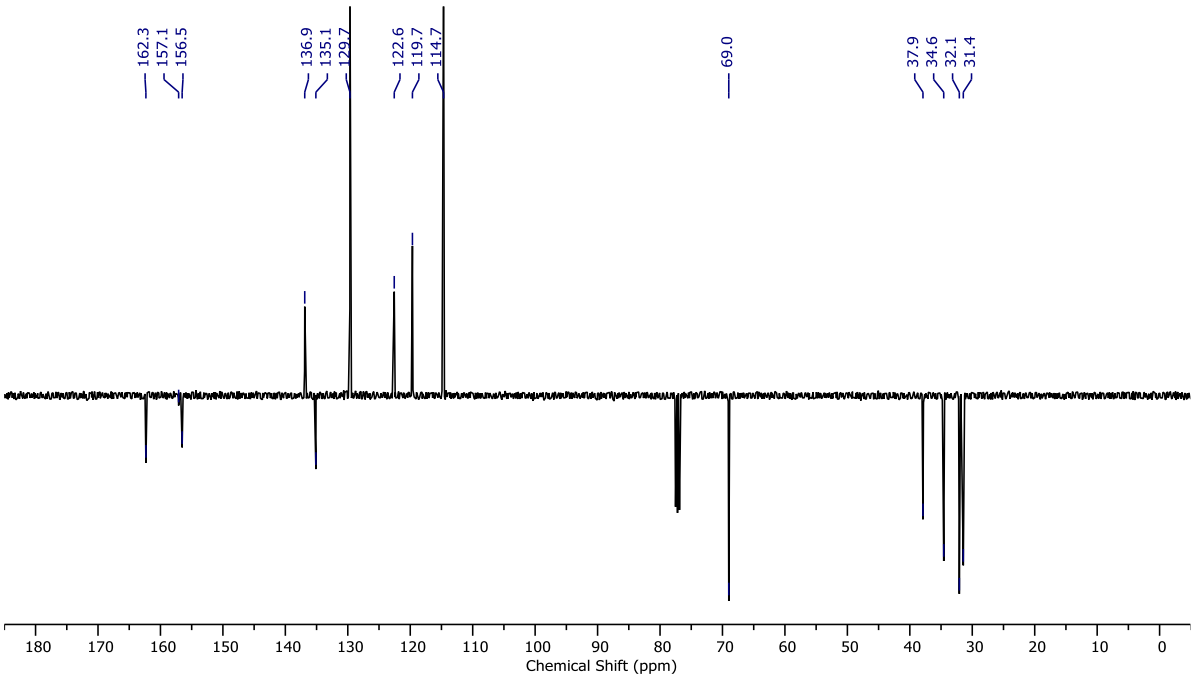

Figure 2.59 - JMOD NMR ($CDCl_3$, 101 MHz) of **4**.

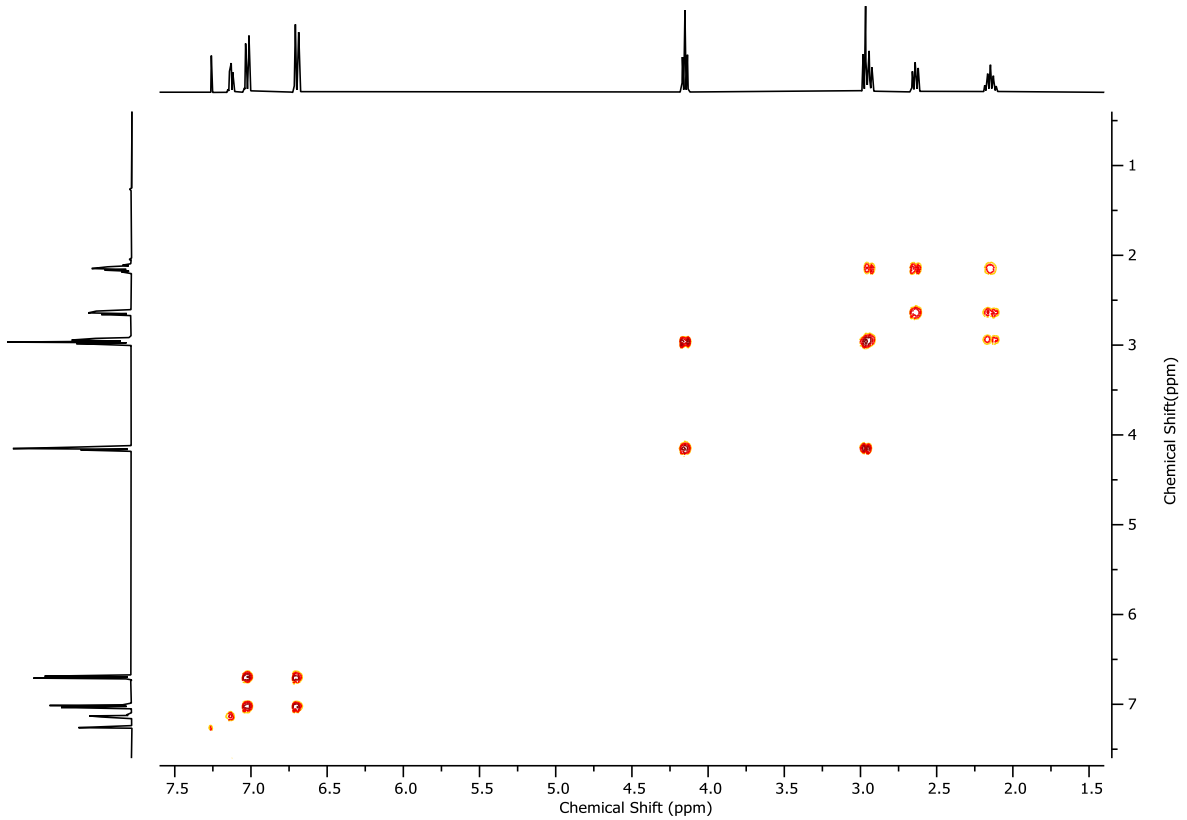

Figure 2.60 - ^{1}H COSY NMR ($CDCl_3$, 400 MHz) of **4**.

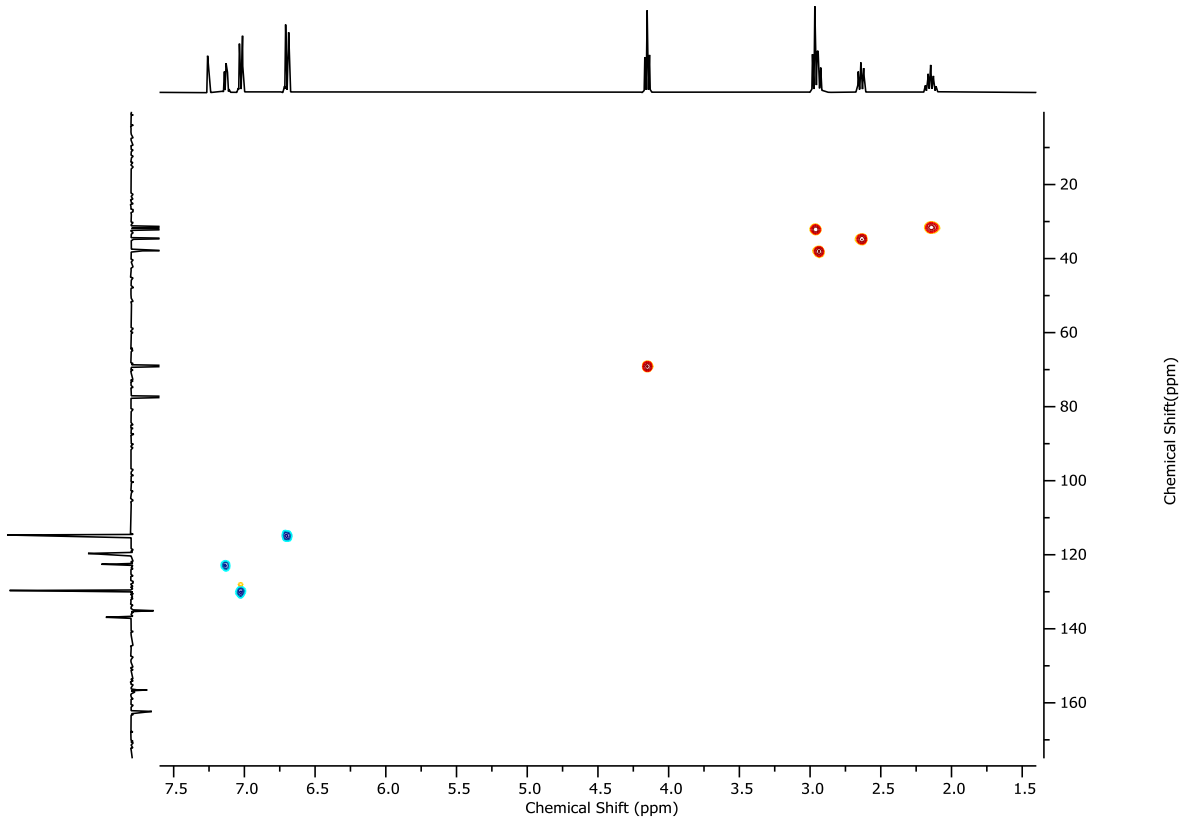

Figure 2.61 - HSQC NMR ($CDCl_3$, 400 MHz) of **4**.

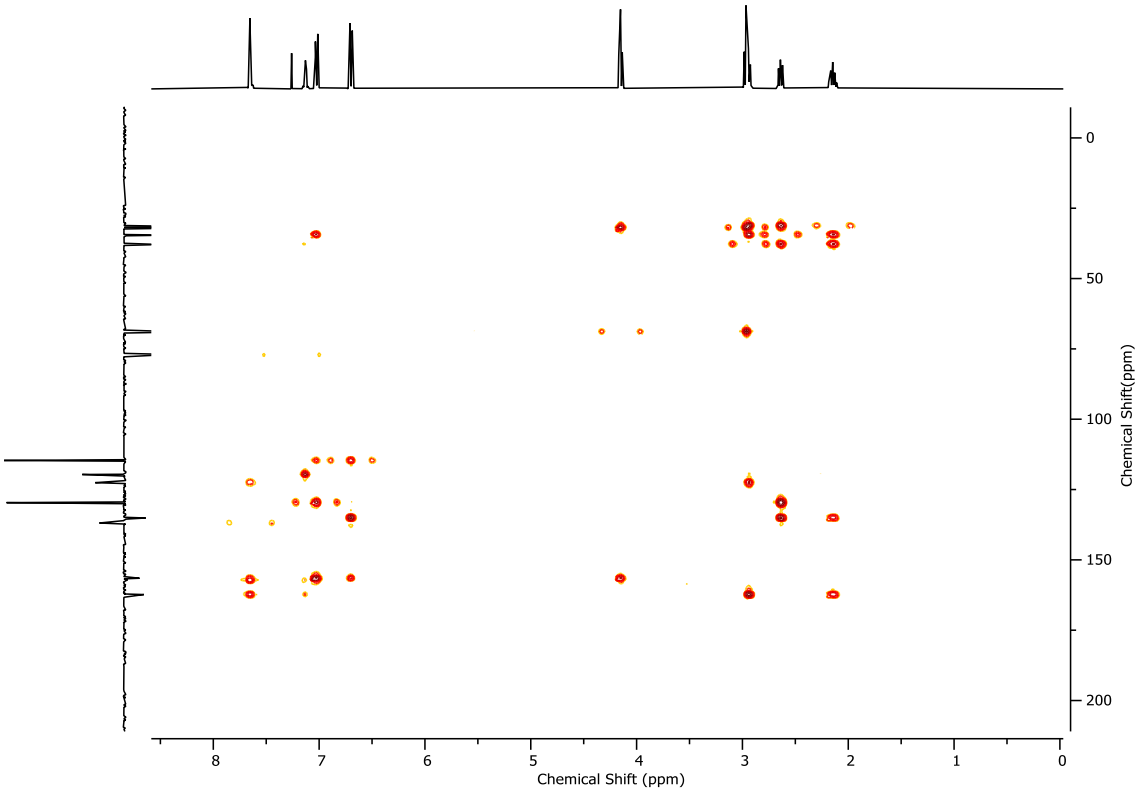

Figure 2.62 - HMBC NMR ($CDCl_3$, 400 MHz) of **4**.

Sulfoxide macrocycle 2

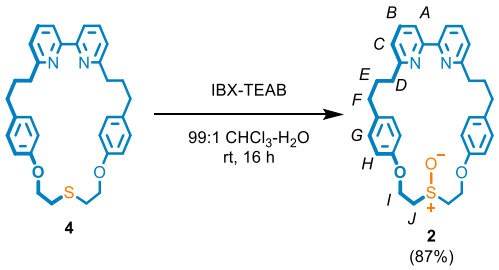

To a solution of **4** (85.5 mg, 0.168 mmol, 1.0 eq.) in 99:1 $CHCl_3/H_2O$ (1.68 mL), was added IBX (52 mg, 0.184 mmol, 1.1 eq) and tetraethylammonium bromide (39 mg, 0.184 mmol, 1.1 eq), and the resulting suspension was stirred for 16 h. The reaction mixture was then diluted with CH_2Cl_2 (10 mL), washed with 10% $NaHSO_3$ (5 mL), saturated $NaHCO_3$ (5 mL) and brine (5 mL), extracting all aqueous layers with CH_2Cl_2 (5 mL). The combined organics were dried over $MgSO_4$, filtered, and concentrated *in vacuo*. The residue was purified by column chromatography (SiO_2, CH_2Cl_2-MeOH 0→10%) to yield **2** (77.2 mg, 0.146 mmol, 87%) as an off-white foam.

δ_H ($CDCl_3$, 400 MHz) 7.71 – 7.56 (m, 4H, H_A, H_B), 7.11 (dd, J = 5.9, 2.8, 2H, H_C), 7.02 (d, J = 8.8, 4H, H_G), 6.63 (d, J = 8.7, 4H, H_H), 4.50 – 4.31 (m, 4H, H_I), 3.42 (ddd, J = 13.2, 8.3, 4.7, 2H, H_J), 3.11 (ddd, J = 13.7, 5.4, 4.0, 2H, H_J), 2.92 (t, J = 7.3, 4H, H_D), 2.72 – 2.58 (m, 4H, H_F), 2.20 – 2.08 (m, 4H, H_E); δ_C ($CDCl_3$, 101 MHz) 162.2, 157.0, 155.5, 136.9, 135.7, 129.7, 122.5, 119.6, 114.9, 60.8, 52.1, 37.7, 34.4, 31.3; HR-ESI-MS (+ve) m/z = 527.2374 $[M+H]^+$ (calc. m/z for $C_{32}H_{35}N_2O_3S$ 527.2363).

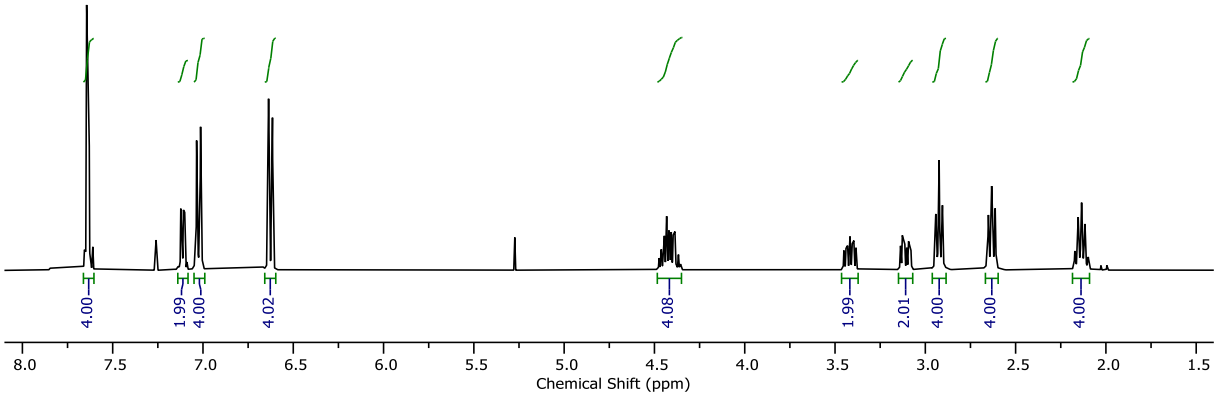

Figure 2.63 - ^{1}H NMR ($CDCl_3$, 400 MHz) of **2**.

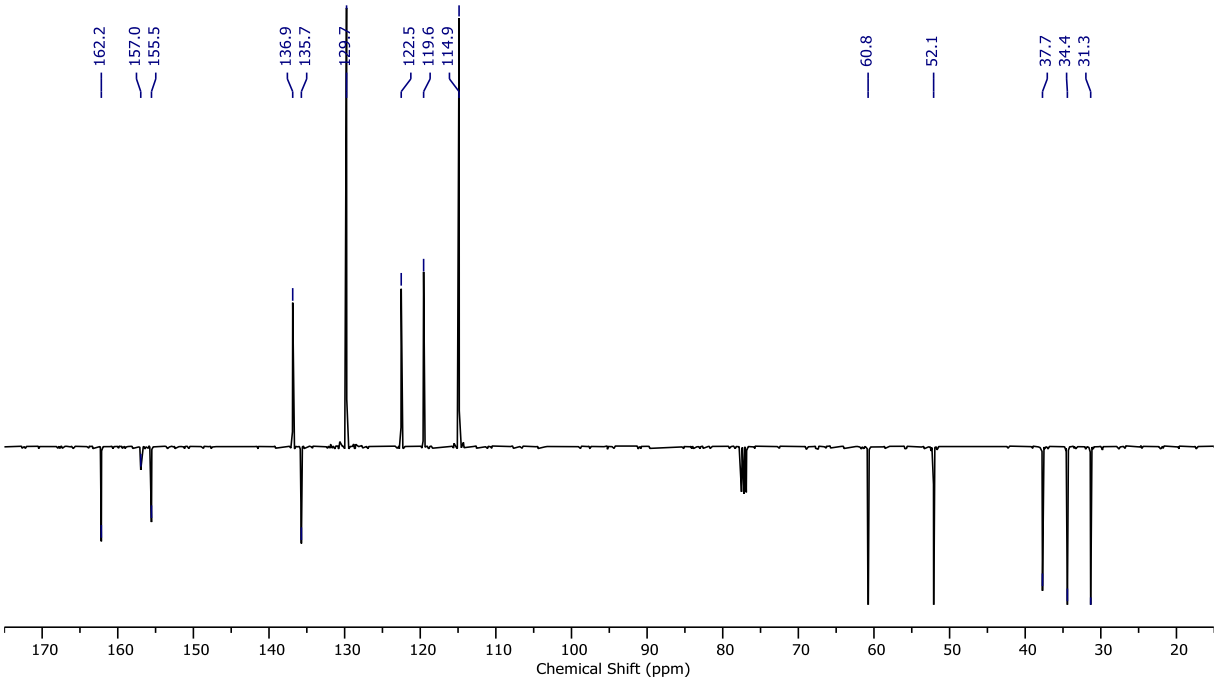

Figure 2.64 - JMOD NMR ($CDCl_3$, 101 MHz) of **2**.

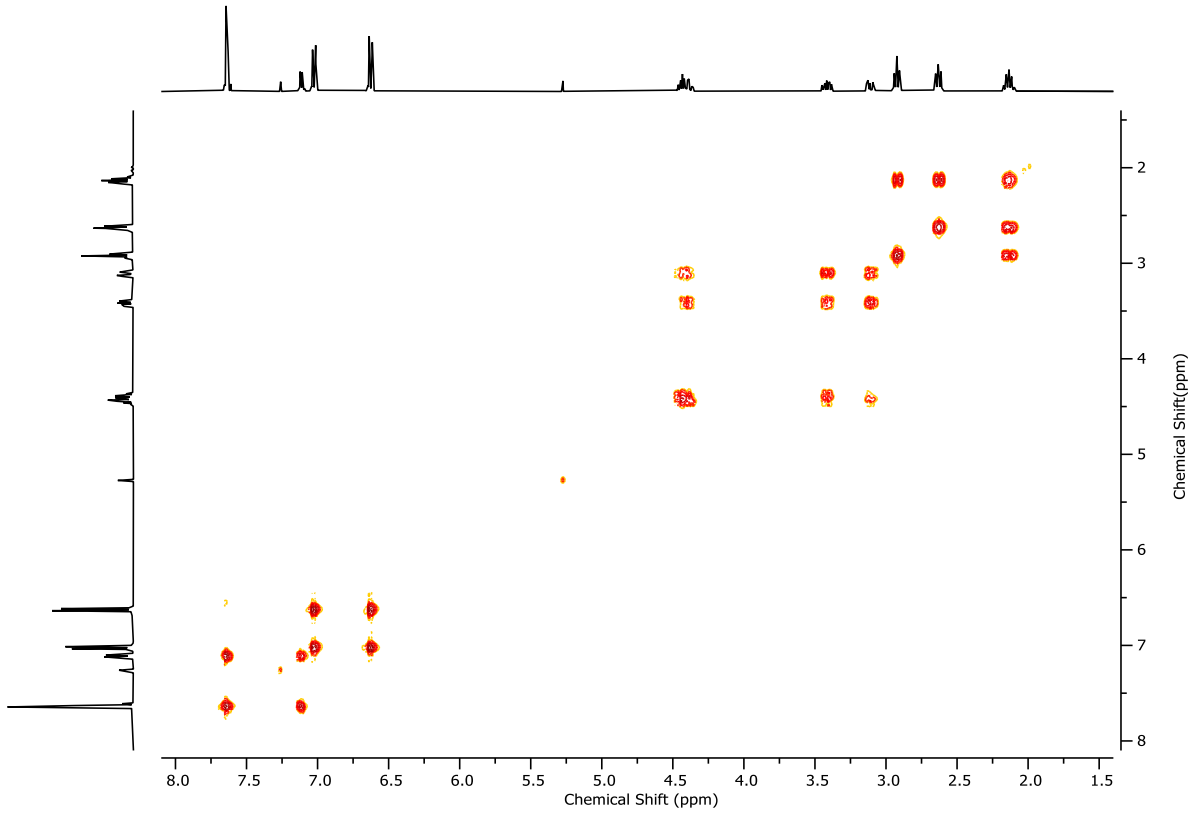

Figure 2.65 - ^{1}H COSY NMR ($CDCl_3$, 400 MHz) of **2**.

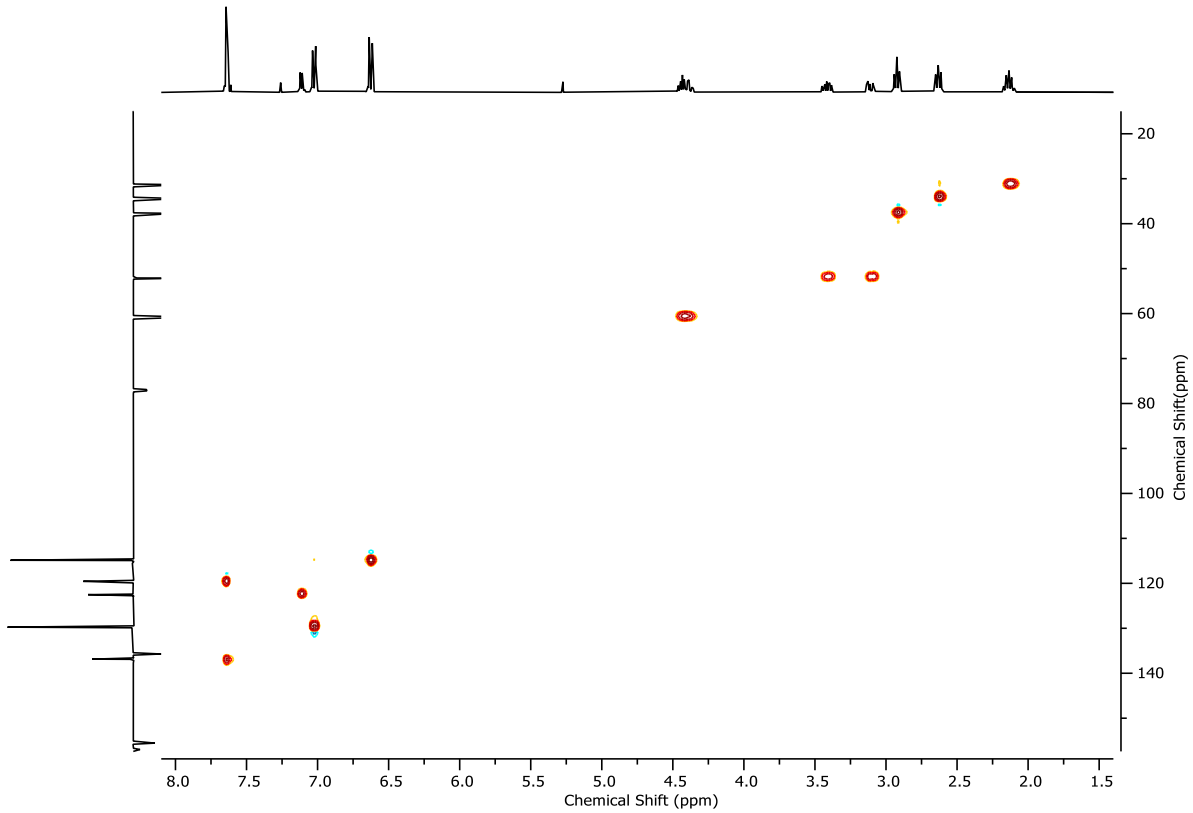

Figure 2.66 - HSQC NMR ($CDCl_3$, 400 MHz) of **2**.

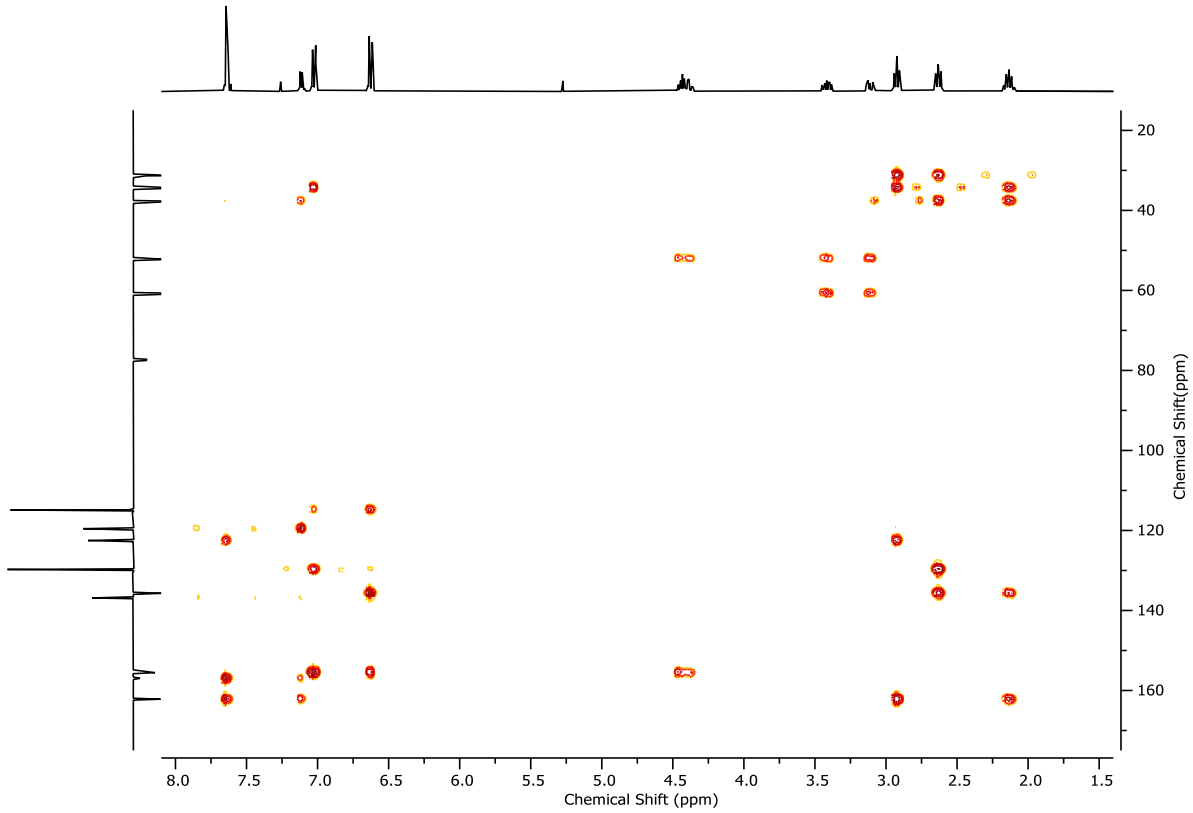

Figure 2.67 - HMBC NMR ($CDCl_3$, 400 MHz) of **2**.

Synthesis of catananes (S_{ma},$R_{co\text{-}c}$)-3 and (R_{ma},$R_{co\text{-}c}$)-3

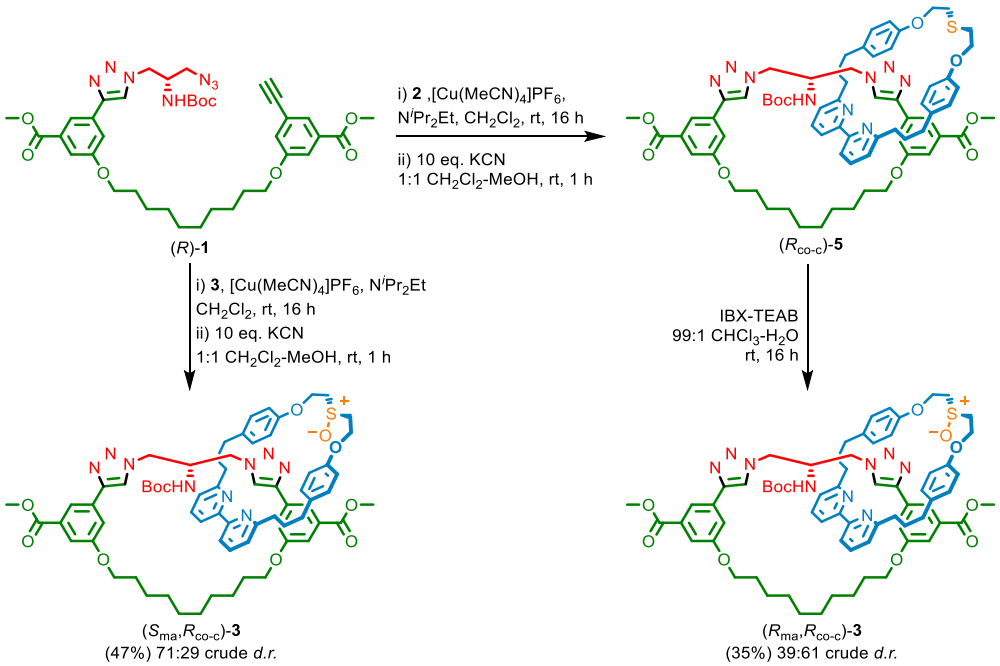

Scheme 2.3 - Synthetic route to mechanically axially chiral epimeric catenanes (S_{ma},$R_{co\text{-}c}$)-**3** and (R_{ma},$R_{co\text{-}c}$)-**3**.

Catenane (S_{ma},$R_{co\text{-}c}$)-3

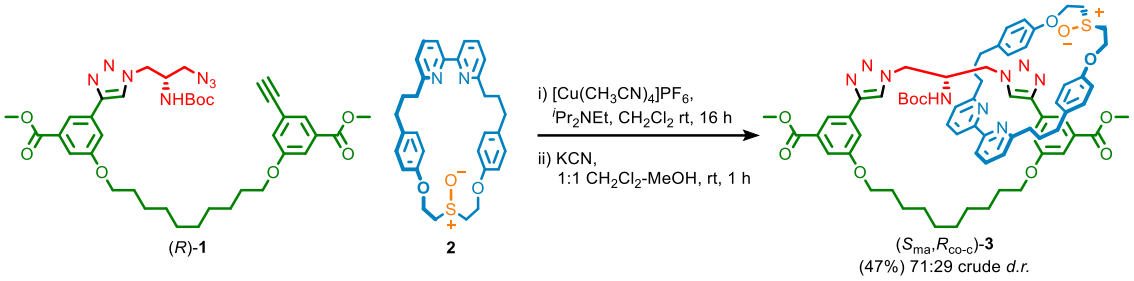

A CEM MW vial was charged with macrocycle **2** (43.1 mg, 0.082 mmol, 1.0 eq.) and $[Cu(CH_3CN)_4]PF_6$ (29.9 mg, 0.080 mmol, 0.98 eq.) and purged with N_2. CH_2Cl_2 (5.95 mL) and $^iPr_2NEt$ (28 µL, 0.164 mmol, 2.0 eq.) were added followed by a solution of pre-macrocycle (*R*)-**1** (65.9 mg, 0.090 mmol, 1.1 eq.) in CH_2Cl_2 (2.0 mL) at ambient temperature over 16 h. Then, MeOH (2.9 mL) and KCN as a solid (53 mg, 0.82 mmol, 10.0 eq.) were added and the resulting mixture was stirred vigorously for 1 h. The crude mixture was diluted with CH_2Cl_2 (8 mL) and washed with H_2O in two portions (10 mL and 5 mL), with separation of aqueous and organic phases. The combined aqueous phase was then extracted with CH_2Cl_2 (3 x 5 mL) and the combined organics were washed with brine (10 mL), dried over $MgSO_4$ and concentrated *in vacuo*. The residue was purified by column chromatography (SiO_2, CH_2Cl_2-CH_3CN 0→100%; CH_3CN-MeOH 0→5%) to yield (S_{ma},$R_{co\text{-}c}$)-**3** (48.3 mg, 0.0384 mmol, 47%, first eluting isomer) as an off-white foam and (R_{ma},$R_{co\text{-}c}$)-**3** (22.6 mg, 0.018 mmol, 22%, second eluting isomer) as a colorless oil. The absolute stereochemistry of the major diatereomer was assigned crystallographically using a sample of rac-(S_{ma},$R_{co\text{-}c}$)-**3** produced by reaction of *rac*-**1** (see 11.1). The mechanical stereochemistry of the minor diastereomer was assigned as opposite to that of the major diastereomer. The co-conformational stereochemistry of both is fixed by the absolute sterechemistry of (*R*)-**1**.

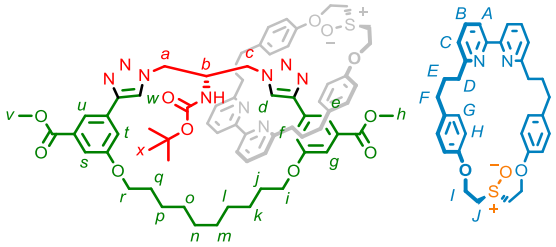

δ_H (400 MHz, $CDCl_3$) 10.34 (1H, s, H_d), 8.32 (1H, s, H_e), 8.10 (1H, s, H_u), 7.79 – 7.60 (2H, m, $H_{B/B'}$), 7.55 (1H, s, H_w), 7.52 – 7.44 (2H, m, $H_{A/A'}$), 7.39 (1H, s, H_s), 7.29 (1H, s, H_g), 7.16 (1H, m, $H_{C'}$), 7.02 (1H, s, H_f), 6.88 (3H, m, H_G, H_C), 6.80 – 6.63 (6H, m, H_H, $H_{H'}$, $H_{G'}$), 6.52 (1H, s, H_t), 5.69 (1H, m, H_{NHBoc}), 4.80 – 4.35 (5H, m, $H_{I/I'}$, H_a), 4.21 – 4.02 (3H, m, H_i, H_b), 4.00 – 3.79 (7H, m, H_h, H_v, H_c), 3.78 – 3.56 (3H, m, H_a, H_J, H_c), 3.53 – 3.22 (3H, m, H_r, H_J), 3.16 (2H, m, $H_{J'}$), 2.66 – 2.23 (8H, m, $H_{D/D'}$, $H_{F/F'}$), 2.15 – 1.67 (4H, m, H_j, $H_{E/E'}$), 1.64 – 1.02 (25H, m, H_q, H_p, H_o, H_n, H_m, H_l, H_k, $H_{E/E'}$, H_x). δ_C (101

MHz, $CDCl_3$) 167.1, 166.9, 163.4, 162.5, 158.9, 156.5, 156.4, 156.3, 156.2, 146.2, 145.9, 137.4, 136.8, 135.6, 133.4, 133.4, 132.8, 132.0, 131.7, 131.3, 129.7, 129.4, 122.1, 121.2, 120.8, 120.4, 119.1, 118.8, 118.3, 116.6, 114.8, 114.6, 114.0, 111.2, 67.8, 67.7, 60.3, 60.2, 52.7, 52.5, 52.1, 50.6, 50.3, 49.8, 36.5, 34.7, 29.8, 29.7, 29.4, 29.3, 29.35, 29.2, 29.0, 28.2, 26.7, 25.9. LR-ESI-MS (+ve) = 1258.6 $[M+H]^+$.

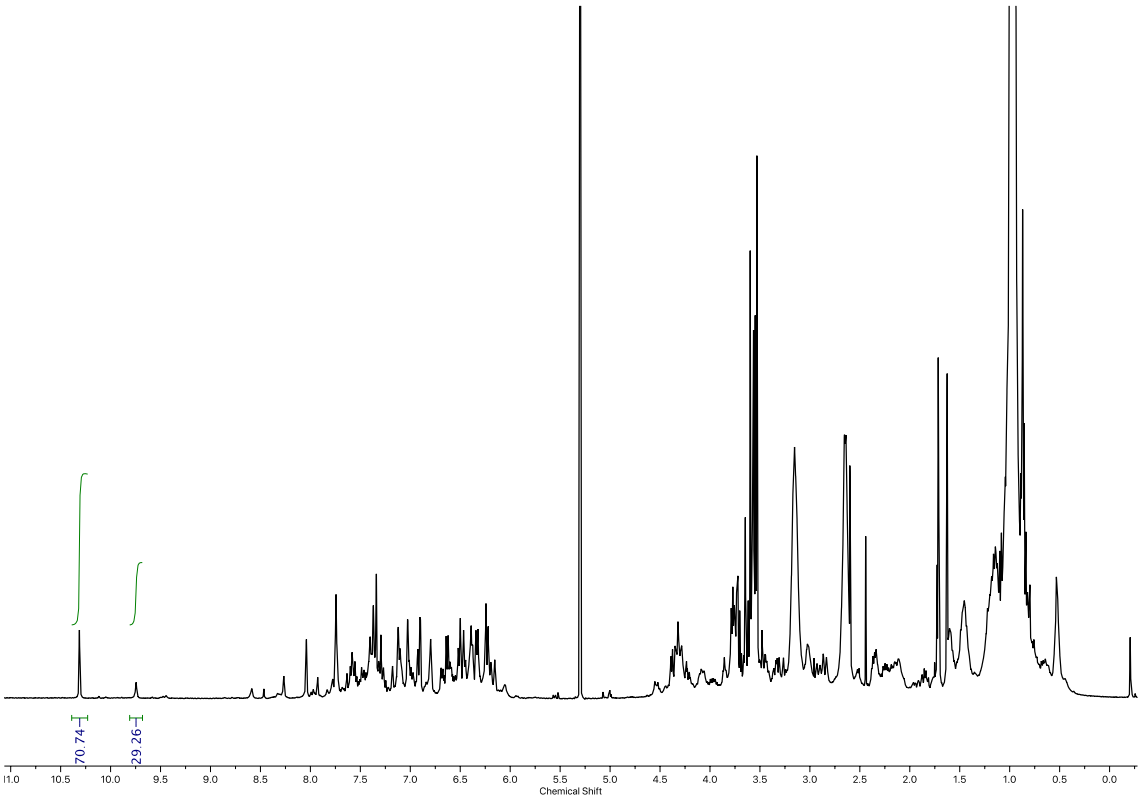

Figure 2.68 - ^1H NMR ($CDCl_3$, 400 MHz) of AT-CuAAC crude leading to major isomer (S_{ma},$R_{co\text{-}c}$)-**3**. Integration of (S_{ma},$R_{co\text{-}c}$)-**3** (10.34 ppm, $\boldsymbol{H}_d$, 70.74H) and (R_{ma},$R_{co\text{-}c}$)-**3** (9.95 ppm, $\boldsymbol{H}_d$, 29.26H).

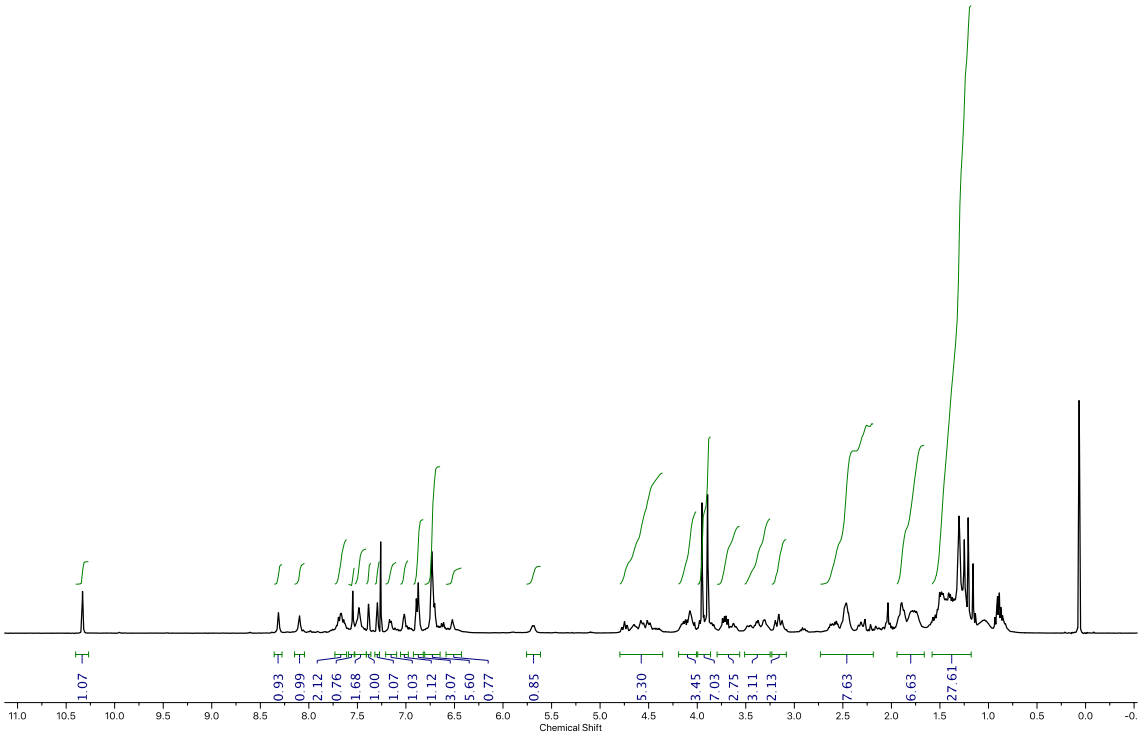

Figure 2.69 - ^{1}H NMR ($CDCl_3$, 400 MHz) of (S_{ma},$R_{co\text{-}c}$)-**3**.

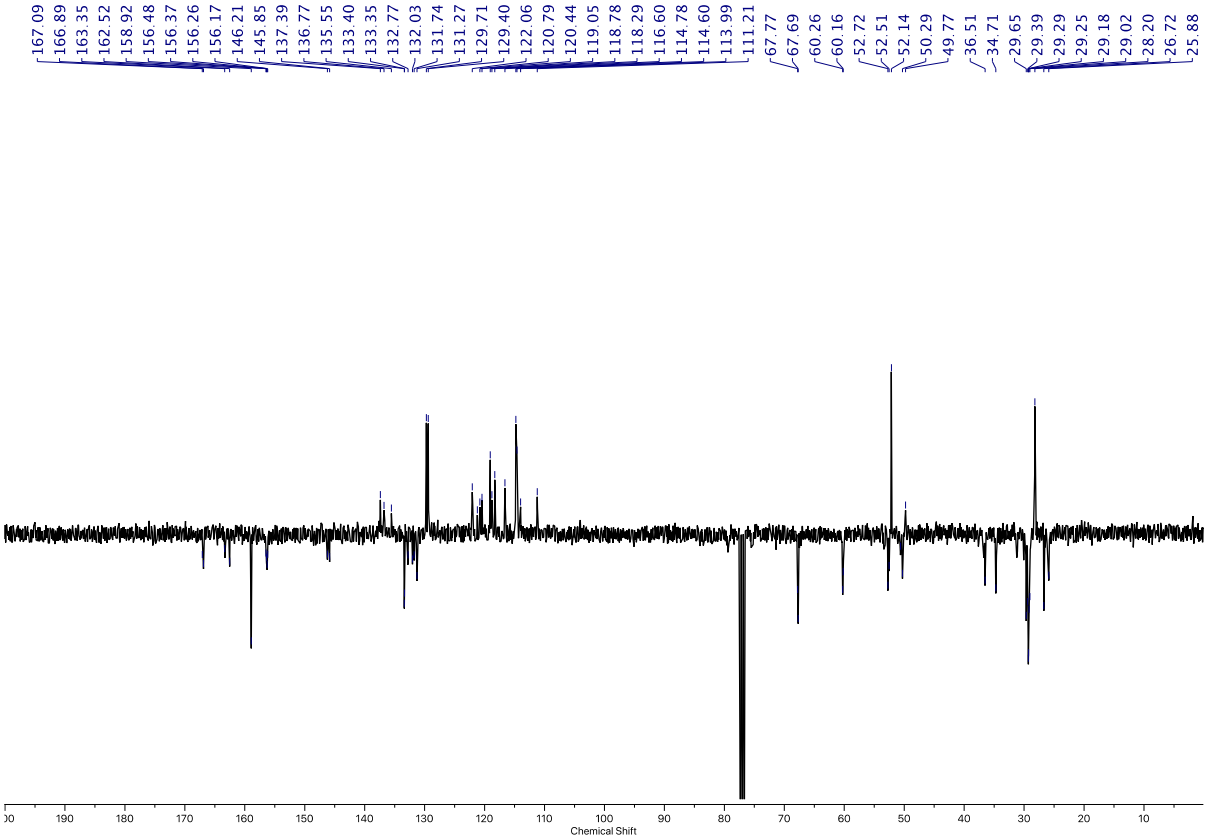

Figure 2.70 - JMOD NMR ($CDCl_3$, 101 MHz) of (S_{ma},$R_{co\text{-}c}$)-**3**.

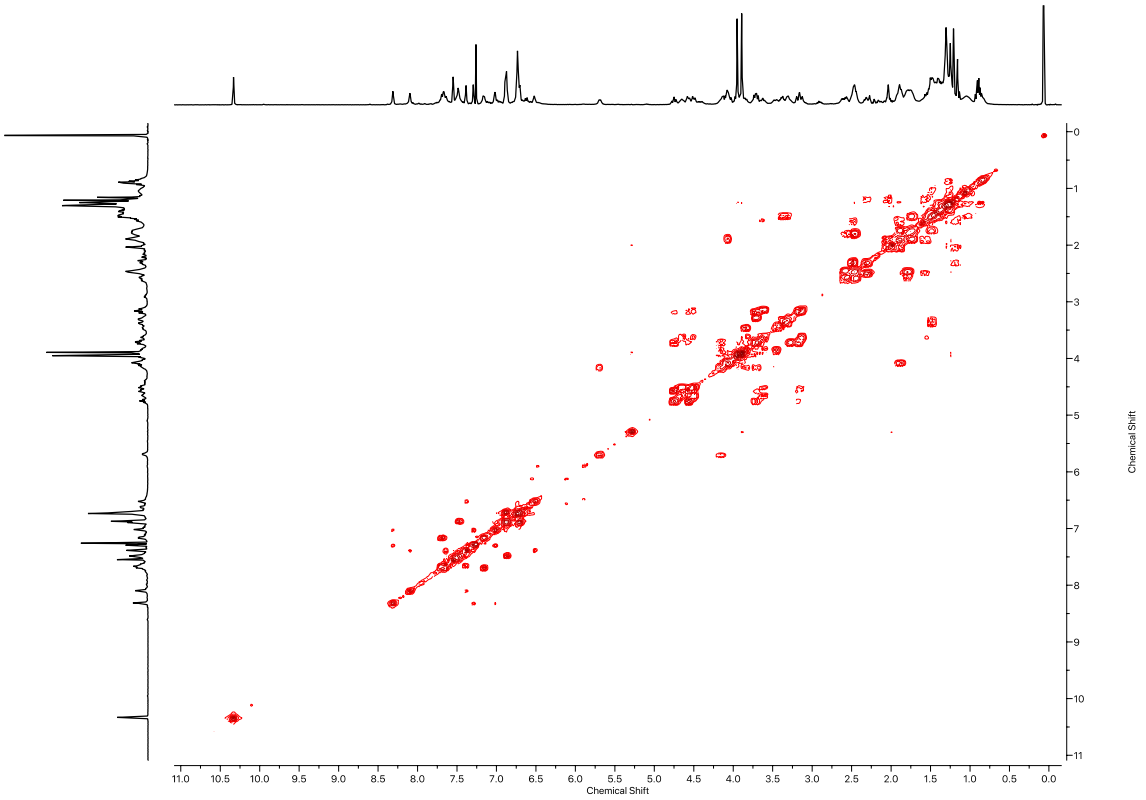

Figure 2.71 - ^{1}H COSY NMR ($CDCl_3$, 400 MHz) of (S_{ma},$R_{co\text{-}c}$)-**3**.

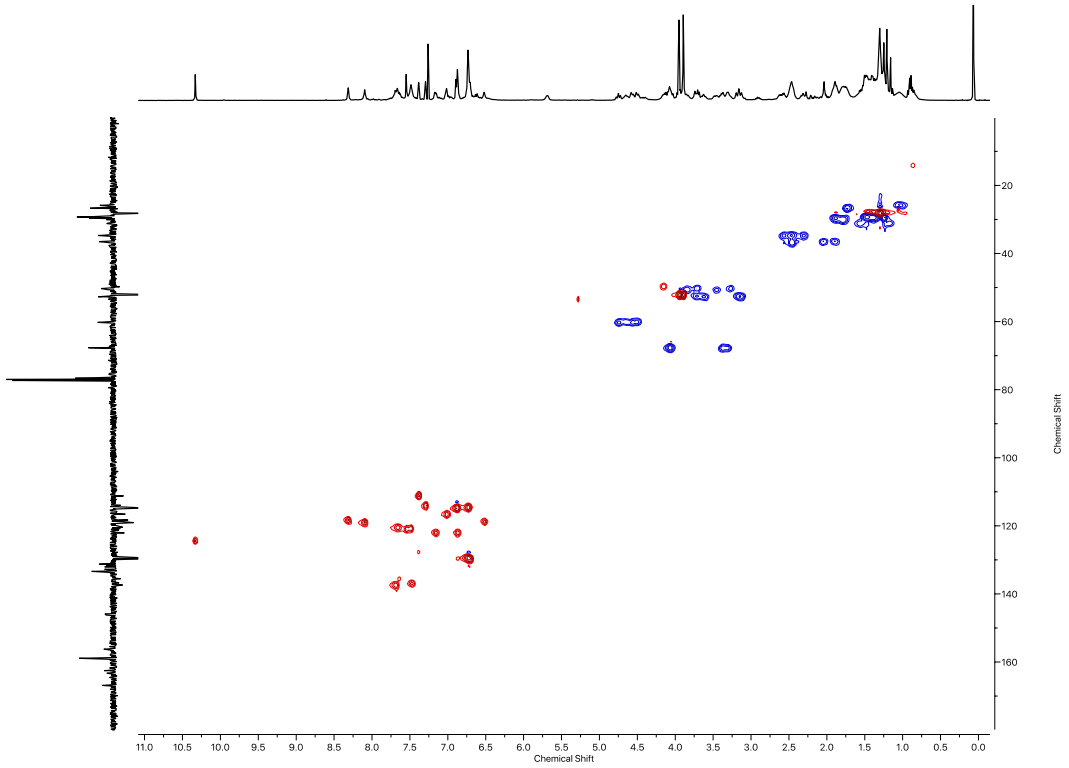

Figure 2.72 - HSQC NMR ($CDCl_3$, 400 MHz) of (S_{ma},$R_{co\text{-}c}$)-**3**.

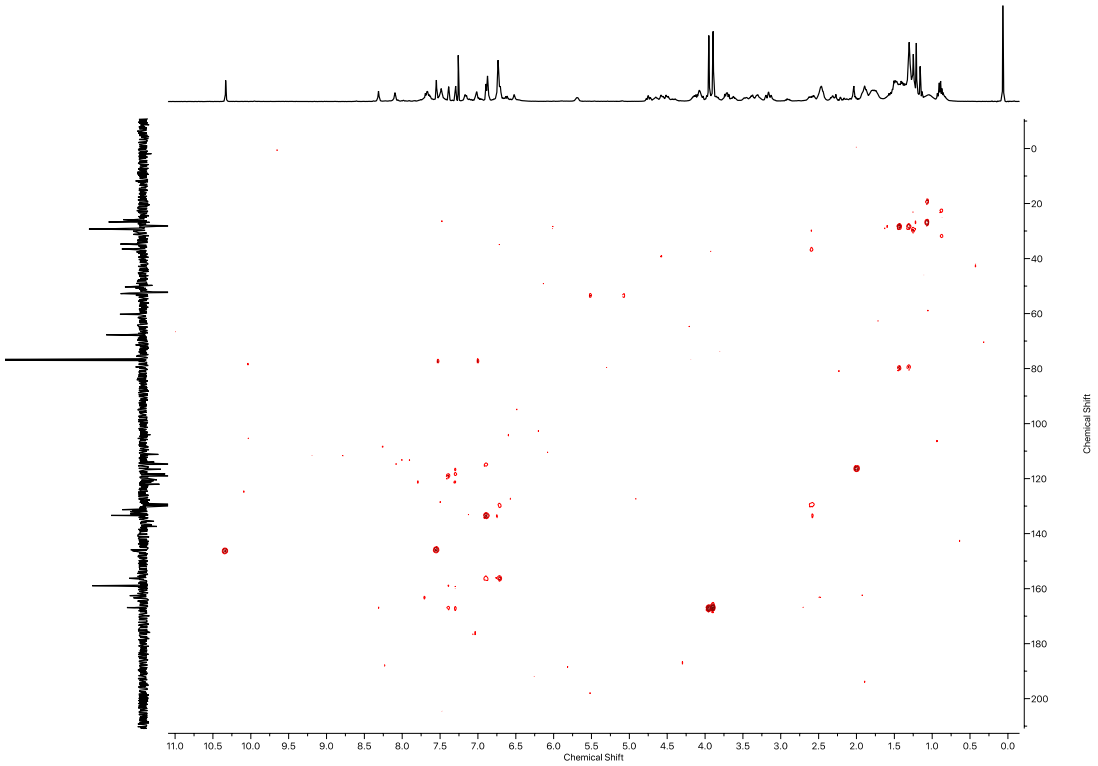

Figure 2.73 - HMBC NMR ($CDCl_3$, 400 MHz) of (S_{ma},$R_{co\text{-}c}$)-**3**.

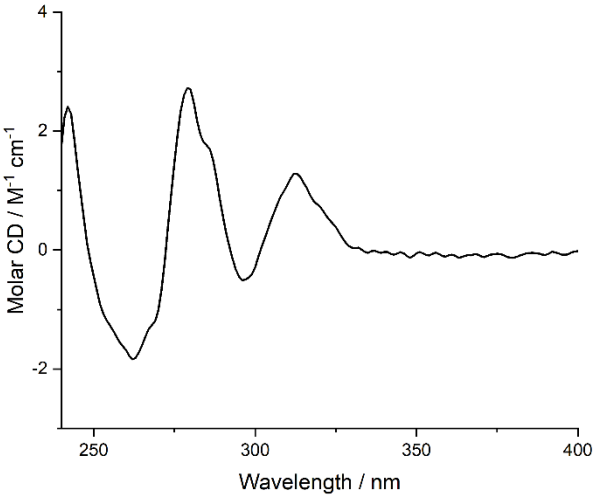

Figure 2.74 - Circular Dichroism Spectra of (S_{ma},$R_{co\text{-}c}$)-**3** (19 µM) at 293 K in $CHCl_3$.

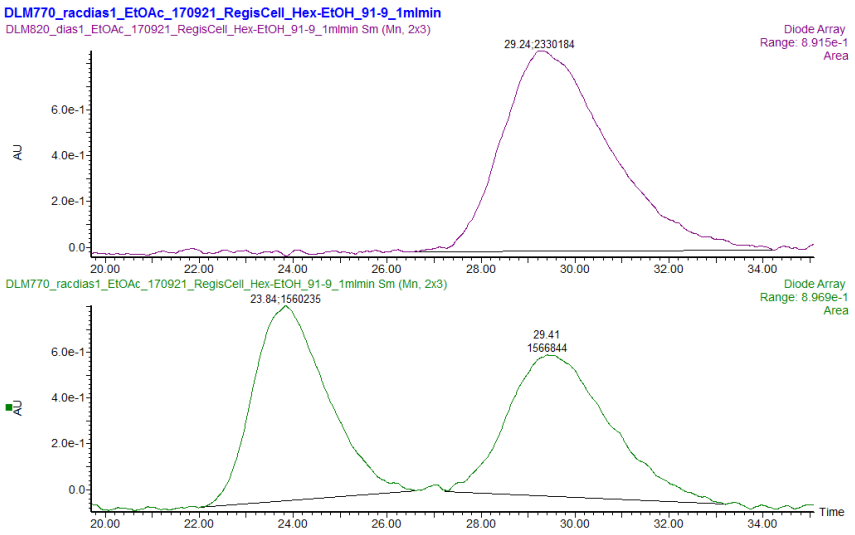

Figure 2.75 - CSP-HPLC of (S_{ma},$R_{co\text{-}c}$)-**3** (loaded in EtOAc). RegisCell, *n*-hexane-EtOH 91 : 9, flowrate 1 mLmin^{-1}. (top) (S_{ma},$R_{co\text{-}c}$)-**3** (29.24 min, 2330184, >99.9%), (R_{ma},$S_{co\text{-}c}$)-**3** (not observed). (bottom) *rac*-**3**, (R_{ma},$S_{co\text{-}c}$)-**3** (23.84 min, 1560235, 49.9%), (S_{ma},$R_{co\text{-}c}$)-**3** (29.41 min, 1566844, 50.1%).

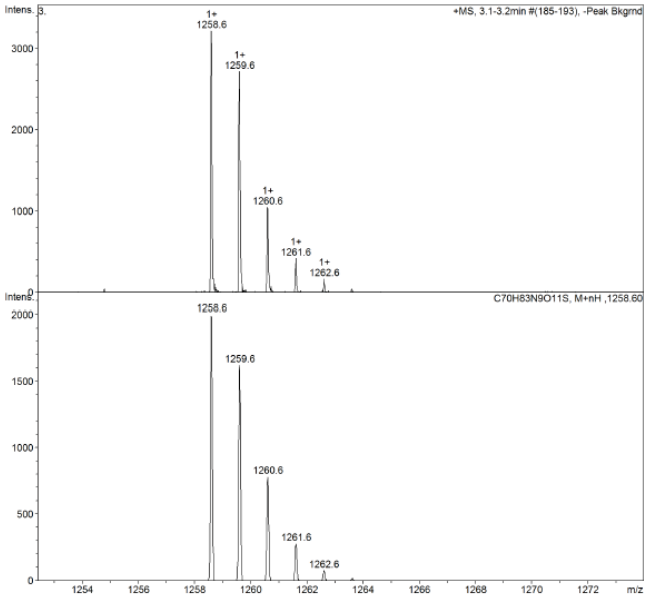

Figure 2.76 - Observed (top) and calculated (bottom) isotopic patterns for (S_{ma},$R_{co\text{-}c}$)-**3**.

Catenane ($R_{co\text{-}c}$)-5

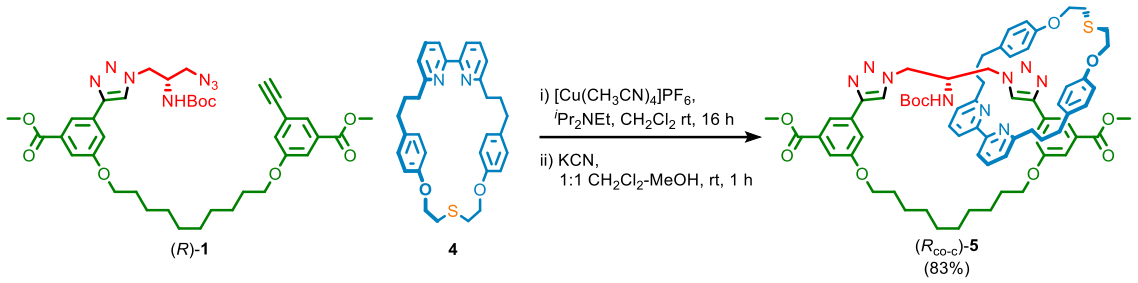

To a stirred solution of **4** (20.0 mg, 0.039 mmol, 1.00 eq.), $[Cu(CH_3CN)_4]PF_6$ (14.3 mg, 0.039 mmol, 0.98 eq.), and DIPEA (14 µL, 0.78 mmol, 2.00 eq.) in CH_2Cl_2 (4.1 mL) was added a solution of (*R*)-**1** (31.6 mg, 0.043 mmol, 1.1 eq.) in CH_2Cl_2 (1.60 mL) via syringe pump over a 16 h period. MeOH (3 mL) was then added, followed by KCN (25.0 mg, 0.39 mmol, 10.0 eq.). After stirring for 1 h, and the loss of deep orange colour, the mixture was diluted with CH_2Cl_2 (15 mL) and H_2O (10 mL). The aqueous and organic phases were separated, and the aqueous was extracted with CH_2Cl_2 (2 x 15 mL). The combined organics were washed with brine (10 mL), dried over $MgSO_4$ and concentrated *in vacuo*. The residue was purified by column chromatography (SiO_2, DCM-EtOAc 0→20%) to yield ($R_{co\text{-}c}$)-**5** (40.0 mg, 0.032 mmol, 83%) as an off-white foam. See 4.1 for a discussion of stereochemical assignment.

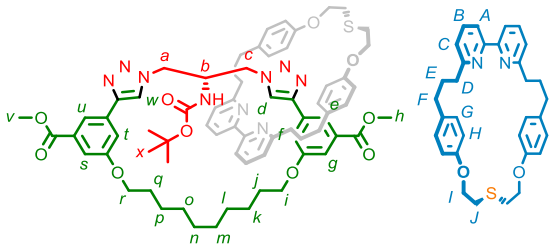

δ_H (400 MHz, $CDCl_3$) 10.07 (1H, s, H_d), 8.33 (1H, s, H_e), 8.09 (1H, s, H_u), 7.92 (1H, s, H_w), 7.65 – 7.54 (2H, m, H_B, $H_{B'}$), 7.53 – 7.46 (2H, m, H_A, $H_{A'}$), 7.41 (1H, dd, J = 2.5, 1.4, H_s), 7.33 (1H, dd, J = 2.5, 1.4, H_g), 7.09 (1H, d, J = 7.4, H_C), 7.06 (1H, dd, J = 2.6, 1.5, H_f), 6.99 (1H, dd, J = 6.3, 2.3, $H_{C'}$), 6.75 – 6.70 (2H, m, H_G), 6.68 – 6.59 (6H, m, $H_{G'}$, H_H, $H_{H'}$), 6.52 (1H, t, J = 2.0, H_t), 5.39 (1H, s, H_{NHBoc}), 4.65 – 4.45 (2H, m, H_l, $H_{l'}$), 4.40 – 4.22 (2H,m, H_l, $H_{l'}$), 4.08 (2H, t, J = 5.4, H_r), 4.00 – 3.75 (9H, m, H_a, H_b, H_h, H_v), 3.63 – 3.53 (2H, m, H_c), 3.50 – 3.42 (2H, m, H_i), 3.38 – 3.11 (4H, m, H_J, $H_{J'}$), 2.57 – 2.10 (8H, m, H_D, $H_{D'}$, H_F, $H_{F'}$), 1.95 – 1.82 (2H, m, H_q), 1.82 – 1.62 (4H, m, H_E, $H_{E'}$), 1.61 – 1.22 (23H, m, H_x, $H_{j\text{-}p}$). δ_C (101 MHz, $CDCl_3$) 167.1, 166.8, 162.6, 162.5, 158.9, 158.9, 156.7, 156.5, 156.4, 156.2, 154.4, 146.3, 146.0, 137.1, 136.9, 132.7, 132.6, 132.3, 131.8, 131.6, 131.3, 129.0, 128.9, 125.0, 122.0, 121.9, 120.8, 120.6, 119.3, 118.9, 118.6, 117.1, 115.0, 114.7, 113.8, 111.6, 68.1, 67.9, 67.8, 67.8, 52.2, 52.2, 50.8, 49.4, 49.1, 36.6, 34.6, 34.6, 31.8, 30.8, 30.4, 29.5, 29.4, 29.3, 29.2, 29.2, 29.1, 28.3, 26.7, 26.0. LR-ESI-MS (+ve) m/z = 1242.6 $[M+H]^+$.

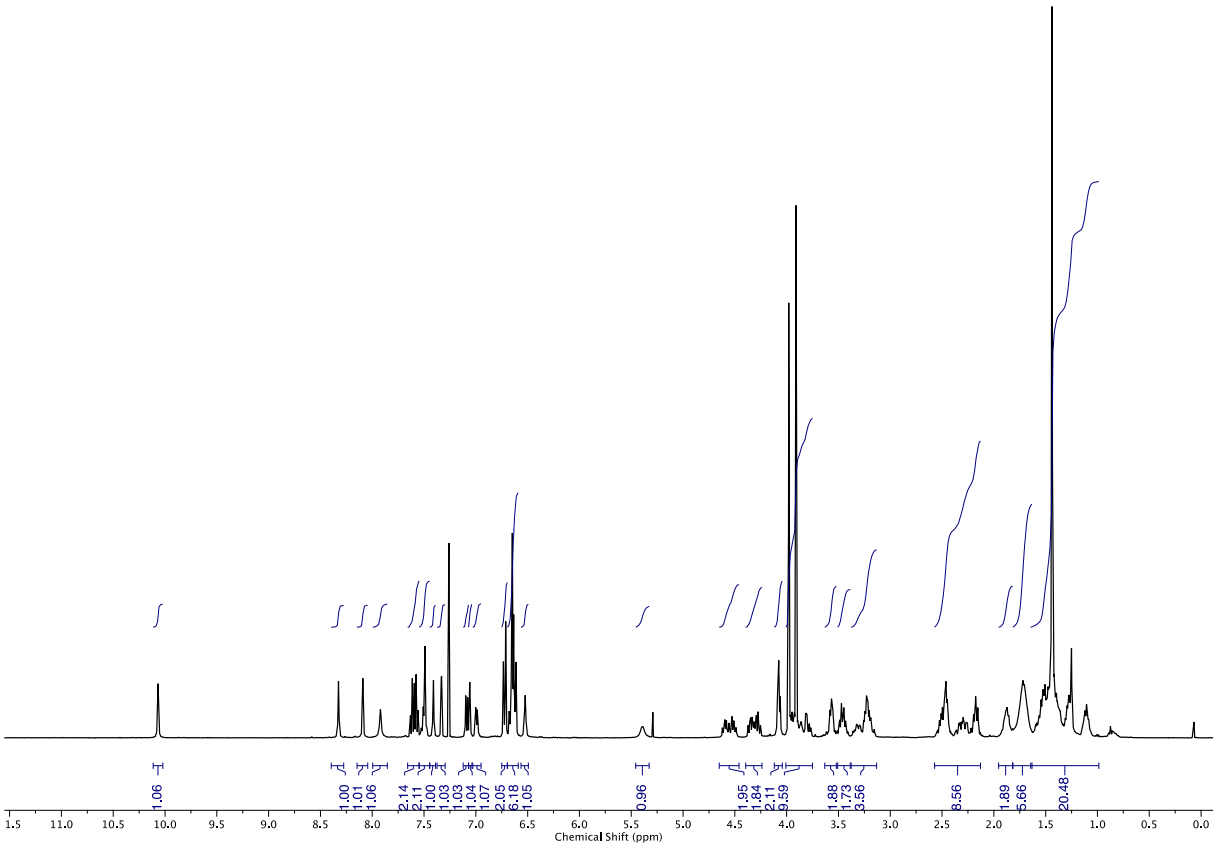

Figure 2.77 - ^{1}H NMR ($CDCl_3$, 400 MHz) of ($R_{co\text{-}c}$)-**5**.

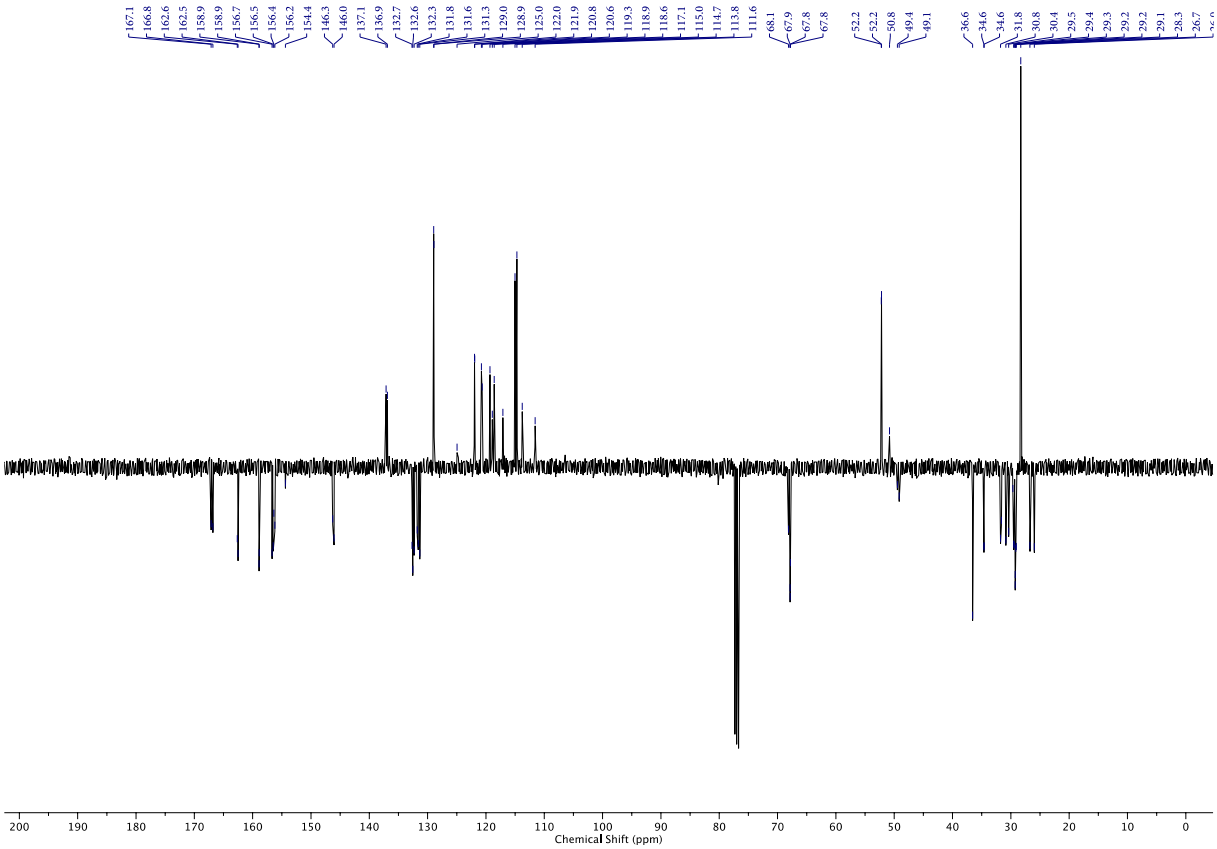

Figure 2.78 - JMOD NMR ($CDCl_3$, 101 MHz) of ($R_{co\text{-}c}$)-**5**.

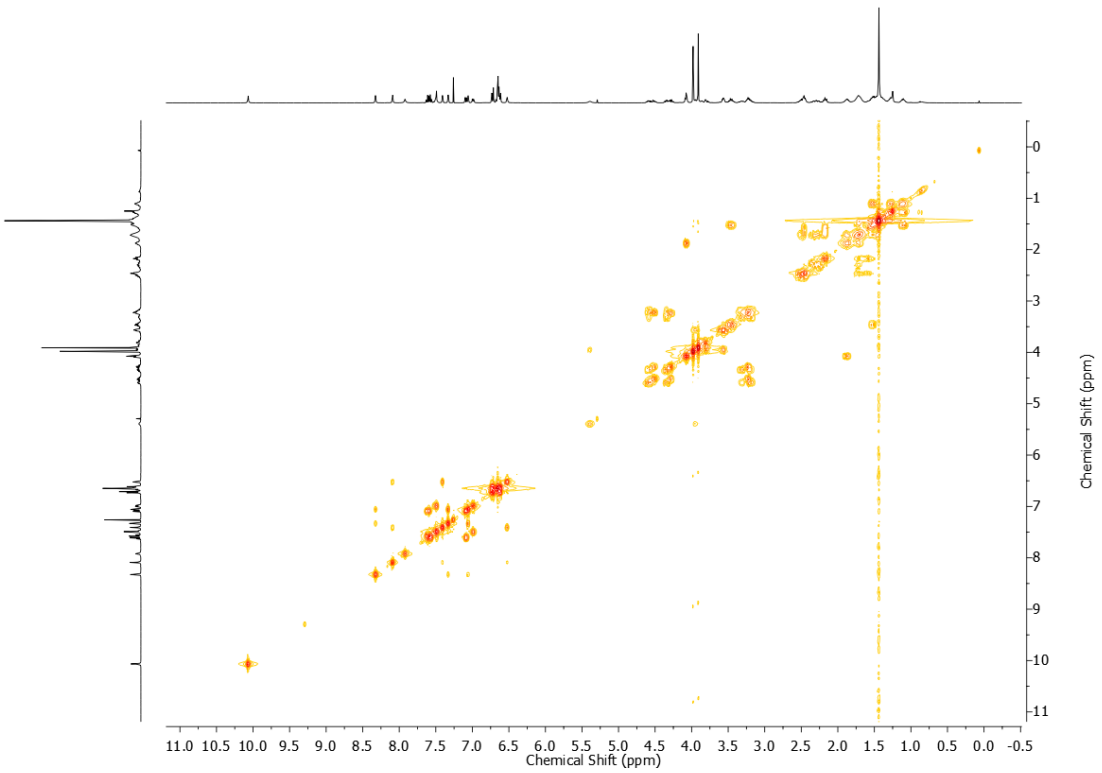

Figure 2.79 - ^{1}H COSY NMR ($CDCl_3$, 400 MHz) of ($R_{co\text{-}c}$)-**5**.

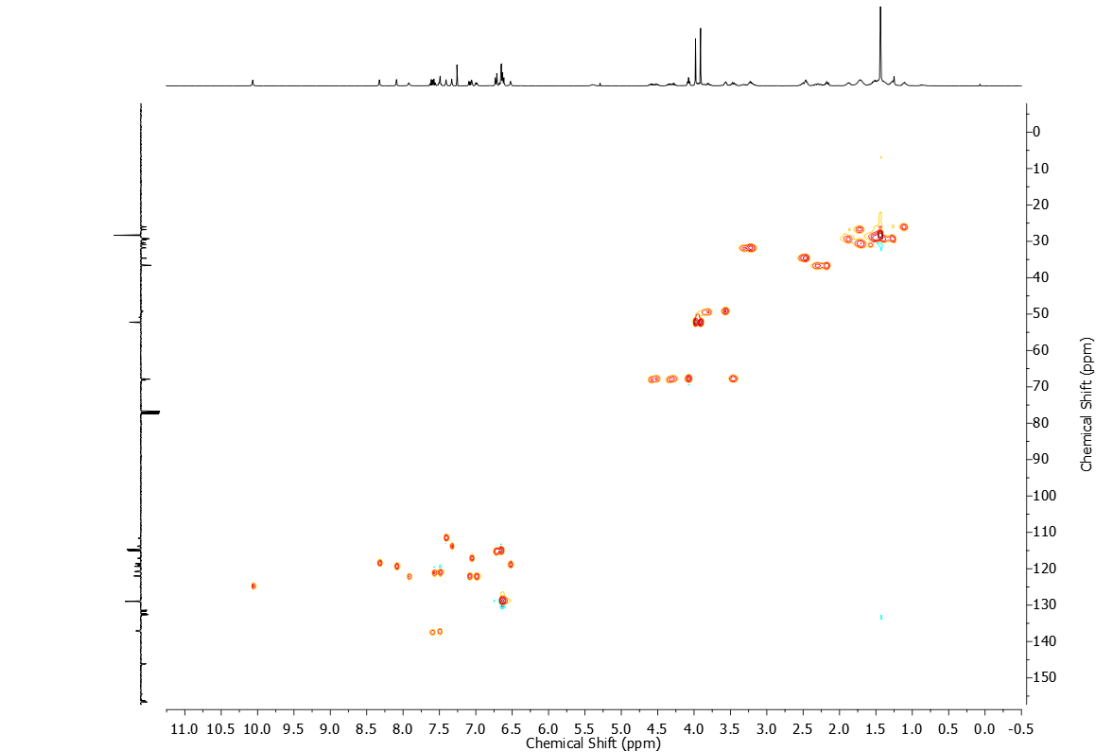

Figure 2.80 - HSQC NMR ($CDCl_3$, 400 MHz) of ($R_{co\text{-}c}$)-**5**.

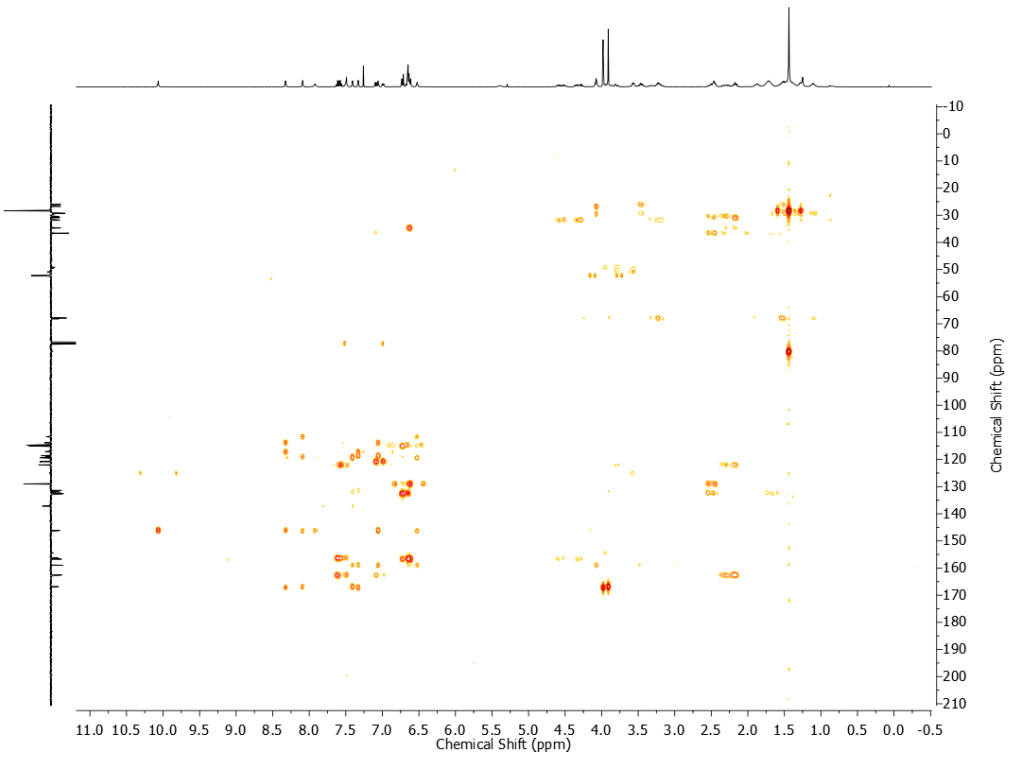

Figure 2.81 - HMBC NMR ($CDCl_3$, 400 MHz) of ($R_{co\text{-}c}$)-**5**.

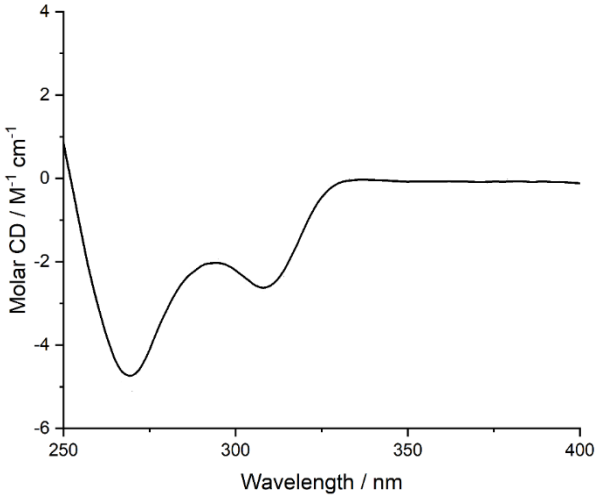

Figure 2.82 - Circular Dichroism Spectrum of ($R_{co\text{-}c}$)-**5** (29 μM) at 293 K in $CHCl_3$.

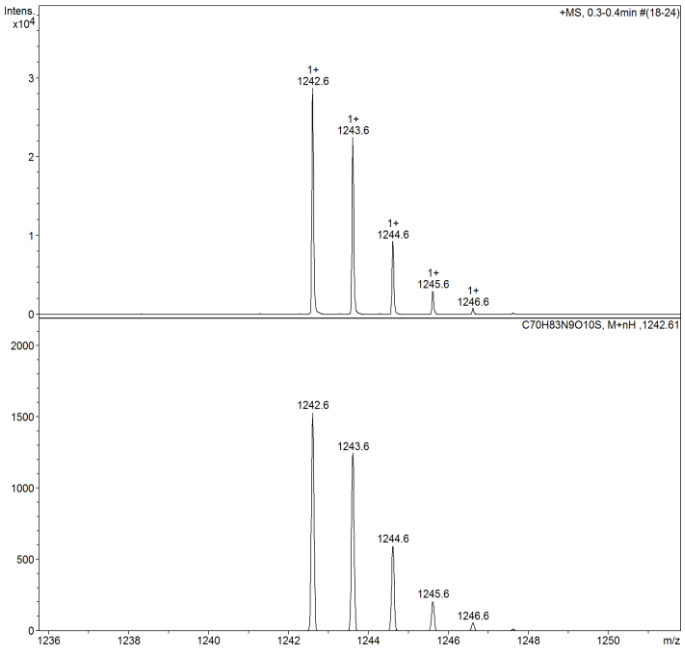

Figure 2.83 - Observed (top) and calculated (bottom) isotopic patterns for ($R_{co\text{-}c}$)-**5**.

Catenane (R_{ma},$R_{co\text{-}c}$)-3

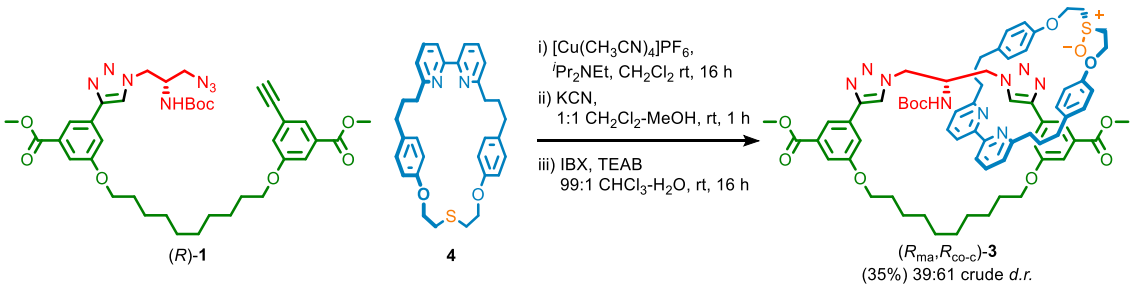

A CEM MW vial was charged with macrocycle **4** (27.3 mg, 0.053 mmol, 1.0 eq.) and $[Cu(CH_3CN)_4]PF_6$ (19.5 mg, 0.052 mmol, 0.98 eq.) and purged with N_2. CH_2Cl_2 (5.5 mL) and $^iPr_2NEt$ (19 µL, 0.11 mmol, 2.0 eq.) were added followed by a solution of pre-macrocycle (*R*)-**1** (43.0 mg, 0.059 mmol, 1.0 eq.) in CH_2Cl_2 (2.2 mL) at ambient temperature over 16 h. Then, MeOH (2.9 mL) and KCN as a solid (35 mg, 0.53 mmol, 10.0 eq.) were added and the resulting mixture was stirred vigorously for 1 h. The crude mixture was diluted with CH_2Cl_2 (5 mL) and washed with H_2O in two portions (10 mL and 5 mL), with separation of aqueous and organic phases. The combined aqueous phase was then extracted with CH_2Cl_2 (3 x 5 mL) and the combined organics were washed with brine (10 mL), dried over $MgSO_4$ and concentrated *in vacuo*. The residue corresponding to ($R_{co\text{-}c}$)-**5** was re-dissolved in 99:1 $CHCl_3/H_2O$ (0.67 µL), then tetraethylammonium bromide (12.3 mg, 0.058 mmol, 1.1 eq.) and IBX (30% of stabilizer, 23.3 mg, 0.058 mmol, 1.1 eq.) were added. The resulting suspension was stirred for 16 h at ambient temperature. The reaction mixture was

then diluted with CH_2Cl_2 (5 mL), washed with 10% $NaHSO_3$ (5 mL), saturated $NaHCO_3$ (5 mL) and brine (5 mL), extracting all aqueous layers with CH_2Cl_2 (2 x 5 mL). The combined organics were dried over $MgSO_4$, filtered, and concentrated *in vacuo*. The residue was purified by column chromatography (SiO_2, CH_2Cl_2-CH_3CN 0→100%; CH_3CN-MeOH 0→5%) to yield (R_{ma},$R_{co\text{-}c}$)-**3** (23.0 mg, 0.0186 mmol, 35%, second eluting isomer) as an off-white foam and (S_{ma},$R_{co\text{-}c}$)-**3** (16.0 mg, 0.013 mmol, 24%, first eluting isomer) as a colorless oil.

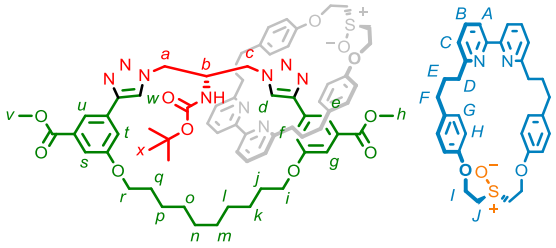

δ_H (400 MHz, $CDCl_3$) 9.96 (1H, s, H_d), 8.06 (2H, s, H_e, H_u), 7.67 – 7.38 (6H, m, $H_{A/A'}$, $H_{B/B'}$, H_w, H_s), 7.34 (1H, dd, J = 2.4, 1.5, H_g), 7.16 – 7.06 (2H, m, $H_{C/C'}$, H_f), 6.98 (1H, d, J = 7.6, $H_{C/C'}$), 6.79 – 6.45 (9H, m, $H_{G/G'}$, $H_{H/H'}$, H_t), 5.45 (1H, d, J = 3.9, -N*H*Boc), 4.76 – 4.49 (4H, m, $H_{I/I'}$), 4.30 (1H, m, H_c), 4.13 (2H, t, J = 5.4, H_r), 4.03 (3H, s, H_h), 3.99 – 3.65 (9H, m, H_v, $H_{J/J'}$, H_a, H_b, $H_{c'}$), 3.53 – 3.25 (4H, m, H_i, $H_{J/J'}$), 2.52 – 2.10 (12H, m, H_D, H_E, H_F, $H_{D'}$, $H_{E'}$, $H_{F'}$), 1.97 – 1.81 (2H, m, H_q), 1.58 – 1.13 (23H, m, $H_{j\text{-}p}$, H_x). δ_C (101 MHz, $CDCl_3$) 167.3, 167.0, 163.0, 162.7, 159.1, 159.1, 156.5, 156.2, 155.9, 155.9, 146.6, 146.3, 137.3, 137.0, 133.3, 133.0, 132.5, 132.0, 131.8, 131.4, 129.1, 128.9, 122.3, 122.1, 120.6, 119.4, 119.1, 118.9, 116.7, 115.1, 115.1, 114.7, 111.9, 80.6, 77.5, 77.2, 76.8, 68.2, 67.8, 61.2, 61.1, 52.4, 52.0, 49.3, 36.9, 36.8, 34.8, 34.7, 30.9, 30.8, 29.8, 29.5, 29.4, 29.2, 28.5, 26.8, 26.1. LR-ESI-MS (+ve) = 1258.6 $[M+H]^+$.

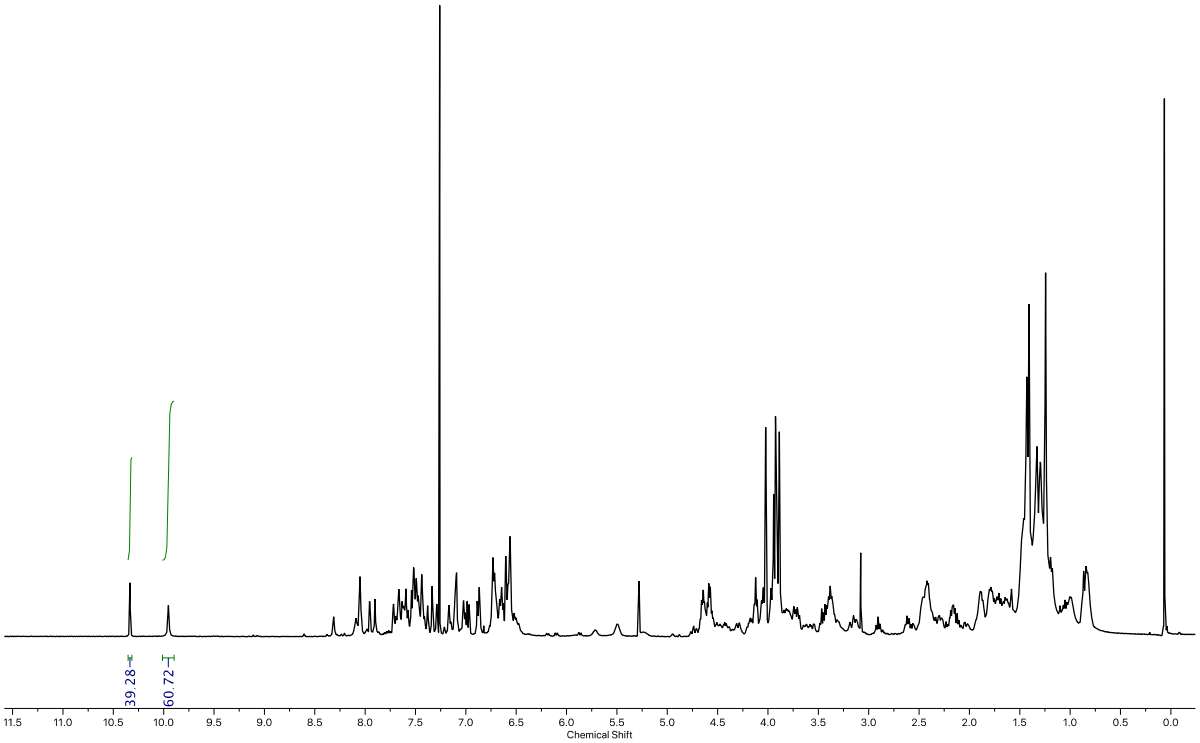

Figure 2.84 - ^{1}H NMR ($CDCl_3$, 400 MHz) of crude oxidation leading to major (R_{ma},$R_{co\text{-}c}$)-**3**. Integration of (S_{ma},$R_{co\text{-}c}$)-**3** (10.34 ppm, $\boldsymbol{H}_d$, 39.28H) and (R_{ma},$R_{co\text{-}c}$)-**3** (9.95 ppm, $\boldsymbol{H}_d$, 60.72H).

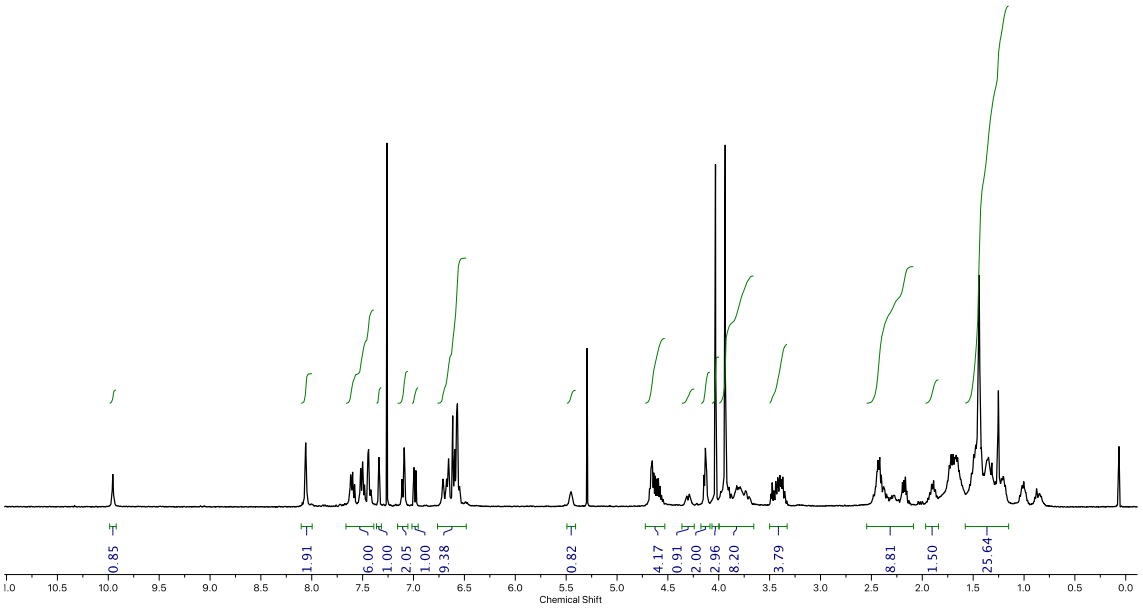

Figure 2.85 - ^{1}H NMR ($CDCl_3$, 400 MHz) of (R_{ma},$R_{co\text{-}c}$)-**3**.

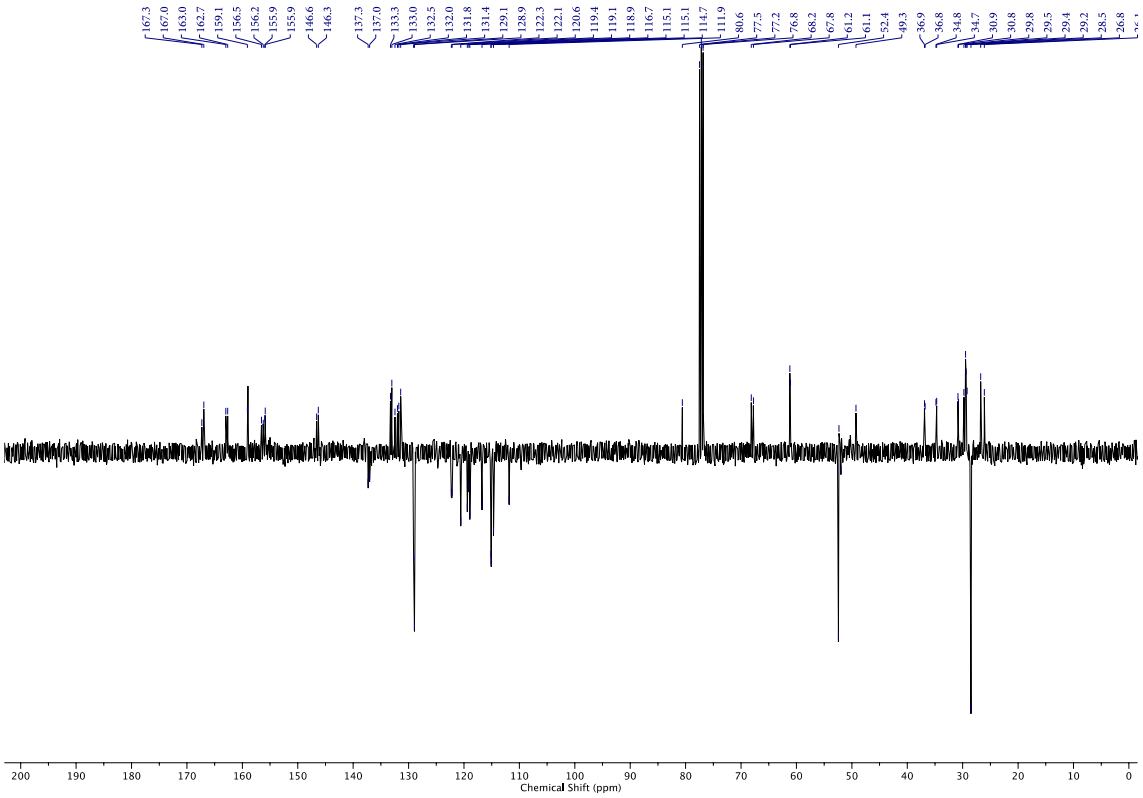

Figure 2.86 - JMOD NMR ($CDCl_3$, 101 MHz) of (R_{ma},$R_{co\text{-}c}$)-**3**.

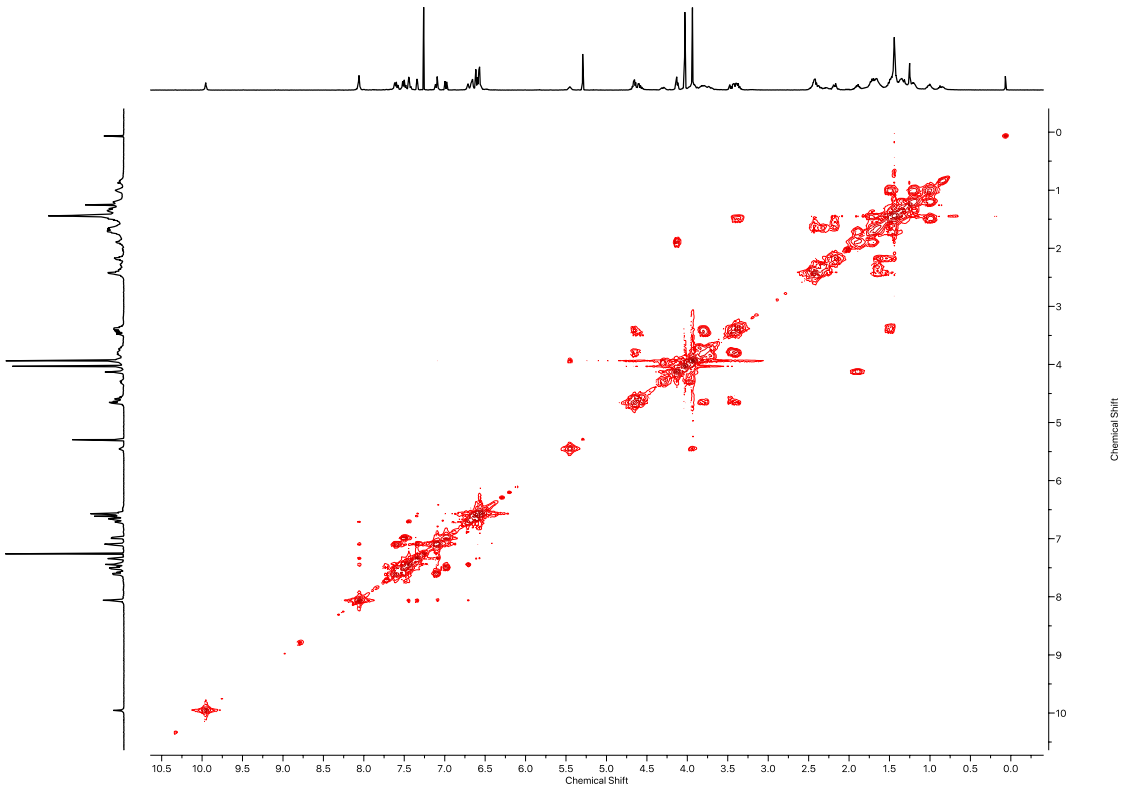

Figure 2.87 - ^{1}H COSY NMR ($CDCl_3$, 400 MHz) of (R_{ma},$R_{co\text{-}c}$)-**3**.

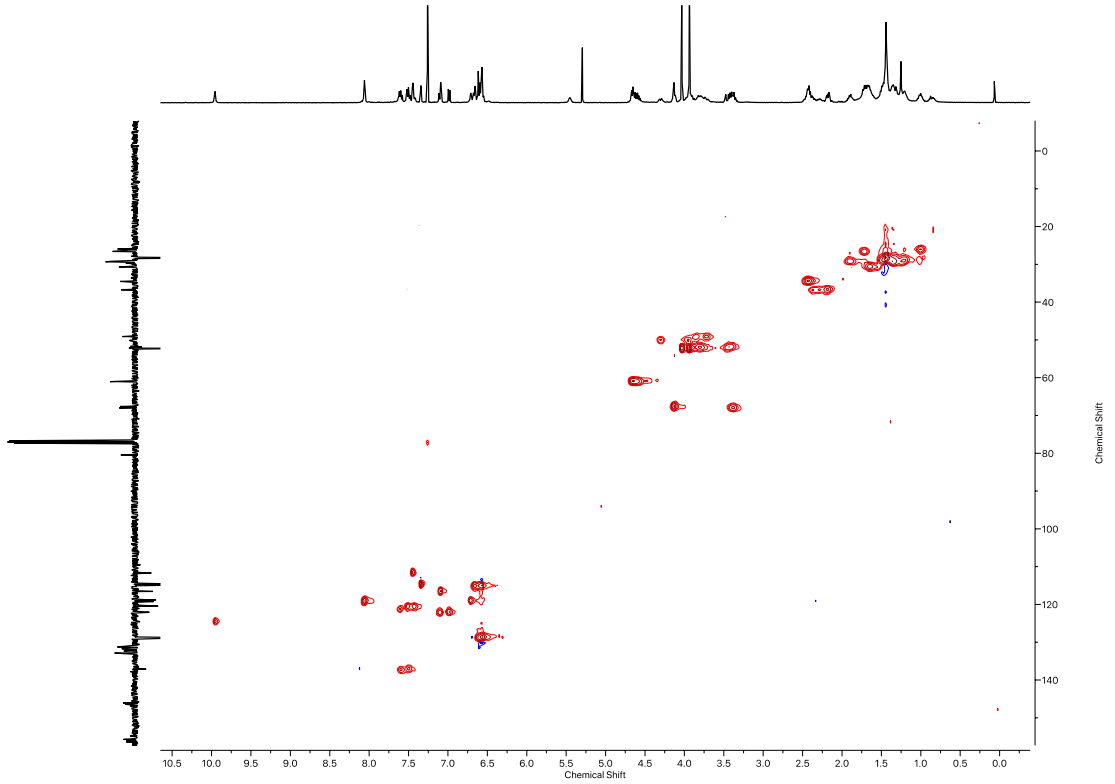

Figure 2.88 - HSQC NMR ($CDCl_3$, 400 MHz) of (R_{ma},$R_{co\text{-}c}$)-**3**.

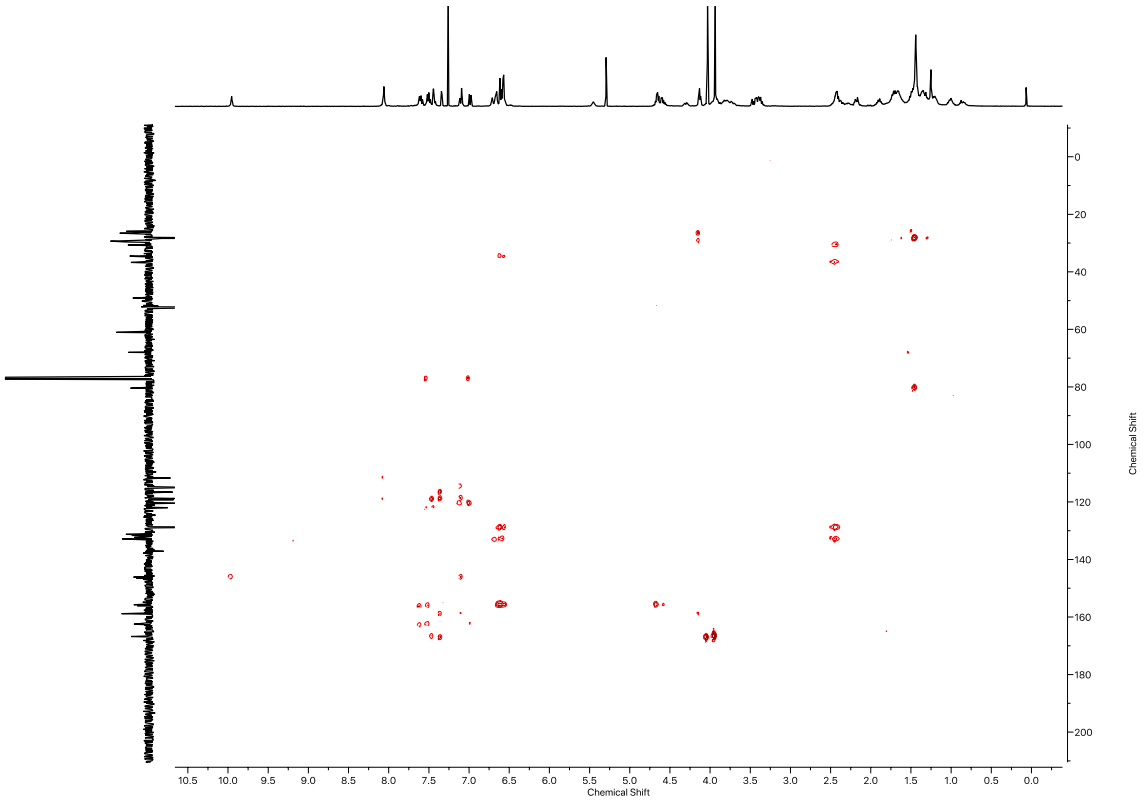

Figure 2.89 - HMBC NMR ($CDCl_3$, 400 MHz) of (R_{ma},$R_{co\text{-}c}$)-**3**.

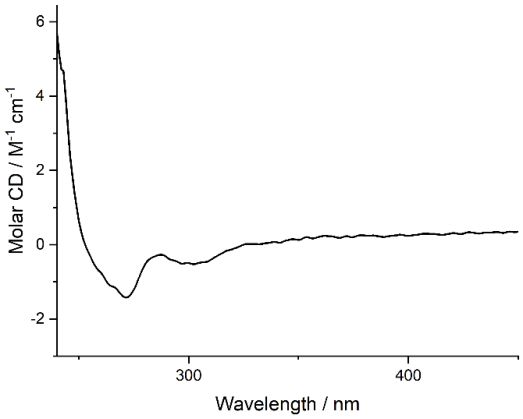

Figure 2.90 - Circular Dichroism Spectra of (R_{ma},$R_{co\text{-}c}$)-**3** (31 µM) at 293 K in $CHCl_3$.

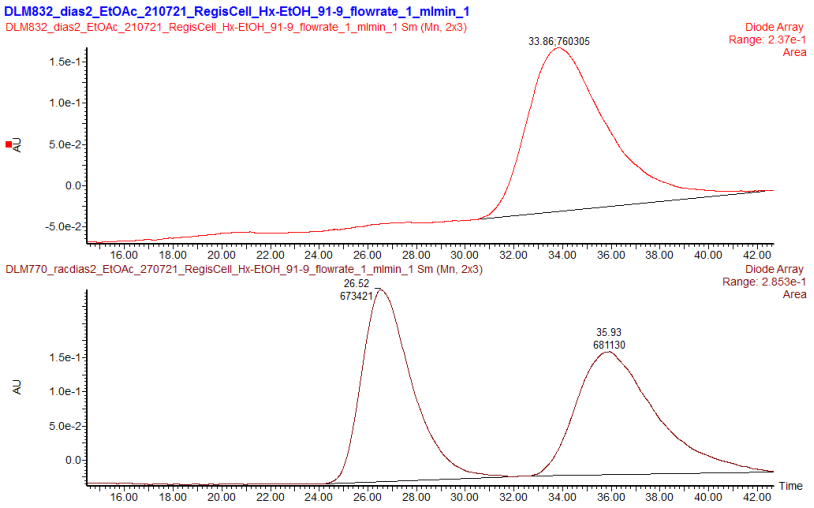

Figure 2.91 - CSP-HPLC of (R_{ma},$R_{co\text{-}c}$)-**3** (loaded in EtOAc). RegisCell, *n*-hexane-EtOH 91 : 9, flowrate 1 $mLmin^{-1}$. (top) (R_{ma},$R_{co\text{-}c}$)-**3** (33.86 min, 760305, >99.9%), (S_{ma},$S_{co\text{-}c}$)-**3** (not observed). (bottom) *rac*-**3**, (S_{ma},$S_{co\text{-}c}$)-**3** (26.52 min, 673421, 49.7%), (R_{ma},$R_{co\text{-}c}$)-**3** (35.93 min, 681130, 50.3%).

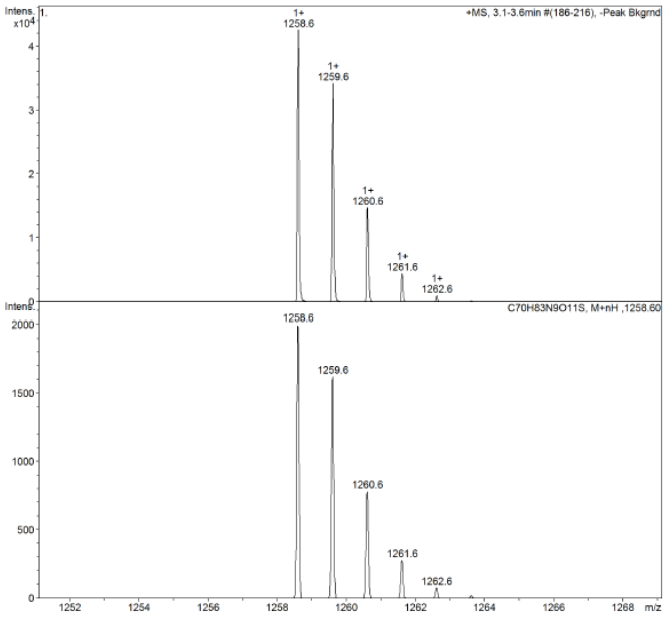

Figure 2.92 - Observed (top) and calculated (bottom) isotopic patterns for (R_{ma},$R_{co\text{-}c}$)-**3**.

Macrocycle S13

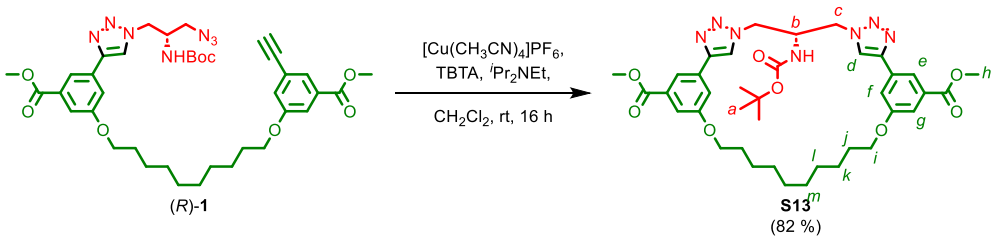

A CEM MW vial was charged with TBTA (3.60 mg, 0.007 mmol, 0.2 eq.), $[Cu(CH_3CN)_4]PF_6$ (2.5 mg, 0.007 mmol, 0.2 eq.), $^{i}Pr_2NEt$ (12 µL, 0.068 mmol, 2.0 eq.), and CH_2Cl_2 (0.5 mL) and was purged with N_2. A solution of pre-macrocycle (*R*)-**1** (25 mg, 0.034 mmol, 1.0 eq.) in CH_2Cl_2 (0.2 mL) was added at ambient temperature over 16 h, and then stirred at ambient temperature for 1 h. The crude mixture was diluted with CH_2Cl_2 (5 mL) and washed with EDTA-NH_3 solution (2 x 10 mL), and the combined organics were washed with brine (10 mL), dried over $MgSO_4$ and concentrated *in vacuo*. The residue was purified by column chromatography (SiO_2, petrol-EtOAc 0→50) to yield macrocycle **S13** (20.3 mg, 0.0277 mmol, 82%) as a white foam.

δ_H ($CDCl_3$, 400 MHz) 8.09 (2H, dd, *J* = 1.3, H_e), 7.96 (2H, s, H_d), 7.52 (2H, m, H_g), 7.49 (2H, m, H_f), 5.9 (1H, d, H_{NHBoc}), 4.55 (3H, m, H_c, H_b), 4.45 (2H, dd, *J* = 16, 8, $H_{c'}$), 4.06 (2H, m, H_i), 3.93 (3H, s, H_h), 1.81 (4H, quint, *J* = 8.0, H_j), 1.48 (13H, m, H_a, H_k), 1.37 (8H, m, H_l, H_m); δ_C ($CDCl_3$, 101 MHz) 166.6, 159.5, 147.1, 132.2, 131.3, 121.9, 118.9, 116.5, 115.5, 68.5, 52.3, 50.8, 50.1, 29.1, 28.9, 28.3, 25.9. LR-ESI-MS (+ve) $[M+H]^+$ m/z (%) 732.7 (100); HR-EI-MS (+ve) $[M+Na]^+$ m/z 754.3534 (calc. for $C_{38}H_{49}N_7O_8Na$ m/z 754.3535).

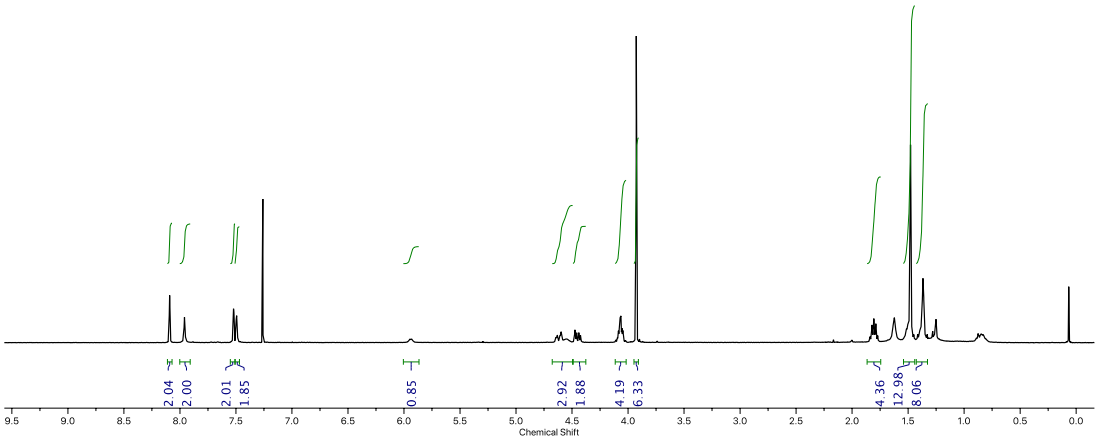

Figure 2.93 - ^{1}H NMR ($CDCl_3$, 400 MHz) of **S13**.

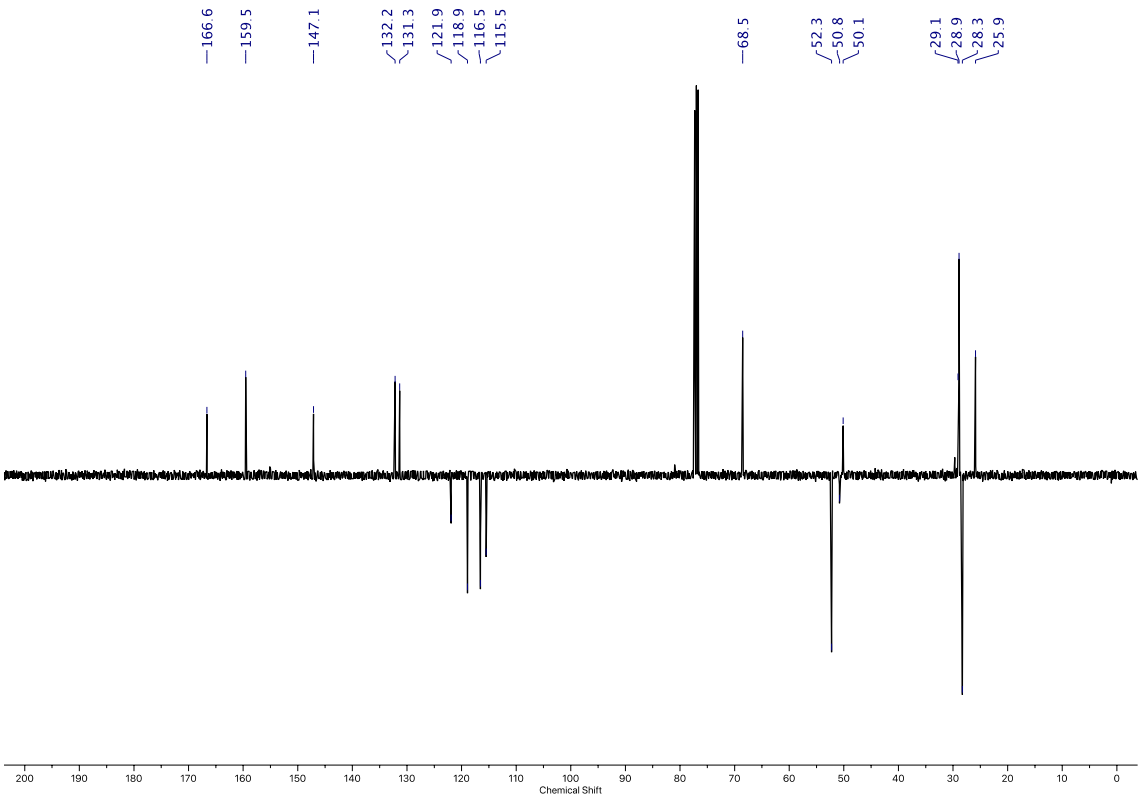

Figure 2.94 - JMOD NMR ($CDCl_3$, 101 MHz) of **S13**.

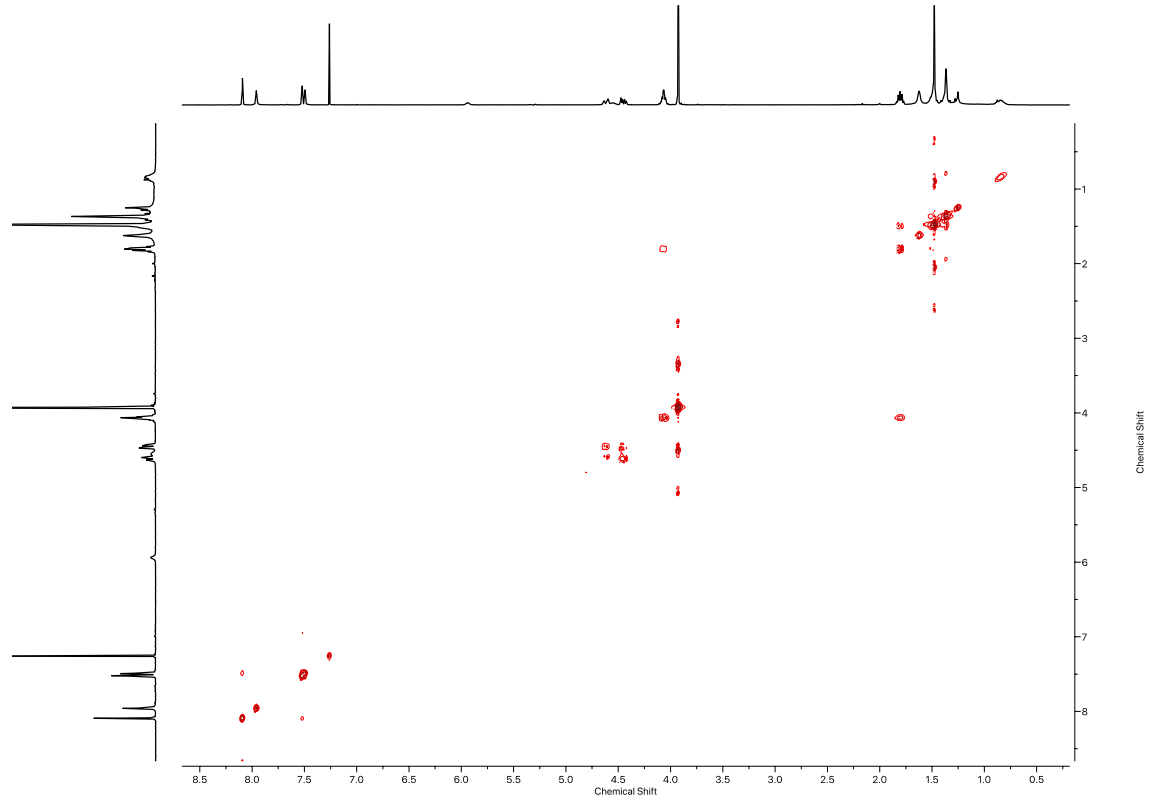

Figure 2.95 - ^{1}H COSY NMR ($CDCl_3$, 400 MHz) of **S13**.

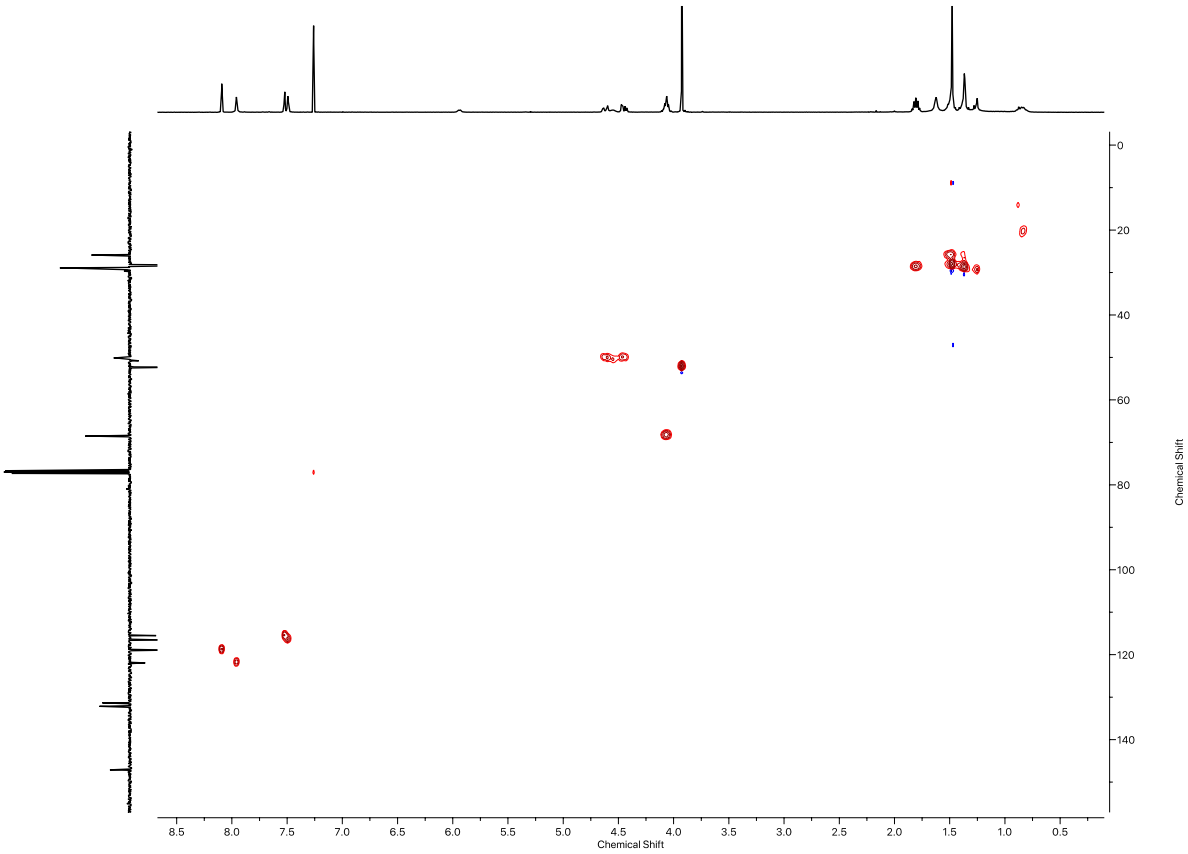

Figure 2.96 - HSQC NMR ($CDCl_3$, 400 MHz) of **S13**.

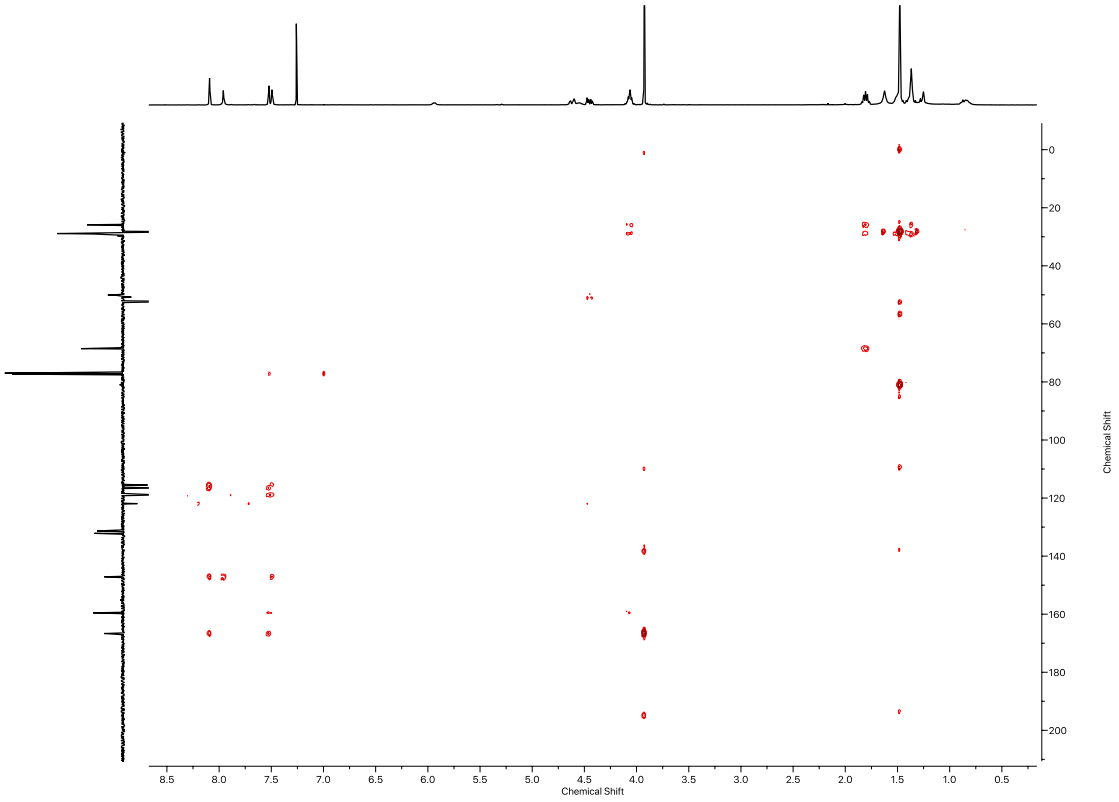

Figure 2.97 - HMBC NMR ($CDCl_3$, 400 MHz) of **S13**.

Synthesis of enantiomeric catenanes (S_{ma})-6 and (R_{ma})-6

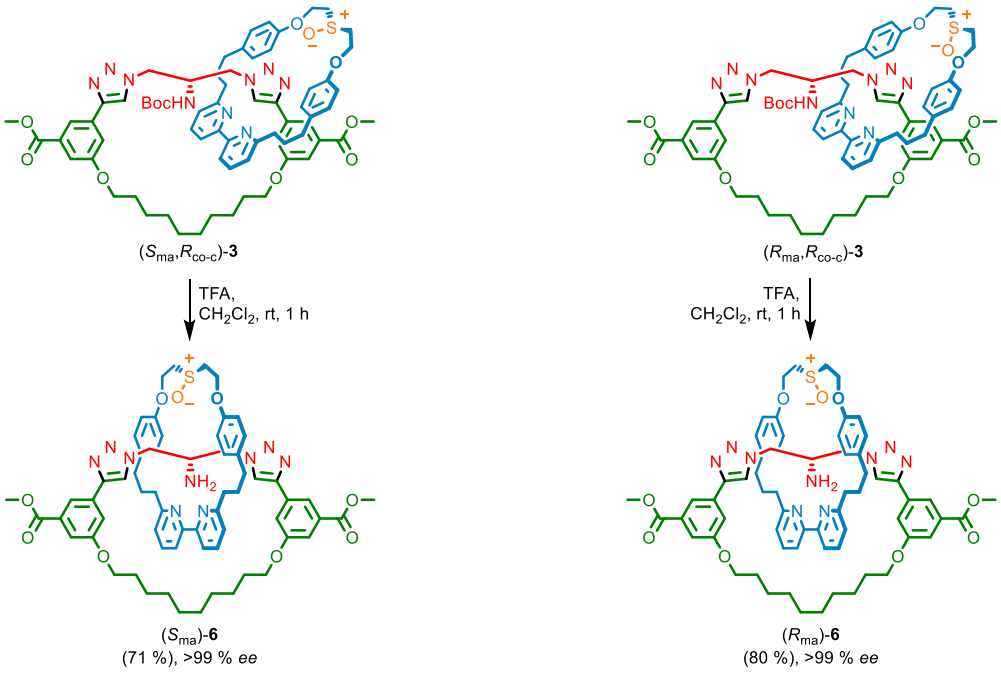

Scheme 2.4 - Synthetic route to mechanically axially chiral enantiomeric catenanes (R_{ma})-**6** and (S_{ma})-**6**.

Catenane (S_{ma})-6

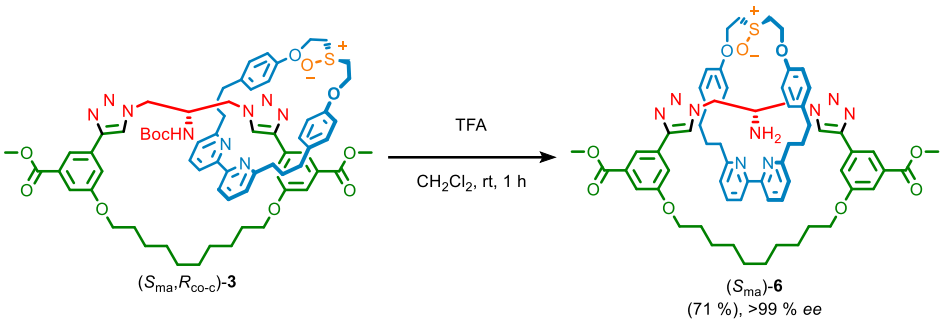

A solution of catenane (S_{ma},$R_{co\text{-}c}$)-**3** (35.7 mg, 0.028 mmol, 1.0 eq.) in CH_2Cl_2 (0.3 mL) was added TFA (65 µL, 0.85 mmol, 30 eq.) dropwise at 0 °C, then stirred at ambient temperature for 1 h. The reaction mixture was then diluted with CH_2Cl_2 (5 mL) and poured into saturated $NaHCO_3$ (5 mL). The aqueous phase was extracted with CH_2Cl_2 (3 x 6 mL) and combined organics were washed with brine (5 mL), dried over $MgSO_4$, filtered and concentrated *in vacuo*. The residue was purified by column chromatography (SiO_2, CH_2Cl_2-MeOH 0→15%) to yield catenane (S_{ma})-**6** (23.4 mg, 0.020 mmol, 71%) as a white foam. The mechanical stereochemistry of the product was assigned by observing that this cannot change during the removal of the Boc group (or if it does, that the resulting product would be racemic, which was not observed).

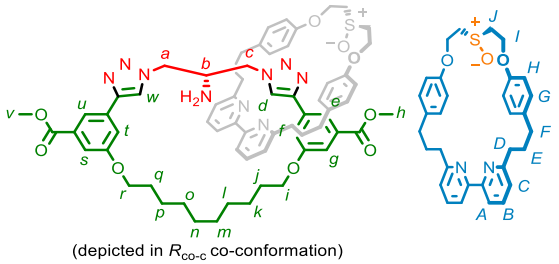

δ_H ($CDCl_3$, 400 MHz) 9.03 (s, 1H, H_d), 8.31 (t, J = 1.4, 1H, H_e), 8.18 (t, J = 1.4, 1H, H_u), 7.97 (s, 1H, H_w), 7.67 (t, J = 7.8, 1H, H_B), 7.56 (dd, J = 7.8, 1.0, 1H, H_A), 7.49 (t, J = 7.7, 1H, $H_{B'}$), 7.43 (dd, J = 2.6, 1.4, 1H, H_s), 7.40 – 7.36 (m, 2H, $H_{A'}$, H_g), 7.15 (dd, J = 7.7, 1.0, 1H, H_C), 6.98 (dd, J = 7.7, 1.0, 1H, H_C), 6.94 (dd, J = 2.6, 1.5, 1H, H_f), 6.87 – 6.78 (m, 5H, H_G, $H_{G'}$, H_t), 6.66 (dd, 4H, H_H, $H_{H'}$), 4.77 – 4.48 (m, 4H, H_I), 3.96 – 3.88 (m, 8H, H_h, H_r, H_v, H_a), 3.80-3.64 (m, 3H, H_J, H_a), 3.55 (t, J = 6.5, 2H, H_i), 3.46 (dd, J = 13.9, 4.7, 1H, H_c), 3.30 (dd, J = 13.9, 8.3, 1H, H_c), 3.25 – 3.15 (m, 2H, H_J), 3.08 (m, 1H, H_b), 2.59 – 2.39 (m, 4H, H_F, $H_{F'}$), 2.37 – 2.29 (m, 2H, H_D), 2.22 (td, J = 13.3, 4.6, 1H, H_D), 2.11 (td, J = 13.3, 5.0, 1H, H_D), 1.84 – 1.47 (m, 8H, H_E, $H_{E'}$, H_j, H_q), 1.43 – 1.11 (m, 12H, H_k, H_l, H_m, H_n, H_o, H_p); δ_C ($CDCl_3$, 101 MHz) 167.1, 162.9, 162.8, 159.2, 159.2, 157.4, 156.7, 156.3, 156.3, 146.6, 146.6, 137.8, 137.1, 133.7, 133.4, 132.6, 132.3, 132.1, 132.0, 129.9, 129.6, 123.0, 122.6, 122.2, 121.4, 121.0, 120.8, 119.2, 118.4, 118.1, 116.7, 115.0, 114.9, 114.4, 112.8, 68.1, 68.0, 61.0, 60.5, 54.0, 53.9, 53.2, 53.0, 52.4, 52.4, 51.9, 37.1, 36.7, 34.8, 31.9, 31.2, 29.8, 29.6, 29.6, 29.5, 29.5, 29.4, 26.7, 26.3; LR-ESI-MS (+ve) = 1158.6 $[M+H]^+$.

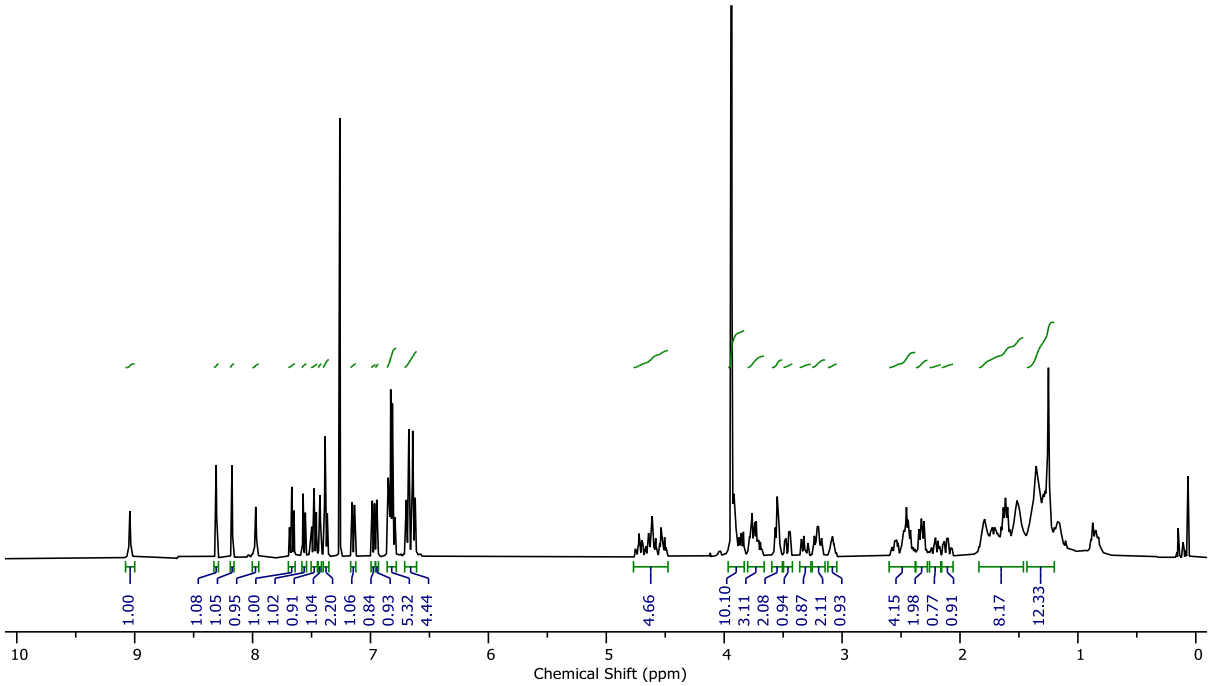

Figure 2.98 - ^{1}H NMR ($CDCl_3$, 400 MHz) of (S_{ma})-**6**.

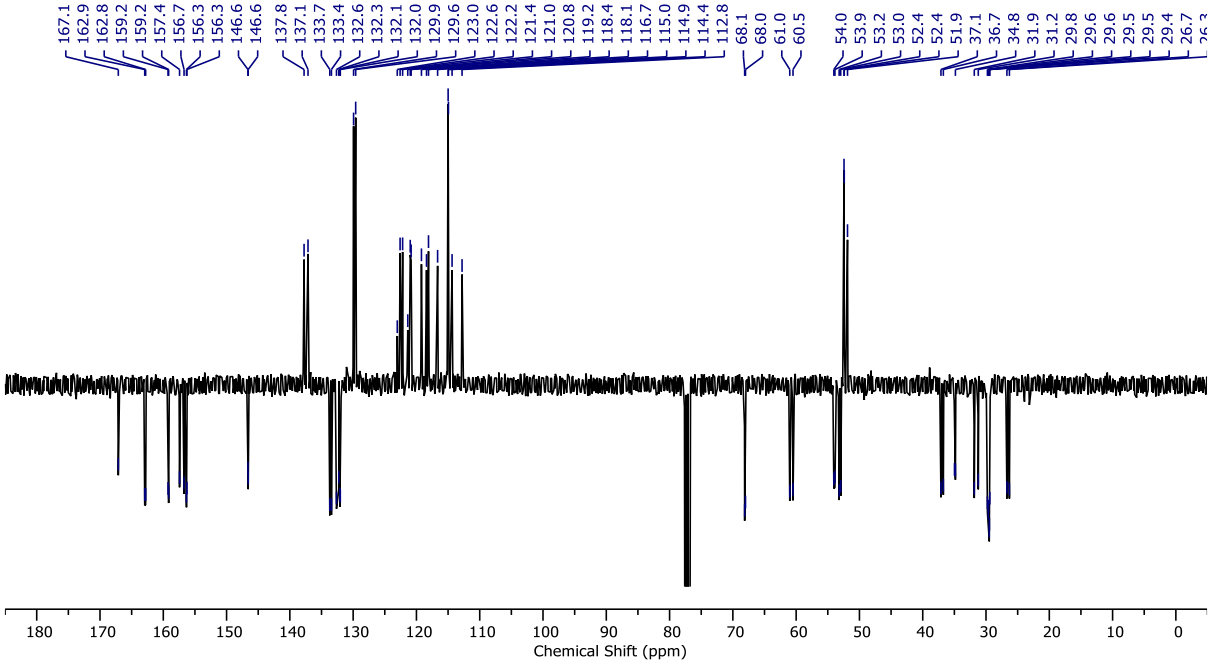

Figure 2.99 - JMOD NMR ($CDCl_3$, 101 MHz) of (S_{ma})-**6**.

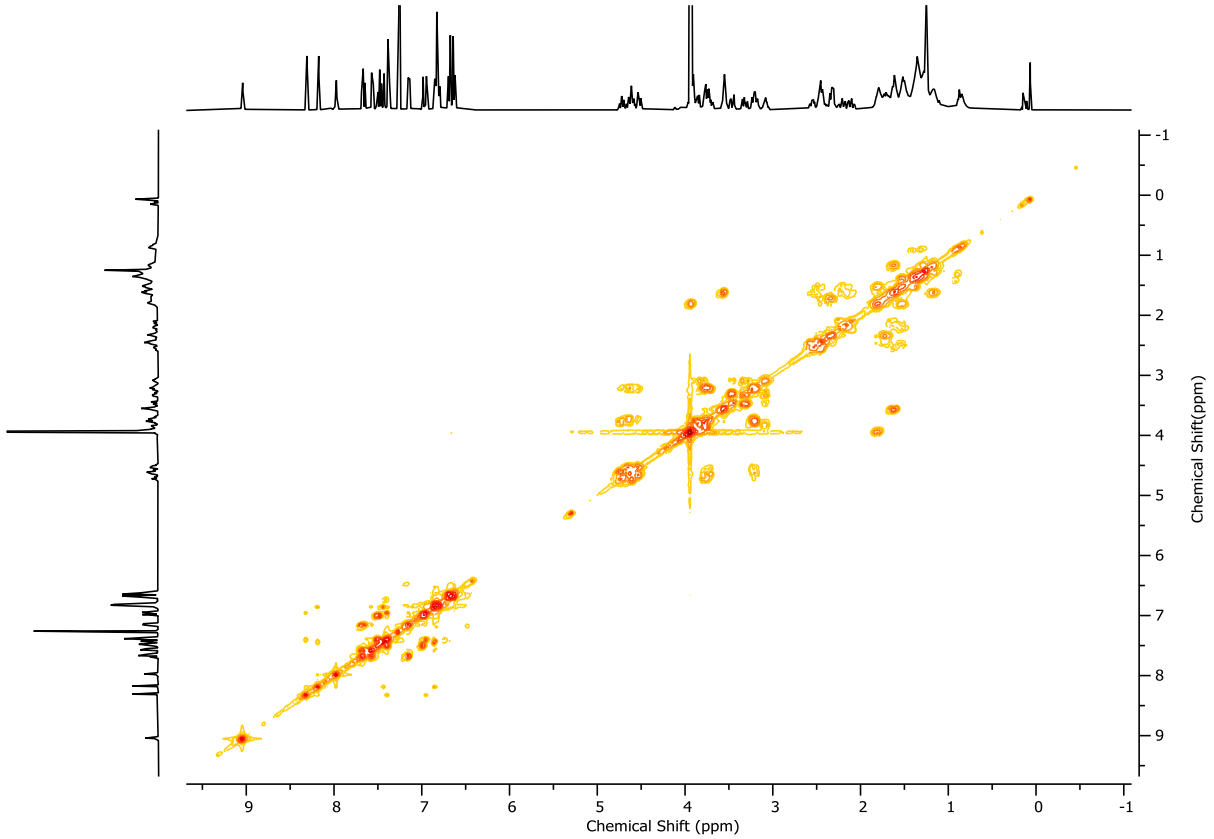

Figure 2.100 - ^{1}H COSY NMR ($CDCl_3$, 400 MHz) of (S_{ma})-**6**.

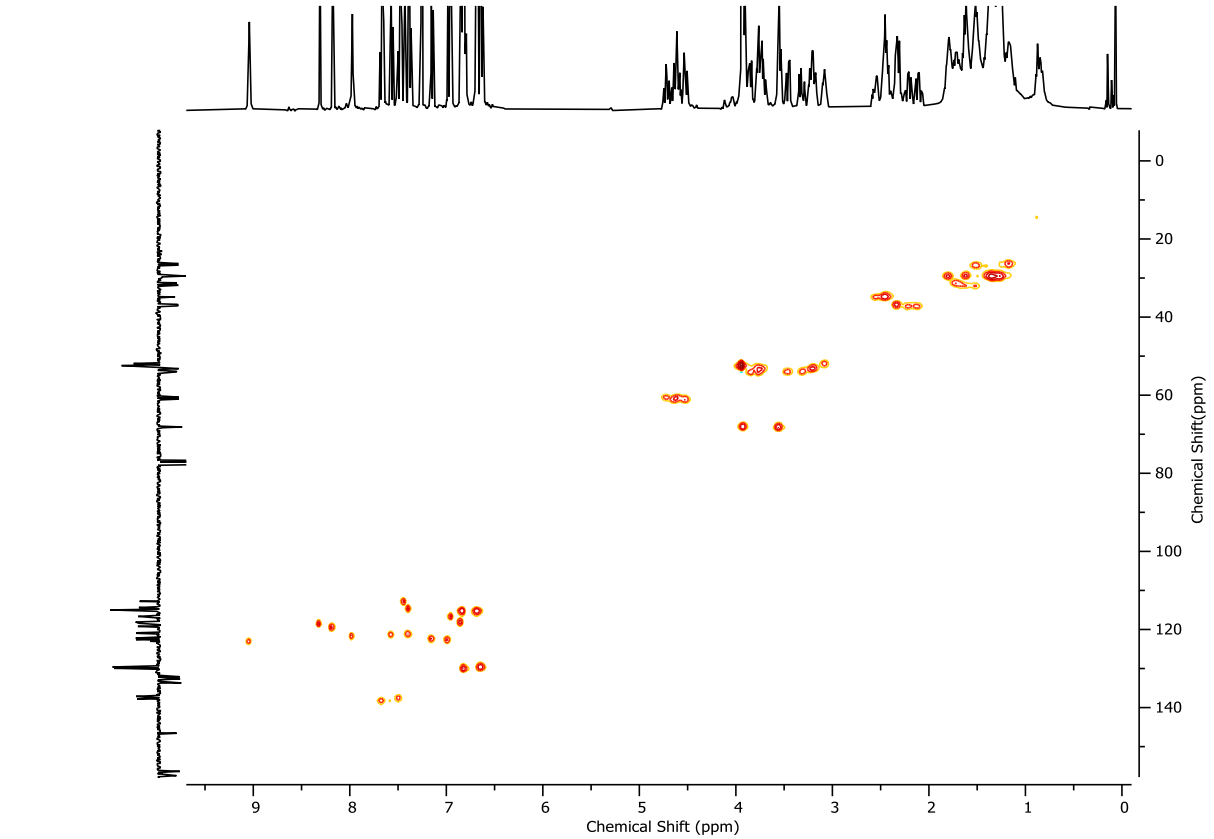

Figure 2.101 - HSQC NMR ($CDCl_3$, 400 MHz) of (S_{ma})-**6**.

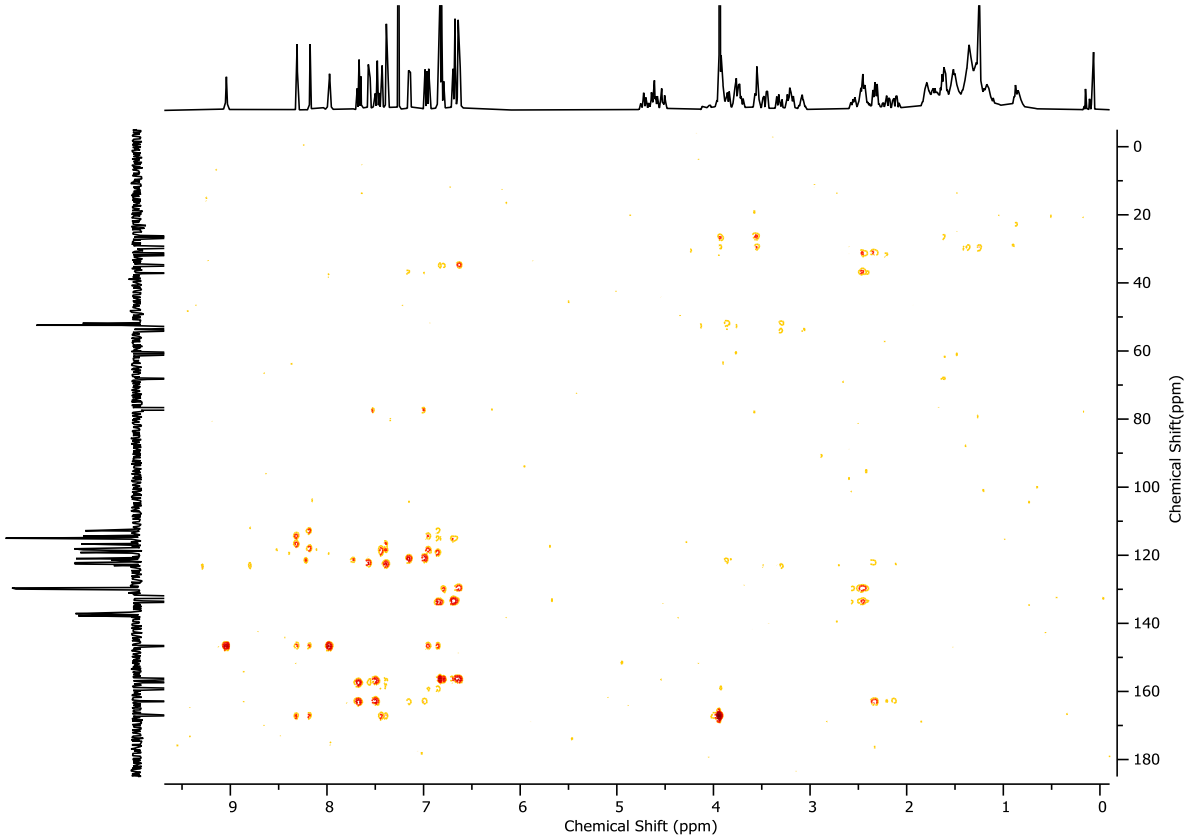

Figure 2.102 - HMBC NMR ($CDCl_3$, 400 MHz) of (S_{ma})-**6**.

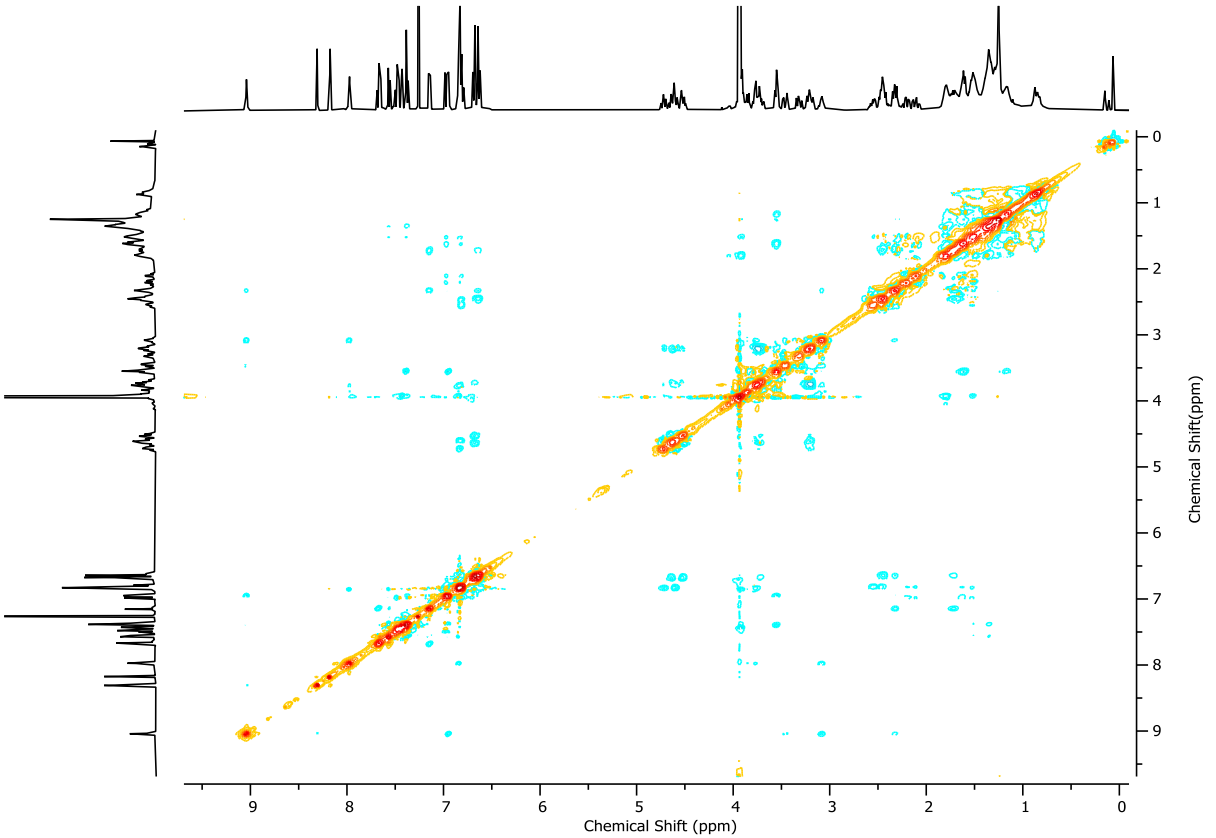

Figure 2.103 - ^1H NOESY NMR ($CDCl_3$, 400 MHz) of (S_{ma})-**6**.

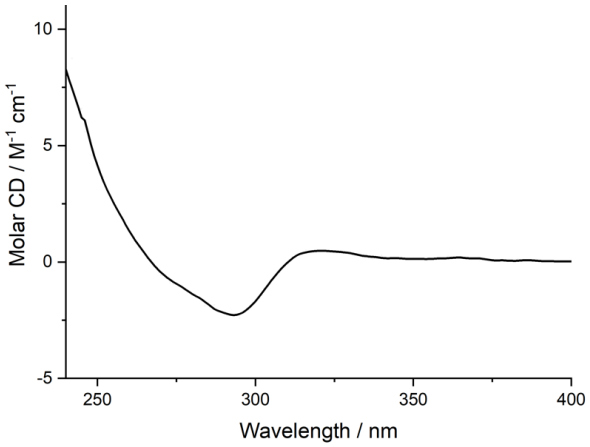

Figure 2.104 - Circular Dichroism Spectra of (S_{ma})-**6** (15 µM) at 293 K in $CHCl_3$.

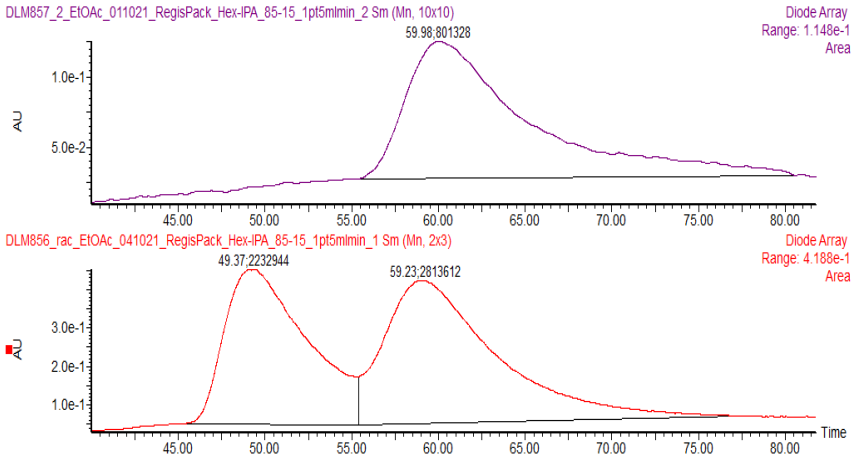

Figure 2.105 - CSP-HPLC of (S_{ma})-**6** (loaded in EtOAc). RegisCell, *n*-hexane-EtOH 85 : 15, flowrate 1.5 mLmin^{-1}. (top) (S_{ma})-**6** (59.98 min, 801328, >99.9%), (R_{ma})-**6** (not observed). (bottom) *rac*-**6**, (R_{ma})-**6** (49.37 min, 2232944, 44.2%), (S_{ma})-**6** (59.23 min, 2813612, 55.8%).

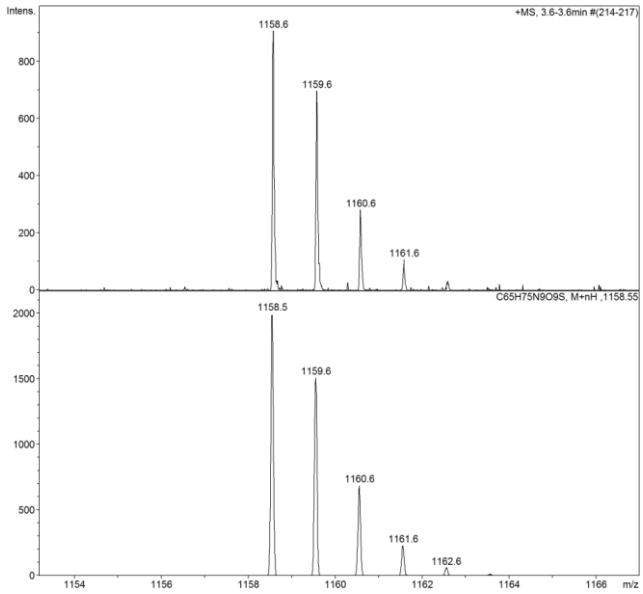

Figure 2.106 - Observed (top) and calculated (bottom) isotopic patterns for (S_{ma})-**6**.

Catenane (R_{ma})-6

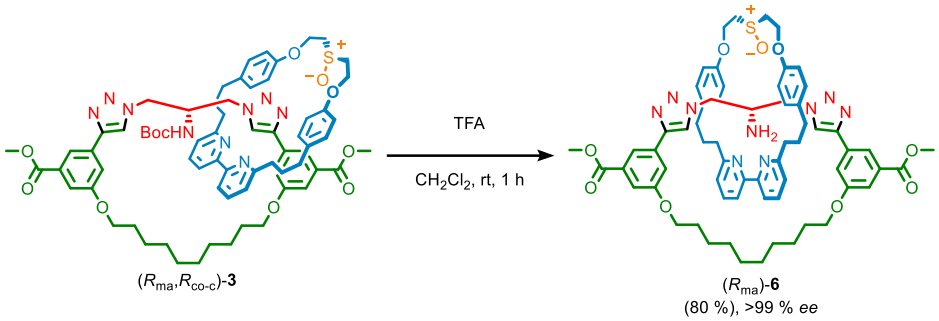

A solution of catenane (R_{ma},$R_{co\text{-}c}$)-**6** (28.2 mg, 0.022 mmol, 1.0 eq.) in CH_2Cl_2 (0.3 mL) was added TFA (51 µL, 0.67 mmol, 30 eq.) dropwise at 0 ºC, then stirred atambient temperature for 1 h. The reaction mixture was then diluted with CH_2Cl_2 (5 mL) and poured into saturated $NaHCO_3$ (5 mL). The aqueous phase was extracted with CH_2Cl_2 (3 x 5 mL) and combined organics were washed with brine (5 mL), dried over $MgSO_4$, filtered and concentrated *in vacuo*. The residue was purified by column chromatography (SiO_2, CH_2Cl_2-MeOH 0→15%) to yield catenane (R_{ma})-**6** (20.8 mg, 0.018 mmol, 80%) as a white foam.

All spectroscopic data is consistent with those reported for (S_{ma})-**6**, with the exception of circular dichroism spectra.

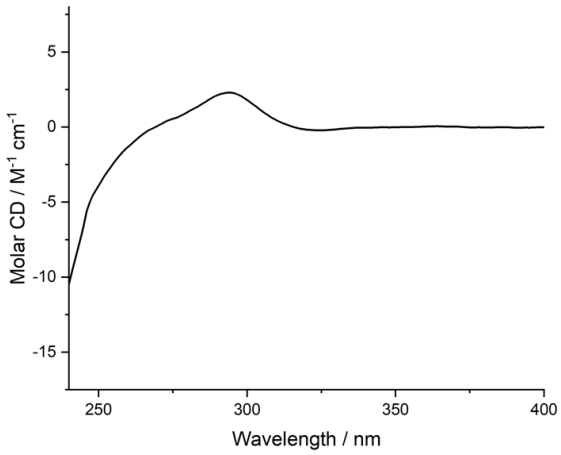

Figure 2.107 - Circular Dichroism Spectra of (R_{ma})-**6** (21 µM) at 293 K in $CHCl_3$.

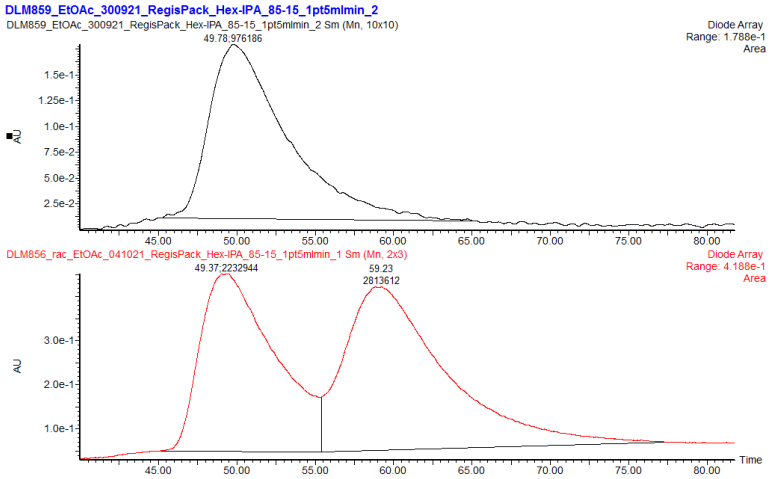

Figure 2.108 - CSP-HPLC of (R_{ma})-**6** (loaded in EtOAc). RegisCell, *n*-hexane-EtOH 85:15, flowrate 1.5 mLmin^{-1}. (top) (R_{ma})-**6** (49.78 min, 976186, >99.9%), (S_{ma})-**6** (not observed); (bottom) *rac*-**6**, (R_{ma})-**6** (49.37 min, 2232944, 44.2%), (S_{ma})-**6** (59.23 min, 2813612, 55.8%).

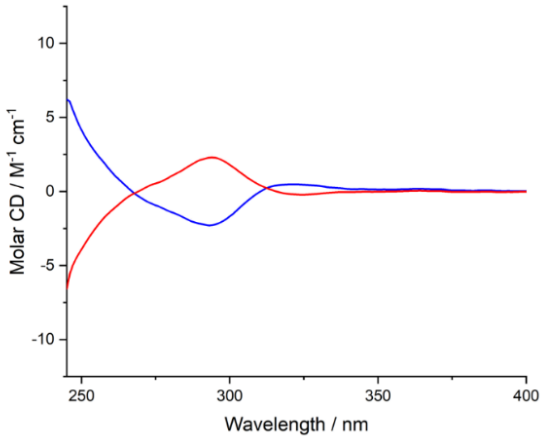

Figure 2.109 - Circular Dichroism Spectra of (R_{ma})-**6** (red, 21 μM) and (S_{ma})-**6** (blue, 15 μM) at 293 K in $CHCl_3$.

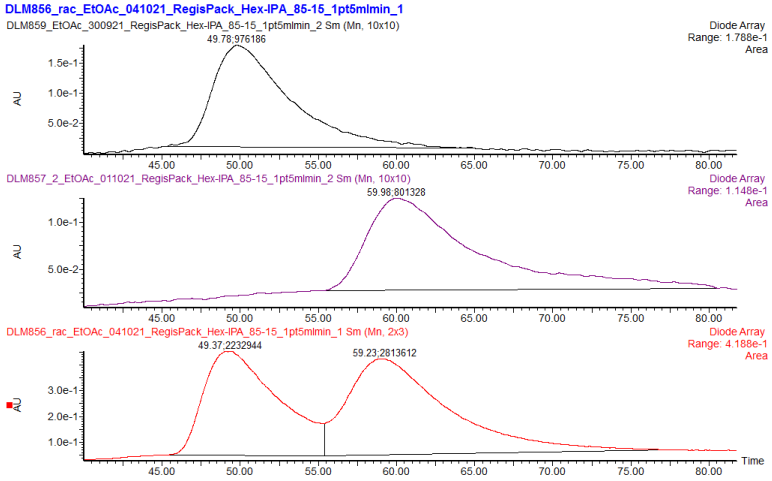

Figure 2.110 - CSP-HPLC of (R_{ma})-**6** and (S_{ma})-**6** (loaded in EtOAc) 286 nm trace. RegisCell, *n*-hexane-EtOH 88:12, flowrate 1 mLmin^{-1}. (top) (R_{ma})-**6** (49.78 min, 976186, >99.9%), (S_{ma})-**6** (not observed); (middle) (S_{ma})-**6** (59.98 min, 801328, >99.9%), (R_{ma})-**6** (not observed).; (bottom) *rac*-**6**, (R_{ma})-**6** (49.37 min, 2232944, 44.2%), (S_{ma})-**6** (59.23 min, 2813612, 55.8%).

Macrocycle S14

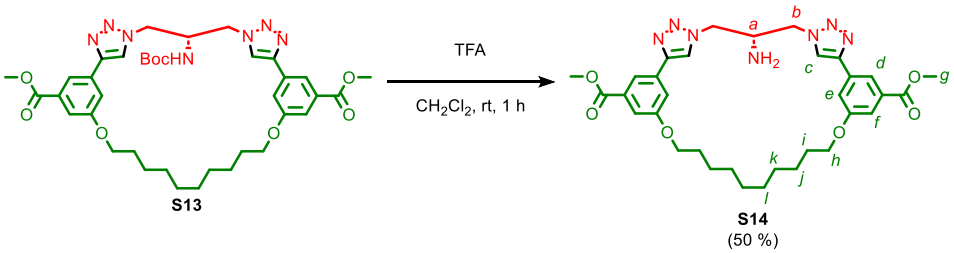

A solution of macrocycle **S13** (37.2 mg, 0.051 mmol, 1.0 eq.) in CH_2Cl_2 (0.5 mL) was added TFA (117 µL, 1.52 mmol, 30 eq.) dropwise then stirred at ambient temperature for 1 h. The reaction mixture was then diluted with CH_2Cl_2 (5 mL) and washed with 5M NaOH (2 x 5 mL). The aqueous phase was extracted with CH_2Cl_2 (3 x 8 mL) and combined organics were washed with brine (5 mL), dried over $MgSO_4$, filtered and concentrated *in vacuo*. The residue was purified by column chromatography (SiO_2, CH_2Cl_2 → EtOAc then CH_2Cl_2 → MeOH 0→15%) to yield **S14** (16.0 mg, 0.025 mmol, 50%) as a white foam.

δ_H ($CDCl_3$, 400 MHz) 8.11 (t, J = 1.4, 2H, H_e), 7.90 (s, 2H, H_c), 7.51 (m, 2H, H_f), 7.47 (m, 2H, H_d), 4.44 (m, 4H, H_b), 4.06 (app t, J = 6.3, 4. H, H_h), 3.97 (t, J = 6.0, 1H, H_a), 3.92 (s, 6H, H_g), 1.80 (quint, J = 7.5, 4H, H_i), 1.50 (m, 2H, -NH_2), 1.31 (m, 12H, H_j, H_k, H_l); δ_C ($CDCl_3$, 101 MHz) 166.7, 159.5, 147.0, 132.2, 131.5, 121.8, 119.0, 116.8, 115.2, 68.5, 53.2, 52.3, 51.8, 29.7, 29.1, 28.9, 25.9; LR-ESI-MS (+ve) $[M+H]^+$ m/z (%) 632.5 (100); HR-EI-MS (+ve) $[M+H]^+$ m/z 632.3193 (calc. for $C_{33}H_{42}N_7O_6$ m/z 632.3191).

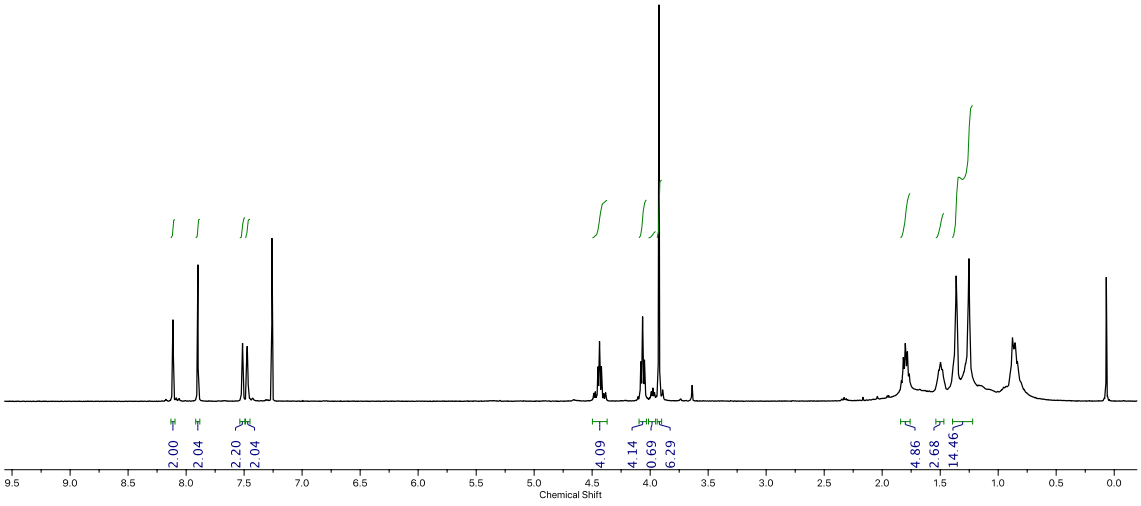

Figure 2.111 - ^{1}H NMR ($CDCl_3$, 400 MHz) of **S14**.

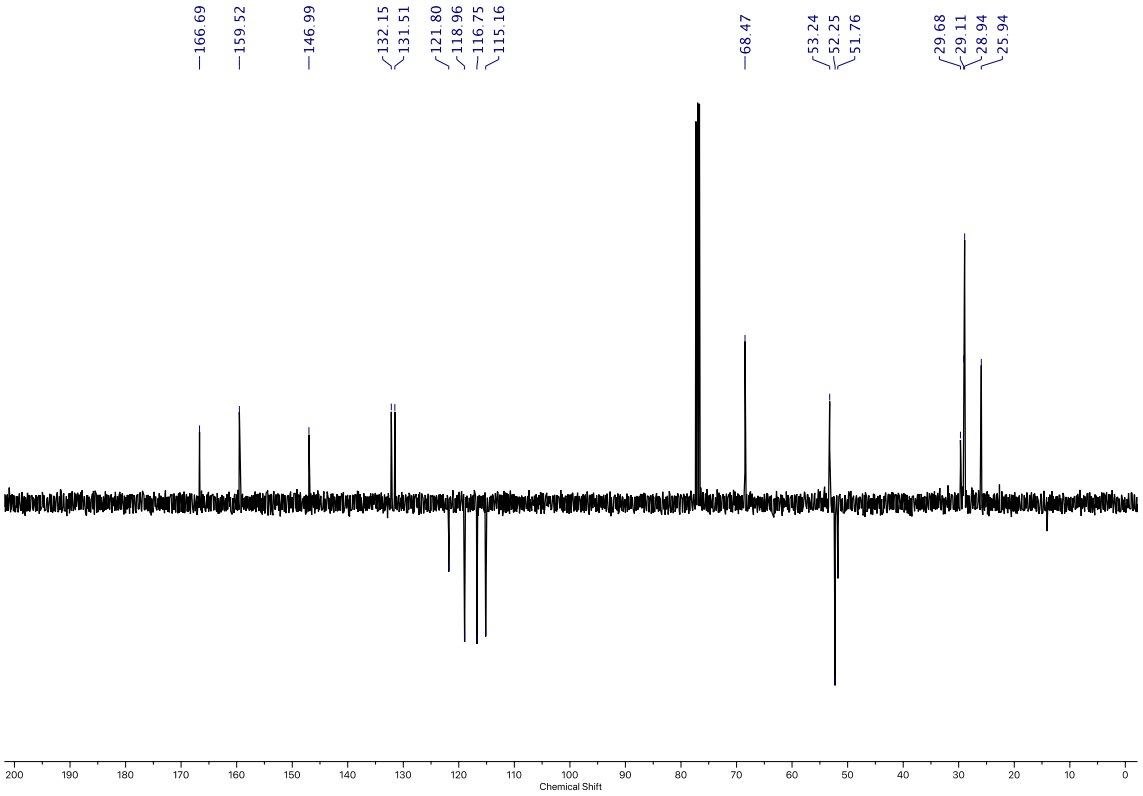

Figure 2.112 - JMOD NMR ($CDCl_3$, 101 MHz) of **S14**.

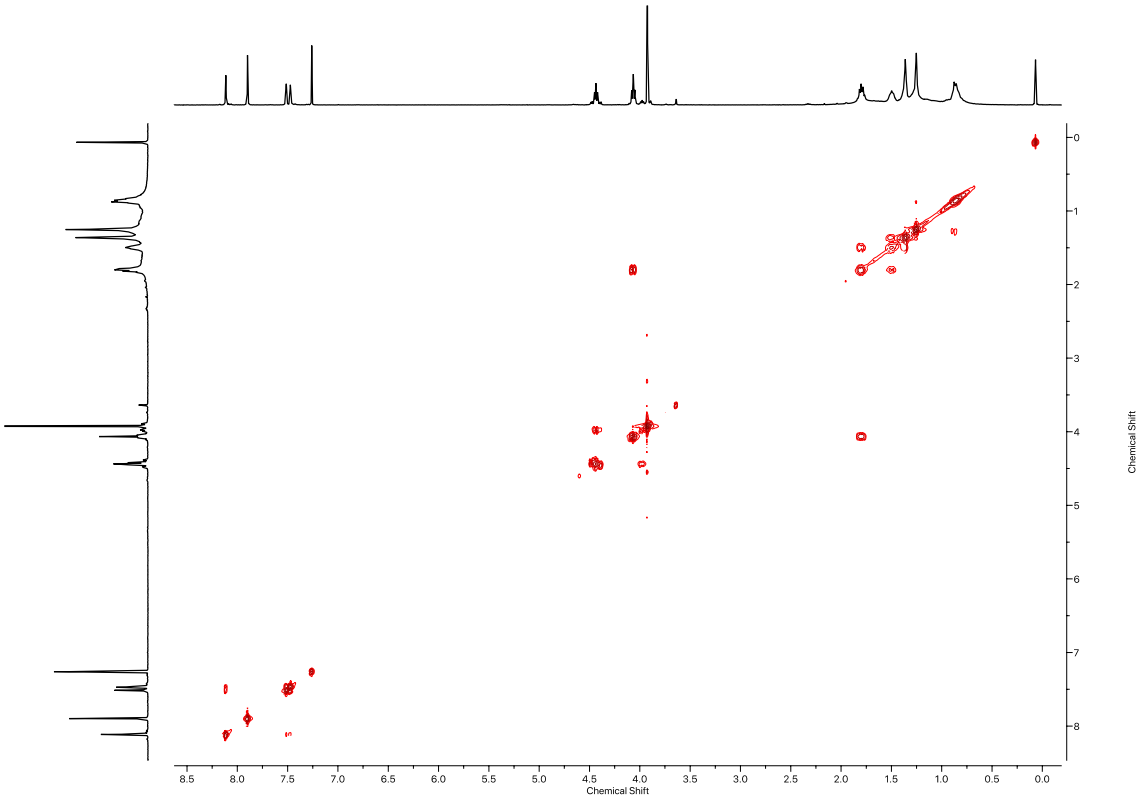

Figure 2.113 - ^1H COSY NMR ($CDCl_3$, 400 MHz) of **S14**.

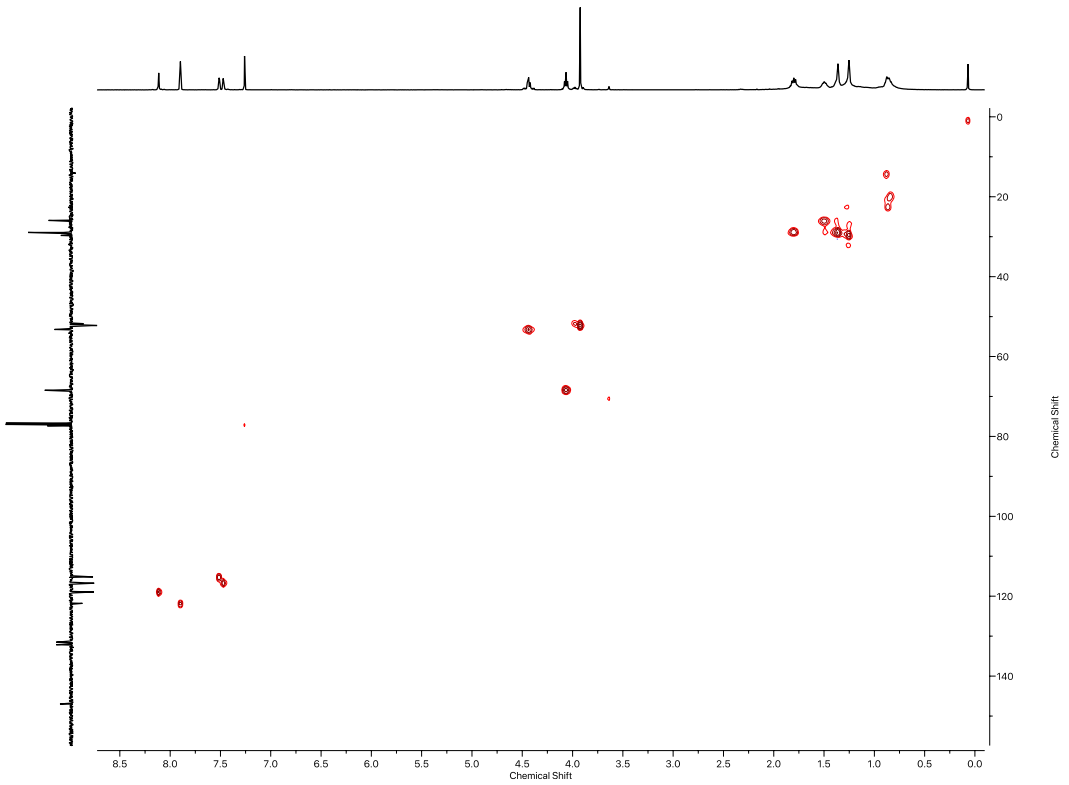

Figure 2.114 - HSQC NMR ($CDCl_3$, 400 MHz) of **S14**.

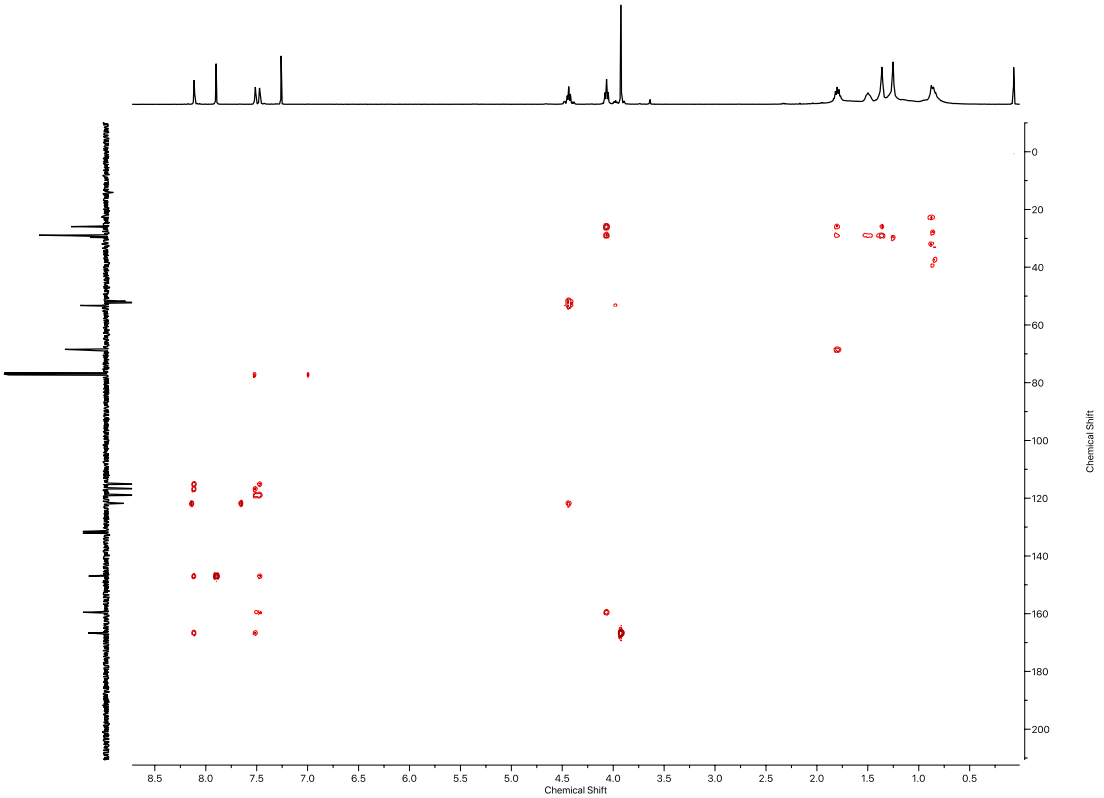

Figure 2.115 - HMBC NMR ($CDCl_3$, 400 MHz) of **S14**.

Synthesis of enantiomeric catenanes (S_{ma})-S15 and (R_{ma})-S15

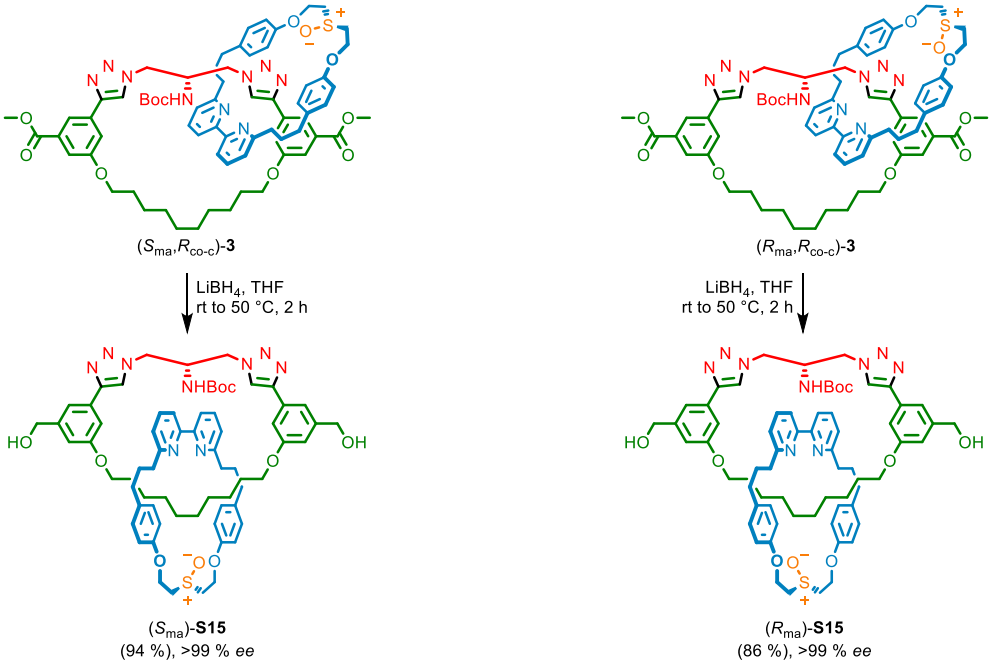

Scheme 2.5 - Synthetic route to mechanically axially chiral enantiomeric catenanes (R_{ma})-**S15** and (S_{ma})-**S15**.

Catenane (S_{ma})-S15

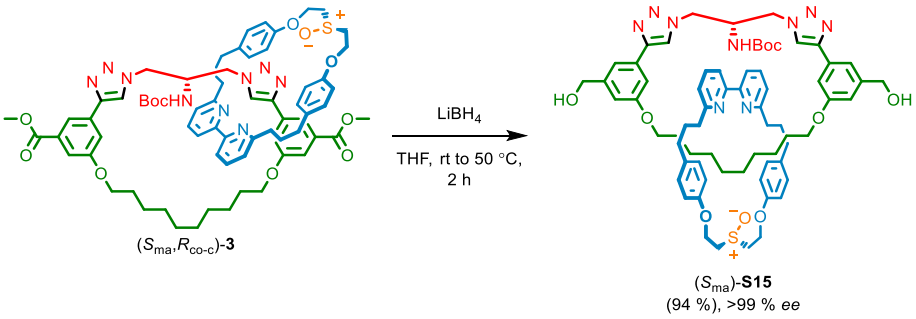

A dry CEM MW vial was charged with catenane (S_{ma},R_{co-c})-**3** (21.9 mg, 0.017 mmol, 1.0 eq.) and THF (0.5 mL). $LiBH_4$ (3.3 mg, 0.09 mmol, 5.0 eq.) was added at ambient temperature, and the solution was stirred for 2 h at 50 °C. The crude mixture was allowed to cool down, EtOAc (4 mL) was added and organics were washed with H_2O in two portions (2 mL and 4 mL), and the combined organics were washed with brine (8 mL), dried over $MgSO_4$ and concentrated *in vacuo*. The residue was purified by column chromatography (SiO_2, CH_2Cl_2-MeOH 0→10%) to yield catenane (S_{ma})-**S15** (19.0 mg, 0.016 mmol, 94%) as a white foam. The mechanical stereochemistry of the product was assigned by observing that this cannot change during the reduction step (or if it does, that the resulting product would be racemic, which was not observed).

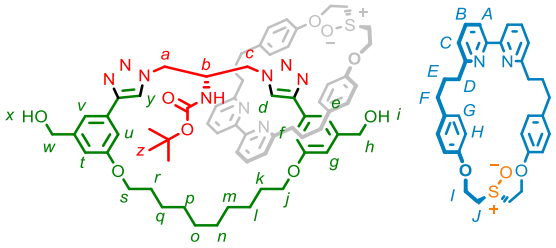

δ_H (DMSO-d_6, 500 MHz) 8.57 (s, 1H, H_d), 8.40 (s, 1H, H_y), 7.74 (t, J = 10, 1H, H_B), 7.70-7.58 (m, 3H, H_A, $H_{A'}$, $H_{B'}$), 7.51-7.47 (m, 2H, H_e, H_v), 7.30-7.12 (m, 4H, H_f, H_C, $H_{C'}$, $H_{\text{-NHBoc}}$), 7.01 (s, 1H, H_u), 6.87-6.77 (m, 5H, H_G, $H_{G'}$, H_g), 6.72-6.52 (m, 5H, H_t, H_H, $H_{H'}$), 5.31 (t, J = 5.5, 1H, H_i), 5.27 (t, J = 6, 1H, H_x), 4.66-4.29 (m, 17H, H_a, H_b, H_c, H_h, H_w, H_s, H_j, H_l, $H_{l'}$), 3.67-3.57 (m, 2H, H_J), 3.51-3.45 (m, 2H, $H_{J'}$), 2.80-2.69 (m, 4H, H_D, H_F), 2.49-2.44 (m, 4H, $H_{D'}$, $H_{F'}$) 1.76-1.61 (m, 4H, H_E, $H_{E'}$), 1.28-1.20 (m, 9H, H_k, H_r, H_l, H_q), 1.14 (m, 9H, H_z), 0.52-0.31 (m, 8H, H_l, H_m); δ_C (DMSO-d_6, 126 MHz) 161.5, 161.5, 159.0, 159.0, 157.2, 157.1, 154.8, 154.2, 154.1, 146.9, 146.9, 145.0, 144.8, 136.9, 136.8, 134.9, 134.8, 131.6, 131.4, 129.6, 129.3, 128.9, 122.1, 122.0, 119.2, 119.1, 115.0, 114.8, 114.8, 111.7, 111.3, 111.1, 110.3, 78.4, 69.8, 67.4, 62.8, 62.8, 59.8, 59.7, 52.5, 51.3, 51.1, 50.8, 37.2, 37.1, 33.4, 33.3, 33.1, 33.0, 32.4, 31.3, 29.0, 27.9, 25.5, 25.2, 25.2, 24.5; LR-ESI-MS (+ve) $[M+H]^+$ m/z (%) 1203.0 (100).

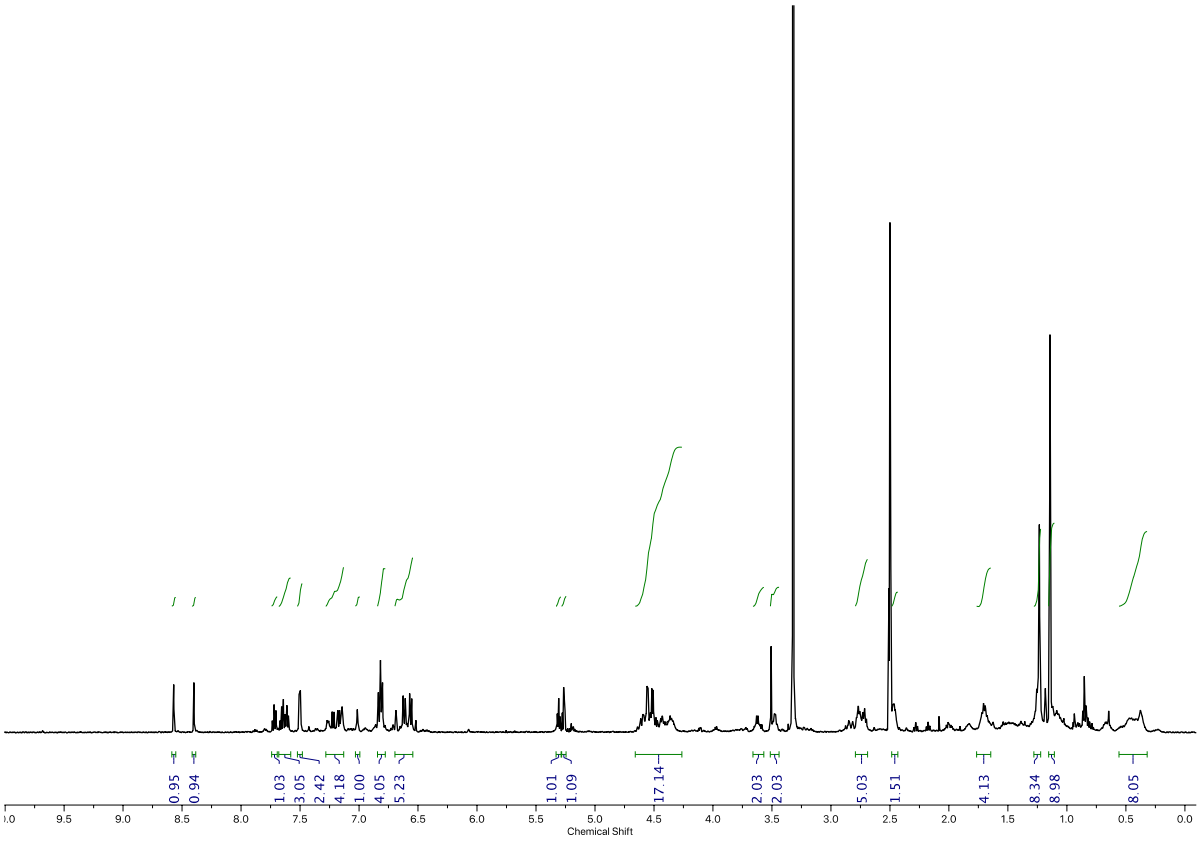

Figure 2.116 - ^{1}H NMR ($CDCl_3$, 500 MHz) of (S_{ma})-**S15**.

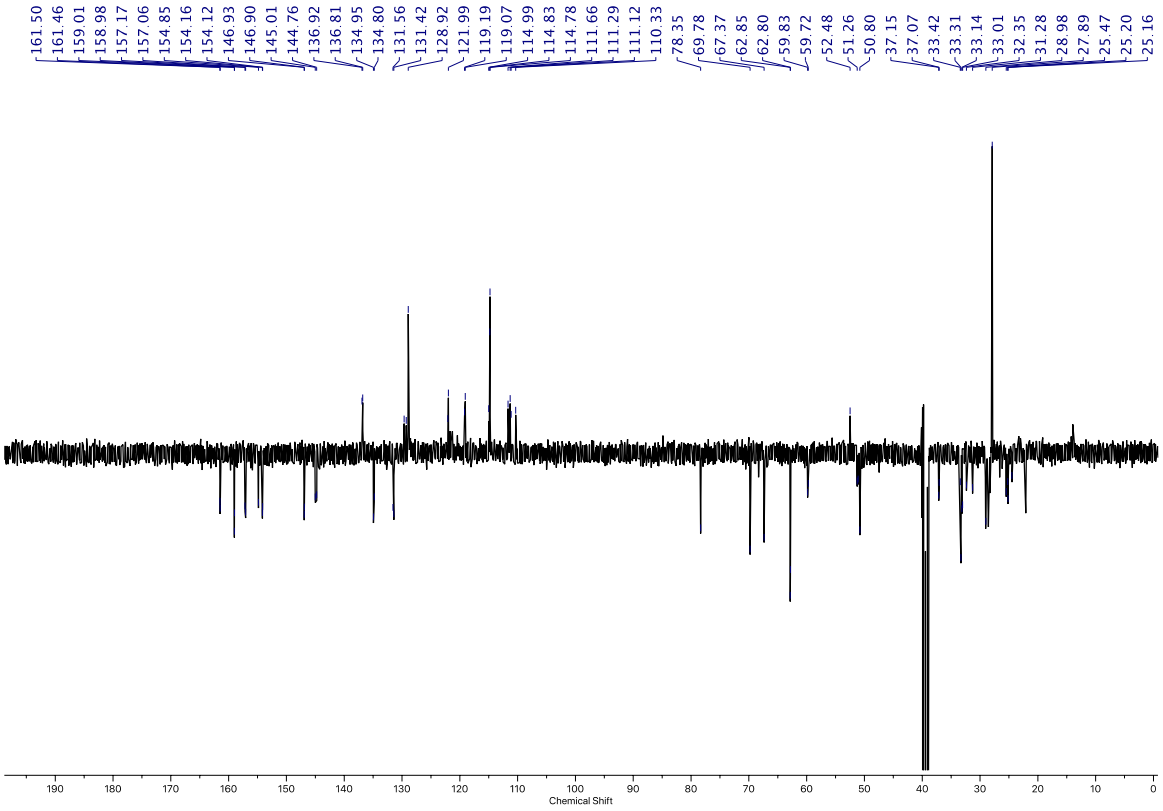

Figure 2.117 - JMOD NMR ($CDCl_3$, 126 MHz) of (S_{ma})-**S15**.

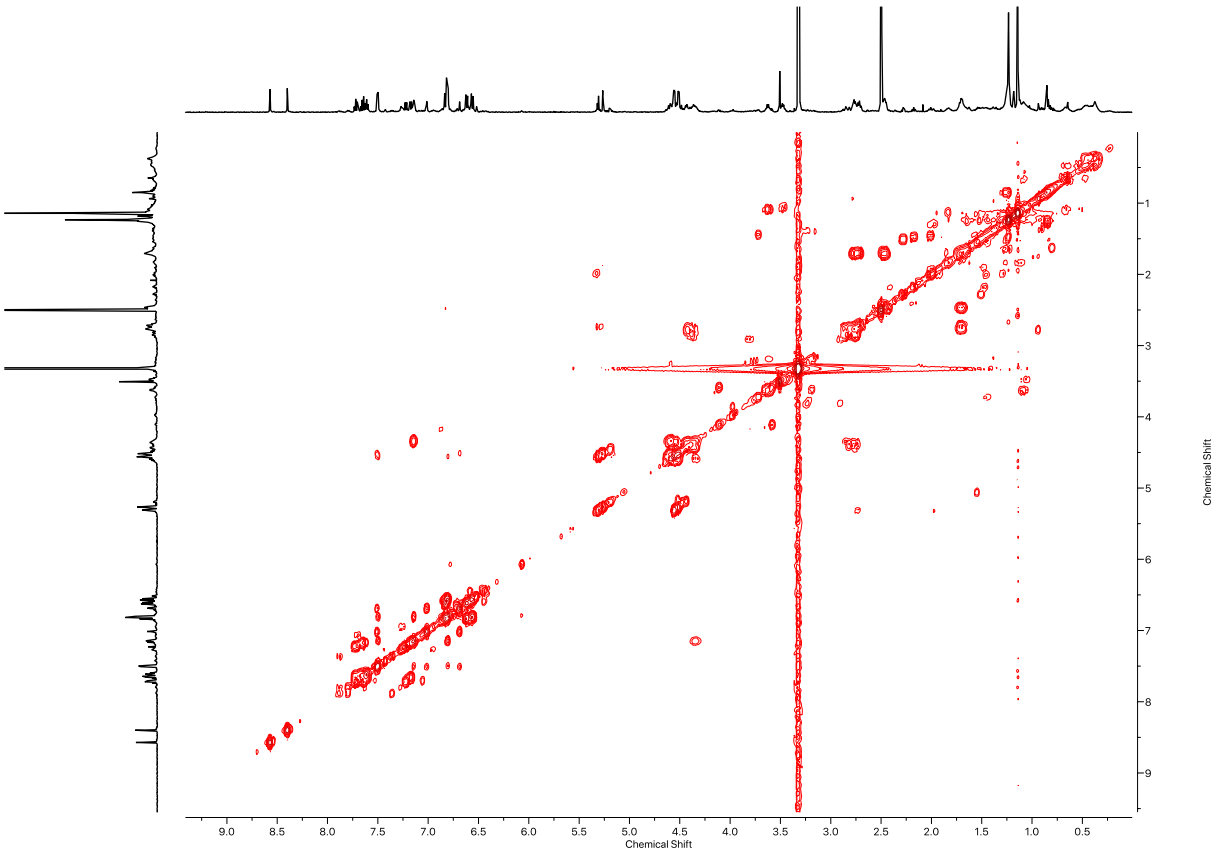

Figure 2.118 - ^1H COSY NMR (DMSO, 500 MHz) of (S_{ma})-**S15**.

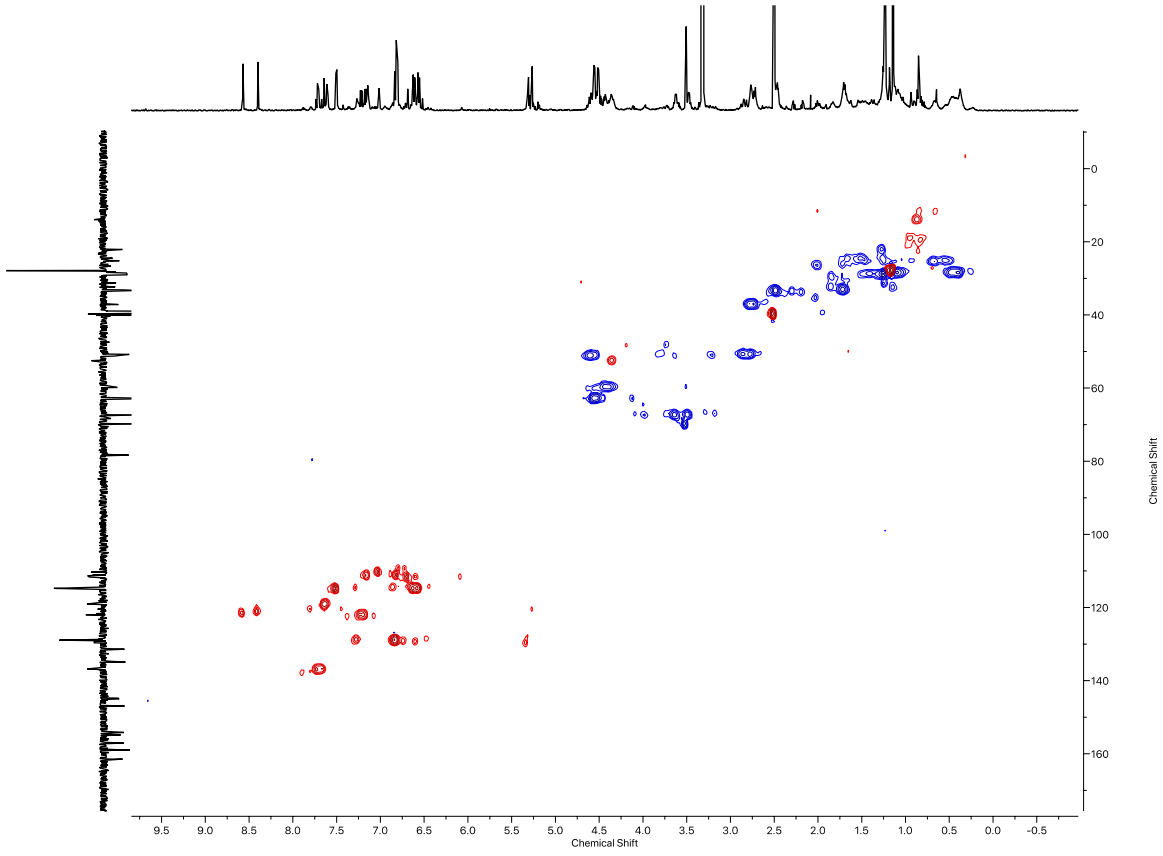

Figure 2.119 - HSQC NMR (DMSO, 500 MHz) of (S_{ma})-**S15**.

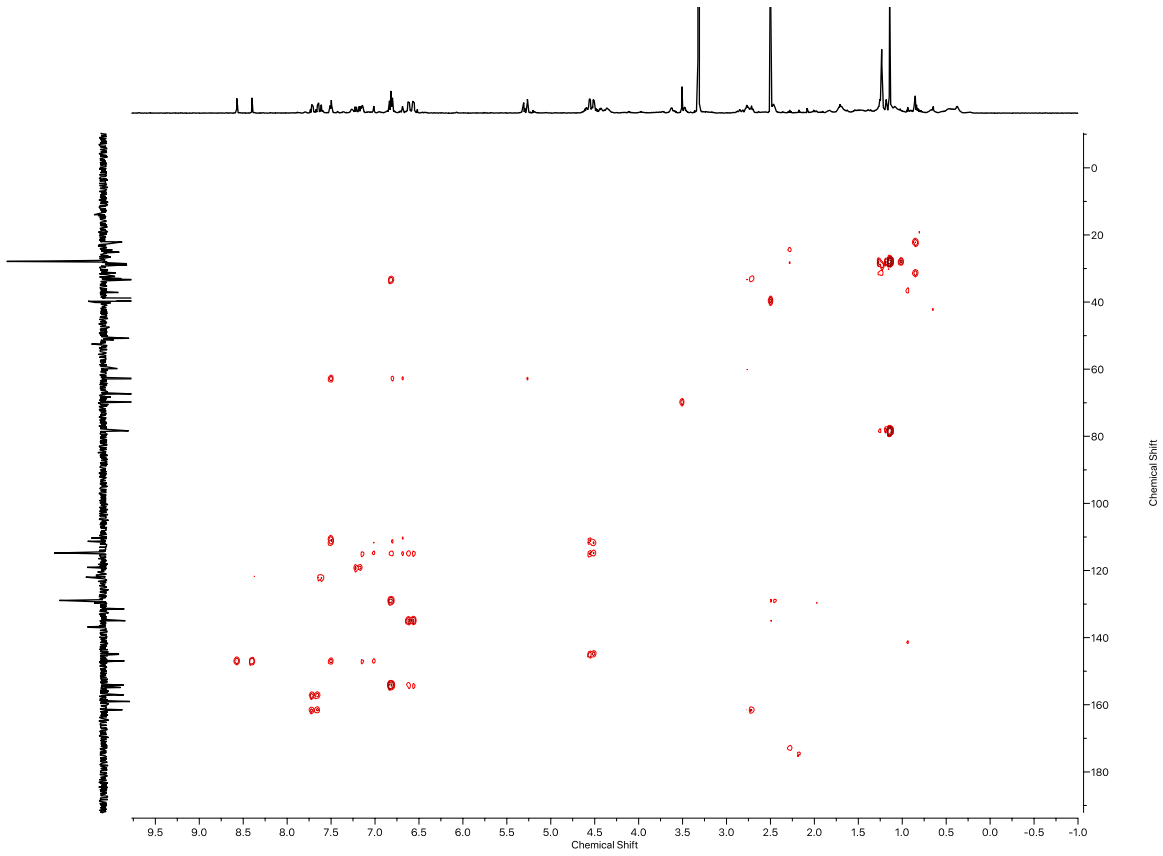

Figure 2.120 - HMBC NMR (DMSO, 500 MHz) of (S_{ma})-**S15**.

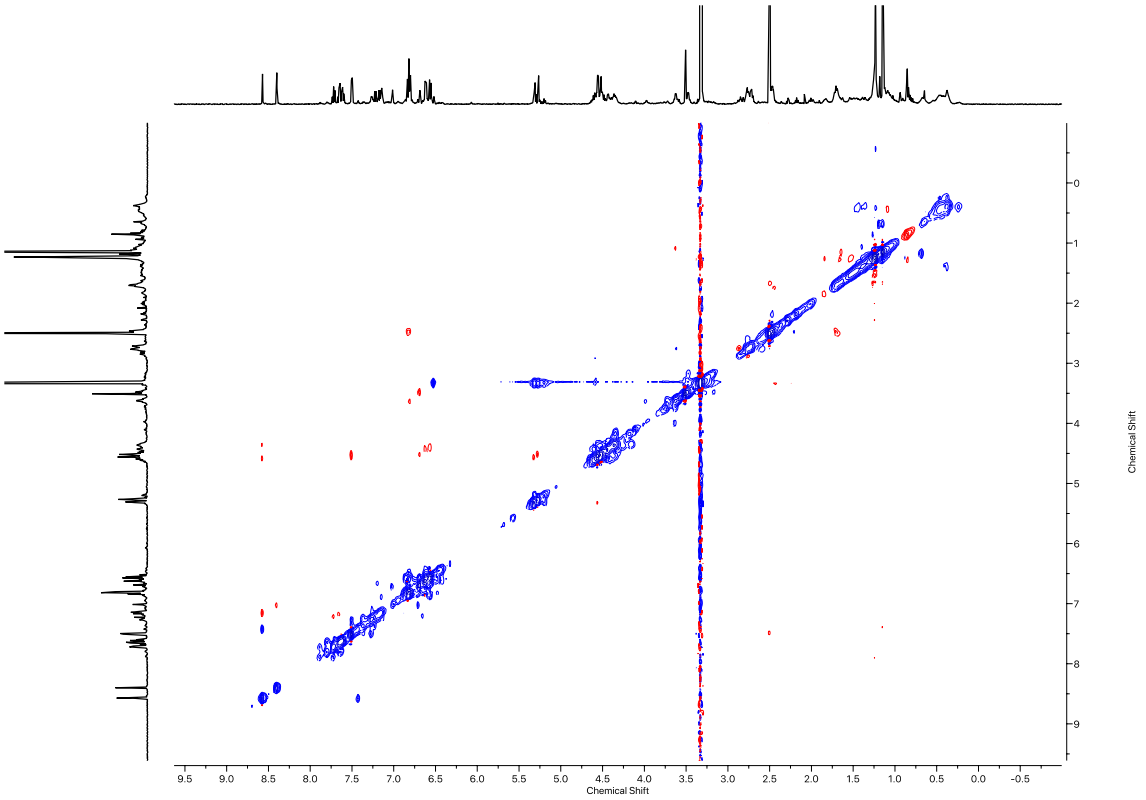

Figure 2.121 - ^{1}H NOESY NMR (DMSO, 500 MHz) of (S_{ma})-**S15**.

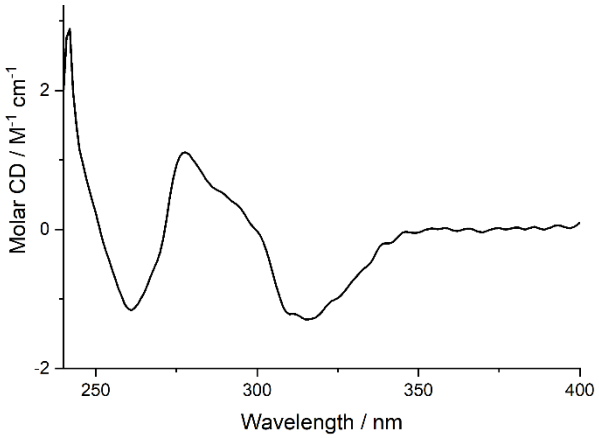

Figure 2.122 - Circular Dichroism Spectra of (S_{ma})-**S15** (18 µM) at 293 K in $CHCl_3$.

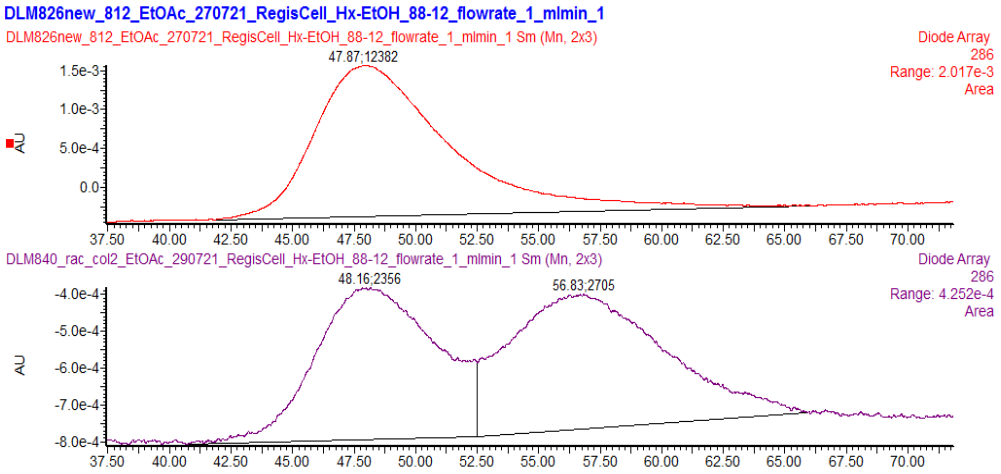

Figure 2.123 - CSP-HPLC of (S_{ma})-**S15** (loaded in EtOAc) 286 nm trace. RegisCell, *n*-hexane-EtOH 88 : 12, flowrate 1 mLmin^{-1}. (top) (S_{ma})-**S15** (47.87 min, 12382, >99.9%), (R_{ma})-**S15** (not observed). (bottom) *rac*-**S15**, (S_{ma})-**S15** (48.16 min, 2356, 50.1%), (R_{ma})-**S15** (56.83 min, 2705, 49.9%).

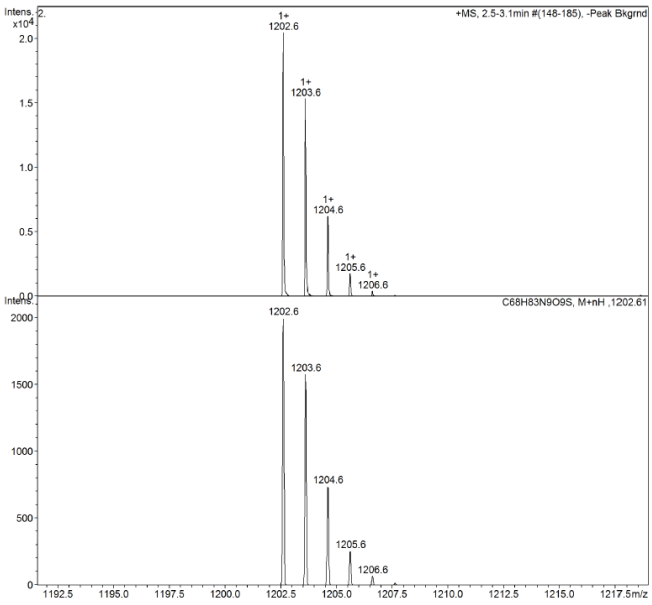

Figure 2.124 - Observed (top) and calculated (bottom) isotopic patterns for *(S_{ma})*-**S15**.

Catenane (R_{ma})-S15

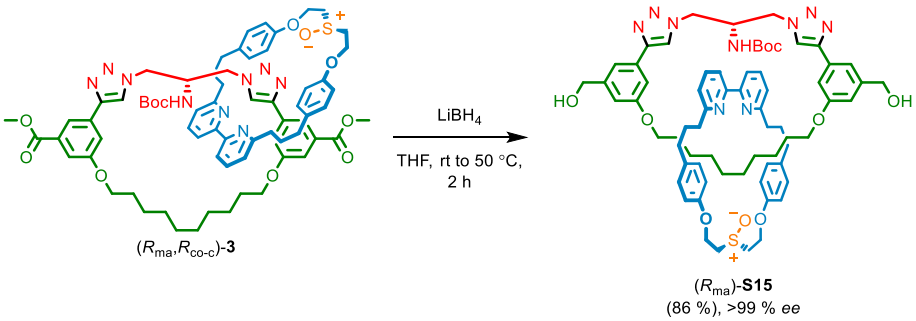

A dry CEM MW vial was charged with catenane (R_{ma},$R_{co\text{-}c}$)-**3** (23.5 mg, 0.019 mmol, 1.0 eq.) and THF (0.5 mL). $LiBH_4$ (3.5 mg, 0.09 mmol, 5.0 eq.) was added at ambient temperature, and the solution was stirred for 2 h at 50 °C. The crude mixture was allowed to cool down, EtOAc (4 mL) was added and organics were washed with H_2O in two portions (2 mL and 4 mL), and the combined organics were washed with brine (8 mL), dried over $MgSO_4$ and concentrated *in vacuo*. The residue was purified by column chromatography (SiO_2, CH_2Cl_2-MeOH 0→10%) to yield catenane (R_{ma})-**S15** (19.3 mg, 0.016 mmol, 85%) as a white foam.

All spectroscopic data is consistent with those reported for (S_{ma})-**S15**, with the exception of circular dichroism spectra.

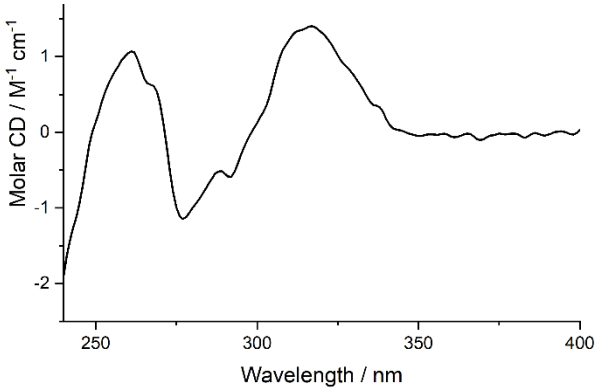

Figure 2.125 - Circular Dichroism Spectra of (R_{ma})-**S15** (16 µM) at 293 K in $CHCl_3$.

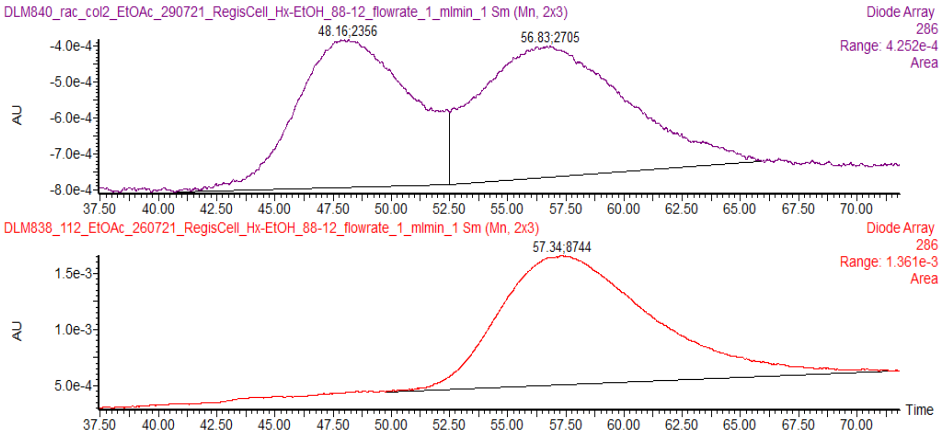

Figure 2.126 - CSP-HPLC of (R_{ma})-**S15** (loaded in EtOAc) 286 nm trace. RegisCell, *n*-hexane-EtOH 88:12, flowrate 1 mLmin^{-1}. (top) *rac*-**S15**, (S_{ma})-**S15** (48.16 min, 2356, 50.1%), (R_{ma})-**S15** (56.83 min, 2705, 49.9%); (bottom) (S_{ma})-**S15** (not observed), (R_{ma})-**S15** (57.34 min, 8744, >99.9%).

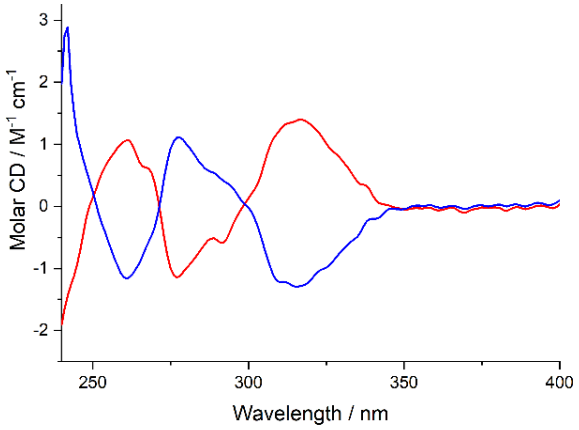

Figure 2.127 - Circular Dichroism Spectra of (S_{ma})-**S15** (red, 16 µM) and (R_{ma})-**S15** (blue, 18.3 µM)at 293 K in $CHCl_3$.

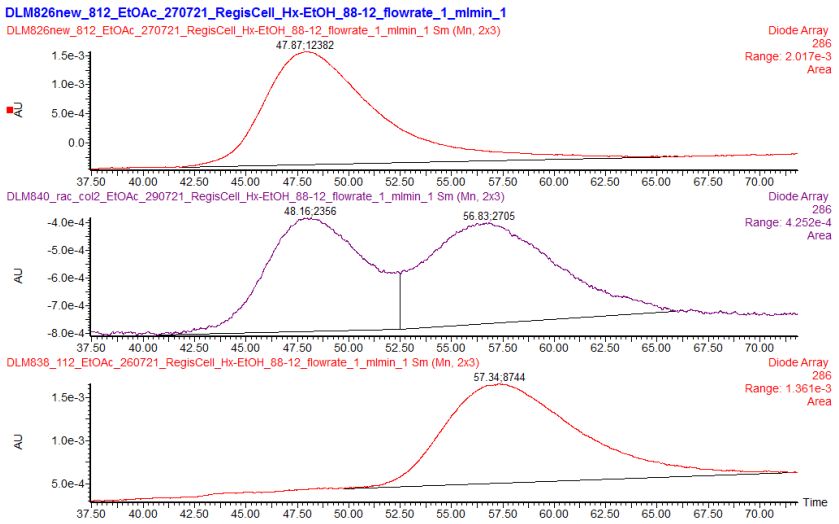

Figure 2.128 - CSP-HPLC of (R_{ma})-**S15** and (S_{ma})-**S15** (loaded in EtOAc) 286 nm trace. RegisCell, *n*-hexane-EtOH 88:12, flowrate 1 mLmin^{-1}. (top) (S_{ma})-**S15** (47.87 min, 12382, >99.9%), (R_{ma})-**S15** (not observed); (middle) *rac*-**S15**, (S_{ma})-**S15** (48.16 min, 2356, 50.1%), (R_{ma})-**S15** (56.83 min, 2705, 49.9%); (bottom) (S_{ma})-**S15** (not observed), (R_{ma})-**S15** (57.34 min, 8744, >99.9%).

Macrocycle S16

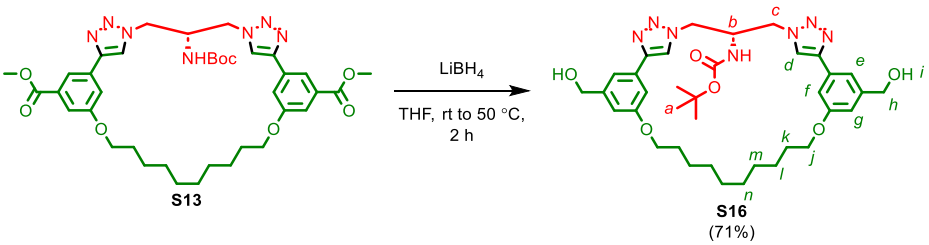

To a solution of macrocycle **S13** (17.7 mg, 0.024 mmol, 1.0 eq.) in THF (0.5 mL) at ambient temperature was added $LiBH_4$ (2.6 mg, 0.121 mmol, 5 eq.), and then the reaction mixture was stirred at 50 °C for 2 h. The reaction mixture was diluted with EtOAc (5 mL) and washed with H_2O (2 x 5 mL). The aqueous phase was extracted with EtOAc (2 x 8 mL) and combined organics were washed with brine (5 mL), dried over $MgSO_4$, filtered and concentrated *in vacuo*. The residue was purified by column chromatography (SiO_2, CH_2Cl_2 → EtOAc then CH_2Cl_2 → MeOH 0→15%) to yield **S16** (11.6 mg, 0.017 mmol, 71%) as a white foam. Two rotamers of **S16** are observed due to slow rotation of -NHBoc group at 298 K, which were equilibrated by VT-NMR (Figure 2.130).

δ_H ($CDCl_3$, 500 MHz) 8.61 (s, 2H, H_d), 7.50 (s, 2H, H_c), 7.19 (d, J = 8.9, 1H, -N*H*Boc), 7.11 (br. s, 2H, H_f), 6.84 (m, 2H, H_d), 5.24 (t, J = 5.5, 2H, H_i), 4.65-4.44 (m, 9H, H_b, H_c, H_h), 4.00 (t, J = 6.5, 4H, H_j), 1.72 (quint., 4H, H_k), 1.45 (m, 4H, H_l), 1.31 (m, 8H, H_m, H_n), 1.23 (s, 9H, H_a); δ_C ($CDCl_3$, 101 MHz) 166.7, 159.5, 147.0, 132.2, 131.5, 121.8, 119.0, 116.8, 115.2, 68.5, 53.2, 52.3, 51.8, 29.7, 29.1, 28.9, 25.9; LR-ESI-MS (+ve) $[M+H]^+$ m/z (%) 632.5 (100); HR-EI-MS (+ve) $[M+H]^+$ m/z 676.3813 (calc. for $C_{36}H_{50}N_7O_6$ m/z 676.3817).

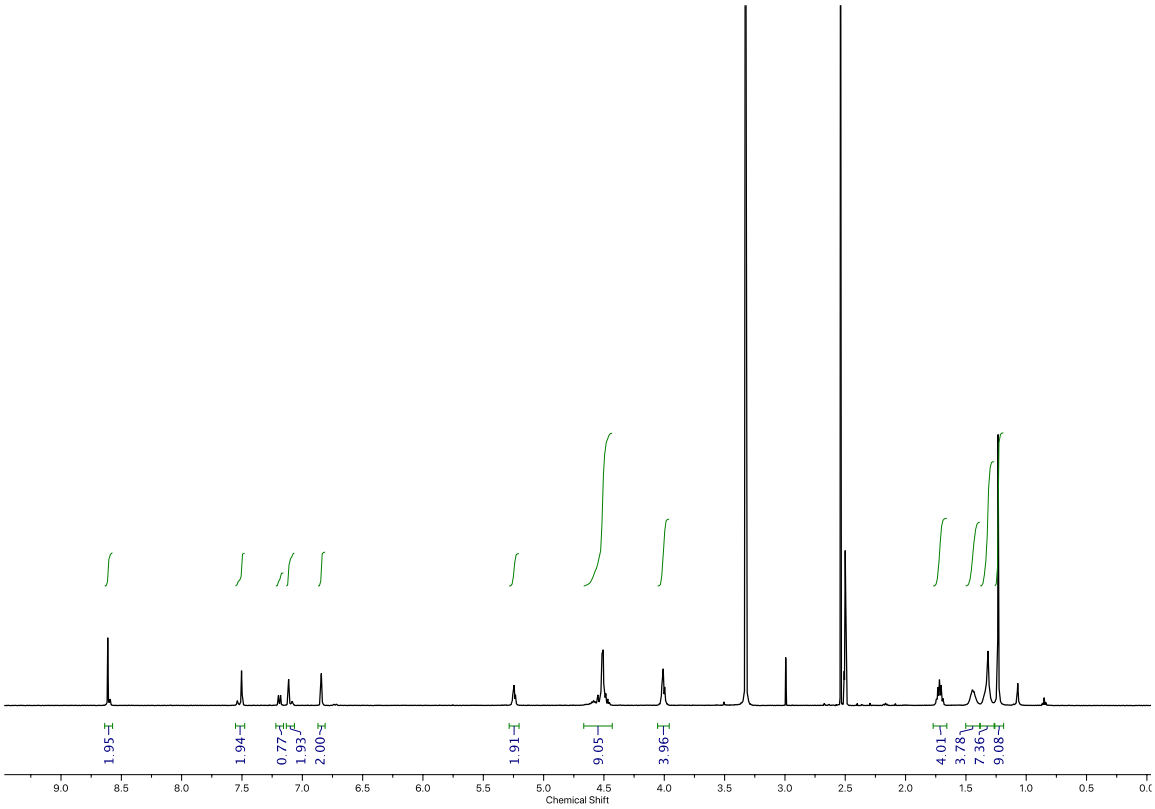

Figure 2.129 - ^{1}H NMR ($CDCl_3$, 500 MHz) of **S16**.

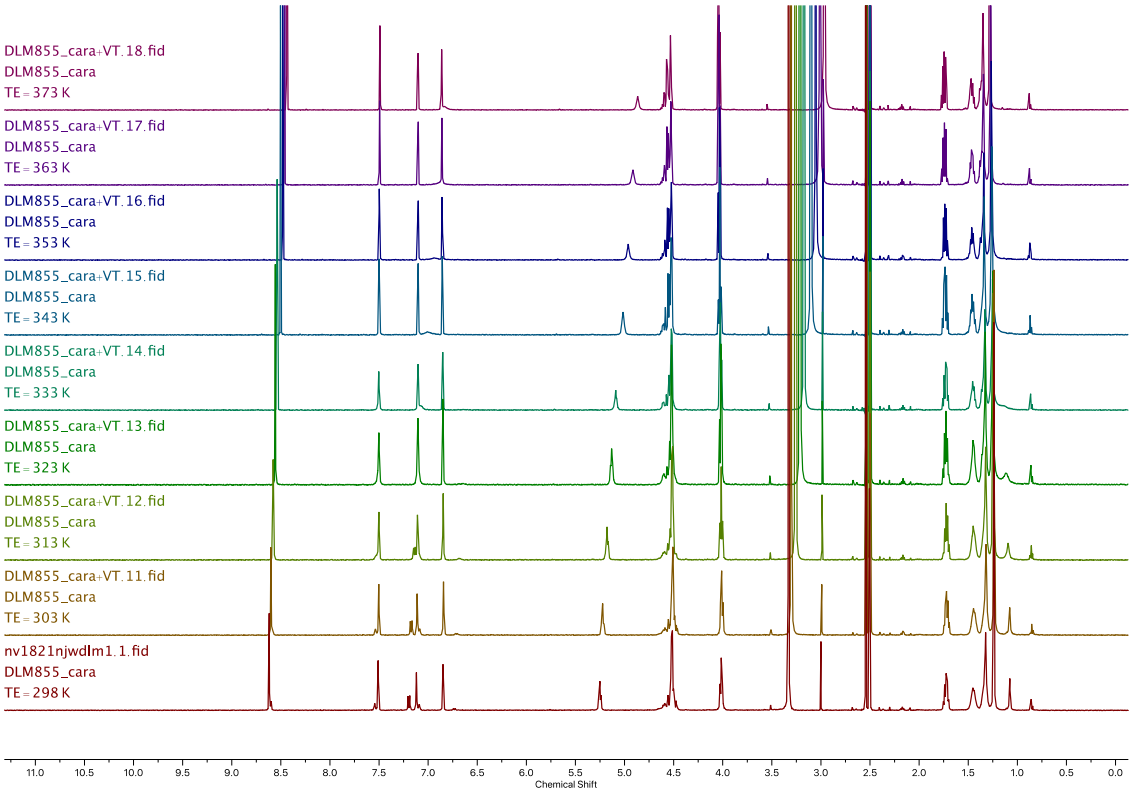

Figure 2.130 - ^{1}H VT-NMR ($CDCl_3$, 500 MHz) of **S16**.

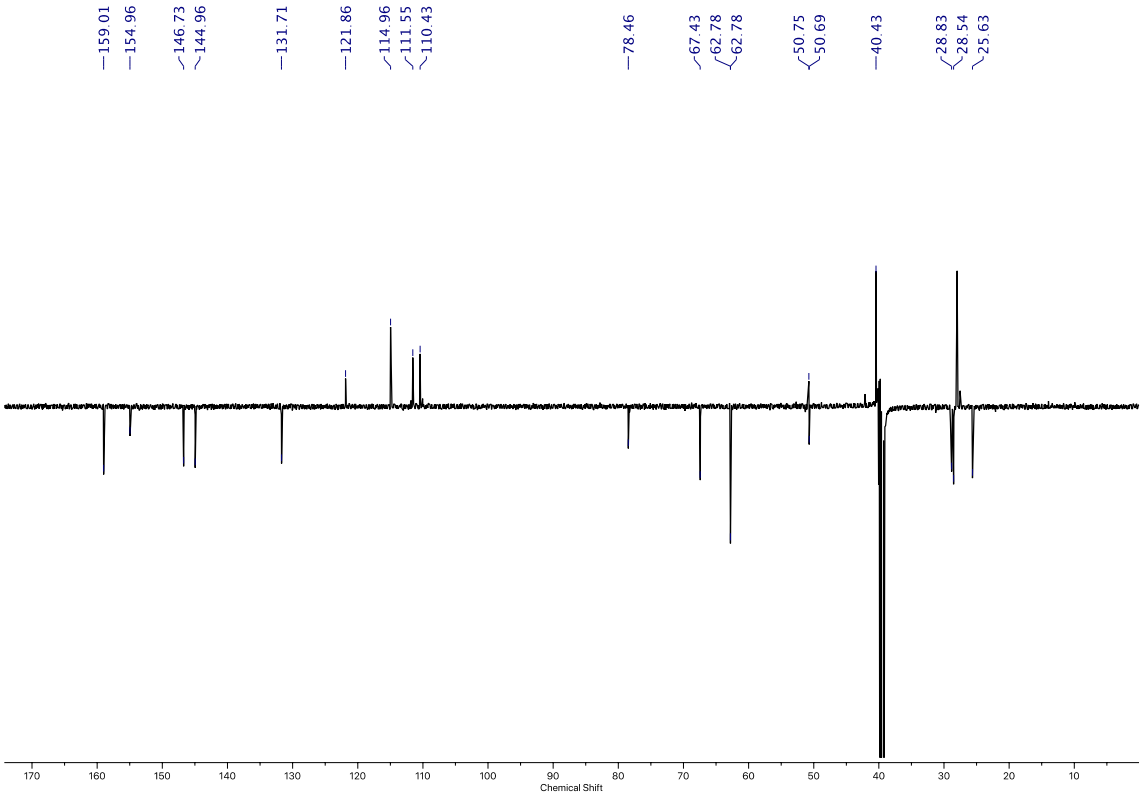

Figure 2.131 - JMOD NMR ($CDCl_3$, 126 MHz) of **S16**.

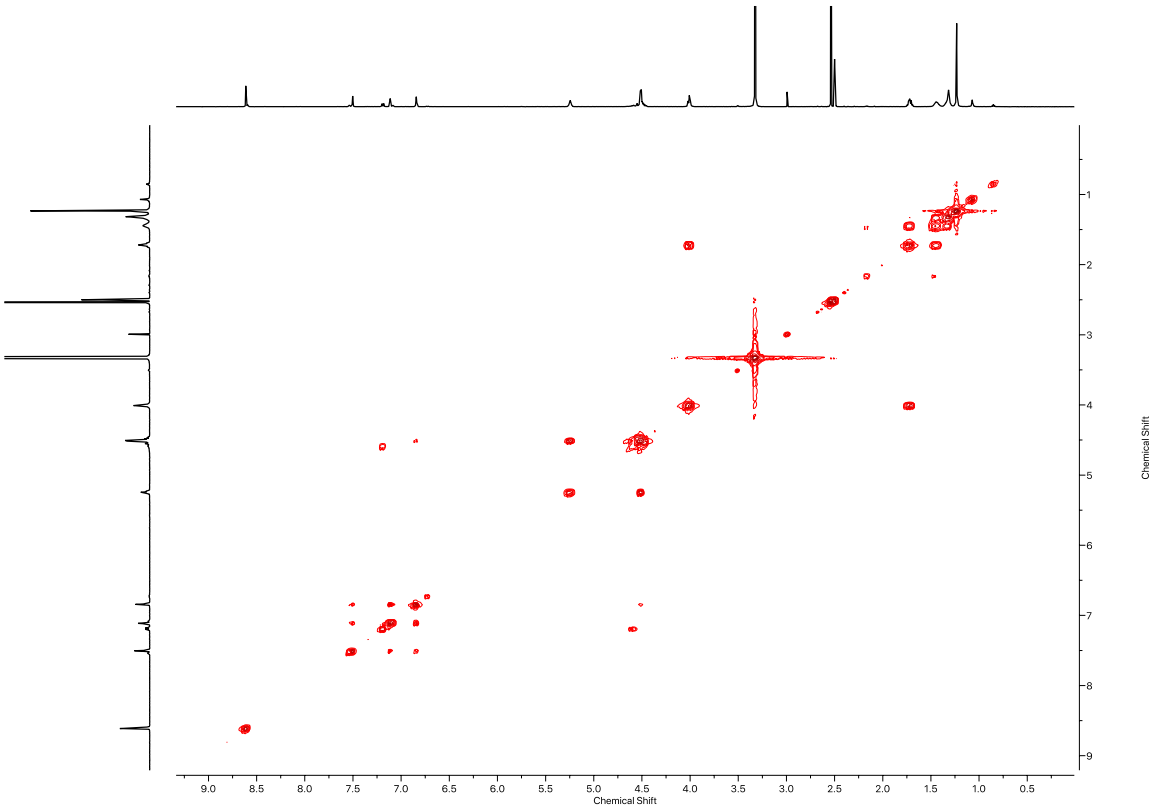

Figure 2.132 - ^1H COSY NMR (DMSO, 500 MHz) of **S16**.

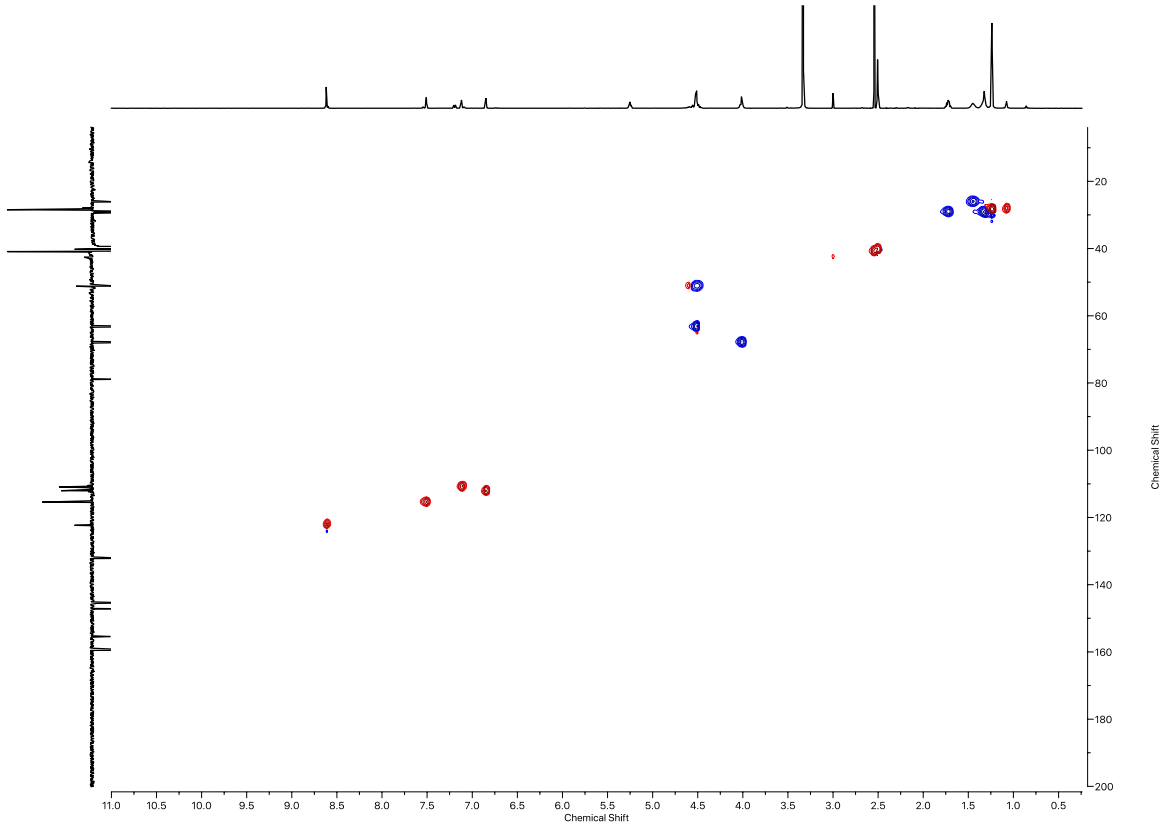

Figure 2.133 - HSQC NMR (DMSO, 500 MHz) of **S16**.

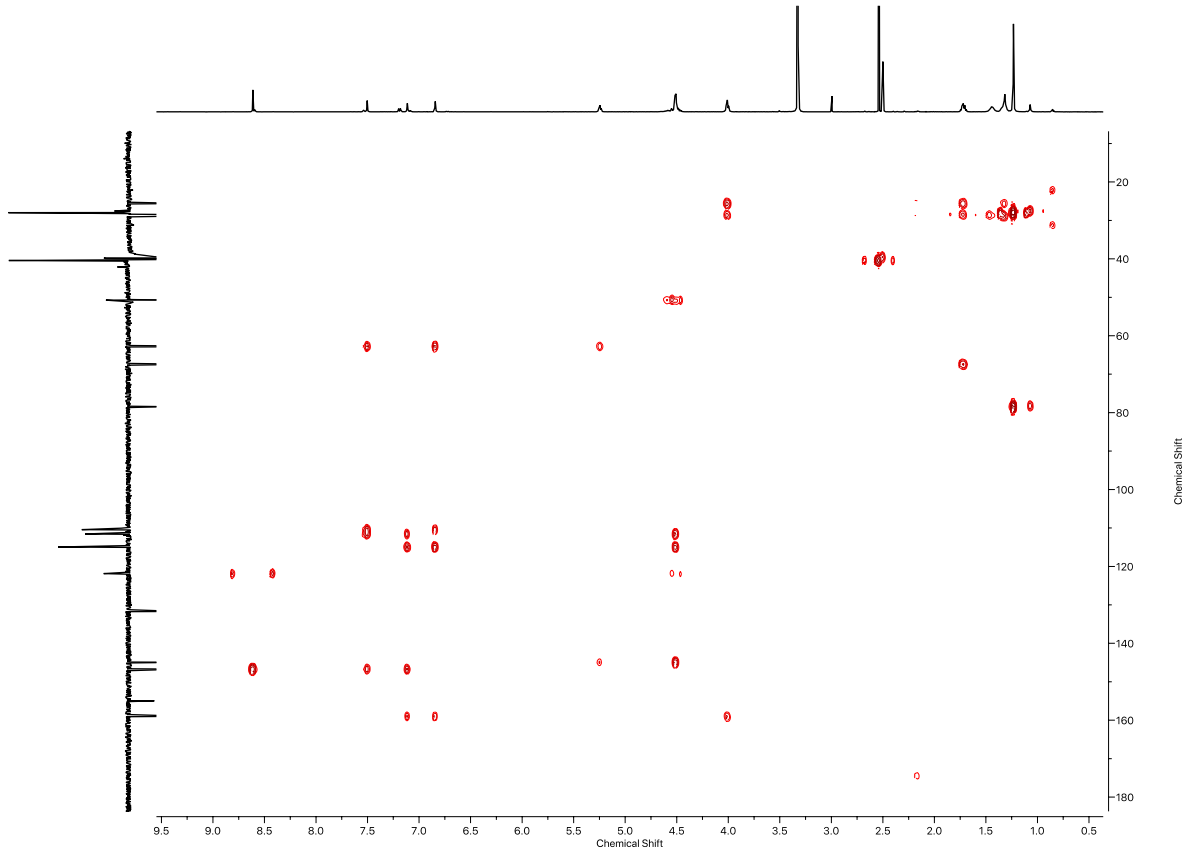

Figure 2.134 - HMBC NMR (DMSO, 500 MHz) of **S16**.

Compounds leading to rotaxane half-axle (*R*)-8

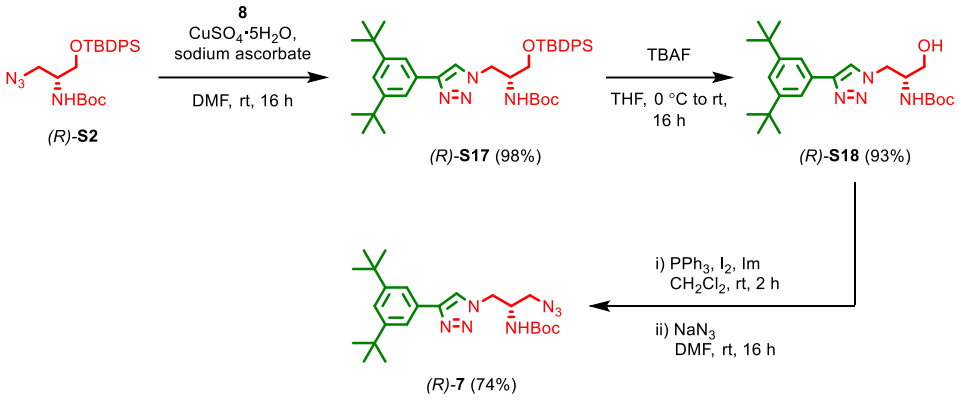

Scheme 2.6 - Synthetic route to rotaxane half axle (*R*)-**7**.

Compound (*R*)-S17

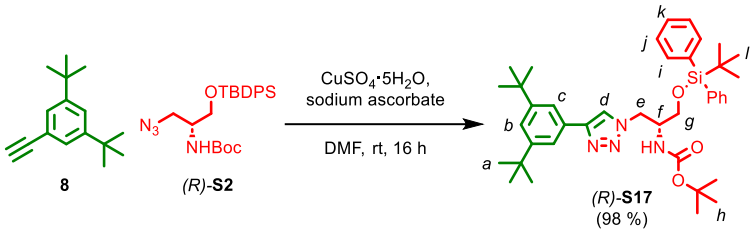

To a solution of *(R)*-**S2** (803.1 mg, 1.77 mmol, 1.0 eq.), alkyne **8** (417.6 mg, 1.95 mmol, 1.1 eq.) and sodium ascorbate (442.4 mg, 1.96 mmol,1.0 eq.) in DMF (7.4 mL) was added copper(II) sulfate pentahydrate (417.6 mg, 1.77 mmol, 1.0 eq.) and stirred at ambient temperature for 16h. The reaction mixture was diluted with EtOAc (10 mL) and washed with a saturated EDTA/NH_3 solution (10 mL). The aqueous layer was extracted with EtOAc (3 x 10 mL). The combined organic fractions were washed with 5% LiCl (3 x 5 mL), and brine (10 mL) then dried over $MgSO_4$, filtered, and concentrated *in vacuo*. The residue was purified by column chromatography (SiO_2, 1:1 petrol-Et_2O 0→20%) to yield (*R*)-**S17** as an off-white foam (1.16 g, 1.73 mmol, 98%).

δ_H ($CDCl_3$, 400 MHz) 7.80 (s, 1H, H_d), 7.67 – 7.57 (m, 6H, H_c, H_i), 7.45 – 7.30 (m, 7H, H_b, H_j, H_k), 5.02 (d, *J* = 8.5, 1H, H_{NHBoc}), 4.65 (d, *J* = 5.6, 2H, H_e), 4.17 (br. s, 1H, H_f), 3.71 (dd, *J* = 10.6, 4.4, 1H, H_g), 3.52 (dd, *J* = 10.1, 6.0, 1H, H_g), 1.40 (s, 9H, H_h), 1.37 (s, 18H, H_a), 1.11 (s, 9H, H_l); δ_C ($CDCl_3$, 101 MHz) 151.5, 148.8, 135.7, 135.6, 132.7, 130.2, 130.2, 129.9, 128.1, 122.5, 120.9, 120.3, 62.9, 52.0, 50.4, 35.1, 31.6, 28.5, 27.1, 19.5; HR-ESI-MS (+ve) m/z = 669.4198 $[M+H]^+$ (calc. m/z for $C_{40}H_{57}N_4O_3Si$ 669.4194).

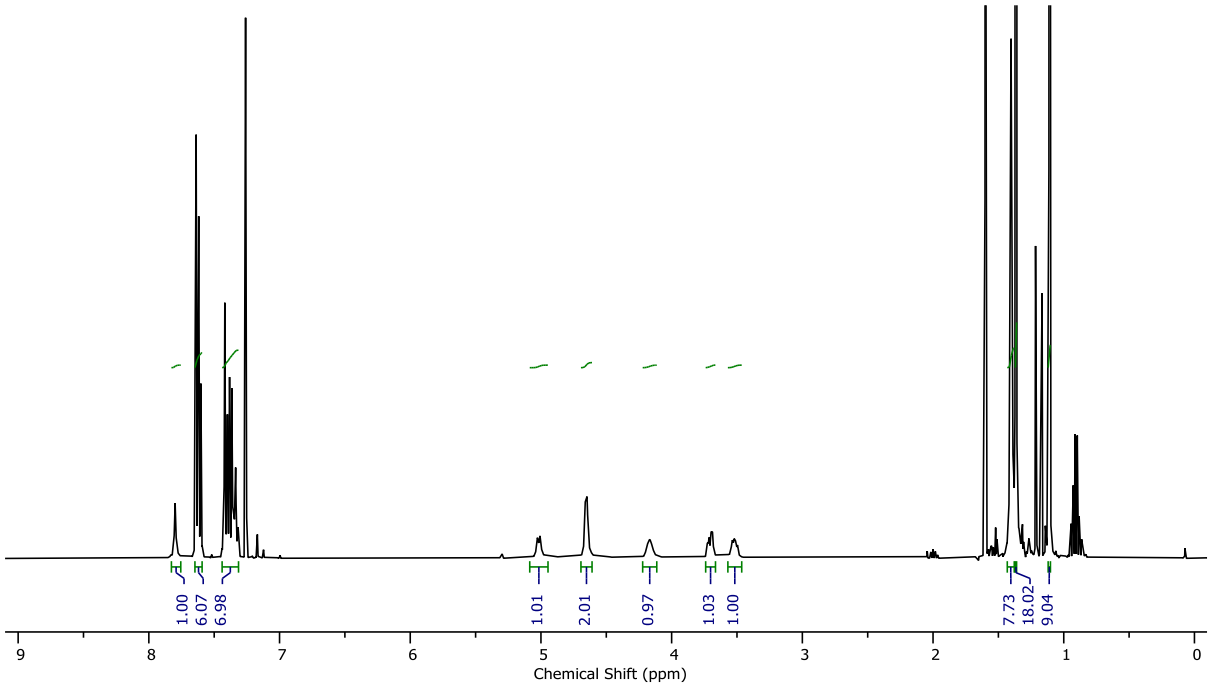

Figure 2.135 - ^{1}H NMR ($CDCl_3$, 400 MHz) of (*R*)-**S17**.

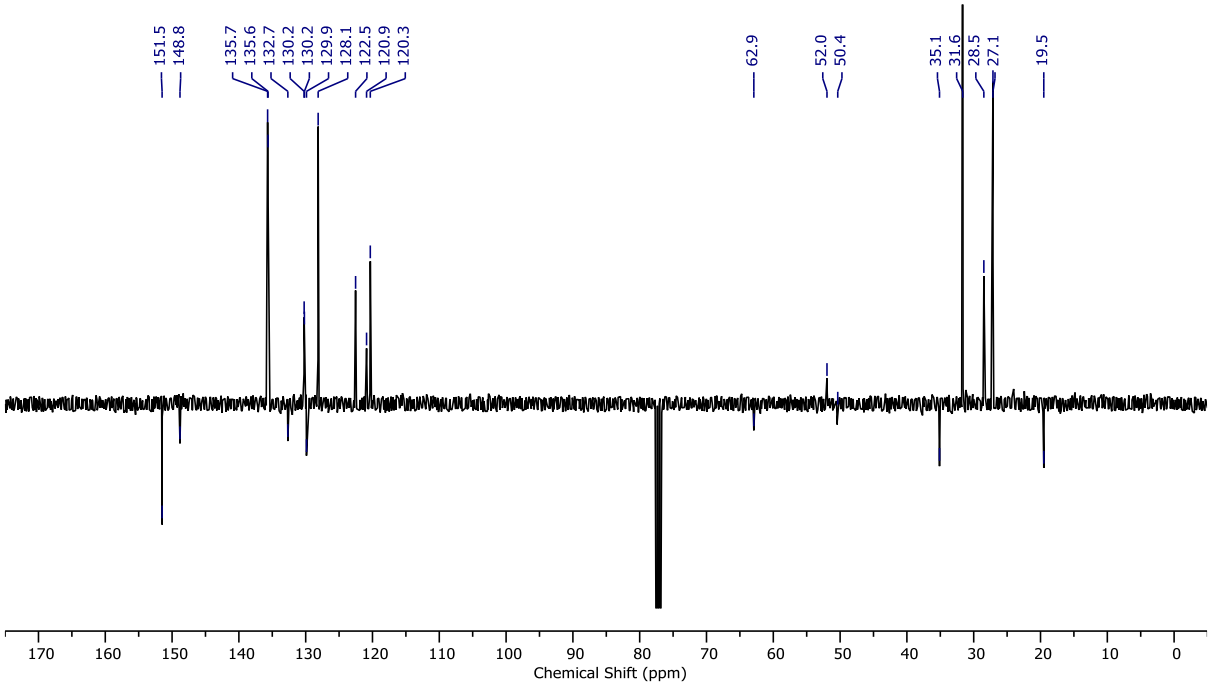

Figure 2.136 - JMOD NMR ($CDCl_3$, 101 MHz) of (*R*)-**S17**.

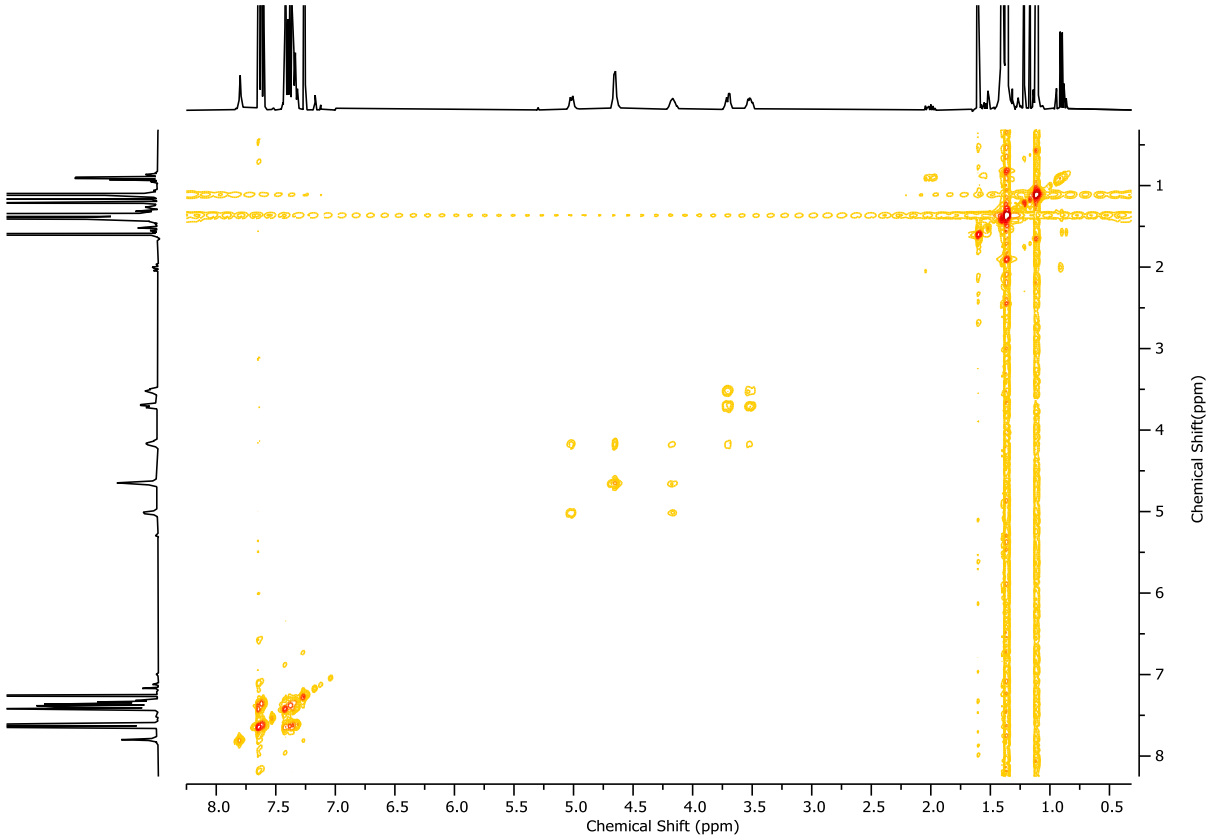

Figure 2.137 - ^{1}H COSY NMR ($CDCl_3$, 400 MHz) of (*R*)-**S17**.

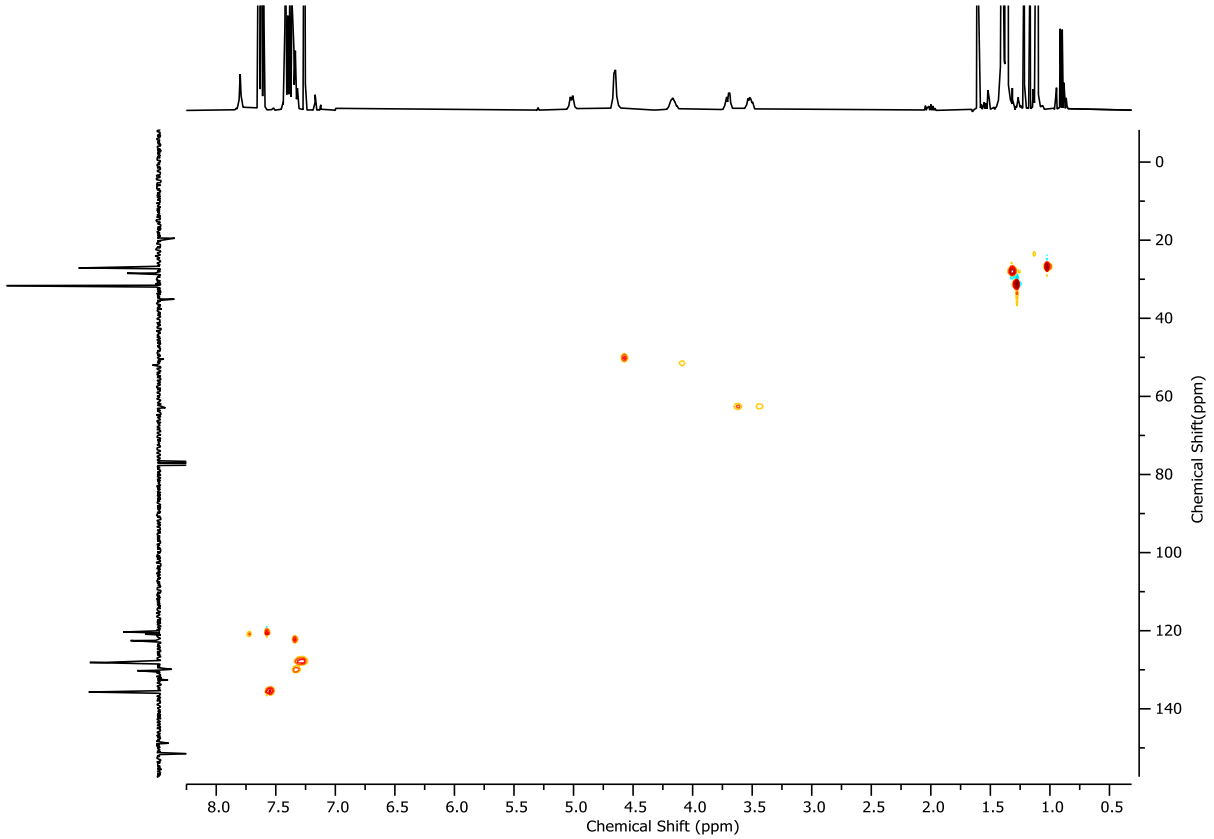

Figure 2.138 - HSQC NMR ($CDCl_3$, 400 MHz) of (*R*)-**S17**

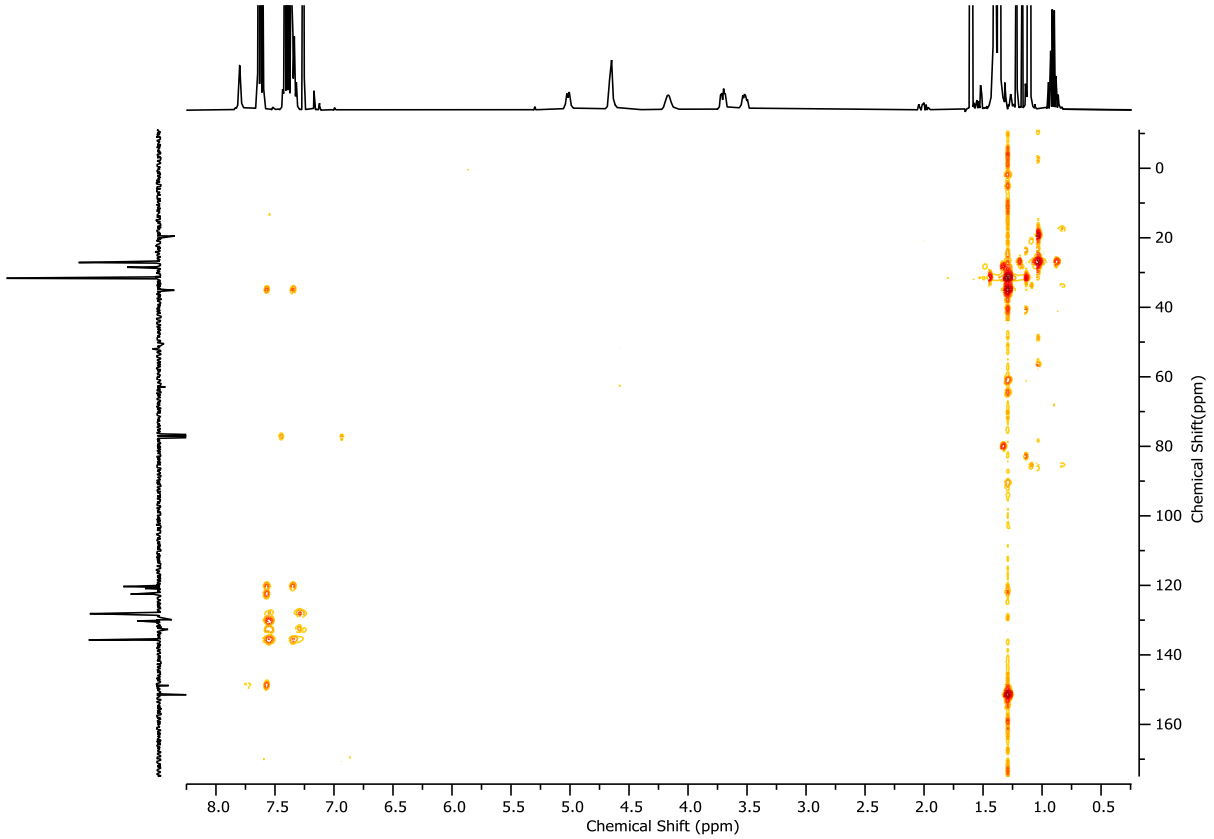

Figure 2.139 - HMBC NMR ($CDCl_3$, 400 MHz) of (*R*)-**S17**.

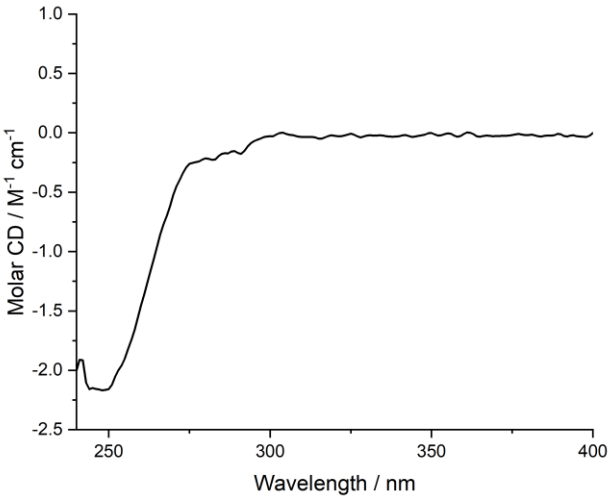

Figure 2.140 - Circular Dichroism Spectra of (*R*)-**S17** (64 µM) at 293 K in $CHCl_3$.

Compound (*R*)-S18

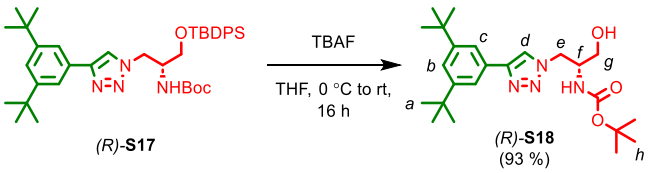

To a solution of (*R*)-**S17** (849.1 mg, 1.27 mmol, 1.0 eq.) in THF (6.3 mL) at 0 °C was added dropwise a 1.0 M solution of TBAF in THF (1.4 mL, 1.40 mmol, 1.1 eq.), and the mixture was allowed to warm to ambient temperature. After 16 h, the crude mixture was concentrated *in vacuo*, the resulting residue dissolved in EtOAc (15 mL) and washed with H_2O (10 mL). The aqueous layer was extracted with EtOAc (3 x 10 mL). The combined organic fractions were washed with brine (10 mL) then dried over $MgSO_4$, filtered, and concentrated *in vacuo*. The residue was purified by column chromatography (SiO_2, CH_2Cl_2- CH_3CN 0→20%) to yield (*R*)-**S18** (508.9 mg, 1.18 mmol, 93%) as a white solid.

δ_H ($CDCl_3$, 400 MHz) 7.88 (s, 1H, H_d), 7.65 (d, *J* = 1.8, 2H, H_c), 7.42 (t, *J* = 1.8, 2H, H_b), 5.35 (d, *J* = 7.9, 1H, H_{NHBoc}), 4.70 (dd, *J* = 13.9, 6.4, 1H, H_e), 4.63 (dd, *J* = 13.9, 5.2, 1H, H_e), 4.09 – 4.00 (m, 1H, H_f), 3.75 – 3.68 (m, 1H, H_g), 3.60 – 3.53 (dd, 1H, H_g), 1.44 (s, 9H, H_h), 1.37 (s, 18H, H_a); δ_C ($CDCl_3$, 101 MHz) 155.9, 151.6, 149.0, 129.5, 123.9, 121.2, 120.3, 80.4, 61.5, 52.2, 50.0, 35.1, 31.6, 28.5; HR-ESI-MS (+ve) m/z = 431.3019 $[M+H]^+$ (calc. m/z for $C_{24}H_{39}N_4O_3$ 431.3017); Melting Point 130-133 °C.

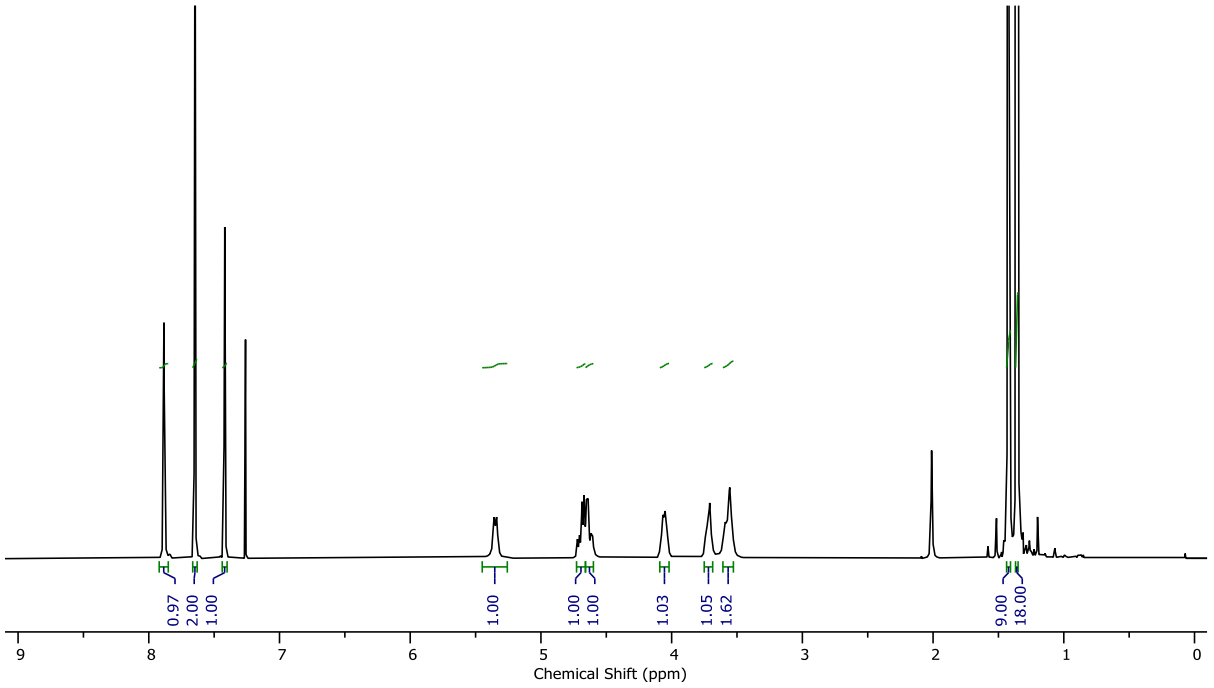

Figure 2.141 - ^1H NMR ($CDCl_3$, 400 MHz) of (*R*)-**S18**.

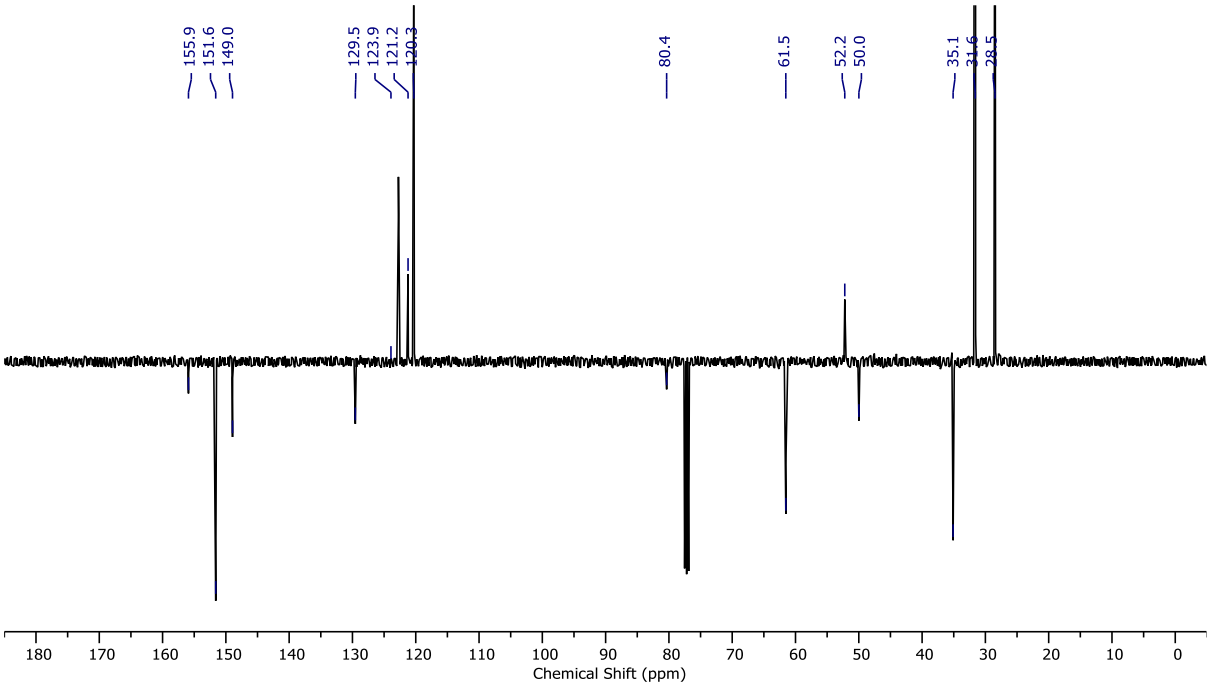

Figure 2.142 - JMOD NMR ($CDCl_3$, 101 MHz) of (*R*)-**S18**.

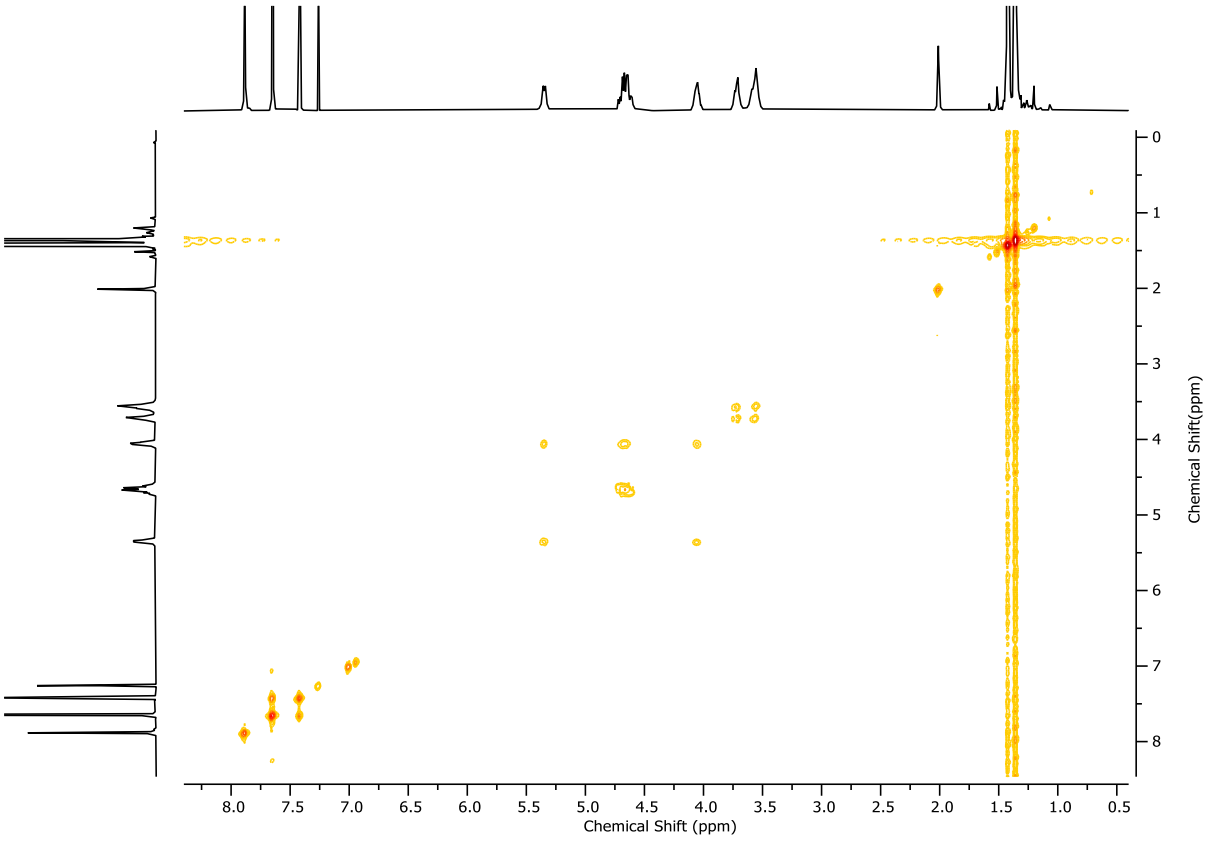

Figure 2.143 - ^1H COSY NMR ($CDCl_3$, 400 MHz) of (*R*)-**S18**.

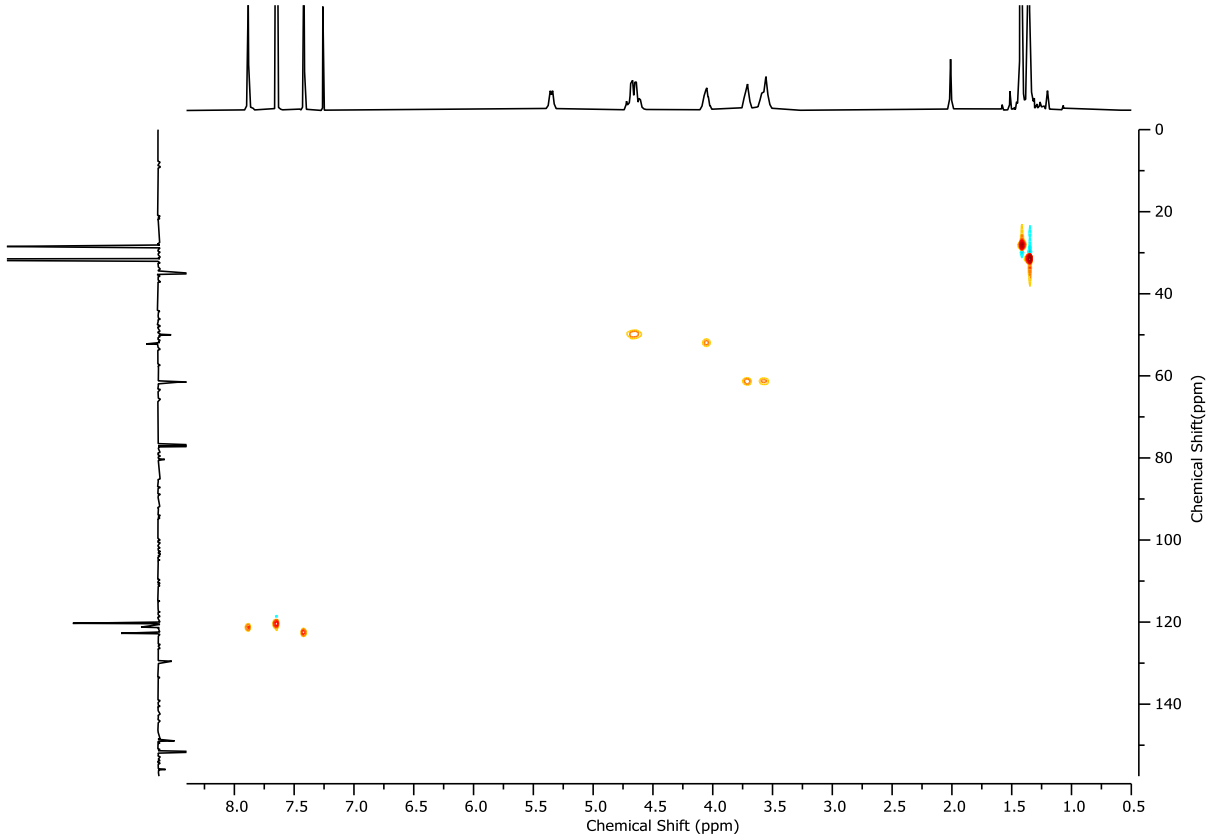

Figure 2.144 - HSQC NMR ($CDCl_3$, 400 MHz) of (*R*)-**S18**.

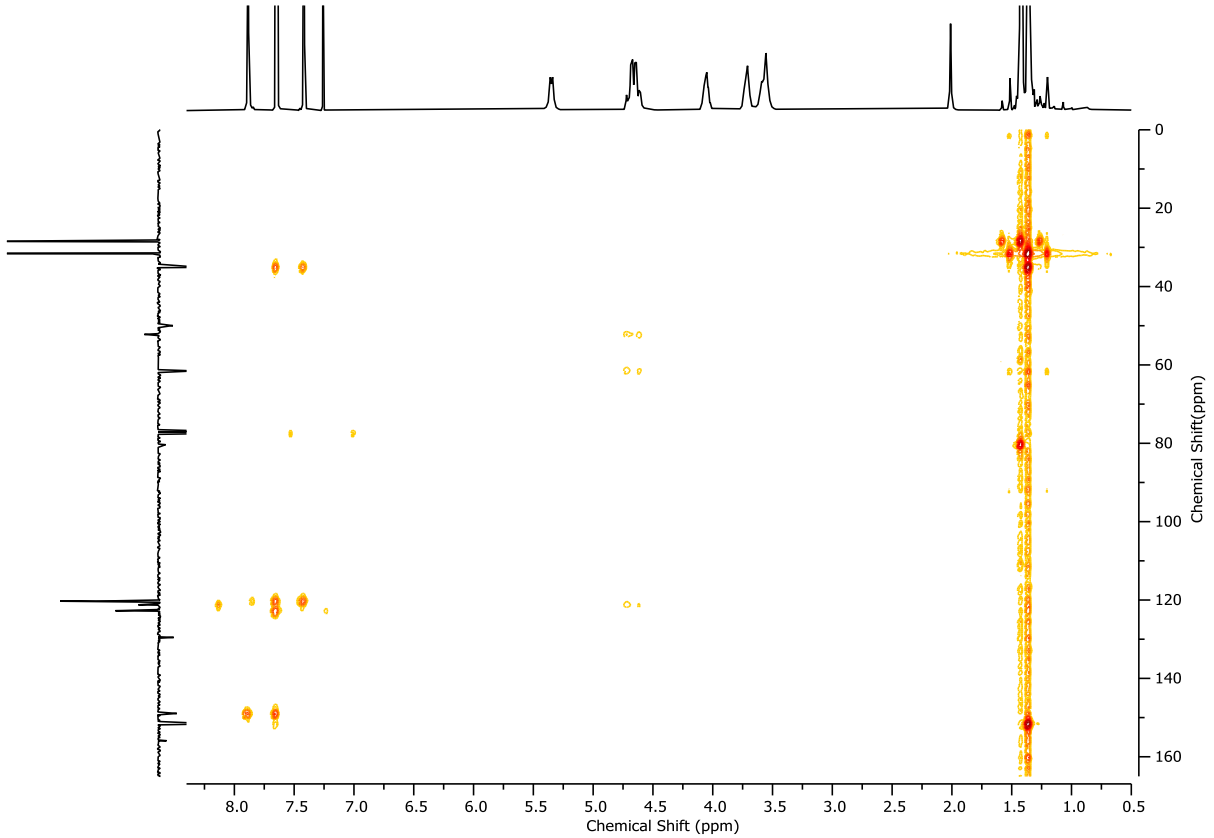

Figure 2.145 - HMBC NMR ($CDCl_3$, 400 MHz) of (*R*)-**S18**.

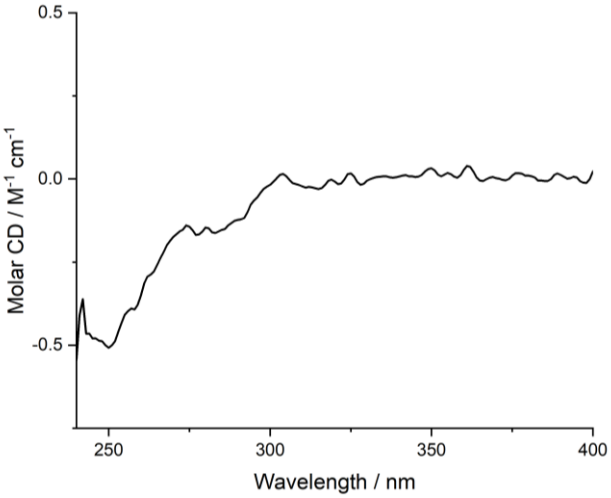

Figure 2.146 - Circular Dichroism Spectra of (*R*)-**S18** (46 μM) at 293 K in $CHCl_3$.

Rotaxane half-axle (*R*)-7

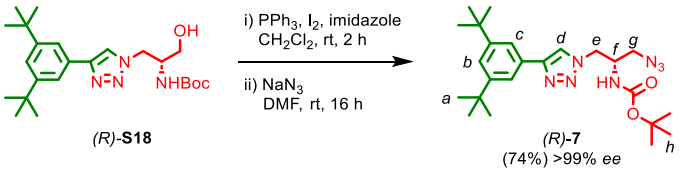

To a solution of PPh_3 (216.0 mg, 0.82 mmol, 3.0 eq.) and imidazole (99.4 mg, 1.46 mmol, 5.0 eq.) in CH_2Cl_2 (1.8 mL) was added I_2 (207.3 mg, 0.82 mmol, 3.0 eq.) in 1 portion at 0 °C. After stirring for 10 min, a solution of (*R*)-**S18** (118.1 mg, 0.27 mmol, 1.0 eq.) in CH_2Cl_2 (1.0 mL) was added dropwise. The reaction mixture was allowed to warm to ambient temperature and stirred for 2 h. The crude mixture was filtered through Celite®, washing with CH_2Cl_2, and concentrated *in vacuo*. The residue was purified by column chromatography (SiO_2, petrol-EtOAc 0→10%). The resultant oil was immediately dissolved in DMF (1.3 mL) and NaN_3 (155.3 mg, 2.39 mmol, 8.9 eq.) was added. After stirring for 16 h at ambient temperature, the reaction mixture was diluted with EtOAc (10 mL) and washed with H_2O (10 mL). The aqueous layer was extracted with EtOAc (3 x 10 mL). The combined organic fractions were washed with 5% LiCl (2 x 15 mL), and brine (15 mL) then dried over $MgSO_4$, filtered, and concentrated *in vacuo*. The residue was purified by column chromatography (SiO_2, petrol-EtOAc 0→20%) to yield (*R*)-**7** (93.1 mg, 0.20 mmol, 74%) as an off-white foam.

δ_H ($CDCl_3$, 400 MHz) 7.82 (s, 1H, H_d), 7.67 (d, J = 1.8, 2H, H_c), 7.42 (t, J = 1.8, 1H, H_b), 5.19 (d, J = 8.3, 1H, H_{NHBoc}), 4.59 (d, J = 5.6, 2H, H_e), 4.23 – 4.10 (m, 1H, H_f), 3.55 (dd, J = 12.4, 5.1, 1H, H_g), 3.33 (dd, J = 12.4, 6.4, 1H, H_g), 1.43 (s, 9H, H_h), 1.37 (s, 18H, H_a); δ_C ($CDCl_3$, 101 MHz) 155.2, 151.6, 149.0, 129.5, 122.8, 120.9, 120.3, 80.7, 51.3, 50.4, 50.3, 35.1, 31.6, 28.4; HR-ESI-MS (+ve) m/z = 456.3082 $[M+H]^+$ (calc. m/z for $C_{24}H_{38}N_7O_2$ 456.3081).

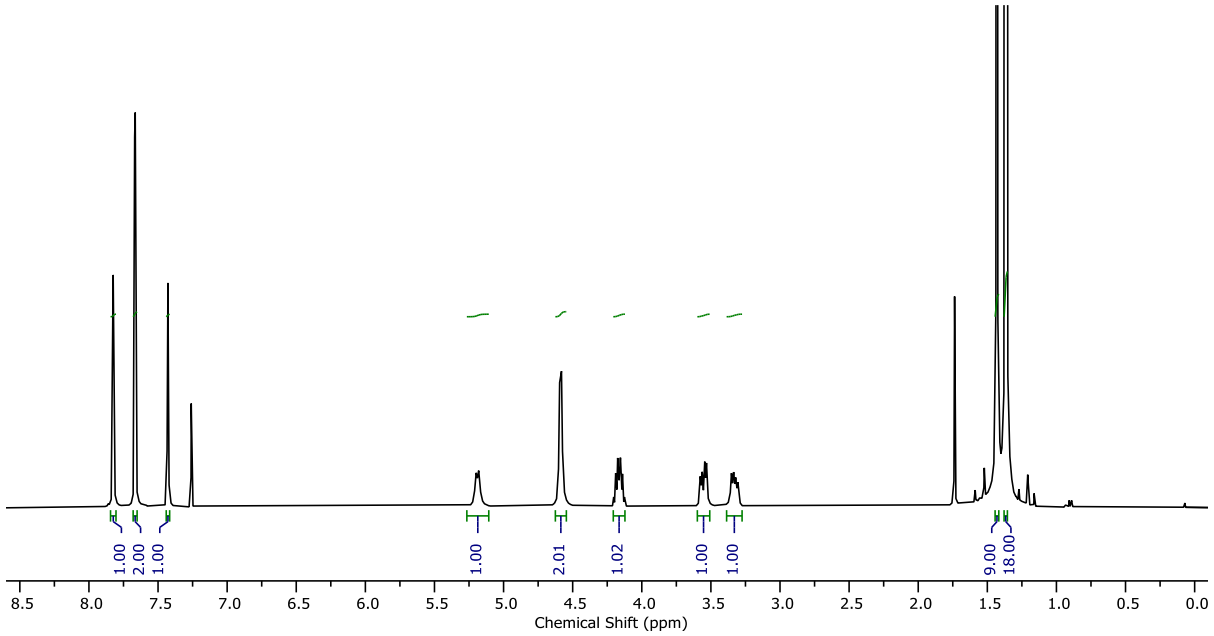

Figure 2.147 - ^{1}H NMR ($CDCl_3$, 400 MHz) of (*R*)-**7**.

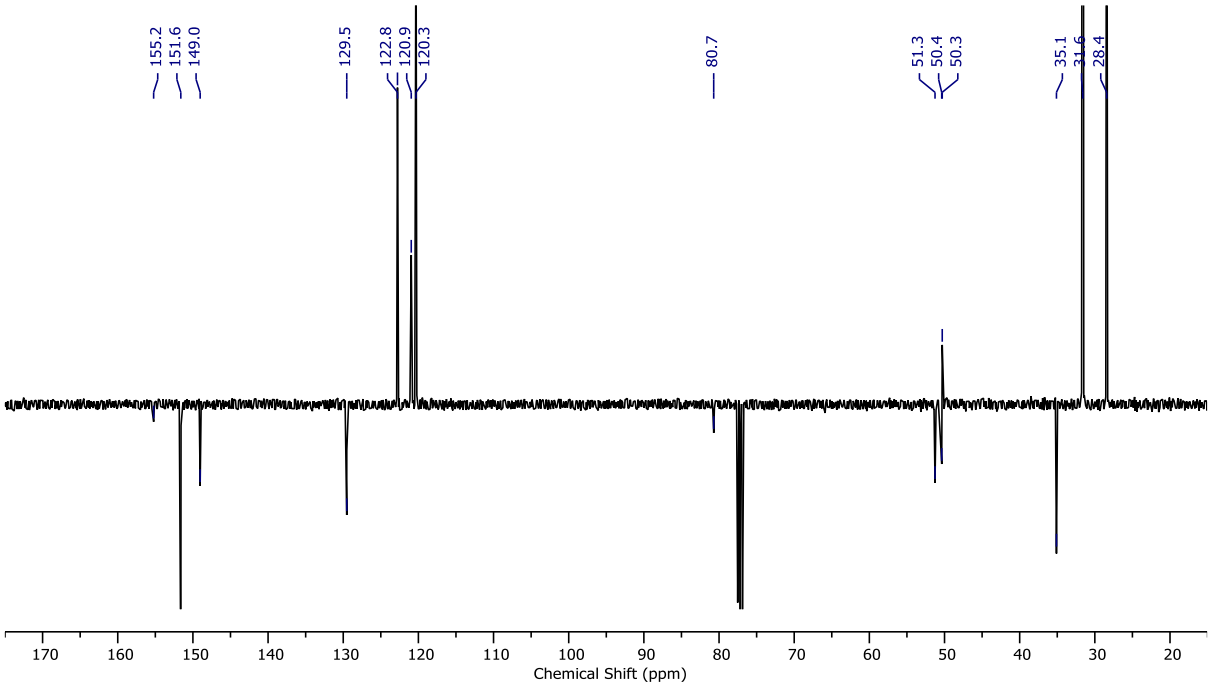

Figure 2.148 - JMOD NMR ($CDCl_3$, 101 MHz) of (*R*)-**7**.

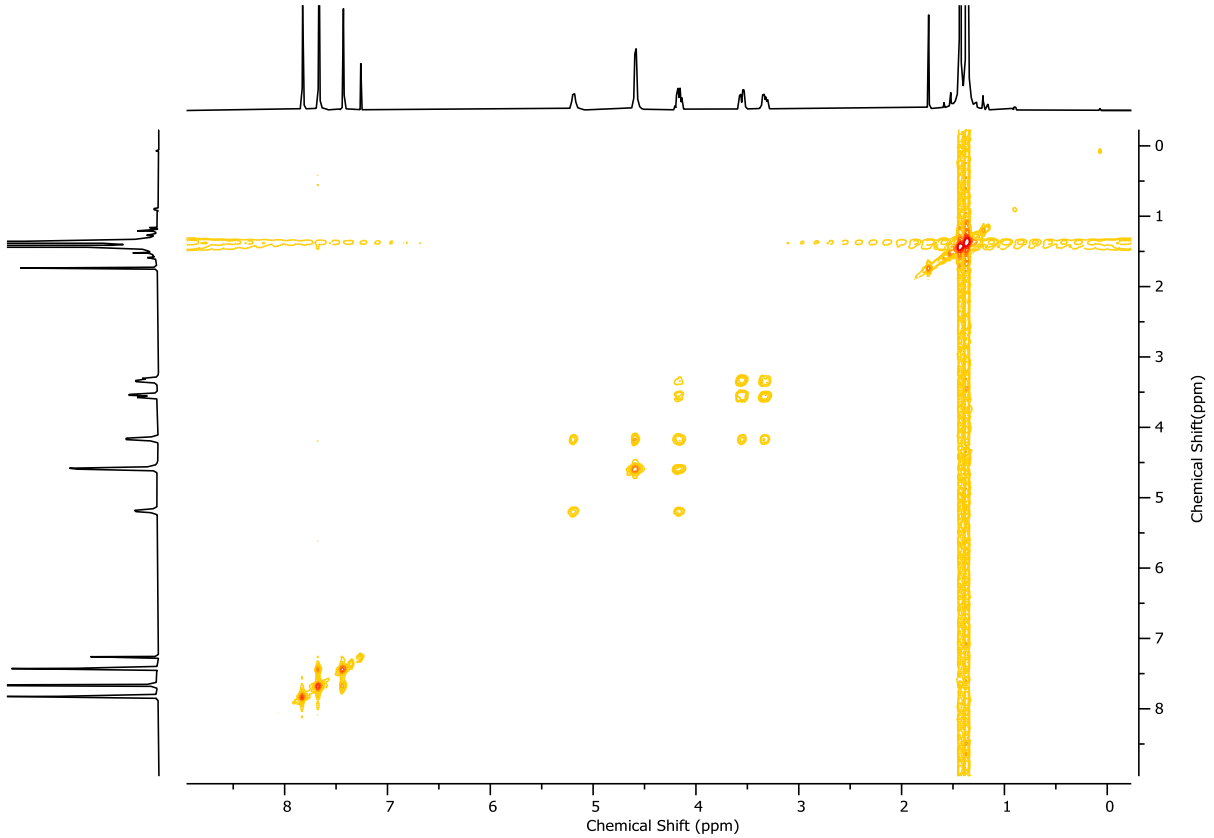

Figure 2.149 - ^{1}H COSY NMR ($CDCl_3$, 400 MHz) of (*R*)-**7**.

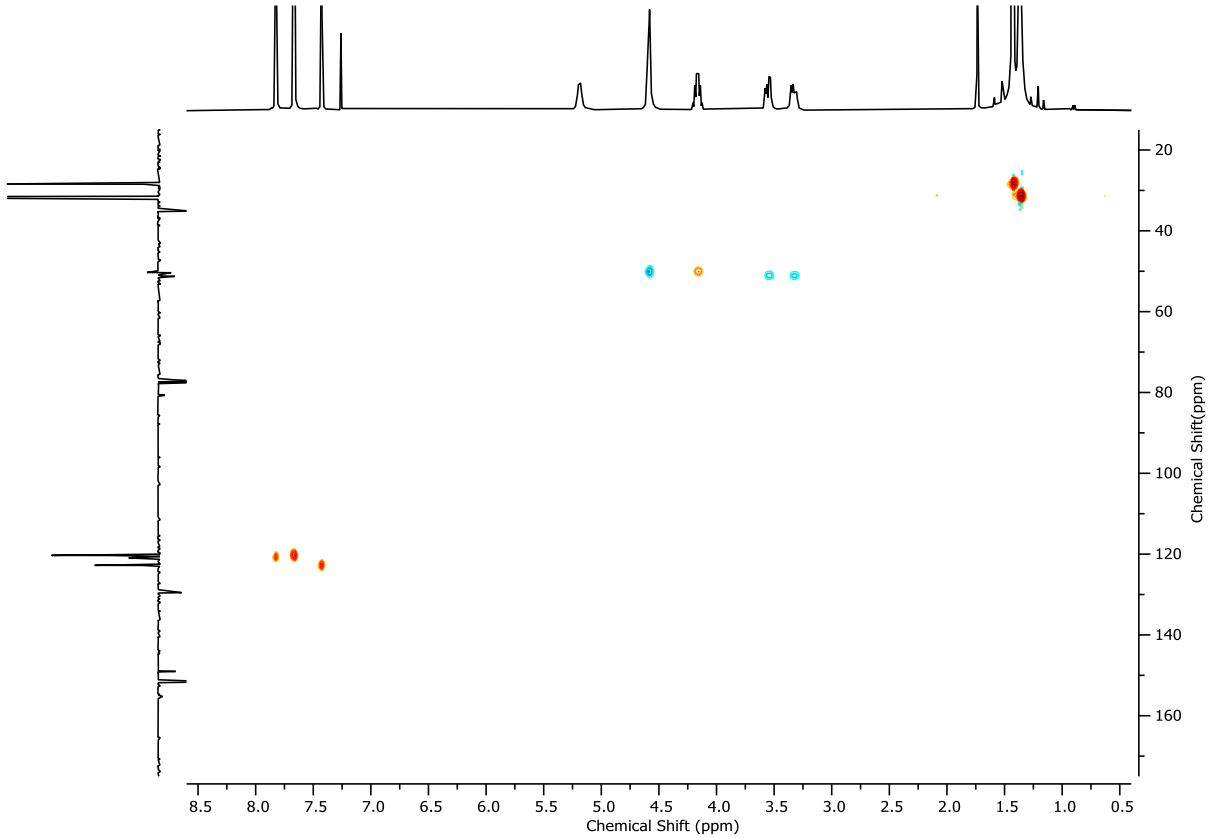

Figure 2.150 - HSQC NMR ($CDCl_3$, 400 MHz) of (*R*)-**7**.

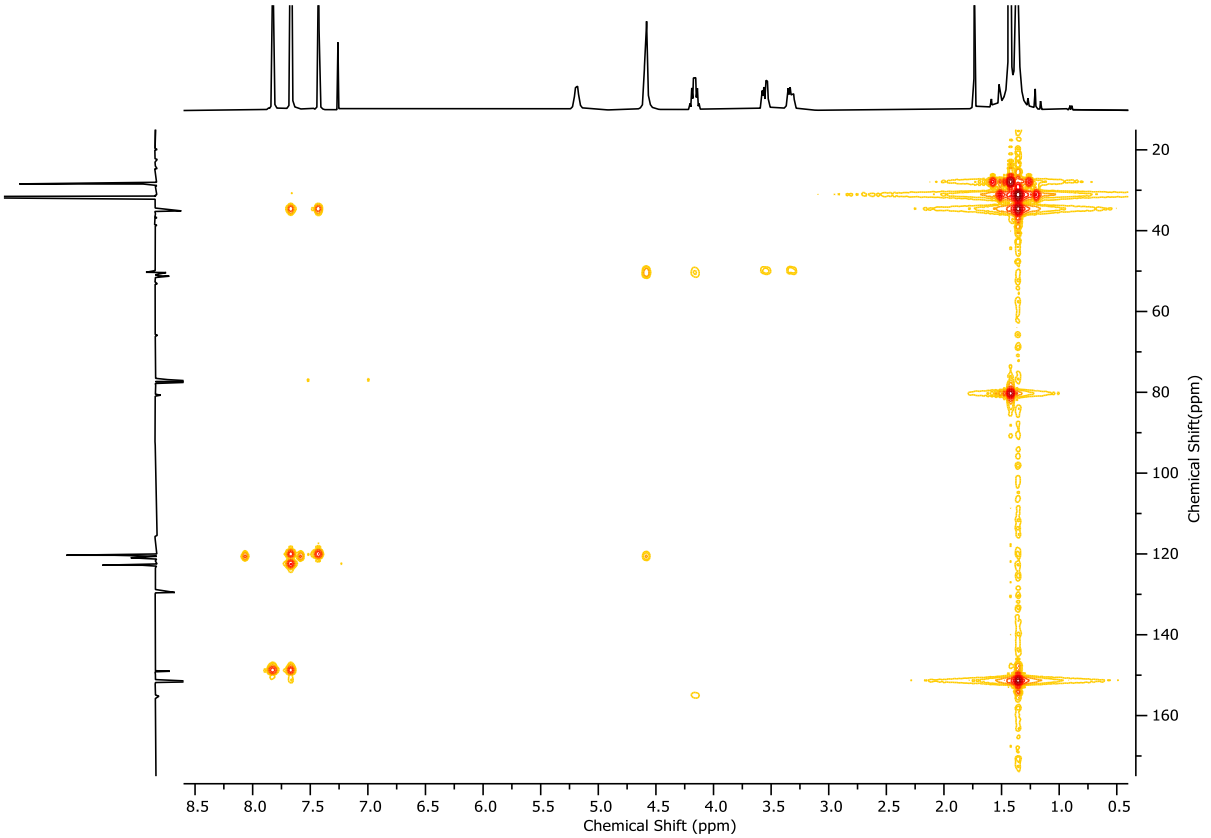

Figure 2.151 - HMBC NMR ($CDCl_3$, 400 MHz) of (*R*)-**7**.

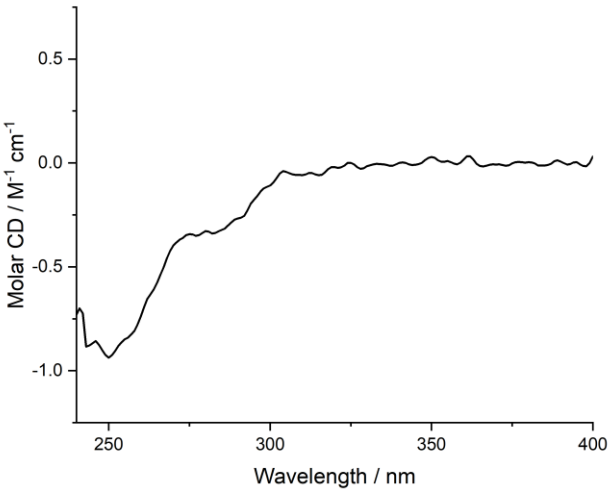

Figure 2.152 - Circular Dichroism Spectra of (*R*)-**7** (41 µM) at 293 K in $CHCl_3$.

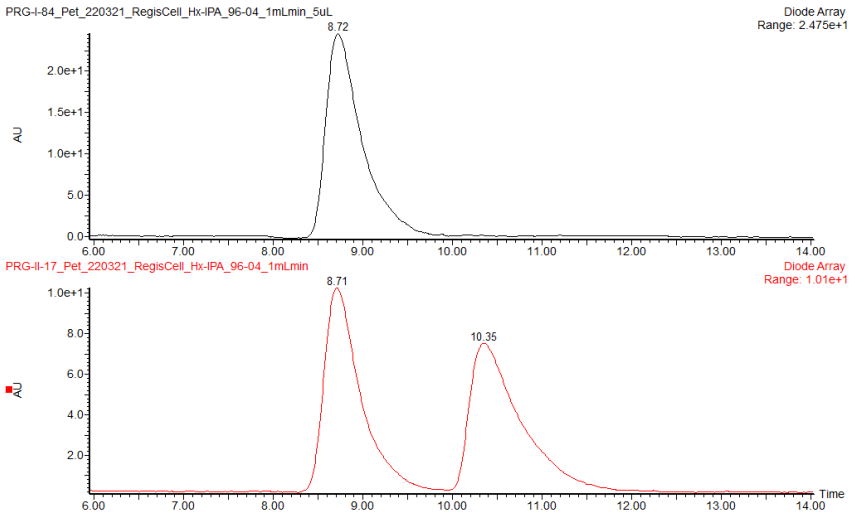

Figure 2.153 - CSP-HPLC of (*R*)-**7** (loaded in Et_2O). RegisCell, *n*-hexane-EtOH 98 : 2, flowrate 1 $mLmin^{-1}$. (top) (*R*)-**7** (8.72 min, 11538817, >99.9%), (*S*)-**7** (not observed). (bottom) *rac*-**7**, (*R*)-**7** (8.71 min, 4729977, 50.1%), (*S*)-**7** (10.35 min, 4710027, 49.9%).

Synthesis of rotaxanes (S_{ma},$R_{co\text{-}c}$)-9 and (R_{ma},$R_{co\text{-}c}$)-9

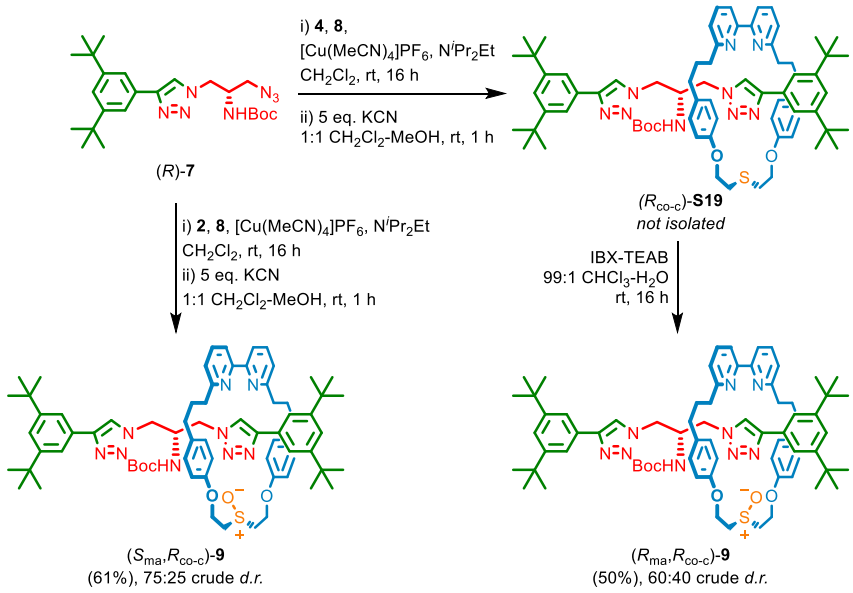

Scheme 2.7 - Synthetic route to mechanically axially chiral epimeric catenanes (R_{ma},$R_{co\text{-}c}$)-**9** and (S_{ma},$R_{co\text{-}c}$)-**9**.

Rotaxane (S_{ma},$R_{co\text{-}c}$)-9

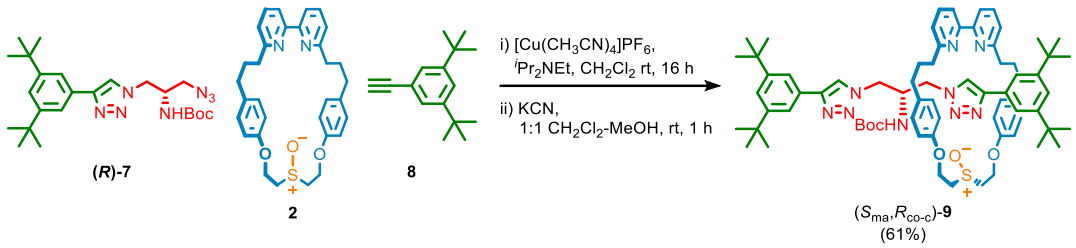

A CEM MW vial was charged with alkyne **8** (18.7 mg, 0.087 mmol, 1.1 eq.), azide (*R*)-**7** (38.3 mg, 0.084 mmol, 1.1 eq.), macrocycle **2** (40.2 mg, 0.076 mmol, 1.0 eq.) and $[Cu(CH_3CN)_4]PF_6$ (27.7 mg, 0.074 mmol, 0.97 eq.) and purged with N_2. CH_2Cl_2 (1.9 mL) and $^iPr_2NEt$ (26 µL, 0.15 mmol, 2.0 eq.) were added and the resulting deep red solution was stirred at ambient temperature for 16 h. Then, MeOH (1.9 mL) and KCN as a solid (25 mg, 0.38 mmol, 5.0 eq.) were added and the resulting mixture was stirred vigorously for 1 h. The crude mixture was diluted with CH_2Cl_2 (5 mL) and washed with H_2O in two portions (10 mL and 5 mL). The combined aqueous phase was then extracted with CH_2Cl_2 (3 x 5 mL) and the combined organics were washed with brine (10 mL), dried over $MgSO_4$ and concentrated *in vacuo*. The residue was purified by column chromatography (SiO_2, petrol-EtOAc 0→50% then petrol-EtOAc (1:1) with MeOH 0→5%) to yield (S_{ma},$R_{co\text{-}c}$)-**9** (55.3 mg, 0.046 mmol, 61%) as a white foam. See 8.2 for a discussion of stereochemical assignment.

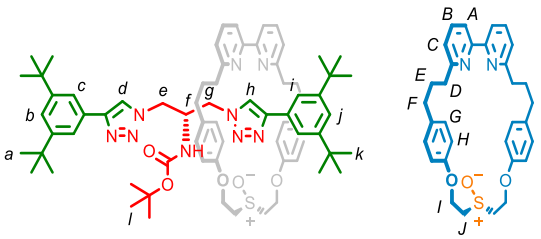

δ_H ($CDCl_3$, 400 MHz) 9.41 (s, 1H, H_h), 7.73 (s, 1H, H_d), 7.67 (d, J = 1.6, 2H, H_c), 7.63 (app. td, J = 8.3, 7.8, 2H, H_B), 7.55 (d, J = 1.8, 2H, H_i), 7.45 (dd, J = 7.7, 0.9, 2H, H_A), 7.40 (t, J = 1.8, 1H, H_b), 7.28 (t, J = 1.8, 1H, H_j), 7.16 – 7.09 (m, 2H, H_C), 6.69 – 6.61 (m, 8H, H_G, H_H), 5.35 (d, J = 6.6, 1H, H_{NHBoc}), 4.74 – 4.63 (m, 2H, H_l), 4.62 – 4.54 (m, 2H, H_l), 4.11 – 3.98 (m, 3H, H_J, H_e), 3.90 (app. q, J = 7.7, 1H, H_e), 3.76 – 3.67 (m, 2H, H_f, H_g), 3.64 – 3.54 (m, 1H, H_g), 3.27 – 3.14 (m, 2H, H_J), 2.60 – 2.50 (m, 2H, H_F), 2.49 – 2.33 (m, 6H, H_D, H_F), 1.83 – 1.65 (m, 4H, H_E), 1.37 (s, 18H, H_a), 1.25 (s, 9H, H_l), 1.22 (s, 18H, H_k); δ_C ($CDCl_3$, 101 MHz) 162.9, 162.9, 157.6, 157.6, 156.0, 155.9, 151.4, 150.9, 148.4, 147.4, 137.1, 133.8, 133.6, 132.3, 132.2, 132.1, 132.1, 130.6, 130.1, 129.5, 129.4, 128.8, 128.6, 122.3, 122.0, 121.6, 120.4, 120.3, 120.0, 79.9, 60.9, 60.9, 53.2, 53.1, 51.1, 50.5, 50.3, 37.2, 37.1, 35.1, 35.0, 34.9, 34.8, 31.7, 31.5, 31.4, 31.0, 30.4, 29.9, 28.4; LR-ESI-MS (+ve) m/z = 1196.7 $[M+H]^+$.

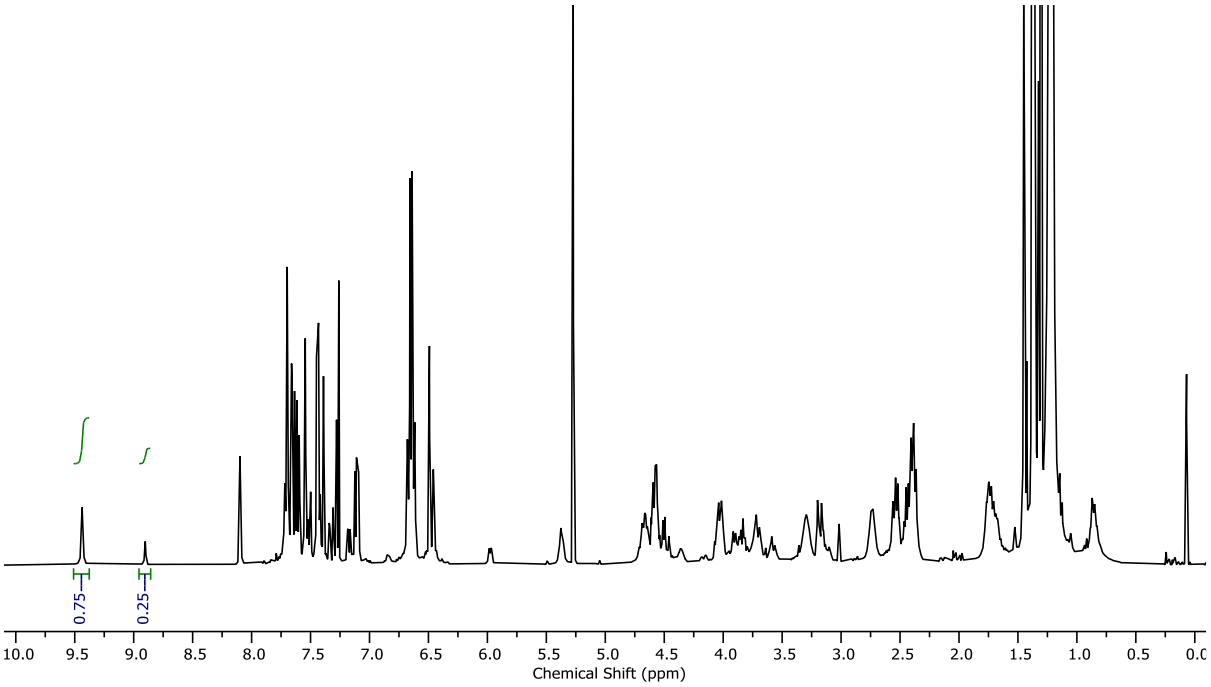

Figure 2.154 - Crude ^{1}H NMR of **9** *via* AT-CuAAC reaction of macrocycle **3** (CDCl3, 400 MHz). Diastereoisomer integration: $\boldsymbol{H}_{h}$ protons (major 9.44 ppm, 0.75, minor 8.89 ppm, 0.25).

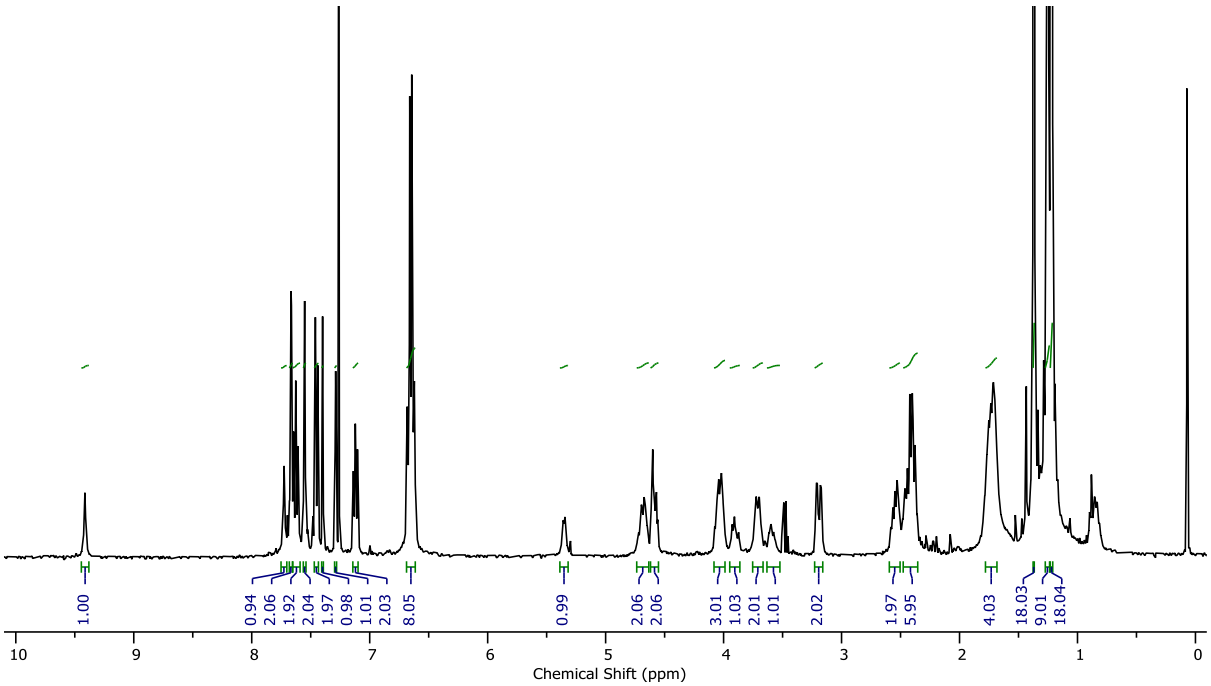

Figure 2.155 - ^{1}H NMR ($CDCl_3$, 400 MHz) of (S_{ma},$R_{co\text{-}c}$)-**9**.

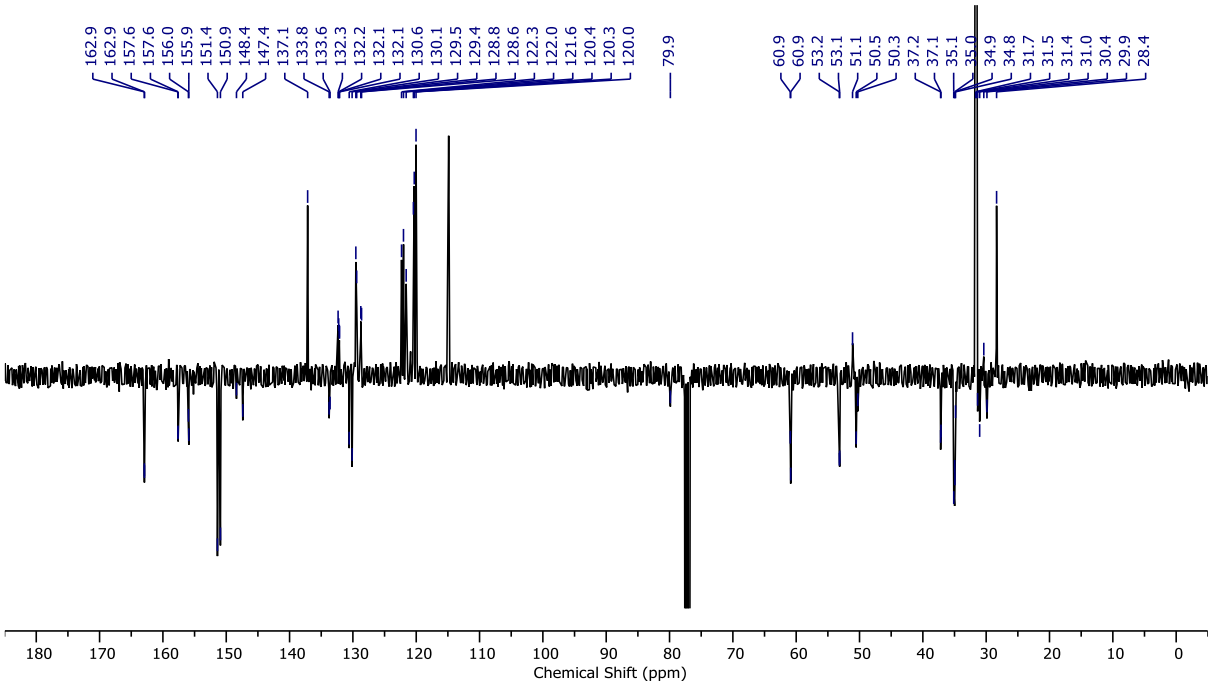

Figure 2.156 - JMOD NMR ($CDCl_3$, 101 MHz) of (S_{ma},$R_{co\text{-}c}$)-**9**.

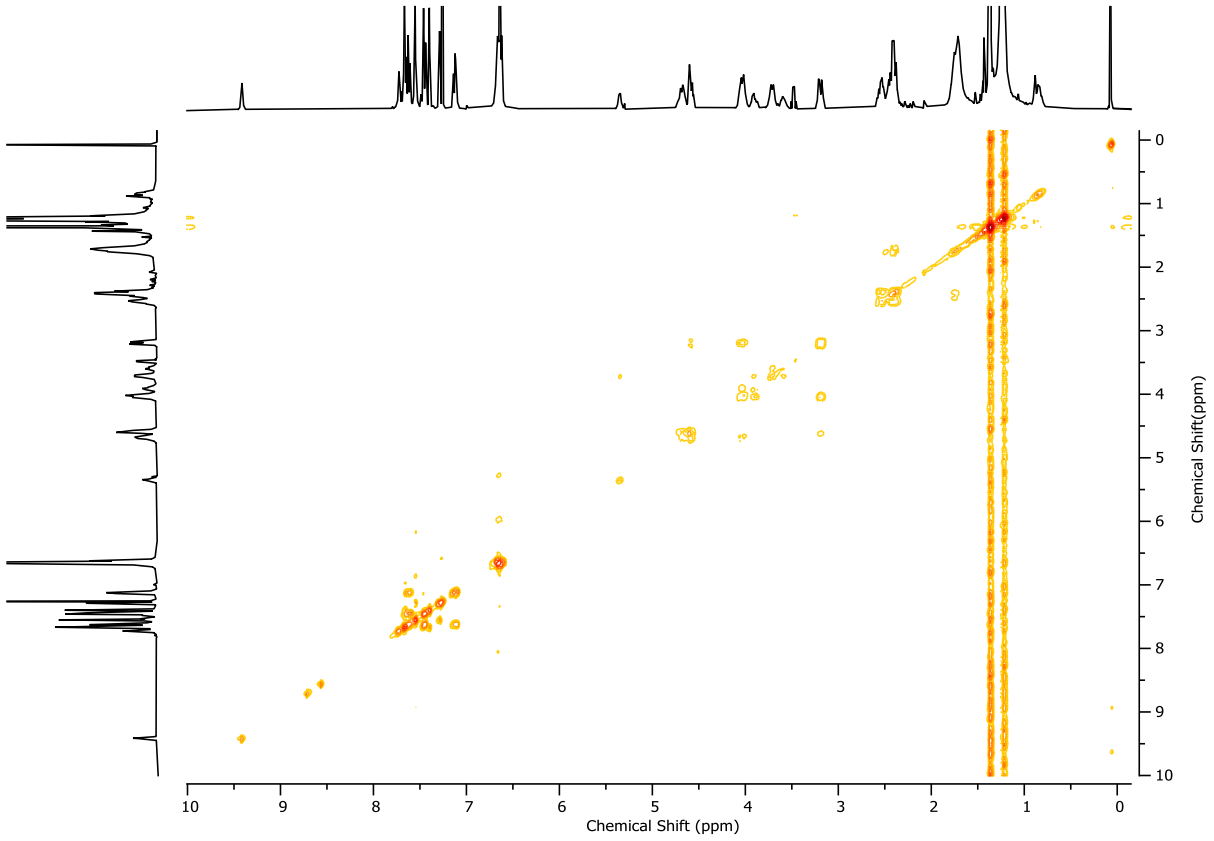

Figure 2.157 - ^{1}H COSY NMR ($CDCl_3$, 400 MHz) of (S_{ma},$R_{co\text{-}c}$)-**9**.

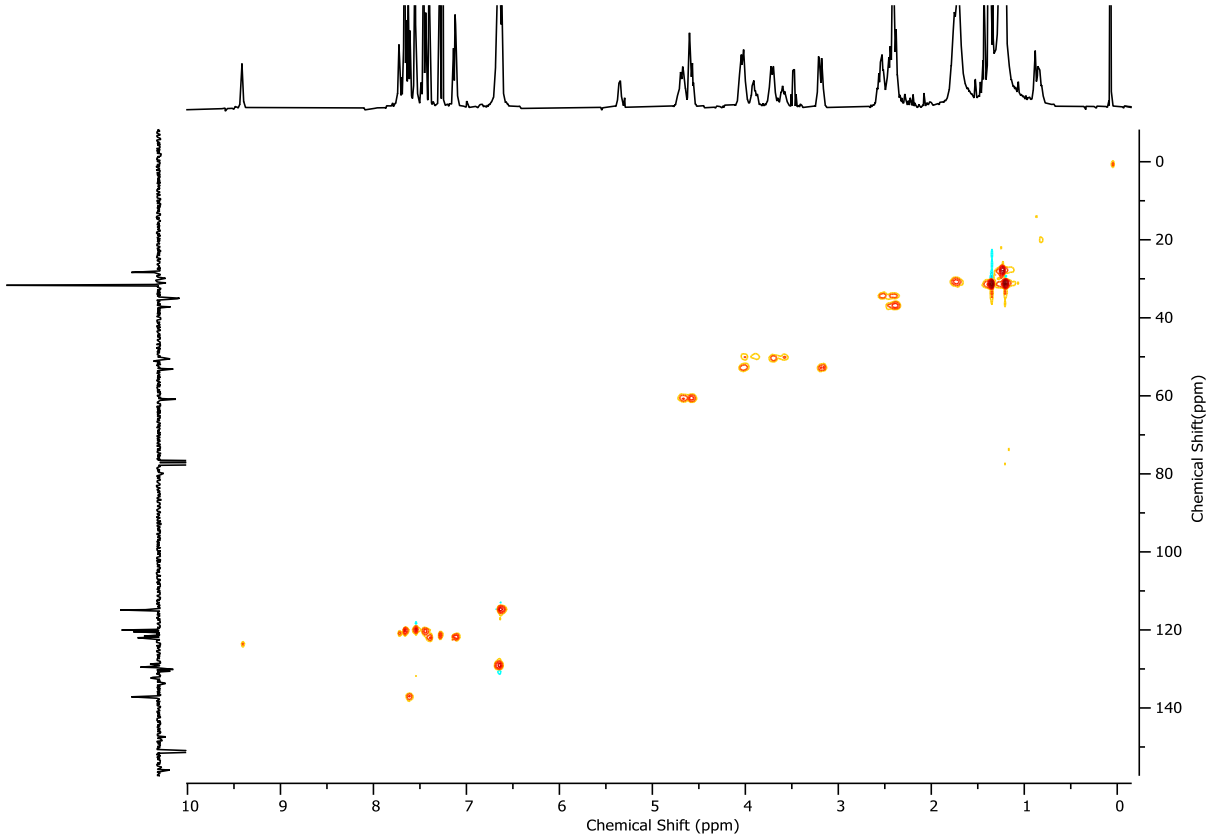

Figure 2.158 - HSQC NMR ($CDCl_3$, 400 MHz) of (S_{ma},$R_{co\text{-}c}$)-**9**.

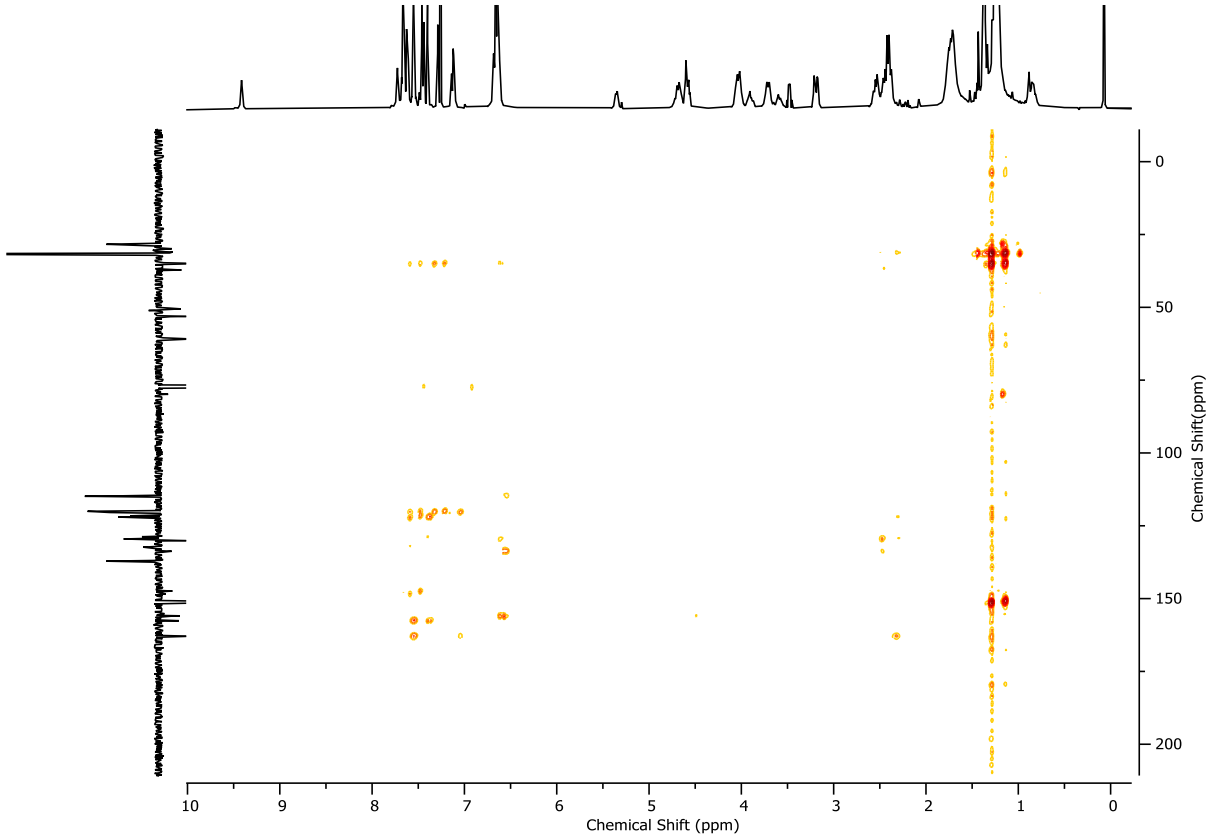

Figure 2.159 - HMBC NMR ($CDCl_3$, 400 MHz) of (S_{ma},$R_{co\text{-}c}$)-**9**.

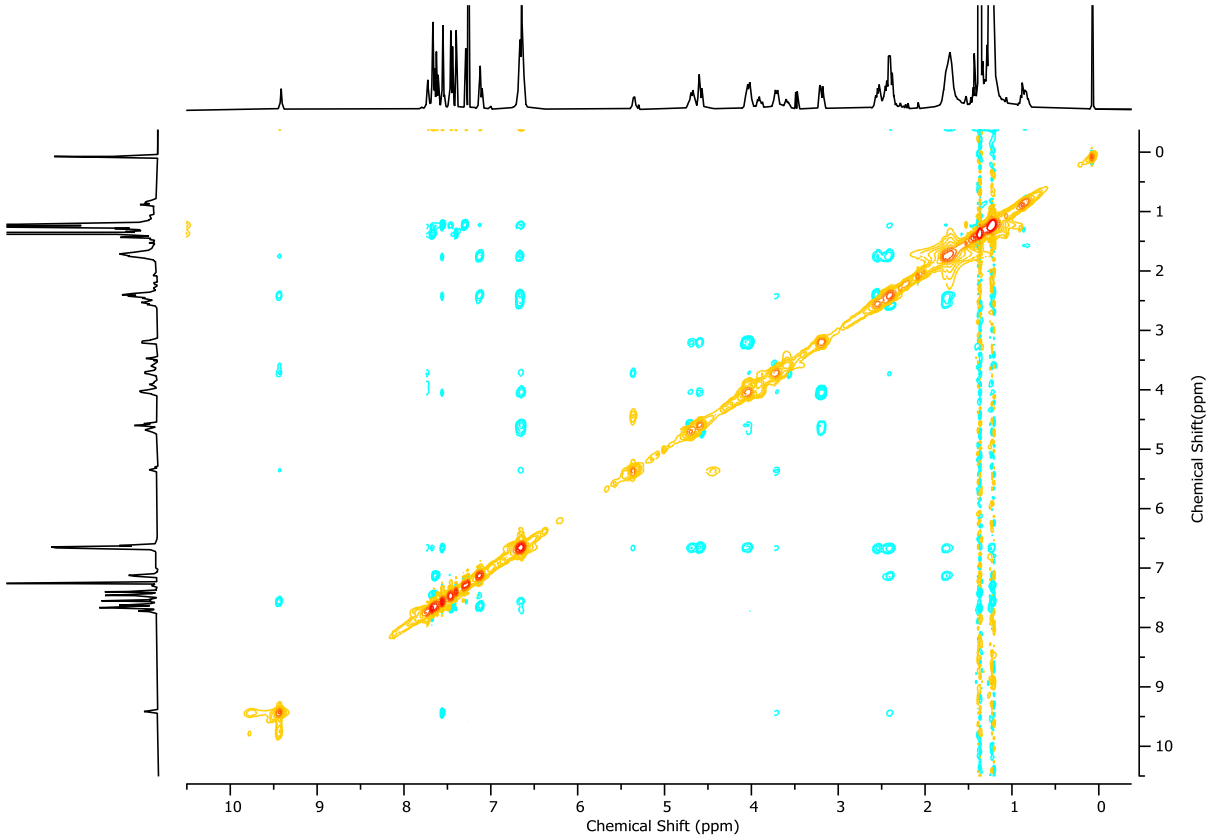

Figure 2.160 - ^{1}H NOESY NMR ($CDCl_3$, 400 MHz) of (S_{ma},$R_{co\text{-}c}$)-**9**.

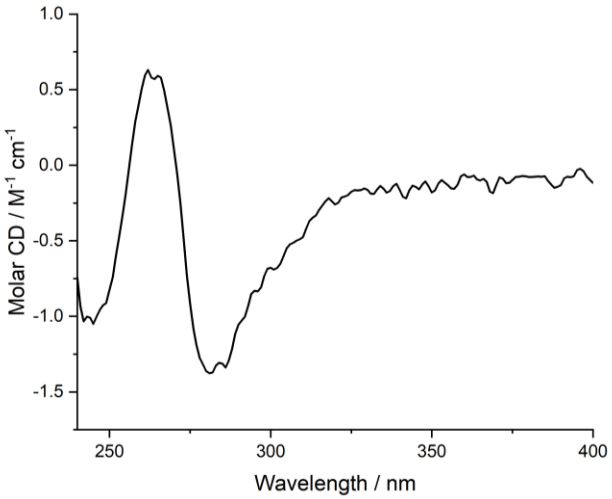

Figure 2.161 - Circular Dichroism Spectra of (S_{ma},$R_{co\text{-}c}$)-**9** (21 μM) at 293 K in $CHCl_3$.

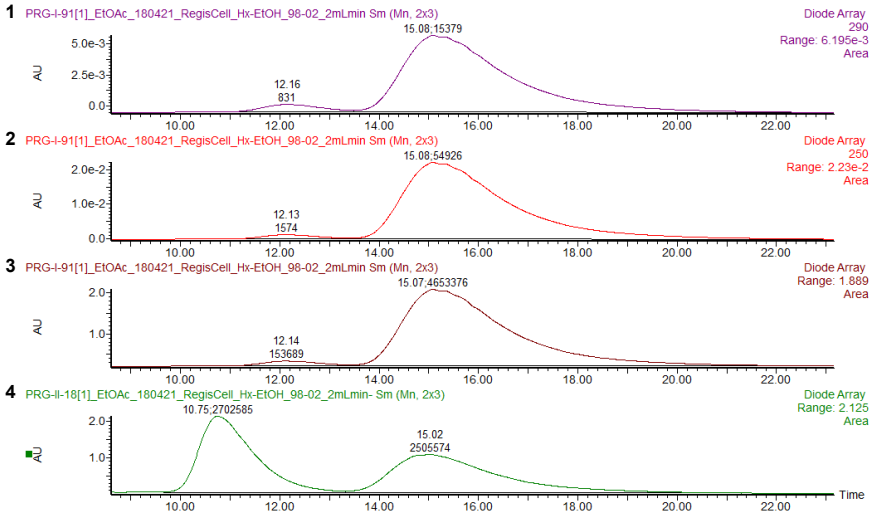

Figure 2.162 - CSP-HPLC of (S_{ma},$R_{co\text{-}c}$)-**9** (loaded in EtOAc) with 290 nm and 250 nm traces. RegisCell, *n*-hexane-EtOH 98 : 2, flowrate 2 mLmin^{-1}. The minor signal observed at ~12.15 min is not consistent with the minor enantiomer (10.75 min); varying the wavelength of detection yielded different relative integrals vs the major enantiomer ((1) 290 nm = 5.1%), (2) 250 nm = 2.8%), (3) diode array = 3.2%). This impurity could not be detected by ^{1}H NMR and could not be completely removed from the sample. On this basis, the enantiopurity of (R_{ma},$S_{co\text{-}c}$)-**9** is estimated to be >99% *ee*. (4) *rac*-**9**, (R_{ma},$S_{co\text{-}c}$)-**9** (10.75 min, 2702585, 51.8%), (S_{ma},$R_{co\text{-}c}$)-**9** (15.02 min, 2505574, 48.2%).

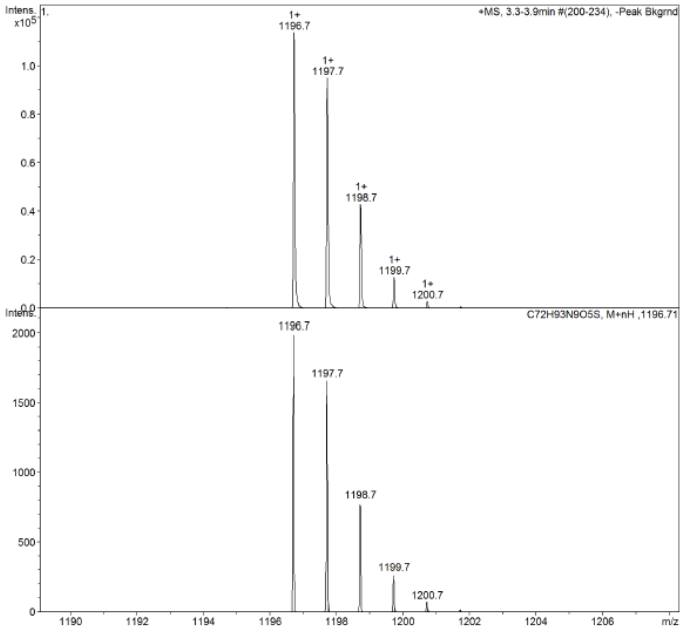

Figure 2.163 - Observed (top) and calculated (bottom) isotopic patterns for (S_{ma},$R_{co\text{-}c}$)-**9**.

Rotaxane (R_{ma},$R_{co\text{-}c}$)-9

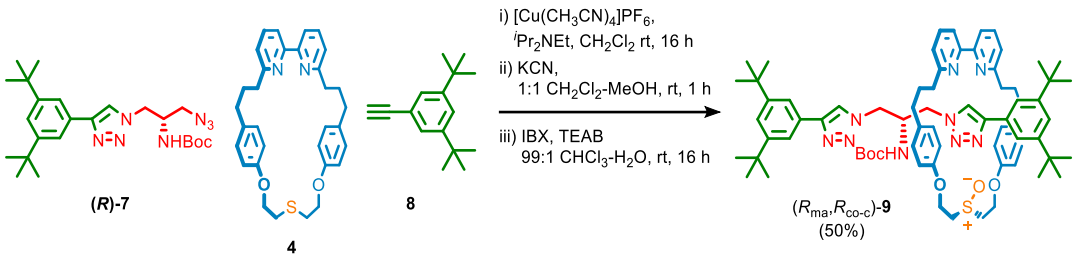

A CEM MW vial was charged with alkyne **8** (18.3 mg, 0.085 mmol, 1.1 eq.), azide (*R*)-**7** (38.2 mg, 0.083 mmol, 1.1 eq.), macrocycle **4** (38.7 mg, 0.076 mmol, 1.0 eq.), and $[Cu(CH_3CN)_4]PF_6$ (27.5 mg, 0.074 mmol, 0.97 eq.) and purged with N_2. CH_2Cl_2 (1.8 mL) and $^iPr_2NEt$ (26 µL, 0.15 mmol, 2.0 eq.) were added and the resulting deep red solution was stirred at ambient temperature for 16 h. Then, MeOH (1.9 mL) and KCN as a solid (25 mg, 0.38 mmol, 5.0 eq.) were added and the resulting mixture was stirred vigorously for 1 h. The crude mixture was diluted with CH_2Cl_2 (5 mL) and washed with H_2O in two portions (10 mL and 5 mL). The combined aqueous phase was then extracted with CH_2Cl_2 (3 x 5 mL) and the combined organics were washed with brine (10 mL), dried over $MgSO_4$ and concentrated *in vacuo*. The residue corresponding to ($R_{co\text{-}c}$)-**S19** was dissolved in 99:1 $CHCl_3/H_2O$ (760 µL), then IBX (23.2 mg, 0.083 mmol, 1.1 eq.) and tetraethylammonium bromide (17.7 mg, 0.084 mmol, 1.1 eq.) were added. The resulting suspension was stirred for 16 h. The reaction mixture was then diluted with CH_2Cl_2 (5 mL), washed with 10% $NaHSO_3$ (5 mL), saturated $NaHCO_3$ (5 mL) and brine (5 mL), extracting all aqueous layers with CH_2Cl_2 (2 x 5 mL). The combined organics were dried over $MgSO_4$, filtered, and concentrated *in vacuo*. The residue was purified by column chromatography (SiO_2, petrol-EtOAc 0→50% then petrol-EtOAc (1:1) with MeOH 0→5%) to yield (R_{ma},$R_{co\text{-}c}$)-**9** (45.7 mg, 0.038 mmol, 50%) as an off-white foam. The absolute stereochemistry of the major diastereomer was assigned crystallographically (see 11.4). The mechanical stereochemistry of the minor diastereomer was assigned as opposite to that of the major diastereomer. The co-conformational stereochemistry of both is fixed by the absolute sterechemistry of (*R*)-**1**.

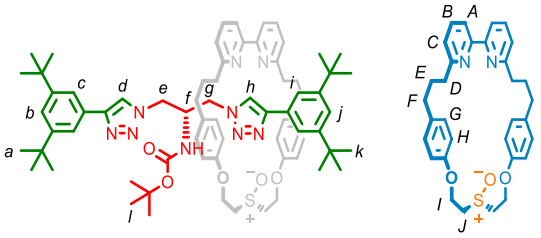

δ_H ($CDCl_3$, 400 MHz) 8.89 (s, 1H, H_h), 7.69 (app. td, J = 7.7, 3.1, 2H, H_B), 7.64 (d, J = 1.9, 2H, H_c), 7.60 (s, 1H, H_d), 7.55 (t, J = 1.3, 1H, H_A), 7.53 (t, J = 1.3, 1H, H_A), 7.51 (d, J = 1.9, 2H, H_i), 7.43 (t, J = 1.8, 1H, H_b), 7.32 (t, J = 1.8, 1H, H_j), 7.19 (dd, J = 2.8, 0.9, 1H, H_C), 7.17 (dd, J = 2.8, 1.0, 1H, H_C), 6.53 – 6.43 (m, 8H, H_G, H_H), 5.34 (d, J = 6.4, 1H, H_{NHBoc}), 4.71 – 4.61 (m, 2H, H_l), 4.60 – 4.49 (m, 2H, H_l), 4.18 (dd, J = 13.9, 4.5, 1H, H_e), 3.94 (dd, J = 13.8, 6.1, 1H, H_e), 3.88 – 3.71 (m, 4H, H_J, H_g), 3.77 – 3.72 (m, 1H, H_f), 3.17 – 3.08 (m, 2H, H_J), 2.65 – 2.49 (m, 4H, H_D), 2.49 – 2.32 (m, 4H, H_F), 1.84 – 1.59 (m, 4H, H_E), 1.38 (s, 18H, H_a), 1.34 (s, 9H, H_l), 1.32 (s, 18H, H_k); δ_C ($CDCl_3$, 101 MHz) 162.9, 162.9, 157.9, 157.9, 155.3, 155.2, 151.6, 150.8, 148.5, 147.5, 137.3, 137.3, 133.6, 133.4, 130.2, 129.9, 128.8, 128.7, 122.6, 122.4, 122.3, 121.5, 120.9, 120.5, 120.2, 120.2, 115.1, 115.0, 80.3, 61.1, 61.0, 52.2, 52.2, 51.1, 50.0, 49.8, 37.5, 35.1, 35.1, 34.7, 34.6, 31.8, 31.7, 31.6, 31.4, 28.4; LR-ESI-MS (+ve) m/z = 1196.7 $[M+H]^+$

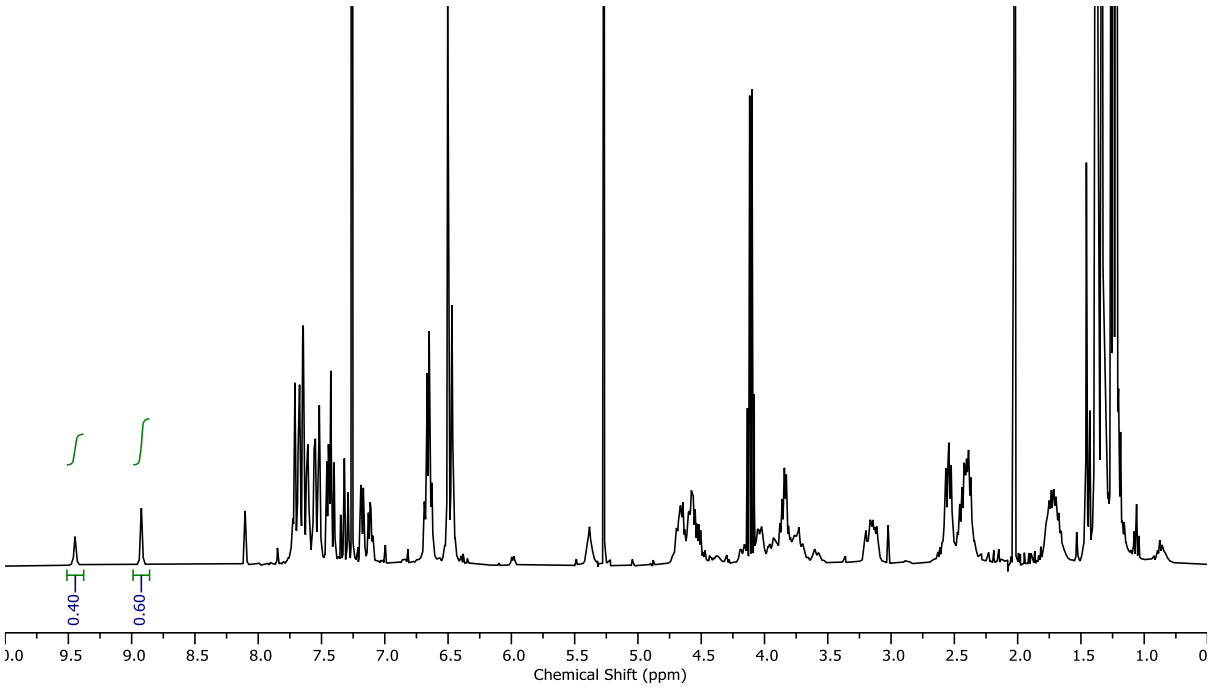

Figure 2.164 - Crude ^{1}H NMR of **9** *via* oxidation of sulfide rotaxane ($R_{co\text{-}c}$)-**9** ($CDCl_3$, 400 MHz). Diastereoisomer integration: ***H***$_h$ protons (major 9.42 ppm, 0.40, minor 8.89 ppm, 0.60).

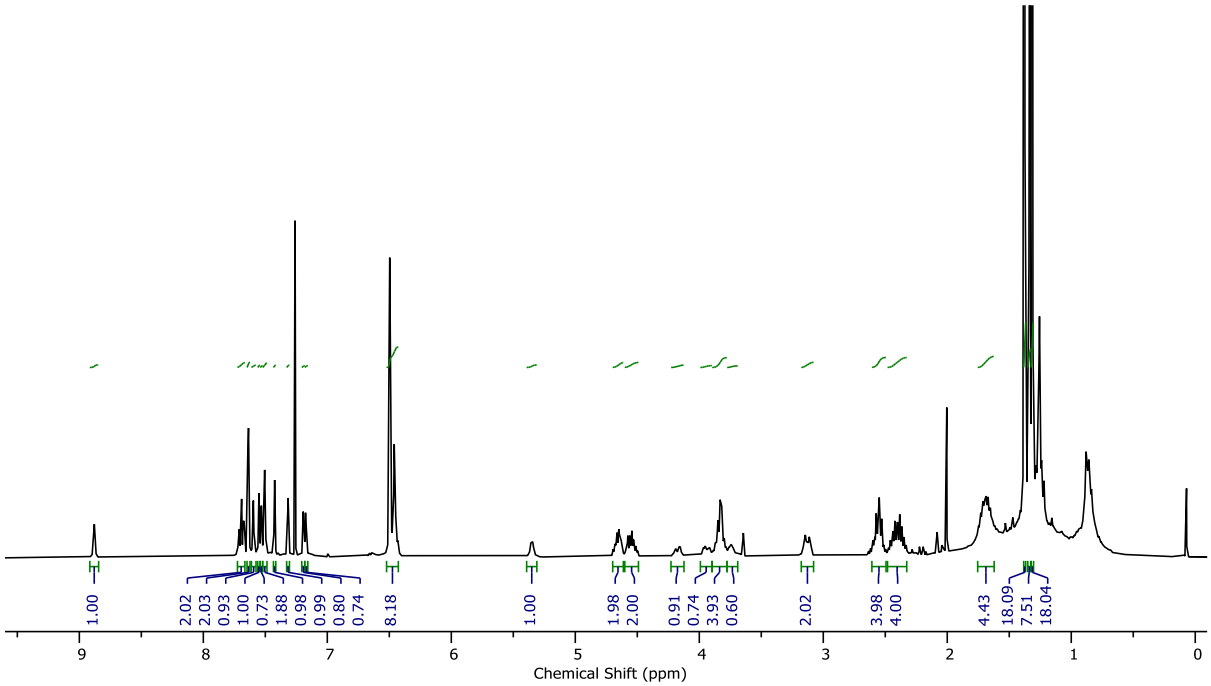

Figure 2.165 - ^{1}H NMR ($CDCl_3$, 400 MHz) of (R_{ma},$R_{co\text{-}c}$)-**9**.

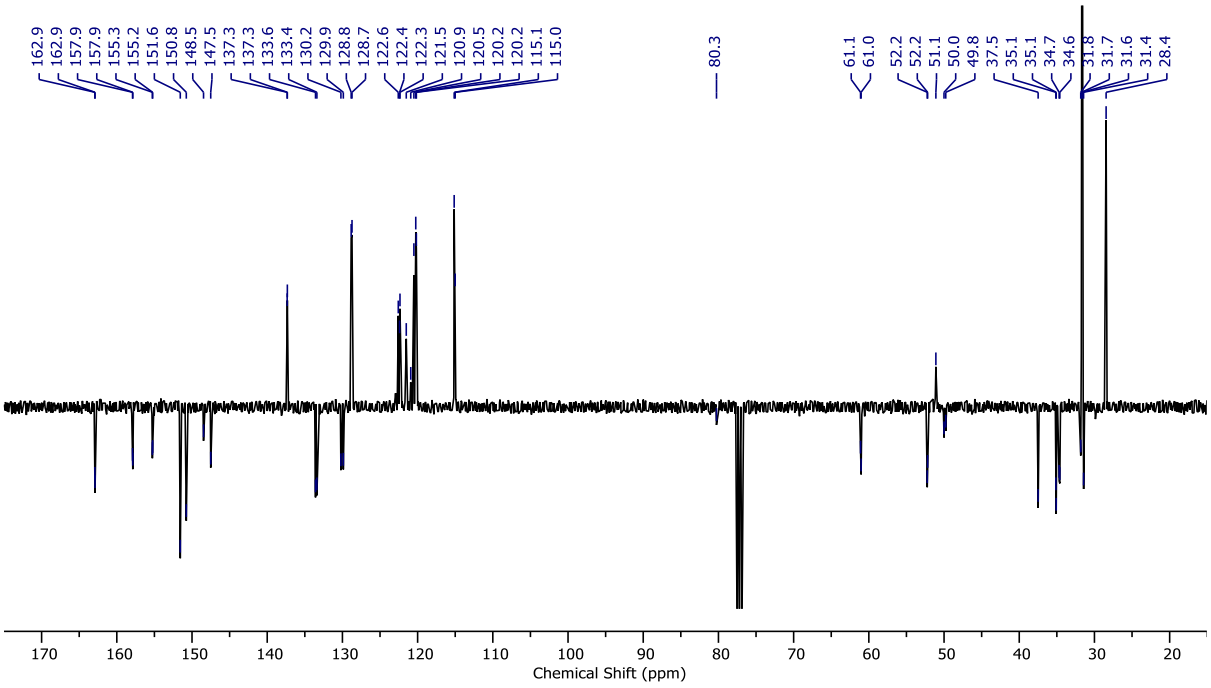

Figure 2.166 - JMOD NMR ($CDCl_3$, 101 MHz) of (R_{ma},$R_{co\text{-}c}$)-**9**.

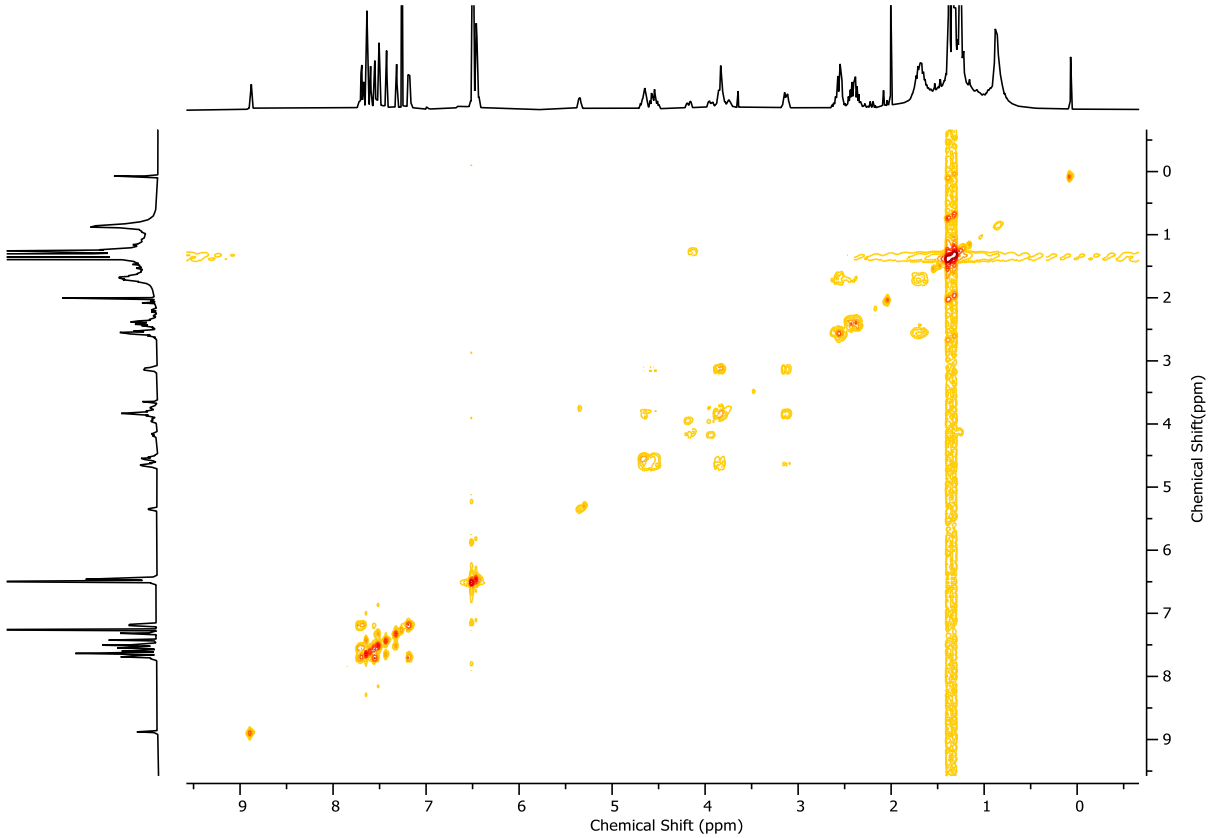

Figure 2.167 - ^{1}H COSY NMR ($CDCl_3$, 400 MHz) of (R_{ma},$R_{co\text{-}c}$)-**9**.

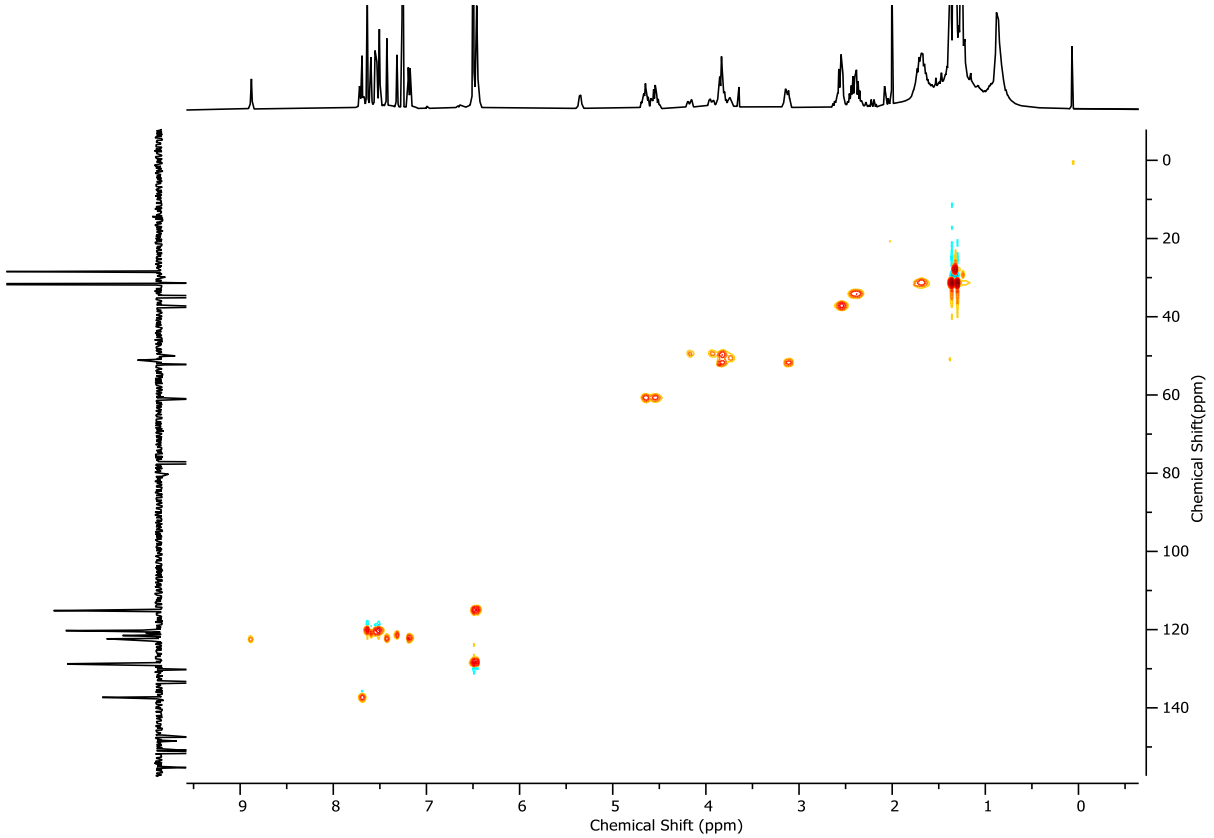

Figure 2.168 - HSQC NMR ($CDCl_3$, 400 MHz) of (R_{ma},$R_{co\text{-}c}$)-**9**.

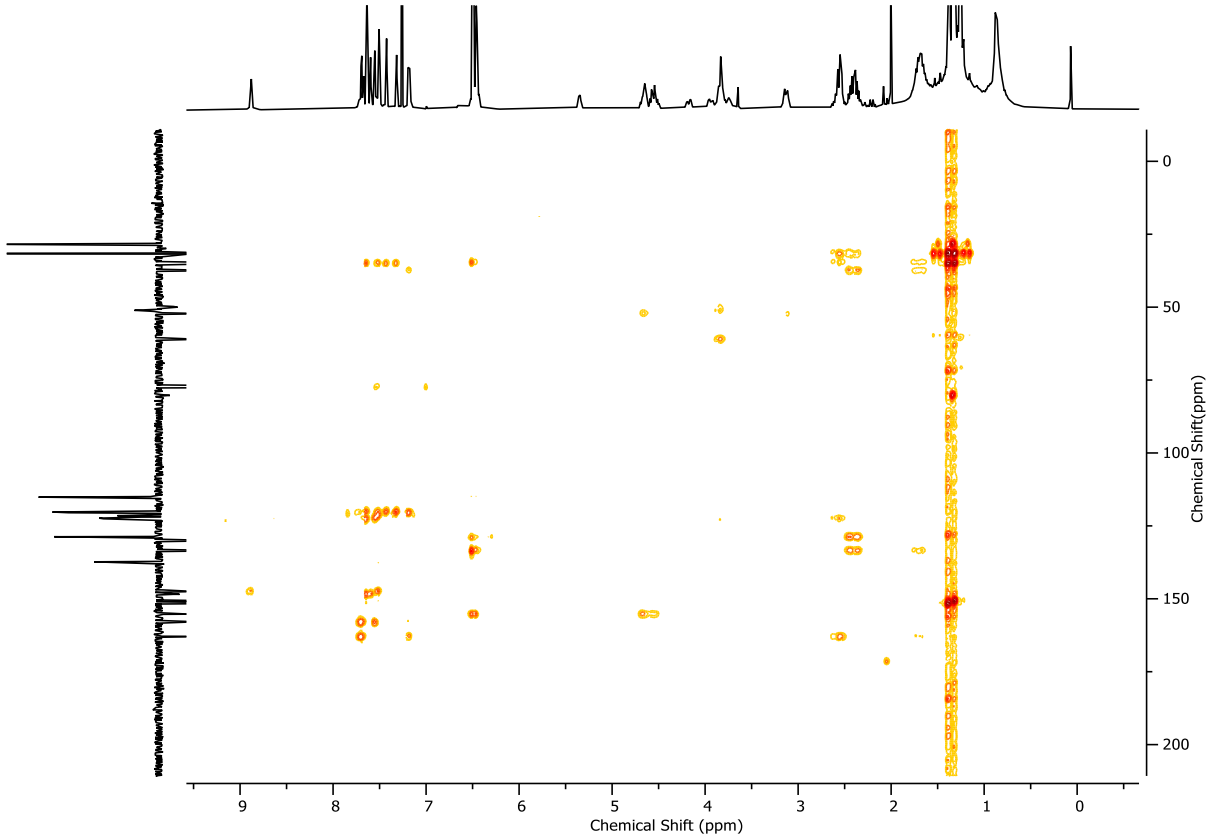

Figure 2.169 - HMBC NMR ($CDCl_3$, 400 MHz) of (R_{ma},R_{co-c})-**9**.

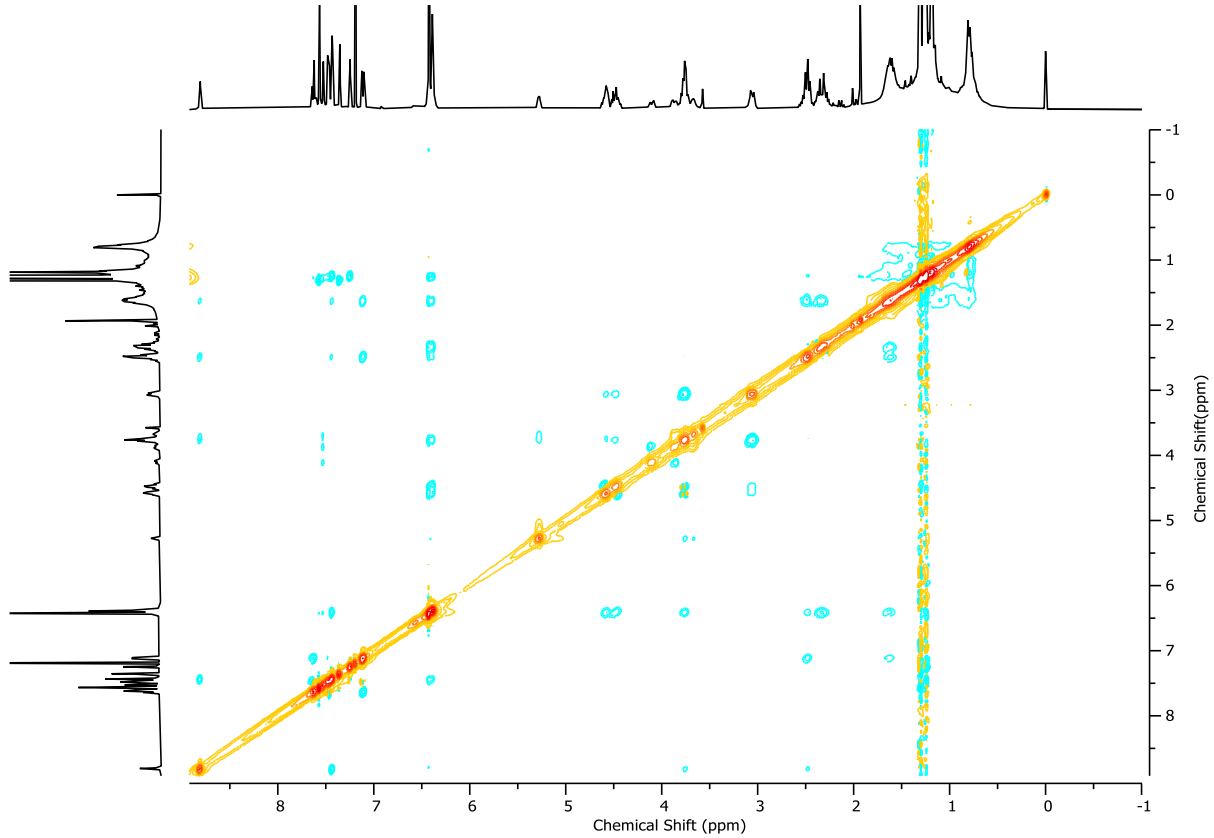

Figure 2.170 - ^{1}H NOESY NMR ($CDCl_3$, 400 MHz) of (R_{ma},R_{co-c})-**9**.

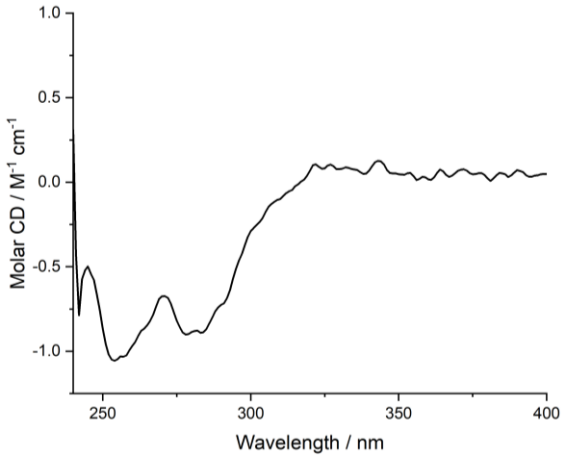

Figure 2.171 - Circular Dichroism Spectra of (R_{ma},$R_{co\text{-}c}$)-**9** (25 µM) at 293 K in $CHCl_3$.

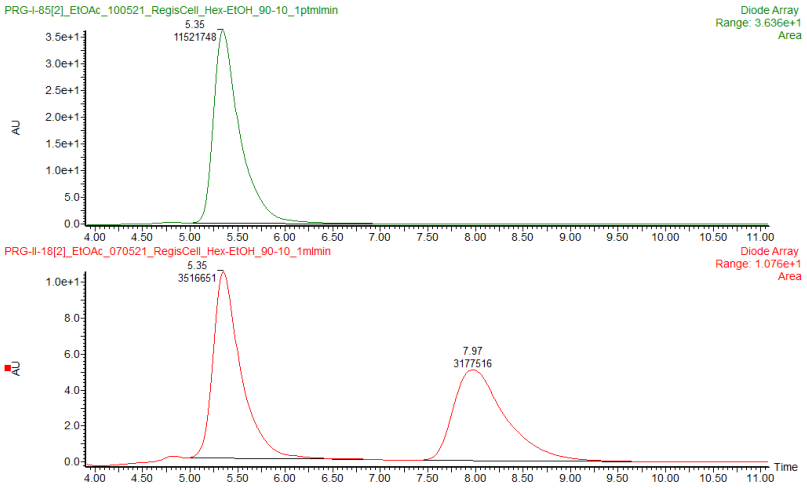

Figure 2.172 - CSP-HPLC of (R_{ma},$R_{co\text{-}c}$)-**9** (loaded in EtOAc). RegisCell, *n*-hexane-EtOH 90 : 10, flowrate 1 mLmin^{-1}. (top) (R_{ma},$R_{co\text{-}c}$)-**9** (5.35 min, 11521748, >99.9%), (S_{ma},$S_{co\text{-}c}$)-**9** (not observed). (bottom) *rac*-**9**, (R_{ma},$R_{co\text{-}c}$)-**9** (5.35 min, 3516651, 52.5%), (S_{ma},$S_{co\text{-}c}$)-**9** (7.97 min, 3177516, 47.5%).

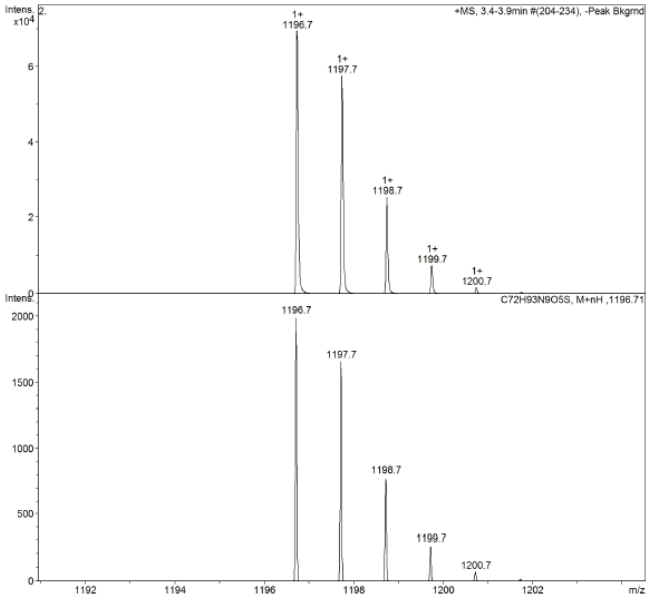

Figure 2.173 - Observed (top) and calculated (bottom) isotopic patterns for (R_{ma},$R_{co\text{-}c}$)-**9**.

Axle S20

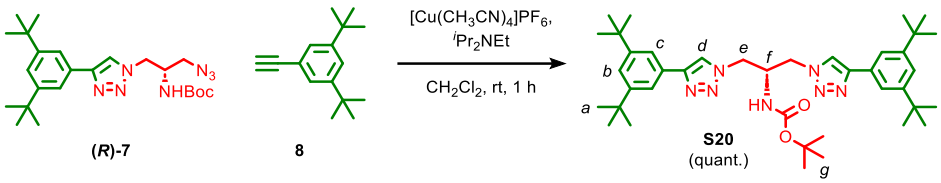

A CEM MW vial was charged with alkyne **8** (6.0 mg, 0.028 mmol, 1.1 eq.), azide (*R*)-**7** (11.4 mg, 0.025 mmol, and $[Cu(CH_3CN)_4]PF_6$ (1.9 mg, 0.005 mmol, 0.2 eq.) and purged with N_2. CH_2Cl_2 (0.5 mL) and $^iPr_2NEt$ (9 µL, 0.15 mmol, 2.0 eq.) then stirred at ambient temperature for 1 h. The crude mixture was diluted with CH_2Cl_2 (5 mL) and washed with EDTA-NH_3 solution (2 x 5 mL), and the combined organics were washed with brine (5 mL), dried over $MgSO_4$ and concentrated *in vacuo*. The residue was purified by column chromatography (SiO_2, petrol-EtOAc 0→30 %) to yield axle **S20** (16.5 mg, 0.025 mmol, quant.) as a white foam.

δ_H ($CDCl_3$, 400 MHz) 8.10 (s, 2H, H_d), 7.71 (d, J = 1.8, 4H, H_c), 7.45 (t, J = 1.8, 2H, H_b) 5.94 (d, J = 7.3, 1H, H_{NHBoc}), 4.58 (dd, J = 14.2, 4.2, 2H, H_e), 4.47 (dd, J = 14.2, 6.4, 2H, H_e), 4.34 (s, 1H, H_f), 1.47 (s, 9H, H_g), 1.38 (s, 36H, H_a); δ_C ($CDCl_3$, 101 MHz) 151.7, 149.2, 129.4, 123.0, 121.8, 120.4, 51.6, 49.5, 35.2, 31.6, 29.9, 28.5; HR-ESI-MS (+ve) m/z = 670.4819 $[M+H]^+$ (calc. m/z for $C_{40}H_{60}N_7O_2$ 670.4803).

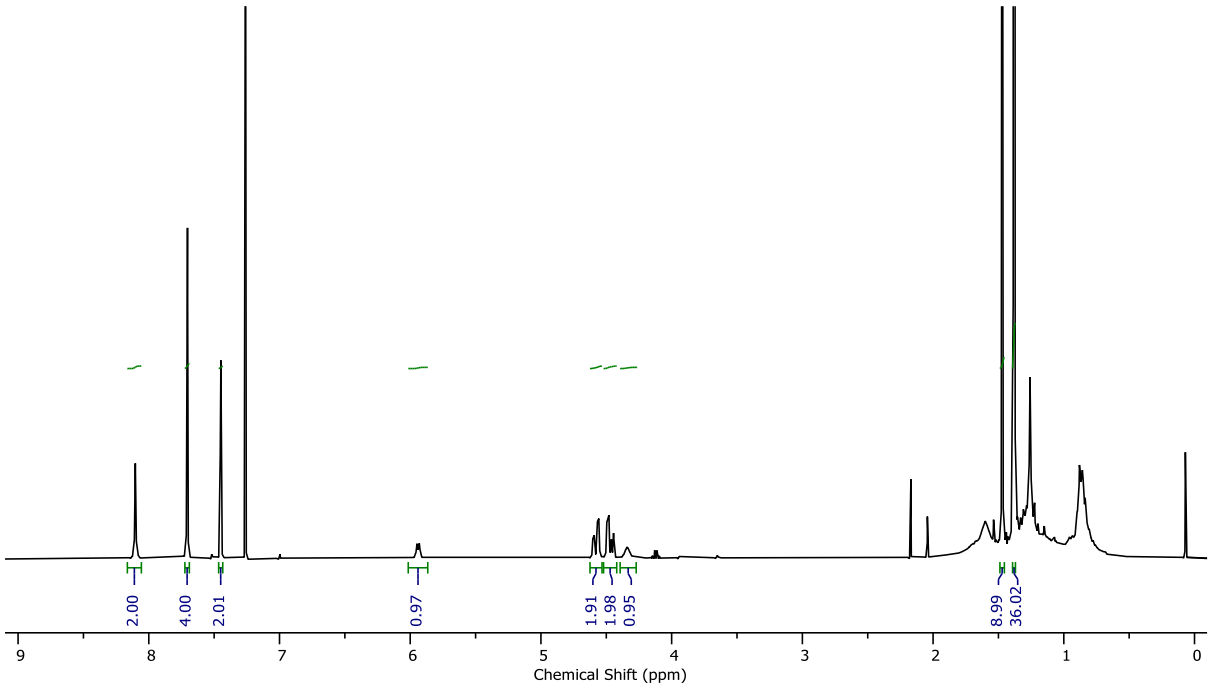

Figure 2.174 - ^1H NMR ($CDCl_3$, 400 MHz) of **S20**.

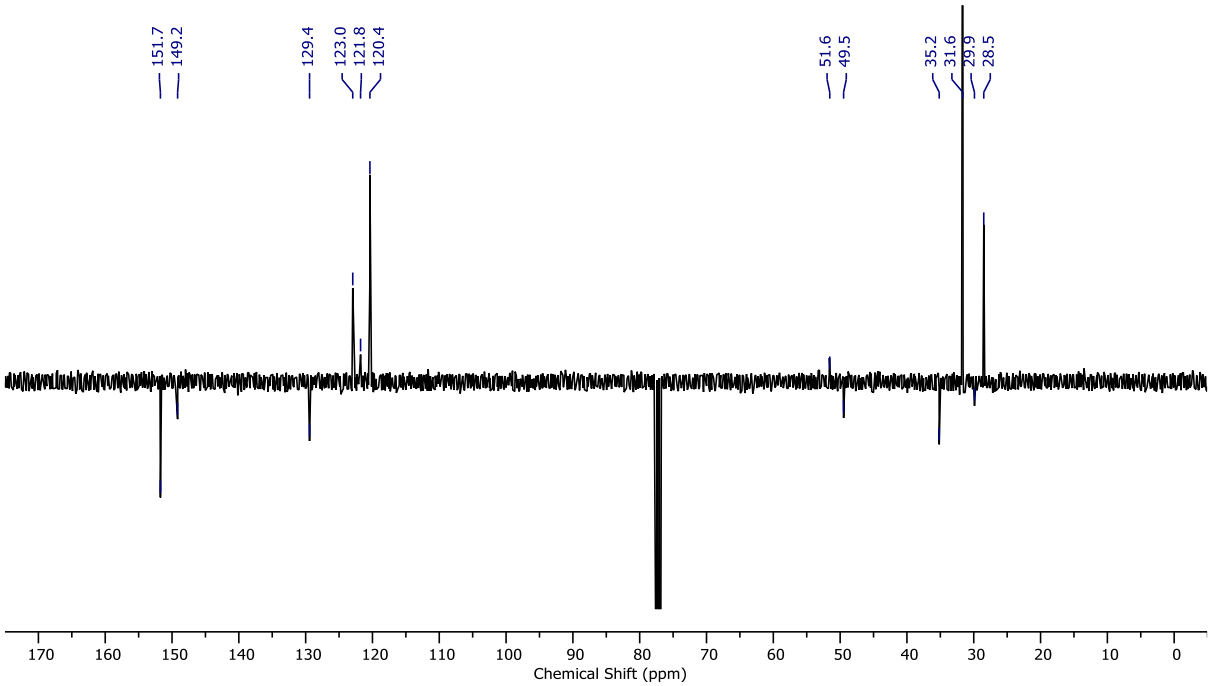

Figure 2.175 - JMOD NMR ($CDCl_3$, 101 MHz) of **S20**.

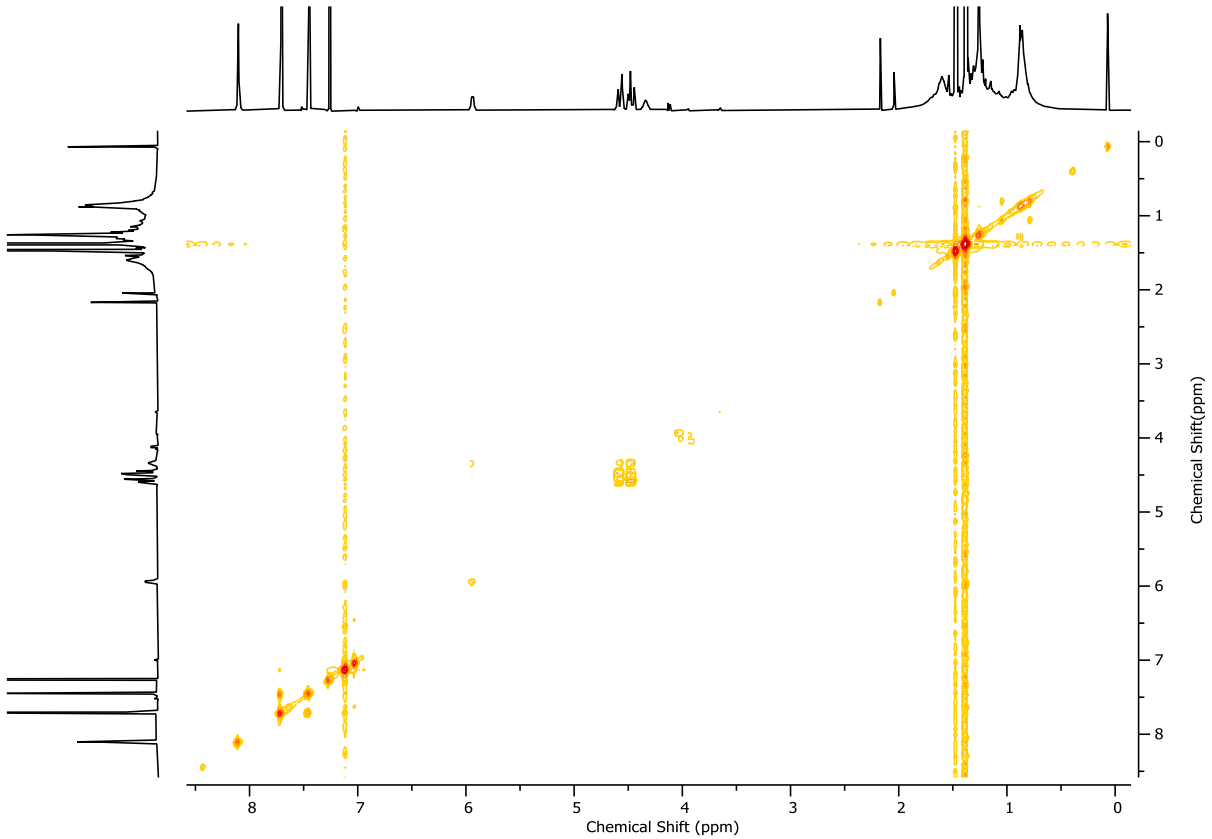

Figure 2.176 - ^1H COSY NMR ($CDCl_3$, 400 MHz) of **S20**.

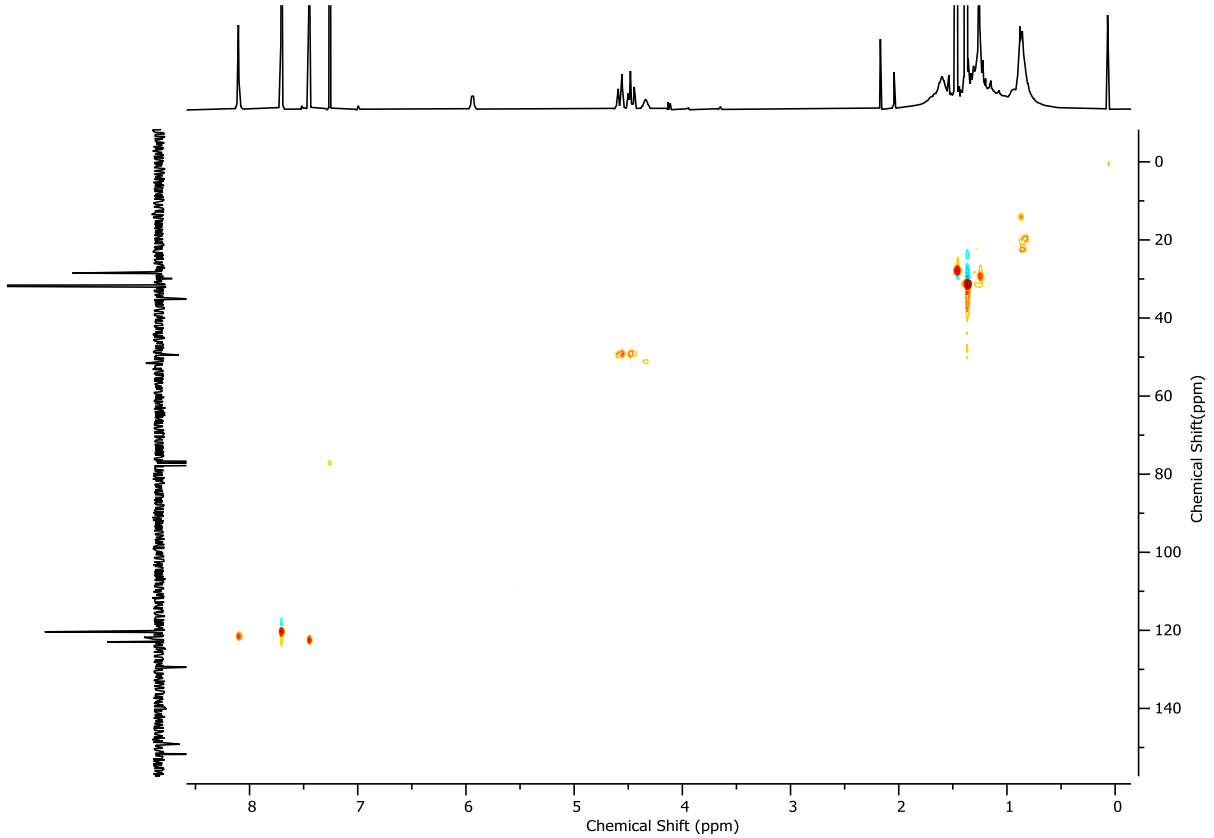

Figure 2.177 - HSQC NMR ($CDCl_3$, 400 MHz) of **S20**.

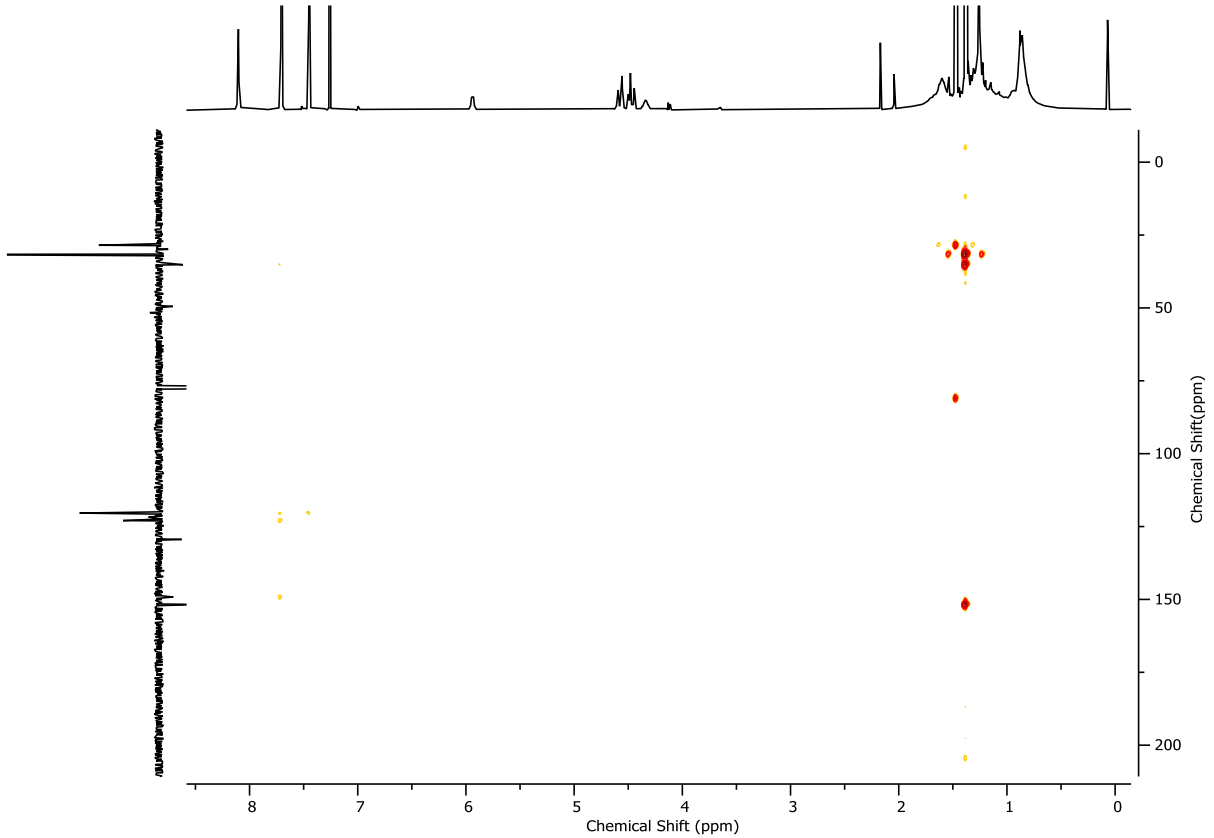

Figure 2.178 - HMBC NMR ($CDCl_3$, 400 MHz) of **S20**.

Synthesis of enantiomeric rotaxanes (S_{ma})-10 and (R_{ma})-10

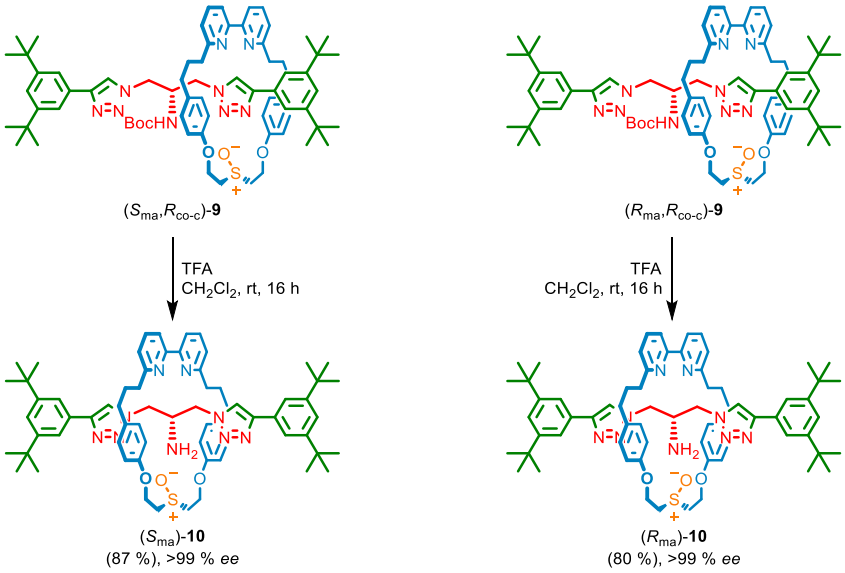

Scheme 2.8 - Synthetic route to mechanically axially chiral enantiomeric rotaxanes (R_{ma})-**10** and (S_{ma})-**10**.

Rotaxane (S_{ma})-10

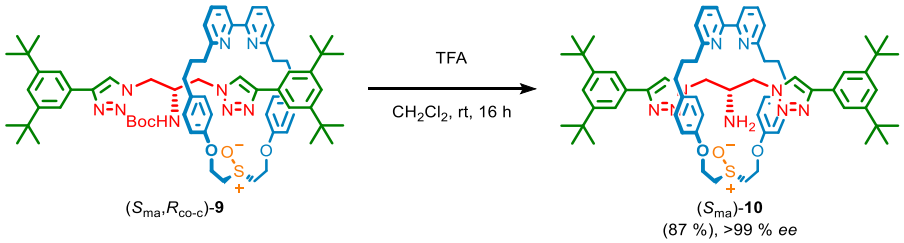

To a solution of rotaxane (S_{ma},$R_{co\text{-}c}$)-**9** (18.0 mg, 0.015 mmol, 1 eq.) in CH_2Cl_2 (300 µL) was added TFA (35 µL, 0.46 mmol, 31 eq.) dropwise, and the reaction mixture was stirred at ambient temperature for 16 h. The reaction mixture was then diluted with CH_2Cl_2 (5 mL) and poured into saturated $NaHCO_3$ (5 mL). The aqueous phase was extracted with CH_2Cl_2 (3 x 5 mL) and combined organics were washed with brine (5 mL), dried over $MgSO_4$, filtered and concentrated *in vacuo*. The residue was purified by column chromatography (SiO_2, CH_2Cl_2-CH_3CN 0→20% then CH_2Cl_2-CH_3CN (3:1) with MeOH 0→10%) to yield rotaxane (S_{ma})-**10** (13.8 mg, 0.013 mmol, 87%) as an off-white foam. The mechanical stereochemistry of the product was assigned by observing that this cannot change during the removal of the Boc group (or if it does, that the resulting product would be racemic, which was not observed).

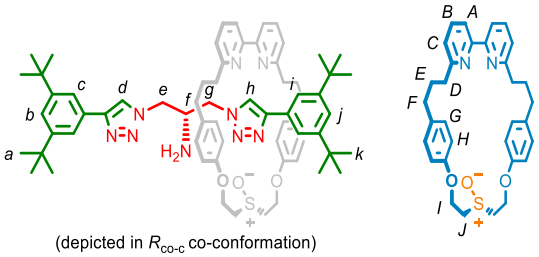

δ_H ($CDCl_3$, 400 MHz) 8.58 (s, 1H, H_h), 8.07 (s, 1H, H_d), 7.66 (d, J = 1.8, 2H, H_c), 7.65 –7.58 (m, 3H, H_I, H_B), 7.46 (dd, J = 2.9, 1.0, 1H, H_A), 7.44 (dd, J = 2.9, 1.0, 1H, H_A), 7.39 (t, J = 1.8, 1H, H_b), 7.35 (t, J = 1.8, 1H, H_j), 7.12 (dd, J = 7.7, 1.0, 1H, H_C), 7.09 (dd, J = 7.8, 1.0, 1H, H_C), 6.72 – 6.62 (m, 6H, H_G, H_H), 6.61 – 6.53 (m, 2H, H_H), 4.73 – 4.61 (m, 2H, H_I), 4.59 – 4.47 (m, 2H, H_I), 3.92 – 3.75 (m, 3H, H_J, H_e), 3.64 – 3.54 (m, 2H, H_e, H_g), 3.22 (dd, J = 13.8, 7.9, 1H, H_g), 3.16 – 3.09 (m, 2H, H_J), 2.70 – 2.63 (m, 1H, H_f), 2.54 – 2.40 (m, 9H, H_F, H_D), 1.79 – 1.67 (m, 4H, H_E), 1.37 (s, 18H, H_a), 1.29 (s, 18H, H_k); δ_C ($CDCl_3$, 101 MHz) 162.7, 162.7, 157.9, 157.8, 155.9, 155.7, 151.3, 148.3, 148.0, 137.3, 137.2, 134.0, 133.9, 130.4, 130.2, 129.5, 129.5, 122.7, 122.2, 122.2, 122.1, 122.0, 121.3, 120.6, 120.6, 120.3, 120.0, 115.0, 114.9, 61.0, 60.9, 54.2, 53.7, 53.1, 53.1, 51.5, 37.4, 37.2, 35.1, 35.1, 34.8, 34.7, 32.0, 31.9, 31.7, 31.6; LR-ESI-MS (+ve) m/z = 1196.7 $[M+H]^+$

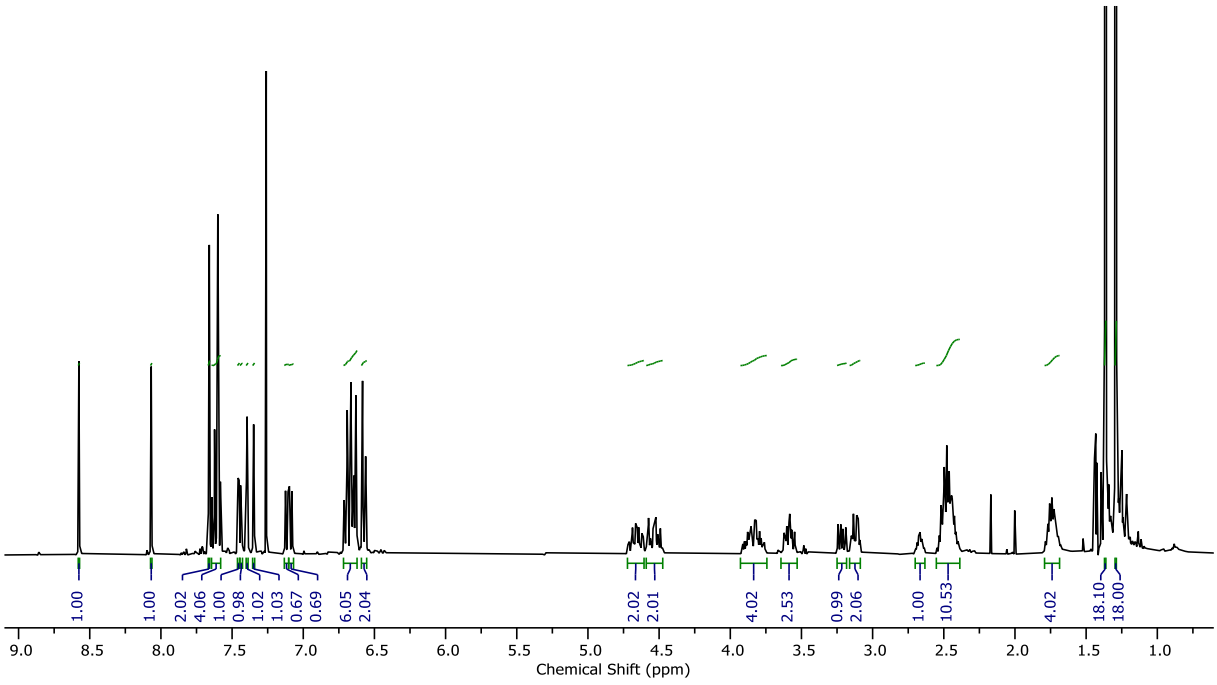

Figure 2.179 - ^{1}H NMR ($CDCl_3$, 400 MHz) of (S_{ma})-**10**.

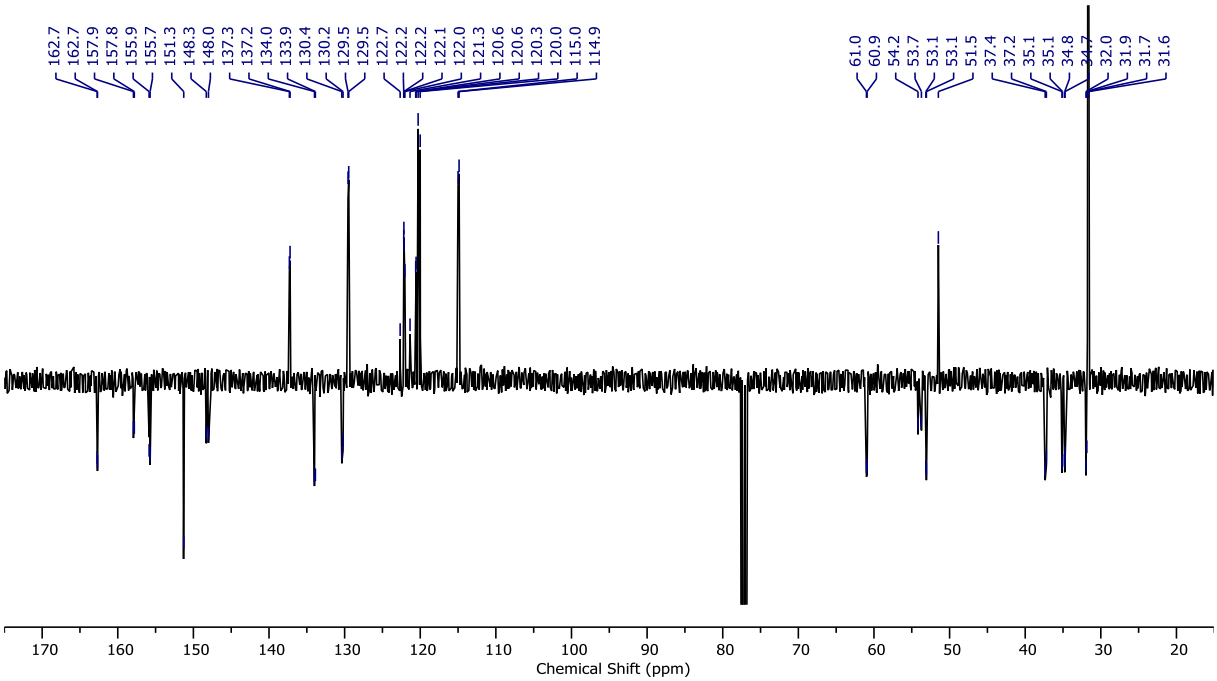

Figure 2.180 - JMOD NMR ($CDCl_3$, 101 MHz) of (S_{ma})-**10**.

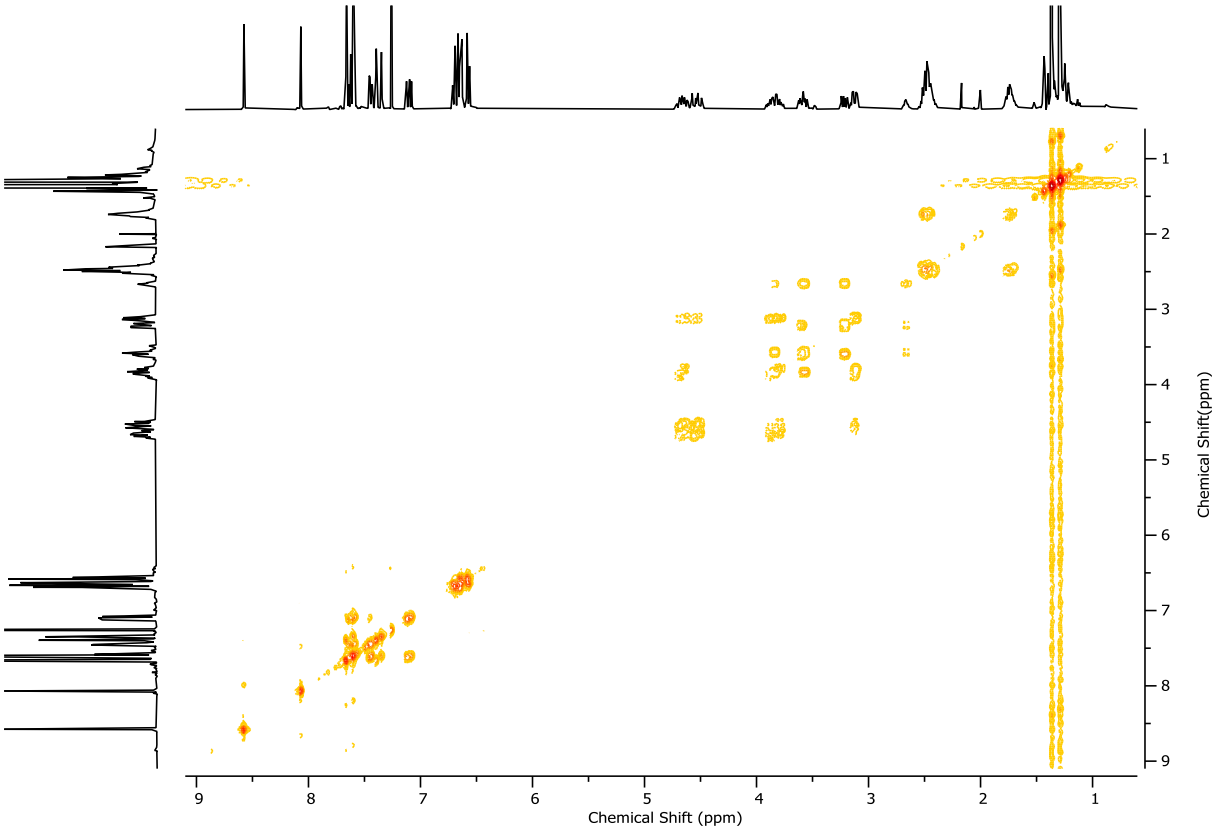

Figure 2.181 - ^1H COSY NMR ($CDCl_3$, 400 MHz) of (S_{ma})-**10**.

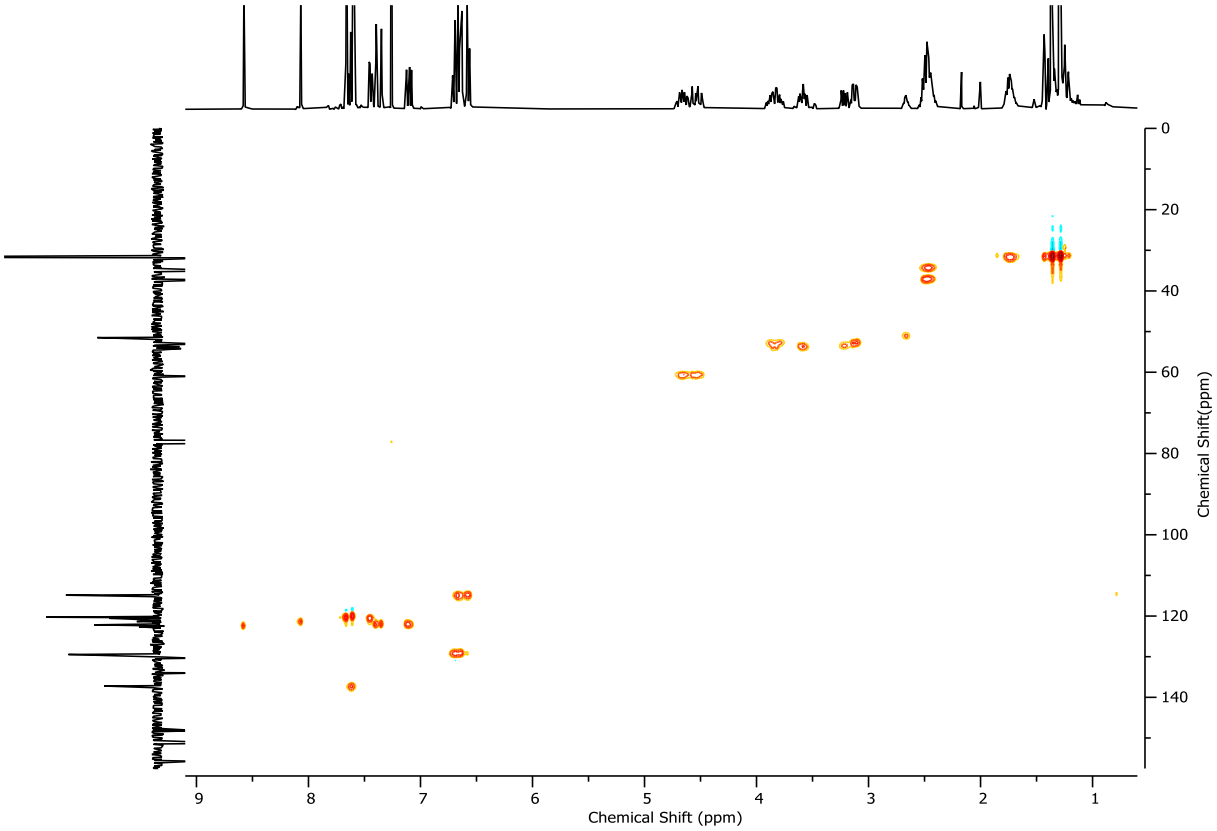

Figure 2.182 - HSQC NMR ($CDCl_3$, 400 MHz) of (S_{ma})-**10**.

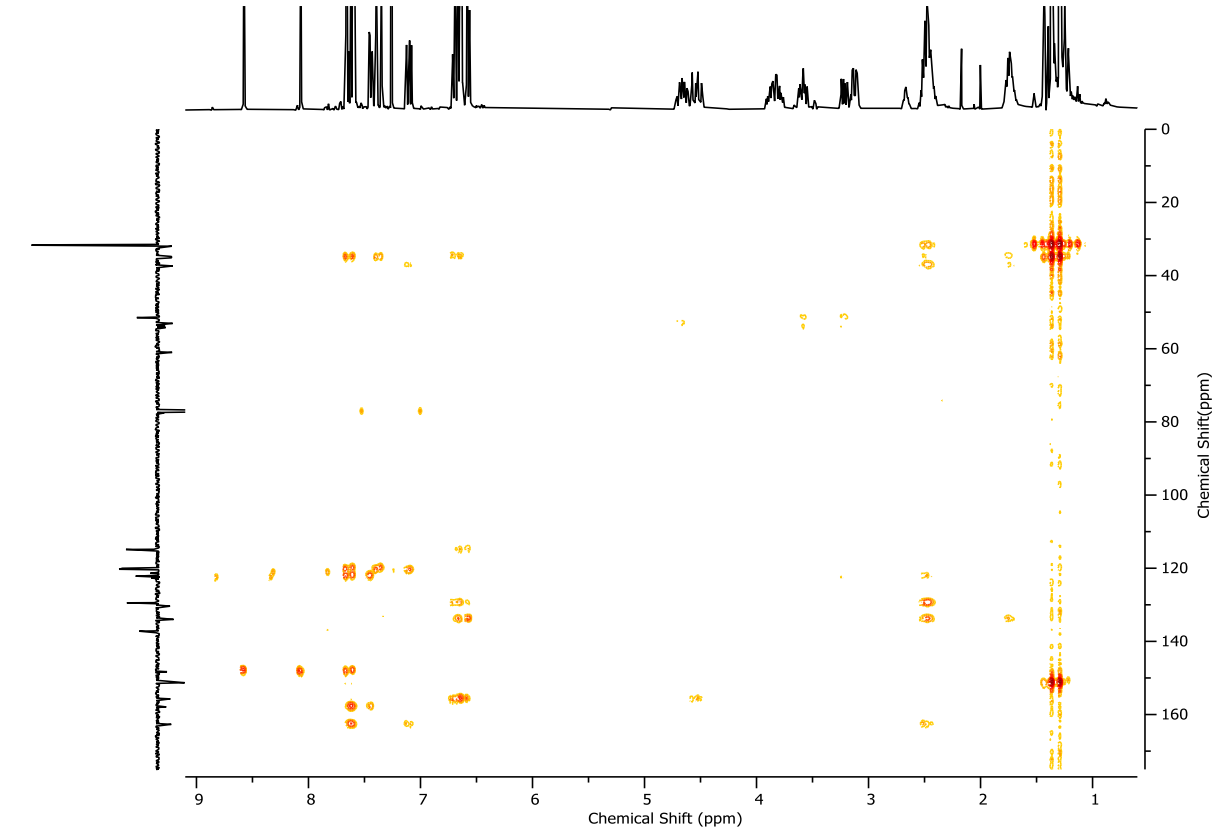

Figure 2.183 - HMBC NMR ($CDCl_3$, 400 MHz) of (S_{ma})-**10**.

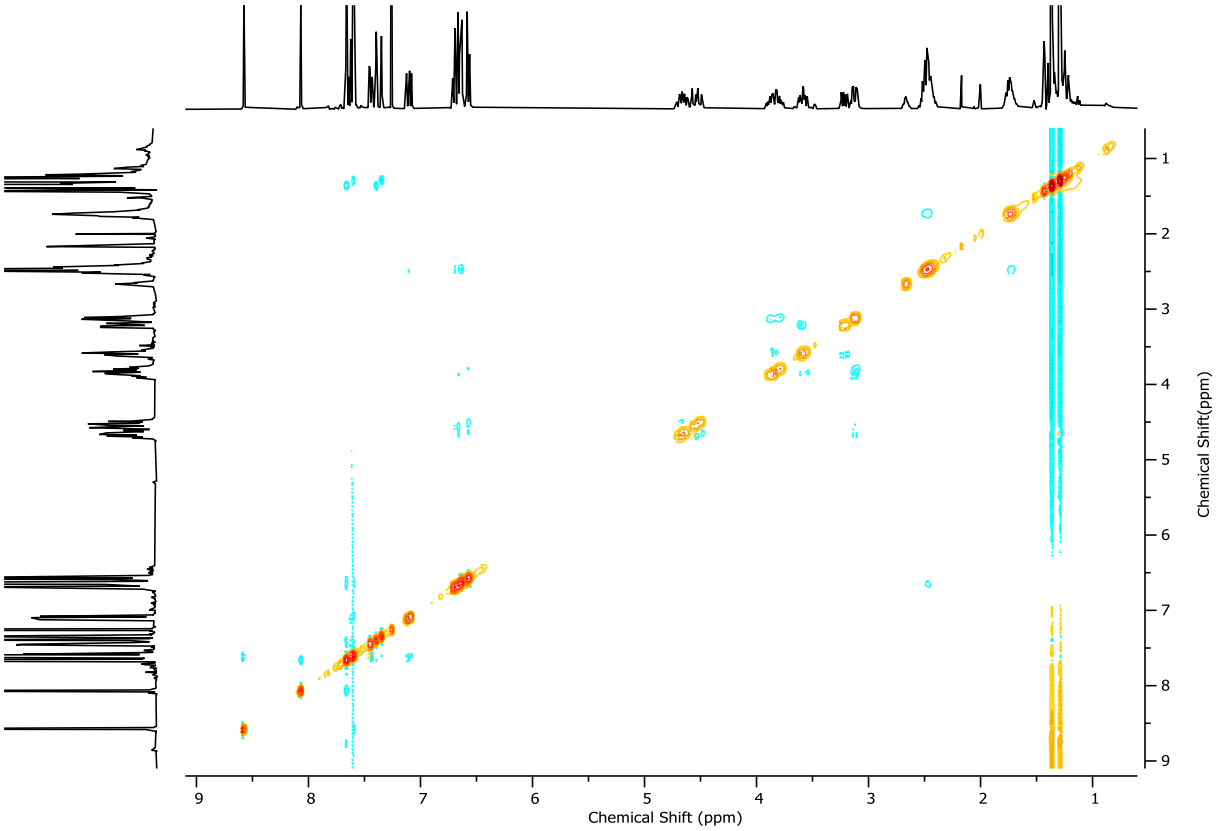

Figure 2.184 - ^{1}H NOESY NMR ($CDCl_3$, 400 MHz) of (S_{ma})-**10**.

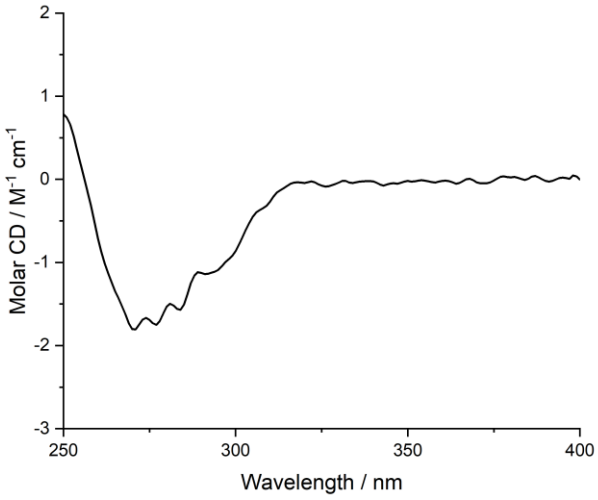

Figure 2.185 - Circular Dichroism Spectra of (S_{ma})-**10** (26 μM) at 293 K in $CHCl_3$.

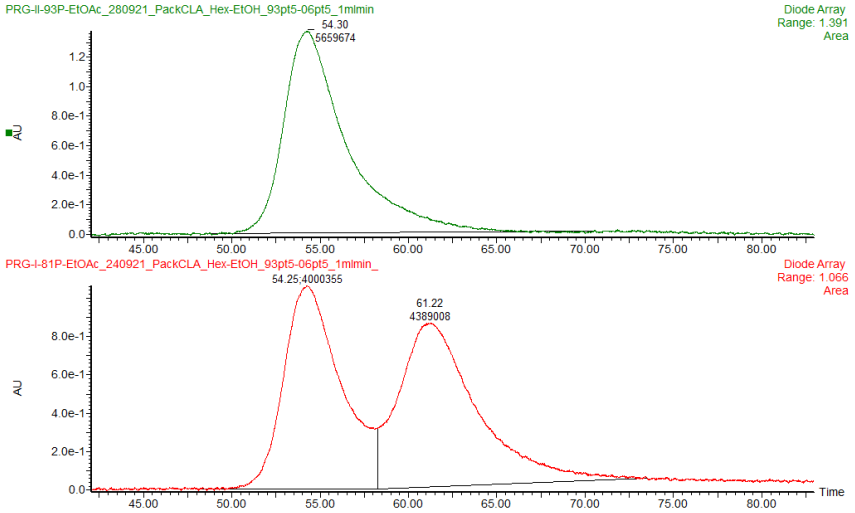

Figure 2.186 - CSP-HPLC of (S_{ma})-**10** loaded in EtOAc). RegisPackCLA-1, *n*-hexane-EtOH 93.5 : 6.5, flowrate 1 mLmin^{-1}. (top) (S_{ma})-**10** (54.30 min, 5659674, >99.9%), (R_{ma})-**10** (not observed). (bottom) *rac*-**10**, (S_{ma})-**10** (54.25 min, 4000355, 47.7%), (R_{ma})-**10** (61.22 min, 4389008, 52.3%).

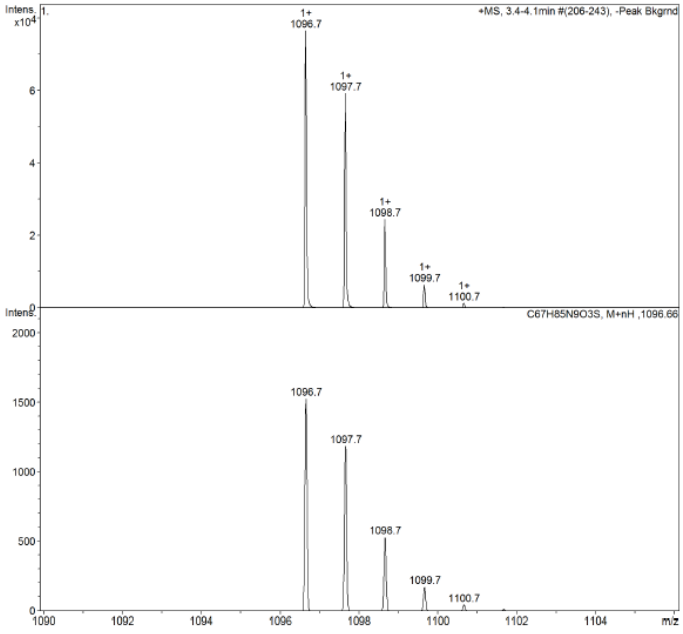

Figure 2.187 - Observed (top) and calculated (bottom) isotopic patterns for (S_{ma})-**10**.

Rotaxane (R_{ma})-10

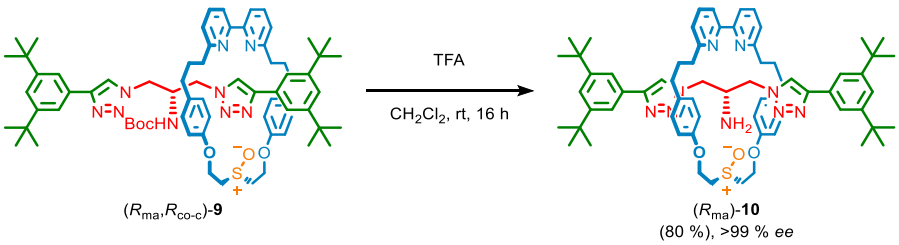

To a solution of rotaxane (R_{ma},$R_{co\text{-}c}$)-**9** (12.2 mg, 0.010 mmol, 1 eq.) in CH_2Cl_2 (200 µL) was added TFA (23 µL, 0.30 mmol, 30 eq.) dropwise, and the reaction mixture was stirred at ambient temperature for 16 h. The reaction mixture was then diluted with CH_2Cl_2 (5 mL) and poured into saturated $NaHCO_3$ (5 mL). The aqueous phase was extracted with CH_2Cl_2 (3 x 5 mL) and combined organics were washed with brine (5 mL), dried over $MgSO_4$, filtered and concentrated *in vacuo*. The residue was purified by column chromatography (SiO_2, CH_2Cl_2-CH_3CN 0→20% then CH_2Cl_2-CH_3CN (3:1) with MeOH 0→10%) to yield rotaxane (R_{ma})-**10** (8.5 mg, 0.008 mmol, 80%) as an off-white foam.

All spectroscopic data is consistent with those reported for (S_{ma})-**10**, with the exception of circular dichroism spectra.

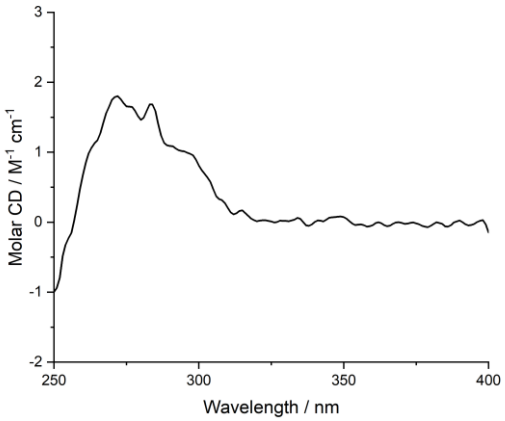

Figure 2.188 - Circular Dichroism Spectra of (R_{ma})-**10** (23 µM) at 293 K in $CHCl_3$.

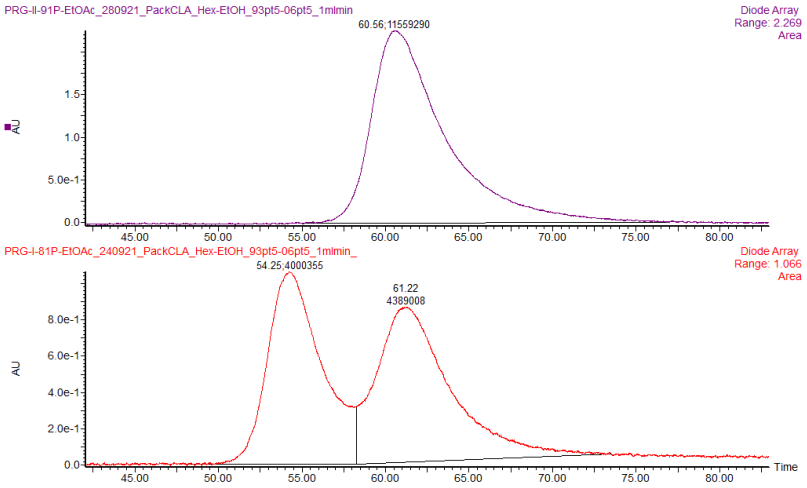

Figure 2.189 - CSP-HPLC of (R_{ma})-**10** loaded in EtOAc). RegisPackCLA-1, *n*-hexane-EtOH 93.5 : 6.5, flowrate 1 mLmin^{-1}. (top) (S_{ma})-**10** (not observed), (R_{ma})-**10** (60.56 min, 11559290, >99%). (bottom) *rac*-**10**, (S_{ma})-**10** (54.25 min, 4000355, 47.7%), (R_{ma})-**10** (61.22 min, 4389008, 52.3%).

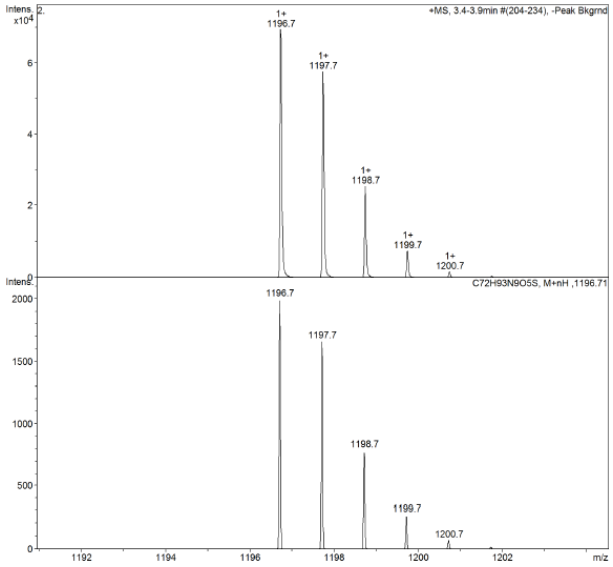

Figure 2.190 - Observed (top) and calculated (bottom) isotopic patterns for (R_{ma})-**10**.

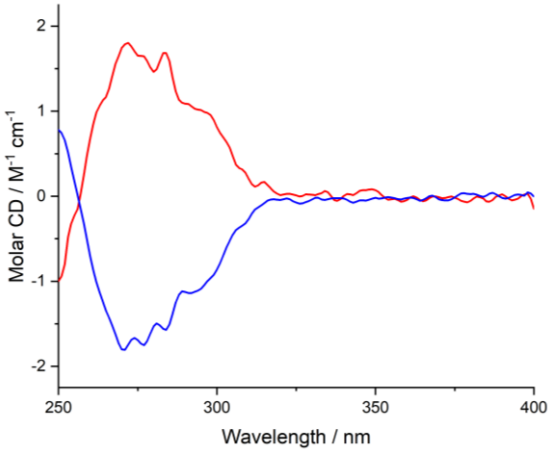

Figure 2.191 - Circular Dichroism Spectra of (R_{ma})-**10** (blue, 23 μM) and (S_{ma})-**10** (red, 26 μM) at 293 K in $CHCl_3$.

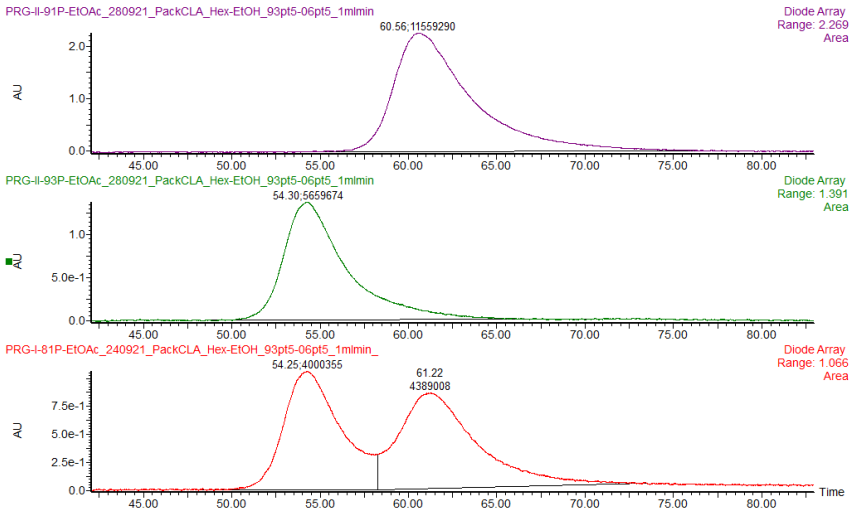

Figure 2.192 - CSP-HPLC of (R_{ma})-**10** and (S_{ma})-**10** (loaded in EtOAc). RegisPackCLA-1, *n*-hexane-EtOH 93.5 : 6.5, flowrate 1 mLmin^{-1}. (top) (R_{ma})-**10** (not observed), (S_{ma})-**10** (60.56 min, 11559290, >99.9%); (middle) (R_{ma})-**10** (54.30 min, 5659674, >99.9%), (S_{ma})-**10** (not observed); (bottom) *rac*-**10**, (S_{ma})-**10** (54.25 min, 4000355, 47.7%), (R_{ma})-**10** (61.22 min, 4389008, 52.3%).

Axle S21

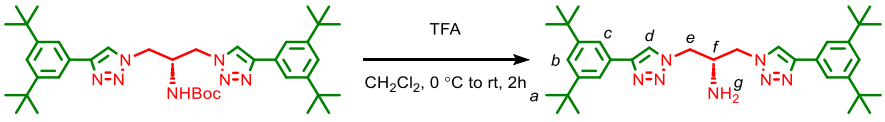

S20 **S21** (quant.)

A solution of **S20** (21.5 mg, 0.032 mmol) in CH_2Cl_2 (480 µL) was cooled to 0 °C, then TFA (160 µL) was added dropwise. After warming to ambient temperature, the reaction mixture was stirred for 2 h. The reaction mixture was then diluted with CH_2Cl_2 (5 mL) and poured into saturated $NaHCO_3$ (5 mL) with separation of aqueous and organic phases. The aqueous phase was extracted with CH_2Cl_2 (3 x 5 mL) and the combined organics were washed with brine (5 mL), dried over $MgSO_4$, filtered and concentrated *in vacuo* to yield **S21** (18.1 mg, 0.032 mmol, quant.) as a white foam without further purification.

δ_H ($CDCl_3$, 400 MHz) 7.99 (s, 2H, H_d), 7.69 (d, J = 1.8, 4H, H_c), 7.44 (t, J = 1.8, 2H, H_b), 4.51 (dd, J = 14.0, 5.6, 2H, H_e), 4.42 (dd, J = 14.0, 5.7, 2H, H_e), 3.92 (p, J = 5.7, 1H, H_f), 1.68 (br. s, 2H, H_{NH2}), 1.37 (s, 36H, H_a); δ_C ($CDCl_3$, 101 MHz) 151.7, 149.0, 129.6, 122.8, 121.4, 120.4, 53.6, 51.9, 35.1, 31.6, 29.9, 17.9; HR-ESI-MS (+ve) m/z = 570.4281 $[M+H]^+$ (calc. m/z for $C_{35}H_{52}N_7$ 570.4279).

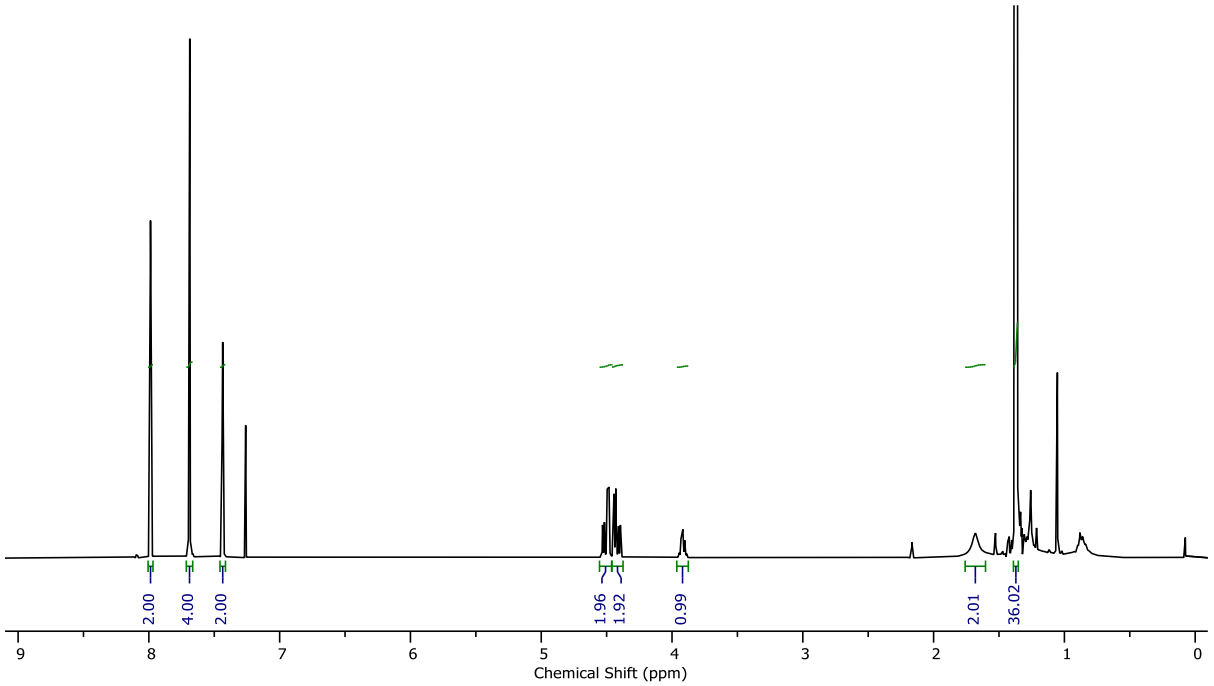

Figure 2.193 - ^{1}H NMR ($CDCl_3$, 400 MHz) of **S21**.

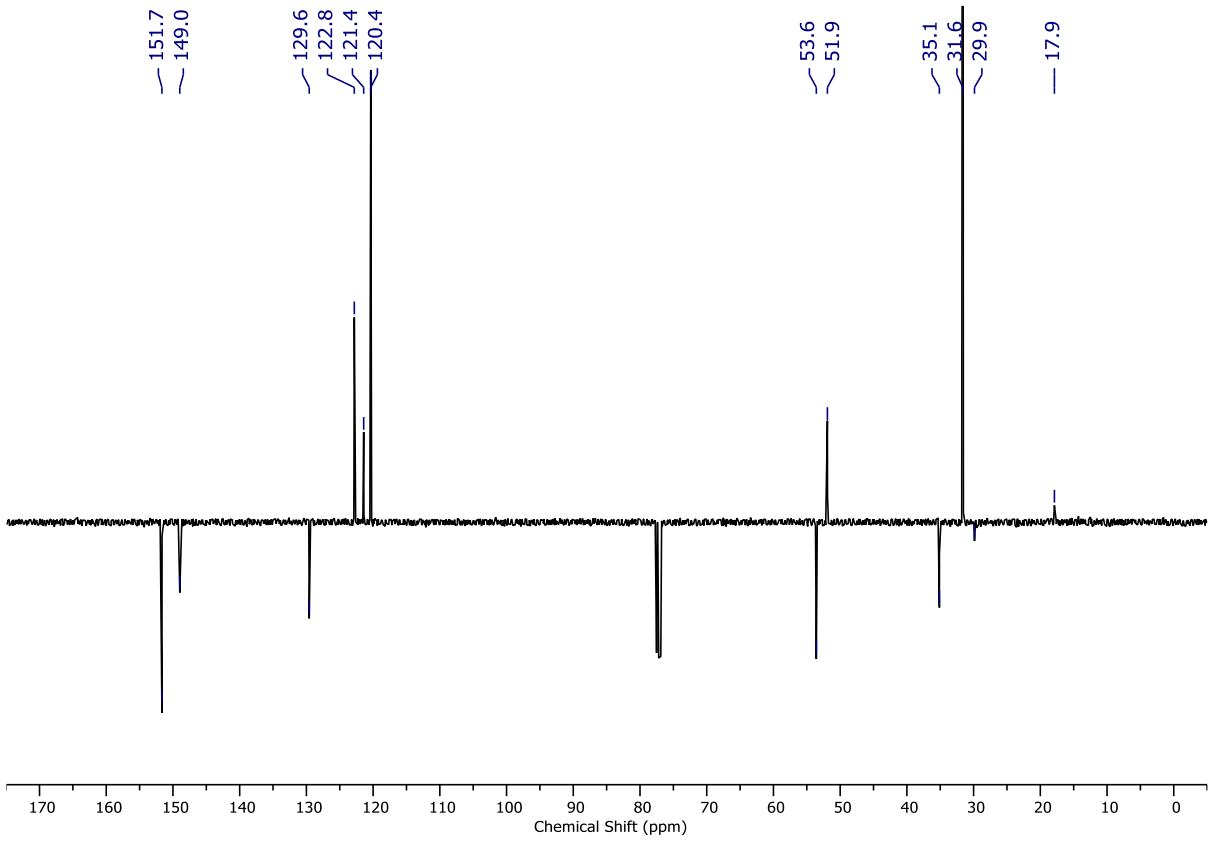

Figure 2.194 - JMOD NMR ($CDCl_3$, 101 MHz) of **S21**.

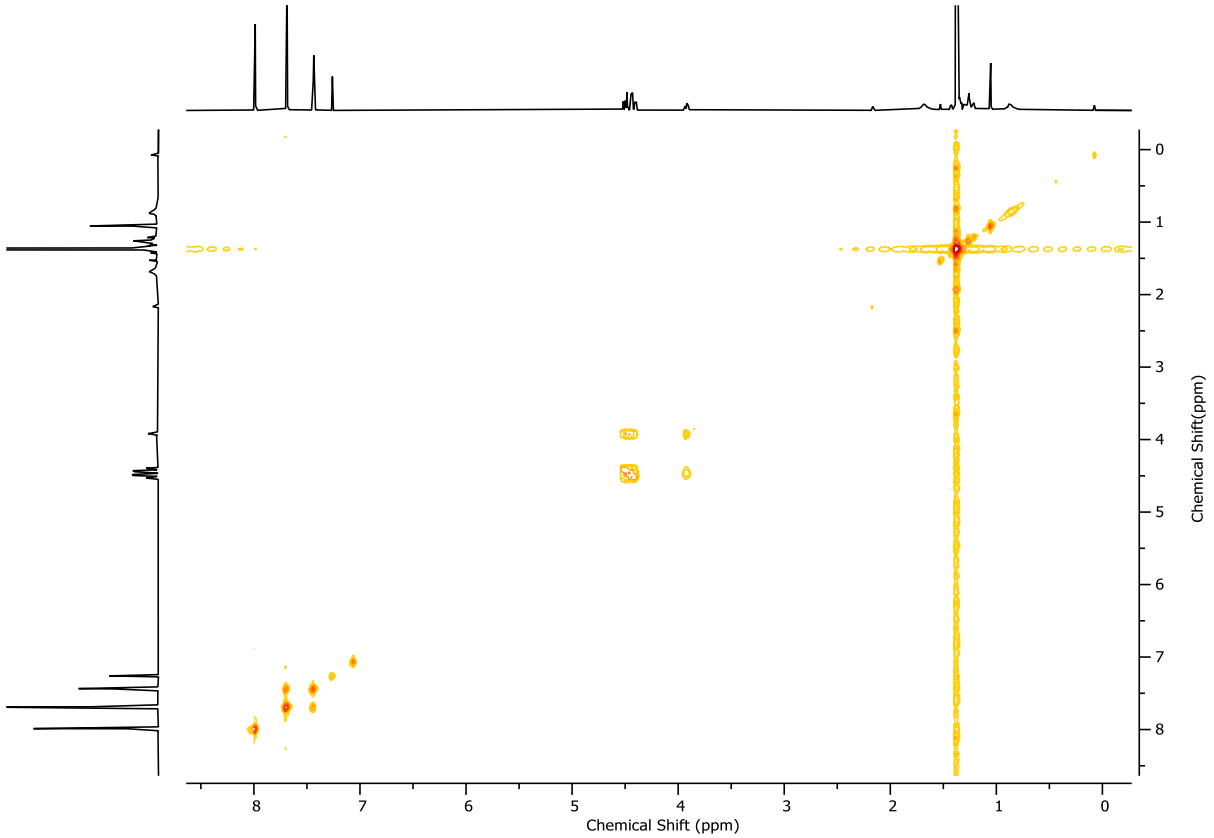

Figure 2.195 - ^{1}H COSY NMR ($CDCl_3$, 400 MHz) of **S21**.

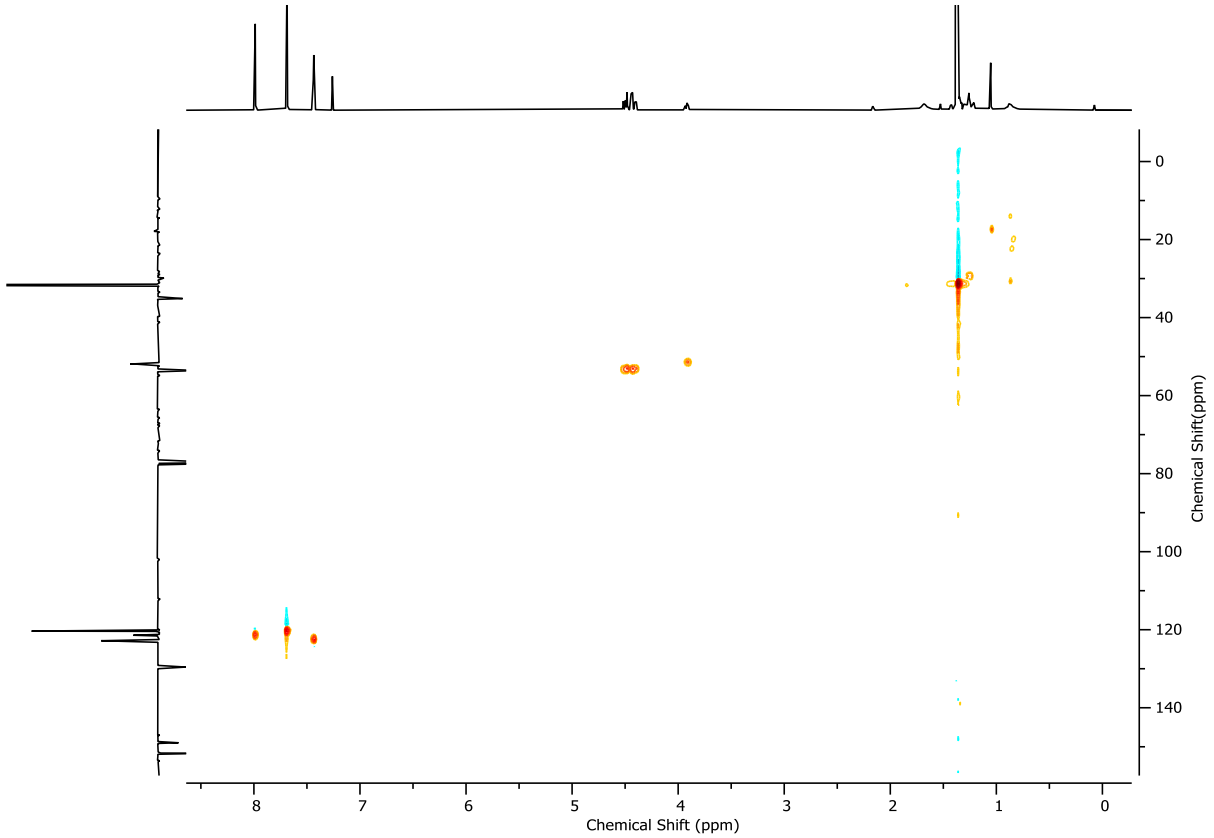

Figure 2.196 - HSQC NMR ($CDCl_3$, 400 MHz) of **S21**.

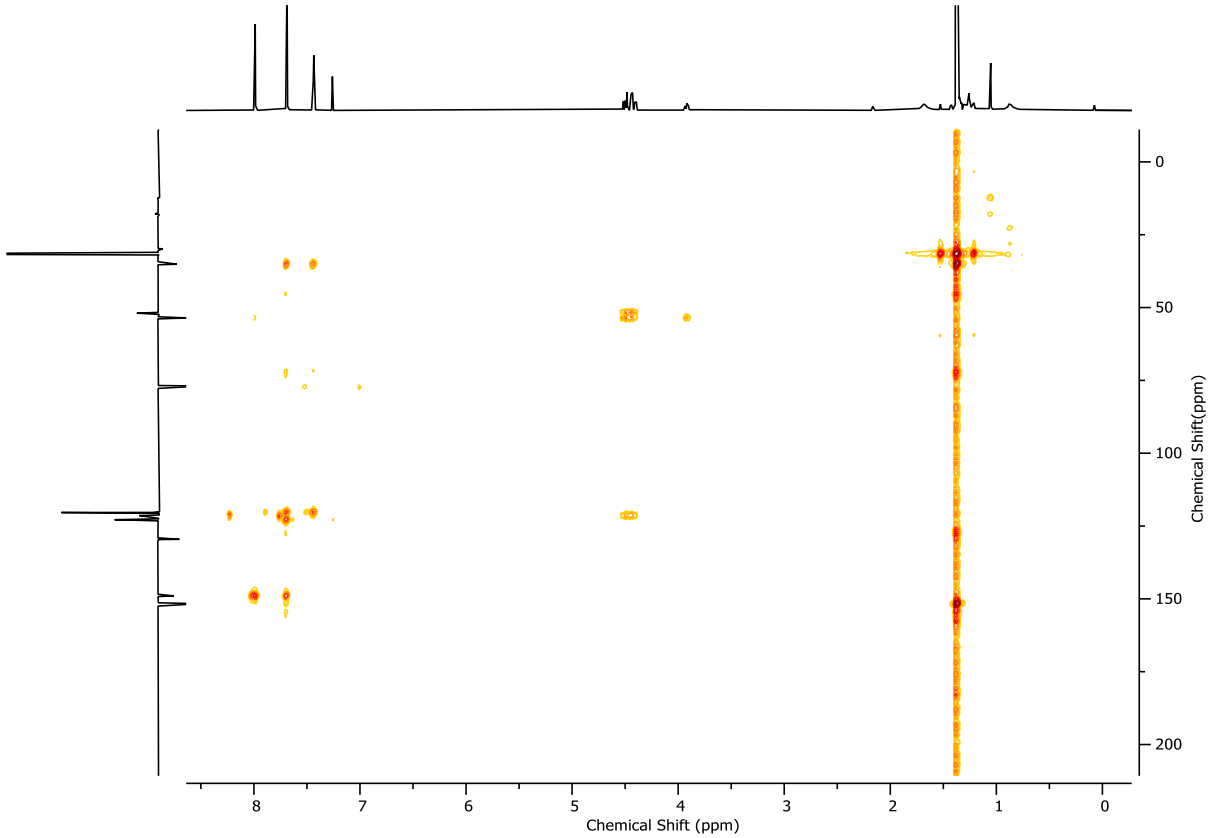

Figure 2.197 - HMBC NMR ($CDCl_3$, 400 MHz) of **S21**.

2.4.2. Effect of conditions in the synthesis of catenane 3 and rotaxane 9

2.4.2.1. Effect of solvent on the direct synthesis of catenane 3 (route a)

Varying the solvent used in the AT-CuAAC synthesis of catenane **3** from pre-macrocycle (*R*)-**1** and macrocycle **1** did not lead to an improvement in the observed stereoselectivity (Table 1).

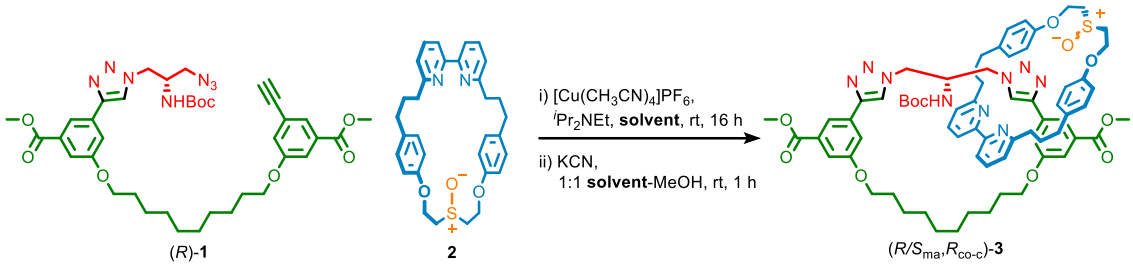

Scheme 2.9 - Synthesis of catenane **3** from (*R*)-**1** and macrocycle **2** (route a)

Table 2.1 - Effect of solvent in the direct synthesis of catenane **3**

Entry	Solvent	%conv.	*d.r.*
1	CH_2Cl_2	100	71 : 29
2	(1:1) CH_2Cl_2-PhMe	100	64 : 36
3	(1:1) CH_3Cl-EtOH	100	63 : 37

2.4.2.2. Oxidant screening for the oxidative synthesis of synthesis of catenane 3 (route b)

A brief screen of oxidants for route b was conducted. Initially mCPBA appeared to give high diastereoselectivity but closer inspection revealed this was at the expense of yield because over oxidation to the sulfone was observed (Table 2.2, entries 1 and 2). Oxone (entry 3) proved unselective but avoided over oxidation. IBX produced catenane **3** in reasonable diastereoselectivity (39 : 61) and with the opposite major stereoisomer to route a (entry 4). The chiral Davis oxaziridine reagent produced the opposite major stereoisomer in reasonable stereoselectivity (entry 5). Conditions reported by Sharpless for the enantioselective oxidation of sulfides did not result in any conversion. IBX oxidation (entry 4) was selected for the preparative reactions as it proceeds with the highest stereoselectivity and gives access to the opposite major stereoisomer from route a, facilitating access to the second enantiomer of **5**.

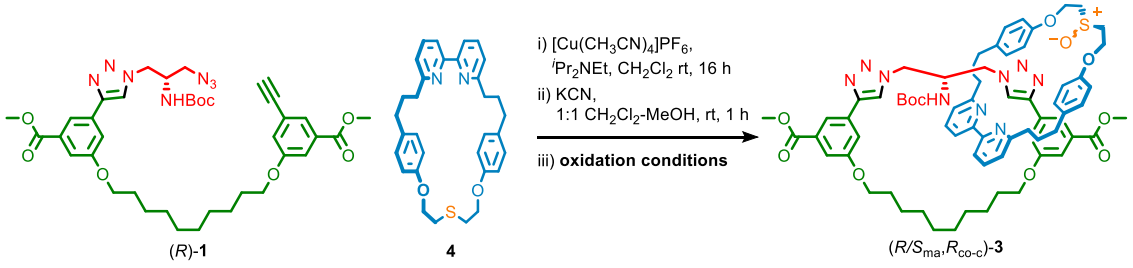

Scheme 2.10 - Synthesis of catenane **3** from (*R*)-**1** and macrocycle **4** via oxidation (route b)

Table 2.2 - Effect of oxidation conditions on the synthesis of catenane **3**

Entry	Conditions	%conv.	%sulfone	*d.r.*
1	mCPBA (1.2), CH_2Cl_2, -30 °C, 16 h	100	54	79 : 21
2	mCPBA (1.2), CH_2Cl_2, 25 °C, 2 h	100	27	58 : 42
3	Oxone (0.7), CH_3CN-H_2O, 25 °C, 16 h[65]	70	0	48 : 52
4	IBX (1.1), TEAB, $CHCl_3$-H_2O, 25 °C, 16 h[39]	100	0	39 : 61
5	Davis oxaziridine[a] (1.0), CH_2Cl_2, 25 °C, 16 h[66]	100	0	56 : 44
6	TBHP (1.0), Ti(O^iPr)$_4$, DET,[b] $ClCH_2CH_2Cl$, -20 °C, 16 h[67]	0	-	-

[a] (+)-(8,8-Dichlorocamphorylsulfonyl)oxaziridine. [b] Diethyltartrate

2.4.2.3. Effect of solvent on the direct synthesis of rotaxane 9 (route a)

Varying the solvent used in the AT-CuAAC synthesis of rotaxane **9** from half axle (*R*)-**7** and macrocycle **1** did not lead to an improvement in the observed stereoselectivity (Table 3).

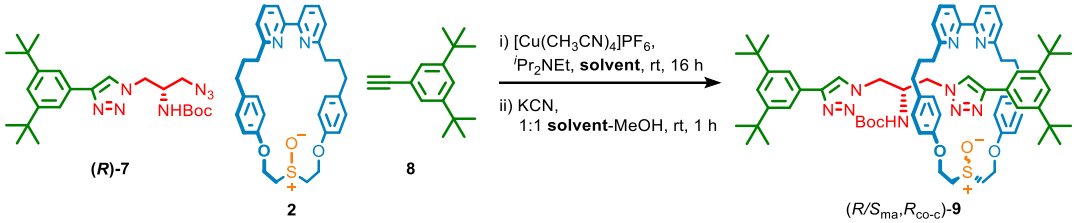

Scheme 2.11- Synthesis of rotaxane **9** from (*R*)-**7**, macrocycle **2** and alkyne **8** (route a)

Table 2.3 - Effect of solvent in the direct synthesis of rotaxane **9**

Entry	Solvent	%conv.	*d.r.*
1	CH_2Cl_2	100	75 : 25
2	(1:1) CH_3Cl-EtOH	100	62 : 38

2.4.2.4. Oxidant screening for the oxidative synthesis of rotaxane 9 (route b)

As with the synthesis of catenane 3, varying the oxidant in the synthesis of rotaxane 9 (route b), resulted in different diastereoselectivity (Table 4). Once again, the use of IBX resulted in the highest diastereoselectivity for the oxidation of the sulfide rotaxane (entry 3) and produced the opposite major stereoisomer to route a. This method was selected for preparative scale reactions.

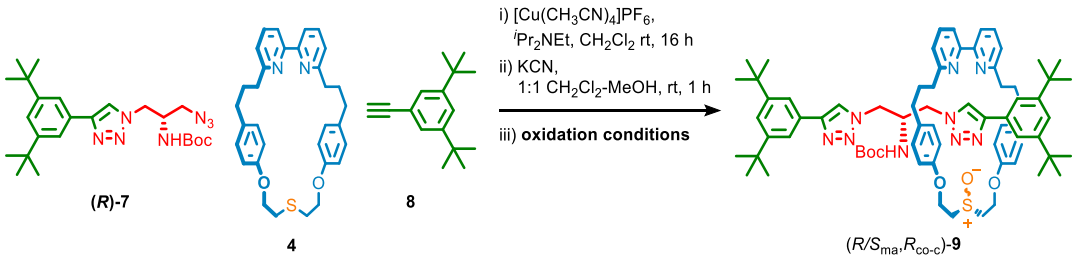

Scheme 2.12 - Synthesis of rotaxane **9** from (*R*)-**7**, macrocycle **4** and alkyne **8** *via* oxidation (route b)

Table 2.4 - Effect of oxidation conditions on the synthesis of rotaxane **9**

Entry	Conditions	%conv.	%sulfone	*d.r.*
1	mCPBA (1.2), CH_2Cl_2, 25 °C, 3 h	90	10	48 : 52
2	NBS (1.1), SiO_2, CH_2Cl_2, 25 °C, 1.5 h[68]	100	0	50 : 50
3	IBX/TEAB (1.1), $CHCl_3$-H_2O, 25 °C, 16 h[39]	100	0	40 : 60
4	Davis oxaziridine[a] (1.0), CH_2Cl_2, 25 °C, 16 h[66]	100	0	56 : 44
5	Ti(O^iPr)$_4$/BINOL/TBHP (2.0), PhMe-H_2O, 25 °C, 16 h[69]	50	9	57 : 43

[a] (+)-(8,8-Dichlorocamphorylsulfonyl)oxaziridine

NMR Stack Plots

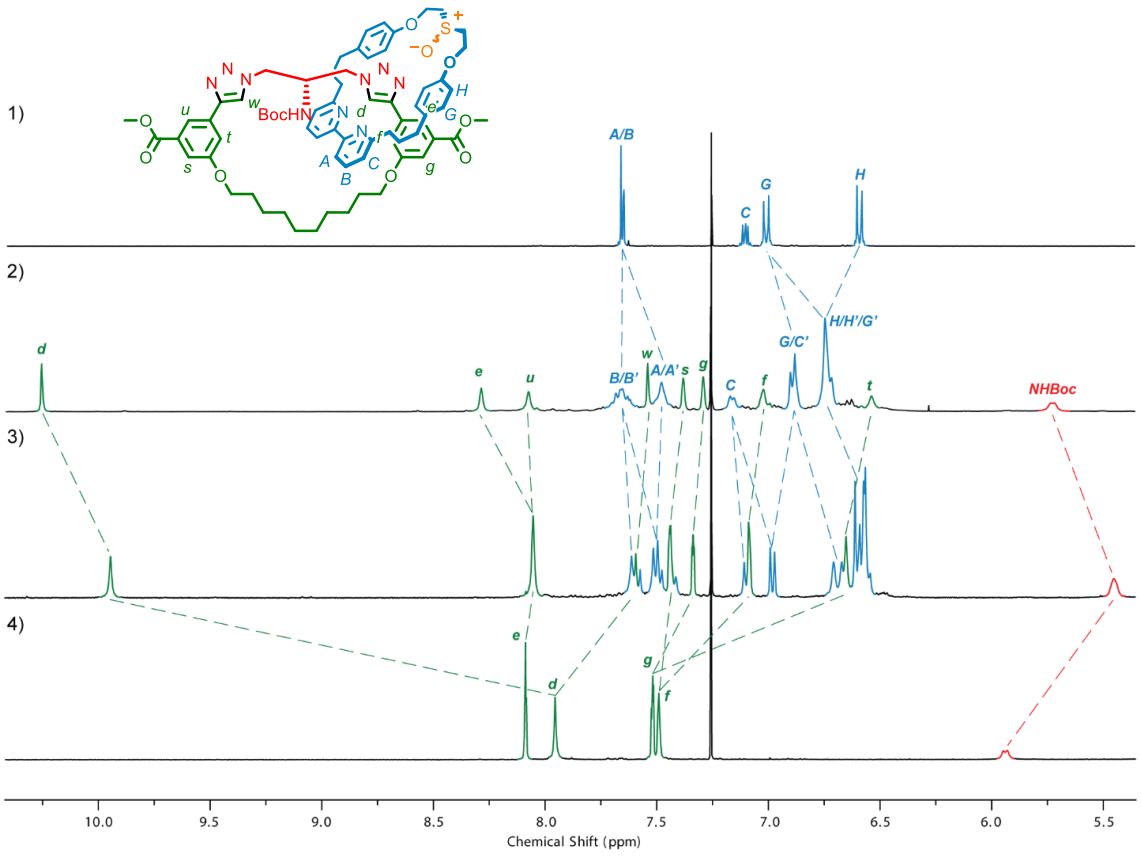

Figure 2.198 - Stacked ^{1}H NMR ($CDCl_3$, 400 MHz): 1) macrocyle **2**, 2) catenane (S_{ma},$R_{co\text{-}c}$)-**3**, 3) catenane (R_{ma},$R_{co\text{-}c}$)-**3**, 4) macrocycle **S13**.

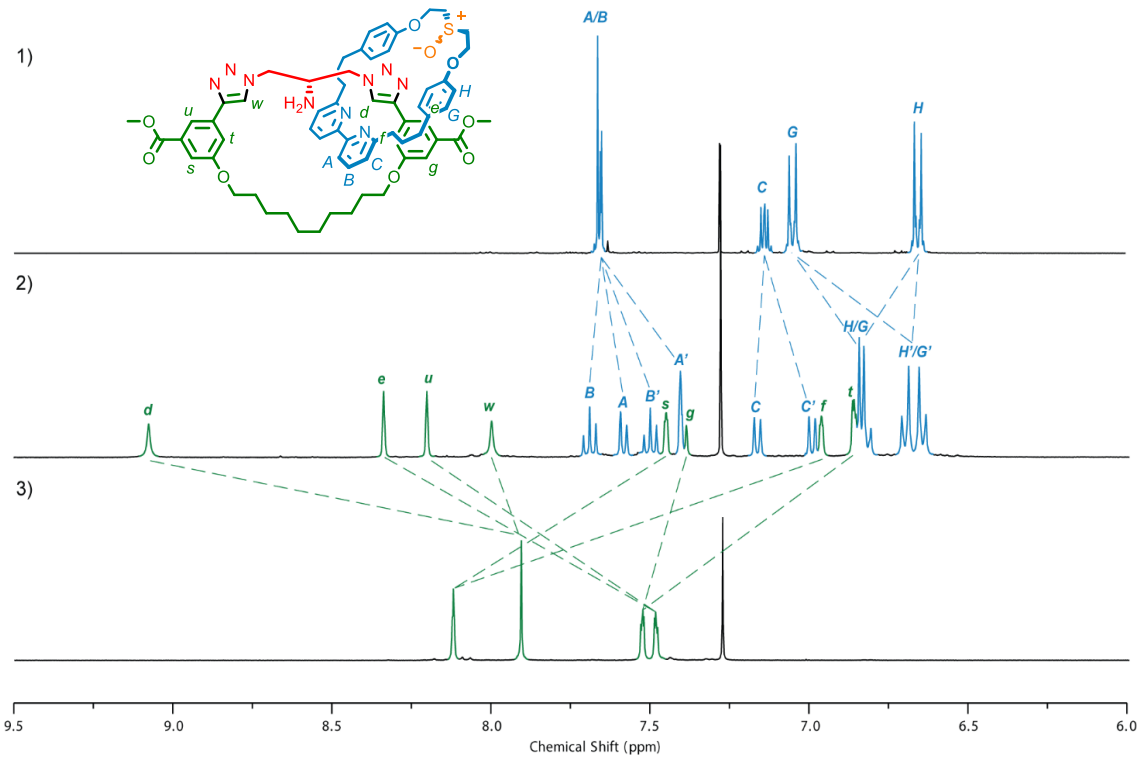

Figure 2.199 - Stacked ^{1}H NMR ($CDCl_3$, 400 MHz): macrocyle **2**, 2) catenane (S_{ma})-**6**, 3) macrocycle **S13**.

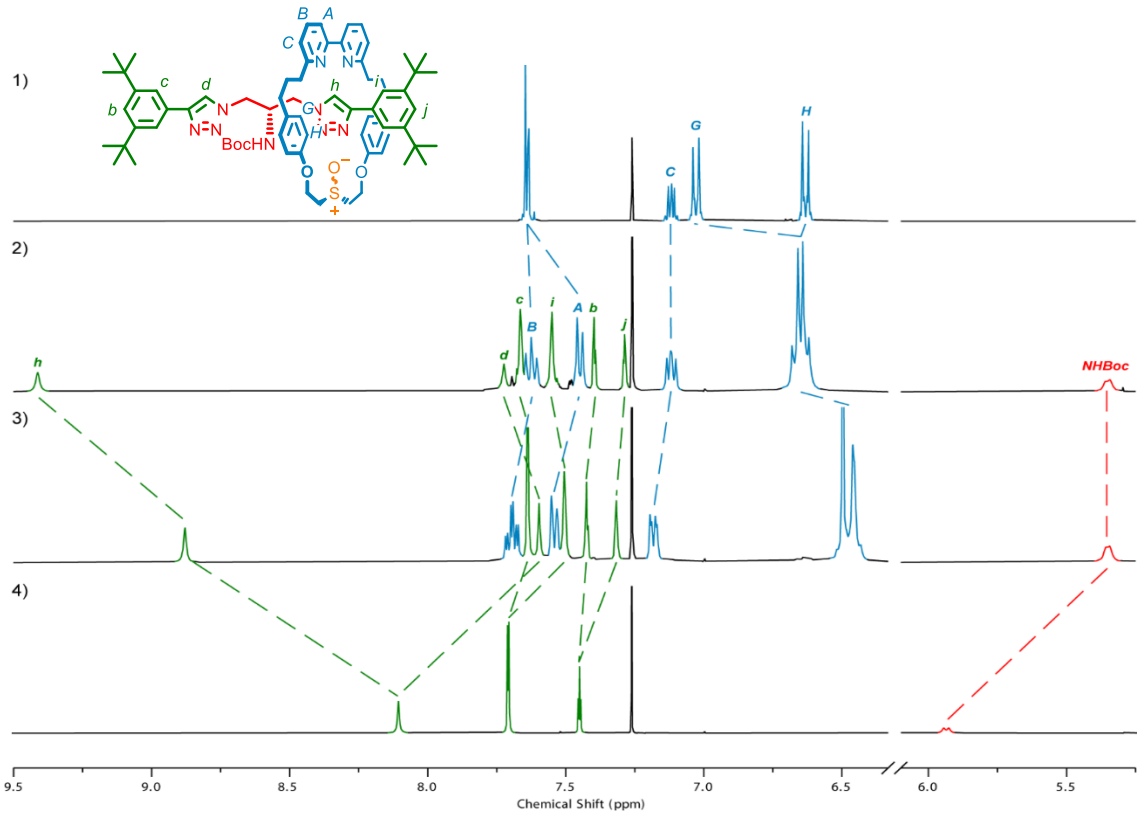

Figure 2.200 - Stacked ^{1}H NMR ($CDCl_3$, 400 MHz): 1) macrocyle **2**, 2) rotaxane (S_{ma},$R_{co\text{-}c}$)-**9**, 3) rotaxane (R_{ma},$R_{co\text{-}c}$)-**9**, 4) axle **S20**.

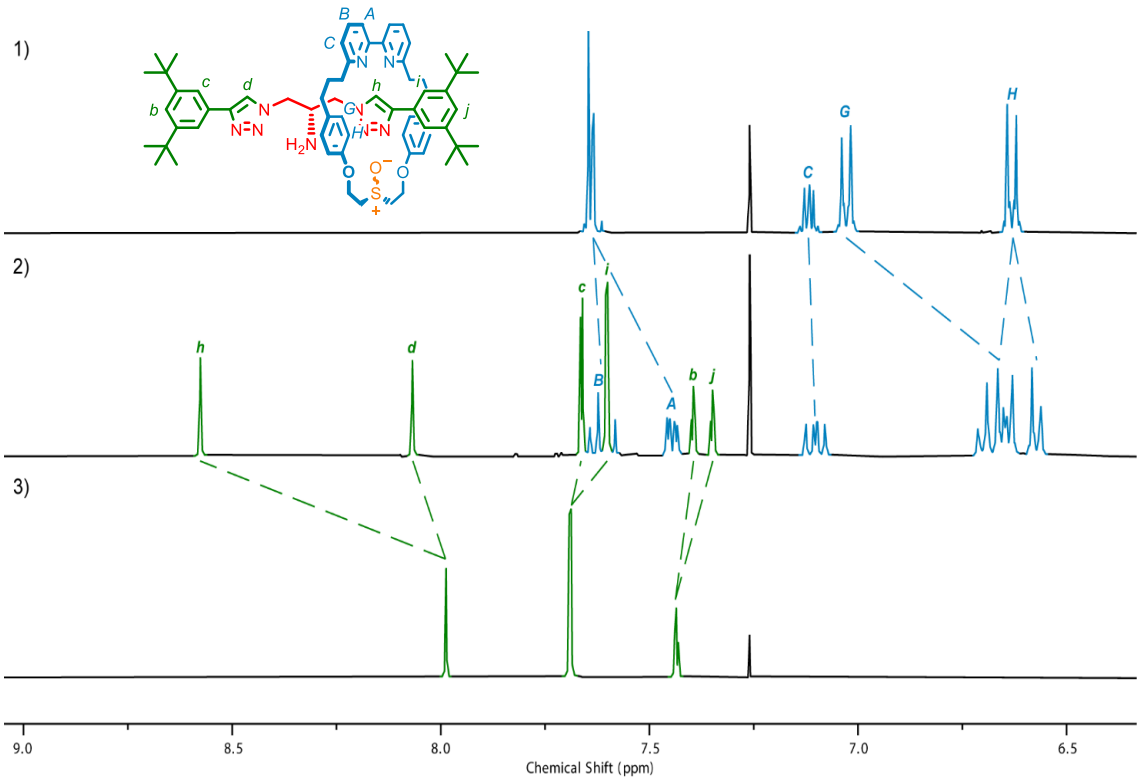

Figure 2.201 - Stacked ^{1}H NMR ($CDCl_3$, 400 MHz): 1) macrocycle **2**, 2) rotaxane (S_{ma})-**10**, 3) axle **S21**

2.4.3. Single crystal X-ray diffraction analysis

Single Crystal X-ray Diffraction Data for Catenane *rac*-(S_{ma},$R_{co\text{-}c}$)-3

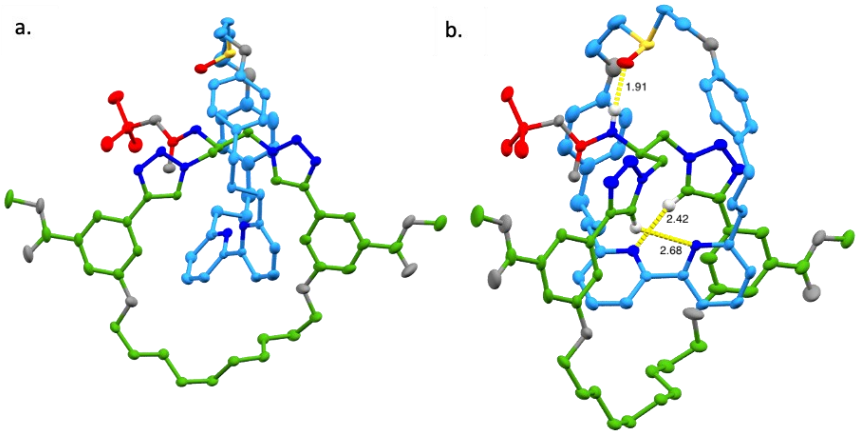

Figure 2.202 - Ellipsoid plot of the asymmetric unit of *rac*-(S_{ma},$R_{co\text{-}c}$)-**3** with hydrogens omitted for clarity (a) and highlighting key interactions (b). Thermal ellipsoids at 50% probability.

Single crystals of racemic *rac*-(S_{ma},$R_{co\text{-}c}$)-**3** were grown by slow vapour diffusion of *n*pentane into a concentrated CH_2Cl_2 solution, yielding large colourless block crystals. Data was collected at 100 K on a Rigaku 007 HF diffractometer equipped with a HyPix 6000HE hybrid pixel array detector. Cell determination, data reduction, cell refinement, and absorption correction were processed by CrysalisPro[70]. The structure was solved within Olex2[71] by refinement by ShelXL[72]. The asymmetric unit contained one molecule of $C_{70}H_{83}N_9O_{11}S$ (R_{ma},$S_{co\text{-}c}$)-**3** and disordered solvent. The unit cell contains both enantiomers related by an inversion centre. The disordered solvent was believed to contain primarily two dichloromethane molecules. There was also some indication of a low occupancy pentane molecule. Modelling of the disordered solvent molecules was attempted, however, the quality of the solution was significantly diminished, and thus the program SQUEEZE[73] implemented within PLATON[74] was used to account for the electron density within this region of the unit cell. SQUEEZE identified solvent accessible voids of 590 Å^3 and 192 electrons per unit cell were recovered.

Table 2.5 - Crystal data and structure refinement for (*rac*)-(S_{ma},$R_{co\text{-}c}$)-**3**

CCDC Number	2109976	r_{calc} g/cm^3	1.120
Empirical Formula	$C_{70}H_{83}N_9O_{11}S$	m/mm^{-1}	0.10
Formula Weight	1258.51	F(000)	1340
Temperature/K	100	Crystal size/mm^3	0.47 ´ 0.25 ´ 0.14
Crystal System	Triclinic	Radiation	Mo *K*a (l=0.71073)
Space Group	*P*-1	2Q range/°	4.0 – 64.2
a/Å	15.2504(3)	Index range	-21 ≤ *h* ≤ 22, -24 ≤ *k* ≤ 25, -24 ≤ *l* ≤ 25

b/Å	17.0326(4)	Reflections Collected	108399
c/Å	17.2393(3)	Independent Reflections	23034
a/°	106.910(2)	Data/parameters/restraints	23034/915/75
b/°	103.444(2)	Goodness-of-fit on F^2	1.025
g/°	110.252(2)	Final R-factor [I ≥ 2s(I)]	0.0616
Volume/Å^3	3732.34(15)	Final R indexes [all data]	R_1 = 0.0830, wR_2 = 0.1698
Z	2	Largest diff. peak/hole e Å^{-3}	0.88/-0.54

Single Crystal X-ray Diffraction Data for Catenane *rac*-6

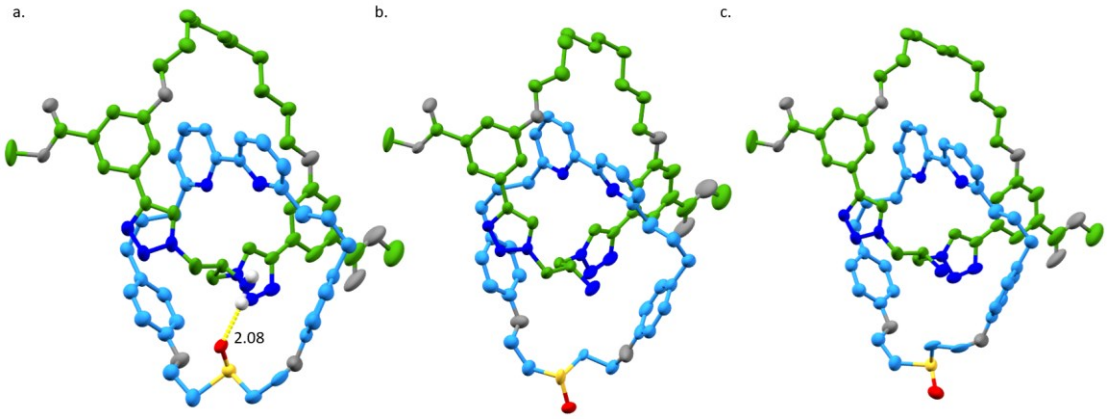

Figure 2.203 - Ellipsoid plots of the asymmetric unit for rac-**6** depicting the three positions modelled for the sulfoxide disorder, which correspond to (a) (S_{ma},R_{co-c})-**6**, (b) (S_{ma},R_{co-c})-**6** and (c) (R_{ma},R_{co-c})-**6** with ~50%, 30% and 20% occupancy respectively. Thermal ellipsoids at 50% probability, hydrogens omitted for clarity. Key intramolecular interactions are highlighted.

Single crystals of *rac*-**6** were grown by slow evaporation of a primarily ethyl acetate solution over a period of three months, yielding large colourless block crystals. Data was collected at 100 K on a Rigaku 007 HF diffractometer equipped with a HyPix 6000HE hybrid pixel array detector. Cell determination, data reduction, cell refinement, and absorption correction were processed by CrysalisPro. The structure was solved within Olex2[71] by ShelXT[73] with refinement by ShelXL[72]. The asymmetric units contained one molecule of $C_{65}H_{75}N_9O_9S$ and disordered solvent. The unit cell contained both enantiomers related by an inversion centre. The serendipity of the crystallization, in combination with disorder, precluded the identification of the solvent. Consequently, the electron density in this region of the unit cell was accounted for using the program SQUEEZE[73] implemented within PLATON[74]. SQUEEZE identified solvent accessible voids of 64 Å^3 and 23 electrons per unit cell were recovered. The sulfoxide group could be modelled reasonably as being disordered over three positions. A residual electron density peak (0.79 electrons) suggested the possibility of a fourth position corresponding to the second co-conformation of the inward pointing sulfoxide. However, this could not be modelled effectively.

Table 2.6 - Single Crystal Diffraction and Refinement Statistics for *rac*-**6**

CCDC Number	2115463	r_{calc} g/cm^3	1.274
Empirical Formula	$C_{65}H_{75}N_9O_9S$	m/mm^{-1}	1.00
Formula Weight	1158.40	F(000)	1232
Temperature/K	100	Crystal size/mm^3	0.45 ´ 0.33 ´ 0.22
Crystal System	Triclinic	Radiation	Cu *Ka* (l=1.54178)
Space Group	*P*-1	2Q range/˚	7.8 – 140.4
a/Å	9.9605(1)	Index range	-10 ≤ h ≤ 11, -15 ≤ k ≤ 16, -27 ≤ l ≤ 26
b/Å	13.4937(1)	Reflections Collected	35260
c/Å	22.5630(2)	Independent Reflections	11057
a/˚	88.176(1)	Data/parameters/restraints	11057/889/306
b/˚	86.450(1)	Goodness-of-fit on F^2	1.041
g/˚	86.543(1)	Final R-factor [I ≥ 2s(I)]	0.0866
Volume/Å^3	3020.03(5)	Final R indexes [all data]	R1 = 0.0895, wR2 = 0.2219
Z	2	Largest diff. peak/hole e Å^{-3}	1.45/-0.65

Single Crystal X-ray Diffraction Data for Catenane *rac*-S15

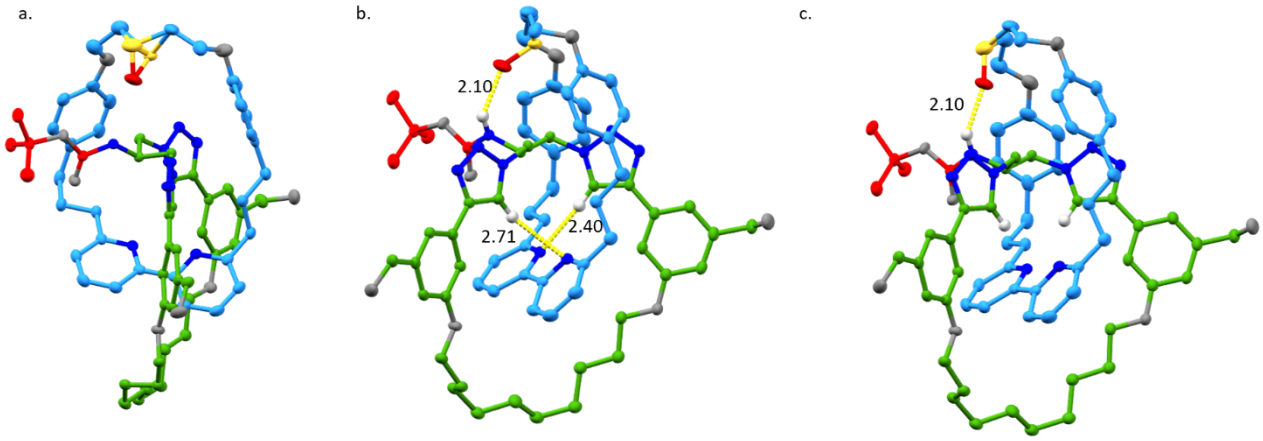

Figure 2.204 - Ellipsoid plot of the asymmetric unit for rac-**S15**. (a) disorder of the sulfur atom between the two diastereomeric positions (hydrogens omitted for clarity), key interactions for (b) (S_{ma},R_{co-c})-**S15** and (c) (R_{ma},R_{co-c})-**S15**. Thermal ellipsoids at 50% probability, methanol solvent omitted for clarity.

Single crystals of *rac*-**S15** were grown by slow evaporation of a concentrated methanol solution, yielding colourless block crystals. Data was collected at 100 K on a Rigaku 007 HF diffractometer equipped with a HyPix 6000HE hybrid pixel array detector. Cell determination, data reduction, cell refinement, and absorption correction were processed by CrysalisPro. The structure was solved within Olex2[71] by ShelXT[73] with refinement by ShelXL[72]. The asymmetric unit contained one molecule of $C_{68}H_{83}N_9O_9S$ (**S15**) and one molecule of methanol. The unit cell contained enantiomeric structures related by an inversion centre. Modelling of the disorder is consistent

with diastereomeric structures (R_{ma},$S_{co\text{-}c}$)-**S15** and (S_{ma},$S_{co\text{-}c}$)-**S15** occupying the same lattice positions with the occupancies refining to a ratio of ~80 : 20. A consequence of this disorder is a number of Hirshfeld test warnings for atom pairs in the alkyl chain, with one reaching a B-level alert on the checkcif report. We could remove these alerts by applying various restraints, however, in the context of the crystal we felt these were excessive. Moreover, the structure presented here agrees with all other experimental data. Therefore, we conclude that these alerts are a result of the disorder and not indicative of an incorrect atom-type assignment.

Table 2.7 - Crystal data and structure refinement for (*rac*)-**S15**

CCDC Number	2109991	ρ_{calc} g/cm^3	1.257
Empirical Formula	$C_{69}H_{87}N_9O_{10}S$	μ/mm^{-1}	0.97
Formula Weight	1234.53	F(000)	1320
Temperature/K	100	Crystal size/mm^3	0.37 × 0.20 × 0.12
Crystal System	Triclinic	Radiation	Cu $K\alpha$ (λ=1.54178)
Space Group	*P*-1	2Θ range/°	6.2 – 140.4
a/Å	11.4186(1)	Index range	-13 ≤ *h* ≤ 13, -18 ≤ *k* ≤ 18, -24 ≤ *l* ≤ 24
b/Å	15.1215(1)	Reflections Collected	60775
c/Å	20.0942(1)	Independent Reflections	12119
α/°	95.432(1)	Data/parameters/restraints	12119/818/3
β/°	100.146(1)	Goodness-of-fit on F^2	1.034
γ/°	105.079(1)	Final R-factor [I ≥ 2σ(I)]	0.0468,
Volume/Å^3	3261.51(4)	Final R indexes [all data]	R_1 = 0.0480, wR_2 = 0.1145
Z	2	Largest diff. peak/hole e Å^{-3}	1.05/-0.42

Single Crystal X-ray Diffraction Data for Rotaxane (R_{ma},$R_{co\text{-}c}$)-9

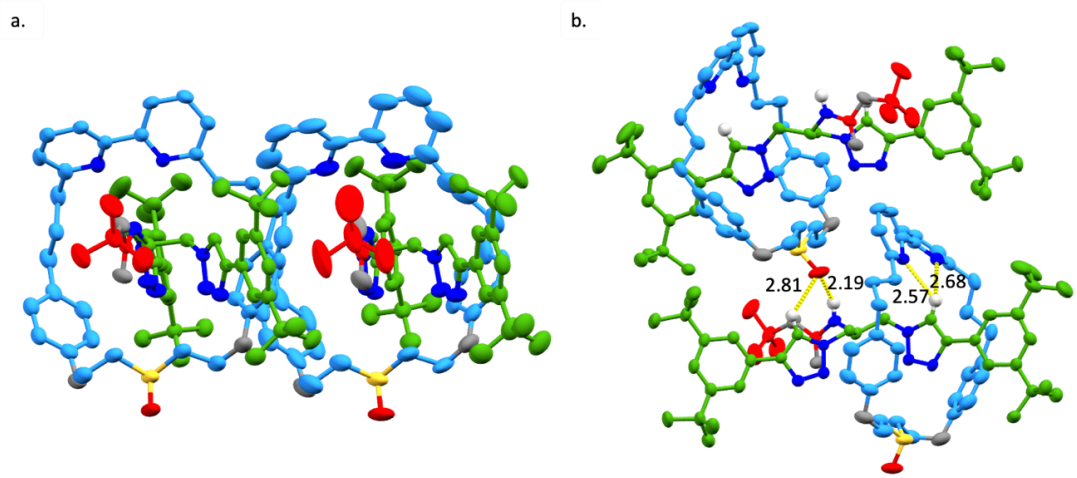

Figure 2.205 - Ellipsoid plot of the asymmetric unit for (R_{ma},$R_{co\text{-}c}$)-**9** (a) and with key interactions (b). Thermal ellipsoids at 50% probability, hydrogens omitted for clarity.

Single crystals of (R_{ma},$R_{co\text{-}c}$)-**9** were grown by slow vapour diffusion of ^{n}pentane into a concentrated CH_2Cl_2 solution of (R_{ma},$R_{co\text{-}c}$)-**9** yielding colourless needle crystals. Data was collected at 100 K on a Rigaku 007 HF diffractometer equipped with a HyPix 6000HE hybrid pixel array detector. Cell determination, data reduction, cell refinement, and absorption correction were processed by CrysalisPro. The structure was solved within Olex2[71] by ShelXT[73] with refinement by ShelXL[72]. The asymmetric unit contained two crystallographically independent molecules of $C_{72}H_{93}N_9O_5S$ (R_{ma},$R_{co\text{-}c}$)-**9** and solvent accessible voids. The voids were accounted for using the program SQUEEZE[73] implemented within PLATON[74]. SQUEEZE identified solvent accessible voids of 565 Å^3 and 18 electrons per unit cell were recovered. The absolute stereochemistry of the structure is consistent with the configuration of the starting materials and supported by by refinement of the Flack parameter.

Table 2.8 - Crystal data and structure refinement for (R_{ma},$R_{co\text{-}c}$)-**9**

CCDC Number	2109992	F(000)	2576
Empirical Formula	$C_{72}H_{93}N_9O_5S$	Crystal size/mm^3	0.48x0.13x0.06
Formula Weight	1196.61	Radiation	Cu Ka (l=1.54178)
Temperature/K	100	2Q range/˚	5.8 – 140.6
Crystal System	Monoclinic	Index range	-22 ≤ h ≤ 23, -23 ≤ k ≤ 20, -24 ≤ l ≤ 16
Space Group	$P2_1$	Reflections Collected	67048
a/Å	19.0015(1)	Independent Reflections	22005
b/Å	19.5618(2)	Data/parameters/restraints	22005/1597/61
c/Å	19.8094(2)	Goodness-of-fit on F^2	1.068
b/˚	102.508(1)	Final R-factor [I ≥ 2s(I)]	0.0496
Volume/Å^3	7188.46(11)	Final R indexes [all data]	R1 = 0.0568, wR2 = 0.1425
Z	4	Flack parameter	0.027(7)
r_{calc} g/cm^3	1.106	Largest diff. peak/hole e Å^{-3}	0.51/-0.31
m/mm^{-1}	0.81		

2.4.4. Discussion of the structural features of mechanically axially chiral molecules

2.4.4.1. Fundamental symmetry properties of the mechanical axial stereogenic unit

A mechanically axially chiral stereogenic unit arises when two covalent subcomponents with permanently distinguishable faces are directly mechanically bonded. The requirement for permanently distinguishable faces of the ring is achieved when its most symmetrical conformation has C_{nv} symmetry (rotational axis and mirror planes are perpendicular to the ring plane). Schematic structure **II** is the minimal representation of an axially chiral catenane (Figure 2.206a), the constituent rings (**I**) of which have $C_{\infty v}$ symmetry. Examining **II** allows us to identify how the mechanical axial stereogenic unit arises; in catenane **II** it is not possible to align any mirror plane of one ring with that of the other, which ensures that no improper symmetry operations of the subcomponents are maintained in the interlocked structure. In other words, it is the orthogonal arrangement of the rings enforced by the mechanical bond that ensures that the resulting structure is chiral.

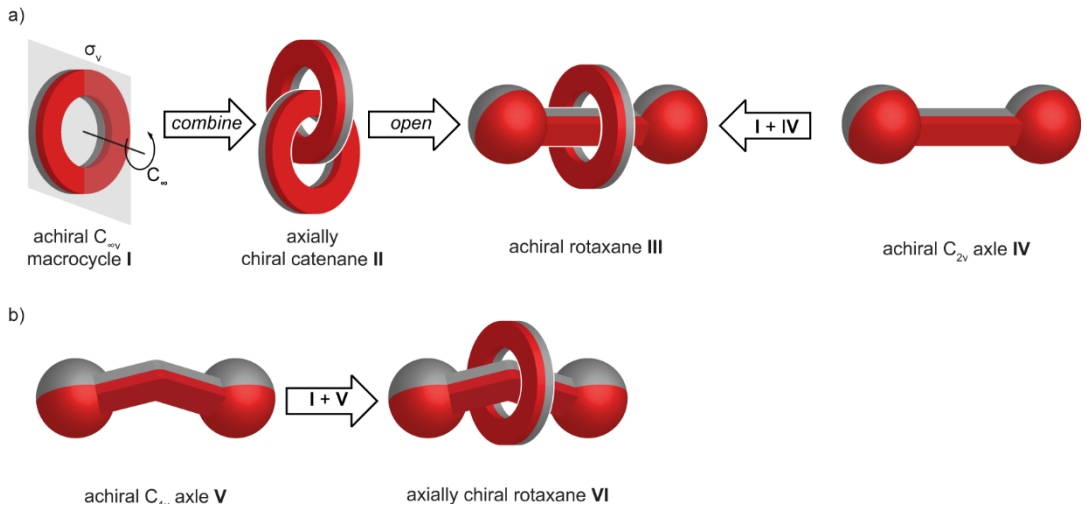

Figure 2.206 - a) Minimal schematic representation of axially chiral catenane **II** based on $C_{\infty v}$ ring **I** and achiral rotaxane **III** that results from the notional ring opening of **II**. b) Minimal schematic respresentation of a mechanically axially chiral rotaxane based on C_{1v} axle **VI**.

Turning to the equivalent rotaxane stereogenic unit, it is tempting to consider the notional ring opening and stoppering of axially chiral catenane structure **II**, but this results in an achiral object (**III**) if the axle (**IV**) is assumed to have a linear structure, as is typical in such schematic representations (Figure 2.206a). Examining the symmetry of axle **IV** reveals the origin of this surprising result; it has C_{2v} symmetry and one of the σ_v mirror planes of the axle can be arranged to be coincident with that of the ring. As a consequence, representation **III** is achiral. An alternative way of considering this problem is simply to recognise that axle **IV** does not have distinguishable faces.

Returning to the definition of the catenane axial stereogenic unit, we can predict that an equivalent stereogenic unit will arise in a rotaxane if the axle component has no mirror planes along its long axis. This is the case if the axle component has C_{1v} symmetry (more commonly referred to as C_s) in which the only symmetry operation is a mirror plane perpendicular to the axle. In schematic form, this can be achieved by requiring that the axle adopts a fixed non-linear structure (**V**), although any structural feature that results in C_{1v} symmetry is sufficient (Figure 2.206b).

Based on the above discussion we define the mechanical axial stereogenic unit of catenanes as arising the mechanical bond between two C_{nv} rings, and the equivalent unit of rotaxanes arising from the combination of a C_{1v} (C_s) axle with a C_{nv} ring.

2.4.4.2. Prochirality in "real" mechanically axially chiral structures

The schematic representations above make no reference to how the required symmetry properties arise. Indeed, representation **I** effectively implies that the structure of the ring is continuous, whereas molecules are made up of atoms bonded together and so are granular.

The axles of mechanically axially chiral rotaxanes are required to be prochiral as this gives rise to the required C_{1v} symmetry. Thus, suitably embedded prochiral centres, axes and planes in the middle of an axle will give rise to a mechanically axially chiral rotaxane (**VI**-**VIII** respectively,Figure 2.207a). Alternatively, a meso structure (e.g. **IX**, Figure 2.207b) in which two or more stereogenic centres are related by a mirror plane that bisects the axle will also give rise to a C_{1v} axle and so mechanical axial chirality. It should be noted that the overall structure of **IX** is also potentially prochiral as any single modification that does not lie on the mirror plane gives rise to a chiral structure.

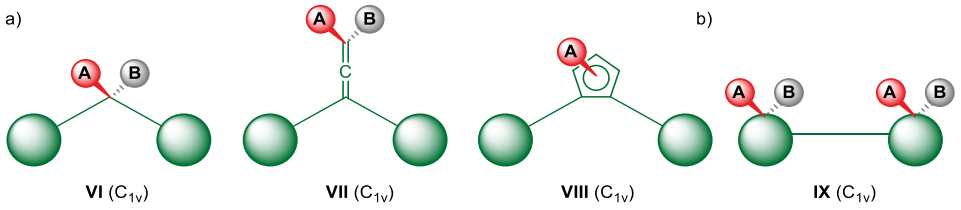

Figure 2.207 - Semi-structural representations of axles suitable for inclusion in mechanically axially chiral rotaxanes based on (a) a single prochiral centre (**VI**), axis (**VII**) or plane (**VIII**) or (b) two stereogenic units related by an internal mirror plane to generate a meso structure (**IX**).

The simplest way to design a ring suitable for inclusion in a mechanically axially chiral structure is also to embed a single prochiral moiety (centre as shown, or axis/plane) such that the associated mirror plane lies perpendicular to the ring to generate a C_{1v} structure (e.g. **X**, Figure 2.208). Achiral rings containing multiple identical prochiral units also give rise to catenanes in

which the mechanical axial stereogenic unit is the sole fixed source of stereochemistry (e.g. **XI**). It is also possible to achieve C_{1v} symmetry when a ring contains two or more stereogenic units related by a mirror plane to give a meso structure (e.g. **XII**). As with **IX**, ring **XII** is potentially prochiral as any modification that does not lie on the symmetry plane results in a chiral structure. If multiple non-identical prochiral units are present, the maximum rotational symmetry is determined by the lowest number in a set; for example, a ring containing two pairs of identical prochiral moieties can exhibit C_{2v} symmetry (e.g. **XIII**). The same groups connected such that the system is meso has C_{1v} symmetry (**XIV**).

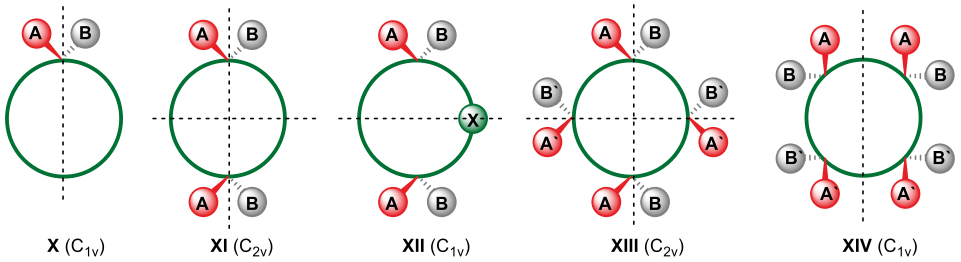

Figure 2.208 - Semi-structural representations of rings suitable for inclusion in mechanically axially molecules based on a single prochiral centre (**X**), two identical prochiral (**XI**), two identical stereogenic units (XII), two pairs of prochiral units (**XIII**) or two pairs of stereogenic units (**XIV**).

Finally, it is interesting to consider if rings can be designed in which prochirality does not arise, as in minimal representation **I**. If a C_{nv} ring containing n identical prochiral moieties is designed such that every atom lies on a mirror plane the overall structure is pro-prochiral (i.e. two modifications are required to render the structure chiral) but can still give rise to mechanically axially chiral structures (e.g. **XV**, Figure 2.209). Although a cyclohexane ring is obviously far too small to include in a catenane structure, the same holds for any cycloalkane substituted as shown. Such rings are obviously a special case, but it is important to note this exception to the general rule that the covalent subcomponents of mechanically axially chiral molecules exhibit prochirality. As n→∞ an equivalent symmetry to **II** would be achieved, although this is unphysical.

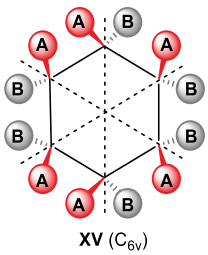

Figure 2.209 - An example of a C_{nv} ring that does not display prochirality - as every atom and bond lies on a mirror plane two modification as required to generate a chiral structure.

2.4.4.3. Co-conformational covalent diastereomerism in mechanically axially chiral structures

Co-conformational covalent stereochemistry arises when the relative positions of the covalent sub-components in an interlocked structure result in the desymmetrisation of one or more covalent pro-stereogenic units (e.g. rotaxane **XVI** exists as an achiral and enantiomeric co-conformations, Figure 2.210). Given that prochirality is a common feature of mechanically axially chiral structures, it is thus unsurprising that they will be expected to display co-conformational diastereomerism (e.g. **XVII**) – although a highly symmetrical representation in which the mechanical axial stereogenic unit is the only source of stereochemistry is possible, it is not required to be the dominant co-conformation. Indeed, it is this property that we have taken advantage of in our approach to mechanically axially chiral rotaxanes and catenanes.

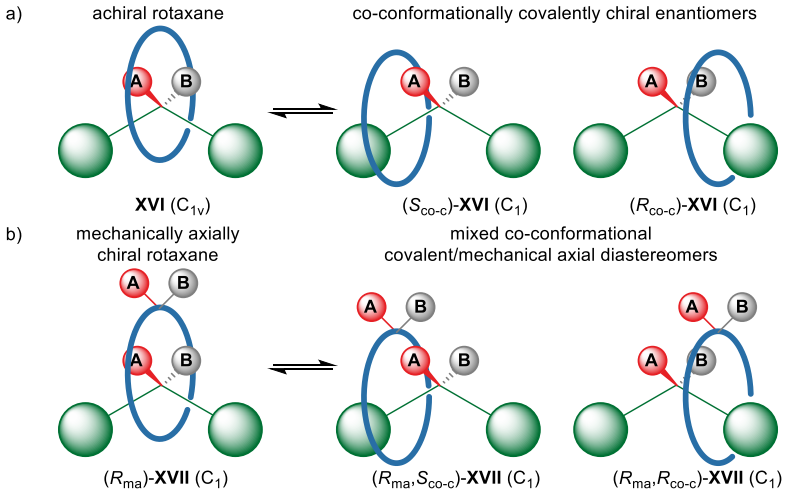

Figure 2.210 - Co-conformational stereoisomerism in rotaxanes based on C_{1v} axles. (a) Co-conformational enantiomerism in rotaxane **XVI**. (b) Co-conformational diastereomerism in mechanically axially chiral rotaxane **XVII**.

The exception to this general rule would appear to be catenanes based on C_{nv} rings that contain n identical prochiral moieties – it has already been noted that such structures are pro-prochiral (Figure 2.209). However, although such molecules require two covalent modifications to generate a chiral structure, co-conformational desymmetrisation, which simply relies on the position of the other covalent subcomponent in space, can still give rise to diastereomers directly – the second component is not required to be located over an atom or a bond midpoint. Thus, although such rings are not prochiral, they can still exhibit co-conformational diastereomerism.

2.4.5. Assigning the absolute stereochemistry of mechanically axially chiral molecules

Although rules for assigning the absolute stereochemistry of mechanically axially chiral molecules have been proposed[13,14], as is often the case, attempts to apply these to real examples

(as opposed to hypothetical cases or examples where the stereochemistry of the products was not determined), revealed their shortcomings. In particular, attempts to assign the stereochemistry of the molecules reported here highlighted that the outcome depended on the conformation of the covalent components considered. Here we propose a detailed approach that takes this complication into consideration.

2.4.5.1. Assigning the absolute stereochemistry of mechanically axially chiral molecules containing (pro)stereogenic centres

We propose that the absolute stereochemistry of axially chiral molecules based on a prochiral centre in each component can be assigned by correctly orienting their substituents. In the case of catenanes (e.g. **I**, Figure 2.211a), the in-plane substituents of the prochiral units should be oriented towards one another, whereas in the case of rotaxanes they should be oriented in the same direction (e.g. **II**, Figure 2.211b). The latter rule is to ensure that the notional ring opening of a catenane results in a rotaxane with the same absolute configuration. This arrangement is then viewed along the axis between prochiral centres to determine the orientation of the vectors connecting the out of plane substituents.

This approach can be readily extended to rings containing multiple identical prochiral moieties as any of these can be selected to achieve an identical result (e.g. **III,** Figure 2.211c). Similarly, catenanes based on rings containing multiple but non-identical prochiral moieties can be assigned by identifying the highest priority centre using CIP priorities for each centre and then following the same approach (e.g. **V**, Figure 2.211d). This approach can be extended to molecules based on a meso ring structure by orienting the in-plane substituents of the highest priority stereogenic units in the same way (e.g. **IV** and **VI**, Figure 2.211c and d respectively).

The step-by-step application of our approach for catenanes (e.g. **I**, Figure 2.211a) is given below. The same approach, with the prochiral moieties oriented in the same direction, can be applied to rotaxanes (e.g. **II**, Figure 2.211b):

Step 1: in each ring, identify the highest priority prochiral group (or stereogenic unit in meso structures) using the Cahn-Ingold-Prelog priority of the central atom.

Step 2: In each ring, identify the highest priority ligand of the identified centre that lie outside of the macrocycle plane, again using CIP priority, and label it as “A”; label the lower priority group “B”.

Step 2: redraw the molecule such that the in-plane substituents of both centres point towards one another with the macrocycles perpendicular to one another.

Step 3: define a vector A→B for each centre.

Step 4: View the relative orientation of the vectors along the axis connecting the centres and consider the direction of rotation from the head of the front vector to the tail of the rear vector, with a right-handed path assigned as (R_{ma}) and a left-handed path assigned as (S_{ma}).

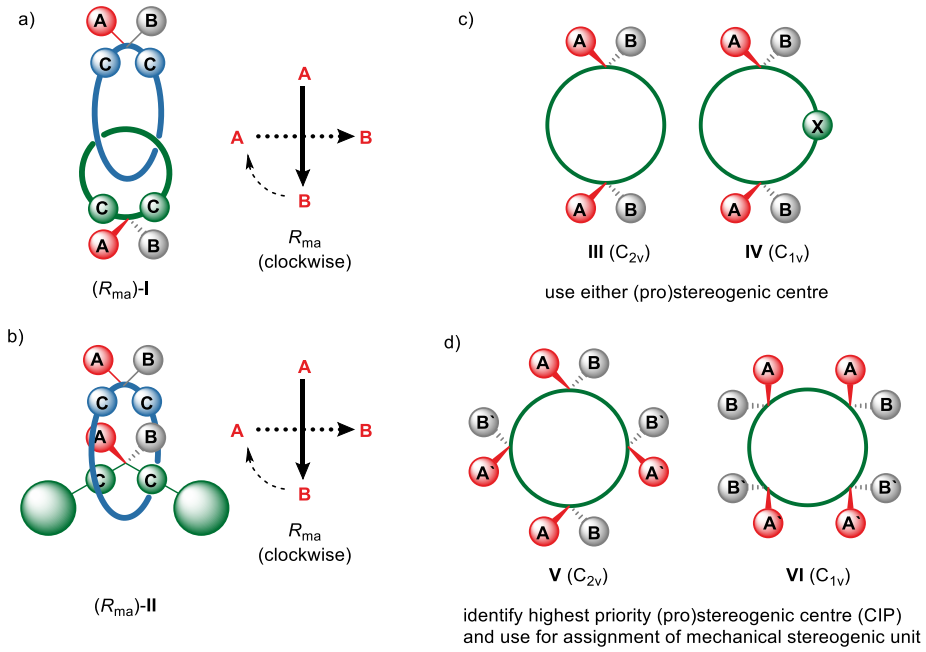

Figure 2.211 - (a) Schematic representation of the method for assigning the stereochemistry of mechanically axially chiral catenane **I** whose rings each contain one prochiral centre. (b) Schematic representation of the method for assigning the stereochemistry of mechanically axially chiral rotaxane **II** whose ring and axle each contain one prochiral centre. (c) Examples of rings containing identical (pro)stereogenic centres - structures based on these rings can be assigned using any of the (pro)stereogenic units. (d) Examples of rings containing non-identical (pro)stereogenic centres - structures based on these rings can be assigned by first identifying the highest priority (pro)stereogenic unit based on the Cahn-Ingold-Prelog priority.

2.4.5.2. Assigning the absolute stereochemistry of mechanically axially chiral molecules based on other (pro)stereogenic units

The approach described above can be extended to rings based on (pro)stereogenic units other than centres (e.g. **VI**) by identifying that these can also be characterized as having (i) in plane substituents and (ii) at least one out of plane substituent. Indeed, this is a requirement for the appearance of permanent facial dissymmetry, the pre-requisite for mechanical axial stereochemistry.

In the case of axial (pro)stereogenic units, the approach can be extended without any significant modifications; the in-plane substituents that connect the (pro)stereogenic unit to the ring structure should be oriented towards one another and the out-of-plane substituents that define the (pro)stereogenic axis ranked using the CIP system, as in the assignment of a covalent axial

stereogenic unit, and labelled A/B as above (e.g. **VII**, Figure 2.212). Planar (pro)stereogenic units (e.g. **VIII**, Figure 2.212) require a single modification to our general approach. Once again, the in-plane substituents that connects the (pro)stereogenic unit to the ring structure should be oriented towards one another. However, the plane is typically desymmetrised on only one face and so it is hard to identify the A and B substituents as in (pro)stereogenic centres and axes. In this case we propose that the A→B vector be replaced by a vector perpendicular to the ring plane pointing from (i.e. this is the tail of the vector) the highest priority out of plane ligand, the "pilot atom" in the context of the assignment of planar covalent stereogenic units, to the opposite face of the ring. Based on these arguments, all three prochiral units shown in Figure 2.212 result in the same **A→B** vector.

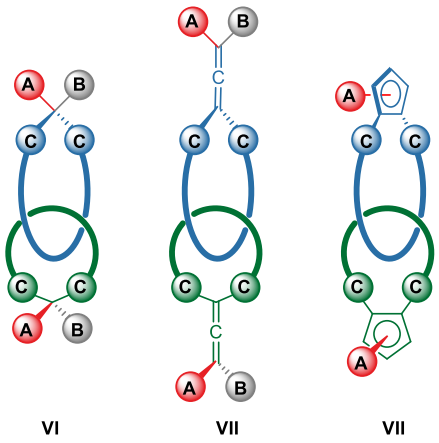

Figure 2.212 - Three mechanically axially chiral catenanes with the same stereolabel based on prochiral centres (**VI**), axes (**VII**) and planes (**VIII**)

2.4.6. Mechanical stereochemistry in molecules containing prochiral and stereogenic centres

2.4.6.1. Stereochemical analysis of catenanes containing one prochiral and one chiral stereogenic unit

Having focused on how mechanical axial stereogenic units arise due to prochiral units, it is worth considering what happens when one of these is replaced by a chiral stereogenic unit (e.g. a stereogenic centre, Figure 2.213). If we consider what happens on substituent permutation[10], we see that such molecules can exist as four stereoisomers, which is consistent with them containing a covalent and a mechanical stereogenic unit. Exchanging C and D inverts the covalent absolute configuration whereas exchanging A` and B` inverts the mechanical absolute configuration. Interestingly, exchanging A and B inverts the absolute configuration of both stereogenic units. Based on this analysis, we propose that catenanes of this form are considered as containing a combination of mechanical axial and covalent stereogenic units and so, if a single

diastereomer could be isolated, are viable precursors to axially chiral catenanes were the in-plane substituents of the stereogenic centre symmetrised through chemical modification.

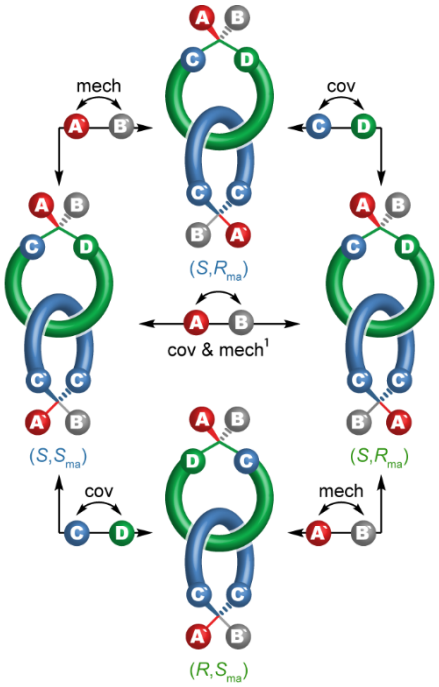

Figure 2.213 - The four stereoisomers of a catenane in which one ring contains a prostereogenic centre and the other contains a stereogenic centre. cov = ligand exchange inverts covalent stereolable, mech = ligand exchange inverts mechanical stereolabel.

2.4.6.2. Catenanes containing one chiral stereogenic unit in each ring

The next logical step is to consider the stereochemistry of a catenane in which both rings contain a covalent stereogenic centre (Figure 2.214). Intuitively, because each ring can exist in two enantiomeric forms, each of which can be interlocked with the other in two orientations, we can anticipate the potential for eight stereoisomeric forms and indeed, using the substituent permutation approach, this is what we find. Based on this, we can conclude that such molecules contain two covalent stereogenic units and one mechanical stereogenic unit but how to describe the mechanical stereochemistry is less obvious. In one interpretation, the facial desymmetrisation provided by the covalent stereogenic centre gives rise to mechanical axial stereochemistry. In the other, the sequence of atoms within each ring as a result of the stereogenic centre gives rise to a topological mechanical stereogenic unit. The labels arising from these interpretations behave differently under substituent permutation; exchanging the in-plane substituents inverts the topological and covalent stereogenic labels but leaves the axial stereodescriptor unchanged. Conversely, exchanging the out of plane substituents inverts the axial and covalent stereodescriptors but the topological label is unchanged.

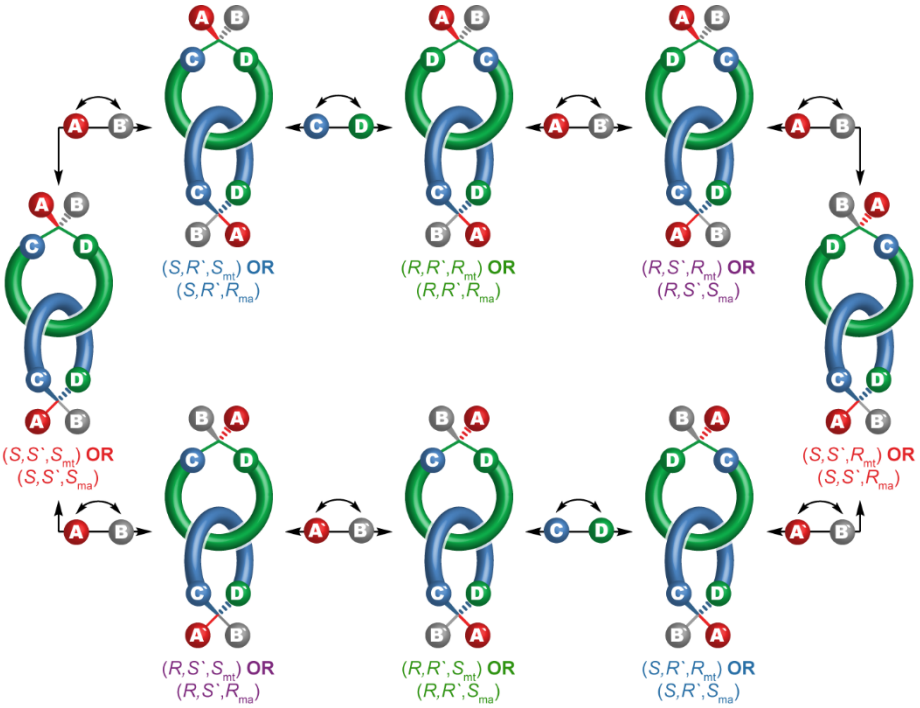

Figure 2.214 - The eight stereoisomers of a catenane in which both rings contain a stereogenic centre. cov = ligand exchange inverts covalent stereolable, mech = ligand exchange inverts mechanical stereolabel. For each structure two mechanical stereolabels are provided, onl one of which is required to specify the structure.

Privileging one of these interpretations over the other is challenging but we propose that the covalent/topological description is more intuitively satisfying as it captures one of the more interesting properties of the system, the topological invariance of the mechanical stereogenic unit in such molecules; even when the Euclidean properties of the system are relaxed (i.e. bond angles and lengths), such catenanes remain chiral objects whereas axially chiral catenanes themselves do not. Indeed, it is chemically possible to epimerise the covalent stereocentres, for example through deprotonation/reprotonation or nucleophilic displacement, which would also invert the mechanical axial stereodescriptor, but a direct chemical process that exchanges the topological epimers is harder to envisage. Regardless of the interpretation, what is undoubtedly true is that the stereochemistry of such molecules can be fully described using two covalent and one mechanical stereolabel, confirming that the mechanical stereogenic unit should only be "counted" once – it would be incorrect to assign both mechanical topologically and axial stereodescriptors simultaneously as this would, in effect, be double counting[75,41].

2.4.7. Other manifestations of mechanical axial stereochemistry

The manuscript describes an approach to molecules containing a fixed mechanical axial stereogenic unit. However, similar dynamic stereogenic units can arise due to co-conformational and conformational isomerism of the covalent subcomponents.

2.4.7.1. Co-conformational mechanical axial chirality

We have previously identified[14] that catenanes can display a co-conformational mechanical axial stereogenic unit when a ring whose highest symmetry representation is of C_{2h} or D_{nd} symmetry is combined with a C_{nv}, C_{2h} or D_{nd} ring. Such structures do not contain a fixed mechanical stereogenic unit but adopt chiral co-conformations that rely on the facial dissymmetry of the constituent rings, hence the analogy with the fixed mechanical axial stereogenic unit qualified by the co-conformational prefix. In schematic form, the required symmetry can be envisaged in rings that contain two or more prochiral moieties where the facial dissymmetry imparted by one is opposed by the other (e.g. **I** and **II**).

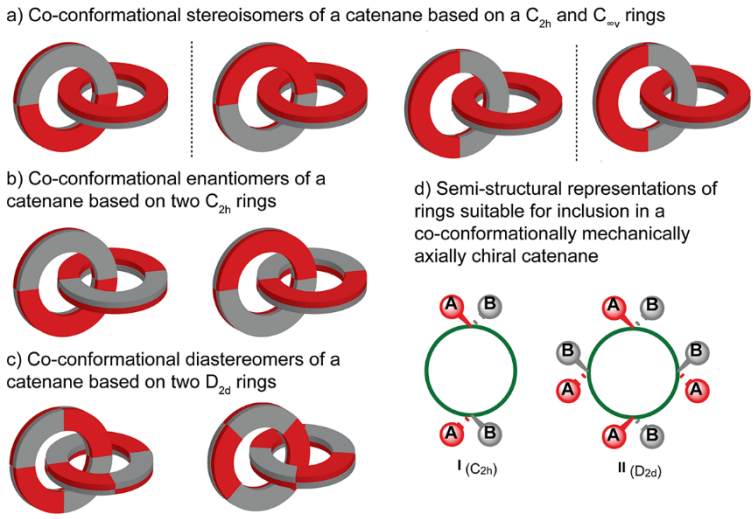

Figure 2.215 - a) Co-conformationally mechanically axially chiral enantiomers and diastereomers of a catenane based on a C_{2h} ring and a $C_{\infty v}$ ring. b) Co-conformationally mechanically axially chiral enantiomers of a catenane based on two C_{2h} rings. c) Co-conformationally mechanically axially chiral diastereomers of a catenane based on two D_{2d} rings. d) Semi-structural representations of a C_{2h} ring containing two prochiral centres and a D_{2d} ring containing 4 prochiral centres.

The only example of such a structure we have been able to identify was reported by Puddephat and co-workers (Figure 2.216)[76]. The isolated ring, **IV**, of catenane **V** can exist in chiral and achiral forms, depending on the configurations of the binapthyl units, which are atropisomeric. When precursor **III** was combined with a Pd^{II} source, the resulting catenane was observed to contain meso rings **III** but the overall structure was found to be chiral, with both enantiomers observed in the solid state. The most symmetrical representation of the meso form of **IV** has C_{2h} symmetry and thus the observed stereochemistry can be recognised as arising from a co-conformationally mechanically axially stereogenic unit. The enantiomers of **V** can thus be exchanged by pirouetting one ring relative to the other.

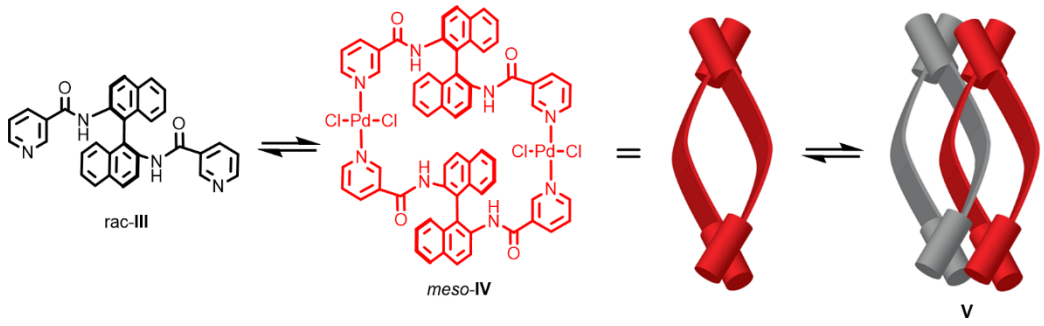

Figure 2.216 - Puddephat's co-conformationally mechanically axially chiral catenane **V** constructed from C_{2h} rings **IV**.

2.4.7.2. Conformational mechanical axial chirality

Rings whose most symmetric representation is of higher symmetry than C_{nv} but whose stable conformations have C_{nv} symmetry can lead to interlocked structures that express what appears to be a mechanical axial stereogenic unit. The simplest example of this are structures containing a suitably embedded biphenyl unit (Figure 2.217). As this moiety adopts a non-planar conformation it behaves as a covalent axial prochiral moiety (e.g. **VI**). Such systems can be conformationally locked (i.e. atropisomeric) and so result in structures that functionally contain a fixed mechanical stereogenic unit, albeit a notional conformational exchange process can invert the enantiomers.

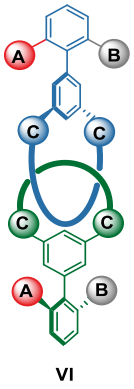

Figure 2.217 - Conformationally mechanically axially chiral catenane **VI** whose stereochemistry relies on prochiral atropisomeric axial units.

Less obviously, any structural feature that enforces a C_{nv} symmetric conformation on the ring structure will result in the appearance of conformational mechanical axial stereochemistry. The earliest example we were able to identify that meets these criteria was reported by Sauvage and co-workers (Figure 2.218); the rings of catenane **VII** are too small to allow the alkyl chain to adopt the most symmetrical conformation in which it bisects the phenanthroline unit and so it is sits to one side. As a result, both rings adopt C_{2v} conformations that are enforced by the mechancial

bond. The chiral nature of **VIII** could be detected when NMR analysis was carried out in the presence of a chiral anion, which led the appearance of diastereomeric signals.

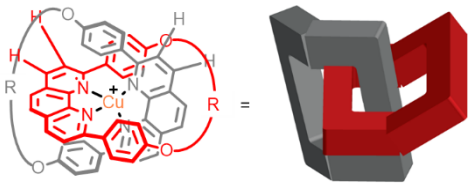

Figure 2.218 - Conformationally mechanically axially chiral catenane **VII** whose stereochemistry arises due to the C_{1v} conformation of the rings that is enforced by the sterically crowded nature of the mechancial bond.

Cougnon and co-workers reported catenane **IX** (Figure 2.219) that displays conformational mechanical axial stereochemistry (Figure 2.219)[54] (note: the schematic representations used in this manuscript suggest that the system displays co-conformational topological stereochemistry and the term "mechanical axial" is also used to describe the observed stereochemistry). The mechanical stereogenic unit arises because the naphthyl side panels of macrocycle **VIII** can adopt planar chiral conformations, the most stable of which is the meso form, at least in the catenane, and so the resulting ring structure has C_{1v} symmetry. The authors demonstrated that the conformational equilibrium could be biased by a chiral counteranion, which resulted in an unequal mixture of two diastereomeric structures. It is less clear whether isomerisation between the enantiomers occurs through bond rotation or if the structure is too crowded for this to occur and instead the isomerisation takes place by opening and closing the rings. It should be noted that the solid-state structure contains molecules in which the rings of the catenane are not perpendicular to one another and so a co-conformational helical stereogenic unit is also present and the meso conformational stereogenic units are also desymmetrised by the relative positions of the two rings.

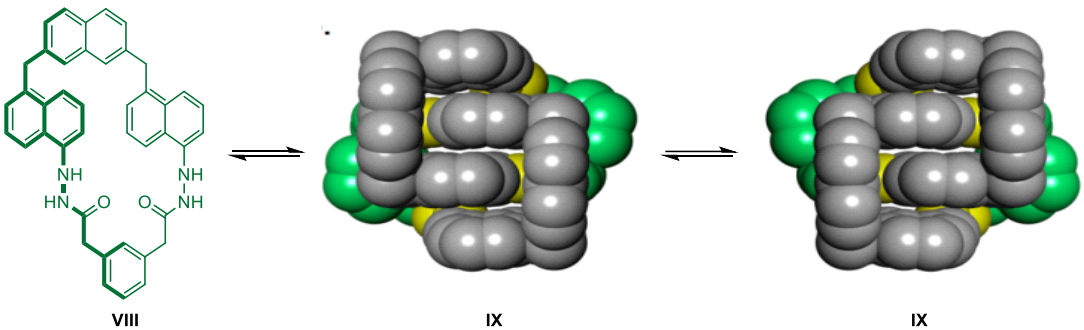

Figure 2.219 - Conformationally mechanically axially chiral catenane IX constructed from macrocycle **VIII** that adopts a C_{1v} conformation.

2.4.7.3. Combining conformational and co-conformational isomerism

Although previously unrecognised (including by us)[14], if a ring adopts a preferred C_{2h} conformation, the resulting catenane can display a co-conformational mechanical axial stereogenic unit. This effect is most striking when the separated rings undergo fast conformational exchange which is slowed significantly in the interlocked structure due to steric crowding. Stoddart and co-workers demonstrated such a system in the case of catenane **XII** (Figure 2.220). The isolated rings of catenane **XII**, **X** and **XI**, are achiral but the naphthyl side panels are conformationally stereogenic. The rings can thus adopt conformations of different symmetry (Figure 2.220b), including an achiral C_{2h} structure, which results in co-conformationally mechanically axially chiral enantiomers that can be exchanged either by covalent bond rotation (i.e. inversion of the conformational stereogenic units) or co-conformational motion (relative rotation of one ring 180°).

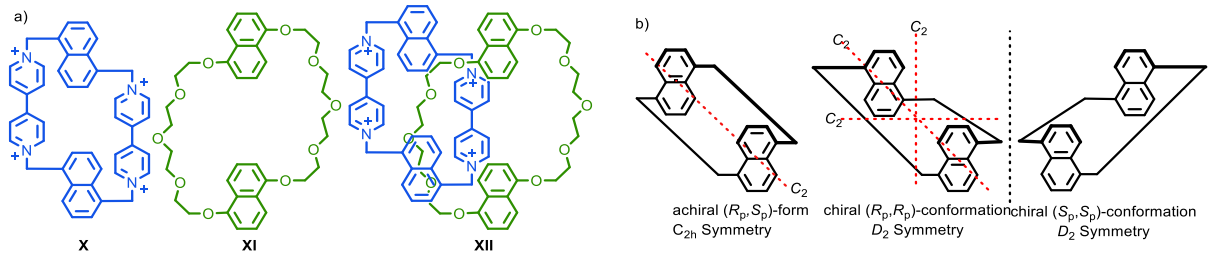

Figure 2.220 - Catenane XII reported by Stoddart and co-workers in which the constituent macrocycles can exist in C_{2h} symmetry conformations, resulting in co-conformational mechanical stereochemistry.

2.5. Bibliography

1 W. T. Kelvin, Baltimore Lectures on Molecular Dynamics and the Wave Theory of Light (C. J. Clay, London, 1904), p. 619

2 D. Zschiesche, P. Papazoglou, S. Schramm, W. C. Beckmann, J. Schaffner-Bielich, H. Stöcker, W. Greiner, *HNPS Proceedings* **2020**, *9*.

3 M. Petitjean, *Symmetry* **2021**, *13*.

4 P. G. Mezey, *Comput. Math. Appl.* **1997**, *34*, 105–112.

5 H. da Motta, *J. Phys.: Conf. Ser.* **2020**, *1558*, 012014.

6 D. B. Diaz, S. D. Appavoo, A. F. Bogdanchikova, Y. Lebedev, T. J. McTiernan, G. Dos Passos Gomes, A. K. Yudin, *Nat. Chem.* **2021**, *13*, 218–225.

7 E. L. Eliel, S. H. Wilen, L. N. Mander, *Stereochemistry of Organic Compounds*, John Wiley and Sons, Inc., New York, **1994**.

8 The Nobel Prize in Chemistry 2001 - NobelPrize.org, accessed 9/11/2021.

9 The Nobel Prize in Chemistry 2021 - NobelPrize.org, accessed 9/11/2021.

10 K. Mislow, J. Siegel, *J. Am. Chem. Soc.* **1984**, *106*, 3319–3328.

11 R. Herges, *Chem. Rev.* **2006**, *106*, 4820–4842.

12 S. D. P. Fielden, D. A. Leigh, S. L. Woltering, *Angew. Chem. Int. Ed.* **2017**, *56*, 11166–11194.

13 C. J. Bruns, J. F. Stoddart, *The Nature of the Mechanical Bond: From Molecules to Machines*, Wiley, **2016**.

14 E. M. G. Jamieson, F. Modicom, S. M. Goldup, *Chem. Soc. Rev.* **2018**, *47*, 5266–5311.

15 H. L. Frisch, E. Wasserman, *J. Am. Chem. Soc.* **1961**, *83*, 3789–3795.

16 G. Schill, *Catenanes, Rotaxanes and Knots*, Academic Press, New York, **1971**.

17 J. R. J. Maynard, S. M. Goldup, *Chem* **2020**, *6*, 1914–1932.

18 J. C. Chambron, C. Dietrich-Buchecker, G. Rapenne, J. P. Sauvage, *Chirality* **1998**, *10*, 125–133.

19 C. Yamamoto, Y. Okamoto, T. Schmidt, R. Jager, F. Vogtle, *J. Am. Chem. Soc.* **1997**, *119*, 10547–10548.

20 K. Hirose, M. Ukimi, S. Ueda, C. Onoda, R. Kano, K. Tsuda, Y. Hinohara, Y. Tobe, *Symmetry* **2018**, *10*, 20.

21 M. Gaedke, F. Witte, J. Anhauser, H. Hupatz, H. V. Schroder, A. Valkonen, K. Rissanen, A. Lutzen, B. Paulus, C. A. Schalley, *Chem. Sci.* **2019**, *10*, 10003-10009.

22 A. Imayoshi, B. V. Lakshmi, Y. Ueda, T. Yoshimura, A. Matayoshi, T. Furuta, T. Kawabata, *Nat. Commun.* **2021**, *12*, 404.

23 C. Tian, S. D. P. Fielden, B. Perez-Saavedra, I. J. Vitorica-Yrezabal, D. A. Leigh, *J. Am. Chem. Soc.* **2020**, *142*, 9803–9808.

24 R. J. Bordoli, S. M. Goldup, *J. Am. Chem. Soc.* **2014**, *136*, 4817–4820.

25 M. A. Jinks, A. de Juan, M. Denis, C. J. Fletcher, M. Galli, E. M. G. Jamieson, F. Modicom, Z. Zhang, S. M. Goldup, *Angew. Chem. Int. Ed.* **2018**, *57*, 14806–14810.

26 A. de Juan, D. Lozano, A. W. Heard, M. A. Jinks, J. M. Suarez, G. J. Tizzard, S. M. Goldup, *Nat. Chem.* **2022**, *14*, 179–187.

27 M. Denis, J. E. M. Lewis, F. Modicom, S. M. Goldup, *Chem* **2019**, *5*, 1512–1520.

28 C. P. McArdle, S. Van, M. C. Jennings, R. J. Puddephatt, *J. Am. Chem. Soc.* **2002**, *124*, 3959–3965.

29 N. C. Habermehl, M. C. Jennings, C. P. McArdle, F. Mohr, R. J. Puddephatt, *Organomet.* **2005**, *24*, 5004–5014.

30 A. Theil, C. Mauve, M.-T. Adeline, A. Marinetti, J.-P. Sauvage, *Angew. Chem. Int. Ed.* **2006**, *45*, 2104–2107.

31 IUPAC. Compendium of Chemical Terminology, 2nd ed. (the "Gold Book"). Compiled by A. D. McNaught and A. Wilkinson. Blackwell Scientific Publications, Oxford (1997). Online version (2019-) created by S. J. Chalk. ISBN 0-9678550-9-8. https://doi.org/10.1351/goldbook.

32 M. Alvarez-Perez, S. M. Goldup, D. A. Leigh, A. M. Slawin, *J. Am. Chem. Soc.* **2008**, *130*, 1836–1838.

33 A. Carlone, S. M. Goldup, N. Lebrasseur, D. A. Leigh, A. Wilson, *J. Am. Chem. Soc.* **2012**, *134*, 8321–8323.

34 Y. Cakmak, S. Erbas-Cakmak, D. A. Leigh, *J. Am. Chem. Soc.* **2016**, *138*, 1749–1751.

35 J. E. M. Lewis, R. J. Bordoli, M. Denis, C. J. Fletcher, M. Galli, E. A. Neal, E. M. Rochette, S. M. Goldup, *Chem.Sci.* **2016**, *7*, 3154–3161.

36 M. Denis, S. M. Goldup, *Nat. Rev. Chem.* **2017**, *1*, 0061.

37 V. Aucagne, K. D. Hanni, D. A. Leigh, P. J. Lusby, D. B. Walker, *J. Am. Chem. Soc.* **2006**, *128*, 2186–2187.

38 J. E. M. Lewis, F. Modicom, S. M. Goldup, *J. Am. Chem. Soc.* **2018**, *140*, 4787–4791.

39 V. G. Shukla, P. D. Salgaonkar, K. G. Akamanchi, *J. Org. Chem.* **2003**, *68*, 5422–5425.

40 H. Lahlali, K. Jobe, M. Watkinson, S. M. Goldup, *Angew. Chem. Int. Ed. Engl.* **2011**, *50*, 4151–4155.

41 H. V. Schroder, Y. Zhang, A. J. Link, *Nat. Chem.* **2021**.

42 D. M. Walba, *Tetrahedron* **1985**, *41*, 3161–3212.

43 P. J. Canfield, I. M. Blake, Z. L. Cai, I. J. Luck, E. Krausz, R. Kobayashi, J. R. Reimers, M. J. Crossley, *Nat. Chem.* **2018**, *10*, 615–624.

44 S. H. Reisberg, Y. Gao, A. S. Walker, E. J. N. Helfrich, J. Clardy, P. S. Baran, *Science* **2020**, *367*, 458–463.

45 O. Lukin, A. Godt, F. Vogtle, *Chemistry* **2004**, *10*, 1878–1883.

46 A. Martinez-Cuezva, A. Saura-Sanmartin, M. Alajarin, J. Berna, *ACS Catal.* **2020**, *10*, 7719–7733.

47 N. Pairault, J. Niemeyer, *Synlett* **2018**, *29*, 689–698.

48 R. Mitra, H. Zhu, S. Grimme, J. Niemeyer, *Angew. Chem. Int. Ed. Engl.* **2017**, *56*, 11456–11459.

49 N. Pairault, H. Zhu, D. Jansen, A. Huber, C. G. Daniliuc, S. Grimme, J. Niemeyer, *Angew. Chem. Int. Ed. Engl.* **2020**, *59*, 5102–5107.

50 M. Dommaschk, J. Echavarren, D. A. Leigh, V. Marcos, T. A. Singleton, *Angew. Chem. Int. Ed. Engl.* **2019**, *58*, 14955–14958.

51 A. W. Heard, S. M. Goldup, *Chem* **2020**, *6*, 994–1006.

52 S. Corra, C. de Vet, J. Groppi, M. La Rosa, S. Silvi, M. Baroncini, A. Credi, *J. Am. Chem. Soc.* **2019**, *141*, 9129–9133.

53 C. S. Wood, T. K. Ronson, A. M. Belenguer, J. J. Holstein, J. R. Nitschke, *Nat. Chem.* **2015**, *7*, 354–358.

54 K. Caprice, D. Pal, C. Besnard, B. Galmes, A. Frontera, F. B. L. Cougnon, *J. Am. Chem. Soc.* **2021**, *143*, 11957–11962.

55 Z. Cui, Y. Lu, X. Gao, H. J. Feng, G. X. Jin, *J. Am. Chem. Soc.* **2020**, *142*, 13667–13671.

56 J. P. Carpenter, C. T. McTernan, J. L. Greenfield, R. Lavendomme, T. K. Ronson, J. R. Nitschke, *Chem* **2021**, *7*, 1534–1543.

57 D. A. Leigh, F. Schaufelberger, L. Pirvu, J. H. Stenlid, D. P. August, J. Segard, *Nature* **2020**, *584*, 562–568.

58 S. Corra, C. de Vet, M. Baroncini, A. Credi, S. Silvi, *Chem* **2021**, *7*, 2137–2150.

59 A. H. G. David, J. F. Stoddart, *Israel Journal of Chemistry* **2021**, *61*, 608–621.

60 P. R. Ashton, S. E. Boyd, S. Menzer, D. Pasini, F. M. Raymo, N. Spencer, J. F. Stoddart, A. J. P. White, D. J. Williams, P. G. Wyatt, *Chem. - A Eur. J.* **1998**, *4*, 299–310.

61 A. Pigorsch, M. Köckerling, *Cryst. Growth Des.* **2016**, *16*, 4240–4246.

62 M. Shibakami, K. Miyawaki, A. Harada, T. Takagi, *Synlett* **2003**, 0349–0352.

63 C. L. Do-Thanh, J. J. Vargas, J. W. Thomas, G. R. Armel, M. D. Best, *J. Agric. Food Chem.* **2016**, *64*, 3533–3537.

64 S. Ogi, T. Ikeda, R. Wakabayashi, S. Shinkai, M. Takeuchi, *Chem. - A Eur. J.* **2010**, *16*, 8285–8290.

65 R. V. Kupwade, S. S. Khot, U. P. Lad, U. V. Desai, P. P. Wadgaonkar, *Res. Chem. Int.* **2017**, *43*, 6875–6888.

66 F. A. Davis, R. ThimmaReddy, M. C. Weismiller, *J. Am. Chem. Soc.* **2002**, *111*, 5964–5965.

67 P. Pitchen, E. Dunach, M. N. Deshmukh, H. B. Kagan, *J. Am. Chem. Soc.* **2002**, *106*, 8188–8193.

68 M. Hashmat Ali, M. Hartman, K. Lamp, C. Schmitz, T. Wencewicz, *Synth. Commun.* **2006**, *36*, 1769–1777.

69 N. Komatsu, Y. Nishibayashi, T. Sugita, S. Uemura, *Tetrahedron Lett.* **1992**, *33*, 5391–5394.

70 CrysAlisPro Software System, Rigaku Oxford Diffraction, (2020).

71 O. V. Dolomanov, L. J. Bourhis, R. J. Gildea, J. A. K. Howard, H. Puschmann, *J. Appl. Cryst.* **2009**, *42*, 339–341.

72 G. M. Sheldrick, *Acta Cryst. C* **2015**, *71*, 3–8.

73 A. L. Spek, *Acta Cryst. C* **2015**, *71*, 9–18.

74 A. L. Spek, *J. Appl. Cryst.* **2003**, *36*, 7–13.

75 Y. Makita, N. Kihara, T. Takata, *Supramolecular Chemistry* **2021**, *33*, 1–7.

76 T. J. Burchell, D. J. Eisler, R. J. Puddephatt, *Dalton Trans* **2005**, 268–272.

Chapter 3: Facial Selectivity in Mechanical Bond Formation: Axially Chiral Enantiomers and Geometric Isomers from a Simple Prochiral Macrocycle

Abstract: In 1971, Schill recognized that a prochiral macrocycle encircling an oriented axle led to geometric isomerism in rotaxanes. More recently, we identified an overlooked chiral stereogenic unit in rotaxanes that arises when a prochiral macrocycle encircles a prochiral axle. Here we show that both stereogenic units can be accessed using equivalent strategies, with a single weak stereo-differentiating interaction sufficient for reasonable stereoselectivity. Using this understanding, we were able to demonstrate the first direct enantioselective (70% *ee*) synthesis of a mechanically axially chiral rotaxane.

Acknowledgements: John R. J. Maynard synthesised, characterised, began initial solvent screening and collected X-ray diffraction data of (Z_m)-**6**, and (E_m)-**6**. Andrea Savoini contributed to the synthesis, purification and characterisation of rotaxanes **7**-**12** and contributed to the synthesis, characterisation and condition optimisation of rotaxanes **4**, **15** and **16**, and relative compounds. Abed Saady contributed to the synthesis of **13**. Patrick Butler collected X-ray diffraction data of **4d** and fully refined its SCXRD data. Graham J. Tizzard collected X-ray diffraction data of (Z_m)-**9**, and (E_m)-**11**, and fully refined their and SCXRD data as well as (Z_m)-**6**, and (E_m)-**6**. I synthesised, purified, characterised and optimised conditions rotaxanes **4**, **15**, **16**, catenane **14** and contributed to the synthesis and screening of rotaxanes **7**-**12**. I also managed the collection of CSP-HPLC data, preparation of manuscript graphics. A. Savoini, A. Saady and I jointly managed the preparation of Supporting Information.

A. Savoini, A. Saady, JRJM, PB, GJT and SMG and I all contributed to the analysis of the results and writing of the manuscript.

Prior publication: This chapter was previously published as:

P. R. Gallagher, A. Savoini, A. Saady, J. R. J. Maynard, P. V. W. Butler, G. J. Tizzard, S. M. Goldup, *J. Am. Chem. Soc.* **2024**, *146*, 9134–9141.

3.1. Introduction

Early in the development of the chemistry of the mechanical bond,[1] Schill recognized that when a macrocycle containing a prochiral centre such that its faces are distinguishable encircles an axle with distinguishable ends, the rotaxane can exist as distinct geometric isomers even though the individual components are stereochemically trivial.[2] Although molecules that correspond to the type 1[3] mechanical geometric isomers (MGI-1) of rotaxanes have been reported, the vast majority where the mechanical bond provides the sole stereogenic unit[4] are constructed from calixarenes[5] or similar macrocycles[6] whose facial dissymmetry arises from the fixed cone-shaped conformation of the threaded ring.[7] The same is true of the corresponding catenane stereogenic unit first reported by Gaeta and Neri.[8] In these cases, facial dissymmetry is expressed over the whole macrocycle, which has been shown to lead to stereoselective formation of the corresponding rotaxanes. However, to our knowledge, the only MGI-1 rotaxanes in which a single covalent prochiral centre differentiates the faces of the ring,[9] as envisaged by Schill, were reported by Bode and Saito,[10] where no stereoselectivity was reported.

More recently,[11] we identified that when a facially dissymmetric macrocycle encircles a prochiral axle an overlooked mechanically axially chiral (MAC)[12] stereogenic unit arises that is analogous to that of catenanes identified by Wasserman and Frisch over 60 years earlier.[13] Having made this observation, we demonstrated that such molecules can be synthesized using a diastereoselective co-conformational chiral auxiliary[14] active template[15] Cu-mediated alkyne-azide cycloaddition (AT-CuAAC[16,17]) approach with a ring whose facial dissymmetry arises from a single prochiral sulfoxide unit.

If we consider a schematic AT-CuAAC retrosynthesis of MGI-1 isomers (Figure 3.1a) and MAC enantiomers (Figure 1b), in which the axle is divided into two half-axle components that couple through the macrocycle in the forward synthesis, the common challenge involved in the stereoselective synthesis of both becomes obvious; we must control which face of the macrocycle is oriented towards which half-axle component in the mechanical bond forming step.

Here, by re-examining our stereoselective synthesis of MAC rotaxanes, we identify that a single H-bond between the sulfoxide unit and one of the two half-axle components plays a key role in the reaction outcome. We use this understanding to develop a stereoselective approach to rotaxane MGI-1 isomers, which can be extended directly to their catenane counterparts. Finally, we apply our understanding to the direct synthesis of MAC rotaxanes without the need to produce diastereomeric intermediates.

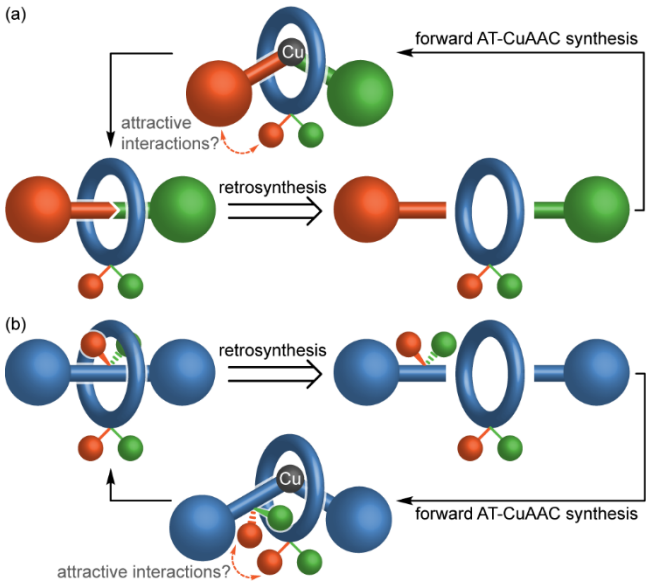

Figure 3.1 - Schematic active template retrosyntheses of the mechanical (a) type 1 geometric isomers and (b) axially chiral enantiomers of rotaxanes highlighting the need to control of facial selectivity in the mechanical bond forming step and the potential for attractive interactions between one face of the macrocycle and one of the half-axles to provide this control.

3.3. Results and Discussion

3.3.1. Effect of conditions and substrate structure in the synthesis of MAC rotaxanes 4

Previously,[11] we found that the AT-CuAAC reaction of azide (*R*)-**1a**, macrocycle **2**, and alkyne **3** gave rotaxane diastereomers (R_{ma},$R_{co\text{-}c}$)[18]-**4a** (major) and (S_{ma},$R_{co\text{-}c}$)-**4a** (minor) in 50% *de* (Scheme 3.1, Table 3.1, entry 1). These products have the same co-conformational covalent configuration[19] (set by the configuration of **1a**) but opposite mechanical axial configuration. They are separable because the steric bulk of the NH Boc group prevents epimerization of the covalent stereocentre by shuttling of the macrocycle between triazole-containing compartments. The solid-state structure obtained by single crystal x-ray diffraction (SCXRD) of an analogous catenane[11] contained a close contact between the polarized NH of the carbamate unit and the O atom of the sulfoxide unit, which suggested that an H-bond between these groups may play a role in the observed stereoselectivity.[20]

Scheme 3.1 - Synthesis of rotaxanes **4**[a]

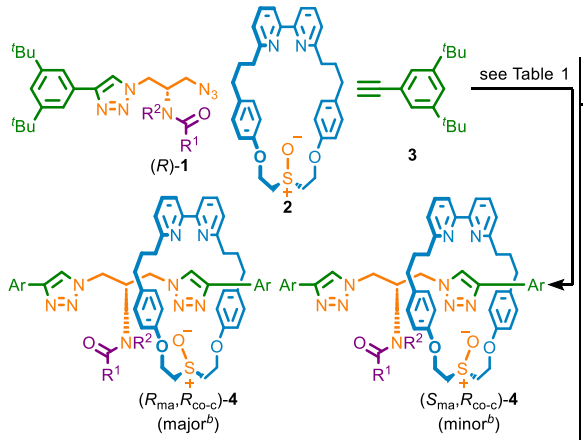

[a]Reagents and conditions (see also Table 1): (*R*)-**1** (1.1 equiv.), **2** (1 equiv.), **3** (1.1 equiv.), $[Cu(CH_3CN)_4]PF_6$ (0.96 equiv.), $^iPr_2NEt$ (2 equiv.). [b]Determined by SCXRD for **1a**[11] and **1d** (Figure 1); **1b**, **c** and **e** are presumed. Ar = 3,5-di-^{t}Bu-C_6H_3.

Table 3.1 - Effect of reaction conditions and substrate on the AT-CuAAC diastereoselective synthesis of rotaxanes **4**

Entry	Substrate	Conditions	Selectivity[a]
1[11]	**1a** (R^1 = O^{t}Bu, R^2 = H)	CH_2Cl_2, rt	50% *de*
2	**1a** (R^1 = O^{t}Bu, R^2 = H)	EtOH, rt	14% *de*
3	**1b** (R^1 = Me, R^2 = H)	CH_2Cl_2, rt	36% *de*
4	**1c** (R^1 = CCl_3, R^2 = H)	CH_2Cl_2, rt	48% *de*
5	**1d** (R^1 = CF_3, R^2 = H)	CH_2Cl_2, rt	70% *de*
6	**1d** (R^1 = CF_3, R^2 = H)	EtOH, rt	16% *de*
7	**1e** (R^1 = CF_3, R^2 = Me)	CH_2Cl_2, rt	10% *de*
8	**1a** (R^1 = O^{t}Bu, R^2 = H)	CH_2Cl_2, -40 °C	72% *de*
9	**1a** (R^1 = O^{t}Bu, R^2 = H)	CH_2Cl_2, -78 °C	80% *de*
10	**1d** (R^1 = CF_3, R^2 = H)	CH_2Cl_2, -40 °C	82% *de*
11	**1d** (R^1 = CF_3, R^2 = H)	CH_2Cl_2, -78 °C	70% *de*

[a]Determined by ^{1}H NMR analysis of the crude reaction product.

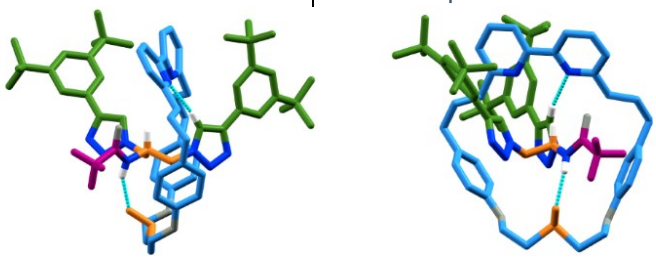

Figure 3.2 - SCXRD structure of [R_{ma},$R_{co\text{-}c}$]-**4d** (major isomer) with key intercomponent interactions highlighted. Colors as in Scheme 3.1, including the sulfoxide (SO) moiety to highlight the differentiation of the macrocycle faces, except N [dark blue], O [grey], H [white]). Majority of H omitted.

To test this proposal, we first compared the outcome of reactions performed in CH_2Cl_2 and EtOH, the latter being a more competitive H-bonding solvent and found that the stereoselectivity was indeed reduced to 14% *de* (Table 3.1, entry 2). Furthermore, the reactions of azides **1b**-**d** to give rotaxanes **4b**-**d** (entries 3-5) proceeded with selectivities that paralleled the polarization of the N-H unit; trifluoro acetamide **1d** produced rotaxane **4d** in the highest selectivity (70% *de*), followed by trichloroacetamide **1c** (48% *de*) then acetamide **1b** (36% *de*). The SCXRD structure of the major isomer of **4d** (Figure 3.2) revealed the same (R_{ma},$R_{co\text{-}c}$) configuration as **4a** with an NH•••O H-bond observed between the amide NH and sulfoxide units. Methylated trifluoroacetamide rotaxane **4e** was produced in 10% *de* (entry 6), which although consistent with the key role of the NH•••O H-bond, suggests that there is some inherent facial bias between the azide and alkyne half-axles in the AT-CuAAC reaction of **2**.

The effect of temperature on the stereoselectivity of the reactions of **1a** and **1d** was more complicated. Whereas reducing the reaction temperature in the synthesis of **4a** from rt (Table 3.1, entry 1), to –40 °C (entry 8), to –78 °C (entry 9) increased the observed selectivity, that for **4d** was higher at –40 °C (entry 10) and then fell at –78 °C (entry 11). We suggest that this slightly counterintuitive observation can be rationalized in broad terms by considering that the AT-CuAAC reaction takes place over several steps,[21] which include an equilibrium between diastereomeric azide/acetylide complexes **I** followed by irreversible formation of the corresponding triazolides **II** (Scheme 3.2).[22] The observed stereoselectivity is thus a composite function of the pre-equilibrium step (K_{eq}) and the relative rates (k_{RR}, k_{SR}) at which intermediates **I** progress to triazolides **II**. The effect of temperature on the reaction to produce **4d** suggests the pre-equilibrium and kinetic resolution steps respond differently to changes in temperature, resulting in the observed behavior.[23]

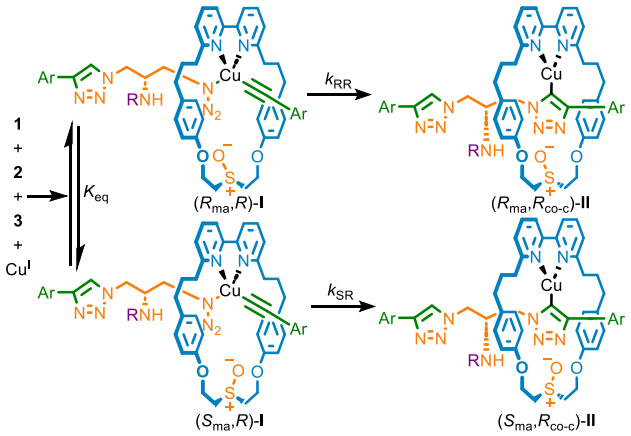

Scheme 3.2 - Proposed AT-CuAAC mechanism highlighting pre-equilibrium and kinetic resolution steps.

3.3.2. Stereoselective synthesis of MGI-1 rotaxanes

Having demonstrated that a single H-bond between the sulfoxide unit and one of the incoming half-axle components appears to be important in the synthesis of rotaxanes **4**, we turned our attention to the synthesis of analogous rotaxanes expressing the MGI-1 stereogenic unit. Intrigued by the small but measurable stereoselectivity observed in the formation of **4e**, which cannot arise due to the proposed stereo-differentiating NH•••O H-bond, we examined the AT-CuAAC coupling between macrocycle **2** and aryl alkyne **3** and aryl azide **5** half-axles, neither of which contain a directing group. At rt in CH_2Cl_2 (Scheme 3.3a, entry 1) geometric isomers (E_m)-**6** and (Z_m)-**6** were formed in low but significant stereoselectivity (24% *de*), confirming that the AT-CuAAC reactions of **2** are not only biased by the H-bond identified in the case of rotaxanes **4**.[24] Analysis of the separated isomers of **6** by SCXRD allowed their absolute stereochemistry to be determined (Figure 3.3a, Figure 3.3b). Replacing the solvent with THF marginally improved the selectivity (28% *de*, entry 2), as did lowering the reaction temperature to –20 °C (40% *de*, entry 3) but, as with **4d**, reduced selectivity was observed at lower temperatures (entries 4 and 5). Using EtOH as solvent was comparable to THF (entry 6).[25]

Although, the selectivities observed in the formation of **4e** and **6** are consistent with some inherent facial bias between the azide and alkyne half-axles in the mechanical bond forming step, when a propargylic alkyne was employed with aryl azide **5** to generate rotaxane **7** no stereoselectivity was observed (Scheme 3.3b). In contrast, the reaction of an alkyl azide and aryl acetylene **3** to give rotaxane **8** proceeded in appreciable stereoselectivity (14% *de*). Thus, although it is clearly possible to achieve low selectivities in the AT-CuAAC reactions of **2** in the absence of obvious directing interactions, this is highly substrate dependent and its origins are unclear at this time.[26]

Returning to our H-bonding-directed approach, when instead a propargylic amide was reacted with **2** to give **9**, a significantly improved stereoselectivity (54% *de*) was obtained, which was reduced in EtOH (40% *de*). The corresponding *N*-methyl amide gave rise to rotaxane **10** in low selectivity (13% *de*). The AT-CuAAC coupling of **3** and an alkyl azide bearing a simple amide gave rotaxane **11** in moderate stereoselectivity (40% *de*), which was reduced in EtOH (19% *de*). Thus, the amide can be placed in either coupling partner. Finally, rotaxane **12**, whose amide NH is expected to be more polarized than that of **11** was produced in good selectivity (72% *de*) at rt, which was improved (90% *de*) when the same reaction was conducted at –40 °C. Reducing the temperature further did not improve the observed stereocontrol and led to a slow reaction. Replacing the reaction solvent with EtOH once again led to reduced selectivity (26% *de*).

Scheme 3.3 – AT-CuAAC synthesis of MGI-1 rotaxanes. (a) Effect of conditions on the formation of rotaxanes **6**.[a] (b) Effect of half-axle structure on the stereoselectivity of mechanical bond formation with macrocycle **2**.[b,c]

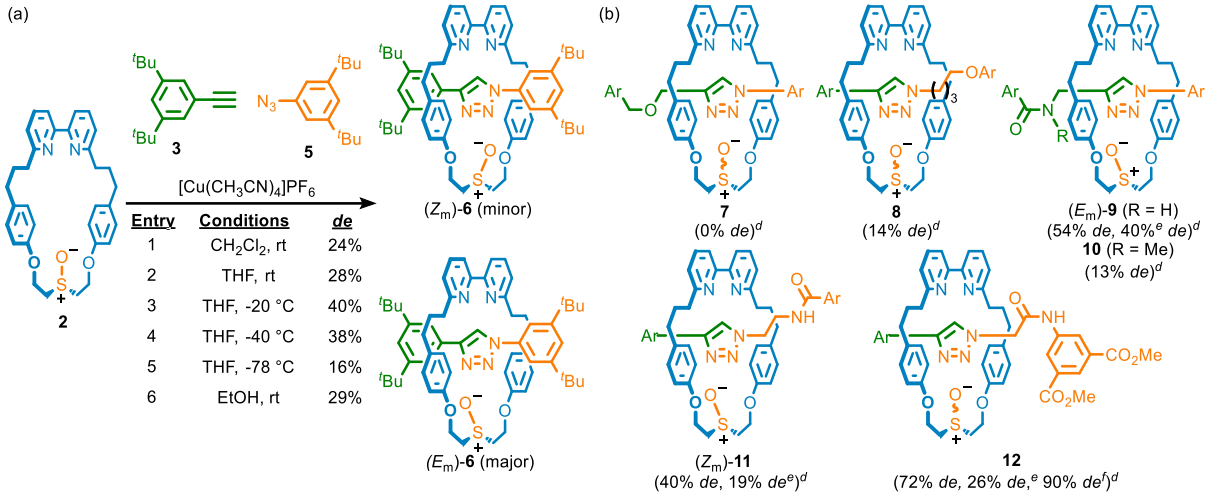

[a]Reagents and conditions: **2** (1 equiv.), **3** (1.1 equiv.), **5** (1.1equiv.), $[Cu(CH_3CN)_4]PF_6$ (0.96 equiv.), $^iPr_2EtN$ (2 equiv.). [b]Synthesized in THF at rt (Scheme 3a, entry 2) unless otherwise stated. [c]Stereochemistry of the major isomer indicated where determined. [d]Determined by ^1H NMR analysis of the crude reaction product. [e]Synthesized in EtOH. [f]Synthesized at –40 °C in THF. Ar = 3,5-di-^{t}Bu-C_6H_3

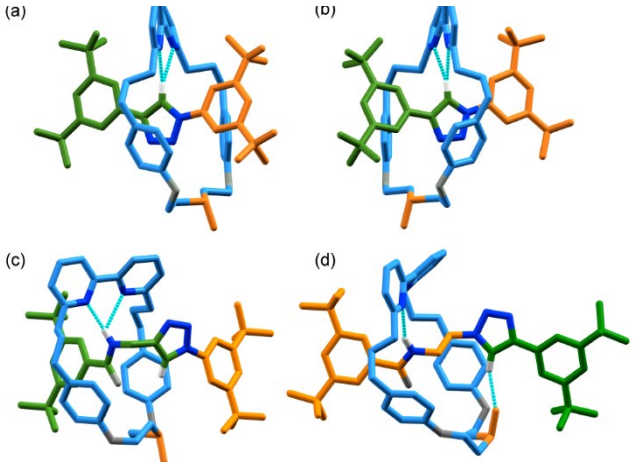

Figure 3.3 - Solid state structures of **(a)** (Z_m)-**6**, **(b)** (E_m)-**6**, **(c)** (Z_m)-**9** and **(d)** (E_m)-**11** with key intercomponent interactions highlighted. Colors as in Scheme 1, including the sulfoxide (SO) moiety to emphasize the macrocycle faces, except O (grey), N (dark blue), H (white). Majority of H omitted for clarity.

As in the case of rotaxanes **4**, the high selectivity observed in the synthesis of **9**, **11** and **12** is consistent with the key role of an NH•••O interaction between the macrocycle and half-axle in controlling the facial selectivity in the AT-CuAAC reactions of macrocycle **2**. However, we previously observed[11] this interaction in the solid-state structures of both diastereomers of epimeric MAC catenanes even though in principle in one diastereomer the S-O bond could be expected to project away from the NH unit, which is possible due to the flexible nature of

macrocycle **2**. The major isomers of rotaxanes **9** and **11** determined by SCXRD (Figure 3.3c and 3.3d respectively) highlight the importance of this flexibility; although both were formed selectively, counterintuitively the ring is oriented in opposite directions with respect to the amide in the major diastereomer of each. Thus, although the NH•••O interaction appears able to direct the synthesis of MGI-1 isomers, the major product depends on the detailed structure of the half-axles used.[27] We also note that whereas an NH•••O interaction is observed in the SCXRD structure of **4d**, in the case of **9** and **11** this is replaced by an NH•••N interaction between the amide proton and one of the bipyridine N atoms, with the SO unit instead interacting with the polarized C-H of the triazole moiety in an inter- or intra-molecular manner respectively, presumably because the NH unit is geometrically accessible to the macrocycle in rotaxanes **9** and **11** whereas it is not in the case of **4d**.

3.3.3. Stereoselective synthesis of an MGI catenane

Having established that a polarised NH unit appears sufficient to control the synthesis of MGI-1 rotaxanes with macrocycle **2**, we briefly investigated whether the same approach could be applied to the related isomers of catenanes. Pre-macrocycle **13**, which contains an activated amide unit analogous to that of **12**, reacted with **2** under our AT-CuAAC catenane-forming conditions (Scheme 3.4)[28] to give **14** with good stereocontrol (80% *de*, entry 1). The same reaction in $CHCl_3$-EtOH gave reduced the selectivity (60% *de*, entry 2) whereas performing the reaction at 0 °C in CH_2Cl_2 increased the selectivity (92% *de*, entry 3). Lowering the temperature further (–40 °C) had no significant effect (90% *de*, entry 4). Thus, unsurprisingly given the similarity of their stereogenic units, MGI-1 rotaxanes and MGI catenanes can be made with good stereocontrol using equivalent strategies.

Scheme 3.4 - Stereoselective synthesis of catenane **14**.[a]

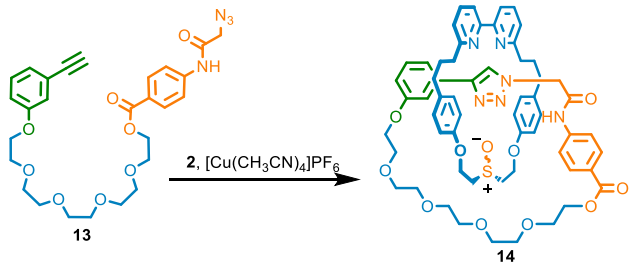

[a]Reagents and conditions: **13** (2 equiv.) was added over the time stated using a syringe pump to **2** (1 equiv.), $[Cu(CH_3CN)_4]PF_6$ (0.97 equiv.), $^iPr_2EtN$ (4 equiv.).

Table 3.2 - Effect of reaction conditions and substrate on the AT-CuAAC diastereoselective synthesis of rotaxanes **4**

Entry	Conditions	Selectivity[a]
1	CH_2Cl_2, rt, 4 h	80 % *de*
2	$CHCl_3$-EtOH (1:1), rt, 4 h	60 % *de*
3	CH_2Cl_2, 0 °C, 16 h	92 % *de*
4	CH_2Cl_2, –40 °C, 16 h	90 % *de*

[a]Determined by ^{1}H NMR analysis of the crude reaction product.

3.3.4. Direct enantioselective synthesis of MAC rotaxanes

Finally, we returned to apply our findings to the stereoselective synthesis of the enantiomers of MAC rotaxanes. In our original report[11] we separated the diastereomers of epimeric rotaxanes **4a** before removing the Boc group to generate rotaxane **15** (Scheme 3.5) in which the MAC stereogenic unit is the only fixed source of stereochemistry. This was necessary as the AT-CuAAC reaction only proceeded in 50% *de*; the ultimate purpose of developing methodologies to produce stereochemically complex mechanically interlocked molecules is so that they can then be investigated in applications such as sensing[29] or catalysis,[30] for which they must be of high stereopurity. Trivially, our optimized conditions for the diastereoselective formation of **4a** (Table 3.1, entry 9) removes the need for the separation of the MAC epimers and so allows the synthesis of highly enantioenriched samples of rotaxane **15** in a two-step, one-pot manner (Scheme 3.5); AT-CuAAC coupling of (*R*)-**1a** followed by TFA-mediated removal of the Boc group gave rotaxane (R_{ma})-**15** in good stereoselectivity (+78% *ee*) in agreement with that observed for **4a** (80% *de*). The same reaction with (*S*)-**1a** gave (S_{ma})-**5** (77% *ee*).

Scheme 3.5 - Two-step, one-pot synthesis of enantioenriched MAC rotaxanes **15**[a]

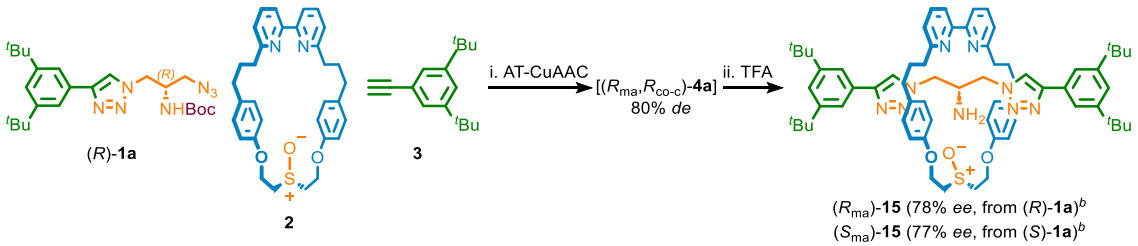

[a]Reagents and conditions: i. **1a** (1.1 equiv.), **2** (1 equiv.), **3** (1.1 equiv.), $[Cu(CH_3CN)]PF_6$ (0.96 equiv.), $^{i}Pr_2NEt$ (2 equiv.), CH_2Cl_2, 16 h, –78 °C; ii. TFA, CH_2Cl_2, –78 °C to rt, 6 h. [b]Determined by analytical CSP-HPLC.

More excitingly, the high stereoselectivity observed in the AT-CuAAC reaction of azides **1** bearing a polarized NH presents the opportunity for the direct synthesis of MAC rotaxanes without the need for first forming separable co-conformational diastereomers; if the N substituent is too small to trap the macrocycle in one triazole-containing compartment, the only fixed stereochemistry in the product is provided by the MAC stereogenic unit (Scheme 3.6). Thus, the reaction of primary amine-containing azide (*R*)-**1f** with macrocycle **2** and alkyne **3** at rt gave MAC rotaxane **15** directly but in low stereoselectivity (16% *ee*, Table 3.3, entry 1), which increased when the reaction was performed at –40 °C (28% *ee*, Table 3.3, entry 2) and improved further still at –78 °C (42% *ee*, entry 3) - CSP-HPLC analysis of a sample of rotaxane (R_{ma})-**15** produced from (*R*)-**1a** (Scheme 3.5) and comparison with the same product from (*R*)-**1f** confirmed that the latter also produces (R_{ma})-**15** as the major product (Figure 3.4a).

When instead formamide-containing azide (*R*)-**1g** was reacted with **2** and **3**, even at rt rotaxane **16**[31] was obtained in reasonable stereopurity (57% *ee*, Table 3.3, entry 3), which was improved further at –40 °C (67% *ee*, entry 4). Conducting this reaction at –78 °C reduced the observed stereoselectivity (59% *ee*, entry 5), suggesting that, as with azide **1d**, the pre-equilibrium and kinetic resolution steps result in an unusual temperature dependence - CSP-HPLC analysis of a sample of rotaxane **16** produced by formylation of a sample of rotaxane (R_{ma})-**15** of known stereopurity and comparison with the same compound produced from (*R*)-**1g** confirmed that the latter produces (R_{ma})-**16** as the major stereoisomer. When (*S*)-**1g** was reacted instead (S_{ma})-**16** was produced (70% *ee*, entry 6). The solid-state structure of **16** obtained by SCXRD (Figure 3.4b) did not display the expected intermolecular NH•••O H-bond; instead, the same interaction was found to occur in an intermolecular fashion within the unit cell.

Scheme 3.6 - Direct synthesis of enantioenriched mechanically axially chiral rotaxanes **15** and **16**[a]

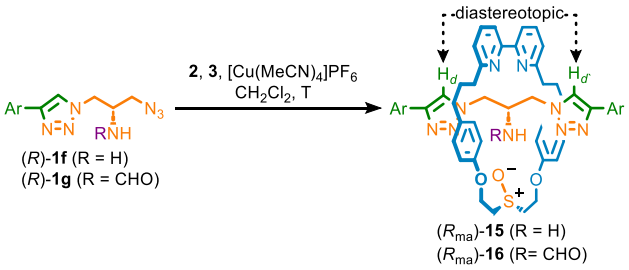

[a]Reagents and conditions: i. **1** (1.1 equiv.), **2** (1 equiv.), **3** (1.1 equiv.), $[Cu(CH_3CN)]PF_6$ (0.96 equiv.), $^{i}Pr_2NEt$ (2 equiv.), CH_2Cl_2, 16 h. Ar = 3,5-di-^{t}Bu-C_6H_3.

Table 3.3 - Effect of substrate and temperature on the AT-CuAAC enantioselective synthesis of rotaxanes **15** and **16**

Entry	Substrate	T	Selectivity[b]
11	(*R*)-**1f**	rt	16% *ee*
2	(*R*)-**1f**	–40 °C	28% *ee*
3	(*R*)-**1f**	–78 °C	42% *ee*
4	(*R*)-**1g**	rt	57% *ee*
5	(*R*)-**1g**	–40 °C	67% *ee*
6	(*R*)-**1g**	–78 °C	59% *ee*
7	(*S*)-**1g**	–40 °C	70% *ee*

[b]Determined by analytical CSP-HPLC of purified reaction products.

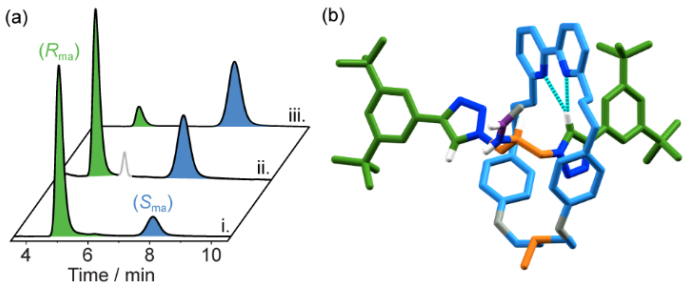

Figure 3.4 - (a) CSP-HPLC analysis of i. (R_{ma})-**16** (67% *ee*) produced from (*R*)-**1g**; ii. (R_{ma})-**16** (21% *ee*) produced from (R_{ma})-**15** (21% ee; minor impurity highlighted in grey), and iii. (S_{ma})-**16** (70% *ee*) produced from (*S*)-**1g**. (b) Solid state structure of *rac*-**16**, in which the N-H•••O bond between the SO unit and the amide is intermolecular (colors as in Scheme 6, including the sulfoxide (SO) moiety to highlight the differentiation of the macrocycle faces, except N [dark blue], O [grey], H [white]).

The different co-conformational behaviors of **4a**, **15** and **16** are clear from analysis of their respective ^{1}H NMR spectra. Diastereomers (R_{ma},$R_{co\text{-}c}$)-**4a** and (S_{ma},$R_{co\text{-}c}$)-**4a** are separable species; heating a mixture diastereomers **4a** resulted in no change in their ratio (Figure 3.51), and heating of diastereomerically pure samples also proceeds without loss of stereopurity, thus confirming that the macrocycle cannot shuttle between the two compartments due to the large NHBoc unit. In contrast, the diastereotopic triazole resonances H_d[32] of amine rotaxane **15** appear as two sharp singlets at 298 K. This is consistent with diastereomeric co-conformations (R_{ma},$R_{co\text{-}c}$)-**15** and (S_{ma},$R_{co\text{-}c}$)-**15** being in fast exchange on the ^{1}H NMR timescale through rapid shuttling of the macrocycle between the two triazole-containing compartments as expected for the smaller NH_2 substituent (Figure 3.194). This is further supported by VT-NMR experiments in which a single set of signals was observed at both lower (–50°C) and higher temperature (+50°C) (Figure 3.215). However, we cannot unequivocally rule out that the system is in slow exchange and strongly biased towards a single co-conformation. The same resonances for formamide rotaxane **16** are broad at 298 K, although once again only two signals are observed (Figure 3.204). This observation is consistent with (R_{ma},$R_{co\text{-}c}$)-**16** and (S_{ma},$R_{co\text{-}c}$)-**16** exchanging on the ^{1}H NMR timescale, albeit more slowly than (R_{ma},$R_{co\text{-}c}$)-**15** and (S_{ma},$R_{co\text{-}c}$)-**15**, in keeping with the larger steric bulk of the formamide group of **16**. Accordingly, increasing the temperature resulted in sharpening of the two resonances corresponding to protons H_d (Figure 3.216).

3.4. Conclusions

In conclusion, we have demonstrated that type 1 rotaxane mechanical geometric isomers and mechanically axially chiral enantiomers can be obtained by controlling facial selectivity in an AT-CuAAC synthesis. Specifically, we show that an H-bonding interaction between a prochiral macrocycle and a functional group contained in one of the two half-axles (rotaxane synthesis) or unsymmetrically disposed in the corresponding pre-macrocycle structure (catenane synthesis) is sufficient to control the reaction outcome. Although the focus of our discussion has been on reaction stereoselectivities, it should be noted that, as is typically the case for AT-CuAAC reactions mediated by bipyridine macrocycles,[33] all of the interlocked structures reported were obtained in good to excellent isolated yield (50 – 90%, see Experimental and Supplementary Information section 3.5.1). The high selectivity observed with optimized substrates allowed us to design a direct enantioselective synthesis of mechanically axially chiral rotaxanes, only the second[34a] example of a direct stereoselective synthesis of a mechanically chiral molecule and the first of this recently identified stereogenic unit. To date, type 1 mechanical geometric isomers of rotaxanes based on calixarenes and similar cone-shaped macrocycles,[5,8b,6d-e] as well as structures expressing combinations of mechanical and covalent stereochemistry[4h] have been investigated as components of molecular switches and motors. Here we have demonstrated that such isomerism can be expressed and controlled in much simpler macrocycles, opening new motifs for study. Similarly, mechanically planar chiral molecules, for which stereoselective methods are known,[14,26,34] have been investigated as enantioselective sensors,[29] catalysts,[30] and chiroptical switches.[35] With methodological concepts now in hand to efficiently synthesize their mechanically axially chiral cousins in high stereopurity, we eagerly anticipate the chemical applications to which molecules containing this stereogenic unit will soon be put.

3.5. Experimental and Supplementary Information

General Experimental Information

Unless otherwise stated, all reagents were purchased from commercial sources (Acros Organics, Alfa Aesar, Fisher Scientific, FluoroChem, Sigma Aldrich and VWR) and used without further purification. $[Cu(CH_3CN)_4]PF_6$ was prepared as described by Pigorsch and Köckerling.[36] Anhydrous solvents were purchased from Acros Organics. Petrol refers to the fraction of petroleum ether boiling in the range 40-60 °C. IPA refers to isopropanol. THF refers to tetrahydrofuran. EDTA-NH_3 solution refers to an aqueous solution of NH_3 (17% w/w) saturated with sodium-ethylenediaminetetraacetate. $CDCl_3$ (without stabilising agent) was distilled over $CaCl_2$ and K_2CO_3 prior to use. Unless otherwise stated, all reaction mixtures were performed in oven dried glassware under an inert N_2 atmosphere with purchased anhydrous solvents. Unless otherwise stated experiments carried out in sealed vessels were performed in CEM microwave vials, with crimped aluminium caps, with PTFE septa. Young's tap vessels and Schlenk techniques were used where specified.

Flash column chromatography was performed using Biotage Isolera-4 or Isolera-1 automated chromatography system. SiO_2 cartridges were purchased commercially Biotage (SNAP or ZIP (50 μm), or Sfär (60 μm) irregular silica, default flow rates). Neutralised SiO_2 refers to ZIP cartridges which were eluted with petrol-NEt_3 (99 : 1, 5 column volumes), followed by petrol (5 column volumes). Analytical TLC was performed on pre-coated silica gel plates on aluminum (0.25 mm thick, 60F254, Merck, Germany) and observed under UV light (254 nm) or visualised with $KMnO_4$ stain.

All melting points were determined using a Griffin apparatus. NMR spectra were recorded on Bruker AV400 or AV500 instrument, at a constant temperature of 298 K. Chemical shifts are reported in parts per million from low to high field and referenced to residual solvent. Coupling constants (*J*) are reported in Hertz (Hz). Standard abbreviations indicating multiplicity were used as follows: m = multiplet, quint = quintet, q = quartet, t = triplet, d = doublet, s = singlet, app. = apparent, br = broad, sept = septet. Signal assignment was carried out using 2D NMR methods (COSY, NOESY, HSQC or HMBC) where necessary. In some cases, complex multiplets with multiple contributing proton signals, exact assignment was not possible. In interlocked compounds, all proton signals corresponding to axle components are in lower case, and all proton signals corresponding to the macrocycle components are in upper case.

Many of the signals analysed to determine diastereopurity were close in ppm and/or broad, which limited the potential to use Q-NMR methodology (https://nmrweb.chem.ox.ac.uk/Data/Sites/70/userfiles/pdfs/quantitative-nmr.pdf). For this reason, we systematically applied the "peak integration" function implemented in MestReNova (v11.0.4, Mestrelab Research S. L.) combined with the GSD peak modelling function (4 rounds of refinement, optimised for broad peaks), which has been shown to be comparable in accuracy to sum integration even when peaks are overlapping (qGSD - quantitative Global Spectral Deconvolution - Mestrelab Resources). Prior to integration, the default polynomial baseline correction was applied. Where possible, the values obtained were improved by comparison of multiple signals. The corresponding values obtained by sum integration are provided for comparison. Residual intensity is included for all peak integrations. Integral curves are included for sum integrations. Full details are included in the captions of the corresponding spectra.

Low resolution mass spectrometry was carried out by the mass spectrometry services at University of Southampton (Waters TQD mass spectrometer equipped with a triple quadrupole analyser with UHPLC injection [BEH C18 column; CH_3CN -H_2O gradient {0.2% formic acid}]). High resolution mass spectrometry was either carried out by the mass spectrometry services at the University of Southampton (MaXis, Bruker Daltonics, with a Time of Flight (TOF) analyser; samples were introduced to the mass spectrometer via a Dionex Ultimate 3000 autosampler and uHPLC pump in a gradient of 20% CH_3CN in *n*-hexane to 100% acetonitrile (0.2% formic acid) over 5-10 min at 0.6 mL/min; column: Acquity UPLC BEH C18 (Waters) 1.7 micron 50 × 2.1mm) or services at University of Birmingham (Waters Synapt G2-S mass spectrometer fitted with a TOF detector).

Circular dichroism spectra were either acquired on an Applied Photo-physics Chirascan spectropolarimeter, recorded using Applied Photophysics software Ver. 4.2.0 or a Jasco J-1500spectropolarimeter in dried spectroscopic grade $CHCl_3$ in a quartz cell of 1 cm path length, at a temperature of 293 K.

Stereochemical purity was determined by Chiral Stationary Phase HPLC on a Waters Acquity Arc Instrument at 303 K, with *n*-hexane-^{i}PrOH or *n*-hexane-EtOH isocratic eluents. Regis Technologies (S,S)-Whelk-O1 (1-(3,5-dinitrobenzamido)-1,2,3,4-tetrahydrophenanthrene stationary phase), RegisCell (tris-(3,5-dimethylphenyl) carbamoyl cellulose stationary phase), Regis Reflect I-Cellulose B (3,5-dimethylphenylcarbamate stationary phase), and Regis Reflect I-Cellulose Z (3-chloro-4-methylphenylcarbamate stationary phase) columns were used throughout (5 micron, column dimensions 25 cm x 4.6 mm). Racemic samples were prepared employing the same synthetic procedures and but starting from *rac*-**1a**.

The following compounds were synthetized according to literature procedures: **1a** ((*R*)-**1a** and (*S*)-**1a**)),[11] **2**,[11] **3**,[37] and **5**.[38]

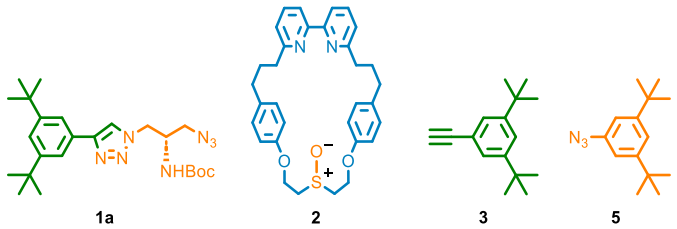

3.5.1. Characterisation of compounds

Synthesis of sulfide macrocycle precursor S3

Macrocycle **2** was synthesised from precursor **S3** according to our previously reported procedure.[11] However, precursor **S3** was produced using a new procedure (below) that avoids the isolation of the corresponding dibromide of **S1**, which is a bifunctional electrophile and thus raises toxicity concerns.

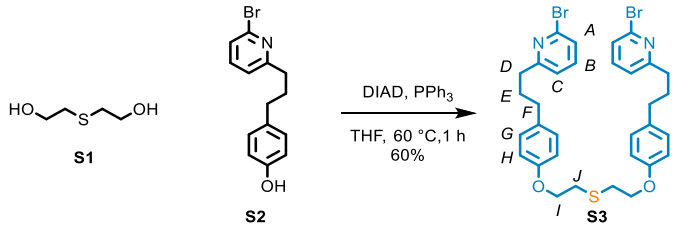

To a solution of PPh_3 (2.6 g, 10.0 mmol) and **S2** (2.9 g, 10.0 mmol) in THF (36 mL) was added **S1** (360 µL, 3.6 mmol), followed by DIAD (1.4 mL, 7.2 mmol) dropwise then the reaction was stirred at 60 °C for 1 h. After cooling to rt, the reaction mixture was washed with H_2O. The aqueous and organic phases were separated, and the aqueous phase was then extracted with EtOAc (3 x 50 mL). The combined organic extracts were washed with brine (100 mL), dried ($MgSO_4$) and concentrated *in vacuo*. Chromatography (petrol:CH_2Cl_2 1 : 1) gave **S3** as a white solid (1.4 g, 60%).

All spectroscopic data is consistent with those reported in literature[11] and previously in Chapter 2 section 3.5.1.

^{1}H NMR (400 MHZ, $CDCl_3$) δ 7.42 (t, *J* = 7.7, 2H, H_B), 7.29 (d, *J* = 7.9, 2H, H_A), 7.12 – 7.03 (m, 6H, H_C, H_G), 6.86 – 6.77 (m, 4H, H_H), 4.16 (t, *J* = 6.6, 4H, H_I), 3.00 (t, *J* = 6.7, 4H, H_J), 2.81 – 2.73 (m, 4H, H_D), 2.65 – 2.57 (m, 4H, H_F), 2.06 – 1.94 (m, 4H, H_E)

^{13}C NMR (100 MHz, CDCl3) δ 163.9, 156.9, 141.7, 138.7, 134.6, 129.6, 125.5, 121.7, 114.7, 68.2, 37.6, 34.7, 31.9, 31.6.

Rotaxanes 4a-e and their precursors

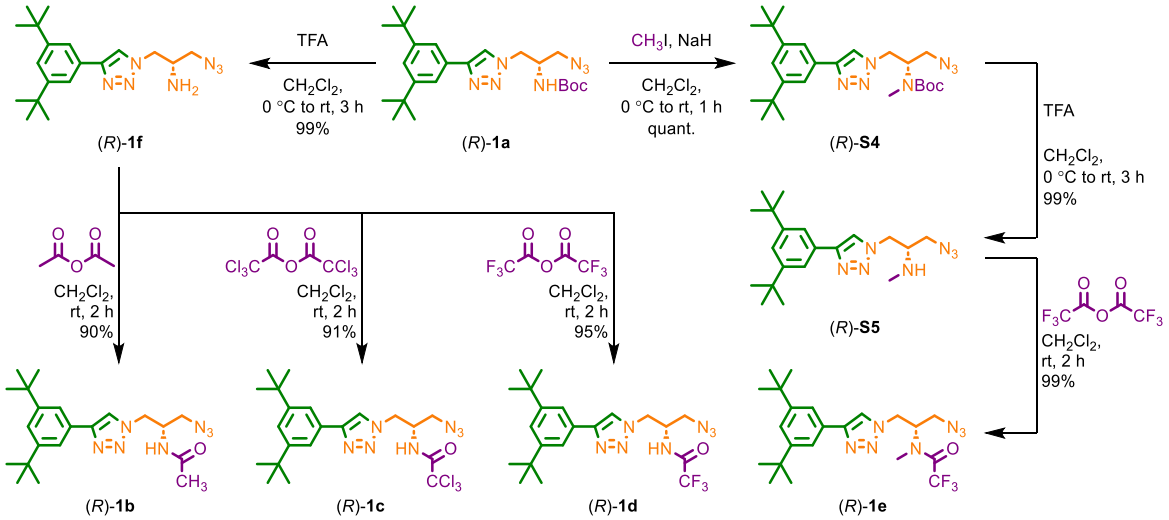

Scheme 3.7 - Synthetic route to azides (*R*)-**1b-e**.

Amine azide (*R*)-1f

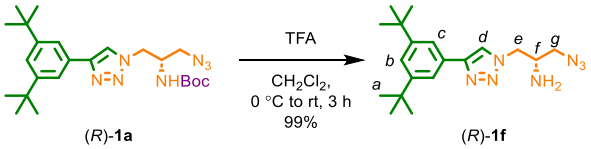

To a solution of (*R*)-**1a** (100.7 mg, 0.22 mmol) in CH_2Cl_2 (2.2 mL) was added TFA (170 µL, 2.22 mmol) at 0 °C. The reaction mixture was allowed to warm to rt and stirred for 3 h. The reaction mixture was then diluted with CH_2Cl_2 (10 mL) and poured slowly into saturated $NaHCO_3$ (10 mL). The aqueous and organic phases were separated, and the aqueous phase was then extracted with CH_2Cl_2 (3 x 5 mL). The combined organic extracts were washed with brine (10 mL), dried ($MgSO_4$) and concentrated *in vacuo* to afford (*R*)-**1f** (78.1 mg, 99%) as a white solid without further purification.

Amine azide (*S*)-**1f** (78.1 mg, quant.) was synthesised using an identical procedure starting from (*S*)-**1f** (100.7 mg, 0.22 mmol). Analytical data was identical to (R)-**1f** with the exeption of their their CD spectra (Figure 3.10) and CSP-HPLC (Figure 3.11).

^{1}H NMR (400 MHz, $CDCl_3$) δ: 7.85 (s, 1H, H_d), 7.67 (d, *J* = 1.8, 2H, H_c), 7.43 (t, *J* = 1.8, 1H, H_b), 4.47 (dd, *J* = 13.8, 4.9, 1H, H_e), 4.36 (dd, *J* = 13.8, 6.8, 1H, $H_{e'}$), 3.54 – 3.39 (m, 2H, H_f, H_g), 3.35 (dd, *J* = 12.1, 5.7, 1H, $H_{g'}$), 1.53 (br. s, 2H, NH_2), 1.37 (s, 18H, H_a);

^{13}C NMR (101 MHz, $CDCl_3$) δ: 151.6, 148.9, 129.7, 122.7, 120.9, 120.3, 55.1, 54.0, 51.4, 35.1, 31.6;

HR-ESI-MS (+ve) m/z = 356.2566 $[M+H]^+$ (calc. m/z for $C_{19}H_{30}N_7$ 356.2557);

$[\alpha]_D^{23}$ +0.6 ((*R*)-**1f**, c 0.72, $CHCl_3$), -0.5 ((*S*)-**1f**, c 0.74, $CHCl_3$);

Melting point 122-124 °C.

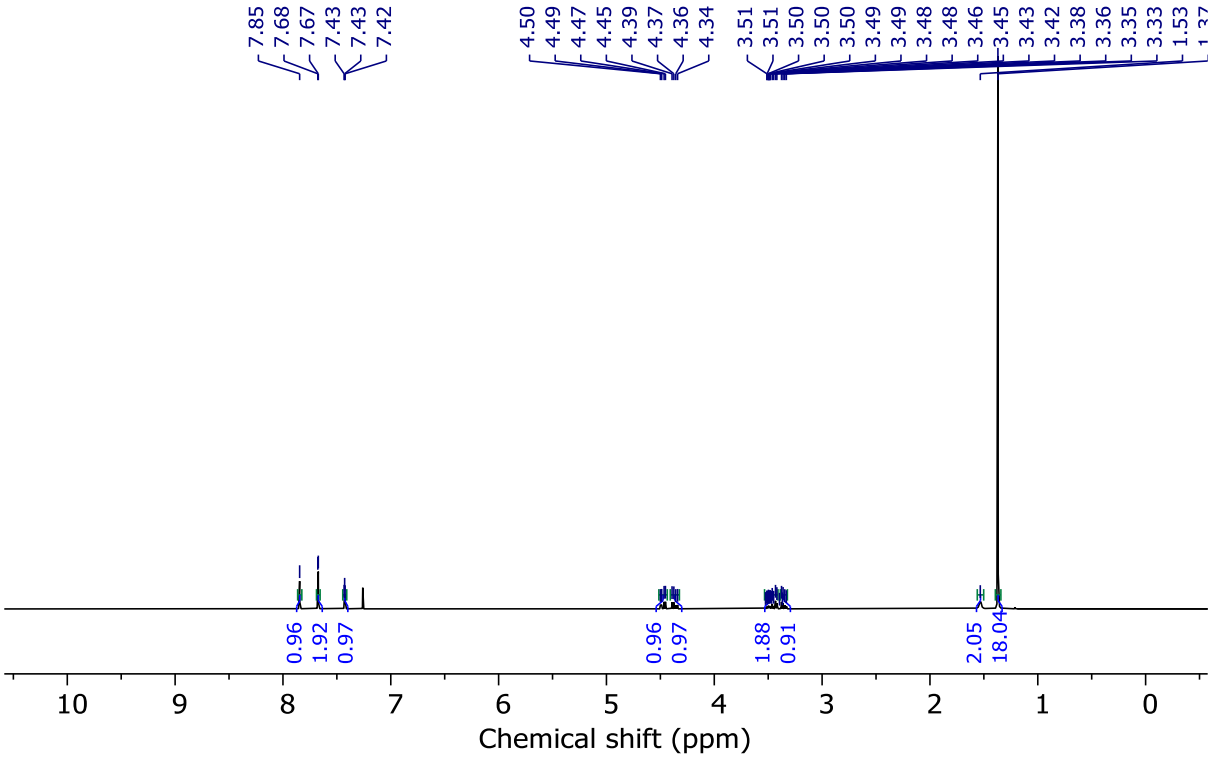

Figure 3.5 - ^{1}H NMR ($CDCl_3$, 400 MHz) of (*R*)-**1f**.

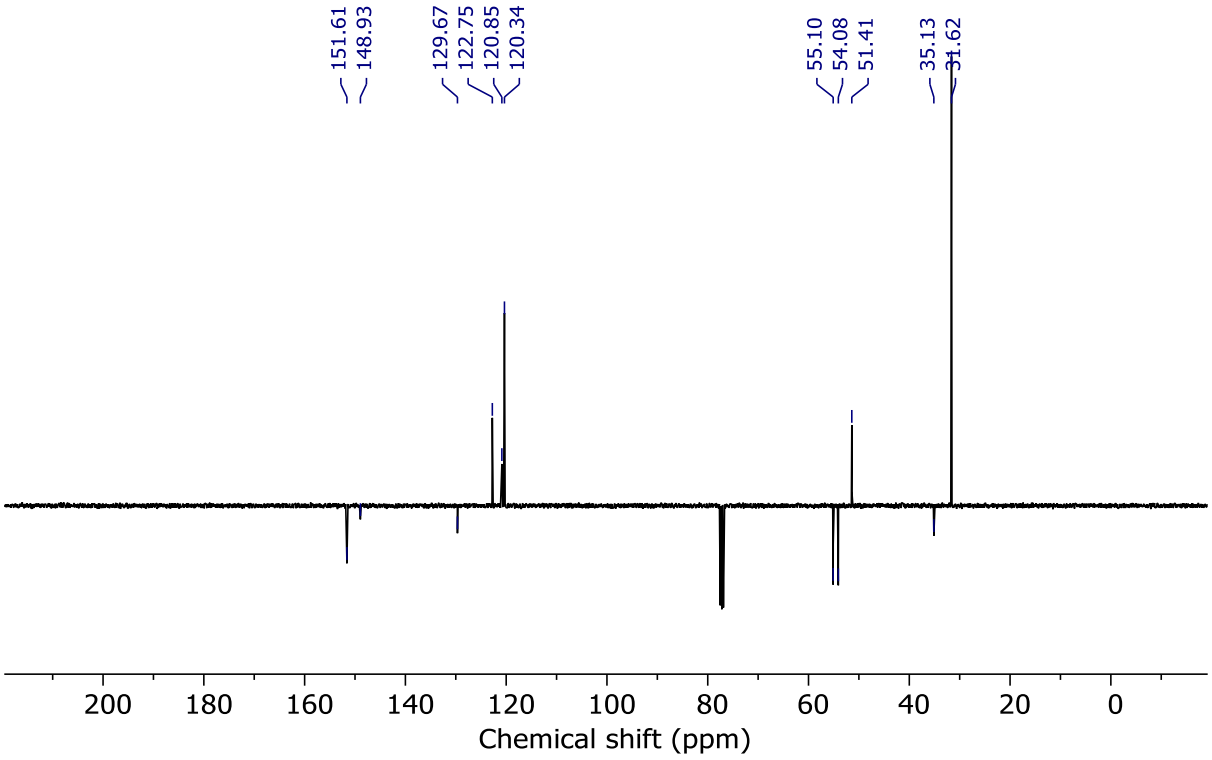

Figure 3.6 - JMOD NMR ($CDCl_3$, 101 MHz) of (*R*)-**1f**.

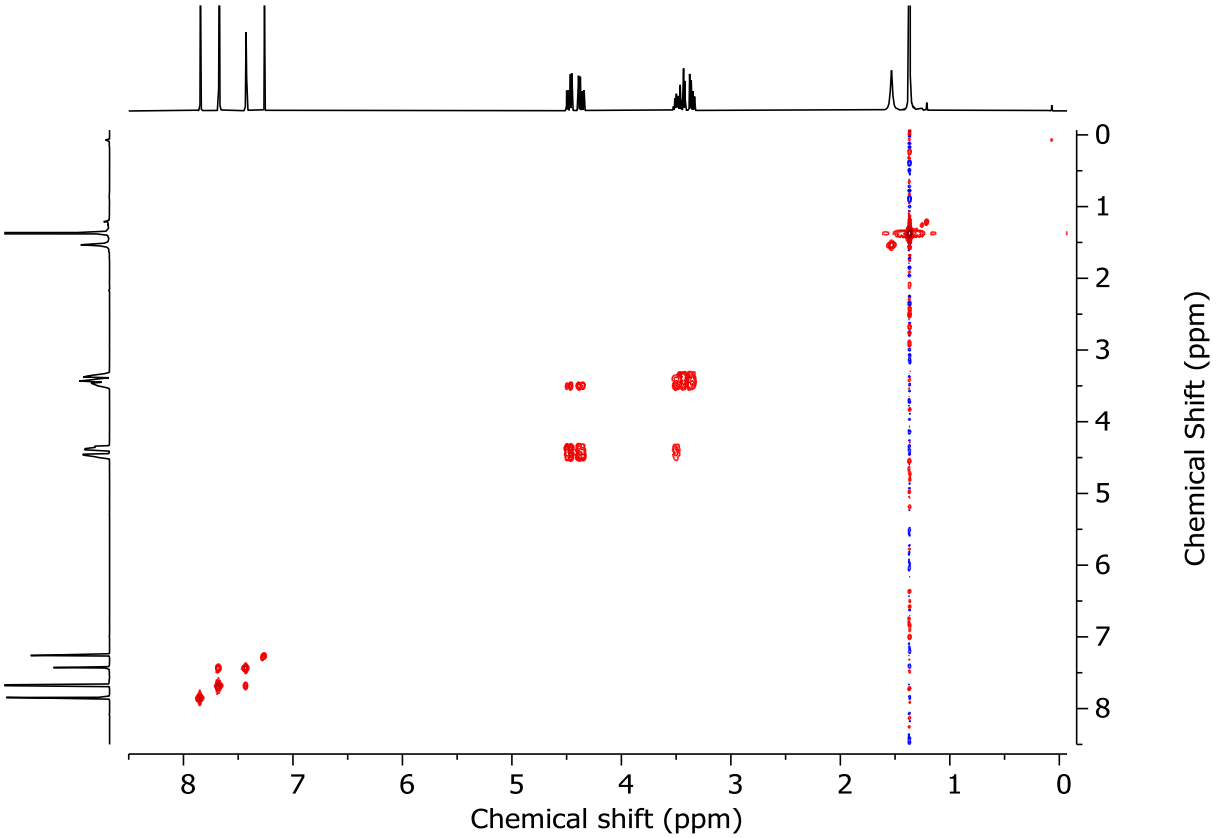

Figure 3.7 - ^{1}H COSY NMR ($CDCl_3$) of (*R*)-**1f**.

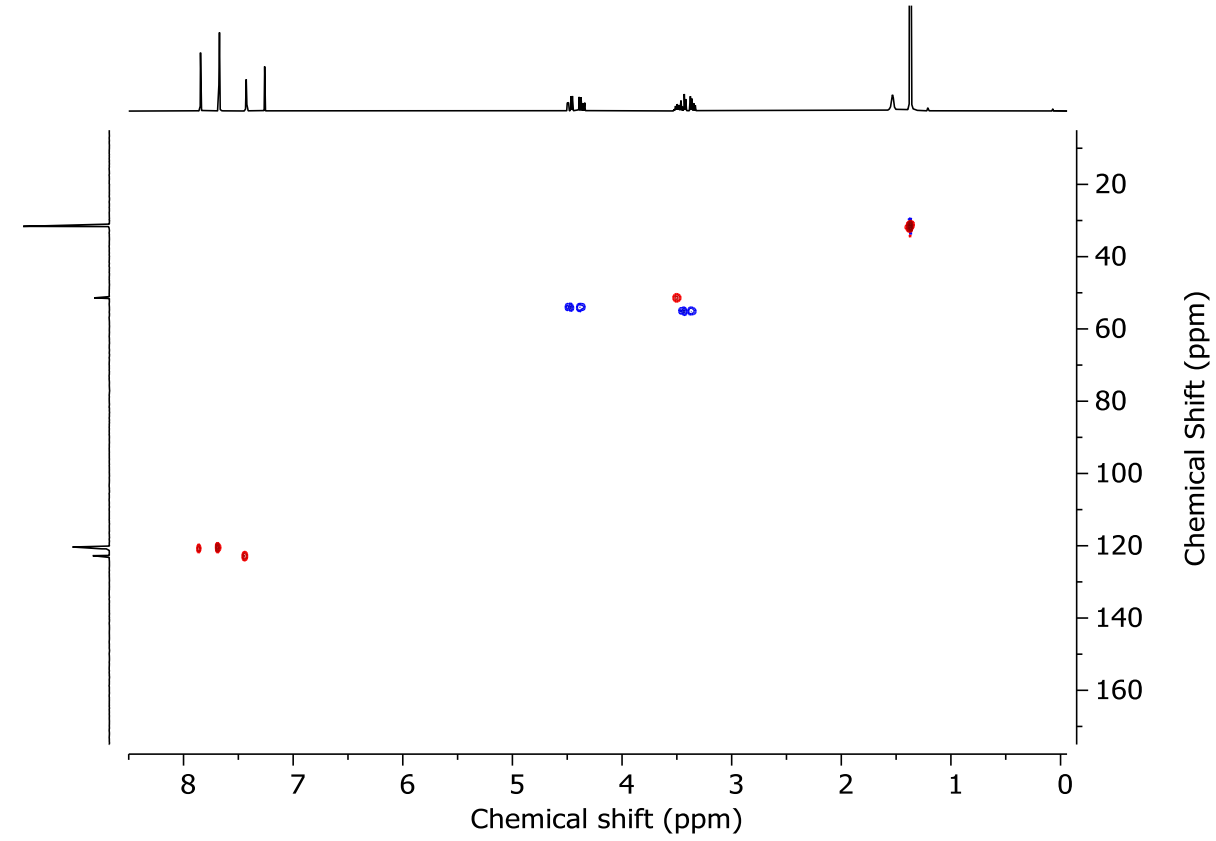

Figure 3.8 - HSQC NMR ($CDCl_3$) of (*R*)-**1f**.

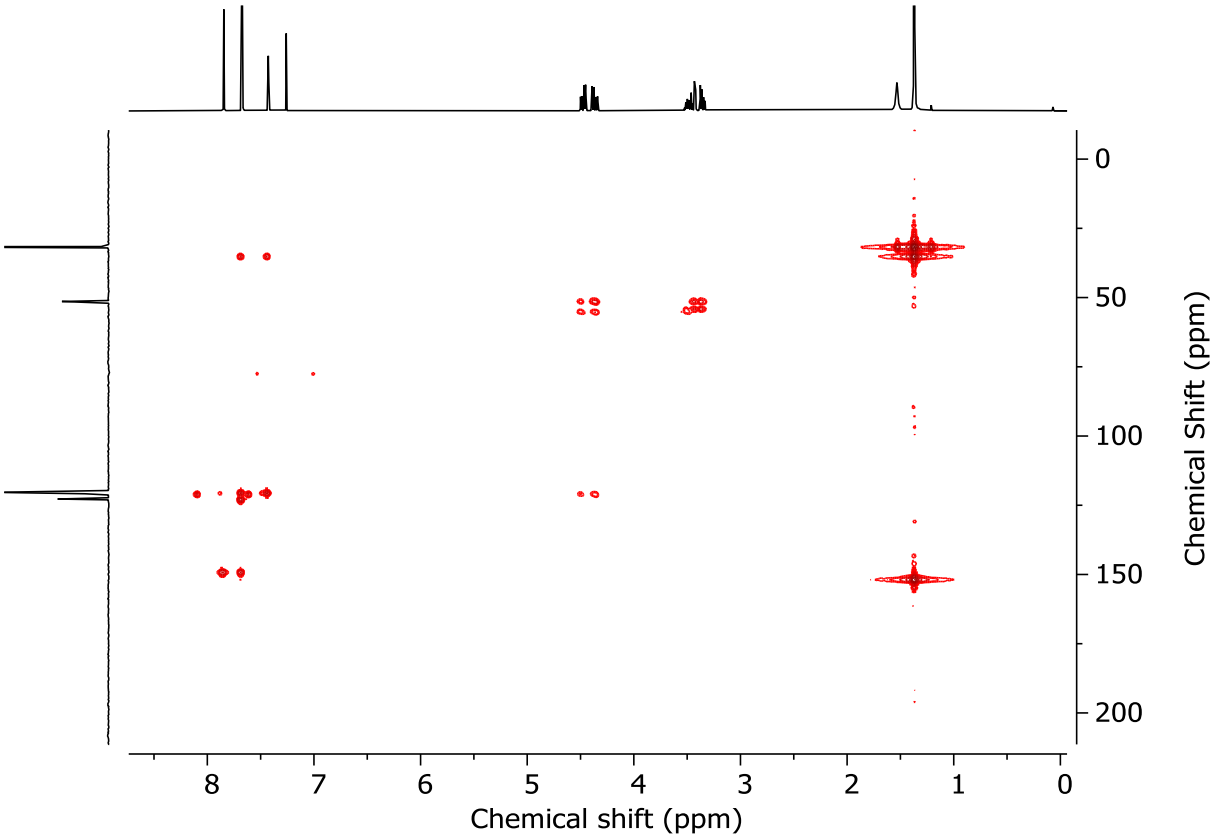

Figure 3.9 - HMBC NMR ($CDCl_3$) of (*R*)-**1f**

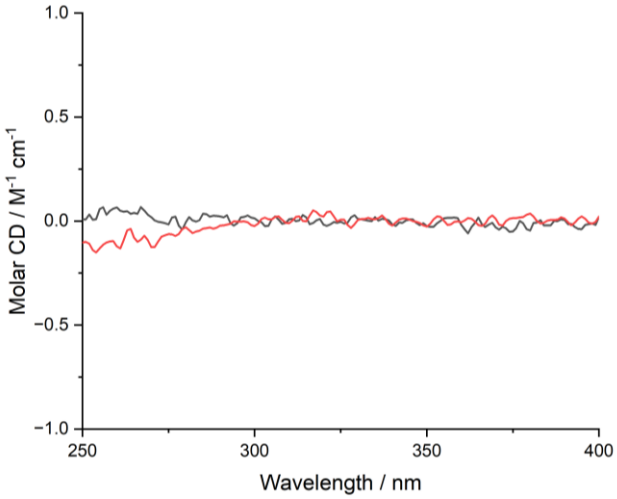

Figure 3.10 - Circular Dichroism Spectra of (*R*)-**1f** (69 µM, grey) and (*S*)-**1f** (69 µM, red) at 293 K in $CHCl_3$. No measurable CD response was observed so the $[\alpha]_D$ of (*R*)-**1f** and (*S*)-**1f** wer measured.

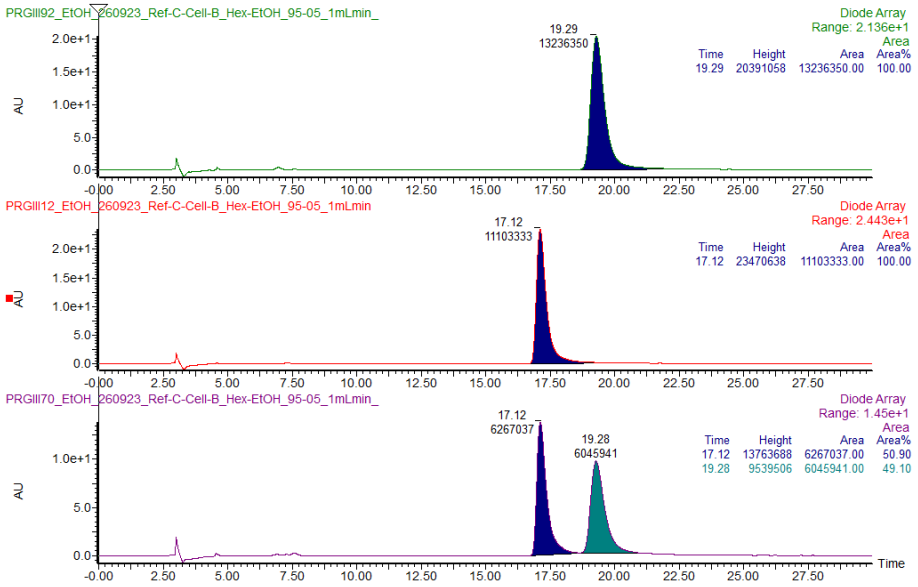

Figure 3.11 - CSP-HPLC of **1f** (loaded in EtOH). Regis Reflect I-Cellulose B, *n*-hexane-EtOH 95 : 5, flowrate 1 mLmin^{-1}. (top) (*R*)-**1f**; (*S*)-**1f** (not observed), (*R*)-**1f** (19.29 min, 13236350, >99.9%). (middle) (*S*)-**1f**; (*S*)-**1f** (17.12 min, 11103333, >99.9%), (*R*)-**1f** (not observed). (bottom) *rac*-**1f**; (*S*)-11f (17.12 min, 6267037, 50.9%), (*S*)-**1f** (19.28 min, 6045941, 49.1%).

Acetamide azide (*R*)-1b

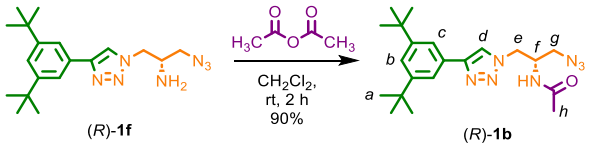

To a solution of (*R*)-**1f** (50.0 mg, 0.14 mmol) in CH_2Cl_2 (1.0 mL) was added acetic anhydride (19.0 µL, 0.20 mmol) dropwise, then allowed to stir at rt for 2 h. The reaction mixture was then diluted with CH_2Cl_2 (2 mL) and poured slowly into sat. $NaHCO_{3\,(aq)}$ (5 mL). The aqueous and organic phases were separated, and the aqueous phase was then extracted with CH_2Cl_2 (3 x 5 mL). The combined organic extracts were washed with brine (5 mL), dried ($MgSO_4$) and concentrated *in vacuo*. Chromatography (petrol-EtOAc 0→50%) gave (*R*)-**1b** (50.1 mg, 90%) as a white solid.

^{1}H NMR (400 MHz, $CDCl_3$) δ: 7.95 (s, 1H, H_d), 7.66 (d, *J* = 1.8, 2H, H_c), 7.44 (t, *J* = 1.9, 1H, H_b), 6.41 (d, *J* = 8.2, 1H, NH), 4.63 (dd, *J* = 5.4, 14.0, H_e), 4.56 (dd, *J* = 5.1, 14.0, $H_{e'}$), 4.48 (app ddt, *J* = 10.0, 5.4, 7.4, 1H, H_f), 3.58 (dd, *J* = 7.4, 12.2, H_g) , 3.25 (dd, *J* = 7.4, 12.2, $H_{g'}$), 2.01 (s, 3H, H_h), 1.37 (s, 18H, H_a) ;

^{13}C NMR (101 MHz, $CDCl_3$) δ: 170.3, 151.6, 149.0, 129.2, 122.8, 121.0, 120.2, 50.6, 50.0, 48.8, 35.0, 31.4, 23.3;

HR-ESI-MS (+ve) m/z = 398.2666 $[M+H]^+$ (calc. 398.2333 m/z for $C_{21}H_{32}N_7O$);

Melting point = 118-120 °C.

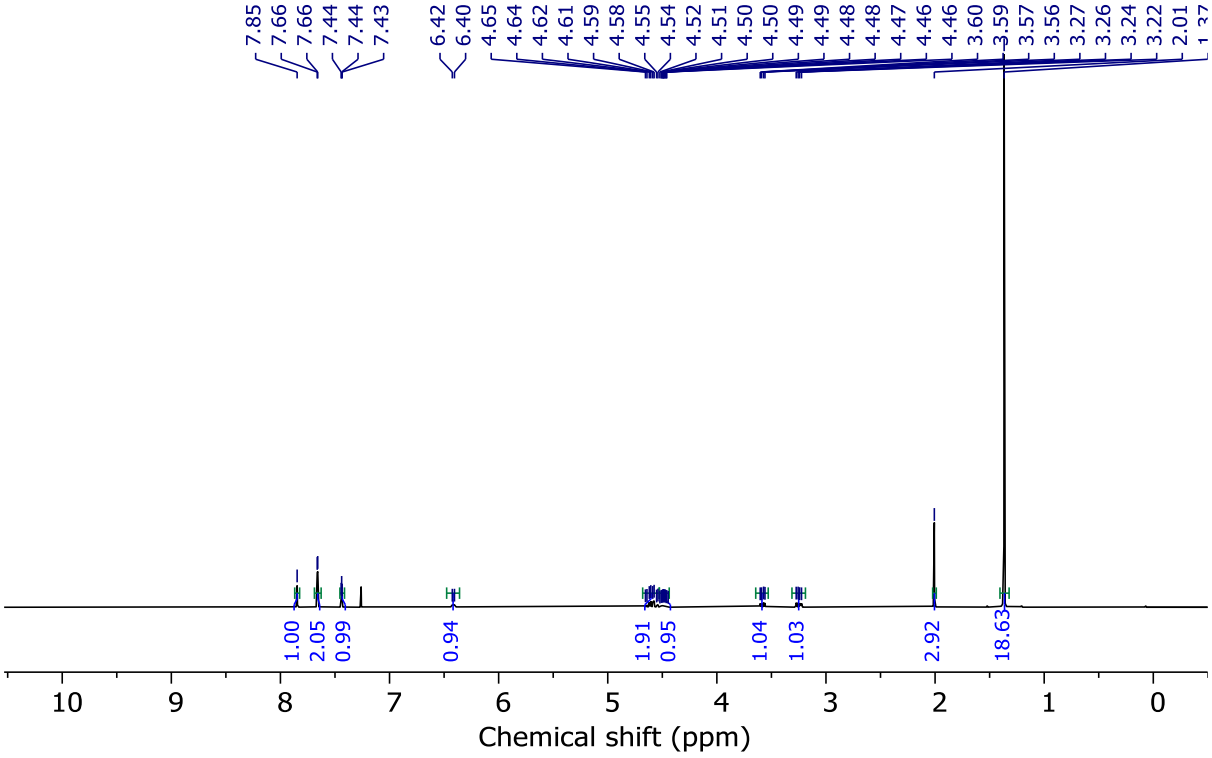

Figure 3.12 - ^{1}H NMR ($CDCl_3$, 400 MHz) of (*R*)-**1b**.

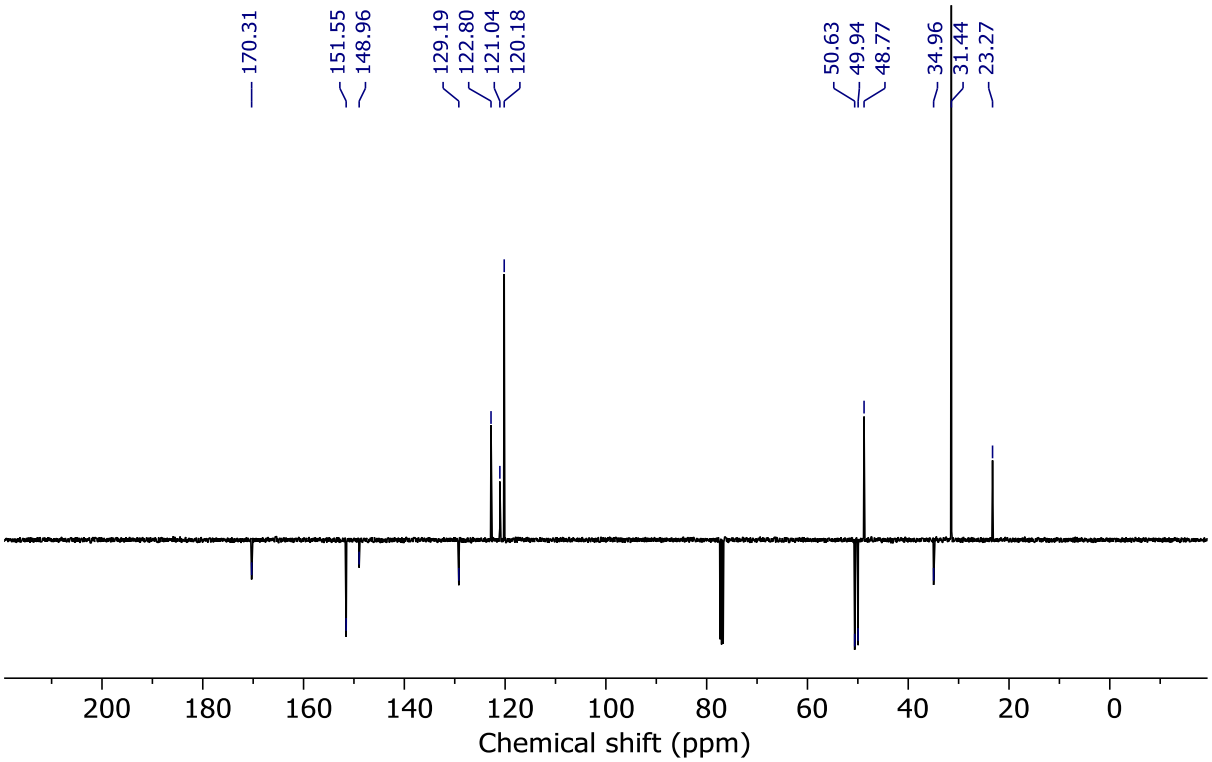

Figure 3.13 - JMOD NMR ($CDCl_3$, 101 MHz) of (*R*)-**1b**

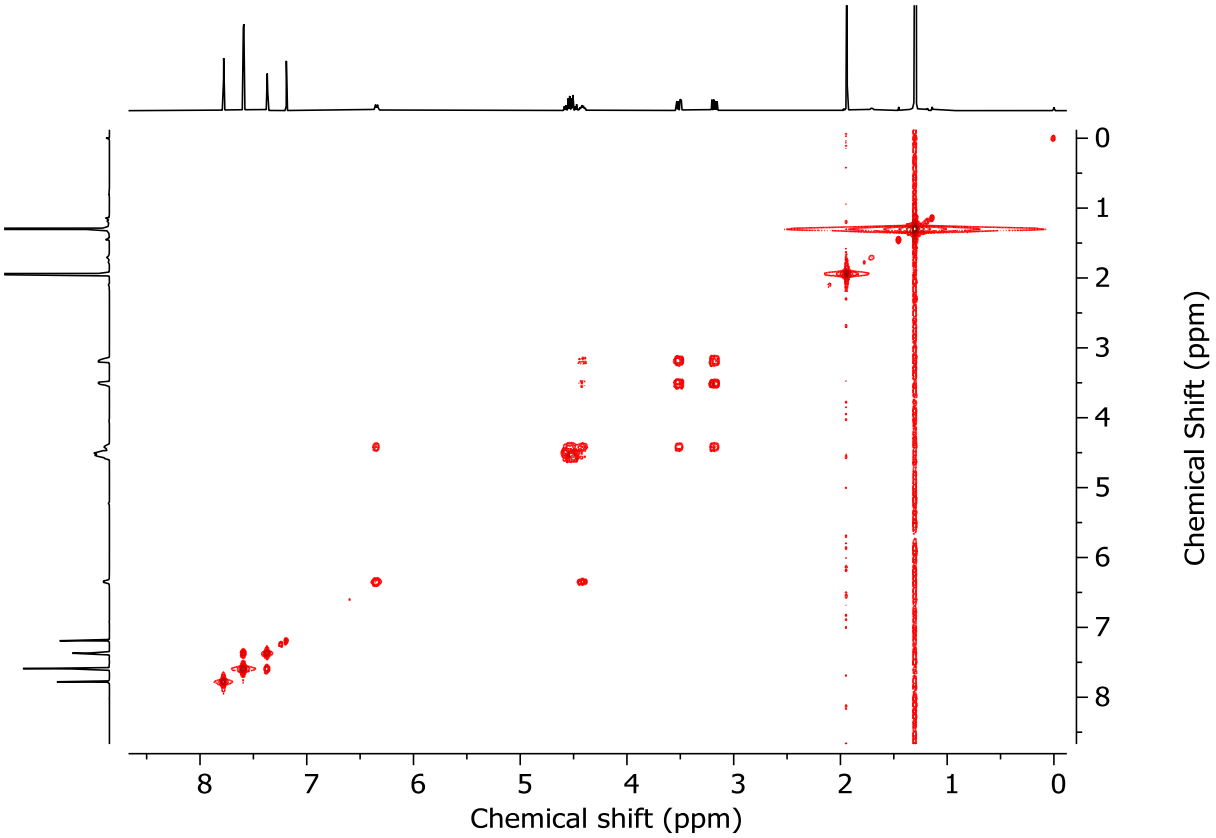

Figure 3.14 - COSY NMR ($CDCl_3$) of (*R*)-**1b**

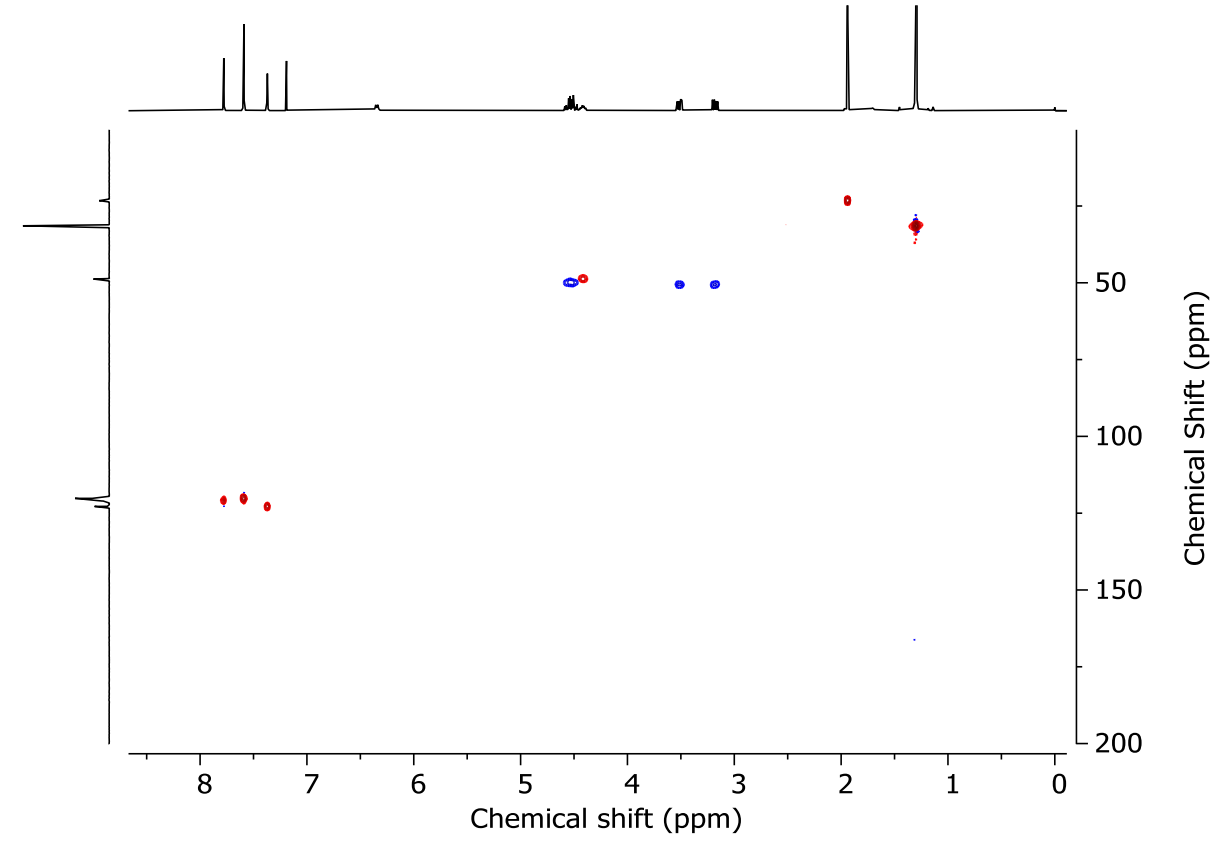

Figure 3.15 - HSQC NMR ($CDCl_3$) of (*R*)-**1b**

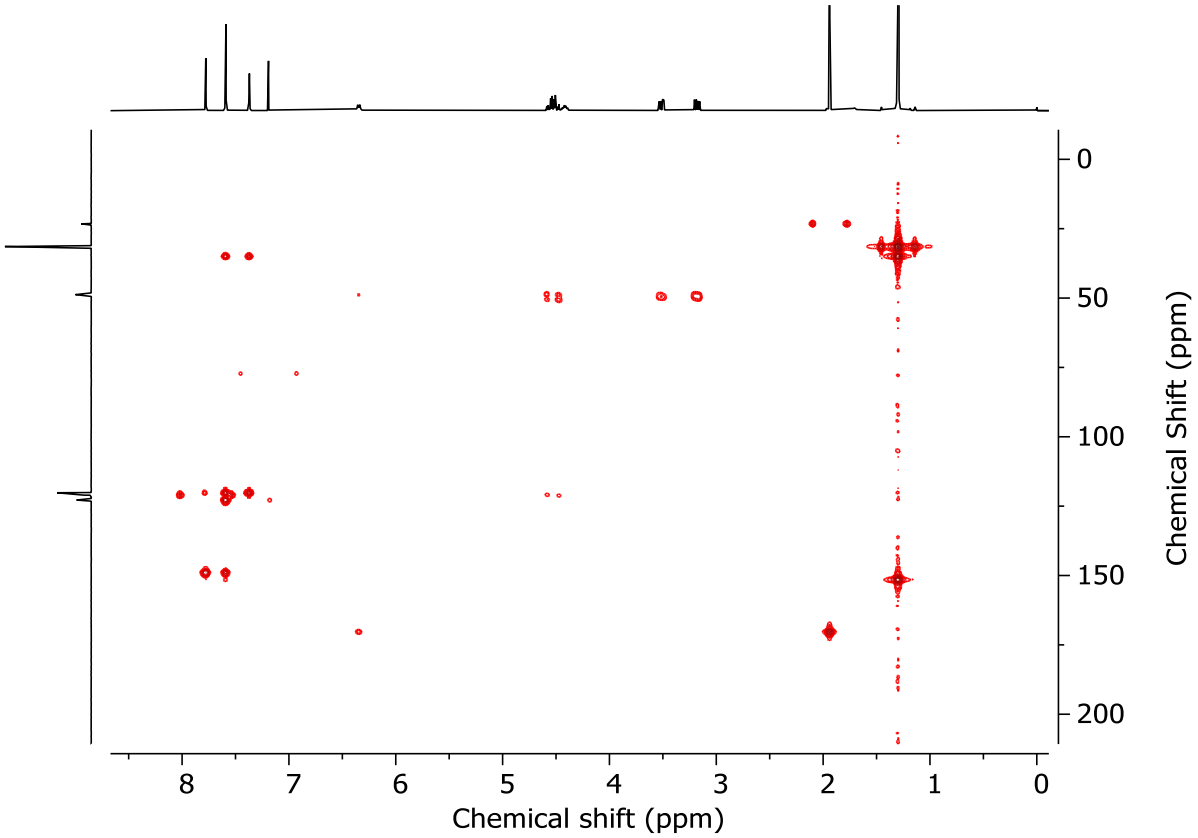

Figure 3.16 - HMBC NMR ($CDCl_3$) of (*R*)-**1b**.

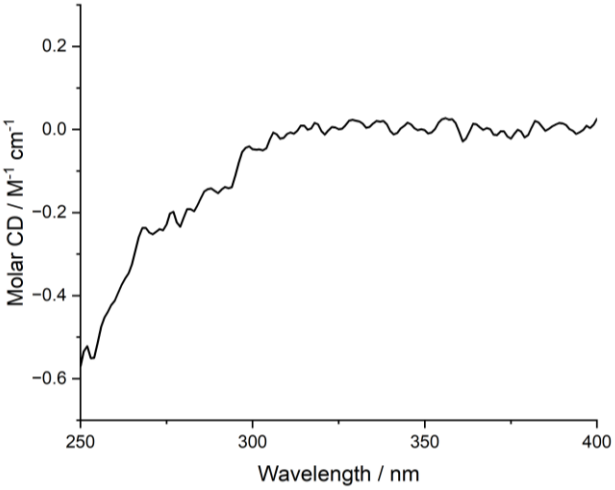

Figure 3.17 - Circular Dichroism Spectra of (R)-**1b** (88 µM) at 293 K in $CHCl_3$.

Trichloroacetamide azide (*R*)-1c

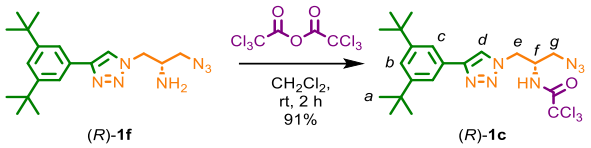

To a solution of (*R*)-**1f** (50.0 mg, 0.14 mmol) in CH_2Cl_2 (1.0 mL) was added trichloroacetic anhydride (38.1 µL, 0.20 mmol) dropwise, then allowed to stir at rt for 2 h. The reaction mixture was then diluted with CH_2Cl_2 (2 mL) and poured slowly into sat. $NaHCO_{3\,(aq)}$ (5 mL). The aqueous and organic phases were separated, and the aqueous phase was then extracted with CH_2Cl_2 (3 x 5 mL). The combined organic extracts were washed with brine (5 mL), dried ($MgSO_4$) and concentrated *in vacuo*. Chromatography (petrol-EtOAc 0→50%) gave (*R*)-**1c** (63.8 mg, 91%) as a white solid.

^{1}H NMR (400 MHz, $CDCl_3$) δ:7.86 (s, 1H, H_d), 7.80 (d, *J* = 7.9, 1H, NH), 7.66 (d, *J* = 1.8, 2H, H_c), 7.45 (t, *J* = 1.8, 1H, H_b), 4.74 (dd, *J* = 5.2, 14.4, H_e), 4.70 (dd, *J* = 5.2, 14.4, $H_{e`}$), 4.51-4.41 (m, 1H, $H_f$), 3.69 (dd, *J* = 5.1, 12.2, $H_g$) , 3.36 (dd, *J* = 7.2, 12.3, $H_{g`}$), 1.37 (s, 18H, H_a);

^{13}C NMR (101 MHz, $CDCl_3$) δ: 162.3, 151.6, 149.1, 129.0, 122.0, 121.3, 120.2, 91.9, 50.7, 50.0, 49.3, 35.0, 31.5;

HR-ESI-MS (+ve) m/z = 500.1493 $[M+H]^+$ (calc. 500.1494 m/z for $C_{21}H_{29}Cl_3N_7O$);

Melting point = 146-148 °C.

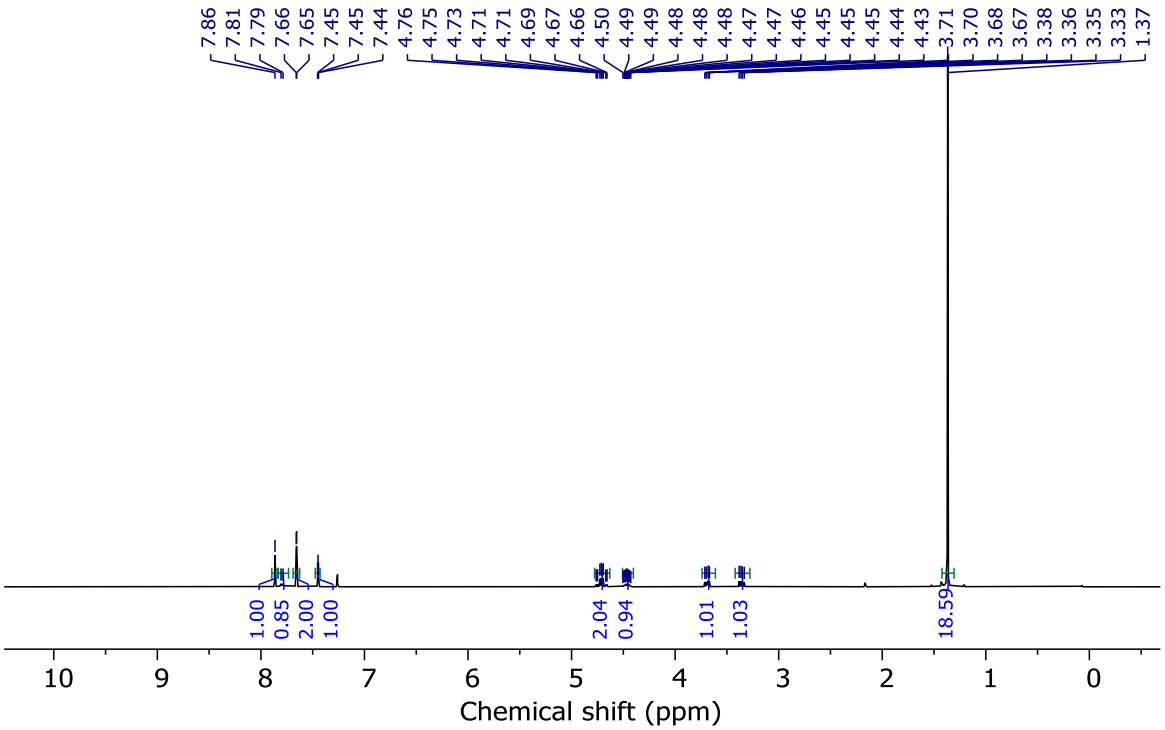

Figure 3.18 - ^{1}H NMR ($CDCl_3$, 400 MHz) of (*R*)-**1c**.

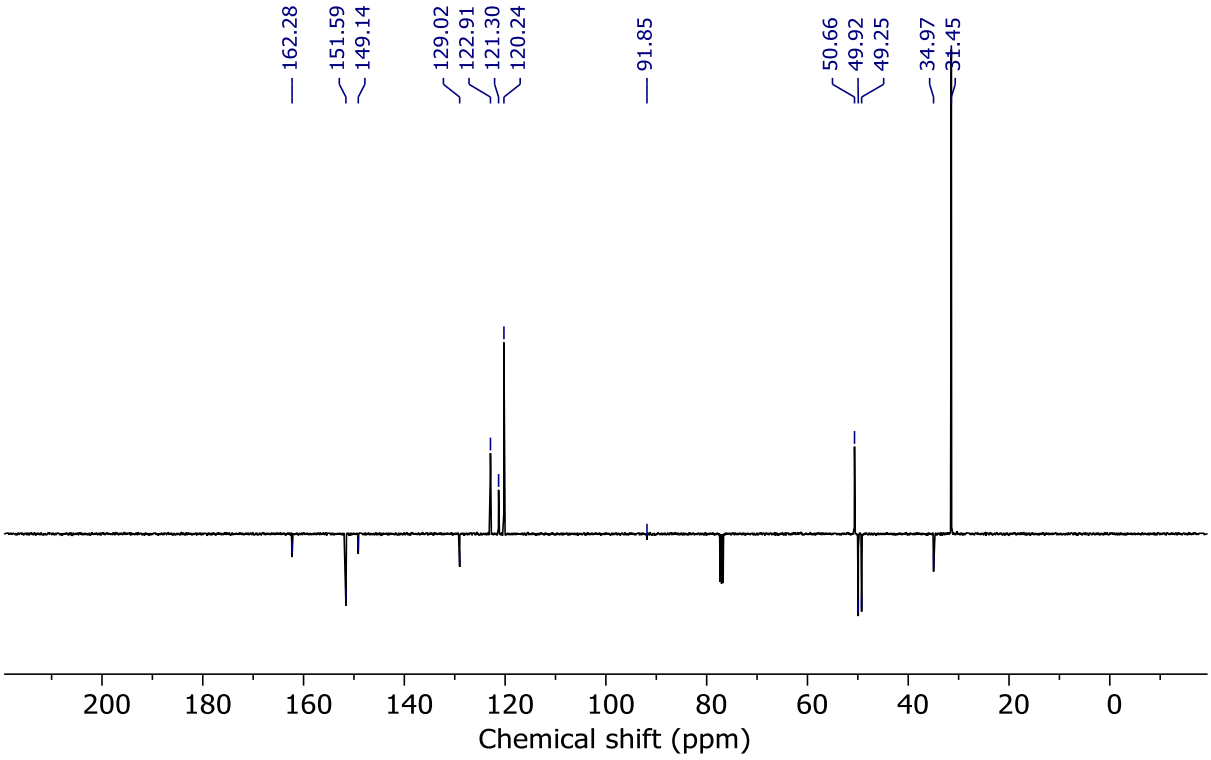

Figure 3.19 - JMOD NMR ($CDCl_3$, 101 MHz) of (*R*)-**1c**.

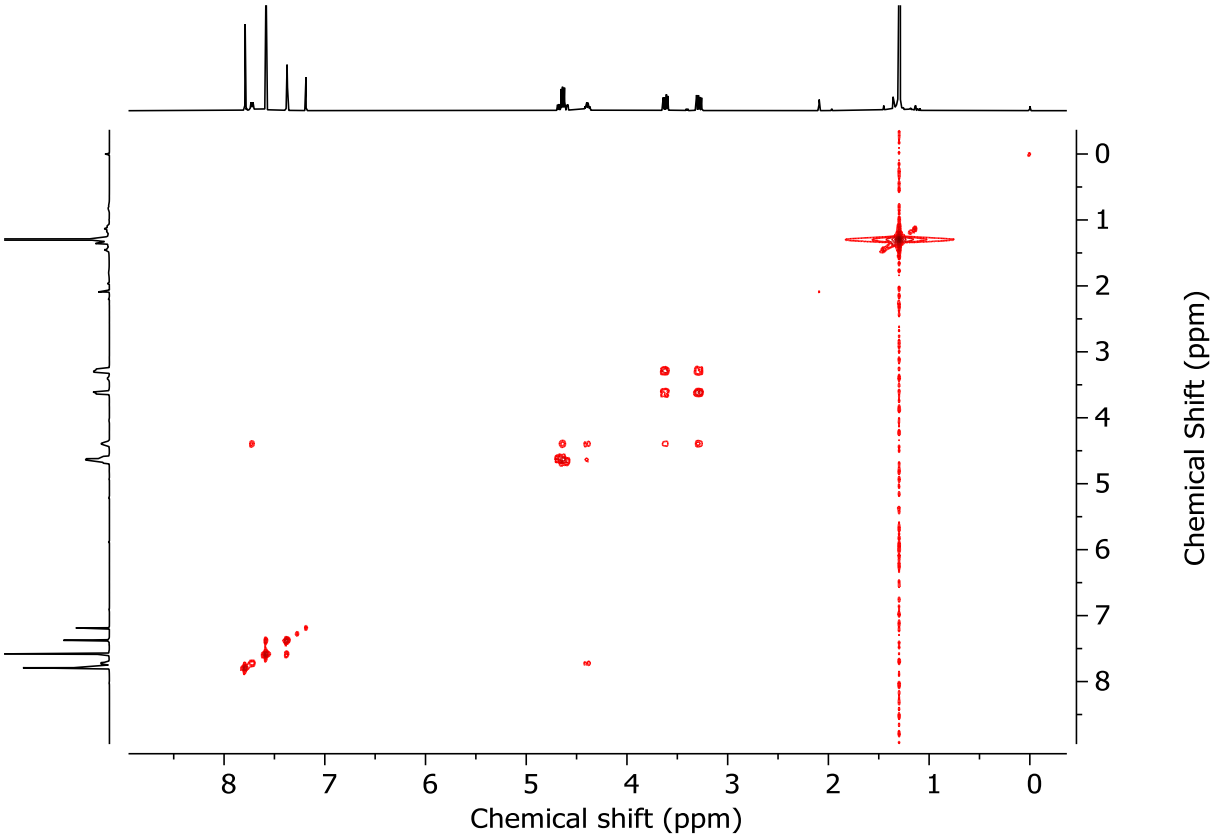

Figure 3.20 – COSY NMR ($CDCl_3$) of (*R*)-**1c**.

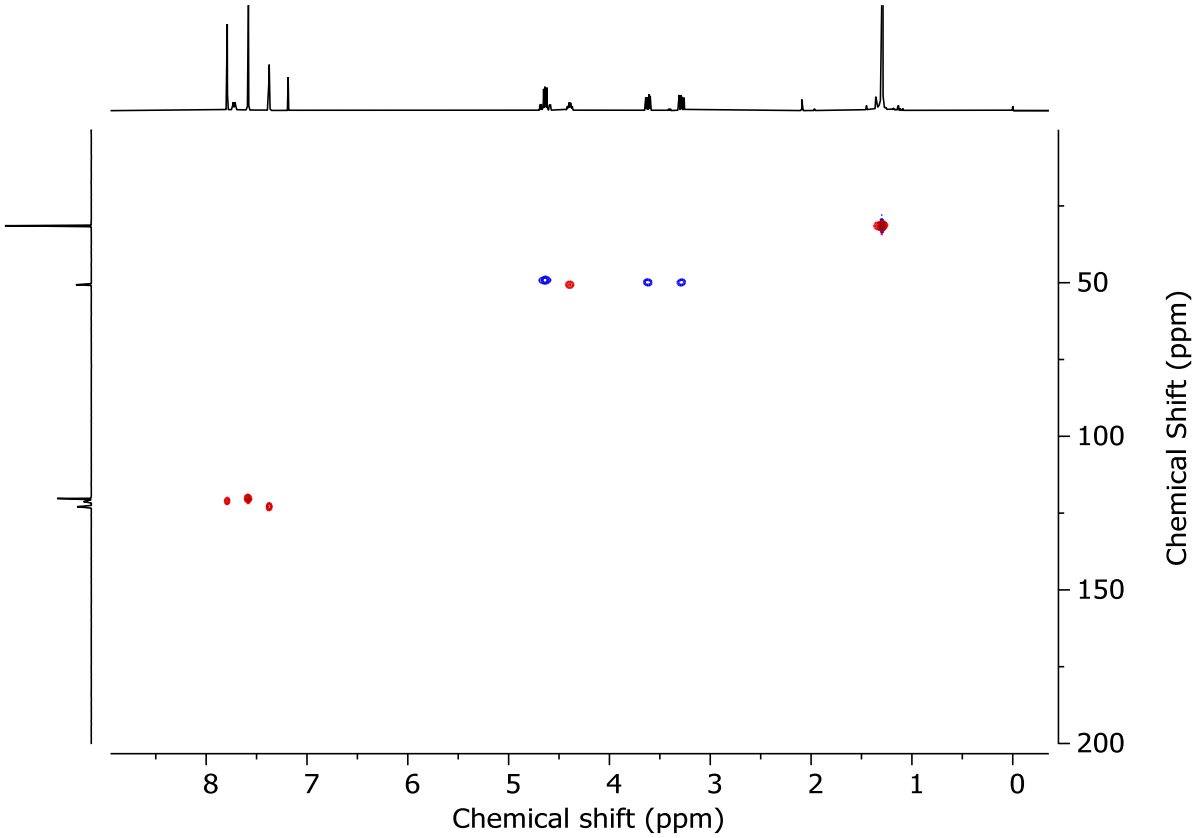

Figure 3.21 - HSQC NMR ($CDCl_3$) of (*R*)-**1c**.

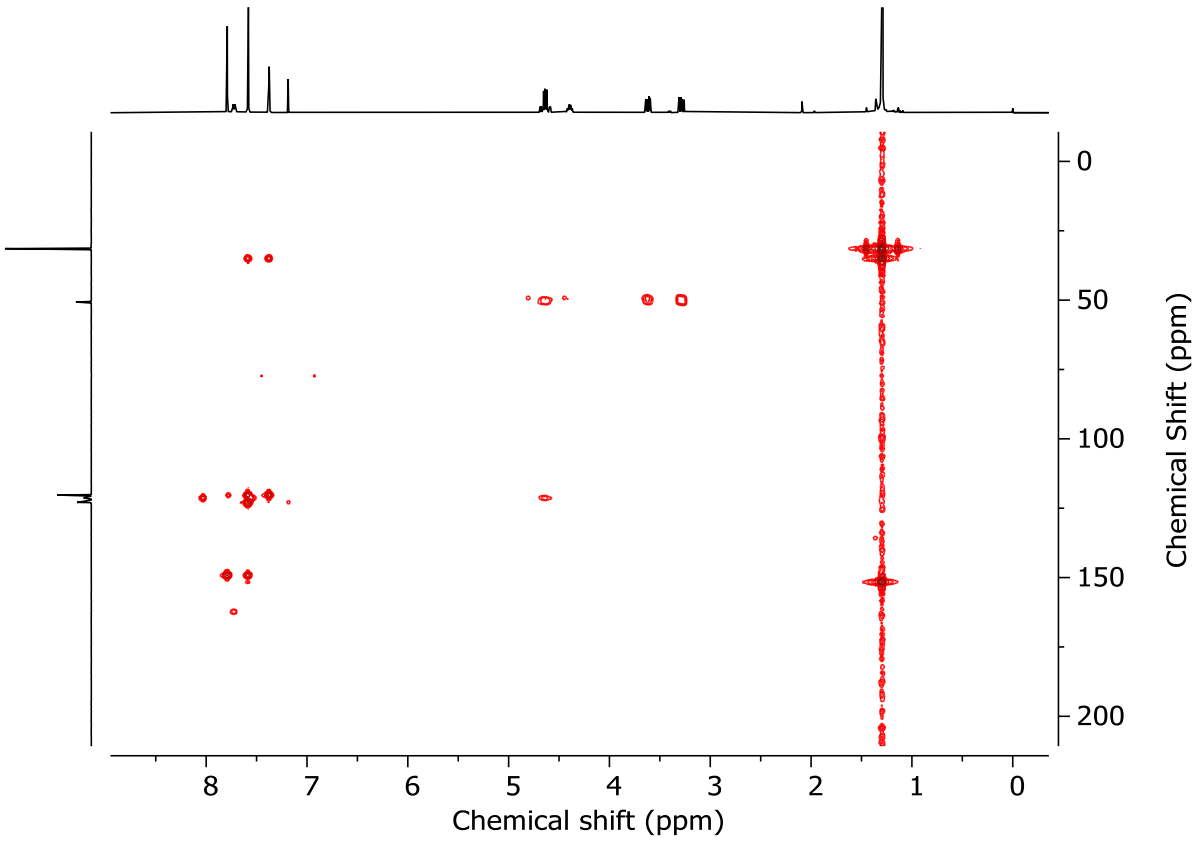

Figure 3.22 - HMBC NMR ($CDCl_3$) of (*R*)-**1c**.

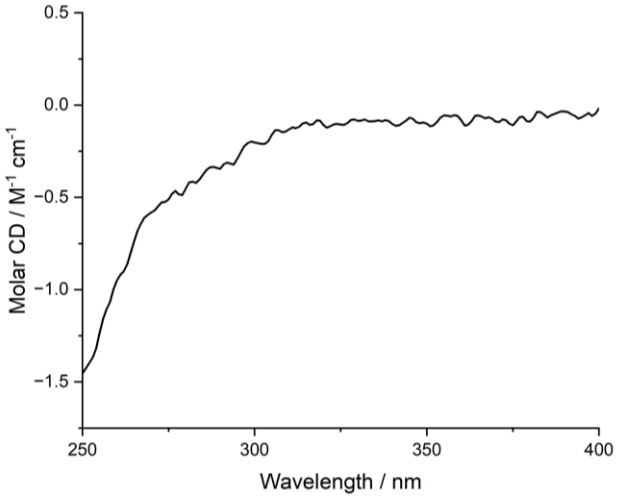

Figure 3.23 - Circular Dichroism Spectra of (*R*)-**1c** (60 µM) at 293 K in $CHCl_3$.

Trifluoroacetamide azide (*R*)-1d

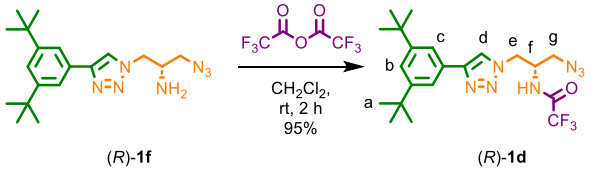

To a solution of (*R*)-**1f** (50.1 mg, 0.14 mmol) in CH_2Cl_2 (0.7 mL) was added trifluoroacetic anhydride (27.4 µL, 0.21 mmol) dropwise, then allowed to stir at rt for 2 h. The reaction mixture was then diluted with CH_2Cl_2 (2 mL) and poured slowly into sat. $NaHCO_{3\,(aq)}$ (5 mL). The aqueous and organic phases were separated, and the aqueous phase was then extracted with CH_2Cl_2 (3 x 5 mL). The combined organic extracts were washed with brine (5 mL), dried ($MgSO_4$) and concentrated *in vacuo*. Chromatography (petrol-EtOAc 0→100%) gave (*R*)-**1d** (60.5 mg, 95%) as a white solid.

^{1}H NMR (400 MHz, $CDCl_3$) δ: 7.98 (d, *J* = 8.1, 1H, NH), 7.88 (s, 1H, H_d), 7.64 (d, *J* = 1.8, 2H, H_c), 7.46 (t, *J* = 1.8, 1H, H_b), 4.67 (qd, *J* = 14.3, 5.4, 2H, H_e), 4.59 – 4.48 (m, 1H, H_f), 3.66 (dd, *J* = 12.6, 5.5, 1H, H_g), 3.39 (dd, *J* = 12.6, 7.1, 1H, $H_{g'}$), 1.36 (s, 18H, H_a);

^{13}C NMR (101 MHz, $CDCl_3$) δ: 157.72 (q, *J* = 38.1), 151.75, 149.28, 129.08, 123.11, 121.39, 120.39, 115.64 (q, *J* = 287.7), 50.11, 49.73, 49.38, 35.07, 31.52;

^{19}F NMR (376 MHz, $CDCl_3$) δ -75.8;

HR-ESI-MS (+ve) m/z = 452.2391 $[M+H]^+$ (calc. m/z for $C_{21}H_{29}F_3N_7O$ 452.2380);

Melting point = 165-167 °C.

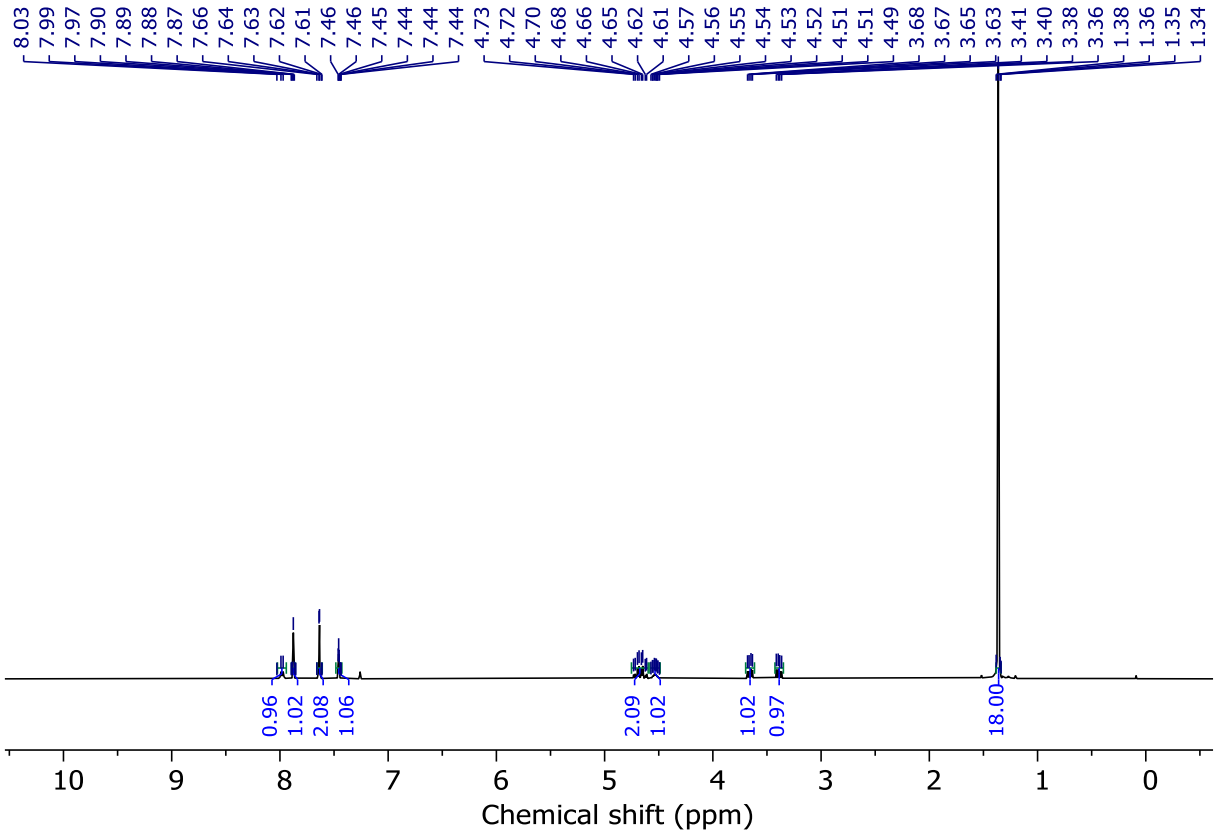

Figure 3.24 - ^{1}H NMR ($CDCl_3$, 400 MHz) of (*R*)-**1d**.

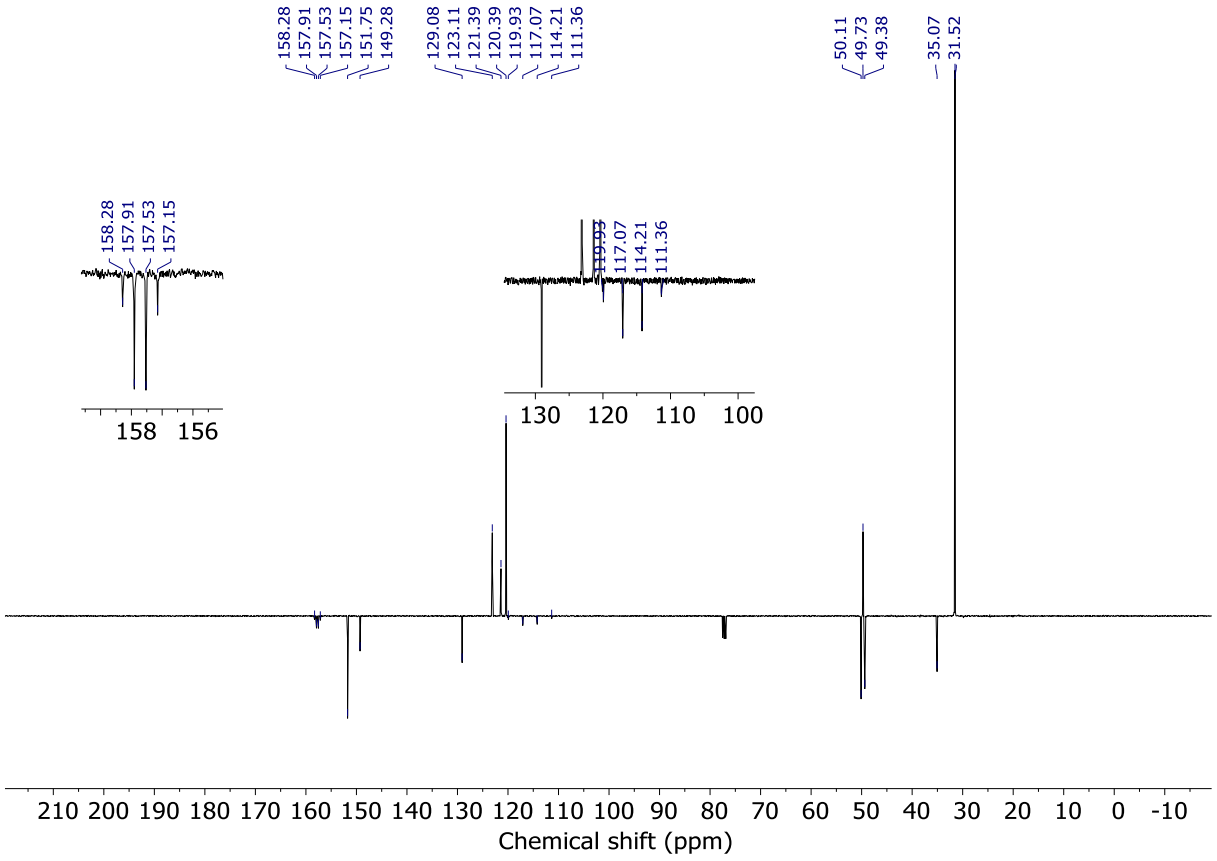

Figure 3.25 - JMOD NMR ($CDCl_3$, 101 MHz) of (*R*)-**1d**.

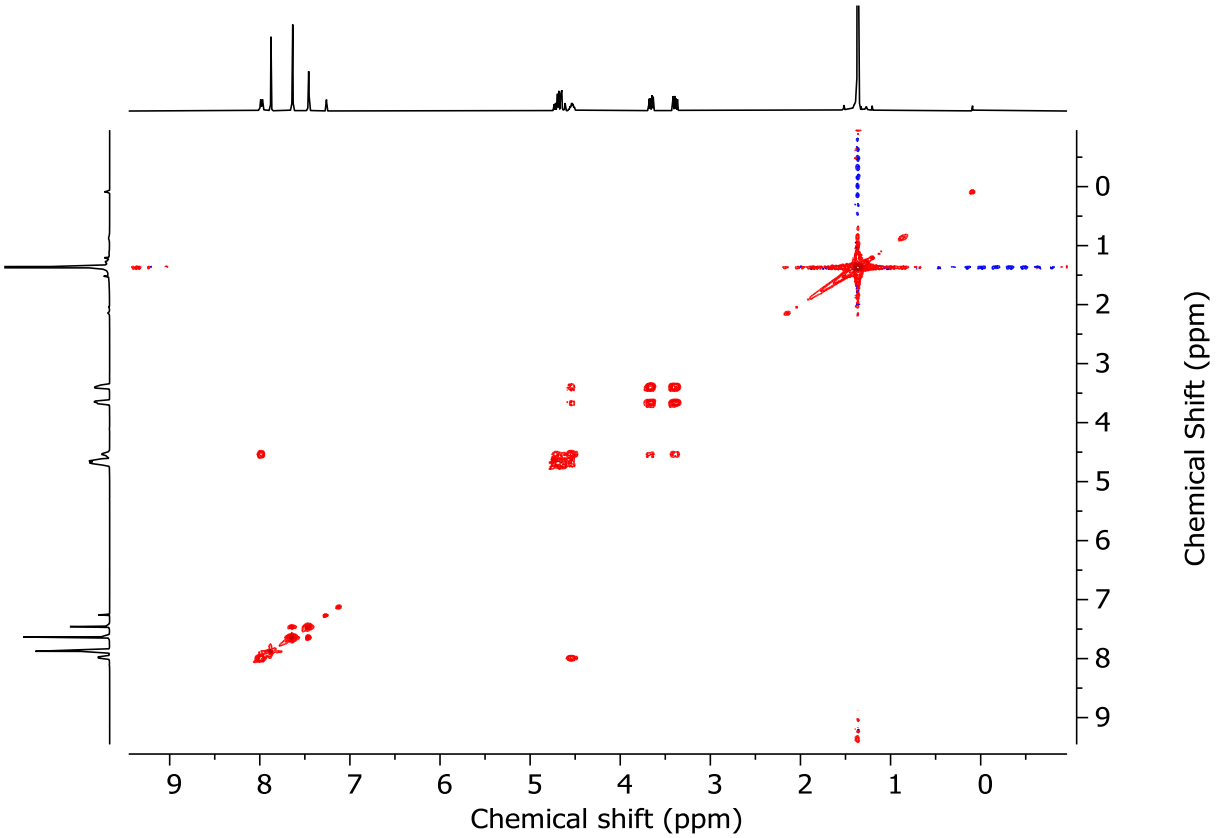

Figure 3.26 - COSY NMR ($CDCl_3$) of (*R*)-**1d**.

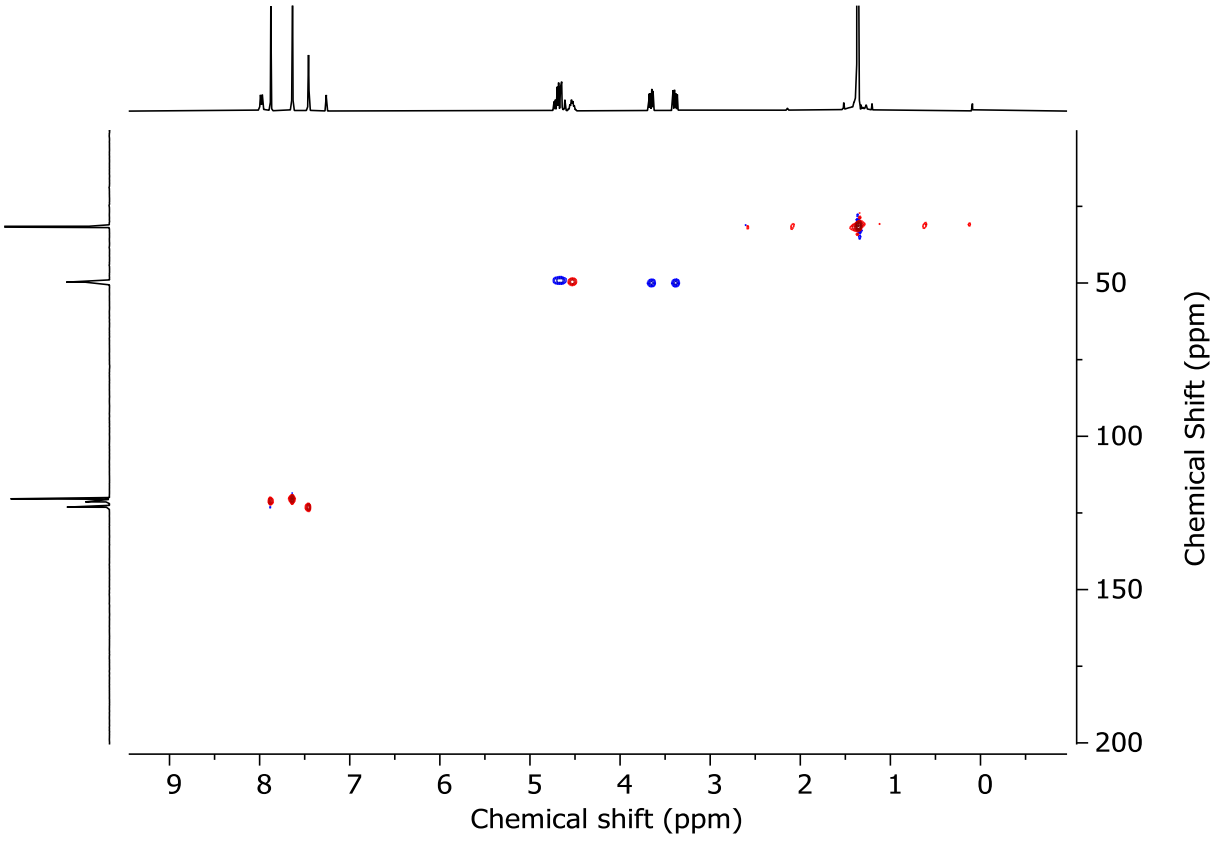

Figure 3.27 - HSQC NMR ($CDCl_3$) of (*R*)-**1d**.

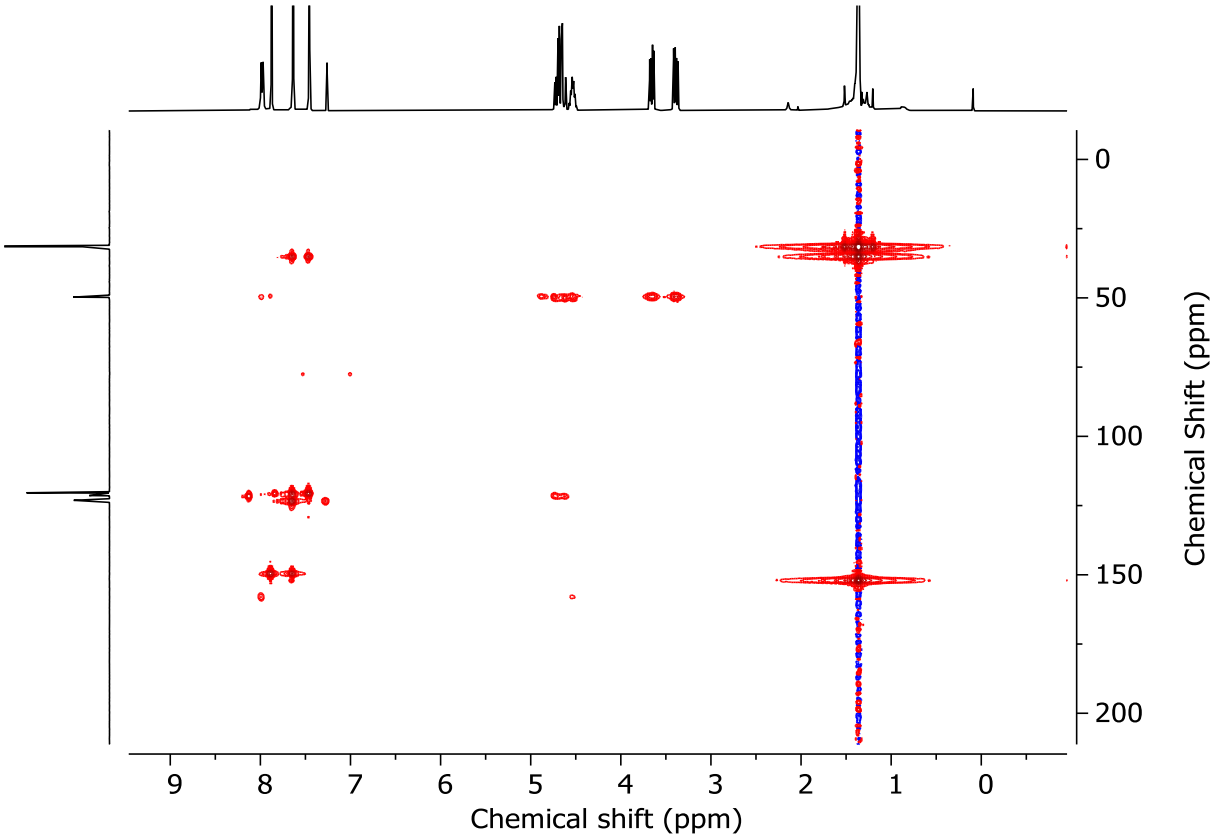

Figure 3.28 - HMBC NMR ($CDCl_3$) of (*R*)-**1d**

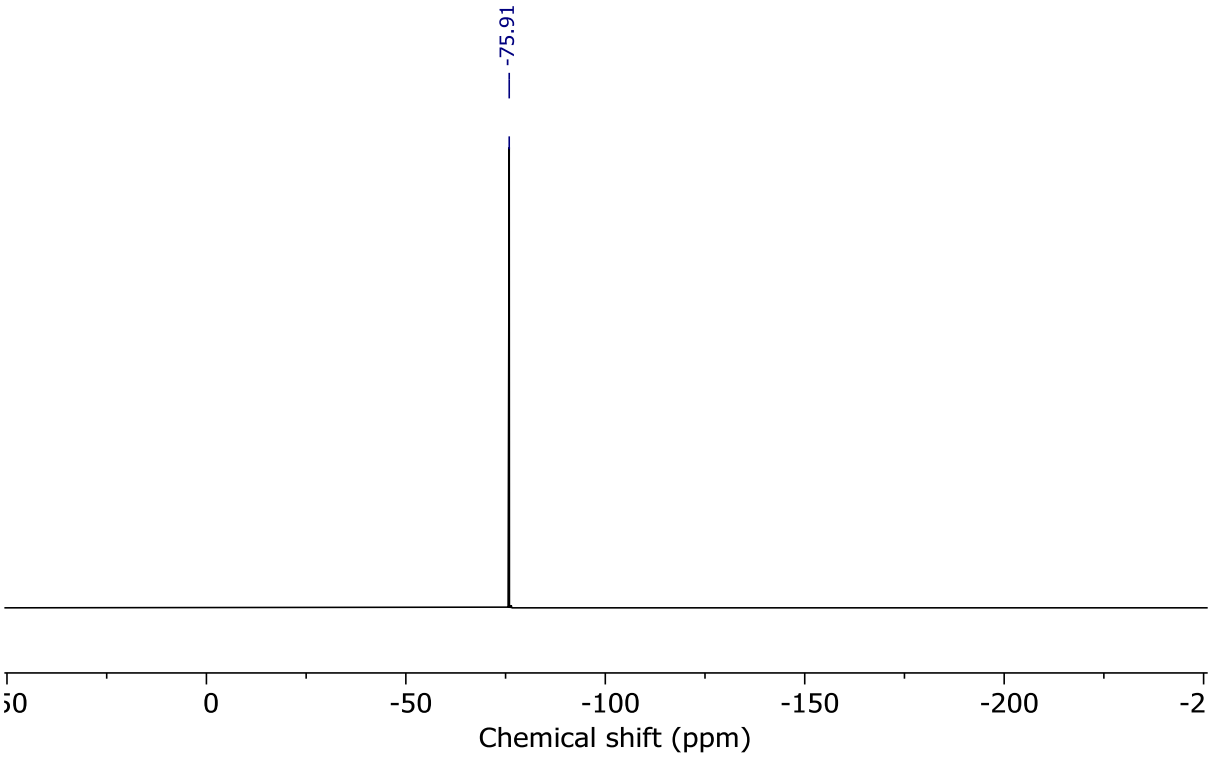

Figure 3.29 - ^{19}F NMR ($CDCl_3$, 376 MHz) of (*R*)-**1d**.

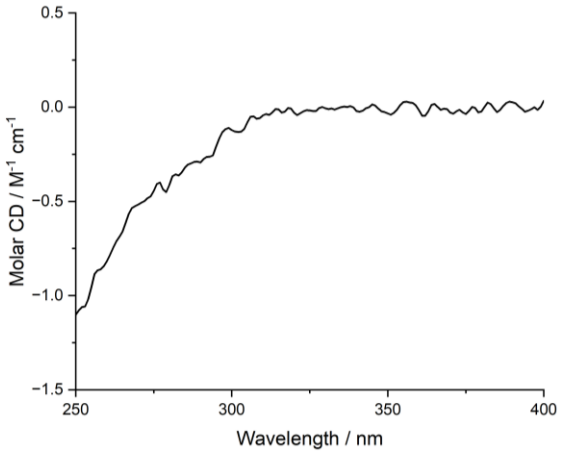

Figure 3.30 - Circular Dichroism Spectra of (*R*)-**1d** (59 µM) at 293 K in $CHCl_3$.

Methylated Boc azide (*R*)-S4

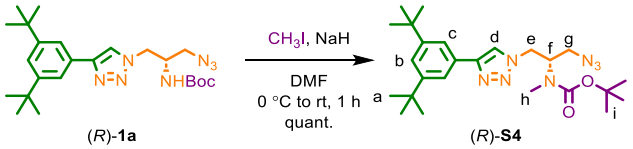

To a suspension of NaH (60% in mineral oil, 17.8 mg, 0.44 mmol) in DMF (2.5 mL) was added (*R*)-**1a** (100.0 mg, 0.22 mmol) in DMF (2.5 mL) dropwise at 0 °C. The reaction mixture was stirred for 10 minutes, then a solution of CH_3I (20 µL, 0.33 mmol) was added dropwise over 10 minutes. The reaction mixture was allowed to warm to rt and stirred for 1 h. The reaction mixture was then quenched by adding H_2O (10 mL) dropwise. The aqueous and organic phases were separated, and the aqueous phase was then extracted with Et_2O (3 x 20 mL). The combined organic extracts were washed with brine (10 mL), dried ($MgSO_4$) and concentrated *in vacuo*. Chromatography (petrol-Et_2O 5→10%) gave (*R*)-**S4** as a colourless oil (103 mg, quant.) as a mixture of rotamers.

^{1}H NMR (400 MHz, $CDCl_3$) δ: 7.81-7.58 (m, 6H, H_c major, H_c minor, H_d major, H_d minor), 7.41 (app t, 2H, H_b major, H_b minor), 4.88-4.78 (m, 2H, H_e major, H_e minor), 4.59-4.50 (m, 2H, H_e major, H_e minor), 4.28-4.16 (m, 2H, H_f major, H_f minor), 3.90-3.80 (m, 2H, H_g major, H_g minor), 4.88-4.78 (m, 2H, H_g major, H_g minor), 2.81 (s, 3H, H_h minor), 2.67 (s, 3H, H_h major), 1.48-1.38 (m, 18H, H_i major, H_i minor), 1.36 (app s, 36H, H_a major, H_a minor)

^{13}C NMR (101 MHz, $CDCl_3$) δ: 155.4, 151.4, 148.7, 129.6, 122.5, 120.4, 120.2, 120.1, 80.7, 58.8, 56.7, 50.5, 50.0, 49.2, 48.8, 34.9, 34.5, 31.5, 28.3.

$[\boldsymbol{\alpha}]_{\boldsymbol{D}}^{\mathbf{23}}$-1.4 (c 0.62, $CHCl_3$)

HR-ESI-MS (+ve) m/z = 470.3252 $[M+H]^+$ (calc. 470.3243 m/z for $C_{25}H_{40}N_7O$);

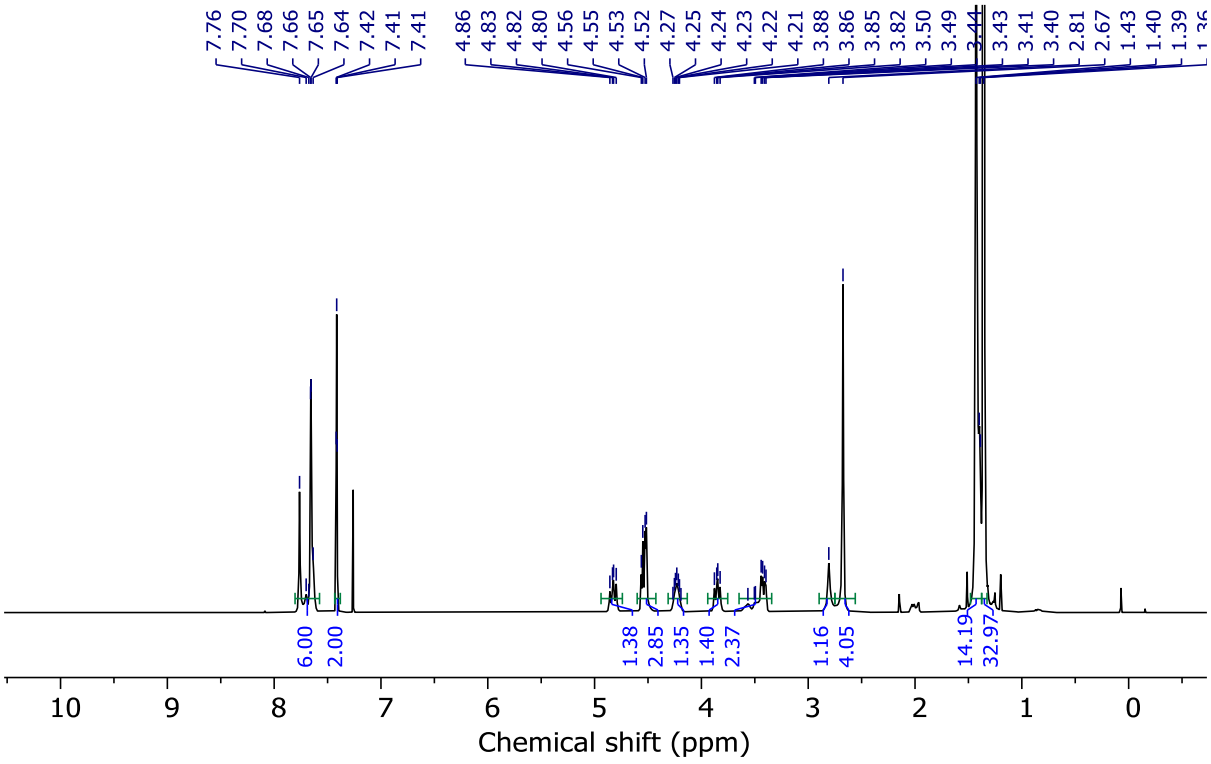

Figure 3.31 - ^{1}H NMR ($CDCl_3$, 400 MHz) of (*R*)-**S4**.

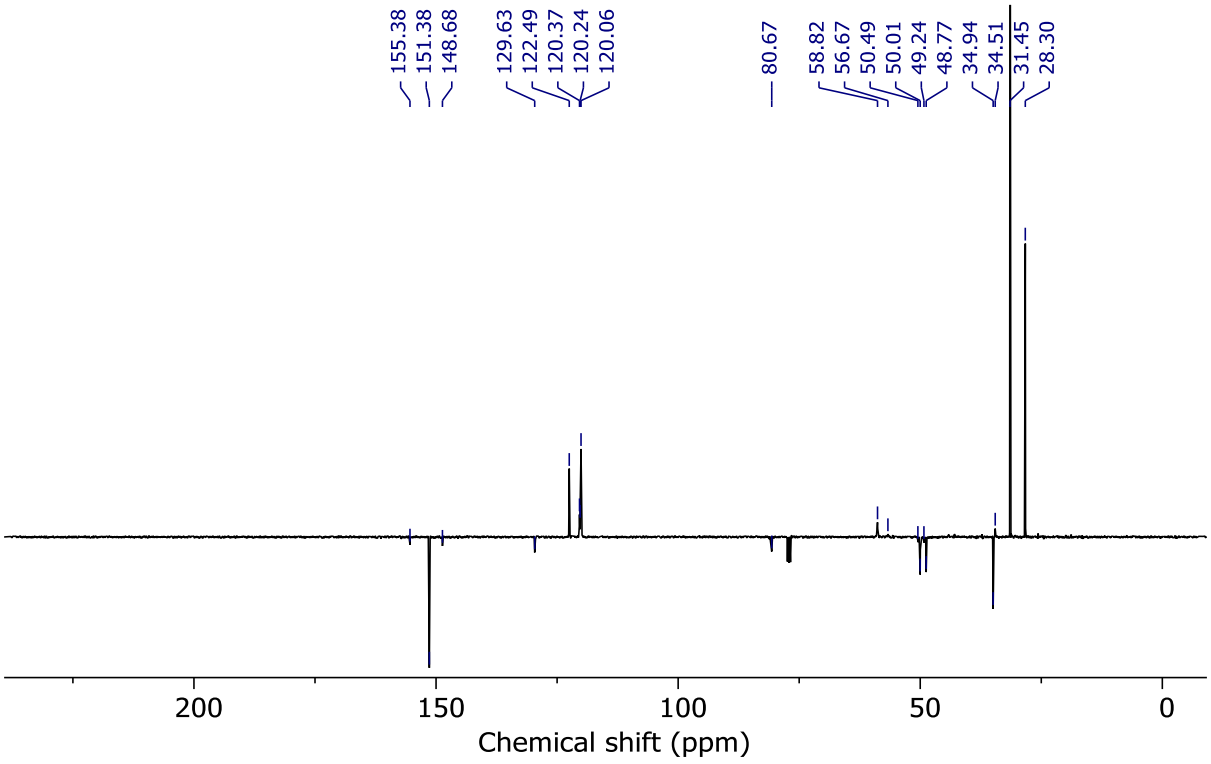

Figure 3.32 - JMOD NMR ($CDCl_3$, 101 MHz) of (*R*)-**S4**.

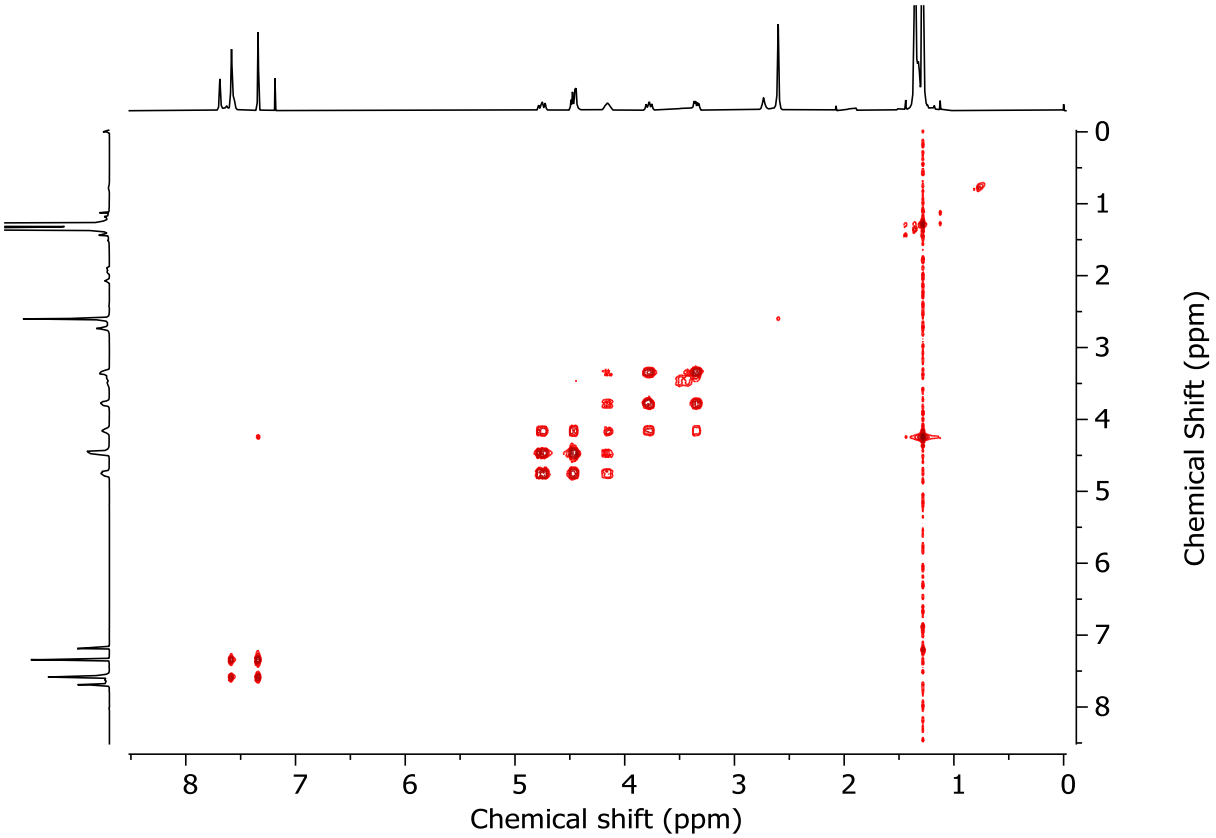

Figure 3.33 - COSY NMR ($CDCl_3$) of (*R*)-**S4**.

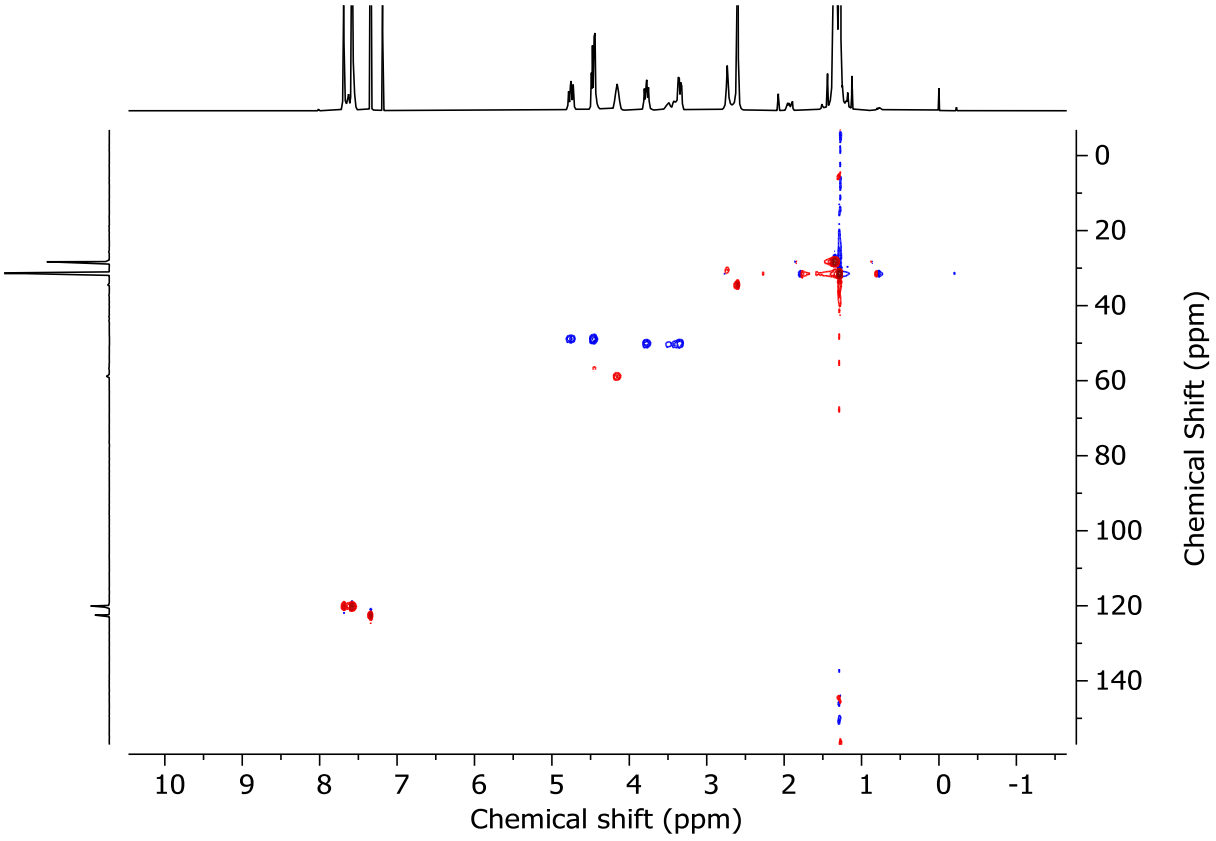

Figure 3.34 - HSQC NMR ($CDCl_3$) of (*R*)-**S4**.

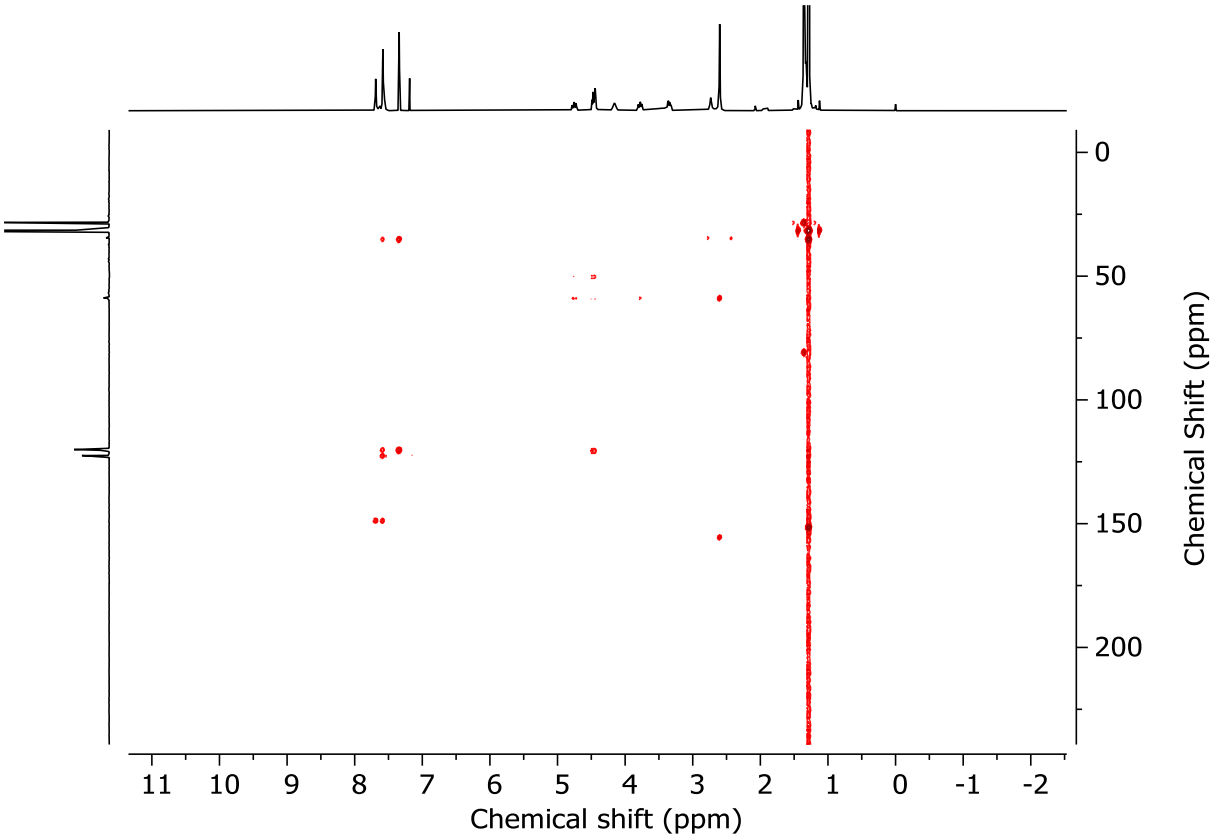

Figure 3.35 - HMBC NMR ($CDCl_3$) of (*R*)-**S4**.

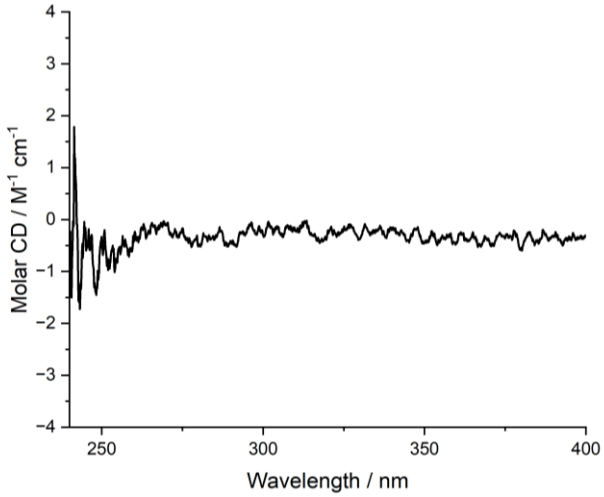

Figure 3.36 - Circular Dichroism Spectra of (*R*)-**S4** (35 μM) at 293 K in $CHCl_3$. No measurable CD response was observed so the $[\alpha]_D$ of (*R*)-**S4** was measured.

Methylated amine azide (*R*)-S5

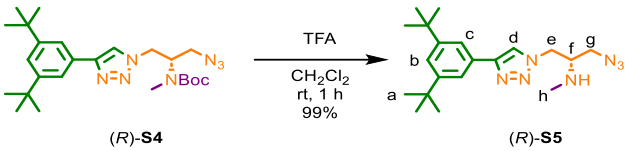

(*R*)-**S4** (*R*)-**S5**

To a solution of (*R*)-**S4** (103 mg, 0.22 mmol) in CH_2Cl_2 (2.2 mL) was added TFA (0.17 mL, 2.2 mmol). The solution was stirred at rt for 1 h. The solution was diluted with CH_2Cl_2 (5 mL) and poured carefully onto a saturated solution of $NaHCO_3$ (15 mL). The aqueous and organic phases were separated, and the aqueous phase was then extracted with CH_2Cl_2 (3 x 10 mL). The combined organic extracts were washed with brine (10 mL), dried ($MgSO_4$) and concentrated *in vacuo* to afford (*R*)-**S5** (81.2 mg, 99%) as a white solid without further purification.

^{1}H NMR (400 MHz, $CDCl_3$) δ: 7.83 (s, 1H, H_d), 7.68 (d, *J* = 1.9, 2H, H_c), 7.43 (t, *J* = 2.0, 1H, H_b), 4.53-4.40 (m, 2H, H_e), 3.44 (dd, *J* = 5.7, 12.7, 1H, H_g), 3.31 (dd, *J* = 5.0, 12.8, 1H, $H_{g'}$), 3.13 (app quint., *J* = 5.6, 1H, H_f), 2.50 (s, 3H, H_h), 1.37 (s, 18H, H_a)

^{13}C NMR (101 MHz, $CDCl_3$) δ: 151.4, 148.7, 129.6, 122.5, 120.8, 120.2, 59.0, 51.3, 50.7, 35.0, 34.0, 31.5.

$[\boldsymbol{\alpha}]_{\boldsymbol{D}}^{\mathbf{23}}$-0.8 (c 0.84, $CHCl_3$)

HR-ESI-MS (+ve) m/z = 370.2750 $[M+H]^+$ (calc. 370.2719 m/z for $C_{20}H_{32}N_7$);

Melting point 133-135°C.

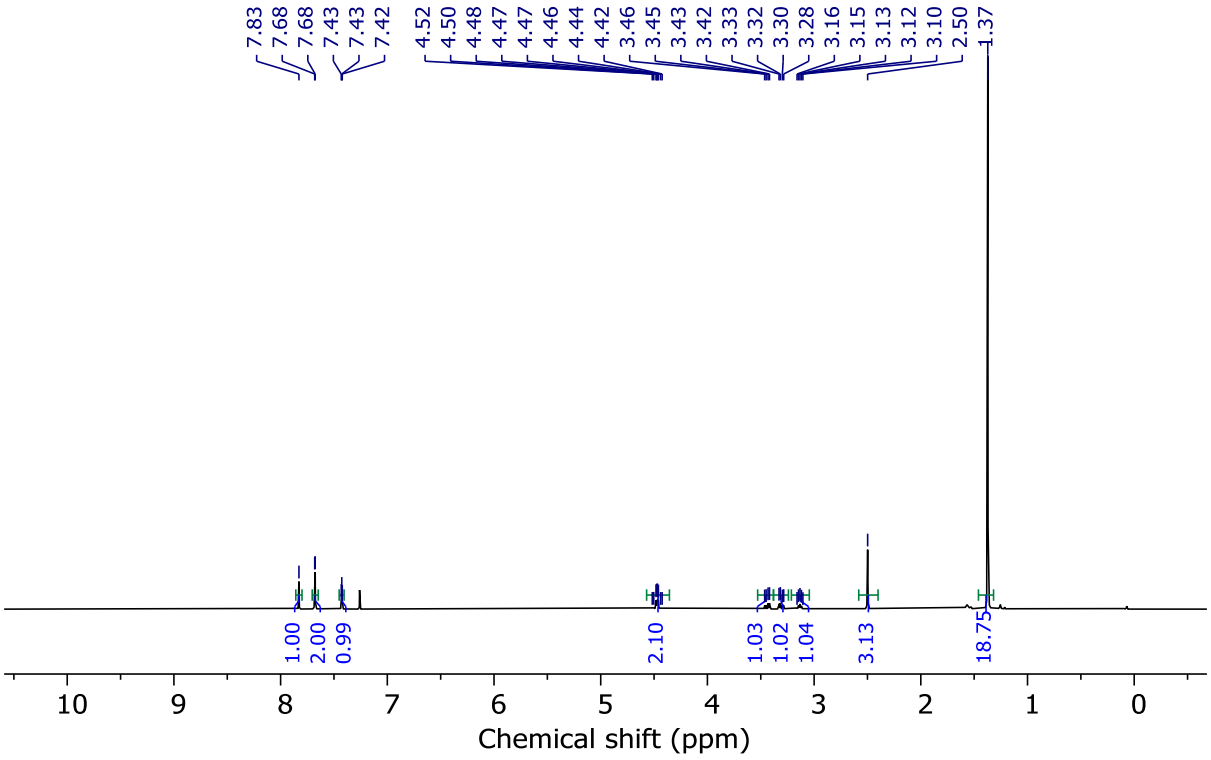

Figure 3.37 - ^{1}H NMR ($CDCl_3$, 400 MHz) of (*R*)-**S5**.

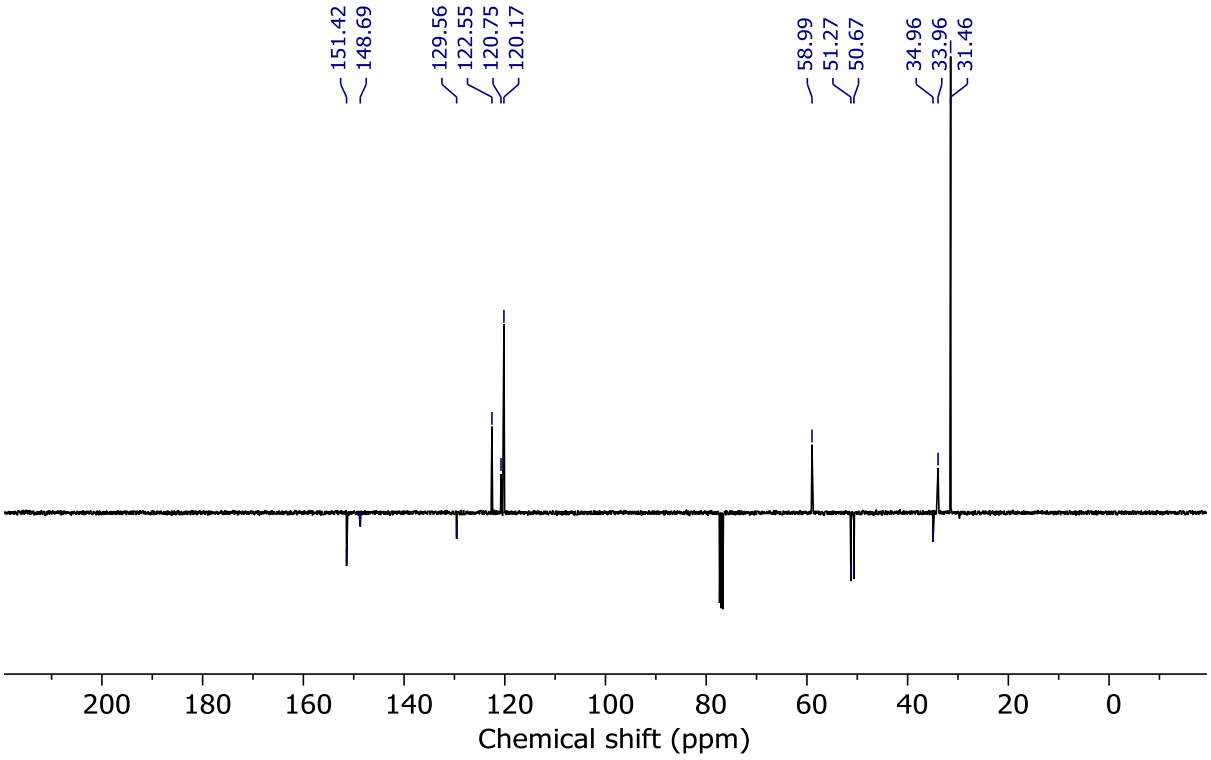

Figure 3.38 - JMOD NMR ($CDCl_3$, 101 MHz) of (*R*)-**S5**.

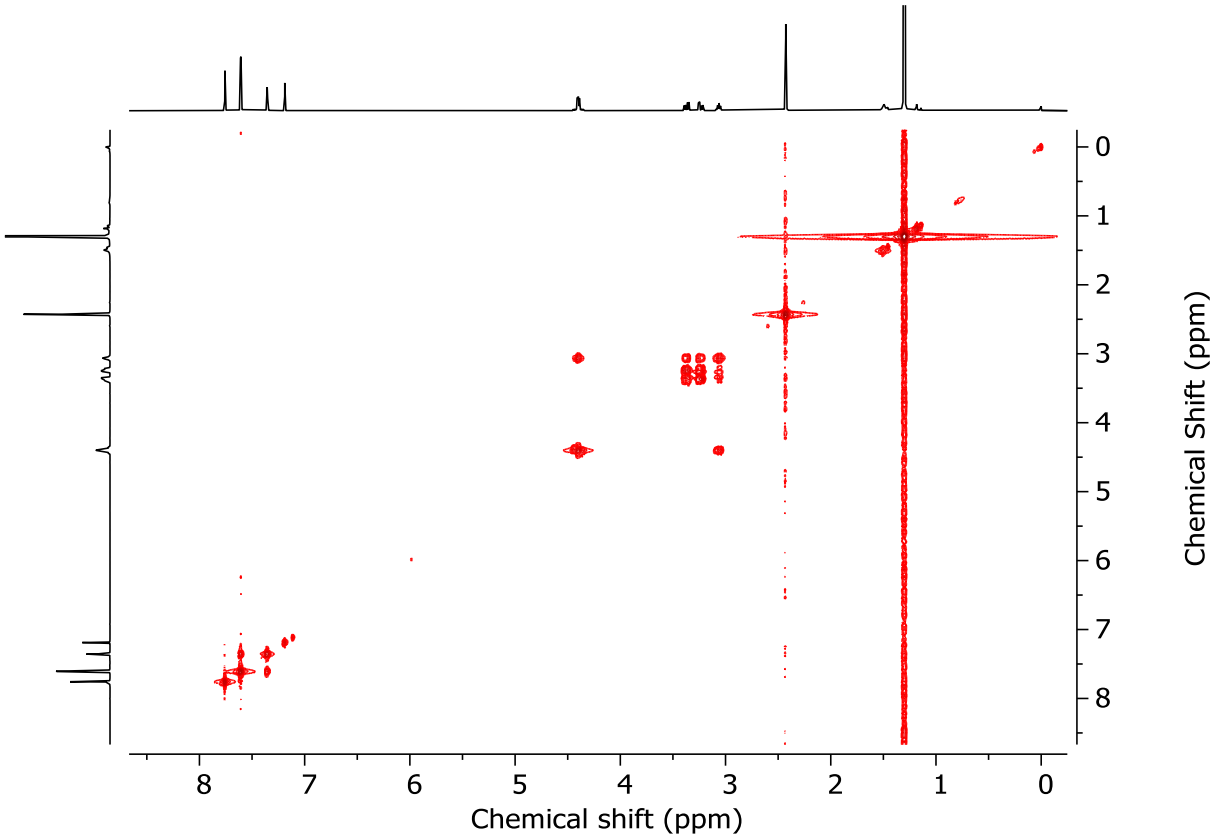

Figure 3.39 - COSY NMR ($CDCl_3$) of (*R*)-**S5**.

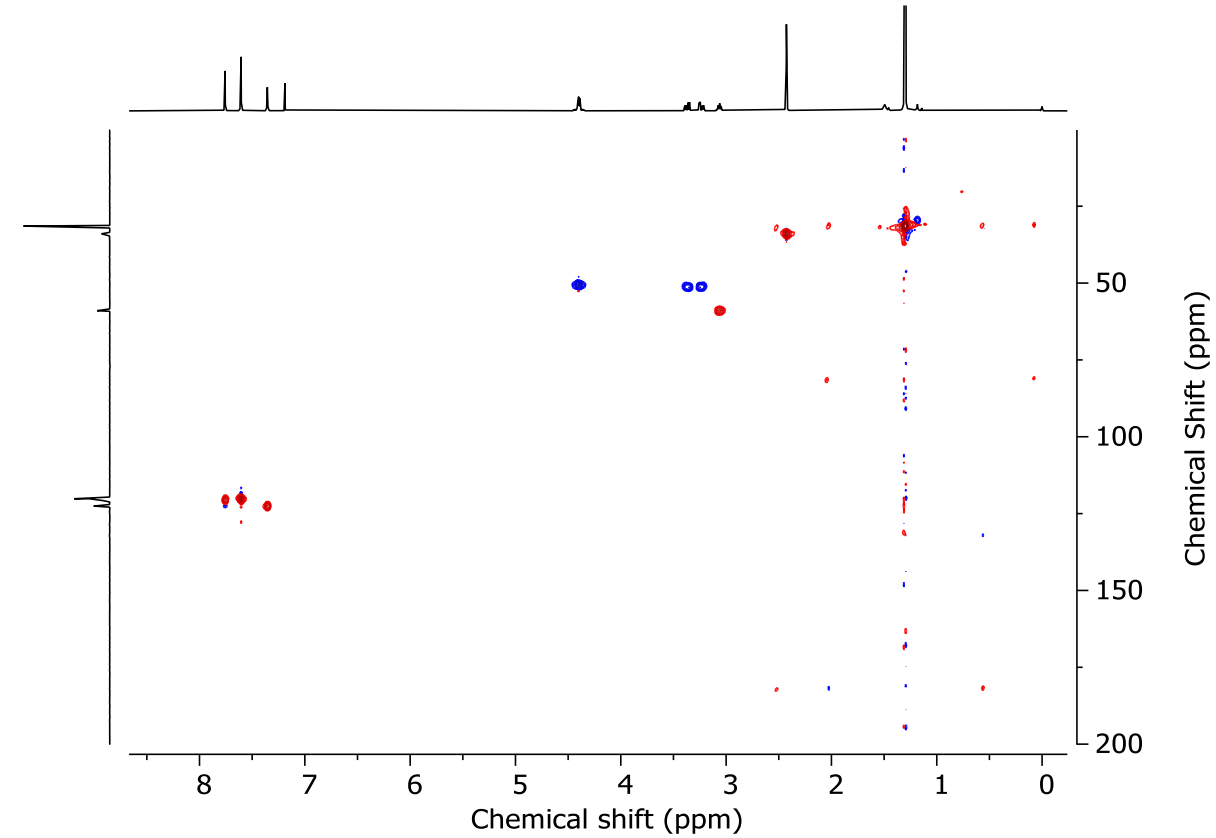

Figure 3.40 - HSQC NMR ($CDCl_3$) of (*R*)-**S5**.

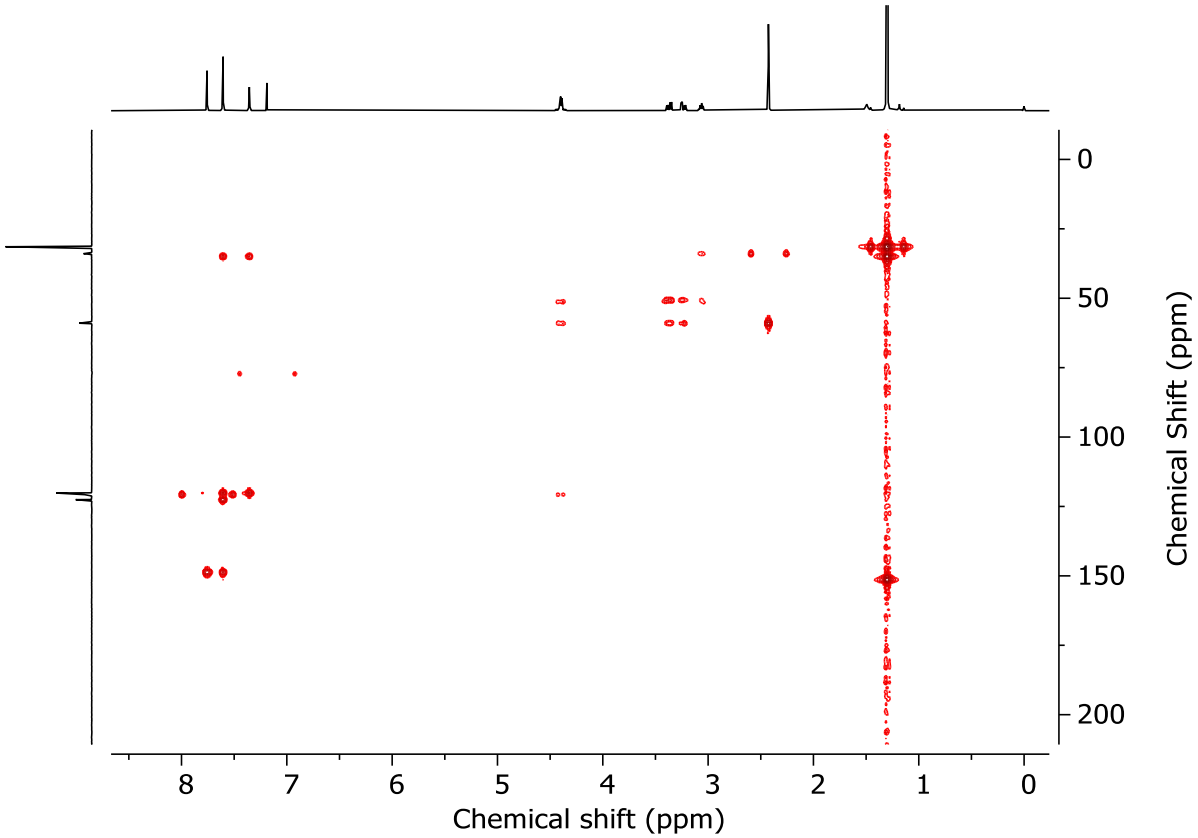

Figure 3.41 - HMBC NMR ($CDCl_3$) of (*R*)-**S5**.

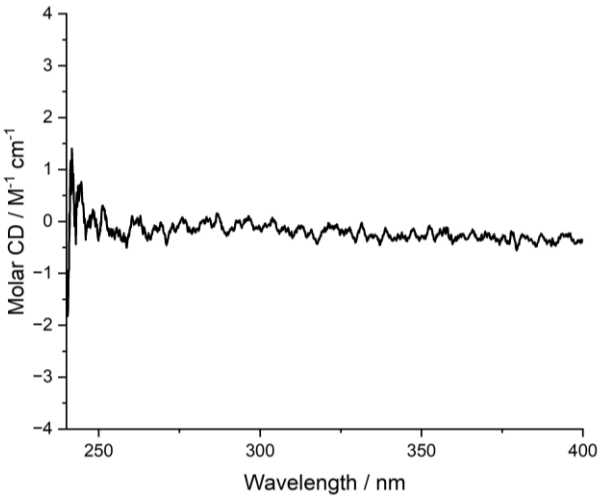

Figure 3.42 - Circular Dichroism Spectra of (*R*)-**S5** (30 μM) at 293 K in $CHCl_3$. No measurable CD response was observed so the $[\alpha]_D$ of (*R*)-**S5** was measured.

Methylated trifluoroacetamide azide (*R*)-1e

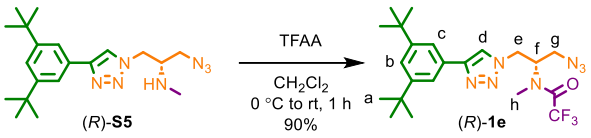

To a solution of (*R*)-**S5** (81.2 mg, 0.22 mmol) in CH_2Cl_2 (2.2 mL) was added trifluoroacetic anhydride (46.6 µL, 0.33 mmol) dropwise, then allowed to stir at rt for 1 h. The reaction mixture was then diluted with CH_2Cl_2 (5 mL) and poured slowly into sat. $NaHCO_{3(aq)}$ (10 mL). The aqueous and organic phases were separated, and the aqueous phase was then extracted with CH_2Cl_2 (3 x 10 mL). The combined organic extracts were washed with brine (15 mL), dried ($MgSO_4$) and concentrated *in vacuo*. Chromatography (petrol-EtOAc 0→100%) gave (*R*)-**1e** (92.1 mg, 90%) as a white foam.

^{1}H NMR (400 MHz, $CDCl_3$) δ: 7.73 (s, 1H, H_d), 7.65 (d, *J* = 1.9, 2H, H_c), 7.44 (t, *J* = 1.9, 1H, H_b), 4.93 (dd, *J* = 8.9, 14.2, 1H, H_e), 4.66 (dd, *J* = 5.8, 14.2, 1H, $H_{e`}$), 4.39 (tt, *J* = 9.2, 5.5, 1H, $H_f$), 4.01 (dd, *J* = 8.5, 12.6, 1H, $H_g$), 3.69 (dd, *J* = 5.6, 12.9, 1H, $H_{g`}$), 2.98 (s, 3H, H_h), 1.37 (s, 18H, H_a)

^{13}C NMR (101 MHz, $CDCl_3$) δ: 158.0 (app. d, $J_{C\text{-}F}$ = 39.8) 157.9, 151.5, 149.2, 129.2, 122.8, 120.4, 120.2, 115.8 (app. d, $J_{C\text{-}F}$ = 290.8), 61.0, 49.1, 47.7, 35.7, 35.0, 31.4.

^{19}F NMR (376 MHz, $CDCl_3$) δ -70.7

HR-ESI-MS (+ve) m/z = 466.2575 $[M+H]^+$ (calc. 466.2542 m/z for $C_{22}H_{30}F_3N_7O$);

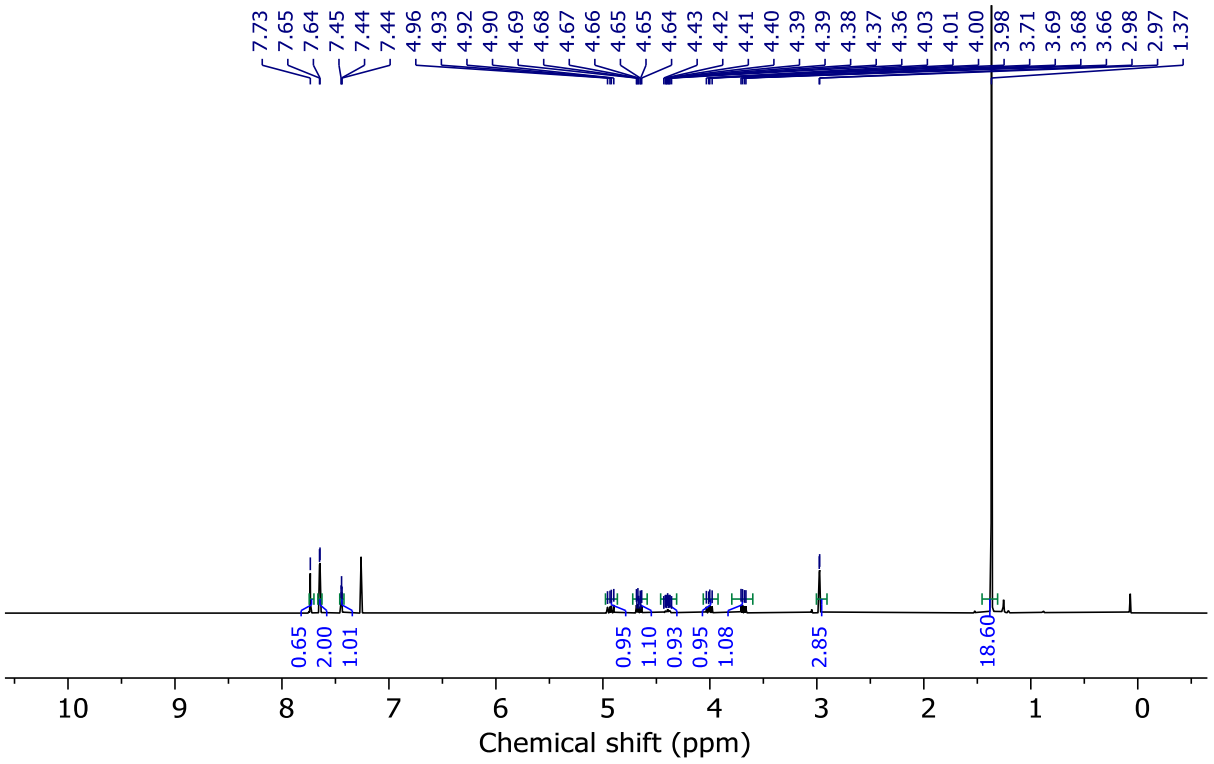

Figure 3.43 - ^{1}H NMR ($CDCl_3$, 400 MHz) of (*R*)-**1e**.

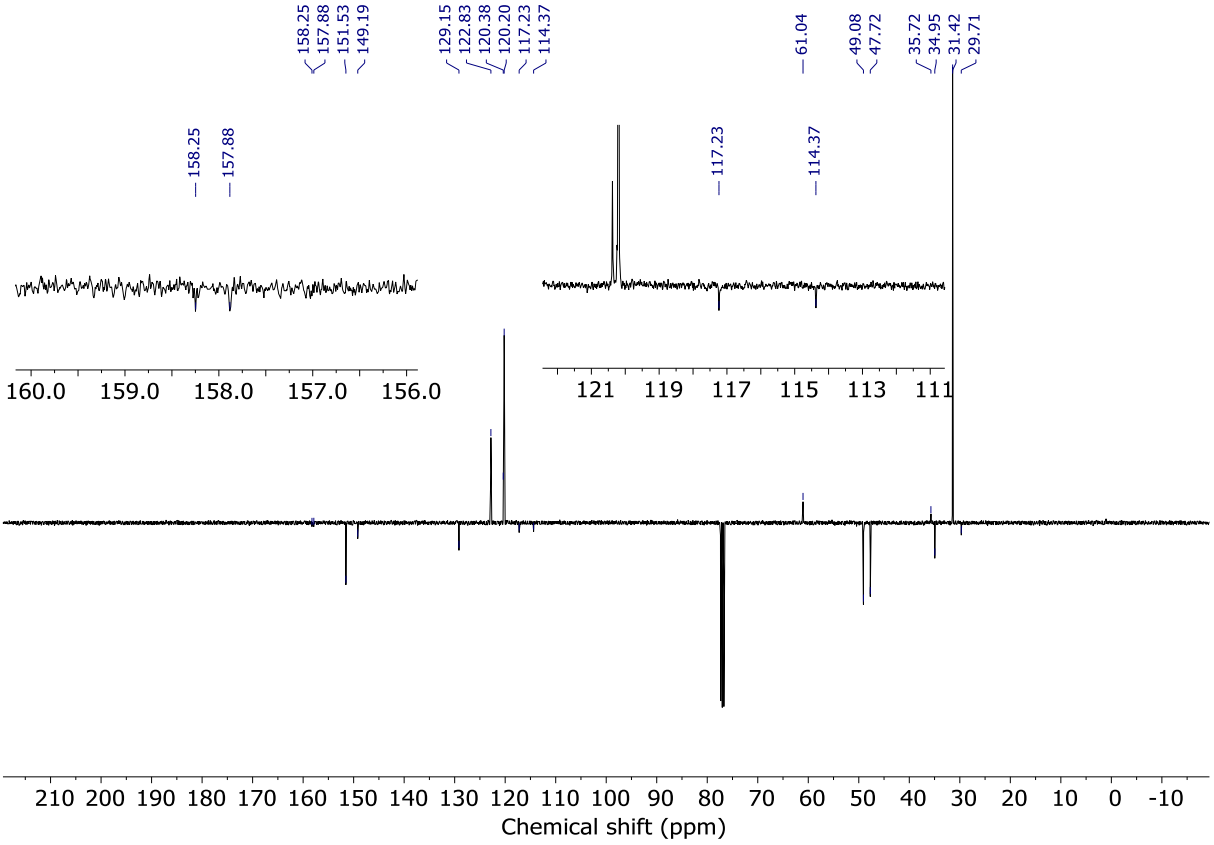

Figure 3.44 - JMOD NMR ($CDCl_3$, 101 MHz) of (*R*)-**1e**.

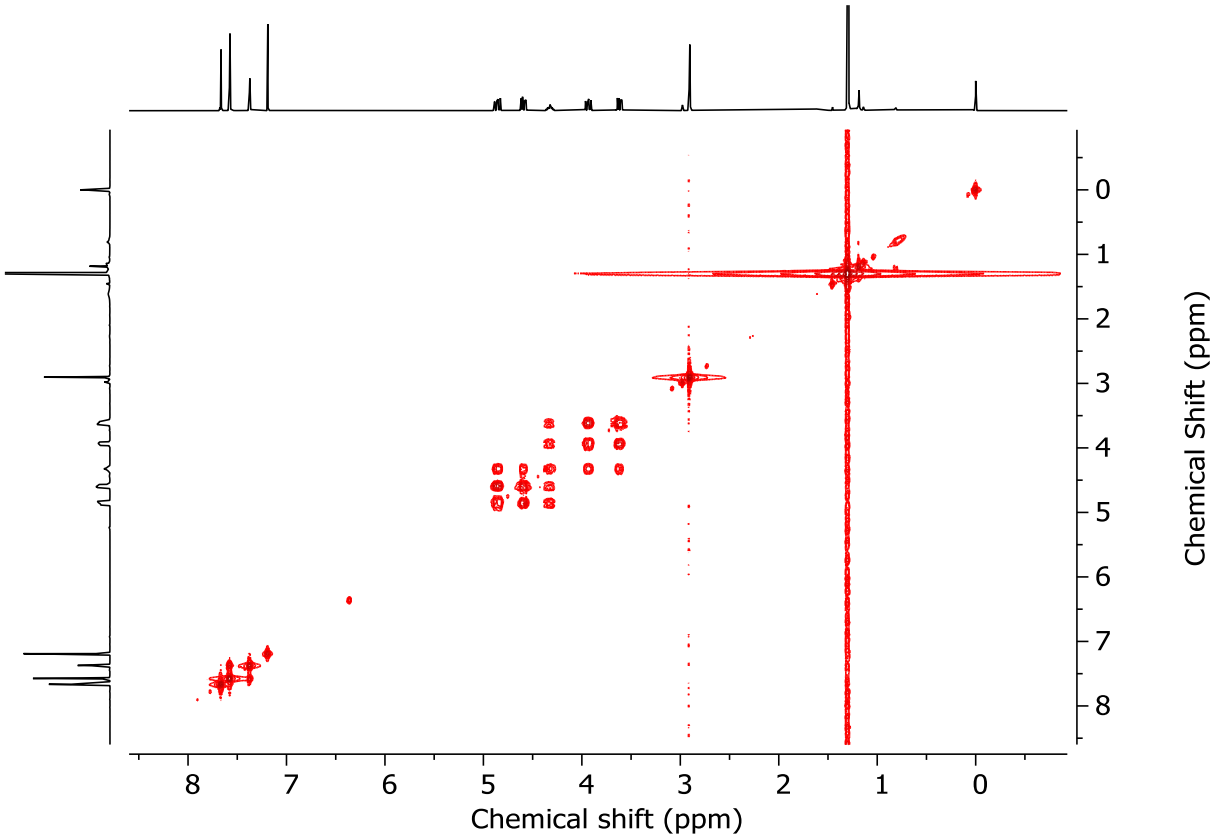

Figure 3.45 - COSY NMR ($CDCl_3$) of (*R*)-**1e**.

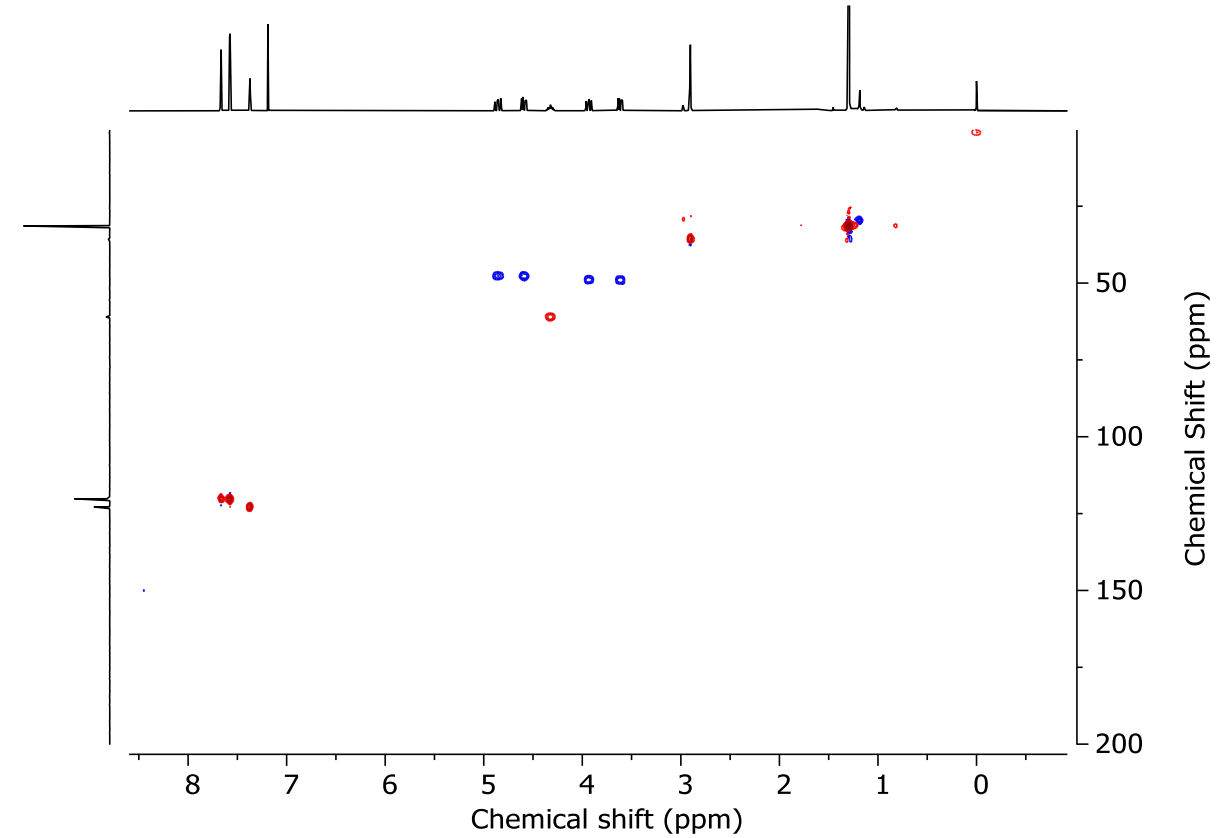

Figure 3.46 - HSQC NMR ($CDCl_3$) of (*R*)-**1e**.

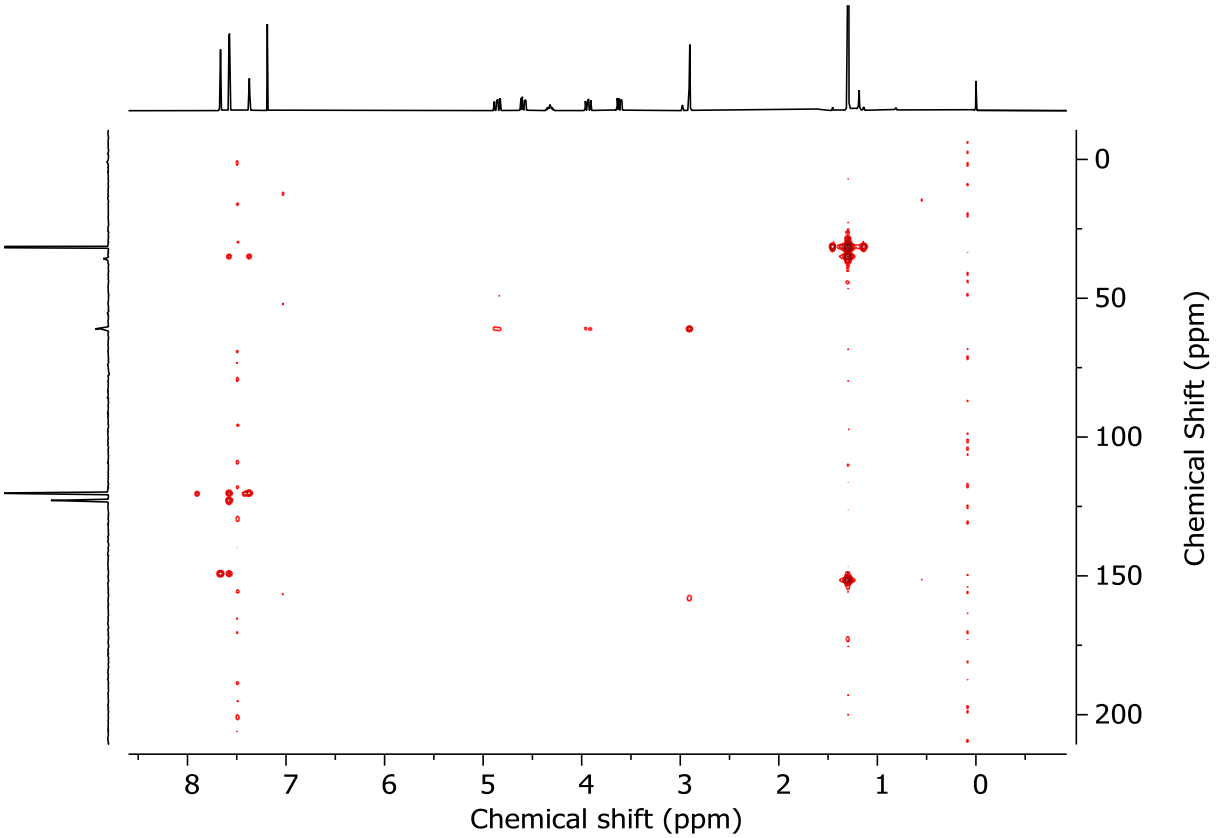

Figure 3.47 - HMBC NMR (CDCl3) of (*R*)-**1e**.

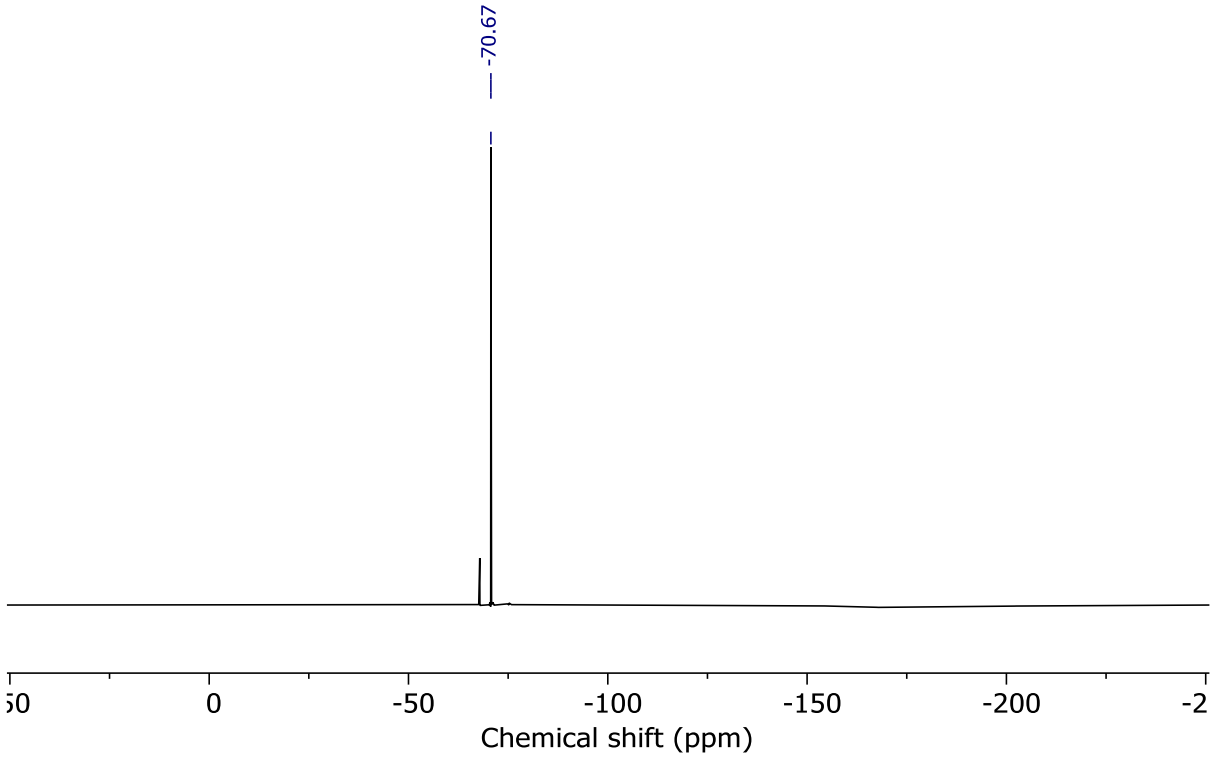

Figure 3.48 - ^{19}F NMR ($CDCl_3$, 376 MHz) of (*R*)-**1e**.

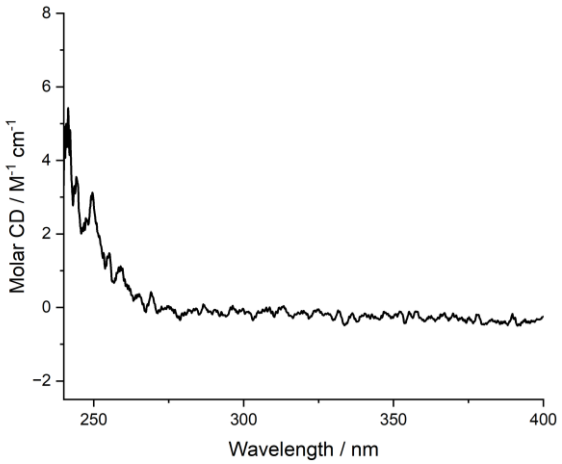

Figure 3.49 - Circular Dichroism Spectra of (*R*)-**1e** (91 µM) at 293 K in $CHCl_3$.

Boc rotaxanes 4a

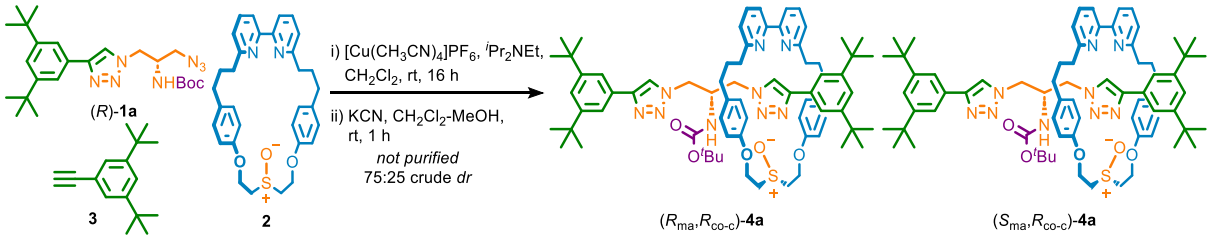

Using the previously reported procedure: [11]

In a CEM vial were added **3** (4.8 mg, 22.4 µmol), (*R*)-**1a** (10.2 mg, 22.4 µmol), **2** (10.5 mg, 19.9 µmol) and $[Cu(CH_3CN)_4PF_6]$ (7.2 mg, 19.3 µmol). The vial was sealed and purged with N_2, then CH_2Cl_2 was added (1.0 mL), followed by $^iPr_2NEt$ (7.0 µL, 39.8 µmol). The solution was stirred at rt for 16 h. MeOH (1 mL) and KCN as a solid (13 mg, 0.20 mmol) were added and the resulting mixture was stirred vigorously for until colourless. The crude mixture was diluted with CH_2Cl_2 (5 mL) and washed with H_2O (5 mL) then EDTA-NH_3 (5 mL), with separation of aqueous and organic phases. The combined aqueous phase was then extracted with CH_2Cl_2 (3 x 5 mL) and the combined organic extracts were washed with brine (10 mL), dried ($MgSO_4$) and concentrated *in vacuo* to give a sample containing **4a** as a mixture of diastereomers (75 : 25 *dr*, Figure 3.50) that was analysed without further purification.

All spectroscopic data is consistent with those reported in literature[11] and previously in Chapter 2 section 3.5.1.

To demonstrate the role of the NHBoc unit as a barrier to co-conformational exchange, the mixture of diastereomers was dissolved in DMSO-d_6 and annealed at 100 °C for 16 h. No change in their ratio was observed, confirming that the macrocycle cannot shuttle between the two triazole containing compartments due to the steric bulk of the NHBoc unit (Figure 3.51).

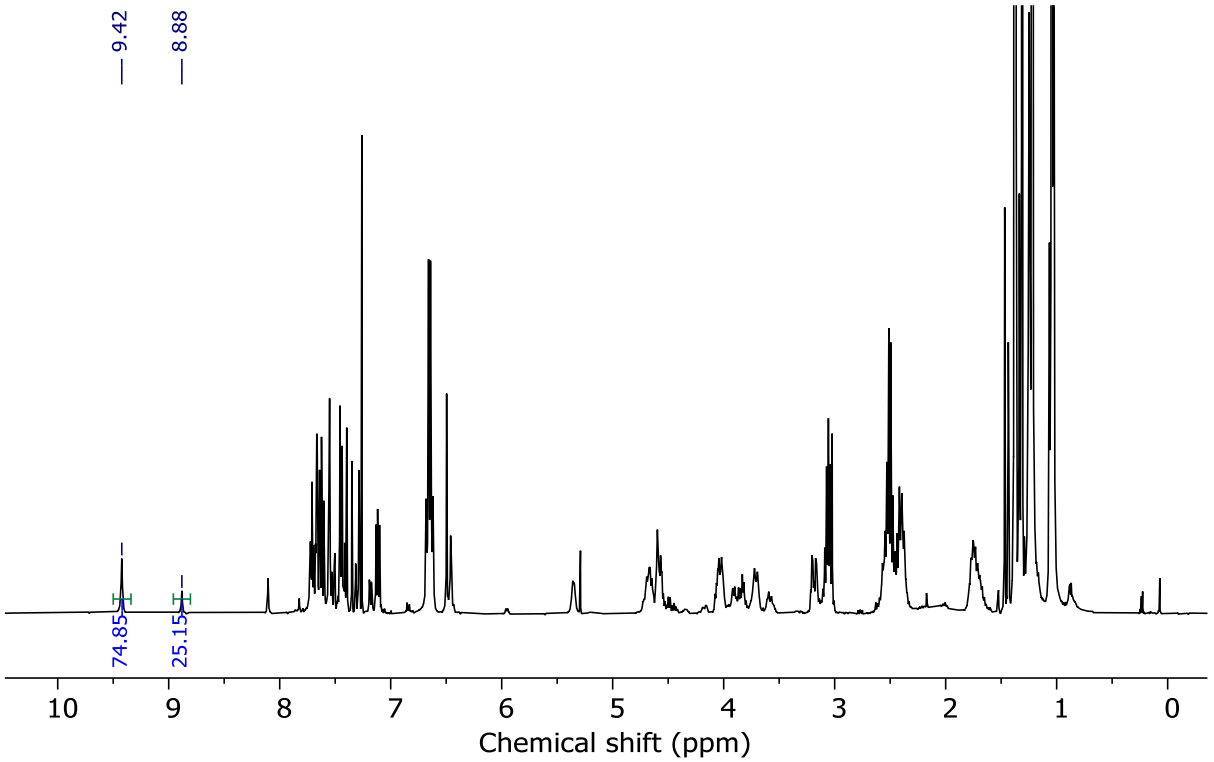

Figure 3.50 - ^{1}H NMR ($CDCl_3$, 400 MHz) of (R_{ma},$R_{co\text{-}c}$)-**4a** and (S_{ma},$R_{co\text{-}c}$)-**4a** analysed without purification.

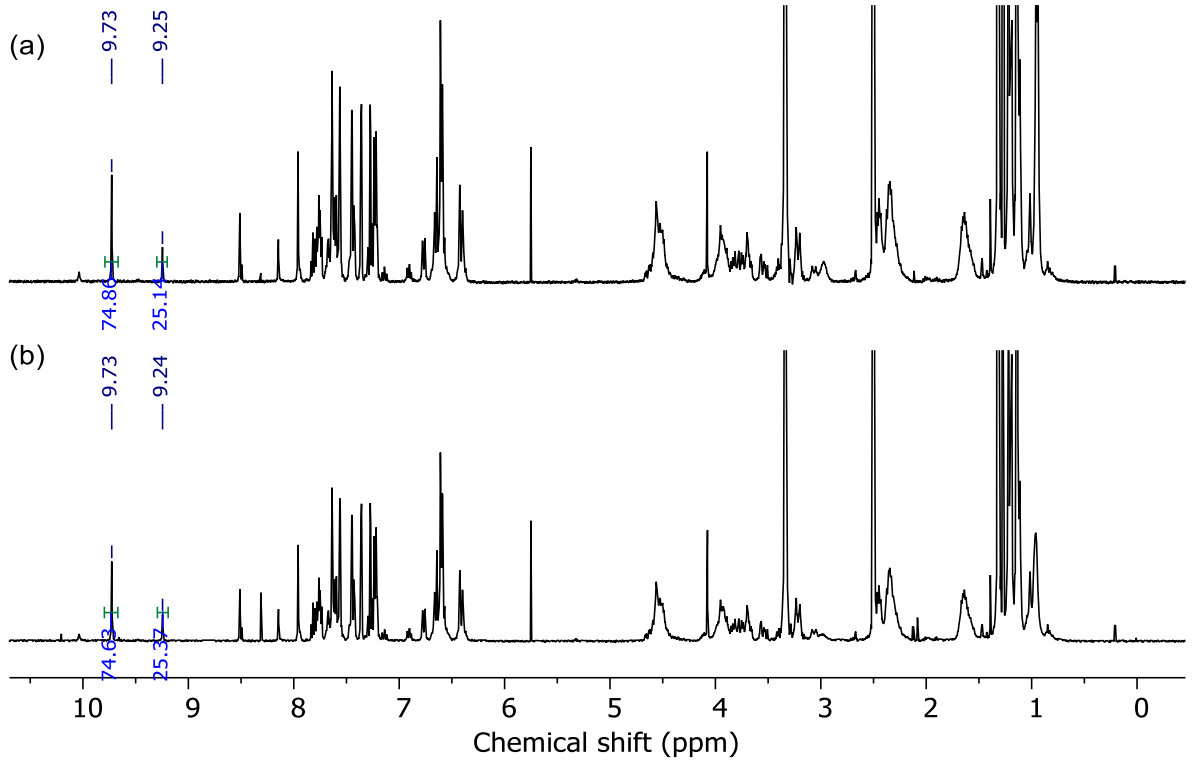

Figure 3.51 - Stacked ^{1}H NMR (DMSO-d_6, 400 MHz) of (R_{ma},$R_{co\text{-}c}$)-**4a** and (S_{ma},$R_{co\text{-}c}$)-**4a**. (a) 75 : 25 *dr* mixture of diastereomers given from the AT-CuAAC synthesis of **4a** (b) 75 : 25 *dr* mixture of rotaxanes **4a** after heating at 100 °C for 16 h.

Acetamide rotaxanes 4b

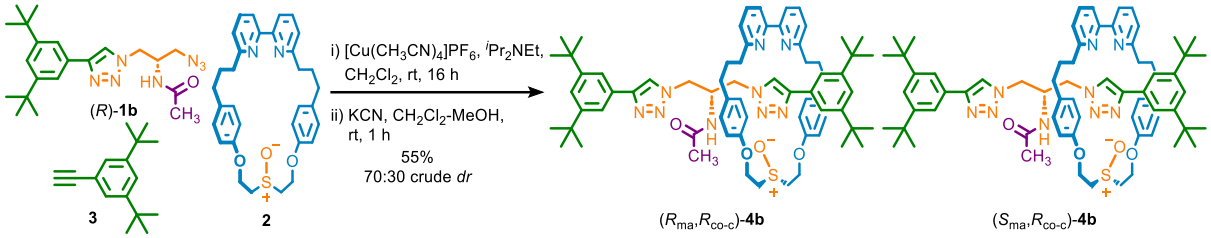

In a CEM vial were added **3** (9.4 mg, 41.7 µmol), (*R*)-**1b** (16.6 mg, 41.7 µmol), **2** (20.0 mg, 38.0 µmol) and $[Cu(CH_3CN)_4PF_6]$ (13.6 mg, 36.0 µmol). The vial was sealed and purged with N_2, then CH_2Cl_2 was added (1.0 mL), followed by $^iPr_2NEt$ (13.2 µL, 75.9 µmol). The solution was stirred at rt for 16 h. MeOH (2 mL mL) and KCN as a solid (24.7 mg, 0.38 mmol) were added and the resulting mixture was stirred vigorously for until colourless. The crude mixture was diluted with CH_2Cl_2 (5 mL) and washed with H_2O (5 mL) then EDTA-NH_3 (5 mL), with separation of aqueous and organic phases. The combined aqueous phase was then extracted with CH_2Cl_2 (3 x 5 mL) and the combined organic extracts were washed with brine (10 mL), dried ($MgSO_4$) and concentrated *in vacuo* to give a sample containing **4b** as a mixture of diastereomers (70 : 30 *dr*, Figure 3.52). Chromatography (CH_2Cl_2-CH_3CN 0→100%) gave **4b** as a white foam (23.8 mg, 55%) as a mixture of diatereomers (2.2 : 1, Figure 3.53).

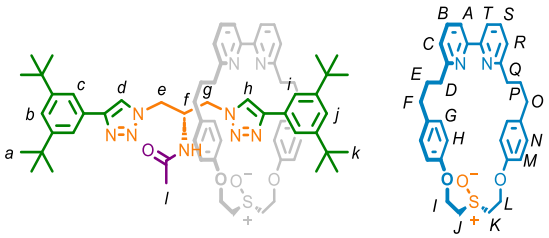

Major diastereoisomer

^{1}H NMR (400 MHz, $CDCl_3$) δ: 9.61 (s, 1H, H_h), 7.73-7.56 (m, 6H, H_B, H_b, H_c, H_d, H_S), 7.52 (d, *J* = 1.8, 2H, H_i), 7.43-7.37 (m, 2H, H_A, H_T), 7.27 (t, *J* = 1.8, 1H, H_j), 7.13-7.07 (m, 2H, H_C, H_R), 6.75 (d, *J* = 8.7, H_G or H_N), 6.71-6.61 (m, 7H, H_G or H_N, H_H, H_M, NH), 4.80-4.42 (m, 4H, H_I, H_L), 4.14-3.87 (m, 4H, H_e or H_g, H_f, H_J, H_K), 3.85-3.62 (m, 2H, H_e or H_g), 3.57 (dd, *J* = 14.5, 4.1, 1H, $H_{e'}$ or $H_{g'}$), 3.19-3.00 (m, 2H, $H_{J'}$, $H_{K'}$), 2.66-2.23 (m, 8H, H_D, H_F, H_O, H_Q), 1.90-1.61 (m, 4H, H_E, H_P superimposed with H_2O), 1.52 (s, 3H, H_l), 1.36 (s, 18H, H_a or H_k), 1.21 (s, 18H, H_a or H_k)

^{13}C NMR (101 MHz, $CDCl_3$) δ: 170.6, 162.9, 162.8, 157.4, 157.1, 156.0, 155.9, 151.2, 151.2, 150.7, 148.2, 147.5, 137.1, 137.0, 133.6, 133.4, 130.4, 129.8, 129.7, 129.4, 128.9, 122.2, 122.0, 121.5, 121.5, 120.5, 120.4, 120.4, 120.1, 119.8, 114.6, 114.5, 60.7, 60.6, 53.5, 53.3, 50.2, 50.0, 49.7, 37.0, 36.7, 34.5, 34.5, 31.6, 31.6, 31.5, 30.6, 30.0, 29.7.

HR-ESI-MS (+ve) m/z = 1138.7 $[M+H]^+$ (calc. m/z for $C_{69}H_{87}N_9O_4S$ 1138.6680);

Minor diastereoisomer

^{1}H NMR (400 MHz, $CDCl_3$) δ: 9.29 (s, 1H, H_h), 7.73-7.56 (m, 3H, H_B, H_d, H_S), 7.54 (d, J = 1.9, 2H, H_i), 7.54-7.47 (m, 2H, H_A, H_T), 7.43-7.37 (m, 3H, H_b, H_c), 7.30 (t, J = 1.9, 1H, H_j), 7.10-7.13 (m, 2H, H_C, H_R), 6.72-6.61 (m, 1H, NH), 6.62-6.50 (m, 8H, H_G, H_H, H_M, H_N), 4.80-4.42 (m, 4H, H_I, H_L), 4.14-3.87 (m, 3H, H_e or H_g, H_f), 3.85-3.62 (m, 4H, H_e or H_g, H_J, H_K), 3.45-3.25 (m, 2H, $H_{J'}$, $H_{K'}$), 2.66-2.23 (m, 8H, H_D, H_F, H_O, H_Q), 1.90-1.61 (m, 4H, H_E, H_P superimposed with H_2O), 1.48 (s, 3H, H_l), 1.38 (s, 18H, H_a or H_k), 1.27 (s, 18H, H_a or H_k)

^{13}C NMR (101 MHz, $CDCl_3$) δ: 170.5, 162.9, 162.8, 157.6, 157.4, 155.4, 155.3, 151.4, 150.7, 148.4, 147.7, 137.3, 137.2, 133.5, 133.4, 130.2, 129.6, 128.9, 123.9, 123.2, 122.5, 122.3, 122.0, 121.4, 120.7, 120.5, 120.1, 120.0, 115.1, 115.0, 61.6, 61.1, 51.8, 51.8, 49.8, 49.8, 49.6, 37.2, 34.9, 34.9, 34.8, 31.4.

HR-ESI-MS (+ve) m/z = 1138.6711 $[M+H]^+$ (calc. m/z for $C_{69}H_{87}N_9O_4S$);

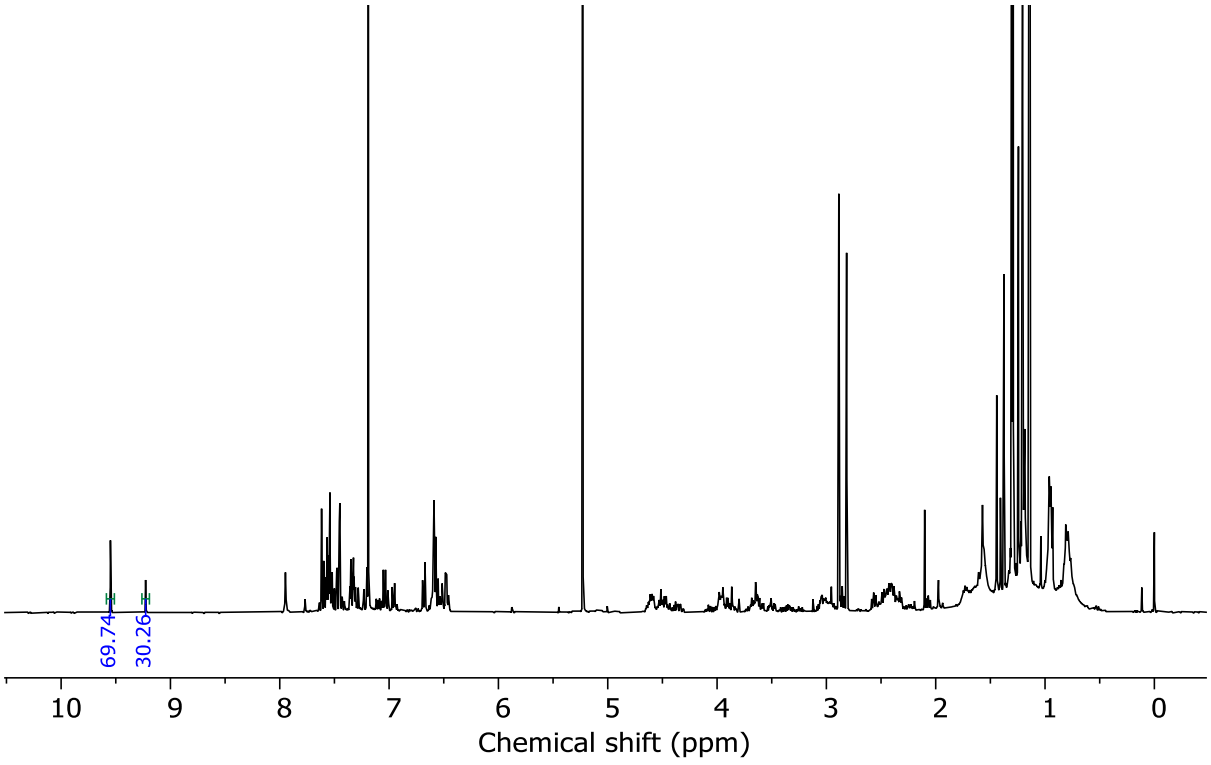

Figure 3.52 - ^{1}H NMR ($CDCl_3$, 400 MHz) of (R_{ma},$R_{co\text{-}c}$)-**4b** and (S_{ma},$R_{co\text{-}c}$)-**4b** prior to purification (70 : 30 *dr*).

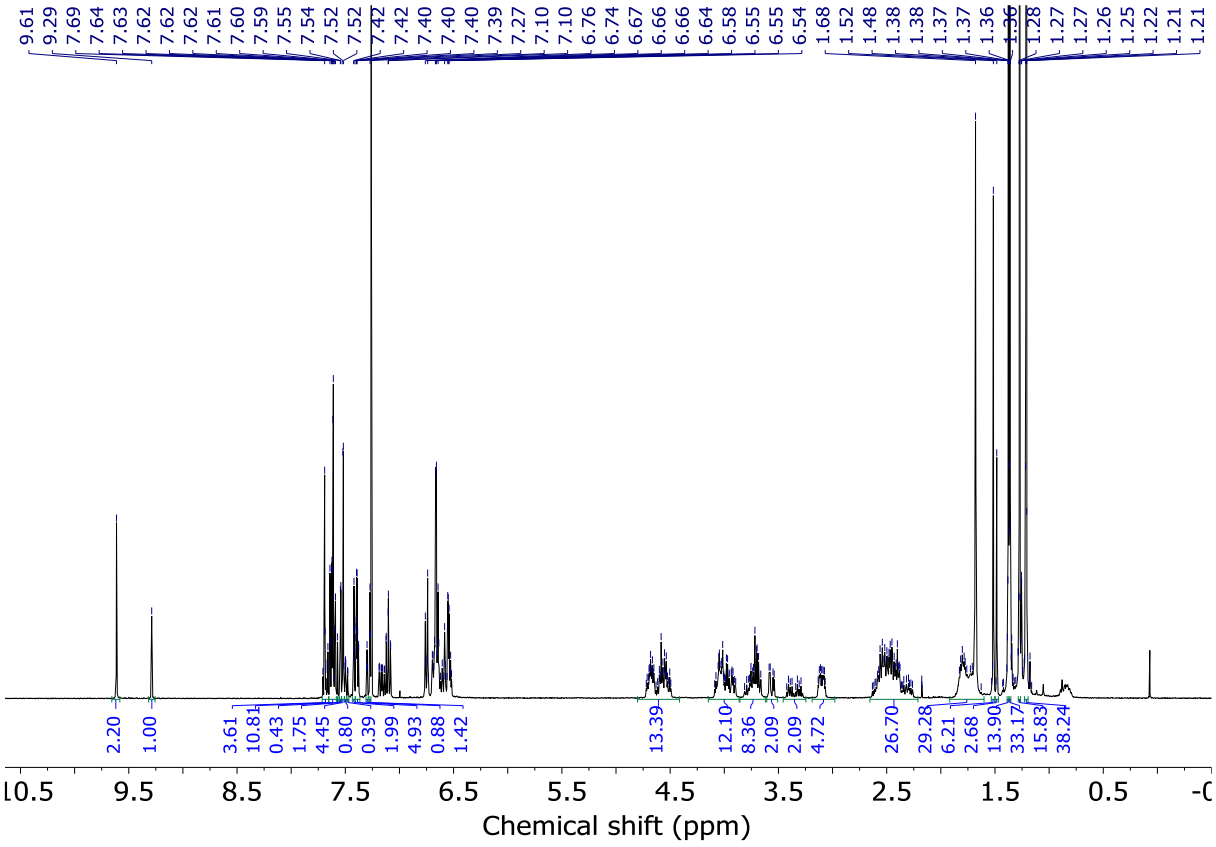

Figure 3.53 - ^{1}H NMR ($CDCl_3$, 400 MHz) of (R_{ma},$R_{co\text{-}c}$)-**4b** and (S_{ma},$R_{co\text{-}c}$)-**4b** (2.2 : 1 *dr*).

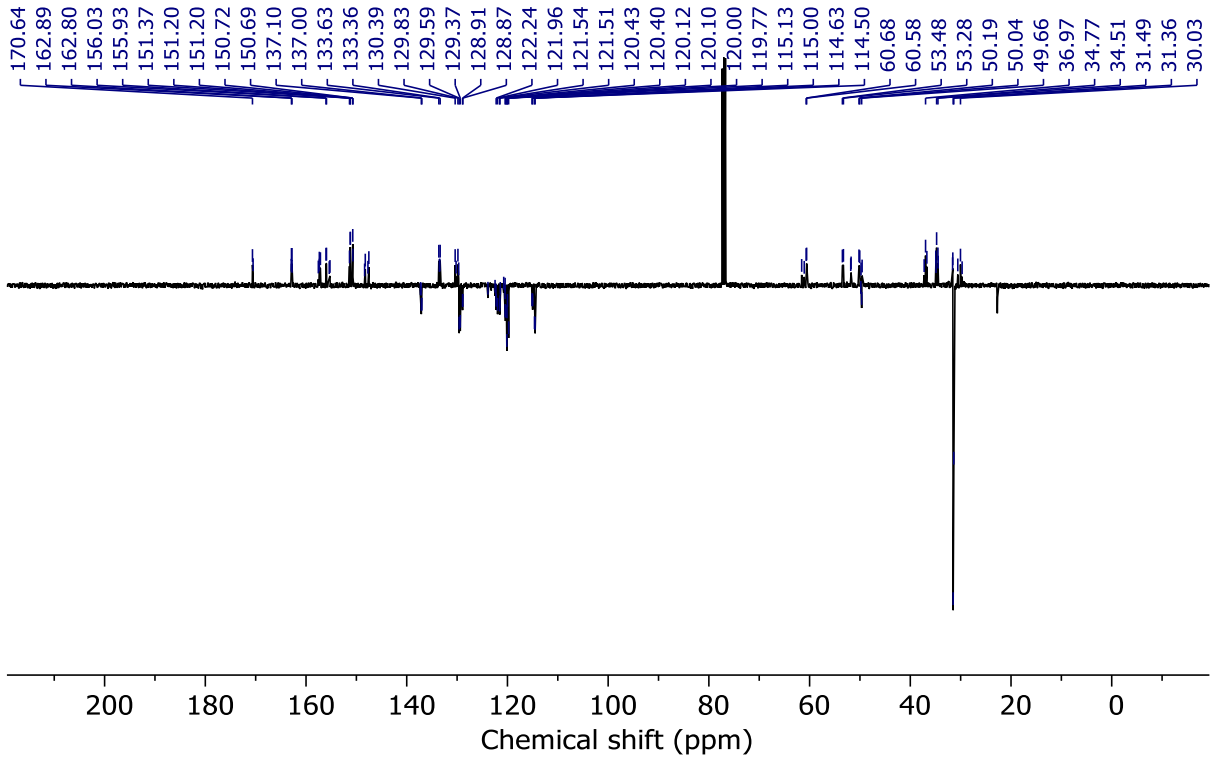

Figure 3.54 - JMOD NMR ($CDCl_3$, 101 MHz) of (R_{ma},$R_{co\text{-}c}$)-**4b** and (S_{ma},$R_{co\text{-}c}$)-**4b** (2.2 : 1 *dr*).

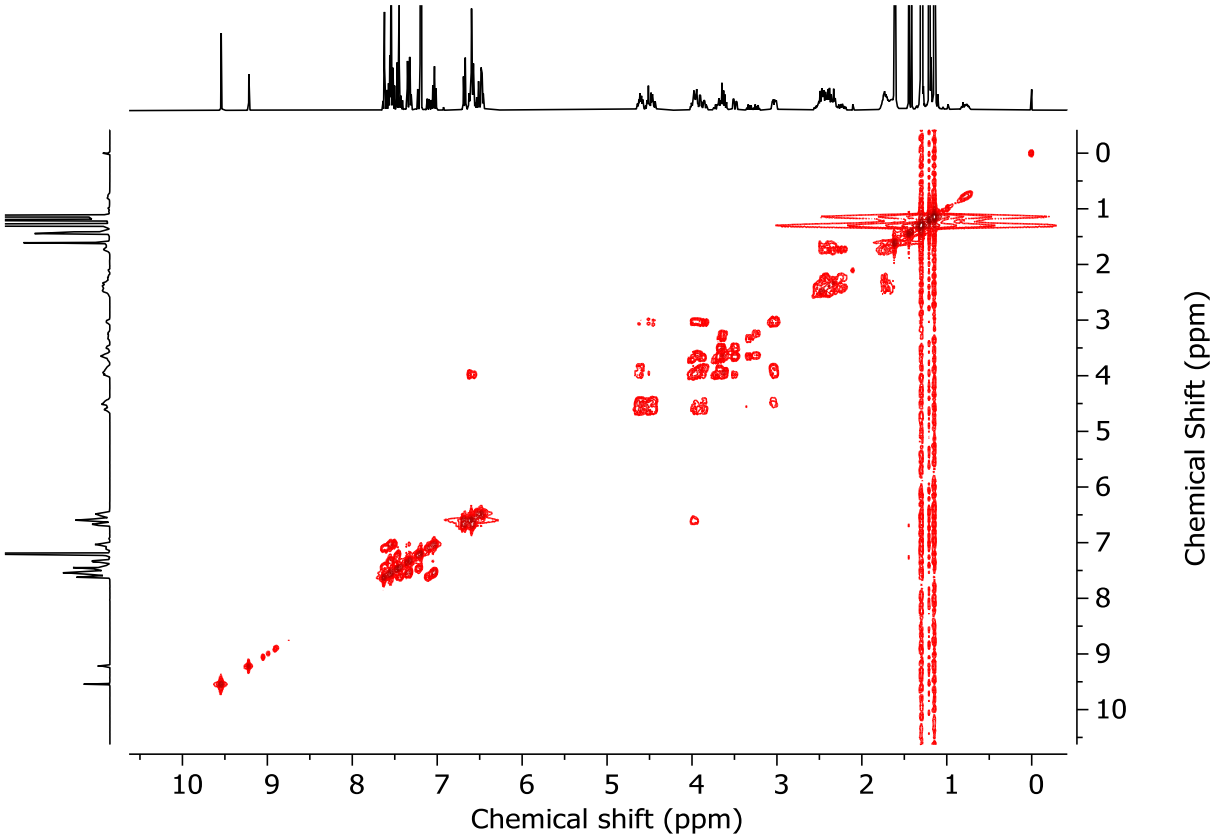

Figure 3.55 - COSY NMR ($CDCl_3$, 400 MHz) of (R_{ma},$R_{co\text{-}c}$)-**4b** and (S_{ma},$R_{co\text{-}c}$)-**4b** (2.2 : 1 *dr*).

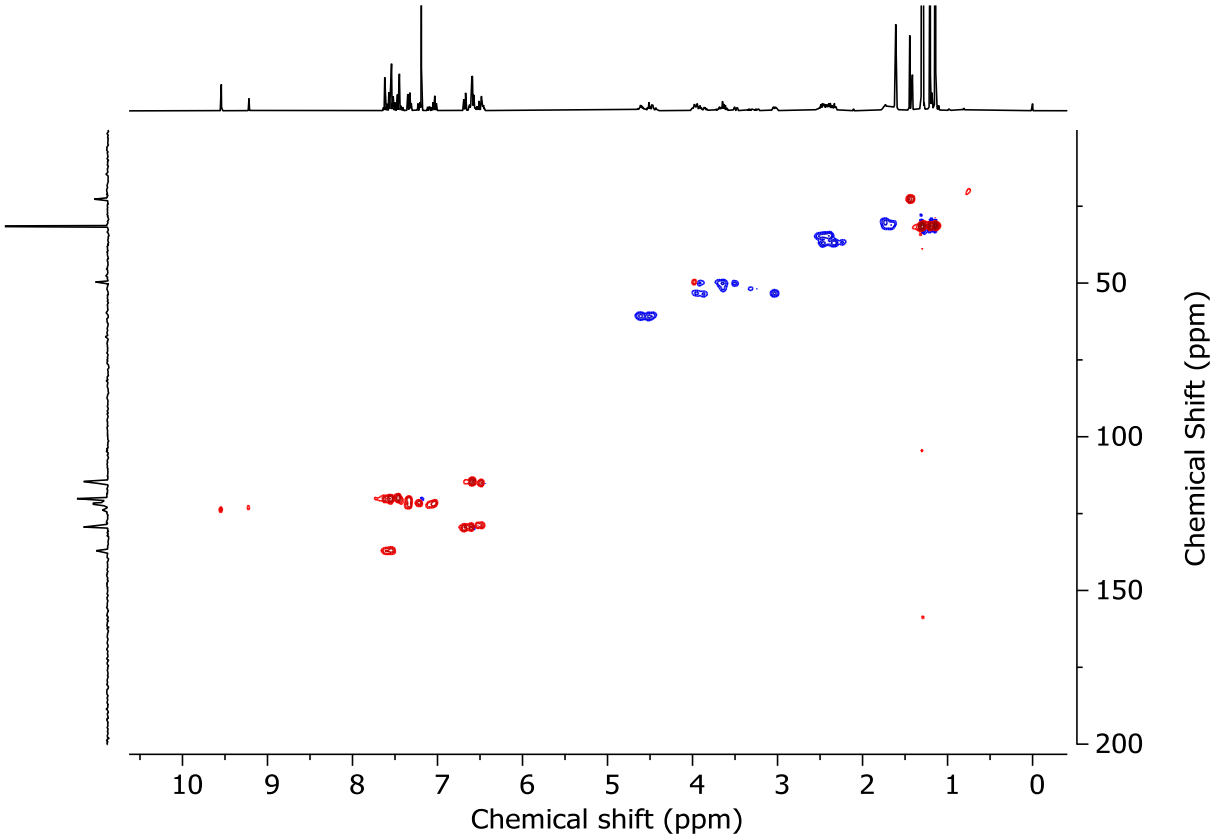

Figure 3.56 - HSQC NMR ($CDCl_3$, 400 MHz) of (R_{ma},$R_{co\text{-}c}$)-**4b** and (S_{ma},$R_{co\text{-}c}$)-**4b** (2.2 : 1 *dr*).

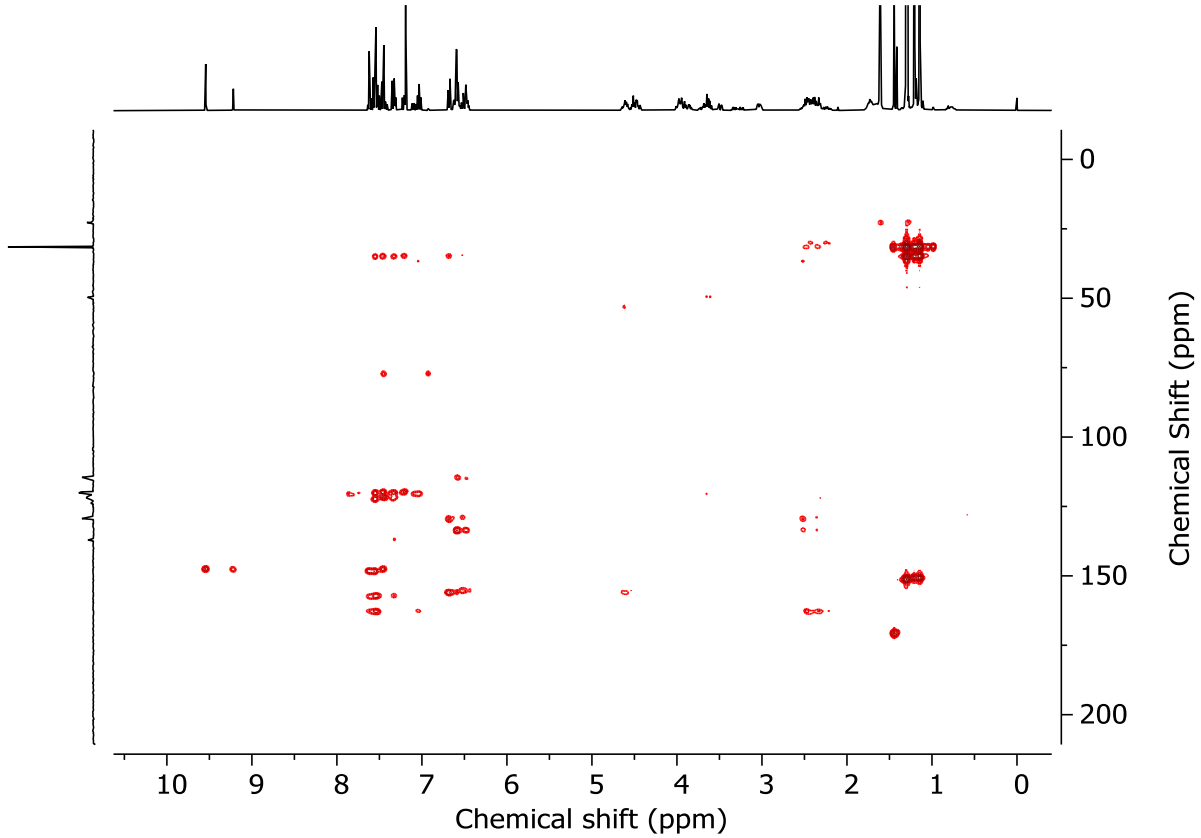

Figure 3.57 - HMBC NMR ($CDCl_3$, 400 MHz) of (R_{ma},$R_{co\text{-}c}$)-**4b** and (S_{ma},$R_{co\text{-}c}$)-**4b** (2.2 : 1 *dr*).

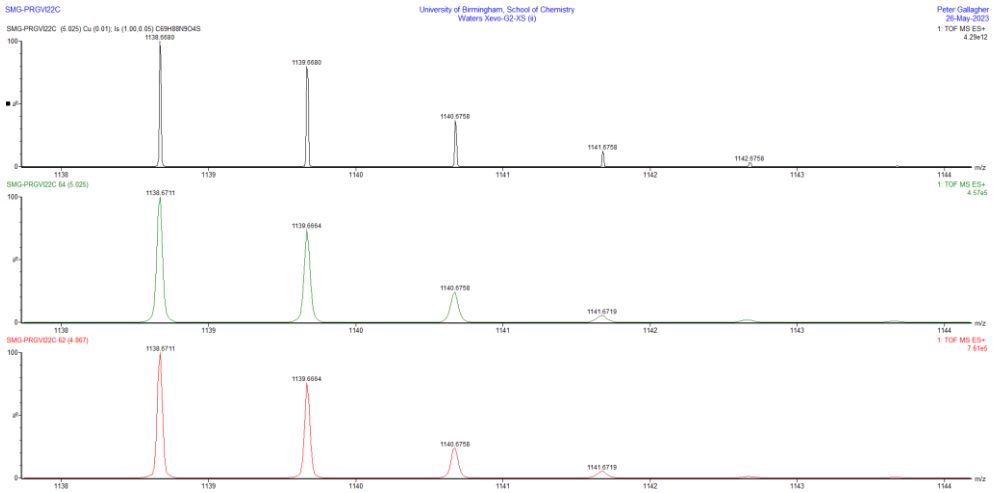

Figure 3.58 - Calculated (top) and observed (middle, bottom) isotopic patterns for rotaxanes **4b**.

Trichloroacetamide rotaxanes 4c

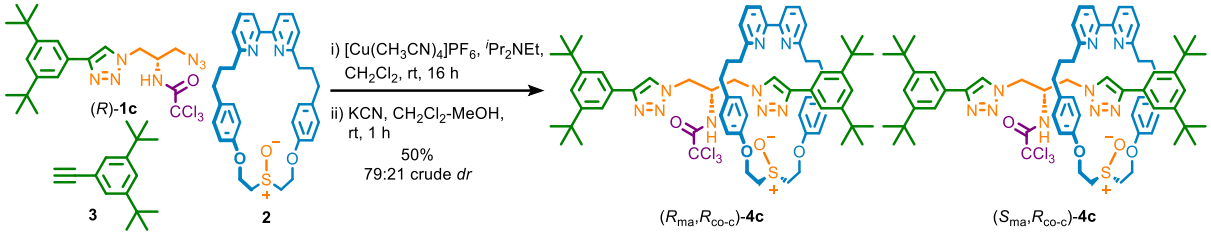

In a CEM vial were added **3** (9.4 mg, 41.7 µmol), (*R*)-**1c** (16.6 mg, 41.7 µmol), **2** (20.0 mg, 38.0 µmol) and $[Cu(CH_3CN)_4PF_6]$ (13.6 mg, 36.0 µmol). The vial was sealed and purged with N_2, then CH_2Cl_2 was added (1.0 mL), followed by $^iPr_2NEt$ (13.2 µL, 75.9 µmol). The solution was stirred at rt for 16 h. MeOH (2 mL mL) and KCN as a solid (24.7 mg, 0.38 mmol) were added and the resulting mixture was stirred vigorously for until colourless. The crude mixture was diluted with CH_2Cl_2 (5 mL) and washed with H_2O (5 mL) then EDTA-NH_3 (5 mL), with separation of aqueous and organic phases. The combined aqueous phase was then extracted with CH_2Cl_2 (3 x 5 mL) and the combined organic extracts were washed with brine (10 mL), dried ($MgSO_{4)}$ and concentrated *in vacuo* to give a sample containing **4c** as a mixture of diastereomers (79 : 21 *dr*, Figure 3.59). Chromatography (CH_2Cl_2-CH_3CN 0→100%) gave **4c** as a white foam (23.5 mg, 50%) as a mixture of diastereoisomers (3.8 : 1 *dr*, Figure 3.60).

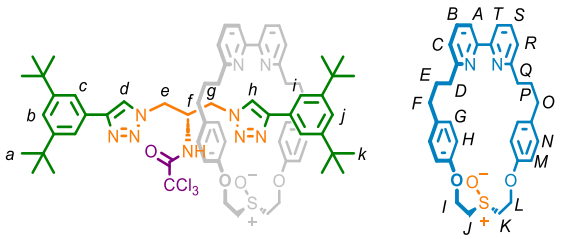

Major Diastereoisomer

^{1}H NMR (500 MHz, $CDCl_3$) δ: 9.58 (s, 1H, H_h), 7.82 (d, *J* = 8.4, 1H, NH), 7.77-7.57 (m, 5H, H_B, H_d, H_i, H_S), 7.54 (d, *J* = 1.8, 2H, H_c), 7.50-7.44 (m, 2H, H_A, H_T), 7.37 (t, *J* = 1.8, 1H, H_b), 7.31 (t, *J* = 2.0, 1H, H_j), 6.74-6.66 (m, 4H, H_G, H_H, H_M or H_N), 6.66-6.58 (m, 4H, H_G, H_H, H_M or H_N), 4.76-4.62 (m, 2H, H_I, H_L), 4.62-4.50 (m, 2H, $H_{I'}$, $H_{L'}$), 4.15 (app. 9plet, *J* = 4.1, 1H, H_f), 4.03-3.61 (m, 5H, H_e, H_g, H_J, H_K), 3.39 (dd, *J* = 14.2, 4.8, 1H, $H_{g'}$), 3.27-3.08 (m, 2H, $H_{J'}$, $H_{K'}$) 2.68-2.23 (m, 8H, H_D, H_F, H_O, H_Q), 1.91-1.51 (m, 4H, H_E, H_P), 1.33 (s, 18H, H_a), 1.24 (s, 18H, H_k)

^{13}C NMR (126 MHz, $CDCl_3$) δ: 162.7, 161.6, 157.5, 157.5, 156.1, 156.0, 151.2, 150.8, 148.3, 147.6, 137.1, 137.1, 133.6, 130.4, 129.7, 129.4, 129.3, 123.6, 122.2, 121.9, 121.8, 121.5, 120.9, 120.5, 120.4, 120.2, 120.0, 114.8, 114.6, 92.0, 60.7, 60.4, 53.2, 52.8, 50.3, 49.2, 49.1, 37.1, 36.9, 34.9, 34.8, 34.7, 34.6, 31.8, 31.5, 31.4, 31.1

Minor Diastereoisomer

^{1}H NMR (500 MHz, $CDCl_3$) δ: 9.02 (s, 1H, H_h), 7.77-7.57 (m, 9H, H_A, H_B, H_c, H_i, H_S, H_T, NH), 7.52 (s, 1H, H_d), 7.42 (t, *J* = 1.7, 1H, H_b), 7.38-7.36 (m, 1H, H_j), 7.21 (d, *J* = 7.7, 1H, H_C), 7.19-7.15 (m, 1H, H_R), 6.56-648. (m, 4H, H_G, H_H, H_M or H_N), 6.48-6.42 (m, 4H, H_G, H_H, H_M or H_N) 4.76-4.62 (m, 2H, H_I, H_L), 4.62-4.50 (m, 2H, $H_{I'}$, $H_{L'}$), 4.07 (dd, *J* = 14.2, 6.5, 1H, H_e or H_g), 4.03-3.61 (m, 6H, H_J, H_K, H_f and H_e and $H_{g'}$ or $H_{e'}$ and H_g), 3.27-3.08 (m, 2H, $H_{J'}$, $H_{K'}$), 2.68-2.23 (m, 8H, H_D, H_F, H_O, H_Q), 1.91-1.51 (m, 4H, H_E, H_P), 1.36 (s, 18H, H_a), 1.34 (s, 18H, H_k)

^{13}C NMR (126 MHz, $CDCl_3$) δ: 162.8, 162.6, 161.8, 157.8, 155.1, 155.1, 151.5, 150.9, 148.6, 147.7, 137.3, 137.3, 133.5, 133.5, 129.9, 129.4, 128.8, 128.7, 123.2, 122.6, 122.3, 122.3, 121.7, 121.0, 120.5, 120.4, 120.3, 120.1, 115.0, 115.0, 91.9, 61.1, 61.1, 52.0, 51.7, 50.9, 48.7, 48.5, 37.4, 37.3, 35.0, 35.0, 34.6, 34.3, 31.9, 31.6, 31.5, 31.0

HR-ESI-MS (+ve) m/z = 1240.5483 $[M+H]^+$ (calc. m/z for $C_{69}H_{85}Cl_3N_9O_4S$ 1240.5510);

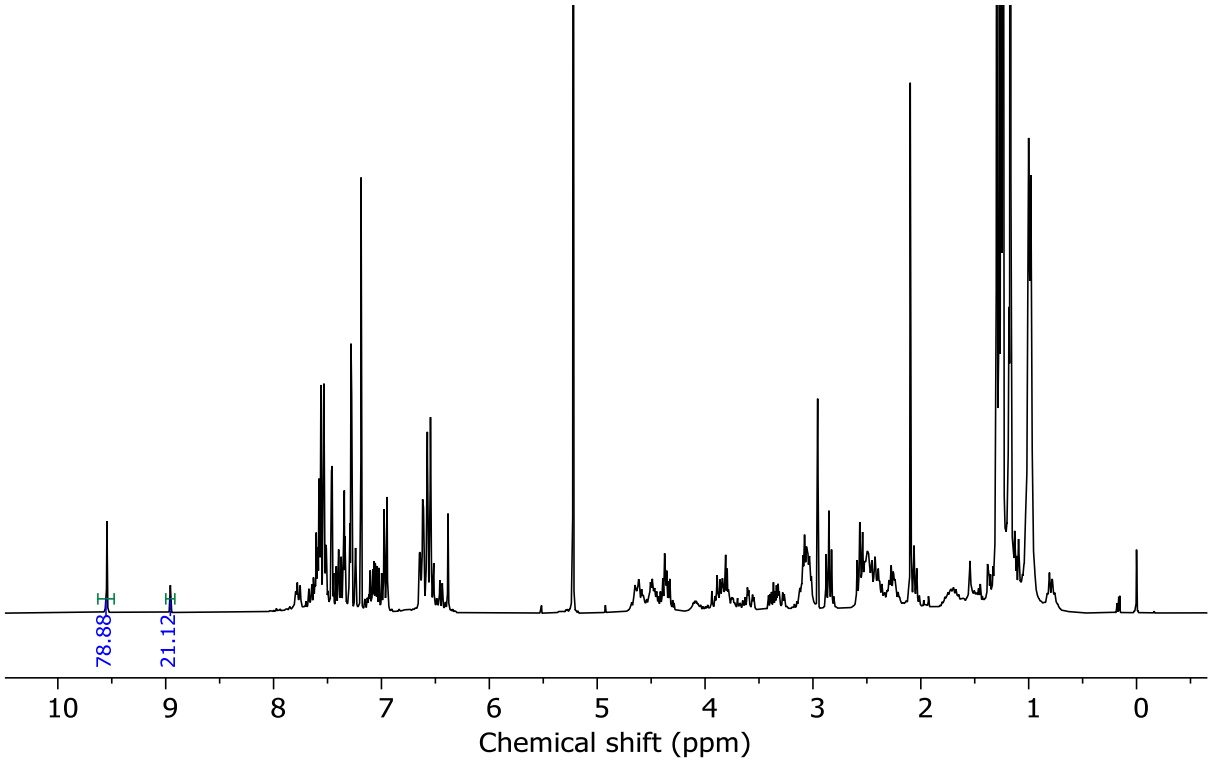

Figure 3.59 - ^{1}H NMR ($CDCl_3$, 400 MHz, 298 K) of (R_{ma},$R_{co\text{-}c}$)-**4c** and (S_{ma},$R_{co\text{-}c}$)-**4c** prior to purification (79 : 21 *dr*).

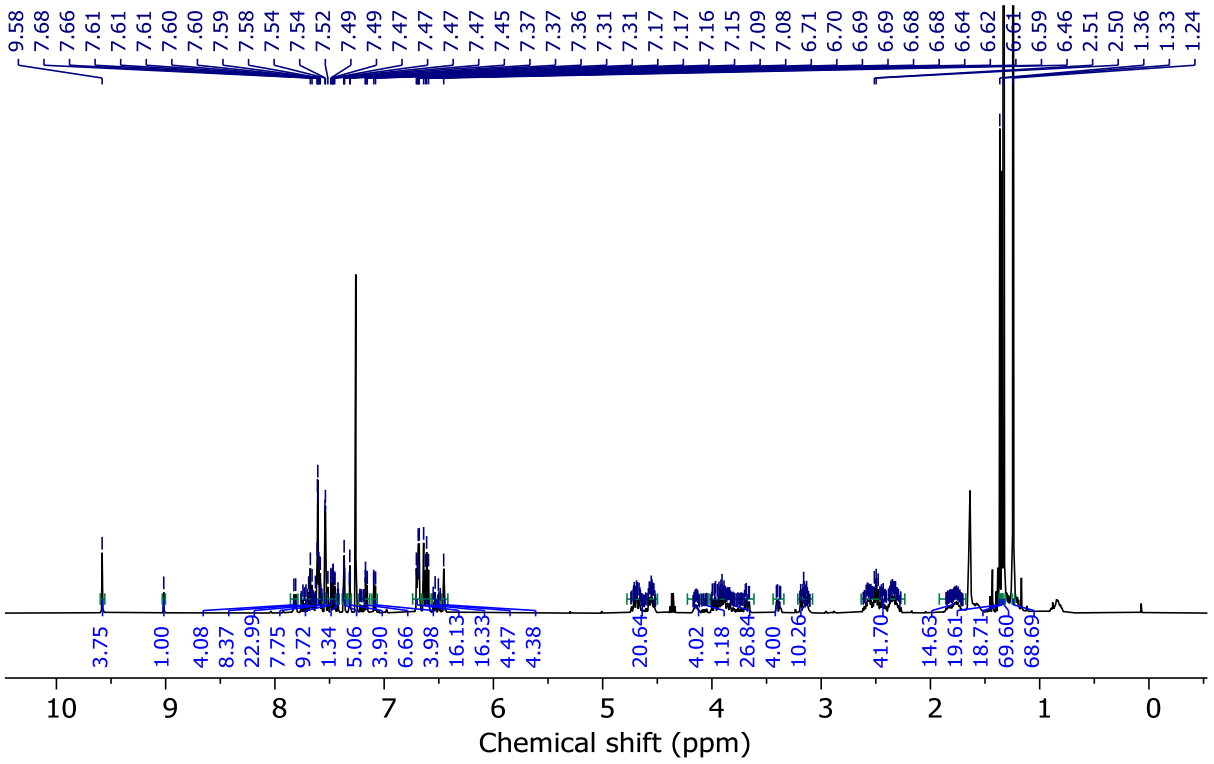

Figure 3.60 - ^{1}H NMR ($CDCl_3$, 500 MHz) of (R_{ma},$R_{co\text{-}c}$)-**4c** and (S_{ma},$R_{co\text{-}c}$)-**4c** (3.8 : 1 *dr*).

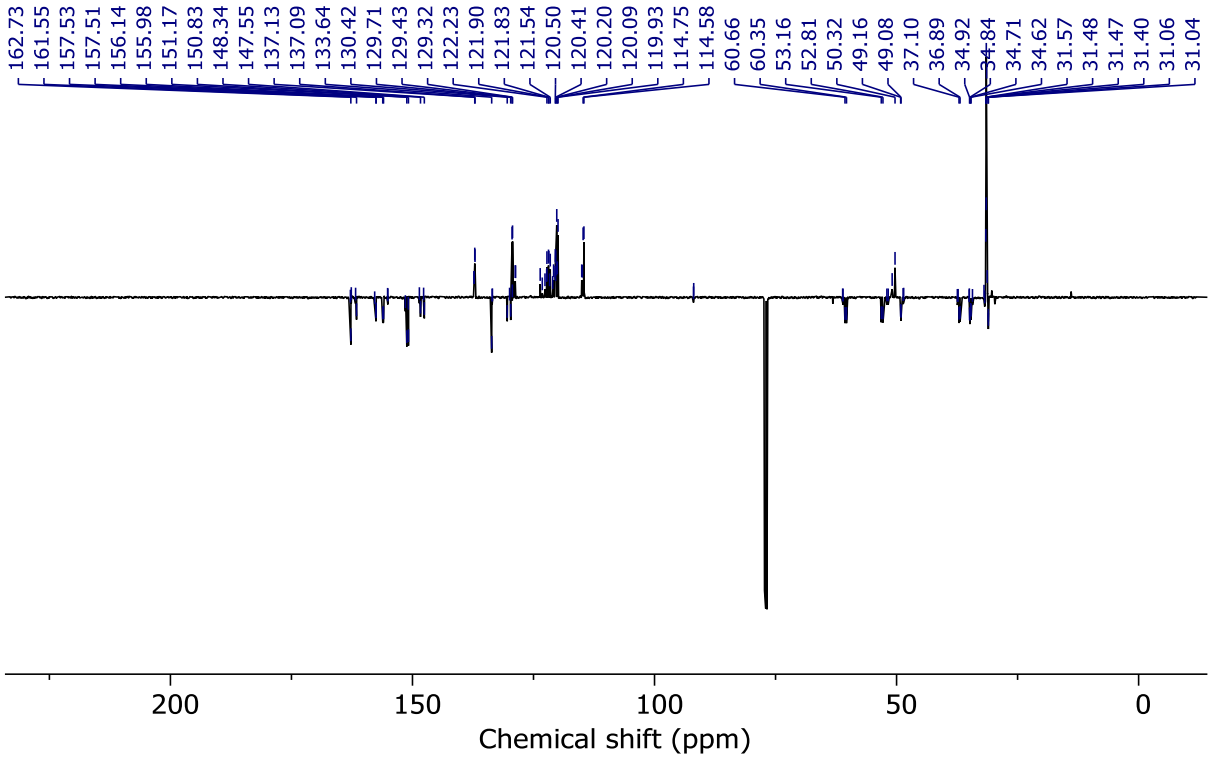

Figure 3.61 - JMOD NMR ($CDCl_3$, 126 MHz) of (R_{ma},$R_{co\text{-}c}$)-**4c** and (S_{ma},$R_{co\text{-}c}$)-**4c** (3.8 : 1 *dr*).

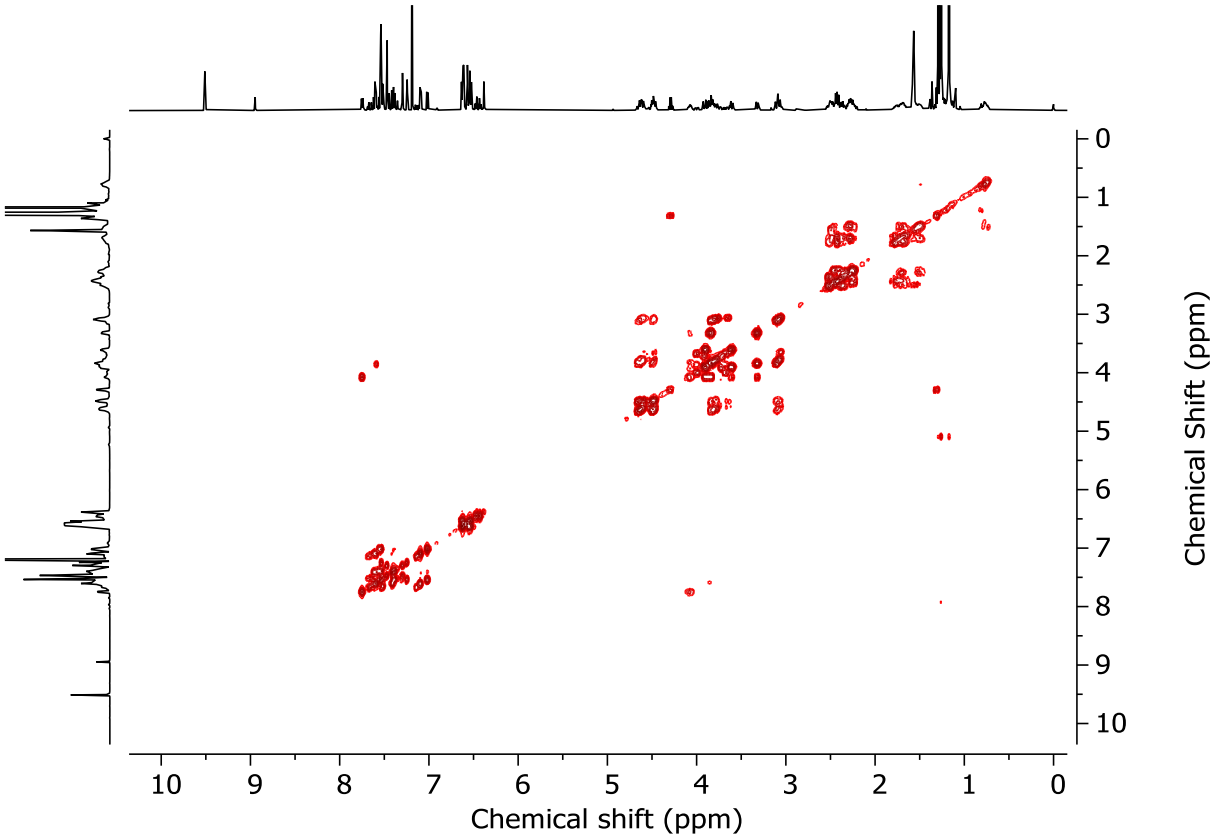

Figure 3.62 - COSY NMR ($CDCl_3$) of (R_{ma},$R_{co\text{-}c}$)-**4c** and (S_{ma},$R_{co\text{-}c}$)-**4c** (3.8 : 1 *dr*).

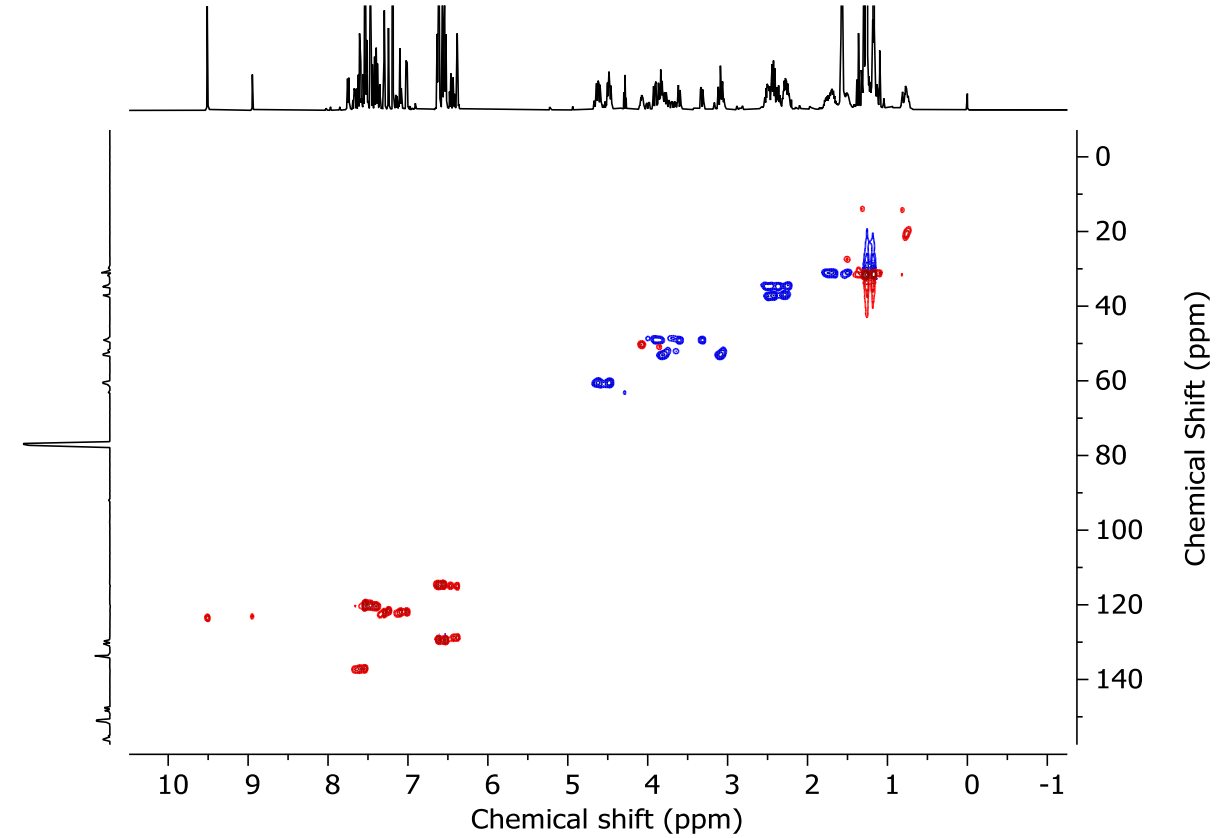

Figure 3.63 - HSQC NMR ($CDCl_3$) of (R_{ma},$R_{co\text{-}c}$)-**4c** and (S_{ma},$R_{co\text{-}c}$)-**4c** (3.8 : 1 *dr*).

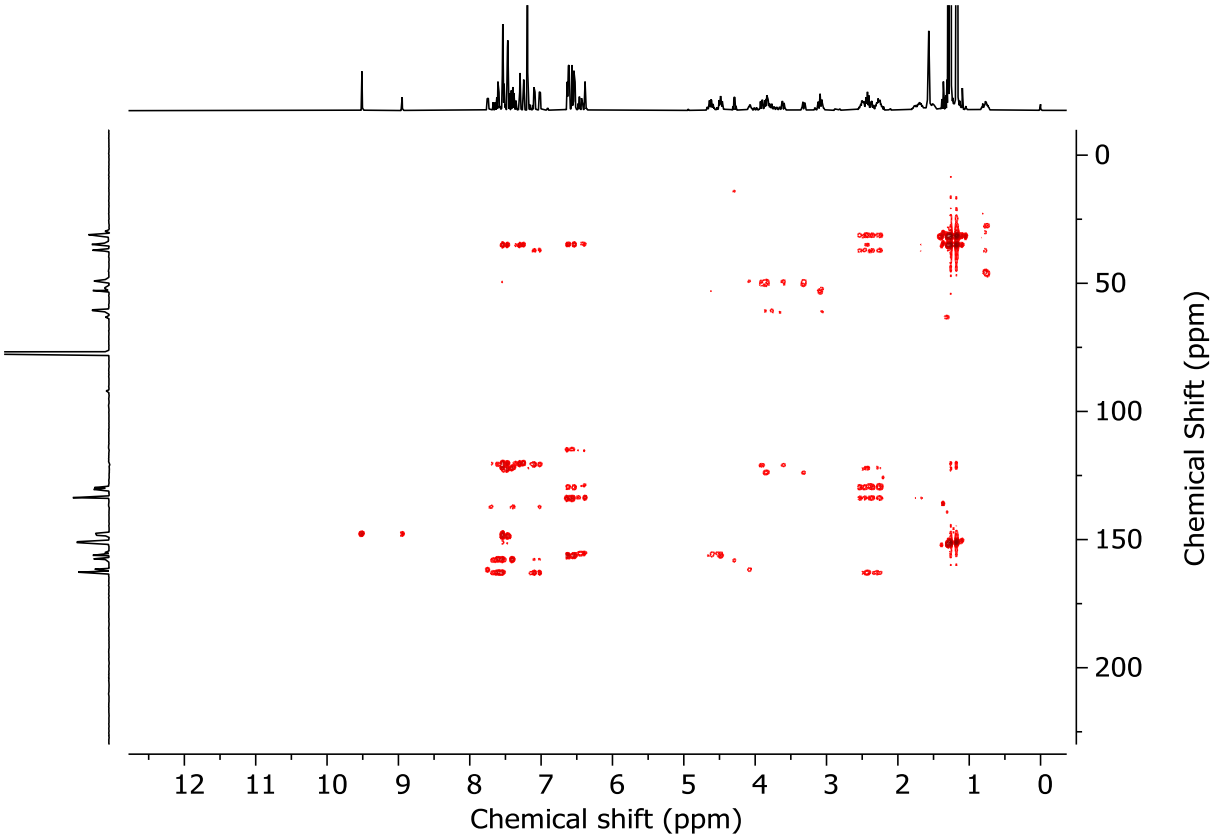

Figure 3.64 - HMBC NMR ($CDCl_3$) of (R_{ma},$R_{co\text{-}c}$)-**4c** and (S_{ma},$R_{co\text{-}c}$)-**4c** (3.8 : 1 *dr*).

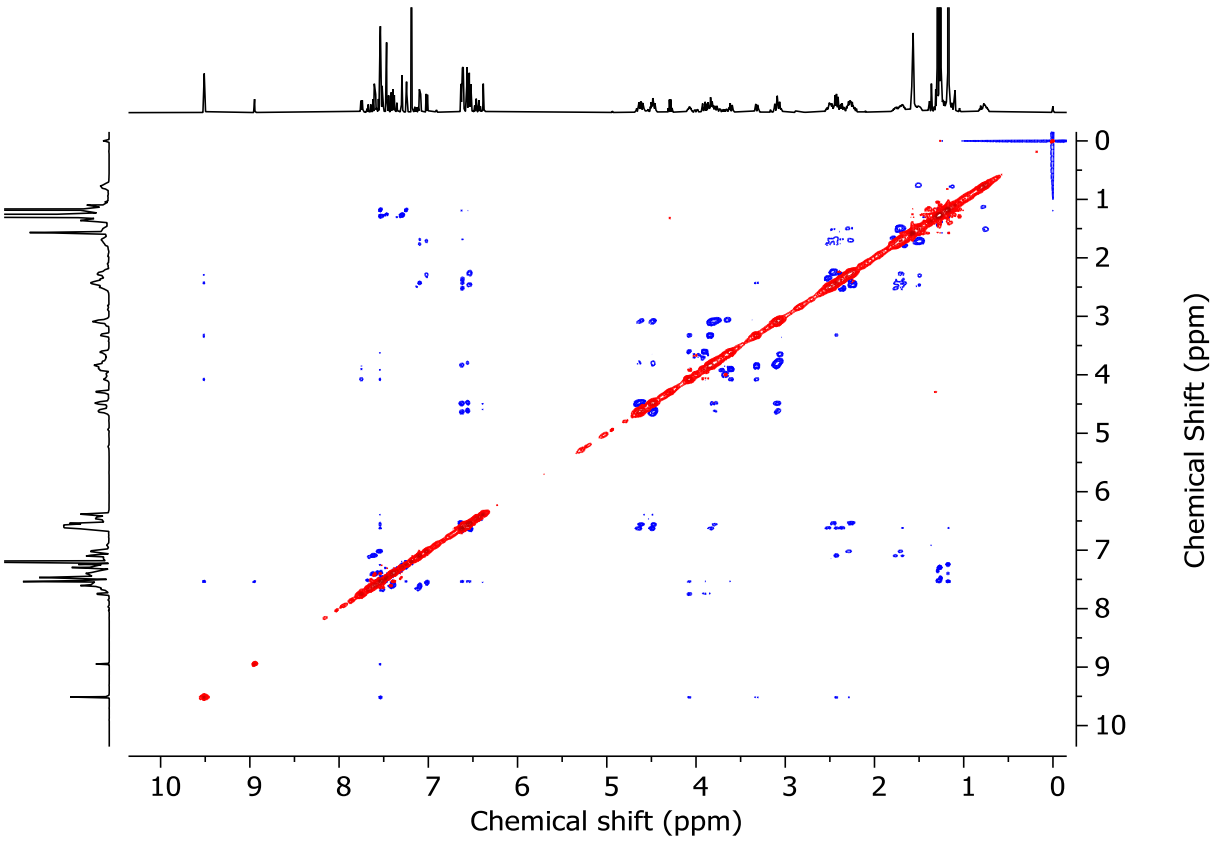

Figure 3.65 - NOESY NMR ($CDCl_3$) of (R_{ma},$R_{co\text{-}c}$)-**4c** and (S_{ma},$R_{co\text{-}c}$)-**4c** (3.8 : 1 *dr*).

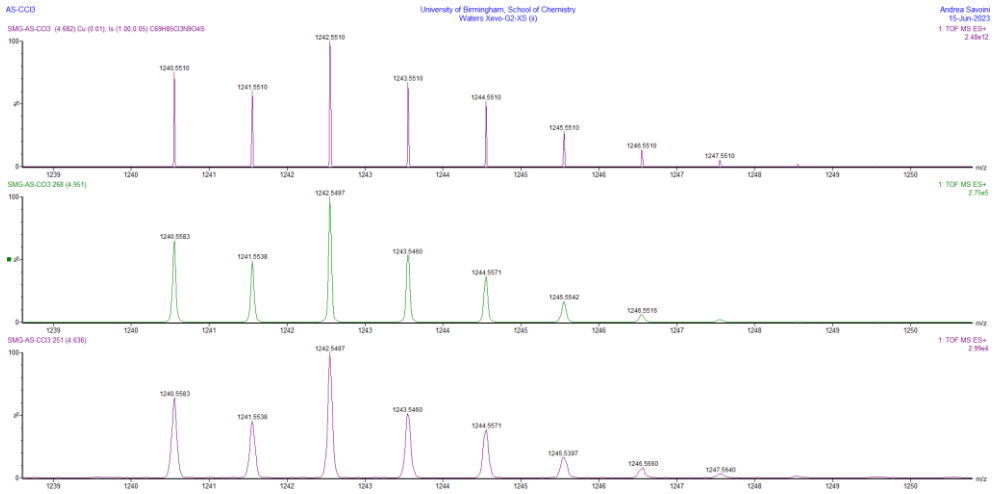

Figure 3.66 - Calculated (top) and observed (middle, bottom) isotopic patterns for rotaxanes **4c**.

Trifluoroacetamide rotaxanes 4d

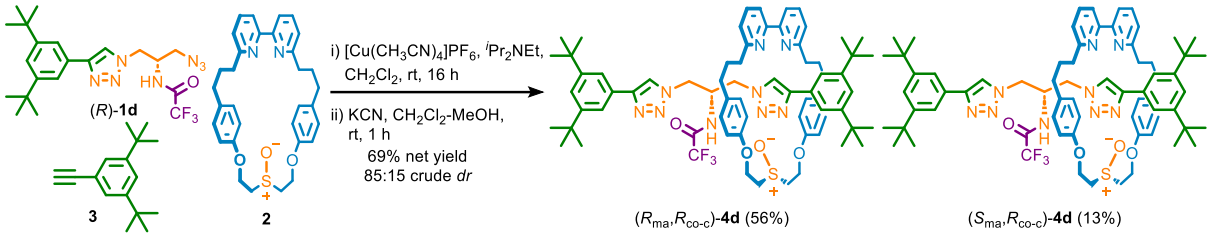

In a CEM vial were added the **3** (18.6 mg, 86.8 µmol), (*R*)-**1d** (39.0 mg, 86.4 µmol), **2** (40.3 mg, 76.5 µmol) and $[Cu(CH_3CN)_4PF_6]$ (27.9 mg, 74.9 µmol). The vial was sealed and purged with N_2, then CH_2Cl_2 was added (1.9 mL), followed by $^{i}Pr_2NEt$ (27 µL, 155 µmol). The solution was stirred at rt for 16 h. MeOH (2 mL mL) and KCN as a solid (49.8 mg, 765 µmol) were added and the resulting mixture was stirred vigorously for until colourless. The crude mixture was diluted with CH_2Cl_2 (5 mL) and washed with H_2O in two portions (10 mL and 5 mL), with separation of aqueous and organic phases. The combined aqueous phase was then extracted with CH_2Cl_2 (3 x 5 mL) and the combined organic extracts were washed with brine (10 mL), dried ($MgSO_4$) and concentrated *in vacuo* to give a sample containing **4d** as a mixture of diastereomers (85 : 15 *dr*, Figure 3.67). Chromatography (CH_2Cl_2-CH_3CN 0→25% then 0→5% MeOH) gave rotaxanes **4d** as white foams; (R_{ma},$R_{co\text{-}c}$)-**4d** (51.1 mg, 42.8 µmol, 56%), (S_{ma},$R_{co\text{-}c}$)-**4d** (12.1 mg, 13%).

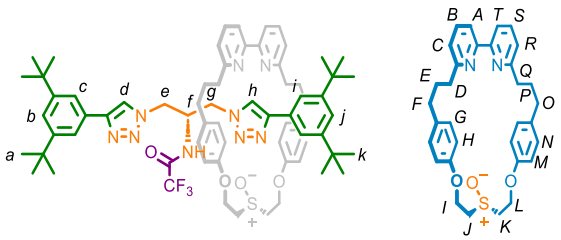

(R_{ma},$R_{co\text{-}c}$)-**4d** - Major diastereoisomer

^{1}H NMR (400 MHz, $CDCl_3$) δ: 10.0 (s, 1H, H_h), 8.30 (d, J = 8.4, 1H, NH), 7.69 (t, J = 7.9, 1H, H_B), 7.60 (d, J = 1.9, 2H, H_c or H_i), 7.55 (t, J = 7.7, 1H, H_S), 7.47 (d, J = 7.7, 1H, H_A), 7.44 (s, 1H, H_d), 7.43-7.39 (m, 3H, H_T, H_c or H_i), 7.33 (t, J = 1.9, 1H, H_b or H_j), 7.28 (t, J = 1.9, 1H, H_b or H_j), 7.21 (d, J = 7.5, 1H, H_C), 7.00, (d, J = 7.7, 1H, H_R), 6.86 (d, J = 8.9, 2H, H_H or H_M), 6.83-7.83 (m, 4H, H_G and H_H or H_M and H_N), 6.65 (d, J = 8.5, 2H, H_G or H_N), 4.82-4.64 (m, 2H, H_I, H_L), 4.59-4.39 (m, 3H, H_f, $H_{I'}$, $H_{L'}$), 3.90 (dd, J = 14.3, 10.0, 1H, H_g), 3.78-3.62 (m, 3H, H_e, H_J, H_K), 3.38 (dd, J = 14.3, 3.6, 1H, $H_{e'}$), 3.19-3.01 (m, 3H, $H_{e'}$, $H_{J'}$, $H_{K'}$), 2.74-2.62 (m, 1H, H_F or H_O), 2.60-2.42 (m, 4H, H_D or H_Q, H_F or H_O and $H_{F'}$ or $H_{O'}$), 2.36-2.09 (m, 2H, H_D or H_O), 2.09-1.66 (m, 4H, H_E, H_P), 1.31 (s, 18H, H_a or H_k), 1.21 (s, 18H, H_a or H_k).

^{13}C NMR (101 MHz, $CDCl_3$) δ: 162.9, 162.7, 157.3, 157.1, 156.9, 156.7 (q, $J_{C\text{-}P}$ = 36.5) 156.6, 156.3, 151.0, 150.8, 148.1, 148.1, 137.3, 137.0, 134.0, 133.8, 130.5, 129.9, 129.7, 129.6, 123.5, 122.0, 121.8, 121.7, 121.5, 120.7, 120.3, 120.1, 120.0, 120.0, 119.9, 115.4 (q, $J_{C\text{-}P}$ = 287.3), 115.0, 114.6, 60.5, 60.1, 53.1, 52.7, 49.6, 49.2, 48.2, 36.8, 36.7, 34.9, 34.8, 34.7, 31.6, 31.5, 31.4, 31.4, 31.4, 31.3, 30.3.

LR-ESI-MS (+ve) m/z = 1192.6 $[M+H]^+$ (calc. m/z for $C_{69}H_{84}F_3N_9O_4S$);

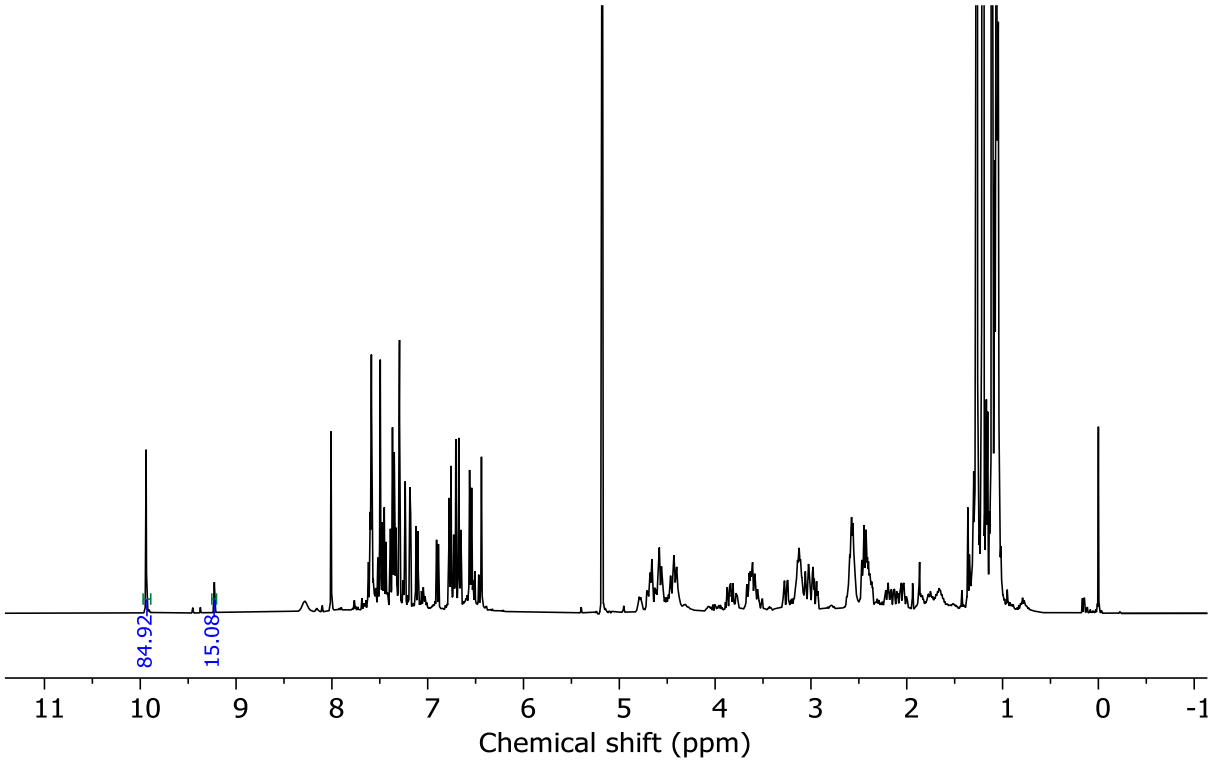

Figure 3.67 - ^{1}H NMR ($CDCl_3$, 400 MHz) of (R_{ma},$R_{co\text{-}c}$)-**4d** and (S_{ma},$R_{co\text{-}c}$)-**4d** prior to purification (85 : 15 *dr*).

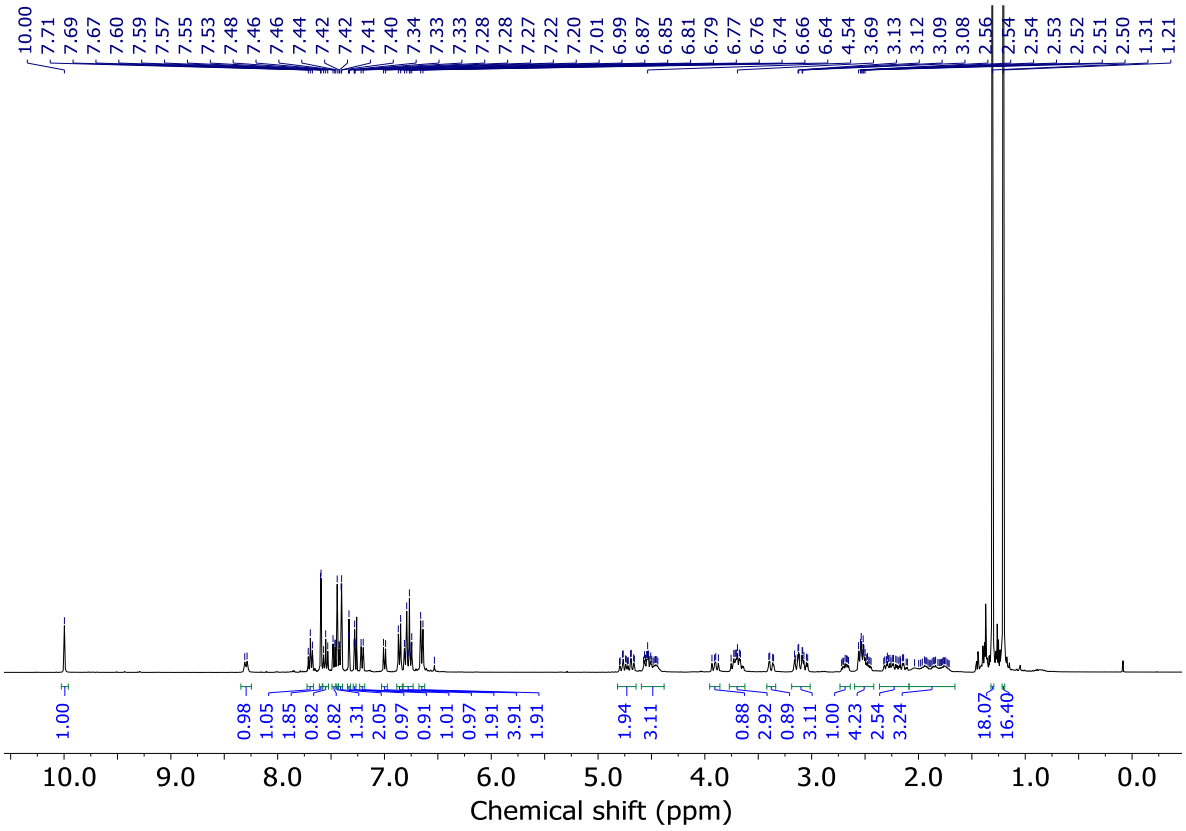

Figure 3.68 - ^{1}H NMR ($CDCl_3$, 400 MHz) of (R_{ma},$R_{co\text{-}c}$)-**4d**.

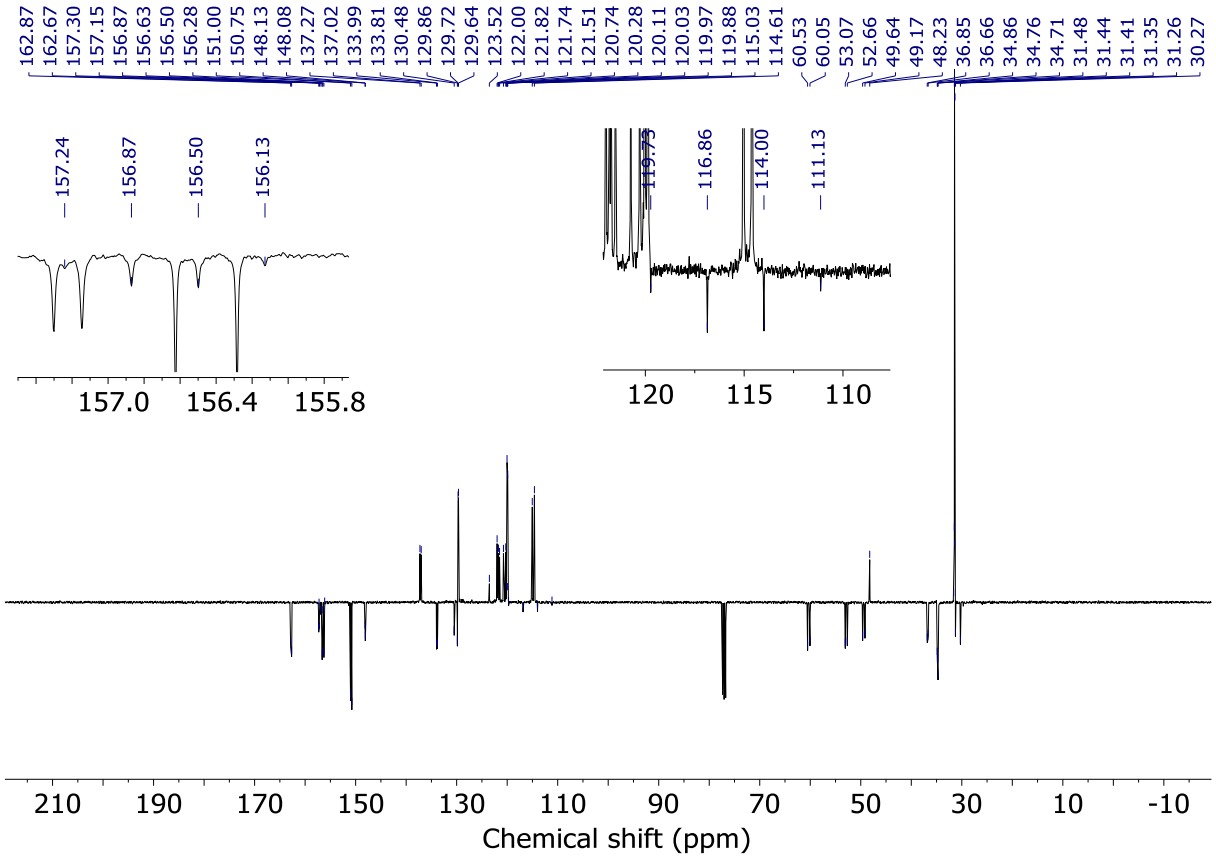

Figure 3.69 - JMOD NMR ($CDCl_3$, 101 MHz) of (R_{ma},$R_{co\text{-}c}$)-**4d**.

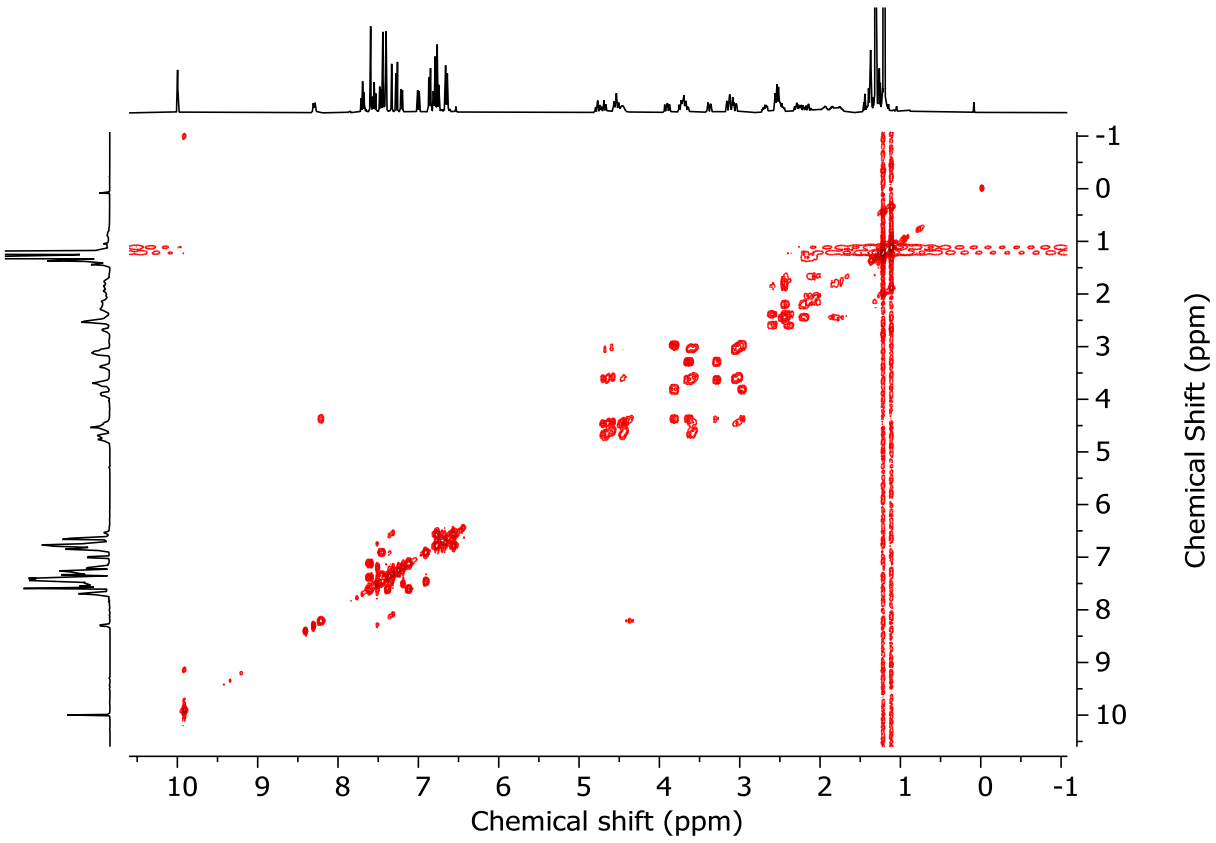

Figure 3.70 - COSY NMR ($CDCl_3$) of (R_{ma},$R_{co\text{-}c}$)-**4d**.

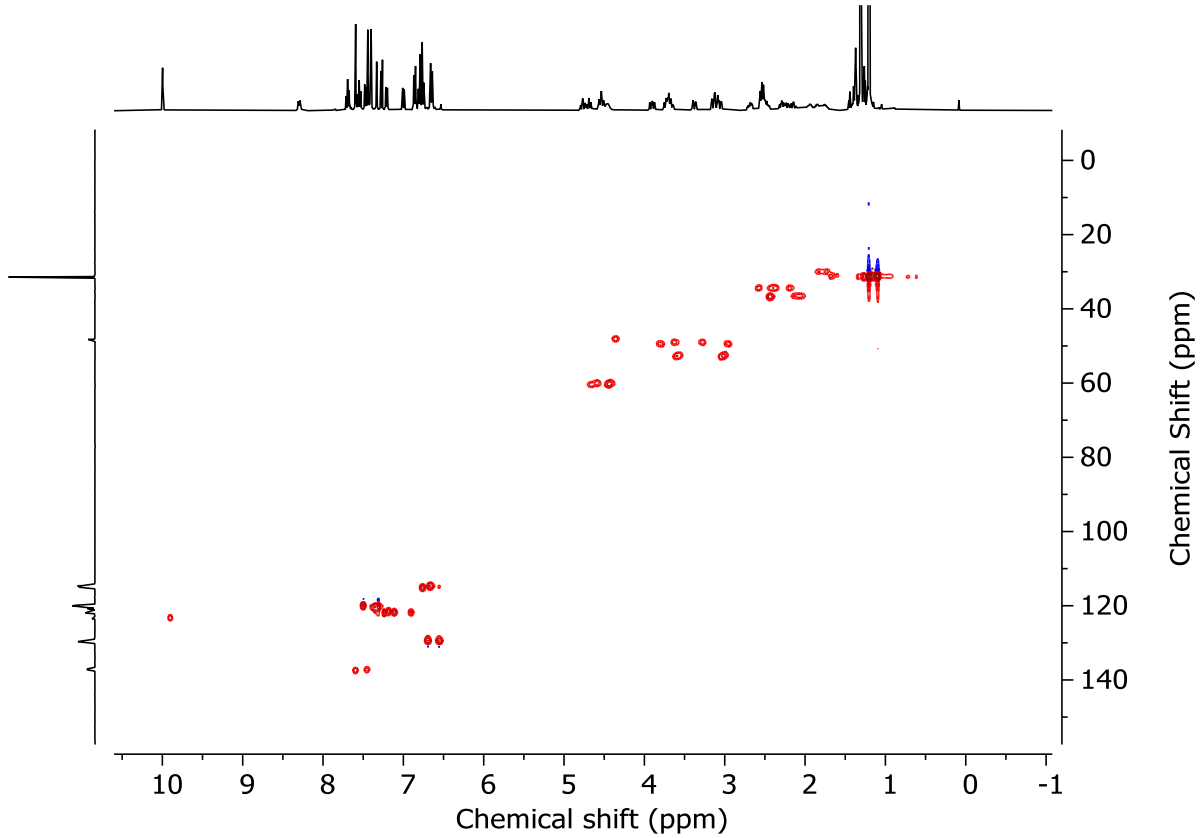

Figure 3.71 - HSQC NMR ($CDCl_3$) of (R_{ma},$R_{co\text{-}c}$)-**4d**.

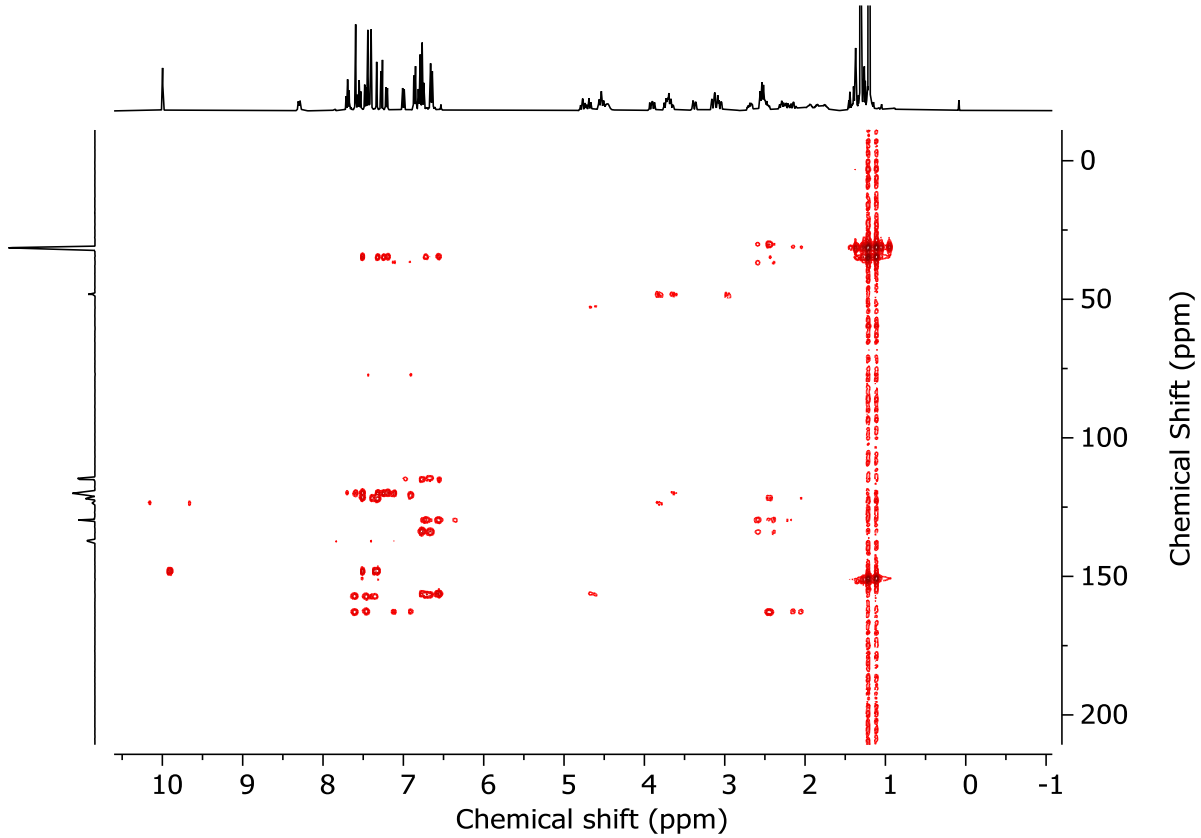

Figure 3.72 - HMBC NMR ($CDCl_3$) of (R_{ma},$R_{co\text{-}c}$)-**4d**.

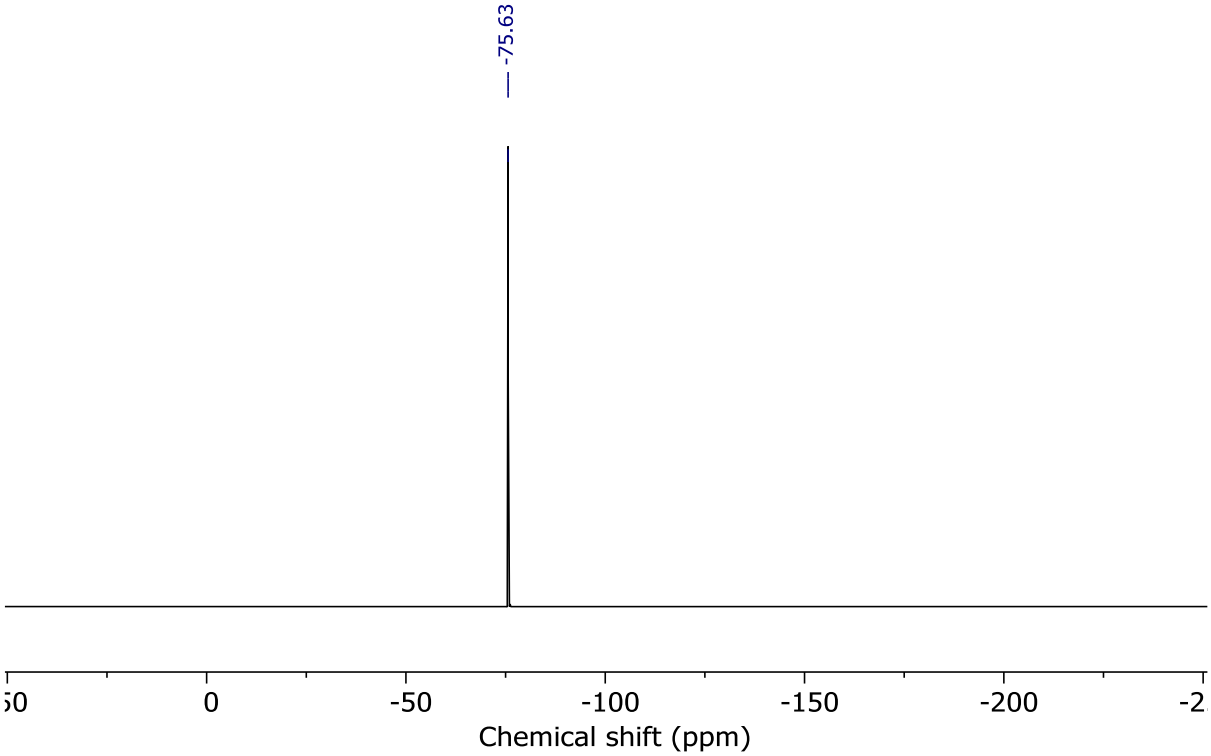

Figure 3.73 - ^{19}F NMR ($CDCl_3$, 376 MHz) of (R_{ma},$R_{co\text{-}c}$)-**4d**.

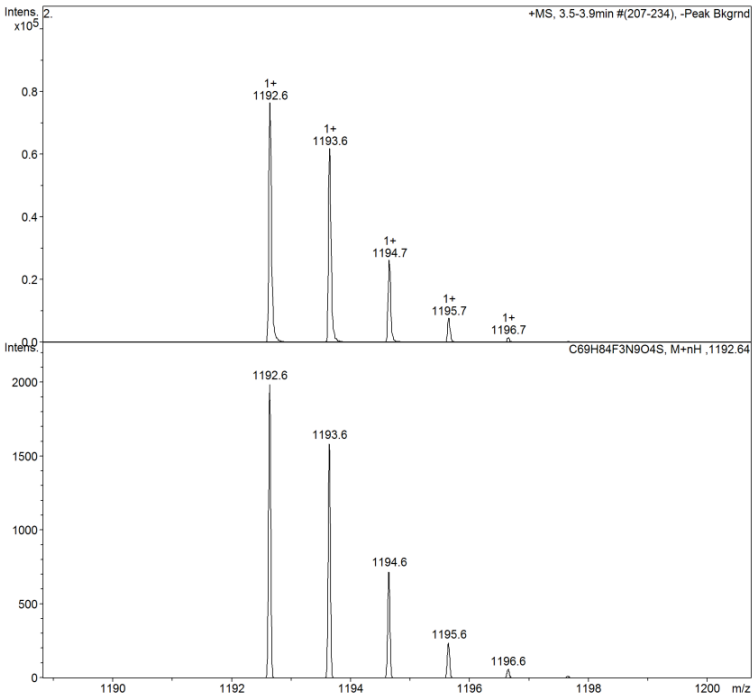

Figure 3.74 - Observed (top) and calculated (bottom) isotopic patterns for rotaxanes (R_{ma},$R_{co\text{-}c}$)-**4d**.

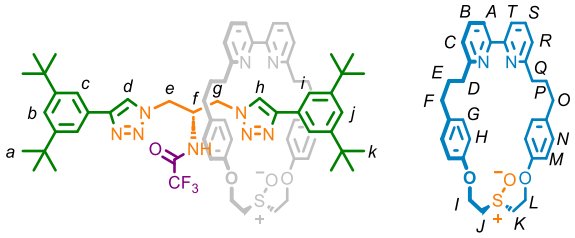

(S_{ma},$R_{co\text{-}c}$)-**4d** - Minor diastereoisomer

^{1}H NMR (500 MHz, $CDCl_3$) δ: 9.28 (s, 1H, H_h), 7.79 (d, J = 7.4, 1H, NH), 7.73 (t, J = 7.9, 1H, H_B), 7.69 (t, J = 7.7, 1H, H_S), 7.60 (d, J = 1.8, 2H, H_i), 7.58-7.55 (m, 3H, H_A, H_c), 7.54 (t, J = 1.1, 1H, H_T), 7.46 (s, 1H, H_d), 7.42 (t, J = 1.7, 1H, H_b), 7.35 (t, J = 1.8, 1H, H_j), 7.21 (d, J = 7.9, 1H, H_C), 7.16 (d, J = 7.9, 1H, H_R), 6.63-6.50 (m, 8H, H_G, H_H, H_M, H_N), 4.74-4.48 (m, 4H, H_I, H_L), 4.12-4.05 (m, 1H, H_f), 4.01 (dd, J = 14.4, 6.6, 1H, H_g), 3.88 (dd, J = 14.6, 4.1, 1H, H_g), 3.77 (dd, J = 14.6, 6.9, 1H, $H_{g`}$), 3.68 (dt, $J$ = 13.3, 6.5, 1H, $H_J$ or $H_K$), 3.66-3.55 (m, 2H, $H_{e`}$, H_J or H_K), 3.39-3.24 (m, 2H, $H_{J`}$, $H_{K`}$), 2.62-2.29 (m, 8H, H_D, H_F, H_O, H_Q), 1.87-1.52 (m, 4H, H_E, H_P), 1.37 (s, 18H, H_a), 1.30 (s, 18H, H_k)

^{13}C NMR (126 MHz, $CDCl_3$) δ: 163.0, 162.8, 157.7, 157.7, 157.2 (q, $J_{C\text{-}F}$ = 37.3), 155.7, 155.6, 154.0, 151.5, 151.3, 151.0, 148.7, 147.9, 137.8, 137.4, 134.7, 133.8, 133.8, 130.8, 130.2, 129.6, 129.2, 129.0, 128.3, 125.2, 125.1, 123.4, 122.7, 122.4, 122.3, 121.8, 120.8, 120.7, 120.6, 120.3, 120.3, 118.8, 115.5 (q, $J_{C\text{-}F}$ = 286.2) 115.4, 115.2, 61.5, 61.3, 52.0, 51.3, 49.8, 48.8, 48.7, 37.3, 37.3, 35.1, 35.1, 34.7, 34.6, 31.6, 31.5, 31.4, 29.9, 29.9.

LR-ESI-MS (+ve) m/z = 1192.6 $[M+H]^+$ (calc. m/z for $C_{69}H_{84}F_3N_9O_4S$);

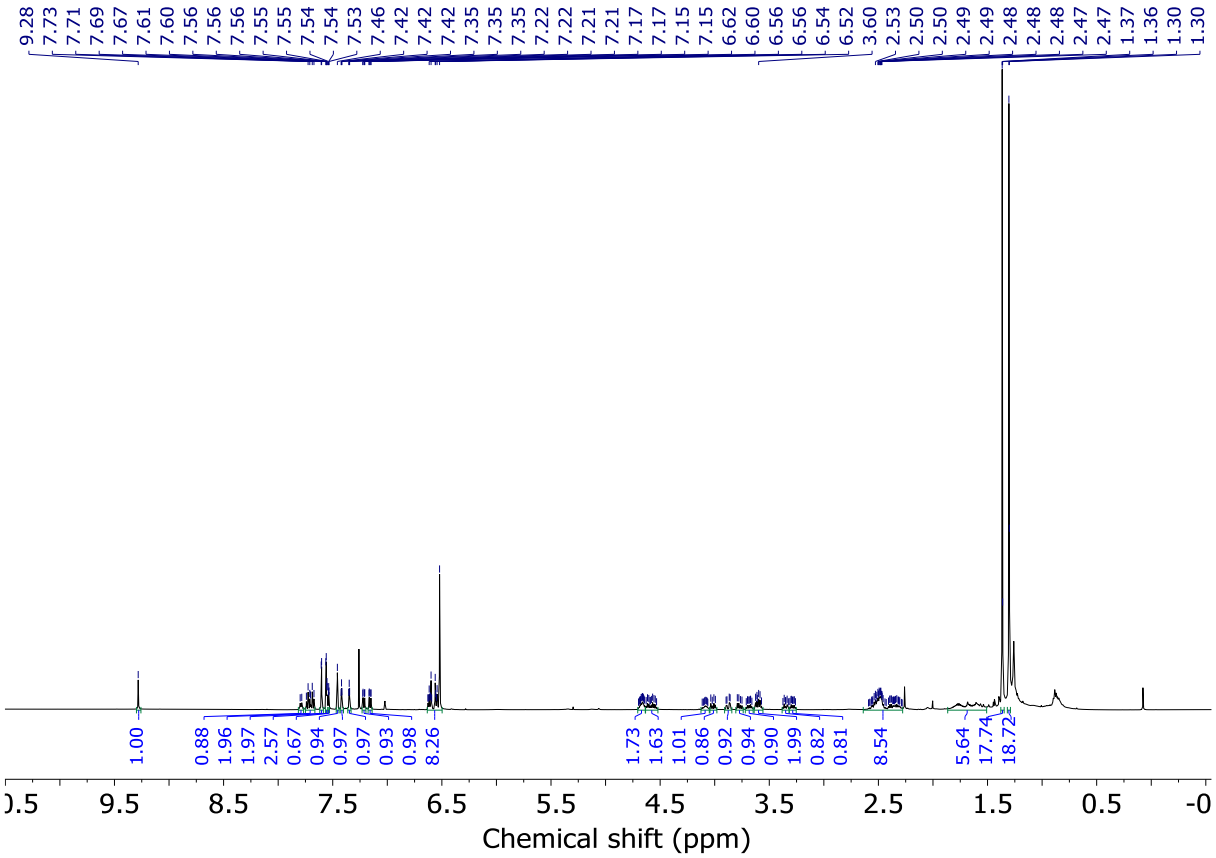

Figure 3.75 - ^{1}H NMR ($CDCl_3$, 500 MHz) of (S_{ma},$R_{co\text{-}c}$)-**4d**.

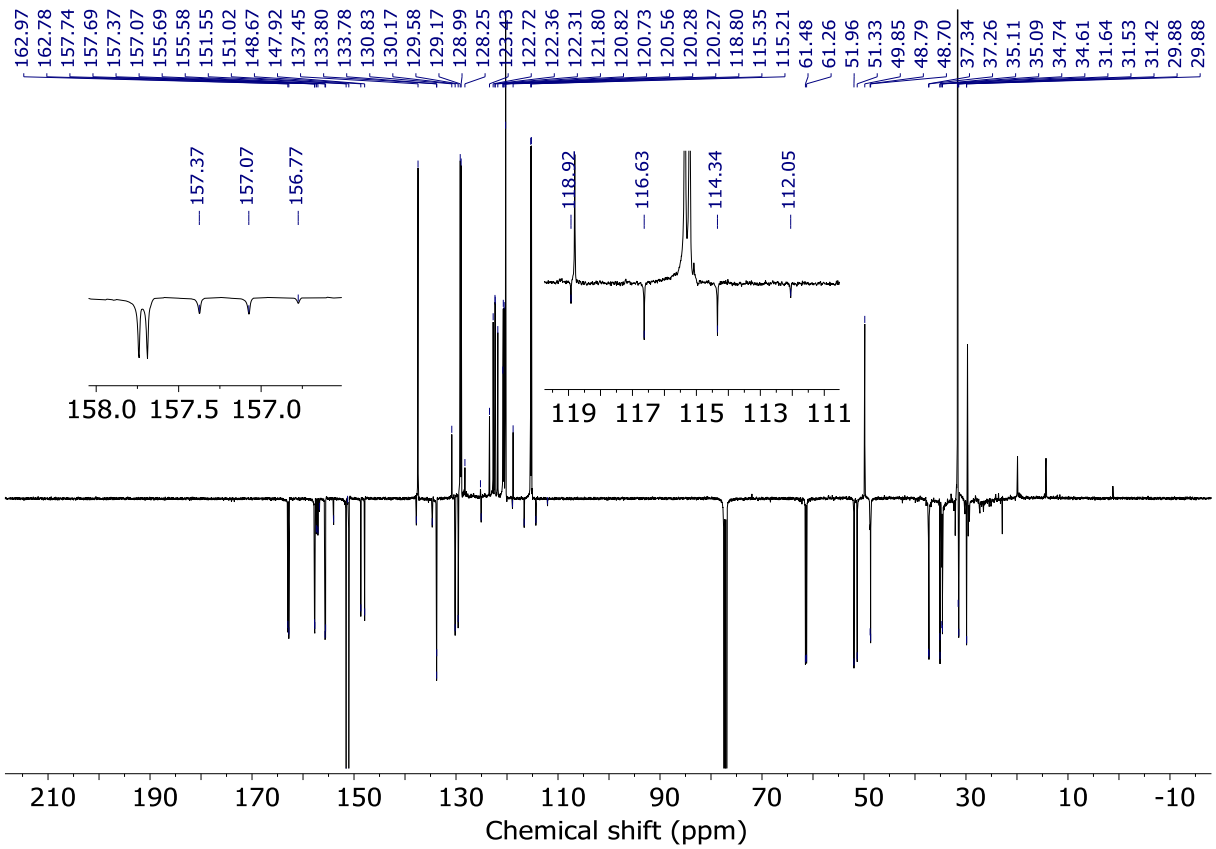

Figure 3.76 - JMOD NMR ($CDCl_3$, 126 MHz) of (S_{ma},$R_{co\text{-}c}$)-**4d**.

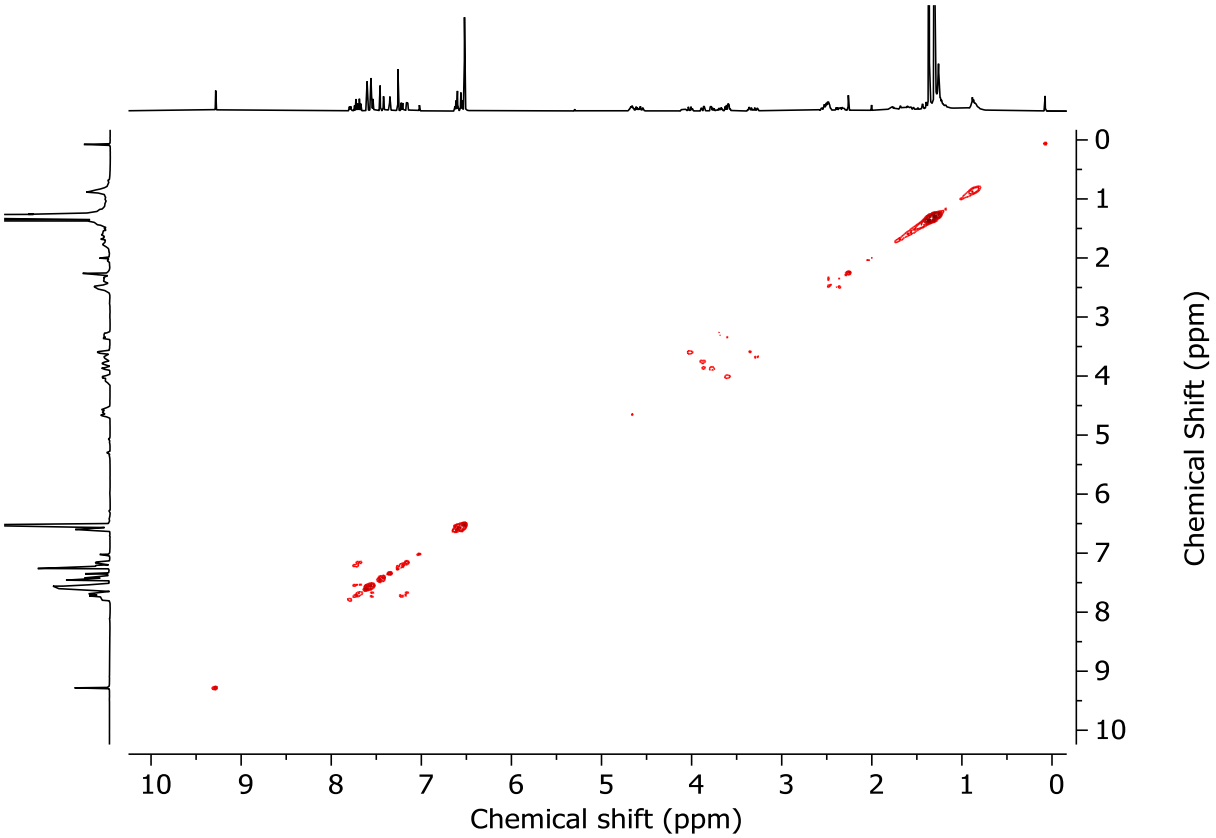

Figure 3.77 - COSY NMR ($CDCl_3$) of (S_{ma},$R_{co\text{-}c}$)-**4d**.

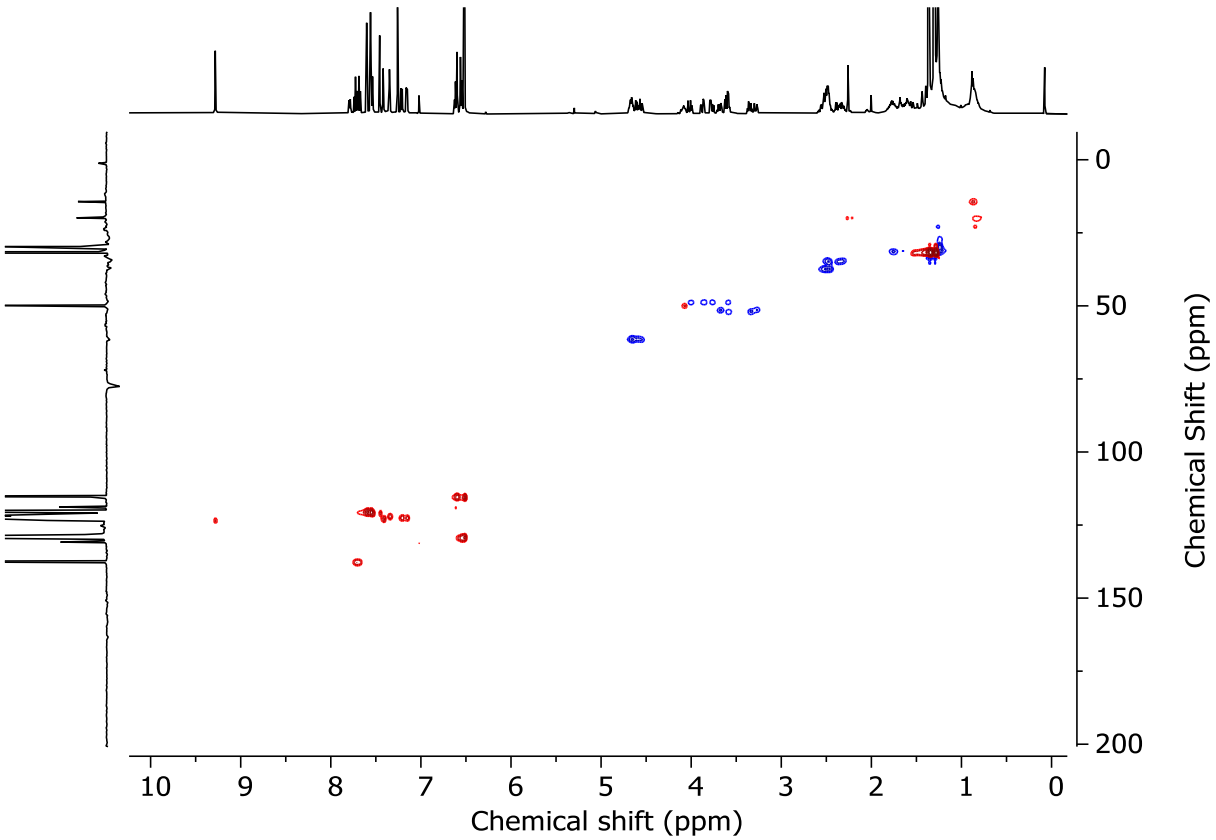

Figure 3.78 - HSQC NMR ($CDCl_3$) of (S_{ma},$R_{co\text{-}c}$)-**4d**.

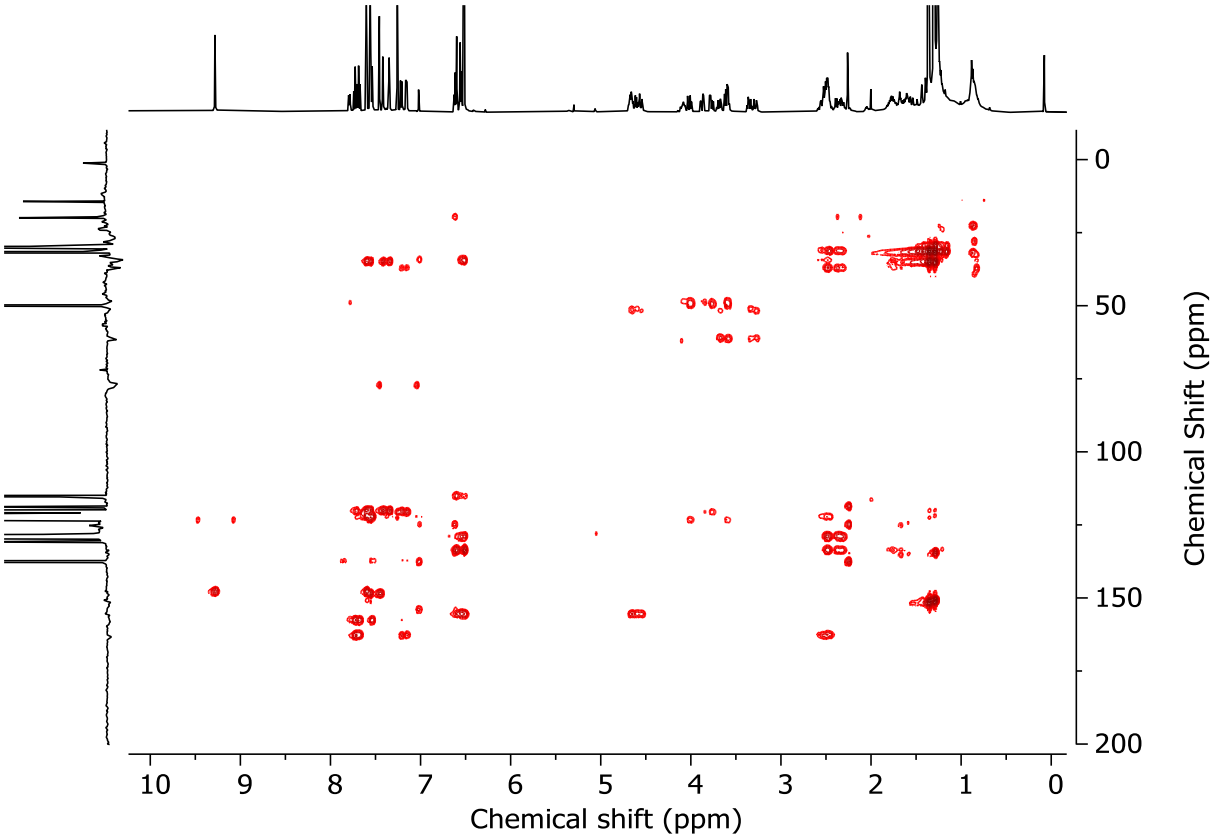

Figure 3.79 - HMBC NMR ($CDCl_3$) of (S_{ma},$R_{co\text{-}c}$)-**4d**.

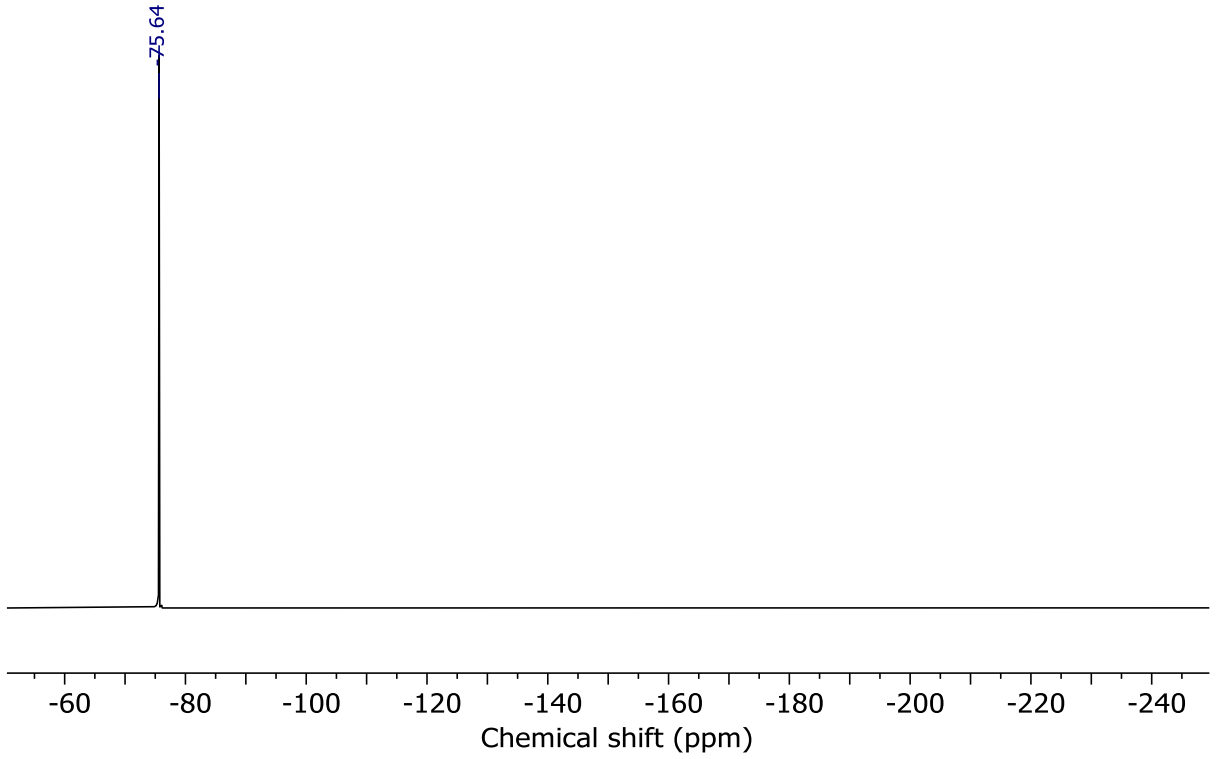

Figure 3.80 - ^{19}F NMR ($CDCl_3$, 470 MHz) of (S_{ma},$R_{co\text{-}c}$)-**4d**.

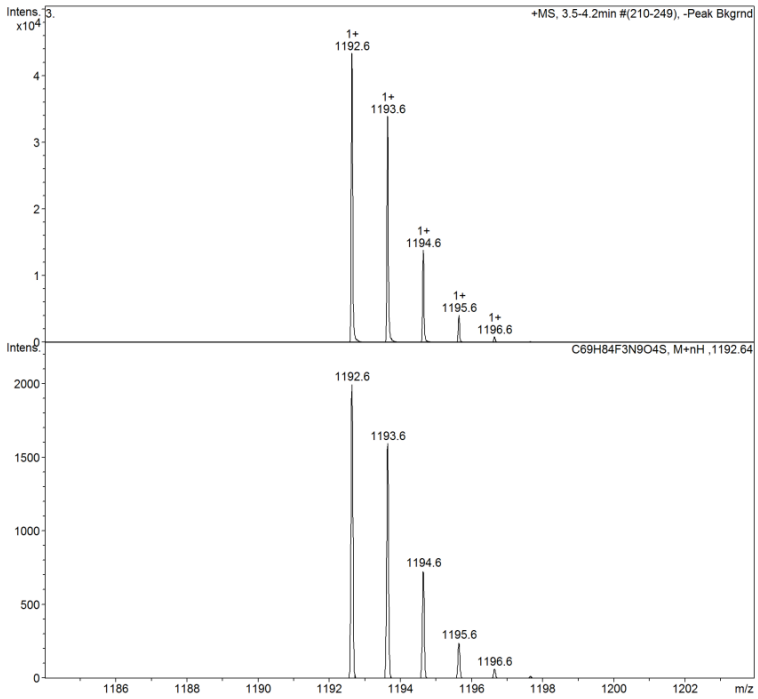

Figure 3.81 - Observed (top) and calculated (bottom) isotopic patterns for (S_{ma},$R_{co\text{-}c}$)-**4d**.

Methylated trifluoroacetamide rotaxanes 4e

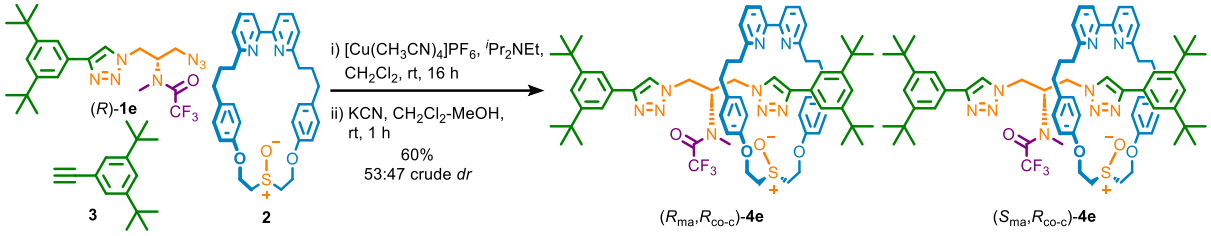

In a CEM vial were added the **3** (11.6 mg, 54.3 µmol), (*R*)-**1e** (25.3 mg, 54.3 µmol), **2** (26.0 mg, 49.4 µmol) and $[Cu(CH_3CN)_4PF_6]$ (17.7 mg, 47.4 µmol). The vial was sealed and purged with N_2, then CH_2Cl_2 was added (1.5 mL), followed by $^iPr_2NEt$ (0.17 mL, 98.8 µmol). The solution was stirred at rt for 16 h. MeOH (2 mL mL) and KCN as a solid (31.9 mg, 0.49 mmol) were added and the resulting mixture was stirred vigorously for until colourless. The crude mixture was diluted with CH_2Cl_2 (5 mL) and washed with H_2O (5 mL) then EDTA-NH_3 (5 mL), with separation of aqueous and organic phases. The combined aqueous phase was then extracted with CH_2Cl_2 (3 x 5 mL) and the combined organic extracts were washed with brine (10 mL), dried ($MgSO_4$) and concentrated *in vacuo* to give a sample containing **4e** as a mixture of diastereomers (53 : 47 *dr*, Figure 3.82). Chromatography (CH_2Cl_2-CH_3CN 0→100%) gave **4e** as a colourless oil (36.0 mg, 60%) as a mixture of diastereoisomers (1.1 : 1, Figure 3.83) and a 97 : 3 mixture of rotamers (the rotameric nature of the compound is highlighted by the EXSY correlation peaks observed in the NOESY spectrum).

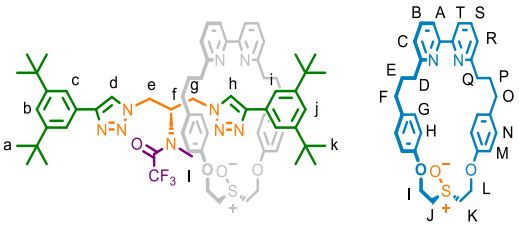

Major Diastereoisomer

^{1}H NMR (500 MHz, $CDCl_3$) δ: 9.44 (s, 1H, H_h), 7.80 (t, *J* = 7.9, 1H, H_B), 7.72-7.64 (m, 3H, H_i, H_S), 7.63-7.56 (m, 3H, H_A, H_c), 7.54 (s, 1H, H_d), 7.48-7.42 (m, 2H, H_b, H_T), 7.40 (t, *J* = 1.8, 1H, H_j), 7.30 (d, *J* = 7.9, 1H, H_C), 7.18 (d, *J* = 7.8, 1H, H_R), 6.72 (d, *J* = 8.6, 2H, H_G or H_M), 6.68 (d, *J* = 8.6, 2H, H_H or H_N), 6.62-6.56 (m, H_G and H_H or H_M and H_N), 4.81-4.40 (m, 5H, H_f, H_I, H_L), 4.20-4.07 (m, 1H, H_J or H_K), 4.07-3.87 (m, 2H, H_g and H_J or H_K), 3.83-3.48 (m, 3H, H_e, $H_{g'}$), 3.27-3.16 (m, 2H, $H_{J'}$ or $H_{K'}$), 2.69-2.24 (m, 11H, H_D, H_F, H_l, H_O, H_Q), 1.93-1.54 (m, 4H, H_E, H_P), 1.39 (s, 18H, H_k), 1.37 (s, 18H, H_a)

^{19}F NMR (470 MHz, $CDCl_3$) δ: 70.79

HR-ESI-MS (+ve) m/z = 1206.6515 $[M+H]^+$ (calc. 1206.7 m/z for $C_{70}H_{87}F_3N_9O_4S$ 1206.6554);

Minor Diastereoisomer

^{1}H NMR (500 MHz, $CDCl_3$) δ: 8.81 (s, 1H, H_h), 7.75 (t, *J* = 7.8, 1H, H_B), 7.72-7.64 (m, 3H, H_i, H_S), 7.63-7.56 (m, 3H, H_A, H_c), 7.49 (s, 1H, H_d), 7.48-7.42 (m, 1H, H_T), 7.41 (t, *J* = 1.9, 1H, H_b), 7.35 (t, *J* = 1.9, 1H, H_j), 7.23 (d, *J* = 7.7, 1H, H_C), 7.20 (d, *J* = 7.8, 1H, H_R), 6.54-6.49 (m, H_G and H_H or H_M and H_N), 6.46-6.38 (m, H_G and H_H or H_M and H_N), 4.81-4.40 (m, 6H, H_e, H_f, H_l, H_L), 4.20-4.07 (m, 2H, H_g), 4.07-3.87 (m, 1H, H_J or H_K), 3.83-3.48 (m, 2H, $H_{e'}$ and H_J or H_K), 3.12-3.01 (m, 2H, $H_{J'}$ or $H_{K'}$), 2.69-2.24 (m, 8H, H_D, H_F, H_O, H_Q), 1.98 (bs, 3H, H_l), 1.93-1.54 (m, 4H, H_E, H_P), 1.36 (s, 18H, H_a), 1.27 (s, 18H, H_k)

^{19}F NMR (470 MHz, $CDCl_3$) δ: 70.69

HR-ESI-MS (+ve) m/z = 1206.6515 $[M+H]^+$ (calc. 1206.7 m/z for $C_{70}H_{87}F_3N_9O_4S$ 1206.6554);

It was not possible to attribute each carbon peak to a single isomer unambiguously, so the complete list of observed peaks is reported below.

^{13}C NMR (126 MHz, $CDCl_3$) δ: 162.9, 162.9, 162.8, 162.8, 157.9, 157.8, 157.8, 157.6, 157.2 (q, $J_{C\text{-}F}$ = 36.0) (x2), 155.9, 155.8, 155.0, 155.0, 151.5, 151.3, 151.0, 151.0, 148.6, 148.2, 147.8, 147.3, 137.6, 137.3, 137.2, 137.2, 133.7, 133.5, 133.5, 133.4, 130.2, 130.1, 129.6, 129.4, 129.3, 129.3, 128.8, 128.6, 123.3, 122.7, 122.5, 122.4, 122.4, 122.3, 122.0, 122.0, 121.8, 121.7, 120.8, 120.6, 120.5, 120.5, 120.3, 120.2, 120.2, 120.1, 120.1, 120.0, 119.8, 115.5 (q, $J_{C\text{-}F}$ = 289.9), 115.5 (q, $J_{C\text{-}F}$ = 289.9), 115.1, 115.1, 114.9, 114.6, 61.3, 61.0, 60.9, 60.8, 53.4, 53.3, 52.4, 51.2, 47.8, 47.2, 47.1, 46.3, 37.6, 37.5, 37.1, 37.1, 36.4 (HMBC), 35.0, 35.0, 34.9, 34.7, 34.7, 34.7, 34.4, 32.4, 31.7, 31.6, 31.5, 31.5, 31.4, 31.4, 31.0, 30.3, 29.7.

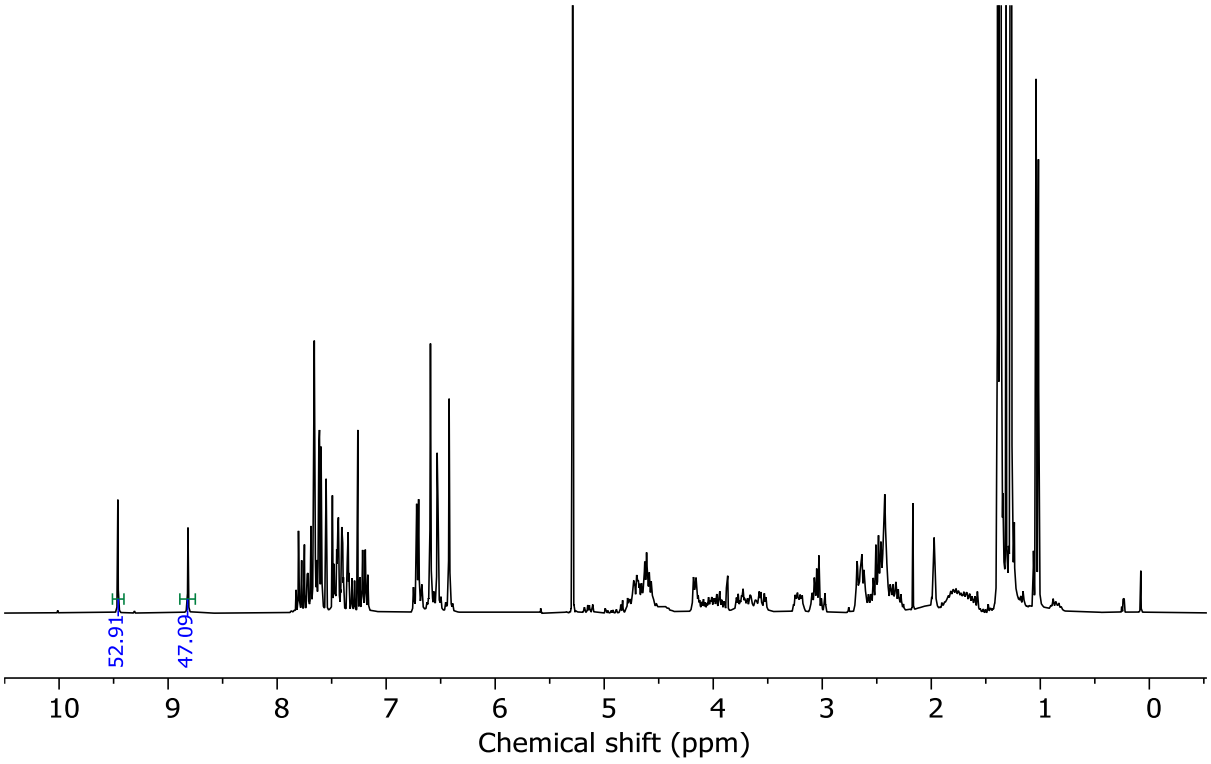

Figure 3.82 - ^{1}H NMR ($CDCl_3$, 400 MHz) of (R_{ma},$R_{co\text{-}c}$)-**4e** and (S_{ma},$R_{co\text{-}c}$)-**4e** prior to purification (97 : 3 mixture of rotamers, 53: 47 *dr*).

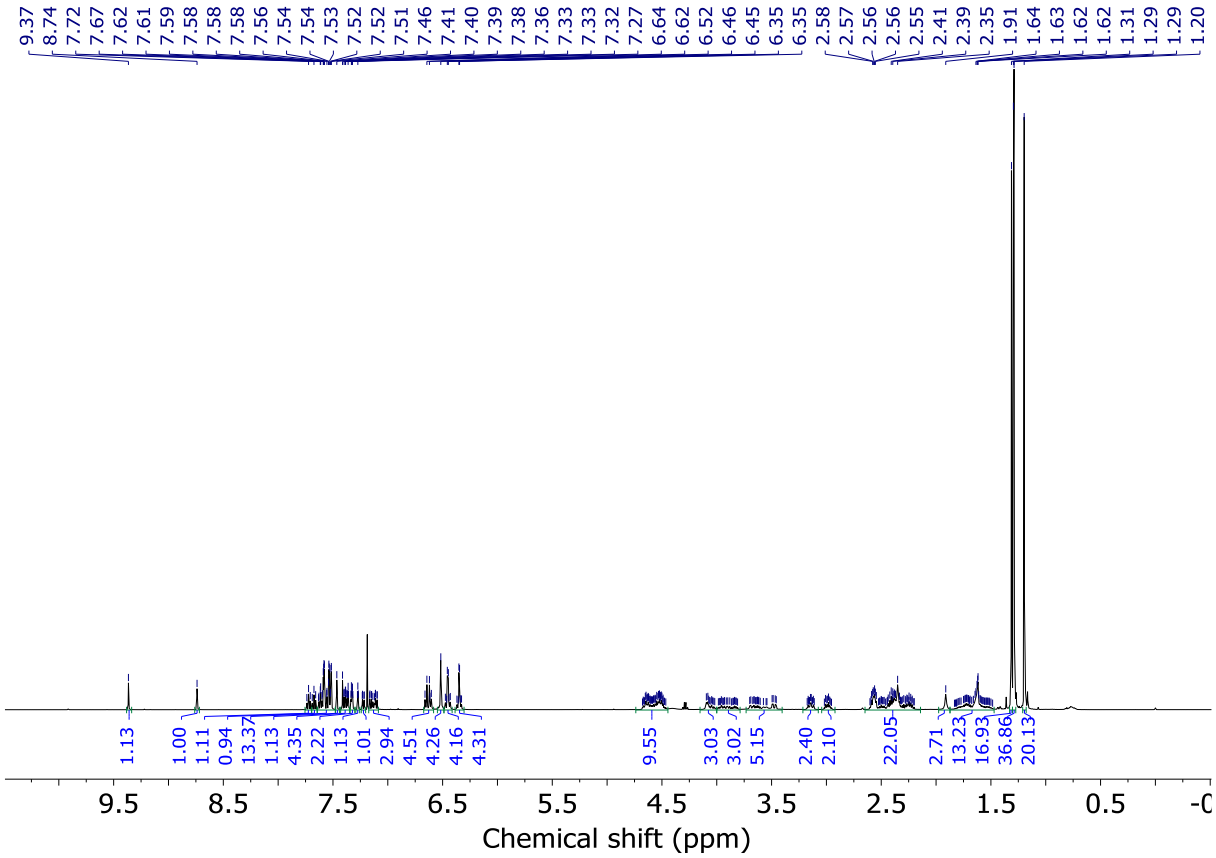

Figure 3.83 - ^{1}H NMR ($CDCl_3$, 500 MHz) of (R_{ma},$R_{co\text{-}c}$)-**4e** and (S_{ma},$R_{co\text{-}c}$)-**4e** (97 : 3 mixture of rotamers, 53: 47 *dr*).

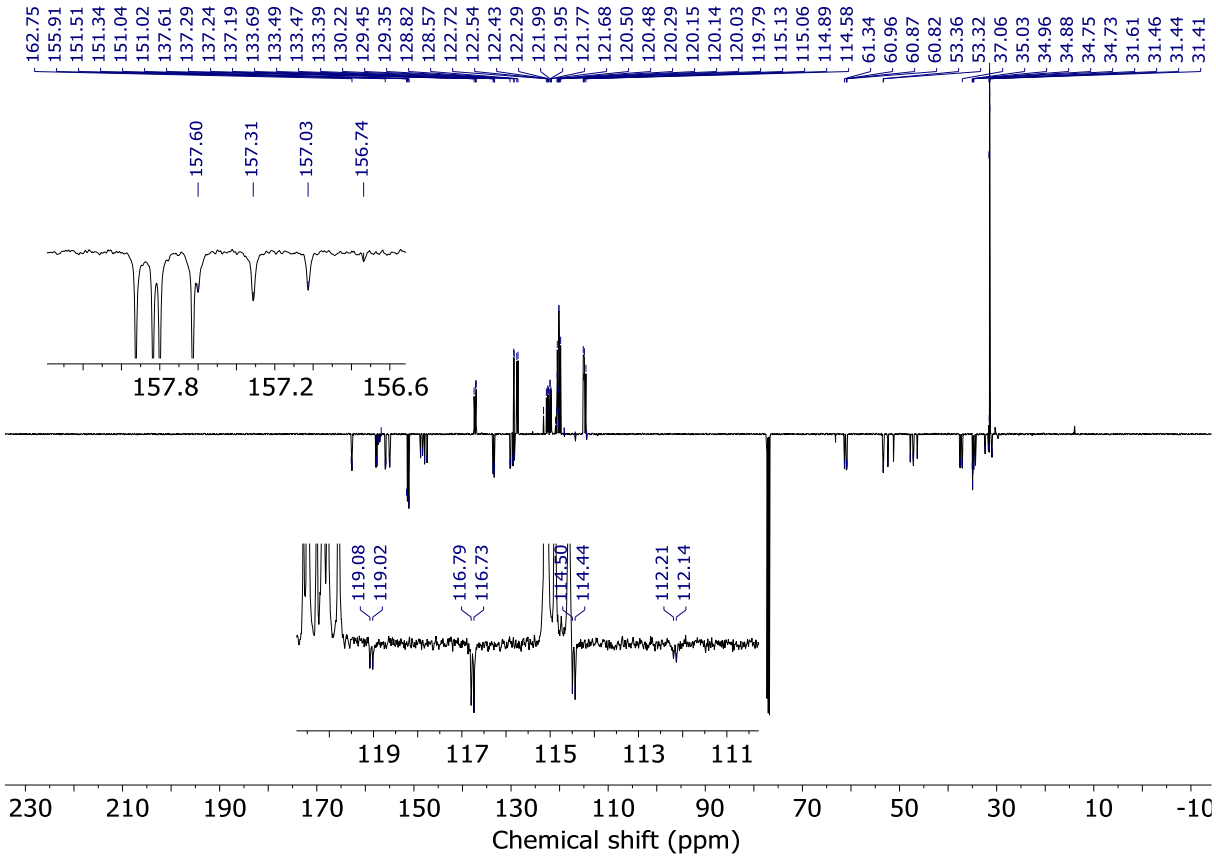

Figure 3.84 - JMOD NMR ($CDCl_3$, 126 MHz) of (R_{ma},$R_{co\text{-}c}$)-**4e** and (S_{ma},$R_{co\text{-}c}$)-**4e** (97 : 3 mixture of rotamers, 53: 47 *dr*).

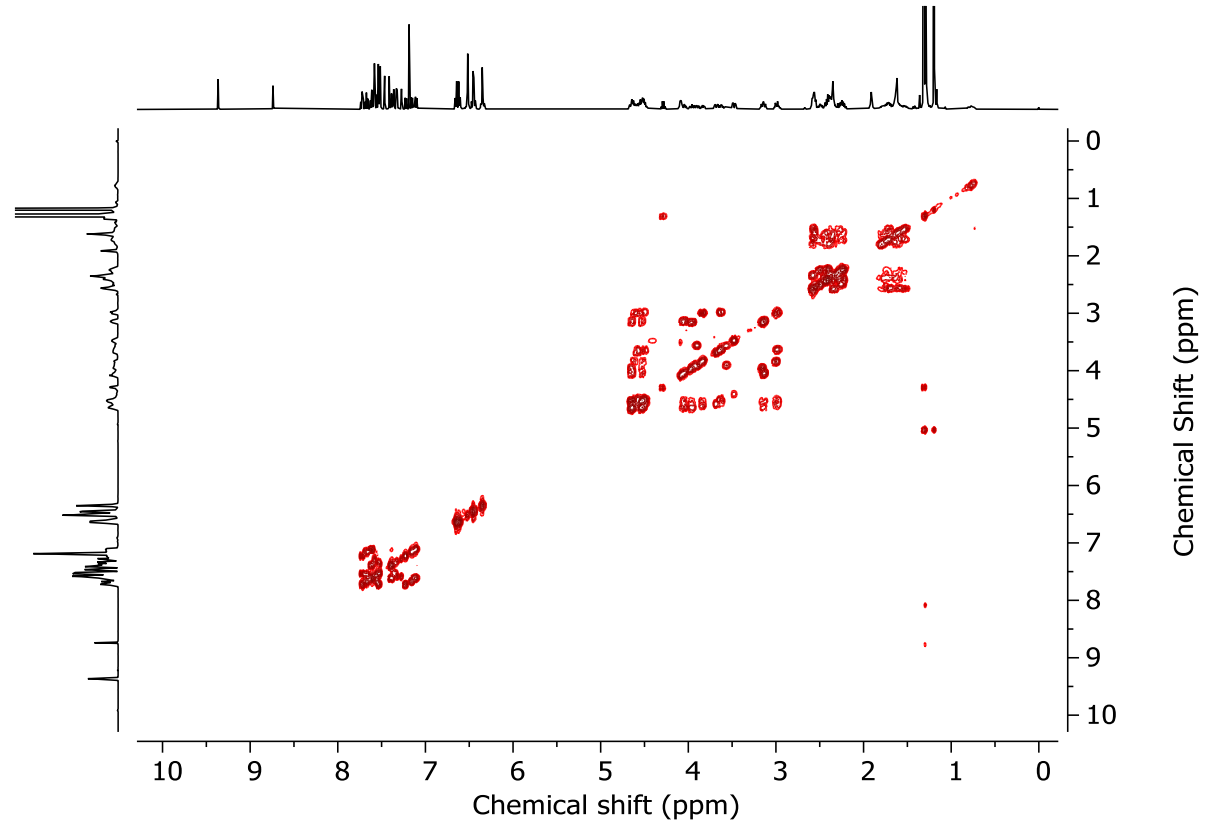

Figure 3.85 - COSY NMR ($CDCl_3$) of (R_{ma},$R_{co\text{-}c}$)-**4e** and (S_{ma},$R_{co\text{-}c}$)-**4e** (97 : 3 mixture of rotamers, 53: 47 *dr*).

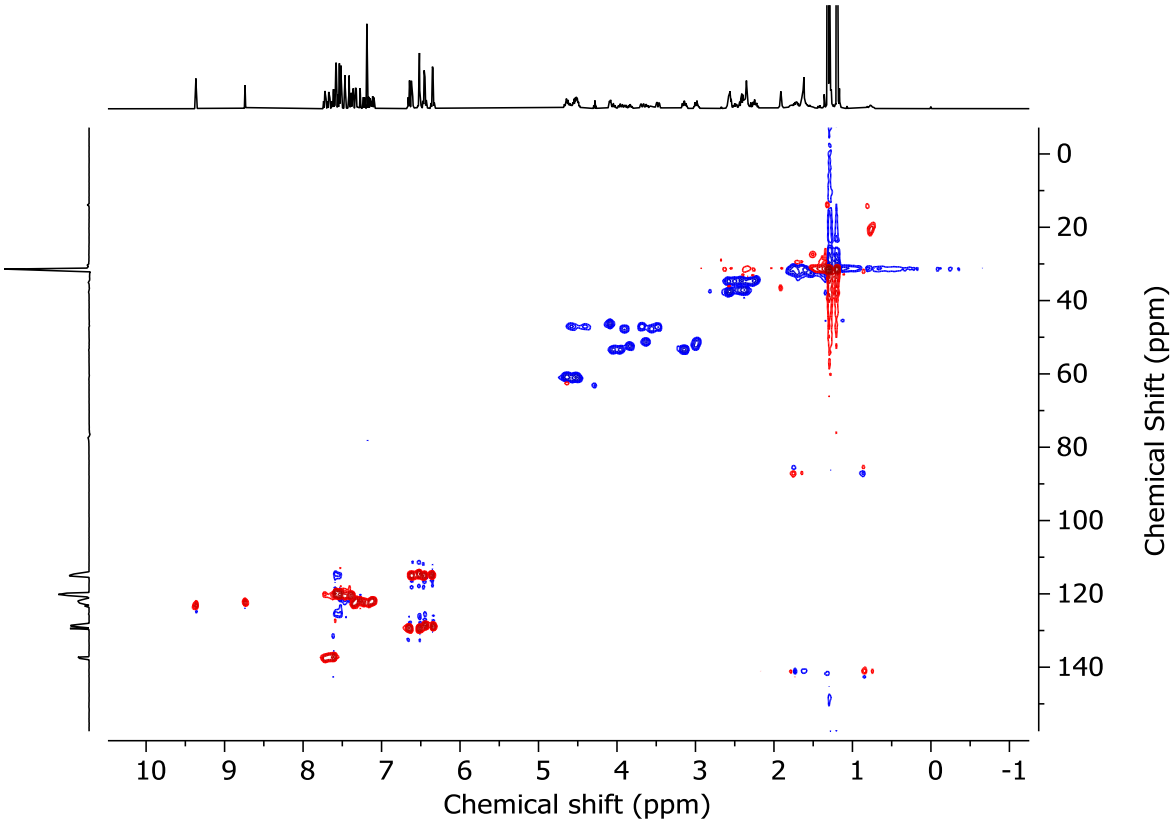

Figure 3.86 - HSQC NMR ($CDCl_3$) of (R_{ma},$R_{co\text{-}c}$)-**4e** and (S_{ma},$R_{co\text{-}c}$)-**4e** (97 : 3 mixture of rotamers, 53: 47 *dr*).

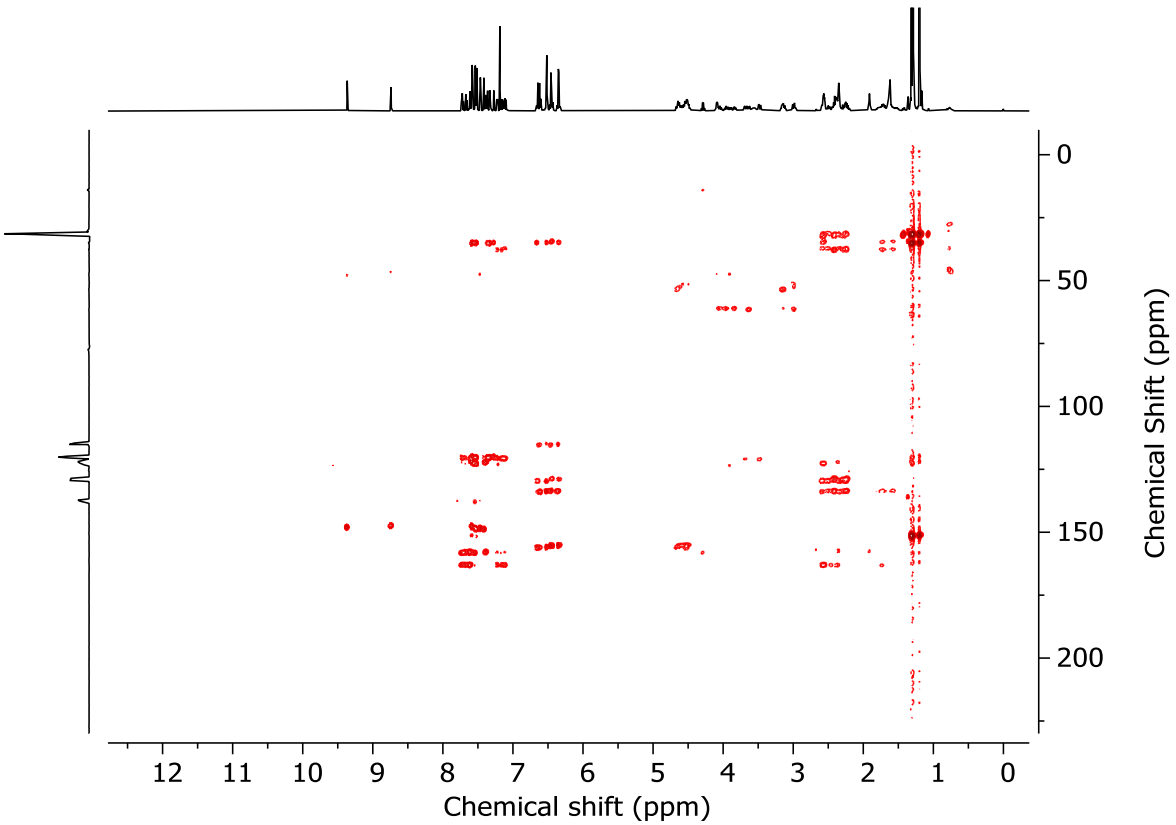

Figure 3.87 - HMBC NMR ($CDCl_3$) of (R_{ma},$R_{co\text{-}c}$)-**4e** and (S_{ma},$R_{co\text{-}c}$)-**4e** (97 : 3 mixture of rotamers, 53: 47 *dr*).

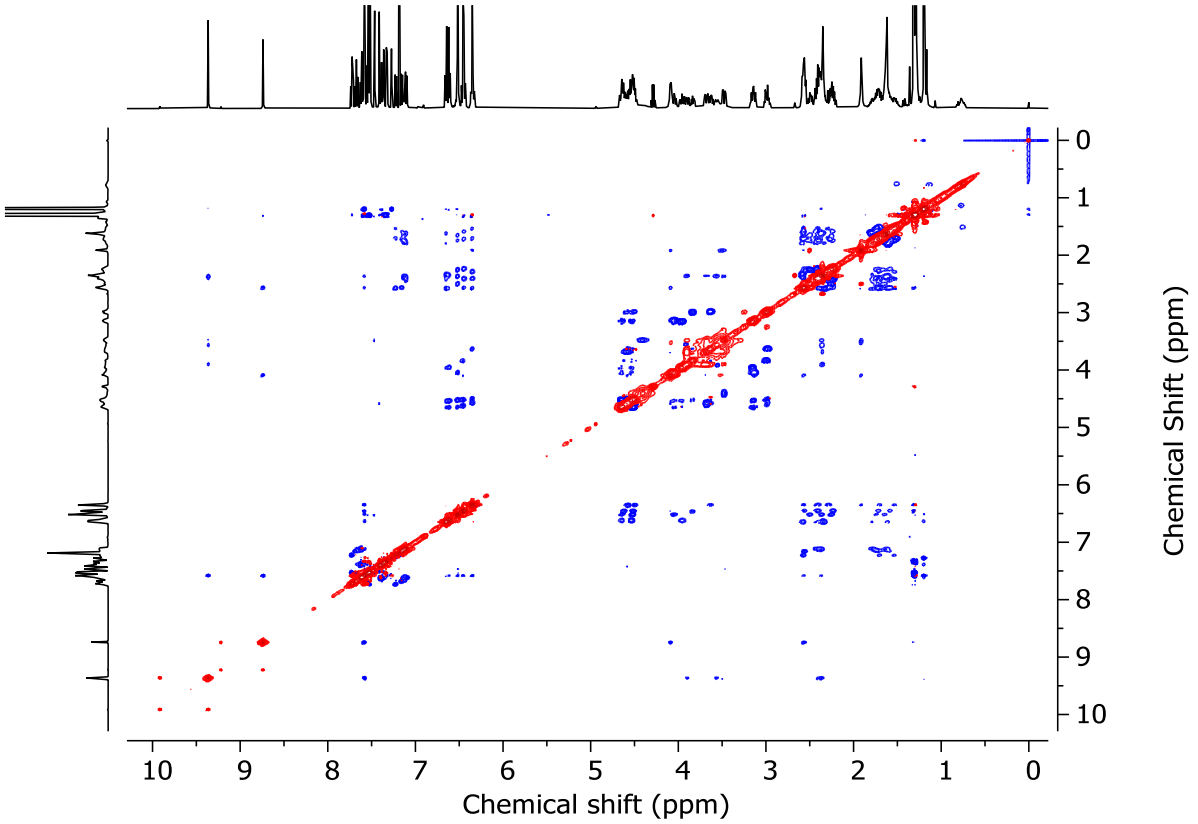

Figure 3.88 - NOESY NMR ($CDCl_3$) of (R_{ma},$R_{co\text{-}c}$)-**4e** and (S_{ma},$R_{co\text{-}c}$)-**4e** (97 : 3 mixture of rotamers, 53: 47 *dr*).

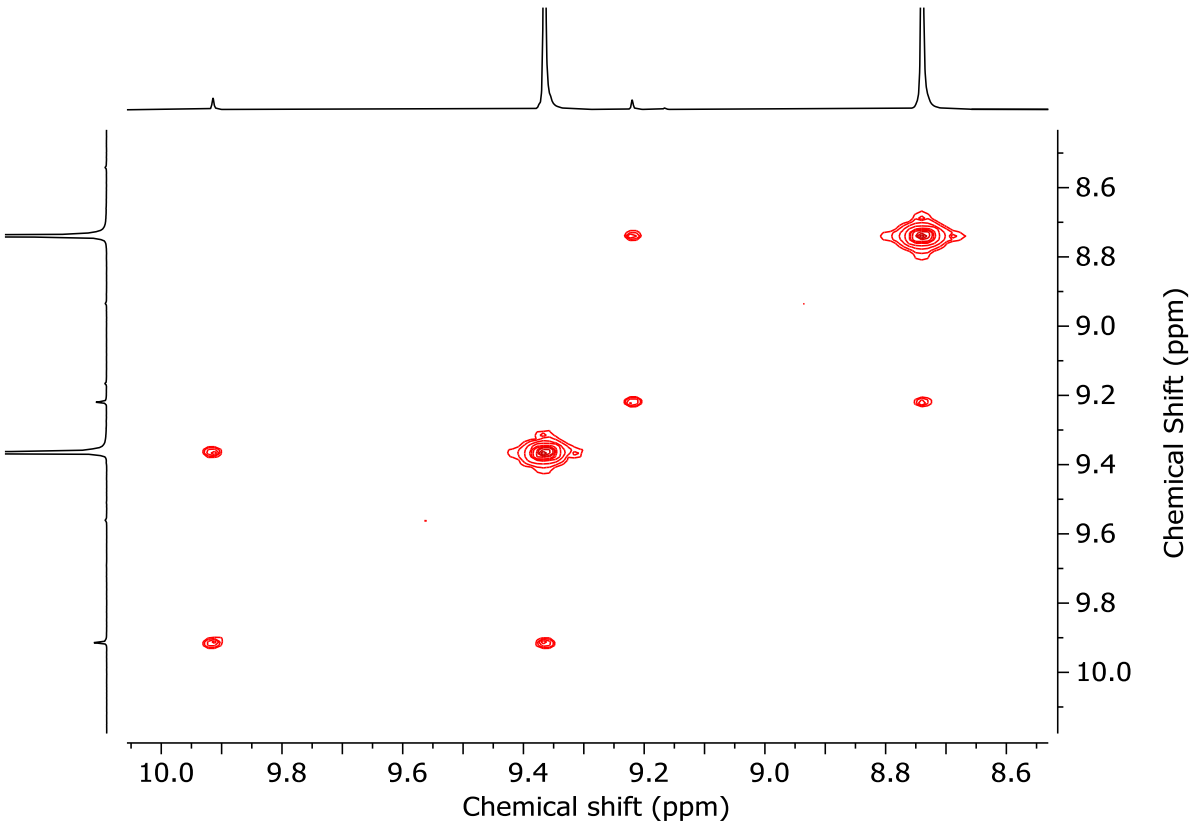

Figure 3.89 - Expansion of NOESY NMR (Figure 3.88) of **4e** highlighting the EXSY cross-peaks observed.

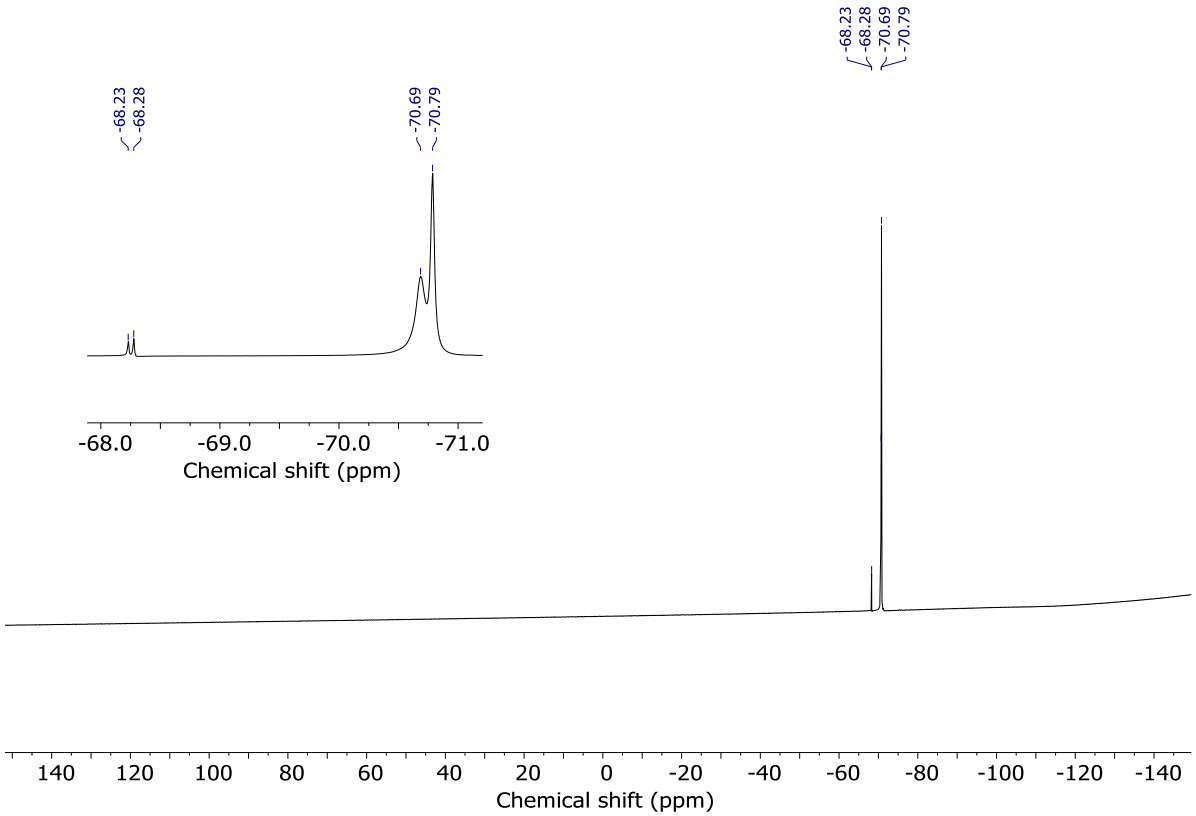

Figure 3.90 - ^{19}F NMR ($CDCl_3$, 470 MHz) of (R_{ma},$R_{co\text{-}c}$)-**4e** and (S_{ma},$R_{co\text{-}c}$)-**4e** (97 : 3 mixture of rotamers, 53: 47 *dr*).

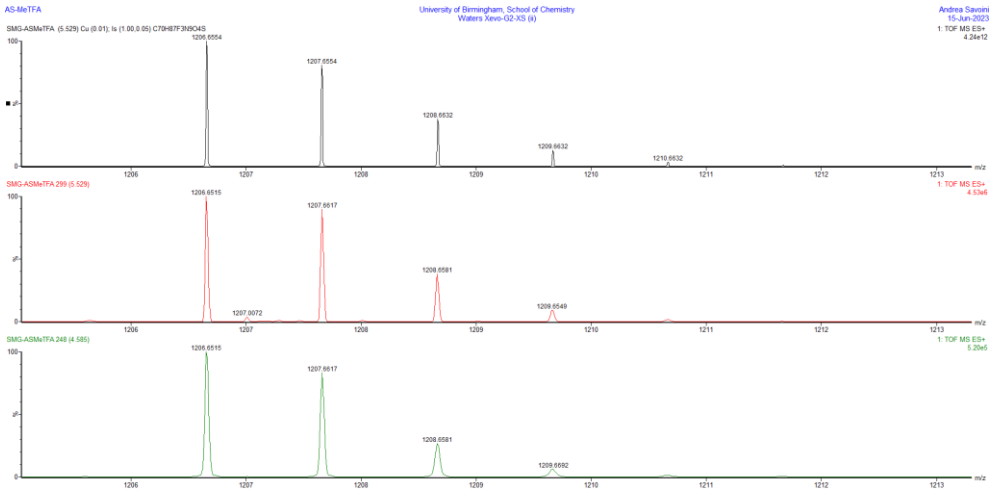

Figure 3.91 - Calculated (top) and observed (middle, bottom) isotopic patterns for rotaxanes **4e**.

Synthesis of rotaxanes 6-12 and associated compounds

Rotaxanes (E_m)-6 and (Z_m)-6

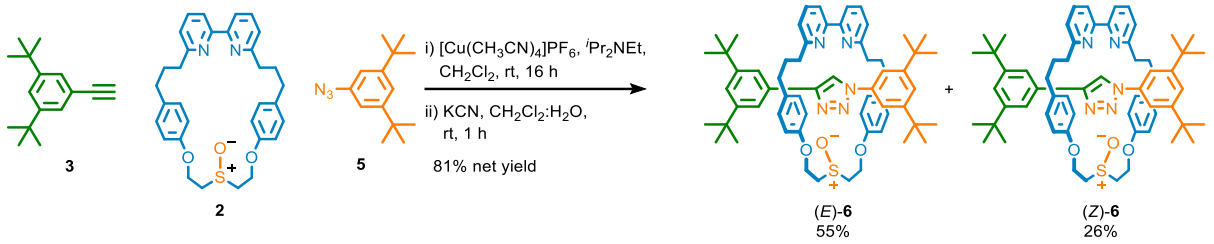

In a CEM vial were added **3** (9.0 mg, 41.7 µmol), **5** (9.7 mg, 41.7 µmol), **2** (20.0 mg, 38.0 µmol) and $[Cu(CH_3CN)_4PF_6]$ (13.6 mg, 36.5 µmol) the vial was sealed and purged with N_2, then CH_2Cl_2 was added (1.0 mL), followed by $^iPr_2NEt$ (13.3 µL, 75.9 µmol). The solution was stirred at rt for 16 h. MeOH (2 mL) and KCN as a solid (24.7 mg, 0.38 mmol) were added and the resulting mixture was stirred vigorously until colourless. The mixture was diluted with CH_2Cl_2 (5 mL) and washed with H_2O (5 mL) then EDTA-NH_3 (5 mL), with separation of aqueous and organic phases. The combined aqueous phase was then extracted with CH_2Cl_2 (3 x 5 mL) and the combined organic extracts were washed with brine (10 mL), dried ($MgSO_4$) and concentrated *in vacuo* to give a residue containing rotaxane **6** (28% de, Figure 3.92). Chromatography (CH_2Cl_2-CH_3CN 0→30%) gave (*E*)-**6** (20.4 mg, 55%) as a white foam and (*Z*)-**6** (9.7 mg, 26%) as a white foam.

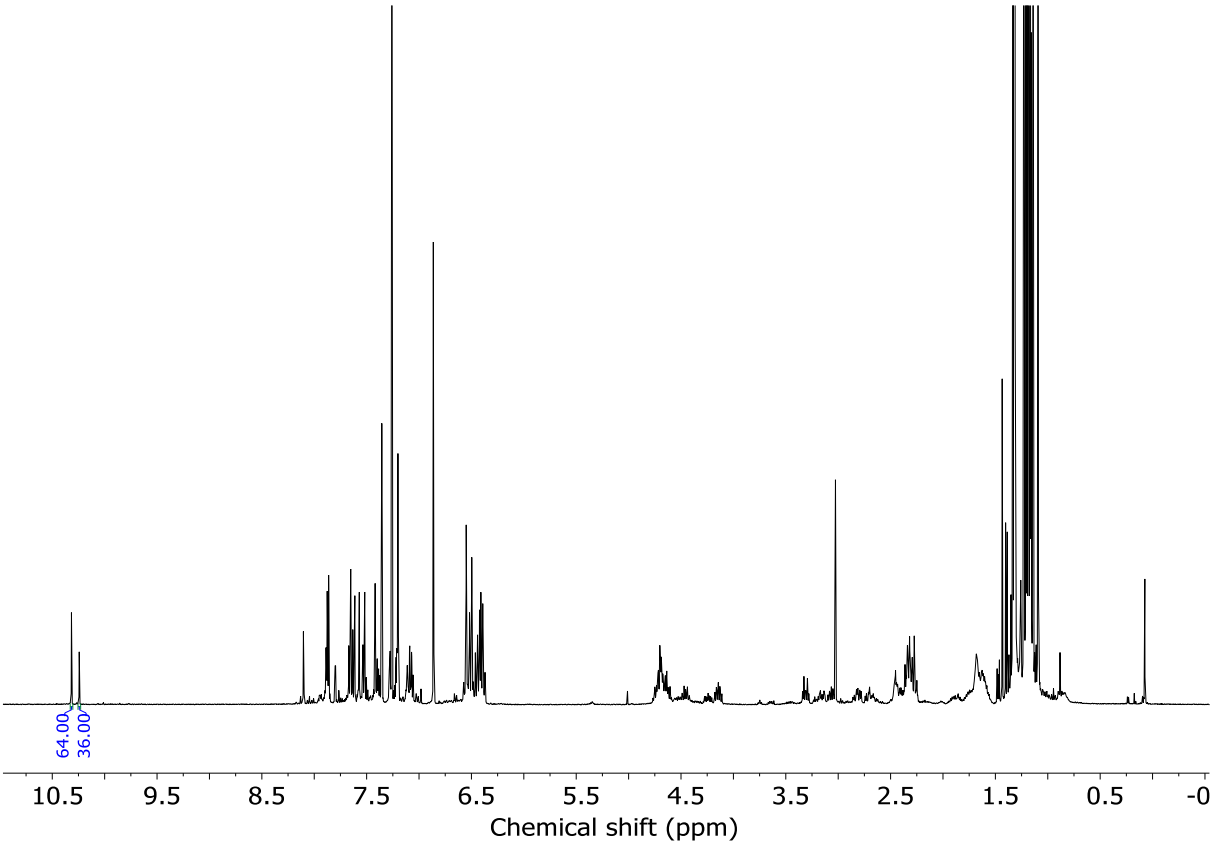

Figure 3.92 - ^1H NMR ($CDCl_3$, 400 MHz) of (E_m)-**6** and (Z_m)-**6** prior to chromatography.

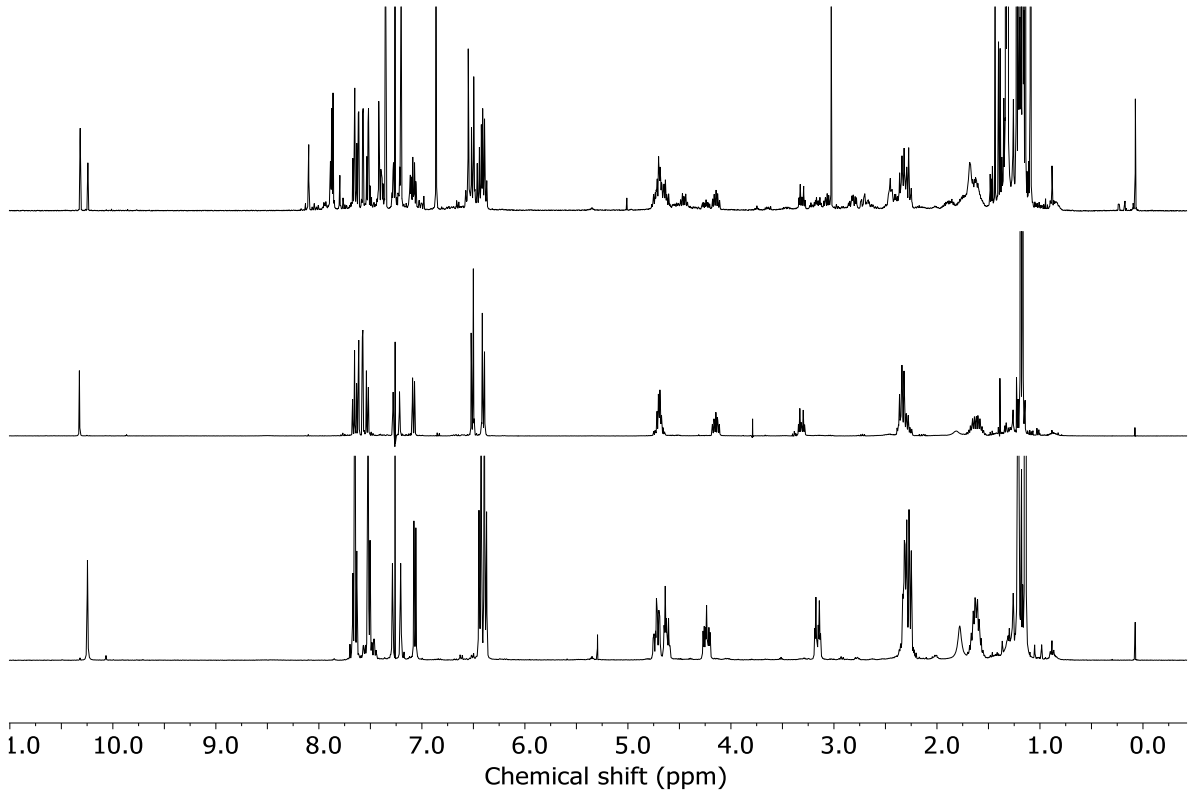

Figure 3.93 - ^{1}H NMR ($CDCl_3$, 400 MHz) of (E_m)-**6** and (Z_m)-**6** prior to chromatography (top), (E_m)-**6** (middle) and (Z_m)-**6** (bottom).

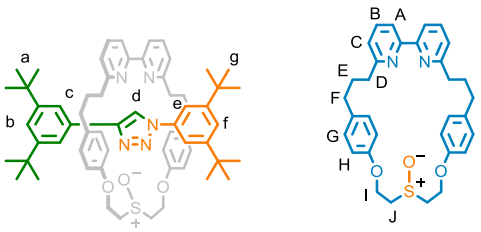

Rotaxane (E_m)-**6**

^{1}H NMR (400 MHz, $CDCl_3$) δ 10.32 (s, 1H, H_d), 7.65 (t, J = 7.8, 2H, H_B), 7.61 (d, J = 1.6, 2H, H_e), 7.58 (d, J = 1.7, 2H, H_c), 7.53 (d, J = 7.7, 2H, H_A), 7.31-7.25 (m, 1H, H_f), 7.24-7.19 (m, 1H, H_b), 7.08 (d, J = 7.6, 2H, H_C), 6.51 (d, J = 8.5, 4H, H_G), 6.40 (d, J = 8.4, 4H, H_H), 4.76-4.59 (m, 4H, H_I), 4.15 (dt, J = 13.4, 6.8, 2H, H_J), 3.31 (dt, J = 13.2, 5.2, 2H, H_J), 2.45 – 2.23 (m, 8H, H_D, H_F), 1.63 (dq, J = 13.9, 8.0, 4H, H_E), 1.19 (s, 19H, H_a), 1.17 (s, 18H, H_g).

^{13}C NMR (101 MHz, $CDCl_3$) δ 163.5, 157.5, 155.2, 151.8, 150.4, 147.3, 137.3, 136.9, 133.0, 130.9, 128.7, 128.7, 122.0, 121.7, 121.1, 120.7, 120.5, 120.0, 114.9, 114.9, 114.6, 60.6, 52.0, 37.2, 35.1, 35.0, 34.9, 31.6, 31.3, 31.1.

HR-ESI-MS (+ve) m/z = 972.5824 $[M+H]^+$ (calc. m/z for $C_{62}H_{78}N_5O_3S$ 972.5820).

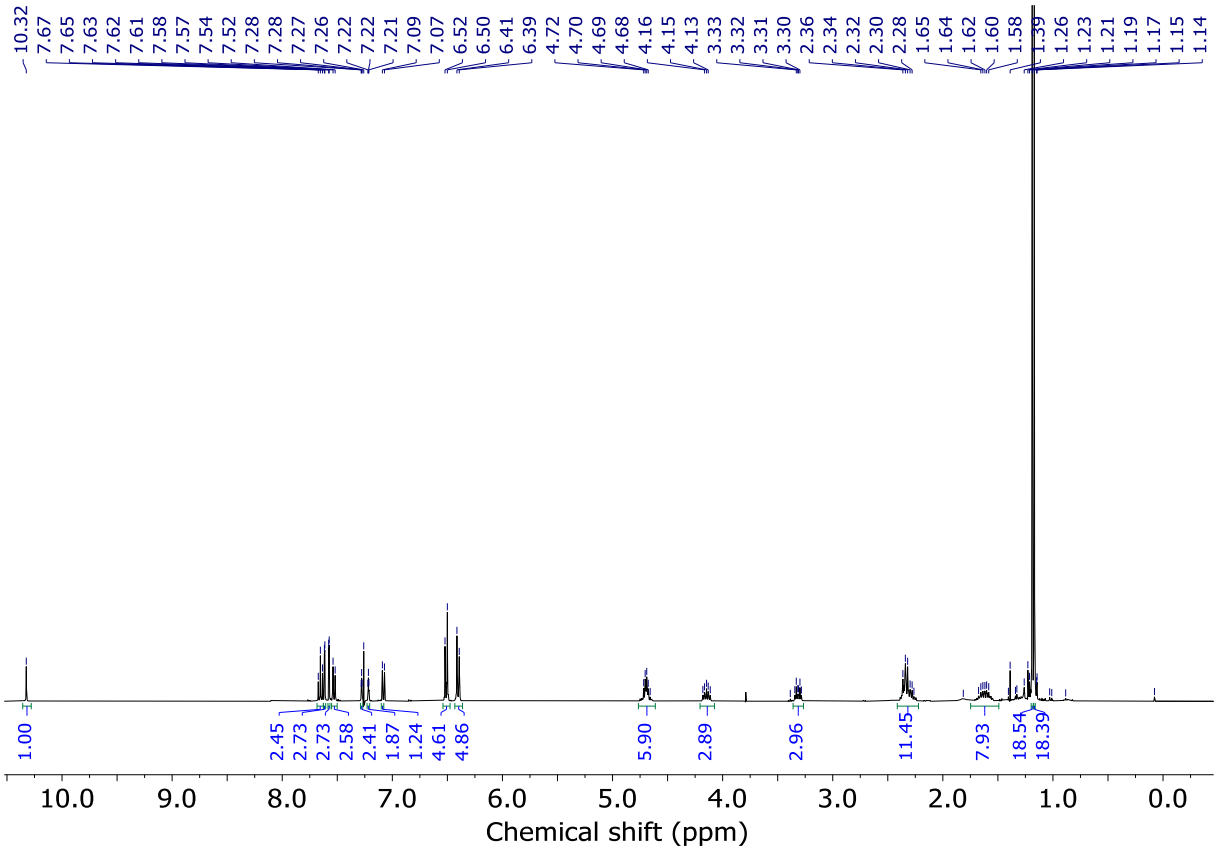

Figure 3.94 - ^{1}H NMR ($CDCl_3$, 400 MHz) of (E_m)-**6**.

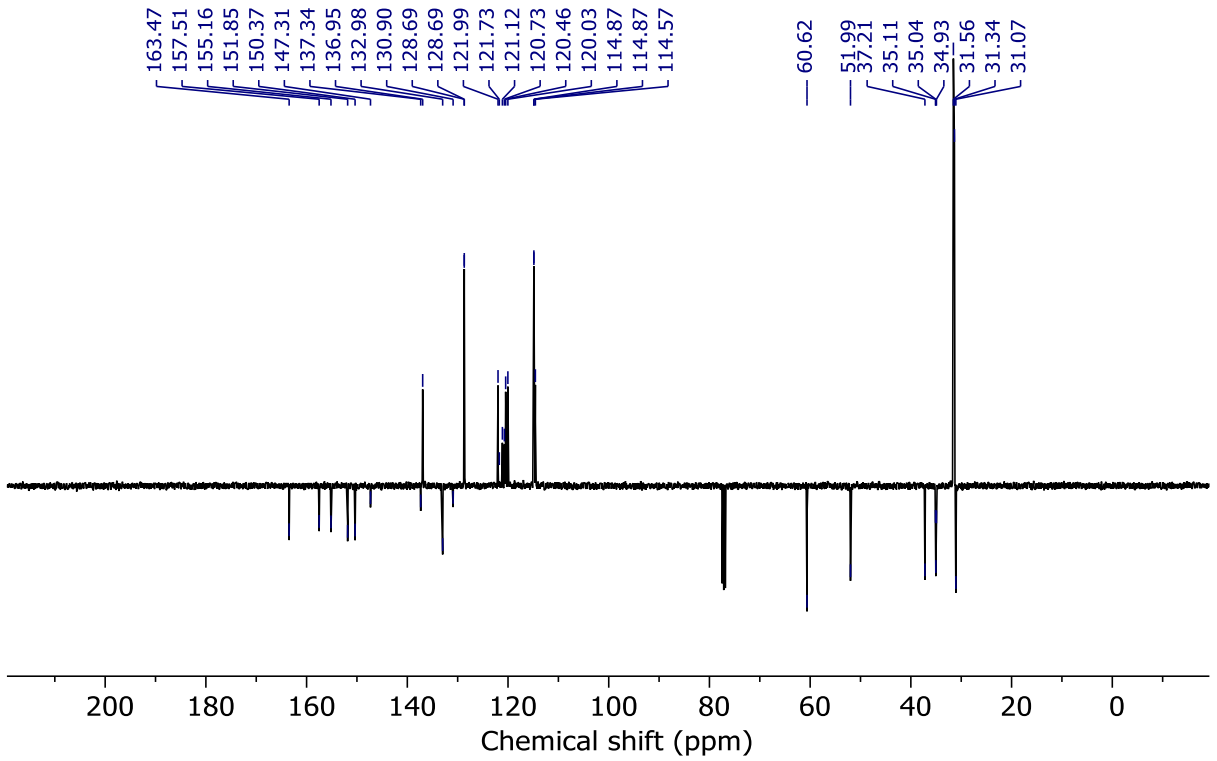

Figure 3.95 - JMOD NMR ($CDCl_3$, 101 MHz) of (E_m)-**6**.

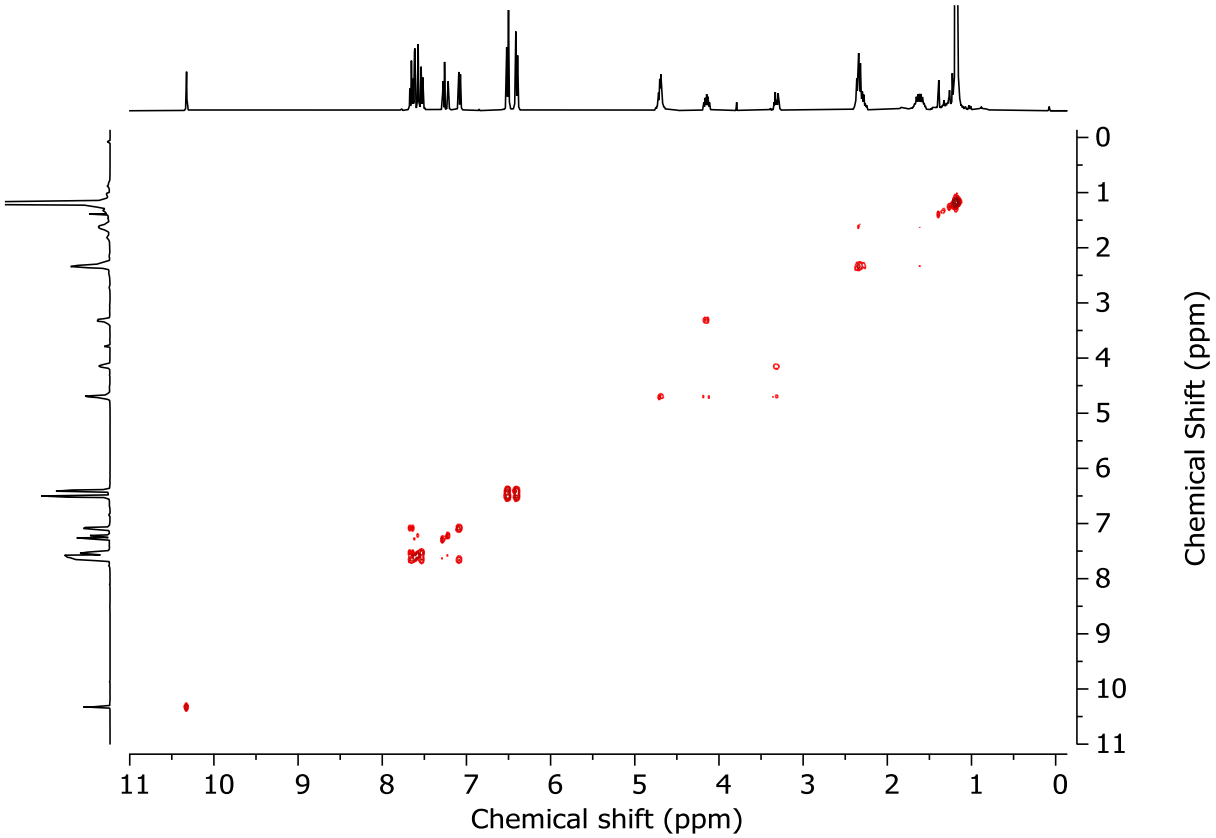

Figure 3.96 - COSY NMR ($CDCl_3$) of (E_m)-**6**.

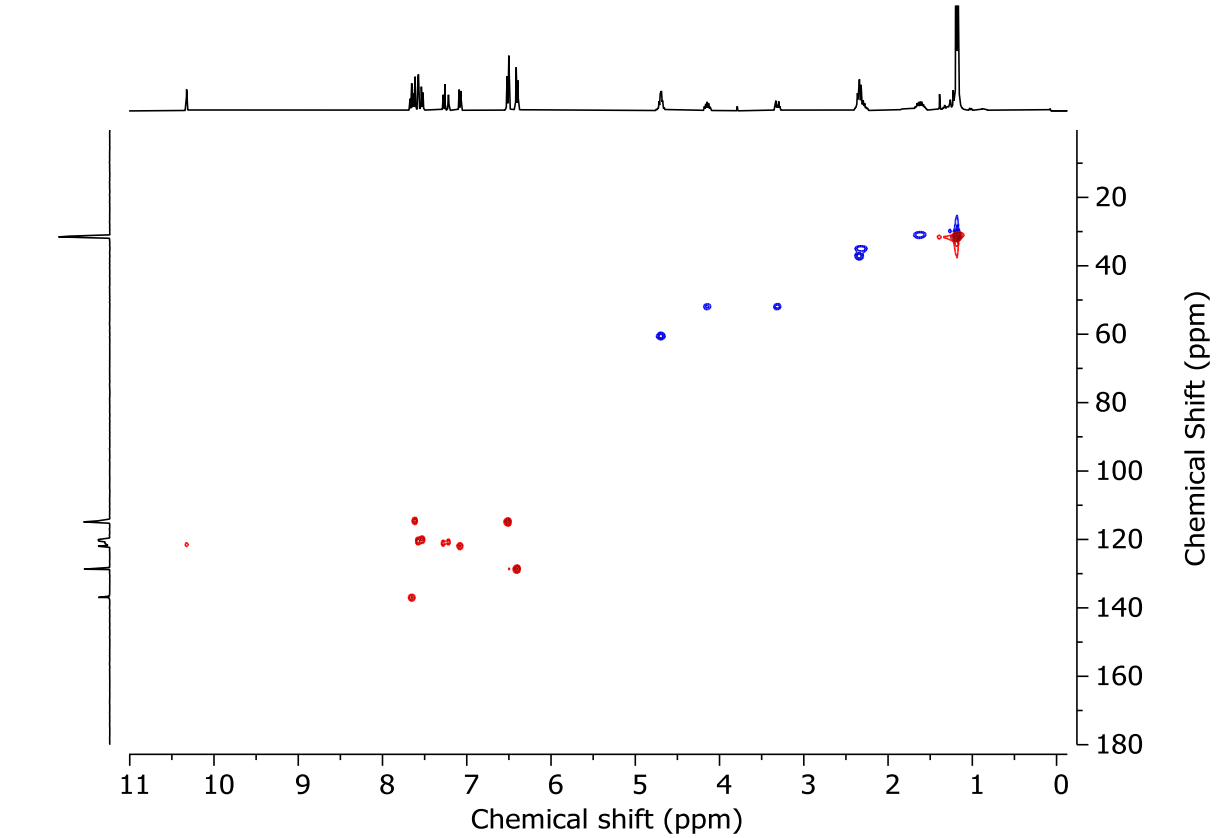

Figure 3.97 - HSQC NMR ($CDCl_3$) of (E_m)-**6**.

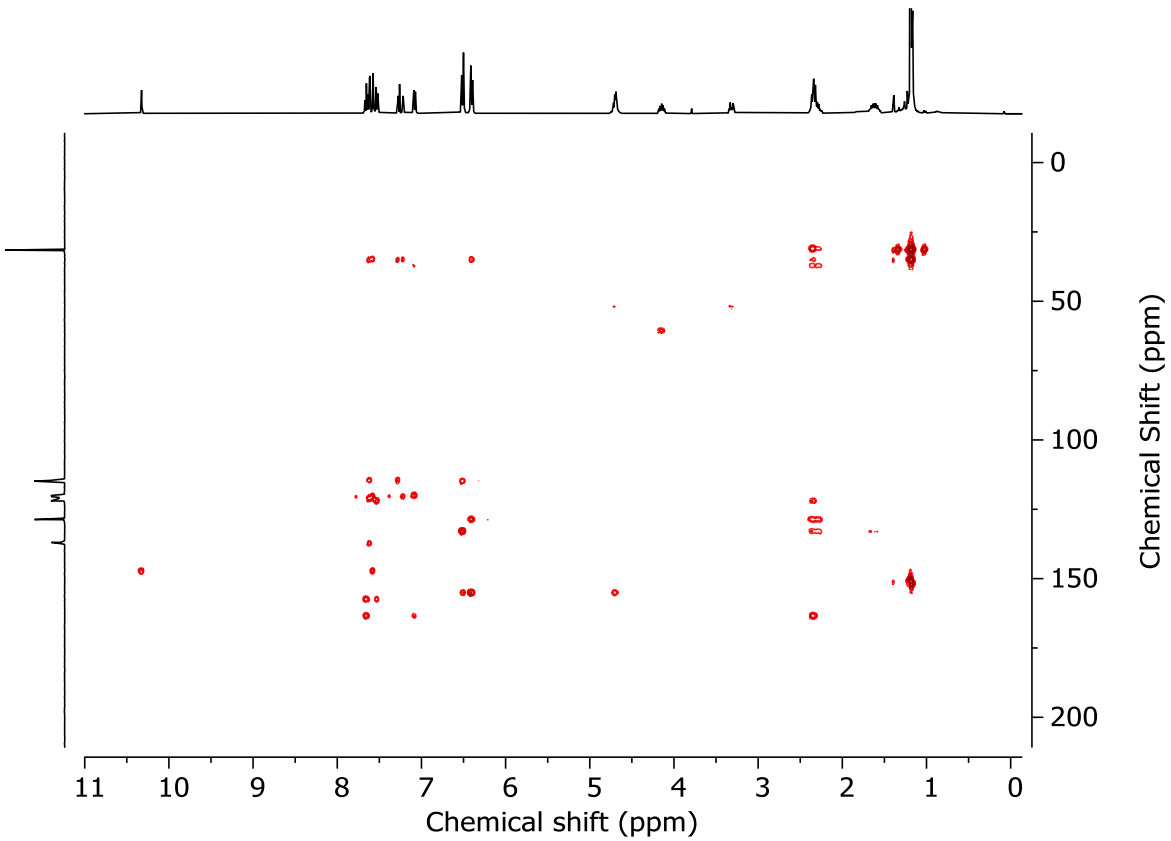

Figure 3.98 - HMBC NMR ($CDCl_3$) of (E_m)-**6**.

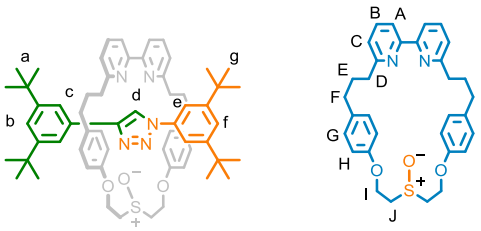

Rotaxane (Z_m)-**6**

^{1}H NMR (400 MHz, $CDCl_3$) δ 10.25 (s, 1H, H_d), 7.72-7.61 (m, 4H, H_B, H_c), 7.54-7.50 (m, 4H, H_A, H_e), 7.29 (t, J = 1.5, 1H, H_b), 7.21 (t, J = 1.5, 1H, H_f), 7.07 (d, J = 7.6, 2H, H_C), 6.43 (d, J = 8.7, 4H, H_G), 6.38 (d, J = 8.7, 4H, H_H), 4.80-4.68 (m, 2H, H_I), 4.66-4.57 (m, 2H, H_I), 4.24 (ddd, J = 13.5, 9.3, 4.5, 2H, H_J), 3.16 (dt, J = 13.2, 4.2, 2H, H_J), 2.28 (dd, J = 17.9, 9.2, 8H, H_D, H_F), 1.62 (dd, J =16.3, 6.2, 4H, H_E), 1.21 (s, 18H, H_a), 1.14 (s, 18H, H_g).

^{13}C NMR (101 MHz, $CDCl_3$) δ 163.6, 157.6, 155.1, 151.6, 150.6, 147.1, 137.2, 137.0, 132.7, 132.3, 132.2, 132.1, 132.1, 131.1, 128.8, 128.8, 128.7, 128.6, 122.1, 121.1, 120.9, 120.1, 120.0, 114.7, 114.5, 60.5, 52.9, 37.3, 35.2, 35.2, 34.8, 31.5, 31.5, 31.5.

HR-ESI-MS (+ve) m/z = 972.5804 $[M+H]^+$ (calc. m/z for $C_{62}H_{78}N_5O_3S$ 972.5820).

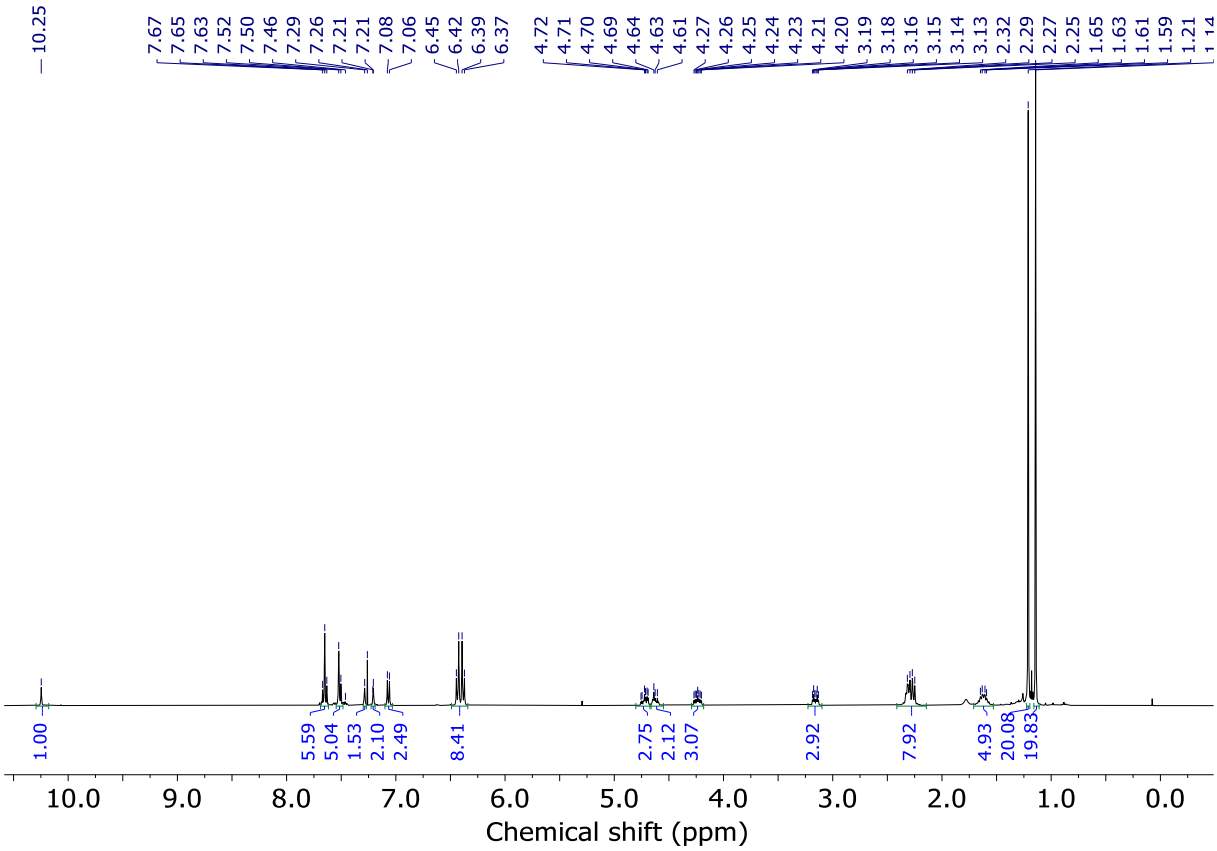

Figure 3.99 - ^{1}H NMR ($CDCl_3$, 400 MHz) of (Z_m)-**6**.

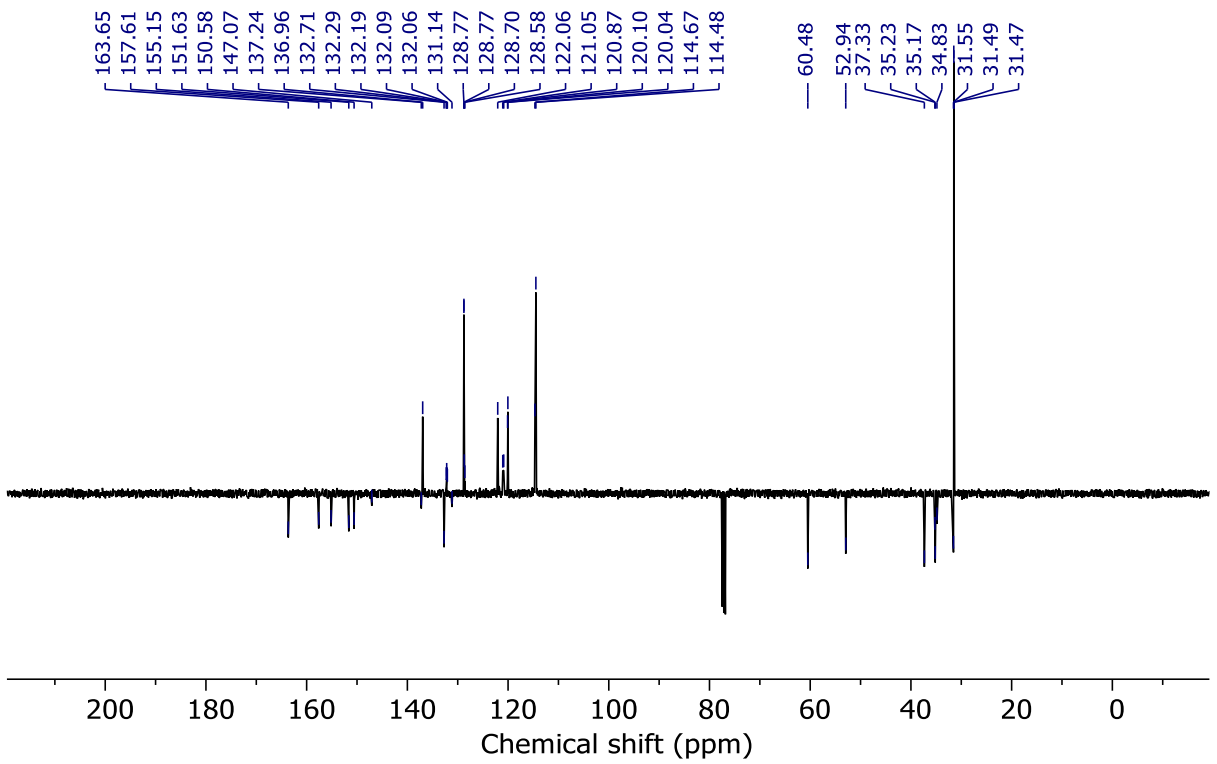

Figure 3.100 - JMOD NMR ($CDCl_3$, 101 MHz) of (Z_m)-**6**.

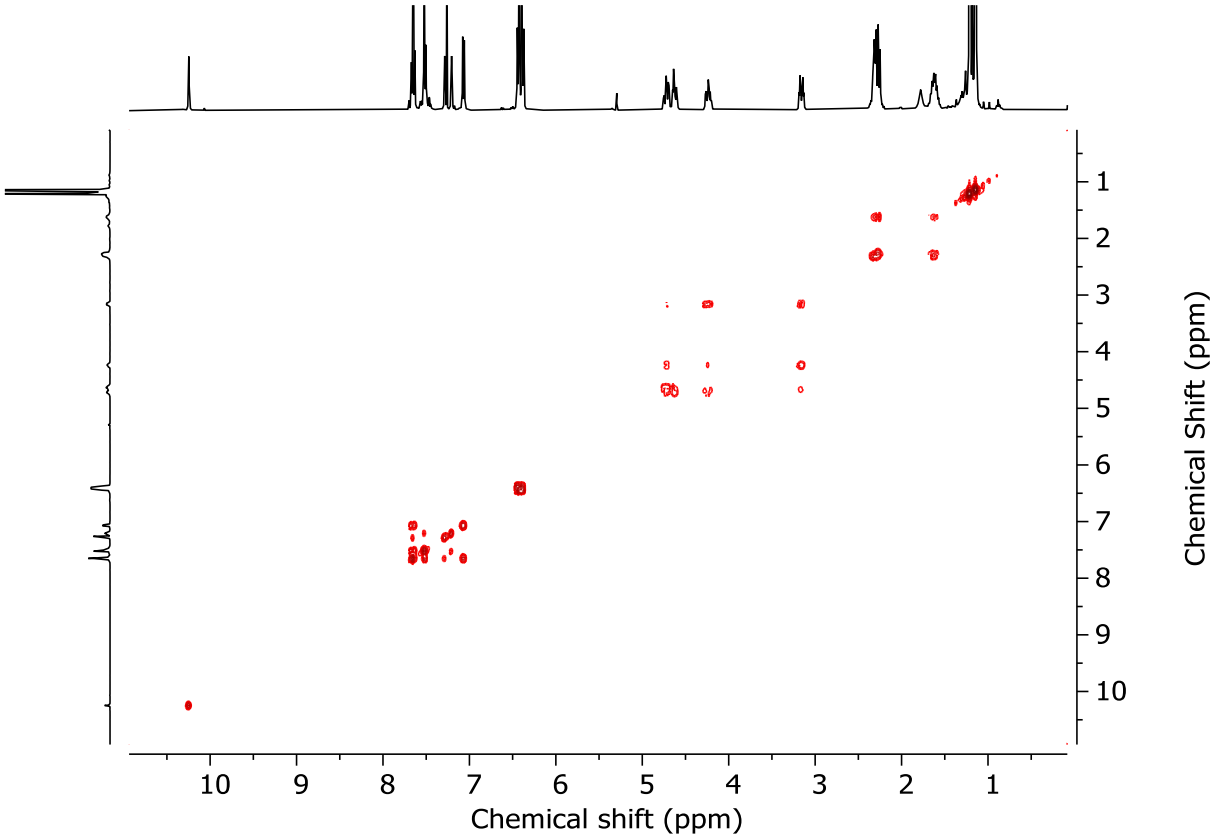

Figure 3.101 - COSY NMR ($CDCl_3$) of (Z_m)-**6**.

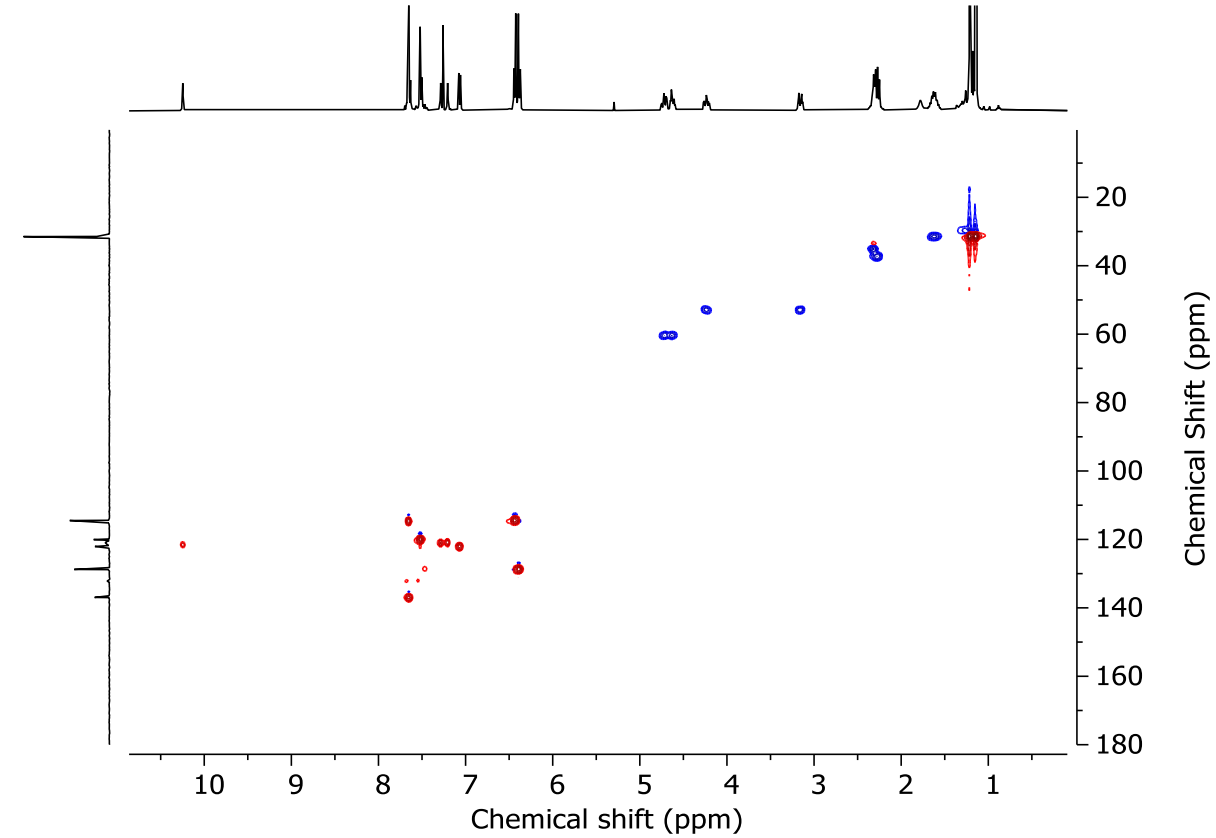

Figure 3.102 - HSQC NMR ($CDCl_3$) of (Z_m)-**6**.

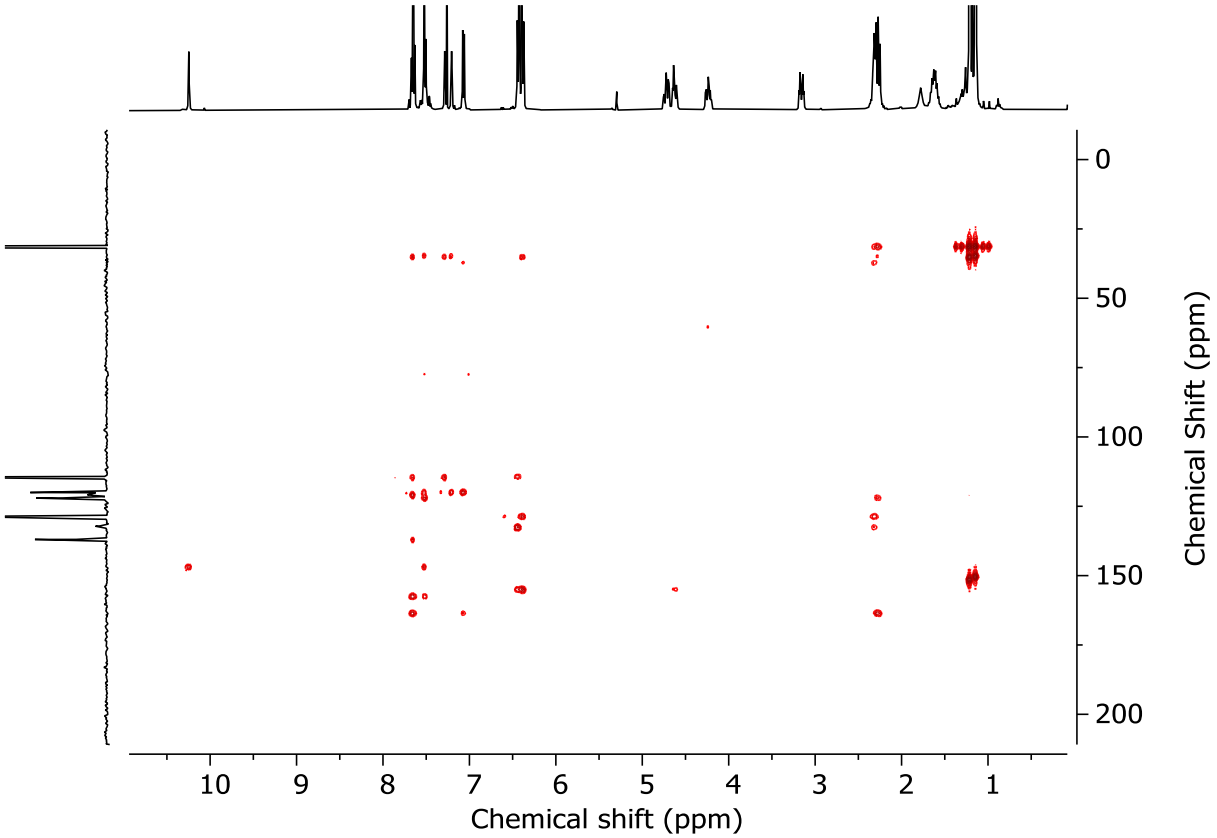

Figure 3.103 - HMBC NMR ($CDCl_3$) of (Z_m)-**6**.

Ether alkyne S8

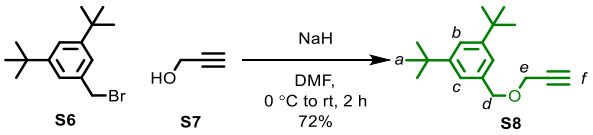

To a suspension of NaH (60% in mineral oil, 320 mg, 8.0 mmol) in DMF (15 mL) was added **S6** (250 mL, 4.0 mmol) dropwise at 0 °C. The reaction mixture was stirred for 10 minutes, then a solution of **S7** (566.4 mg, 2.0 mmol) in DMF (5 mL) was added dropwise over 10 minutes. The reaction mixture was allowed to warm to rt and stirred for 2 h. The reaction mixture was then quenched by adding H_2O (10 mL) dropwise. The aqueous and organic phases were separated, and the aqueous phase was then extracted with Et_2O (3 x 20 mL). The combined organic extracts were washed with brine (10 mL), dried ($MgSO_4$) and concentrated *in vacuo*. Chromatography (petrol-Et_2O 5→10%) gave **S8** as a colourless oil (372.1 mg, 72%).

All spectroscopic data in consitsant with the reported data.[26a]

^{1}H NMR (400 MHz, $CDCl_3$) δ: 7.37 (t, *J* = 1.9, 1H, H_b), 7.19 (dt, *J* = 2.0, 0.5, 2H, H_c), 4.60 (d, *J* = 0.5, 2H, H_d), 4.19 (d, *J* = 2.4, 2H, H_e), 2.47 (t, *J* = 2.3, 1H, H_f), 1.33 (s, 18H, H_a)

^{13}C NMR (101 MHz, $CDCl_3$) δ: 150.9, 136.3, 122.5, 122.0, 80.4, 74.5, 72.4, 57.2, 34.8, 31.5.

Ether rotaxanes (E_m)-7 and (Z_m)-7

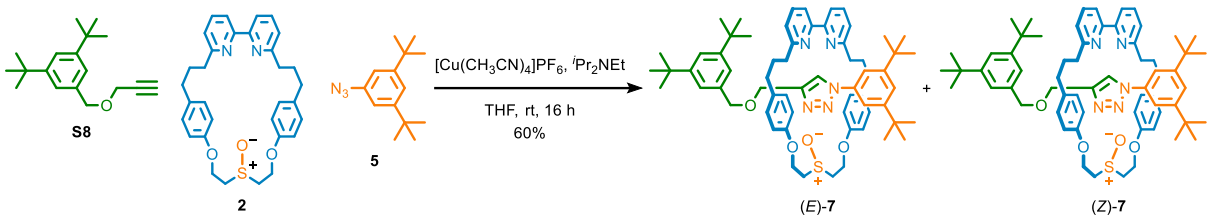

In a CEM vial were added **S8** (10.8 mg, 41.7 µmol), **5** (9.7 mg, 41.7 µmol), **2** (20.0 mg, 38.0 µmol) and $[Cu(CH_3CN)_4PF_6]$ (13.6 mg, 36.5 µmol). The vial was sealed and purged with N_2, then THF was added (1.0 mL), followed by $^iPr_2NEt$ (13.3 µL, 75.9 µmol). The solution was stirred at rt for 16 h. the solution was diluted with CH_2Cl_2 (2 mL), then EDTA-NH_3 (5 mL) was added. The solution was vigorously stirred until complete decolouration. The aqueous and organic phases were separated, and the aqueous phase was then extracted with CH_2Cl_2 (3 x 10 mL). The combined organic extracts were washed with brine (10 mL), dried ($MgSO_4$) and concentrated *in vacuo* to give a sample containing **7** as a mixture of diastereomers (49 : 51 *dr*, Figure 3.104). Chromatography (CH_2Cl_2-CH_3CN 0→100% then CH_3CN-MeOH 0→20%) gave **7** as an off-white foam (23.1 mg, 60%) as a mixture of diastereoisomers (1 : 0.9 *dr*, Figure 3.105).

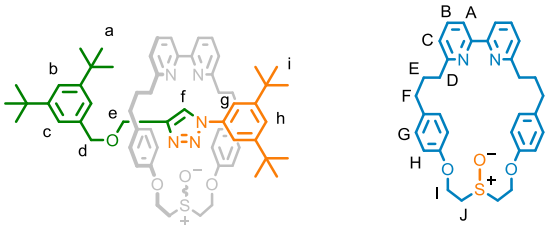

1st diastereoisomer

^{1}H NMR (400 MHz, $CDCl_3$) δ: 9.39 (s, 1H, H_f), 7.65 (t, *J* = 7.5, 2H, H_B), 7.55-7.47 (m, 4H, H_A, H_g), 7.32 (t, *J* = 1.8, 1H, H_h) 7.30 (t, *J* = 1.9, 1H, H_b), 7.08 (d, *J* = 5.4, 2H, H_C) ,7.02 (d, *J* = 1.8, 2H, H_c), 6.46-6.34 (m, 8H, H_G, H_H) 4.70-4.46 (m, 4H, H_I), 4.11 (s, 2H, H_e), 4.08 (s, 2H, Hd), 3.98 (ddd, *J* = 14.2, 9.3, 4.5, 2H, H_J) 3.01 (app dt, *J* = 13.6, 4.5, 2H, $H_{J'}$), 2.53-2.23 (m, 8H, H_D, H_F), 1.77-1.54 (m, 4H, H_E), 1.28 (s, 18H, H_i), 1.27 (s, 18H, H_a)

^{13}C NMR (101 MHz, $CDCl_3$) δ: 163.0, 157.6, 155.2, 154.9, 151.9, 150.4, 143.2, 137.5, 132.9, 128.8, 123.7, 121.9, 121.9, 120.0, 115.2, 115.0, 114.6, 114.4, 72.3, 72.2, 63.1, 63.0, 60.4, 52.8, 37.3, 35.2, 34.7, 34.6, 31.7, 29.7.

LR-ESI-MS (+ve) *m/z* = 1016.6 $[M+H]^+$, for isotopic pattern see Figure 3.111.

2nd diastereoisomer

^{1}H NMR (400 MHz, $CDCl_3$) δ: 9.19 (s, 1H, H_f), 7.59 (t, *J* = 7.7, 2H, H_B), 7.55-7.47 (m, 2H, H_A), 7.38 (t, *J* = 1.8, 1H, H_h) 7.28 (t, *J* = 1.9, 1H, H_b), 7.06 (d, *J* = 5.4, 2H, H_C) ,6.96 (d, *J* = 1.8, 2H, H_c), 6.56 (app. s, 8H, H_G, H_H) 4.70-4.46 (m, 4H, H_l), 3.91 (s, 2H, H_e), 3.83 (s, 2H, H_d), 3.76 (ddd, *J* = 14.2, 9.3, 4.5, 2H, H_J) 3.15 (app dt, *J* = 13.6, 4.5, 2H, $H_{J'}$), 2.53-2.23 (m, 8H, H_D, H_F), 1.77-1.54 (m, 4H, H_E), 1.27 (s, 18H, H_i), 1.23 (s, 18H, H_a)

^{13}C NMR (101 MHz, $CDCl_3$) δ: 162.7, 157.6, 155.2, 151.6, 150.5, 143.9, 136.7, 133.6, 128.5, 123.7, 121.9, 121.8, 121.7, 121.33, 120.0, 115.2, 115.0, 114.6, 114.4, 72.3, 72.2, 63.1, 63.0, 60.7, 51.8, 37.2, 35.2, 34.8, 31.4, 29.7.

LR-ESI-MS (+ve) *m/z* = 1016.6 $[M+H]^+$, for isotopic pattern see Figure 3.111.

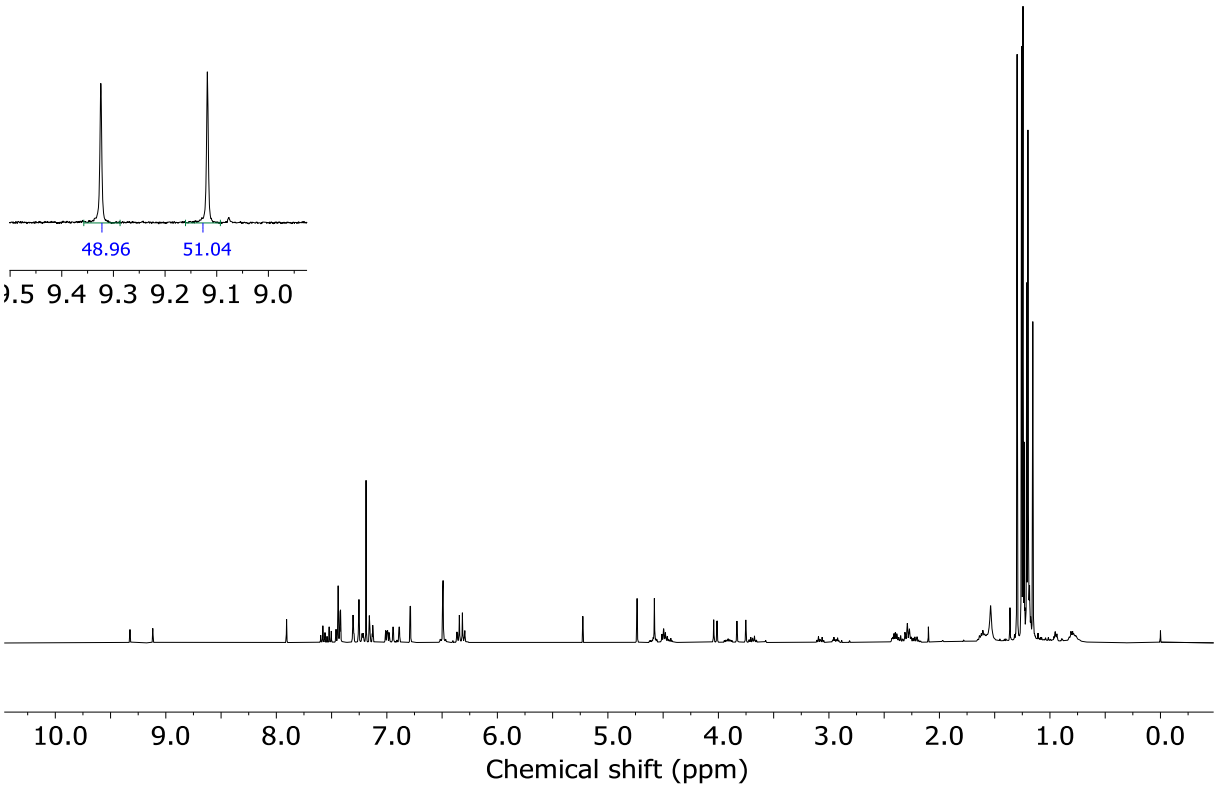

Figure 3.104 - ^{1}H NMR ($CDCl_3$, 400 MHz) of of (E_m)-**7** and (Z_m)-**7** prior to chromatography (49 : 51 *dr*).

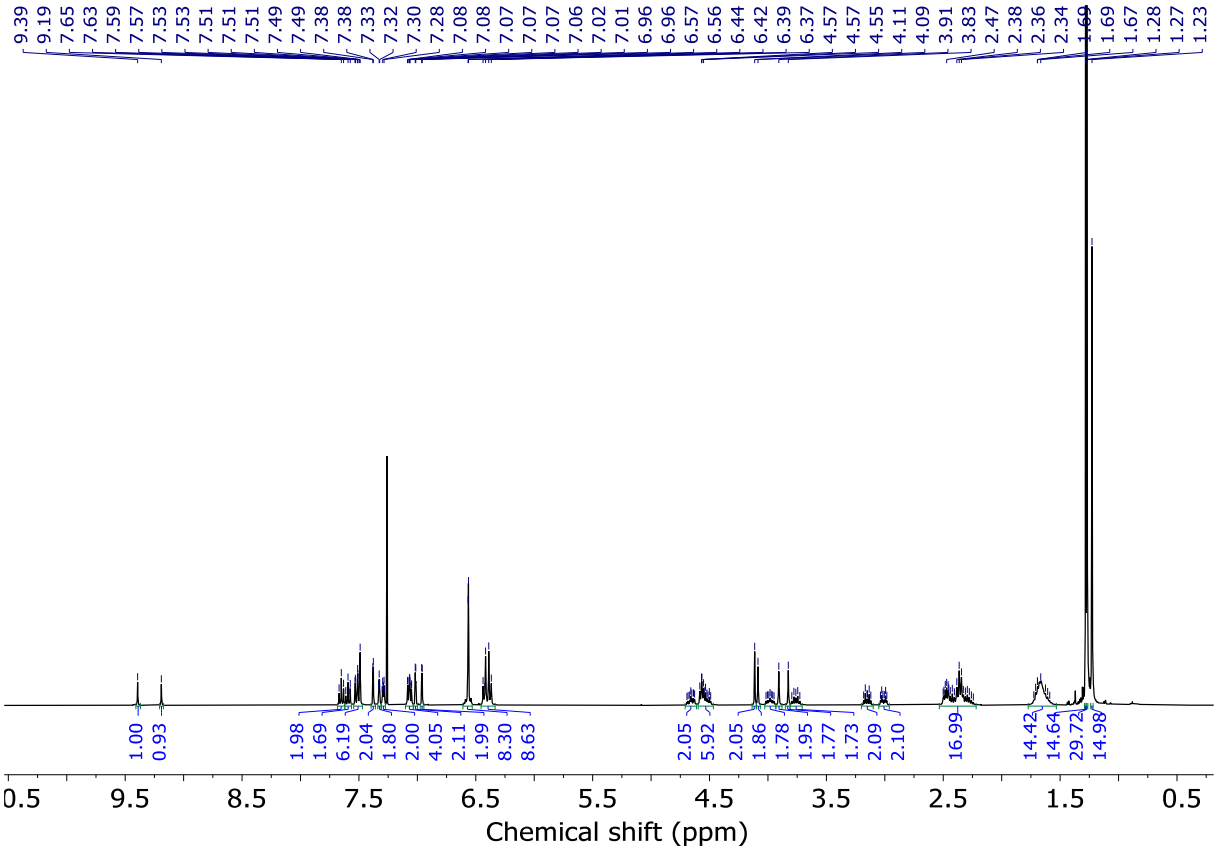

Figure 3.105 - ^{1}H NMR ($CDCl_3$, 400 MHz) of (E_m)-**7** and (Z_m)-**7** (1 : 0.9 *dr*).

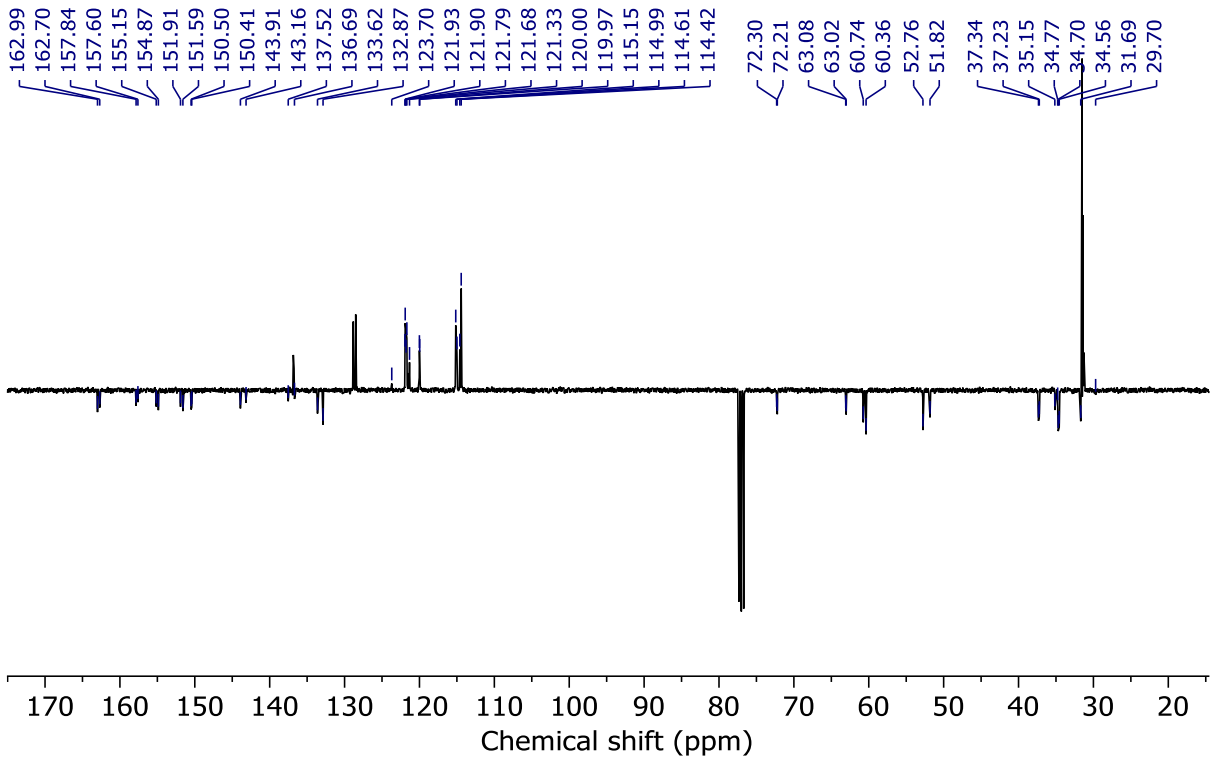

Figure 3.106 - JMOD NMR ($CDCl_3$, 101 MHz) of (E_m)-**7** and (Z_m)-**7** (1 : 0.9 *dr*).

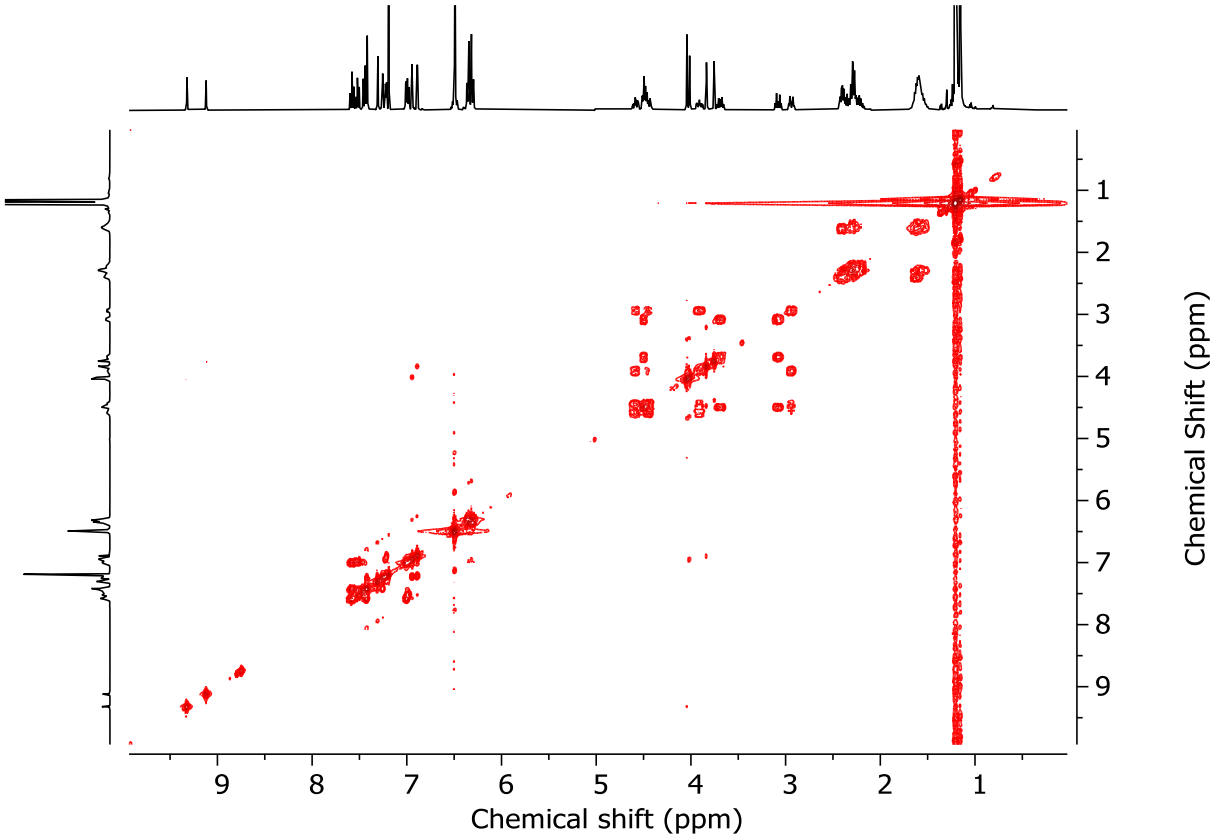

Figure 3.107 - COSY NMR ($CDCl_3$) of (E_m)-**7** and (Z_m)-**7** (1 : 0.9 *dr*).

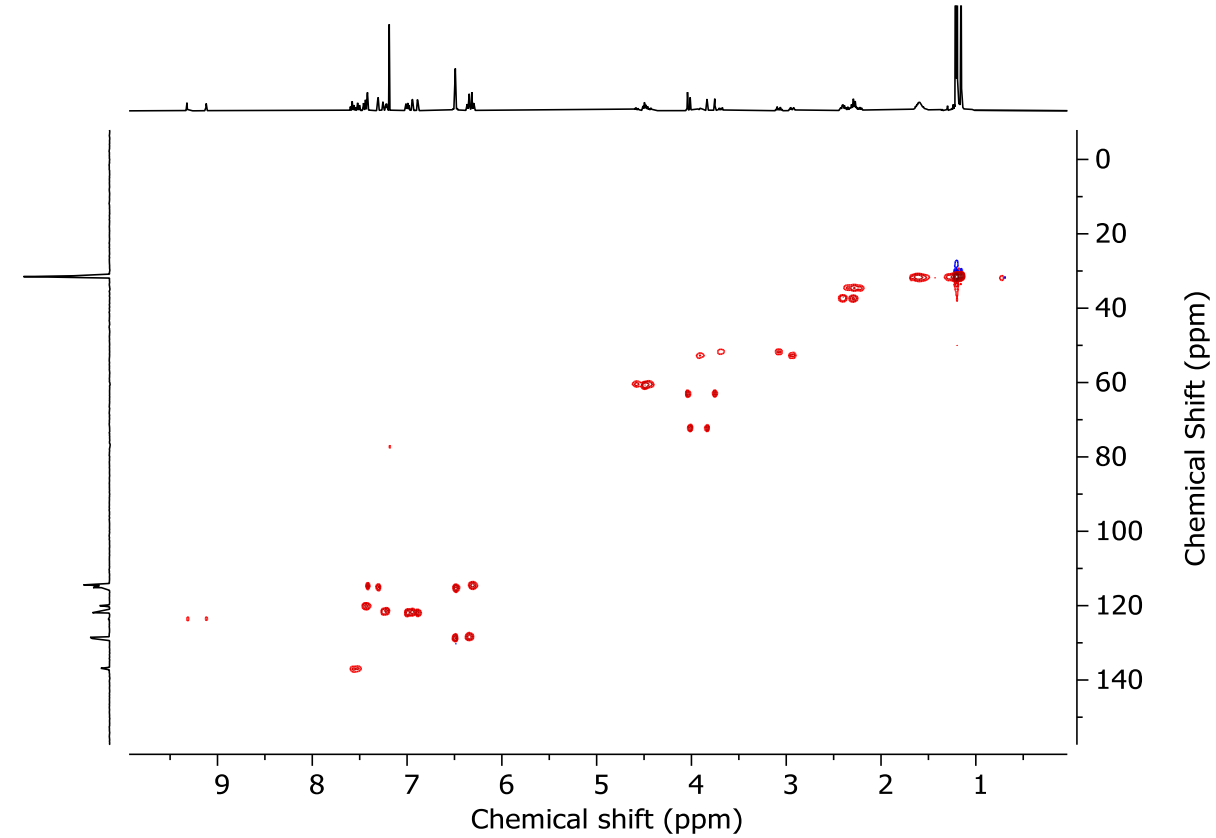

Figure 3.108 - HSQC NMR ($CDCl_3$) of (E_m)-**7** and (Z_m)-**7** (1 : 0.9 *dr*).

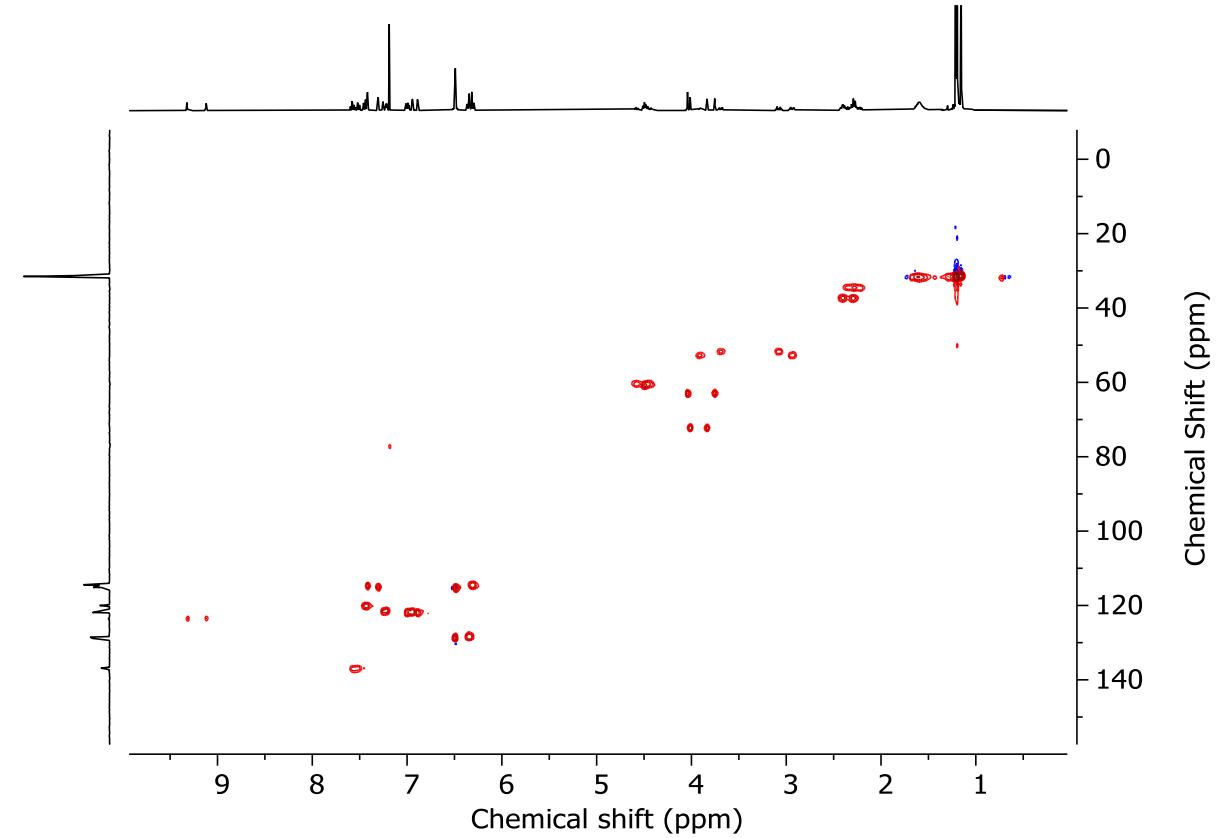

Figure 3.109 - HMBC NMR ($CDCl_3$) of (E_m)-**7** and (Z_m)-**7** (1 : 0.9 *dr*).

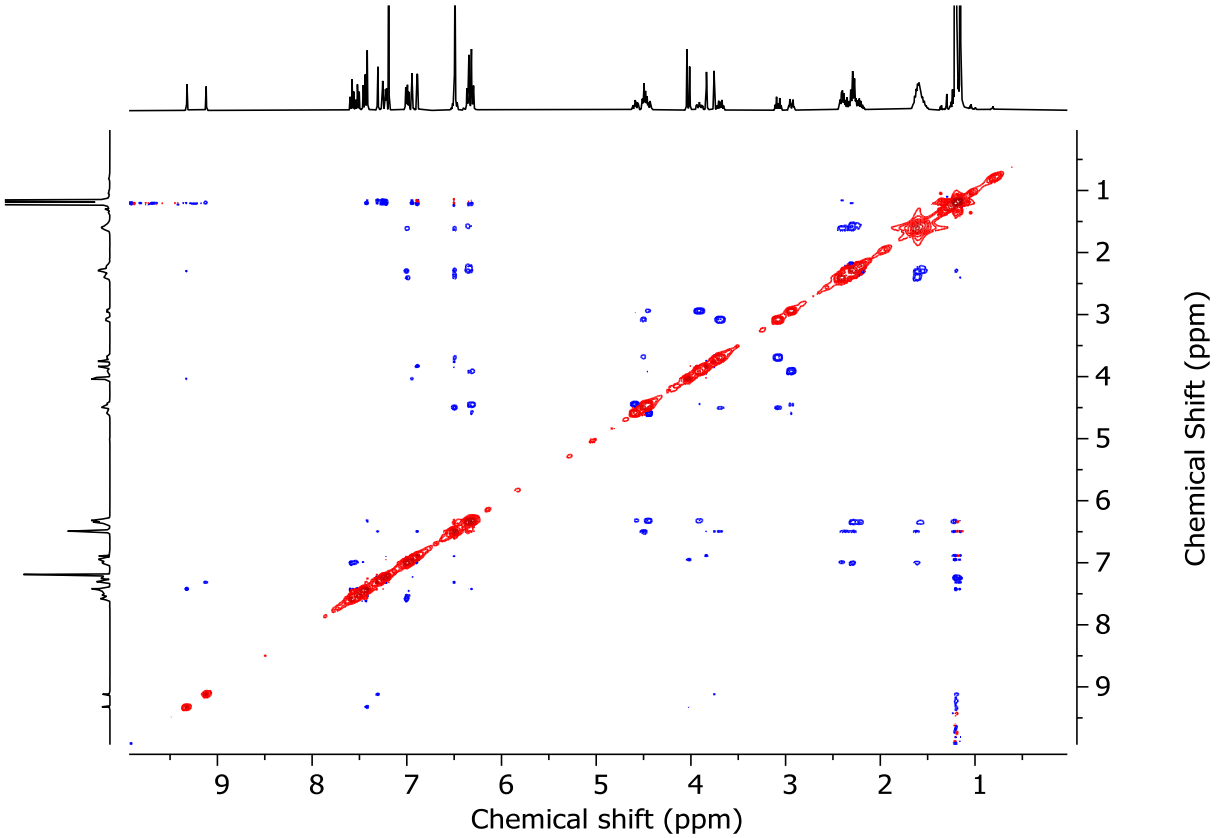

Figure 3.110 - NOESY NMR ($CDCl_3$) of (E_m)-**7** and (Z_m)-**7** (1 : 0.9 *dr*).

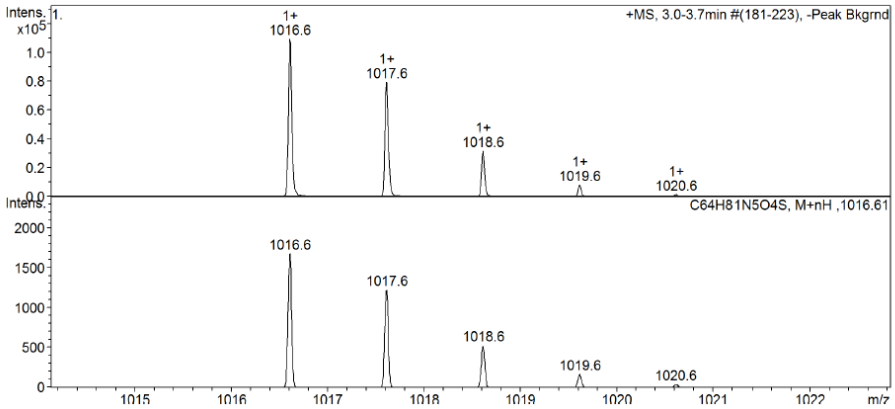

Figure 3.111 - Calculated (top) and observed (bottom) isotopic patterns for (E_m)-**7** and (Z_m)-**7**.

Alkyl bromide S10

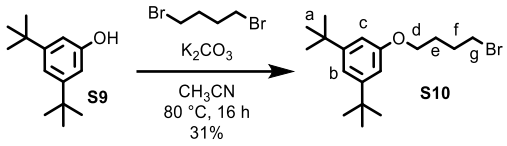

A suspension of **S9** (206 mg, 1.0 mmol), K_2CO_3 (552.8 mg, 4.0 mmol) and 1,4-dibromobutane (459 µL, 4.0 mmol) was stirred at 85 °C for 16 h. H_2O (10 mL) was added, then the aqueous and organic phases were separated, and the aqueous phase was then extracted with CH_2Cl_2 (3 x 20 mL). The combined organic extracts were washed with brine (10 mL), dried ($MgSO_4$) and concentrated *in vacuo*. Chromatography (petrol-EtOAc 0→10%) gave **S10** as a colourless liquid (106 mg, 31%).

^{1}H NMR (400 MHz, $CDCl_3$) δ: 7.02 (t, *J* = 1.6, 1H, H_b), 6.76 (d, *J* = 1.7, 2H, H_c), 4.01 (t, *J* = 6.1, 2H, H_d), 3.51 (t, *J* = 6.7, 2H, H_g), 2.09 (tt, *J* = 9.8, 6.5, 2H, H_f), 1.95 (tt, *J* = 5.9, 8.6, 2H, H_e), 1.32 (s, 18H, H_a)

^{13}C NMR (101 MHz, $CDCl_3$) δ: 158.4, 152.2, 115.1, 108.8, 66.6, 35.0, 33.6, 31.5, 29.6, 28.1.

HR-EI-MS (+ve) *m/z* = 340.1398 $[M+H]^+$ (calc. 340.1402 *m/z* for $C_{18}H_{29}BrO$).

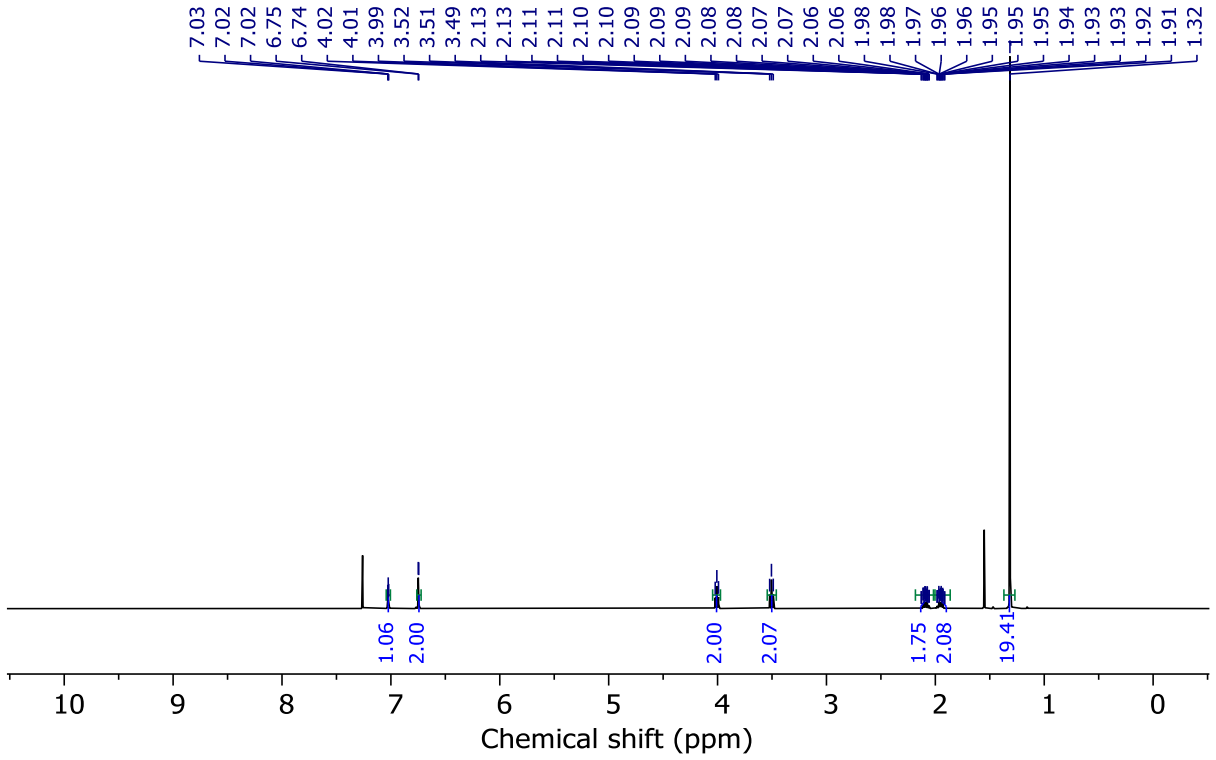

Figure 3.112 - ^{1}H NMR ($CDCl_3$, 400 MHz) of **S10**.

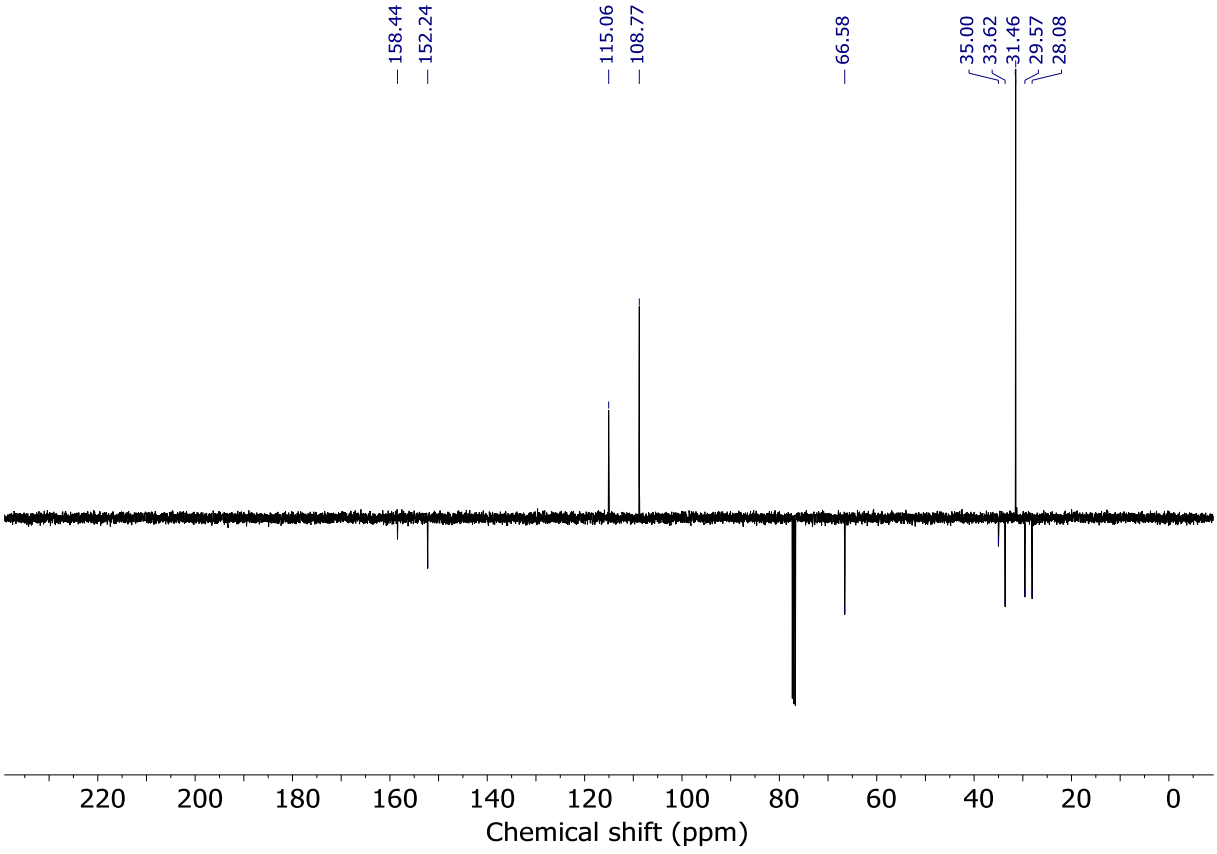

Figure 3.113 - JMOD NMR ($CDCl_3$, 101 MHz) of **S10**.

Azide S11

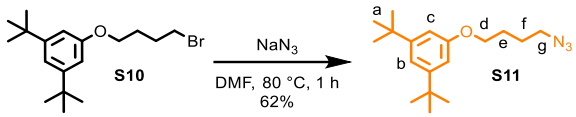

A suspension of **S10** (108.1 mg, 0.31 mmol) and NaN_3 (80.6 mg, 1.24 mmol) in DMF (2 mL) was stirred ad 80 °C for 1 h. 5% $LiCl_{(aq)}$ (5 mL) was added, then the aqueous and organic phases were separated, and the aqueous phase was then extracted with EtOAc (3 x 10 mL). The combined organic extracts were washed with brine (10 mL), dried ($MgSO_4$) and concentrated *in vacuo*. Chromatography (petrol-EtOAc 90 : 10) gave **S11** as a colourless liquid (58.0 mg, 62%).

^{1}H NMR (400 MHz, $CDCl_3$) δ: 7.05 (t, *J* = 1.6, 1H, H_b), 6.77 (d, *J* = 1.7, 2H, H_c), 4.02 (t, *J* = 6.0, 2H, H_d), 3.39 (t, *J* = 6.5, 2H, H_g), 1.95-1.77 (m, 4H, H_e, H_f), 1.33 (s, 18H, H_a).

^{13}C NMR (101 MHz, $CDCl_3$) δ: 158.5, 152.2, 115.1, 108.8, 66.9, 51.3, 35.0, 31.5, 26.7, 25.9.

HR-EI-MS (+ve) *m/z* = 303.2306 $[M+H]^+$ (calc. 303.2311 *m/z* for $C_{18}H_{29}N_3O$).

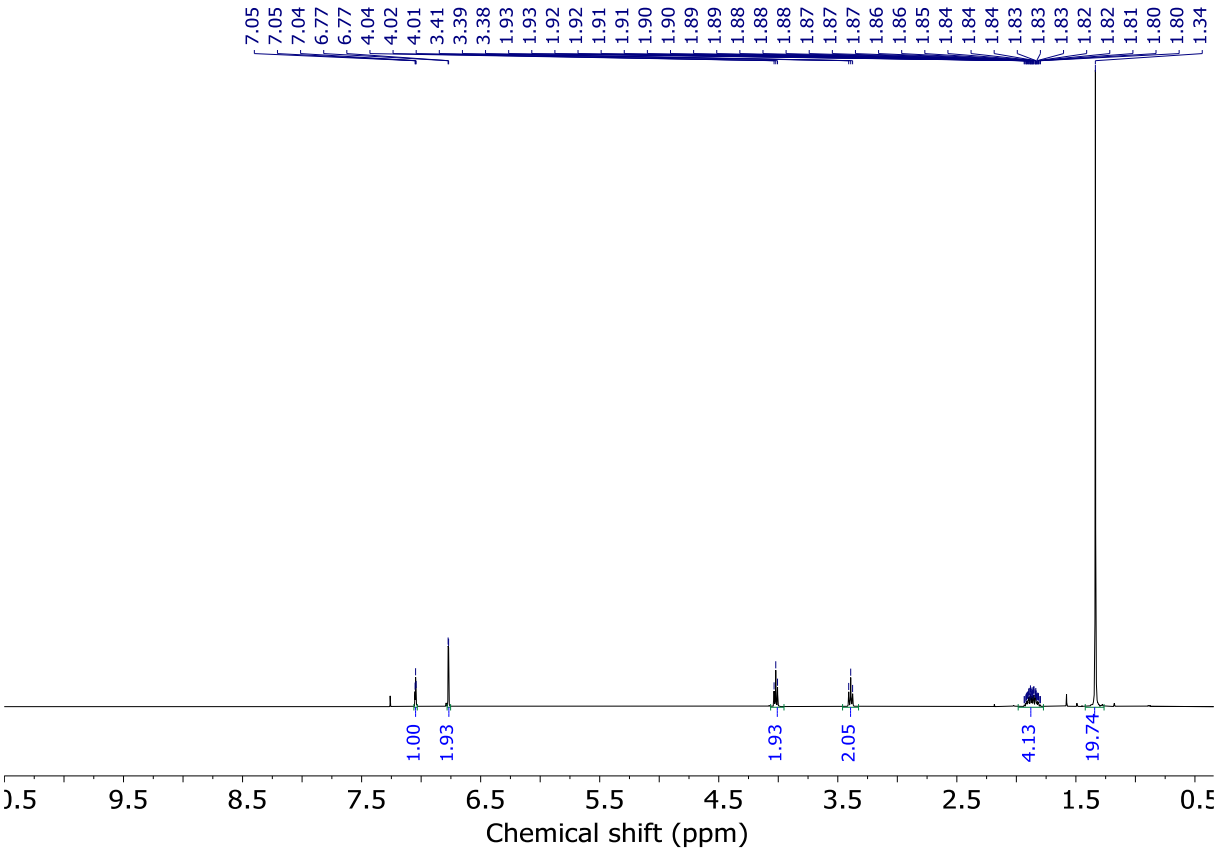

Figure 3.114 - ^{1}H NMR ($CDCl_3$, 400 MHz) of **S11**.

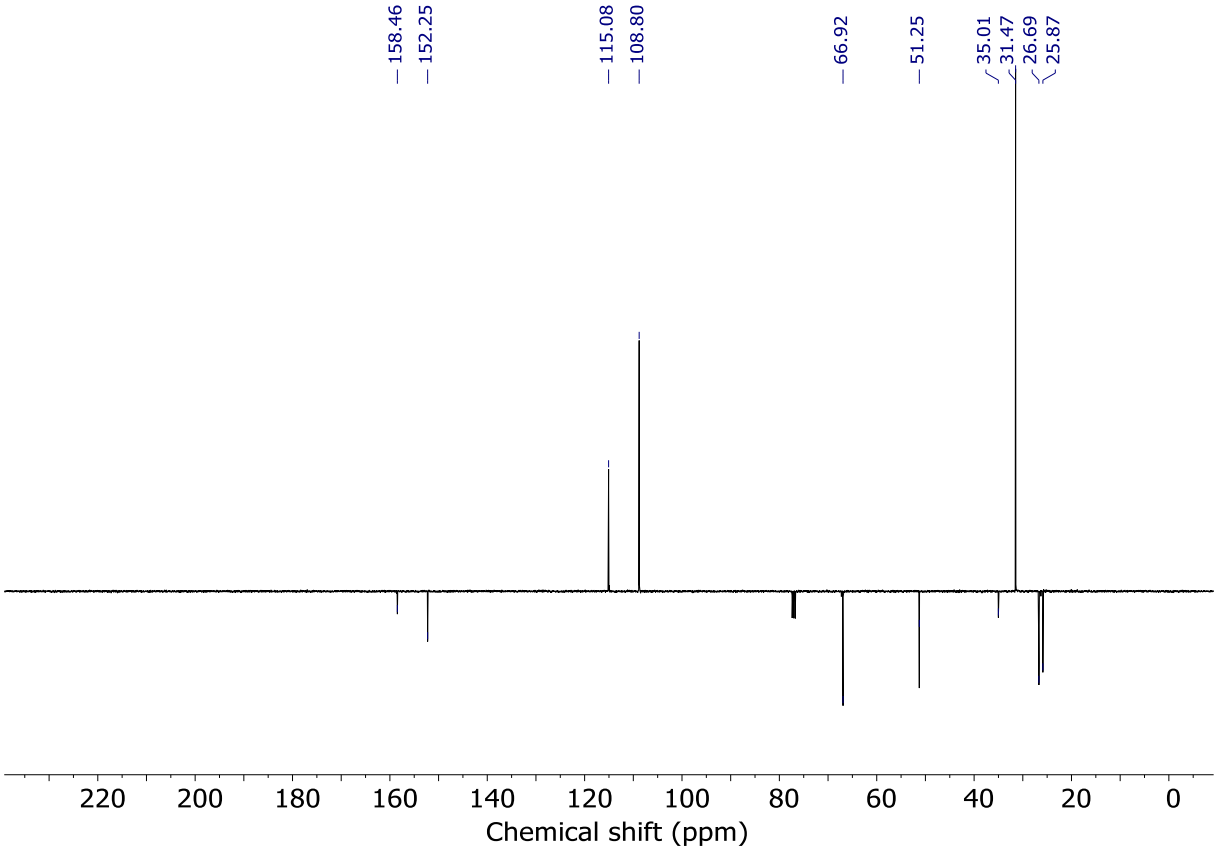

Figure 3.115 - JMOD NMR ($CDCl_3$, 101 MHz) of **S11**.

Phenolic Rotaxanes (E_m)-8 and (Z_m)-8

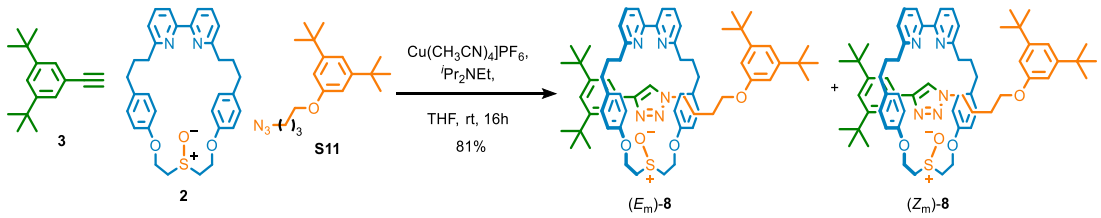

In a CEM vial were added **3** (2.1 mg, 10.3 µmol), **S11** (3.1 mg, 10.3 µmol), **2** (5.0 mg, 9.5 µmol) and $[Cu(CH_3CN)_4PF_6]$ (3.4 mg, 9.1 µmol). The vial was sealed and purged with N_2, then THF was added (1.0 mL), followed by $^iPr_2NEt$ (3.3 µL, 19.0 µmol). The solution was stirred at rt for 16 h. the solution was diluted with CH_2Cl_2 (2 mL), then EDTA-NH_3 (5 mL) was added. The solution was vigorously stirred until complete decolouration. The aqueous and organic phases were separated, and the aqueous phase was then extracted with CH_2Cl_2 (3 x 10 mL). The combined organic extracts were washed with brine (10 mL), dried ($MgSO_4$) and concentrated *in vacuo* to give a sample containing **8** as a mixture of diastereomers (61 : 39 *dr*, Figure 3.116). Chromatography (CH_2Cl_2-CH_3CN 0→100%) gave **8** as a colourless oil (8.1 mg, 82%) as a mixture of diastereoisomers (1.4 : 1 *dr*, Figure 3.117).

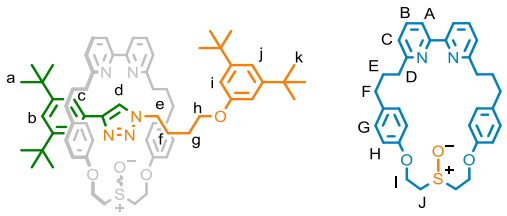

1st diastereoisomer

^{1}H NMR (500 MHz, $CDCl_3$) δ: 8.60 (s, 1H, H_d), 7.63-7.54 (m, 4H, H_B, H_c), 7.51 (d, *J* = 7.6, 2H, H_A), 7.31(t, *J* = 1.8, 1H, H_b), 7.10 (d, *J* = 7.7, 2H, H_C), 7.04-7.00 (m, 1H, H_j), 6.70 (d, *J* = 8.0, 4H, H_G), 6.67 (d, *J* = 1.6, 2H, H_i), 6.62 (d, *J* = 8.0, 4H, H_H), 4.65-4.58 (m, 2H, H_J), 4.57-4.48 (m, 2H, $H_{J'}$), 3.79 (ddd, *J* = 14.3, 9.8, 4.5, 2H, H_I), 3.56-3.48 (m, 2H, H_h), 3.10-2.98 (m, 4H, $H_{I'}$, H_e), 2.61-2.31 (m, 8H, H_D, H_F), 1.86-1.62 (m, 4H, H_E), 1.34 (s, 18H, H_k), 1.26 (s, 18H, H_a), 1.21-0.75 (m, 4H, H_f, H_g).

^{13}C NMR (126 MHz, $CDCl_3$) δ: 162.6, 158.5, 157.8, 155.5, 152.1, 150.9, 147.5, 136.9, 133.9, 139.6, 129.3, 122.1, 121.9, 121.5, 120.2, 119.8, 114.7, 114.7, 108.7, 66.5, 60.3, 53.1, 48.6, 37.4, 35.0, 34.5, 31.9, 31.5, 31.4, 26.2, 26.0

LR-ESI-MS (+ve) *m/z* = 1044.6 $[M+H]^+$, for isotopic pattern see Figure 3.123.

2nd diastereoisomer

^{1}H NMR (500 MHz, $CDCl_3$) δ: 8.25 (s, 1H, H_d), 7.65 (t, *J* = 7.6, 2H, H_B), 7.63-7.54 (m, 4H, H_A, H_c), 7.33 (t, *J* = 1.4, H_b), 7.12 (d, *J* = 7.7, 2H, H_C), 7.04-7.00 (m, 1H, H_j), 6.65 (d, *J* = 1.6, 2H, H_i), 6.53 (app. s, 8H, H_G, H_H), 4.65-4.58 (m, 2H, H_J), 4.57-4.48 (m, 2H, $H_{J'}$), 3.72 (dt, *J* = 13.6, 7.0, 2H, H_I), 3.56-3.48 (m, 2H, H_e), 3.40 (t, *J* = 7.5, 2H, H_h), 3.10-2.98 (m, 2H, $H_{I'}$), 2.64 (t, *J* = 8.5, 4H, H_D), 2.61-2.31 (m, 4H, H_F), 1.35 (s, 18H, H_a), 1.86-1.62 (m, 4H, H_E), 1.33 (s, 18H, H_k) 1.21-0.75 (m, 4H, H_f, H_g)

^{13}C NMR (126 MHz, $CDCl_3$) δ: 162.6, 158.4, 157.9, 155.0, 152.2, 150.7, 147.2, 136.9, 133.9, 130.7, 128.7, 122.0, 121.2, 121.2, 120.2, 120.1, 115.2, 114.9, 108.6, 66.5, 61.0, 51.8, 48.8, 37.6, 35.0, 34.3, 32.0, 31.6, 31.5, 26.2, 26.1

HR-ESI-MS (+ve) *m/z* = 1044.6 $[M+H]^+$, for isotopic pattern see Figure 3.123.

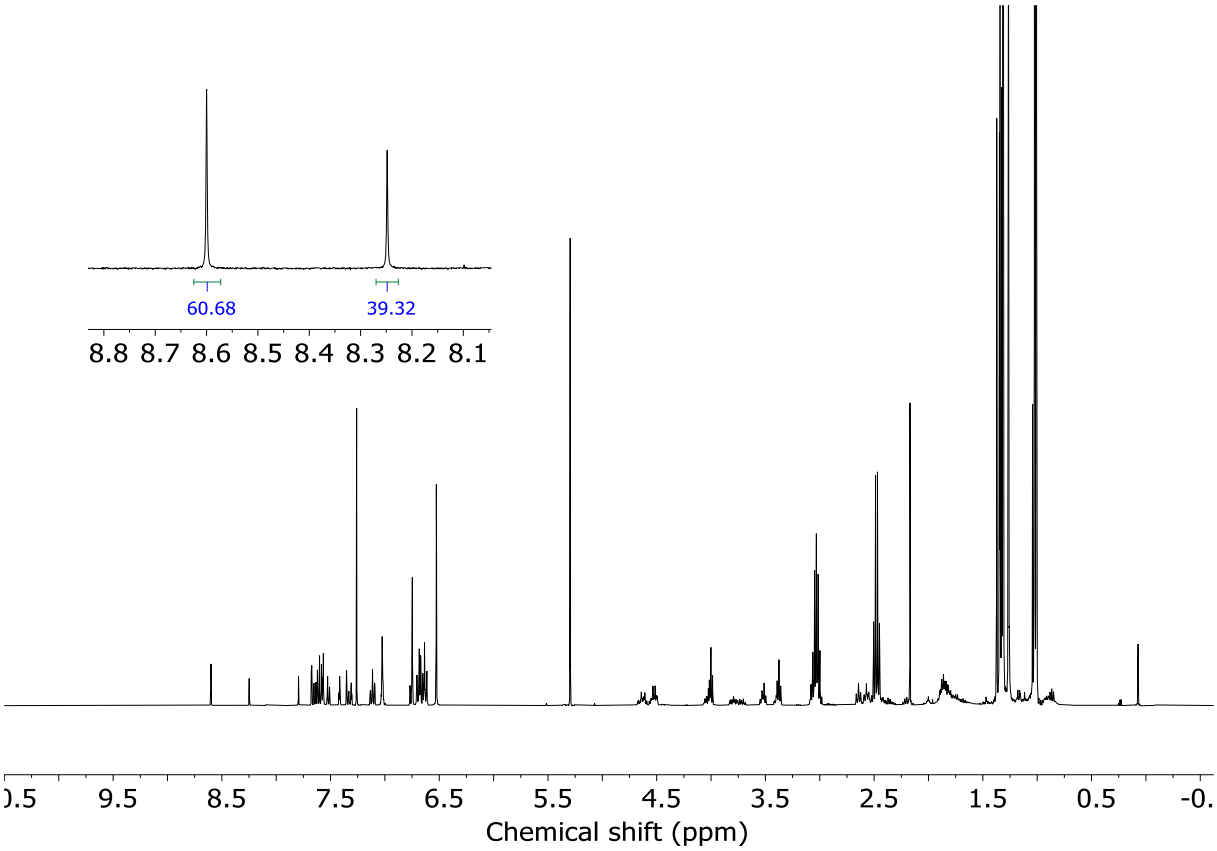

Figure 3.116 - ^{1}H NMR ($CDCl_3$, 400 MHz) of of (E_m)-**8** and (Z_m)-**8** prior to chromatography (61 : 39 *dr*).

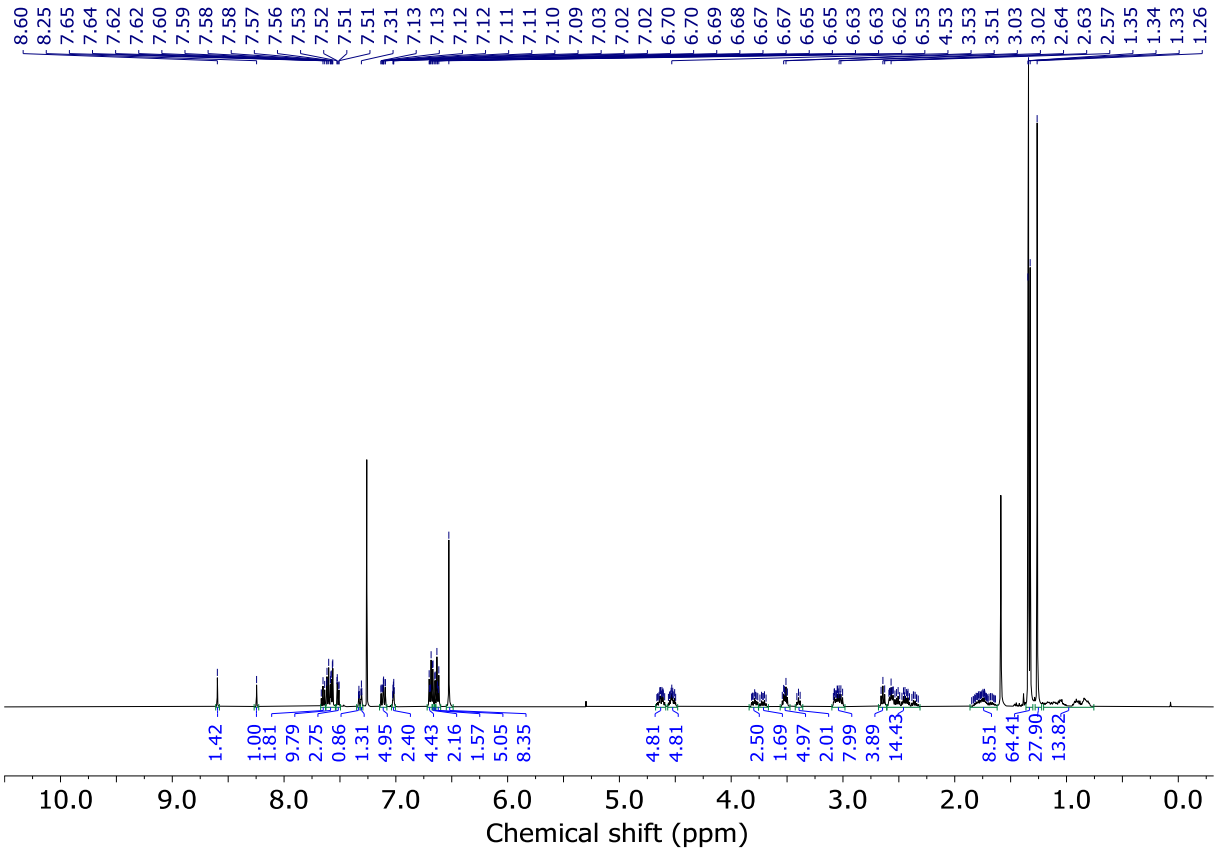

Figure 3.117 - ^{1}H NMR ($CDCl_3$, 500 MHz) of (E_m)-**8** and (Z_m)-**8** (1.4 : 1 *dr*).

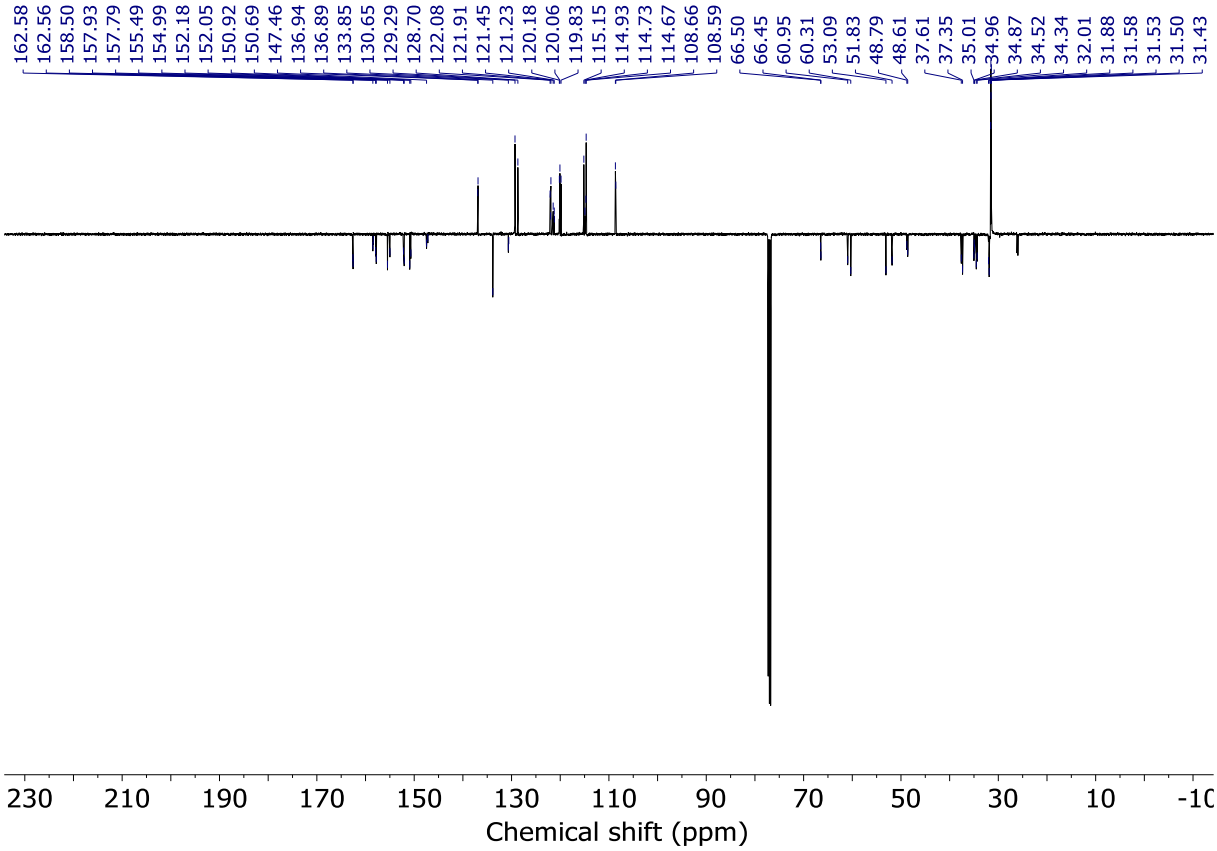

Figure 3.118 - JMOD NMR ($CDCl_3$, 126 MHz) of (E_m)-**8** and (Z_m)-**8** (1.4 : 1 *dr*).

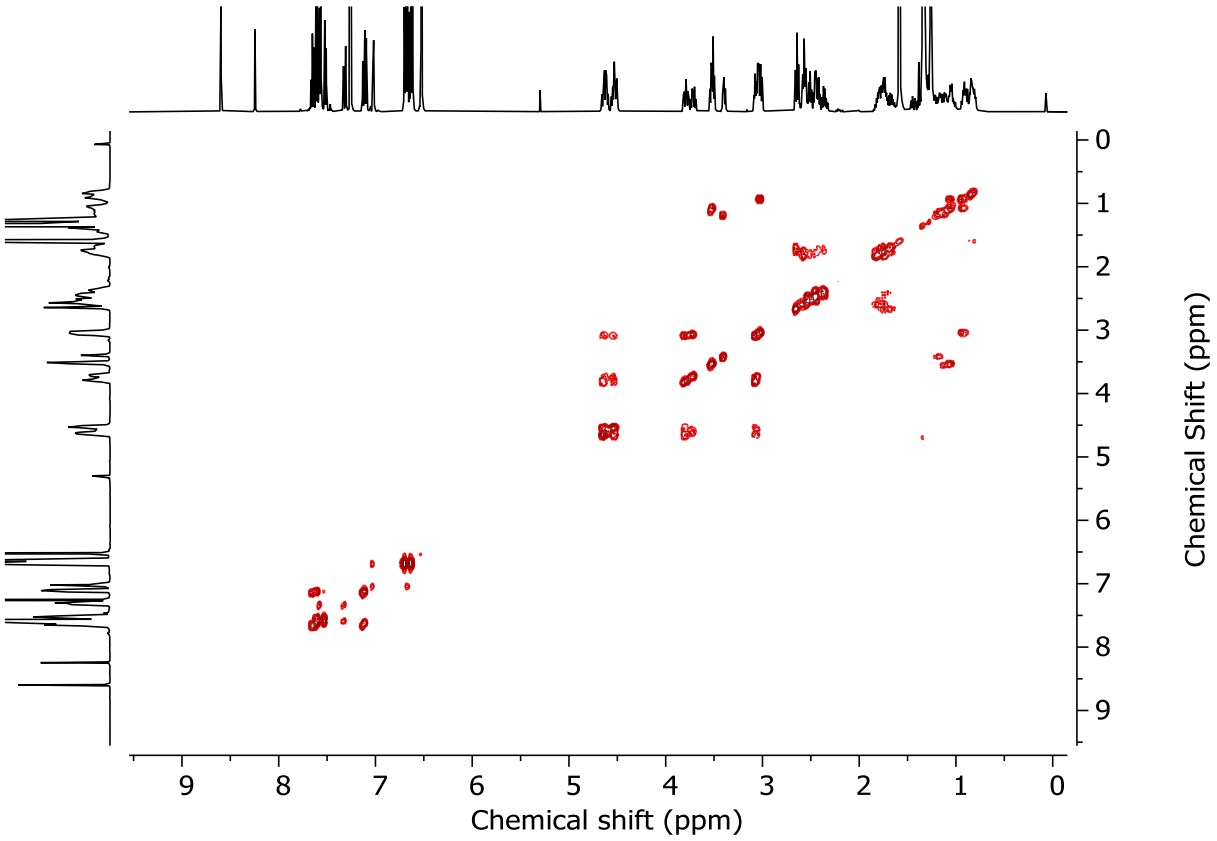

Figure 3.119 - COSY NMR ($CDCl_3$) of (E_m)-**8** and (Z_m)-**8** (1.4 : 1 *dr*).

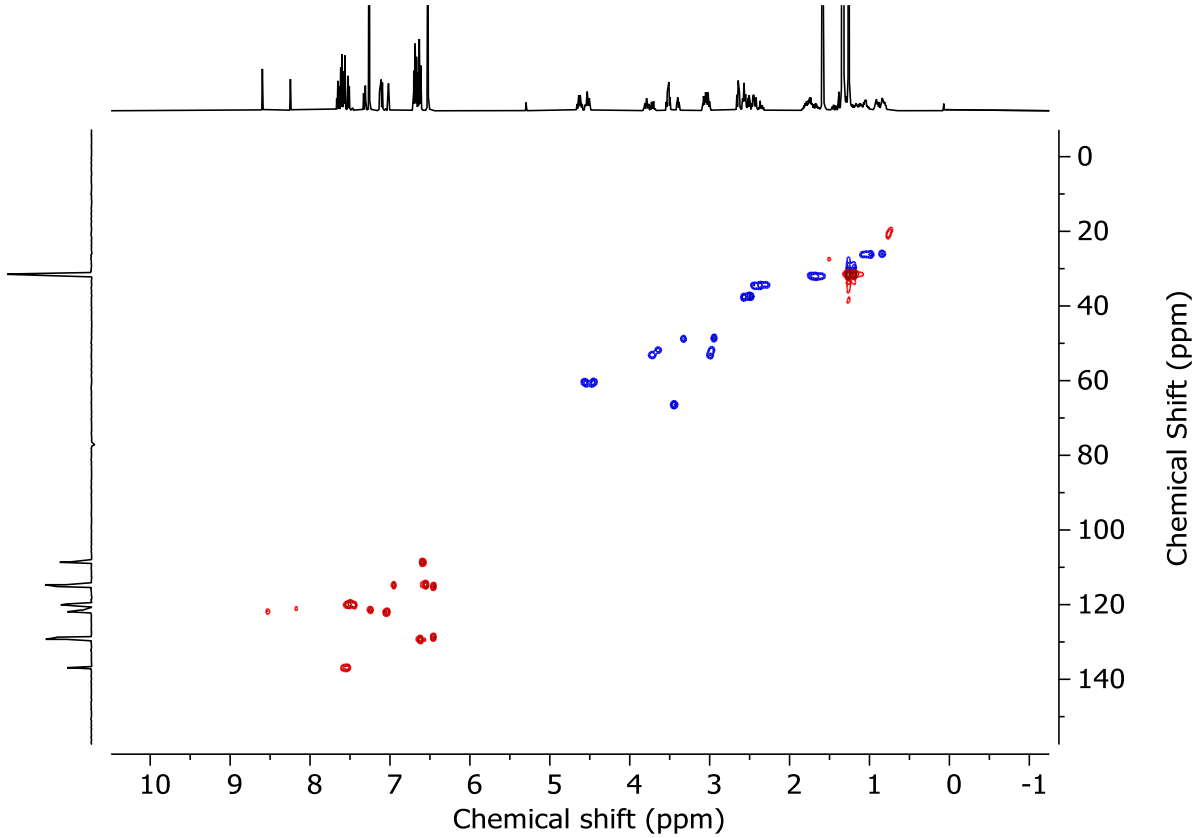

Figure 3.120 - HSQC NMR ($CDCl_3$) of (E_m)-**8** and (Z_m)-**8** (1.4 : 1 *dr*).

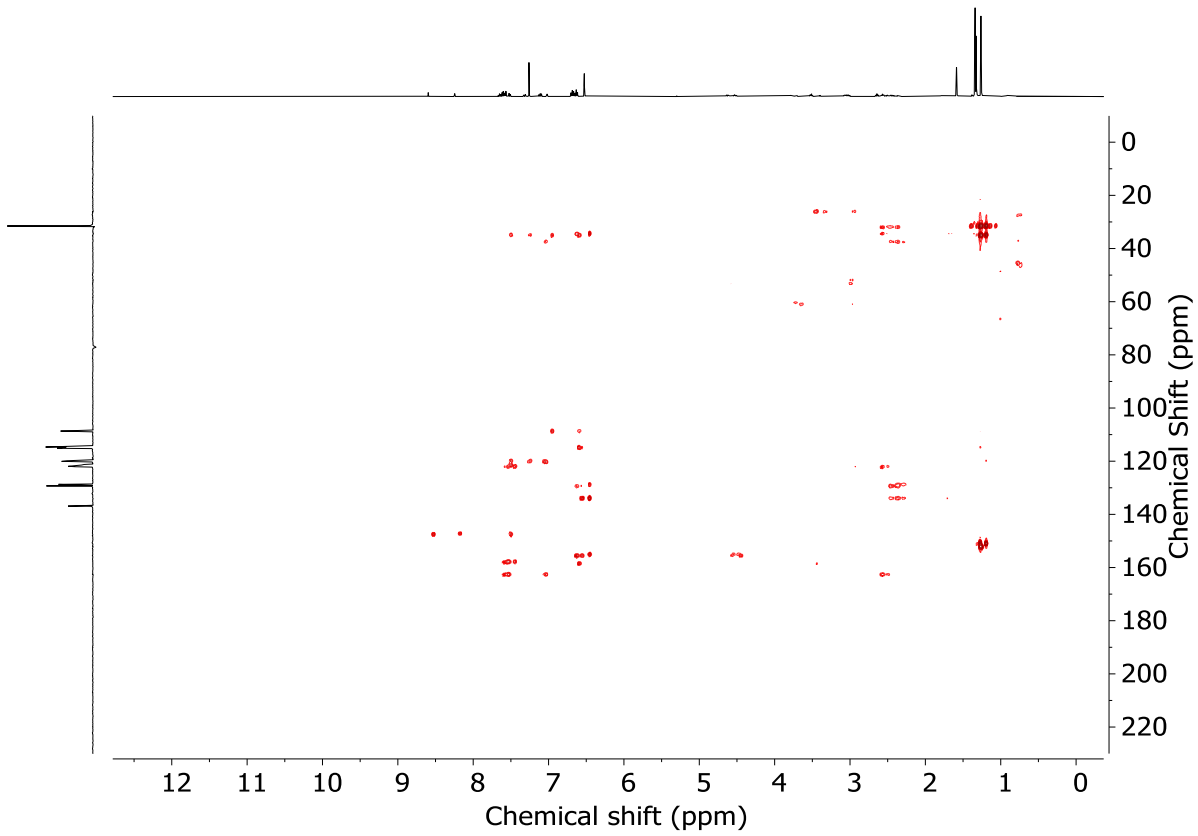

Figure 3.121 - HMBC NMR ($CDCl_3$) of (E_m)-**8** and (Z_m)-**8** (1.4 : 1 *dr*).

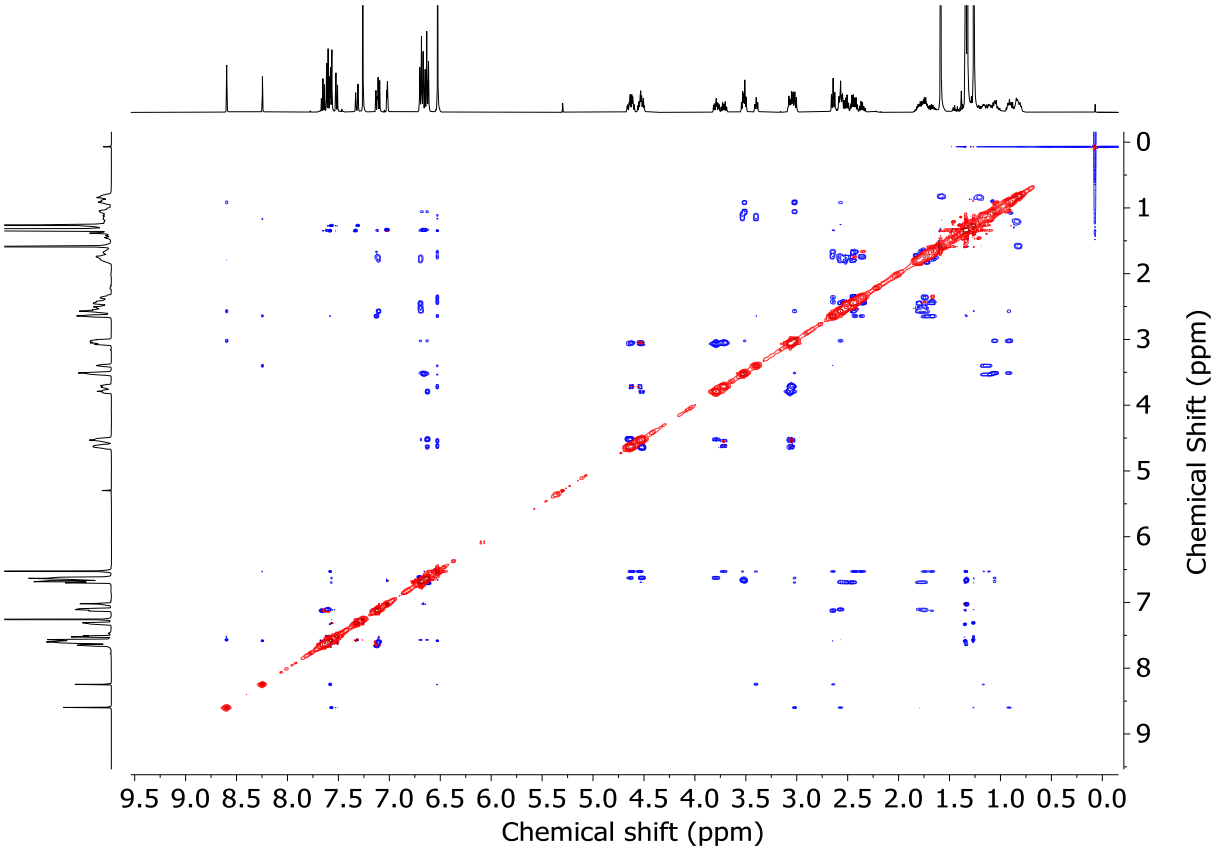

Figure 3.122 - NOESY NMR ($CDCl_3$) of (E_m)-**8** and (Z_m)-**8** (1.4 : 1 *dr*).

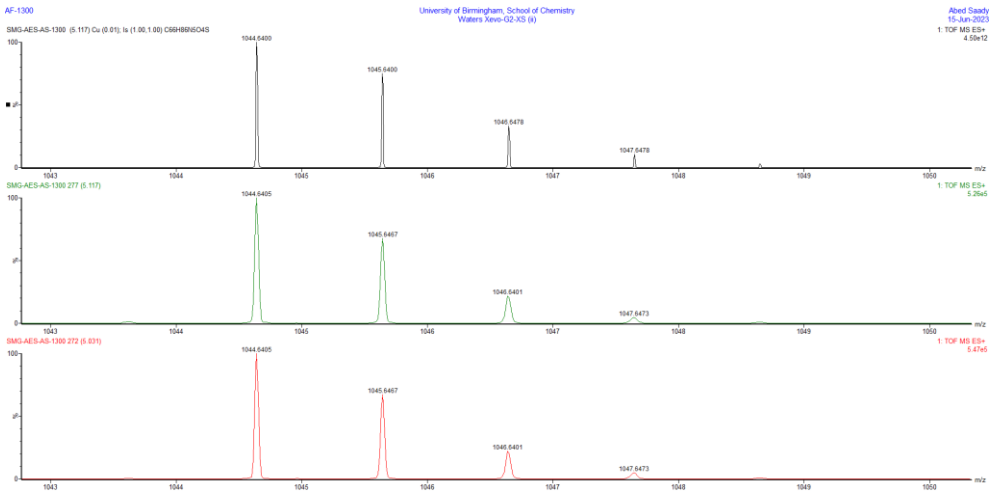

Figure 3.123 - Calculated (top) and observed (middle, bottom) isotopic patterns for (E_m)-**8** and (Z_m)-**8**.

Amide functionalised alkyne S14

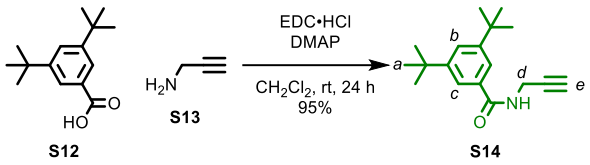

A CEM MW vial was charged with **S12** (140.6 mg, 0.60 mmol), **S13** (40.5 µL, 0.50 mmol), EDC · HCl (191.7 mg, 1.0 mmol), DMAP (2 crystals) and CH_2Cl_2 (5 mL). The reaction mixture was stirred at rt for 24 h. H_2O (10 mL) was added, then the aqueous and organic phases were separated, and the aqueous phase was then extracted with CH_2Cl_2 (3 x 20 mL). The combined organic extracts were washed with brine (10 mL), dried ($MgSO_4$) and concentrated *in vacuo*. Chromatography (petrol-EtOAc 0→60%) gave **S14** as a white solid (141 mg, 95%).

^{1}H NMR (400 MHz, $CDCl_3$) δ: 7.59 (t, *J* = 1.8, 1H, H_b), 7.57 (d, *J* = 1.8, 2H, H_c), 6.34 (t, *J* = 5.2, 1H, NH), 4.26 (dd, *J* = 2.5, 5.4, 2H, H_d), 2.28 (t, *J* = 2.5, 1H, H_e), 1.34 (s, 18H, H_a).

^{13}C NMR (101 MHz, $CDCl_3$) δ: 168.2, 151,4, 133.4, 126.0, 121.2, 79.8, 71.7, 35.0, 31.4, 29.7.

HR-ESI-MS (+ve) *m/z* = 294.1841 $[M+Na]^+$ (calc. 294.1828 *m/z* for $C_{18}H_{25}NaNO$).

Melting point 135-137 °C.

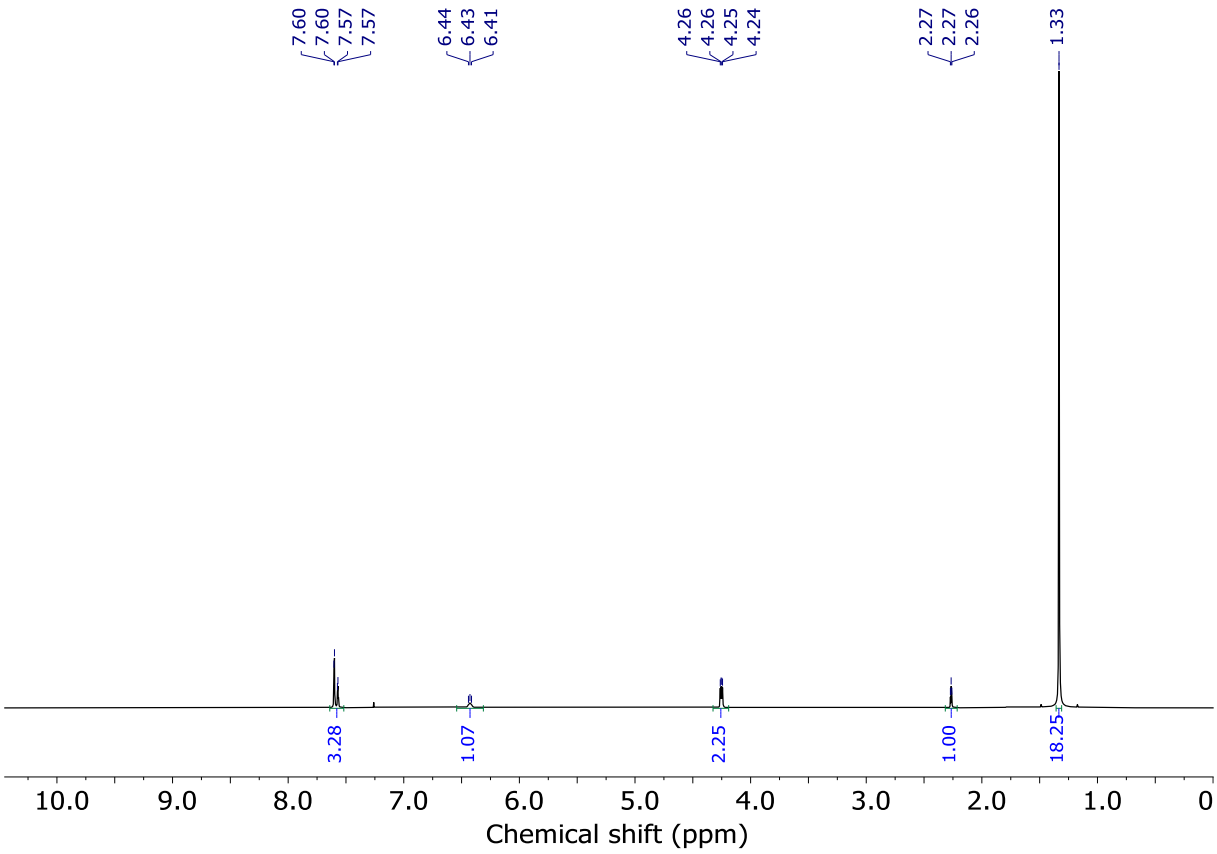

Figure 3.124 - ^{1}H NMR ($CDCl_3$, 400 MHz) of **S14**.

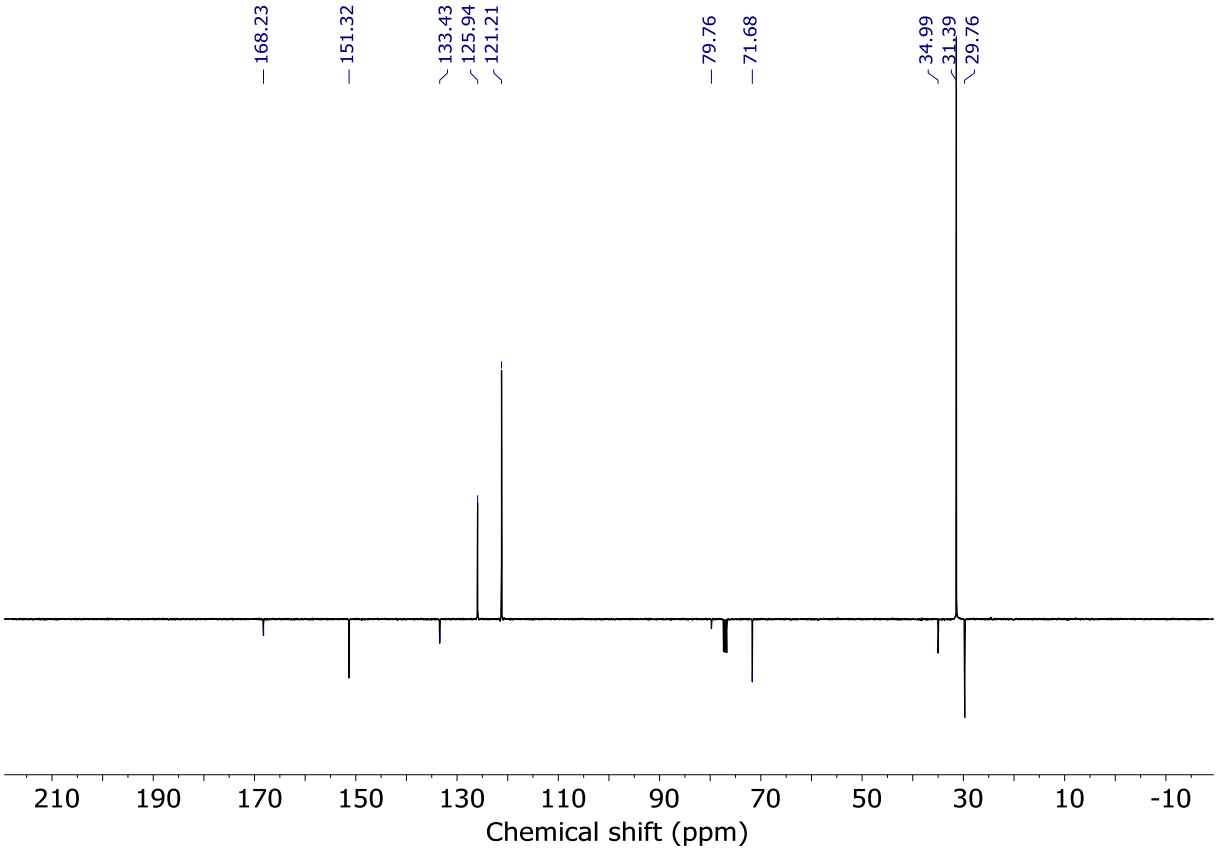

Figure 3.125 - JMOD NMR ($CDCl_3$, 101 MHz) of **S14**.

Amide Rotaxanes (E_m)-9 and (Z_m)-9

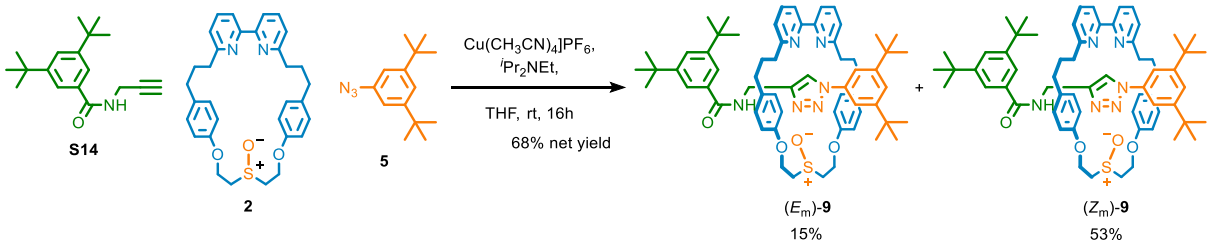

In a CEM vial were added **S14** (11.3 mg, 41.7 µmol), **5** (9.7 mg, 41.7 µmol), **2** (20.0 mg, 38.0 µmol) and [$Cu(CH_3CN)_4PF_6$] (13.6 mg, 36.5 µmol). The vial was sealed and purged with N_2, then THF was added (1.0 mL), followed by $^iPr_2NEt$ (13.3 µL, 75.9 µmol). The solution was stirred at rt for 16h. the solution was diluted with CH_2Cl_2 (10 mL), then EDTA-NH_3 (5 mL) was added. The solution was vigorously stirred until complete decolouration. The aqueous and organic phases were separated, and the aqueous phase was then extracted with CH_2Cl_2 (3 x 10 mL). The combined organic extracts were washed with brine (10 mL), dried ($MgSO_4$) and concentrated *in vacuo* to give a sample containing **9** as a mixture of diastereomers (19 : 81 *dr*, Figure 3.126). Two rounds of chromatography (CH_2Cl_2-CH_3CN 0→100% then CH_3CN-MeOH 0→20% followed by petrol-acetone 0→100%) gave (E_m)-**9** as a white foam (5.9 mg, 15%) and (Z_m)-**9** as a white foam (20.6 mg, 53%).

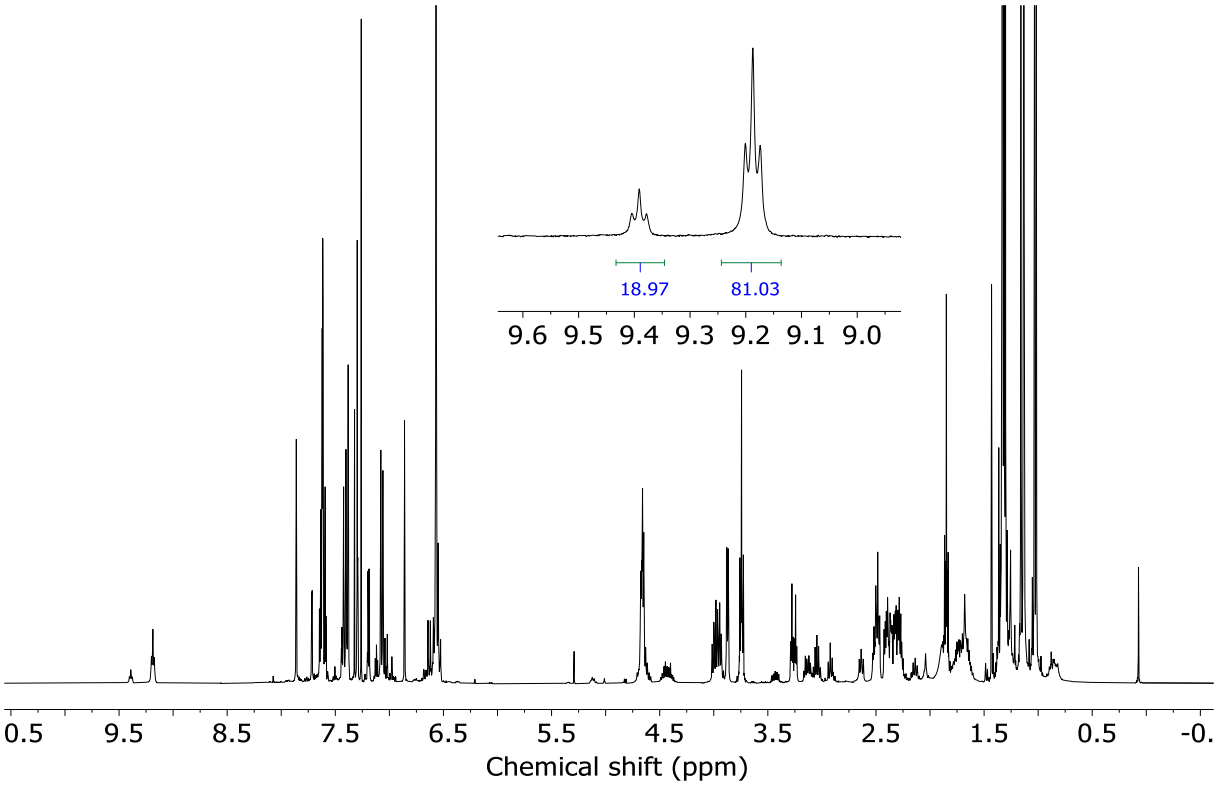

Figure 3.126 - ^{1}H NMR ($CDCl_3$, 400 MHz) of (E_m)-**9** and (Z_m)-**9** prior to chromatography (19 : 81 *dr*).

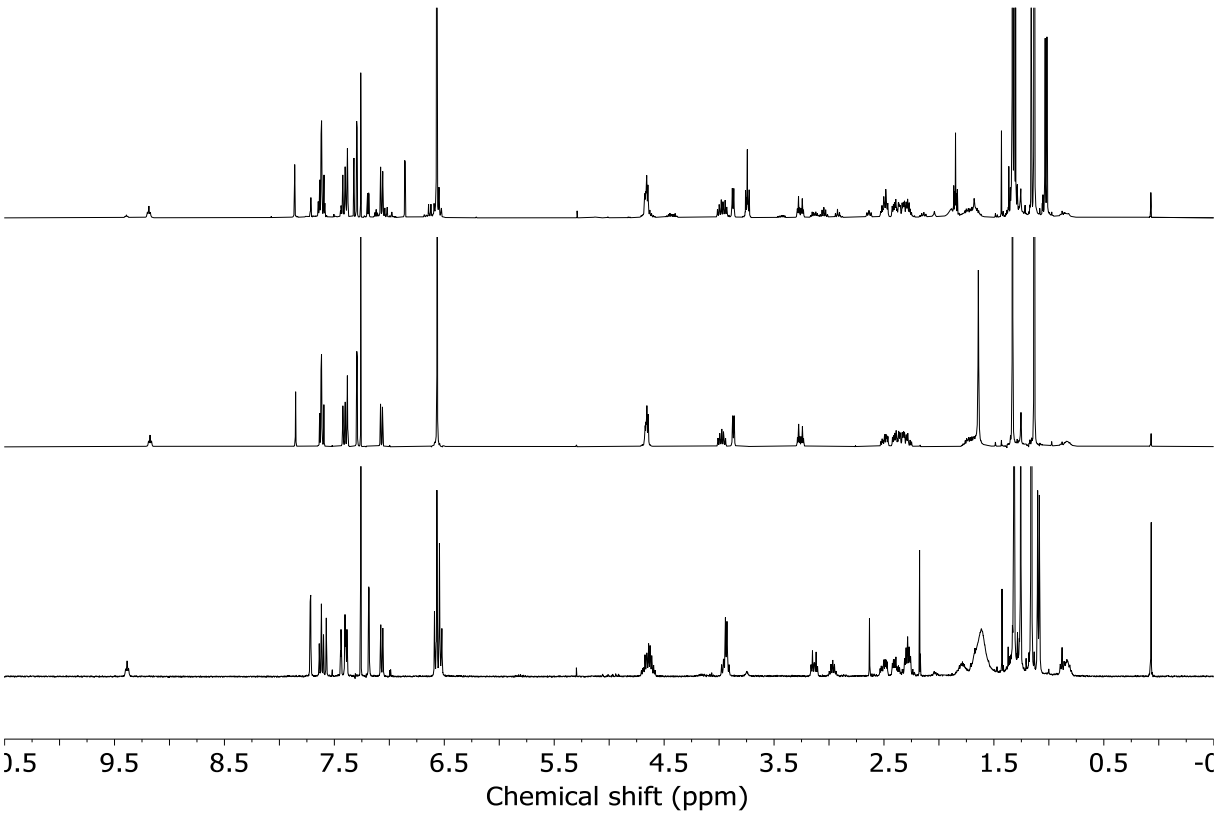

Figure 3.127 - ^{1}H NMR ($CDCl_3$, 400 MHz) of (E_m)-**9** and (Z_m)-**9** prior to chromatography (top), (E_m)-**9** (middle) and (Z_m)-**9** (bottom).

(Z_m)-**9**

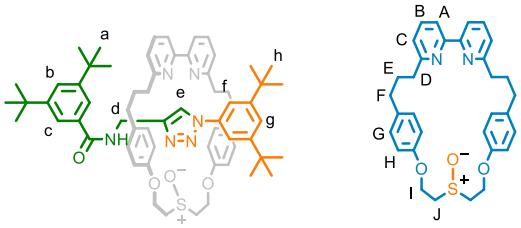

^{1}H NMR (400 MHz, $CDCl_3$) δ: 9.18 (t, *J* = 6.0, 1H, NH), 7.85 (s, 1H, H_e), 7.64-7.58 (m, 4H, H_c, H_B), 7.42 (t, *J* = 1.8, H_g), 7.41-7.37 (m, 3H, H_A, H_b), 7.29 (d, *J* = 1.8, H_f), 7.07 (dd, *J* = 7.6, 0.9, H_C), 6.56 (s, 8H, H_G, H_H), 4.71-4.61 (m, 4H, H_I), 3.98 (ddd, *J* = 13.8, 7.8, 6.1, 2H, H_J), 3.87 (d, *J* = 5.0, 2H, H_d), 3.26 (app. dt, *J* = 13.8, 4.2, 2H, $H_{J'}$), 2.54-2.44 (m, 2H, H_F), 2.44-2.22 (m, 6H, H_D, $H_{F'}$), 1.81-1.59 (m, 4H, H_E), 1.33 (s, 9H, H_h), 1.13 (s, 9H, H_a).

^{13}C NMR (101 MHz, $CDCl_3$) δ: 167.0, 163.2, 156.9, 155.2, 152.3, 150.0, 145.4, 137.1, 136.9, 134.2, 133.1, 129.2, 124.8, 122.2, 122.0., 121.9, 121.4, 120.0, 115.3, 114.7, 59.8, 51.3, 36.5, 35.1, 35.0, 34.8, 34.8, 31.5, 31.4, 31.3, 29.7.

LR-ESI-MS (+ve) *m/z* = 1029.6 $[M+H]^+$, for isotopic pattern see Figure 3.134.

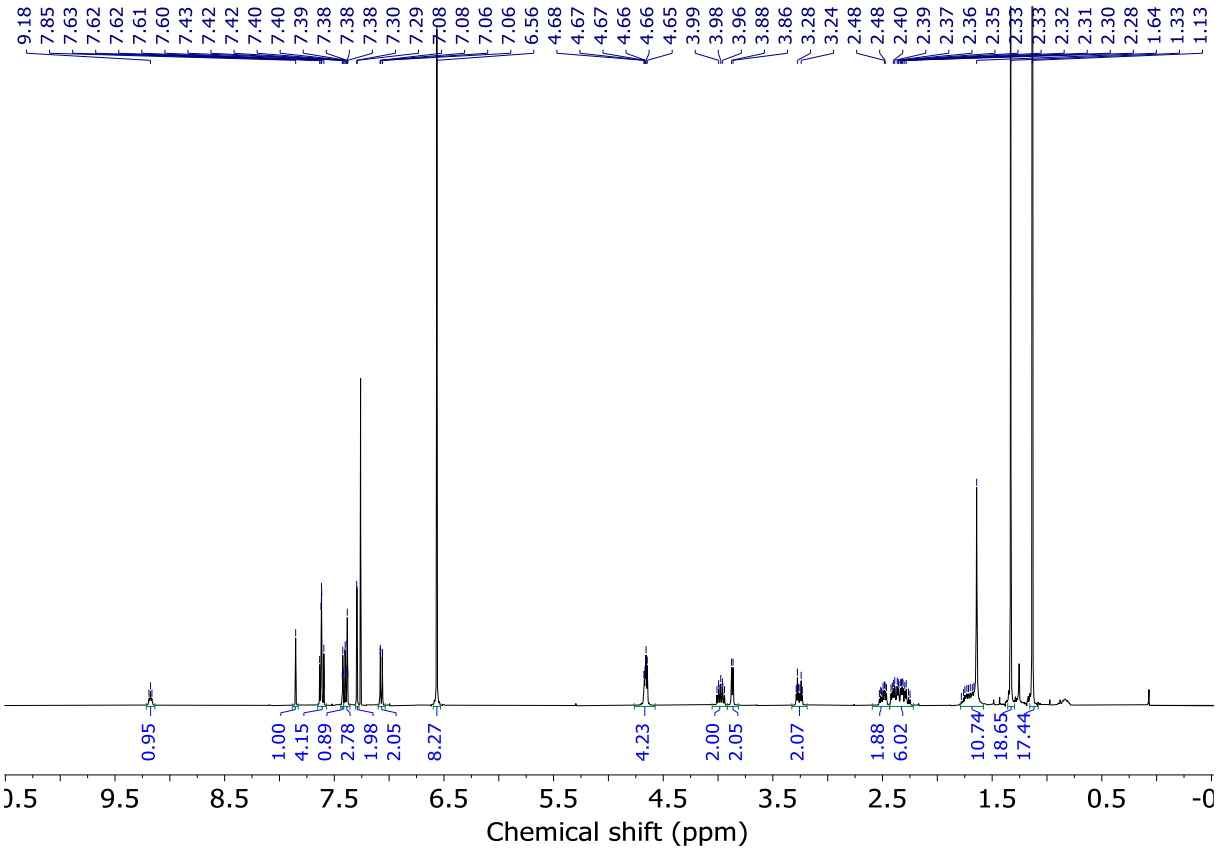

Figure 3.128 - ^{1}H NMR ($CDCl_3$, 400 MHz) of (Z_m)-**9**.

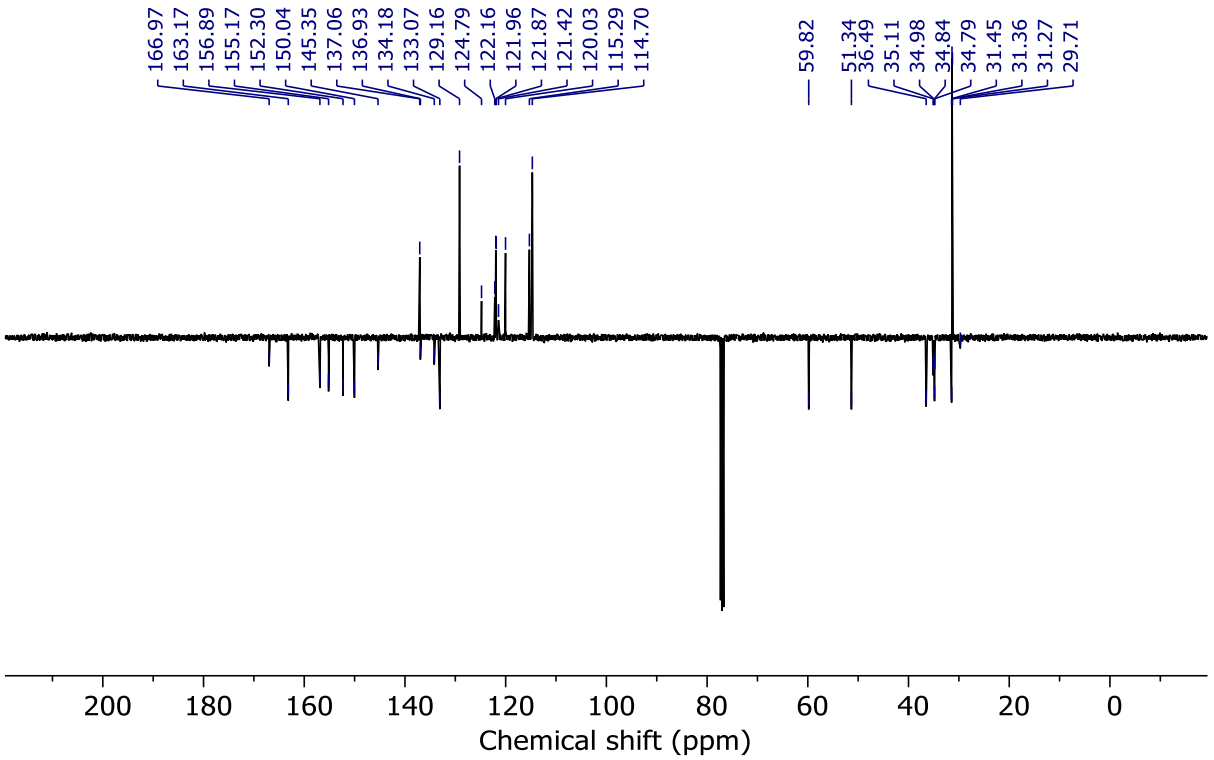

Figure 3.129 - JMOD NMR ($CDCl_3$, 101 MHz) of (Z_m)-**9**.

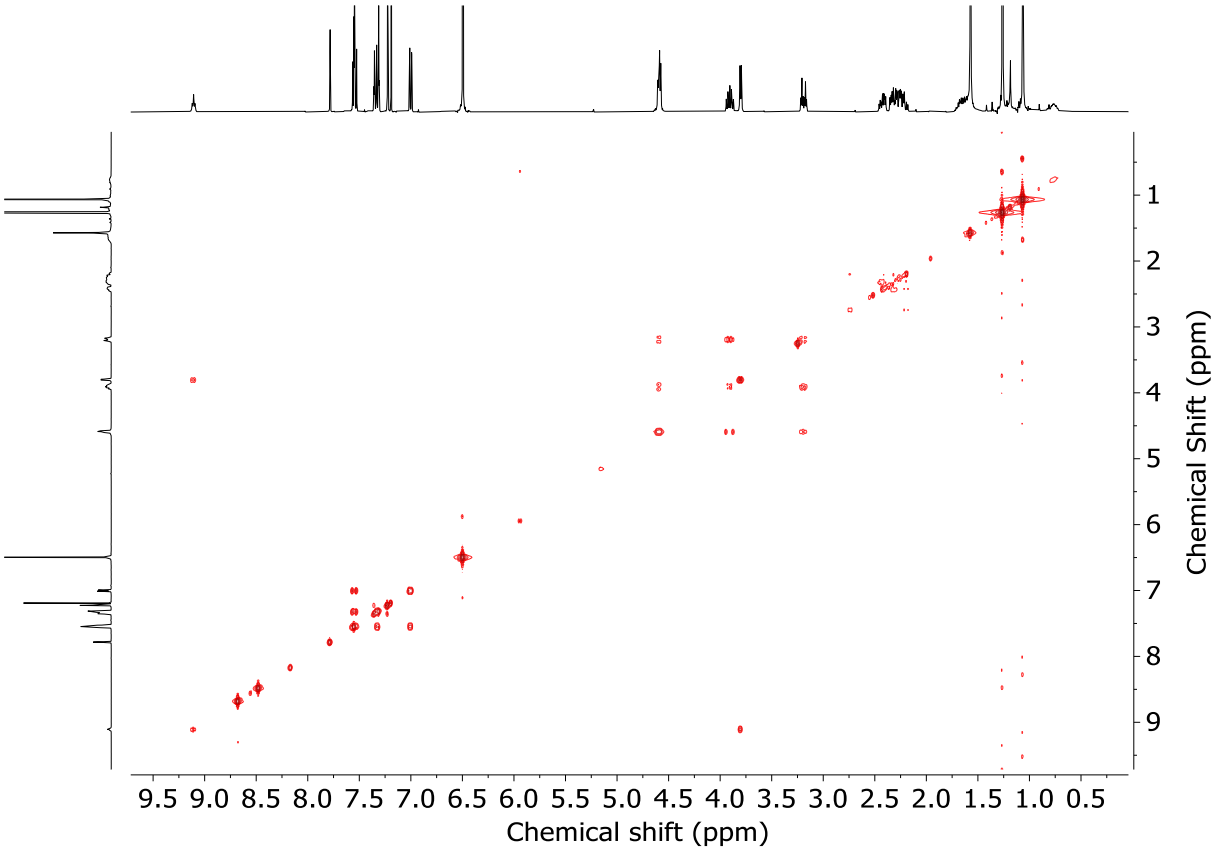

Figure 3.130 - COSY NMR ($CDCl_3$) of (Z_m)-**9**.

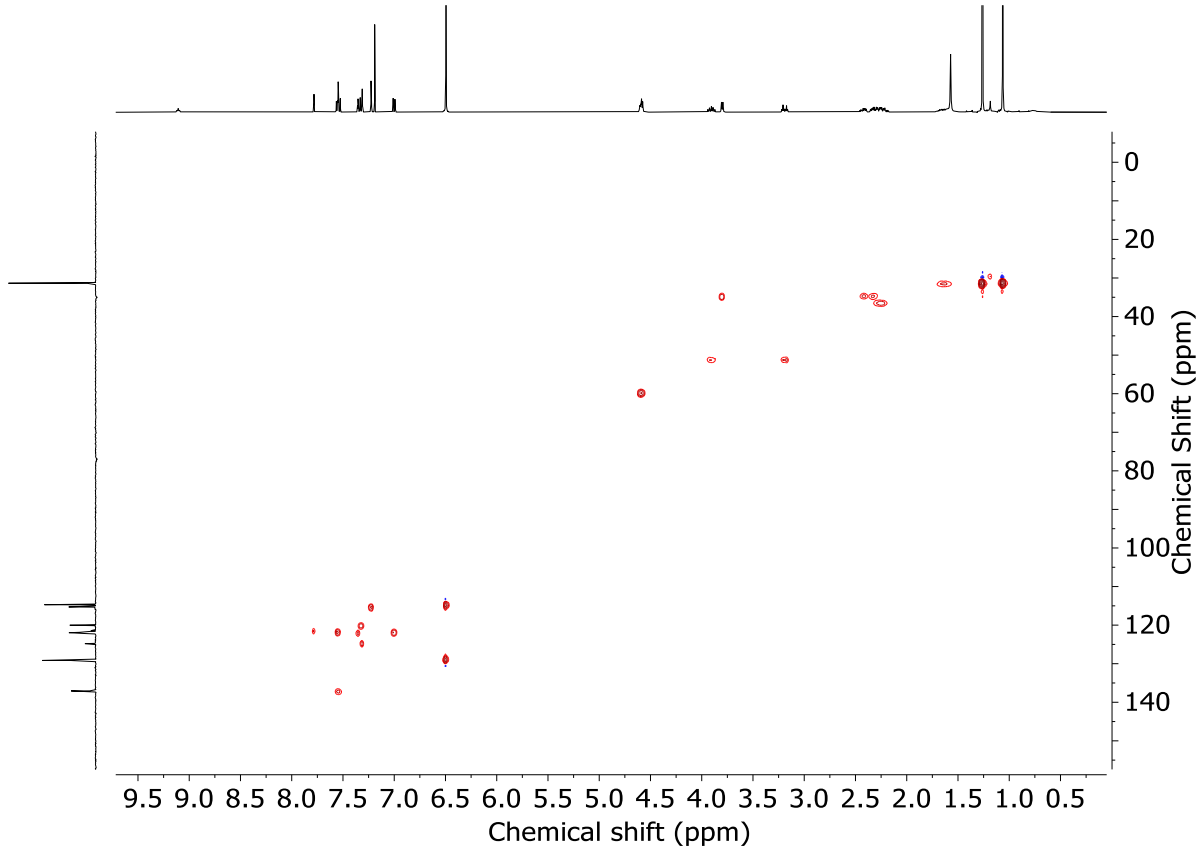

Figure 3.131 - HSQC NMR ($CDCl_3$) of (Z_m)-**9**.

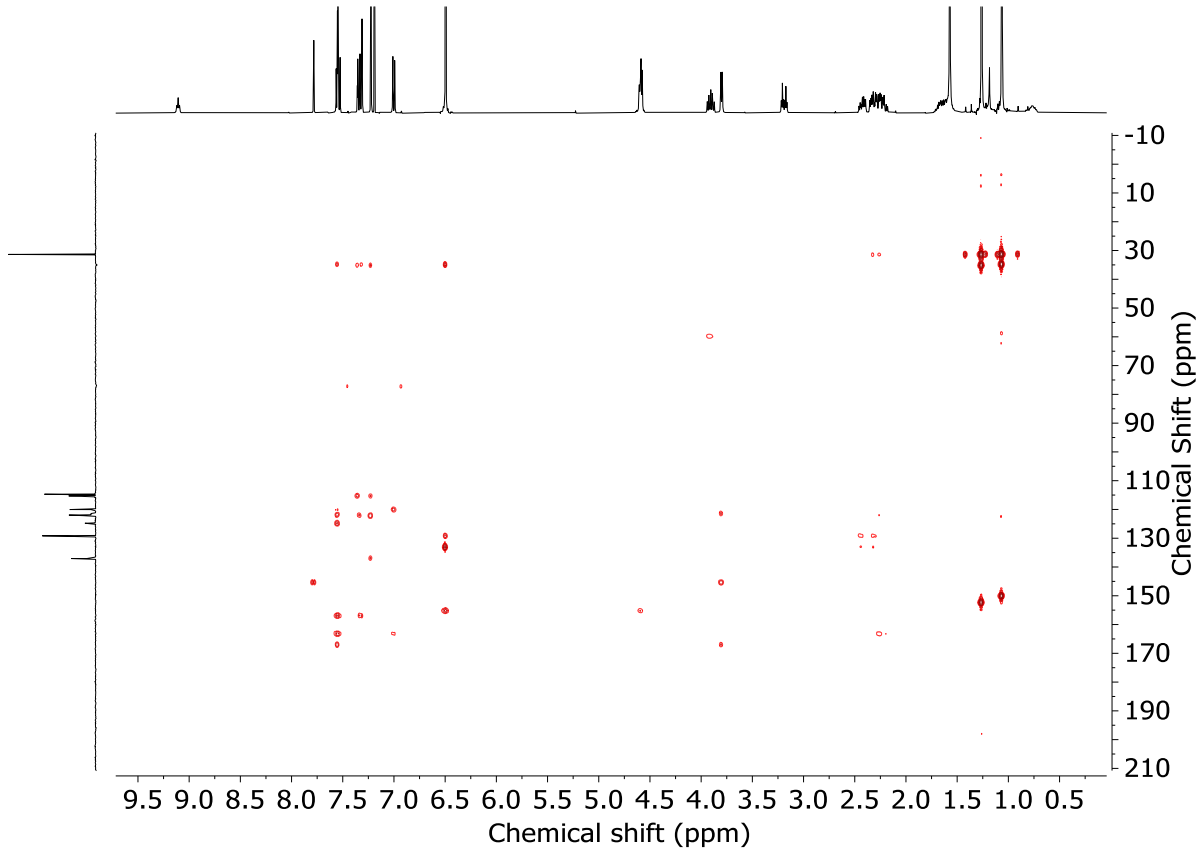

Figure 3.132 - HMBC NMR ($CDCl_3$) of (Z_m)-**9**.

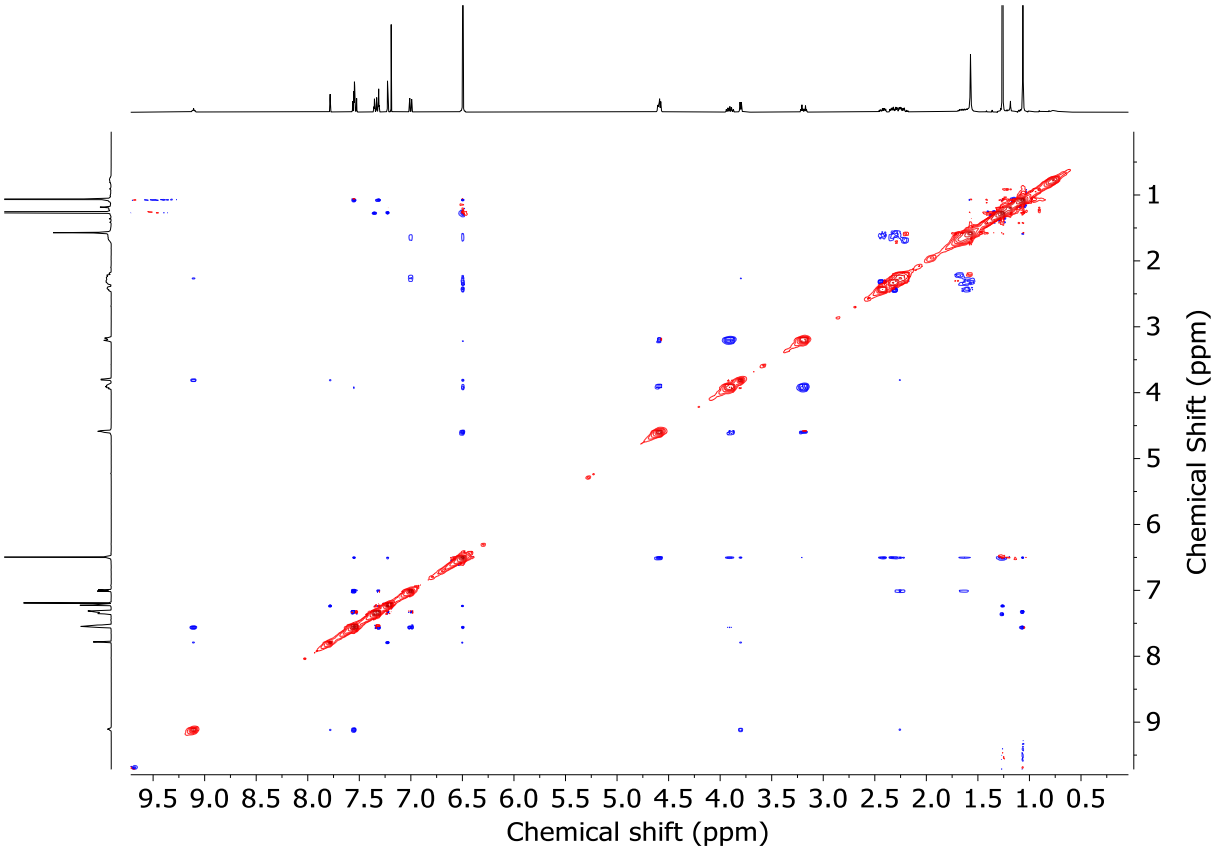

Figure 3.133 - NOESY NMR ($CDCl_3$) of (Z_m)-**9**.

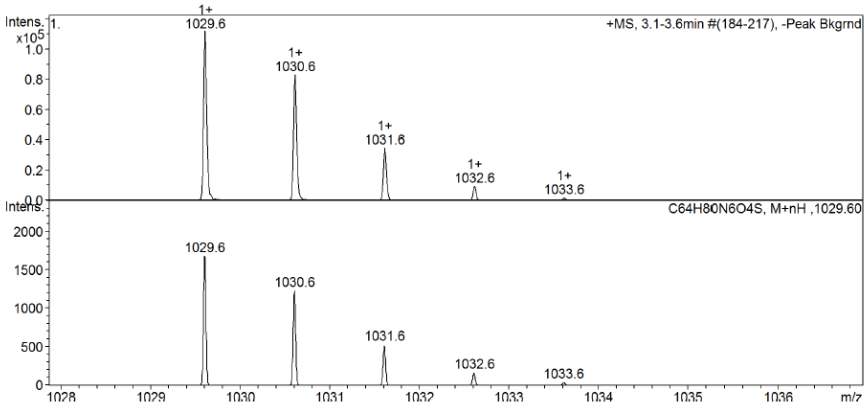

Figure 3.134 - Calculated (top) and observed (bottom) isotopic patterns (Z_m)-**9**.

(E_m)-**9**

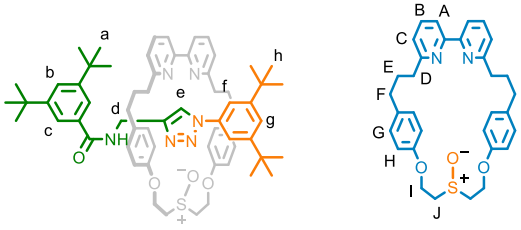

^{1}H NMR (400 MHz, $CDCl_3$) δ: 9.18 (t, *J* = 5.8, 1H, NH), 7.72 (d, *J* = 2.0, 2H, H_c), 7.62 (t, *J* = 7.9, 2H, H_B), 7.57 (s, 1H, H_e), 7.44 (t, *J* = 2.0, 1H, H_g), 7.42-7.36 (m, 3H, H_b, H_A), 7.19 (d, *J* = 1.7, 2H, H_f), 7.07 (d, *J* = 8.0, 2H, H_C), 6.61 (m, 8H, H_G, H_H), 5.73-4.56 (m, 4H, H_I), 4.00-3.89 (m, 4H, H_d, H_J), 3.13 (app dt, *J* = 13.0, 5.8, 2H, $H_{J'}$), 2.56-2.45 (m, 2H, H_F), 2.45-2.23 (m, 6H, H_D $H_{F'}$), 1.86-1.59 (m, 4H, H_E), 1.32 (s, 18H, H_h), 1.18 (s, 18H, H_a).;

^{13}C NMR (101 MHz, $CDCl_3$) δ: 166.8, 163.2, 156.7, 155.1, 152.4, 149.9, 146.1, 137.1, 133.8, 133.0, 129.1, 124.8, 122.5, 122.2, 121.9, 120.0, 115.5, 115.1, 60.7, 51.5, 36.5, 35.3, 35.1, 34.9, 34.9, 31.4, 31.4, 31.1, 29.3.

LR-ESI-MS *m/z* = 1029.6 $[M+H]^+$, for isotopic pattern see Figure 3.141.

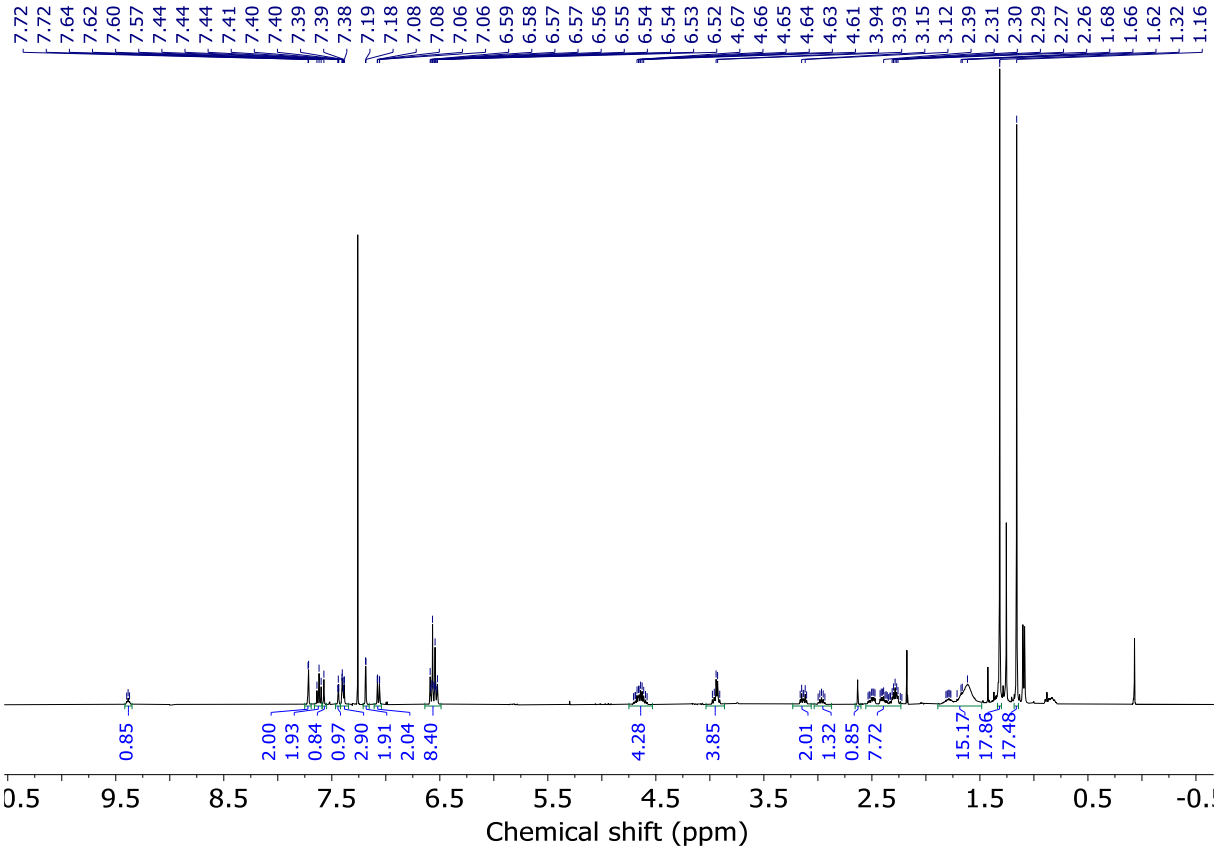

Figure 3.135 - ^{1}H NMR ($CDCl_3$, 400 MHz) of (E_m)-**9**.

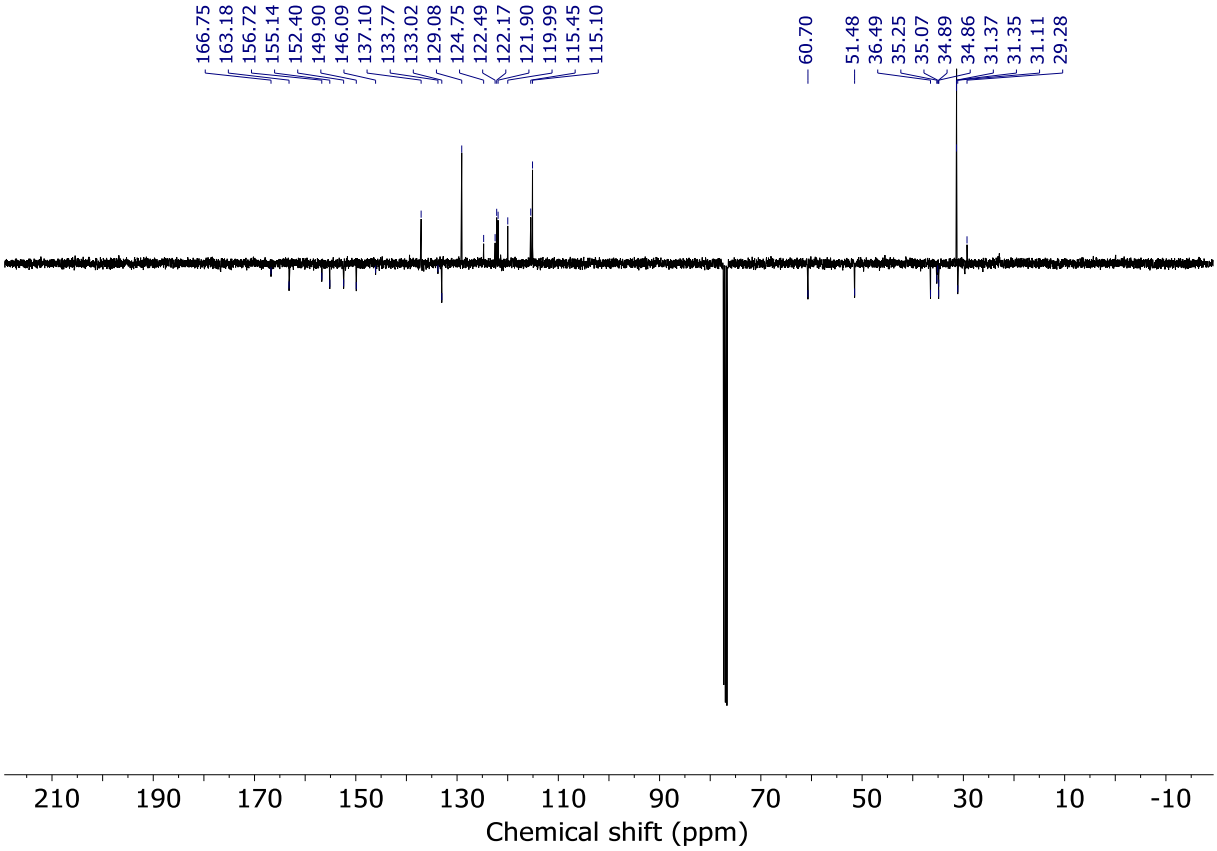

Figure 3.136 - JMOD NMR ($CDCl_3$, 101 MHz) of (E_m)-**9**.

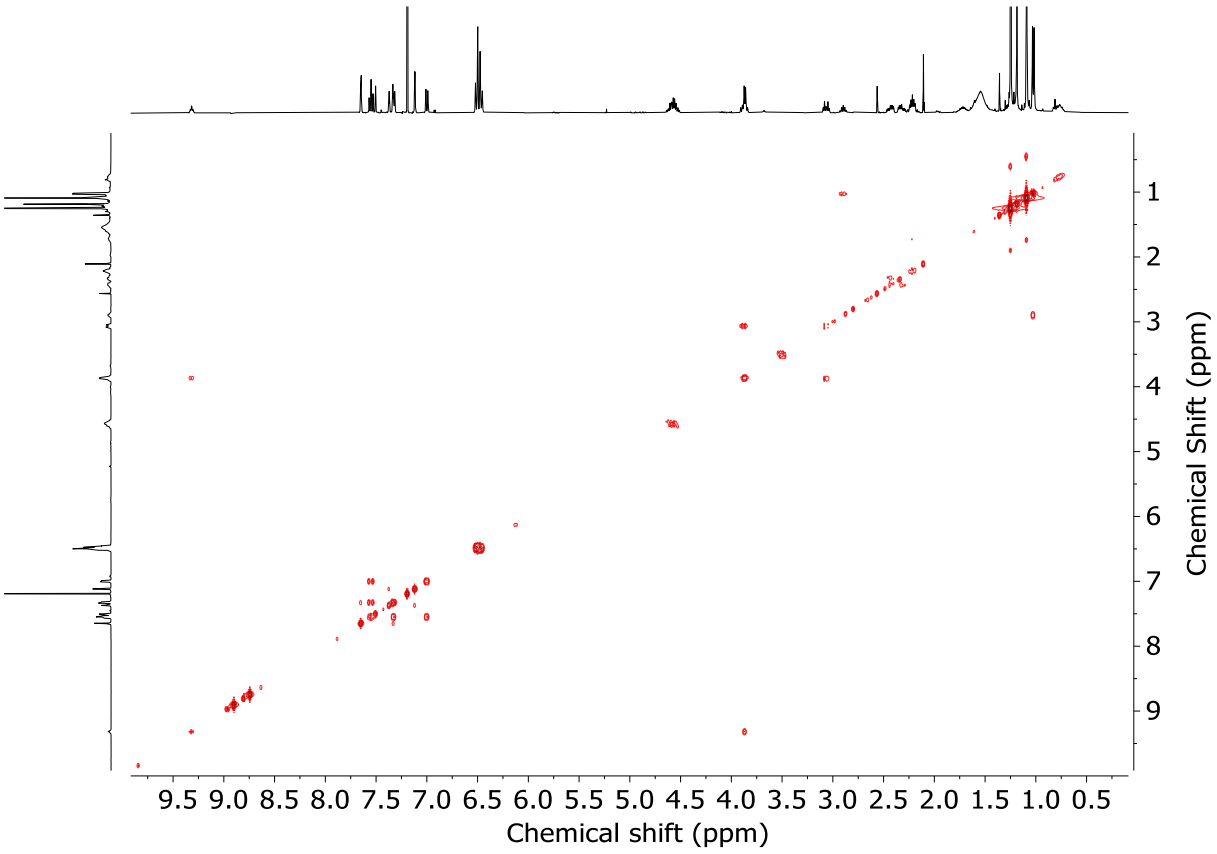

Figure 3.137 - COSY NMR ($CDCl_3$) of (E_m)-**9**.

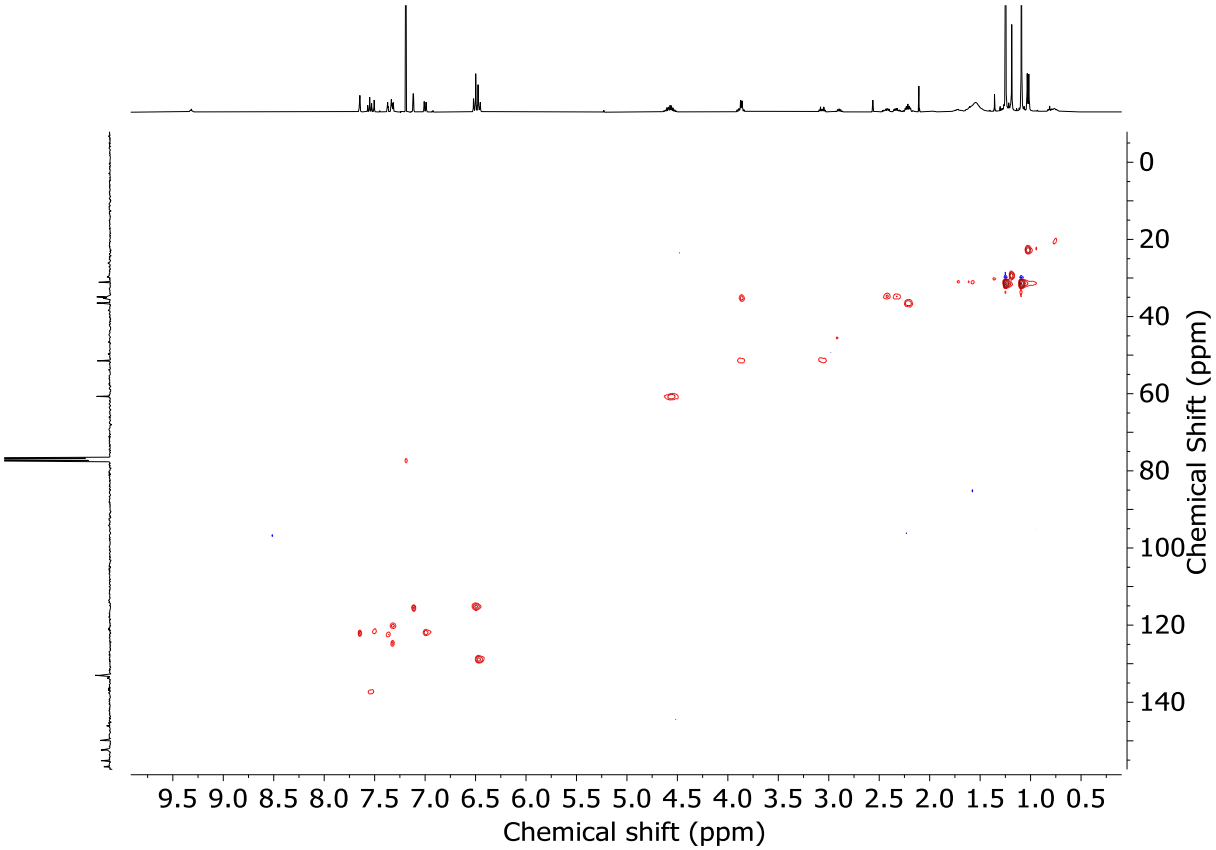

Figure 3.138 - HSQC NMR ($CDCl_3$) of (E_m)-**9**.

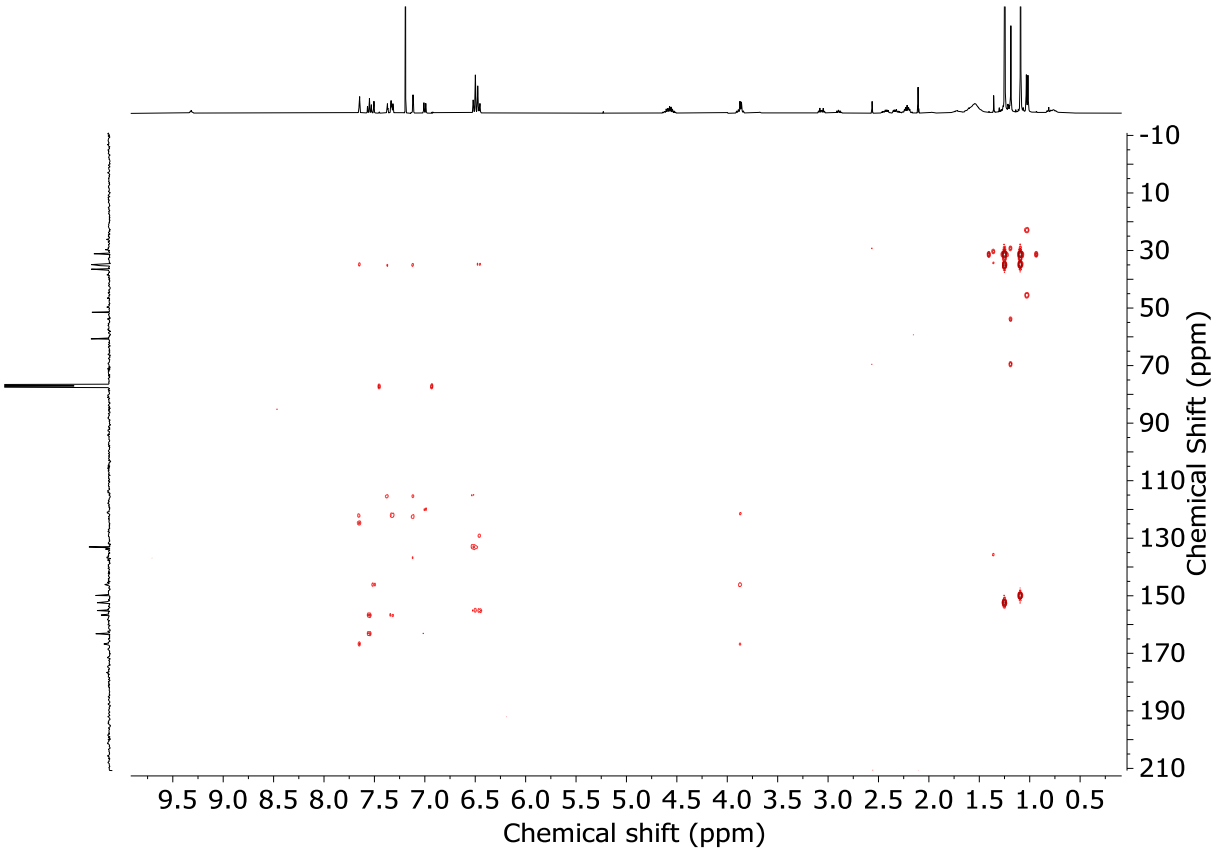

Figure 3.139 - HMBC NMR ($CDCl_3$) of (E_m)-**9**.

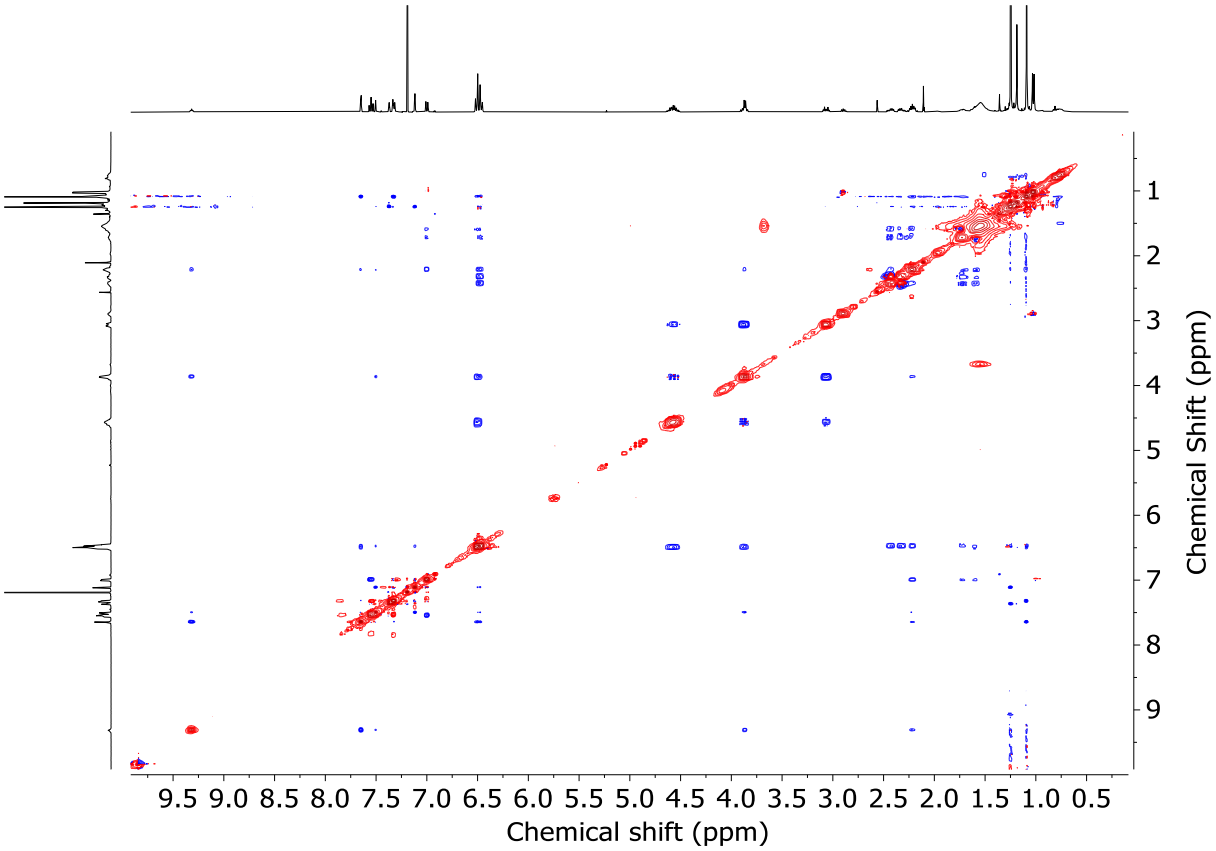

Figure 3.140 - NOESY NMR ($CDCl_3$) of (E_m)-**9**.

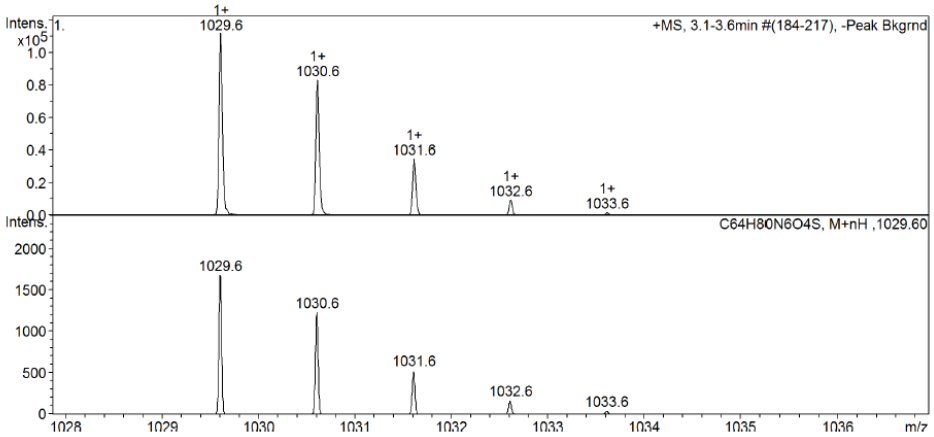

Figure 3.141 - Calculated (top) and observed (middle, bottom) isotopic patterns for (E_m)-**9**.

Methylated amide alkyne S15

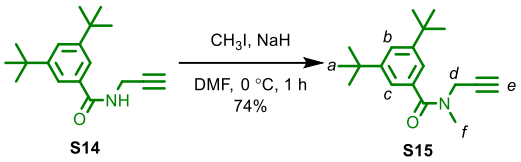

To a suspension of NaH (60% in mineral oil, 12.6 mg, 0.37 mmol) in DMF (2 mL) was added a solution of **S14** (50 mg, 0.18 mmol) in DMF (1 mL) dropwise at 0 °C. The reaction mixture was stirred for 10 minutes, then CH_3I (17.2 µL, 0.27 mmol) was added. The reaction mixture was allowed to warm to rt and stirred for 1 h. The reaction mixture was then quenched by adding H_2O (5 mL) dropwise. The aqueous and organic phases were separated, and the aqueous phase was then extracted with Et_2O (3 x 20 mL). The combined organic extracts were washed with brine (10 mL), dried ($MgSO_4$) and concentrated *in vacuo*. Chromatography (petrol-EtOAc 0→100%) gave **S15** as a colourless oil (37.9 mg, 74%) as a mixture of rotamers.

^{1}H NMR (400 MHz, $CDCl_3$) δ: 7.45 (t, *J* = 2.0, 2H, H_b, $H_{b'}$), 7.41-7.13 (m, 4H, H_c, $H_{c'}$), 4.53-3.79 (m, 4H, H_d, $H_{d'}$), 3.23-2.89 (m, 6H, H_f, $H_{f'}$), 2.43-2.20 (m, 2H, H_f, $H_{f'}$), 1.30 (s, 36H, H_a, $H_{a'}$)

^{13}C NMR (101 MHz, $CDCl_3$) δ: 172.3, 150.9, 134.6, 124.0, 121.3, 78.9, 72.9, 72.1, 72.1, 41.7, 36.9, 36.4, 35.0, 32.8, 31.4.

HR-ESI-MS (+ve) *m/z* = 286.2167 $[M+H]^+$ (calc. 286.2165 *m/z* for $C_{18}H_{28}NO$).

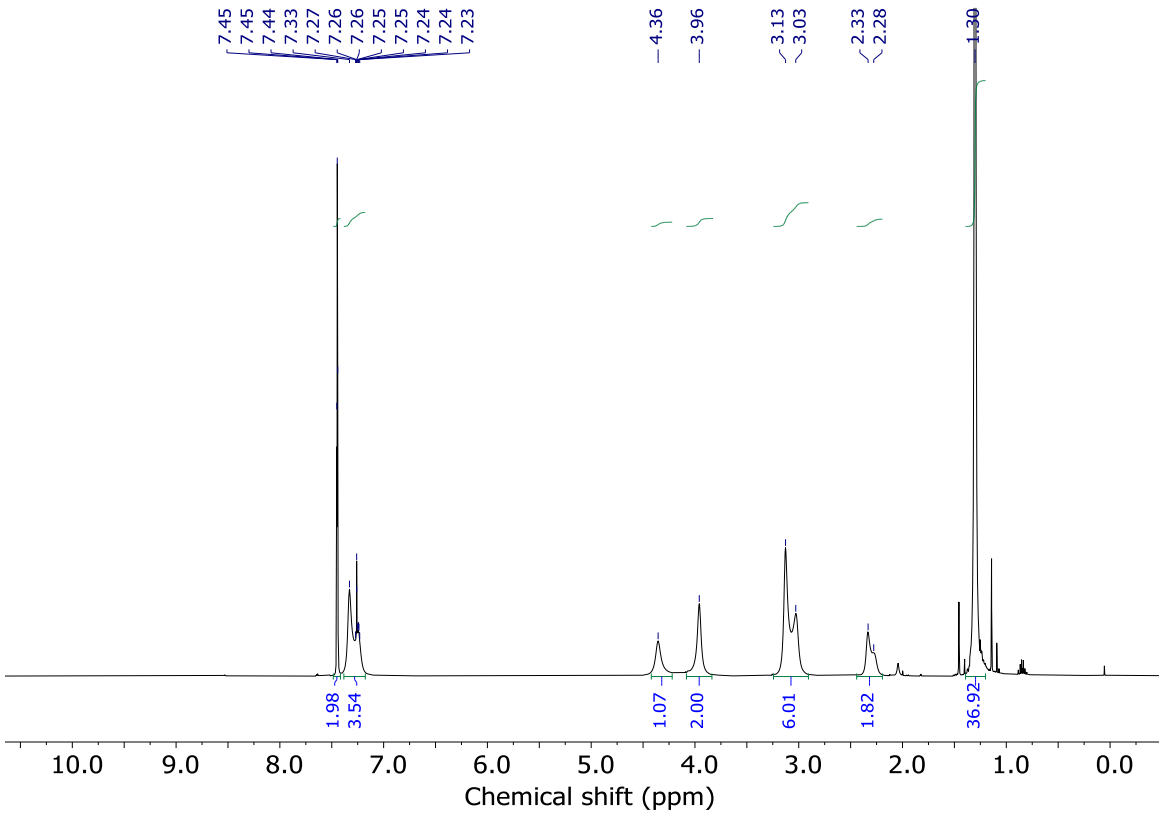

Figure 3.142 - ^{1}H NMR ($CDCl_3$, 400 MHz) of **S15**.

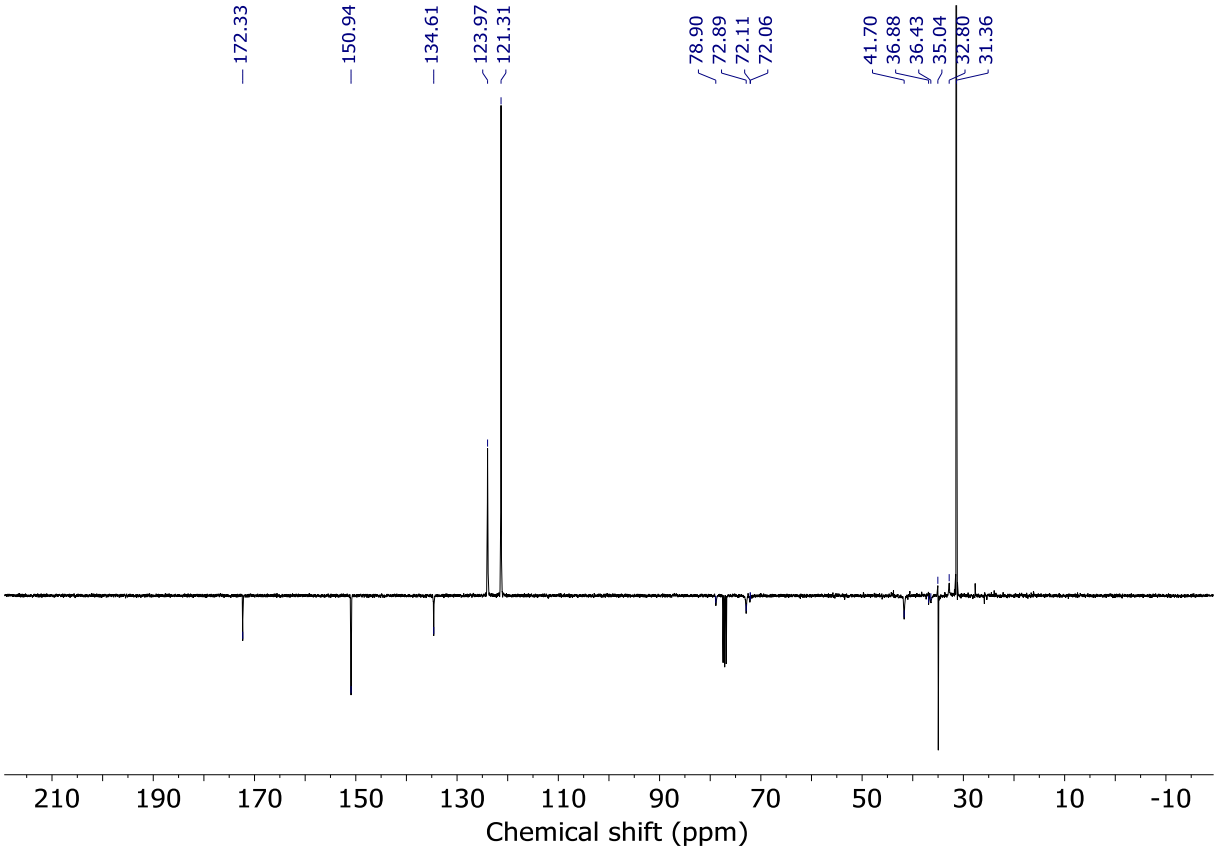

Figure 3.143 - JMOD NMR ($CDCl_3$, 101 MHz) of **S15**.

Methylated Amide Rotaxanes (E_m)-10 and (Z_m)-10

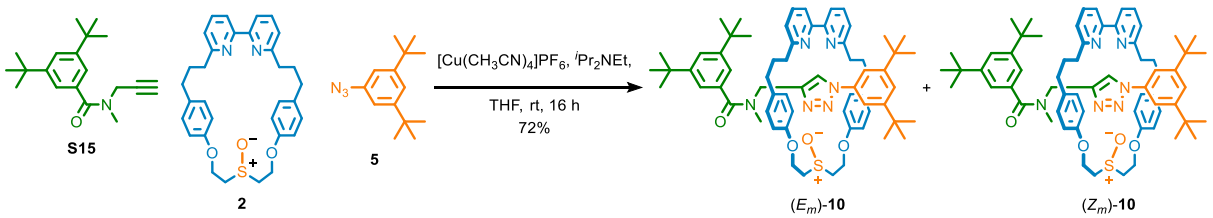

In a CEM vial were added the **S15** (11.9 mg, 41.7 µmol), **5** (9.7 mg, 41.7 µmol), **2** (20.0 mg, 38.0 µmol) and $[Cu(CH_3CN)_4PF_6]$ (13.6 mg, 36.5 µmol). The vial was sealed and purged with N_2, then THF was added (1.0 mL), followed by $^iPr_2NEt$ (13.3 µL, 75.9 µmol). The solution was stirred at rt for 16h. the solution was diluted with CH_2Cl_2 (5 mL), then EDTA-NH_3 (5 mL) was added. The solution was vigorously stirred until complete decolouration. The aqueous and organic phases were separated, and the aqueous phase was then extracted with CH_2Cl_2 (3 x 10 mL). The combined organic extracts were washed with brine (10 mL), dried ($MgSO_4$) and concentrated *in vacuo* to give a sample containing **10** as a mixture of diastereomers (44 : 56 *dr*, Figure 3.144). Chromatography (CH_2Cl_2-CH_3CN 0→100% then CH_3CN-MeOH 0→20%) gave rotaxane **10** as a mixture of (E_m)-**10** and (Z_m)-**10** (28.6 mg, 72%) as a colourless oil. Analytical samples of the single diastereoisomers were obtained *via* column chromatography (*n*-hexane-acetone 0→100%).

Due to the presence of complex rotameric mixture it wasn't possible to assign the NMR spectra of the compounds. However, the purity of the compound was confirmed by LR-MS of the separated fractions (Figure 3.147). The diastereoisomeric ratios observed in the solvent screening were assigned by integrating the de-shielded peaks corresponding to the rotameric mixture of the isolated species.

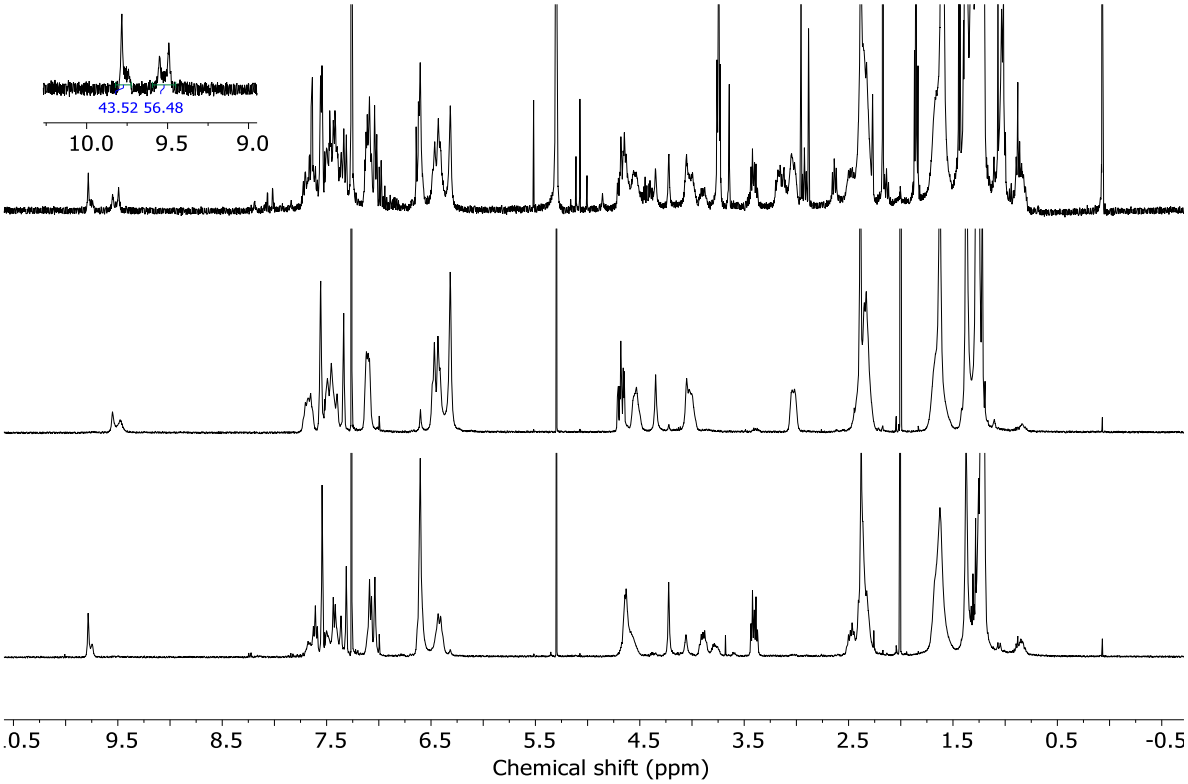

Figure 3.144 - ^{1}H NMR ($CDCl_3$, 400 MHz) of (E_m)-**10** and (Z_m)-**10** prior to chromatography (top), (E_m)-**10** (middle) and (Z_m)-**10** (bottom).

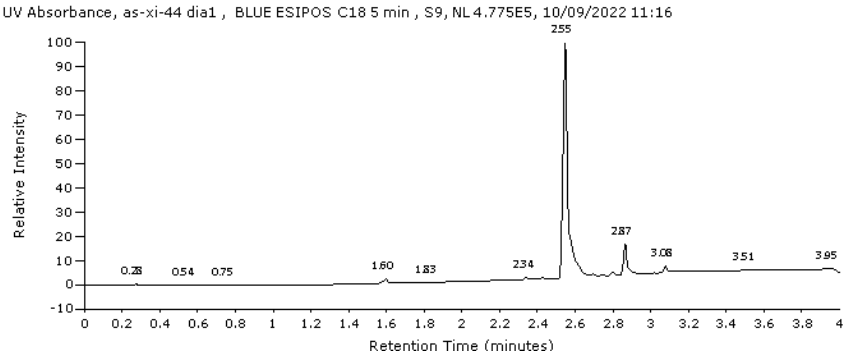

Figure 3.145 - LC-MS of **10** (retention times: 2.55 mins, *m/z* = 1044.0 and 2.87 mins, *m/z* = 1044.0)

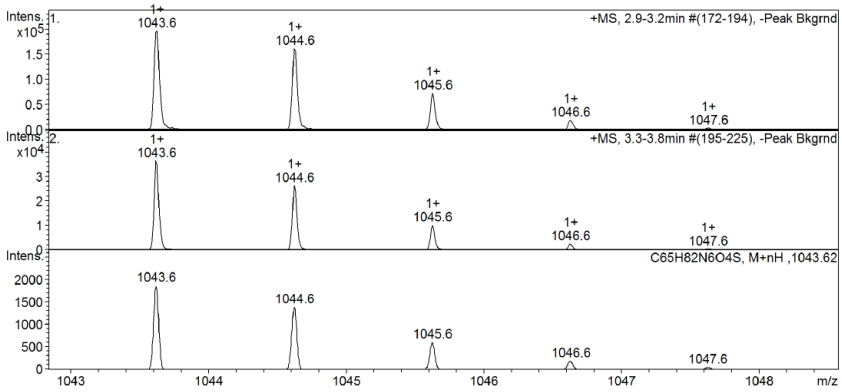

Figure 3.146 - ESI-HR-MS of one the isolated isomer for **10** and experimental and calculated isotopic pattern.

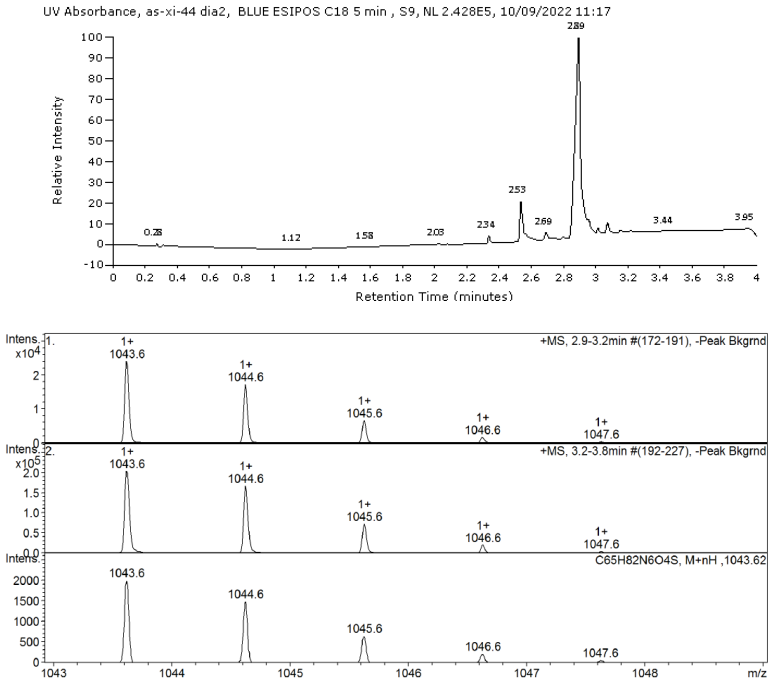

Figure 3.147 - LC-MS (retention times: 2.53 mins, *m/z* = 1044.0 and 2.89 mins, *m/z* = 1044.0) and ESI-HR-MS of one the isolated isomer for **10** and experimental and calculated isotopic pattern.

Amide azide S17

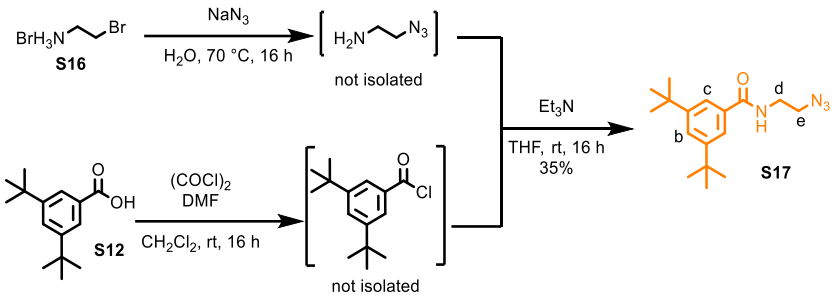

A solution of NaN_3 (476.2 mg, 7.3 mmol) and **S16** (500.0 mg, 2.4 mmol) in H_2O (5 mL) was heated at 70 °C for 16 h. The solution was cooled to 0 °C, then KOH (224 mg, 4.0 mmol) was added portion-wise and the resulting solution stirred at 0 °C for 15 min. The aqueous phases were extracted with Et_2O (3 x 5 mL), dried ($MgSO_4$) and filtered. The product, 2 azido-ethylamine, was stored as a solution of Et_2O at 0 °C. The yield was assumed to be quantitative.

In separate CEM vial was added **S12** (703 mg, 3.0 mmol), the vial sealed and flushed with N_2, then CH_2Cl_2 (6 mL), $(COCl)_2$ (0.77 mL, 9.0 mmol) and DMF (1 drop) were added. The solution was stirred at rt for 16 h, then the solvent and the excess $(COCl)_2$ were removed *in vacuo*. The residue was dissolved in THF (3 mL), the solution of 2-azidoethylamine prepared above and Et_3N (1.30 mL, 9.0 mmol) were added, and the solution was stirred at rt for 16 h, then cooled at 0 °C and H_2O added (5 mL). The phases were separated, and the aqueous phase was then extracted with EtOAc (3 x 20 mL). The combined organic extracts were washed with brine (20 mL), dried ($MgSO_4$) and concentrated *in vacuo*. Chromatography (petrol-EtOAc 0→50%) gave **S17** as a white foam (254.1 mg, 35%).

^{1}H NMR (400 MHz, $CDCl_3$) δ: 6.63-7.55 (m, 3H, H_b, H_c), 6.47 (t, J = 6.1, 1H, NH), 3.68-3.61 (m, 2H, H_d), 3.60-3.54 (m, 2H, H_e), 1.34 (s, 18H, H_a)

^{13}C NMR (101 MHz, $CDCl_3$) δ: 168.8, 151.4, 133.8, 125.9, 121.1, 51.1, 39.6, 35.0, 31.4.

HR-ESI-MS (+ve) *m/z* = 303.2190 $[M+H]^+$ (calc. 303.2180 *m/z* for $C_{17}H_{27}N_4O$);

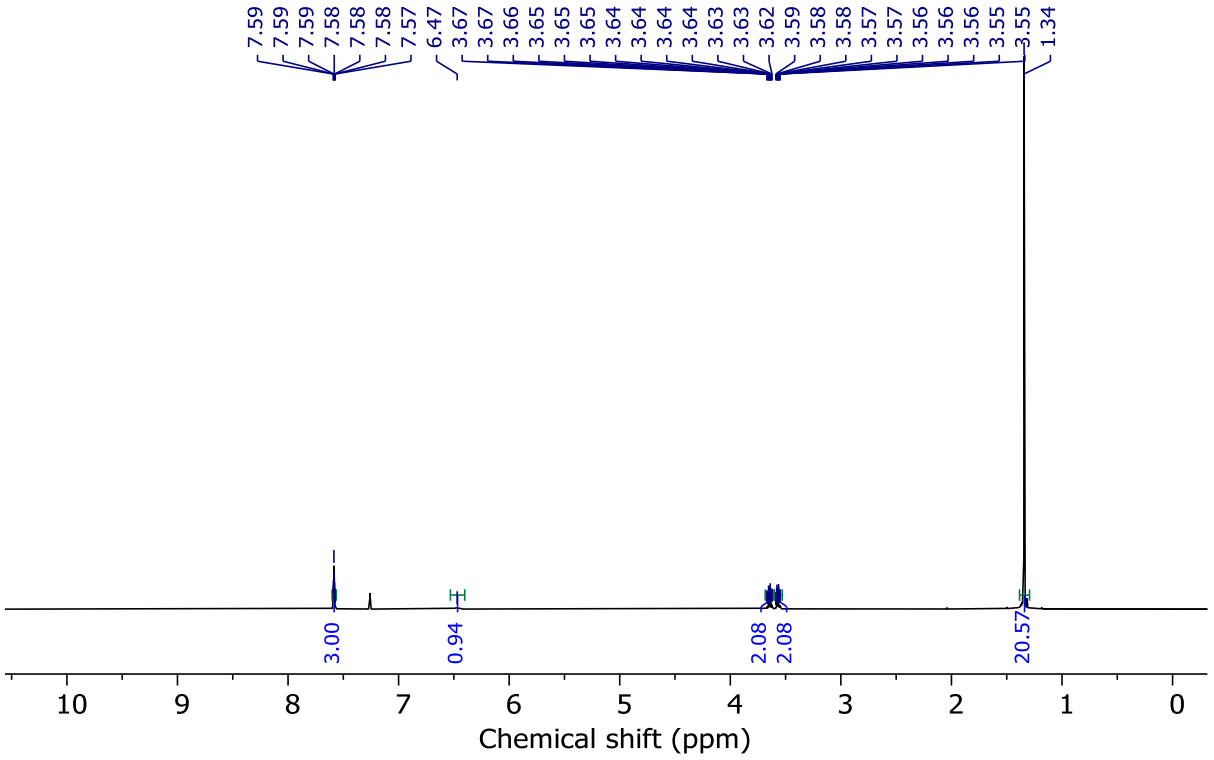

Figure 3.148 - ^{1}H NMR ($CDCl_3$, 400 MHz) of **S17**.

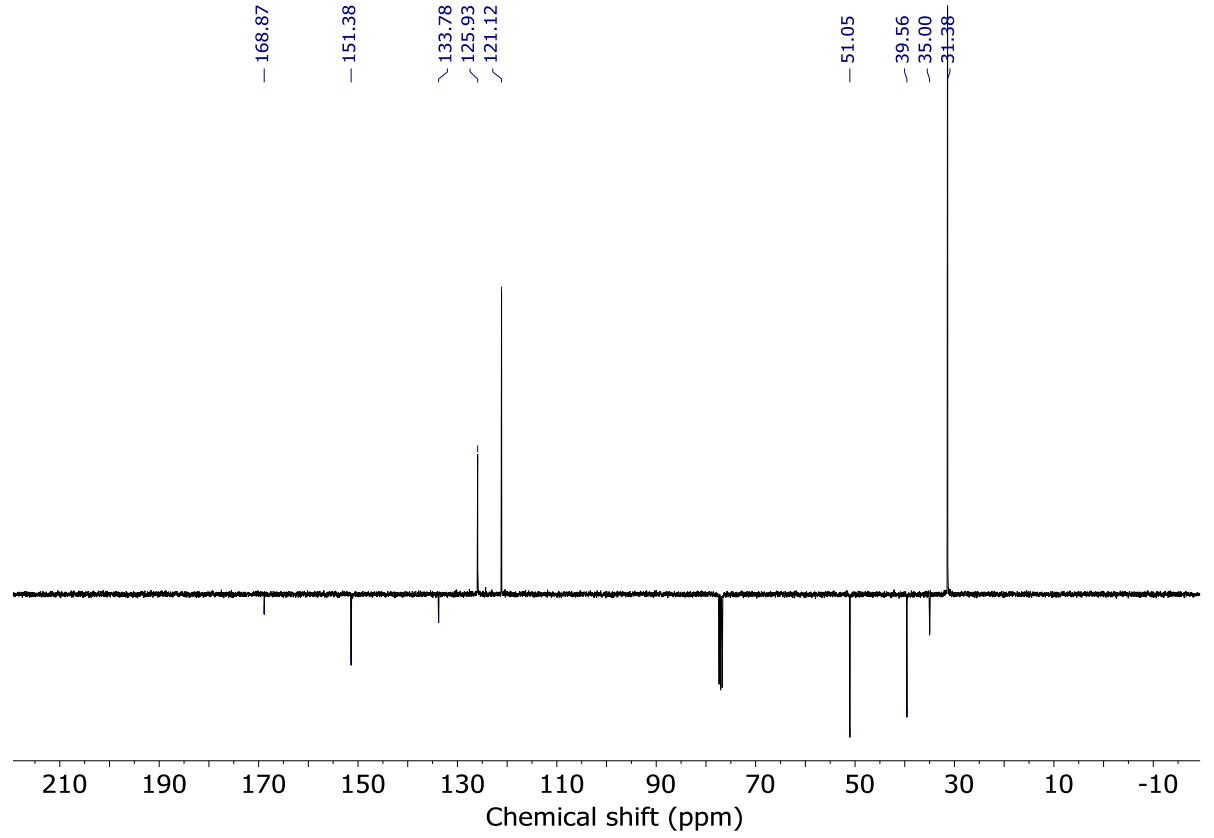

Figure 3.149 - JMOD NMR (**$CDCl_3$**, 101 MHz) of **S17**.

Amide Rotaxanes (E_m)-11 and (Z_m)-11

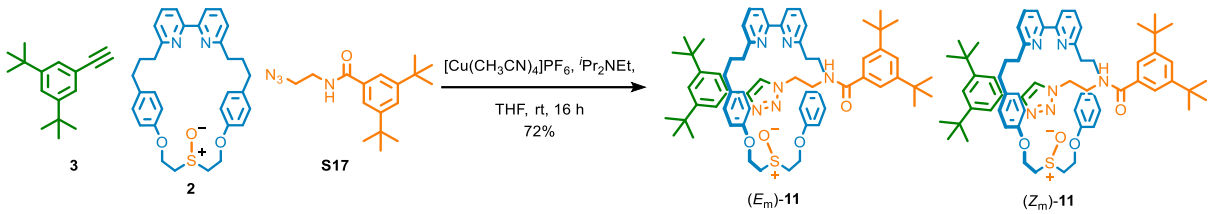

In a CEM vial were added **3** (8.9 mg, 41.7 µmol), **S17** (12.6 mg, 41.7 µmol), **2** (20.0 mg, 38.0 µmol) and $[Cu(CH_3CN)_4PF_6]$ (13.6 mg, 36.5 µmol). The vial was sealed and purged with N_2, then THF was added (1.0 mL), followed by $^{i}Pr_2NEt$ (13.3 µL, 75.9 µmol). The solution was stirred at rt for 16 h. the solution was diluted with CH_2Cl_2 (5 mL), then EDTA-NH_3 (5 mL) was added. The solution was vigorously stirred until complete decolouration. The aqueous and organic phases were separated, and the aqueous phase was then extracted with CH_2Cl_2 (3 x 10 mL). The combined organic extracts were washed with brine (10 mL), dried ($MgSO_4$) and concentrated *in vacuo* to give a sample containing **11** as a mixture of diastereomers (72 : 28 *dr*, Figure 3.150). Chromatography (CH_2Cl_2-CH_3CN 0→100%) gave **11** as a colourless oil as (28.5 mg, 72%) as a mixture of diastereoisomers (2.4: 1 *dr*, Figure 3.151). An analytical sample of the major diastereoisomer was obtained *via* column chromatography (*n*-hexane-acetone 50→80%)

Major diastereoisomer (E_m)-**11**

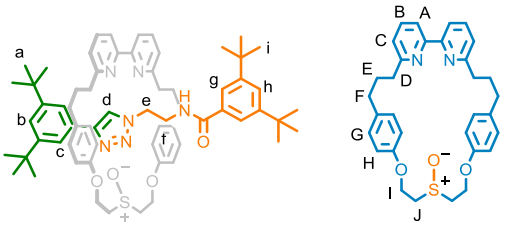

^{1}H NMR (500 MHz, $CDCl_3$) δ: 9.41 (t, *J* = 5.8, 1H, NH), 7.75 (s, 1H, H_d), 7.68 (d, *J* = 1.8, 2H, H_g), 7.66-7.60 (m, 2H, H_B), 7.53 (d, *J* = 1.9, 2H, H_c), 7.45-7.39 (m, 3H, H_A, H_h), 7.36 (t, *J* = 1.9, 1H, H_b), 7.11 (d, *J* = 7.7, 2H, H_C), 6.74-6.69 (m, 8H, H_G, H_H), 4.69-4.61 (m, 4H, H_I), 3.80 (dt, *J* = 13.0, 6.7, 2H, H_J), 3.52 (dd, *J* = 8.3, 6.6, 2H, H_e), 3.30 (dt, *J* = 13.0, 6.7, 2H, $H_{J'}$), 2.91 (dt, *J* = 8.0, 6.0, 2H, H_f), 2.75-2.49 (m, 2H, H_F), 2.50-2.39 (m, 4H, $H_{F'}$, H_D), 2.39-2.27 (m, 2H, $H_{D'}$), 1.91-1.80 (m, 2H, H_E), 1.80-1.67 (m, 2H, $H_{D'}$), 1.33 (s, 18H, H_a), 1.15 (s, 18H, H_i)

^{13}C NMR (126 MHz, $CDCl_3$) δ: 167.2, 163.0, 156.7, 155.4, 151.2, 150.1, 148.2, 137.2, 133.4, 133.3, 130.0, 129.5, 125.0, 122.2, 122.1, 122.0, 120.3, 120.0, 115.1, 60.7, 51.1, 48.9, 39.2, 36.5, 34.9, 34.9, 34.8, 31.5, 31.3, 31.3

LR-ESI-MS (+ve) *m/z* = 1043.6 $[M+H]^+$ for isotopic pattern see Figure 3.156.

Minor diastereoisomer (Z_m)-**11**

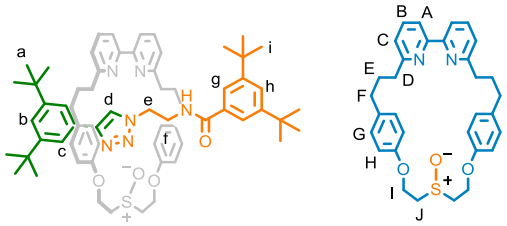

^{1}H NMR (500 MHz, $CDCl_3$) δ: 9.30 (t, *J* = 5.8, 1H, NH), 7.79 (s, 1H, H_d), 7.73 (d, *J* = 1.9, 2H, H_g), 7.66-7.60 (m, 4H, H_b, H_c, H_C), 7.45-7.39 (m, 5H, H_A, H_B, H_h), 6.78 (d, *J* = 8.6, 4H, H_G or H_H), 6.74-6.69 (m, 4H, H_G or H_H), 4.75 (ddd, *J* = 13.4, 10.5, 3.5, 2H, H_I), 4.69-4.61 (m, 2H, $H_{I'}$), 3.98 (ddd, *J* = 13.8, 10.5, 4.7, 2H, H_J), 3.45-3.39 (m, 2H, H_f), 3.14 (dt, *J* = 13.5, 3.6, 2H, $H_{J'}$), 2.75-2.49 (m, 6H, H_e, H_F), 2.50-2.39 (m, 4H, $H_{F'}$, H_D), 2.39-2.27 (m, 2H, $H_{D'}$), 1.91-1.80 (m, 2H, H_E), 1.80-1.67 (m, 2H, $H_{D'}$), 1.40 (s, 18H, H_i), 1.12 (s, 18H, H_a)

^{13}C NMR (126 MHz, $CDCl_3$) δ: 167.5, 162.9, 156.8, 155.5, 151.2, 150.2, 148.2, 137.1, 134.0, 133.6, 130.1, 129.7, 124.9, 121.9, 121.8, 120.3, 120.3, 120.2, 114.6, 60.0, 52.2, 48.3, 39.1, 36.3, 35.0, 34.8, 34.8, 31.5, 31.2, 31.0

HR-ESI-MS (+ve) *m/z* = 1043.6 $[M+H]^+$ for isotopic pattern see Figure 3.156.

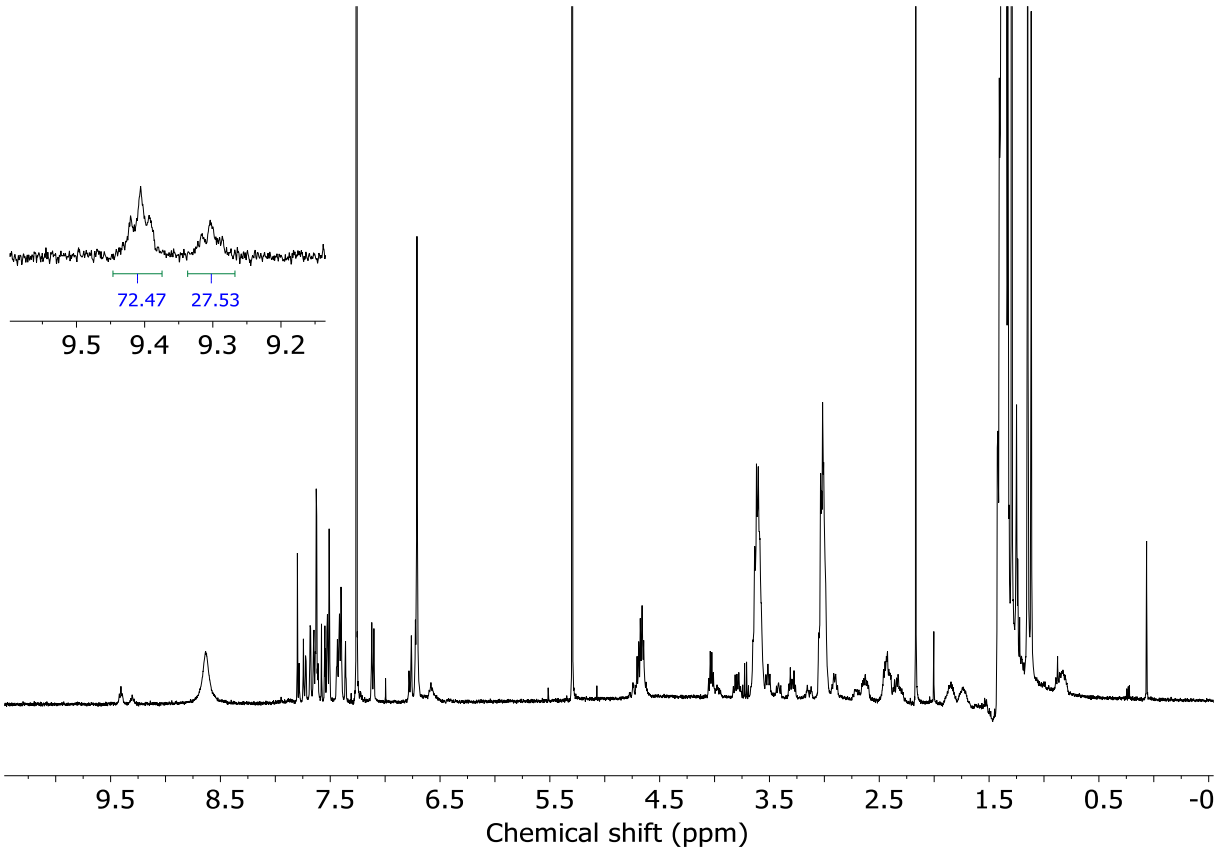

Figure 3.150 - ^{1}H NMR ($CDCl_3$, 400 MHz) of (E_m)-**11** and (Z_m)-**11** prior to chromatography (72 : 28 *dr*).

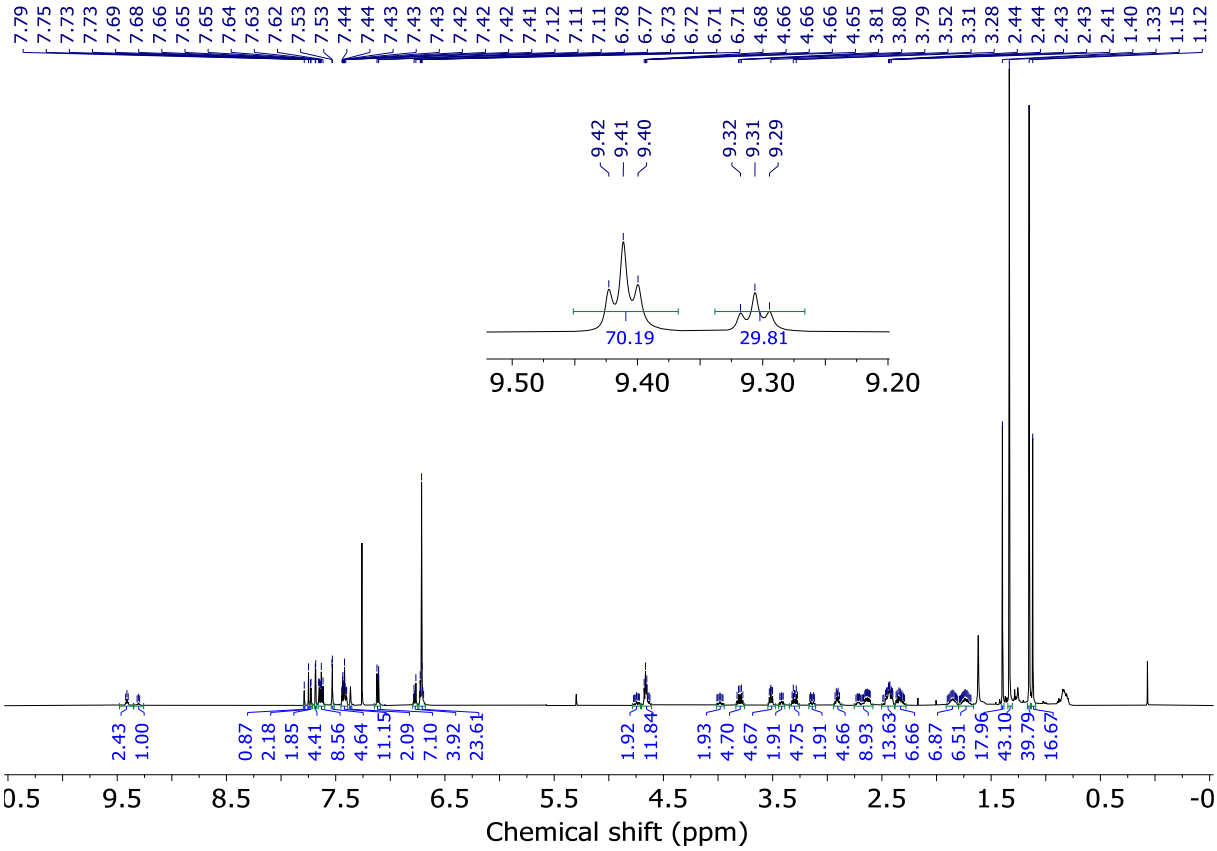

Figure 3.151 - ^{1}H NMR ($CDCl_3$, 400 MHz) of (E_m)-**11** and (Z_m)-**11** (2.4 : 1 *dr*).

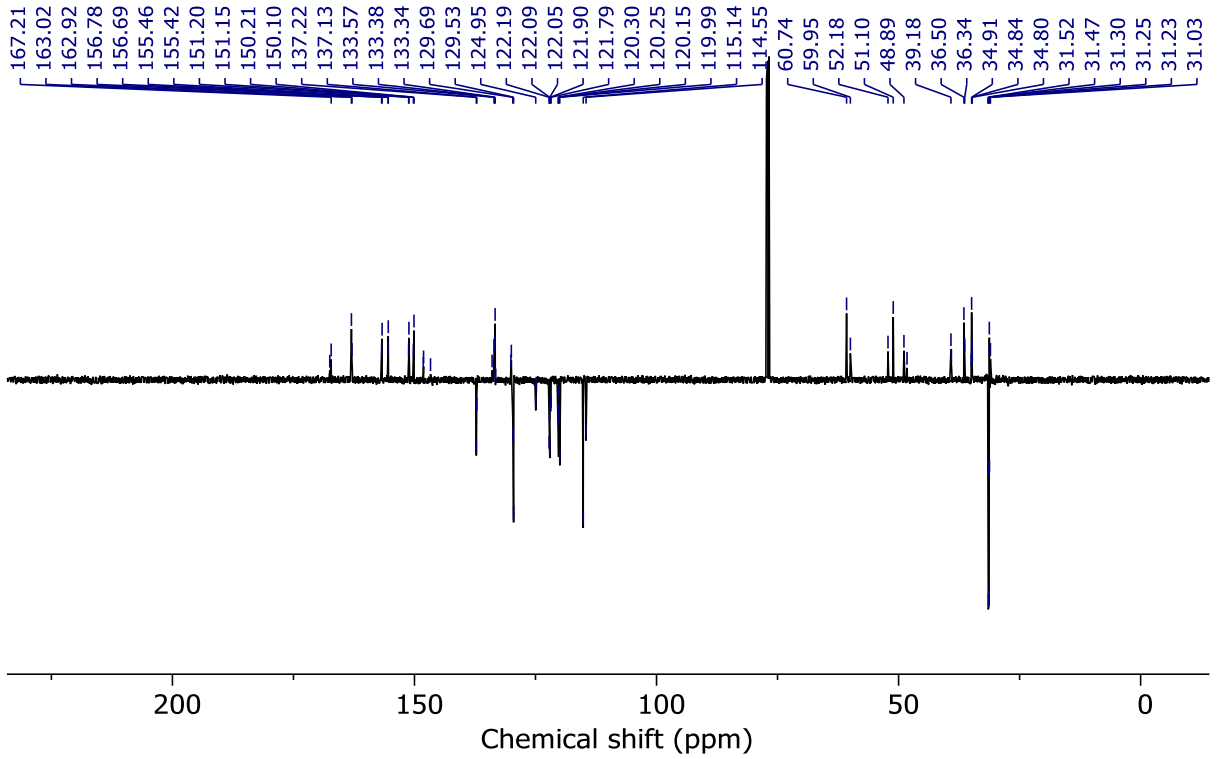

Figure 3.152 - JMOD NMR ($CDCl_3$, 101 MHz) of (E_m)-**11** and (Z_m)-**11** (2.4 : 1 *dr*).

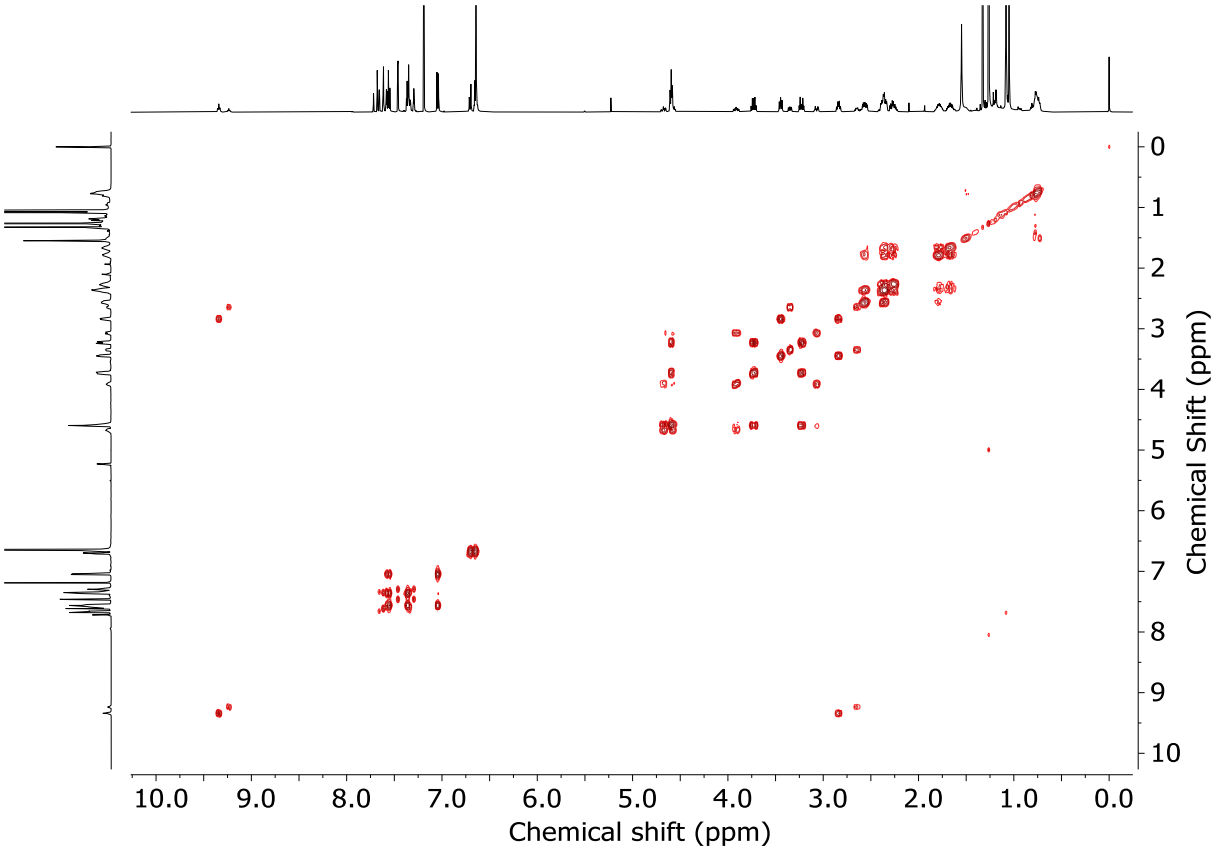

Figure 3.153 - COSY NMR ($CDCl_3$) of (E_m)-**11** and (Z_m)-**11** (2.4 : 1 *dr*).

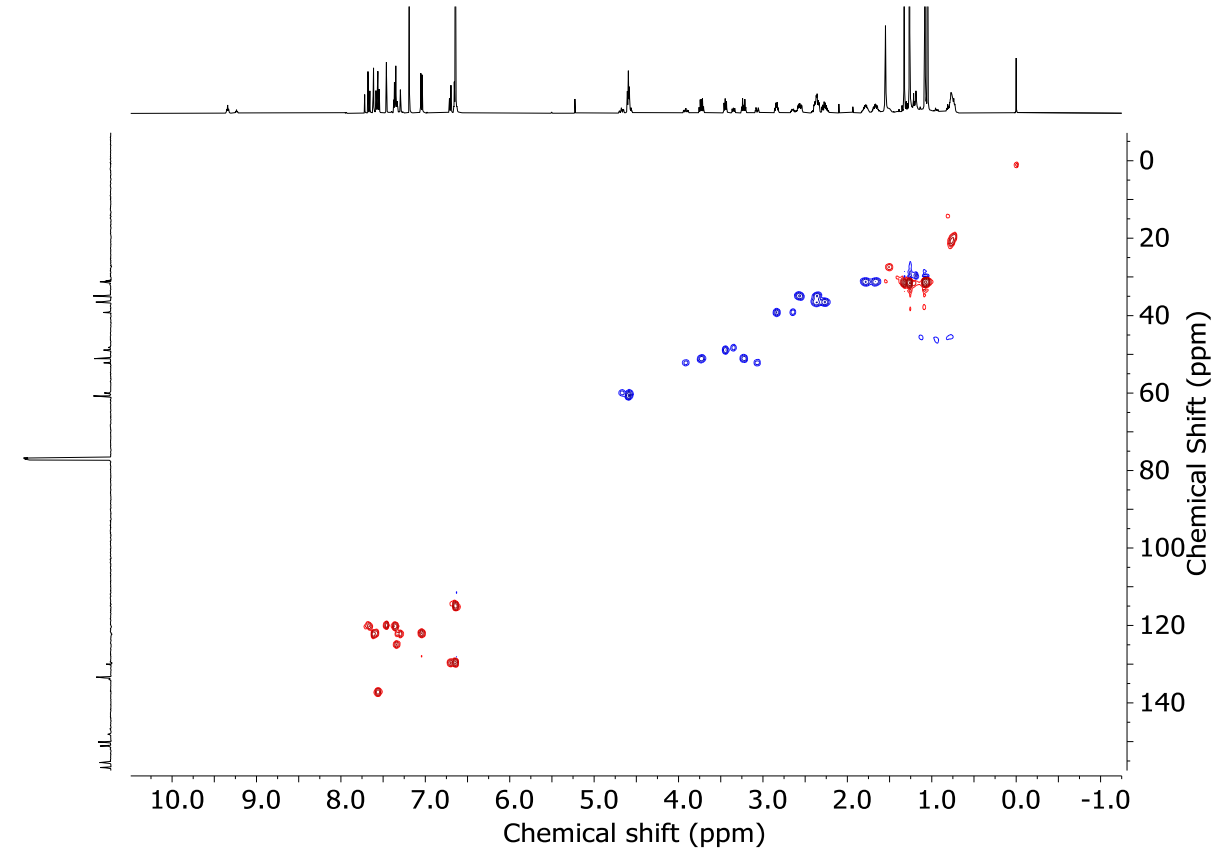

Figure 3.154 - HSQC NMR ($CDCl_3$) of (E_m)-**11** and (Z_m)-**11** (2.4 : 1 *dr*).

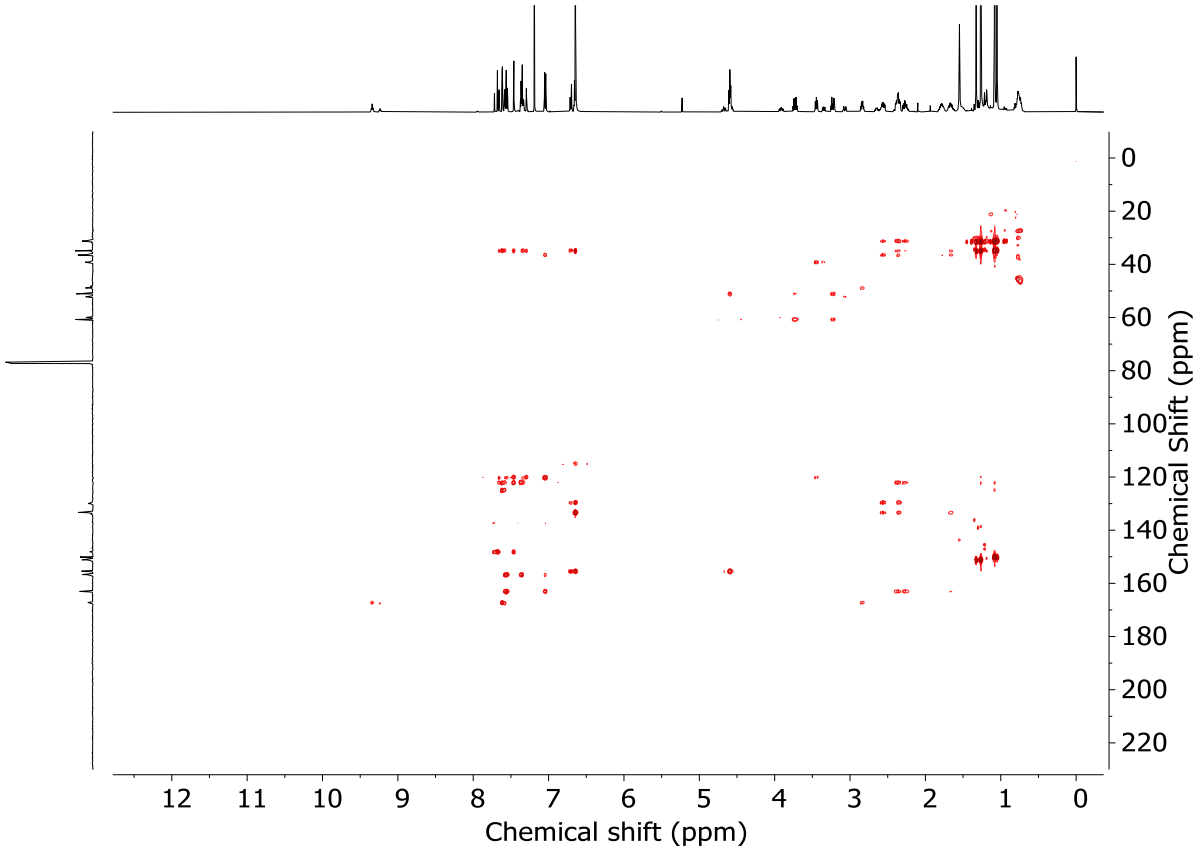

Figure 3.155 - HMBC NMR ($CDCl_3$) of (E_m)-**11** and (Z_m)-**11** (2.4 : 1 *dr*).

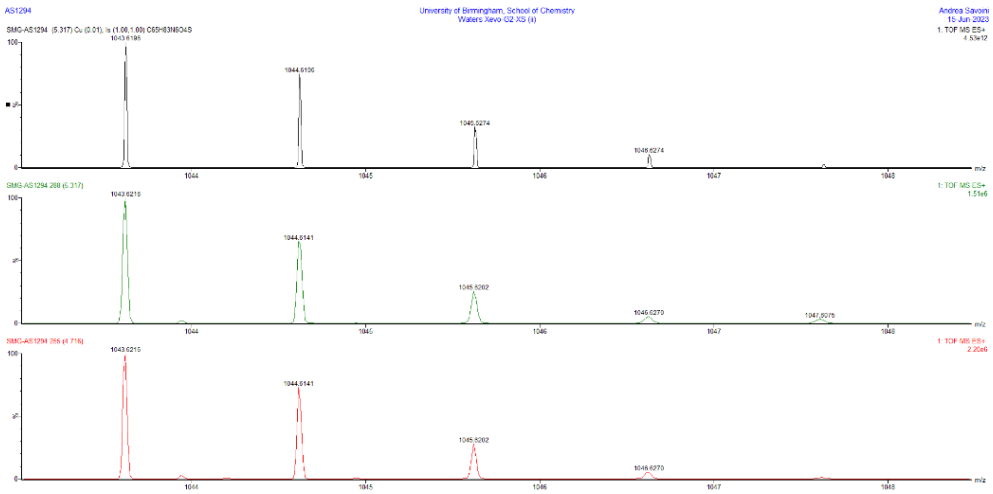

Figure 3.156 - Calculated (top) and observed (middle, bottom) isotopic patterns for (E_m)-**11** and (Z_m)-**11.**

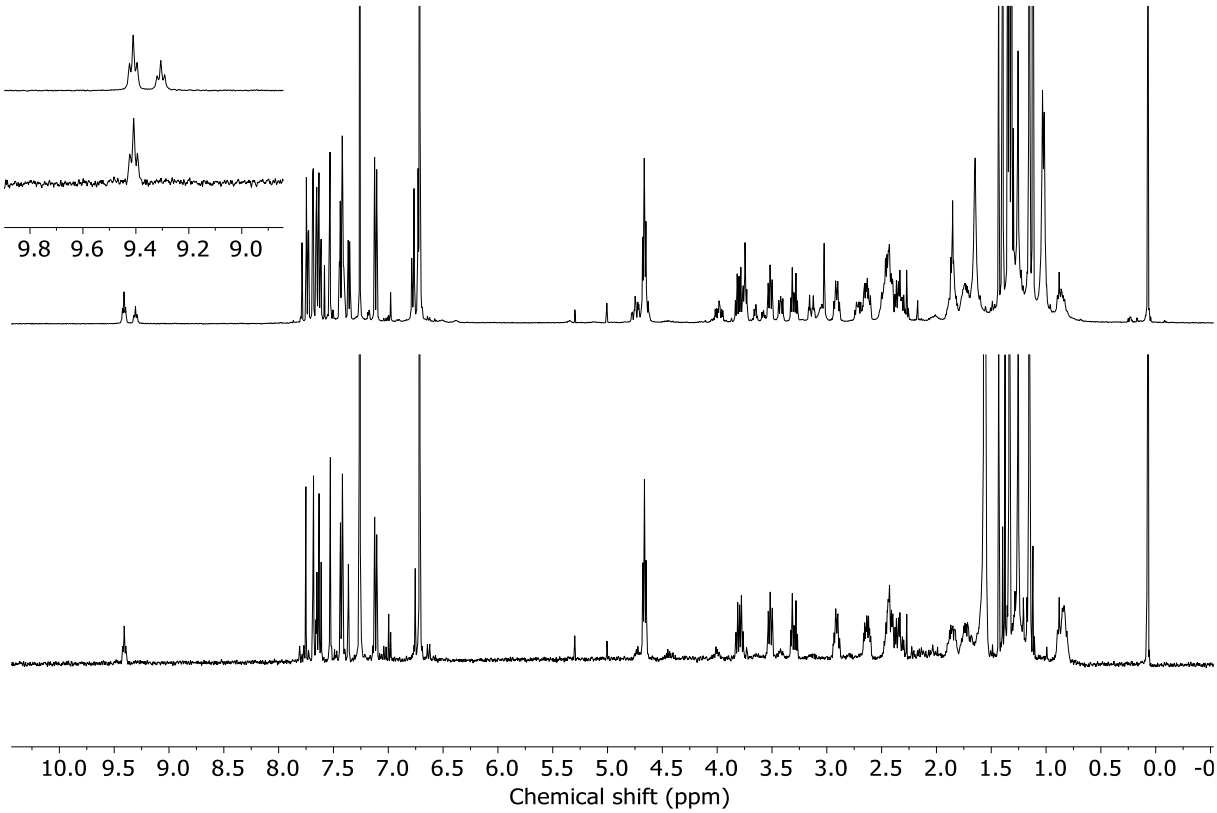

Figure 3.157 - ^{1}H NMR ($CDCl_3$, 400 MHz) of (E_m)-**11** and (Z_m)-**11** (top), analytical sample of (E_m)-**11** obtained after second round of chromatography for SC-XRD (bottom, apodised with standard Gaussian function, 1.00 GB [Hz])

Aniline azide S19

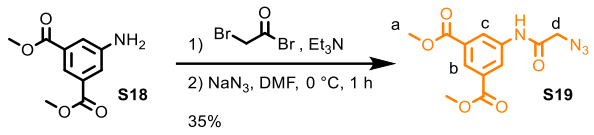

To a solution of **S18** (509.1 mg, 2.4 mmol) in DMF (5 mL) at 0 °C is added Et_3N (0.34 mL, 2.4 mmol) bromoacetyl bromide (0.19 mL, 2.2 mmol) dropwise. The solution turns red and in is stirred at 0 °C for 30 minutes. NaN_3 (238.2 mg, 3.7 mmol) is then added portion wise at 0 °C. The solution is allowed to warm at rt, then it was stirred for 1h. The reaction mixture was then quenched by adding H_2O (10 mL) dropwise. The aqueous and organic phases were separated, and the aqueous phase was then extracted with Et_2O (3 x 20 mL). The combined organic extracts were washed with brine (10 mL), dried ($MgSO_4$) and concentrated *in vacuo*. Chromatography (petrol-Et_2O 0→50%) gave **S19** as a white powder (247.5 mg, 35%).

^{1}H NMR (400 MHz, $CDCl_3$) δ: 8.48 (t, *J* = 1.5, 1H, H_b), 8.41 (d, *J* = 1.5, 2H, H_c), 8.21 (bs, 1H, NH), 4.20 (s, 2H, H_d), 3.95 (s, 6H, H_a).

^{13}C NMR (101 MHz, $CDCl_3$) δ: 165.8 (HMBC), 164.7 (HMBC), 137.3, 131.6, 127.1, 125.0, 52.9, 52.6.

HR-ESI-MS (+ve) *m/z* = 315.0704 $[M+Na]^+$ (calc. *m/z* for $C_{12}H_{12}NaN_4O_5$ 315.0705).

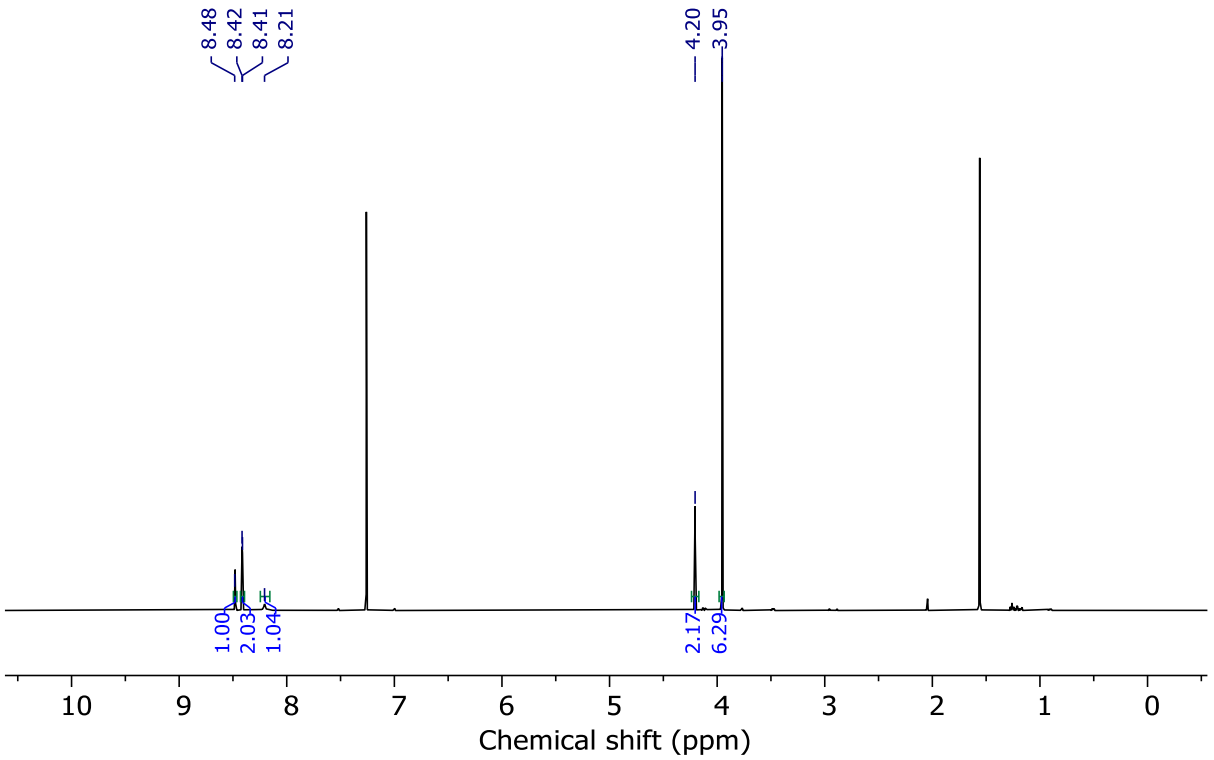

Figure 3.158 - ^{1}H NMR ($CDCl_3$, 400 MHz) of **S19**.

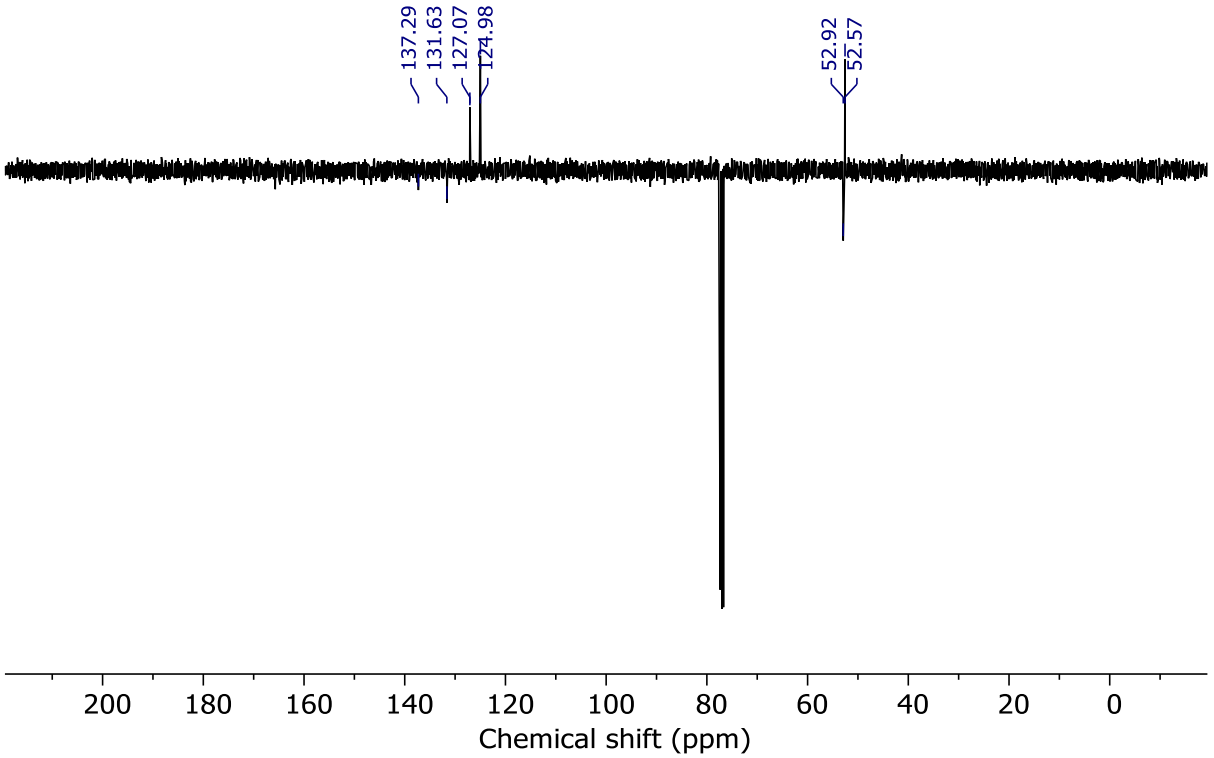

Figure 3.159 - JMOD NMR ($CDCl_3$, 101 MHz) of **S19**.

Aniline Rotaxanes (E_m)-12 and (Z_m)-12

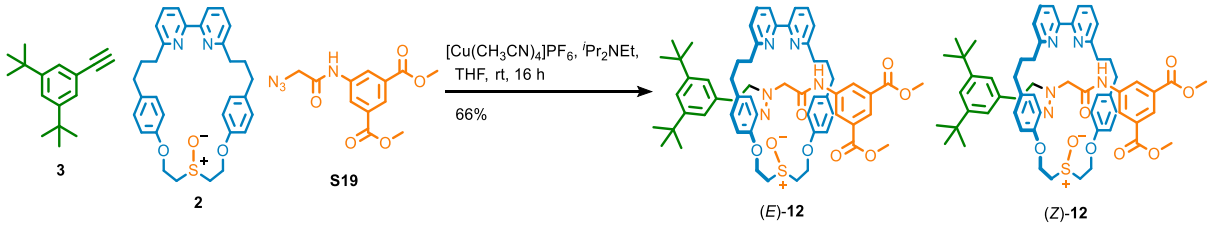

In a CEM vial were added the **3** (2.1 mg, 10.3 µmol), **S19** (3.0 mg, 10.3 µmol), **2** (5.0 mg, 9.4 µmol) and $[Cu(CH_3CN)_4PF_6]$ (3.4 mg, 9.1 µmol). The vial was sealed and purged with N_2, then THF was added (1.0 mL), followed by $^iPr_2NEt$ (3.3 µL, 19.0 µmol). The solution was stirred at rt for 16 h. the solution was diluted with CH_2Cl_2 (2 mL), then EDTA-NH_3 (5 mL) was added. The solution was vigorously stirred until complete decolouration. The aqueous and organic phases were separated, and the aqueous phase was then extracted with CH_2Cl_2 (3 x 10 mL). The combined organic extracts were washed with brine (10 mL), dried ($MgSO_4$) and concentrated *in vacuo* to give a sample containing **12** as a mixture of diastereomers (13 : 87 *dr*, Figure 3.160). Chromatography (CH_2Cl_2-CH_3CN 0→100%) gave **12** as a colourless oil (6.4 mg, 66%) as a mixture of diastereoisomers (1 : 6.1 *dr*, **Figure 3.161**).

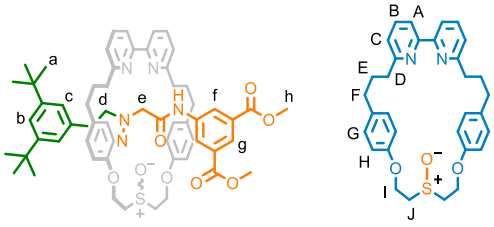

Major diastereoisomer

^{1}H NMR (500 MHz, $CDCl_3$) δ: 11.45 (s, 1H, H_d), 8.40 (t, *J* = 1.5, 1H, H_g), 8.13 (d, *J* = 1.6, 2H, H_f) 7.82-7,75 (m, 2H, H_B)7.70 (d, *J* = 1.9, 2H, H_c), 7.65 (d, *J* = 7.9, 2H, H_A), 7.46 (t, *J* = 1.8, 1H, H_b), 7.38 (s, 1H, NH), 7.29-7.23 (m, 2H, H_C superimposed with $CDCl_3$), 6.68 (dt, *J* = 8.5, 2.5, 4H, H_G), 6.61 (dt, *J* = 8.5, 2.0, 4H, H_H), 4.65 (s, 2H, H_e), 4.49 (ddd, *J* = 13.0, 8.8, 4.5, 2H, H_I), 4.32 (dt, *J* =12.6, 5.1, 2H, $H_{I'}$), 3.96 (s, 6H, H_h), 3.20 (ddd, *J* = 13.8, 8.8, 5.3, 2H, H_J), 2.75 (dt, *J* = 13.5, 4.6, 2H, $H_{J'}$), 2.68-2.41 (m, 8H, H_D, H_F), 1.92-1.72 (m, 4H, H_E), 1.42 (s, 18H, H_a)

^{13}C NMR (126 MHz, $CDCl_3$) δ: 166.1, 163.1, 162.5, 156.2, 155.4, 151.6, 148.4, 138.9, 137.9, 133.2, 130.8, 129.7, 129.3, 125.7, 124.4, 122.6, 122.5, 121.1, 120.3, 119.9, 115.4, 60.4, 52.5, 51.2, 36.6, 35.0, 34.8, 31.6, 31.0.

HR-ESI-MS (+ve) *m/z* = 1033.5 $[M+H]^+$ for isotopic pattern see Figure 3.166.

Minor diastereoisomer

^{1}H NMR (500 MHz, $CDCl_3$) δ: 11.62 (s, 1H, H_d), 8.37 (t, *J* = 1.5, 1H, H_g), 8.12 (d, *J* = 1.5, 2H, H_f), 7.82-7,75 (m, 4H, H_B, H_c), 7.64 (d, *J* = 8.0, 2H, H_A), 7.46 (t, *J* = 1.8, 1H, H_b), 7.43 (s, 1H, NH), 7.29-7.23 (m, 2H, H_C superimposed with $CDCl_3$) 6.64 (s, 8H, H_G, H_H), 4.70-4.62 (m, 2H, H_I), 4.59 (s, 2H, H_e), 4.45 (ddd, *J* = 13.0, 8.8, 4.5, 2H, $H_{I'}$) 3.92 (s, 6H, H_h), 3.40 (ddd, *J* = 14.1, 8.6, 3.9, 2H, H_J), 3.07 (ddd, *J* = 14.2, 5.5, 3.4, 2H, $H_{J'}$), 2.68-2.41 (m, 8H, H_D, H_F), 1.92-1.72 (m, 4H, H_E), 1.45 (s, 18H, H_a)

^{13}C NMR (126 MHz, $CDCl_3$) δ: 166.0, 163.2, 162.5, 156.2, 155.3, 151.5, 148.6, 139.0, 137.8, 132.9, 130.6, 129.8, 129.4, 125.5, 124.6, 122.6, 121.1, 120.3, 120.2, 114.7, 58.9, 52.4, 52.0, 49.6, 36.7, 34.9, 31.6, 31.4

HR-ESI-MS (+ve) *m/z* = 1033.5 $[M+H]^+$ for isotopic pattern see Figure 3.166.

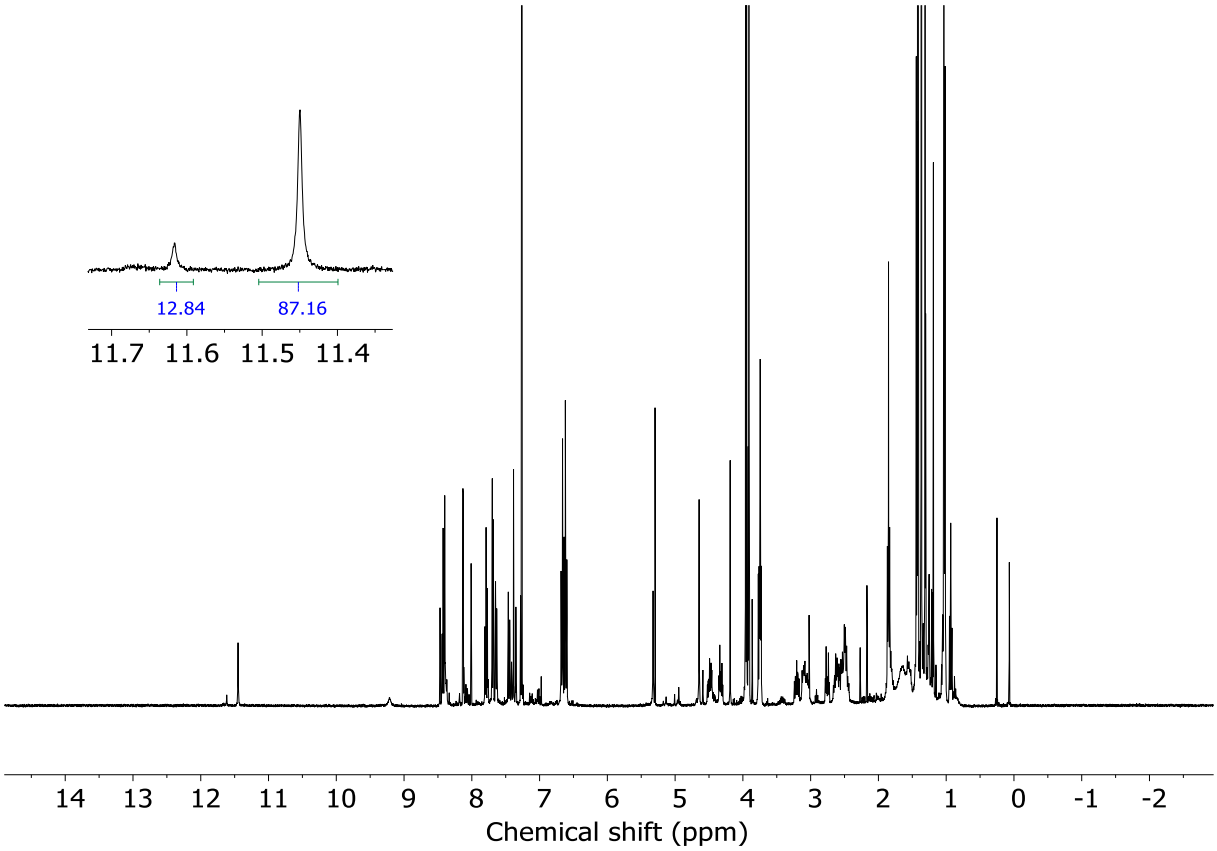

Figure 3.160 - ^{1}H NMR ($CDCl_3$, 400 MHz) of (E_m)-**12** and (Z_m)-**12** prior to chromatography (13:87 *dr*).

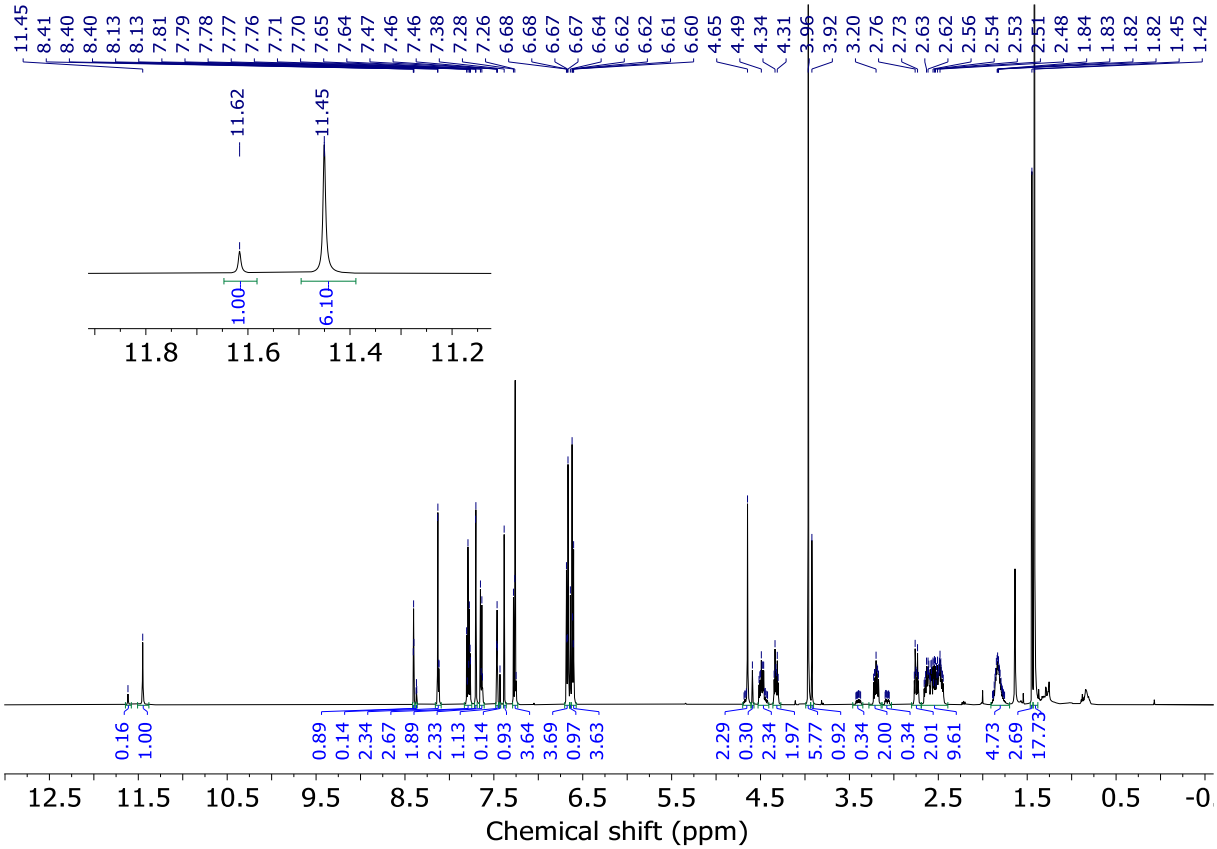

Figure 3.161 - ^{1}H NMR ($CDCl_3$, 400 MHz) of (E_m)-**12** and (Z_m)-**12** (1 : 6.1 *dr*).

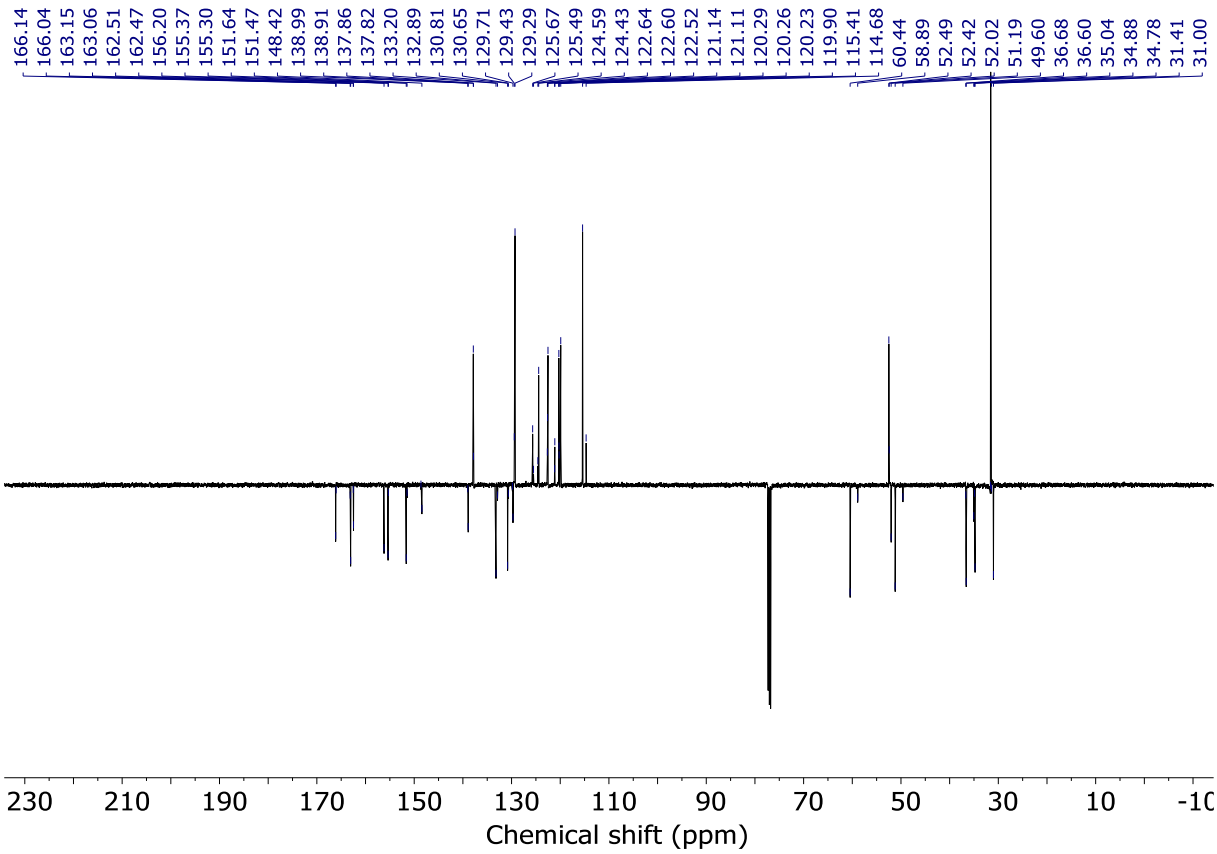

Figure 3.162 - JMOD NMR ($CDCl_3$, 101 MHz) of (E_m)-**12** and (Z_m)-**12** (1 : 6.1 *dr*).

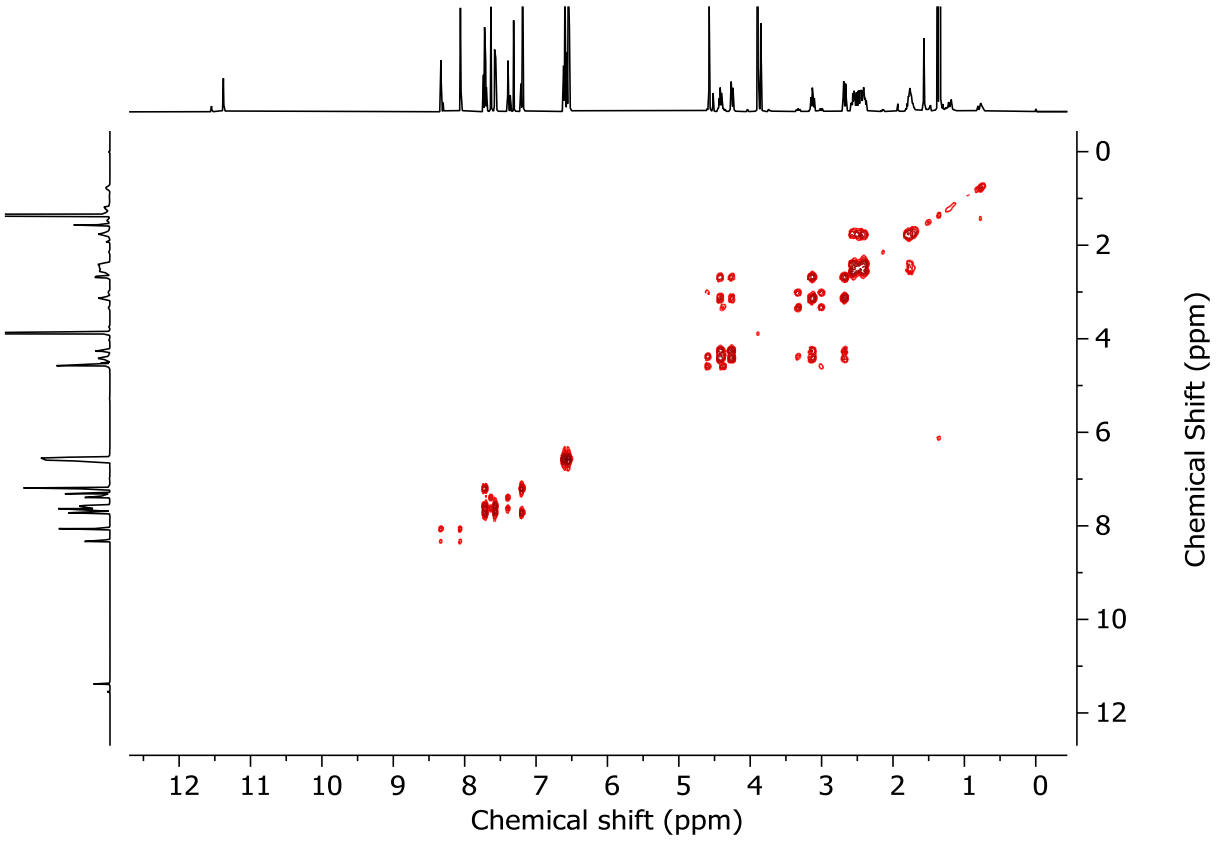

Figure 3.163 - COSY NMR ($CDCl_3$) of (E_m)-**12** and (Z_m)-**12** (1 : 6.1 *dr*).

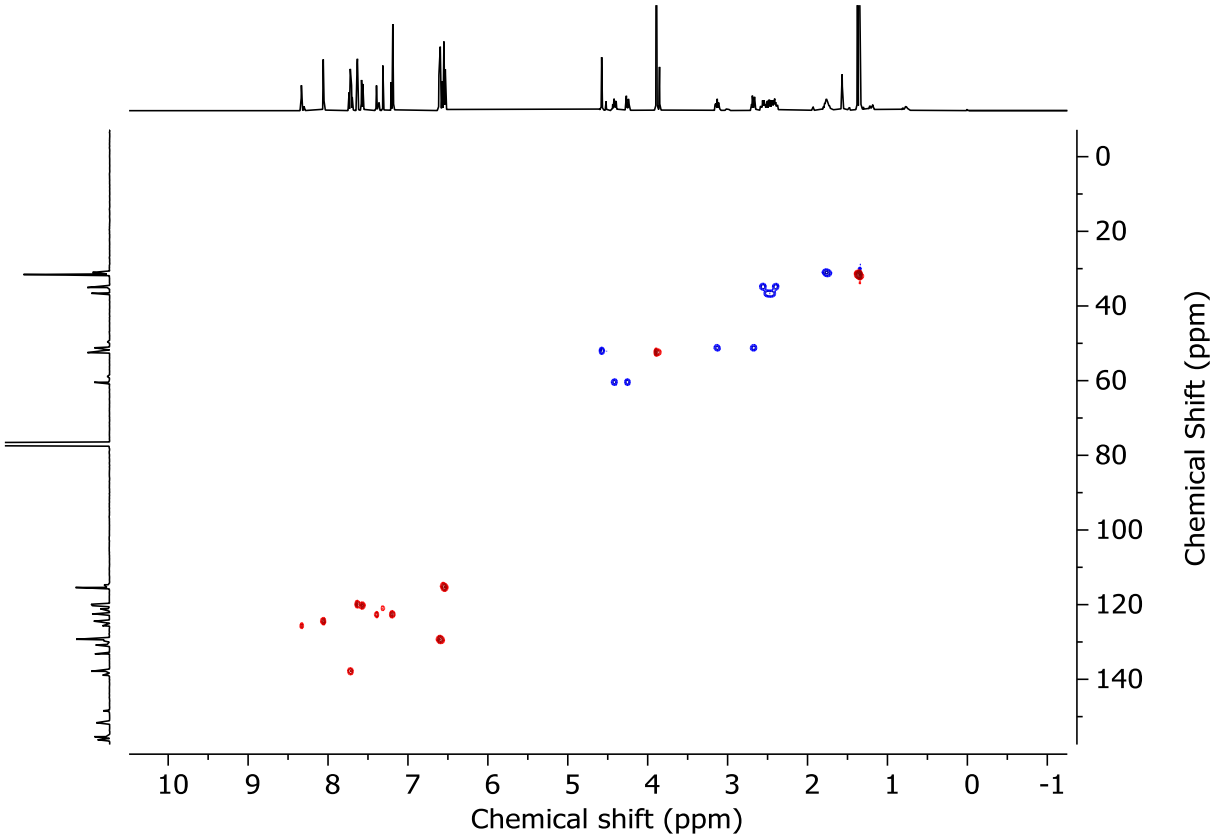

Figure 3.164 - HSQC NMR ($CDCl_3$) of (E_m)-**12** and (Z_m)-**12** (1 : 6.1 *dr*).

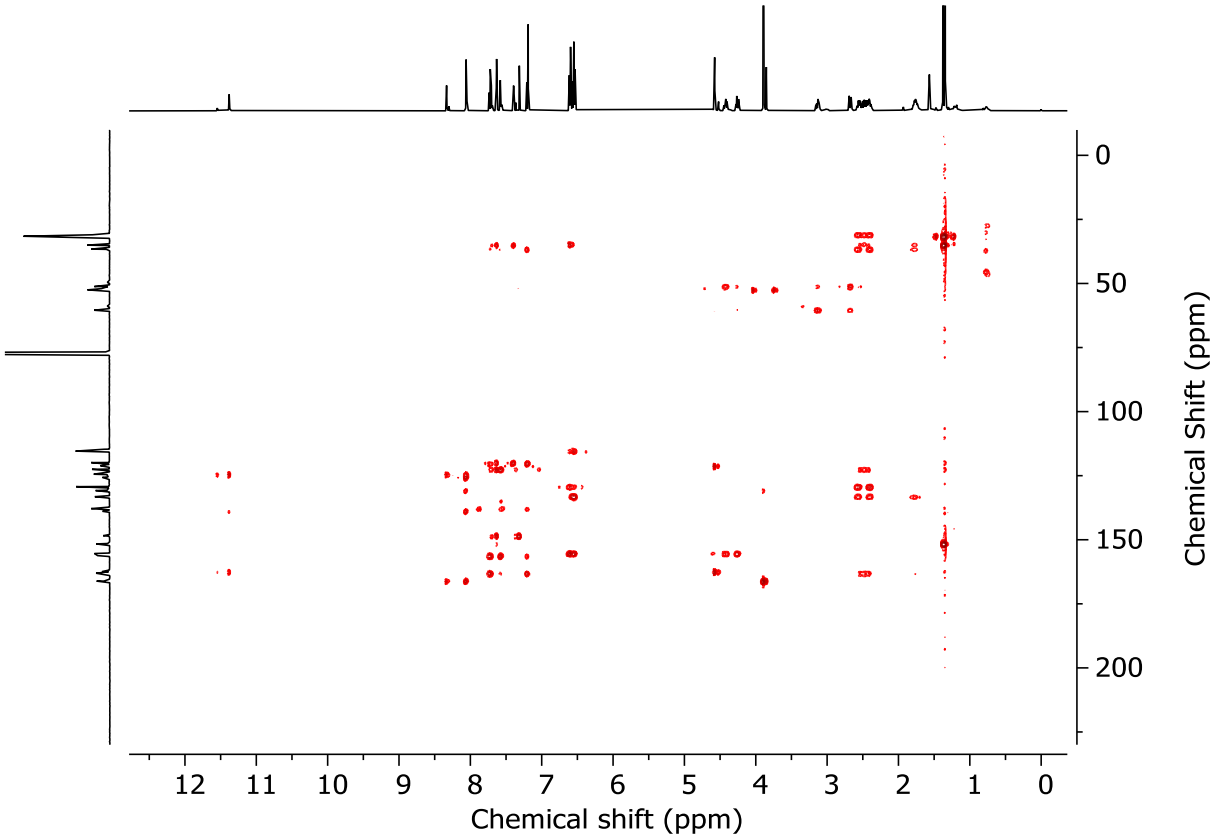

Figure 3.165 - HMBC NMR ($CDCl_3$) of (E_m)-**12** and (Z_m)-**12** (1 : 6.1 *dr*).

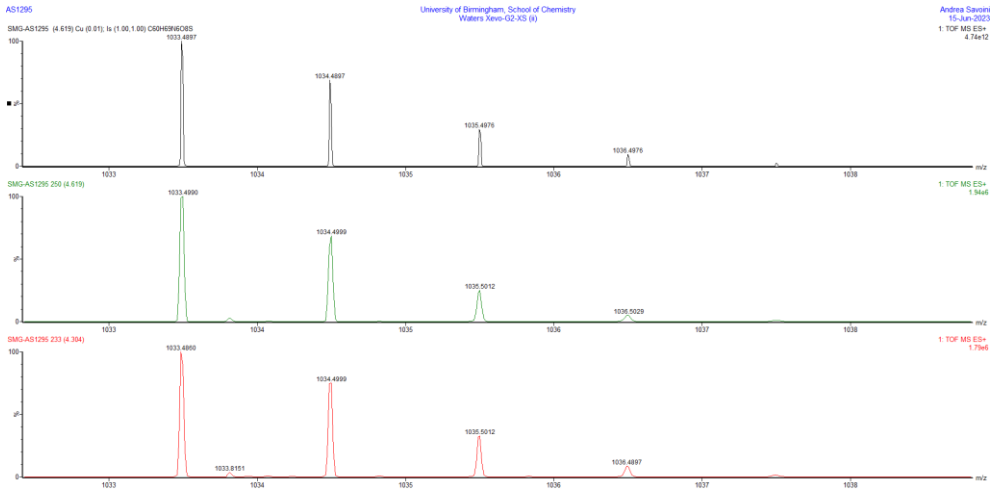

Figure 3.166 - Calculated (top) and observed (middle, bottom) isotopic patterns for (E_m)-**12** and (Z_m)-**12**.

Synthesis of catenane 14 and associated compounds

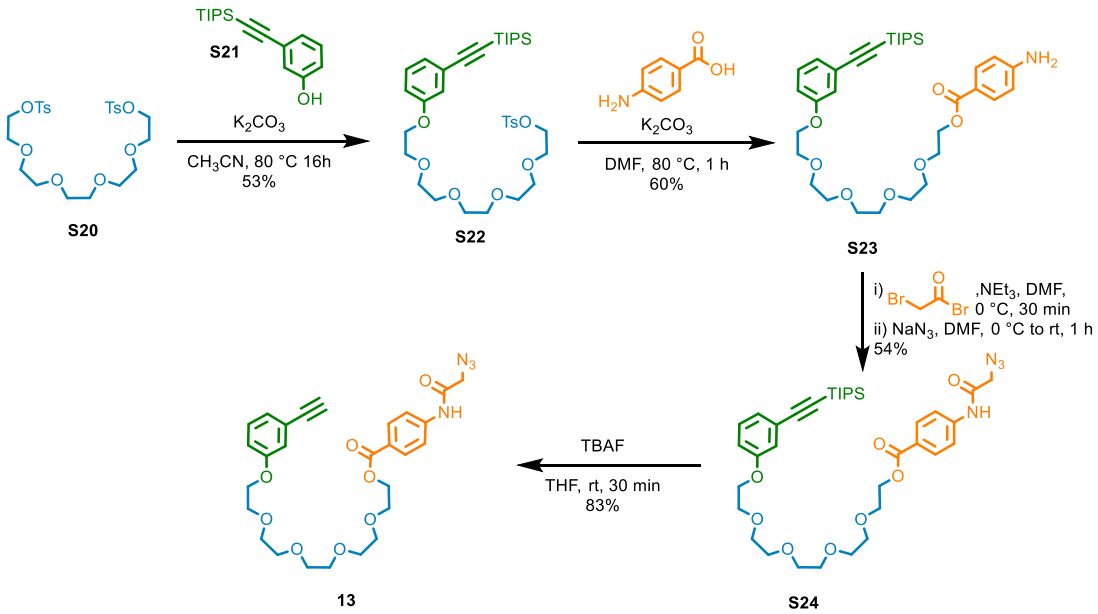

Scheme 3.8 - Synthetic route to macrocycle precursor **13**.

TIPS aryl ether S22

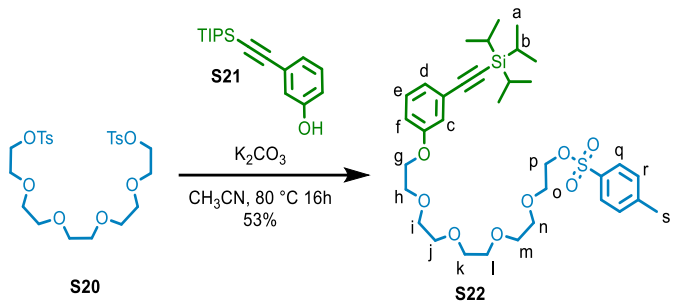

S21 (1.5 g, 4.6 mmol), **S20** (5.0 g, 9.2 mmol) and K_2CO_3 (2.6 g, 18.3 mmol) were suspended in CH_3CN (250 mL) and the resulting suspension was heated at reflux for 16 h. H_2O (100 mL) was added, then the aqueous and organic phases were separated, and the aqueous phase was then extracted with EtOAc (3 x 100 mL). The combined organic extracts were washed with brine (150 mL), dried ($MgSO_4$) and concentrated in vacuo. Chromatography (petrol : EtOAc 0→60%) gave **S22** as a colourless oil (1.6 g, 53%).

^{1}H NMR (400 MHz, $CDCl_3$) δ: 7.79 (dt, J = 8.3, 1.9, 2H, H_q), 7.39-7.29 (m, 2H, H_r), 7.19 (t, J = 7.8, 1H, H_e), 7.07 (dt, J = 7.6, 1.2, 1H, H_f), 7.00 (dd, J = 2.6, 1.4, 1H, H_c), 6.87 (ddd, J = 8.4, 2.7, 1.0, 1H, H_d), 4.21-4.06 (m, 4H, H_g, H_p), 3.87-3.80 (m, 2H, H_h), 3.74-3.49 (m, 14H, H_i, H_j, H_k, H_l, H_m, H_n, H_o), 2.44 (s, 3H, H_s), 1.12 (app.s, 21H, H_a, H_b)

^{13}C NMR (101 MHz, $CDCl_3$) δ: 173.9, 158.4, 144.8, 129.8, 129.3, 128.0, 124.8, 124.5 117.7, 115.4, 106.9, 90.4, 70.9, 70.8 (×3), 70.7, 70.5, 69.7, 69.2, 68.7, 67.5, 29.7, 21.6, 18.7, 11.3.

HR-ESI-MS (+ve) m/z = 649.3242 $[M+H]^+$ (calc. 648.3225 m/z for $C_{34}H_{53}O_8SSi$);

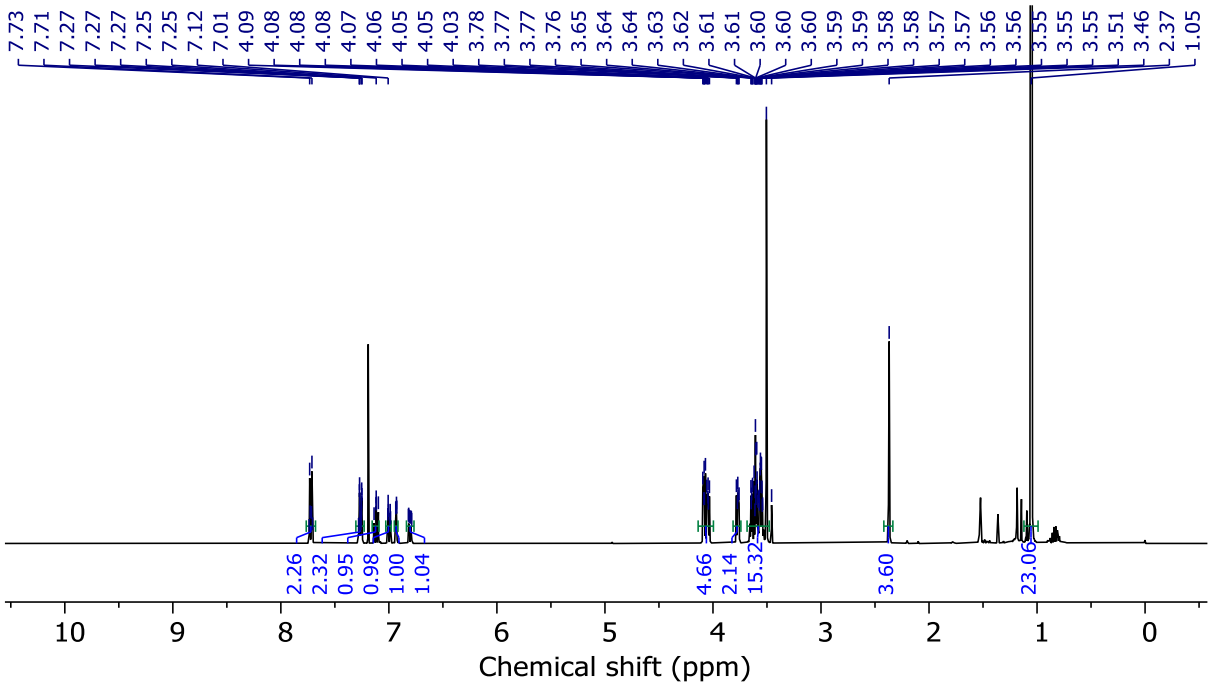

Figure 3.167 - ^{1}H NMR ($CDCl_3$, 400 MHz) of **S22**.

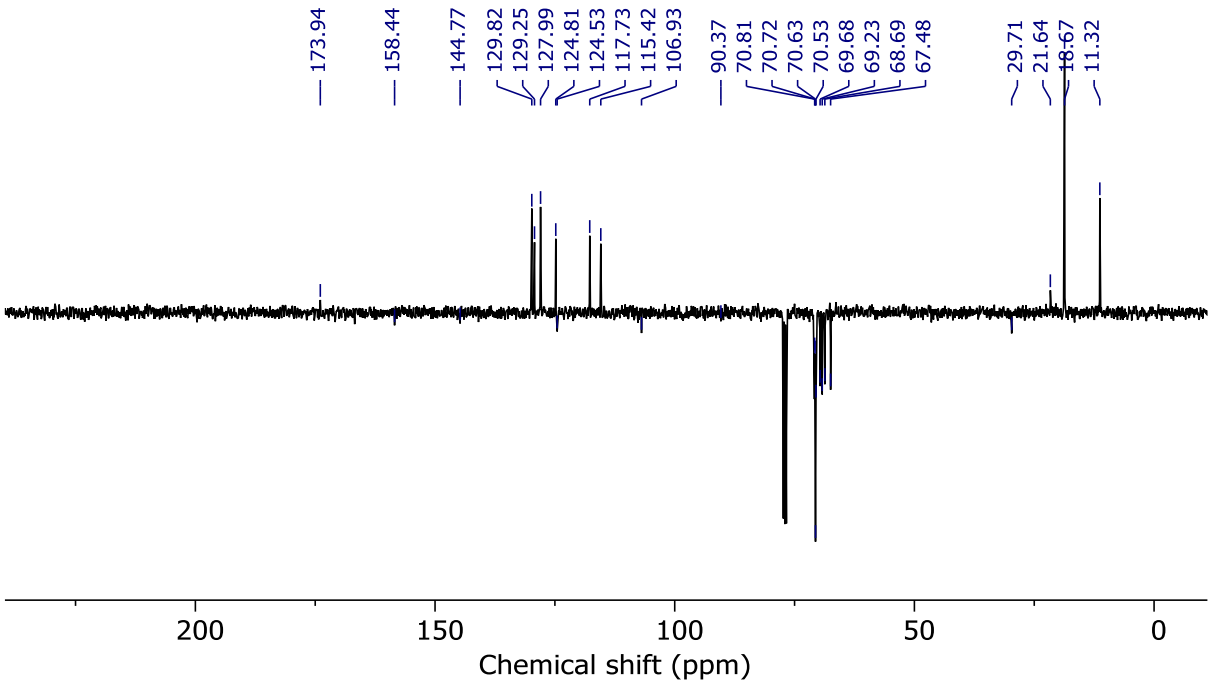

Figure 3.168 - JMOD NMR ($CDCl_3$, 101 MHz) of **S22**.

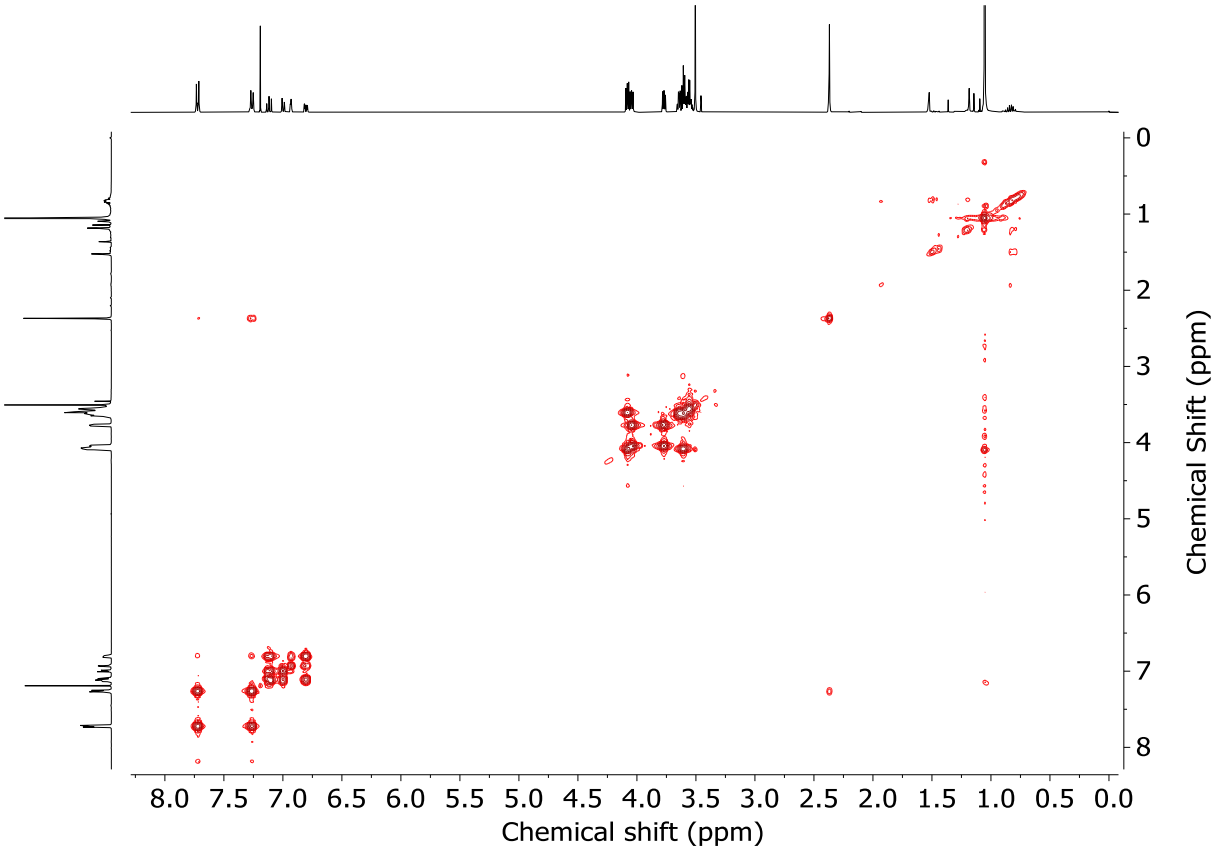

Figure 3.169 - COSY NMR ($CDCl_3$) of **S22**.

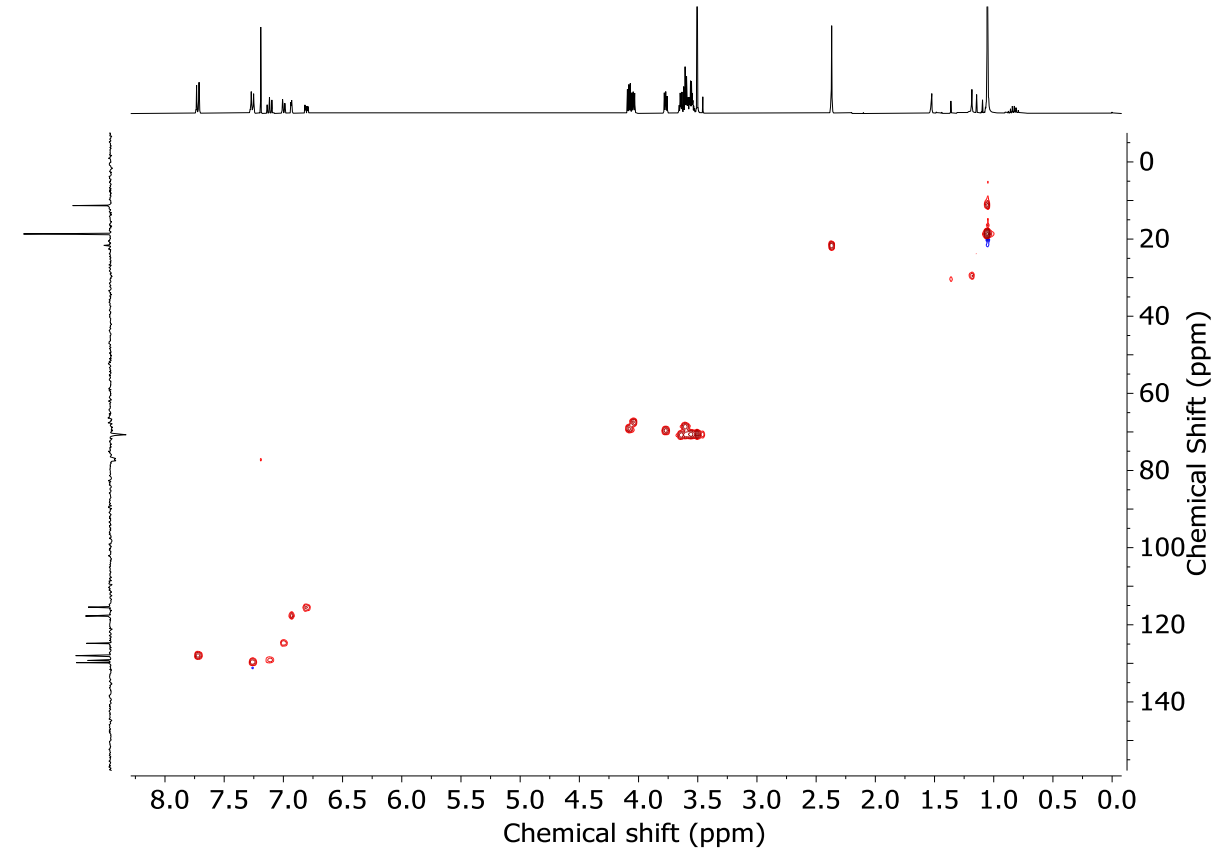

Figure 3.170 - HSQC NMR ($CDCl_3$) of **S22**.

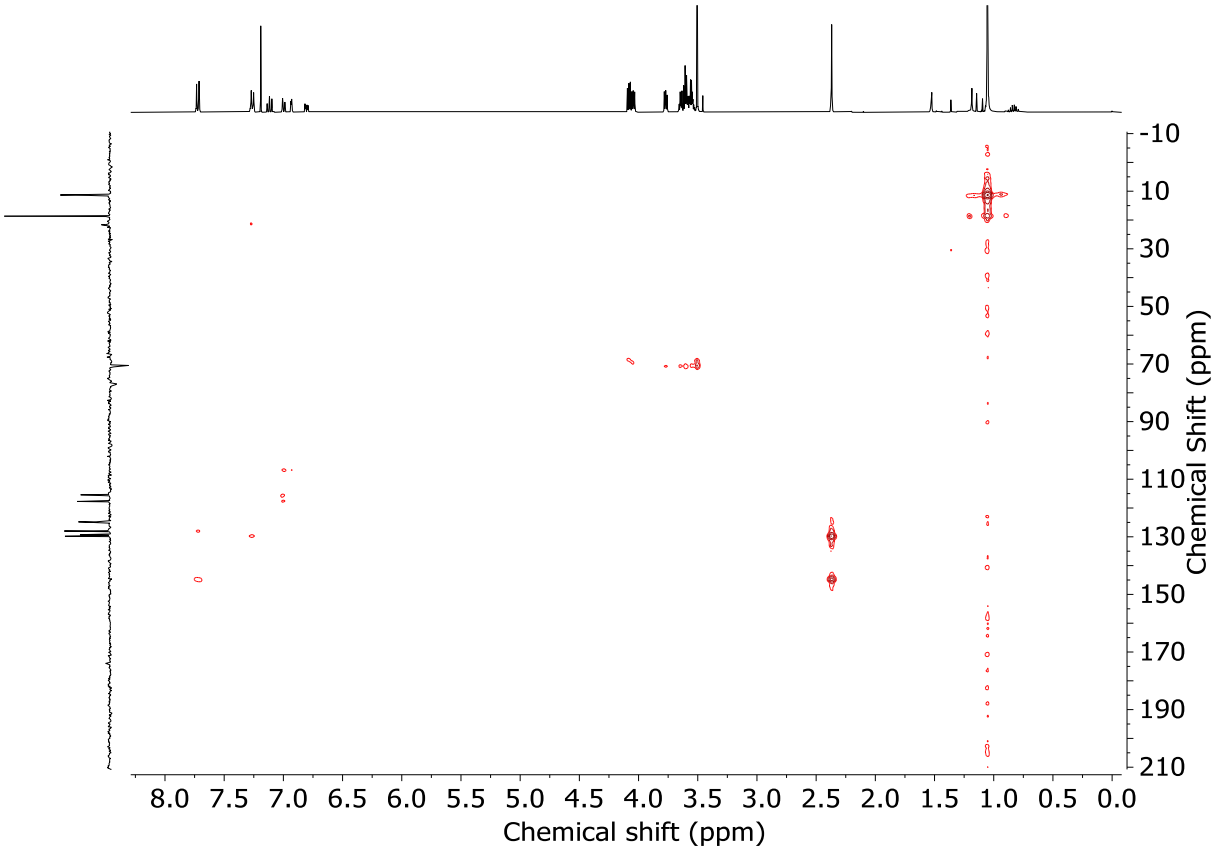

Figure 3.171 - HMBC NMR ($CDCl_3$) of **S22**.

Amine TIPS aryl ether S23

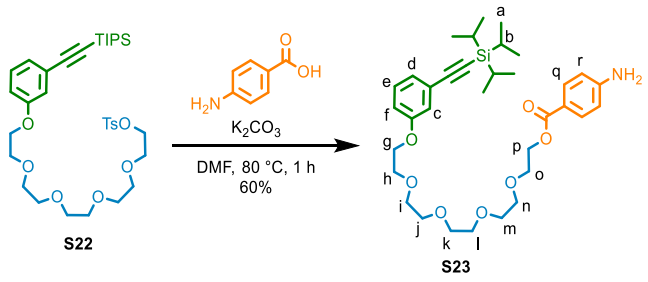

4-aminobenzoic acid (0.82 g, 6.0 mmol) and K_2CO_3 (1.1 g, 8.0 mmol) were suspended in DMF (5 mL) and the resulting suspension was heated at 80 °C for 15 min. A solution of **S22** (1.3 g, 2.0 mmol) in DMF (5 mL) was added and the reaction mixture was stirred at 80 °C for 1 h. The reaction mixture was poured onto sat. $NaHCO_{3\,(aq)}$ (20 mL) then extracted with EtOAc (3 x 20 mL). The organic phases are washed with 5% $LiCl_{(aq)}$ solution (3 x 5 mL), washed with brine (20 mL), dried ($MgSO_4$) and concentrated *in vacuo*. Chromatography (petrol-Et_2O, 50→100%) gave **S23** as a yellow oil (754 mg, 59%).

^{1}H NMR (400 MHz, $CDCl_3$) δ: 7.85 (dt, J = 8.8, 2.1, 2H, H_q), 7.18 (t, J = 8.0, 1H, H_e), 7.06 (dt, J = 7.5, 1.2, 1H, H_f), 7.00 (dd, J = 2.5, 1.4, 1H, H_c), 6.87 (ddd, J = 8.4, 2.7, 1.0, 1H, H_d), 4.43-4.37 (m, 2H,

H_p), 4.16-3.98 (m, 4H, H_g, NH_2), 3.86-3.76 (m, 4H, H_o, H_h), 3.74-3.59 (m, 12H, H_i, H_j, H_k, H_l, H_m, H_n), 1.12 (app s, 21H, H_a, H_b)

^{13}C NMR (101 MHz, $CDCl_3$) δ: 166.6, 158.4, 150.9, 131.7, 129.3, 124.8, 124.5, 119.6, 117.7, 115.5, 113.7, 106.9, 90.4, 70.8, 70.6 (×5), 69.7, 69.4, 67.5, 63.6, 18.7, 11.3.

HR-ESI-MS (+ve) *m/z* = 636.3351 $[M+Na]^+$ (calc. 636.3327 *m/z* for $C_{34}H_{51}NNaO_7Si$);

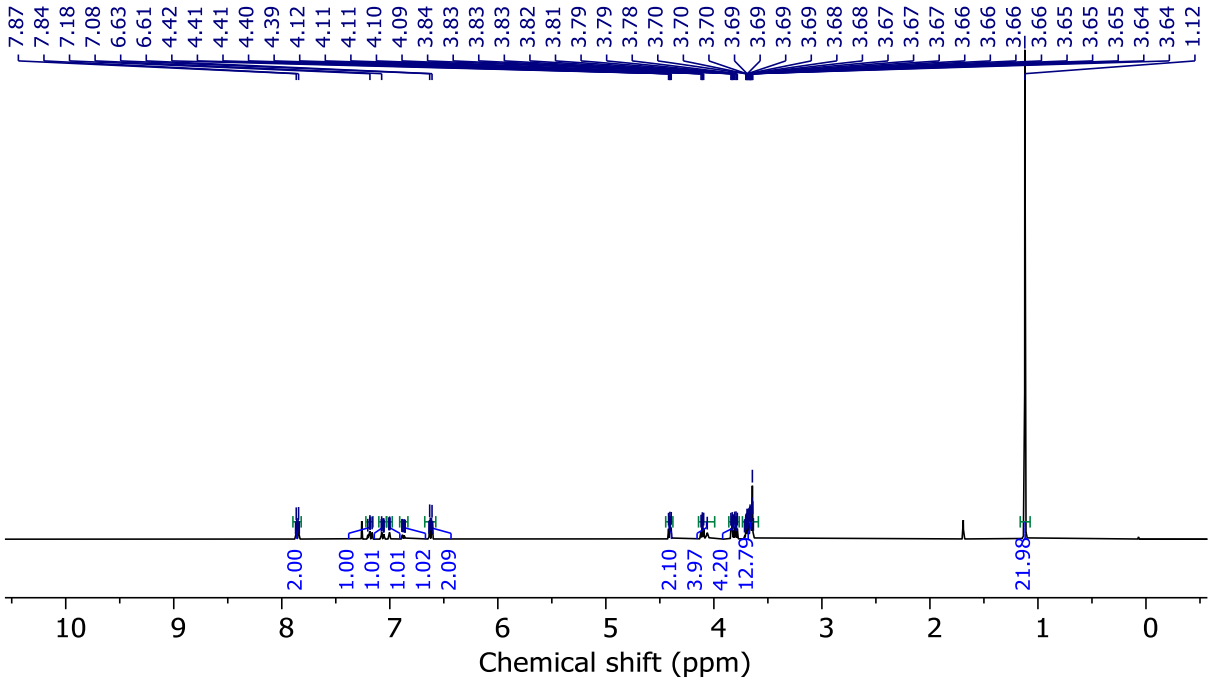

Figure 3.172 - ^{1}H NMR ($CDCl_3$, 400 MHz) of **S23**.

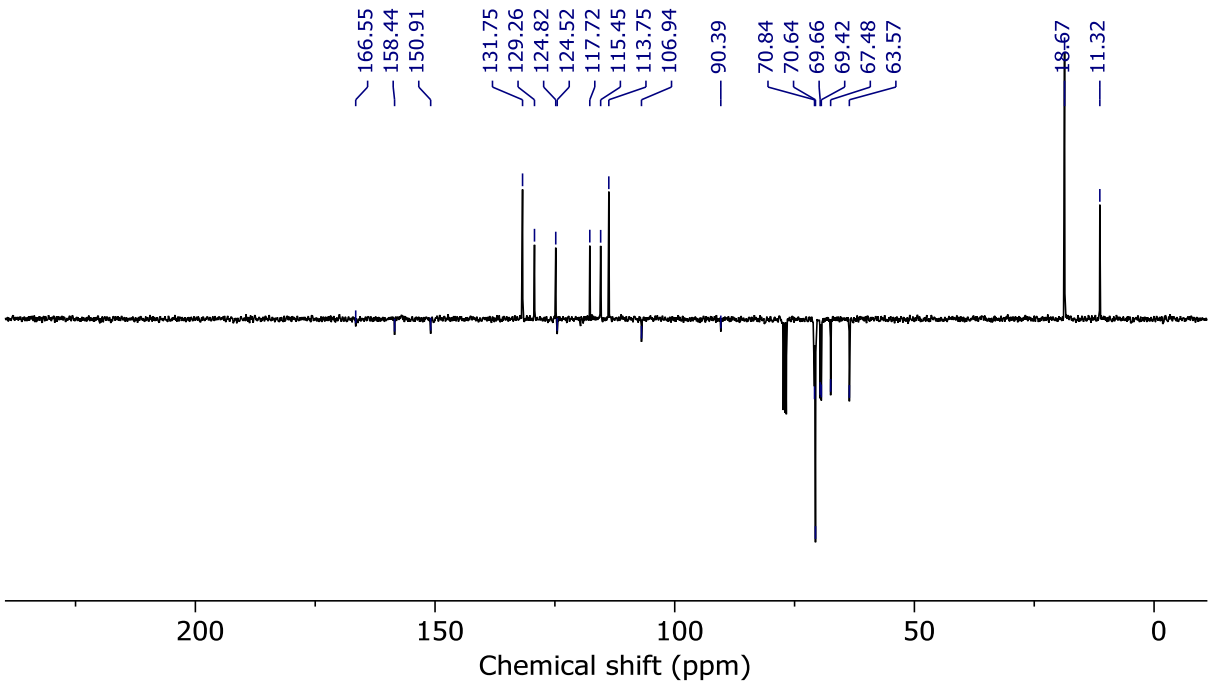

Figure 3.173 - JMOD NMR ($CDCl_3$, 101 MHz) of **S23**.

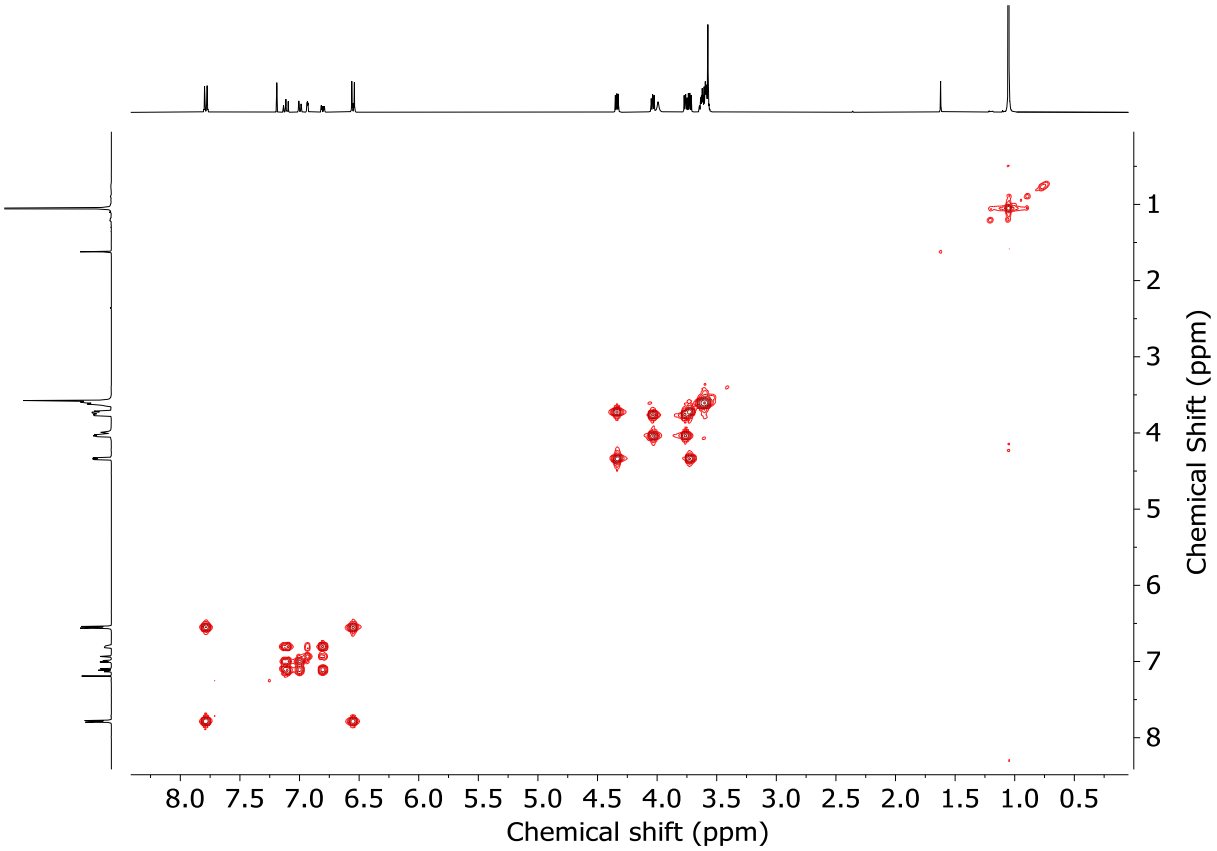

Figure 3.174 - COSY NMR ($CDCl_3$) of **S23**.

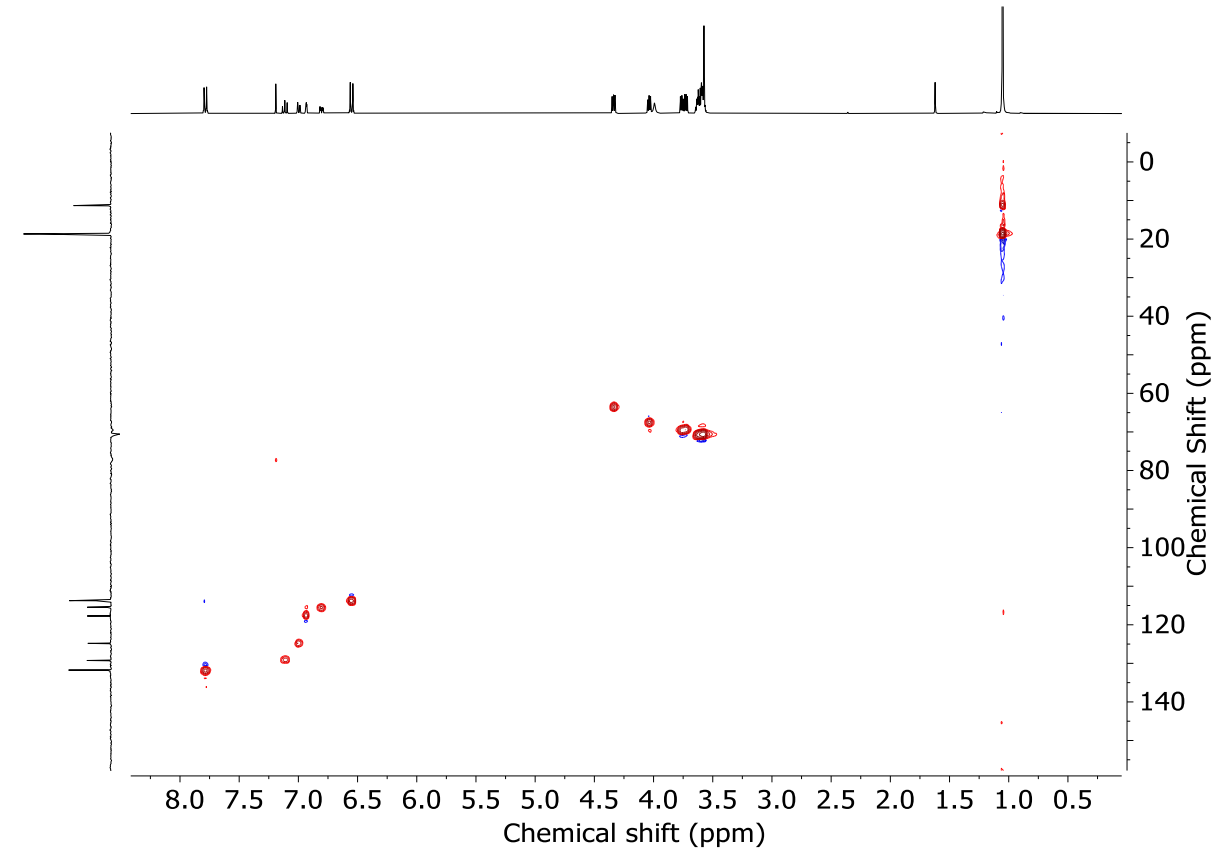

Figure 3.175 - HSQC NMR ($CDCl_3$) of **S23**.

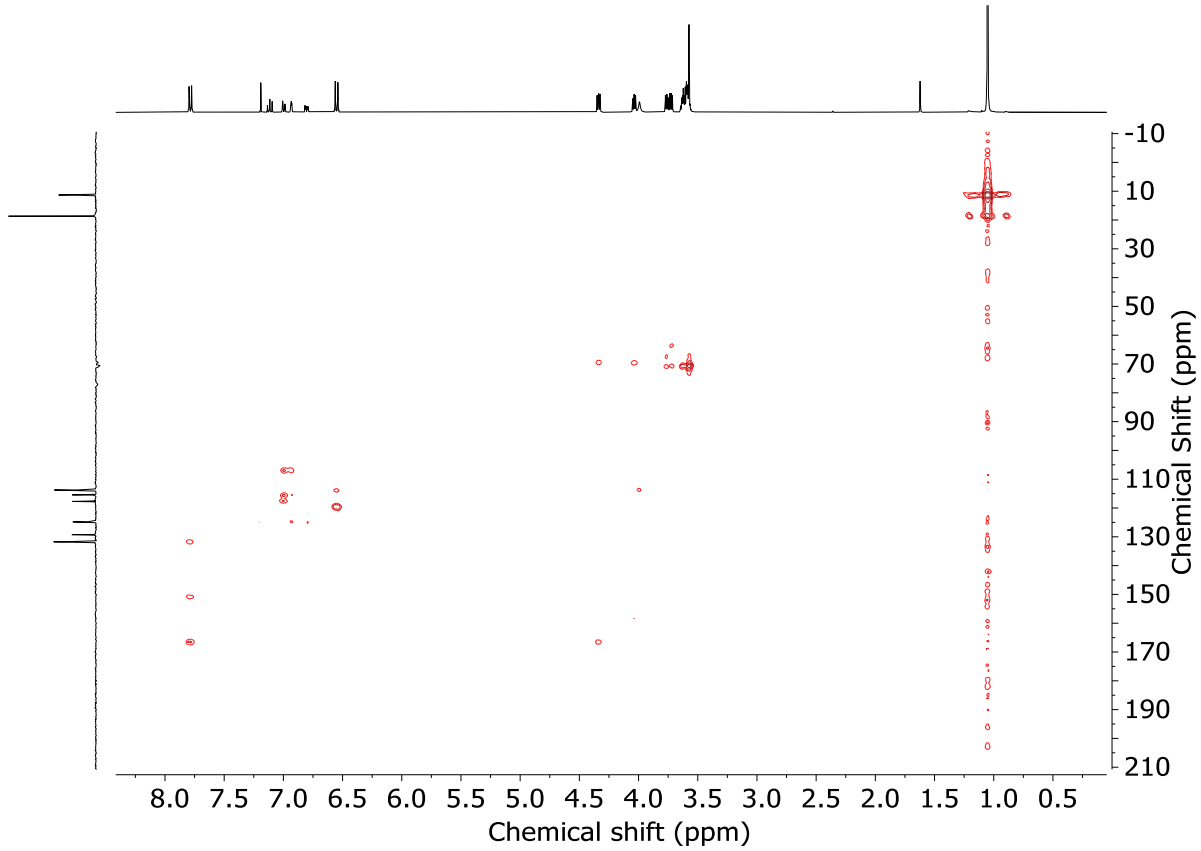

Figure 3.176 - HMBC NMR ($CDCl_3$) of **S23**.

Azide TIPS aryl ether S24

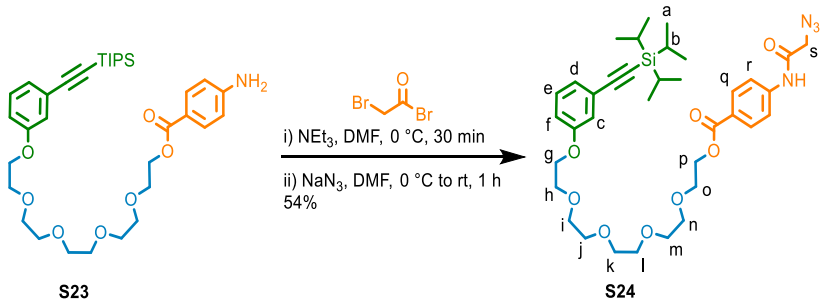

To a solution of **S23** (690 mg, 1.12 mmol) in DMF (5 mL) at 0 °C was added Et_3N (0.63 mL, 4.5 mmol) bromoacetyl bromide (0.15 mL, 1.7 mmol) dropwise. The solution turns red and was stirred at 0 °C for 30 minutes. NaN_3 (219 mg, 3.4 mmol) was then added portion wise at 0 °C. The solution was allowed to warm at rt and it was stirred for 1 h. The reaction mixture was then quenched by adding H_2O (10 mL) dropwise. The aqueous and organic phases were separated, and the aqueous phase was then extracted with EtOAc (3 x 20 mL). The combined organic extracts were washed with 5% $LiCl_{(aq)}$ (3 x 5 mL), brine (10 mL), dried ($MgSO_4$) and concentrated *in vacuo*. Chromatography (petrol-Et_2O 70→100%) gave **S24** as a yellow oil (432.4 mg, 54%).

^{1}H NMR (500 MHz, $CDCl_3$) δ: 8.16 (bs, 1H, NH), 8.05 (dt, J = 8.8, 2.0, 2H, H_q), 7.64 (dt, J = 8.8, 2.0, 2H, H_r), 7.18 (app. t, J = 8.0, 1H, H_e), 7.07 (dt, J = 7.5, 1.1, 1H, H_f), 7.00 (dd, J = 2.5, 1.4, 1H, H_c), 6.87 (ddd, J = 8.4, 2.7, 1.0, 1H, H_d), 4.48-4.43 (m, 2H, H_p), 4.17 (s, 2H, H_s), 4.14-4.09, (m, 2H, H_g), 3.86-3.76 (m, 4H, H_o, H_h), 3.75-3.59 (m, 12H, H_i, H_j, H_k, H_l, H_m, H_n), 1.12 (app s, 21H, H_a, H_b).

^{13}C NMR (126 MHz, $CDCl_3$) δ: 165.9, 164.7, 158.4, 140.9, 131.0, 129.3, 126.4, 124.8, 124.5, 119.1, 117.7, 115.4, 106.9, 90.4, 70.8, 70.7, 70.7, 70.6, 70.6, 69.7, 69.2, 67.5, 64.1, 53.0, 18.7, 11.3.

HR-ESI-MS (+ve) m/z = 697.3598 $[M+H]^+$ (calc. 697.3627 m/z for $C_{36}H_{53}N_4O_8Si$);

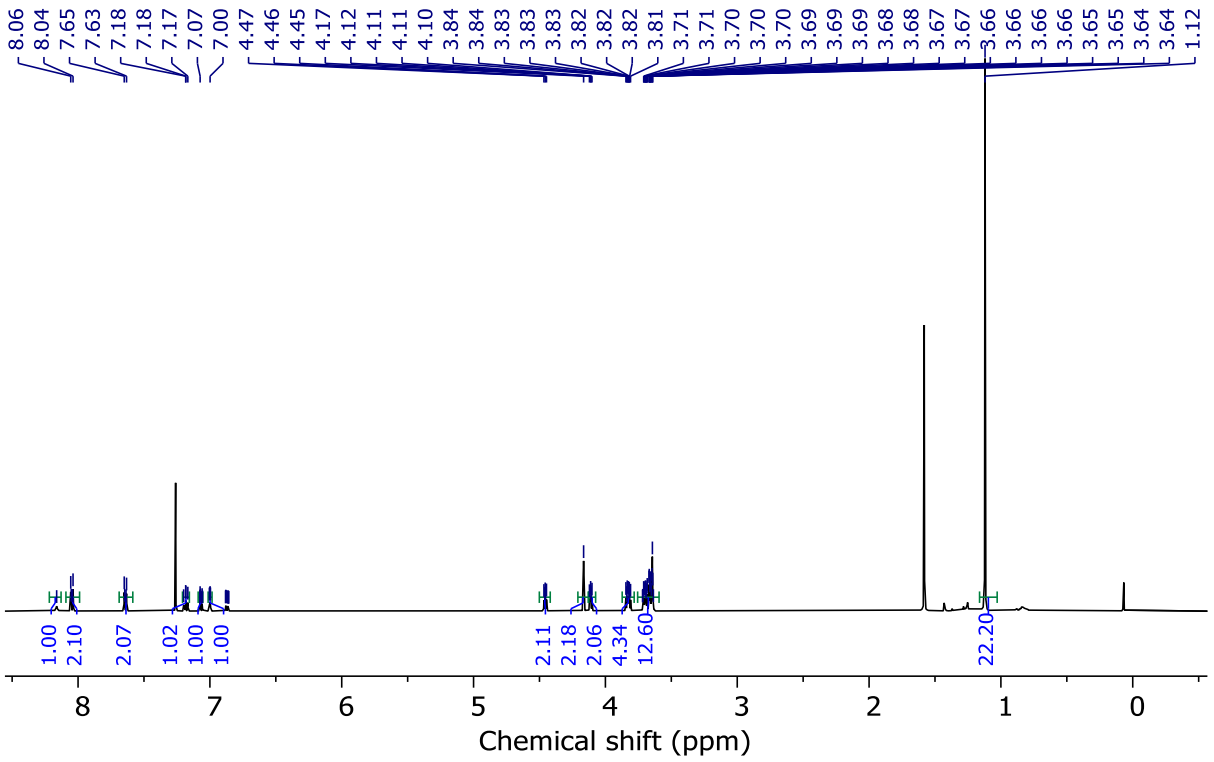

Figure 3.177 - ^{1}H NMR ($CDCl_3$, 500 MHz) of **S24**.

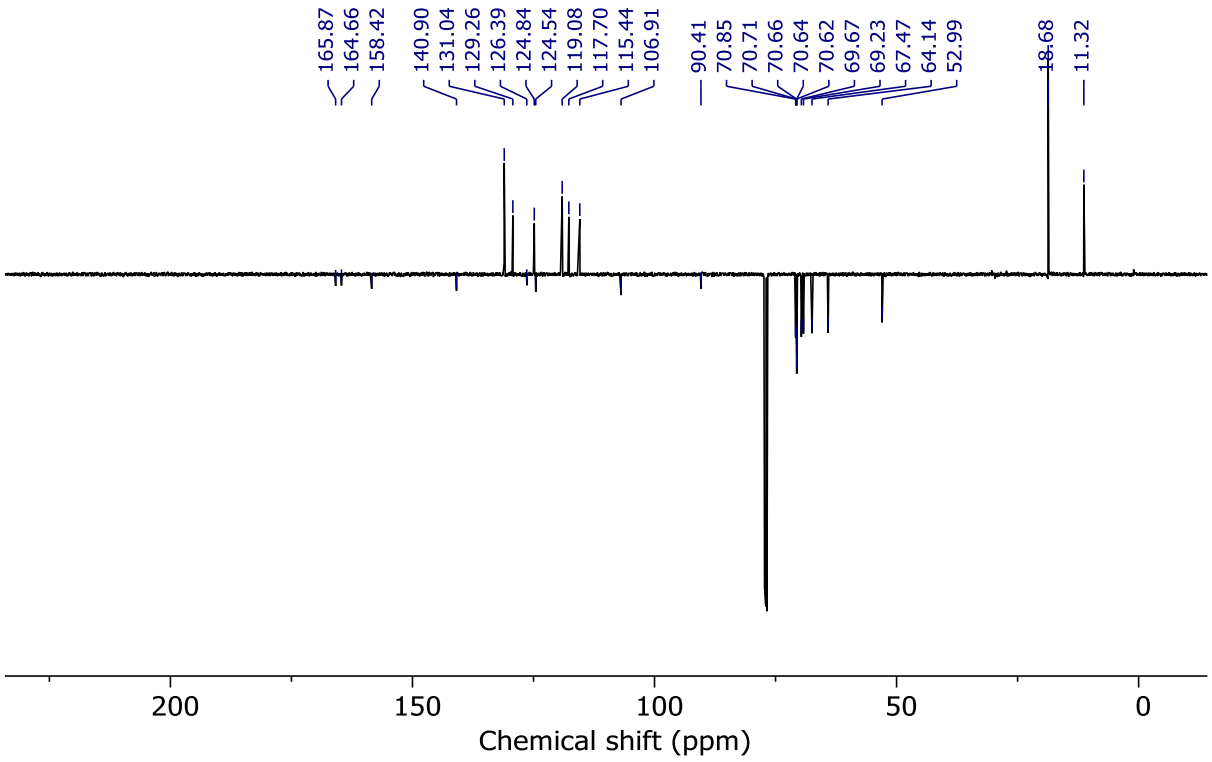

Figure 3.178 - JMOD NMR ($CDCl_3$, 126 MHz) of **S24**.

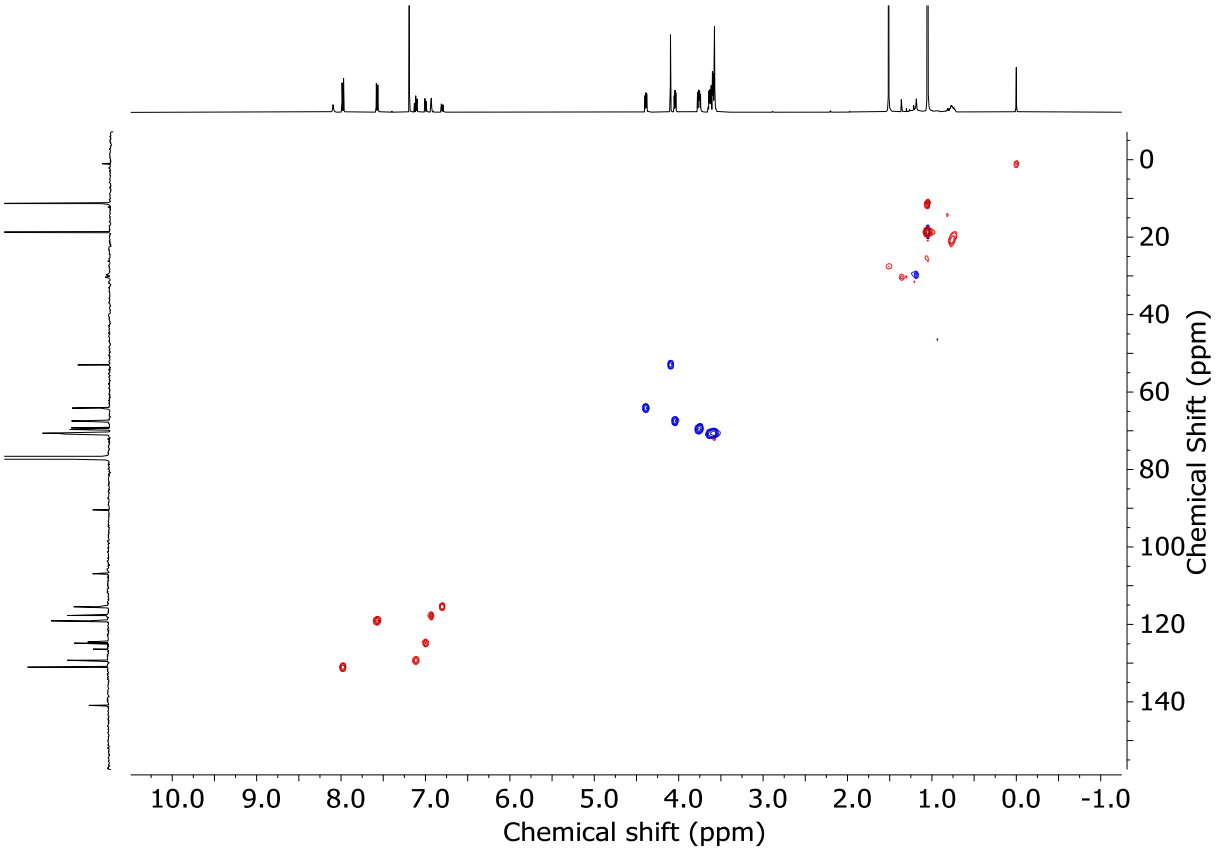

Figure 3.179 - HSQC NMR ($CDCl_3$) of **S24**.

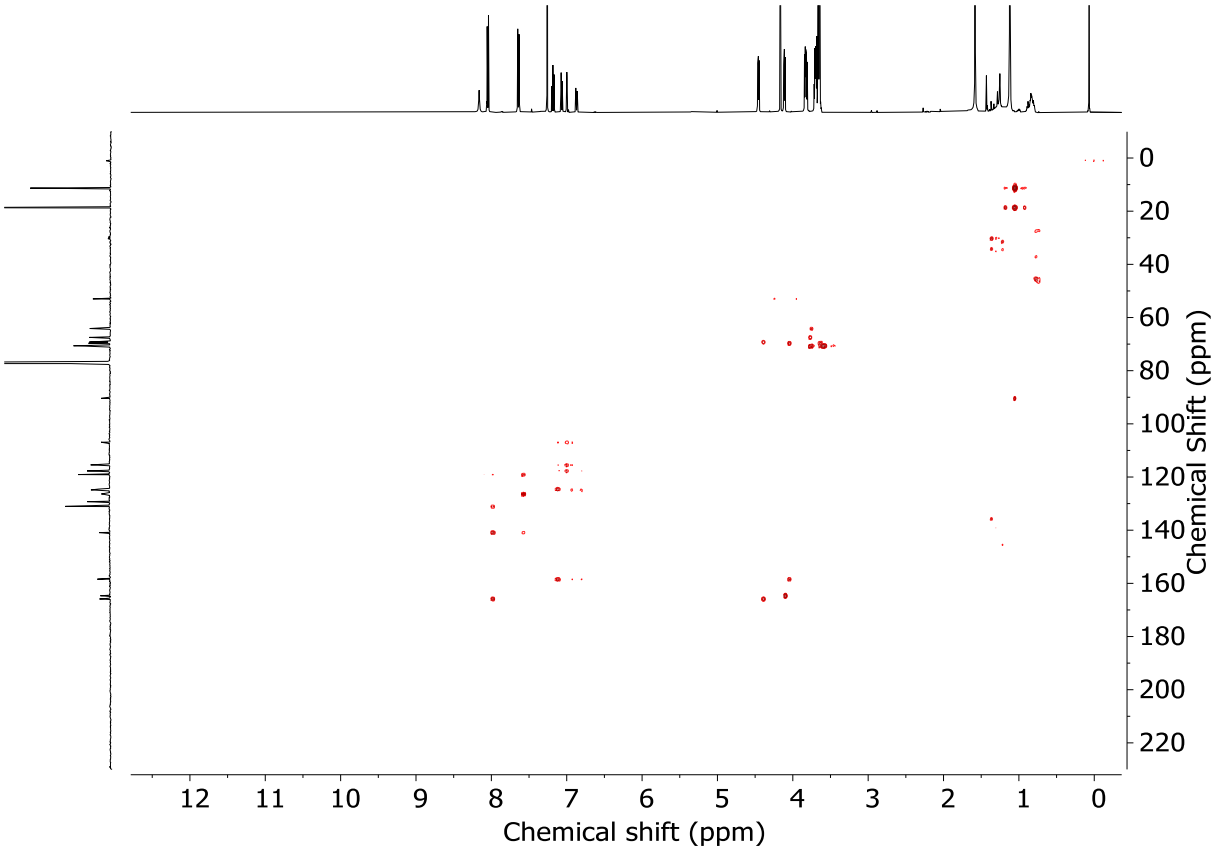

Figure 3.180 - HMBC NMR ($CDCl_3$) of **S24**.

Macrocycle precursor 13

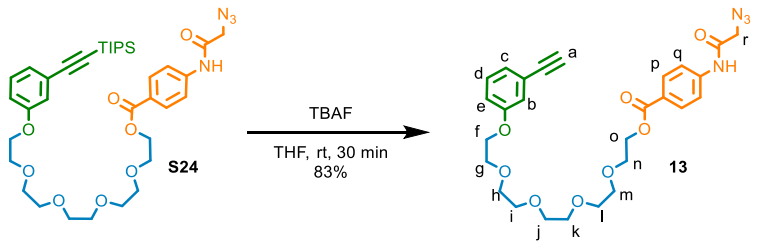

To a solution of **S24** (432 mg, 0.62 mmol) in THF (6 mL) was added a 1M solution of TBAF in THF (0.86 mL, 0.86 mmol). The solution was stirred at rt for 30 min. The reaction mixture was partitioned between H_2O (10 mL) and EtOAc (20 mL), the phases separated, and the organic layer extracted with EtOAc (2 x 20 mL). The collected organic fractions were then washed with brine (20 mL), dried ($MgSO_4$) and the solvent was removed *in vacuo*. Chromatography (*n*-hexane-EtOAC 0 → 60%) gave **14** as a colourless oil (253 mg, 83%).

^{1}H NMR (500 MHz, $CDCl_3$) δ: 8.29 (bs, 1H, NH), 8.01 (dt, J = 9.0, 2.2, 2H, H_p), 7.63 (dt, J = 8.8, 2.0, 2H, H_q), 7.19 (app. t, J = 8.2, 1H, H_d) 7.07 (dt, J = 7.6, 1.2, 1H, H_c) 7.00 (dd, J = 2.6, 1.4, 1H, H_b) 6.89 (ddd, 8.3, 2.7, 0.9, 1H, H_e), 4.47-4.41 (m, 2H, H_o), 4.13 (s, 2H, H_r), 4.11-4.05 (m, 2H, H_f), 3.84-3.78 (m, 4H, H_g, H_n), 3.73-3.60 (m, 12H, H_h, H_i, H_j, H_k, H_l, H_m) 3.05 (s, 1H, H_a).

^{13}C NMR (126 MHz, $CDCl_3$) δ: 165.9, 164.9, 158.5, 141.1, 131.0, 129.4, 126.2, 124.9, 123.1, 119.1, 117.7, 116.0, 83.5, 70.8, 70.7, 70.6, 70.6, 70.6, 70.6, 69.6, 69.2, 67.5, 64.1, 52.9.

HR-ESI-MS (+ve) *m/z* = 563.2148 $[M+Na]^+$ (calc. 563.2112 *m/z* for $C_{27}H_{32}N_4NaO_8$).

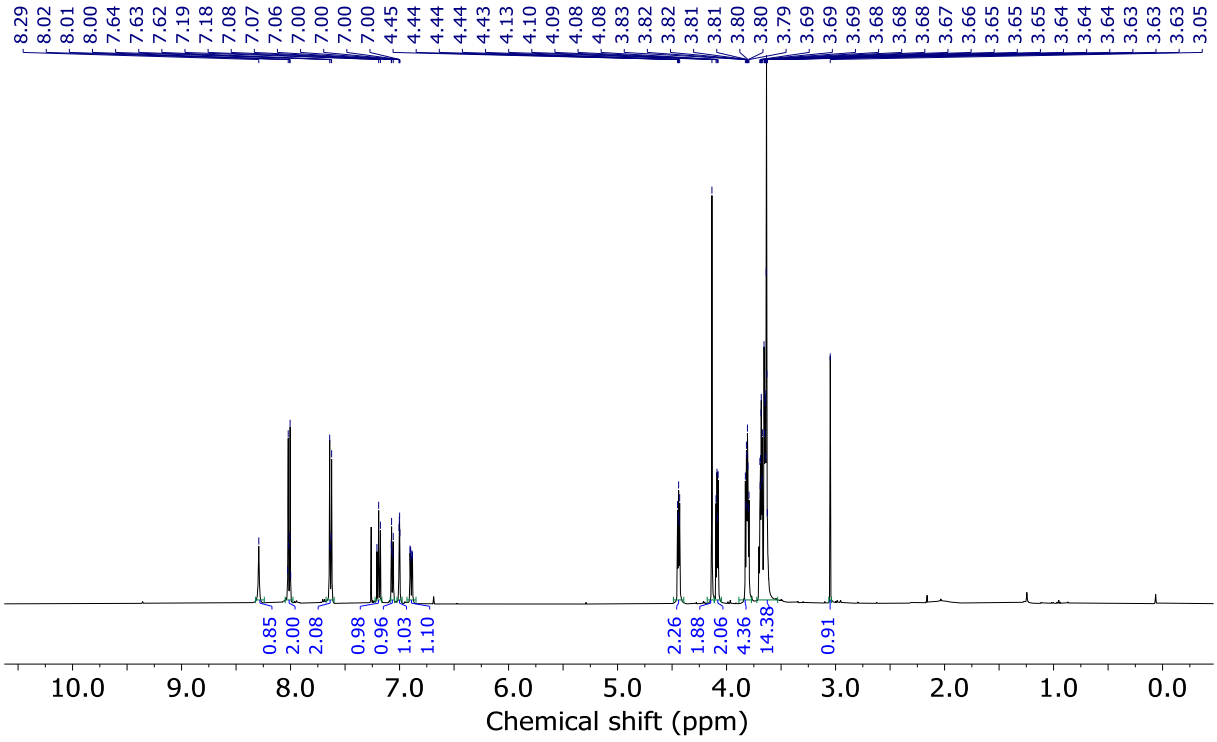

Figure 3.181 - ^{1}H NMR ($CDCl_3$, 500 MHz) of **13**.

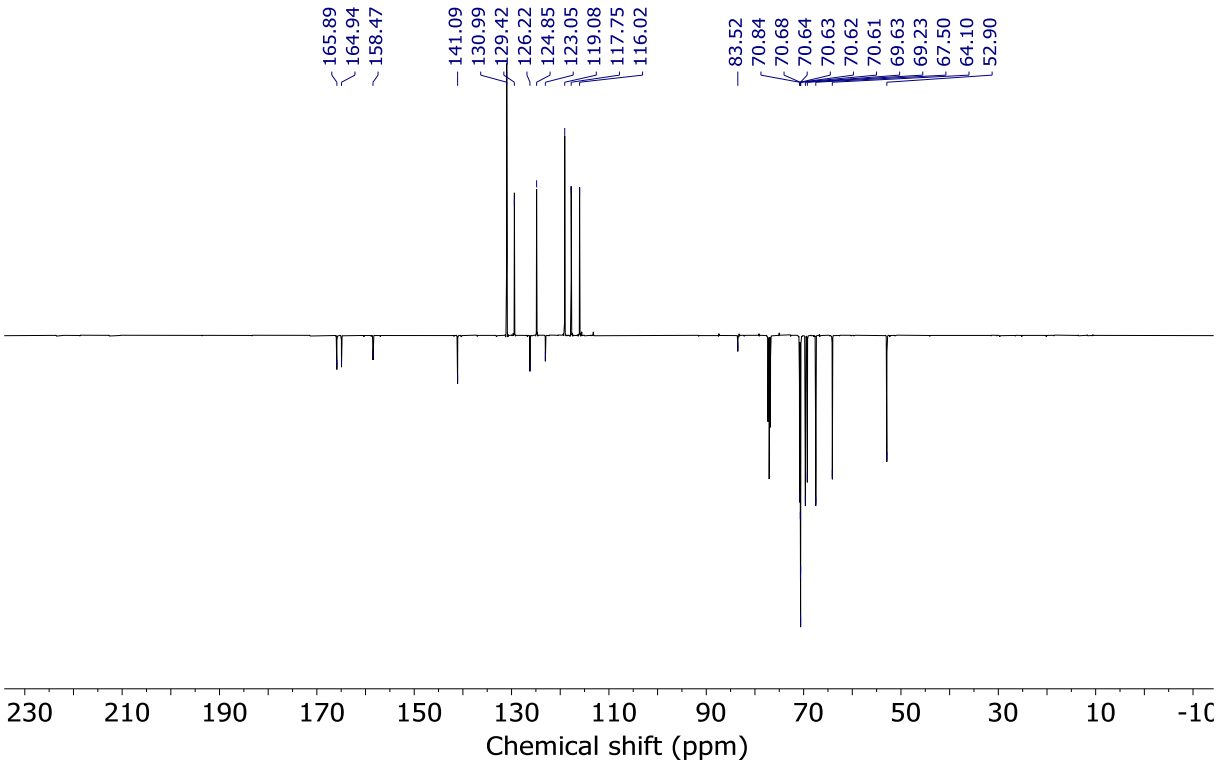

Figure 3.182 - JMOD NMR ($CDCl_3$, 126 MHz) of **13**.

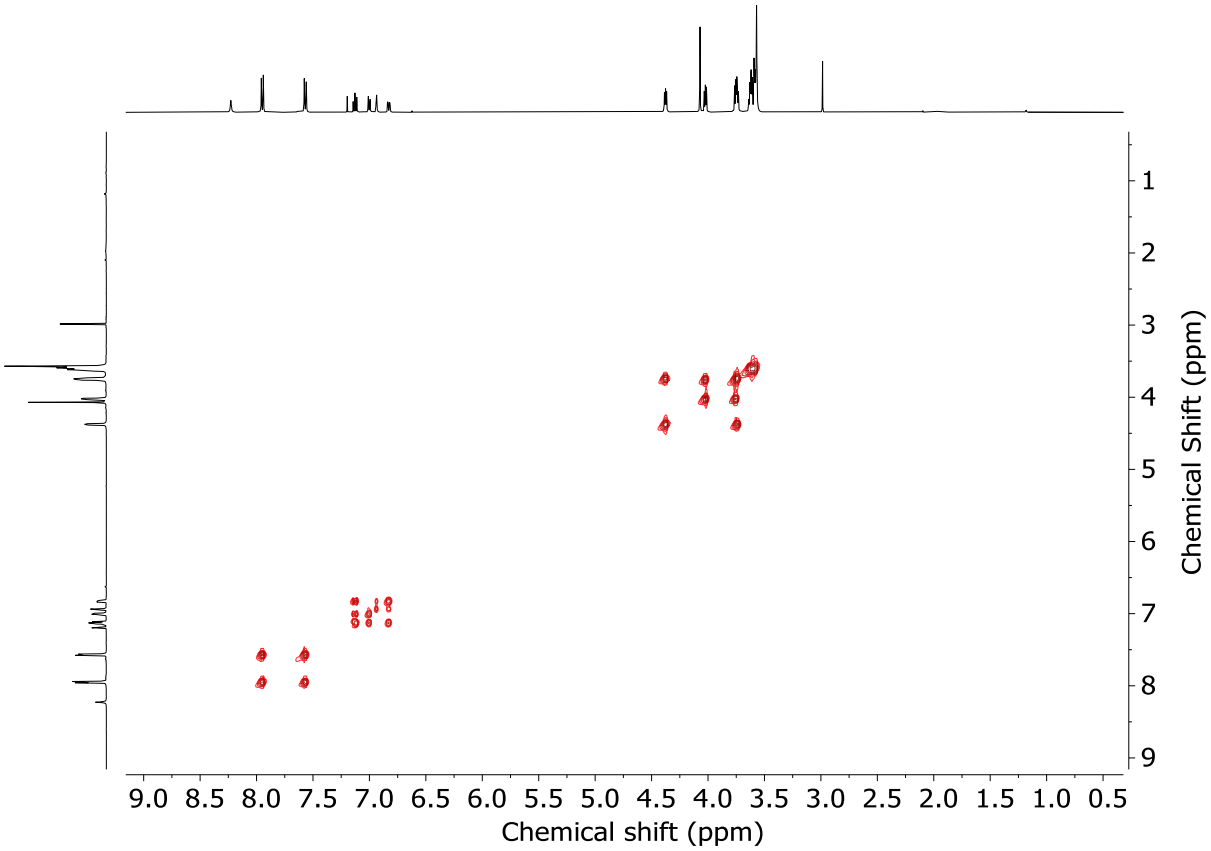

Figure 3.183 - COSY NMR ($CDCl_3$) of **13**.

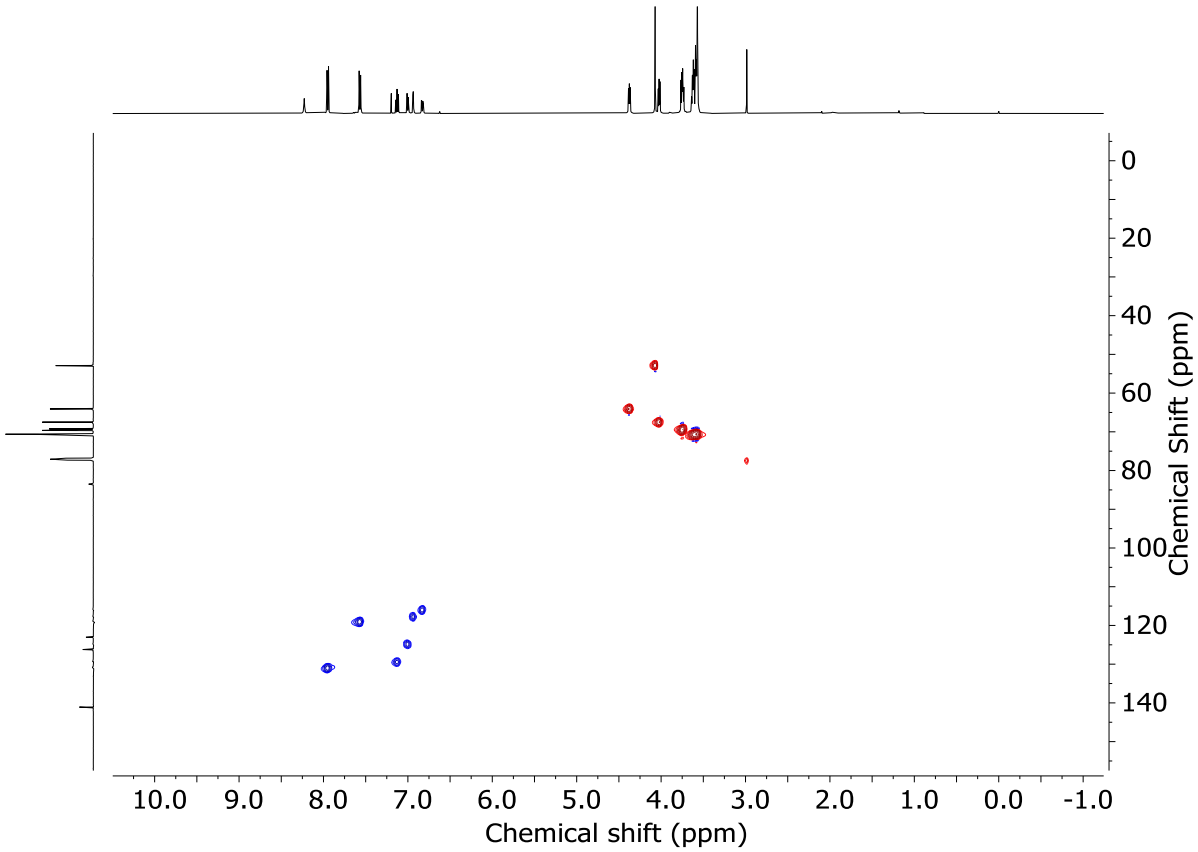

Figure 3.184 - HSQC NMR ($CDCl_3$) of **13**.

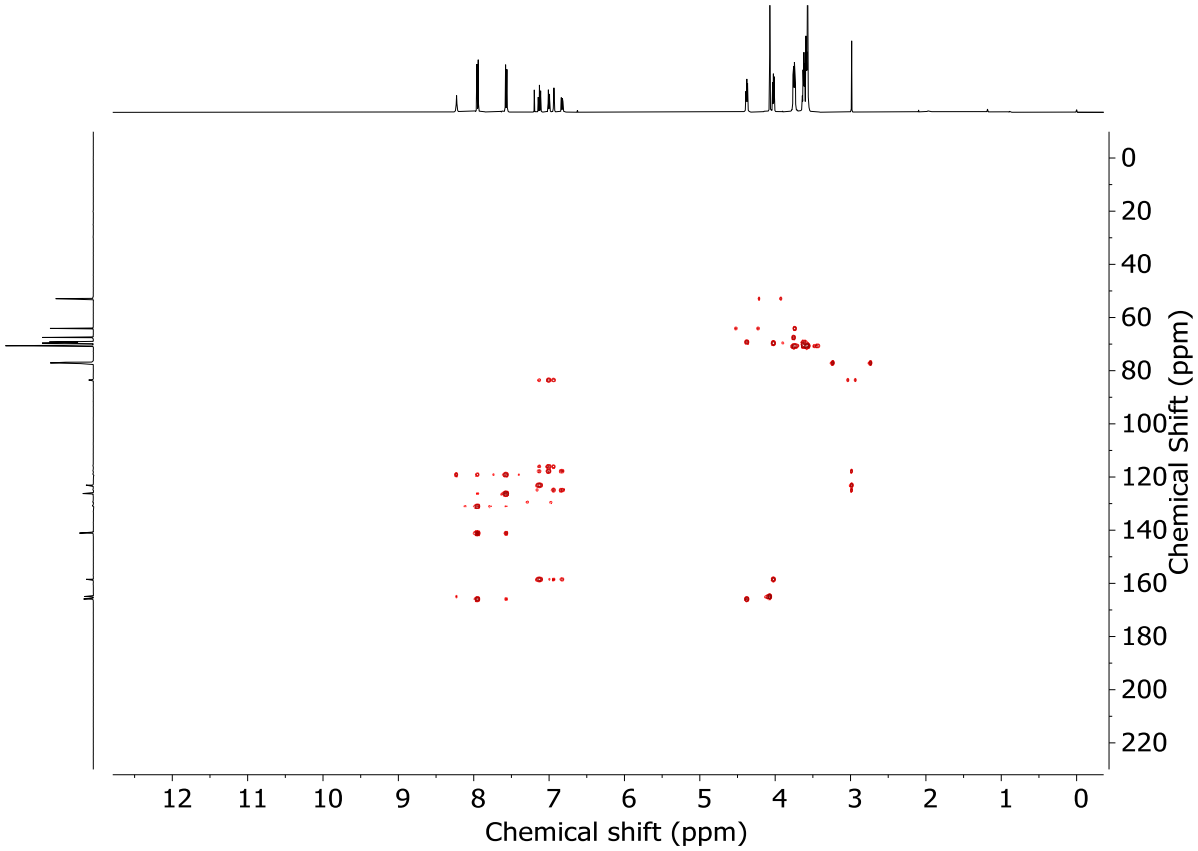

Figure 3.185 - HMBC NMR ($CDCl_3$) of **13**.

Catenanes (E_m)-14 and (Z_m)-14

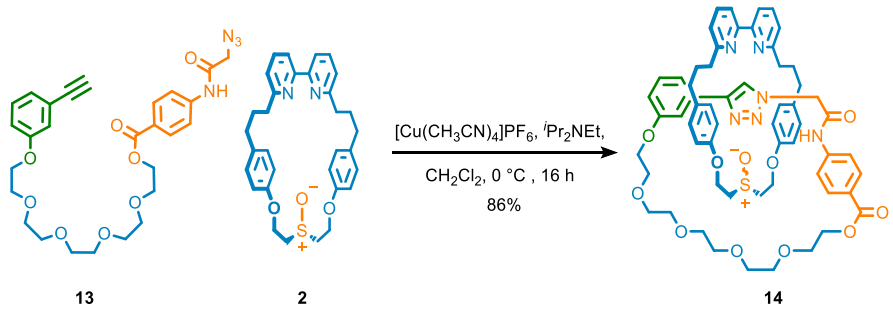

To a solution of **2** (19.0 mg, 36 µmol), $[Cu(CH_3CN)_4]PF_6$ (13.1 mg, 35 µmol) and $^iPr_2NEt$ (25 µL, 140 µmol) in CH_2Cl_2 (3.6 mL) at 0 °C was added a solution of **13** (39.2 mg, 73 µmol) in CH_2Cl_2 over 16 hours. Once addition had finished, to the reaction mixture at 0 °C was added TFA (500 µL) and stirred for 1 hour until complete decolouration. The crude mixture was diluted with CH_2Cl_2 (5 mL) and carefully poured onto EDTA-NH_3 (5 mL), with separation of aqueous and organic phases. The combined aqueous phase was then extracted with CH_2Cl_2 (3 x 5 mL) and the combined organic extracts were washed with brine (10 mL), dried ($MgSO_4$) and concentrated *in vacuo* to give a sample containing **14** as a mixture of diastereomers (95 : 5 *dr*, Figure 3.186). Chromatography

([1:1 CH_2Cl_2-PhMe]-acetone 0→100% with 2% EtOH) gave catenanes-**14** as a white foam (32.8 mg, 86%) as a mixture of diastereoisomers (4.9 : 1 *dr*, Figure 3.187).

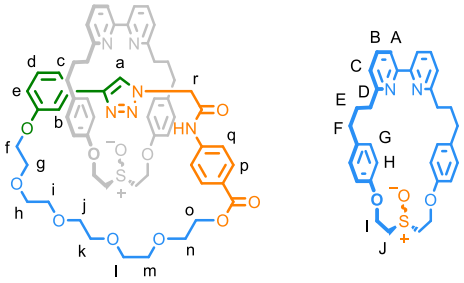

Major diastereoisomer

^{1}H NMR (500 MHz, $CDCl_3$) δ: 11.38 (s, 1H, NH), 7.90 (dt, J = 8.7, 1.9, 2H, H_p), 7.78 (t, J = 7.7, 2H, H_B), 7.67 (dt, J = 7.8, 1.3, 1H, H_b), 7.64-7.58 (m, 2H, H_A), 7.38 (app.t, J = 7.8, 1H, H_d), 7.35-7.22 (m, 5H, H_a, H_C, H_q superimposed with $CDCl_3$), 6.98-6.94 (m, 1H, H_e), 6.88-6.82 (m, 1H, H_d), 6.77-6.69 (m, 8H, H_G, H_H), 4.70-4.55 (m, 4H, H_I, H_r), 4.54-4.48 (m, 2H, H_o), 4.44 (dt, J = 12.9, 4.2, 2H, $H_{I'}$), 4.14-4.09 (m, 2H, H_f), 3.86-3.74 (m, 4H, H_g, H_n), 3.72-3.57 (m, 2H, H_m), 3.55 (t, J = 5.5, 2H, H_h), 3.51-3.35 (m, 4H, H_i, H_l), 3.35-3.25 (m, 4H, H_j, H_k), 3.24-3.12 (m, 2H, H_J), 2.70-2.57 (m, 4H, H_F, $H_{J'}$), 2.56-2.28 (m, 6H, $H_{F'}$, H_D), 1.88-1.72 (m, 4H, H_E)

^{13}C NMR (126 MHz, $CDCl_3$) δ: 166.4, 163.1, 162.6, 158.9, 156.2, 155.3, 147.4, 142.2, 138.0, 133.1, 131.7, 130.4, 130.2, 129.3, 125.4, 122.6, 120.9, 120.4, 119.7, 117.9, 115.7, 113.6, 112.8, 70.5, 70.5, 70.2, 70.2, 69.7, 69.7, 69.6, 67.3, 64.4, 60.2, 52.9, 52.1, 36.5, 34.7, 31.2.

LR-ESI-MS m/z = 1016.5 $[M+H]^+$ for isotopic pattern see Figure 3.193

Minor diastereoisomer

^{1}H NMR (500 MHz, $CDCl_3$) 11.36 (s, 1H, NH), 7.84 (dt, J = 8.8, 2.0, 2H, H_p), 7.73 (t, J = 7.8, 2H, H_B), 7.64-7.58 (m, 1H, H_b), 7.55-7.51 (m, 3H, H_A, H_a), 7.35-7.22 (m, 3H, H_c, H_q, superimposed with $CDCl_3$), 7.18 (d, J =7.7, 2H, H_C), 6.98-6.94 (m, 1H, H_e), 6.88-6.82 (m, 1H, H_d), 6.77-6.69 (m, 8H, H_G, H_H), 4.70-4.55 (m, 2H, H_I), 4.54-4.47 (m, 6H, $H_{I'}$, H_o, H_r), 4.03 (t, J = 5.2, 2H, H_f), 3.86-3.74 (m, 4H, H_g, H_n), 3.72-3.57 (m, 8H, H_h, H_i, H_l, H_m), 3.51-3.35 (m, 4H, H_J, H_j or H_k), 3.35-3.25 (m, 2H, H_j or H_k), 3.24-3.12 (m, 2H, $H_{J'}$), 2.70-2.57 (m, 4H, H_F), 2.56-2.28 (m, 8H, H_F, H_D), 1.88-1.72 (m, 4H, H_E)

^{13}C NMR (126 MHz, $CDCl_3$) 166.2, 162.9, 162.7, 158.8, 156.2, 155.6, 147.5, 142.5, 137.9, 133.0, 131.8, 130.1, 129.9, 129.5, 125.3, 122.6, 121.3, 120.5, 119.9, 118.1, 114.9, 114.2, 112.7, 50.5, 70.5, 70.3, 70.2, 69.6, 67.0, 64.4, 59.5, 52.8, 50.2, 36.5, 34.8, 31.3.

HR-ESI-MS (+ve) m/z = 1067.5 $[M+H]^+$ for isotopic pattern see Figure 3.193

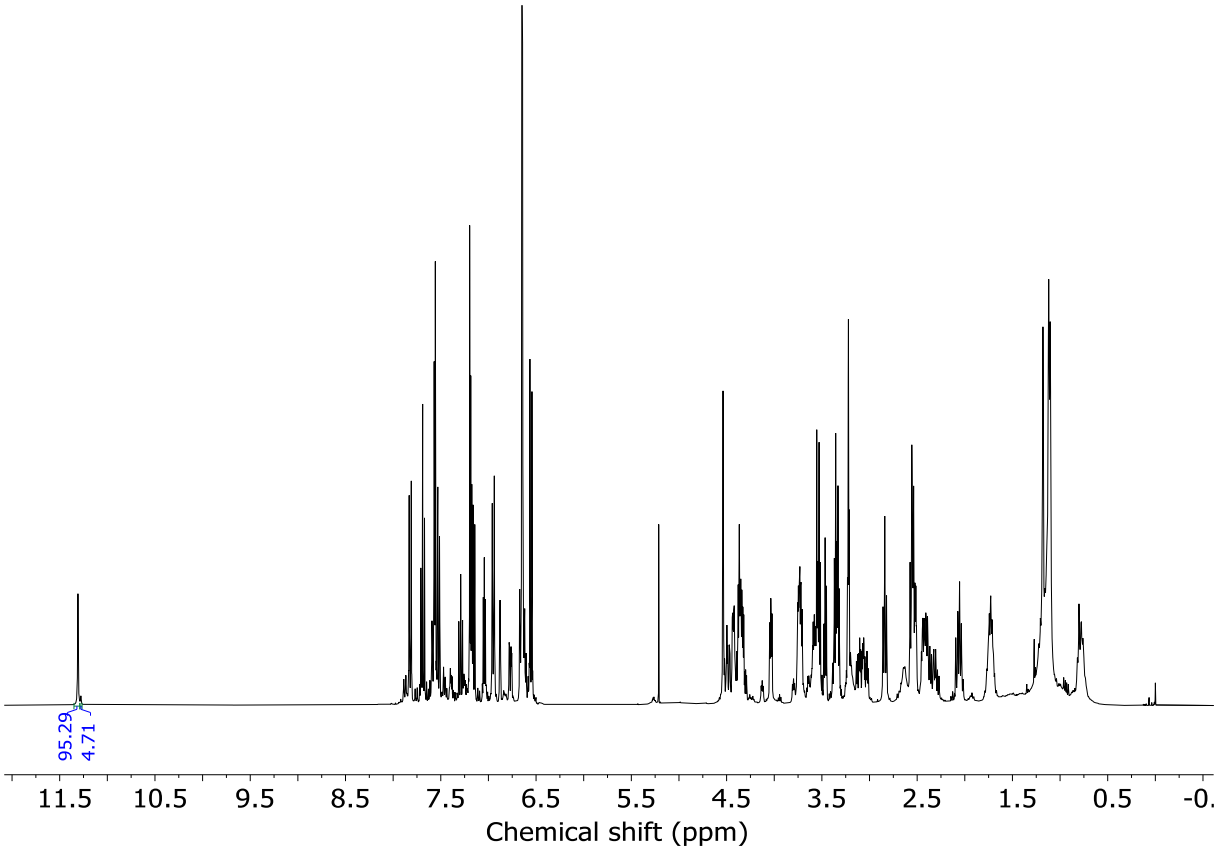

Figure 3.186 - ^{1}H NMR ($CDCl_3$, 500 MHz) of catenanes **14** prior to chromatography (95 : 5 *dr*).

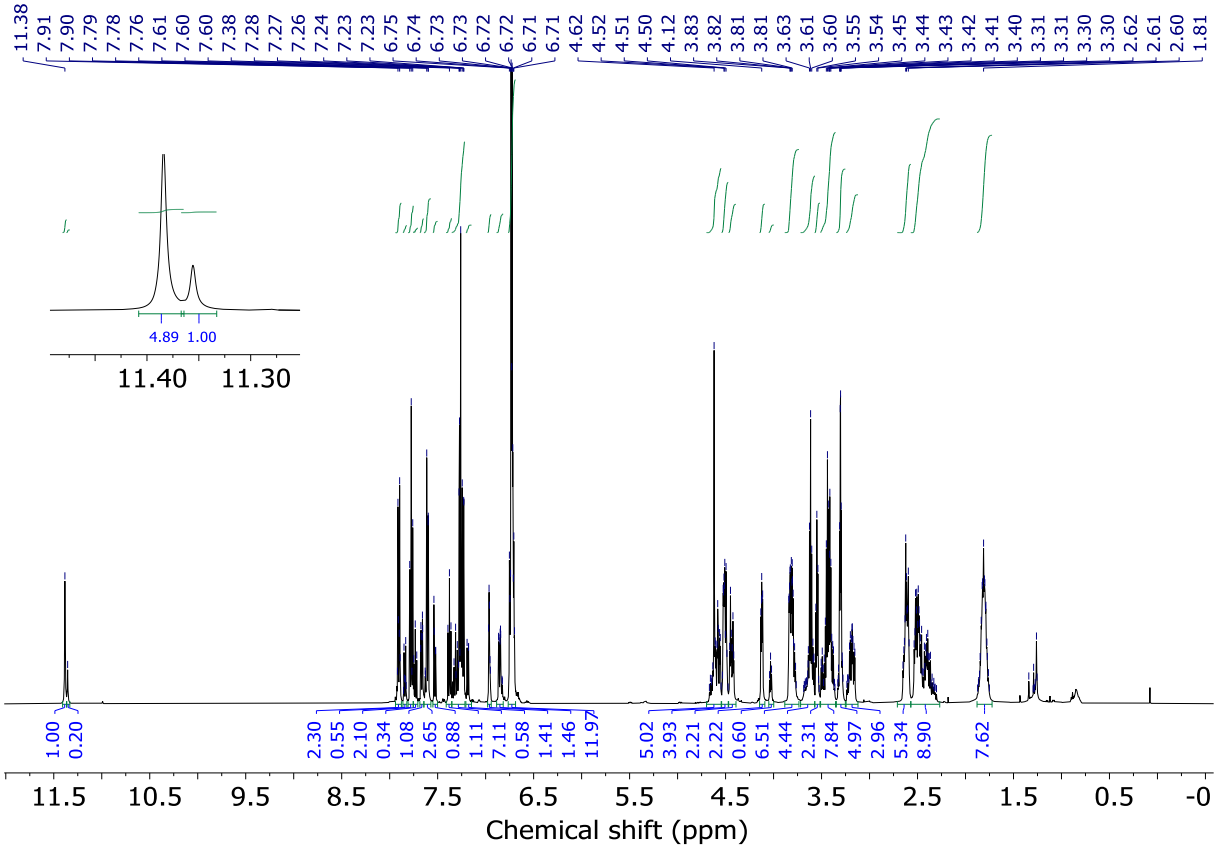

Figure 3.187 - ^{1}H NMR ($CDCl_3$, 500 MHz) of (E_m)-**14** and (Z_m)-**14** (4.9 : 1 *dr*).

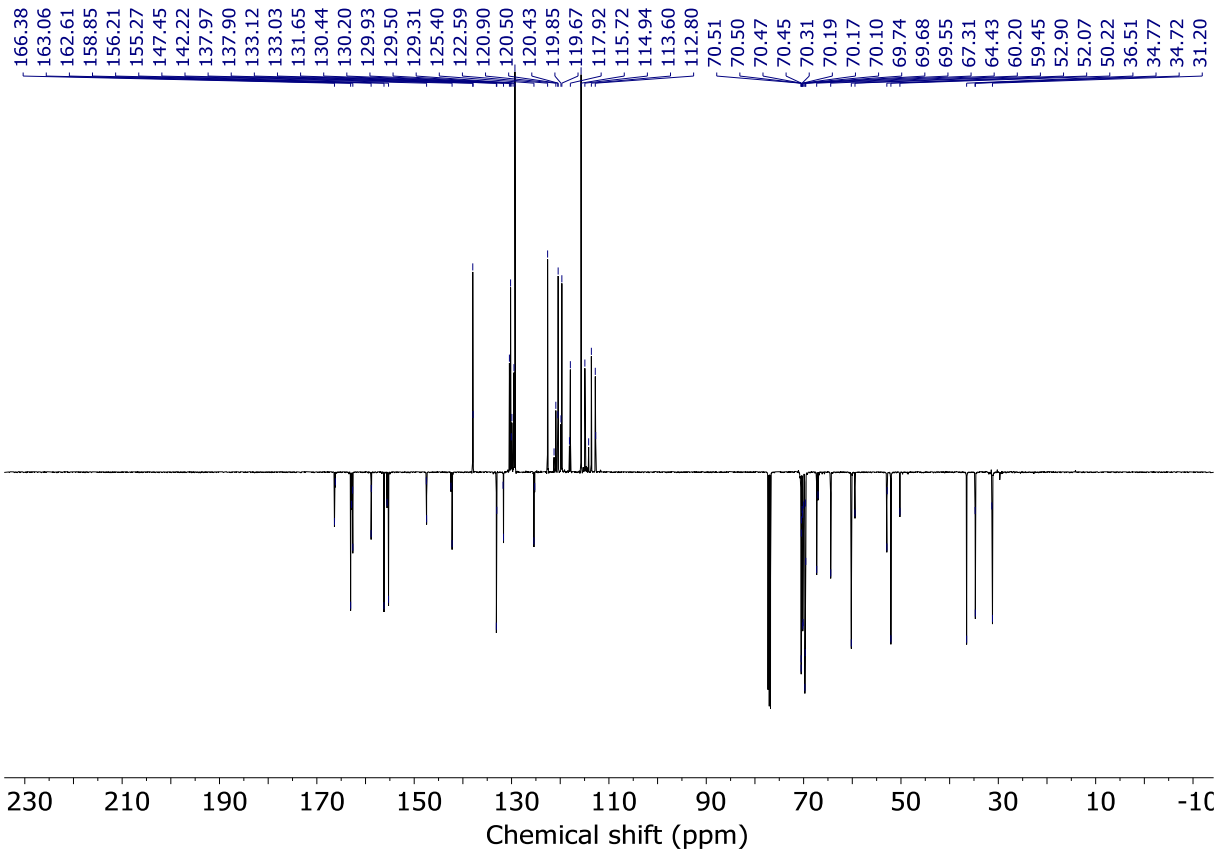

Figure 3.188 - JMOD NMR ($CDCl_3$, 126 MHz) of (E_m)-**14** and (Z_m)-**14** (4.9 : 1 *dr*).

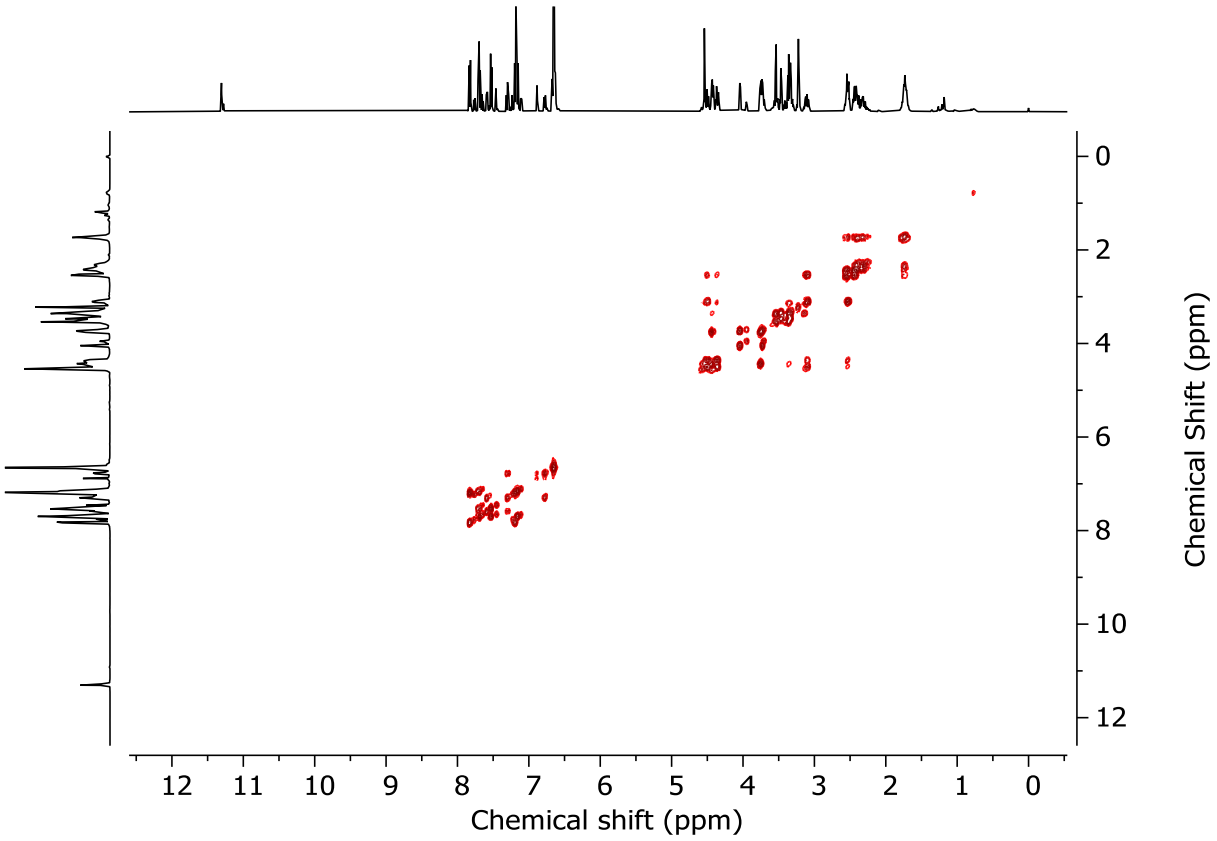

Figure 3.189 - COSY NMR ($CDCl_3$) of (E_m)-**14** and (Z_m)-**14** (4.9 : 1 *dr*).

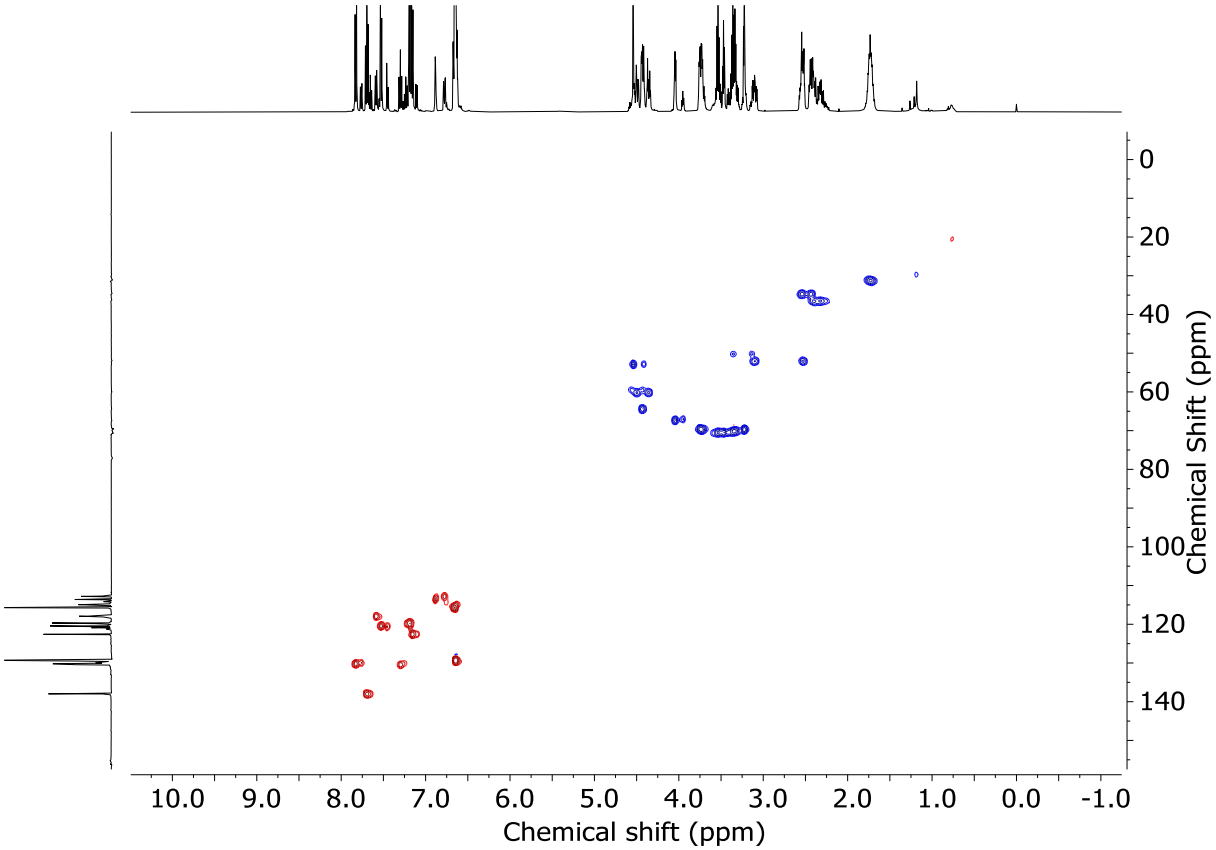

Figure 3.190 - HSQC NMR ($CDCl_3$) of (E_m)-**14** and (Z_m)-**14** (4.9 : 1 *dr*).

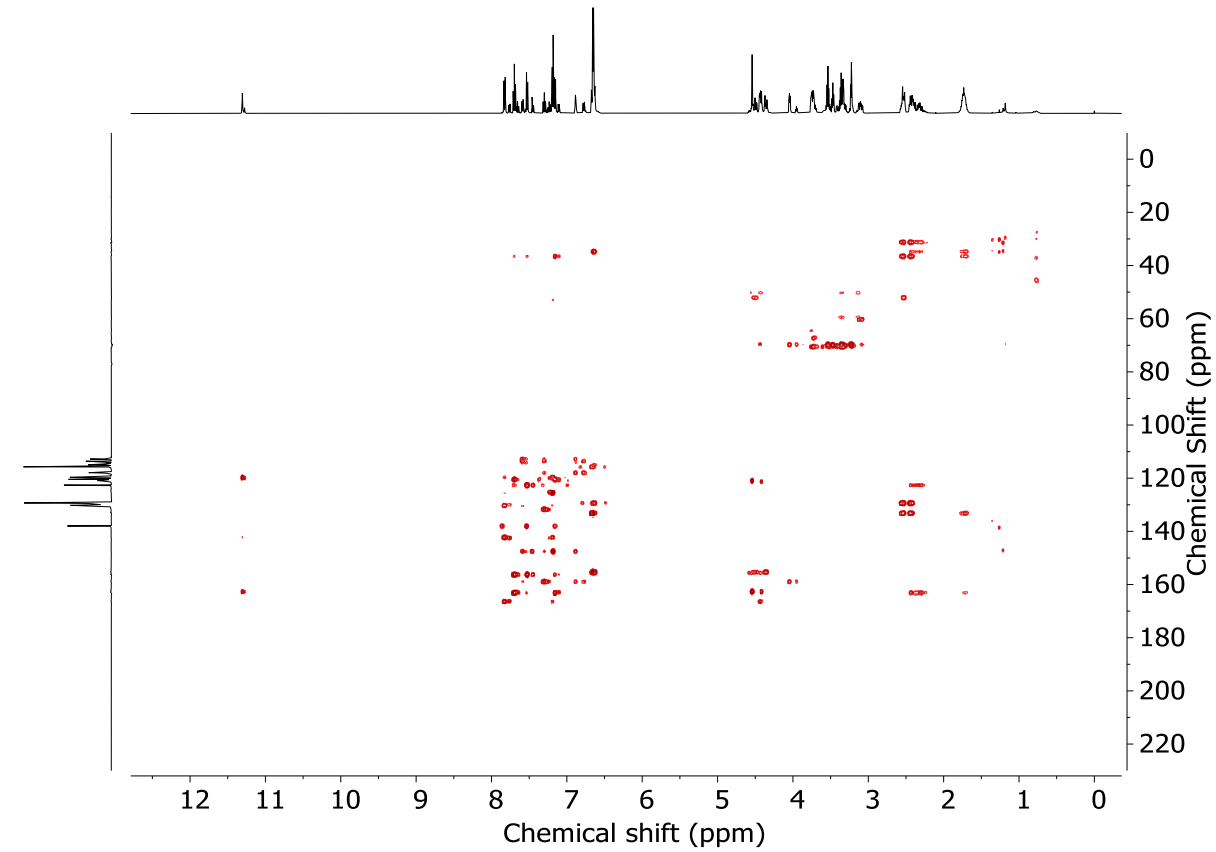

Figure 3.191 - HMBC NMR ($CDCl_3$) of (E_m)-**14** and (Z_m)-**14** (4.9 : 1 *dr*).

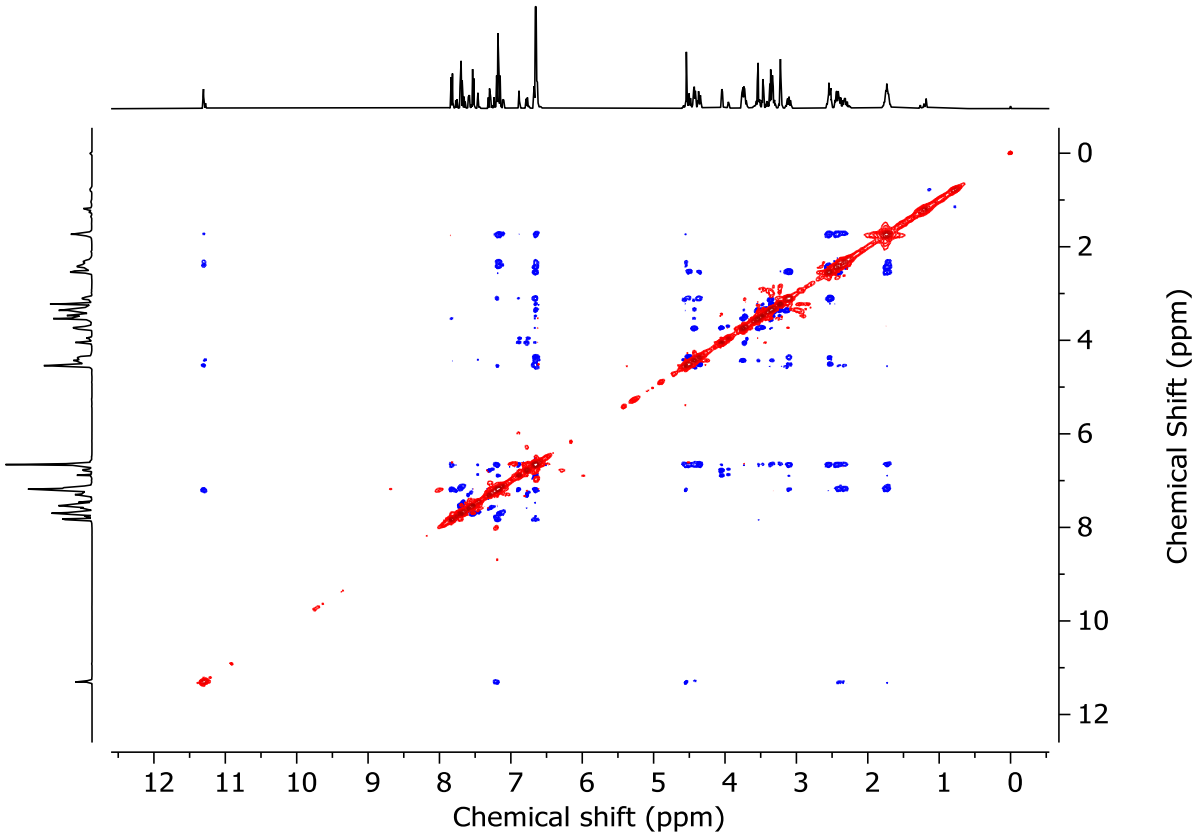

Figure 3.192 - NOESY NMR ($CDCl_3$) of (E_m)-**14** and (Z_m)-**14** (4.9 : 1 *dr*).

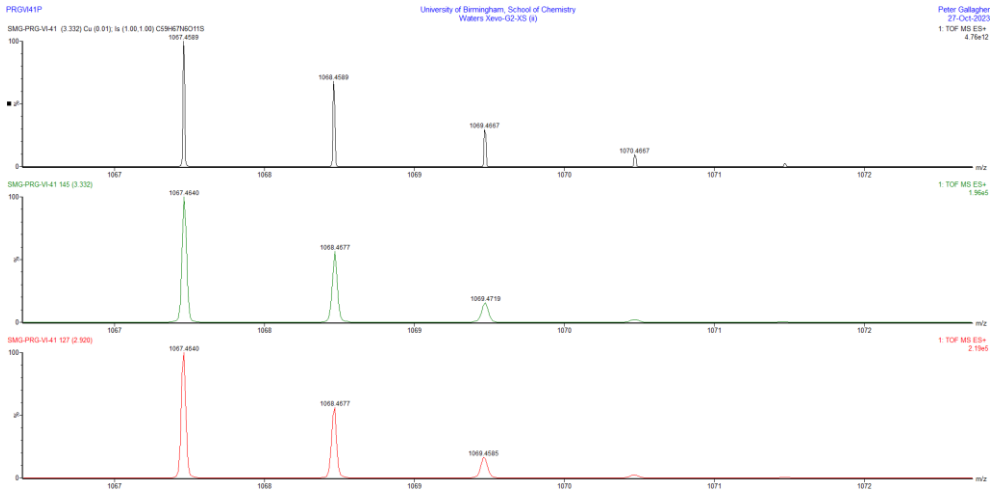

Figure 3.193 - Calculated (top) and observed (middle, bottom) isotopic patterns for (E_m)-**14** and (Z_m)-**14.**

Rotaxanes 15 and 16, and their precursors

Amine rotaxane (R_{ma})-15 from (*R*)-1a

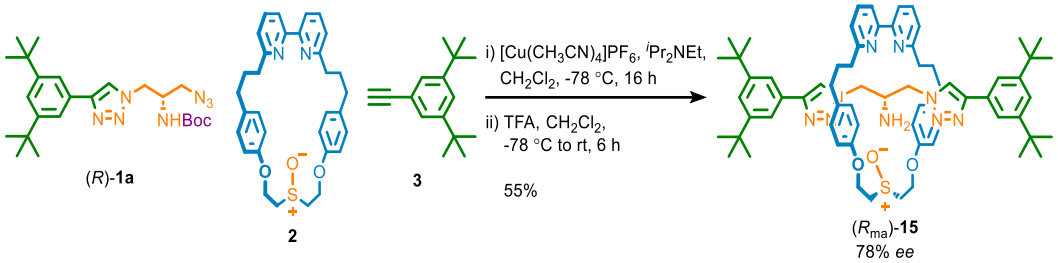

In a CEM vial were added **3** (2.8 mg, 13.1 µmol), (*R*)-**1a** (5.5 mg, 12.1 µmol), **2** (5.8 mg, 11.0 µmol) and $[Cu(CH_3CN)_4PF_6]$ (3.9 mg, 10.5 µmol). The vial was sealed and purged with N_2, then CH_2Cl_2 was added (250 µL). The solution was cooled to -78 °C, then $^{i}Pr_2NEt$ (4 µL, 23 µmol) was added. The solution was stirred at -78 °C for 16 h. TFA (170 µL, 1 mmol) was added and the resulting mixture was allowed to warm to rt and stirred vigorously for 6h. The crude mixture was diluted with CH_2Cl_2 (5 mL) and carefully poured onto EDTA-NH_3 (5 mL), with separation of aqueous and organic phases. The combined aqueous phase was then extracted with CH_2Cl_2 (3 x 5 mL) and the combined organic extracts were washed with brine (10 mL), dried ($MgSO_4$) and concentrated *in vacuo*. Chromatography (CH_2Cl_2-CH_3CN 0→20% then [(3:1) CH_2Cl_2-CH_3CN]-MeOH 0→10%) gave (R_{ma})-**15** as a white foam (6.7 mg, 55%, 78% *ee* see Figure 3.195).

All spectroscopic data is consistent with those reported in literature[11] and previously in Chapter 2 section 3.5.1.

Amine rotaxane (S_{ma})-**15** (29.9 mg, 68%, 77% *ee*) was synthesised using an identical procedure starting from (*S*)-**1a** (16.9 mg, 44.1 µmol). Analytical data were identical to (R_{ma})-**15** with the exception CSP-HPLC (Figure 3.195).

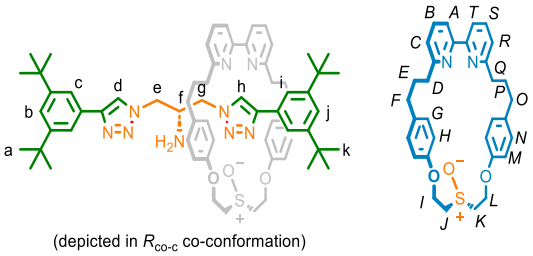

^{1}H NMR (500 MHz, $CDCl_3$) δ: 8.58 (s, 1H, H_h), 8.06 (s, 1H, H_d), 7.66 (d, *J* = 1.8 Hz, 2H, H_C), 7.65-7.58 (m, 3H, H_i, H_B), 7.46 (d, *J* = 2.9 Hz, 1H, H_A), 7.44 (d, *J* = 2.9 Hz, 1H, H_A), 7.39 (t, *J* = 1.8 Hz, 1H, H_b), 7.35 (t, *J* = 1.9 Hz, 1H, H_j), 7.12 (d, *J* = 8.0 Hz, 1H, H_C), 7.09 (d, *J* = 7.7 Hz, 1H, H_C), 6.73-6.61 (m, 6H, H_G, H_H), 6.59-6.55 (m, 2H, H_H), 4.73-4.60 (m, 2H, H_I), 4.60-4.45 (m, 2H, H_I), 3.94-3.74 (m, 3H, H_J, H_e), 3.67-3.52 (m, 2H, H_e, H_g),

3.21 (dd, *J* = 13.8, 7.9 Hz, 1H, H_g), 3.17-3.06 (m, 2H, H_J), 2.70-2.62 (m, 1H, H_f), 2.57-2.38 (m, 9H, H_F, H_D), 1.81-1.66 (m, 4H, H_E), (s, 18H, H_a), 1.29 (s, 18H, H_k);

^{13}C NMR (126 MHz, $CDCl_3$) δ: 162.7, 162.7, 157.9, 157.8, 155.8, 155.7, 151.3, 148.3, 148.0, 137.3, 137.2, 134.0, 133.9, 130.4, 130.2, 129.5, 129.4, 122.6, 122.2, 122.1, 122.1, 122.0, 121.3, 120.6, 120.5, 120.3, 120.0, 115.0, 114.9, 61.0, 60.9, 53.7, 53.1, 53.0, 51.5, 37.3, 37.2, 35.1, 35.0, 34.7, 34.7, 31.9, 31.8, 31.7, 31.6.

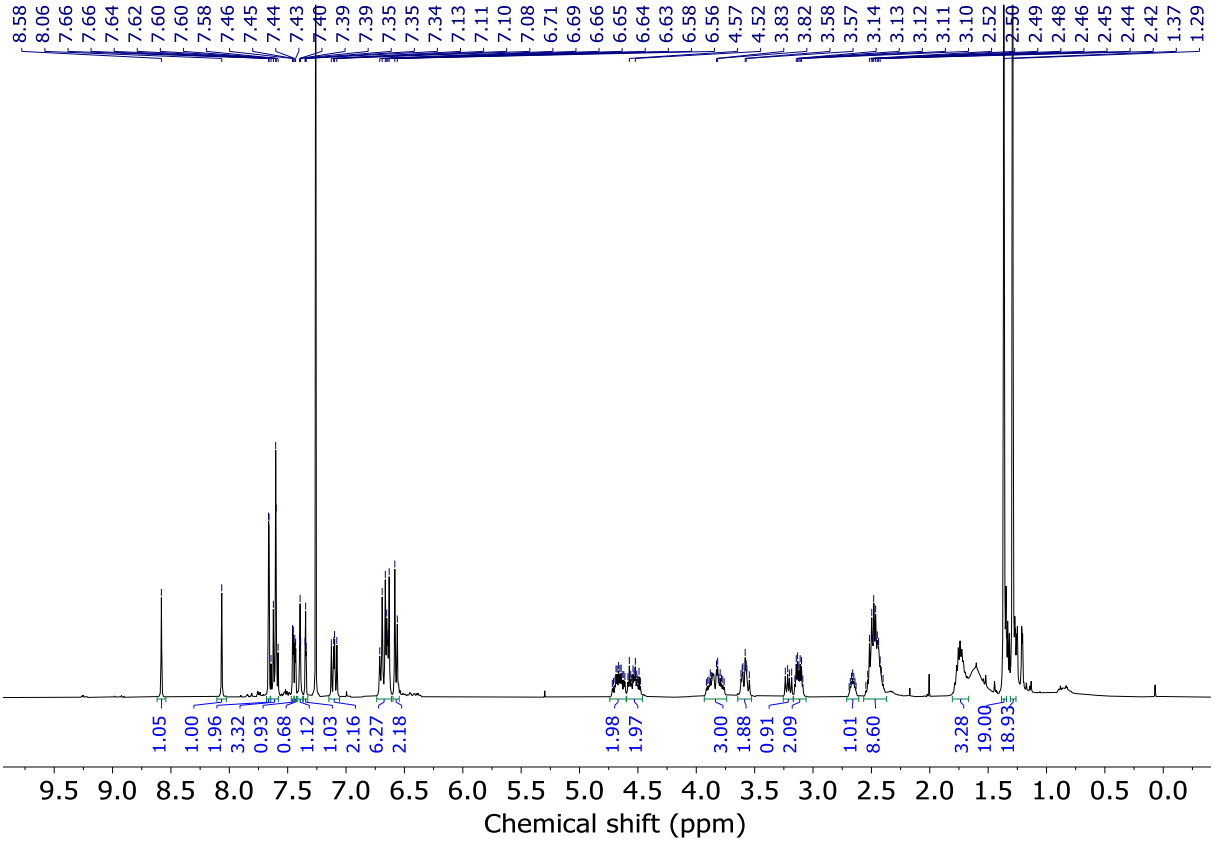

Figure 3.194 - ^{1}H NMR ($CDCl_3$, 400 MHz) of (R_{ma})-**15**.

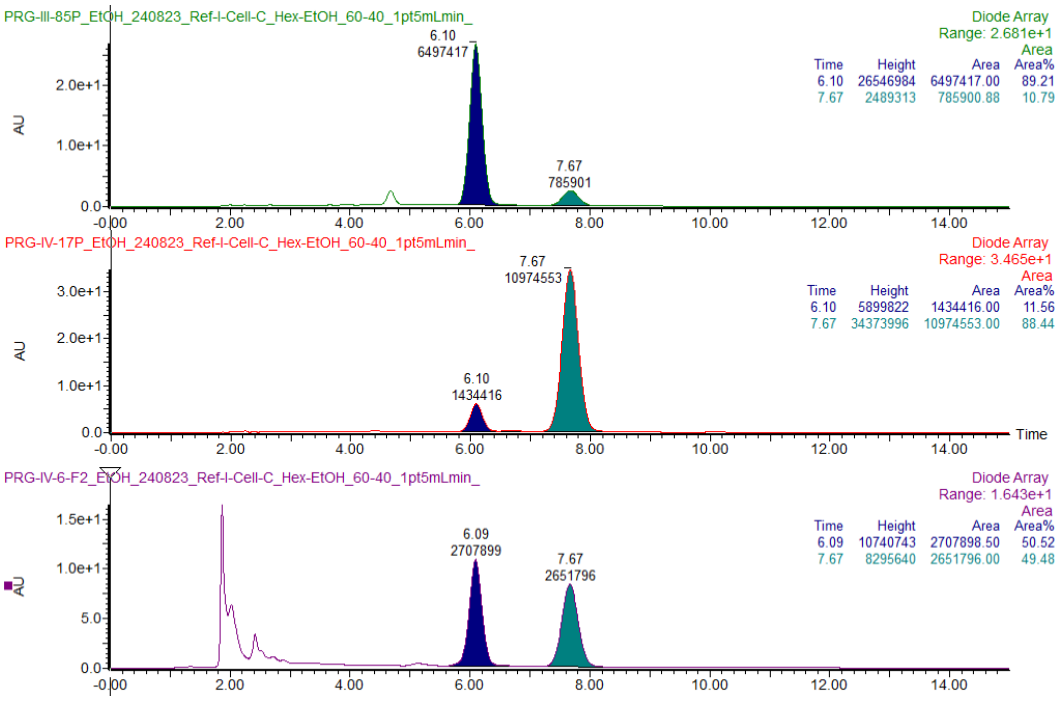

Figure 3.195 - CSP-HPLC of **15** from **1a** (loaded in EtOH). Regis Reflect I-Cellulose C, *n*-hexane-EtOH 60 : 40, flowrate 1.5 mLmin^{-1}. (top) (R_{ma})-**15** from (R)-**1a**; (R_{ma})-**15** (6.10 min, 6497417, 89.21%), (S_{ma})-**15** (7.67 min, 785901, 10.79%). (middle) (S_{ma})-**15** from (*S*)-**1a**; (R_{ma})-**15** (6.10 min, 1434416, 11.56%), (S_{ma})-**15** (7.67 min, 10974553, 88.44%). (bottom) *rac*-**15**; (R_{ma})-**15** (6.09 min, 2707899, 50.52%), (S_{ma})-**15** (7.67 min, 2651796, 49.48%).

Amine rotaxane (R_{ma})-15 from (*R*)-1f

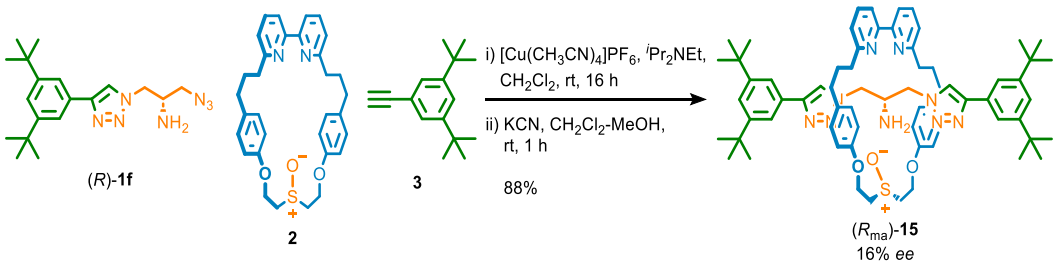

In a CEM vial were added **3** (4.7 mg, 21.9 µmol), (*R*)-**1f** (7.8 mg, 21.9 µmol), **2** (10.5 mg, 20.0 µmol) and [Cu(CH_3CN)$_4$$PF_6$] (7.1 mg, 19.3 µmol). The vial was sealed and purged with N_2, then CH_2Cl_2 was added (1.0 mL), followed by $^{i}Pr_2NEt$ (7 µL, 40.1 µmol). The solution was stirred at rt for 16 h. MeOH (2 mL mL) and KCN as a solid (13 mg, 0.20 mmol) were added and the resulting mixture was stirred vigorously for until colourless. The crude mixture was diluted with CH_2Cl_2 (5 mL) and washed with H_2O (5 mL) then EDTA-NH_3 (5 mL), with separation of aqueous and organic phases. The combined aqueous phase was then extracted with CH_2Cl_2 (3 x 5 mL) and the combined organic extracts were washed with brine (10 mL), dried ($MgSO_4$) and concentrated *in vacuo*. Chromatography (CH_2Cl_2-CH_3CN 0→20% then [(3:1) CH_2Cl_2-CH_3CN]-MeOH 0→10%) gave (R_{ma})-**15** as a white foam (19.3 mg, 88%, 16.10% *ee* see Figure 3.196).

All spectroscopic data are identical to those reported for rotaxane (R_{ma})-**5** reported previously.[11]

Amine rotaxane (S_{ma})-**5** (18.1 mg, 83%, 16.70% *ee*) was synthesised using an identical procedure starting from (*S*)-**1f** (7.7 mg, 21.7 µmol). Analytical data were identical to (R_{ma})-**5** with the exception CSP-HPLC (Figure 3.196).

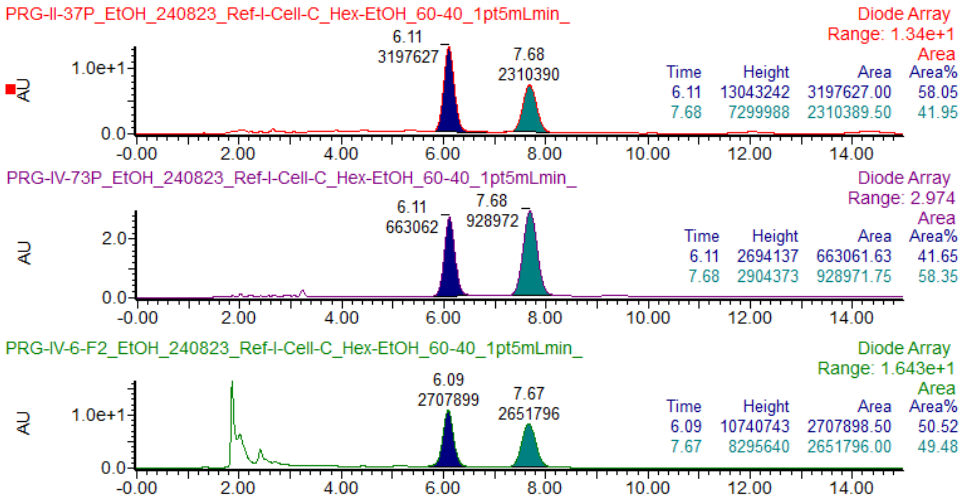

Figure 3.196 - CSP-HPLC of **15** from **1f** (loaded in EtOH). Regis Reflect I-Cellulose C, *n*-hexane-EtOH 60 : 40, flowrate 1.5 mLmin^{-1}. (top) (R_{ma})-**15** from (*R*)-**1f**; (R_{ma})-**15** (6.11 min, 3197627, 58.05%), (S_{ma})-**15** (7.68 min, 2310390, 41.95%). (middle) (S_{ma})-**15** from (*S*)-**1f**; (R_{ma})-**15** (6.11 min, 663062, 41.65%), (S_{ma})-**15** (7.68 min, 928972, 58.35%). (bottom) *rac*-**15**; (R_{ma})-**15** (6.09 min, 2707899, 50.52%), (S_{ma})-**15** (7.67 min, 2651796, 49.48%).

Formamide azide (*R*)-1g

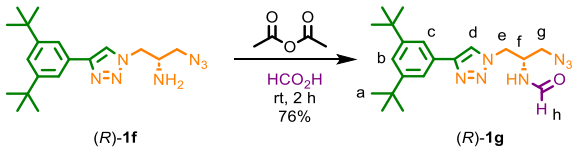

To a solution of (*R*)-**1f** (30.0 mg, 0.084 mmol) in HCO_2H (800 µL) was added acetic anhydride (63.8 µL, 0.68 mmol). The solution was stirred at rt for 2 h, then the solution was diluted with CH_2Cl_2 (5 mL) and H_2O (2 mL) was added. The aqueous and organic phases were separated, and the aqueous phase was then extracted with CH_2Cl_2 (3 x 10 mL). The combined organic extracts were washed with brine (15 mL), dried ($MgSO_4$) and concentrated *in vacuo*. Chromatography (petrol-EtOAc 0→50%) gave (*R*)-**1g** (21.4 mg, 76%) as a white solid.

Formamide azide (*S*)-**1g** (17.4 mg, 82%) was synthesised using an identical procedure starting from (*S*)-**1f** (21.1 mg, 0.055 mmol). Analytical data was identical to (R)-**1g** with the exeption of their CD spectra (Figure 3.202) and CSP-HPLC (Figure 3.203).

^{1}H NMR (400 MHz, $CDCl_3$) [note: the labelling scheme used here differs from that in Scheme 6; see main text and associated footnote] δ: 8.20 (s, 1H, H_h), 7.85 (s, 1H, H_d), 7.65 (d, *J* = 1.8, 2H, H_c), 7.44 (t, *J* = 1.8, 1H, H_b), 6.63 (d, *J* = 7.7, 1H, NH), 4.71-4.51 (m, 3H, H_e, H_f), 3.62 (dd, *J* = 12.5, 4.8 Hz, 1H H_g), 3.32 (dd, *J* = 12.5, 6.7 Hz, 1H $H_{g'}$), 1.36 (s, 18H H_a);

^{13}C NMR (100 MHz, $CDCl_3$) δ: 161.3, 151.6, 149.0, 129.1, 122.9, 121.1, 120.2, 50.6, 49.9, 47.6, 35.0, 31.4

HR-ESI-MS (+ve) m/z = 384.2513 $[M+H]^+$ (calc. 384.2506 m/z for $C_{20}H_{30}N_7O$);

Melting point = 152-154 °C.

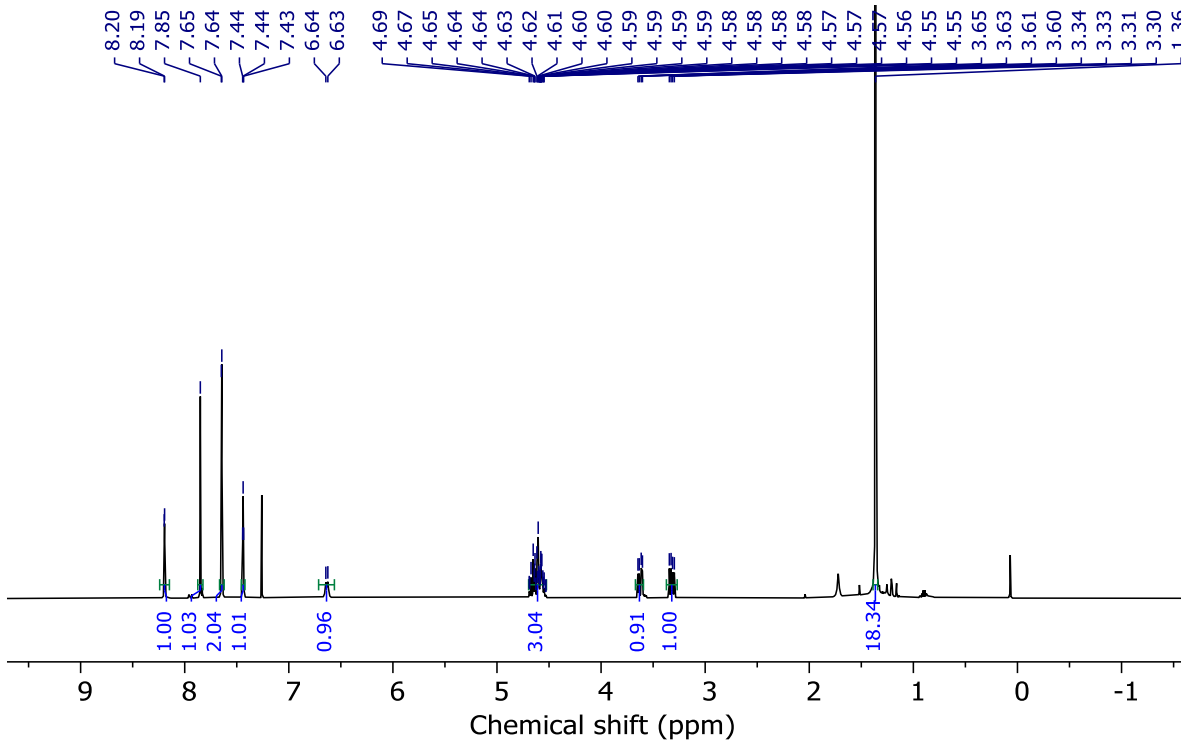

Figure 3.197 - ^{1}H NMR ($CDCl_3$, 400 MHz) of (*R*)-**1g**.

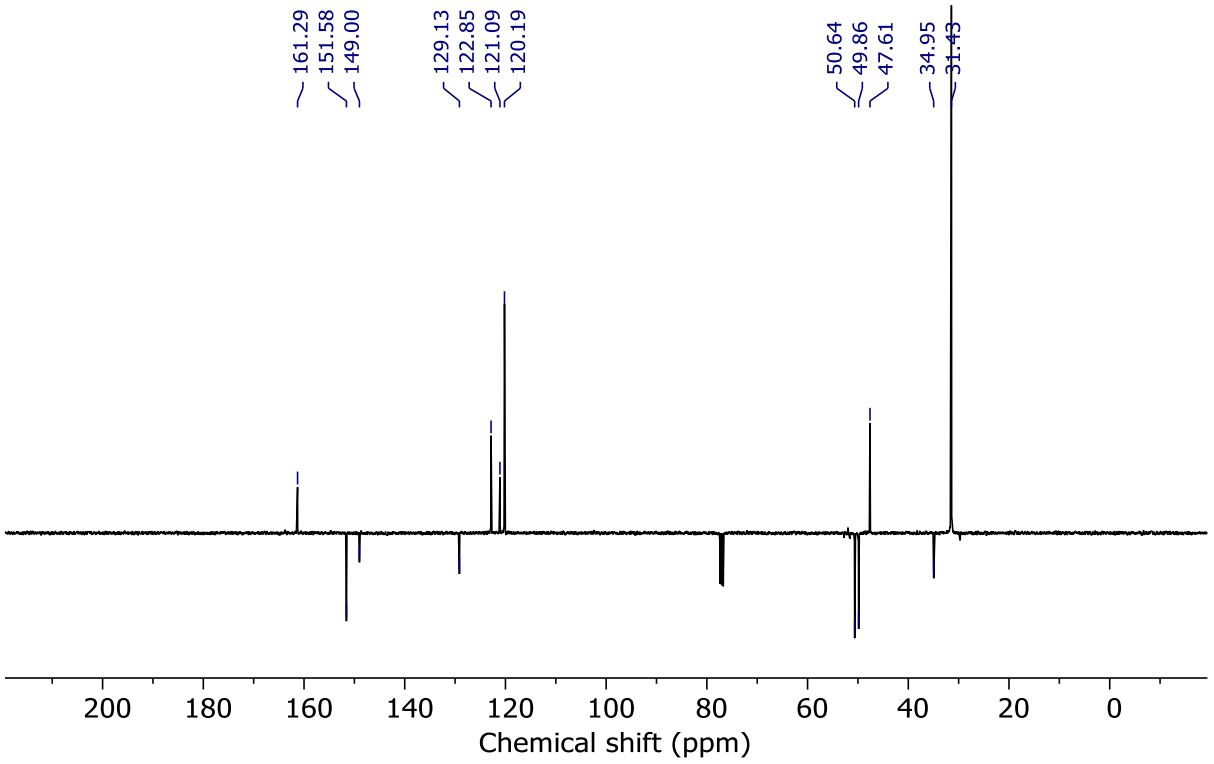

Figure 3.198 - JMOD NMR ($CDCl_3$, 101 MHz) of (*R*)-**1g**.

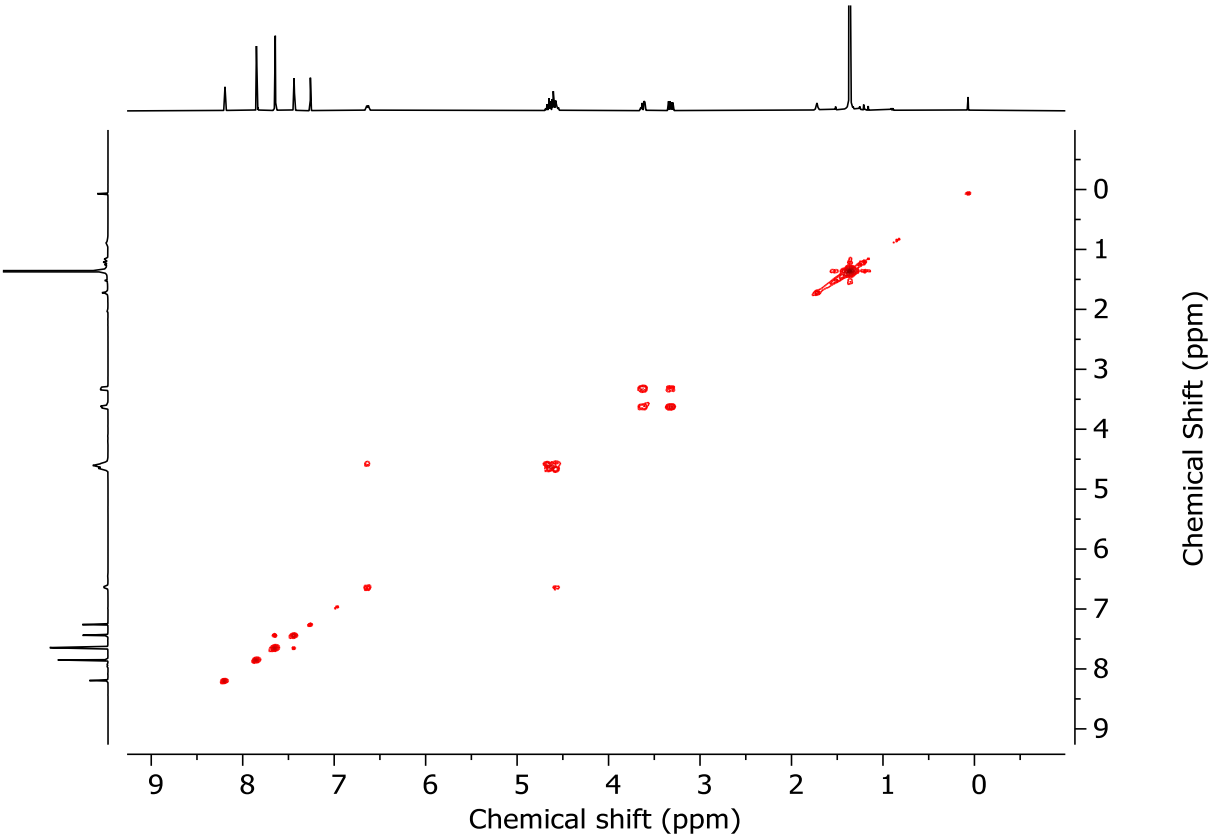

Figure 3.199 - COSY NMR ($CDCl_3$) of (*R*)-**1g**.

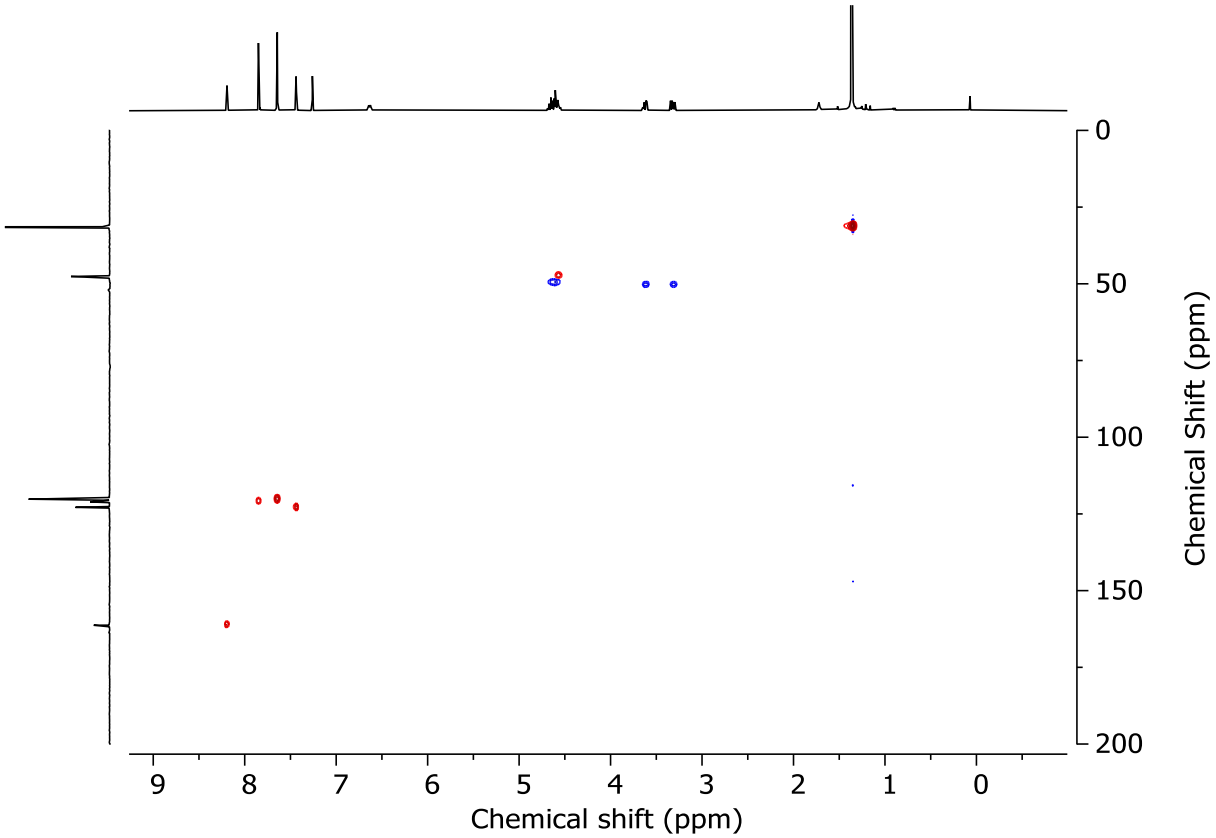

Figure 3.200 - HSQC NMR ($CDCl_3$) of (*R*)-**1g**.

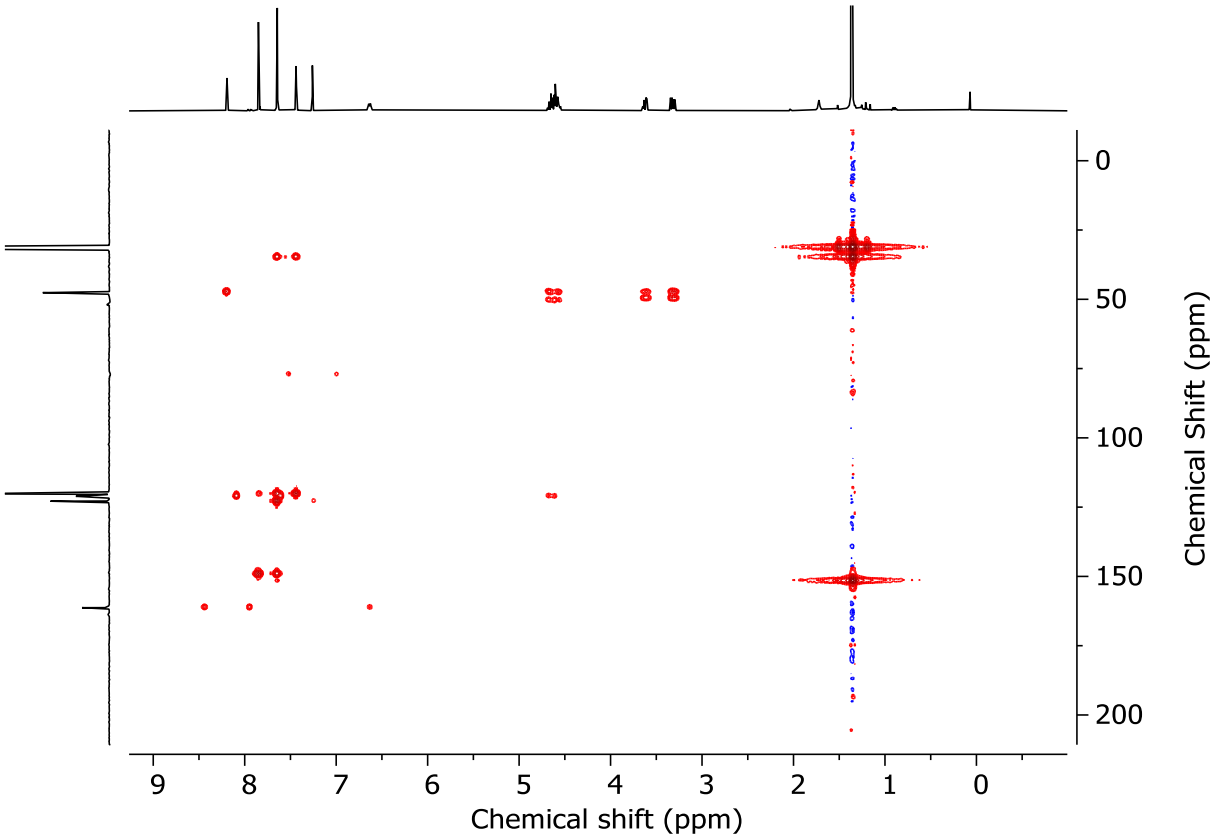

Figure 3.201 - HMBC NMR ($CDCl_3$) of (*R*)-**1g.**

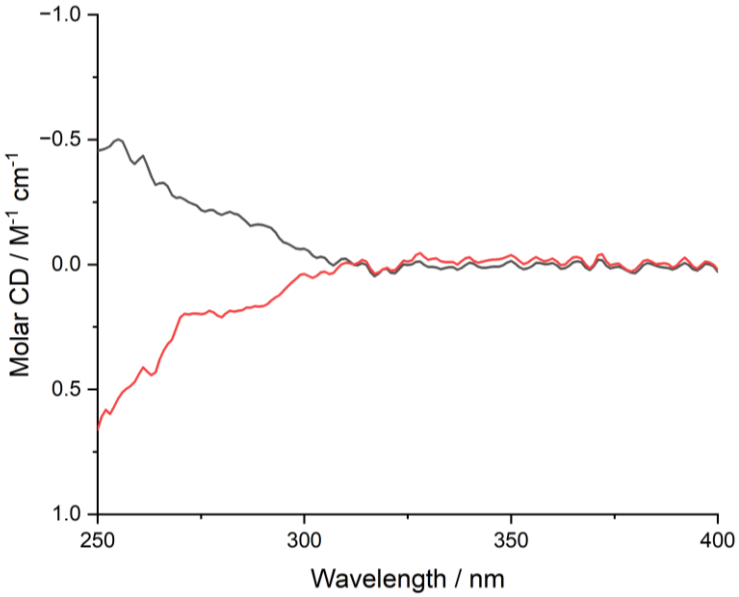

Figure 3.202 - Circular Dichroism Spectra of (*S*)-**1f** (64 µM, grey) and (*R*)-**1f** (82 µM, red) at 293 K in $CHCl_3$.

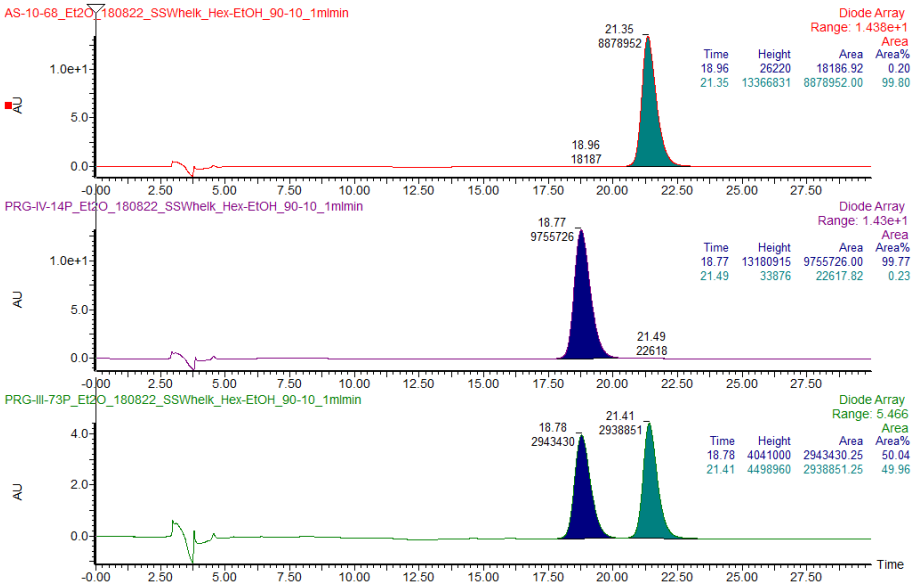

Figure 3.203 - CSP-HPLC of **1g** (loaded in Et_2O). SSWhelk, *n*-hexane-EtOH 90 : 10, flowrate 1 $mLmin^{-1}$. (top) (R)-**1g**; (*S*)-**1g** (18.96 min, 18187, 0.20%), (R)-**1g** (21.49 min, 8878952, 99.80%). (middle) (*S*)-**1g**; (*S*)-**1g** (18.77 min, 9755726, 99.77%), (*S*)-**1g** (21.49 min, 22618, 0.23%). (bottom) *rac*-**1g**, (*S*)-**1g** (18.78 min, 2943430, 50.04%), (R)-**1f** (10.35 min, 2938851, 49.96%).

Formamide rotaxane (R_{ma})-16

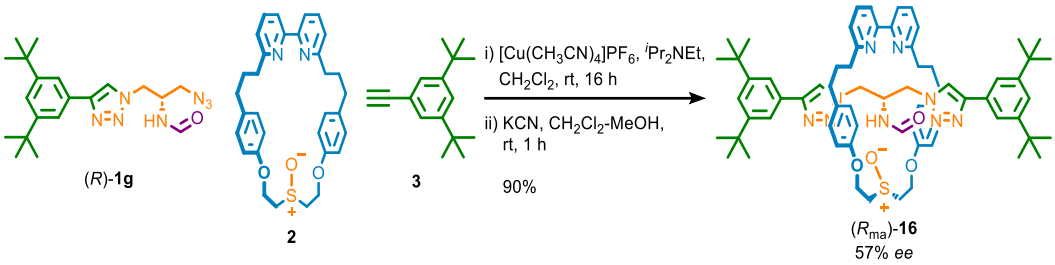

In a CEM vial were added **3** (4.7 mg, 21.9 µmol), (*R*)-**1g** (8.4 mg, 21.9 µmol), **2** (10.5 mg, 20.0 µmol) and $[Cu(CH_3CN)_4PF_6]$ (7.1 mg, 19.0 µmol). The vial was sealed and purged with N_2, then CH_2Cl_2 was added (500 µL), followed by $^iPr_2NEt$ (7 µL, 40.1 µmol). The solution was stirred at rt for 16 h. MeOH (2 mL mL) and KCN as a solid (13 mg, 0.20 mmol) were added and the resulting mixture was stirred vigorously for until colourless. The crude mixture was diluted with CH_2Cl_2 (5 mL) and washed with H_2O (5 mL) then EDTA-NH_3 (5 mL), with separation of aqueous and organic phases. The combined aqueous phase was then extracted with CH_2Cl_2 (3 x 5 mL) and the combined organic extracts were washed with brine (10 mL), dried ($MgSO_4$) and concentrated *in vacuo*. Chromatography (CH_2Cl_2-CH_3CN 0→100%) gave (R_{ma})-**16** as a white foam (20.6 mg, 90%, 57% *ee* see Figure 3.211).

Formamide rotaxane (S_{ma})-**16** (29.9 mg, 68%, 61.84% *ee*) was synthesised using an identical procedure starting from (*S*)-**1g** (16.9 mg, 44.1 µmol). Analytical data were identical to (R_{ma})-**16** with the exception CSP-HPLC (Figure 3.211).

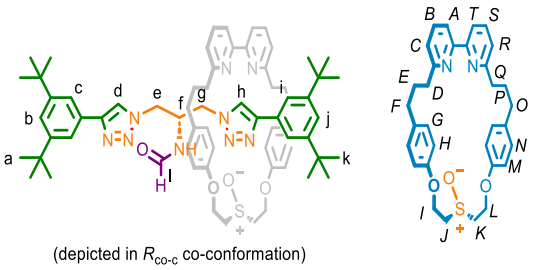

^{1}H NMR (500 MHz, CD_2Cl_2) [note: the labelling scheme used here differs from that in Scheme 3.6; see main text and associated footnote] δ: 9.08 (bs, 1H, H_h), 8.21 (bs, 1H, H_d), 7.68 (t, *J* = 7.8, 1H, H_B), 7.63 (t, *J* = 7.6, 1H, H_S), 7.60-7.53 (m, 5H, H_c, H_i, NH), 7.47-7.39 (m, 2H, H_A, H_T), 7.38 (t, *J* = 1.9, 1H, H_b or H_j), 7.32 (t, *J* = 1.9, 1H, H_b or H_j), 7.19 (dd, *J* = 7.8, 1.0, 1H, H_C), 7.13-7.08 (m, 2H, H_L, H_R), 6.78 (d, *J* = 8.6, 2H, H_G or H_N), 6.75-6.67 (m, 4H, H_G and H_H or H_M and H_N), 6.60 (d, *J* = 8.5, 2H, H_H or H_M), 4.69-4.55 (m, 2H, H_I and $H_{I'}$ or H_L and $H_{L'}$), 4.52 (dd, *J* = 12.2, 9.2, 3.6, 1H, H_I or H_L), 4.43 (dt, *J* = 12.0, 4.7, 1H, $H_{I'}$ or $H_{L'}$), 4.17-4.08 (m, 1H, H_f), 3.98 (dd, *J* = 14.6, 3.4, 1H, H_e), 3.92-3.65 (m, 4H, $H_{e'}$, H_g, H_J or H_K), 3.61 (ddd, *J* = 13.8, 9.3, 4.4, 1H, H_J or H_K), 3.21-3.05 (m, 2H, $H_{J'}$, $H_{K'}$), 2.67-2.38

(m, 6H, H_F, H_O, H_D or H_Q), 2.37-2.20 (m, 2H, H_D or H_Q), 1.95-1.67 (m, 4H, H_E, H_P, superimposed with residual H_2O), 1.33 (s, 18H, H_a), 1.26 (s, 18H, H_k)

^{13}C NMR (126 MHz, CD_2Cl_2) δ: 163.0, 162.8, 161.3, 157.4, 157.3, 156.2, 151.3, 151.1, 148.1, 148.0, 137.5, 137.4, 133.8, 133.6, 130.5, 130.2, 129.6, 129.5, 122.9, 122.3, 122.1, 121.8, 121.8, 121.4, 120.8, 120.7, 120.0, 119.8, 115.1, 114.6, 61.4, 60.7, 53.0, 50.1, 49.9, 48.7, 37.0, 36.6, 34.9, 34.8, 34.8, 31.9, 31.3, 31.3, 31.3, 30.2

LR-ESI-MS (+ve) m/z = 1124.7 $[M+H]^+$ (calc. m/z for $C_{68}H_{85}N_9O_4S$ 1124.7);

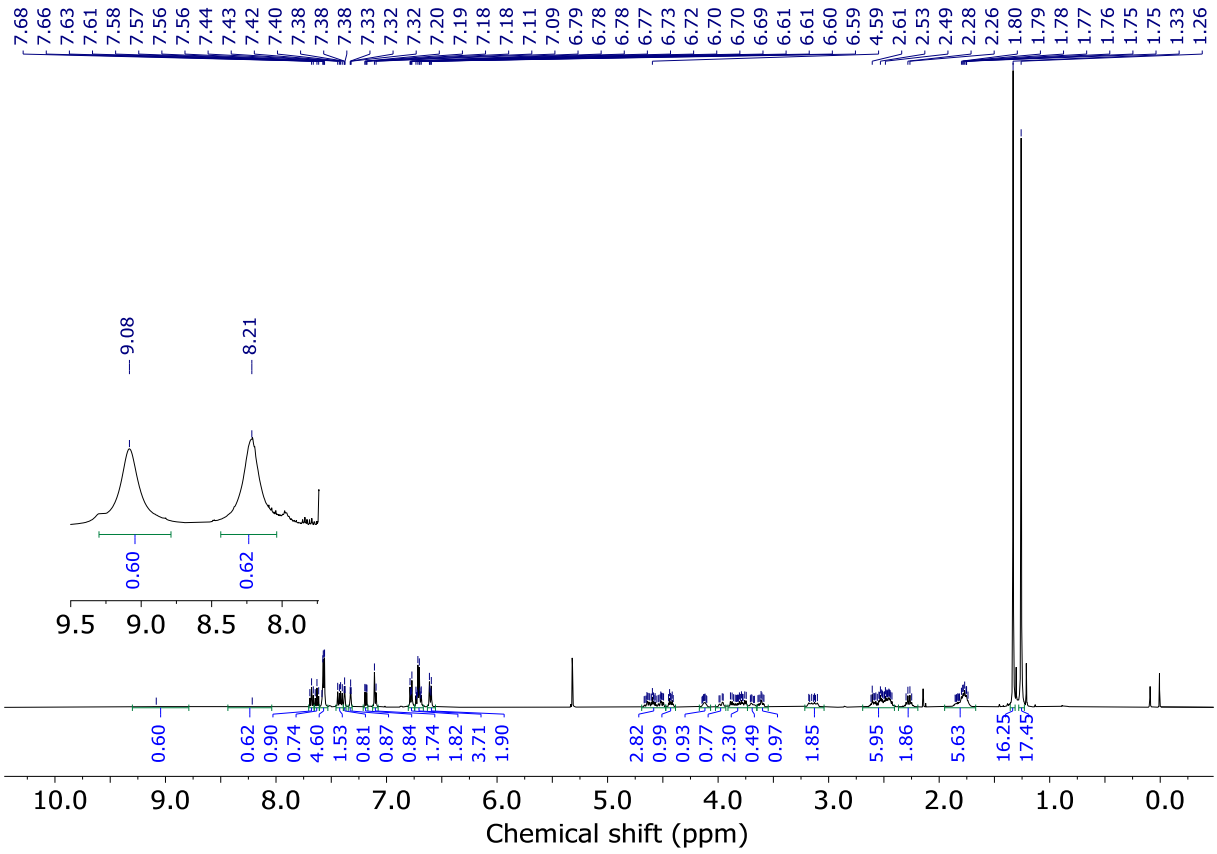

Figure 3.204 - ^{1}H NMR (CD_2Cl_2, 500 MHz) of (R_{ma})-**16**.

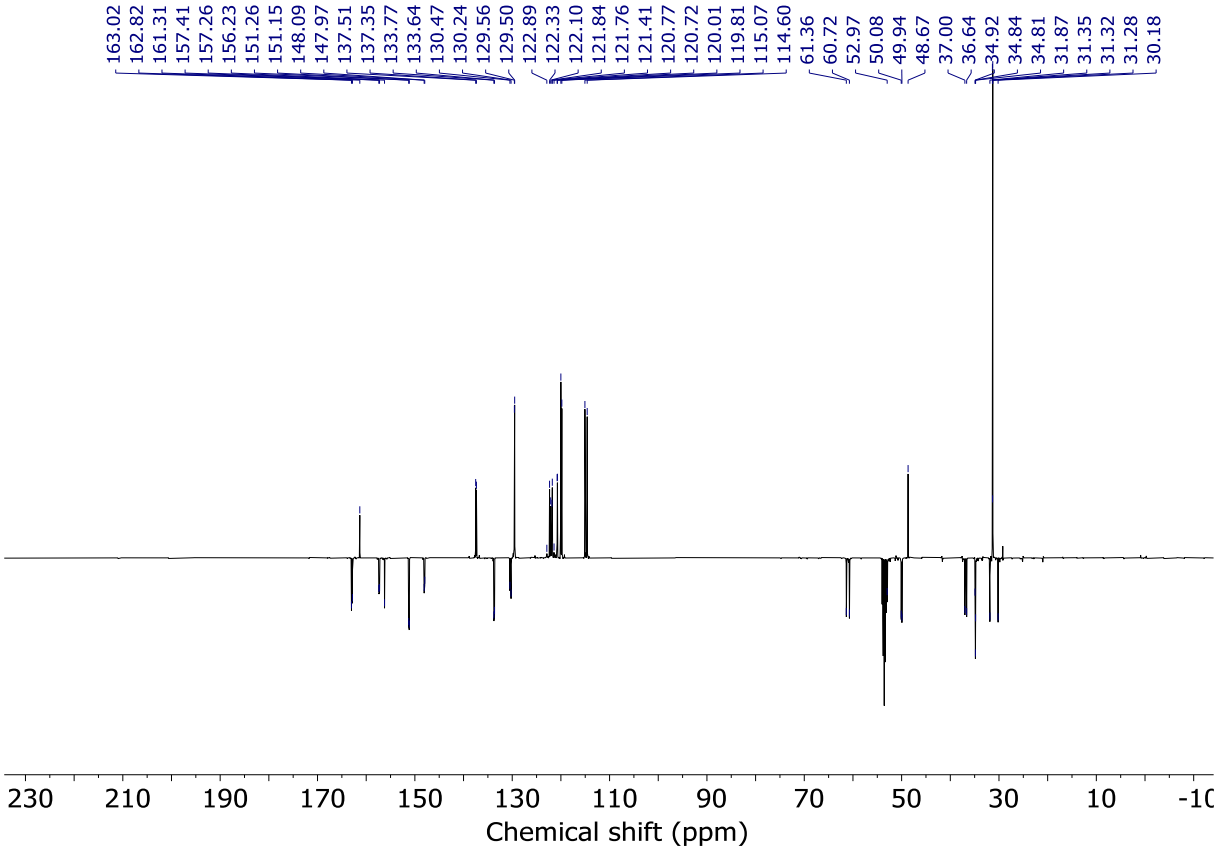

Figure 3.205 - JMOD NMR (CD_2Cl_2, 126 MHz) of (R_{ma})-**16**.

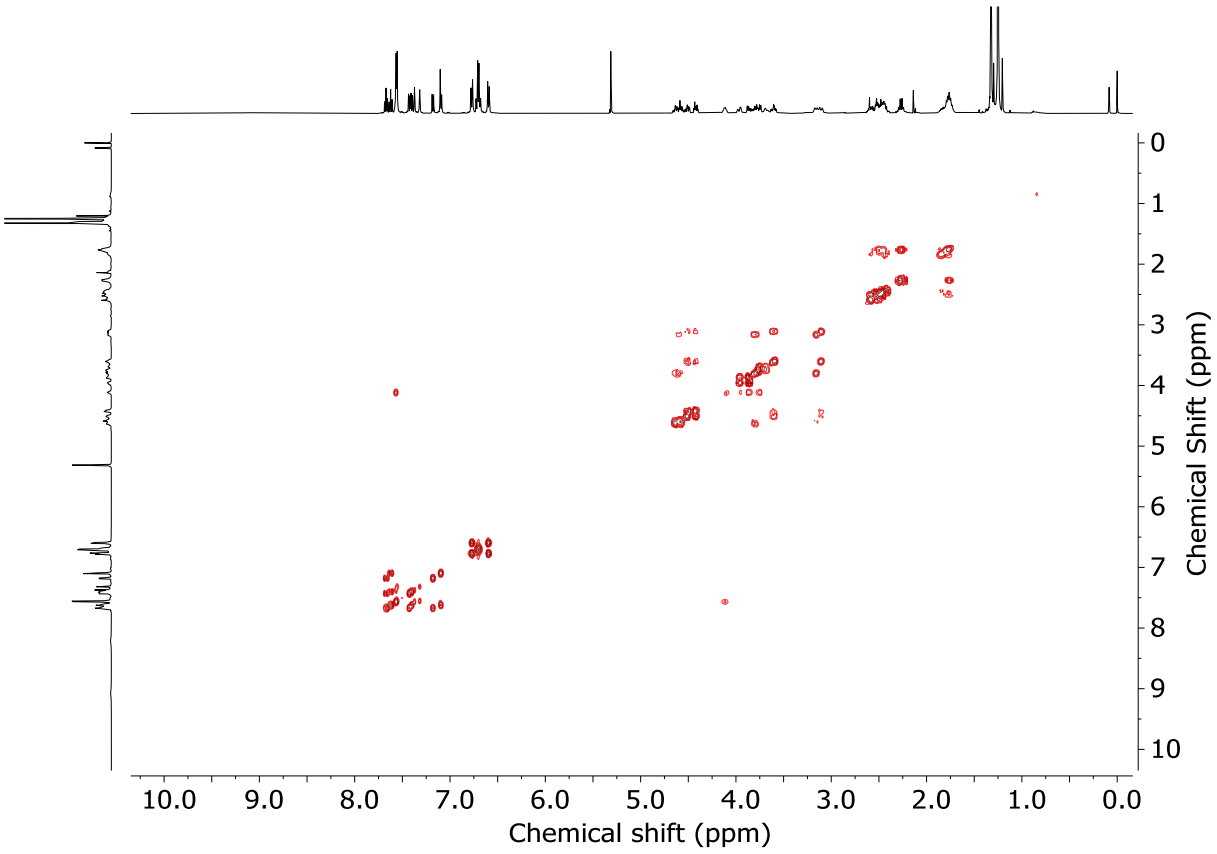

Figure 3.206 - COSY NMR (CD_2Cl_2) of (R_{ma})-**16**.

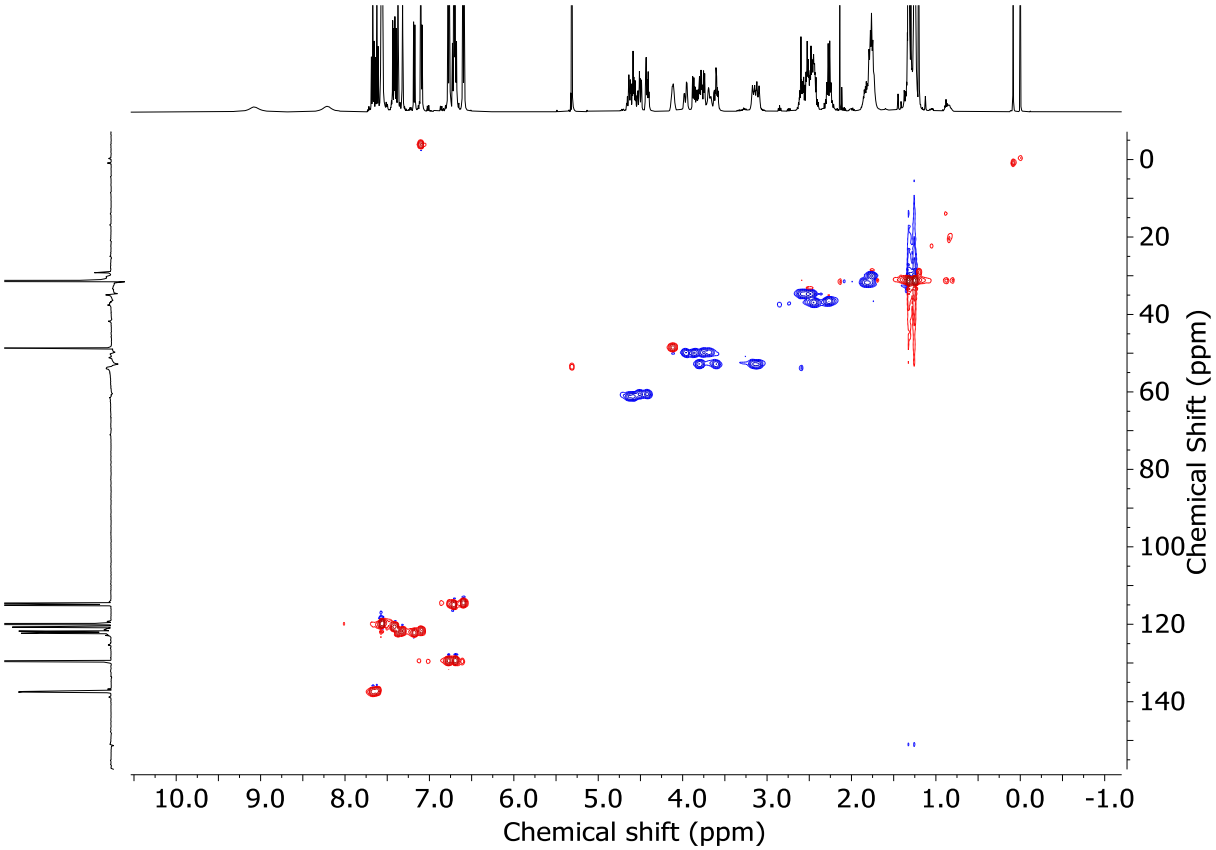

Figure 3.207 - HSQC NMR (CD_2Cl_2) of (R_{ma})-**16**.

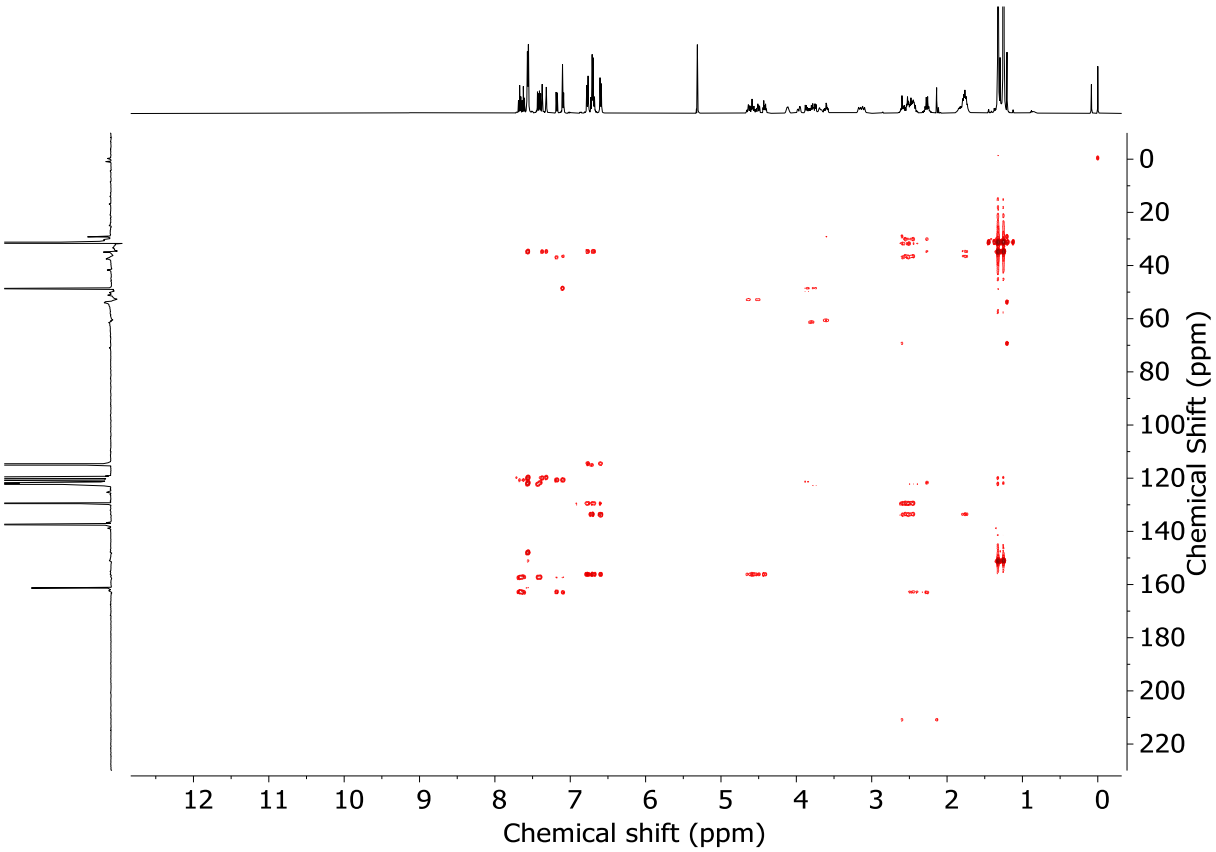

Figure 3.208 - HMBC NMR (CD_2Cl_2) of (R_{ma})-**16**.

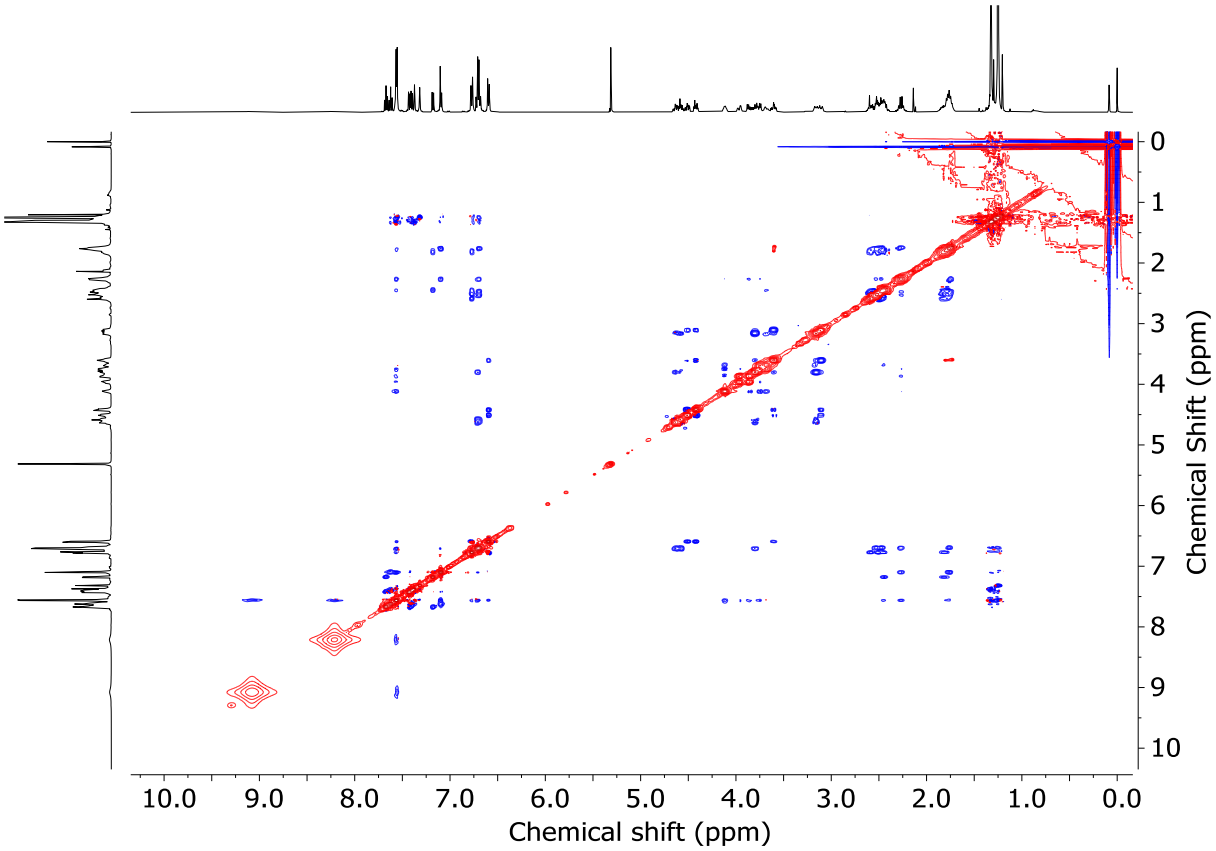

Figure 3.209 - NOESY NMR (CD_2Cl_2) of (R_{ma})-**16**.

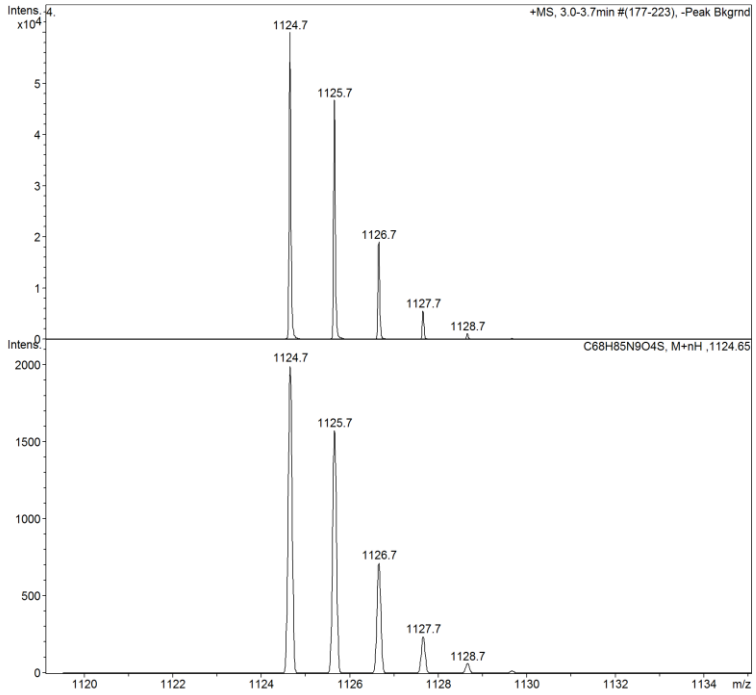

Figure 3.210 - Observed (top) and calculated (bottom) isotopic patterns for rotaxanes **16**.

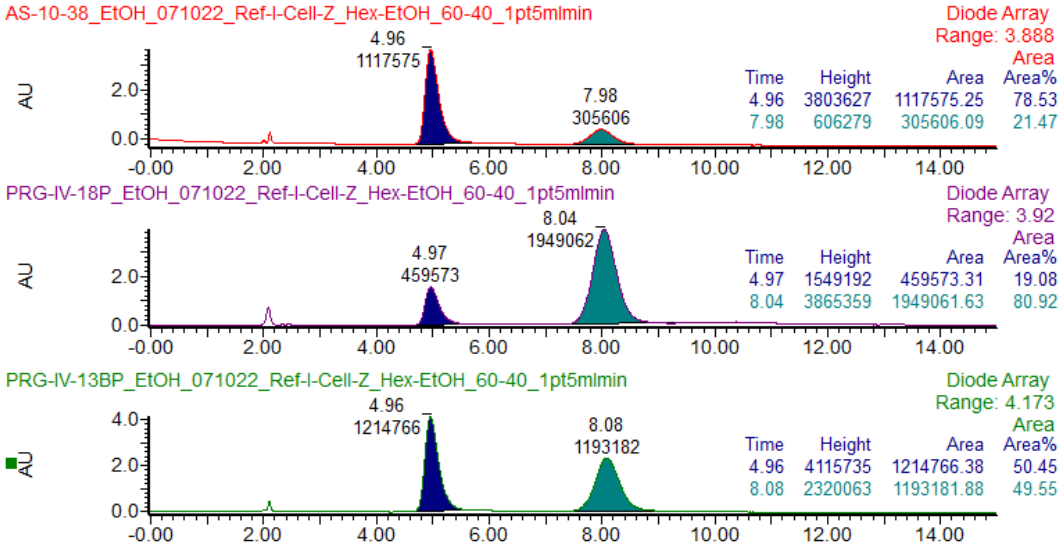

Figure 3.211 - CSP-HPLC of **16** (loaded in EtOH). Regis Reflect I-Cellulose Z, *n*-hexane-EtOH 60 : 40, flowrate 1.5 mLmin^{-1}. (top) (R_{ma})-**16** from (*R*)-**1g**; (R_{ma})-**6** (4.96 min, 1117575, 78.53%), (S_{ma})-**16** (7.98 min, 305606, 21.47%). (middle) (S_{ma})-**16** from (*S*)-**1g**; (R_{ma})-**16** (4.97 min, 459573, 19.08%), (S_{ma})-**16** (8.04 min, 1949062, 80.92%). (bottom) *rac*-**16**, (R_{ma})-**16** (4.96 min, 1214766, 50.45%), (S_{ma})-**16** (8.08 min, 1193182, 49.55%).

Determination of the major stereoisomer of rotaxane 16 produced from 1g

In order to determine the absolute stereochemistry of major stereoisomer of rotaxane **16** produced directly from **1g**, an analytical sample of rotaxane (R_{ma})-**16** was prepared formylation of a sample amine rotaxane (R_{ma})-**15** of known stereopurity (21% *ee*), as described below, which allowed us to assign the retention time of the enantiomers of **16**.

Rotaxanes 16 *via* formylation of rotaxanes 15

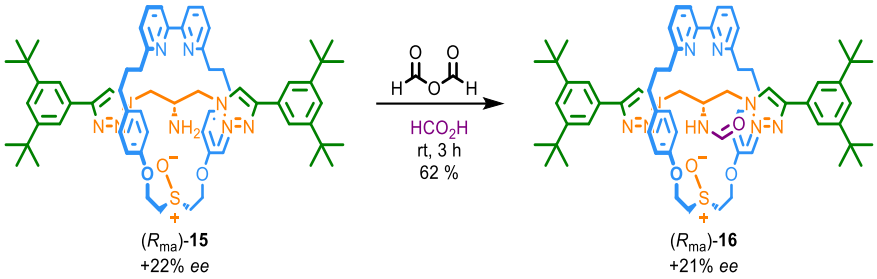

To a solution of (R_{ma})-**15** (3.5 mg, 3.2 µmol, 21% *ee*, Figure 3.212) in HCO_2H (250 µL) was added acetic anhydride (18.0 µL, 19.0 µmol). The solution was stirred at rt for 3 h, then the solution was diluted with CH_2Cl_2 (5 mL) and H_2O (2 mL) was added. The aqueous and organic phases were separated, and the aqueous phase was then extracted with CH_2Cl_2 (3 x 10 mL). The combined organic extracts were washed with brine (15 mL), dried ($MgSO_4$) and concentrated *in vacuo*. Chromatography (CH_2Cl_2-CH_3CN 0→100%) gave (R_{ma})-**16** (2.2 mg, 62%, +21% *ee*, Figure 3.212) as a white foam. All spectroscopic data were identical to those reported for rotaxane (R_{ma})-**16** above.

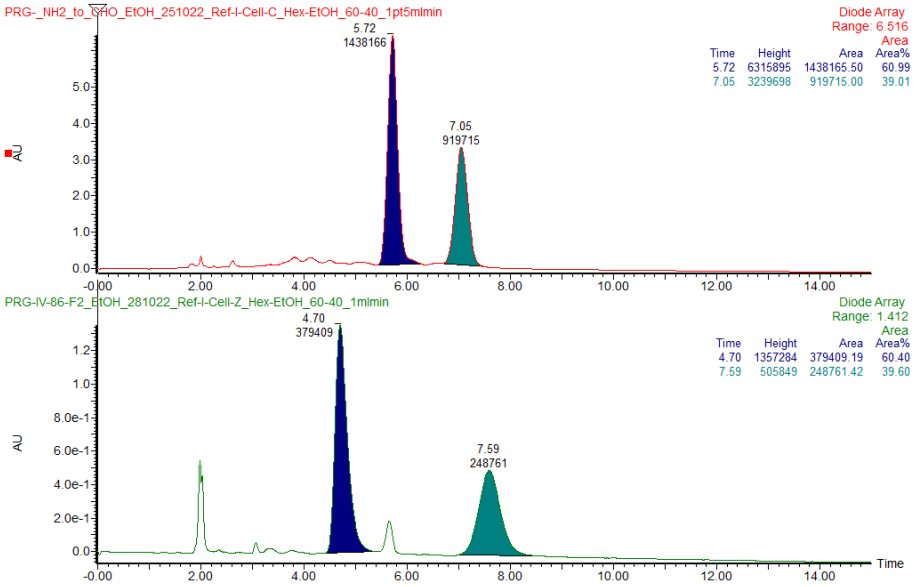

Figure 3.212 - CSP-HPLC to determine the absolute stereochemistry of rotaxanes **16**. (top) amine rotaxane (R_{ma})-**15** starting material (+21.98% *ee*). (bottom) formamide rotaxane (R_{ma})-**16** product (+20.80% *ee*).

3.5.2. Absolute stereochemical assignment of interlocked compounds

Methods to assign the absolute stereochemistry of interlocked molecules are still in development. However, we have previously proposed methods for the assignment of absolute stereochemistry in mechanically planar chiral catenanes and rotaxanes, which are based on oriented covalent sub-units[12a] and mechanically axially chiral catenanes and rotaxanes, which are based on facially dissymmetric components.[11] In all cases we make use of Cahn-Ingold-Prelog (CIP)-derived atom priorities to unambiguously assign vectors associated the bilateral dissymmetry of the covalent sub-components. Here we extend these rules to mechanical geometric isomers. We also propose a revision to the method for assigning the MAC stereogenic unit of rotaxanes and catenanes. In all cases, the stereochemical assignment is achieved by considering the relative orientation of the vectors associated with the individual components. Those vectors can be identified by a step-by-step approach based on the rules outlined below.

3.5.2.1. A note on the assignment of the MAC stereogenic unit – the need for revision

Recently, we proposed a method to assign the absolute stereochemistry of interlocked molecules with mechanical axial stereochemistry.[11] Our original method to assign mechanically axially chiral (MAC) catenanes was based on a previous proposal by Stoddart and Bruns.[1] A particular challenge with assigning the absolute stereochemistry of MAC rotaxanes is that the outcome depends on the relative orientation of the axle within the cavity of the ring (c.f., deciding which orientation to observe a covalent stereocentre to assign the stereolabel). This is obviously an arbitrary decision and originally, we defined the orientation such that the MAC catenane and rotaxane stereogenic units obtained through the notional ring opening of the former to generate the latter were assigned the same stereolabel (i.e., R_{ma} catenane generates R_{ma} rotaxane). However, when the same arbitrary axle orientation convention was applied to a recently identified non-canonical mechanical geometric stereogenic unit, we found that this created a contradiction; the type II mechanical geometric stereogenic unit of a rotaxane generated by ring opening of the corresponding catenane geometric isomer was assigned the opposite stereolabel (i.e., Z_m catenane generates E_m rotaxane).[3]

In light of this, here we propose a revised method for the assignment of absolute stereochemistry of the MAC stereogenic unit of catenanes and rotaxanes that still results in the same stereolabel if a notional ring opening of the former to generate the latter is followed. Importantly, this method allows the same arbitrary axle orientation to be applied in both MAC and MGI rotaxanes and catenanes, with the same rules that have already been established for the assignment of mechanical planar stereochemistry.[0]

The revision changes the position from which the vectors associated with the facial dissymmetry is viewed and thus effectively inverts the stereolabels of all previously assigned MAC rotaxanes and catenanes.

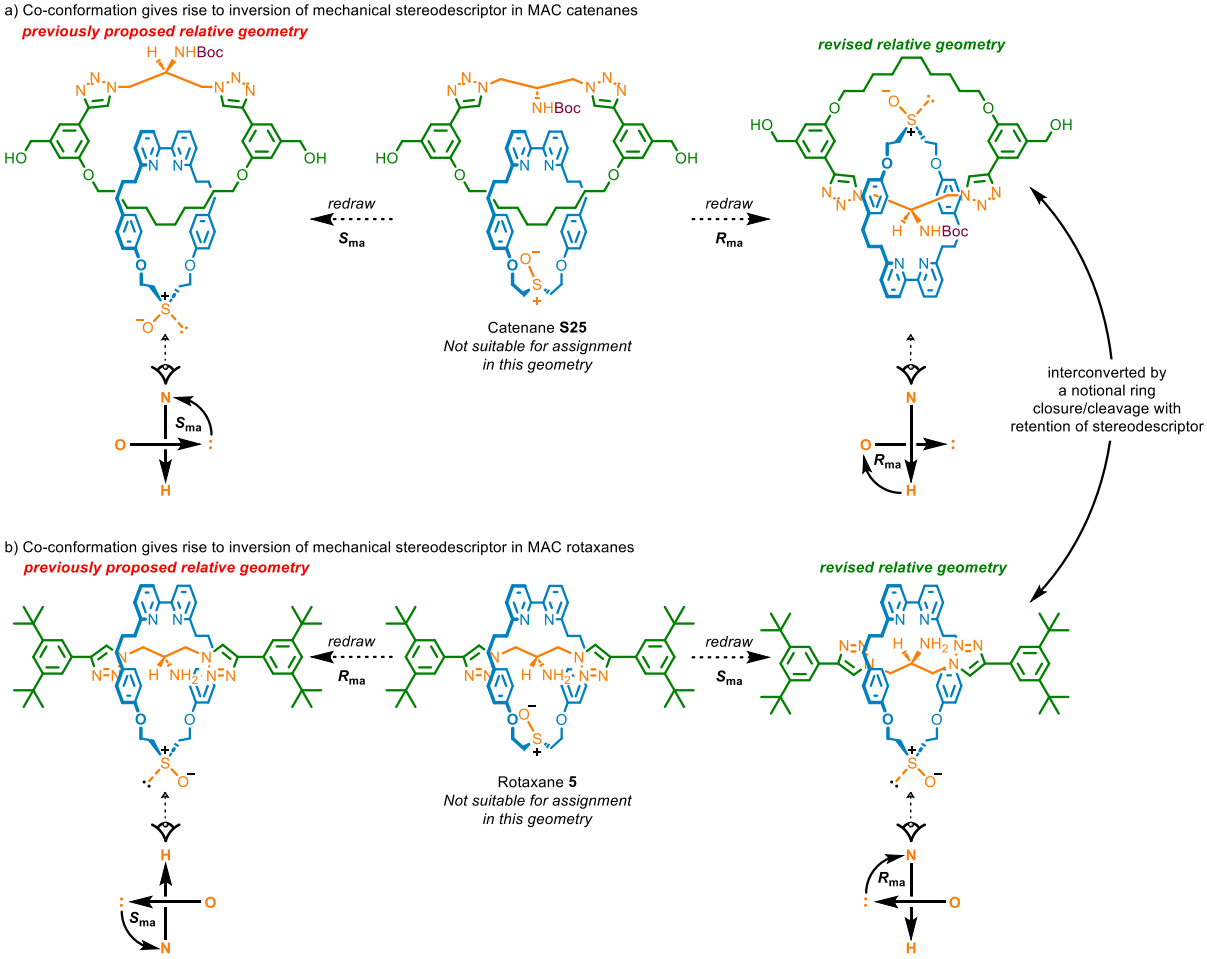

3.5.2.2. Revised rules for the assignment of mechanically axially chiral catenanes

To assign the absolute stereochemistry of mechanically axially chiral catenanes it is necessary to consider the relative orientation of the vectors associated with the individual components. These vectors can be identified by a step-by-step approach based on the following rules:

Step 1: In each ring, identify the highest priority prochiral group (or stereogenic unit in meso structures) using the Cahn-Ingold-Prelog priority of the central atom. Redraw the rings such that the in-plane substituents of the prochiral centres point into the centre of the respective macrocycle.

Step 2: In each ring, identify the highest priority ligand of the selected centre that lie outside of the macrocycle plane, again using CIP priority, and label it as "**A**"; label the lower priority group "**B**".

Step 3: Redraw the molecule such that the prochiral group of each ring lies within the cavity of the other.

Step 4: View the relative orientation of the **A→B** vectors at the crossing point of the two rings and consider the direction of rotation from the head of the front vector to the tail of the rear vector. A right-handed path assigned as (R_{ma}) and a left-handed path assigned as (S_{ma}).

Worked example - catenane S25

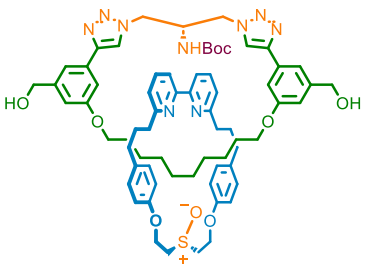

(R_{ma})-**S25**

Step 1: The highest CIP prochiral centres in each component are the carbon bearing the substituted amine in the axle and the sulfoxide sulfur in the macrocycle. Currently the in plane substituents of the prochiral units point out of the cavity. Redraw the structure such that these point into the centre of the ring.

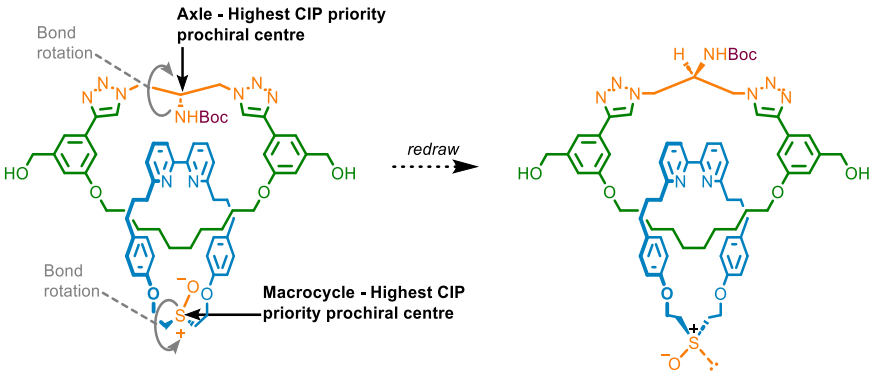

Step 2: The highest priority exocyclic atom bonded to the sulfoxide according to CIP rules is the oxygen, which is labelled as "**A**", while the lone pair is labelled as "**B**". The highest priority exocyclic atom bonded to the prochiral carbon of the triazole-containing macrocycle according to CIP rules is the amine nitrogen, which is labelled as "**A**", while the proton is labelled as "**B**".

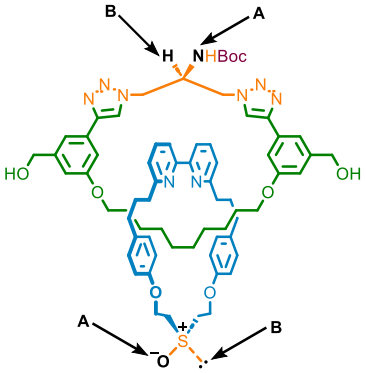

Step 3: Redraw the structure such that the prochiral centre of each ring lies within the cavity of the other.

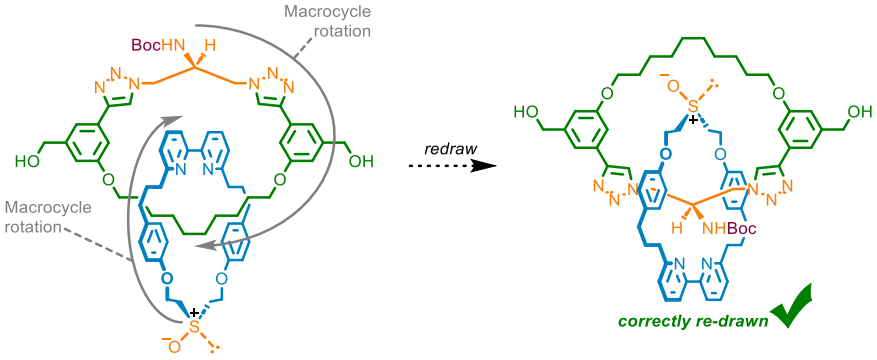

Step 4: View the relative orientation of the **A→B** vectors at the crossing point between the rings. As a clockwise path is taken to the head of the vector defined by the sulfoxide, the stereoisomer of catenane **S25** shown is labelled as (R_{ma})-**S25.**

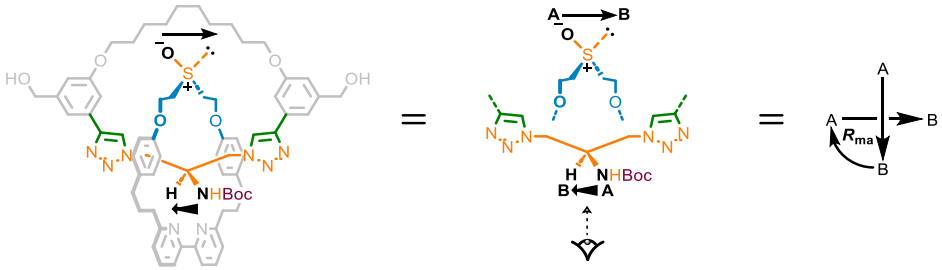

3.5.2.3. Revised rules for the assignment of mechanically axially chiral rotaxanes

To assign the absolute stereochemistry of mechanically axially chiral rotaxanes it is necessary to consider the relative orientation of the vectors associated with the individual components. These vectors can be identified by a step-by-step approach based on the following rules:

Step 1: In the ring, identify the highest priority prochiral group (or stereogenic unit in meso structures) using the Cahn-Ingold-Prelog priority of the central atom. Redraw the ring such that the in-plane substituents of the prochiral centre points into the centre of the macrocycle.

Step 2: Identify the highest priority ligand of the selected centre that lies outside of the macrocycle plane, again using CIP priority, and label it as "**A**"; label the lower priority group "**B**".

Step 3: In the axle, identify the highest priority prochiral group (or stereogenic unit in *meso* structures) using the CIP priority of the central atom. Identify the highest priority out of plane ligand of the identified centre, again using CIP priority, and label it as "**C**"; label the lower priority group "**D**".

Step 4: View the assembly with the in-plane substituents of macrocycle pointing away from the observer and the in plane substituents of the axle prochiral pointing towards the observer.

Step 5: View the relative orientation of the **A→B** and **C→D** vectors and consider the direction of rotation from the head of the front vector to the tail of the rear vector. A right-handed path assigned as (R_{ma}) and a left-handed path assigned as (S_{ma}).

Worked example – rotaxane 15

Step 1: The highest CIP prochiral centre in the macrocycle is the sulfoxide unit. This is then redrawn such that the in-plane methylene units point into the cavity of the ring.

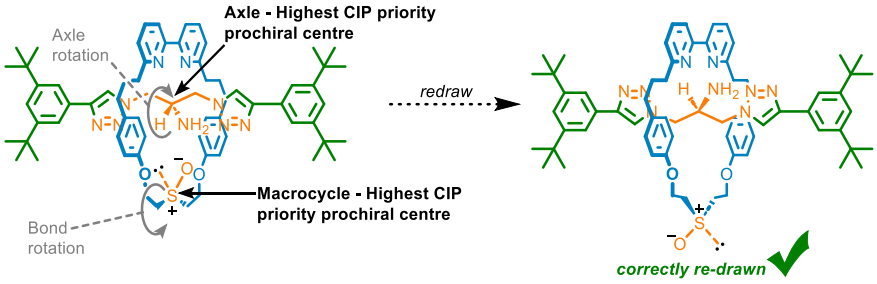

Step 2: The highest priority exocyclic atom bonded to the sulfoxide according to CIP rules is the oxygen, which is labelled as "**A**", while the lone pair is labelled as "**B**".

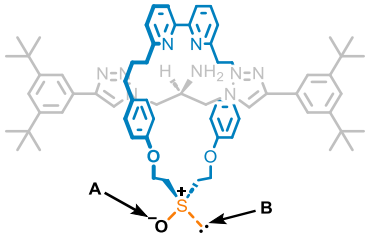

Step 3: The highest priority prochiral centre in the axle is the carbon bearing the amine unit. The highest priority exocyclic atom bonded to the prochiral carbon is the amine nitrogen, which is labelled as "**C**", while the proton is labelled as "**D**".

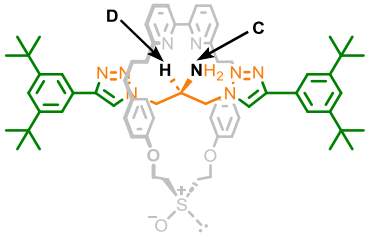

Step 4: Viewing the assembly with the in-plane substituents of the macrocycle pointing away from the observer and those of the axle pointing towards the observer an anticlockwise path is taken to the head of the vector defined by **C→D** vector from the tail of the **A→B** vector. Thus the stereoisomer of rotaxane **5** shown (S_{ma})-**5.**

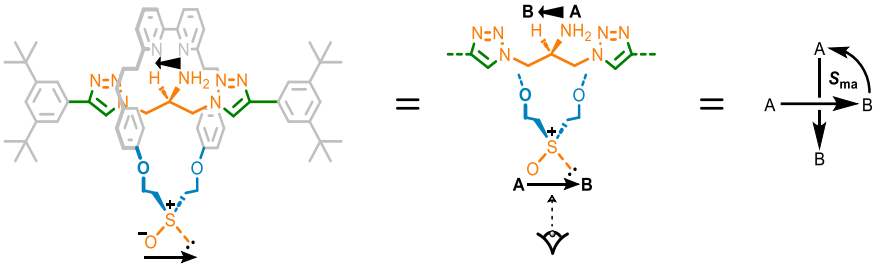

3.5.2.4. Absolute stereochemical assignment of type I rotaxane mechanical geometric isomers

Step 1: In the axle, identify the highest priority atom using the (CIP) priority rules and label it as "**A**".

Step 2: Moving outward from **A** in spheres, as per the CIP method for assigning covalent stereogenic centres, determine the highest priority atom (CIP) that can be used to define an orientation of the axle (typically a ligand of **A**) and label it as "**B**". The orientation of the axle is defined by the vector **A→B**, which, where relevant, passes through the intervening atoms (i.e., follows the bonds).

Step 3: In the macrocycle, identify the highest priority prochiral group (or stereogenic unit in *meso* structures) using the CIP priority of the central atom. Redraw the macrocycle such that the in-plane substituents of the prochiral centre point towards the centre of the ring.

Step 4: Identify the highest priority ligand of the identified centre that lie outside of the macrocycle plane, again using CIP priority, and label it as "**C**"; label the lower priority group "**D**".

Step 5: View the relative orientation of the vectors **A**→**B** and **C**→**D**. If the vectors point in the same direction, the molecule will be labelled as (Z_m). If they point toward opposite directions, the molecule will be labelled as (E_m).

Worked example - rotaxane 6

Step 1: The atom of the axle with the highest priority is N_2, which is labelled as **A.**

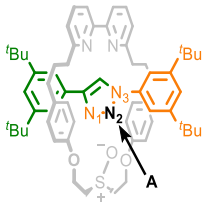

Step 2: The highest priority ligand of **A** is N_3, which allows the orientation of the axle to be assigned, and so is labelled **B**.

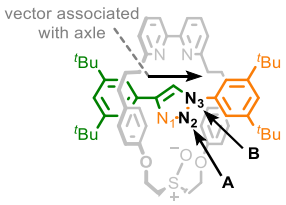

Step 3: The sulfoxide moiety is the only prochiral unit in the macrocycle. The macrocycle is redrawn such that the in-plane methylene substituents of the prochiral centre point towards the axle.

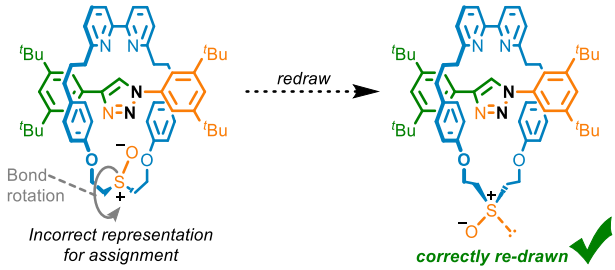

Step 4: The highest priority exocyclic atom bonded to the prochiral unit is the oxygen, which is labelled **C**. The lone pair is labelled **D**, allowing the vector associated with the macrocycle to be defined.

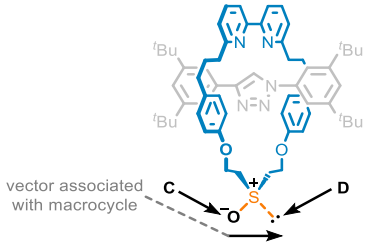

Step 5: The vectors **A→B** (associated with the axle) and **C→D** (associated with the macrocycle) point in the same direction and so the stereoisomer of rotaxane **6** shown is labelled as (Z_m)-**6**.

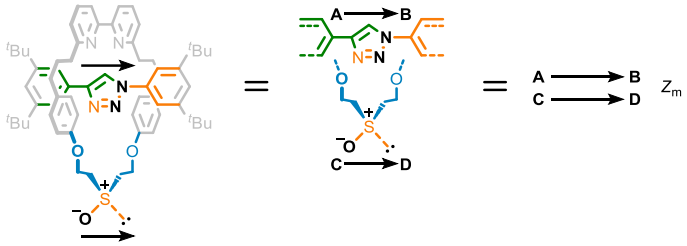

3.5.2.5. Absolute stereochemical assignment of catenane mechanical geometric isomers

Step 1: Identify the highest priority atom in the oriented macrocycle using the CIP priority rules and label it as "**A**".

Step 2: Moving outward from **A** in spheres, as per the CIP method for assigning covalent stereogenic centres, determine the highest priority atom (CIP) that can be used to define an orientation of the axle (typically a ligand of **A**) and label it as "**B**". The orientation of the macrocycle is defined by the vector **A→B**, which, where relevant, passes through the intervening atoms (i.e., follows the bonds).

Step 3: In the facially dissymmetric macrocycle, identify the highest priority prochiral group (or stereogenic unit in *meso* structures) using the CIP priority of the central atom. Redraw the macrocycle such that the in-plane substituents of the prochiral centre point towards the centre of the ring.

Step 4: Identify the highest priority exocyclic ligand of the identified prochiral centre, again using CIP priority, and label it as "**C**"; label the lower priority group "**D**".

Step 5: Redraw the assembly such that the vector **A→B** passes through the cavity of the facially dissymmetric macrocycle and the prochiral centre is in the in the cavity of the oriented ring.

Step 6: View the relative orientation of the vectors **A→B** and **C→D** at the crossing point between the rings. If the vectors point in the same direction, the molecule will be labelled as (Z_m). If they point in opposite directions, the molecule will be labelled as (E_m).

Worked example - catenane 14

Step 1: The highest atom according to the CIP rules in the oriented, triazole-containing macrocycle is the oxygen of the ester moiety, which is labelled as "**A**".

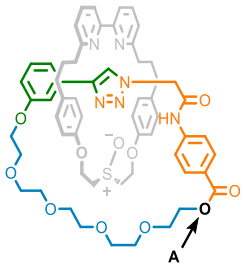

Step 2: Moving outwards, the highest priority atom defining an orientation of the ring is the carbon of the carboxylic moiety. This is labelled as "**B**", and allows to identify the vector **A→B.**

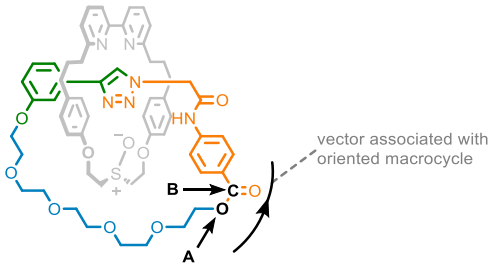

Step 3: The sulfoxide moiety is the only prochiral unit in the facially dissymmetric macrocycle so the macrocycle needs to be drawn such that the methylene units attached to S point into the cavity of the ring.

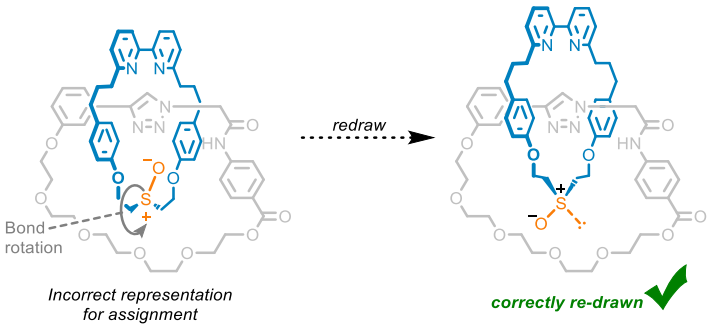

Step 4: The highest priority atom on the prochiral unit lying on the oriented macrocycle plane is the oxygen, which is labelled as "**C**". The lower priority group is the lone pair, which is labelled as "**D**".

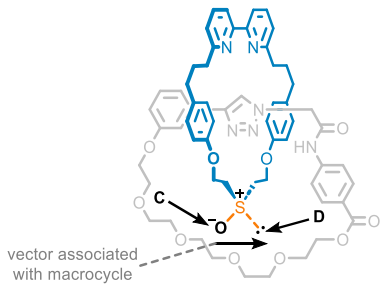

Step 5: Redraw the assembly such that the vector A→B passes through the facially dissymmetric macrocycle and the prochiral unit is in the centre of the oriented macrocycle.

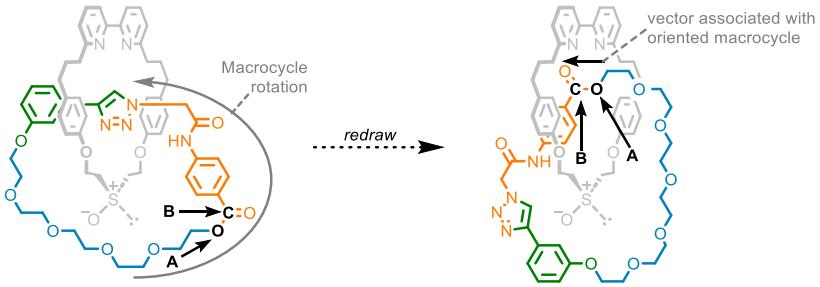

Step 6: View the relative orientations of the vectors **A→B** and **C→D** at the crossing point between the rings. As they point in opposite directions, the stereoisomer of catenene **14** shown is labelled as (E_m)-**14.**

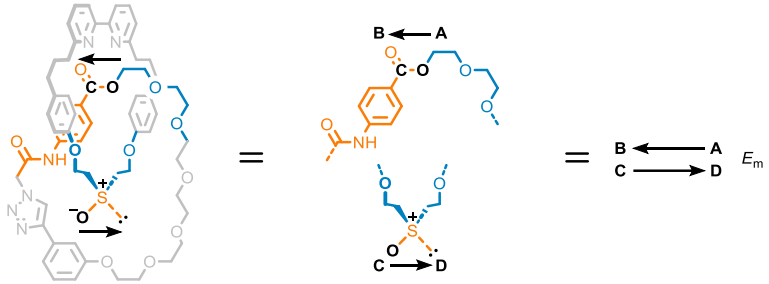

3.5.3. Effect of conditions on the diastereoselective synthesis of rotaxanes 6

Varying the solvent used in the AT-CuAAC synthesis of rotaxanes **6** showed a minor effect on the selectivity, whith the *dr* ranging between 20 and 29% with the exception of CH_3CN, which led to a drop in selectivity (Table 3.4, entry 4). A stronger effect could be observed by varying the temperature. A higher temperature (60 °C) led to a lower *de* (20%, Table 3.4, entry 8), while running the reaction at -20 °C led to an increase of the *de* to 40% (Table 3.4, entry 9). Furtherly lowering the temperature was detrimental to the selectivity, with a 37% *de* observed after running the reaction at -40 °C and a 16% *de* at -78 °C.

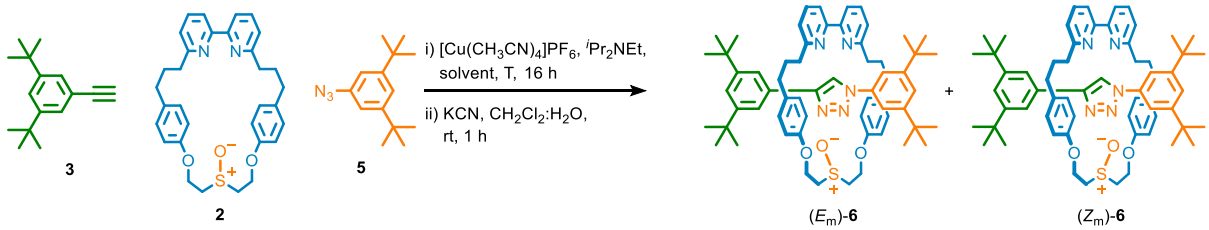

Scheme 3.9 - AT-CuAAC synthesis of rotaxanes **6**

Table 3.4 - Effect of solvent and temperature on the diastereoselectivity of rotaxane **6**

Entry	Solvent	Temperature [°C]	Selectivity[a]
1	CH_2Cl_2	rt	24% *de*
2	$CHCl_3$	rt	22% *de*
3	1:1 PhMe : CH_2Cl_2	rt	24% *de*
4	CH_3CN	rt	10% *de*
5	THF	rt	28% *de*
6	EtOH	rt	29% *de*
7	9:1 THF:H_2O	rt	25% *de*
8	THF	60	20% *de*
9	THF	-20	40% *de*
10	THF	-40	37% *de*
11	THF	-78	16% *de*

[a]Determined by ^{1}H-NMR analysis of the crude reaction mixture after demetallation

3.5.4. Effect of conditions on the enantioselectivity of the AT-CuAAC reaction

3.5.4.1. Effect of temperature on the direct enantioselective synthesis of rotaxanes 15

Varying the temperature of the AT-CuAAC synthesis of rotaxanes **15** led to an increased enantioselectivity at lower temperatures. This was evident for both enantiomers of **1f** and maximum *ee* values of +41.52% and -41.48% were achieved when (*R*)-**1f** and (*S*)-**1f** were used at -78 °C (Table 3.5, entries 3 and 6).

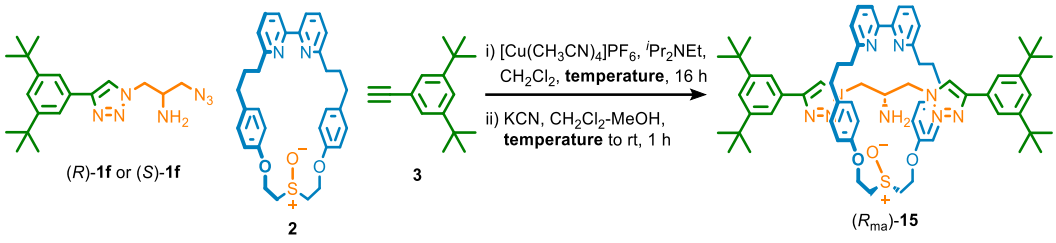

Scheme 3.10 - AT-CuAAC synthesis of rotaxanes **15**

Table 3.5 - Effect of temperature on the enantioselective synthesis of rotaxanes **15**

entry	Substrate	Conditions	Selectivity[a]
1	(*R*)-**1f**	CH_2Cl_2, rt	+16.10% *ee*
2	(*R*)-**1f**	CH_2Cl_2, –40 °C	+28.44% *ee*
3	(*R*)-**1f**	CH_2Cl_2, –78 °C	+41.52% *ee*
4	(*S*)-**1f**	CH_2Cl_2, rt	-16.70% *ee*
5	(*S*)-**1f**	CH_2Cl_2, –40 °C	-25.46 % *ee*
6	(*S*)-**1f**	CH_2Cl_2, –78 °C	-41.48% *ee*

[a]Determined by CSP-HPLC analysis of purified products as seen in Figure 3.213

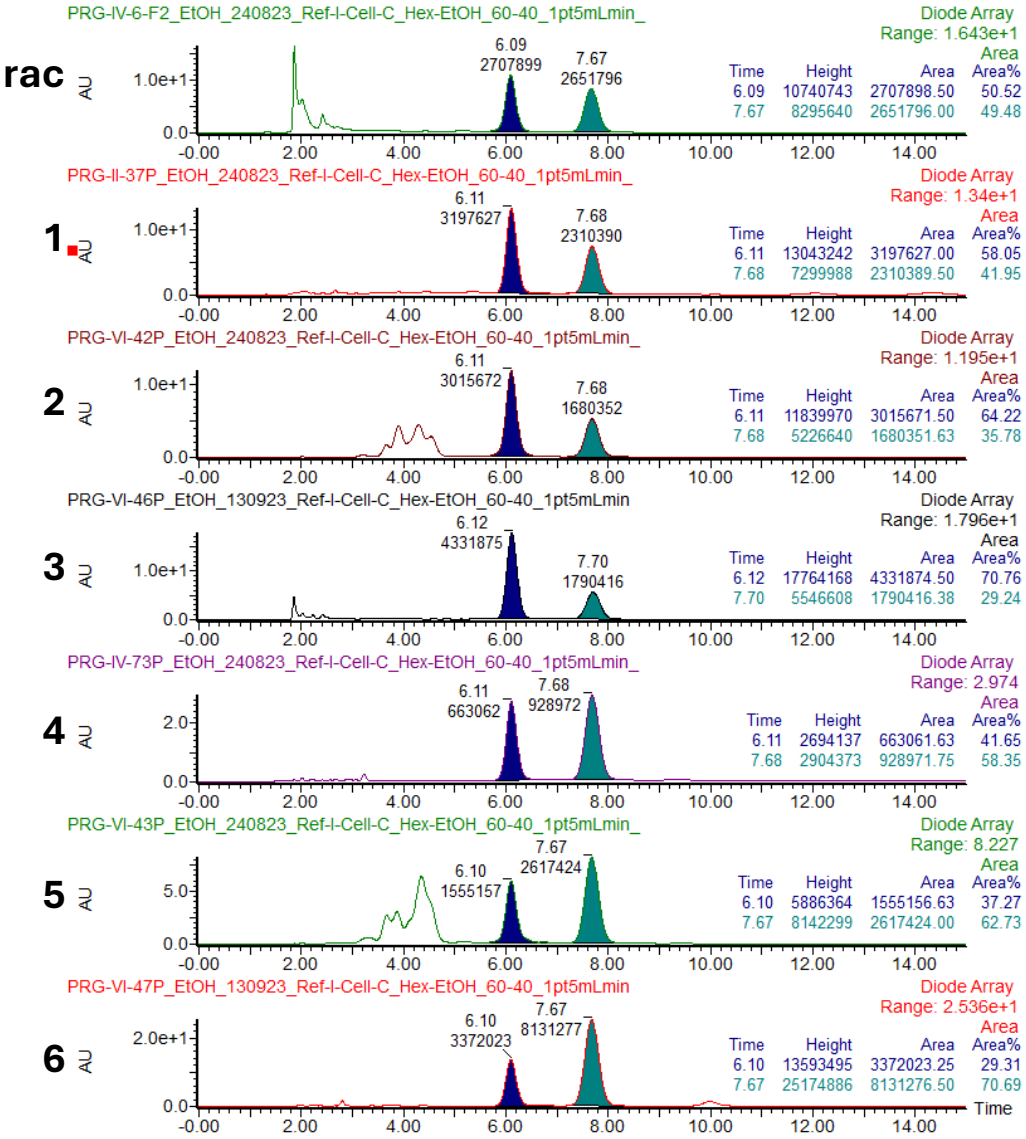

Figure 3.213 - CSP-HPLC analysis of rotaxane **15** produced under different conditions (numbers indicate the relevant entry in Table 3.5). Samples loaded in EtOH, Regis Reflect I-Cellulose C, *n*-hexane-EtOH 60 : 40, flowrate 1.5 $mLmin^{-1}$.

3.5.4.2. Effect of temperature on the enantioselective synthesis of rotaxanes 16

Varying the temperature of the AT-CuAAC synthesis of rotaxanes **16** led to an increased enantioselectivity at lower temperatures. This was evident for both enantiomers of **1g** and maximum *ee* values of +67.26% and -69.94% were achieved when (*R*)-**1g** and (*S*)-**1g** were used at -40 °C (Table 3.6, entries 2 and 5).

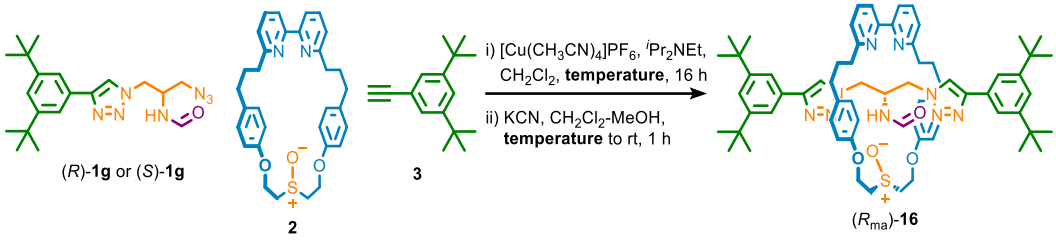

Scheme 3.11 - AT-CuAAC synthesis of rotaxanes **16**

Table 3.6 - Effect of temperature on the enantioselective synthesis of rotaxanes **16**

entry	Substrate	Conditions	Selectivity[a]
1	(*R*)-**1g**	CH_2Cl_2, rt	+57.06% *ee*
2	(*R*)-**1g**	CH_2Cl_2, –40 °C	+67.26% *ee*
3	(*R*)-**1g**	CH_2Cl_2, –78 °C	+58.70% *ee*
4	(*S*)-**1g**	CH_2Cl_2, rt	-61.94% *ee*
5	(*S*)-**1g**	CH_2Cl_2, –40 °C	-69.94 % *ee*
6	(*S*)-**1g**	CH_2Cl_2, –78 °C	-63.60% *ee*

[a]Determined by CSP-HPLC analysis of purified products as seen in Figure 3.214

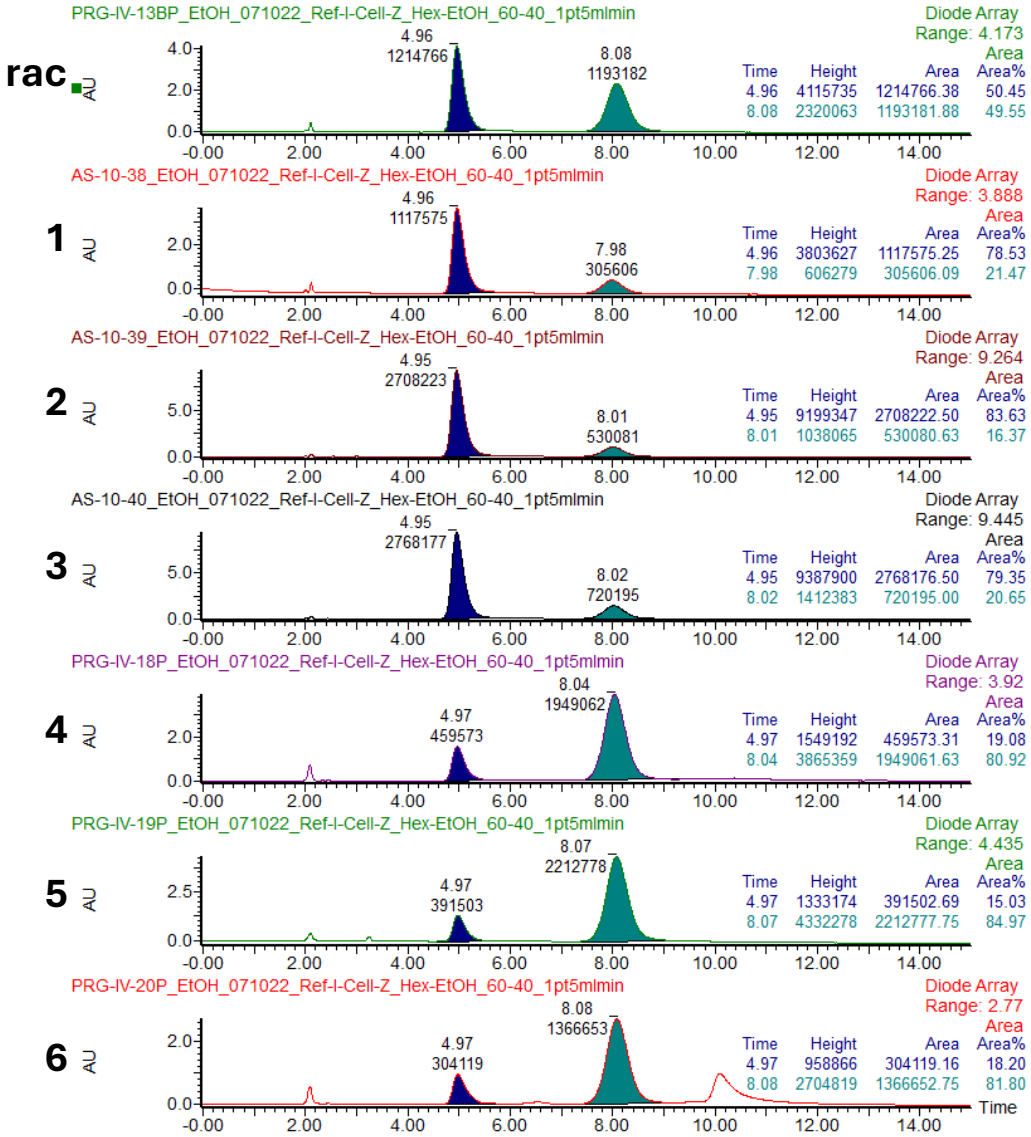

Figure 3.214 - CSP-HPLC analysis of rotaxane **16** produced under different conditions (numbers indicate the relevant entry in Table 3.6). Samples loaded in EtOH, Regis Reflect I-Cellulose Z, *n*-hexane-EtOH 60 : 40, flowrate 1.5 mLmin^{-1}.

3.5.5. Variable temperature NMR analysis

Rotaxanes **15** and **16** can exist as two diastereomeric co-conformations depending on whether the macrocycle is displaced across the amine or formamide unit to render the prochiral centre $R_{co\text{-}c}$ or $S_{co\text{-}c}$. If these co-conformations are in fast exchange, we would expect to see a single set of signals corresponding to weighted average of the spectra of the two diastereomers. If they are in slow exchange, we expect to see two sets of signals corresponding to the two diastereomeric co-conformations, the ratio between which is not required to be unity as they are not necessarily equienergetic.

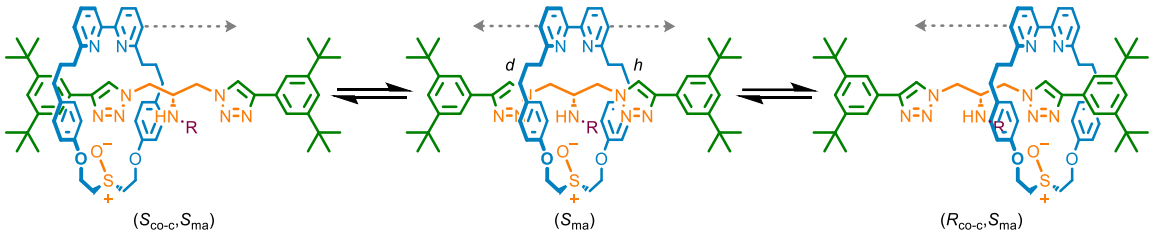

Scheme 3.12 - Illustration of the shuttling process in rotaxane **15** and **16** to afford diastereomeric co-conformations.

3.5.5.1. Variable temperature NMR analysis of rotaxane 15

At 298K, two sharp signals are observed corresponding to the triazole protons H_d and H_h, indicating that diastereomeric co-conformations (R_{ma},$R_{co\text{-}c}$)-**15** and (S_{ma},$R_{co\text{-}c}$)-**15** are either in fast exchange (with these signals corresponding to the weighted average of spectra for both co-conformers), or that they are in slow exchange with a significant preference for a single conformer (such that signals for only one co-conformer is observed). While we cannot unequivocally rule out that the system is in slow exchange, as the smaller NH_2 substituent is not expected to provide a prohibitive steric barrier to shuttling over the prochiral centre and that only a single pair of signals corresponding to H_d and H_h are observed at both lower (–50°C) and higher temperature (+50°C) rotaxane **15** is assumed to be under fast-exchange (Figure 3.215).

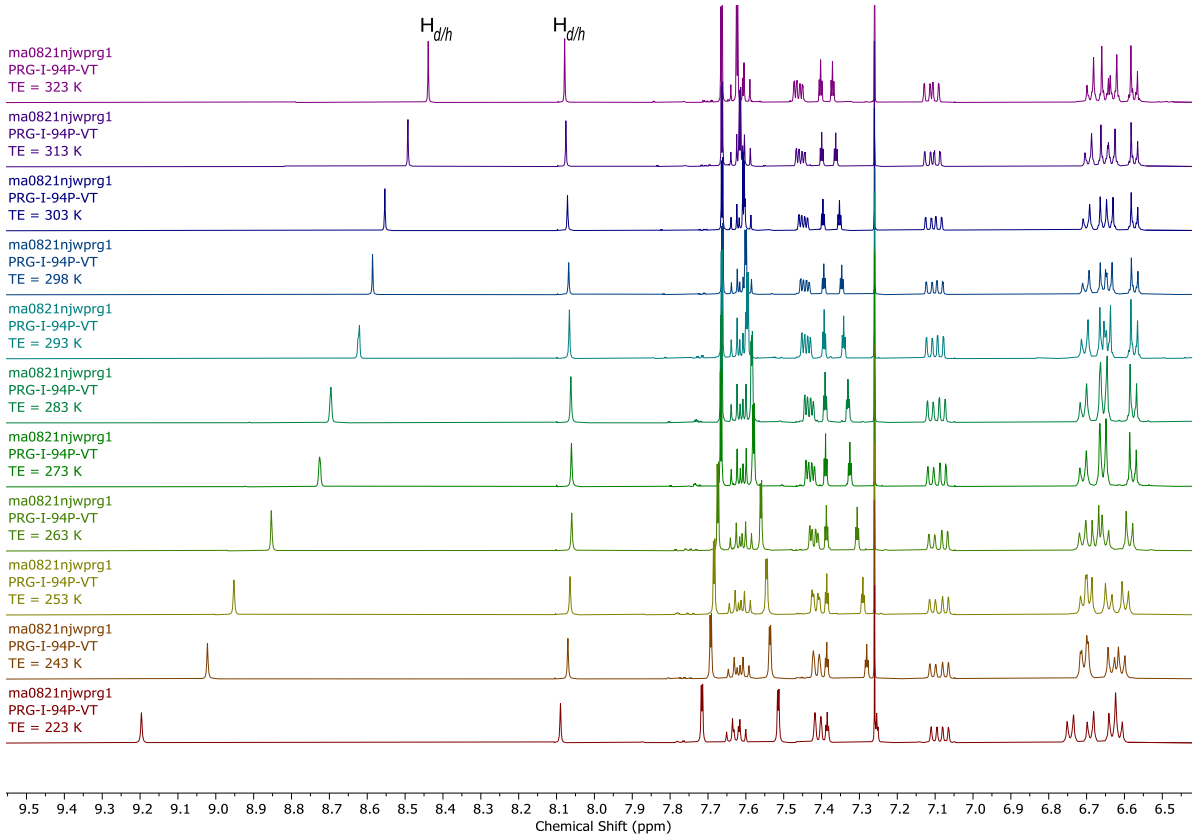

Figure 3.215 - Partial ^{1}H VT-NMR ($CDCl_3$, 500 MHz) of amine rotaxane **15**.

3.5.5.2. Variable temperature NMR analysis of rotaxane 16

^{1}H NMR analysis (Figure 3.216) suggests that at 298 K exchange between these co-conformations is relatively slow on the NMR timescale - the peaks corresponding to triazole protons H_d and H_h appear as two broad resonances rather than two sharp signals (fast exchange) or two sets of two signals (slow exchange). In keeping with this, raising the temperature resulted in a sharpening of the signals corresponding to H_d and H_h, suggesting that at 298 K the spectrum is above the coalescence temperature. Conversely, cooling the sample caused the two signals observed at 298 K to broaden and shift (one to higher ppm, one to lower). At low temperature (223 K) one becomes sharper and stabilises around 9.85 ppm. The other seems to be obscured by other resonances. Also, as the temperature is lowered, a broad doublet that we assign as the NH of the formamide unit shifts to higher ppm and broadens before sharpening again. At 223 K, a minor second set of signals appears that could correspond to the occupied triazole and NH of the second diastereomeric co-conformation. If this is the correct interpretation, one of the diastereomeric co-conformations of rotaxane **16** is significantly preferred.

Based on this analysis, we are confident that the formamide unit is small enough to permit the macrocycle to shuttle between the compartments at rt, confirming that the only fixed stereogenic unit is the mechanical axial unit. Further work is required to fully establish the co-conformational behaviour of the mechanical axial stereogenic unit.

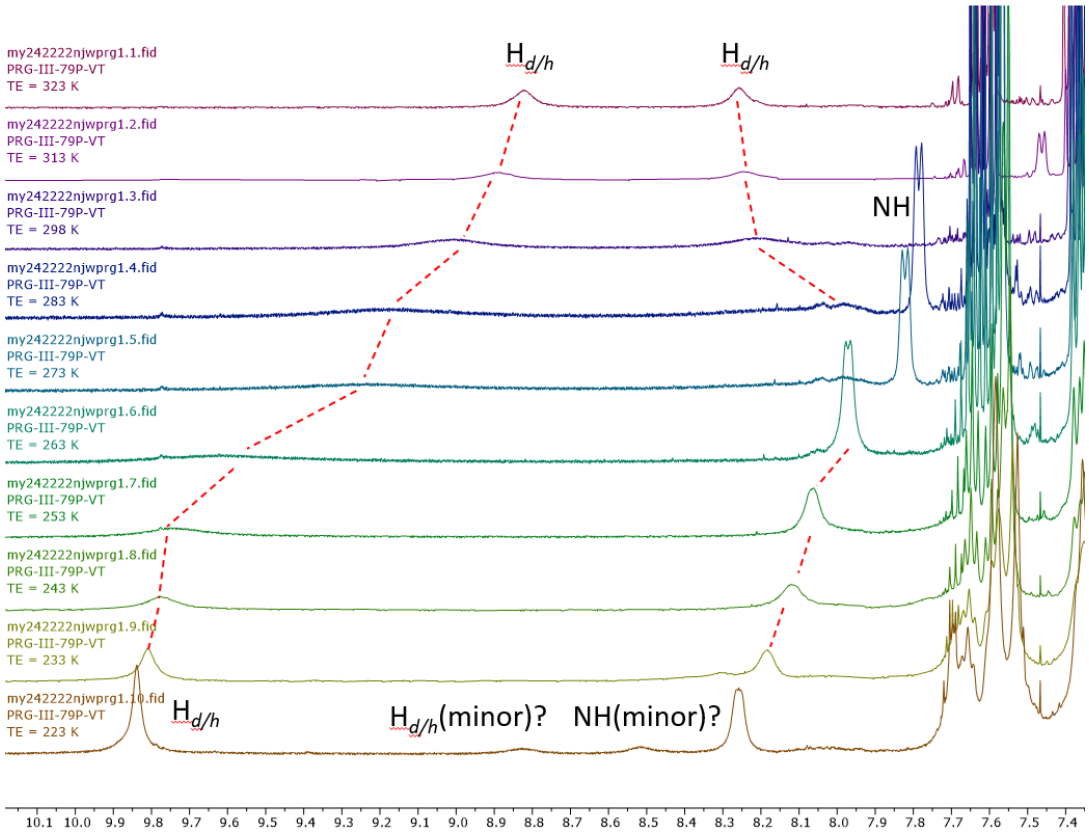

Figure 3.216 - Partial ^{1}H VT-NMR ($CDCl_3$, 500 MHz) of formamide rotaxane **16**.

3.5.6. Single crystal X-ray diffraction analysis

Single Crystal X-ray Diffraction Data for rotaxane (R_{ma},$R_{co\text{-}c}$)-4d

Single crystals of (R_{ma},$R_{co\text{-}c}$)-**4d** were grown by slow vapour diffusion of n-pentane into a concentrated CH_2Cl_2 solution of (R_{ma},$R_{co\text{-}c}$)-**4d**, yielding large colourless plate crystals. Data was collected at 100 K on a Rigaku 007 HF diffractometer equipped with a HyPix 6000HE hybrid pixel array detector. Cell determination, data reduction, cell refinement, and absorption correction were processed by CrysalisPro[39] The structure was solved within Olex2[40] by ShelXT[41] with refinement by ShelXL.[42] The asymmetric cell contained two molecules of $C_{69}H_{84}N_9O_4F_3S$ and disordered solvent. Modelling of the solvent suggested the presence of three dichloromethane molecules and one pentane molecule. The disorder of the solvent, however, was found to preclude a satisfactory solution and so the program SQUEEZE[43] implemented within PLATON[44] was used to account for the electron density within this region of the unit cell. Solvent accessible voids of 1593Å^3 were identified and 469 electrons per unit cell were recovered.

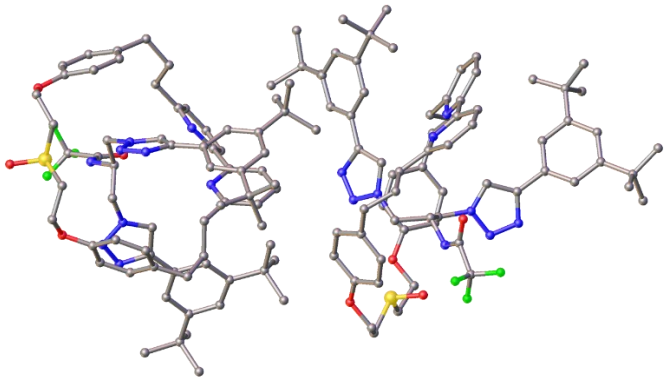

Figure 3.217 - Solid state structurer of (R_{ma},$R_{co\text{-}c}$)-**4d** shown in ball and stick mode with H-atoms and disorder omitted for clarity. N.B. this is a Z'=2 structure with two crystallographically independent rotaxanes in the asymmetric unit.

Table 3.7 - Crystal data and structure refinement for (R_{ma},$R_{co\text{-}c}$)-**4d**

CCDC Number	2303663	Z/Z`	4/2
Empirical Formula	$C_{69}H_{84}N_9O_4F_3S$	r_{calc} g/cm^3	1.039
Formula Weight	1192.51	m/mm^{-1}	0.096
Temperature/K	100	Crystal size/mm^3	0.36×0.22×0.08
Crystal System	Triclinic	Radiation	Mo Ka
Space Group	*P*-1	2Q range/˚	1.6 – 29.2
a/Å	18.6219	Reflections Collected	148929
b/Å	19.1615	Independent Reflections	34957
c/Å	22.3951	Data/parameters/restraints	22248/1621/1084
α/˚	85.885	Goodness-of-fit on F^2	1.015
β/˚	77.745	Final R-factor [I ≥ 2s(I)]	0.0498
γ/˚	77.691	Final R indexes [all data]	R1 = 0.1404, wR2 = 0.2527
Volume/Å^3	7188.46	Largest diff. peak/hole e Å^{-3}	1.13/-0.88

Single Crystal X-ray Diffraction Data for rotaxane (Z_m)-6

Single colourless block-shaped crystals of (Z_m)-**6** were grown by slow evaporation of an Et_2O-petrol solution. A suitable crystal 0.60×0.19×0.11 mm^3 was selected and mounted on a MITIGEN holder in oil on a Rigaku 007HF diffractometer with HF Varimax confocal mirrors, an AFC11 goniometer and HyPix 6000HE detector. The crystal was kept at a steady T = 100(2) K during data collection. The structure was solved with the ShelXT 2018/2[42] structure solution program using the using dual methods solution method and by using Olex2 1.5-alpha as the graphical interface.[40] The model was refined with version of olex2.refine 1.5-alpha using full matrix least squares minimisation on F^2 minimisation.[45] All non-hydrogen atoms were refined anisotropically. Hydrogen atom positions were calculated geometrically and refined using the riding model. Thermal restraints applied to solvent isohexane.

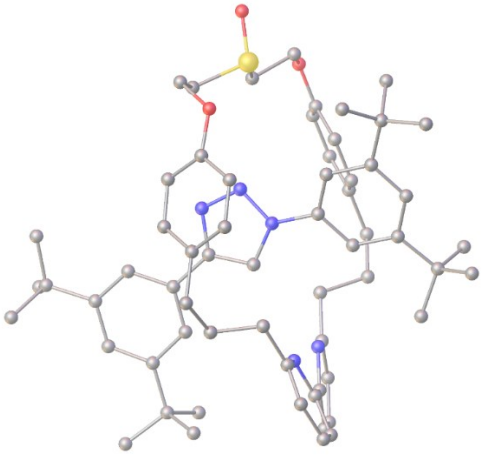

Figure 3.218 - Solid state structure of (Z_m)-**6** shown in ball and stick mode with the solvent isohexane molecule and H-atoms omitted and minor disorder component 'ghosted' for clarity.

Table 3.8 - Crystal data and structure refinement for (Z_m)-**6**

CCDC Number	2303663	Z/Z`	4/1
Empirical Formula	$C_{69}H_{84}N_9O_4F_3S$	r_{calc} g/cm^3	1.115
Formula Weight	1058.58	m/mm^{-1}	0.819
Temperature/K	100	Crystal size/mm^3	0.60×0.19×0.11
Crystal System	monoclinic	Radiation	Cu Ka
Space Group	$P2_1/n$	2Q range/˚	3.39 – 70.33
a/Å	17.5926	Reflections Collected	59812
b/Å	16.1257	Independent Reflections	11798
c/Å	22.3794	Data/parameters/restraints	10779/709/30
α/˚	90	Goodness-of-fit on F^2	1.0411
β/˚	96.449	Final R-factor [I ≥ 2s(I)]	0.0302
γ/˚	90	Final R indexes [all data]	R1 = 0.0567, wR2 = 0.1495
Volume/$Å^3$	6308.70	Largest diff. peak/hole e $Å^{-3}$	0.8447/-0.6096

Single Crystal X-ray Diffraction Data for rotaxane (E_m)-6

Single colourless needle-shaped crystals of (E_m)-**6** were grown by slow evaporation of an Et_2O-petrol solution. A suitable crystal 0.27×0.02×0.01 mm^3 was selected and mounted on a MITIGEN holder in oil on a Rigaku 007HF diffractometer with HF Varimax confocal mirrors, an AFC11 goniometer and HyPix 6000HE detector. The crystal was kept at a steady T = 100(2) K during data collection. The structure was solved with the ShelXT 2018/2[7] structure solution program using the using dual methods solution method and by using Olex2 1.5-alpha[8] as the graphical interface. The model was refined with version of olex2.refine 1.5-alpha[9] using full matrix least squares minimisation on F^2 minimisation. All non-hydrogen atoms were refined anisotropically. Hydrogen atom positions were calculated geometrically and refined using the riding model. Thermal restraints applied to solvent isohexane.

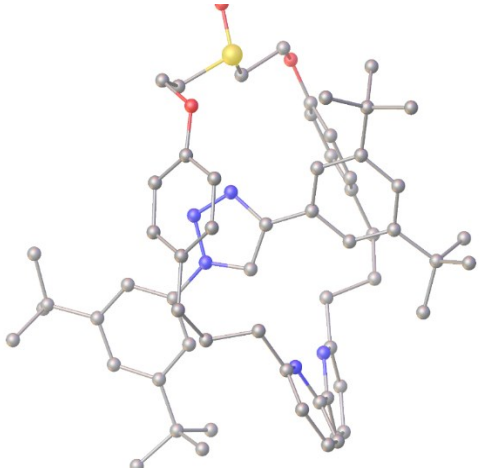

Figure 3.219 - Solid state structure of (E_m)-**6** shown in ball and stick mode with the solvent isohexane molecule and H-atoms omitted and minor disorder component 'ghosted' for clarity.

Table 3.9 - Crystal data and structure refinement for (E_m)-**6**

CCDC Number	2307122	Z/Z`	4/1
Empirical Formula	$C_{68}H_{91}N_5O_3S$	r_{calc} g/cm^3	1.118
Formula Weight	1058.578	m/mm^{-1}	0.822
Temperature/K	100	Crystal size/mm^3	0.27×0.02×0.01
Crystal System	monoclinic	Radiation	Cu Ka
Space Group	$P2_1/n$	2Q range/˚	3.03 – 51.08
a/Å	17.6111	Reflections Collected	36644
b/Å	16.0502	Independent Reflections	6846
c/Å	22.3898	Data/parameters/restraints	6099/709/30
α/˚	90	Goodness-of-fit on F^2	1.0674
β/˚	96.445	Final R-factor [I ≥ 2s(I)]	0.0506
γ/˚	90	Final R indexes [all data]	R1 = 0.0684, wR2 = 0.1754
Volume/$Å^3$	6288.7	Largest diff. peak/hole e $Å^{-3}$	0.8008/-0.4720

Single Crystal X-ray Diffraction Data for rotaxane (Z_m)-9

Single colourless slab-shaped crystals of (Z_m)-**9** were recrystallised from a mixture of ^{n}pentane and CH_2Cl_2 by solvent layering. A suitable crystal was selected and mounted on a MITIGEN holder in oil on a Rigaku 007HF diffractometer equipped with Arc)Sec VHF Varimax confocal mirrors and a UG2 goniometer and HyPix 6000HE detector. The crystal was kept at a steady T = 100(2) K during data collection. The structure was solved with the ShelXT 2018/2[7] structure solution program using the using dual methods solution method and by using Olex2 1.5-alpha[8] as the graphical interface. The model was refined with ShelXL 2018/3 (Sheldrick, 2015)[41] using full matrix least squares minimisation on F^2 minimisation. All non-hydrogen atoms were refined anisotropically. Hydrogen atoms positions were calculated geometrically except amine H-atoms which were located in the difference map. All hydrogen atoms were refined with the riding model.

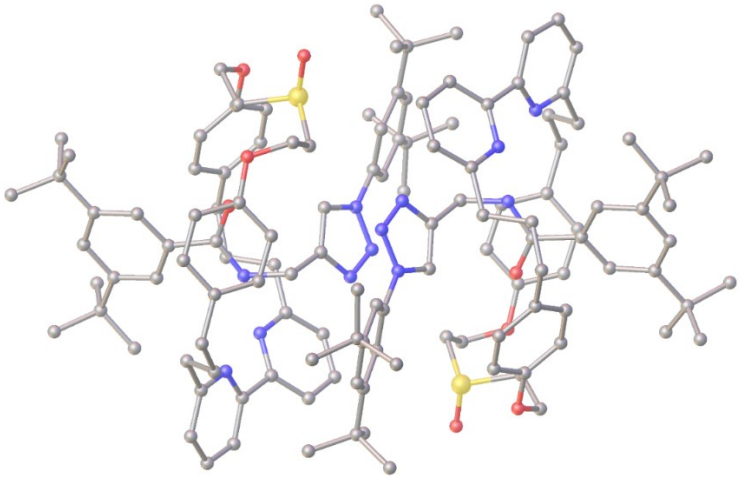

Figure 3.220 - Solid state structurer of (Z_m)-**9** shown in ball and stick mode with H-atoms omitted for clarity. N.B. this is a Z'=2 structure with two crystallographically independent rotaxanes in the asymmetric unit.

Table 3.10 - Crystal data and structure refinement for (Z_m)-**9**

CCDC Number	2307119	Z/Z`	8/2
Empirical Formula	$C_{64}H_{80}N_6O_4S$	r_{calc} g/cm^3	1.185
Formula Weight	1029.40	m/mm^{-1}	0.903
Temperature/K	100	Crystal size/mm^3	0.10×0.09×0.02
Crystal System	monoclinic	Radiation	Cu Ka
Space Group	monoclinic	2Q range/°	2.490 – 75.129
a/Å	$P2_1/n$	Reflections Collected	123562
b/Å	26.6812	Independent Reflections	23477
c/Å	13.15830	Data/parameters/restraints	18146 /1381/0
α/°	34.4438	Goodness-of-fit on F^2	1.024
β/°	90	Final R-factor [I ≥ 2s(I)]	0.0302
γ/°	107.3140	Final R indexes [all data]	R1 = 0.0736, wR2 = 0.1594
Volume/Å^3	90	Largest diff. peak/hole e Å^{-3}	0.600/-0.507

Single Crystal X-ray Diffraction Data for rotaxane (*E*$_m$)-11

Single colourless slab-shaped crystals of (*E*$_m$)-**11** were grown by slow evaporation of a CH_2Cl_2 solution at room temperature. A suitable crystal was selected and mounted on a MITIGEN holder in oil on a Rigaku 007HF diffractometer equipped with Arc)Sec VHF Varimax confocal mirrors and a UG2 goniometer and HyPix 6000HE detector. The crystal was kept at a steady *T* = 100(2) K during data collection. The structure was solved with the ShelXT 2018/2[7] structure solution program using the using dual methods solution method and by using Olex2 1.5-alpha[8] as the graphical interface. The model was refined with ShelXL 2018/3[10] using full matrix least squares minimisation on F^2 minimisation. All non-hydrogen atoms were refined anisotropically. Hydrogen atoms positions were calculated geometrically except amine H-atoms which were located in the difference map. All hydrogen atoms were refined with the riding model. One tBu group was modelled as disordered with equal distance 1,2 and 1,3 geometric restraints applied to equivalent atom pairs of each disorder component. Thermal restraints were applied to all disorder components.

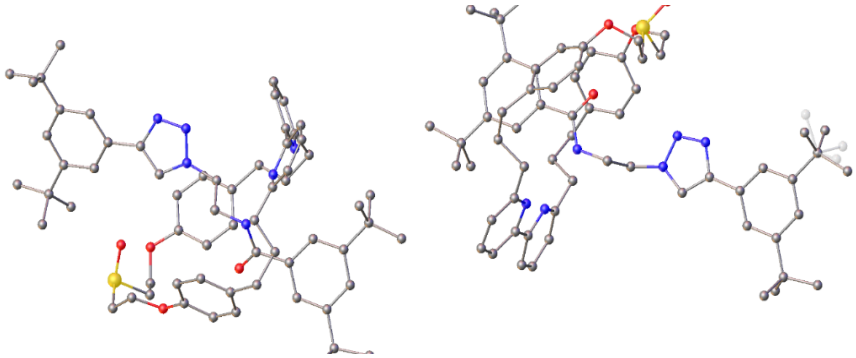

Figure 3.221 - Solid state structure of (*E*$_m$)-**11** shown in ball and stick mode with H-atoms omitted and minor disorder component 'ghosted' for clarity. N.B. this is a Z'=2 structure with two crystallographically independent rotaxanes in the asymmetric unit.

Table 3.11 - Crystal data and structure refinement for (*E*$_m$)-**11**

CCDC Number	2303663	Z/Z`	16/2
Empirical Formula	$C_{65}H_{82}N_6O_4S$	r_{calc} g/cm^3	1.177
Formula Weight	1043.42	m/mm^{-1}	0.892
Temperature/K	100	Crystal size/mm^3	0.11×0.11×0.04
Crystal System	orthorhombic	Radiation	Cu Ka
Space Group	*Pbca*	2Q range/˚	3.719 – 66.595
a/Å	16.2520	Reflections Collected	102466
b/Å	19.8197	Independent Reflections	20372
c/Å	73.1056	Data/parameters/restraints	15040 /1430/39
α/˚	90	Goodness-of-fit on F^2	1.062
β/˚	90	Final R-factor [I ≥ 2s(I)]	0.1019
γ/˚	90	Final R indexes [all data]	R1 = 0.1245, wR2 = 0.2545
Volume/Å^3	23548.0	Largest diff. peak/hole e Å^{-3}	0.745/-0.479

Single Crystal X-ray Diffraction Data for rotaxane *rac*-16

Single colourless lath-shaped crystals of *rac*-**16** were grown by slow evaporation of a Et_2O solution at in a fridge (*ca*. 5 °C). A suitable crystal was selected and mounted on a MITIGEN holder in oil on a Rigaku 007HF diffractometer equipped with Arc)Sec VHF Varimax confocal mirrors and a UG2 goniometer and HyPix 6000HE detector. The crystal was kept at a steady T = 100(2) K during data collection. The structure was solved with the ShelXT 2018/2[42] structure solution program using the using dual methods solution method and by using Olex2 1.5-alpha as the graphical interface.[40] The model was refined with olex2.refine 1.5-alpha using full matrix least squares minimisation on F^2 minimisation.[45] All non-hydrogen atoms were refined anisotropically. Hydrogen atom positions were calculated geometrically and refined using the riding model. The disorder in the macrocycle and triazole was assumed to be linked and modelled accordingly (ca.78:22). Additional disorder in the iPr groups was modelled independently (ca. 84:16 and ca, 63:37). Equivalent 1,2 and 1,3 pairs of atoms of each disorder component have had equal distance restraints applied. RIGU thermal restraints were applied to all atoms. ISOR thermal restraints were applied to minor disorder component triazole N-atoms.

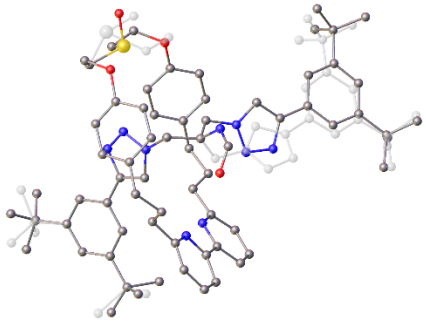

Figure 3.222 - Solid state structurer of *rac*-**16** shown in ball and stick mode with H-atoms omitted and minor disorder component 'ghosted' for clarity.

Table 3.12 - Crystal data and structure refinement for *rac*-**16**

CCDC Number	2307076	Z/Z`	8/1
Empirical Formula	$C_{68}H_{84}N_9O_4S$	r_{calc} g/cm^3	1.193
Formula Weight	1123.549	m/mm^{-1}	0.890
Temperature/K	100	Crystal size/mm^3	0.65×0.04×0.01
Crystal System	monoclinic	Radiation	Cu Ka
Space Group	*C*2/*c*	2Q range/˚	2.75 – 66.60
a/Å	36.4756	Reflections Collected	52802
b/Å	10.6634	Independent Reflections	11009
c/Å	32.8280	Data/parameters/restraints	7468/1043/1141
α/˚	90	Goodness-of-fit on F^2	1.0793
β/˚	101.629	Final R-factor [I ≥ 2s(I)]	0.0817
γ/˚	90	Final R indexes [all data]	R1 = 0.1259, wR2 = 0.2964
Volume/Å^3	12506.5	Largest diff. peak/hole e Å^{-3}	1.4952/-0.8568

3.6. Bibliography

1 C. J. Bruns, J. F. Stoddart, *The Nature of the Mechanical Bond: From Molecules to Machines*, John Wiley & Sons, Hoboken, New Jersey, **2017**.

2 G. Schill, *Catenanes, Rotaxanes and Knots*, Academic Press, New York, **1971**.

3 We have recently identified a second form of rotaxane geometric stereochemistry and so have proposed that these are disambiguated by the addition of the type 1/2 label: A. Savoini, P. R. Gallagher, A. Saady, S. M. Goldup, *J. Am. Chem. Soc.* **2024**, *146*, 8472–8479

4 The stereochemistry of rotaxanes and catenanes whose macrocycle contains one or more covalent stereogenic centre in the main chain (e.g., as found in cyclodextrin rings) and whose axle/second ring respectively are oriented can be fully described by a covalent stereodescriptor and either a mechanical planar stereolable or mechanical geometric stereolabel. We prefer the mechanically planar description as, in the case of catenanes, this typically although not always[34g] refers to a topological source of stereochemistry, one of the unusual properties of such systems. For selected examples of structures that conform to this class of molecule see - (a) D. Armspach, P. R. Ashton, R. Ballardini, V. Balzani, A. Godi, C. P. Moore, L. Prodi, N. Spencer, J. F. Stoddart, M. S. Tolley, T. J. Wear, D. J. Williams, *Chem. Eur. J.* **1995**, *1*, 33–55. (b) M. R. Craig, M. G. Hutchings, T. D. W. Claridge, H. L. Anderson, *Angew. Chem. Int. Ed.* **2001**, *40*, 1071–1074. (c) Q. C. Wang, X. Ma, D. H. Qu, H. Tian, *Chem. Eur. J.* **2006**, *12*, 1088–1096. (d) Bruns, *Symmetry* **2019**, *11*, 1249. (e) Y. Makita, N. Kihara, T. Takata, *Supramol. Chem.* **2021**, *33*, 1–7. (f) H. V. Schroder, Y. Zhang, A. J. Link, *Nat. Chem.* **2021**, *13*, 850–857. (g) C. Lopez-Leonardo, A. Saura-Sanmartin, M. Marin-Luna, M. Alajarin, A. Martinez-Cuezva, J. Berna, *Angew. Chem. Int. Ed.* **2022**, *61*, e202209904. (h) E. Liu, S. Cherraben, L. Boulo, C. Troufflard, B. Hasenknopf, G. Vives, M. Sollogoub, *Chem* **2023**, *9*, 1147–1163.

5 Selected examples - (a) A. Arduini, F. Ciesa, M. Fragassi, A. Pochini, A. Secchi, *Angew. Chem. Int. Ed.* **2005**, *44*, 278-281. (b) A. Arduini, R. Bussolati, A. Credi, G. Faimani, S. Garaudee, A. Pochini, A. Secchi, M. Semeraro, S. Silvi, M. Venturi, *Chem. Eur. J.* **2009**, *15*, 3230–3242. (c) T. Pierro, C. Gaeta, C. Talotta, A. Casapullo, P. Neri, *Org. Lett.* **2011**, *13*, 2650–2653. (d) A. Arduini, R. Bussolati, A. Credi, A. Secchi, S. Silvi, M. Semeraro, M. Venturi, *J. Am. Chem. Soc.* **2013**, *135*, 9924–9930. (e) R. Ciao, C. Talotta, C. Gaeta, L. Margarucci, A. Casapullo, P. Neri, *Org. Lett.* **2013**, *15*, 5694–5697. (f) V. Zanichelli, G. Ragazzon, A.

Arduini, A. Credi, P. Franchi, G. Orlandini, M. Venturi, M. Lucarini, A. Secchi, S. Silvi, *Eur. J. Org. Chem.* **2016**, *2016*, 1033–1042. (g) P. La Manna, C. Talotta, C. Gaeta, A. Soriente, M. De Rosa, P. Neri, *J. Org. Chem.* **2017**, *82*, 8973–8983. (h) M. Bazzoni, L. Andreoni, S. Silvi, A. Credi, G. Cera, A. Secchi, A. Arduini, *Chem. Sci.* **2021**, *12*, 6419–6428. (i) G. Cera, A. Arduini, A. Secchi, A. Credi, S. Silvi, *Chem. Rec.* **2021**, *21*, 1161–1181. (j) L. Andreoni, F. C. Bonati, J. Groppi, D. Balestri, G. Cera, A. Credi, A. Secchi, S. Silvi, *Chem. Commun.* **2023**, *59*, 4970–4973.

6 Selected examples - (a) M. Xue, Y. S. Su, C. F. Chen, *Chem. Eur. J.* **2010**, *16*, 8537–8544. (b) Y.-X. Xia, T. Xie, Y. Han, C.-F. Chen, *Org. Chem. Front.* **2014**, *1*. (c) H. X. Wang, Z. Meng, J. F. Xiang, Y. X. Xia, Y. Sun, S. Z. Hu, H. Chen, J. Yao, C. F. Chen, *Chem. Sci.* **2016**, *7*, 469–474. (d) J. S. Cui, Q. K. Ba, H. Ke, A. Valkonen, K. Rissanen, W. Jiang, *Angew. Chem. Int. Ed.* **2018**, *57*, 7809–7814. (e) K. A. Li, Z. Wang, C. D. Xie, T. Chen, H. Qiang, Y. A. Liu, X. S. Jia, W. B. Hu, K. Wen, *Org. Biomol. Chem.* **2019**, *17*, 4975–4978.

7 (a) K. A. Li, Z. Wang, C. D. Xie, T. Chen, H. Qiang, Y. A. Liu, X. S. Jia, W. B. Hu, K. Wen, *Org. Biomol. Chem.* **2019**, *17*, 4975–4978. (b) X. Wang, Q. Gan, B. Wicher, Y. Ferrand, I. Huc, *Angew. Chem. Int. Ed.* **2019**, *58*, 4205–4209.

8 (a) C. Gaeta, C. Talotta, S. Mirra, L. Margarucci, A. Casapullo, P. Neri, *Org. Lett.* **2013**, *15*, 116–119. (b) V. Zanichelli, L. Dallacasagrande, A. Arduini, A. Secchi, G. Ragazzon, S. Silvi, A. Credi, *Molecules* **2018**, *23*, 1156.

9 For a detailed discussion of facial dissymmetry in interlocked structures see ref. 11.

10 F. Saito, J. W. Bode, *Chem. Sci.* **2017**, *8*, 2878–2884.

11 J. R. J. Maynard, P. Gallagher, D. Lozano, P. Butler, S. M. Goldup, *Nat. Chem.* **2022**, *14*, 1038–1044.

12 (a) E. M. G. Jamieson, F. Modicom, S. M. Goldup, *Chem. Soc. Rev.* **2018**, *47*, 5266–5311. (b) N. Pairault, J. Niemeyer, *Synlett* **2018**, *29*, 689–698. (c) N. H. Evans, *Chem. Eur. J.* **2018**, *24*, 3101–3112.

13 H. L. Frisch, E. Wasserman, *J. Am. Chem. Soc.* **1961**, *83*, 3789–3795.

14 J. R. J. Maynard, S. M. Goldup, *Chem* **2020**, *6*, 1914–1932.

15 M. Denis, S. M. Goldup, *Nat. Rev. Chem.* **2017**, *1*, 0061.

16 V. Aucagne, K. D. Hanni, D. A. Leigh, P. J. Lusby, D. B. Walker, *J. Am. Chem. Soc.* **2006**, *128*, 2186–2187.

17 A. Saady, S. M. Goldup, *Chem* 2023, *9*, 2110–2127.

18 The suffix "ma" indicates that the label refers to the mechanical axial stereogenic unit. The suffix "co-c" indicates that the stereochemical label refers to the co-conformational covalent stereogenic unit.[11]

19 We note that others have referred to such co-conformational covalent stereochemistry as "mechanical point chirality" (Y. Cakmak, S. Erbas-Cakmak, D. A. Leigh, *J. Am. Chem. Soc.* **2016**, *138*, 1749). We introduced the co-conformational covalent description[12a] as it is more precise and information rich; it highlights that that the stereogenic unit arises due to desymmetrization of a covalent pro-stereogenic unit and that these stereoisomers can in principle be converted by co-conformational movement. One of the reviewers of this manuscript suggested the term "co-configurational isomers" might be more useful and clearer for a non-expert. We hesitate to adopt it here as changes in nomenclature should be properly discussed and put in the wider context of the field. However, we wanted to give credit to our anonymous reviewer for this intriguing suggestion and will consider its use in future.

20 We note that the previously reported SCXRD structure of minor diastereomer (*S*ma,*R*co-c)-**4a**[11] contains the same interaction but in this case it occurs intermolecularly between neighboring molecules in the unit cell, as observed for **4d** (Figure 3.2).

21 (a) E. A. Neal, S. M. Goldup, *Chem. Sci.* **2015**, *6*, 2398-2404. (b) E. A. Neal, S. M. Goldup, *Angew. Chem. Int. Ed.* **2016**, *55*, 12488–12493. (b) F. Modicom, E. M. G. Jamieson, E. Rochette, S. M. Goldup, *Angew. Chem. Int. Ed.* **2019**, *58*, 3875–3879.

22 J. Winn, A. Pinczewska, S. M. Goldup, *J. Am. Chem. Soc.* **2013**, *135*, 13318-13321.

23 We note that our results cannot rule out that either K_{eq} or $k_{SS}/_{SR}$ depends on a large negative entropy of reaction or activation respectively, which may also account for the unexpected temperature dependence of the AT-CuAAC reaction.

24 The subscript is intended to indicate the mechanical origin of the stereochemistry. For a detailed discussion of how the mechanical stereogenic unit is assigned in such systems, see Supporting Information section 3.5.2.

25 Other combinations of solvent and temperature did not improve the reaction stereoselectivity. See Supporting Information section 3.5.3 for further details.

26 (a) M. A. Jinks, A. de Juan, M. Denis, C. J. Fletcher, M. Galli, E. M. G. Jamieson, F. Modicom, Z. Zhang, S. M. Goldup, *Angew. Chem. Int. Ed.* **2018**, *57*, 14806–14810. (b) A. de Juan, D. Lozano, A. W. Heard, M. A. Jinks, J. M. Suarez, G. J. Tizzard, S. M. Goldup, *Nat. Chem.* **2022**, *14*, 179–187.

27 Unfortunately, we were unable to determine the absolute stereochemistry of rotaxane **10** as crystals suitable for SCXRD analysis were not forthcoming.

28 J. E. M. Lewis, F. Modicom, S. M. Goldup, *J. Am. Chem. Soc.* **2018**, *140*, 4787–4791.

29 K. Hirose, M. Ukimi, S. Ueda, C. Onoda, R. Kano, K. Tsuda, Y. Hinohara, Y. Tobe, *Symmetry* **2018**, *10*, 20.

30 A. W. Heard, S. M. Goldup, *Chem* **2020**, *6*, 994–1006.

31 ^{1}H NMR analysis of **16** confirmed that the ring is able to shuttle past the formamide unit. See Supporting Information section 3.5.5.

32 The ^{1}H spectra of rotaxanes **15** and **16** are extremely complicated because the mechanical bond renders any nuclei not related by single bond rotation (e.g., the ^{t}Bu groups of the axle unit) magnetically inequivalent; for example, all the methylene protons flanking the amine unit in the axle are magnetically inequivalent. For this reason, when assigning the ^{1}H NMR spectra of these molecules (see ESI) we took the decision to assign different letters to carbon atoms (and the associated protons) whose equivalence is lifted by the mechanical bond and reserved prime notation to differentiate diastereotopic geminal protons. Thus, although the triazole protons of rotaxanes **15** and **16** are labelled in Scheme 3.6 as H_d and $H_{d'}$ in accordance with standard practice for diastereotopic signals to aid an intuitive understanding of the diagram, they are assigned as H_d and H_h in their characterization data

33 For recent examples of functionalized and functional molecules synthesized in good to excellent yield using the AT-CuAAC reaction mediated by bipyridine macrocycles see - (a) Z. Zhang, G. J. Tizzard, J. A. G. Williams, S. M. Goldup, *Chem. Sc.* **2020**, *11*, 1839–1847. (b) A. Acevedo-Jake, A. T. Ball, M. Galli, M. Kukwikila, M. Denis, D. G. Singleton, A. Tavassoli, S. M. Goldup, *J. Am. Chem. Soc.* **2020**, *142*, 5985–5990. (c) M. Cirulli, E. Salvadori, Z. H. Zhang, M. Dommett, F. Tuna, H. Bamberger, J. E. M. Lewis, A. Kaur, G. J. Tizzard, J. van Slageren, R.

Crespo-Otero, S. M. Goldup, M. M. Roessler, *Angew. Chem. Int. Ed.* **2021**, *60*, 16051–16058. (d) P. Rajamalli, F. Rizzi, W. Li, M. A. Jinks, A. K. Gupta, B. A. Laidlaw, I. D. W. Samuel, T. J. Penfold, S. M. Goldup, E. Zysman-Colman, *Angew. Chem. Int. Ed.* **2021**, *60*, 12066–12073. (e) J. R. J. Maynard, B. Galmes, A. D. Stergiou, M. D. Symes, A. Frontera, S. M. Goldup, *Angew. Chem. Int. Ed.* **2022**, *61*, e202115961. (g) A. Saady, G. Malcolm, M. Fitzpatrick, N. Pairault, G. Tizzard, S. Mohammed, A. Tavassoli, S. M. Goldup, *Angew. Chem. Int. Ed.* **2024**, e202400344.

34 (a) M. Denis, J. E. M. Lewis, F. Modicom, S. M. Goldup, *Chem* **2019**, *5*, 1512–1520. (c) C. Tian, S. D. P. Fielden, B. Perez-Saavedra, I. J. Vitorica-Yrezabal, D. A. Leigh, *J. Am. Chem. Soc.* **2020**, *142*, 9803–9808. (c) A. Imayoshi, B. V. Lakshmi, Y. Ueda, T. Yoshimura, A. Matayoshi, T. Furuta, T. Kawabata, *Nat. Commun.* **2021**, *12*, 404. (d) M. F. Li, X. L. Chia, C. Tian, Y. Zhu, *Chem* **2022**, *8*, 2843–2855. (e) A. Rodriguez-Rubio, A. Savoini, F. Modicom, P. Butler, S. M. Goldup, *J. Am. Chem. Soc.* **2022**, *144*, 11927–11932. (f) S. Zhang, A. Rodríguez-Rubio, A. Saady, G. J. Tizzard, S. M. Goldup, *Chem* **2023**, *9*, 1195–1207. (g) N. Pairault, F. Rizzi, D. Lozano, E. M. G. Jamieson, G. J. Tizzard, S. M. Goldup, *Nat. Chem.* **2023**, *15*, 781–786.

35 (a) M. Gaedke, F. Witte, J. Anhauser, H. Hupatz, H. V. Schroder, A. Valkonen, K. Rissanen, A. Lutzen, B. Paulus, C. A. Schalley, *Chem. Sci.* **2019**, *10*, 10003–10009. (b) Y. Wang, J. Gong, X. Wang, W. J. Li, X. Q. Wang, X. He, W. Wang, H. B. Yang, *Angew. Chem. Int. Ed.* **2022**, e202210542.

36 A. Pigorsch, M. Köckerling, *Cryst. Growth Des.* **2016**, *16*, 4240–4246.

37 S. Ogi, T. Ikeda, R. Wakabayashi, S. Shinkai, M. Takeuchi, *Chemistry* **2010**, *16*, 8285–8290.

38 N. Kobayashi, M. Kijima, *J. Mater. Chem.* **2008**, *18*, 1037–1045.

39 CrysAlisPro Software System, Rigaku Oxford Diffraction, (2021).

40 O. V. Dolomanov, L. J. Bourhis, R. J. Gildea, J. A. K. Howard, H. Puschmann, *J. Appl. Cryst.* **2009**, *42*, 339–341.

41 G. M. Sheldrick, *Acta Cryst. C* **2015**, *A71*, 3–8.

42 G. M. Sheldrick, *Acta Cryst. C* **2015**, *C*71, 3–8

43 A. L. Spek, *Acta Cryst. C* **2015**, *C71*, 9–18.

44 A. L. Spek, **2005**, PLATON, A Multipurpose Crystallographic Tool, Utrecht University, Utrecht, The Netherlands.

45 L. J. Bourhis, O. V. Dolomanov, R. V. Gildea, J. A. K. Howard, H. Puschmann, *Acta Cryst. A*, **2015**, *A71*, 59–71.

Chapter 4: The Final Stereogenic Unit of [2]Rotaxanes: Type 2 Geometric Isomers

Abstract: Mechanical stereochemistry arises when the interlocking of stereochemically trivial covalent subcomponents results in a stereochemically complex object. Although this general concept was identified in 1961, the stereochemical description of these molecules is still under development to the extent that new forms of mechanical stereochemistry are still being identified. Here we present a simple analysis of rotaxane and catenane stereochemistry that allowed us to identify the final missing simple mechanical stereogenic unit, an overlooked form of rotaxane geometric isomerism, and demonstrate its stereoselective synthesis.

Acknowledgements: Andrea Savoini contributed to the synthesis and characterisation of unselective MGI rotaxanes **4**, **5**, and compounds leading to (*S*)-**7**. Abed Saady synthesised rotaxanes **10** and **11** *via* the interlocking auxiliary approach and contributed to the synthesis and characterisation of compounds leading to (*S*)-**7**. I contributed to the synthesis, screening and characterisation of rotaxanes unselective MGI **4** and **5**, and compounds leading to (*S*)-**7**. I also managed the preparation of manuscript graphics, Supporting Information, and contributed to the analysis of mechanical stereochemistry and preparation of Supporting Information section 1 with Stephen M. Goldup.

A. Savoini, A. Saady, SMG and I all contributed to the analysis of the results and writing of the manuscript.

Prior publication: This chapter was previously published as:

A. Savoini, P. R. Gallagher, A. Saady, S. M. Goldup, *J. Am. Chem. Soc.* **2024**, *146*, 8472–8479.

4.1. Introduction

In 1961,[1] Wasserman and Frisch recognized that interlocking two non-stereogenic rings can result in a chiral catenane where the enantiomers are related by inverting the relative orientations of the two rings.[2] A decade later,[3] Schill identified a similar phenomenon when a ring encircles an axle in a rotaxane, and that geometric isomerism is also possible in such systems. Since these first reports, the pantheon of mechanical stereogenic units in simple [2]catenanes and [2]rotaxanes has expanded beyond those envisaged by Wassermann and Frisch, and Schill; in 2013,[4] Gaeta and Neri recognized that catenanes can also express mechanical geometric isomerism and more recently, we identified a previously overlooked class of mechanically chiral rotaxanes,[5a] and re-analyzed the planar chiral stereochemistry of catenanes to show that, although they were hitherto simply described as "topologically chiral", this is not an essential characteristic of this stereogenic unit.[6]

The recent discovery of new conditional[7]mechanical stereogenic units contrasts with covalent organic stereochemistry where, although new pathways of isomerization[8] and previously overlooked expressions of atropisomerism[9] have recently been reported, the archetypal stereogenic units (centres, axes, planes, helices and multiple bonds)[10] are long-established. This raises an obvious question; are there any mechanical stereogenic units of [2]catenanes and [2]rotaxanes still lying undetected? Here we provide a simple stereochemical analysis that shows the answer is yes; working from first principles we identify a previously overlooked rotaxane geometric stereogenic unit, but also demonstrate that this is the final one to be found - our pantheon is now complete (Figure 4.2). Using concepts developed for the synthesis of mechanically planar chiral molecules we demonstrate the first stereoselective synthesis of these new type 2 rotaxane mechanical geometric isomers.

4.2. Results and discussion

4.2.1. Examining the achiral building blocks of [2]catenanes confirms the set of stereogenic units is complete

We first recognize that the highest symmetry ring point group, $D_{\infty h}$, contains the achiral D_{nd}, C_{nh}, C_{nv} and S_{2n} subgroups and that therefore rings of these symmetries are the complete set of building blocks of catenane mechanical stereochemistry (see Supplementary section 4.4.1 for further discussion). Second, we recognize that any ring that has a C_2 axis in the macrocycle plane ($C_{2(x)}$)[11] cannot give rise to a conditional mechanical stereogenic unit because this symmetry operation of the separated rings corresponds to the notional process of switching their relative orientations in the corresponding [2]catenane (Figure 4.1a). Although this observation appears obvious, to our knowledge, this is the first time it has been stated explicitly.[12] Thus, we can discard rings of D_{nd}, and $C_{2v(x)}$ and $C_{2h(x)}$ symmetry.[11,13,14]

The visually tractable D_{4h} point group contains the C_{4v}, C_{4h} and S_4 subgroups, representative of C_{nv}, C_{nh} and S_{2n}, and so we modified a D_{4h} ring to generate these structures by adding 4 equally spaced, equivalent vectors perpendicular and/or tangential to the ring plane in different relative orientations to highlight the key features of these achiral macrocycles (Figure 4.1b). Taking this approach, we find that to ensure that $C_{2(x)}$ is not a symmetry operation of the ring it must either be oriented (C_{nh} or S_{2n}; characterised by vectors tangential to the ring circumference that define its direction), or facially dissymmetric (C_{nv}; characterised vectors perpendicular to the ring plane that differentiate its faces).

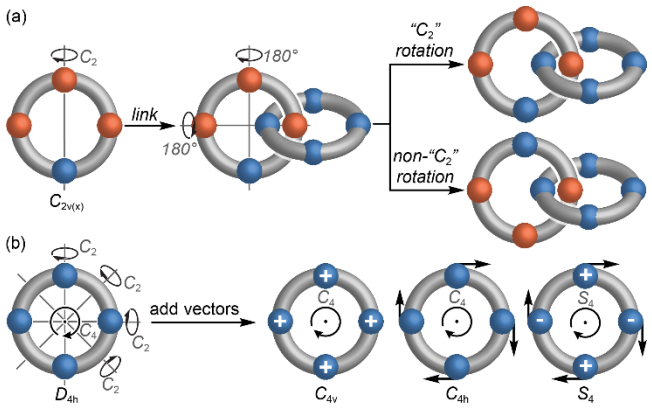

Figure 4.1 - (a) Schematic demonstration that the $C_{2(x)}$[11] symmetry operation of a non-interlocked ring corresponds to the notional process of inverting the relative ring orientations in a [2]catenane; hence, any ring for which $C_{2(x)}$ is a symmetry operation cannot give rise to conditional mechanical stereoisomers. (b) Conversion of a D_{4h} symmetric structure to rings of C_{4v}, C_{4h} and S_4 symmetry, which we propose to be representative of the complete set of oriented (C_{nh} and S_{2n}) and facially dissymmetric (C_{nv}) building blocks of catenane stereochemistry, by the addition of simple vectors (+/- refer to vectors projecting up/down respectively perpendicular to the plane of the ring).

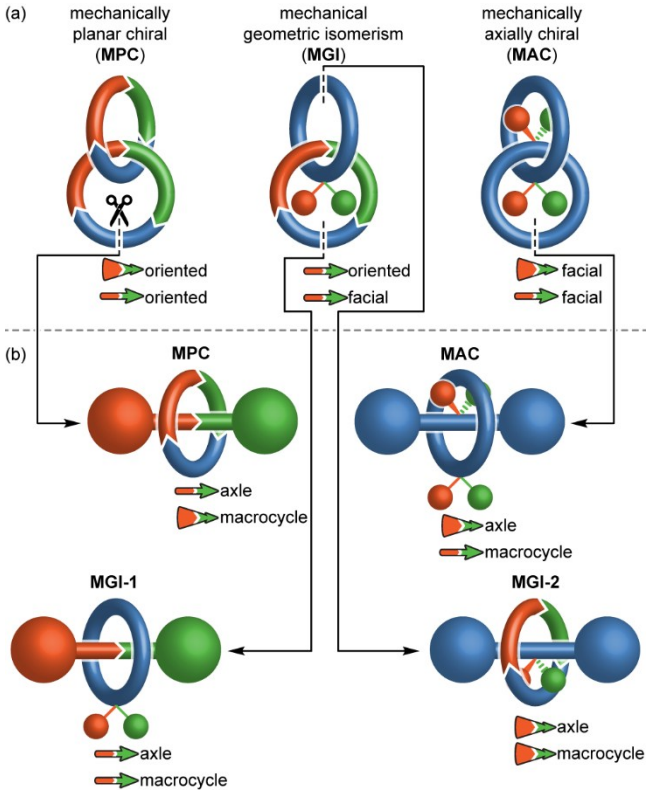

Figure 4.2 - (a) The complete set of catenane mechanical stereogenic units that can be constructed from the archetypal rings identified (Figure 1) and their relationship with the (b) mechanical stereogenic units of rotaxanes *via* a notional ring-opening-and-stoppering operation, including the newly identified "type 2" rotaxane mechanical geometric unit. The vectors shown characterise their stereochemistry and their relationship to the components that gives rise to them defines the stereogenic unit.

The requirement for the rings of a [2]catenane to be oriented or facially dissymmetric for mechanical stereochemistry to arise is not a new observation; combining two oriented C_{nh} rings or two facially dissymmetric C_{nv} rings gives rise to the chiral catenanes originally identified by Wasserman and Frisch,[1] illustrated here using rings of C_{1h} and C_{1v} symmetry[15] respectively (Figure 4.2a). The vectors associated with the orientation or facial dissymmetry of the individual rings can never become coplanar in the resultant catenanes and thus the stereochemistry of such structures can be defined using the resulting oriented skew lines.[16] The skew lines lie parallel to the associated ring when two oriented rings are combined but perpendicular to the rings when two facially dissymmetric rings are combined, which defines the canonical mechanically planar chiral (MPC) and mechanically axially chiral (MAC) stereogenic units of [2]catenanes, respectively. Thus, the only surprising result from our analysis is that S_{2n} symmetric rings are oriented and thus give rise to a mechanical stereogenic unit, which to our knowledge has not previously been noted. However, we suggest that combining two S_{2n} macrocycles (or a combination of S_{2n} and C_{nh} rings) gives rise to the MPC stereogenic unit, as defined by the orientation of the skew lines associated with the rings, rather than a new form of mechanical

stereochemistry.[17] Finally, combining one facially dissymmetric C_{nv} ring and one oriented C_{nh} (or S_{2n}) ring results in an achiral structure because the associated skew lines can be made co-planar, in the interlocked structure. However, two mechanical geometric isomers (MGI) are possible because the vectors can be arranged *syn* (Z_m) or *anti* (E_m) (Figure 4.2a).[18]

4.2.2. Analysing the achiral building blocks of rotaxanes reveals the final mechanical stereogenic unit

The same analysis can be used to identify the axle point group symmetries that can give rise to mechanical stereochemistry in a rotaxane and thus the complete set of rotaxane stereogenic units (see Supplementary section 4.4.2). However, the same result is reached more intuitively by identifying that rotaxanes and catenanes are interconverted by a notional ring-opening-and-stoppering operation (Figure 4.2b), which, as previously noted, leads to the conclusion that MPC catenanes and rotaxanes are directly related,[6] as are the MAC pair.[5a] Once again, these rotaxane stereogenic units can be differentiated by considering the relative orientation of the skew lines that characterise their configuration; the MPC stereogenic unit of rotaxanes is defined as arising when the vector associated with the axle lies along its axis, whereas the MAC stereogenic unit arises when the vector associated with the axle is perpendicular to its axis. These axle vectors lie perpendicular to the vector associated with the ring when interlocked with oriented or facially dissymmetric rings respectively.

It is when we turn to the MGI stereogenic unit of catenanes that we find a surprise. Because the two rings are distinct there are two possible products of the opening-and-stoppering sequence, one of which is the canonical MGI rotaxane stereogenic unit identified by Schill, and the other is a previously overlooked form of rotaxane geometric isomerism. The former is characterized by the co-planar vectors associated with the two components lying parallel to the axle whereas in the latter these vectors lie perpendicular to the axle. We propose that the labels “type 1” and “type 2” are used to distinguish between the canonical and non-canonical geometric isomers of rotaxanes (MGI-1 and MGI-2 respectively), with the numeral assigned by the order in which they were identified.

4.2.3. Catenane and rotaxane stereochemistry – conclusions

Our simple, first principles approach has allowed us to identify all the possible conditional stereogenic units of rotaxanes and catenanes, and confirm that, now that a previously overlooked MGI-2 rotaxane stereochemistry has been found, the pantheon of unique stereogenic units is complete. Based on this analysis, methods exist to stereoselectively synthesise all conditional mechanical stereogenic units of [2]catenanes and [2]rotaxanes apart from MGI-2 rotaxanes;

although until 2014,[19] chiral stationary phase HPLC was required to produce enantioenriched samples of mechanically chiral molecules,[20] since this time methodologies[21] for the stereoselective synthesis of MPC[6,13,22,23] and MAC[5] catenanes and rotaxanes have been disclosed. Similarly, the first stereoselective synthesis of MGI-1 rotaxanes was reported in 2005[24] using calixarene rings and since then many examples based on cone-shaped macrocycles,[25] and more recently simple prochiral[26] rings,[5b,27] have been reported. The corresponding MGI catenanes are less well studied but yield to similar strategies to the corresponding rotaxanes.[4,5b,28]

4.2.4. Retrosynthetic analysis of the "new" MGI-2 stereogenic unit

Having identified the MGI-2 stereogenic unit, we considered what strategies could be used for its selective synthesis. Notionally, the challenge in the synthesis of MGI-2 rotaxanes is the same as that of MPC rotaxanes – how to thread an oriented ring onto an axle with control over their relative orientation (Figure 4.3a). We previously achieved this for MPC rotaxanes[22a,e] using an active template[29] Cu-mediated alkyne-azide cycloaddition (AT-CuAAC[30,31]) approach in which the intermediates leading to the different enantiomers are diastereomeric due to a covalent chiral auxiliary. This analysis suggests that a similar approach is possible in the case of MGI-2 rotaxanes (Figure 4.3b). Although it may seem counterintuitive to synthesise the achiral MGI-2 stereogenic unit using chiral starting materials, it should be noted that almost regardless of where the prochiral axle is subdivided,[32] a chiral starting material is produced. This is symmetrised during mechanical bond formation and so no additional auxiliary removal step is required. Furthermore, a racemic mixture of starting materials would lead to the same MGI-2 product mixture using this direct approach.

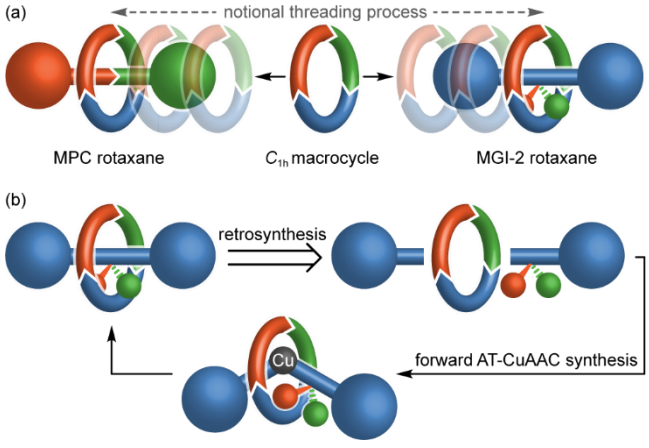

Figure 4.3 - (a) Comparison of the MGI-2 and MPC stereogenic units highlighting the common challenge of selectively threading of an oriented ring onto an oriented or facially dissymmetric axle, respectively. (b) Retrosynthesis of the MGI-2 stereogenic unit using a direct AT-CuAAC approach. The forward reaction proceeds *via* two possible diastereomeric intermediates (one shown). Although one of the half-axle units is chiral, this is symmetrized in the forward reaction and the same achiral, diastereomeric mixture is produced whether the starting material is enantiopure or racemic.

4.2.5. Attempted direct synthesis of MGI-2 rotaxanes 5

Thus, we initially attempted a synthesis of a rotaxane expressing the MGI-2 stereogenic unit using a stepwise AT-CuAAC approach. Reaction of oriented macrocycle **1**,[33] alkyne **2** and serine-based azide (*S*)-**3** under our AT-CuAAC conditions[22a] in CH_2Cl_2 gave rotaxane **4** as a mixture of diastereomers (17% *de*,[34] Scheme 4.1, entry 1) that differ in their MGI-2 configuration but have the same co-conformational covalent configuration, which is fixed due to the bulky NHBoc unit that prevents the macrocycle from shuttling between the two triazole compartments. The same reaction in THF (entry 2) or EtOH (entry 3) gave lower selectivity (3% and 16% *de* respectively), whereas lower temperatures (entries 4 and 5) gave increased selectivity at the expense of reduced conversion. Unfortunately, the (Z_m,$S_{co\text{-}c}$)-**4** and (E_m,$S_{co\text{-}c}$)-**4** diastereomers proved hard to separate; the best we could achieve was a 59% *de* sample starting from a 17% *de* sample after several rounds of chromatography. We were also unable to separate rotaxanes **5**, which only express the MGI-2 stereogenic unit, obtained by removal of the Boc group from the mixture of rotaxanes **4**.

Scheme 4.1 - Poorly selective direct AT-CuAAC synthesis of type 2 rotaxane geometric isomers **5** *via* chiral diastereomers **4**.[a]

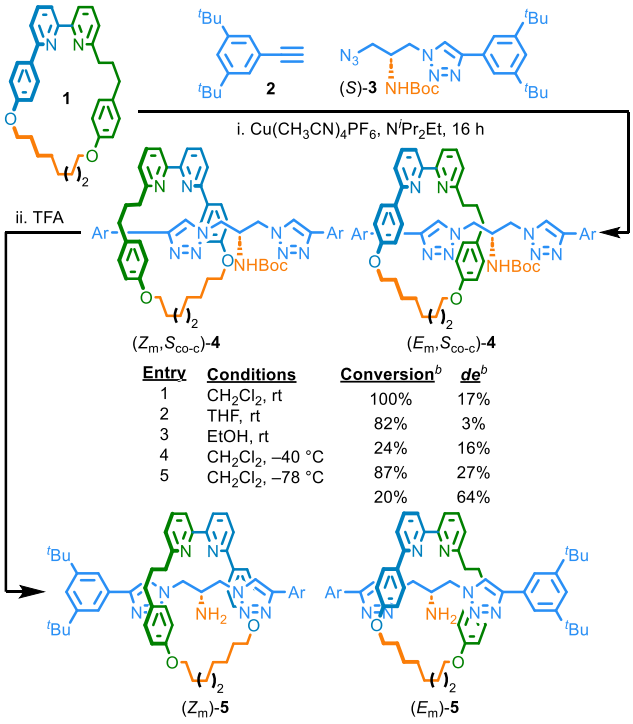

[a]Reagents and conditions: i. **11** (1 equiv.), (*S*)-**2** (1.1 equiv.), **2** (1.1 equiv.), $[Cu(CH_3CN)_4]PF_6$ (0.97 equiv.), $^iPr_2EtN$ (2 equiv.). ii. TFA, CH_2Cl_2, rt, 1 h. [b]Determined by ^1H NMR analysis of the crude reaction product. Ar = 3,5-di-^{t}Bu-C_6H_3.

The disappointing stereoselectivity in the formation of rotaxanes **4** is perhaps unsurprising; we have previously identified that AT-CuAAC auxiliary approaches to MPC rotaxanes, which are analogous to the direct approach to the achiral MGI-2 stereogenic units presented here, only proceed efficiently when a sterically hindered α-chiral azide half-axle is used.[22a,e] This is hard to realize practically in the case of the MGI-2 stereogenic unit as it would nominally require iterative CuAAC couplings of a 1,1-bis-azide synthon. Thus, we returned to our comparison of the MPC and MGI-2 stereogenic units and recognized that our chiral interlocking auxiliary strategy,[19f] which reliably loads macrocycle **1** onto the axle of almost any rotaxane in a specific orientation that is determined by the absolute stereochemistry of the amino acid-derived azide used, corresponds to the desired notional oriented threading process (Figure 4.3a).

4.2.6. Stereoselective synthesis of MGI-2 rotaxanes 11 using an interlocking auxiliary approach

Coupling of azide (*S*)-**6** with *o*-Me acetylene half-axle (*S*)-**7** in the presence of macrocycle **1** gave rotaxane (*S*,*S*,R_{mp})-**8** (Scheme 2), in which the macrocycle preferentially encircles the less hindered triazole unit, in excellent stereoselectivity (94% *de*). Subsequent Suzuki coupling produced rotaxane (*S*,*S*,R_{mp})-**9** as the major co-conformational isomer. Transesterification with MeOH gave rotaxane (E_m,$S_{co\text{-}c}$)-**10**, which contains an MGI-2 and a co-conformational stereogenic unit, in excellent stereopurity (92% *de*).[35] Removal of the Boc group provided rotaxane (E_m)-**11** that only expresses MGI-2 stereochemistry, again in high stereopurity (94% *de*). The same synthesis starting from (*R*)-**6** and (*S*)-**7** gave (Z_m,$S_{co\text{-}c}$)-**10** (94% *de*) which was converted to (Z_m)-**11** (92% *de*).

We note that the absolute MGI-2 configuration of the product of this interlocking auxiliary approach depends not on the enantiomer of chiral auxiliary **6** used but instead on the diastereomer of the axle produced in the first coupling step; the reaction of the (*S*)-**6**/(*S*)-**7** (Scheme 4.2) or (*R*)-**6**/(*R*)-**7** (not shown) pairs to give (*S*,*S*,R_{mp})-**8** or (*R*,*R*,S_{mp})-**8** respectively, would both ultimately produce (E_m)-**11**. However, unlike in the case of a direct AT-CuAAC synthesis (Figure 4.3b, Scheme 4.1), a racemic mixture of starting materials would always lead to an equal mixture of MGI isomers using this approach.

Scheme 4.2 - A chiral interlocking auxiliary synthesis of MGI-2 rotaxanes **10** and **11**[a]

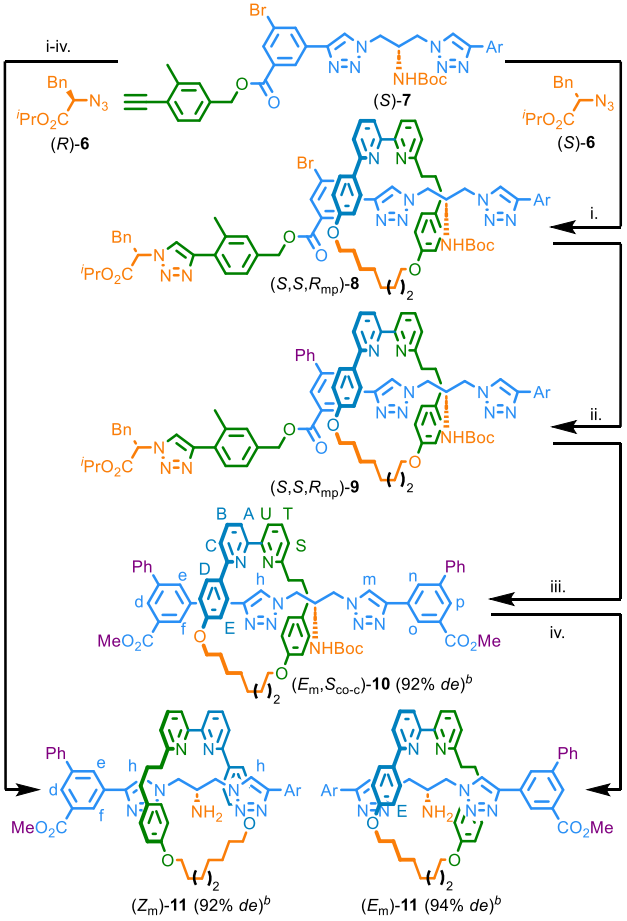

[a]Reagents and conditions: i. (*S*)-**7** (1.1 equiv.), **1** (1 equiv.), **6** (1.1 equiv.), $[Cu(CH_3CN)_4]PF_6$ (0.99 equiv.), $^iPr_2EtN$ (2 equiv.), CH_2Cl_2, rt, 16 h. ii. $PhB(OH)_2$, $Pd(PPh_3)_4$, K_2CO_3, acetone-^{i}PrOH-H_2O (2 : 1 : 1), 60 °C, 3 h iii. K_2CO_3, CH_2Cl_2:MeOH, rt, 3 h. iv. TFA, CH_2Cl_2, rt, 1 h. [b]Determined by ^{1}H NMR. Ar = 3-CO_2Me-5-Ph-C_6H_3.

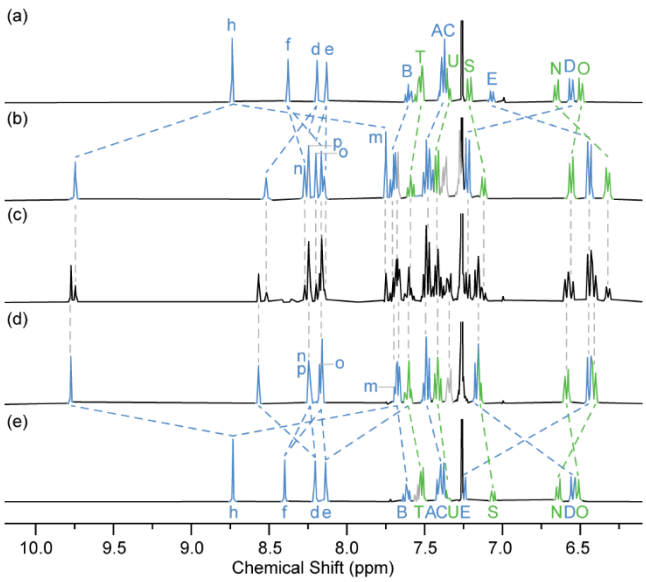

Figure 4.4 - Partial ^{1}H NMR (400 MHz, $CDCl_3$, 298 K) spectra of (a) (Z_m)-**11** (92% *de*); (b) (Z_m,S_{co-c})-**10** (94% *de*); (c) **10** (16% *de*, obtained by a direct AT-CuAAC coupling, see ESI section 6), (d) (E_m,S_{co-c})-**10** (92% *de*) (e) (E_m)-**11** (94% *de*). Peak assignment and colors as in Scheme 4.2.

4.2.7. Analysis of rotaxanes 10 and 11

Rotaxanes (E_m,$S_{co\text{-}c}$)-**10** and (Z_m,$S_{co\text{-}c}$)-**10** have distinct ^{1}H NMR spectra (Figures 4.4b and 4.4d respectively) that each correspond to one of the inseparable isomers obtained using a direct AT-CuAAC approach to the same molecules (Figure 4.4c). The ^{1}H NMR spectra of the two geometric isomers of rotaxanes **11** (Figures 4.4a and 4e) are also distinct from one another but they suggest molecules of much higher symmetry than rotaxanes **10**. This is not because the macrocycle preferentially encircles the amine unit; the high chemical shift of triazole protons H_h in rotaxanes **11** is consistent with the macrocycle exchanging between the two triazole containing compartments where it engages in a C-H•••N H-bond.[36] Instead, and in contrast with MAC rotaxanes,[5] based on a similar prochiral axle, the two co-conformers of rotaxanes **11** are enantiomeric and so the H_h pair are enantiotopic and isochronous.

Interestingly, the absolute stereochemistry of the co-conformations of rotaxane **11** (Scheme 4.3), and that of static diastereomers **4** and **10**, can be fully described using two of three possible stereolabels, of which we strongly prefer the co-conformational covalent and MGI-2 description as this captures the desymmetrization of the axle component upon shuttling and the sole fixed stereogenic unit of the molecule. The co-conformational MPC/MGI-2 description fails to capture the former and the co-conformational covalent/co-conformational MPC description obscures the fixed MGI-2 unit, with both stereolabels inverting under co-conformational exchange (see Supplementary section 4.4.5 for an extended discussion).

Scheme 4.3 - Co-conformational exchange between the enantiomeric co-conformations of rotaxane (Z_m)-11 highlighting the different stereochemical labels that can be applied to fully assign their absolute stereochemistry.

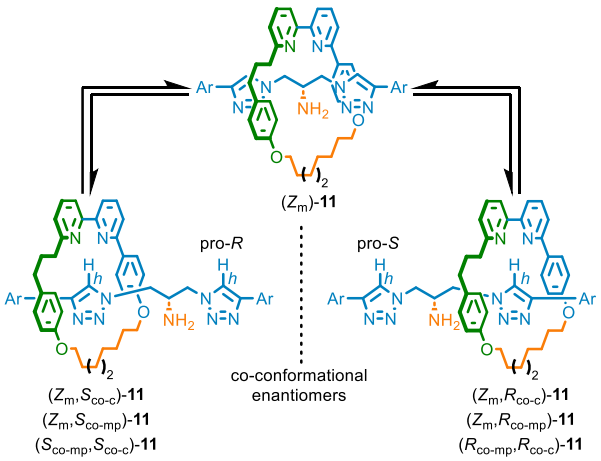

4.3. Conclusions

In conclusion, we have presented a simple stereochemical analysis to identify the complete set of [2]catenane and [2]rotaxane mechanical stereoisomers and, in doing so, recognized a new form of rotaxane geometric isomerism. Furthermore, retrosynthetic analysis of the non-canonical type 2 geometric stereogenic unit allowed us to make the link to the mechanical planar chiral stereogenic unit of rotaxanes, which led to the first stereoselective synthesis of such molecules.

Now that all of the mechanical stereogenic units of simple [2]catenanes and [2]rotaxanes have been delineated and concepts developed to allow their stereoselective synthesis,[4,5,6,44,22,23,24,25,28] it is reasonable to propose that, 62 years after such systems were first discussed,[1] we have finally reached the end of the beginning of the study of mechanical stereochemistry. Such molecules have already been used as the basis of molecular machines,[14d] enantioselective sensors[37] and catalysts,[38] and chiroptical switches,[39] work which will only accelerate as methods to synthesize them improve. Moreover, we suggest it is time now to set our sights beyond these simple structures and develop methodologies for the systematic synthesis of structures whose stereochemistry arises due to the presence of additional crossing points[40] or larger numbers of interlocked components[41] so that the potential benefits of such architectures can also be explored.

4.4. Experimental and Supplementary Information

4.4.1. Stereochemical analysis to identify the fundamental catenane stereogenic units

4.4.1.1. The achiral ring point groups – the building blocks of mechanically chiral catenanes

By conditional mechanical stereochemistry arises in [2]catenanes when two achiral rings are interlocked such that the resulting structure expresses stereochemistry, even in its highest symmetry representation, that is invariant with co-conformational motion. If the stereochemistry of the catenane varies with co-conformation, a co-conformational stereogenic unit is present, which can be either covalent, if the position of one ring desymmetrizes the other such that a pro-stereogenic unit becomes stereogenic, or mechanical if the position of one ring desymmetrises the other such that a mechanical stereogenic unit arises.

The highest possible symmetry of a macrocycle is $D_{\infty h}$, which is easily represented by a simple ring (Figure 1). The key symmetry properties of this point group are a principal rotation axis perpendicular to the ring plane, a horizontal mirror plane perpendicular to the principal axis, and an infinite number of C_2 axes in the plane of the ring and an infinite number of reflection planes perpendicular to the ring plane. Interlocking two $D_{\infty h}$ rings does not result in a fixed mechanical stereogenic unit; the highest symmetry representation of the corresponding catenane has achiral D_{2d} point group symmetry. It should be noted that such structures do express co-conformational stereochemistry; when the two rings are not perpendicular to one another, a co-conformational helical stereogenic unit is present.

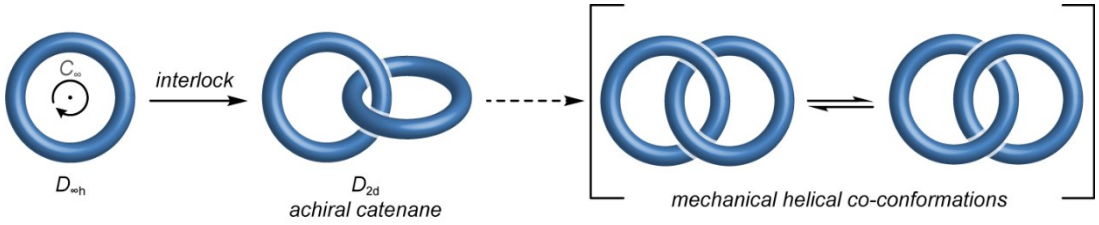

Figure 4.5 - Schematic representation of a $D_{\infty h}$ ring and the corresponding catenane highlighting the lack of conditional mechanical stereochemistry but the potential for co-conformational stereochemistry.

As discussed in the manuscript, the $D_{\infty h}$ point group contains the D_{nd}, C_{nh}, C_{nv} and S_{2n} subgroups, which therefor represent the achiral point group symmetries possible for macrocycles and are thus the candidate building blocks of catenane mechanical stereochemistry. Given that mechanical stereoisomers are related by changing the relative orientation of the two rings, which corresponds to notional process of rotating one ring by 180° through the other about an axis in the

plane of the ring, we can then eliminate D_{nd}, $C_{2h(x)}$ and $C_{2v(x)}$ as this process corresponds to a symmetry operation of such rings, leaving the structure unchanged.

This leaves us with $C_{nh(z)}$, $C_{nv(z)}$ and S_{2n} symmetric rings as the candidate building blocks of catenane stereochemistry. To make this problem visually tractable, we considered C_{4h}, C_{4v} and S_4, which can be derived from a D_{4h} symmetric structure by addition of sets of 4 equivalent vectors either tangential or perpendicular to the ring.

From D_{4h} to C_{4h}. The C_{4h} point group is derived from D_{4h} if the structure is modified such that the reflection planes perpendicular to the ring are removed. This can be achieved simply by adding four equivalent, equidistant vectors evenly distributed around the rotation axis in the plane of the ring, which for convenience we represent as tangents at the circumference of the macrocycle, which ensures that $C_{2(x)}$ symmetry is lost. This is a general property of macrocycles in the C_{nh} point group – they can all be described as "oriented". By oriented we mean that as the ring is rotated about the principal axis an observer would see all the vectors pointing in the same direction (left or right) as they pass in front of them. We note that C_{1h} is more properly named as $C_{s(xy)}$ (z-axis is defined as perpendicular to the ring) with the orientation defining the mirror plane as in the plane of the ring. We prefer to use $C_{1h(z)}$ as it emphasises the family (C_{nh}) to which these macrocycles belong.

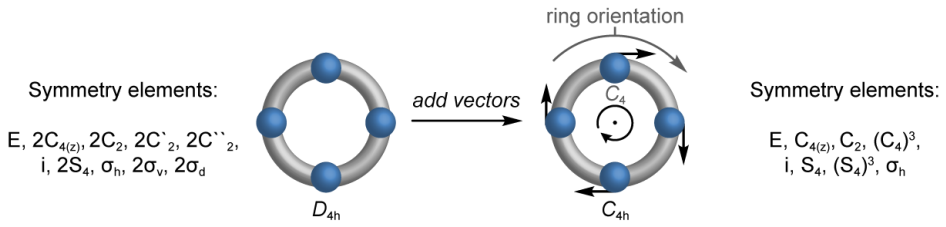

Figure 4.6 - Schematic representation of the descent in symmetry from D_{4h} to C_{4h}.

Chemically, the C_{nh} symmetry can be achieved if the ring has a distinguishable sequence of atoms that, for C_{4h} symmetry, repeats four times, equally spaced around the principal axis. More commonly the rings used in rotaxanes and catenanes have C_{1h} symmetry.

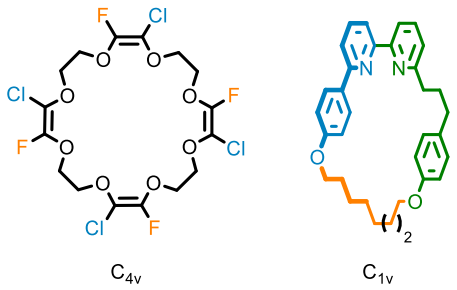

Figure 4.7 - Chemical structure that corresponds to C_{4h} and C_{1h} symmetry.

From D_{4h} to C_{4v}. The C_{4v} point group is derived from D_{4h} by desymmetrizing the two faces of the ring without removing the reflection planes perpendicular to the ring or the principal rotation axis. This can be achieved simply by adding four equivalent vectors perpendicular to the plane of the ring and distributed evenly around the ring circumference. The same approach can be taken starting from any D_{nh} ring and thus, all macrocycles in the C_{nv} (principal axis perpendicular to the ring plane) point group can be described as "facially dissymmetric". Practically, facial dissymmetry means that as the ring is rotated about the principal axis an observer would see all of the vectors pointing in the same direction (up or down) as they pass in front of them. We note that C_{1v} is more properly named as $C_{s(xz)}$ (z-axis is defined as perpendicular to the ring) with the orientation defining the mirror plane as perpendicular to the ring. We prefer to use $C_{1v(z)}$ as it emphasises the family (C_{nv}) to which these macrocycles belong.

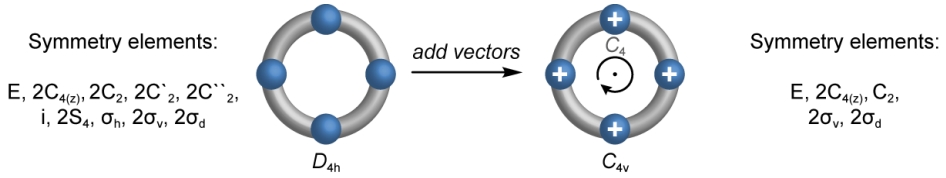

Figure 4.8 - Schematic representation of the descent in symmetry from D_{4h} to C_{4v}.

Chemically, C_{nv} symmetry can be achieved if the ring contains prochiral centres paired either side of a σ_v reflection plane, which in the case of C_{4v} symmetry requires four such centres. More commonly the rings used in rotaxanes and catenanes have C_{1v} symmetry.

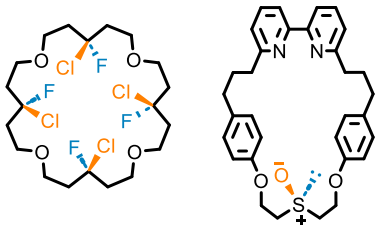

Figure 4.9 - Chemical structure that corresponds to C_{4v} and C_{1v} symmetry

From D_{4h} to S_4 (Figure 6). The S_4 point group is derived from D_{4h} by desymmetrizing the structure both in the plane of the ring and facially such that the principal rotation axis is reduced from 4-fold to 2-fold and all reflection symmetry is lifted, but such that an improper rotation axis is maintained. Examining the symmetry properties of the S_4 structure, we see that if the ring is rotated about its principal axis an observer would see the vectors perpendicular to the ring alternating in direction (up then down, then up…) but the vectors parallel to the ring would be seen as pointing in the same direction (left or right) as they pass in front of and so rings of this symmetry can be described as oriented.

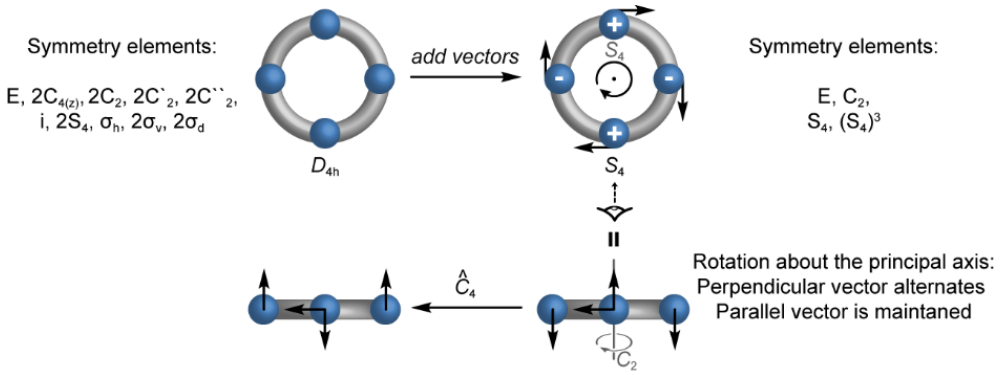

Figure 4.10 - Schematic representation of the descent in symmetry from D_{4h} to S_4.

Chemically, S_{2n} symmetry can be achieved if the ring has 2n equivalent stereogenic centres arranged around the S_{2n} axis alternating in their configuration. For example, S_4 symmetry requires four such centres whereas S_2 symmetry (more properly C_i symmetry) requires two such centres. We could not identify any rotaxanes or catenanes composed of S_{2n} symmetric rings.

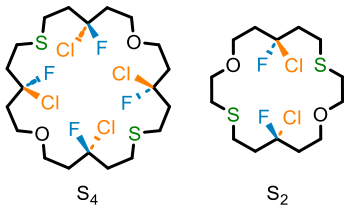

Figure 4.11 - Chemical structure that corresponds to S_4 and S_2 symmetry

4.4.1.2. The stereogenic units of [2]catenanes

Having developed representative models of the achiral macrocycle point groups we considered the stereochemical outcome of interlocking to determine if the known set of mechanical stereogenic units is complete.

Interlocking two facially dissymmetric (C_{nv}) rings – the mechanical axial stereogenic unit: When two C_{nv} rings are interlocked, the resulting structure has no improper symmetry operations because the mechanical bond prevents the rings from becoming coplanar and thus the is no relative orientation in which the σ_v reflection plane of one ring is a symmetry operation of the corresponding catenane. The facial dissymmetry of the rings can be used to characterise this stereogenic unit by observing that the vectors that differentiate the faces can never become co-planar and thus correspond to oriented skew lines. The mechanically axially chiral stereogenic unit is thus defined as that which arises when these skew lines are perpendicular to the rings.

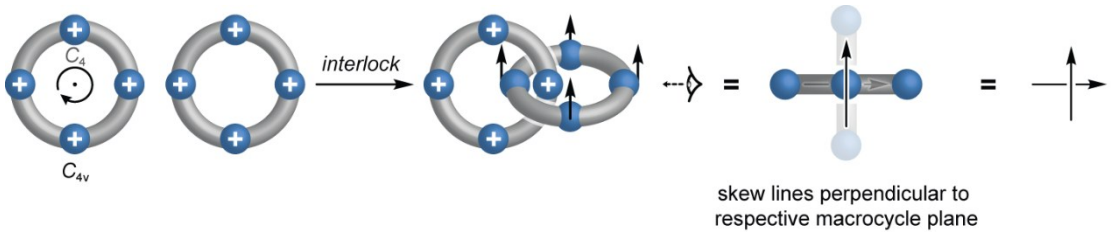

Figure 4.12 - Schematic representation of the interlocking of two C_{4v} symmetric rings, which gives rise to a mechanically axially chiral catenane whose stereochemistry is characterized by the oriented skew lines of the rings lying perpendicular to one another and also the associated ring.

Interlocking two oriented rings (C_{nh} or S_{2n} symmetry) – the mechanically planar chiral stereogenic unit: When two C_{nh} rings are interlocked, the resulting structure has no improper symmetry operations because the mechanical bond prevents the rings from becoming coplanar and thus the is no relative orientation in which the σ_h reflection plane of one ring is a symmetry operation of the corresponding catenane. The orientation of the rings can be used to characterise this stereogenic unit by observing that the vectors that define the orientations can never become co-planar and thus correspond to oriented skew lines. The mechanically planar chiral stereogenic unit is thus defined as when these skew lines are parallel to the rings.

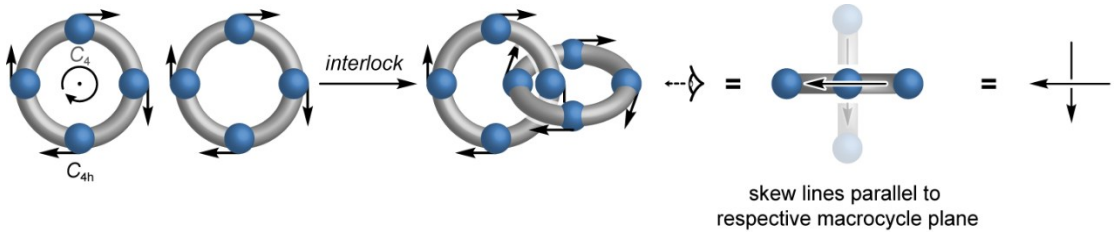

Figure 4.13 - Schematic representation of the interlocking of two C_{4h} symmetric rings, which gives rise to a mechanically planar chiral catenane whose stereochemistry is characterized by the oriented skew lines of the rings lying perpendicular to one another and coplanar associated ring.

Similarly, when two S_{2n} rings are interlocked, the resulting structure has no improper symmetry operations because the improper S_n axis of one ring cannot be an operation of the corresponding catenane. The orientation of the rings can be used to characterise this stereogenic unit by observing that the vectors that define the ring orientations can never become co-planar and thus correspond to oriented skew lines. Because these skew lines are coplanar with the rings, we propose that interlocking S_{2n} rings results in a special case of the mechanically planar chiral stereogenic unit, rather than a new form of mechanical stereochemistry. We note that if one ring is rotated relative to the other, the skew line pair in the plane of the rings that define the mechanical planar stereogenic unit is unaltered but the skew lines that arise from the vector pair perpendicular to the rings inverts, and thus such structures display a dynamic co-conformational stereogenic unit as well.

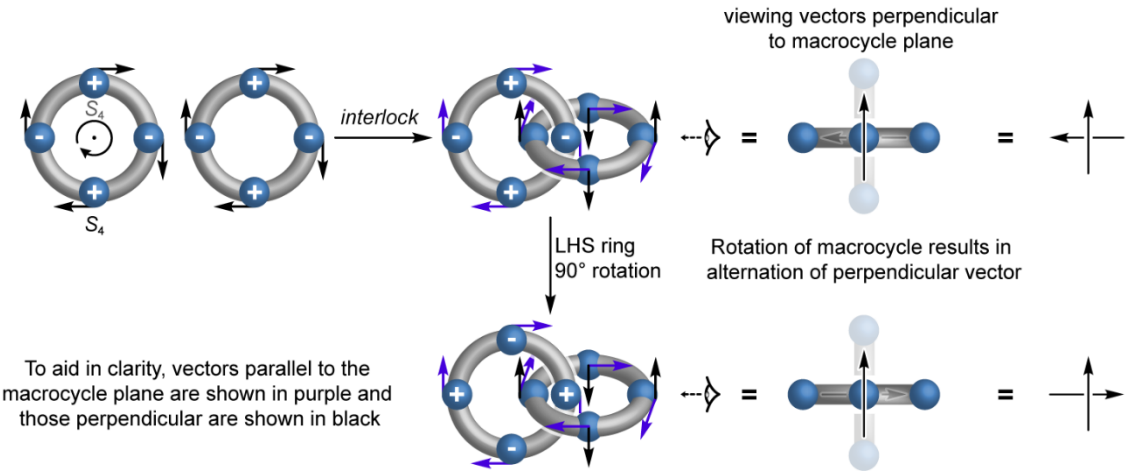

Figure 4.14 - Schematic representation of the interlocking of two S_4 symmetric rings, which gives rise to a mechanically planar chiral catenane whose stereochemistry is characterized by the oriented skew lines of the rings lying perpendicular to one another and coplanar associated ring. Such structures also display co-conformational stereochemistry, which is characterized by the vectors perpendicular to the rings alternating in orientation with respect to the observer as they are rotated relative to one another.

Interlocking one oriented (C_{nh} or S_{2n}) and one facially dissymmetric (C_{nv}) ring – the geometric stereogenic unit of catenanes: When one oriented and one facially dissymmetric ring are interlocked the resulting structure expresses a geometric stereogenic unit because the vector(s) associated with the oriented ring in the plane of the macrocycle can be made co-planar with the vector(s) associated with facially dissymmetric macrocycle perpendicular to this ring. We note that the S_{2n}/C_{nv} pair also expresses a co-conformational mechanically axially chiral stereogenic unit, making the stereochemistry of these structure extremely rich.

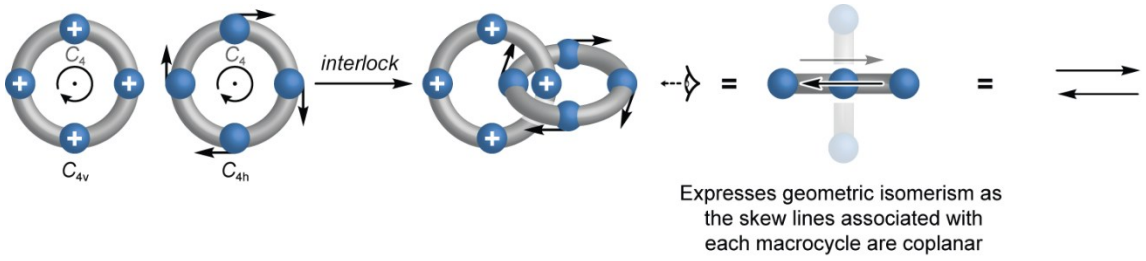

Figure 4.15 - Schematic representation of the interlocking of one C_{4v} and one C_{4h} symmetric ring, which gives rise to a mechanical geometric stereogenic unit that is characterized by the oriented skew lines of the rings lying coplanar to one another in either a parallel or antiparallel fashion.

Summary. The above analysis has allowed us to confirm that the set of known conditional mechanical stereogenic units of [2]catenanes is complete. The only new result from the discussion above is the observation that the achiral S_{2n} symmetric rings are oriented and so can be considered as components of mechanically planar chiral or mechanical geometric isomers.

4.4.2. Stereochemical analysis to identify the fundamental rotaxane stereogenic units

4.4.2.1. The achiral axles

As with macrocycles, the highest symmetry axle has $D_{\infty h}$ point group symmetry which thus contains the D_{nd}, C_{nh}, C_{nv} and S_{2n} subgroups that we can consider to be our fundamental building blocks of rotaxane mechanical stereochemistry. Once again, given that rotaxane mechanical stereoisomers are related by changing the relative orientation of the ring and axle, which corresponds to notional process of rotating either the ring or axle by 180° through the other about an axis in the plane of the ring or perpendicular to the axle, we can eliminate D_{nd}, $C_{2h(x)}$ and $C_{2v(x)}$ symmetric rings and axles as this process corresponds to one of their symmetry operations, leaving the structure unchanged. This leaves us with the C_{nh}, C_{nv} and S_{2n} symmetric rings discussed above and C_{nh}, C_{nv} and S_{2n} symmetric axles as the candidate building blocks of rotaxane stereochemistry.

From $D_{\infty h}$ to C_{nv} (principal axis along the axle): The symmetry of the $D_{\infty h}$ axle can be reduced to $C_{\infty v}$ simply by adding a vector parallel to the long axis of the axle, which removes all $C_{2(x)}$ axes and horizontal mirror planes. Lower C_{1h} symmetry is achieved simply by allowing the axle to deviate from linearity. We note that C_{1h} is more properly named as $C_{s(xy)}$ (z-axis is defined as perpendicular to the ring) with the orientation defining the mirror plane as in the plane of the ring. We prefer to use C_{1h} as it emphasises the family (C_{nh}) to which these axles belong.

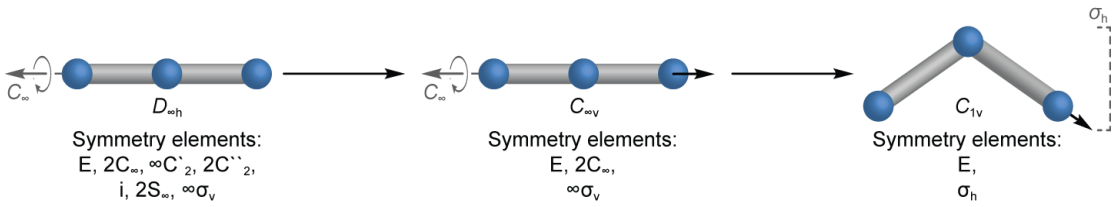

Figure 4.16 - Schematic representation of the descent in symmetry from $D_{\infty h}$ to $C_{\infty v}$ and C_{1v}

Chemically, C_{nv} symmetry can be achieved if the two ends of the axle are different, which effectively ensures that the axle must have a defined sequence of atoms.

Figure 4.17 - Chemical structure of axles that corresponds to $C_{\infty v}$ and C_{1v} symmetry

From $D_{\infty h}$ to C_{1h} (principal axis along the axle): Converting our $D_{\infty h}$ axle model to C_{nh} symmetry requires that we desymmetrize the structure such that a single reflection plane remains perpendicular to the axle and all $C_{2(x)}$ axes are removed. Although any value of n is technically possible, practically and of greatest chemical relevance, the easiest example to construct is C_{1h} (more properly $C_{s(xy)}$) by adding two non-colinear, non-equivalent vectors to the centre of the axle. Alternatively, the same vectors can be added in the same orientation to both ends of the axle or a single vector added to the centre of a non-linear axle. All of these achieve C_{1h} symmetry.

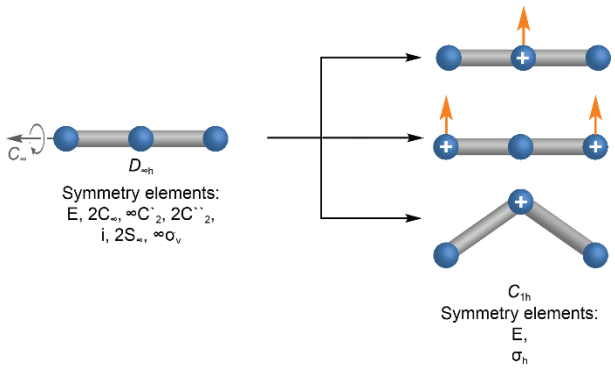

Figure 4.18 - Schematic representation of the descent in symmetry from $D_{\infty h}$ to C_{1h}. The vectors in the plane of the page (orange) and perpendicular (+/-) are inequivalent and perpendicular to one another.

Chemically, the first example corresponds to an axle with a single prochiral centre in the middle of the axle, whereas the second corresponds to two equivalent stereogenic centres at either end of the axle such that the highest symmetry structure is meso. The non-linear axle model corresponds to a pro planar chiral axle.

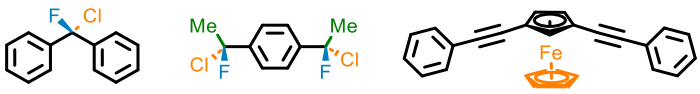

Figure 4.19 - Chemical structure of axles that corresponds to C_{1h}

From $D_{\infty h}$ to S_{2n} (principal axis along the axle): Converting our $D_{\infty h}$ axle model to C_{nh} symmetry requires that we remove all reflection symmetry and $C_{2(x)}$ axes while maintaining a rotation and rotation-reflection parallel to the axle. Although any value of n is technically possible, practically and of greatest chemical relevance, the easiest example to construct is S_2, which is more properly referred to as C_i, by adding two non-colinear, non-equivalent vectors to either end of the axle such that they are related by a centre of inversion.

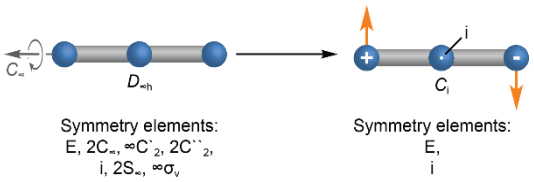

Figure 4.20 - Schematic representation of the descent in symmetry from $D_{\infty h}$ to S_2 (more properly C_i). The vectors in the plane of the page (orange) and perpendicular (+/-) are inequivalent and perpendicular to one another.

Chemically this can be achieved by including equivalent stereogenic centres at either end of the axle, as in the case of the meso C_{1v} structure above but with a central unit of axle designed to lift the reflection symmetry (we note that the meso axle shown can also adopt a C_i conformation).

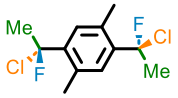

Figure 4.21 - Chemical structure of an axle that corresponds to C_i symmetry

4.4.2.2. The stereogenic units of rotaxanes

"Orientation" and "facial dissymmetry" of axles: The achiral rings that we identified as the building blocks of catenane stereochemistry were described as either oriented (C_{nh} or S_{2n}) or facially dissymmetric (C_{nv}). Axles with C_{nv} symmetry can also be readily seen to be oriented – the vector used to desymmetrize the $D_{\infty h}$ model clearly defines the orientation of the axle.

Facial dissymmetry is harder to discern in an axle but is still possible to define for C_{1v} and C_i symmetric structures if we apply arbitrary rules that determine the orientation in which an axle should be viewed. For example, if we define that the C_{1v} structure based on a bent axle always be viewed with the ends of the axle pointing down, we see that the vector perpendicular to axle plane can either be pointing towards or away from the observer and that these views are interconverted by the C_2 operation that we have previously identified as equivalent to interchanging the relative orientation of the components in a [2]rotaxane.

Figure 4.22 - Schematic to demonstrate that a C_{1v} axle based on a non-linear structure can be described as facially dissymmetric if we define the axle to always be viewed with the apex pointing up.

Similarly, the C_{1v} structure based on two inequivalent vectors on the centre of the axle can be defined as being viewed with the orange vector pointing up, upon which we see that the orthogonal vector can either point towards or away from the viewer. A similar rule can be applied to the meso C_{1v} structure.

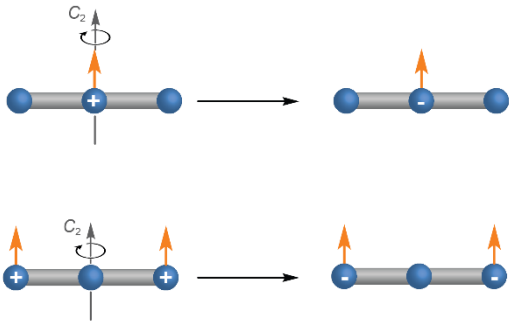

Figure 4.23 - Schematic to demonstrate that C_{1v} axles based inequivalent perpendicular vectors either at the middle (prochiral) or ends (meso) can be defined as facially dissymmetric if we define that the orange vectors point up.

Finally, the C_i structure can be also defined as facially dissymmetric but in this case we must define orientation to view the axle as that in which the left-most orange vector points upwards in the plane of the page with the axle face determined by the direction of the vector perpendicular to the page. Thus, applying a C_2 rotation about an axis perpendicular to the axle (which corresponds to switching the relative orientation of axle and macrocycle in a rotaxane) followed by a C_2 rotation along the axle axis (which corresponds to a pirouetting motion in a rotaxane) confirms that the leftmost perpendicular vector is inverted.

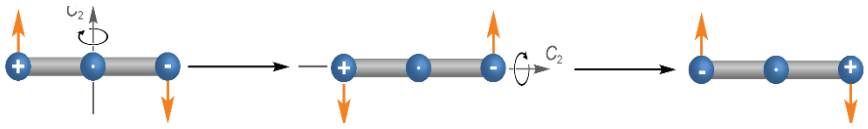

Figure 4.24 - Note on direction that axle is viewed from.

Interlocking an oriented (C_{nh} or S_{2n}) ring with an oriented (C_{nv}) axle – the mechanically planar chiral stereogenic unit: When an oriented ring encircles a C_{nv} axle, the resulting structure has no improper symmetry operations because the mechanical bond prevents the ring and axle from becoming coplanar and thus the is no relative orientation in which the σ_h reflection plane of the ring (in the C_{nh} case) is a symmetry operation of the corresponding rotaxane. The orientation of the ring and axle can be used to characterise this stereogenic unit by observing that the vectors that define the orientations of the components can never become co-planar and thus correspond to oriented skew lines. The mechanically planar chiral stereogenic unit of rotaxanes is thus defined as arising when these skew lines are parallel to the ring circumference and axle axis respectively.

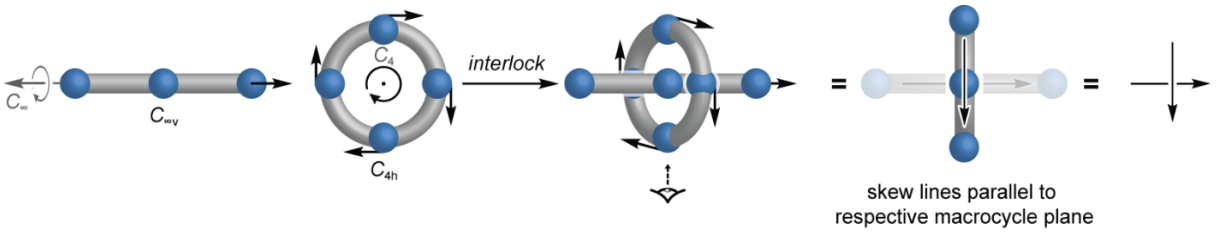

Figure 4.25 - Schematic representation of the interlocking of a C_{4h} ring and a $C_{\infty v}$, which gives rise to a mechanical planar chiral stereogenic unit that is characterised by the associated oriented skew lines of each component lying along the circumference of the ring and along the axle axis respectively

Interlocking a facially dissymmetric (C_{nv}) ring with a facially dissymmetric (C_{nh} or S_{2n}) axle – the mechanically axially chiral stereogenic unit: When a C_{nv} ring encircles a C_{nh} or S_{2n} axle, the resulting structure has no improper symmetry operations because the mechanical bond prevents the ring and axle from becoming coplanar and thus there is no relative orientation in which the σ_v reflection planes of the ring or σ_h plane of the axle (in the C_{nh} case) are a symmetry operation of the corresponding rotaxane. The facial dissymmetry of the ring and axle (see above discussion) can be used to characterise this stereogenic unit by observing that the vectors that define the ring and axle faces can never become co-planar and thus correspond to oriented skew lines. The mechanically axially chiral stereogenic unit of rotaxanes is thus defined as when these skew lines are perpendicular to the ring and axle respectively.

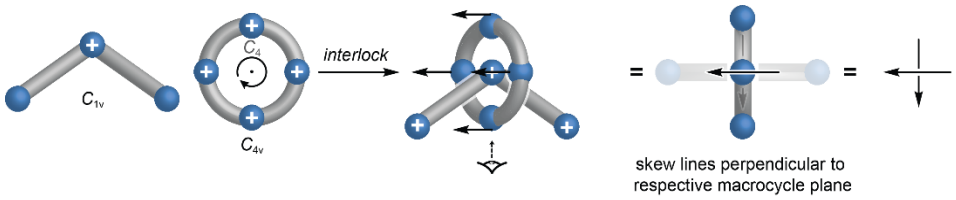

Figure 4.26 - Schematic representation of the interlocking of a C_{4h} ring and a C_{1h} axle, which gives rise to a mechanical axial chiral stereogenic unit that is characterised by the associated oriented skew lines of each component lying perpendicular to the ring and axle respectively

Interlocking a facially dissymmetric (C_{nv}) ring with an oriented (C_{nv}) axle – the type 1 mechanical geometric stereogenic unit: When a C_{nv} ring encircles a C_{nv} axle, the resulting structure is achiral because it is possible for the σ_v reflection planes of the ring and axle to be made coincident. However, the co-planar vectors associated with the components can either be arranged parallel or antiparallel, giving rise to a type 1 mechanical geometric stereogenic unit, which we propose is characterised by the vectors associated with the components lying parallel to the axle.

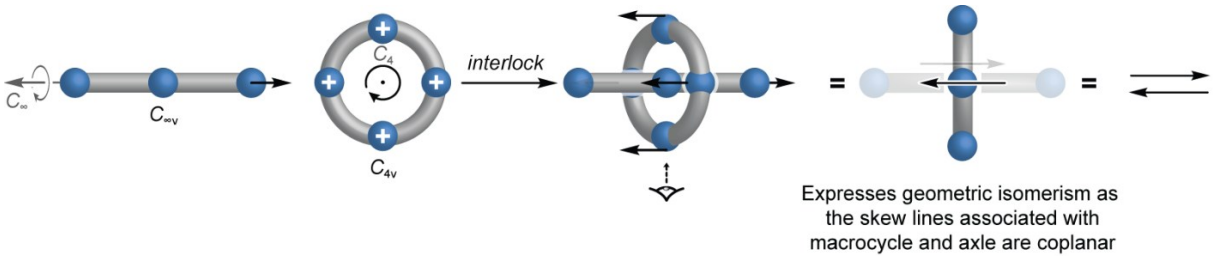

Figure 4.27 - Schematic representation of the interlocking of a C_{4v} ring and a $C_{\infty v}$ axle, which gives rise to a type 1 mechanical geometric stereogenic unit that is characterised by the associated oriented skew lines of both components lying parallel to the axle axis

Interlocking an oriented (C_{nh} or S_{2n}) ring with a facially dissymmetric (C_{nh} or S_{2n}) axle – the type 2 mechanical geometric stereogenic unit: When a facially dissymmetric axle is encircled by an oriented ring, the resulting structure is achiral because it is possible for the σ_h reflection planes of the ring and axle (C_{nh} combination) to be made coincident. However, the co-planar vectors associated with the components can either be arranged parallel or antiparallel, giving rise to a type 2 mechanical geometric stereogenic unit, which we propose is characterised by the vectors associated with the components lying perpendicular to the axle.

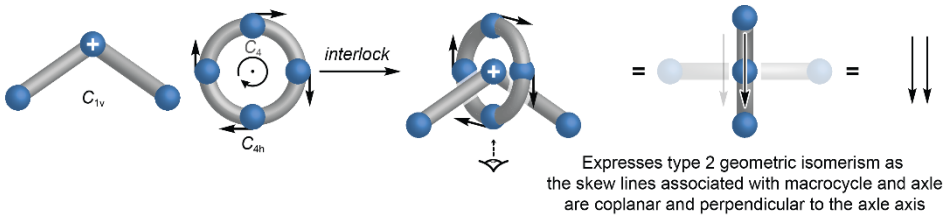

Figure 4.28 - Schematic representation of the interlocking of a C_{4h} ring and a C_{1h} axle, which gives rise to a type 2 mechanical geometric stereogenic unit that is characterised by the associated oriented skew lines of both components lying perpendicular to the axle axis

Summary. The above analysis has allowed us to identify the missing type 2 mechanical geometric stereogenic unit of rotaxanes and also that this is the last stereogenic unit to be found. In addition, we have identified that S_{2n} symmetric axles, of which the most chemically relevant is S_2 symmetry (more properly C_i), are facially dissymmetric and so can give rise to mechanical axial or type 2 mechanical geometric stereochemistry.

General Experimental Information

Unless otherwise stated, all reagents were purchased from commercial sources (Acros Organics, Alfa Aesar, Fisher Scientific, FluoroChem, Sigma Aldrich and VWR) and used without further purification. $[Cu(CH_3CN)_4]PF_6$ was prepared as described by Pigorsch and Köckerling.[42] Anhydrous solvents were purchased from Acros Organics. Petrol refers to the fraction of petroleum ether boiling in the range 40-60 °C. IPA refers to isopropanol. THF refers to tetrahydrofuran. EDTA-NH_3 solution refers to an aqueous solution of NH_3 (17% w/w) saturated with sodium-ethylenediaminetetraacetate. $CDCl_3$ (without stabilising agent) was distilled over $CaCl_2$ and K_2CO_3 prior to use. Unless otherwise stated, all reaction mixtures were performed in oven dried glassware under an inert N_2 atmosphere with purchased anhydrous solvents. Unless otherwise stated experiments carried out in sealed vessels were performed in CEM microwave vials, with crimped aluminium caps, with PTFE septa. Young's tap vessels and Schlenk techniques were used where specified.

Flash column chromatography was performed using Biotage Isolera-4 or Isolera-1 automated chromatography system. SiO_2 cartridges were purchased commercially Biotage (SNAP or ZIP (50 μm), or Sfär (60 μm) irregular silica, default flow rates). Neutralised SiO_2 refers to ZIP cartridges which were eluted with petrol-NEt_3 (99 : 1, 5 column volumes), followed by petrol (5 column volumes). Analytical TLC was performed on pre-coated silica gel plates on aluminum (0.25 mm thick, 60F254, Merck, Germany) and observed under UV light (254 nm) or visualised with $KMnO_4$ stain.

All melting points were determined using a Griffin apparatus. NMR spectra were recorded on Bruker AV400 or AV500 instrument, at a constant temperature of 298 K. Chemical shifts are reported in parts per million from low to high field and referenced to residual solvent. Coupling constants (*J*) are reported in Hertz (Hz). Standard abbreviations indicating multiplicity were used as follows: m = multiplet, quint = quintet, q = quartet, t = triplet, d = doublet, s = singlet, app. = apparent, br = broad, sept = septet. Signal assignment was carried out using 2D NMR methods (COSY, NOESY, HSQC or HMBC) where necessary. In some cases, complex multiplets with multiple contributing proton signals, exact assignment was not possible. In interlocked compounds, all proton signals corresponding to axle components are in lower case, and all proton signals corresponding to the macrocycle components are in upper case.

Many of the signals analysed to determine diastereopurity were close in ppm and/or broad, which limited the potential to use Q-NMR methodology (https://nmrweb.chem.ox.ac.uk/Data/Sites/70/userfiles/pdfs/quantitative-nmr.pdf). For this

reason, we systematically applied the "peak integration" function implemented in MestReNova (v11.0.4, Mestrelab Research S. L.) combined with the GSD peak modelling function (4 rounds of refinement, optimised for broad peaks), which has been shown to be comparable in accuracy to sum integration even when peaks are overlapping (qGSD - quantitative Global Spectral Deconvolution - Mestrelab Resources). Prior to integration, the default polynomial baseline correction was applied. Where possible, the values obtained were improved by comparison of multiple signals. The corresponding values obtained by sum integration are provided for comparison. Residual intensity is included for all peak integrations. Integral curves are included for sum integrations. Full details are included in the captions of the corresponding spectra.

Low resolution mass spectrometry was carried out by the mass spectrometry services at University of Southampton (Waters TQD mass spectrometer equipped with a triple quadrupole analyser with UHPLC injection [BEH C18 column; CH_3CN -H_2O gradient {0.2% formic acid}]). High resolution mass spectrometry was either carried out by the mass spectrometry services at the University of Southampton (MaXis, Bruker Daltonics, with a Time of Flight (TOF) analyser; samples were introduced to the mass spectrometer via a Dionex Ultimate 3000 autosampler and uHPLC pump in a gradient of 20% CH_3CN in *n*-hexane to 100% acetonitrile (0.2% formic acid) over 5-10 min at 0.6 mL/min; column: Acquity UPLC BEH C18 (Waters) 1.7 micron 50 × 2.1mm) or services at University of Birmingham (Waters Synapt G2-S mass spectrometer fitted with a TOF detector).

Circular dichroism spectra were either acquired on an Applied Photo-physics Chirascan spectropolarimeter, recorded using Applied Photophysics software Ver. 4.2.0 or a Jasco J-1500spectropolarimeter in dried spectroscopic grade $CHCl_3$ in a quartz cell of 1 cm path length, at a temperature of 293 K.

Stereochemical purity was determined by Chiral Stationary Phase HPLC on a Waters Acquity Arc Instrument at 303 K, with *n*-hexane-^{i}PrOH or *n*-hexane-EtOH isocratic eluents. A RegisCell (tris-(3,5-dimethylphenyl) carbamoyl cellulose stationary phase) column was used (5 micron, column dimensions 25 cm x 4.6 mm).

The following compounds were synthetized according to literature procedures: **1**,[22e] **2**,[43] (*S*)-**3**[5a], (*S*)-**1**[5a], **S7**,[22e] **S10**,[44] **6** ((*S*)-**6** and (*R*)-**6**)).[22a]

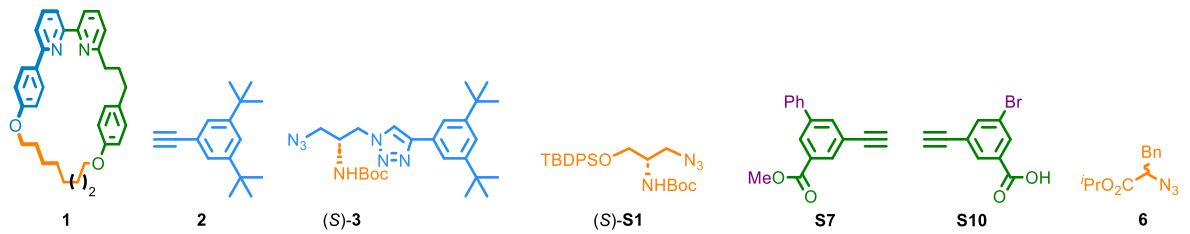

4.4.3. Characterisation of compounds

Synthesis of rotaxane 5 and associated compounds (Scheme 1)

NHBoc Rotaxanes 4

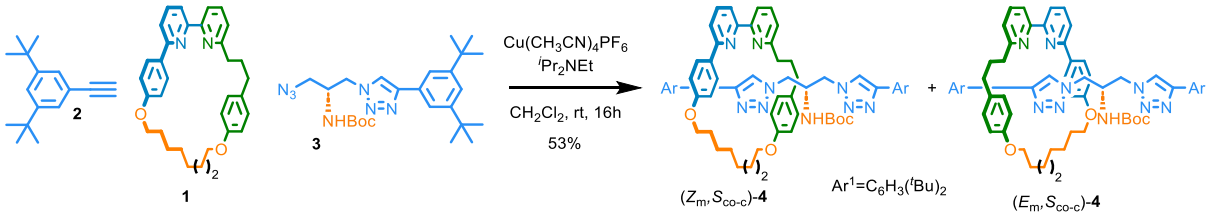

In a CEM vial were added **2** (9.4 mg, 43.9 µmol), (*S*)-**3** (20.0 mg, 43.9 µmol), **1** (19.7 mg, 40.2 µmol) and [$Cu(CH_3CN)_4PF_6$] (14.5 mg, 38.9 µmol). The vial was sealed and purged with N_2, then CH_2Cl_2 was added (2.0 mL), followed by iPr2NEt (14 µL, 80 µmol). The solution was stirred at rt for 16 h. Then, MeOH (2.0 mL) and KCN as a solid (13 mg, 0.20 mmol) were added and the resulting mixture was stirred vigorously for 1 h. The crude mixture was diluted with CH_2Cl_2 (5 mL) and washed with H_2O in two portions (10 mL and 5 mL). The combined aqueous phase was then extracted with CH_2Cl_2 (3 x 5 mL) and the combined organic extracts were washed with brine (10 mL), dried ($MgSO_4$) and concentrated *in vacuo* to give a sample containing **4** as a mixture of diastereomers (58 : 42 *dr*, Figure 25). Two rounds of chromatography (1st: *n*-hexane-acetone 0→100%; 2nd: CH_2Cl_2-CH_3CN 0→100%;) gave **4** as a colourless oil (23.5 mg, 53%) as a partially enriched mixture of diastereoisomers (1.43 : 1 *dr*, Figure 26).

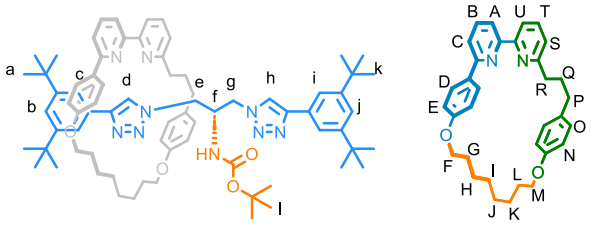

Major diastereomer

^{1}H NMR (500 MHz, $CDCl_3$) **F**δ: 9.71 (s, 1H, H_d), 7.80-7.69 (m, 4H, H_B, H_c, H_T), 7.65-7.51 (m, 5H, H_A, H_C, H_h, H_i), 7.43 (d, J = 7.8, 1H, H_U), 7.41-7.38 (m, 1H, H_j), 7.32-7.27 (m, 4H, H_b, H_D, H_S), 6.67-6.56 (m, 2H, H_O), 6.50-6.41 (m, 4H, H_E, H_N), 5.54 (d, J = 7.5, 1H, NH), 4.39-4.20 (m, 1H, H_M), 4.14-3.97 (m, 2H, H_F), 3.97-3.58 (m, 5H, H_e, H_f, H_g, $H_{M'}$), 3.52 (dd, J = 14.6, 4.1, 1H, $H_{e'}$), 2.85-2.43 (m, 4H, H_P, H_R), 2.09-1.46 (m, 14H, H_G, H_H, H_I, H_J, H_K, H_L, H_Q, superimposed with residual H_2O), 1.38-1.36 (m, 18H, H_k), 1.20 (s, 18H, H_a), 1.17 (bs, 9H, H_l)

Minor diastereomer

^{1}H NMR (500 MHz, $CDCl_3$): 9.63 (s, 1H, H_d), 7.80-7.69 (m, 4H, H_B, H_c, H_T), 7.65-7.51 (m, 4H, H_A, H_C, H_i), 7.49 (d, J = 8.0, 1H, H_U), 7.41-7.38 (m, 1H, H_j) , 7.34 (s, 1H, H_h), 7.32-7.27 (m, 2H, H_b, H_S), 7.20 (dt, J = 8.6, 1.9, 2H, H_D), 6.67-6.56 (m, 2H, H_O), 6.50-6.41 (m, 2H, H_E), 6.38 (d, J = 7.9, 2H, H_N), 5.50 (d, J = 8.0, 1H, NH), 4.39-4.20 (m, 1H, H_M), 4.14-3.97 (m, 4H, H_F, H_g), 3.97-3.58 (m, 4H, H_e, H_f, $H_{M'}$), 2.85-2.43 (m, 4H, H_P, H_R), 2.09-1.46 (m, 14H, H_G, H_H, H_I, H_J, H_K, H_L, H_Q, superimposed with residual H_2O), 1.38-1.36 (m, 18H, H_k), 1.23 (bs, 9H, H_l), 1.21 (s, 18H, H_a)

It was not possible to attribute each carbon peak to a single isomer unambiguously, so the complete list of observed peaks is reported below.

^{13}C NMR (126 MHz, $CDCl_3$): 163.4, 163.3, 159.2, 159.2, 158.9, 157.9, 157.7, 157.5, 157.2, 157.2, 157.2, 155.2, 155.0, 151.3, 151.3, 150.8, 150.8, 148.2, 148.1, 147.9, 147.6, 137.4, 137.4, 137.3, 132.2, 132.0, 131.5, 131.2, 131.2, 130.1, 130.1, 129.3, 129.1, 128.8, 124.6, 124.4, 122.8, 122.6, 122.3, 122.2, 121.3, 121.2, 120.8, 120.5, 120.4, 120.4, 120.2, 120.2, 120.1, 115.0, 114.8, 114.1, 114.0, 79.7, 79.4, 68.0, 67.9, 66.8, 66.7, 51.0, 50.6, 50.6, 50.2, 50.1, 42.0, 42.0, 41.9, 41.9, 37.8, 37.7, 37.4, 35.3, 35.1, 34.9, 32.1, 32.1, 31.6, 31.5, 29.8, 29.5, 29.4, 29.3, 28.7, 28.7, 28.6, 28.5, 28.5, 28.4, 28.3, 28.3, 26.1, 26.1, 25.7, 25.6.

HR-ESI-MS (+ve) m/z = 1162.7 $[M+H]^+$, for isotopic pattern see Figure 4.36.

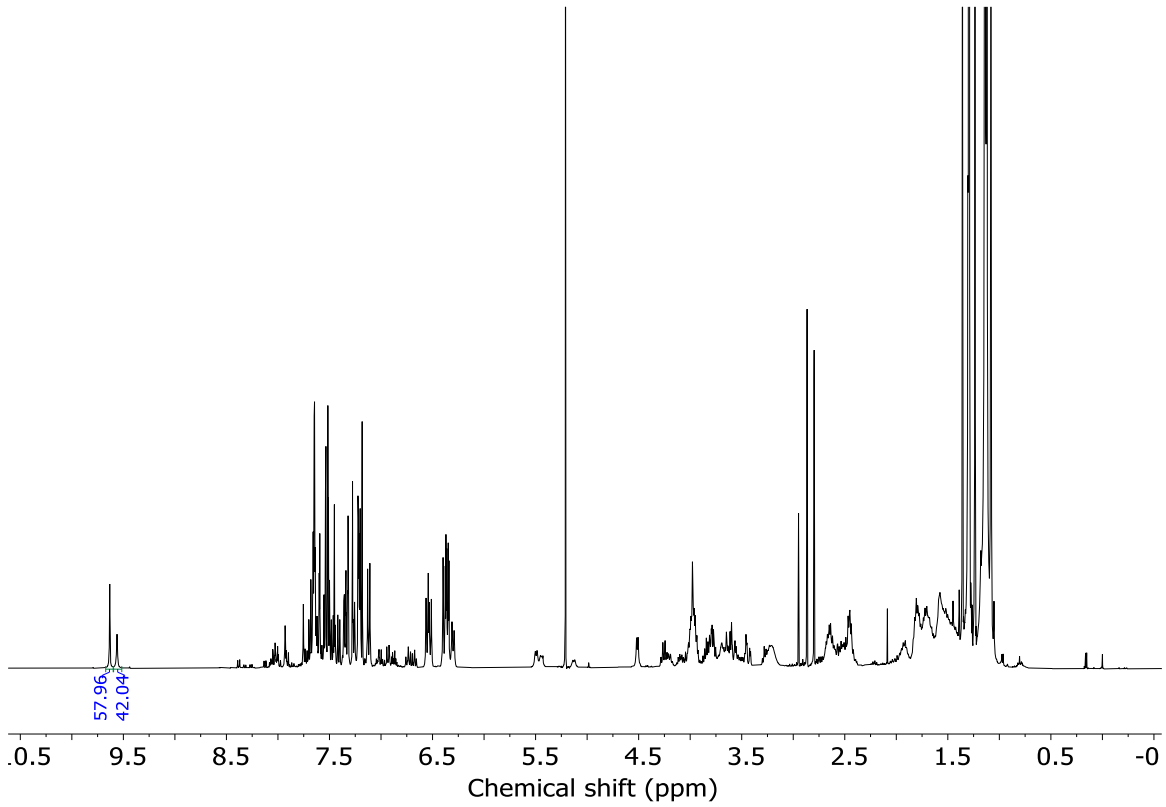

Figure 4.29 - ^{1}H NMR ($CDCl_3$, 400 MHz) of rotaxanes **4** prior to chromatography (58 : 42 *dr*).

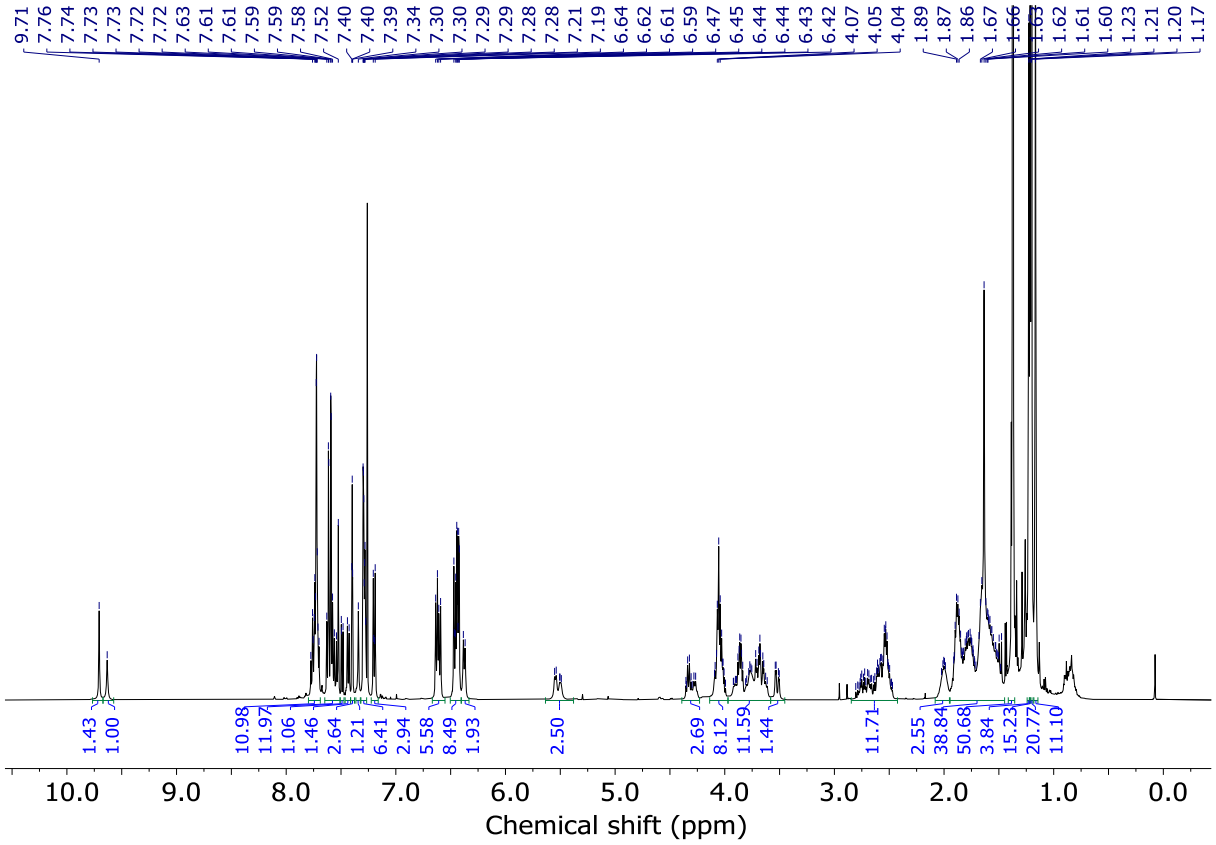

Figure 4.30 - ^{1}H NMR ($CDCl_3$, 500 MHz) of (Z_m,$S_{co\text{-}c}$)-**4** and (E_m,$S_{co\text{-}c}$)-**4** (1.4 : 1 *dr*).

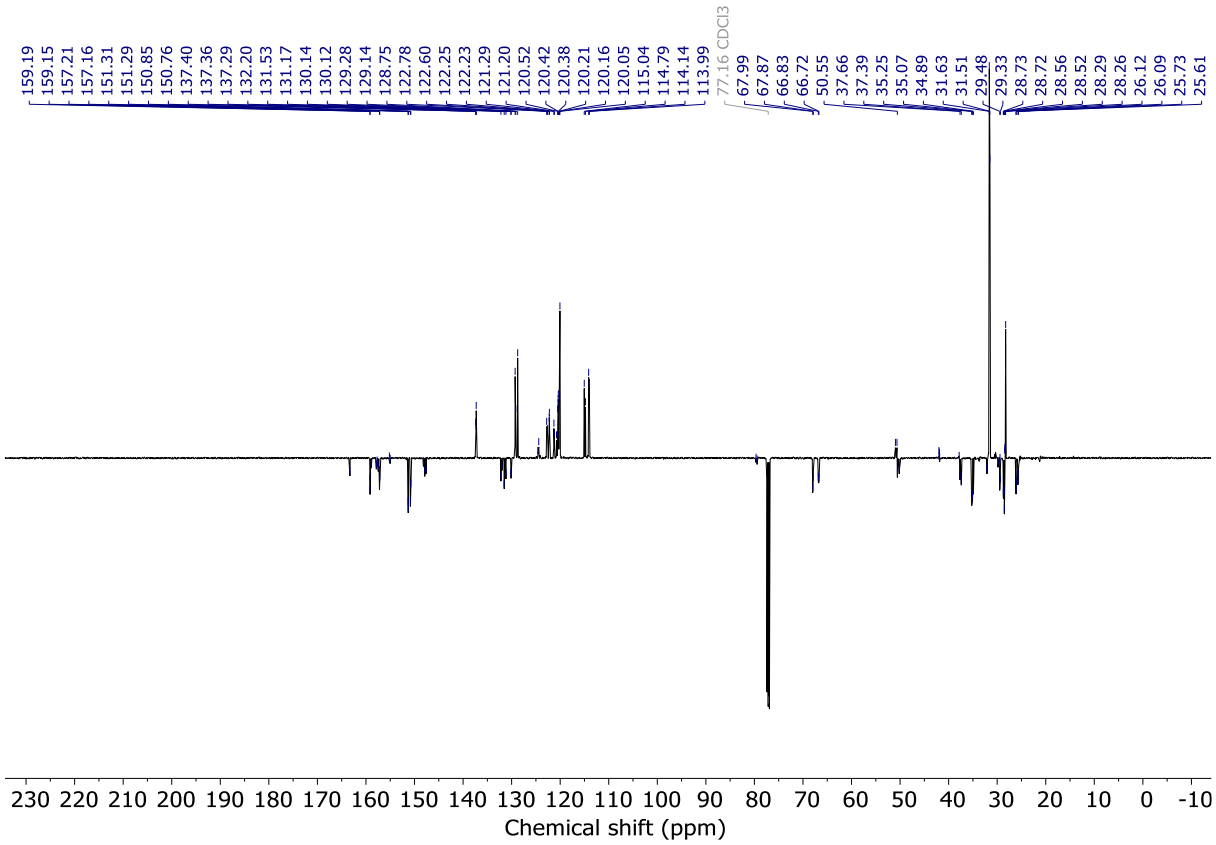

Figure 4.31 - JMOD NMR ($CDCl_3$, 126 MHz) of (Z_m,$S_{co\text{-}c}$)-**4** and (E_m,$S_{co\text{-}c}$)-**4** (1.4 : 1 *dr*).

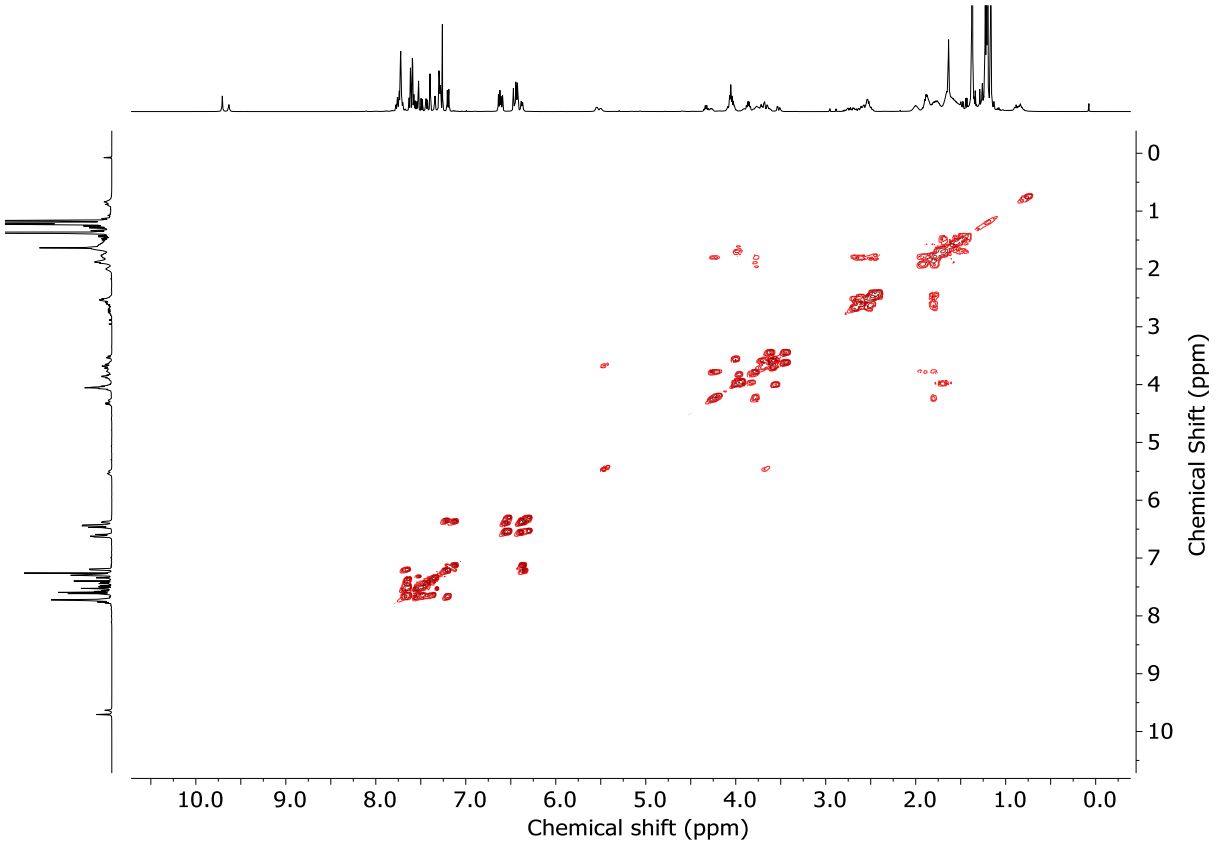

Figure 4.32 - COSY NMR ($CDCl_3$) of (Z_m,$S_{co\text{-}c}$)-**4** and (E_m,$S_{co\text{-}c}$)-**4** (1.4 : 1 *dr*).

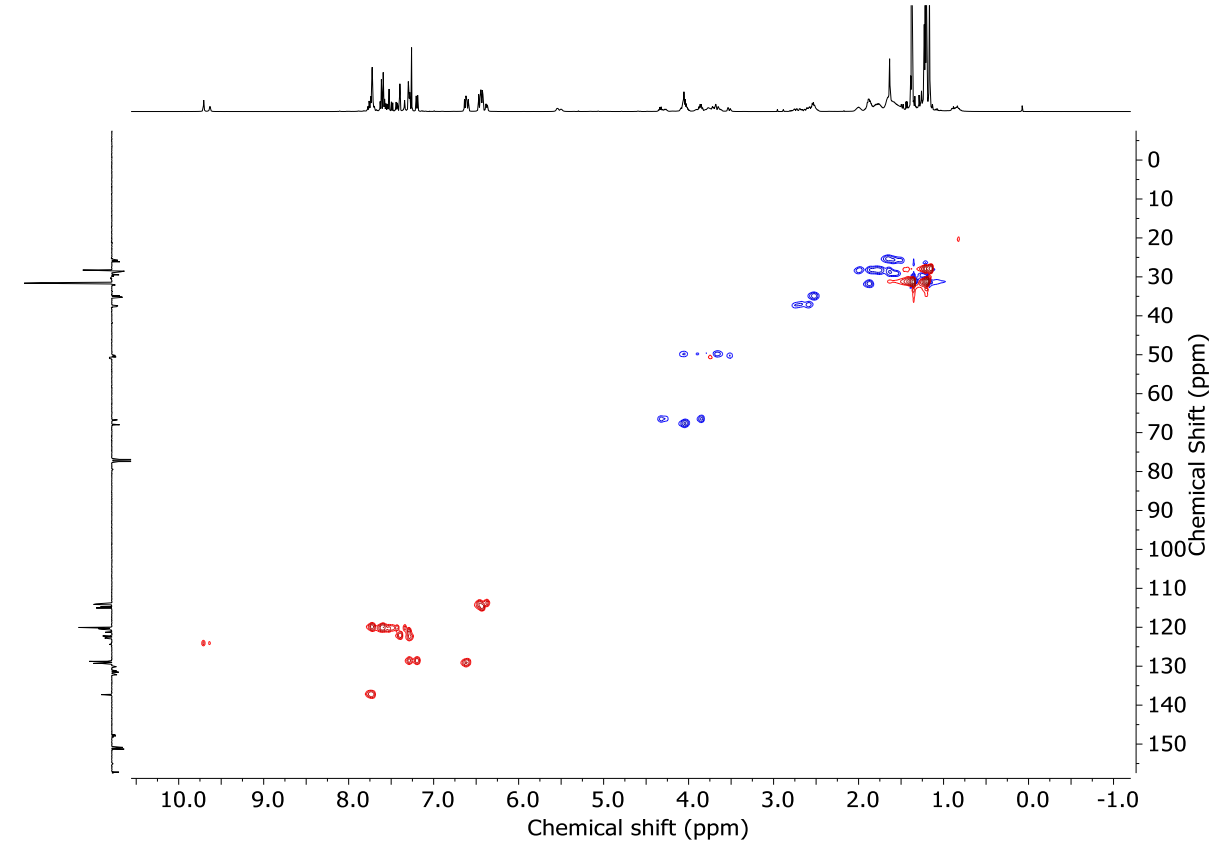

Figure 4.33 - HSQC NMR ($CDCl_3$) of (Z_m,$S_{co\text{-}c}$)-**4** and (E_m,$S_{co\text{-}c}$)-**4** (1.4 : 1 *dr*).

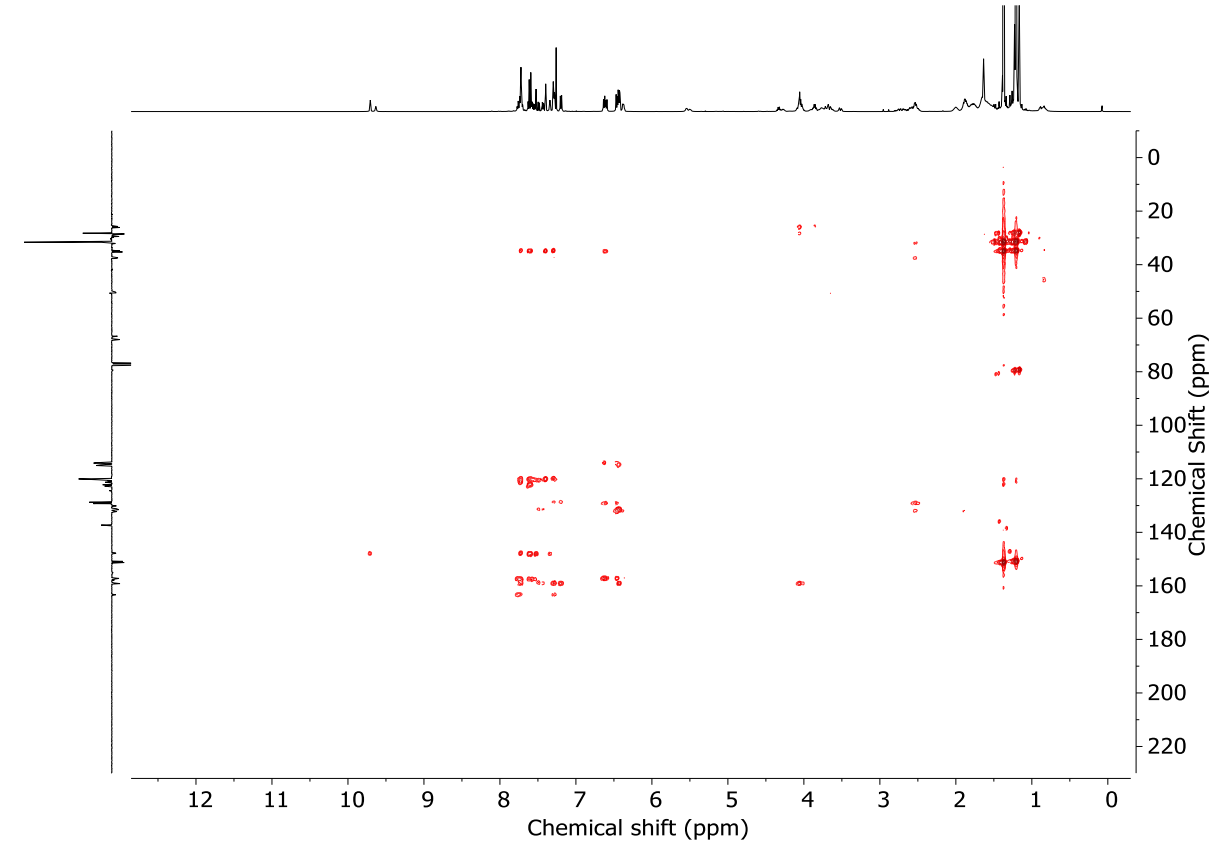

Figure 4.34 - HMBC NMR ($CDCl_3$) of (Z_m,$S_{co\text{-}c}$)-**4** and (E_m,$S_{co\text{-}c}$)-**4** (1.4 : 1 *dr*).

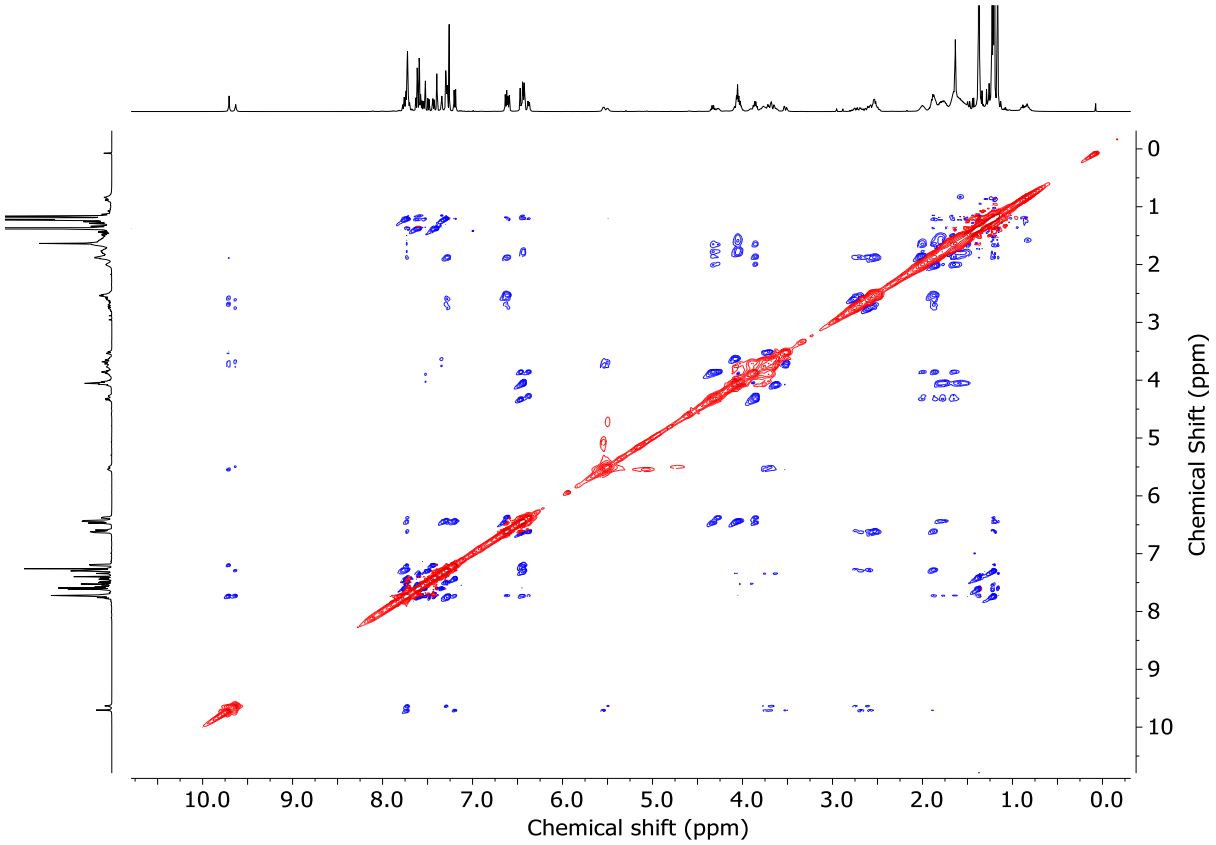

Figure 4.35 - NOESY NMR ($CDCl_3$) of (Z_m,$S_{co\text{-}c}$)-**4** and (E_m,$S_{co\text{-}c}$)-**4** (1.4 : 1 *dr*).

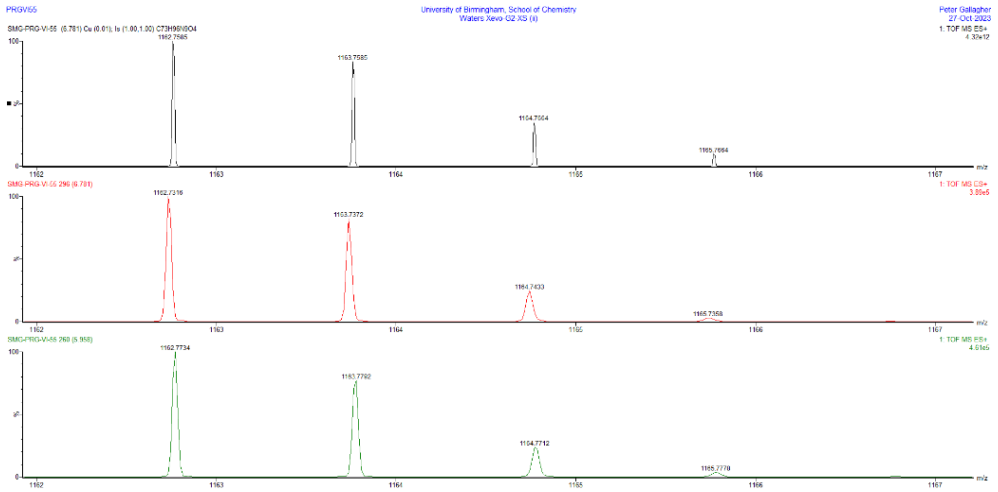

Figure 4.36 - Calculated (top) and observed (middle, bottom) isotopic patterns for (Z_m,$S_{co\text{-}c}$)-**4** and (E_m,$S_{co\text{-}c}$)-**4**.

Amine Rotaxanes 5

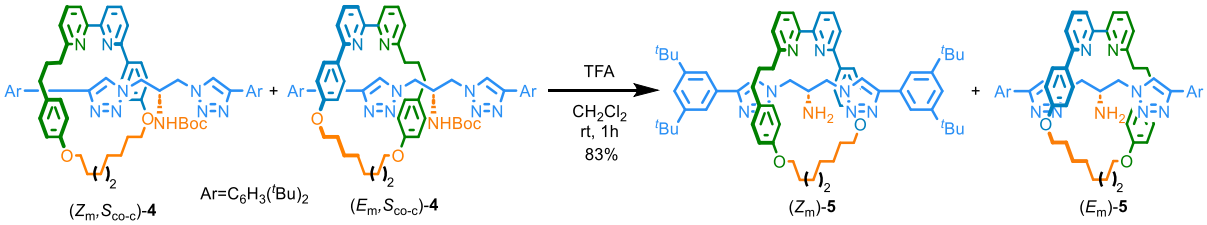

A vessel was charged with a mixture of rotaxanes **4** (16.4 mg, 0.014 mmol, 55:45 *dr*), TFA (25.0 µL, 0.21 mmol), and CH_2Cl_2 (1 mL). The reaction mixture was stirred at rt for 1 h. CH_2Cl_2 (10 mL) was added, washed with sat. $NaHCO_3$ solution (10 mL), brine (10 mL), and the combined organic extracts were dried ($MgSO_4$) and concentrated *in vacuo* to give rotaxanes **5** as a white foam (12.3 mg, 83%, 57:43 *dr*) that were characterised without further purification.

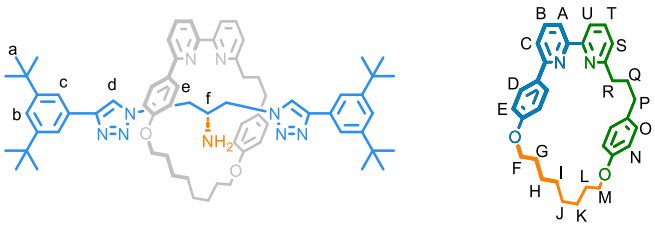

Major diastereomer

^{1}H NMR (500 MHz, $CDCl_3$) δ: 8.54 (s, 2H, H_d), 7.73 (app. T, J = 8.2, 1H, H_T), 7.70-7.63 (m, 5H, H_c, H_B), 7.60-7.55 (m, 1H, H_U), 7.52-7.48 (m, 1H, H_A or H_C), 7.45-7.39 (m, 1H, H_A or H_C), 7.37-7.34 (m, 2H, H_b), 7.30-7.19 (m, 3H, H_S and H_D or H_E, superimposed with residual $CHCl_3$), 6.71-6.63 (m, 2H, H_O), 6.58 (dt, J = 8.4, 2.5, 2H, H_N), 6.51-6.46 (m, 2H, H_D or H_E), 4.22-3.99 (m, 4H, H_F, H_M), 3.88-3.70 (m, 2H, H_e), 3.29 (dd, J = 14.0, 7.6, 2H, $H_{e'}$), 2.65-2.40 (m, 5H, H_f, H_P, H_R), 1.97-1.44 (m, 14H, H_G, H_H, H_I, H_J, H_K, H_L, H_Q, superimposed with residual H_2O), 1.29 (s, 36H, H_a).

Minor diastereomer

^{1}H NMR (500 MHz, $CDCl_3$) δ: 8.54 (s, 2H, H_d), 7.73 (app. T, J = 8.2, 1H, H_T), 7.70-7.63 (m, 5H, H_c, H_B), 7.60-7.55 (m, 1H, H_U), 7.52-7.48 (m, 1H, H_A or H_C), 7.45-7.39 (m, 1H, H_A or H_C), 7.37-7.34 (m, 2H, H_b), 7.30-7.19 (m, 3H, H_S and H_D or H_E, superimposed with residual $CHCl_3$), 6.71-6.63 (m, 2H, H_O), 6.58 (dt, J = 8.4, 2.5, 2H, H_N), 6.51-6.46 (m, 2H, H_D or H_E), 4.22-3.99 (m, 4H, H_F, H_M), 3.88-3.70 (m, 2H, H_e), 3.29 (dd, J = 14.0, 7.6, 2H, $H_{e'}$), 2.65-2.40 (m, 5H, H_f, H_P, H_R), 1.97-1.44 (m, 14H, H_G, H_H, H_I, H_J, H_K, H_L, H_Q, superimposed with residual H_2O), 1.29 (s, 36H, H_a).

It was not possible to attribute each carbon peak to a single isomer unambiguously, so the complete list of observed peaks is reported below.

^{13}C NMR (126 MHz, $CDCl_3$) δ: 163.1, 159.1, 159.1, 159.0, 157.5, 157.1, 151.1, 151.0, 147.9, 147.9, 137.4, 137.3, 137.3, 137.2, 132.5, 132.3, 131.9, 131.8, 130.4, 129.4, 129.3, 129.0, 128.8, 122.7, 122.6, 122.2, 122.0, 121.8, 121.8, 120.6, 120.5, 120.5, 120.3, 120.2, 120.0, 119.9, 115.0, 115.0, 114.2, 114.1, 67.7, 67.5, 66.7, 66.5, 50.5, 50.4, 37.4, 37.3, 35.1, 35.1, 34.9, 32.7, 32.4, 31.4, 29.7, 29.7, 29.4, 29.4, 29.4, 28.8, 28.6, 28.6, 28.4, 28.4, 26.0, 25.7, 25.6

HR-ESI-MS (+ve) m/z = 1062.7061 $[M+H]^+$, for isotopic pattern see Figure 4.42.

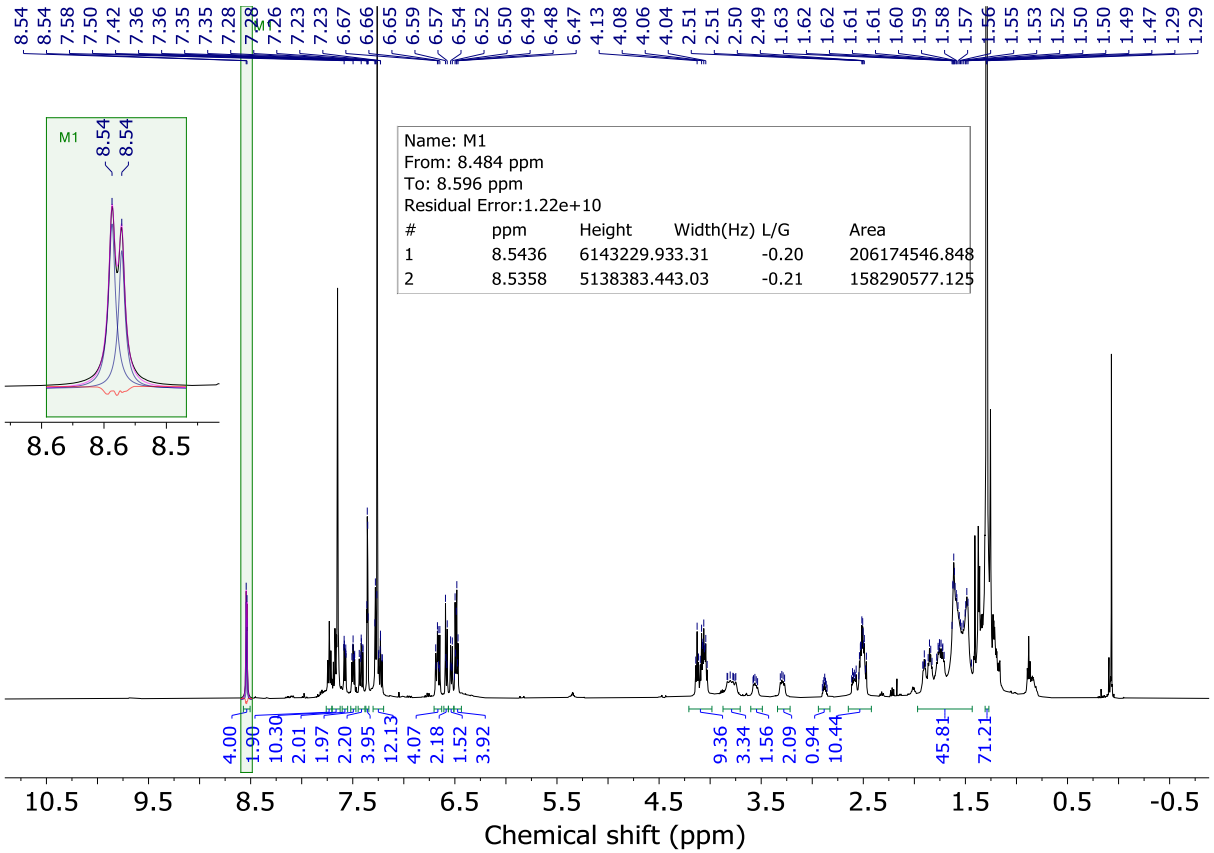

Figure 4.37 - ^{1}H NMR ($CDCl_3$, 500 MHz) of (Z_m)-**5** and (E_m)-**5** (1.3 : 1 *dr*).

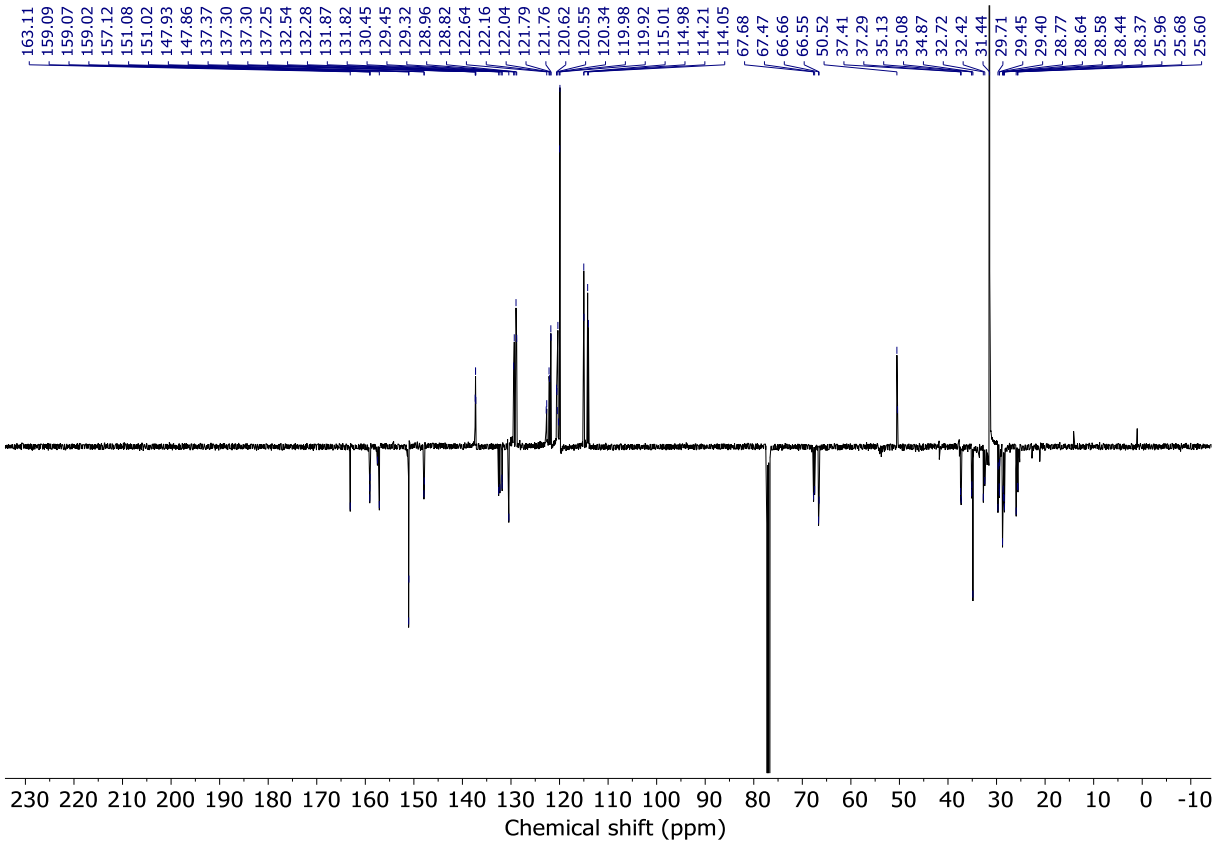

Figure 4.38 - JMOD NMR ($CDCl_3$, 126 MHz) of (Z_m)-**5** and (E_m)-**5** (1.3 : 1 *dr*).

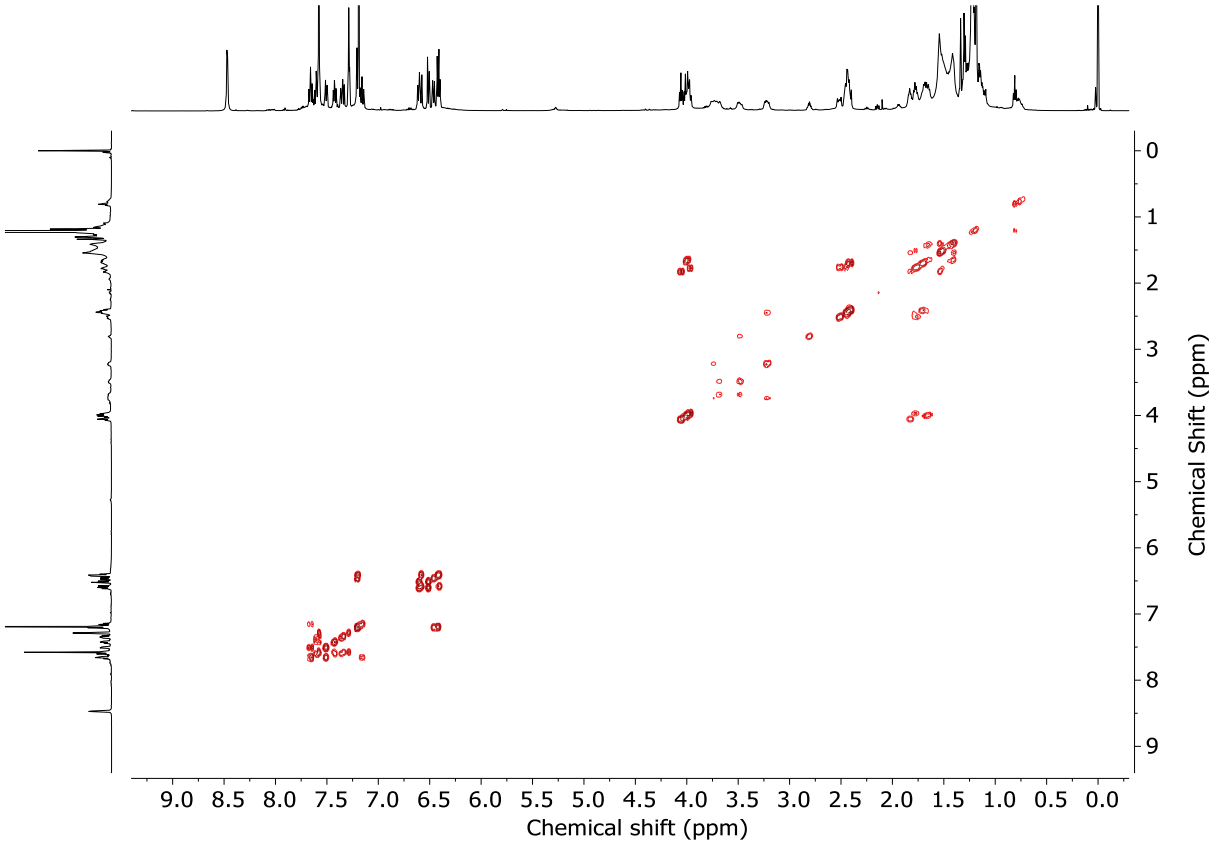

Figure 4.39 - COSY NMR ($CDCl_3$) of (Z_m)-**5** and (E_m)-**5** (1.3 : 1 *dr*).

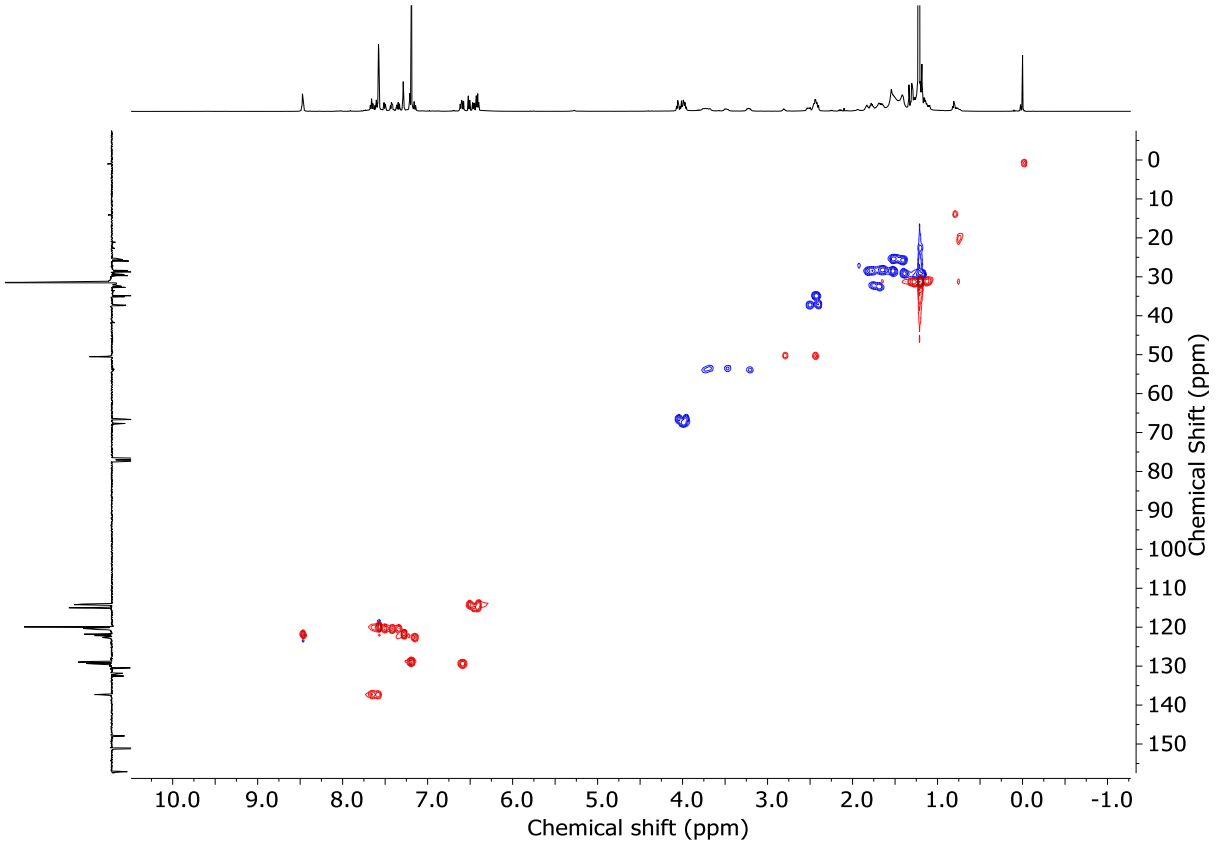

Figure 4.40 - HSQC NMR ($CDCl_3$) of (Z_m)-**5** and (E_m)-**5** (1.3 : 1 *dr*).

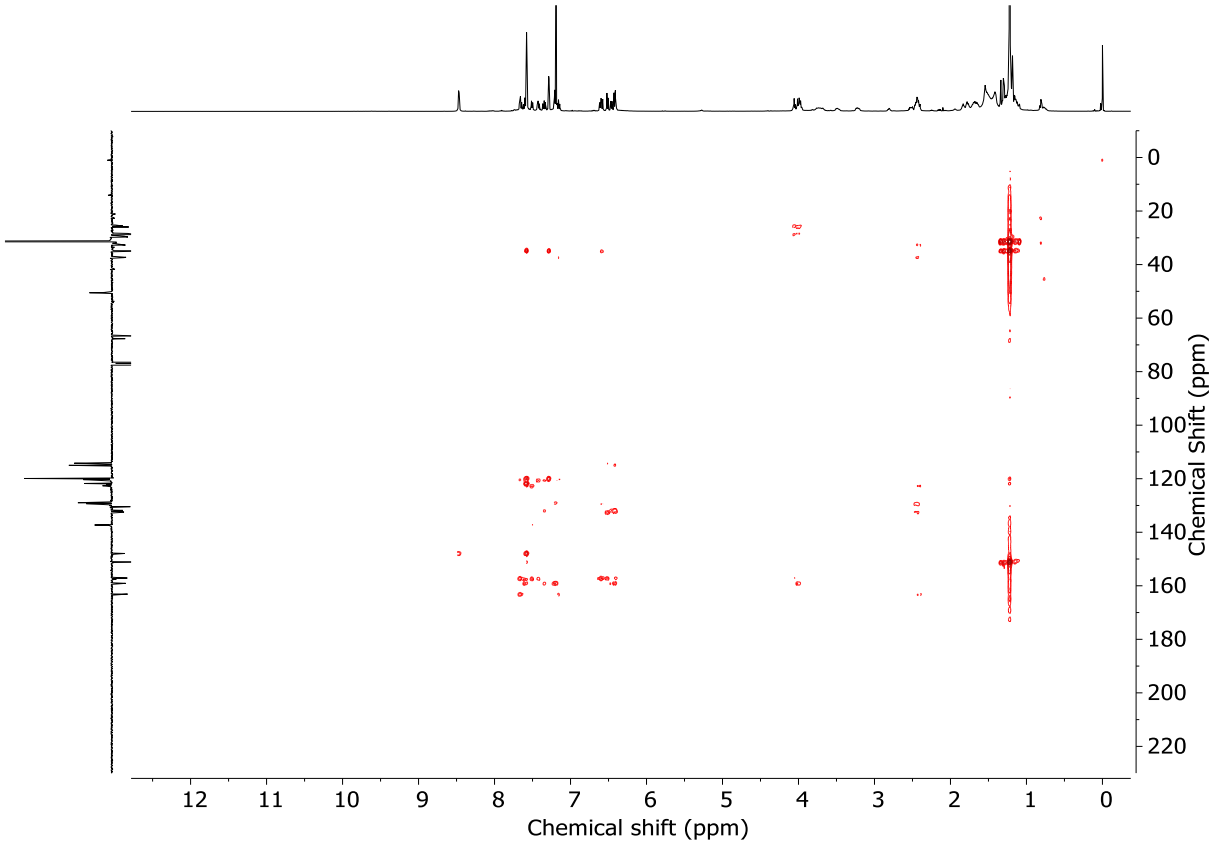

Figure 4.41 - HMBC NMR ($CDCl_3$) of (Z_m)-**5** and (E_m)-**5** (1.3 : 1 *dr*).

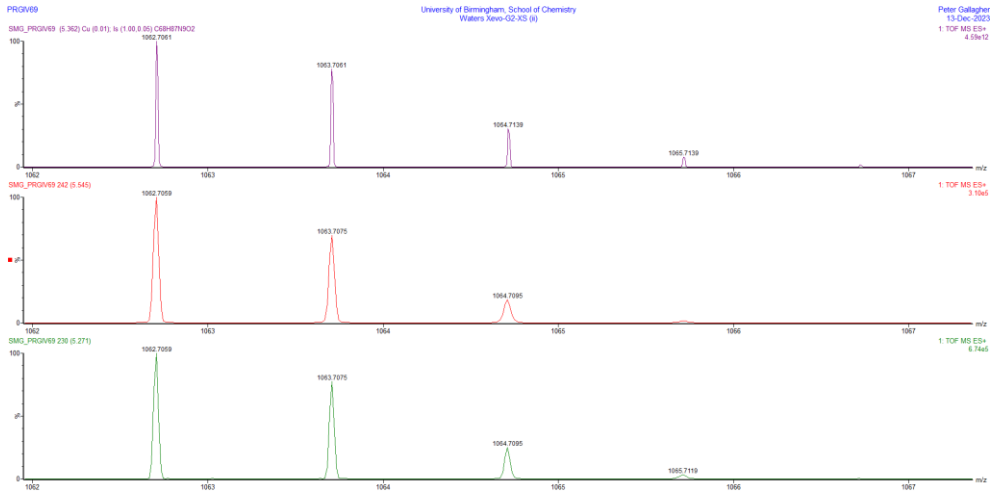

Figure 4.42 - Calculated (top) and observed (middle, bottom) isotopic patterns for (Z_m)-**5** and (E_m)**5**.

Synthesis of rotaxane 11 and associated compounds (Scheme 2)

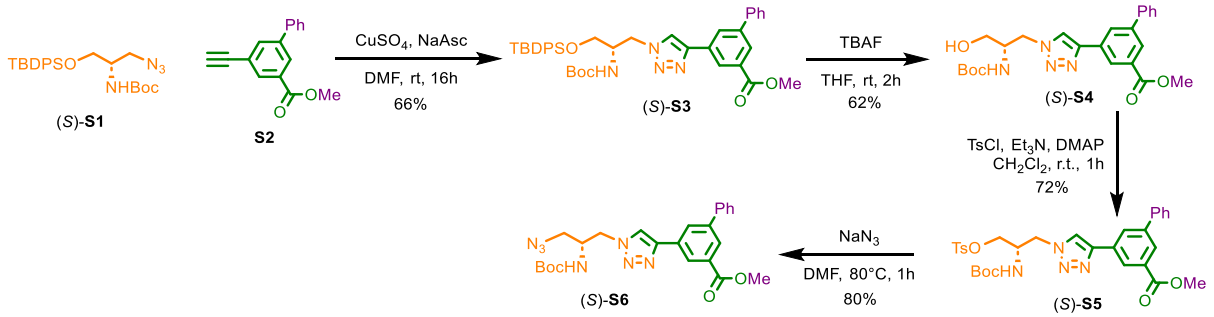

Scheme 4.4 - Synthetic route to azide (*S*)-**S6.**

Silyl ether (*S*)-S3

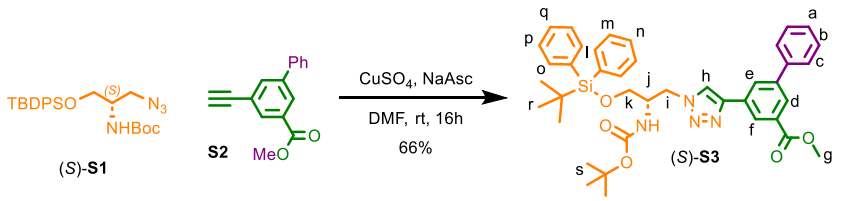

A suspension of (*S*)-**S1** (1.20g, 2.64 mmol), **S2** (623 mg, 2.64 mmol), $CuSO_4$ (42.2 mg, 0.26 mmol) and sodium ascorbate (78.4 mg, 0.39 mmol) in DMF (30 mL) is degassed by bubbling N_2 for 10 min. The solution turns brown, and it is stirred at rt for 16h. The reaction mixture is poured into a NH_3-EDTA (100 mL) then extracted with Et_2O (3 x 50 mL). The organic phases are washed with a 5% LiCl solution (50 mL), washed with brine (50 mL), dried ($MgSO_4$) and concentrated *in vacuo*. Chromatography (petrol-EtOAc 0→20%) gave (*S*)-**S3** as a white foam (1.2 g, 66%).

^{1}H NMR (400 MHz, $CDCl_3$) δ: 8.35 (t, *J* = 1.4, 1H, H_f), 8.31 (t, *J* = 1.8, 1H, H_e) 8.26 (t, *J* = 1.7, 1H, H_d) 7.84 (bs, 1H, H_h), 7.71-7.66 (m, 2H, H_b), 7.66-7.59 (m, 4H, H_p, H_m *or* H_o, H_l) 7.51-7.45 (m, 2H, H_c) 7.44-7.35 (m, 7H, H_a, H_n, H_o and H_l, H_o *or* H_p, H_m), 5.01 (d, *J* = 8.42, 1H, NH), 4.64 (d, *J* = 6.2, 2H, H_k, $H_{k`}$) 4.19 (app bs, 1H, $H_j$), 3.97 (s, 3H, $H_g$), 3.79-3.69 (m, 1H, $H_i$ or $H_{i`}$), 3.67-3.53 (m, 1H, H_i or $H_{i`}$), 1.40 (bs, 9H, H_s), 1.11 (s, 9H, H_r)

^{13}C NMR (101 MHz, $CDCl_3$) δ: 166.8, 146.8, 142.2, 139.8, 139.8, 135.6, 135.6, 135.5, 132.7, 132.5, 131.4, 131.3, 130.1, 130.1, 128.9, 128.6, 128.0, 128.0, 127.9, 127.2, 125.5, 121.2, 79.7 (HMBC), 62.9, 52.3, 51.9, 50.7, 28.3, 27.0, 23.9, 19.3.

HR-ESI-MS (+ve) *m/z* = 691.3317 $[M+H]^+$ (calc. 691.3310 *m/z* for $C_{40}H_{46}N_4O_5Si$);

$[\alpha]_D^{23}$+1.2 (c 0.65, $CHCl_3$);

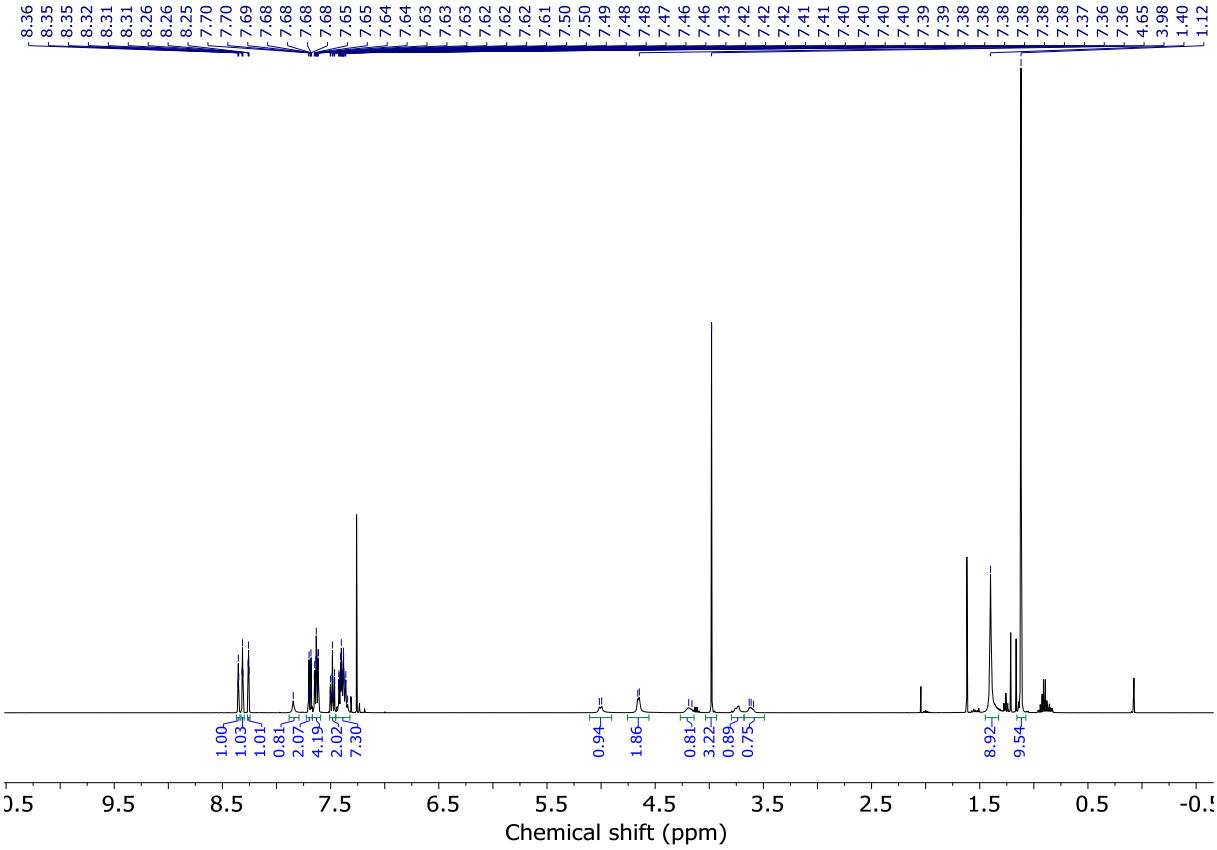

Figure 4.43 - ^{1}H NMR ($CDCl_3$, 400 MHz) of (*S*)-**S3**.

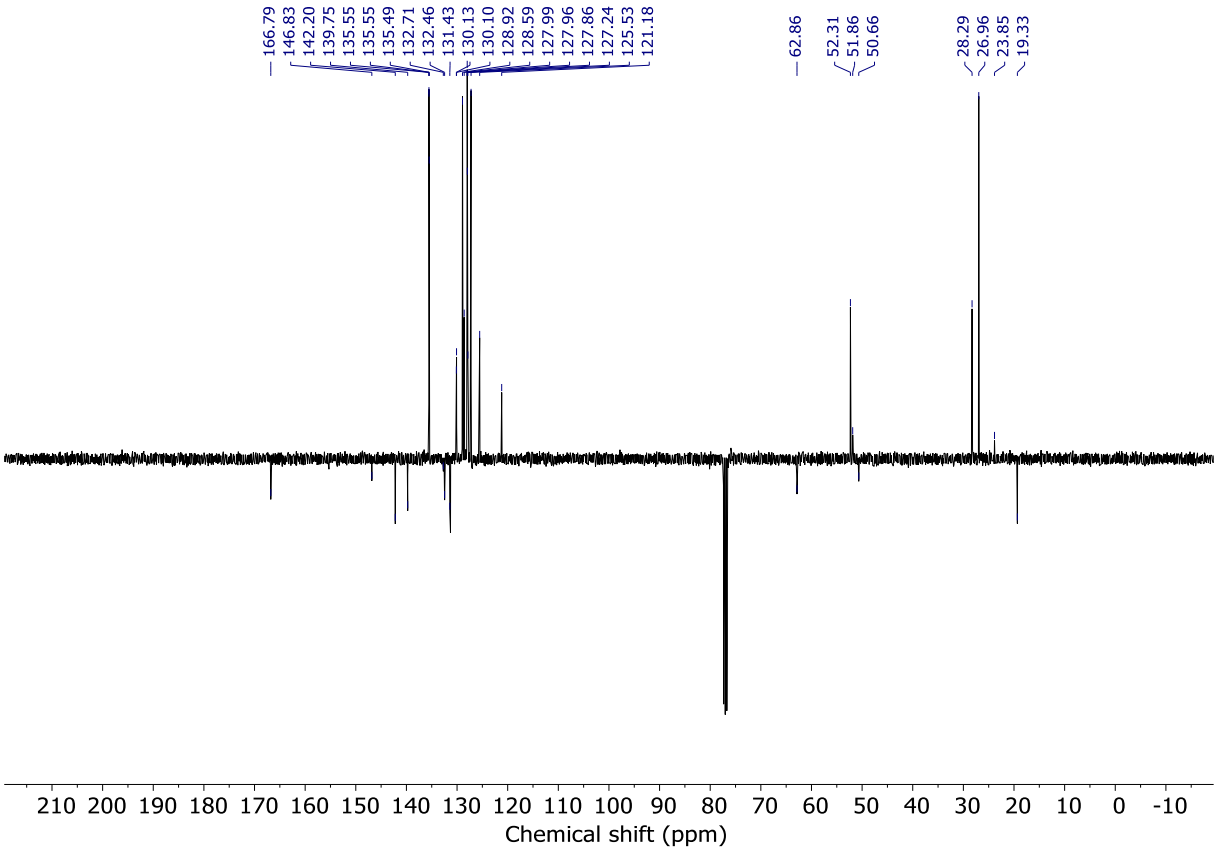

Figure 4.44 - JMOD NMR ($CDCl_3$, 101 MHz) of (*S*)-**S3**.

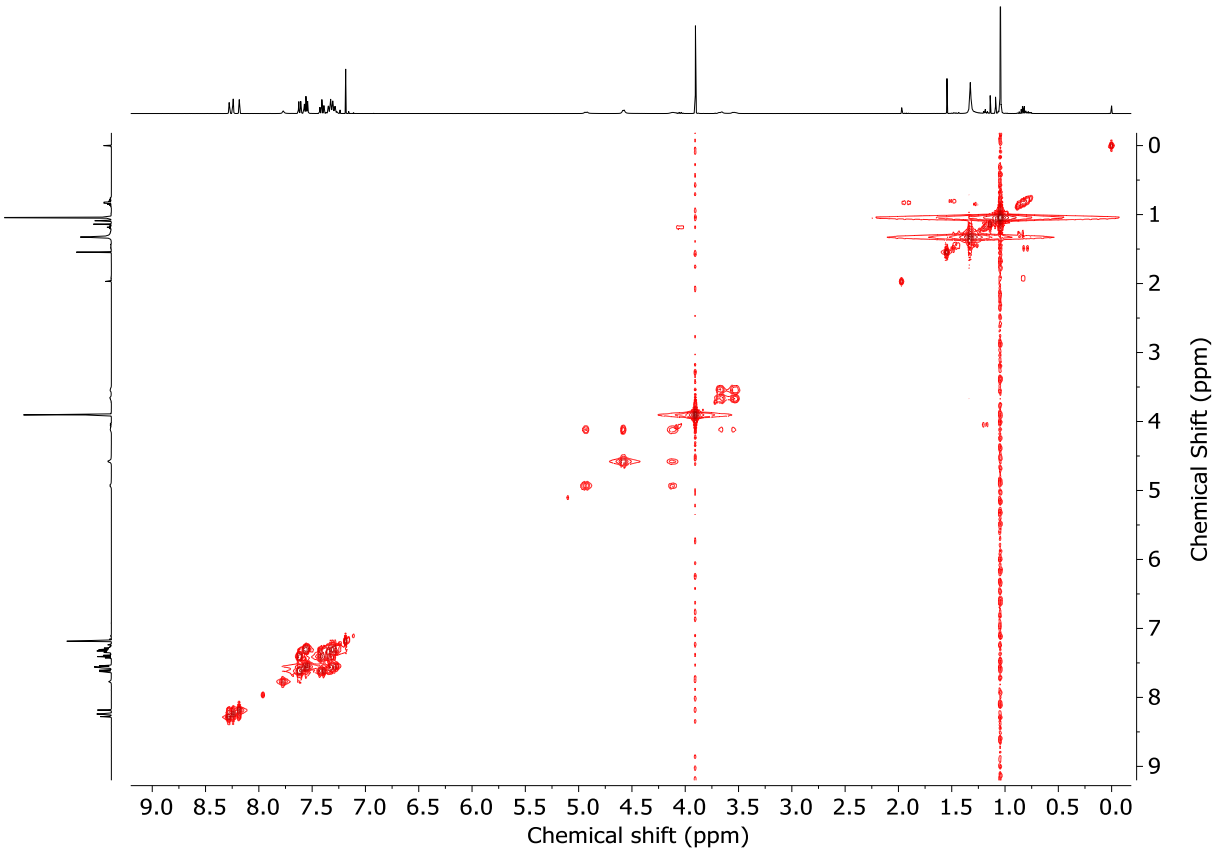

Figure 4.45 - COSY NMR ($CDCl_3$) of (*S*)-**S3**.

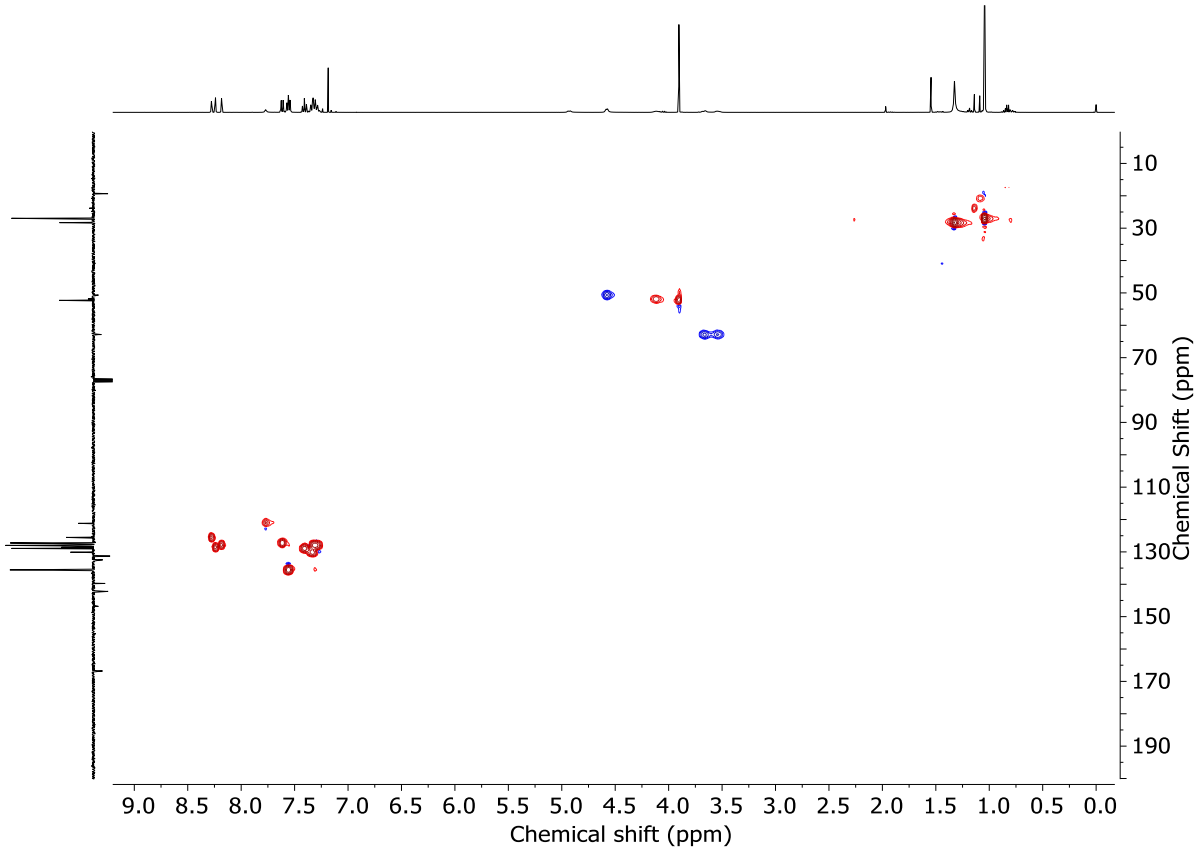

Figure 4.46 - HSQC NMR ($CDCl_3$) of (*S*)-**S3**.

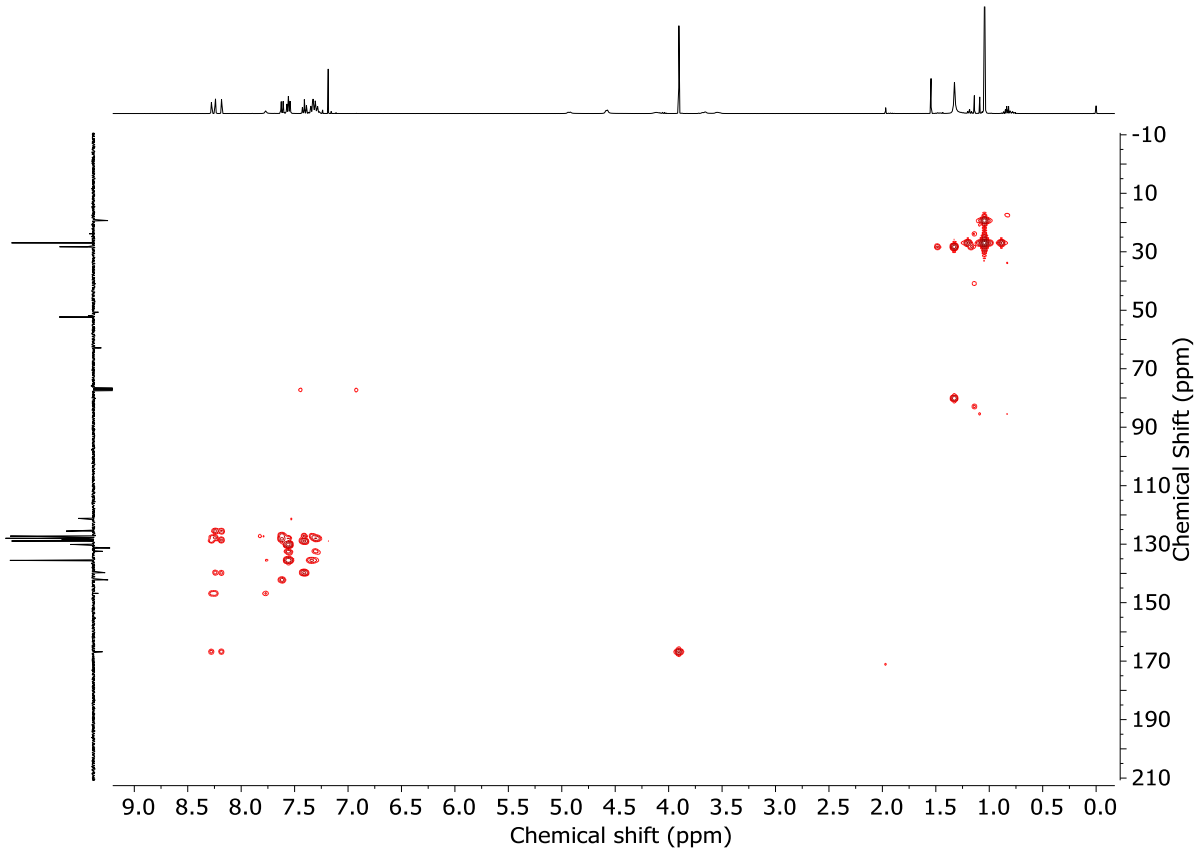

Figure 4.47 - HMBC NMR ($CDCl_3$) of (*S*)-**S3**.

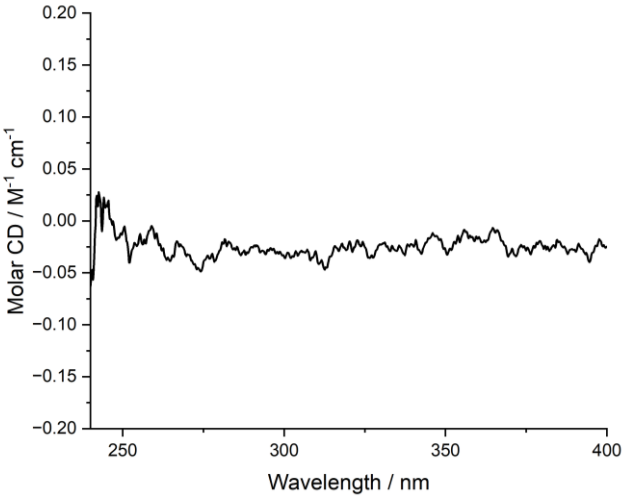

Figure 4.48 - Circular dichroism spectra of (*S*)-**S3** (63.5 µM) at 293 K in $CHCl_3$. No measurable CD response was observed so the $[\alpha]_D$ of (*S*)-**S3** was measured.

Alcohol (*S*)-S4

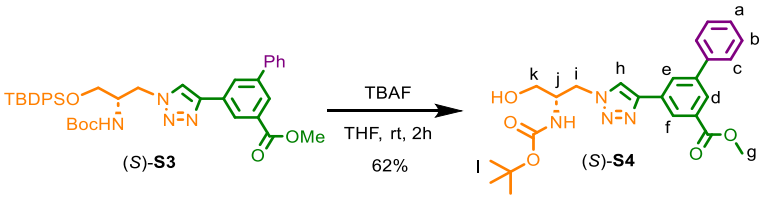

To a suspension of (*S*)-**S3** (1.20 g, 1.74 mmol) in THF (20 mL) was added a 1M solution of TBAF in THF (3.5 mL). The solution is stirred at rt for 2 h. The reaction mixture was partitioned between H_2O (20 mL) and EtOAc (50 mL), the phases separated, and the organic layer extracted with EtOAc (2 x 50 mL). The collected organic fractions were then washed with brine (50 mL), then dried ($MgSO_4$). The solvent was removed *in vacuo* and the crude was purified by column chromatography (CH_2Cl_2-CH_3CN 0→80%) to give (*S*)-**S4** as a white foam (486 mg, 62%).

^{1}H NMR (400 MHz, $CDCl_3$) δ: 8.38 (t, *J* = 1.60, 1H, H_f), 8.35 (t, *J* = 1.60, 1H, H_e), 8.26 (t, *J* = 1.60, 1H, H_d), 7.99 (s, 1H, H_h), 7.71-7.66 (m, 2H, H_c) 7.51-7.45 (m, 2H, H_b) 7.40 (app. tt, *J* = 7.4, 1.1, 1H, H_a) 5.18 (d, *J* = 7.6, 1H, NH), 4.77-4.62 (m, 2H, H_k, $H_{k'}$) 4.09 (app. sept., 1H, H_j), 3.97 (s, 3H, H_g), 3.77 (dd, *J* = 15.0, 4.8, 1H, H_i or $H_{i'}$), 3.62 (dd, *J* = 11.6, 4.8, 1H, H_i or $H_{i'}$), 1.44 (s, 9H, H_l)

^{13}C NMR (101 MHz, $CDCl_3$) δ: 166.8, 147.0 (HMBC) 142.3, 139.7, 131.4, 131.2, 128.9, 128.6, 128.0, 128.0, 127.2, 125.5, 121.6, 80.4 (HMBC), 61.8, 52.3, 52.0, 50.0 28.3.

HR-ESI-MS (+ve) *m/z* = 453.2133 $[M+H]^+$ (calc. 453.2132 *m/z* for $C_{24}H_{29}N_4O_5$);

$[\alpha]_D^{23}$-0.8 (c 0.74, $CHCl_3$)

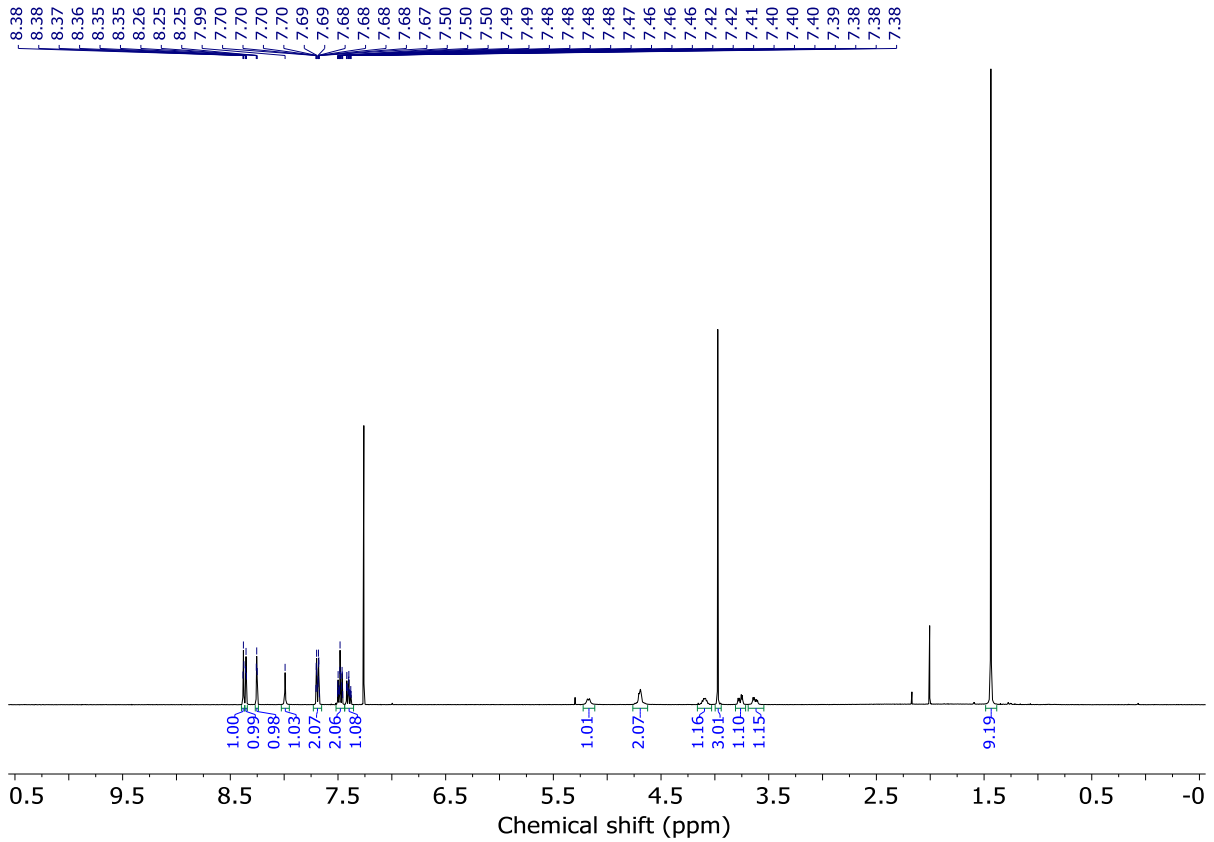

Figure 4.49 - ^{1}H NMR ($CDCl_3$, 400 MHz) of (*S*)-**S4**.

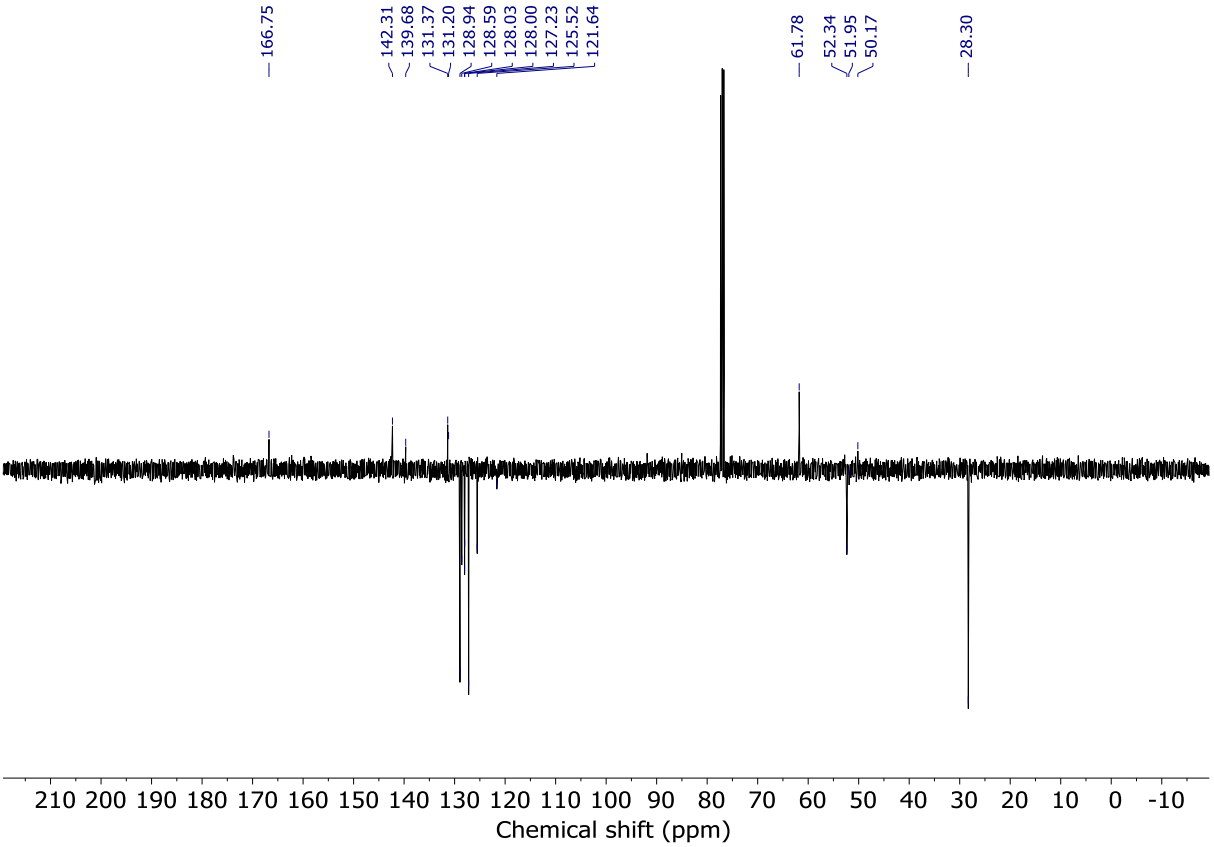

Figure 4.50 - JMOD NMR ($CDCl_3$, 101 MHz) of (*S*)-**S4**.

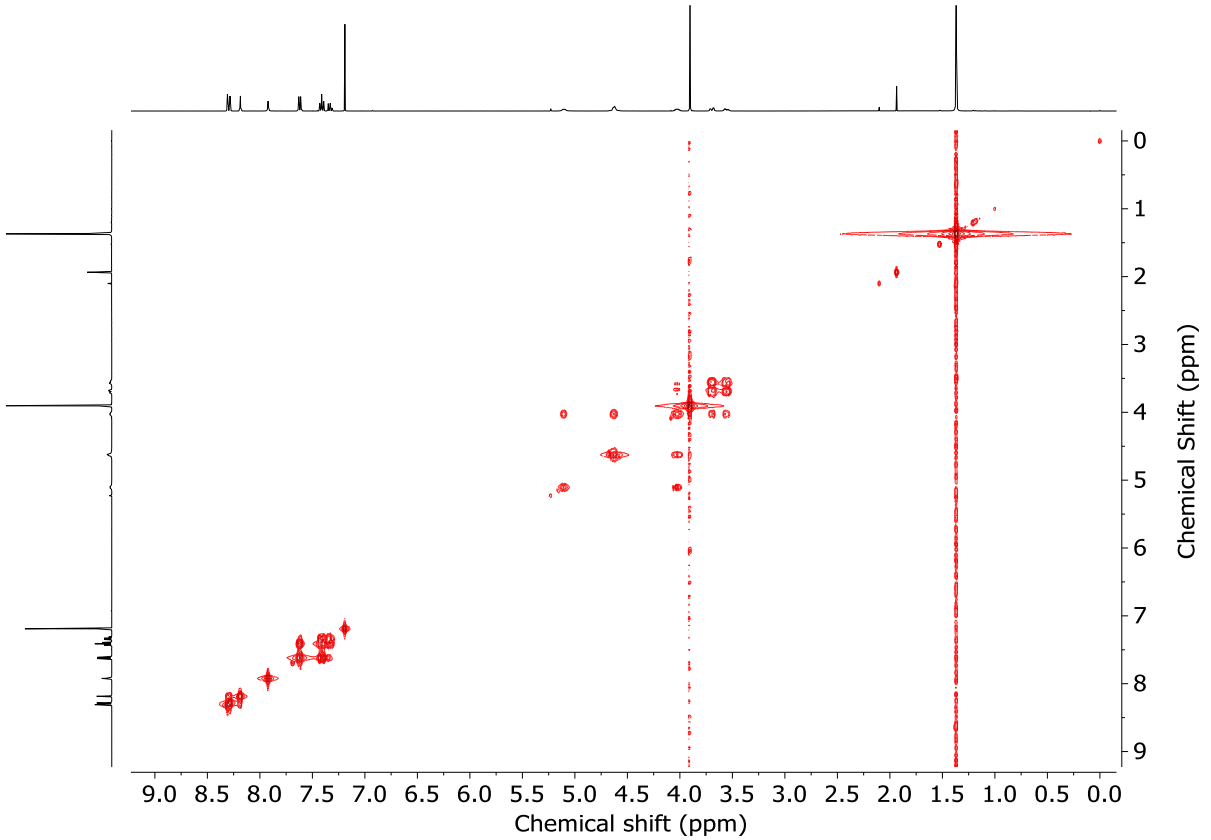

Figure 4.51 - COSY NMR ($CDCl_3$) of (*S*)-**S4**.

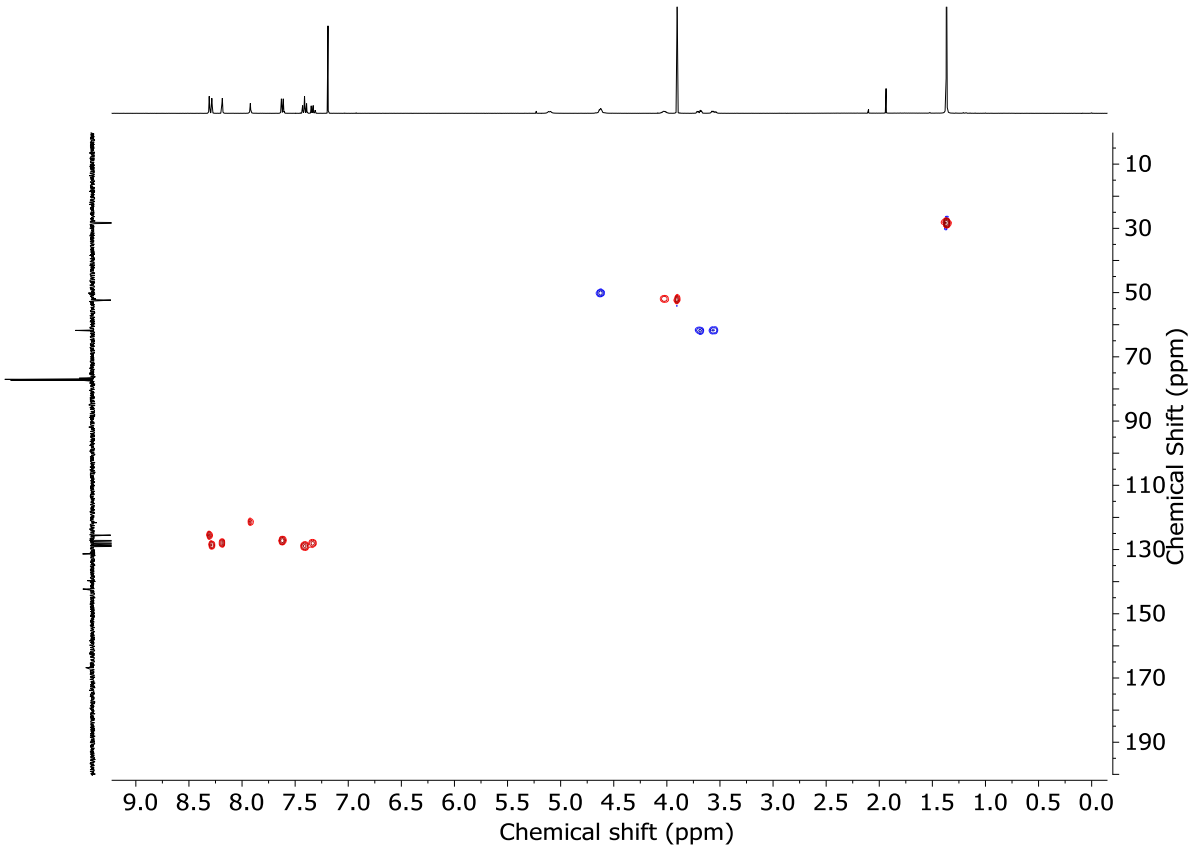

Figure 4.52 - HSQC NMR ($CDCl_3$) of (*S*)-**S4**.

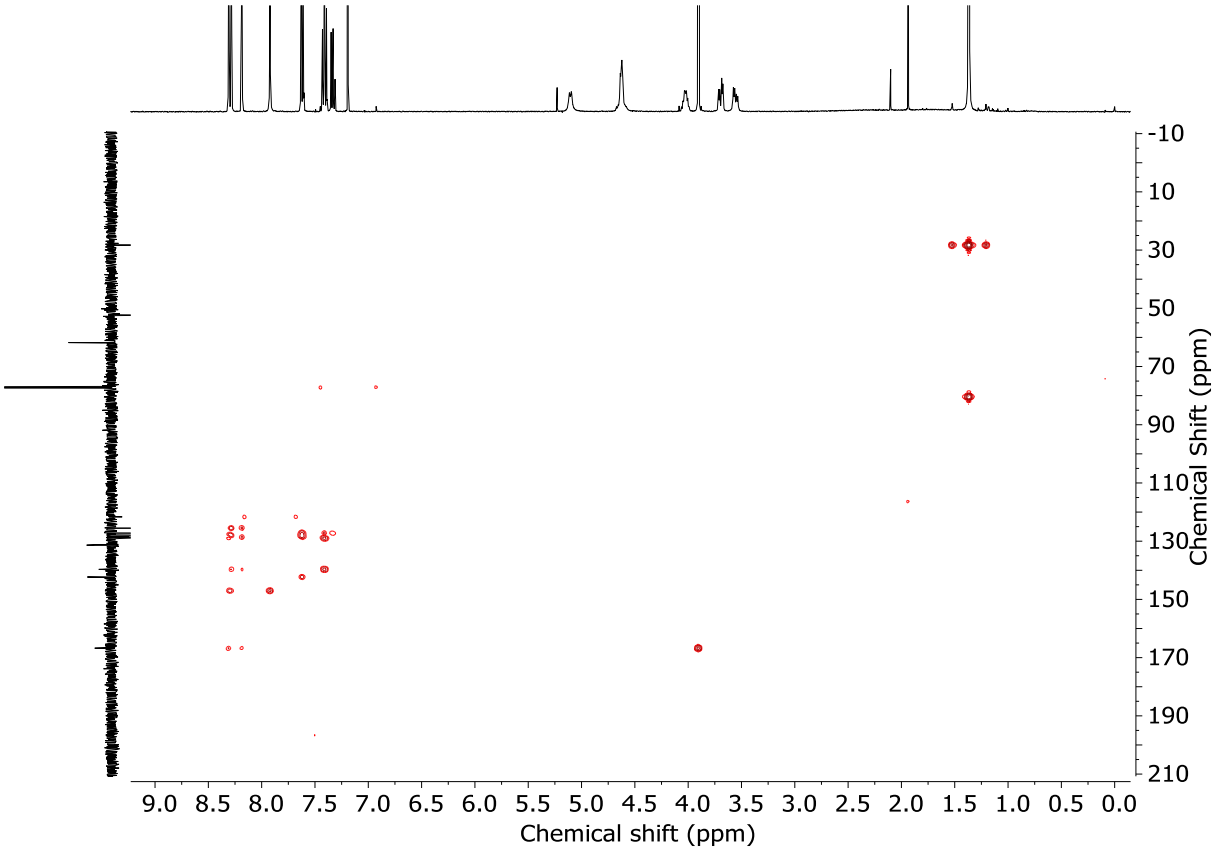

Figure 4.53 - HMBC NMR ($CDCl_3$) of (*S*)-**S4**.

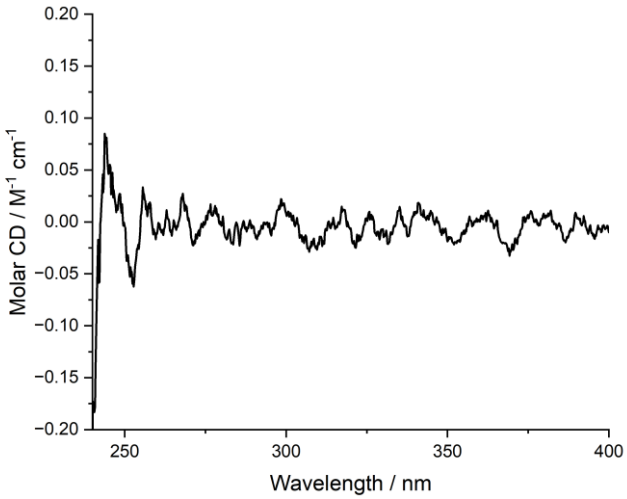

Figure 4.54 - Circular dichroism spectra of (*S*)-**S4** (63.5 μM) at 293 K in $CHCl_3$. No measurable CD response was observed so the $[\alpha]_D$ of (*S*)-**S4** was measured.

Tosylate (*S*)-S5

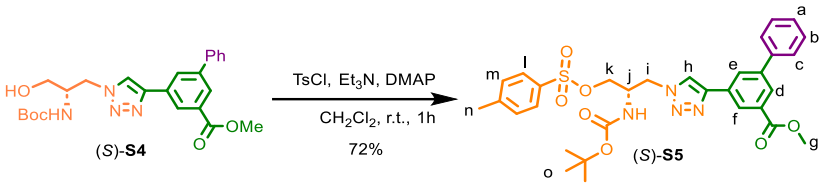

To a solution of (*S*)-**S4** (480 mg, 1.06 mmol), DMAP (13.0 mg, 0.11 mmol), and Et_3N (0.59 mL, 4.24 mmol) in CH_2Cl_2 (10 mL) was added TsCl (404.6 mg, 2.12 mmol). The solution turned yellow and was stirred at rt for 1h. H_2O (20 mL) was added, the phases separated, and the organic layer extracted with CH_2Cl_2 (2 x 50 mL). The collected organic fractions were then washed with brine (50 mL), then dried ($MgSO_4$). The solvent was removed *in vacuo* and the crude was purified by column chromatography (petrol-EtOAC 0→50%) to give (*S*)-**S5** as a white foam (460.4 mg, 72%). Decomposition of the product was observed upon standing in solution of CD_3CN (See Figure 52). The sample was too unstable to collect CD data.

^{1}H NMR (400 MHz, CD_3CN) δ: 8.42 (t, *J* = 1.5, 1H, H_f), 8.30 (t, *J* = 1.8, 1H, H_e), (t, *J* = 1.70, 1H, H_d), 8.20 (s, 1H, H_h), 7.81 (dt, *J* = 8.3, 2.0, 2H, H_l), 7.78-7.74 (m, 2H, H_c) 7.57-7.51 (m, 2H, H_b), 7.49-7.41 (m, 3H, H_a, H_m), 5.58 (d, *J* = 9.0, 1H, NH), 4.61-4.41 (m, 2H, H_i or H_k), 4.35-4.24 (m, 1H, H_j), 4.16-4.04 (m, 2H, H_i or H_k), 3.96 (s, 3H, H_g), 2.40 (s, 3H, H_n), 1.32 (bs, 9H, H_o)

^{13}C NMR (101 MHz, CD_3CN) δ: 167.0, 142.7, 140.1, 132.7, 132.5, 132.3, 130.7, 129.7, 128.8, 128.7, 128.5, 127.7, 126.5, 125.5, 123.0, 79.4 (HMBC), 69.6, 67.6, 53.6, 52.3, 50.6, 50.5, 28.0, 21.2

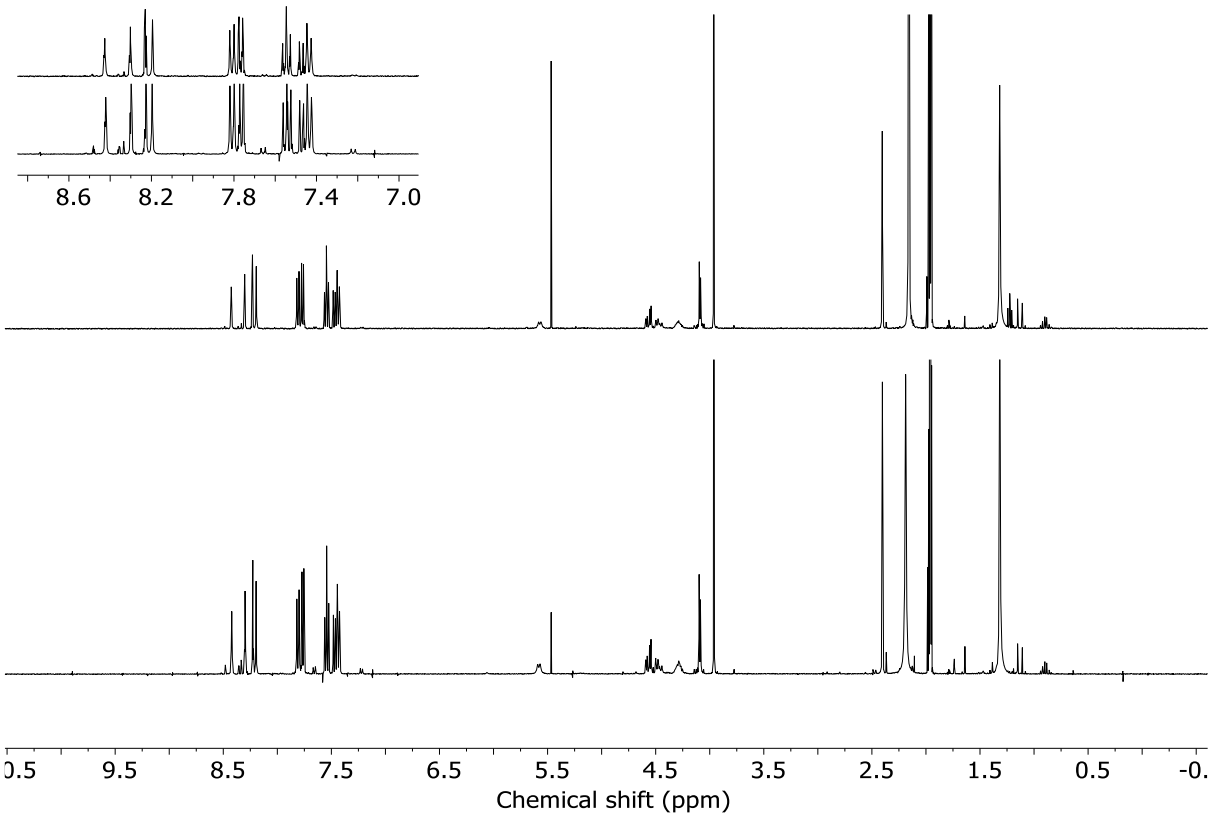

Figure 4.55 - Stacked ^{1}H NMR spectrum of purified (*S*)-**S5** (top) and ^{1}H NMR spectrum of the same sample after 1 hour at room temperature to indicate degradation (bottom, 400 MHz, CD_3CN)

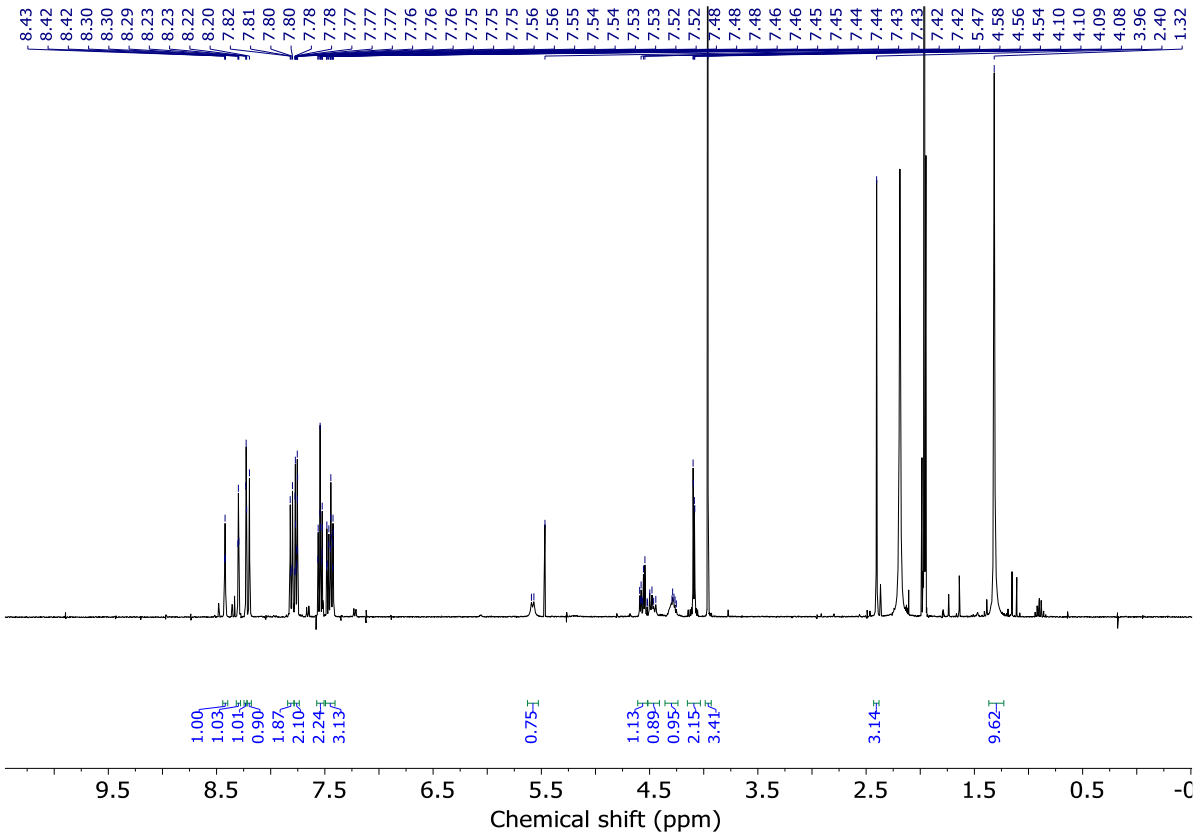

Figure 4.56 - ^{1}H NMR (CD_3CN, 400 MHz) of (*S*)-**S5**.

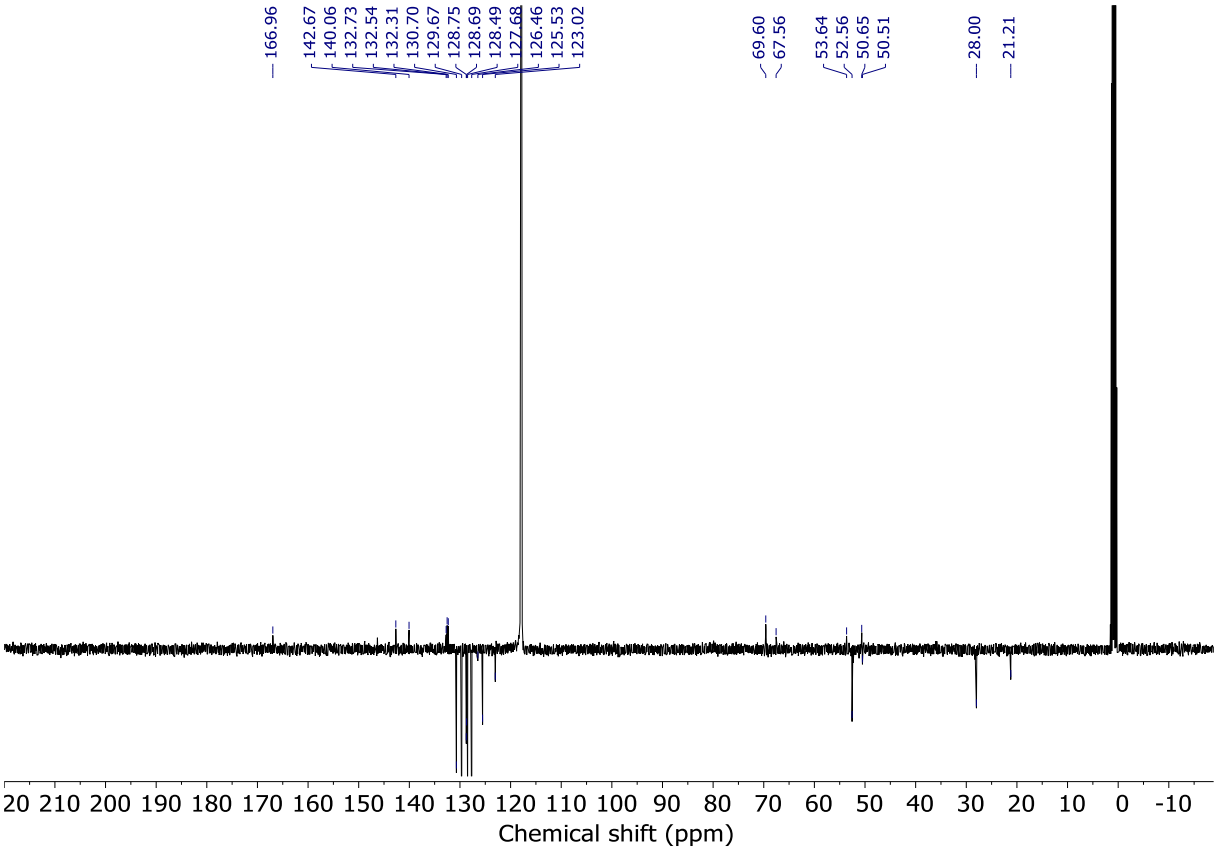

Figure 4.57 - JMOD NMR (CD_3CN, 101 MHz) of (*S*)-**S5**.

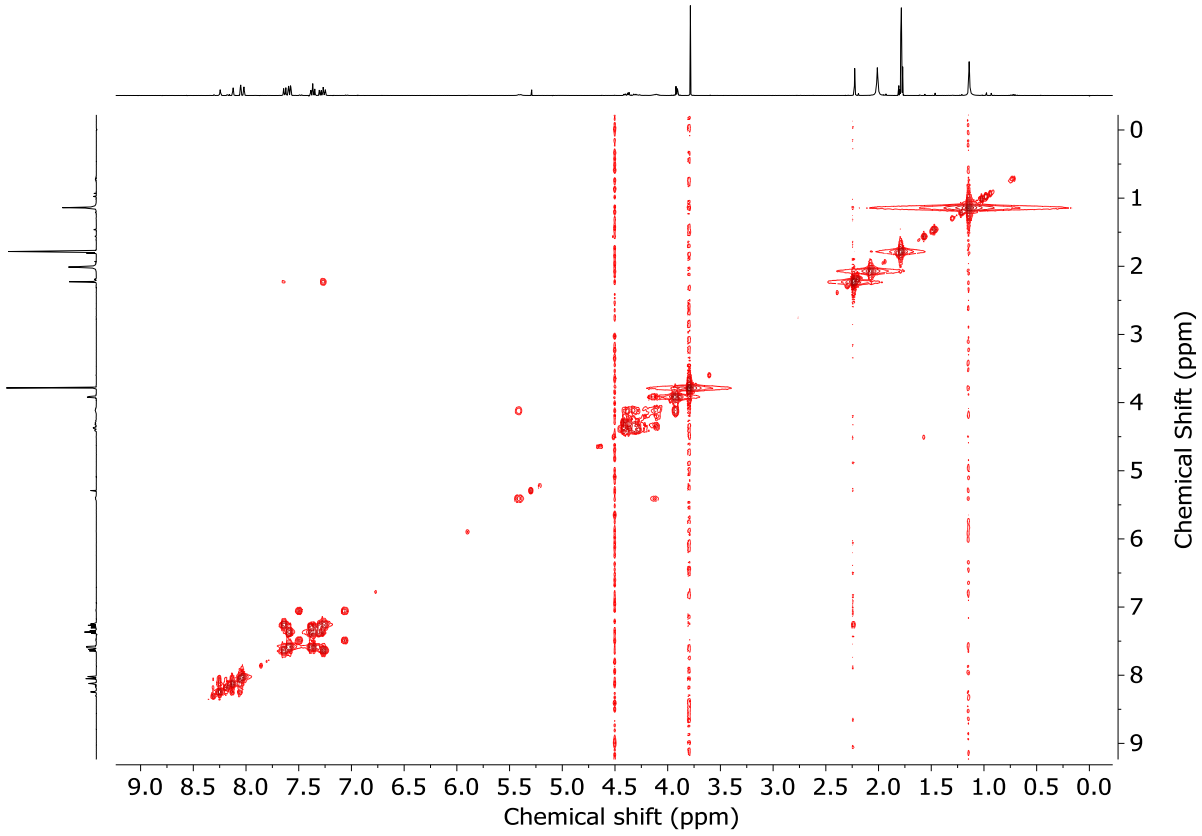

Figure 4.58 - COSY NMR (CD_3CN) of (*S*)-**S5**.

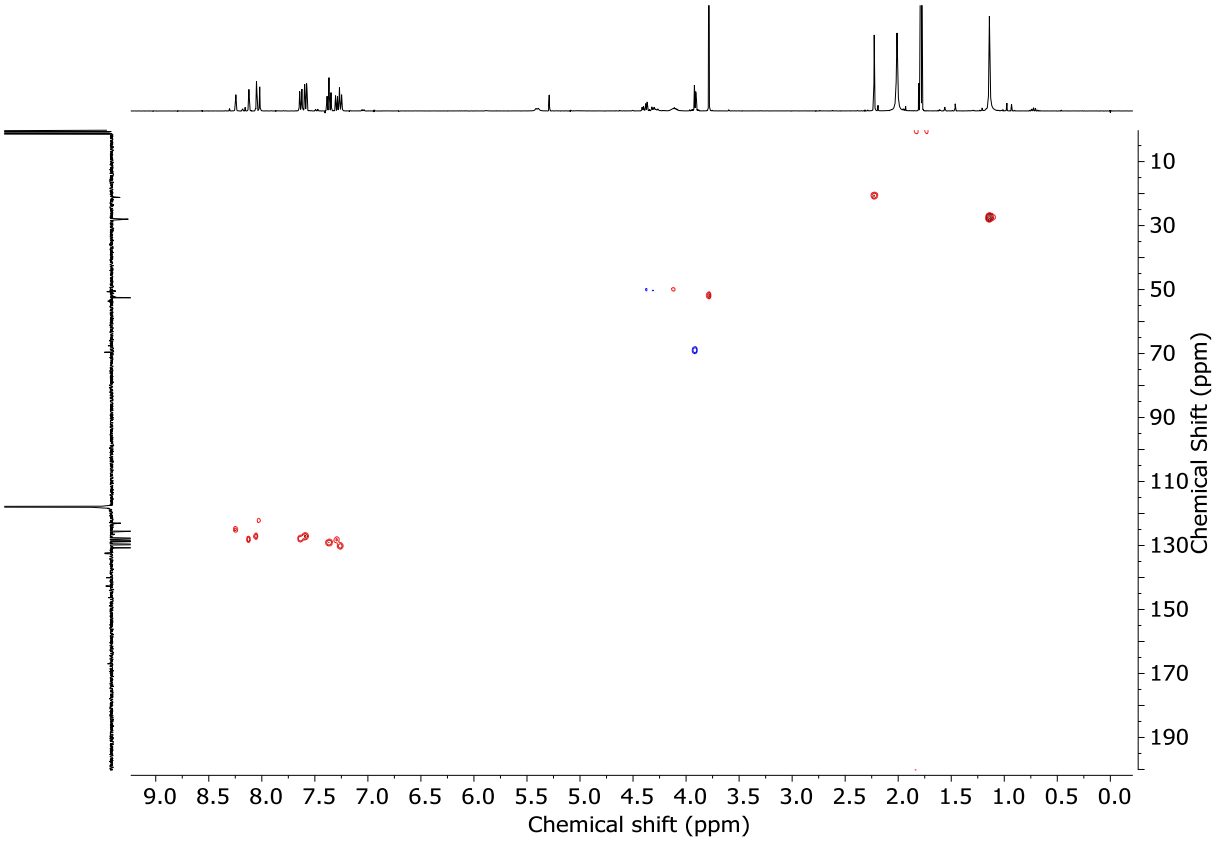

Figure 4.59 - HSQC NMR (CD_3CN) of (*S*)-**S5**.

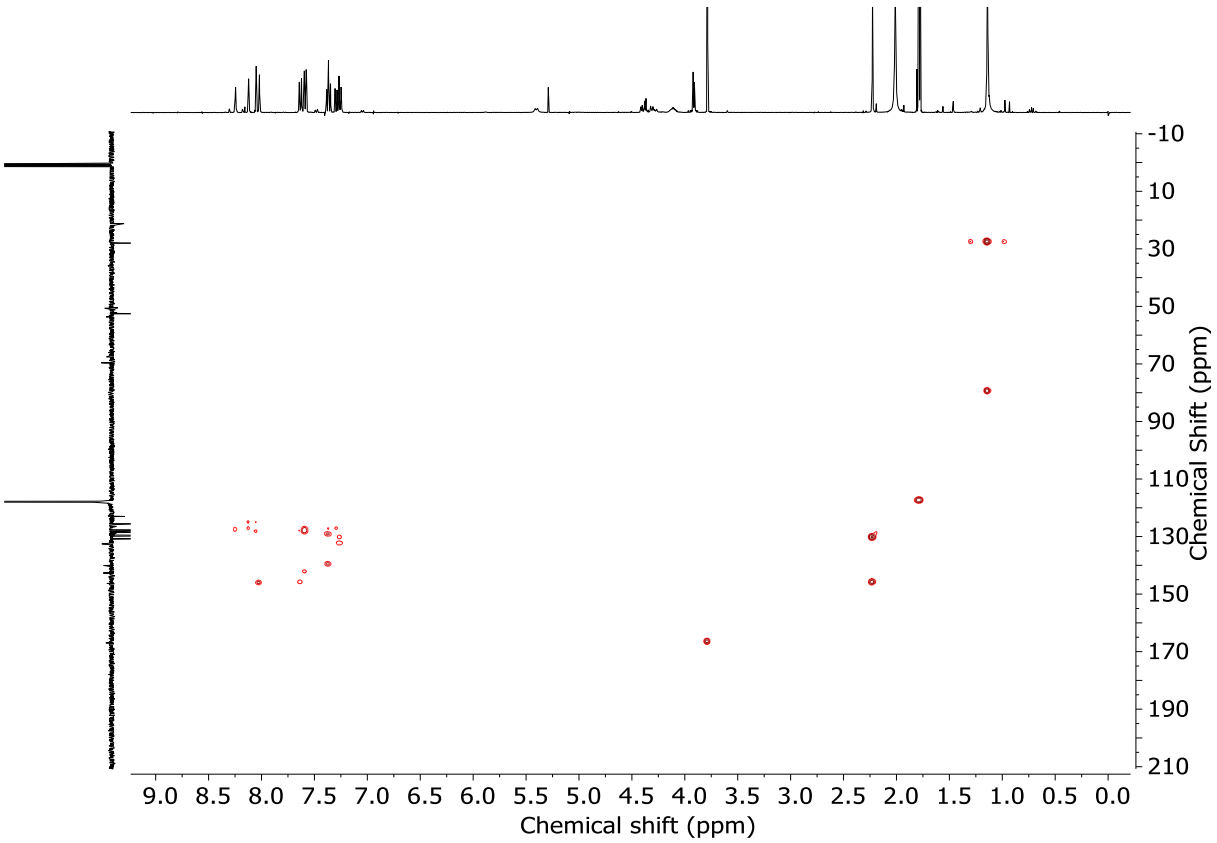

Figure 4.60 - HMBC NMR (CD_3CN) of (*S*)-**S5**.

Azide (*S*)-S6

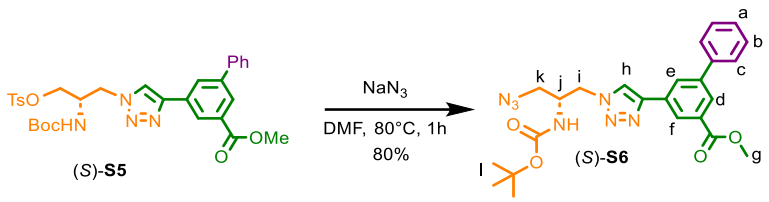

To a solution of (*S*)-**S5** (200 mg, 0.34 mmol) in DMF (4.0 mL) was carefully added NaN_3 (86 mg, 1.32 mmol). The suspension was heated at 80 °C for 1 h, then let cool down. 5% LiCl (10 mL) and Et_2O (15 mL) were added, the phases separated, and the organic layer extracted with Et_2O (2 x 15 mL). The collected organic fractions were then washed with brine (10 mL), then dried ($MgSO_4$). The solvent was removed *in vacuo* and the crude was purified by column chromatography (petrol-EtOAC 0→50%) to give (*S*)-**S6** as a white foam (129.3 mg, 80%).

^{1}H NMR (400 MHz, $CDCl_3$) δ: 8.38 (t, *J* = 1.6, 1H, H_f), 8.36 (t, *J* = 1.7, 1H, H_e), 8.26 (t, *J* = 1.6, 1H, H_f) 7.96 (s, 1H, H_h), 7.69 (dt, *J* = 7.5, 1.5, 2H, H_c), 7.48 (tt, *J* = 7.6, 1.4, 2H, H_b) 7.40 (tt, *J* = 7.4, 1.2, 1H, H_a), 5.13 (d, *J* = 8.8, 1H, NH), 4.61 (d, *J* = 5.7, 2H, H_i), 4.21 (app tq, *J* = 8.3, 5.6, 1H, H_j), 3.98 (s, 3H, H_g), 3.59 (dd, *J* = 12.6, 5.0, 1H, H_k), 3.39 (dd, 12.7, 6.5, 1H, $H_{k'}$), 1.43 (s, 9H, H_l)

^{13}C NMR (101 MHz, $CDCl_3$) δ: 166.7, 142.3, 139.7, 131.4, 131.1, 129.0, 128.6, 128.1, 128.1, 127.2, 125.5, 121.4, 80.7 (HMBC) 52.4, 51.3, 50.6, 50.1, 28.3.

HR-ESI-MS (+ve) *m/z* = 478.2201 $[M+H]^+$ (calc. 478.2197 *m/z* for $C_{24}H_{28}N_7O_4$);

$[\boldsymbol{\alpha}]_{\boldsymbol{D}}^{\mathbf{23}}$+5.4 (c 0.55, $CHCl_3$)

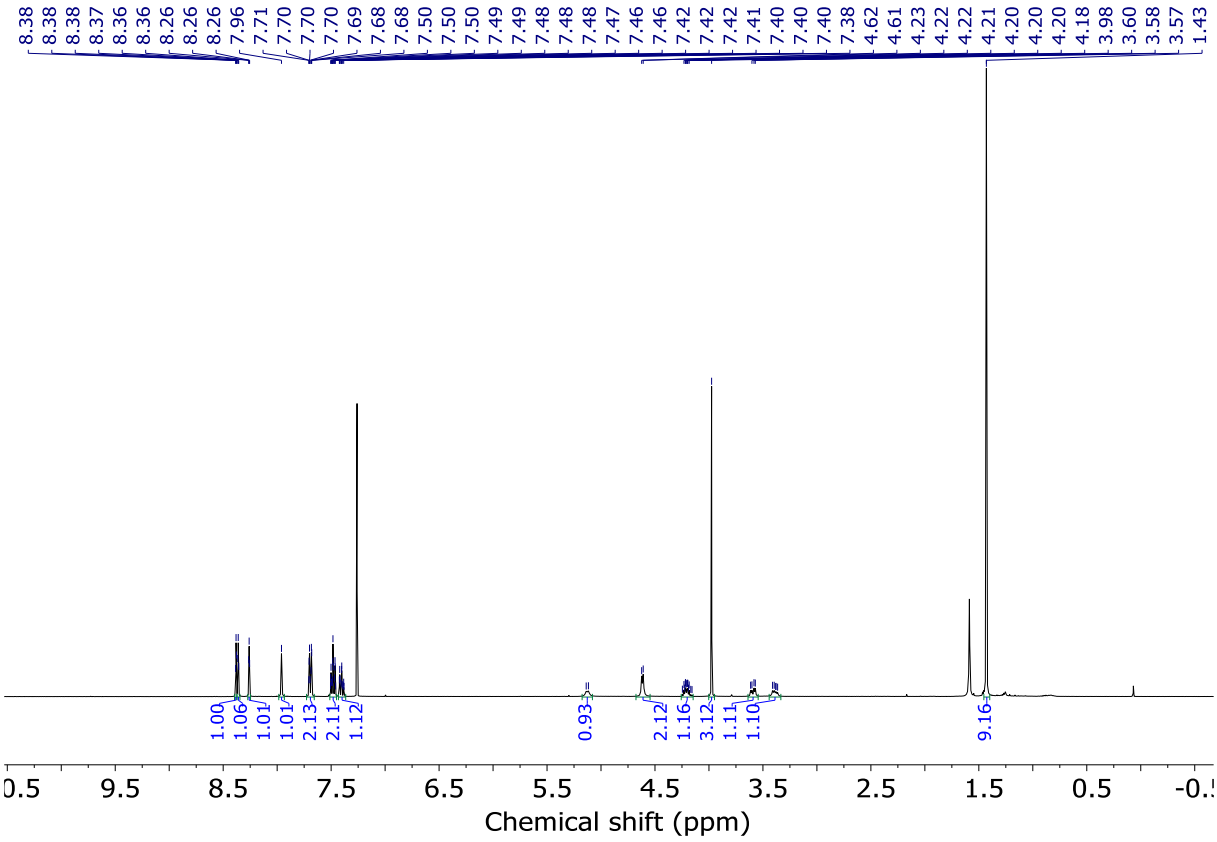

Figure 4.61 - ^{1}H NMR ($CDCl_3$, 400 MHz) of (*S*)-**S6**.

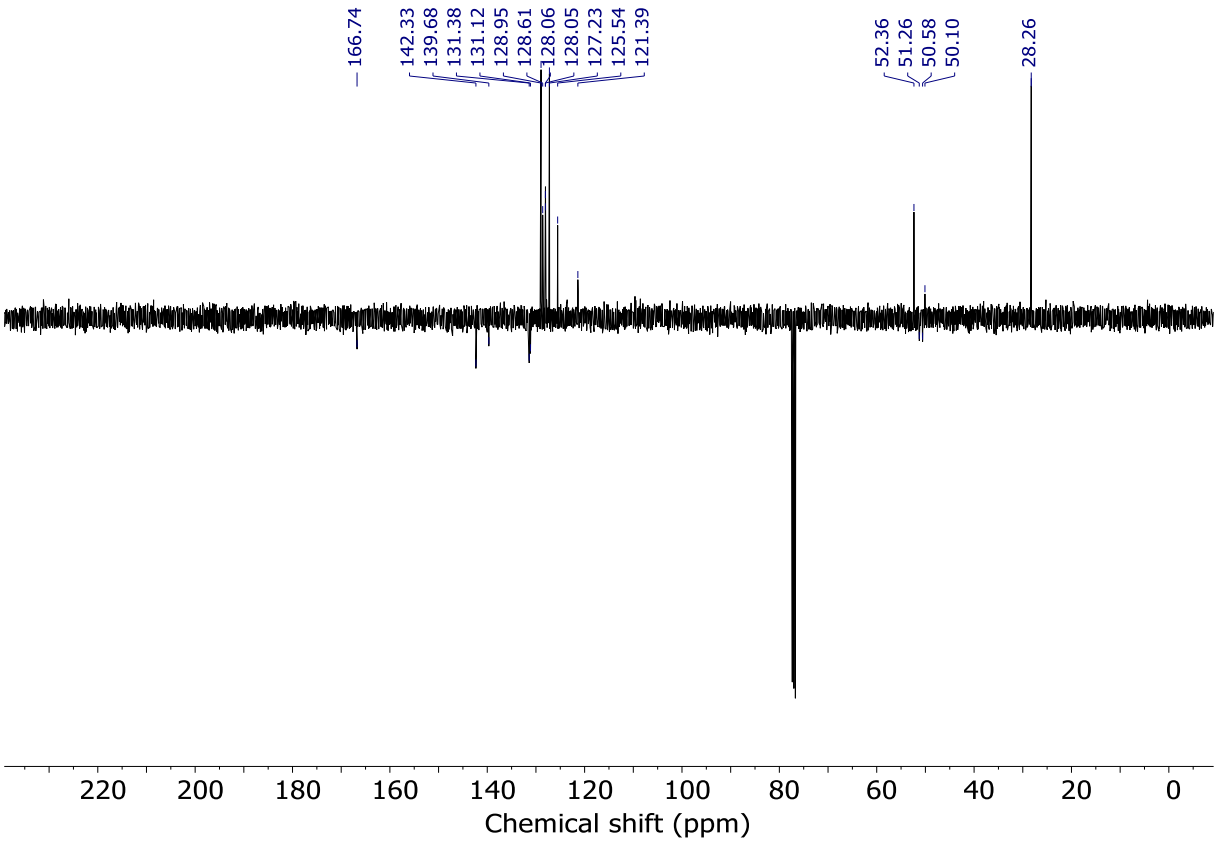

Figure 4.62 - JMOD NMR ($CDCl_3$, 101 MHz) of (*S*)-**S6**.

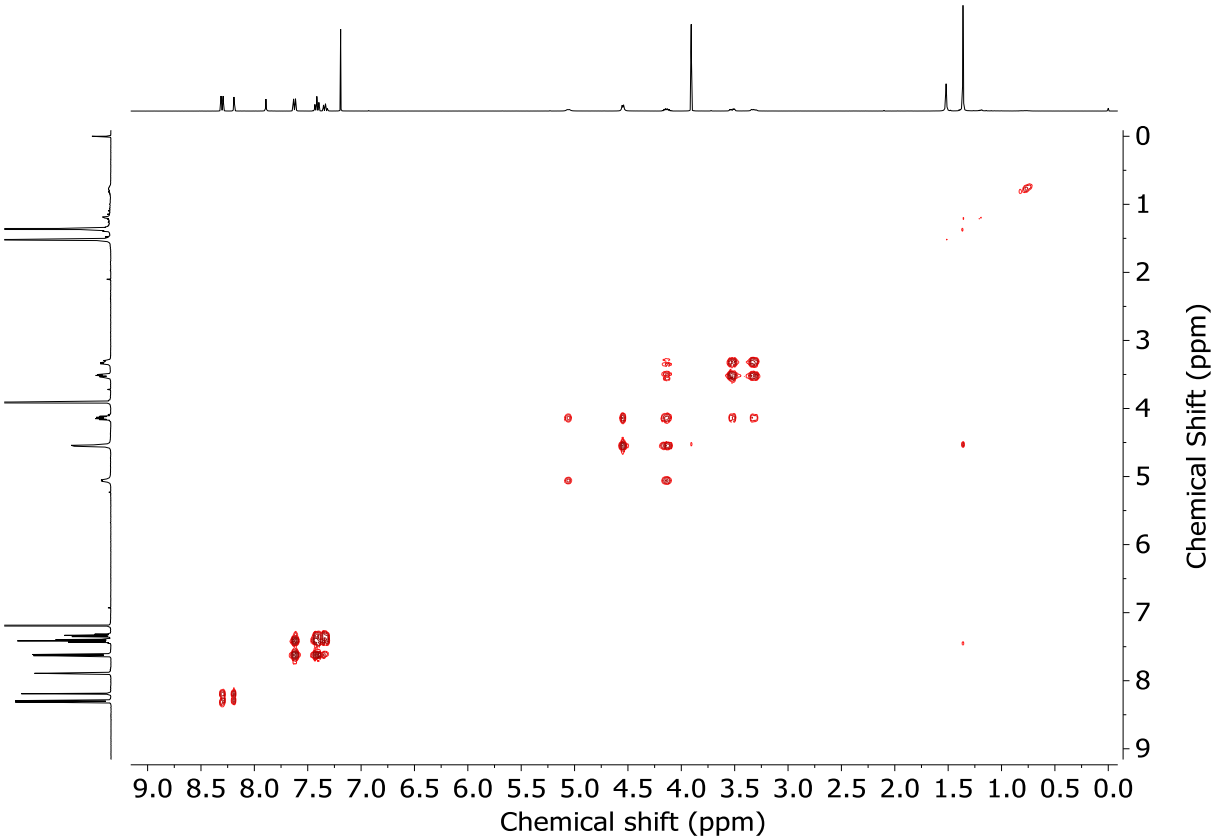

Figure 4.63 - COSY NMR ($CDCl_3$) of (*S*)-**S6**.

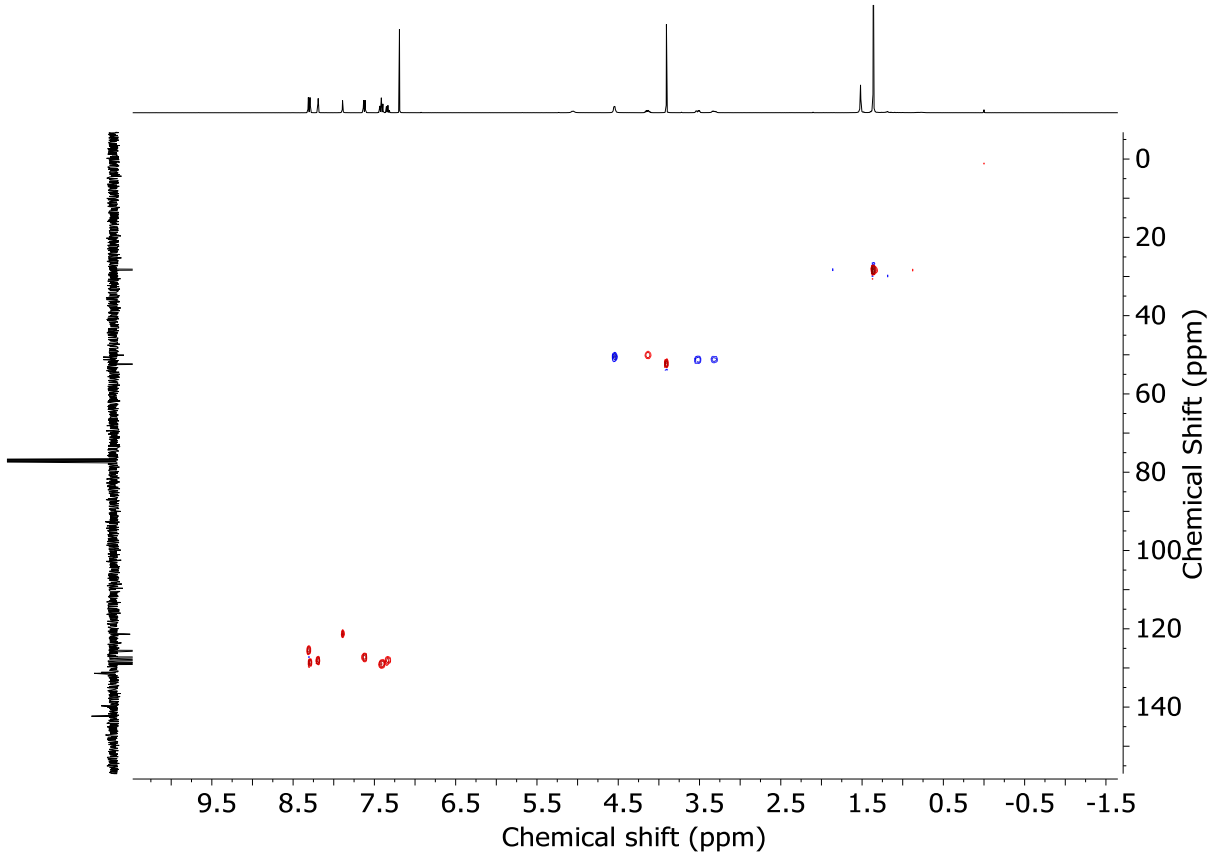

Figure 4.64 - HSQC NMR ($CDCl_3$) of (*S*)-**S6**.

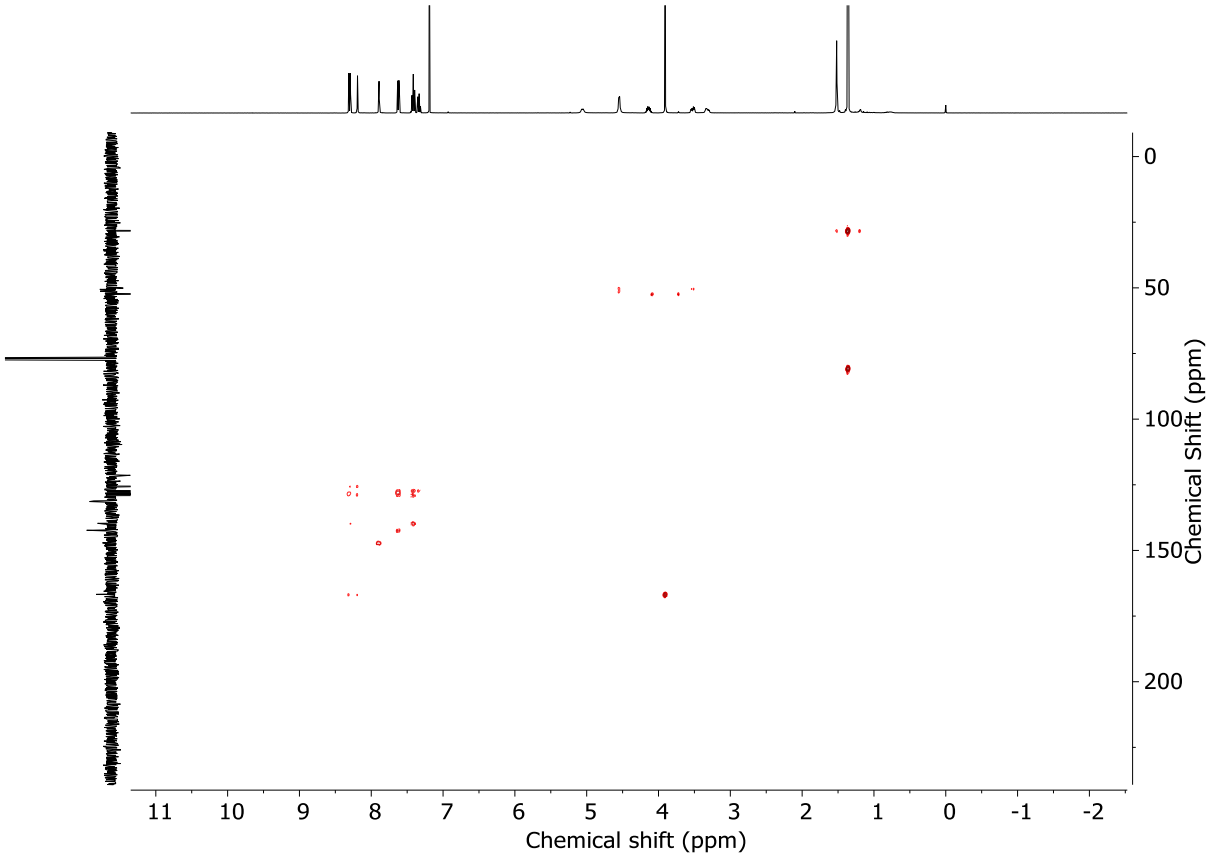

Figure 4.65 - HMBC NMR ($CDCl_3$) of (*S*)-**S6**.

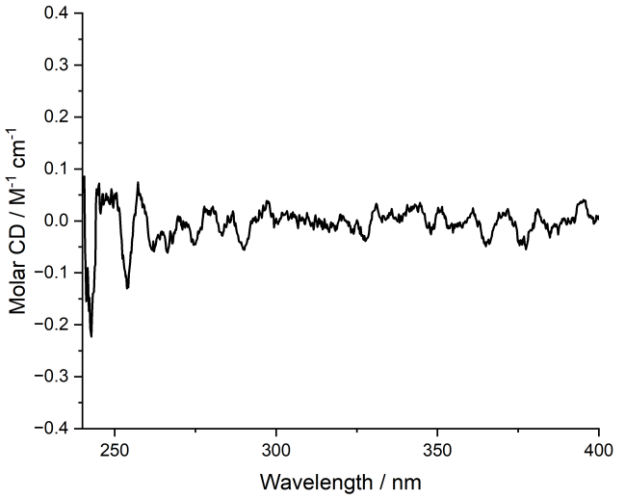

Figure 4.66 - Circular dichroism spectra of (*S*)-**S6** (63.5 μM) at 293 K in $CHCl_3$. No measurable CD response was observed so the $[\alpha]_D$ of (*S*)-**S6** was measured.

Rotaxanes (E_m,$S_{co\text{-}c}$)-10 and (Z_m,$S_{co\text{-}c}$)-10 from (*S*)-S6

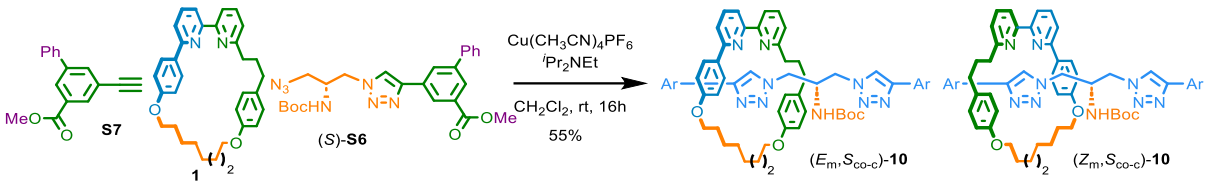

In a CEM vial were added (*S*)-**S6** (9.0 mg, 41.7 µmol), **S7** (9.7 mg, 41.7 µmol), **1** (20.0 mg, 38.0 µmol) and [$Cu(CH_3CN)_4PF_6$] (13.6 mg, 36.5 µmol). The vial was sealed and purged with N_2, then CH_2Cl_2 was added (1.0 mL), followed by $^iPr_2NEt$ (13.3 µL, 75.9 µmol). The solution was stirred at rt for 16 h. MeOH (2 mL mL) and KCN as a solid (24.7 mg, 0.38 mmol) were added and the resulting mixture was stirred vigorously until complete decolouration. The crude mixture was diluted with CH_2Cl_2 (5 mL) and washed with H_2O (5 mL) then EDTA-NH_3 (5 mL), with separation of aqueous and organic phases. The combined aqueous phase was then extracted with CH_2Cl_2 (3 x 5 mL) and the combined organic extracts were washed with brine (10 mL), dried ($MgSO_4$) and concentrated *in vacuo* to give a sample containing **10** as a mixture of diastereomers (58 : 42 *dr*, Figure 64).

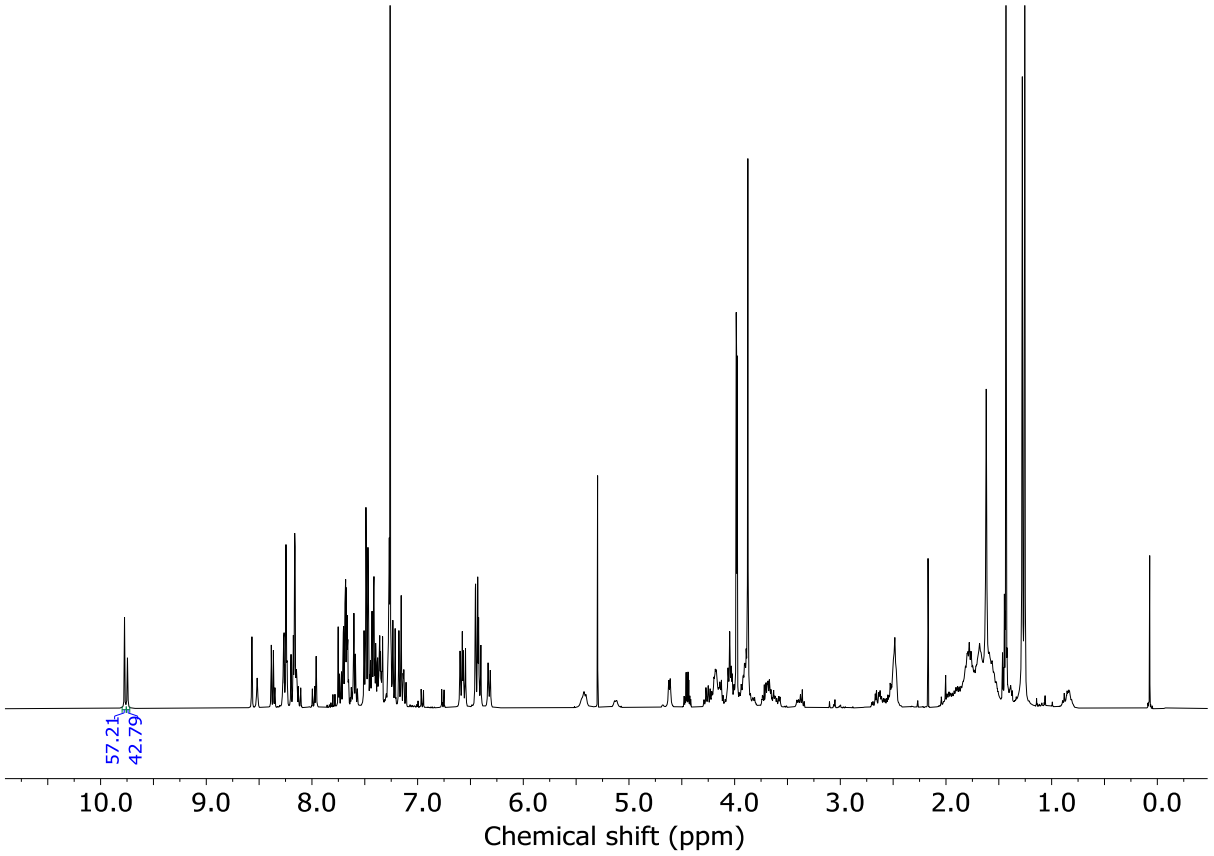

Figure 4.67 - ^1H NMR ($CDCl_3$, 400 MHz) of (E_m)-**10** and (Z_m)-**10** prior to chromatography (57 : 43 *dr*).

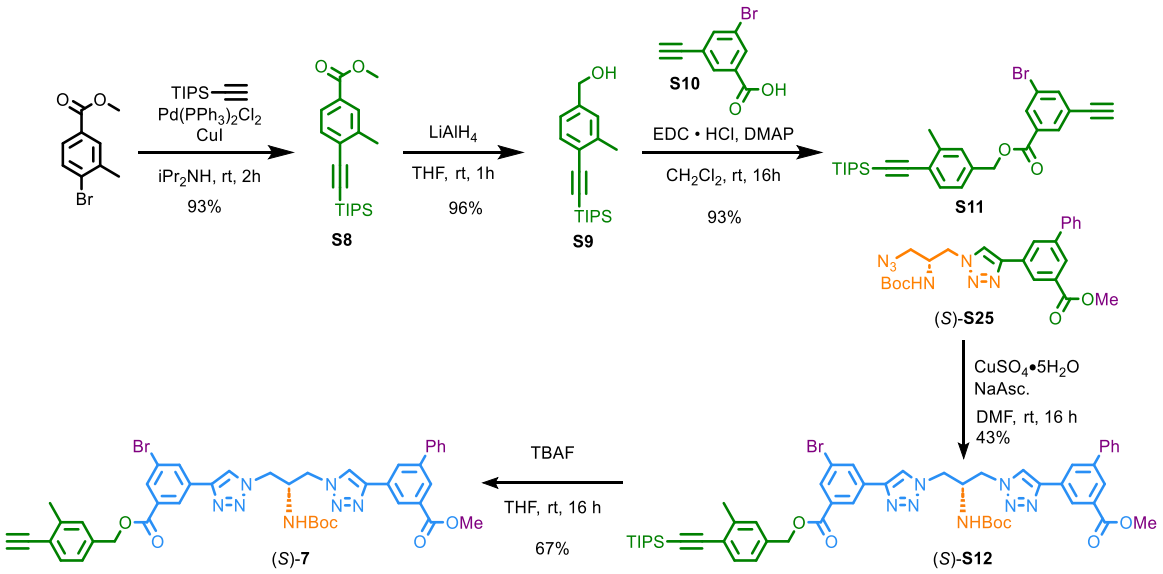

Scheme 4.5 - Synthetic route to shuttle alkyne (*S*)-**7**.

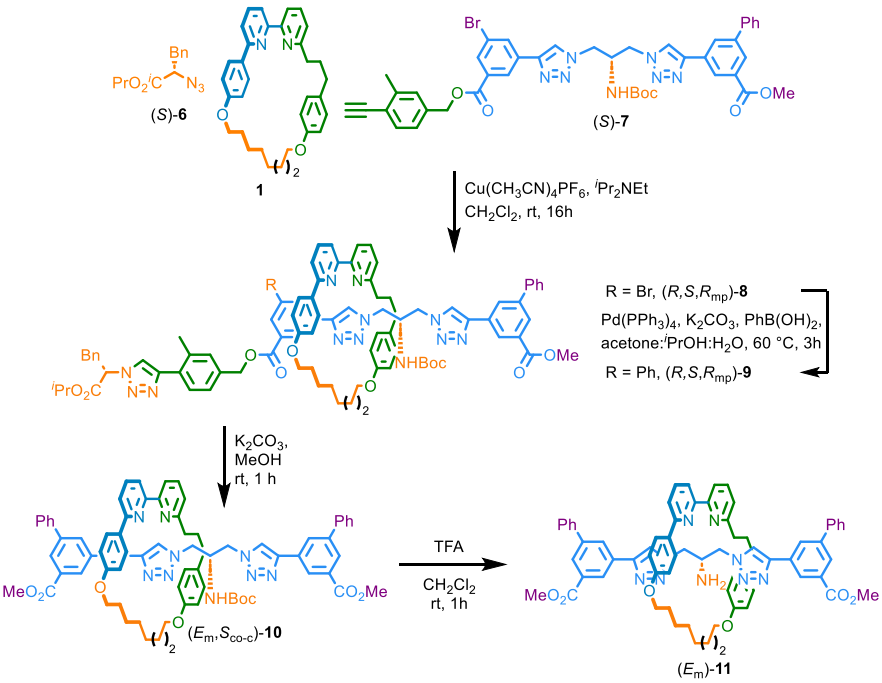

Scheme 4.6 - Synthetic route to diastereoenriched rotaxanes **11** *via* a shuttling approach. Synthesis of (E_m)-**11** shown.

TIPS alkyne S8

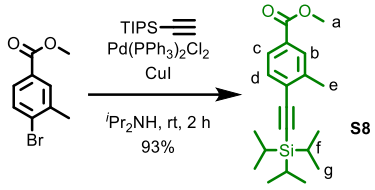

Methyl 4-bromo-3-methylbenzoate (2.5 g, 10.9 mmol), $PdCl_2(PPh_3)_2$ (387 mg, 0.546 mmol), and CuI (214 mg, 1.09 mmol) were suspended in a mixture of $^{i}Pr_2NH$ (8 ml, 54.6 mmol) and THF (25 ml), before the reaction vessel was purged with nitrogen. Ethynyltri*iso*propylsilane (3ml, 13.1 mmol) was then added to the vessel before the reaction was heated at 80 °C overnight. The reaction mixture was allowed to cool, filtrated through celite®, washed with Et_2O, and dried *in vacuo*. Chromatography (petrol-EtOAc 0→5%) gave **S8** (3.347 g, 93%) as a brown oil.

^{1}H NMR (400 MHz, $CDCl_3$) δ: 7.88 (dq, *J* = 1.7, 0.7, 1H, H_b), 7.78 (ddq, *J* = 8.0 1.6, 0.6, 1H, H_c), 7.49 (app. dt, 8.0, 0.4, 1H, H_d), 3.91 (s, 3H, H_a), 2.50 (s, 3H, H_e), 1.16-1.11 (m, 21H, H_f, H_g)

^{13}C NMR (101 MHz, $CDCl_3$) δ: 166.8, 140.7, 132.3, 130.3, 129.4, 128.0, 126.6, 104.9, 98.3, 52.2, 20.9, 18.7, 11.3.

HR-ESI-MS (+ve) *m/z* = 330.2090 $[M+H]^+$ (calc. 330.2081 *m/z* for $C_{20}H_{30}O_2Si$);

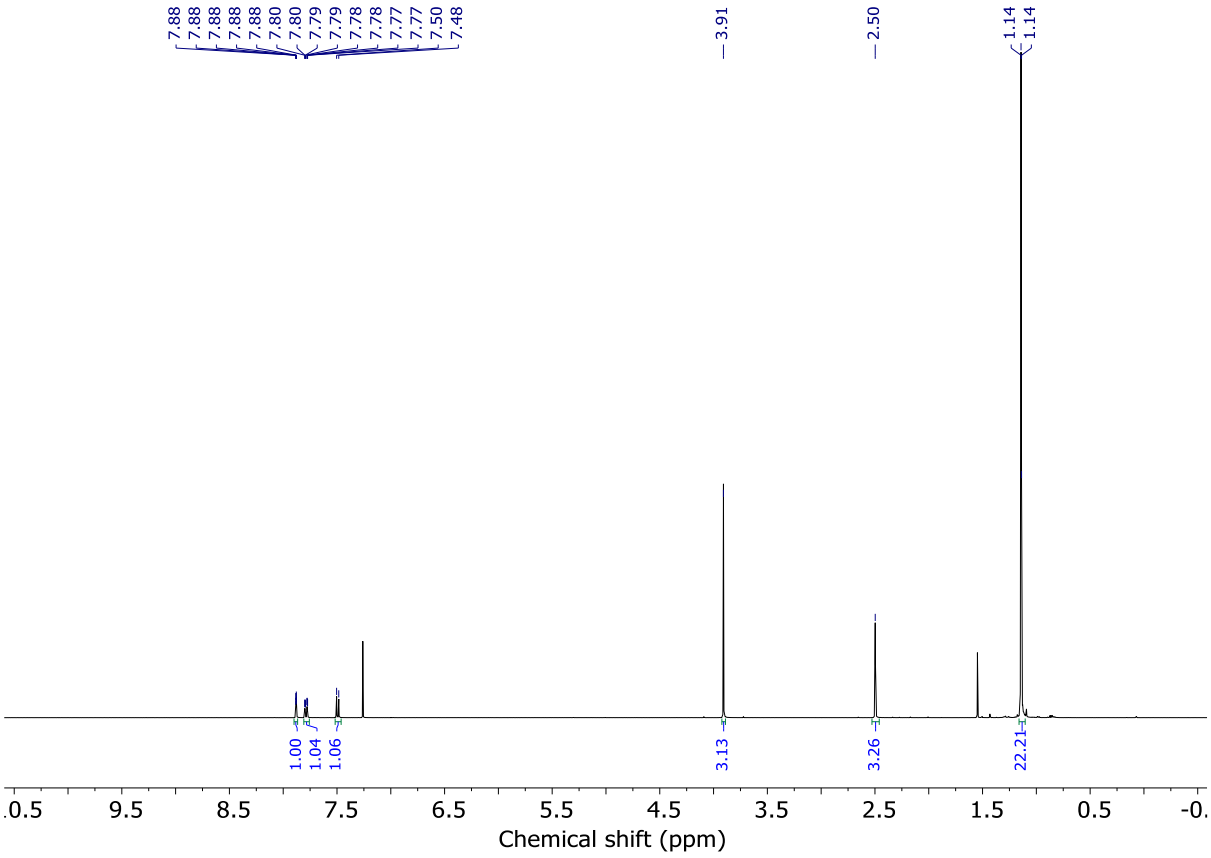

Figure 4.68 - ^{1}H NMR ($CDCl_3$, 400 MHz) of **S8**.

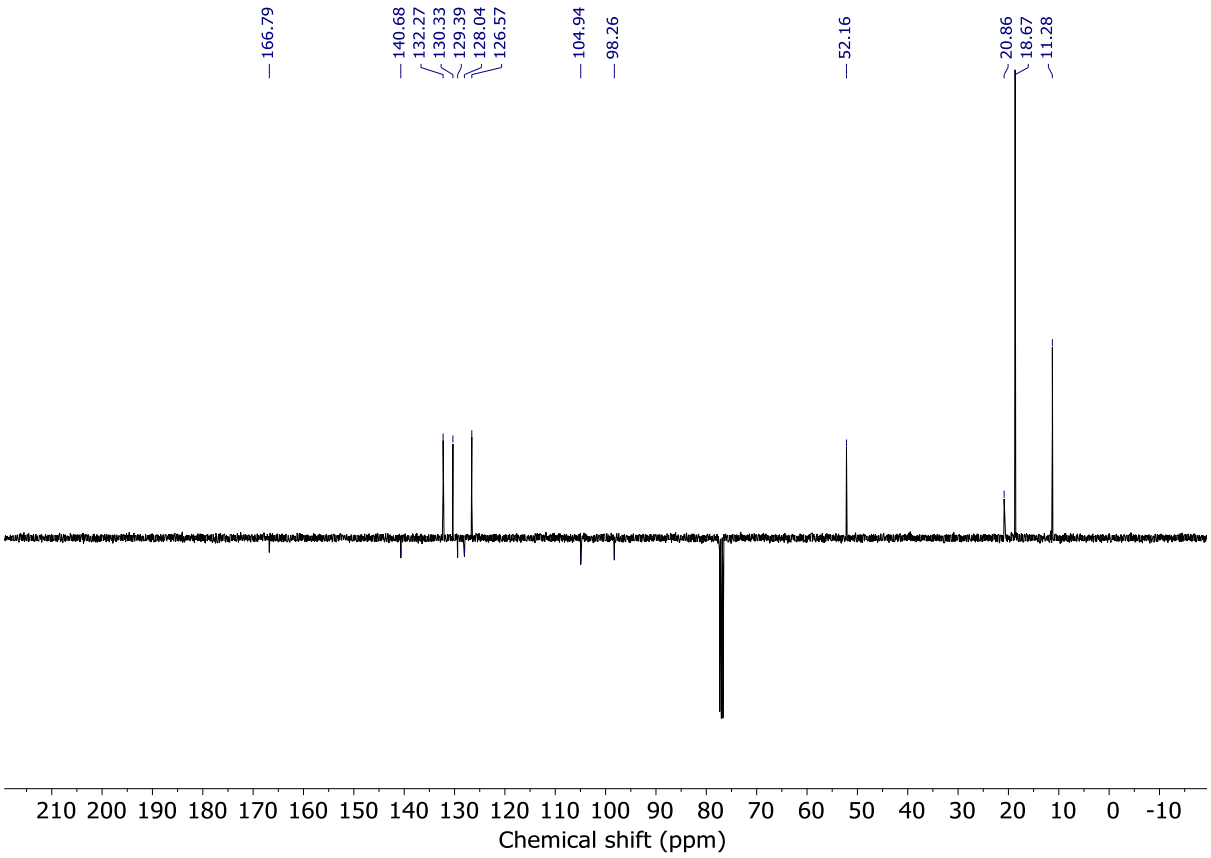

Figure 4.69 - JMOD NMR ($CDCl_3$, 101 MHz) of **S8**.

TIPS alkyne S9

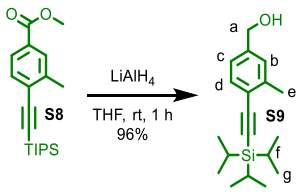

$LiAlH_4$ (695 mg, 18.2 mmol) was suspended in THF (30 ml) and was cooled to 0 °C. **S8** (3.0 g, 9.08 mmol) was added and the reaction mixture was stirred at rt. for 30 mins. The reaction was then quenched using a 1 M HCl/EtOAc/ice mixture to destroy excess $LiAlH_4$. The organic layer was then extracted using EtOAc (100 ml). The combined organic layers were dried ($MgSO_4$), and solvents removed *in vacuo*. Chromatography (petrol-EtOAc 0→10%) gave the product **S9** (2.628 g, 96%) as a yellow oil.

^{1}H NMR (400 MHz, $CDCl_3$) δ: 7.44 (d, *J* = 7.9, 1H, H_d), 7.20 (app. 8plet, *J* = 0.6, 1H, H_b), 7.12 (ddq, *J* = 7.9, 1.8, 0.6, 1H, H_c) 4.65 (d, *J* = 5.9, 2H, H_a), 2.47 (s, 3H, H_e), 1.68 (t, *J* = 6.0, 1H, OH), 1.14 (app. s, 21H, H_f, H_g)

^{13}C NMR (101 MHz, $CDCl_3$) δ: 141.0, 132.6, 127.9, 123.9, 122.7, 105.6, 94.6, 65.1, 20.9, 18.7, 11.3.

HR-ESI-MS (+ve) *m/z* = 302.2066 $[M+H]^+$ (calc. 302.2053 *m/z* for $C_{19}H_{30}OSi$).

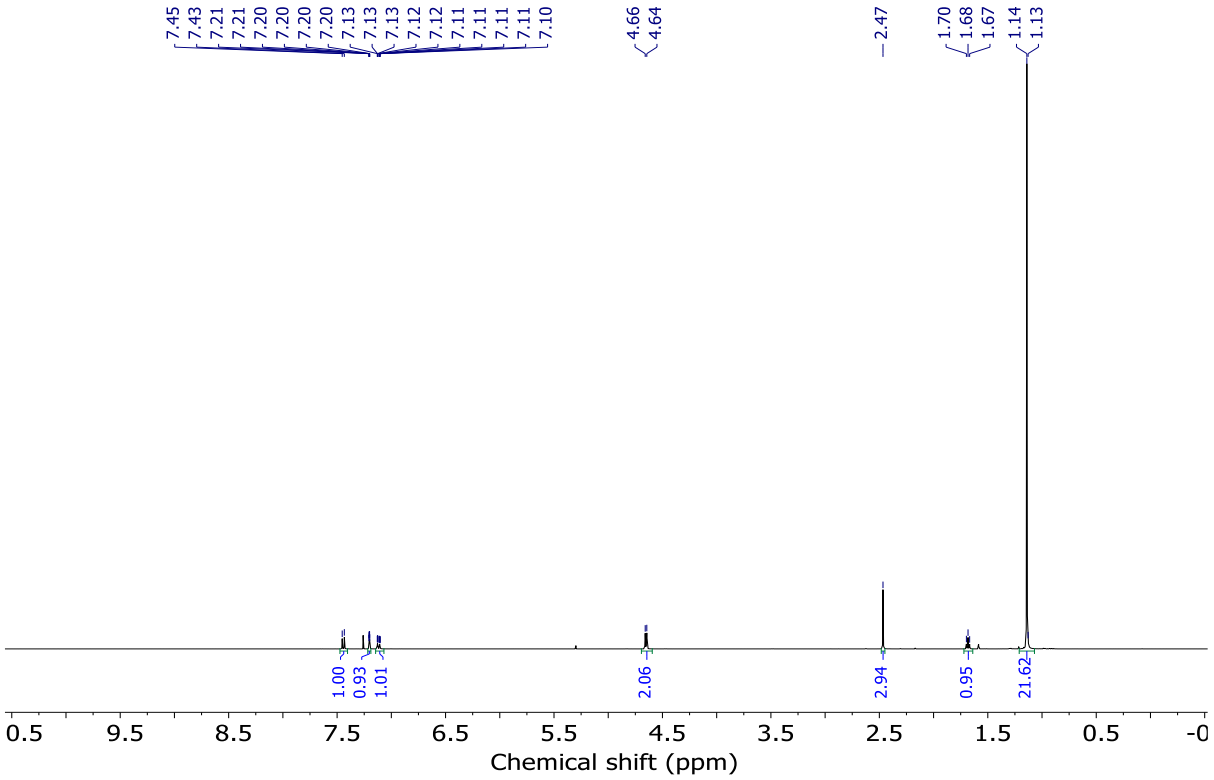

Figure 4.70 - ^{1}H NMR ($CDCl_3$, 400 MHz) of **S9**.

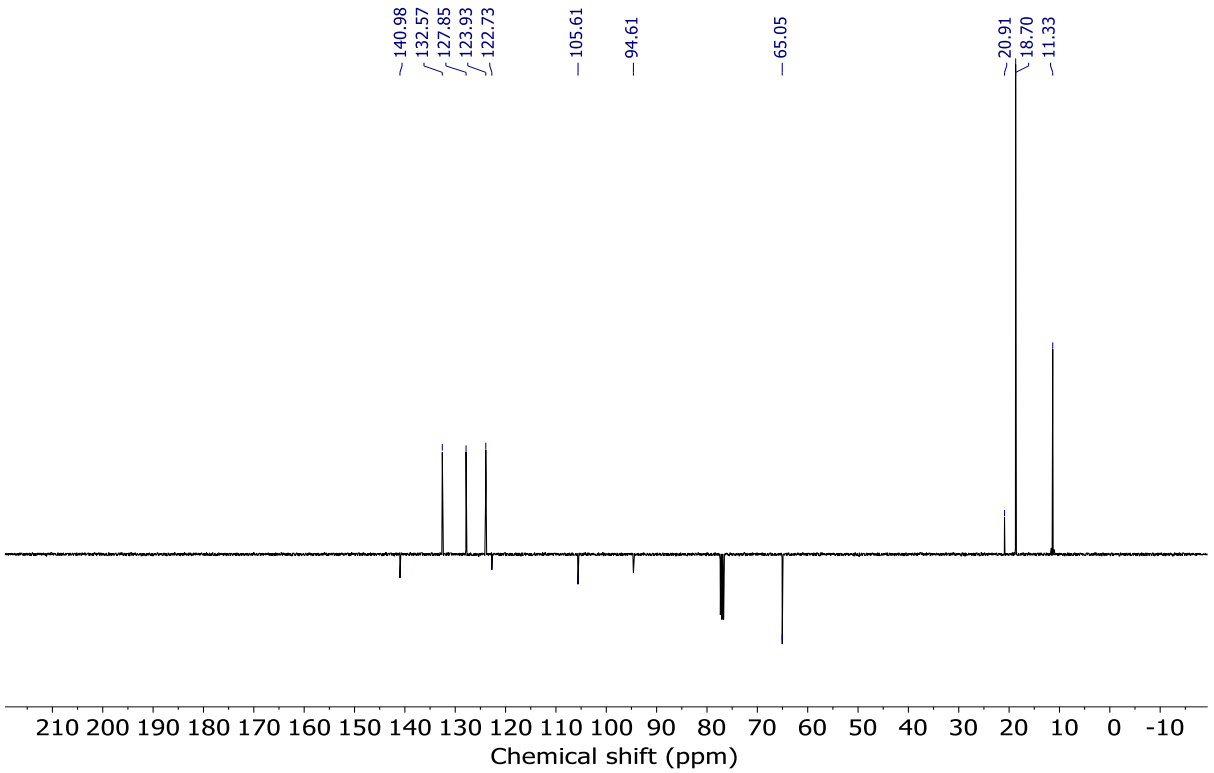

Figure 4.71 - JMOD NMR ($CDCl_3$, 101 MHz) of **S9**.

TIPS alkyne S11

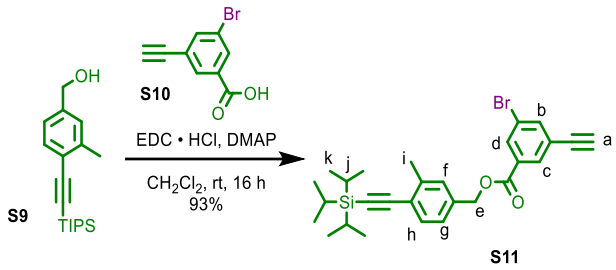

To a solution of **S9** (2.5 g, 7.6 mmol), **S10** (1.8 g, 8.4 mmol), DMAP (92.9 mg, 0.76 mmol) and CH_2Cl_2 (100 mL) was added EDC · HCl (3.0 g, 15.2 mmol). The reaction mixture was stirred at rt for 16 h. H_2O (50 mL) was added, then the aqueous and organic phases were separated, and the aqueous phase was then extracted with CH_2Cl_2 (3 x 50 mL). The combined organic extracts were washed with brine (100 mL), dried ($MgSO_4$) and concentrated *in vacuo*. Chromatography (petrol-EtOAc 0→5%) gave **S11** as a white solid (3.6 g, 93%).

^{1}H NMR (400 MHz, $CDCl_3$) δ: 8.15 (t, *J* = 1.6, 1H, H_d), 8.08 (t, *J* = 1.5, 1H, H_c), 7.79 (t, *J* = 1.6, 1H, H_b), 7.48 (d, *J* = 7.9, 1H, H_h), 7.28-7.24 (m, 1H, H_f superimposed with $CHCl_3$), 7.20 (d, *H* = 8.1, 1H, H_g) 5.22 (s, 2H, H_e), 3.09 (s, 1H, H_a), 2.40 (s, 3H, H_i), 1.06 (app. s, 21H, H_f, H_g)

^{13}C NMR (101 MHz, $CDCl_3$) δ: 164.3, 141.0, 138.9, 135.3, 132.9, 132.7, 132.0, 131.9, 129.5, 125.6, 124.4, 123.8, 122.2, 105.3, 95.5, 81.1, 79.6, 79.0, 67.1, 20.9, 18.7, 11.3.

HR-ESI-MS (+ve) *m/z* = 509.5614 $[M+H]^+$ (calc. 509.5609 *m/z* for $C_{28}H_{33}BrO_2Si$).

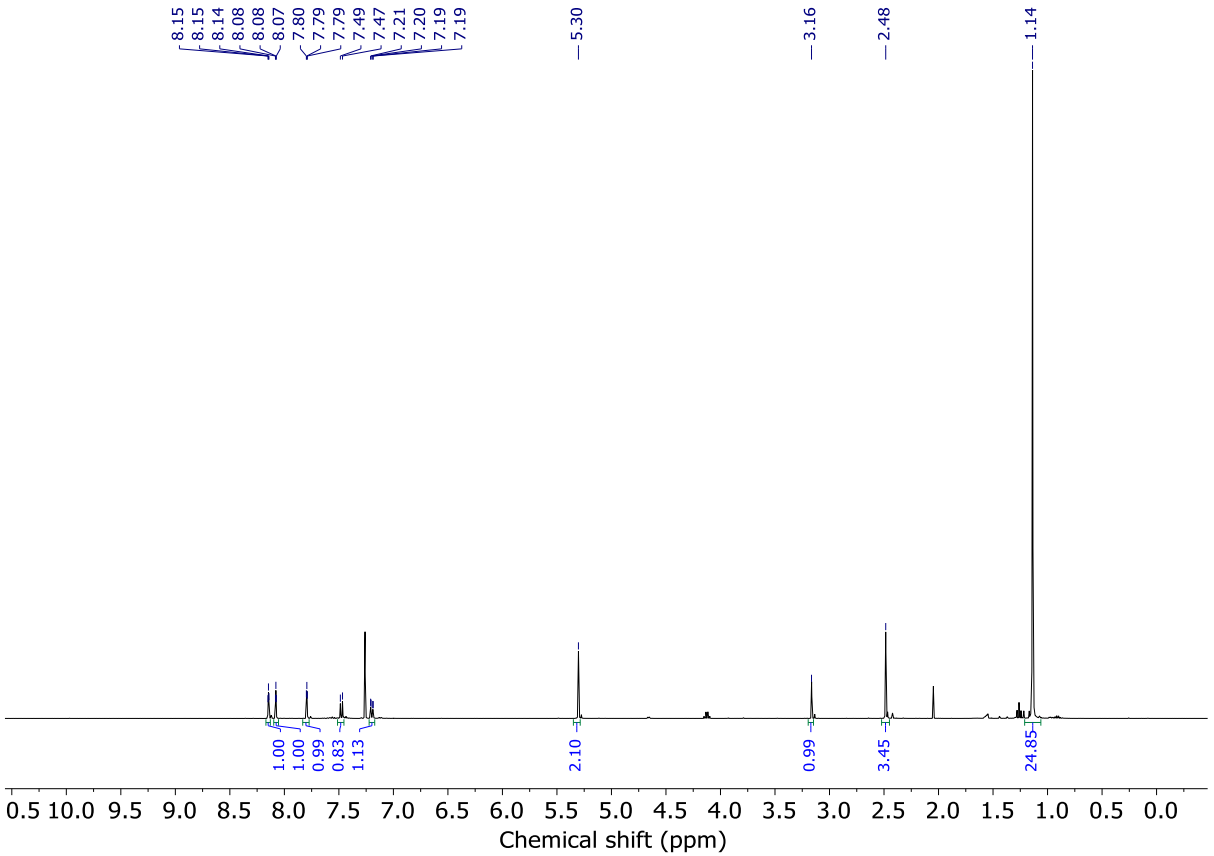

Figure 4.72 - ^{1}H NMR ($CDCl_3$, 400 MHz) of **S11**.

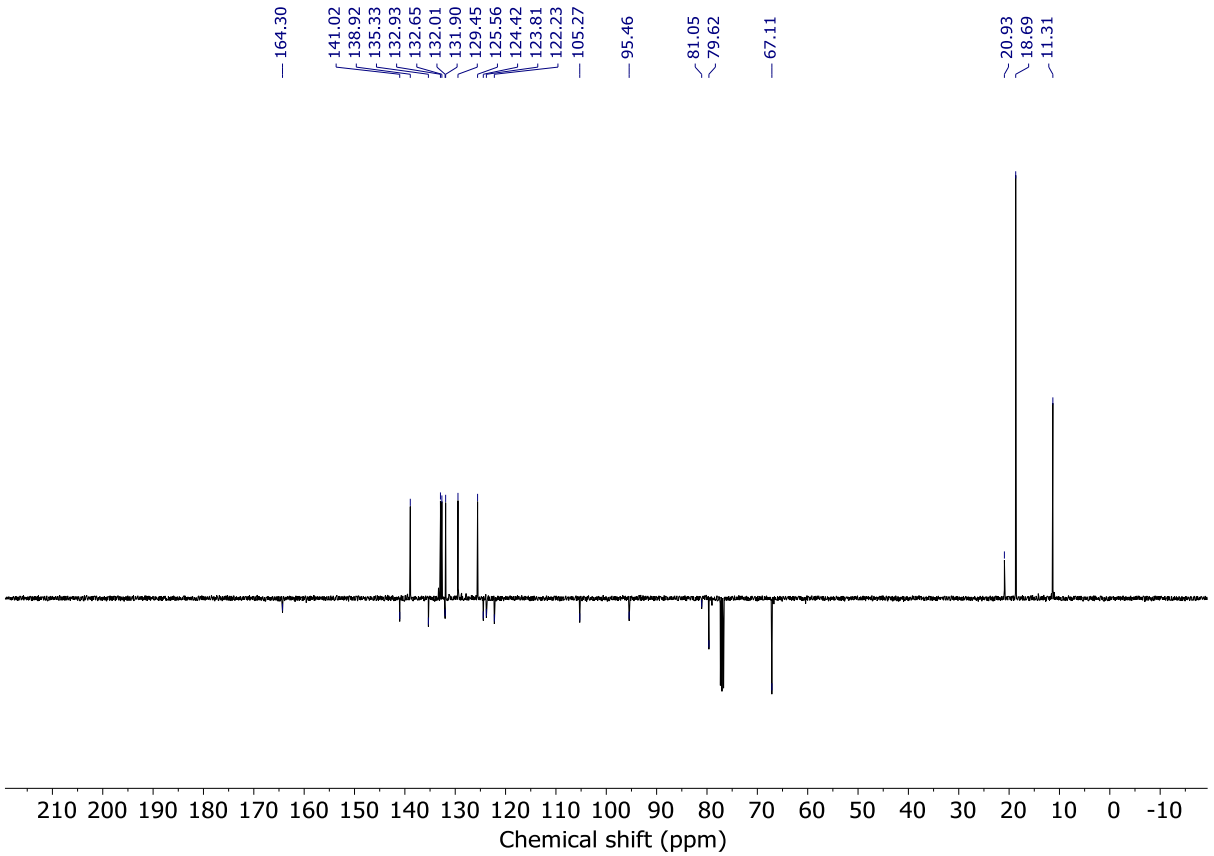

Figure 4.73 - JMOD NMR ($CDCl_3$, 101 MHz) of **S11**.

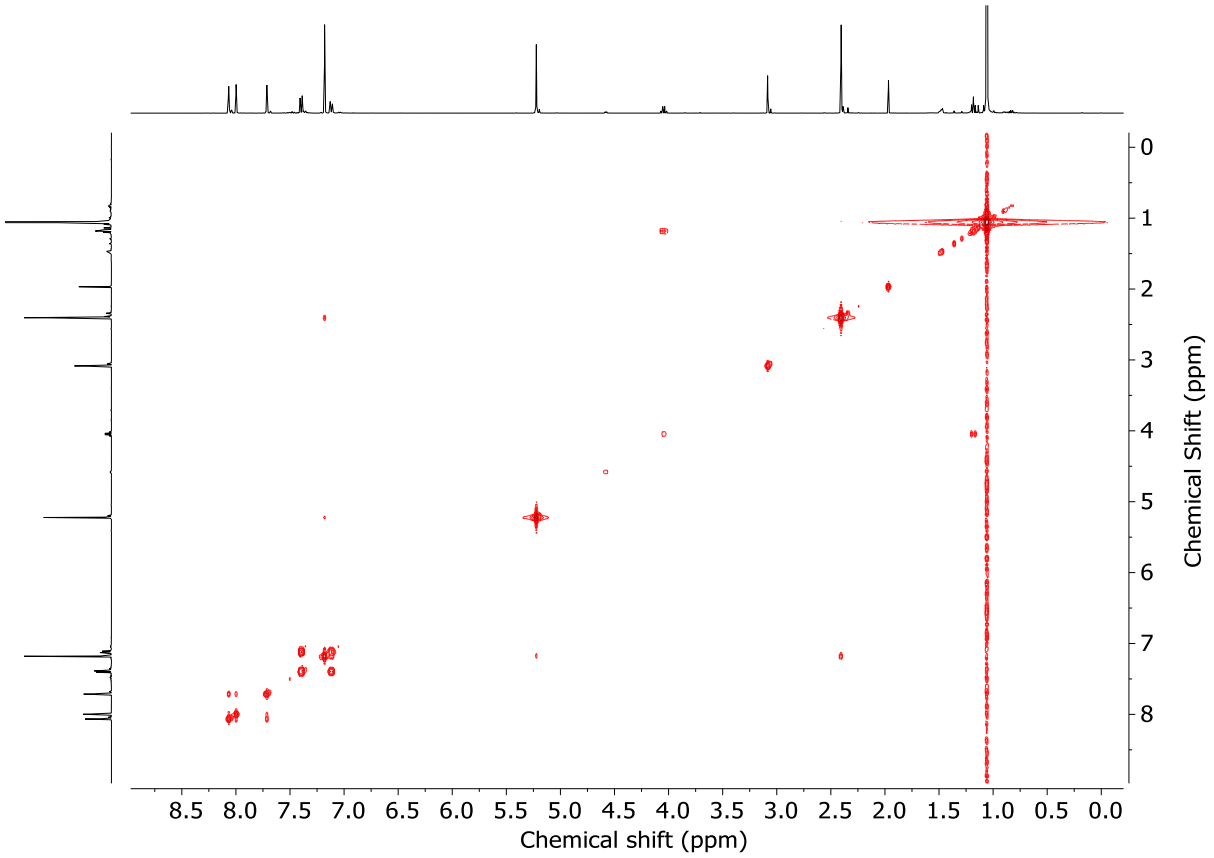

Figure 4.74 - COSY NMR ($CDCl_3$) of **S11**.

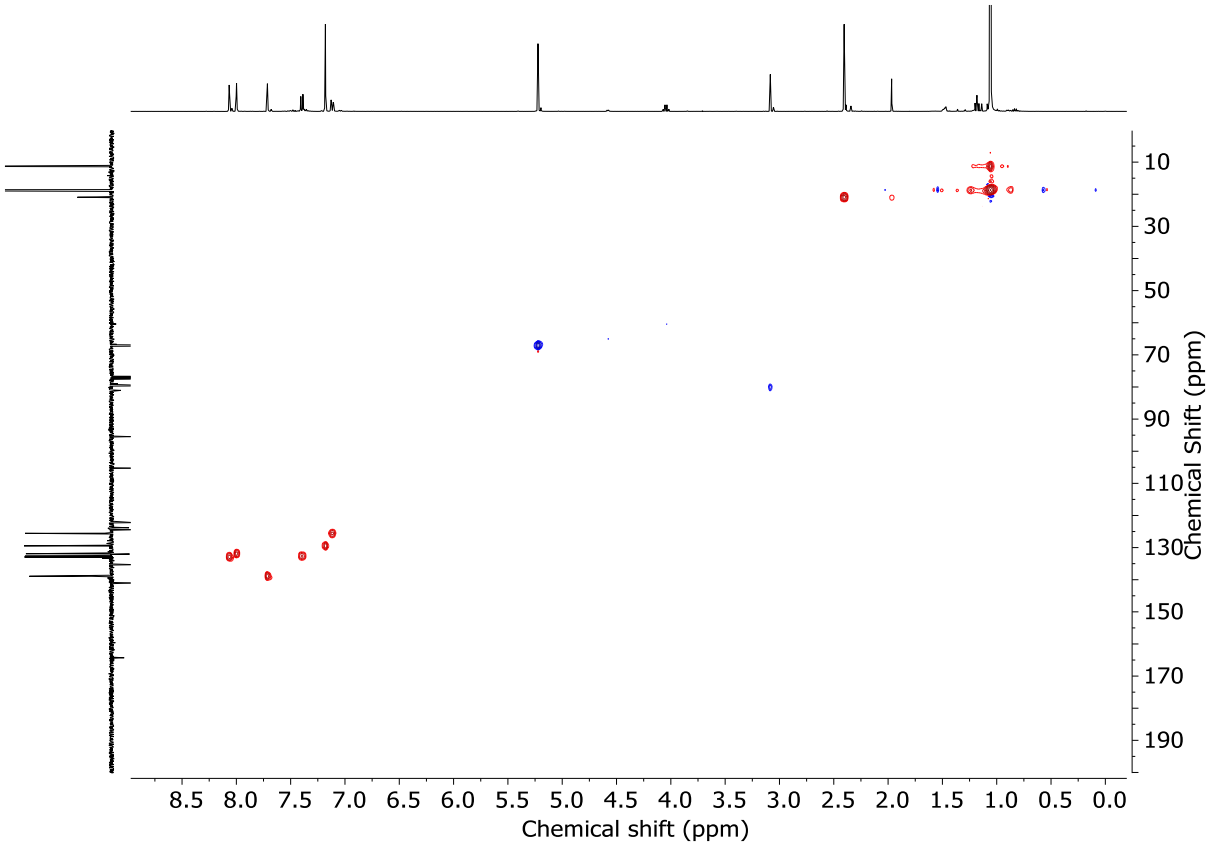

Figure 4.75 - HSQC NMR ($CDCl_3$) of **S11**.

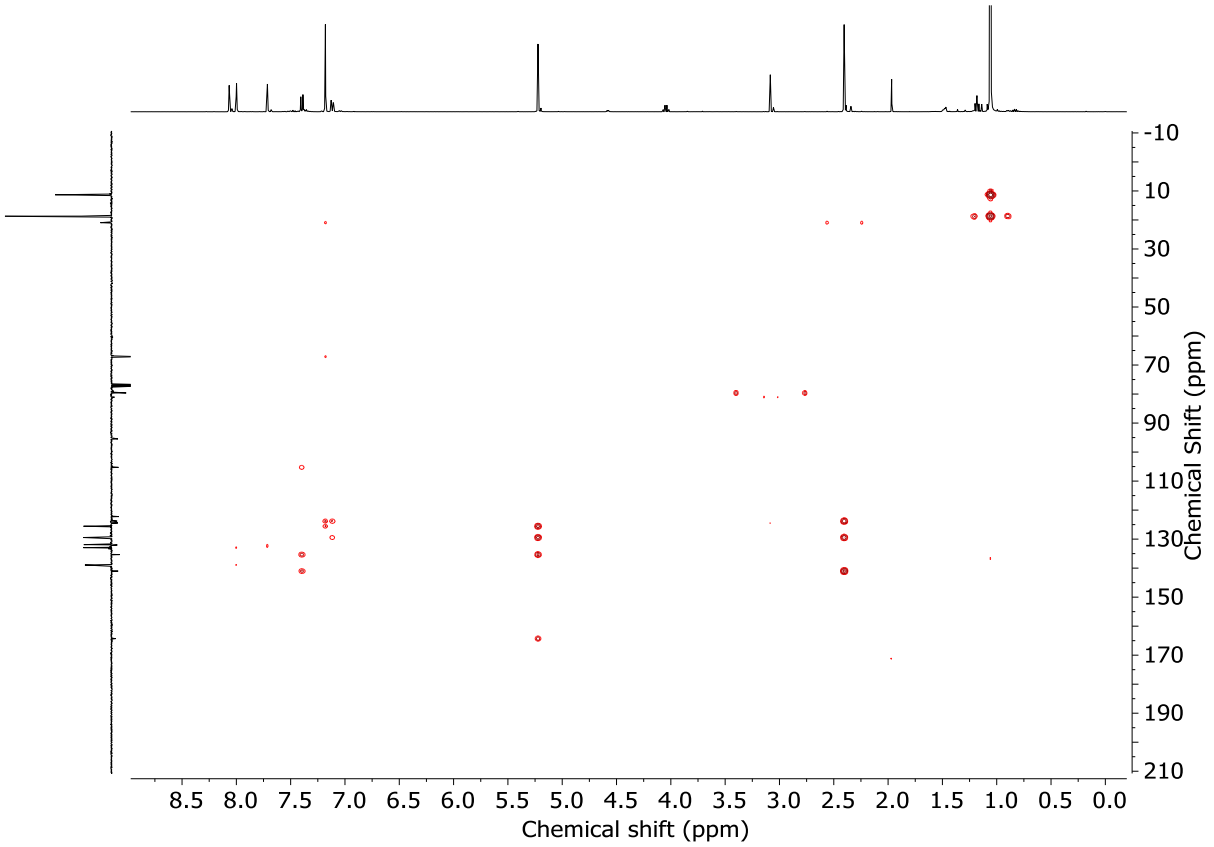

Figure 4.76 - HMBC NMR ($CDCl_3$) of **S11**.

Alkyne precursor (*S*)-S12

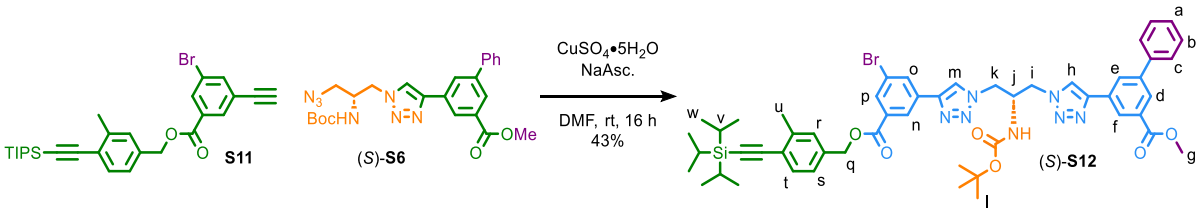

A suspension of (*S*)-**S6** (130 mg, 0.27 mmol), **S11** (138.7 mg, 0.27 mmol), $CuSO_4 \cdot 5\ H_2O$ (4.3 mg, 0.027 mmol) and sodium ascorbate (8.3 mg, 0.041 mmol) in DMF (3 mL) is degassed by bubbling N_2 for 10 min. The solution turns brown, and it is stirred at rt for 16 h. The reaction mixture is poured into a NH_3-EDTA (10 mL) then extracted with EtOAc (3 x 20 mL). The organic phases were washed with a 5% LiCl solution (50 mL), washed with brine (20 mL), dried ($MgSO_4$) and concentrated *in vacuo*. Chromatography (petrol-EtOAc 0→50%) gave (*S*)-**S12** as a white foam (116.0 mg, 43%).

^{1}H NMR (400 MHz, $CDCl_3$) δ: 8.33 (app. s, 1H, H_f), 8.29 (s, 1H, H_n or H_p), 8.27 (app. s, 1H, H_e), 8.21 (app. s, 1H, H_d), 8.19 (s, 1H, H_h) 8,18-8.15 (m, 2H, H_o, H_m), 8.07 (H_n or H_p), 7.68-7.62 (m, 2H, H_b), 7.51-7.43 (m, 3H, H_c, H_t), 7.42-7.36 (m, 1H, H_a) 7.28 (bs, 1H, H_r), 7.14 (s, 1H, H_s) 5.98 (d, *J* = 7.4, 1H, NH), 5.31 (s, 2H, H_q), 4.76-4.44 (m, 5H, H_i, H_j, H_k) 3.96 (s, 3H, H_g), 2.48 (s, 3H, H_u), 1.42 (s, 9H, H_l), 1.13 (m, 21H, H_v, H_w)

^{13}C NMR (101 MHz, $CDCl_3$) δ: 166.6, 164.7, 155.3, 147.1, 145.7, 142.2, 141.0, 139.5, 135.5, 132.7, 132.7, 132.4, 132.3, 132.2, 131.3, 129.6, 128.9, 128.4, 128.1, 127.2, 125.7, 125.4, 125.3, 123.8, 123.1, 122.4, 122.1, 105.3, 95.4, 80.9, 67.1, 52.4, 51.2, 50.1, 50.0, 40.9, 33.9, 33.8, 28.3, 23.9, 20.9, 18.7, 11.3.

HR-ESI-MS (+ve) *m/z* = 1008.3 $[M+Na]^+$ for isotopic pattern see Figure 4.82.

$[\alpha]_D^{23}$-2.3 (c 0.72, $CHCl_3$)

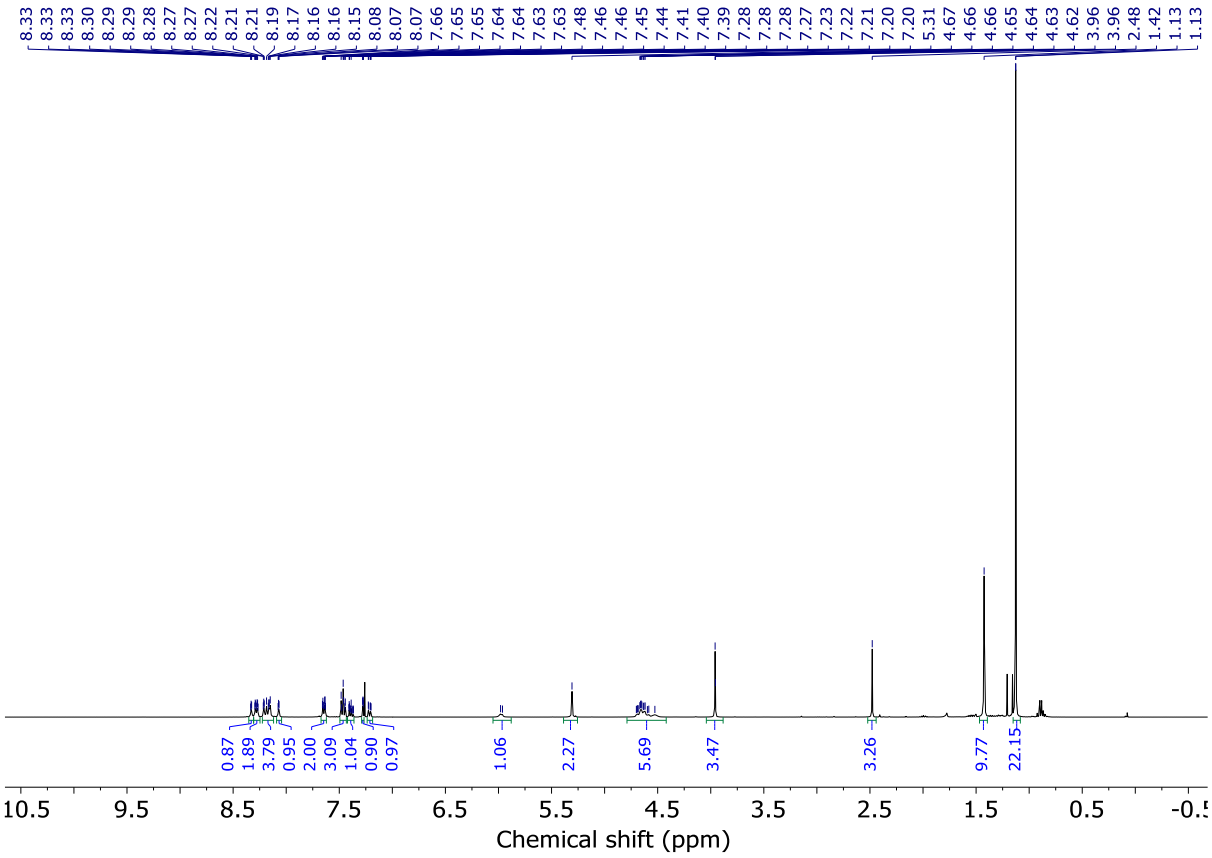

Figure 4.77 - ^{1}H NMR ($CDCl_3$, 400 MHz) of (*S*)-**S12**.

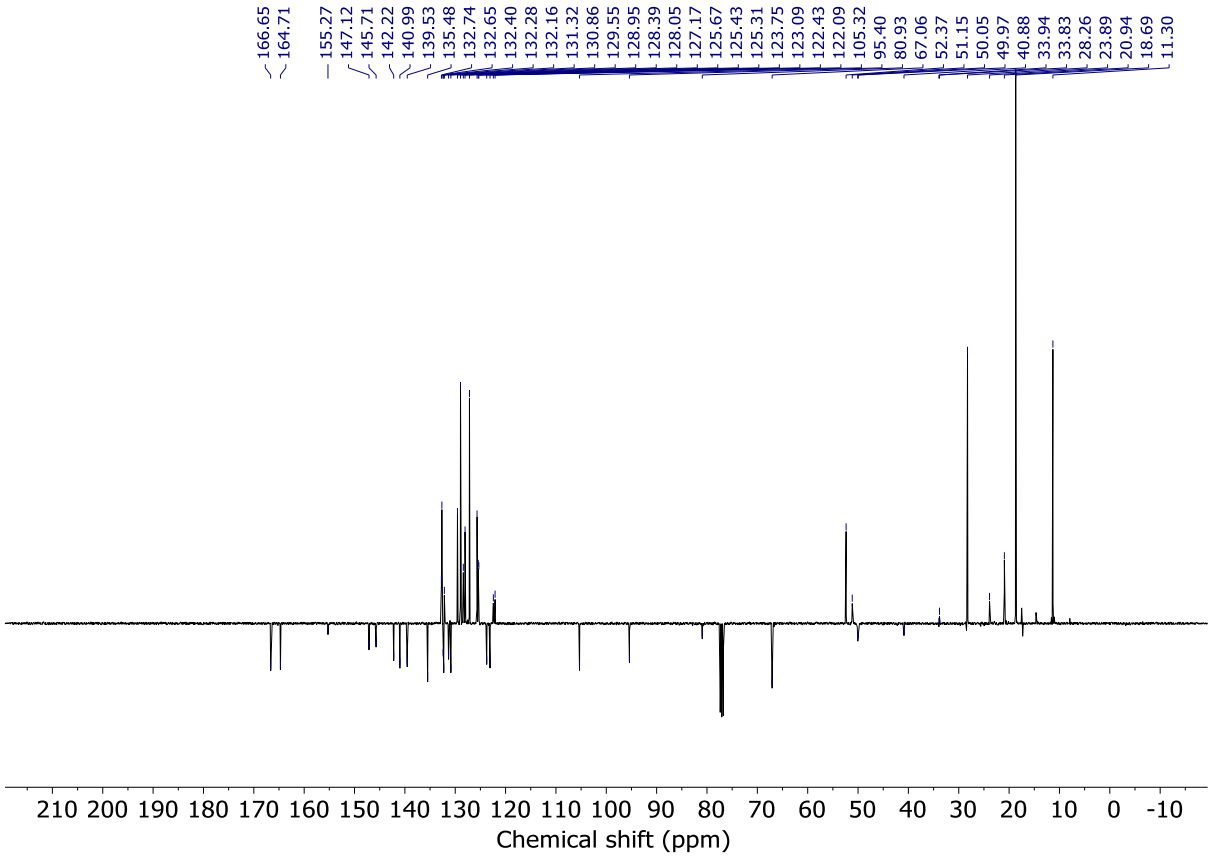

Figure 4.78 - JMOD NMR ($CDCl_3$, 101 MHz) of (*S*)-**S12**.

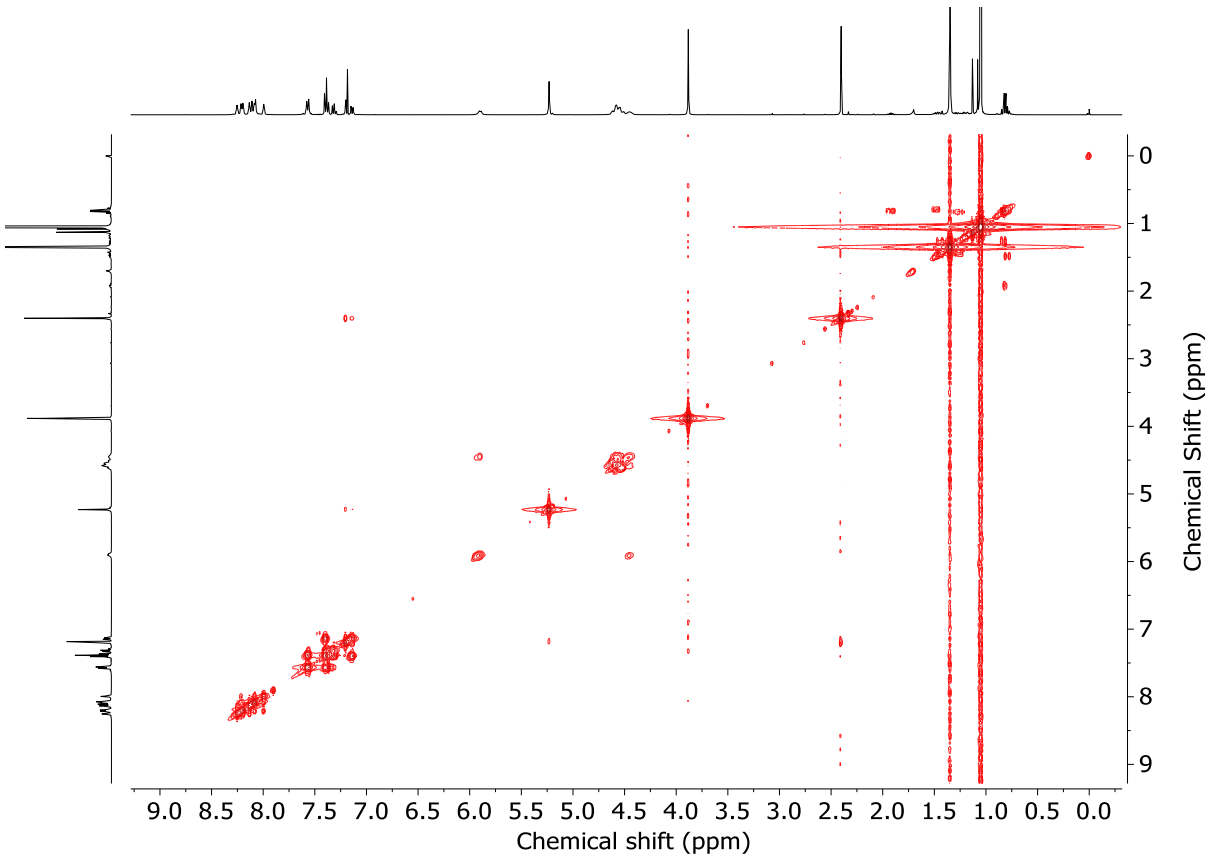

Figure 4.79 - COSY NMR ($CDCl_3$) of (*S*)-**S12**.

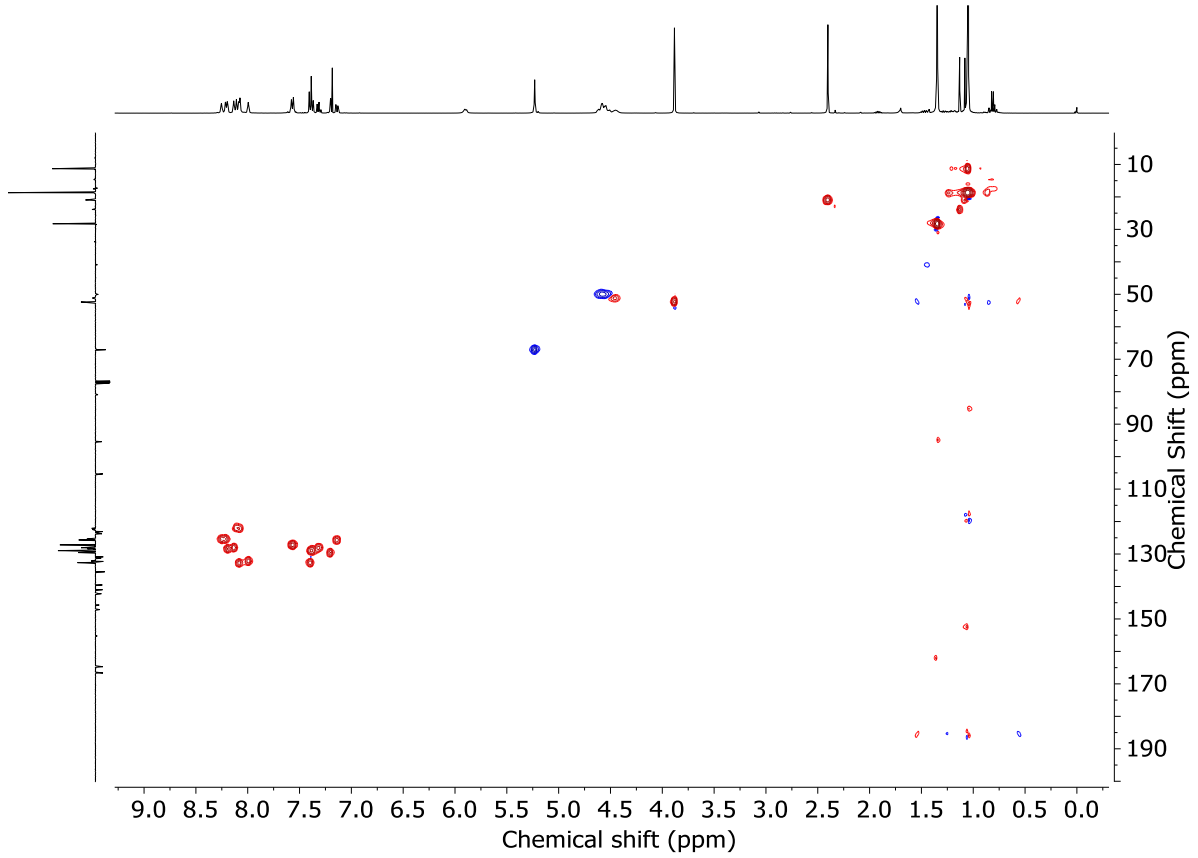

Figure 4.80 - HSQC NMR ($CDCl_3$) of (*S*)-**S12**.

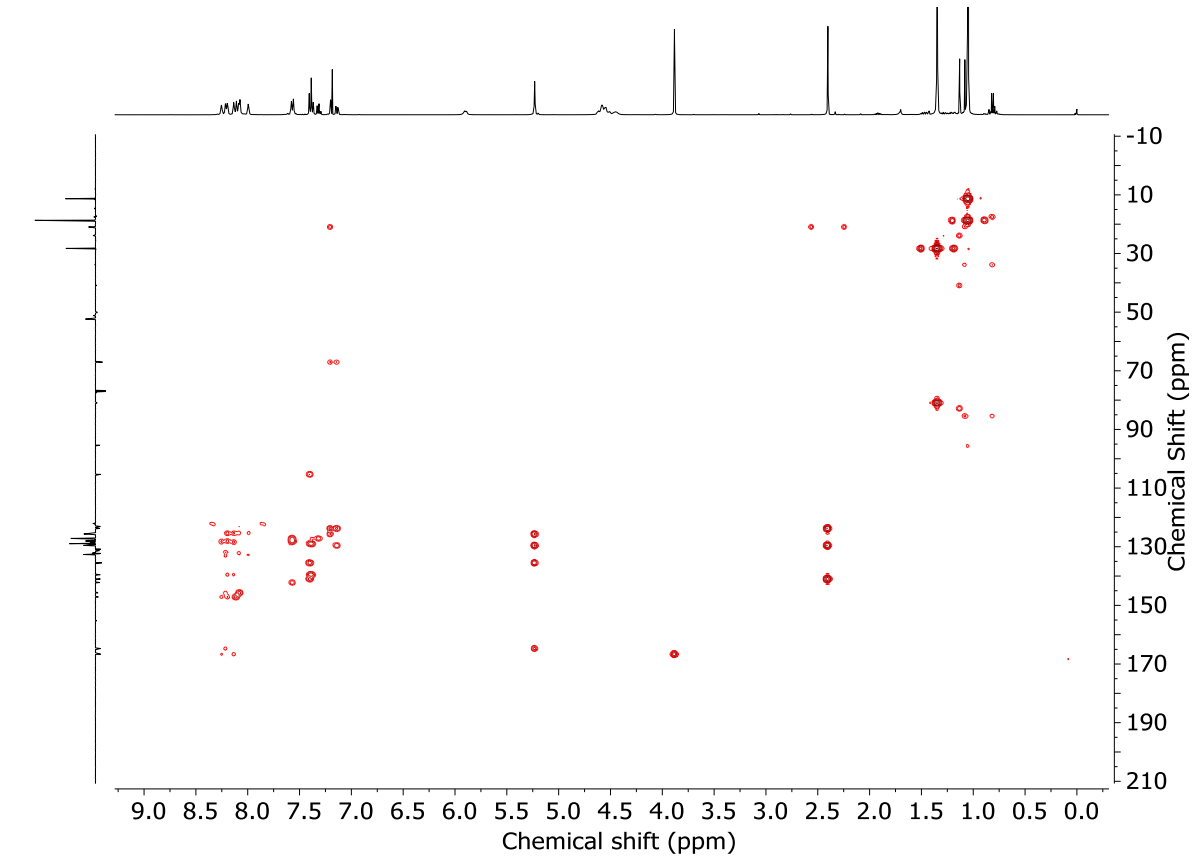

Figure 4.81 - HMBC NMR ($CDCl_3$) of (*S*)-**S12**.

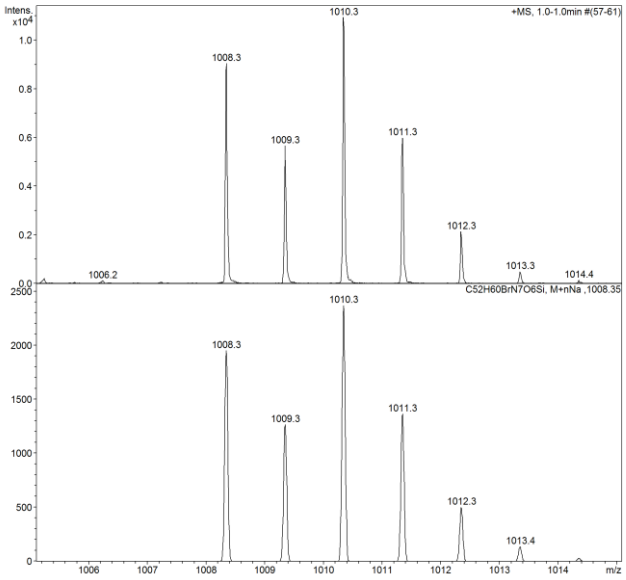

Figure 4.82 - Calculated (top) and observed (bottom) isotopic patterns for (*S*)-**S12**.

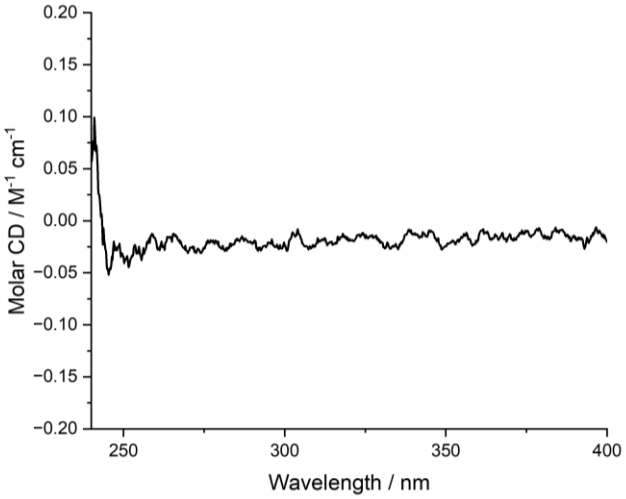

Figure 4.83 - Circular dichroism spectra of (*S*)-**S12** (63.5 μM) at 293 K in $CHCl_3$. No measurable CD response was observed so the $[\alpha]_D$ of (*S*)-**S12** was measured.

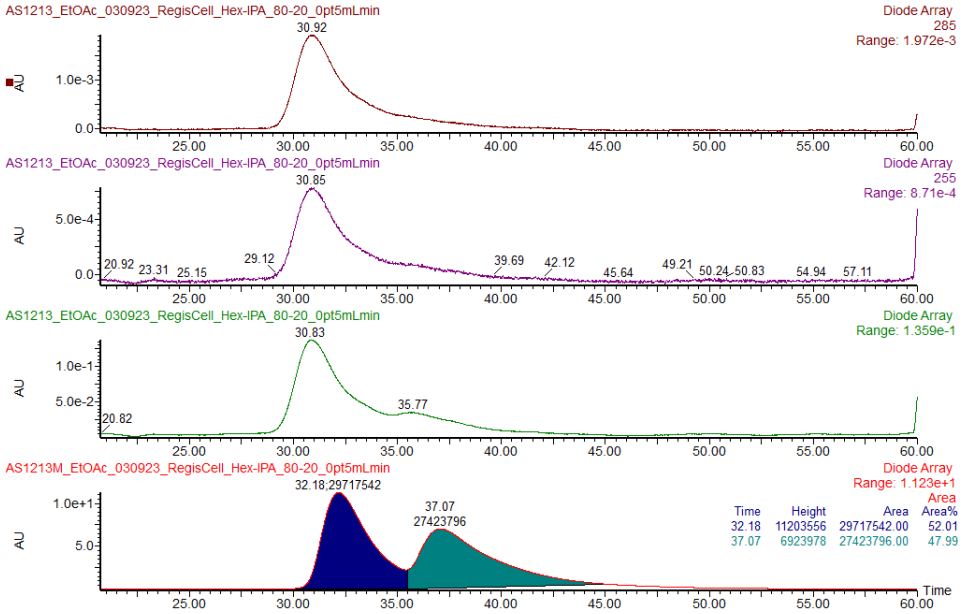

Figure 4.84 - CSP-HPLC of (S)-**S12** (loaded in EtOAc) with 285 and 255 nm traces. RegisCell, *n*-hexane-^{i}PrOH 80 : 20, flowrate 0.5 mLmin^{-1}. The minor signal observed at ~35.77 min is not consistent with the minor enantiomer; varying the wavelength of detection yielded a different relative intensity vs the major enantiomer. This impurity could not be detected by ^{1}H NMR and could not be completely removed from the sample. On this basis, the enantiopurity of (*S*)-**S12** is estimated to be >99% ee. (bottom) *rac*-**S12**, (*S*)-**S12** (32.18 min, 29717542, 52.01%), (*R*)-**S12** (37.07 min, 27423796, 47.99%).

Alkyne (*S*)-13

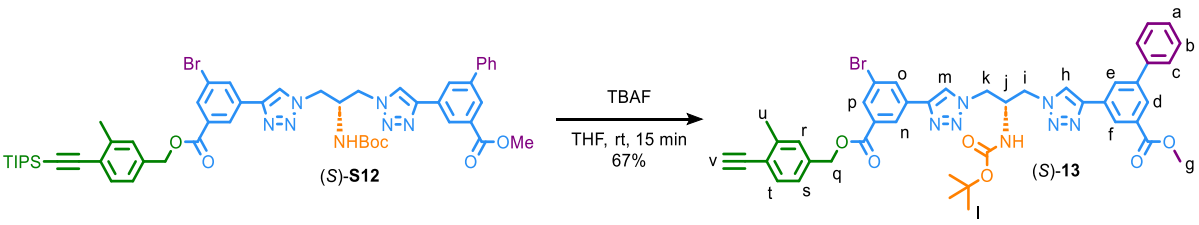

To a solution of (*S*)-**S12** (110 mg, 0.11 mmol) in THF (2 mL) was added a 1M solution of TBAF in THF (0.22 mL). The solution is stirred at rt for 15 min. The reaction mixture was partitioned between H_2O (10 mL) and EtOAc (10 mL), the phases separated, and the organic layer extracted with EtOAc (2 x 10 mL). The collected organic fractions were then washed with brine (10 mL), then dried ($MgSO_4$). The solvent was removed *in vacuo*. Chromatography (petrol-EtOAC 0→50%) gave (*S*)-**13** as a white foam (61.2 mg, 67%).

^{1}H NMR (400 MHz, $CDCl_3$) δ: 8.39 (t, *J* = 1.6, 1H, H_f), 8.36 (t, *J* = 1.5, 1H, H_n or H_p), 8.33 (t, *J* =1.7, 1H, H_e), 8.26 (t, *J* = 2.0, 1H, H_d), 8.23 (t, *J* = 1.6, H, H_n or H_p) 8.18-8.10 (m, 3H, H_h, H_m, H_o), 7.72-7.66 (m, 2H, H_a) ,7.53-7.45 (m, 3H, H_b, H_t) 7.44-7.38 (m, 1H, H_a), 7.29 (app. sept., *J* = 0.6, 1H, H_r), 7.25-7.21 (m, 1H, H_s), 5.83 (d, *J* = 7.7, 1H, NH), 5.34 (s, 2H, H_q), 4.70-4.50 (m, 4H, H_i, H_k), 4.45 (app. quint., *J* = 5.2, 1H, H_j), 3.98 (s, 3H, H_g), 3.29 (s, 1H, H_v), 2.47 (s, 3H, H_u), 1.45 (s, 9H, H_l).

^{13}C NMR (101 MHz, $CDCl_3$) δ: 166.7, 164.7, 155.2, 147.3, 145.8, 142.3, 141.3, 139.6, 132.9, 132.9, 132.5, 132.3, 132.3, 131.5, 130.8, 129.5, 129.0, 128.5, 128.2, 128.1, 127.2, 125.6, 125.5, 125.4, 123.2, 122.4, 122.0, 82.1, 81.5, 81.1, 66.9, 52.4, 51.2, 49.9, 49.8, 28.3, 23.8, 20.5

HR-ESI-MS (+ve) *m/z* = 830.2290 $[M+H]^+$ (calc. 830.2296 *m/z* for $C_{43}H_{40}BrN_7O_6$);

$[\alpha]_D^{23}$-8.5 (c 0.80, $CHCl_3$);

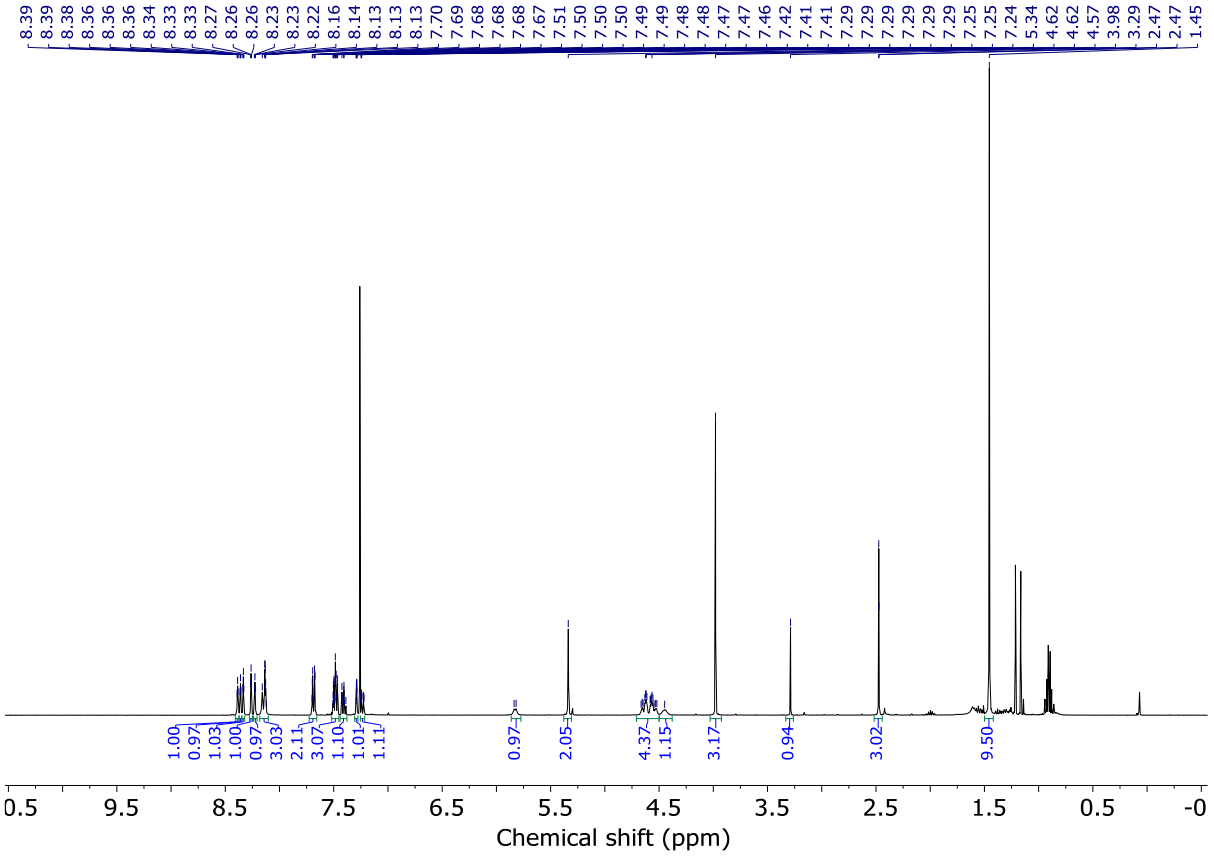

Figure 4.85 - ^{1}H NMR ($CDCl_3$, 400 MHz) of (*S*)-**13**.

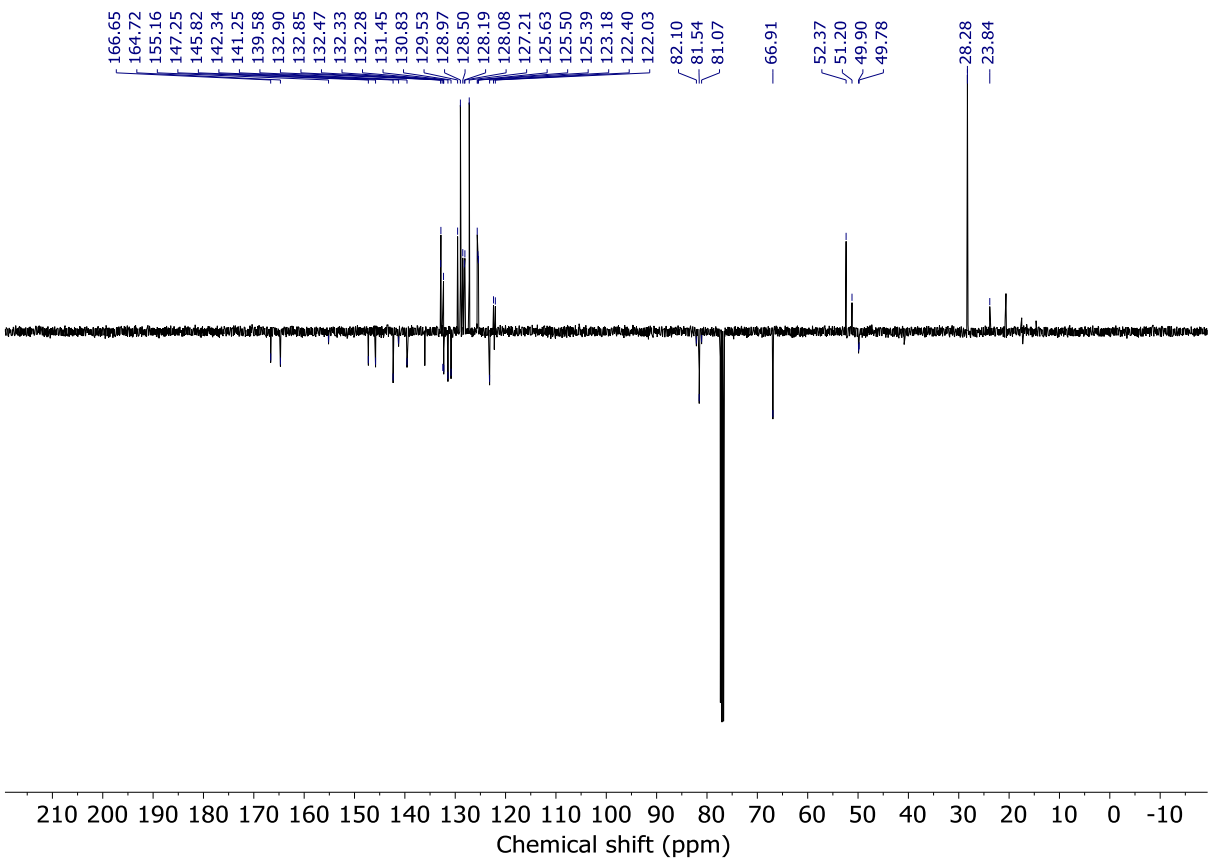

Figure 4.86 - JMOD NMR ($CDCl_3$, 101 MHz) of (*S*)-**13**.

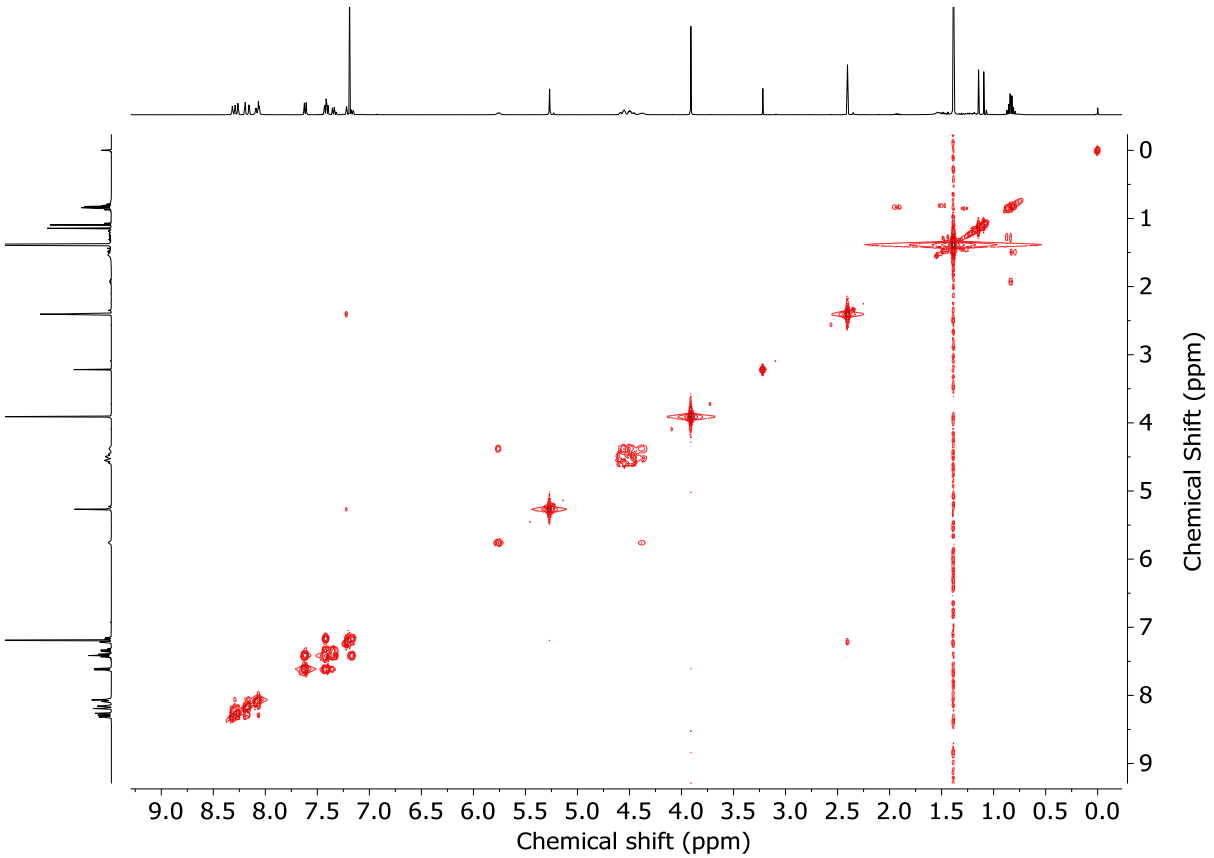

Figure 4.87 - COSY NMR ($CDCl_3$) of (*S*)-**13**.

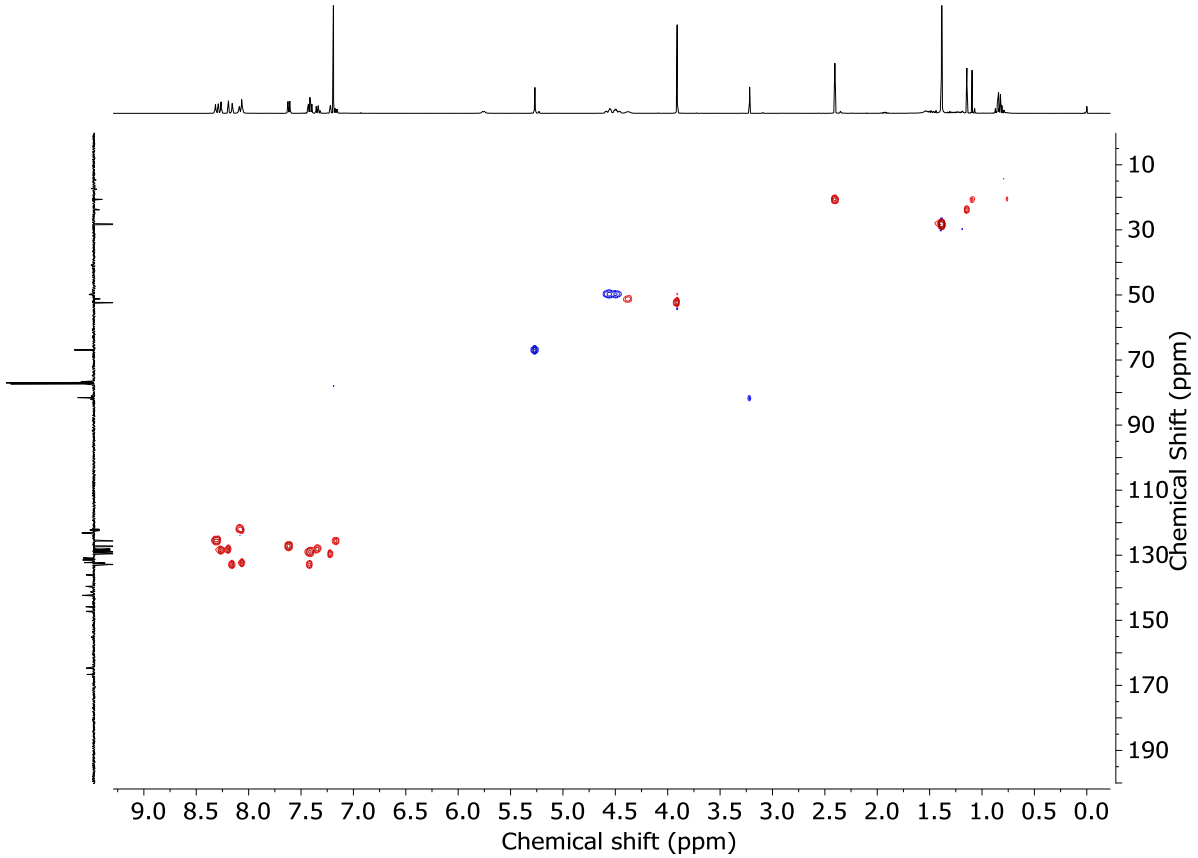

Figure 4.88 - HSQC NMR ($CDCl_3$) of (*S*)-**13**.

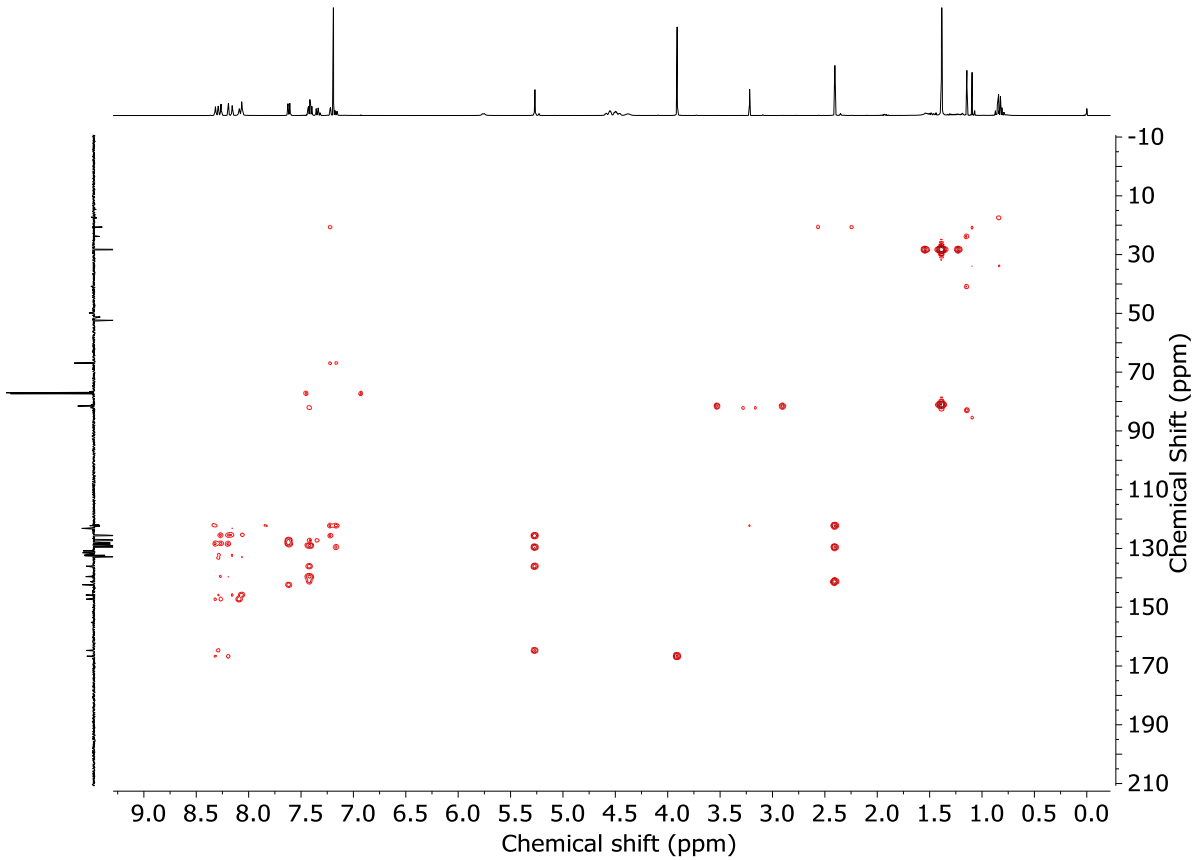

Figure 4.89 - HMBC NMR ($CDCl_3$) of (*S*)-**13**.

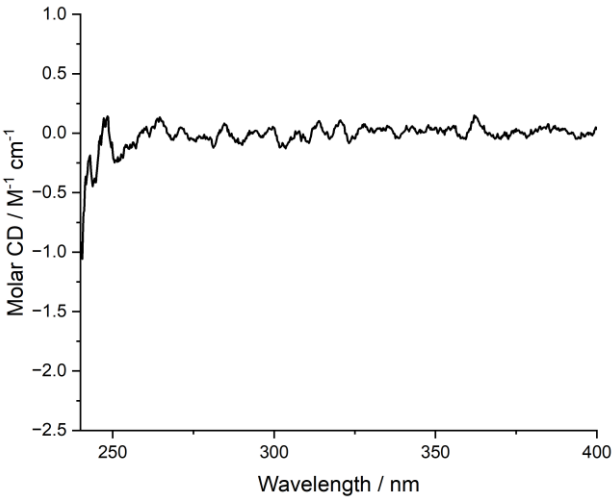

Figure 4.90 - Circular dichroism spectra of (*S*)-**13** (63.5 µM) at 293 K in $CHCl_3$. No measurable CD response was observed so the $[\alpha]_D$ of (*S*)-**13** was measured.

Rotaxane (E_m,$S_{co\text{-}c}$)-10

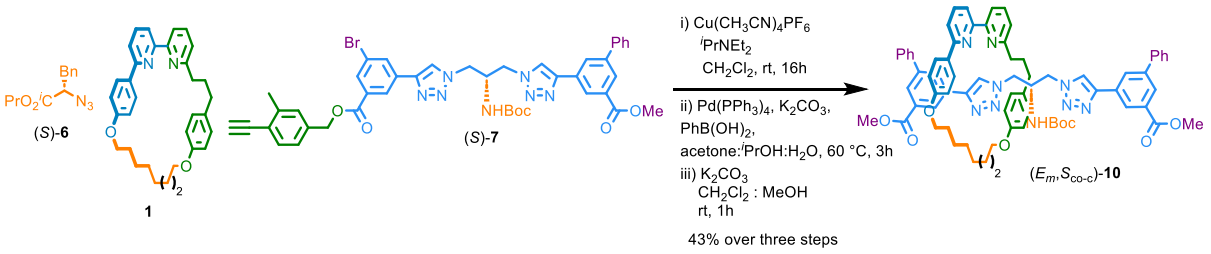

A dry sealed vessel was charged with (*S*)-**7** (50 mg, 60.2 µmol), (*S*)-**6** (14 mg, 60.0 µmol), **1** (27 mg, 55.0 µmol), $[Cu(CH_3CN)_4]PF_6$ (20.3 mg, 54.5 µmol), $^{i}Pr_2NEt$ (39.2 µL, 0.21 mmol), and CH_2Cl_2 (5 mL). The reaction mixture was stirred at rt for 16 h. The solution was diluted with CH_2Cl_2 (5 mL), then EDTA-NH_3 (5 mL) was added. The solution was vigorously stirred until complete decolouration. The aqueous and organic phases were separated, and the aqueous phase was then extracted with CH_2Cl_2 (3 x 10 mL). The combined organic extracts were washed with brine (10 mL), dried ($MgSO_4$) and concentrated *in vacuo* to give a sample containing a mixture of diastereomers (97 : 3 *dr*, Figure 88). The residue was used in the next step without further purification. The crude reaction mixture, $PhB(OH)_2$ (25.5 mg, 0.2 mmol), K_2CO_3 (29 mg, 0.2 mmol), and $Pd(PPh_3)_4$ (6 mg, 51.9 µmol) were dissolved in solvents mixture acetone:iPrOH:H_2O (2:1:1, 4 mL) (degassed) and stir for 3 h at 60 °C. After colling down to room temperature, the solution was diluted with CH_2Cl_2 (5 mL). The aqueous and organic phases were separated, and the aqueous phase was then extracted with CH_2Cl_2 (3 x 5 mL). The combined organic extracts were washed with brine (5 mL), dried over $MgSO_4$ and concentrated in vacuo and used without further

purification. Then dissolved in MeOH:CH_2Cl_2 (1:1, 10 mL) and K_2CO_3 (30 mg, 0.2 mmol) was added and stir for 1h. Solvents were removed, and the crude was purified via silica-gel chromatography (petrol : EtOAc 7:4, 0→40%), gave (E_m,$S_{co\text{-}c}$)-**10** as a colourless oil (27.1 mg, 43% over three steps, 92% *de*).

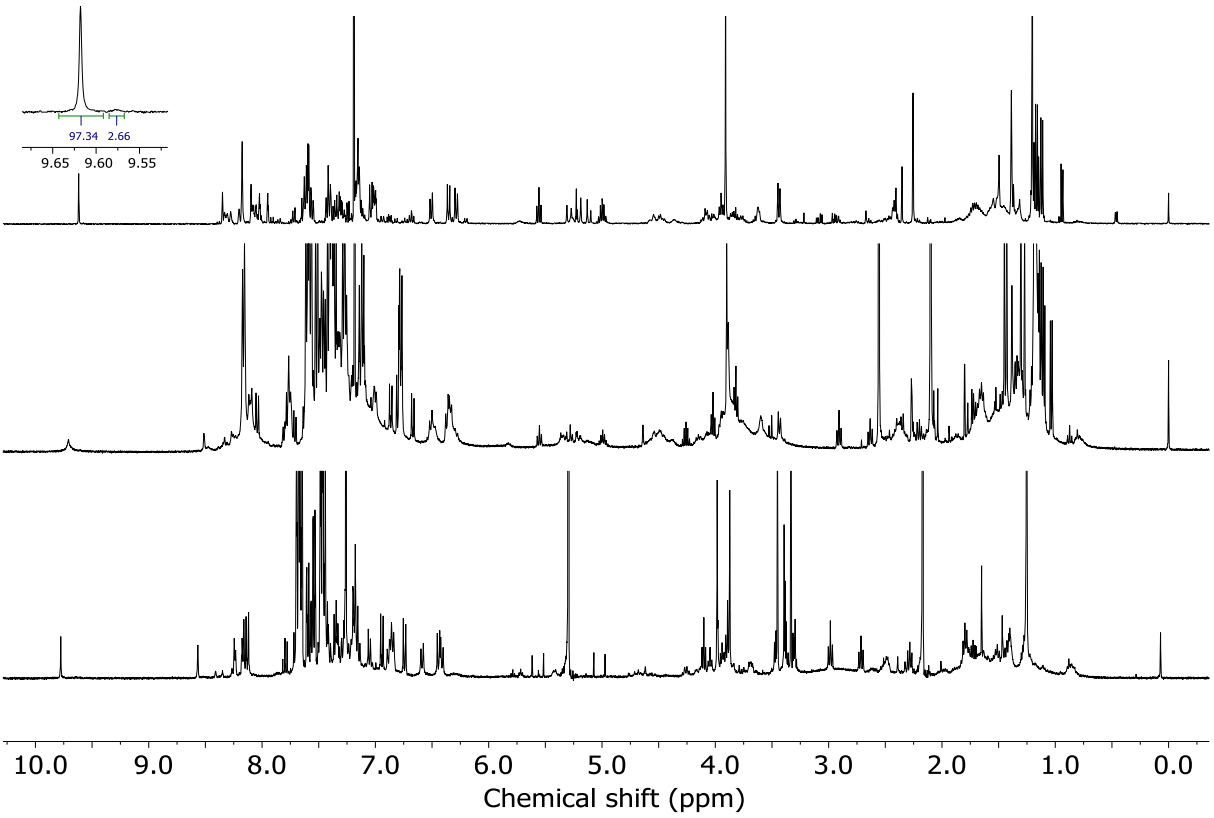

Figure 4.91 - ^{1}H NMR ($CDCl_3$, 400 MHz) of steps towards (E_m,$S_{co\text{-}c}$)-**10** prior to chromatography; first step (top), second step (middle) and third step (bottom).

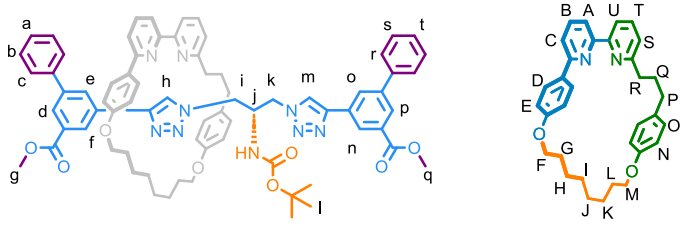

^{1}H NMR (500 MHz, $CDCl_3$) δ: δ: 9.77 (s, 1H, H_h), 8.57 (t, *J* = 1.6, 1H, H_d), 8.25 (t, *J* = 1.6, 1H, H_n), 8.24 (t, *J* = 1.7, 1.1H, H_p), 8.18 (t, *J* = 1.7, 1H, H_o), 8.16 (t, *J* = 1.6 Hz, 1H, H_f), 7.69-7.66 (m, 4H, H_B, H_m H_r or H_s), 7.59 (t, *J* = 7.9, 2H, H_e ,H_T), 7.51-7.41 (m, 6H, H_A, H_C, H_r or H_s, H_t, H_U), 7.35-7.33 (m, 2H, H_b or H_c), 7.29-7.25 (m, 3H, H_a, H_b or H_c, superimposed with $CDCl_3$), 7.16 (t, *J* = 8.7 Hz, 2H, H_D), 7.12 (d, *J* = 7.8 Hz, 1H, H_S), 6.59 (d, *J* = 8.5, 2H, H_O), 6.44 (d, *J* = 8.9, 2H, H_E), 6.41 (d, *J* = 8.4 Hz, 2H, H_N), 5.41 (d, *J* = 6.1, 1H, NH), 4.28-4.10 (m, 3H, H_k, H_M), 4.08-4.00 (m, 5H, H_F, H_q), 3.99-3.79

(m, 6H, H_g, H_i, H_j, $H_{M'}$), 3.69 (m, 1H, $H_{i'}$), 2.61 (td, J = 13.7, 4.4, 1H, H_R), 2.57-2.44 (m, 3H, H_P, $H_{R'}$), 2.03-1.48 (m, 12H, H_G, H_H, H_I, H_J, H_K, H_L, H_Q, superimposed with H_2O), 1.26 (s, 9H, H_l).

^{13}C NMR (126 MHz, $CDCl_3$) δ: 167.1, 166.7, 162.9, 159.2, 158.8, 157.7, 157.01, 157.0, 146.4, 146.0, 142.1, 141.2, 139.7, 139.7, 137.3, 137.0, 132.5, 132.1, 131.5, 131.3, 131.2, 130.9, 129.0, 128.9, 128.6, 128.4, 128.0, 127.7, 127.4, 127.2, 126.8, 125.5, 125.3, 122.4, 121.2, 120.4, 120.3, 120.2, 114.6, 113.8, 67.7, 66.5, 52.3, 52.1, 50.2, 49.9, 37.2, 34.9, 31.9, 29.7, 29.2, 28.5, 28.5, 28.4, 28.1, 25.8, 25.5.

HR-ESI-MS (+ve) *m/z* = 1206.6 $[M+H]^+$ for isotopic pattern see Figure 4.97.

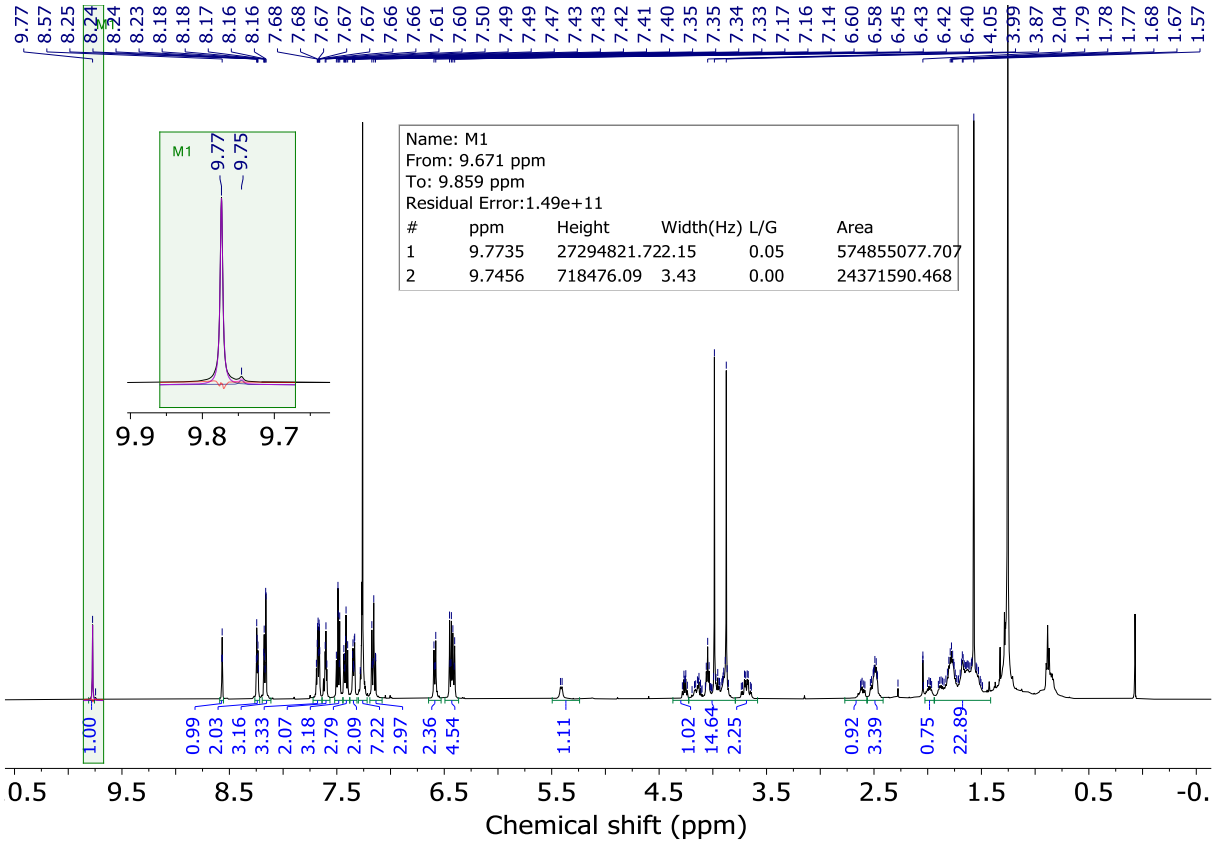

Figure 4.92 - ^{1}H NMR ($CDCl_3$, 500 MHz) of (E_m,$S_{co\text{-}c}$)-**10** (96 : 4 *dr*).

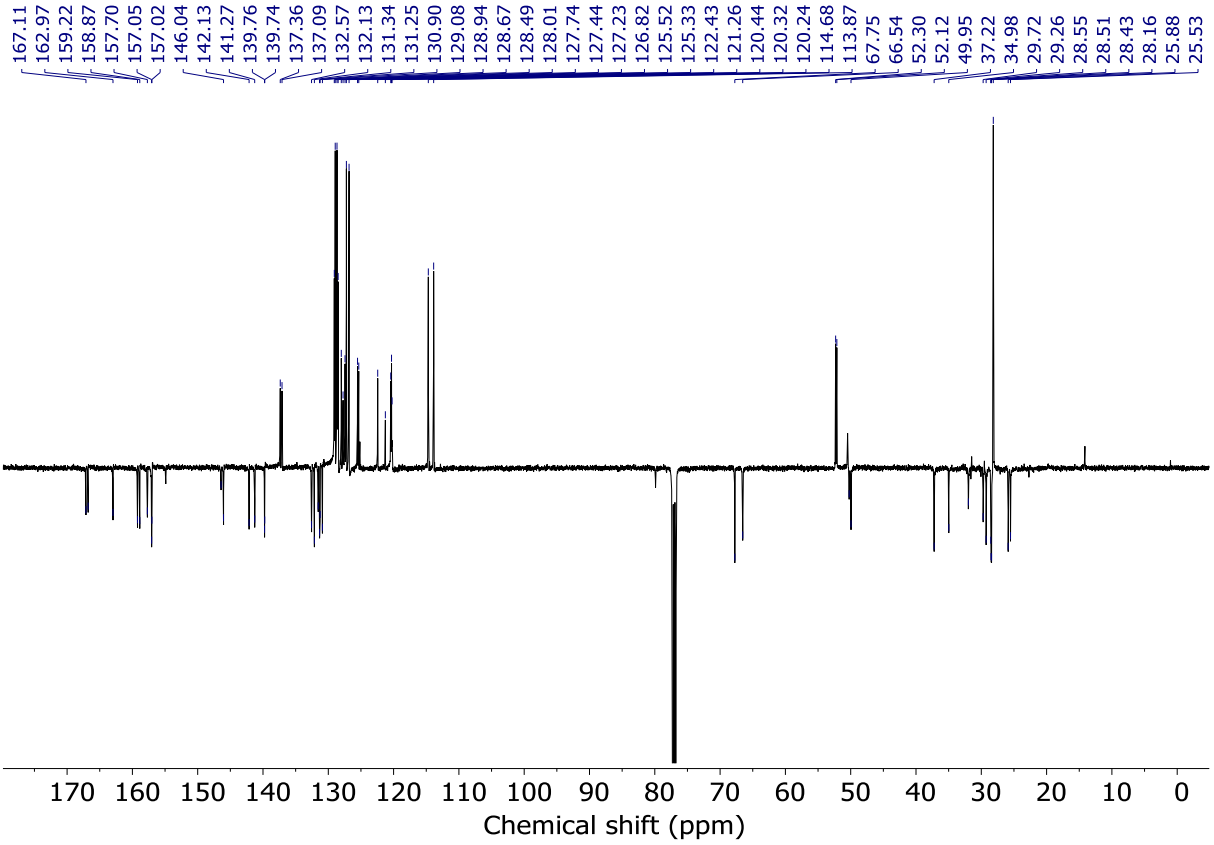

Figure 4.93 - JMOD NMR ($CDCl_3$, 126 MHz) of (E_m,$S_{co\text{-}c}$)-**10** (96 : 4 *dr*).

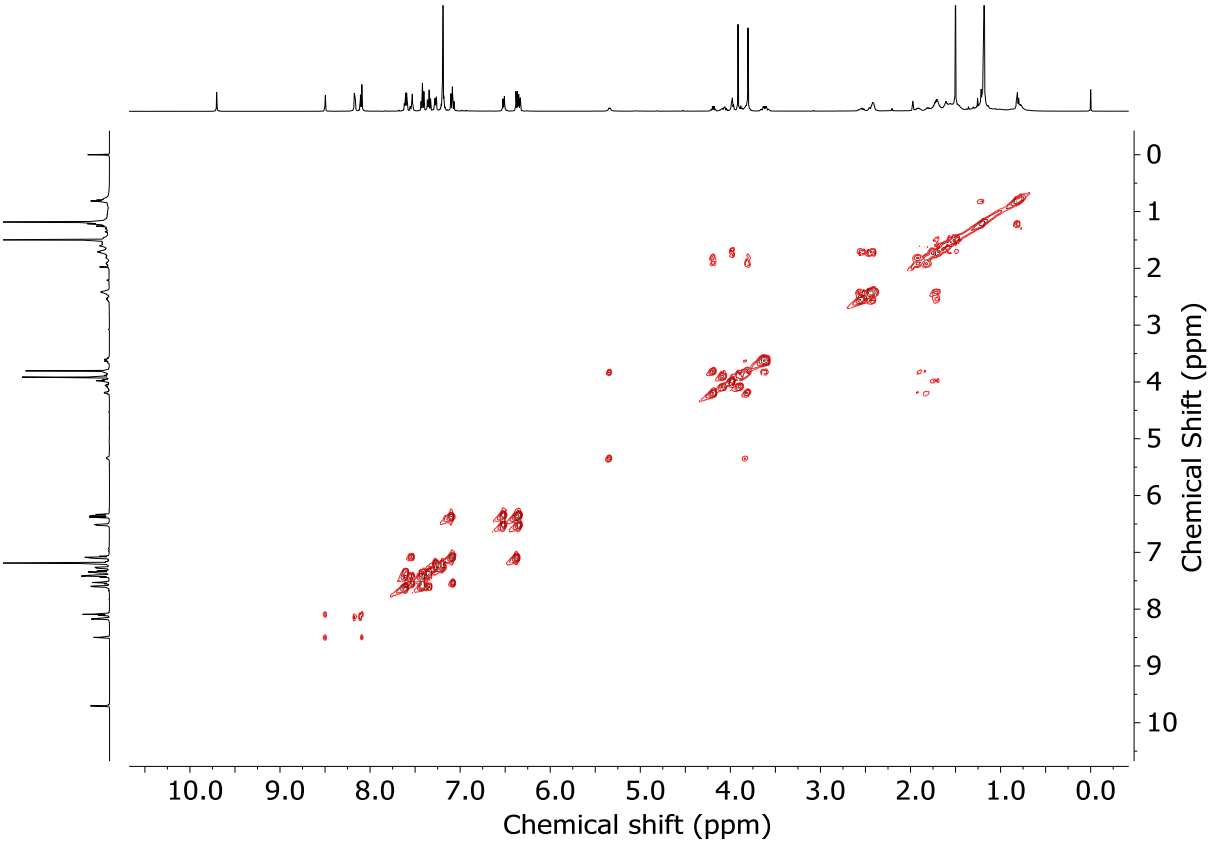

Figure 4.94 - COSY NMR ($CDCl_3$) of (E_m,$S_{co\text{-}c}$)-**10** (96 : 4 *dr*).

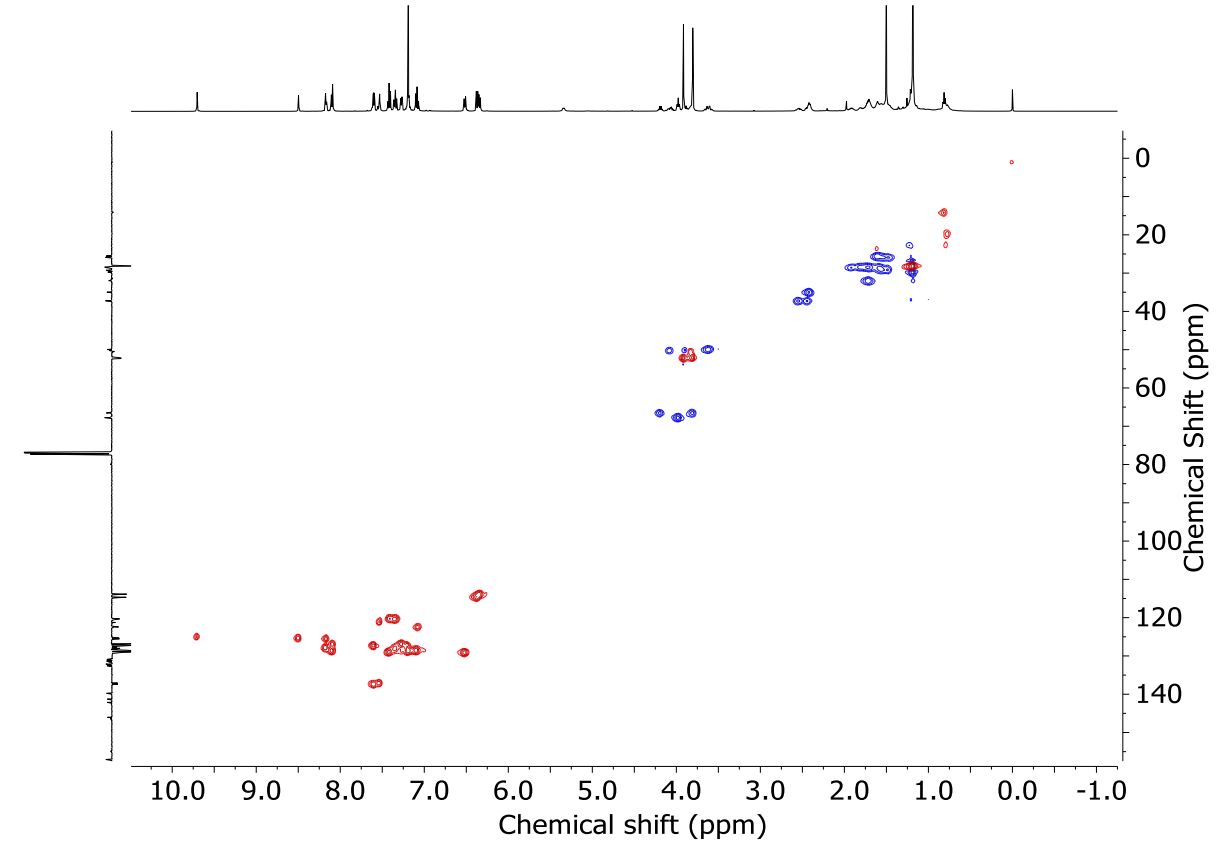

Figure 4.95 - HSQC NMR ($CDCl_3$) of (E_m,$S_{co\text{-}c}$)-**10** (96 : 4 *dr*).

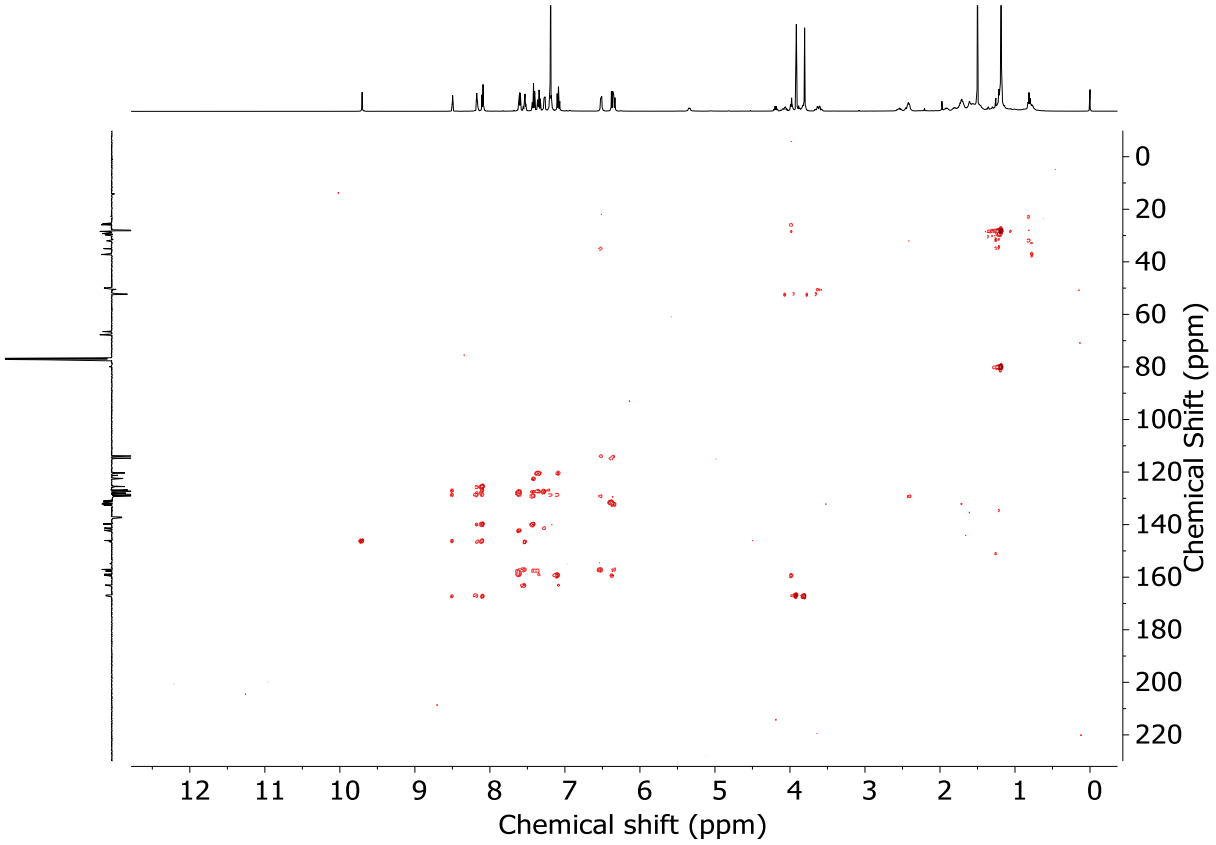

Figure 4.96 - HMBC NMR ($CDCl_3$) of (E_m,$S_{co\text{-}c}$)-**10** (96 : 4 *dr*).

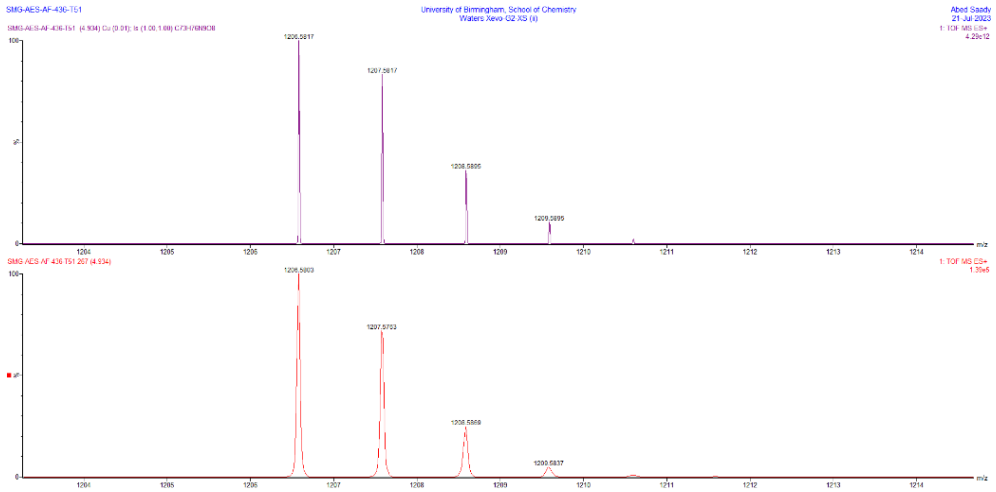

Figure 4.97 - Calculated (top) and observed (bottom) isotopic patterns for (E_m,$S_{co\text{-}c}$)-**10**.

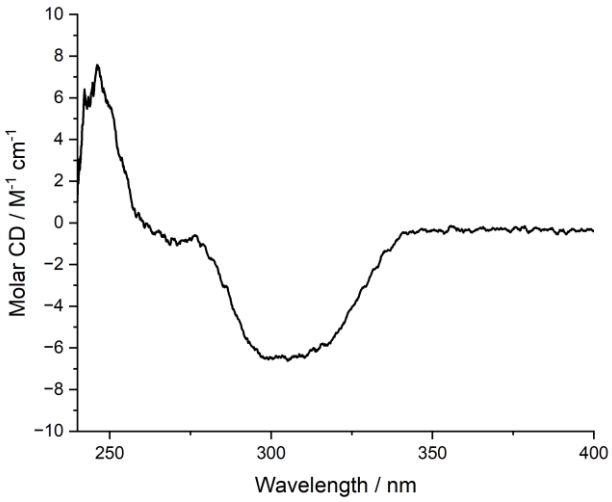

Figure 4.98 - Circular dichroism spectra of (E_m,$S_{co\text{-}c}$)-**10** (63.5 μM) at 293 K in $CHCl_3$

Rotaxane (E_m)-11

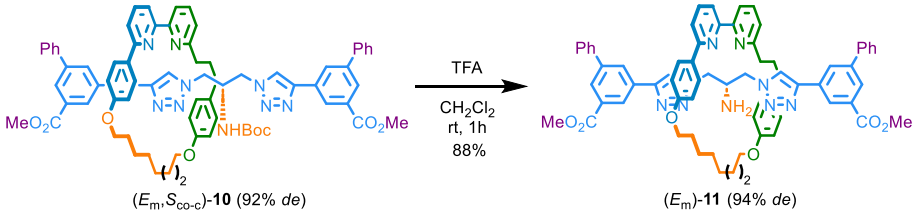

(E_m,$S_{co\text{-}c}$)-**10** (92% *de*) (E_m)-**11** (94% *de*)

A vessel was charged with rotaxane (E_m,$S_{co\text{-}c}$)-**10** (15.0 mg, 0.012 mmol, 92% *de*), TFA (21.4 μL, 0.18 mmol), and CH_2Cl_2 (1 mL). The reaction mixture was stirred at rt for 1 h. CH_2Cl_2 (10 mL) was added, washed with sat. $NaHCO_3$ solution (10 mL), brine (10 mL), and the combined organic extracts were dried ($MgSO_4$) and concentrated *in vacuo*. The residue was purified by column chromatography (*n*-hexane-EtOAc 0→40%) gave rotaxane (E_m)-**11** as a white foam (12.1 mg, 88%, 94% *de*).

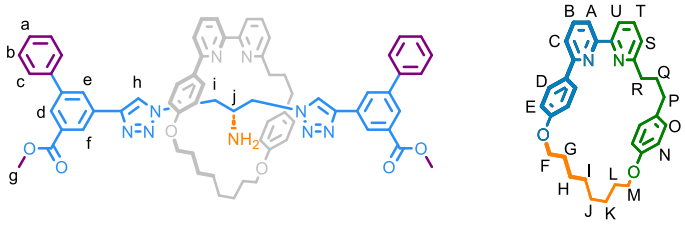

^{1}H NMR (500 MHz, $CDCl_3$) δ: δ: 8.73 (s, 2H, H_h), 8.40 (t, *J* = 1.7, 2H, H_f), 8.20 (t, *J* = 1.7, 2H, H_d), 8.14 (t, *J* = 1.7, 2H, H_e), 7.62 (app t, *J* = 7.8, 1H, H_B),7.56-7.50 (m, 5H, H_b or H_c, H_T), 7.42-7.33 (m, 9H, H_a, H_b or H_c, H_A, H_C, H_U), 7.25 (d, *J* = 8.6, 2H, H_E), 7.07 (d, *J* = 7.8, 1H, H_S), 6.64 (d, *J* = 8.4, 2H, H_N), 6.55 (d, *J* = 8.6, 2H, H_D), 6.52 (d, *J* = 8.4, 2H, H_O), 4.14-4.05 (m, 5H, H_F, H_M), 3.93 (s, 6H, H_g), 3.87 (dd, *J* = 14.4, 4.2, 2H, H_i), 3.42-3.35 (m, 3H, $H_{i'}$, NH), 2.86 (t, *J* = 5.3, 2H, H_R), 2.64 (app. sept. *J* = 3.5, 1H, H_j), 2.52-2.38 (m, 2H, H_P) 1.91 (t, *J* = 5.4, 2H, H_L), 1.80-1.43 (m, 12H, H_G, H_H, H_I, H_J, H_K, H_Q, superimposed with H_2O)

^{13}C NMR (125 MHz, $CDCl_3$) δ: 167.3, 163.3, 159.6, 159.4, 158.1, 157.6, 157.4, 146.6, 142.3, 140.2, 137.9, 137.5, 132.9, 132.5, 132.1, 131.7, 129.8, 129.3, 128.8, 128.2, 127.8, 127.5, 125.6, 125.2, 124.9, 124.8, 123.9, 123.3, 122.9, 121.0, 120.9, 120.7, 119.6, 119.5, 119.3, 115.4, 114.5, 67.9, 67.0, 65.1, 54.5, 52.7, 51.0, 37.6, 37.0, 35.4, 33.1, 32.4, 32.0, 30.8, 30.6, 30.1, 28.8, 26.4, 26.1.

HR-ESI-MS (+ve) *m/z* = 1106.5 $[M+H]^+$ for isotopic pattern see Figure 4.104.

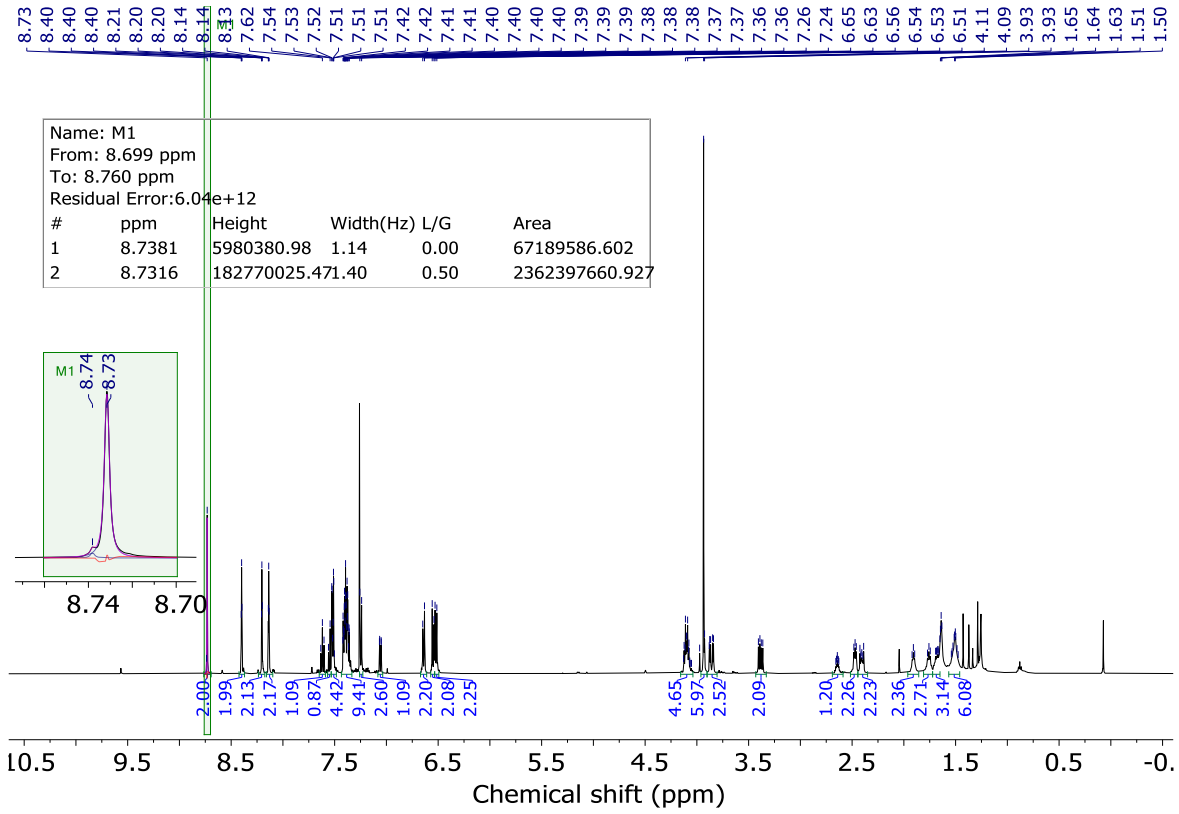

Figure 4.99 - ^{1}H NMR ($CDCl_3$, 500 MHz) of (E_m)-**11** (97: 3 *dr*).

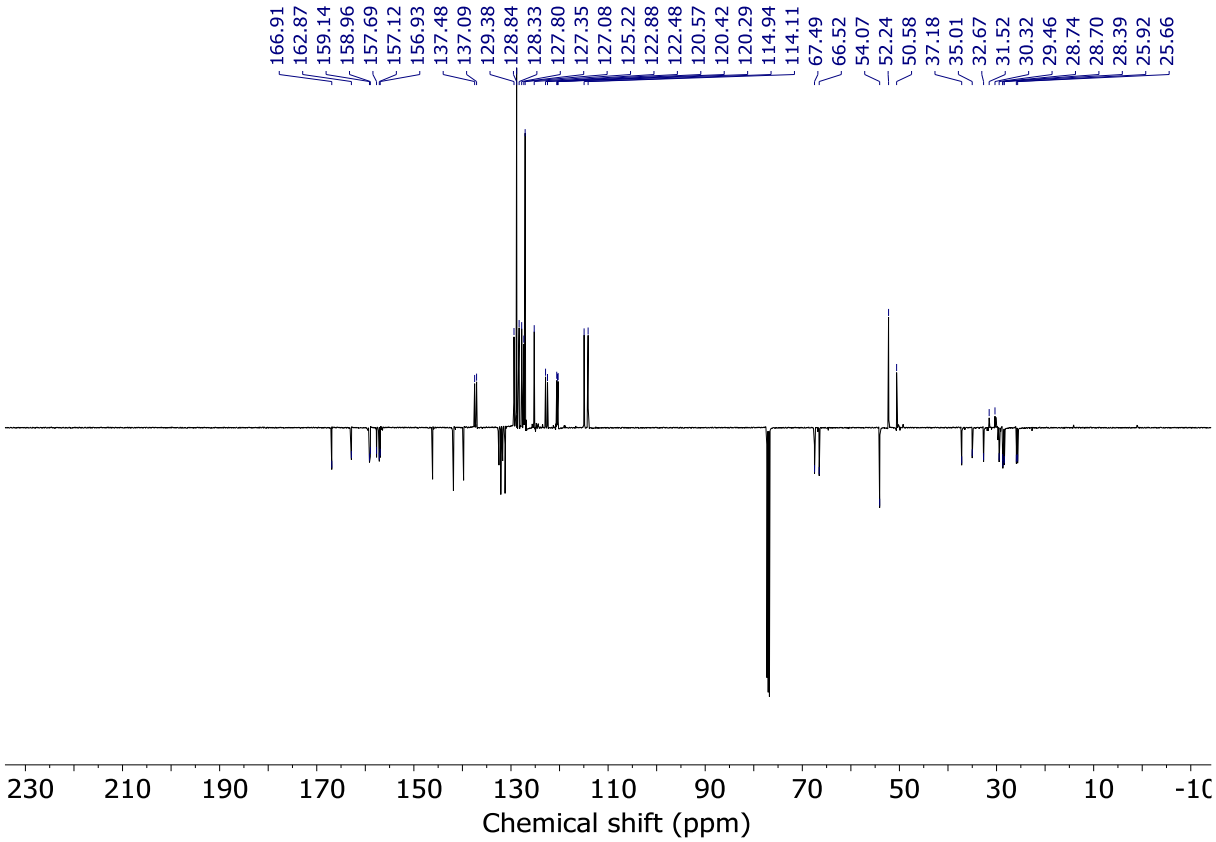

Figure 4.100 - JMOD NMR ($CDCl_3$, 126 MHz) of (E_m)-**11** (97: 3 *dr*).

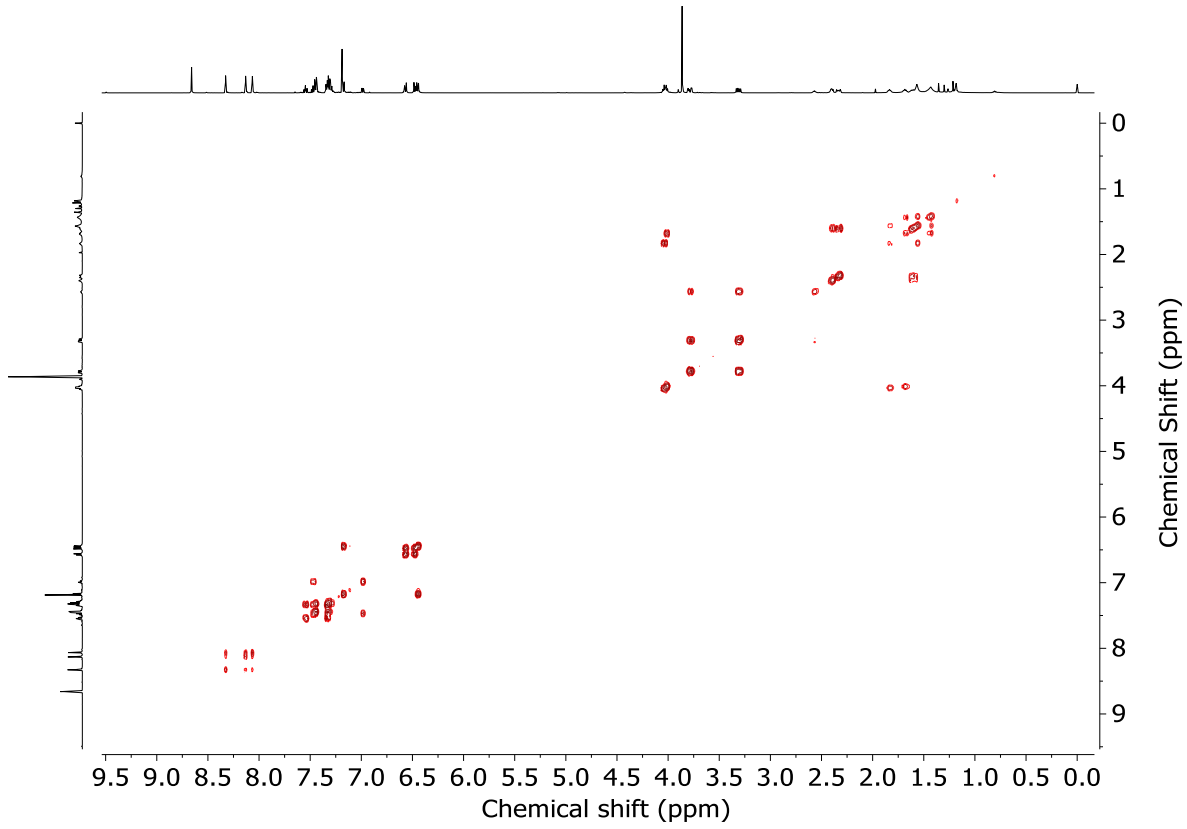

Figure 4.101 - COSY NMR ($CDCl_3$) of (E_m)-**11** (97: 3 *dr*).

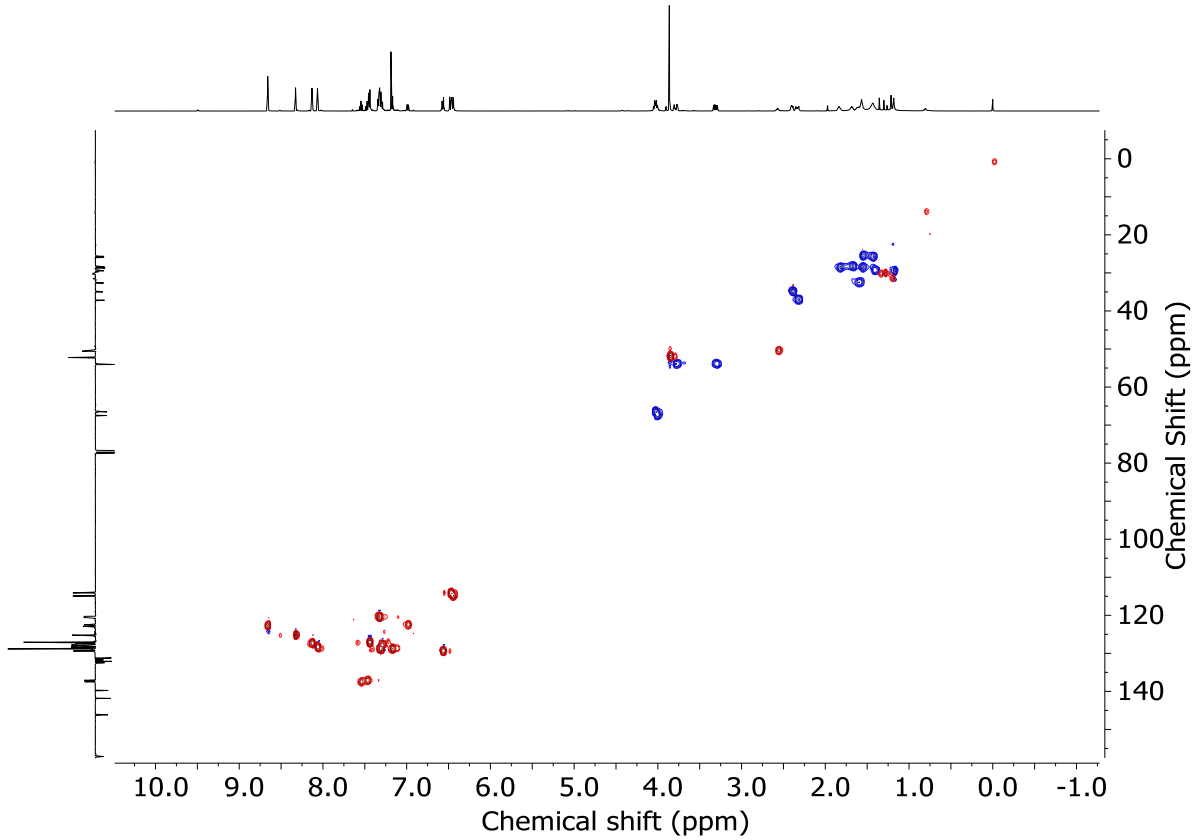

Figure 4.102 - HSQC NMR ($CDCl_3$) of (E_m)-**11** (97: 3 *dr*).

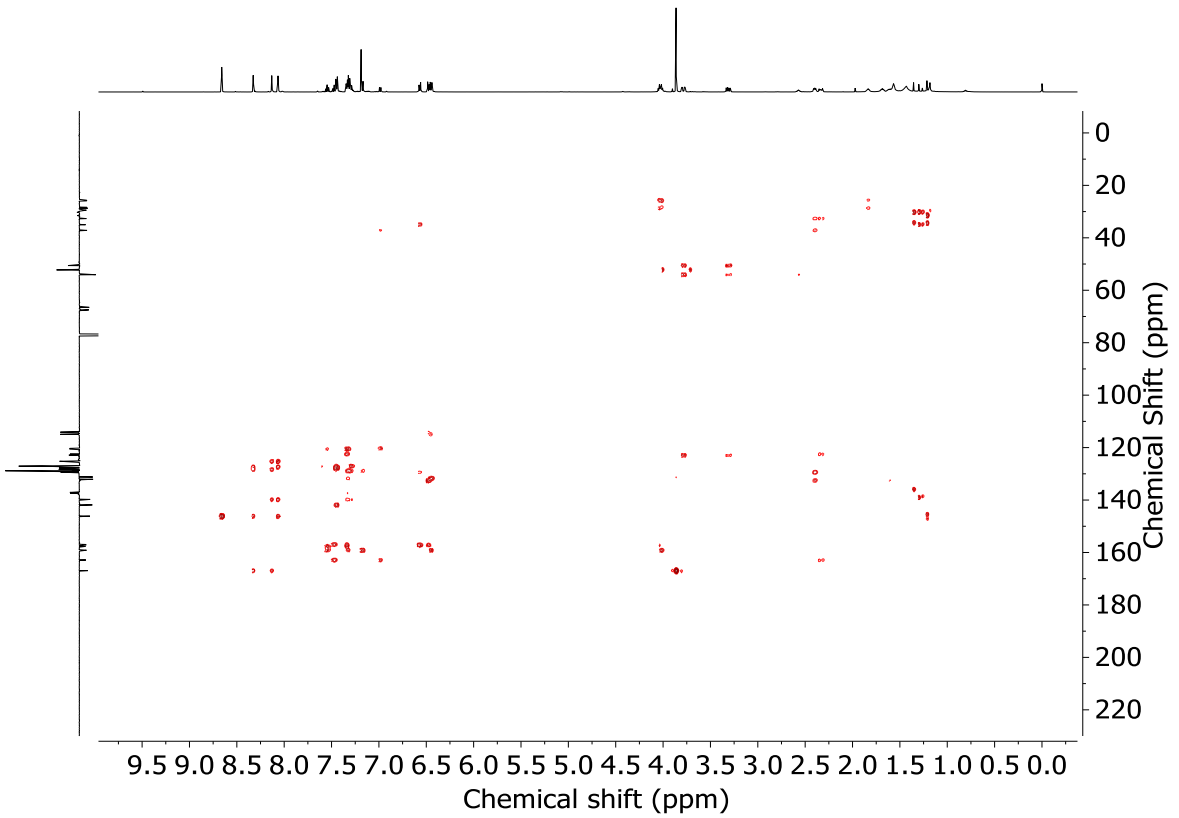

Figure 4.103 - HMBC NMR ($CDCl_3$) of (E_m)-**11** (97: 3 *dr*).

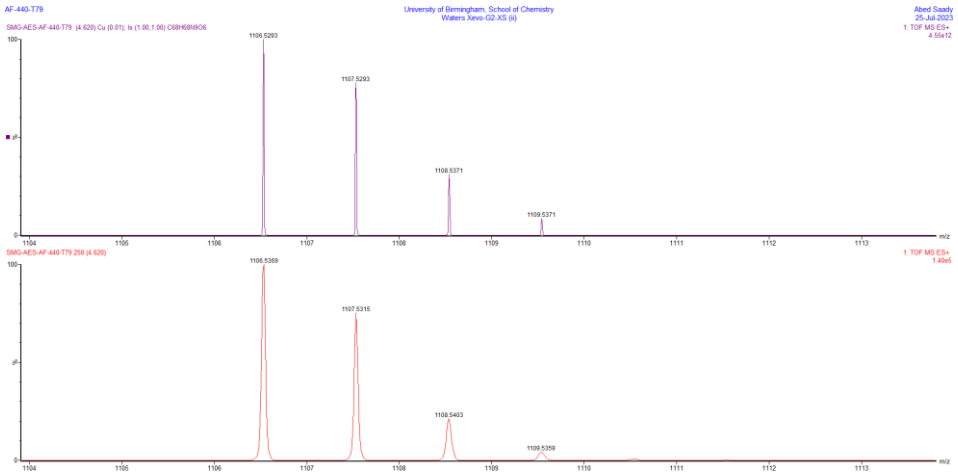

Figure 4.104 - Calculated (top) and observed (bottom) isotopic patterns for (E_m)-**11**.

Rotaxane (Z_m,$S_{co\text{-}c}$)-10

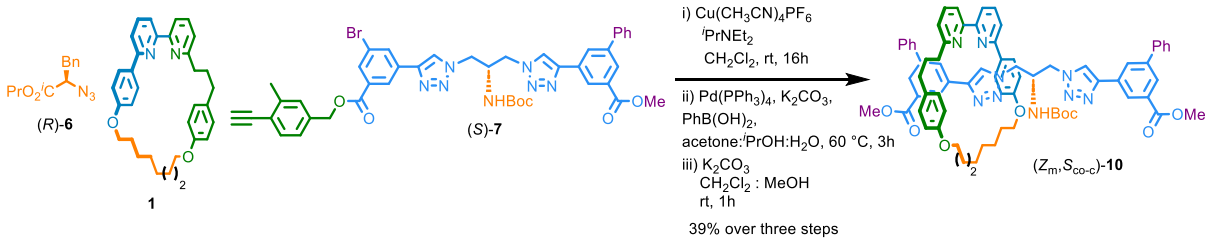

A dry sealed vessel was charged with (*S*)-**7** (50 mg, 60.2 µmol), (*R*)-**6** (14 mg, 60.0 µmol), **1** (27 mg, 55.0 µmol), $[Cu(CH_3CN)_4]PF_6$ (20.3 mg, 54.5 µmol), $^iPr_2NEt$ (39.2 µL, 0.21 mmol), and anhydrous CH_2Cl_2 (5 mL). The reaction mixture was stirred at rt for 16 h. The solution was diluted with CH_2Cl_2 (5 mL), then EDTA-NH_3 (5 mL) was added. The solution was vigorously stirred until complete decolouration. The aqueous and organic phases were separated, and the aqueous phase was then extracted with CH_2Cl_2 (3 x 10 mL). The combined organic extracts were washed with brine (10 mL), dried ($MgSO_4$) and concentrated *in vacuo* to give a sample containing a mixture of diastereomers (2 : 98 *dr*, Figure 102). The residue was used in the next step without further purification. The crude reaction mixture, $PhB(OH)_2$ (25.5 mg, 0.2 mmol), K_2CO_3 (29 mg, 0.2 mmol), and $Pd(PPh)_4$ (6 mg, 51.9 µmol) were dissolved in solvents mixture acetone:*i*PrOH:H_2O (2:1:1, 4 mL) (degassed) and stir for 3 h at 60 °C. After cooling to rt, the solution was diluted with CH_2Cl_2 (5 mL). The aqueous and organic phases were separated, and the aqueous phase was then extracted with CH_2Cl_2 (3 x 5 mL). The combined organic extracts were washed with brine (5 mL), dried ($MgSO_4$) and concentrated *in vacuo,* then dissolved in MeOH:CH_2Cl_2 (1:1, 10 mL) and K_2CO_3 (30 mg, 0.2 mmol) was added. The suspension was stirred at rt for 1 h, then solvents were removed *in vacuo*. Chromatography (petrol-EtOAc 0→30%) gave (Z_m,$S_{co\text{-}c}$)-**10** as a colourless oil (25.8 mg, 39% over three steps, 94% *de*).

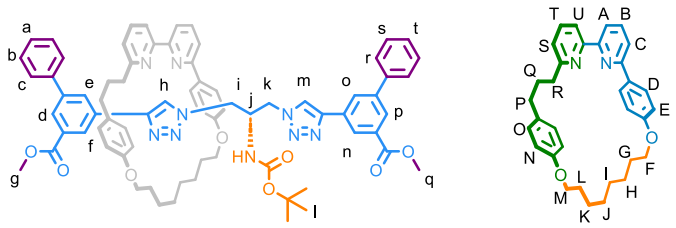

^{1}H NMR (500 MHz, $CDCl_3$) δ: 9.75 (s, 1H, H_h), 8.52 (bs, 1H, H_d), 8.27 (t, *J* = 1.6, 1H, H_n), 8.25 (t, *J* = 1.7, 1.1H, H_p), 8.20 (t, *J* = 1.7, 1H, H_o), 8.16 (t, *J* = 1.6 Hz, 1H, H_f), 8.14 (bs, 1H, H_e), 7.75 (s, 1H, H_m), 7.73-7.65 (m, 3H, H_B, H_r or H_s), 7.59 (t, *J* = 7.9, 1H, H_T), 7.53-7.39 (m, 6H, H_A, H_C, H_r or H_s, H_t, H_U), 7.39-7.35 (m, 2H, H_b or H_c), 7.29-7.25 (m, 3H, H_a, H_b or H_c, superimposed with $CDCl_3$), 7.22 (d, *J* = 8.7 Hz, 2H, H_D), 7.12 (d, *J* = 7.8 Hz, 1H, H_S), 6.56 (d, *J* = 8.5, 2H, H_O), 6.44 (d, *J* = 8.9, 2H, H_E), 6.32 (d, *J* = 8.4 Hz, 2H, H_N), 5.44 (d, *J* = 6.1, 1H, NH), 4.26-4.10 (m, 3H, H_k, H_M), 4.10-3.95 (m, 5H, H_F, H_q), 3.94-3.77 (m, 6H, H_g, H_i, H_j, $H_{M'}$), 3.64 (dd, *J* = 14.4, 4.1, 1H, $H_{i'}$), 2.66 (td, *J* = 13.7, 4.4, 1H, H_R), 2.57-2.44 (m, 3H, H_P, $H_{R'}$), 2.01-1.48 (m, 12H, H_G, H_H, H_I, H_J, H_K, H_L, H_Q, superimposed with H_2O), 1.28 (s, 9H, H_l)

^{13}C NMR (126 MHz, $CDCl_3$) δ: 167.6, 167.3, 163.4, 159.7, 159.2, 158.0, 157.6, 157.5, 146.9, 146.3, 142.6, 141.7, 140.3, 140.2, 137.8, 137.5, 133.1, 132.5, 132.0, 131.8, 131.7, 131.3, 129.4, 129.1, 129.1, 129.0, 128.9, 128.5, 128.2, 127.9, 127.7, 127.3, 127.3, 126.0, 125.8, 122.7, 121.8, 120.9, 120.8, 120.6, 115.0, 114.2, 97.8, 80.5, 77.5, 77.2, 68.2, 66.9, 52.8, 52.6, 51.5, 50.8, 50.1, 37.7, 35.4, 29.6, 28.9, 28.9, 28.8, 28.6, 26.4, 25.9.

HR-ESI-MS (+ve) *m/z* = 1206.6 $[M+H]^+$, for isotopic pattern see Figure 4.111.

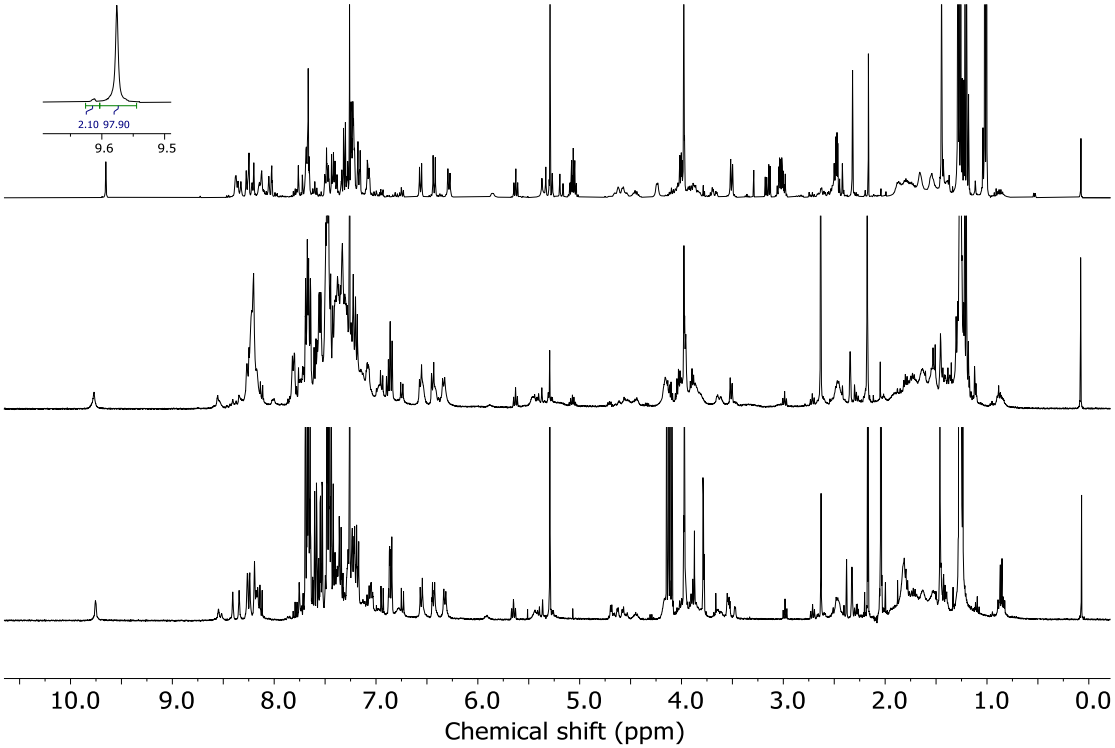

Figure 4.105 - ^{1}H NMR ($CDCl_3$, 400 MHz) of steps towards (Z_m,$S_{co\text{-}c}$)-**10** prior to chromatography; first step (top), second step (middle) and third step (bottom).

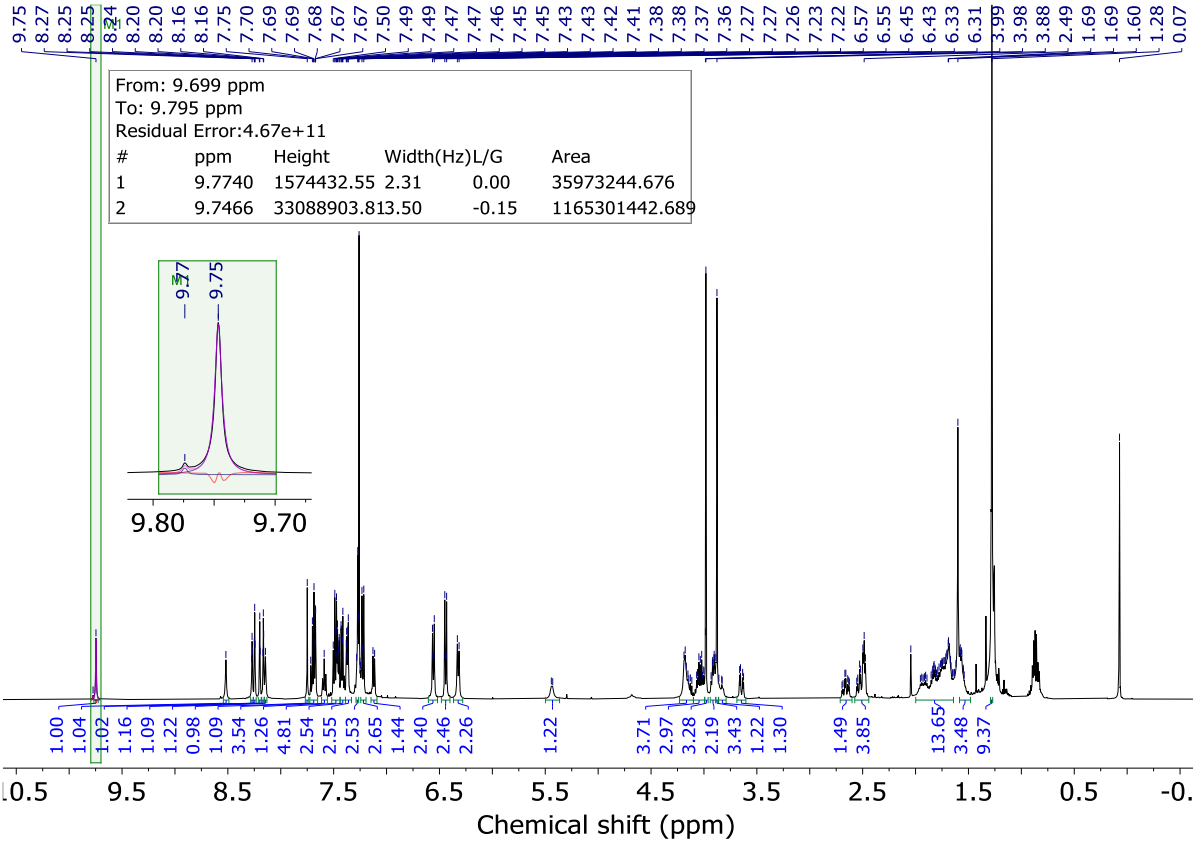

Figure 4.106 - ^{1}H NMR ($CDCl_3$, 500 MHz) of (Z_m,$S_{co\text{-}c}$)-**10** (97 : 3 *dr*).

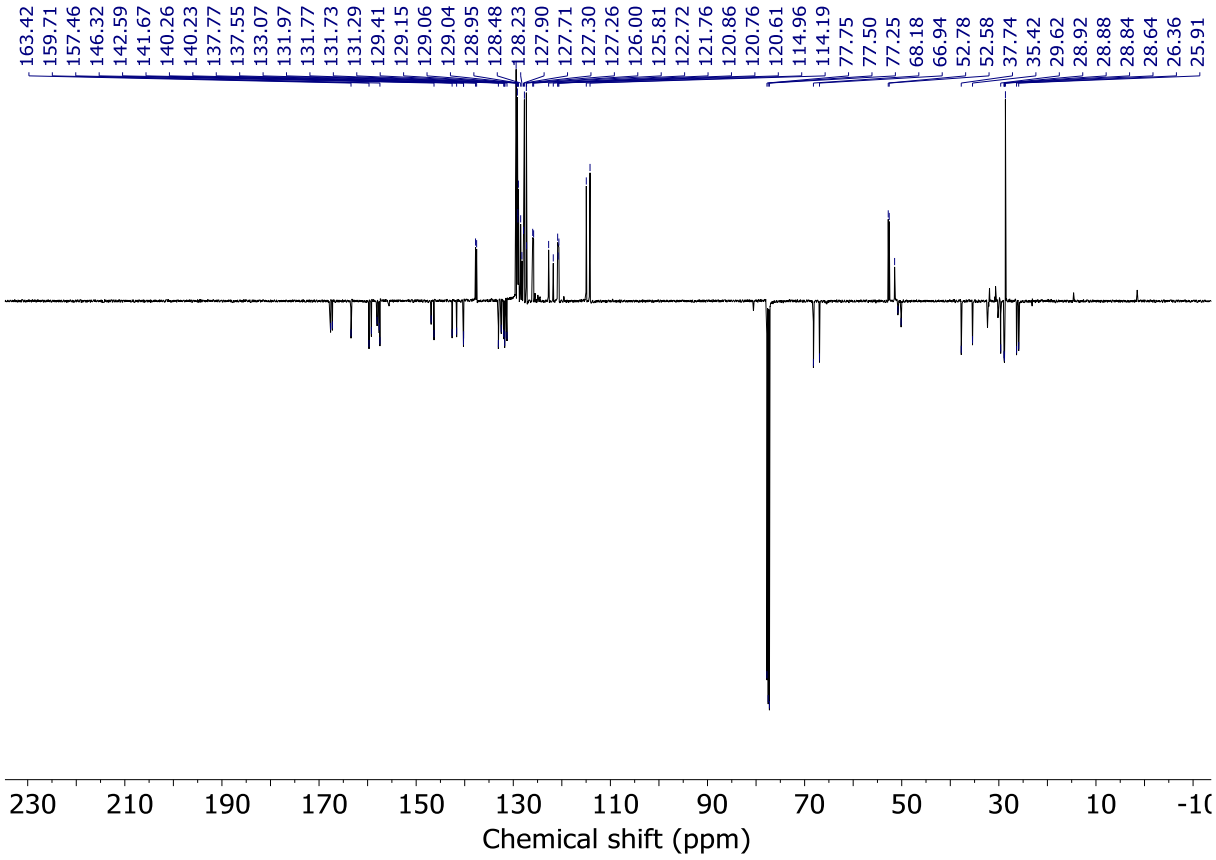

Figure 4.107 - JMOD NMR ($CDCl_3$, 126 MHz) of (Z_m,$S_{co\text{-}c}$)-**10** (97 : 3 *dr*).

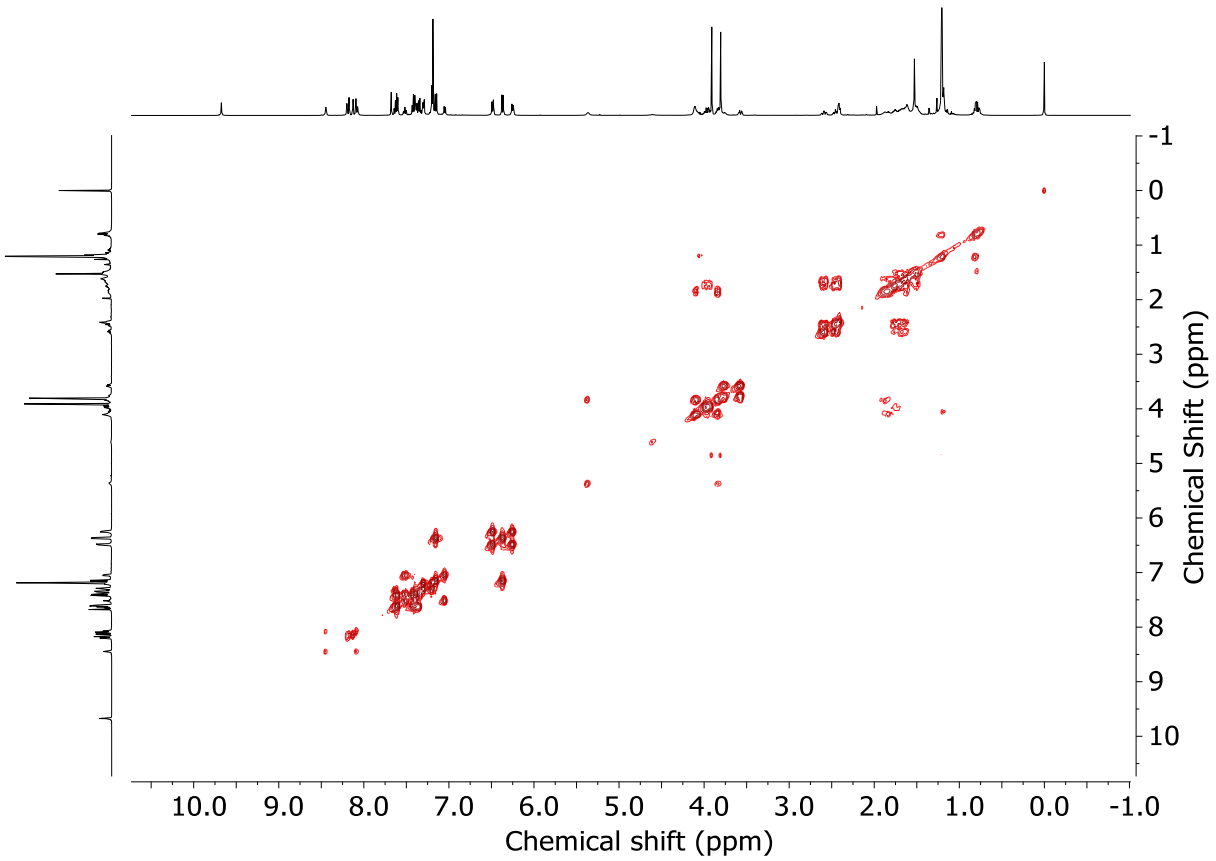

Figure 4.108 - COSY NMR ($CDCl_3$) of (Z_m,$S_{co\text{-}c}$)-**10** (97 : 3 *dr*).

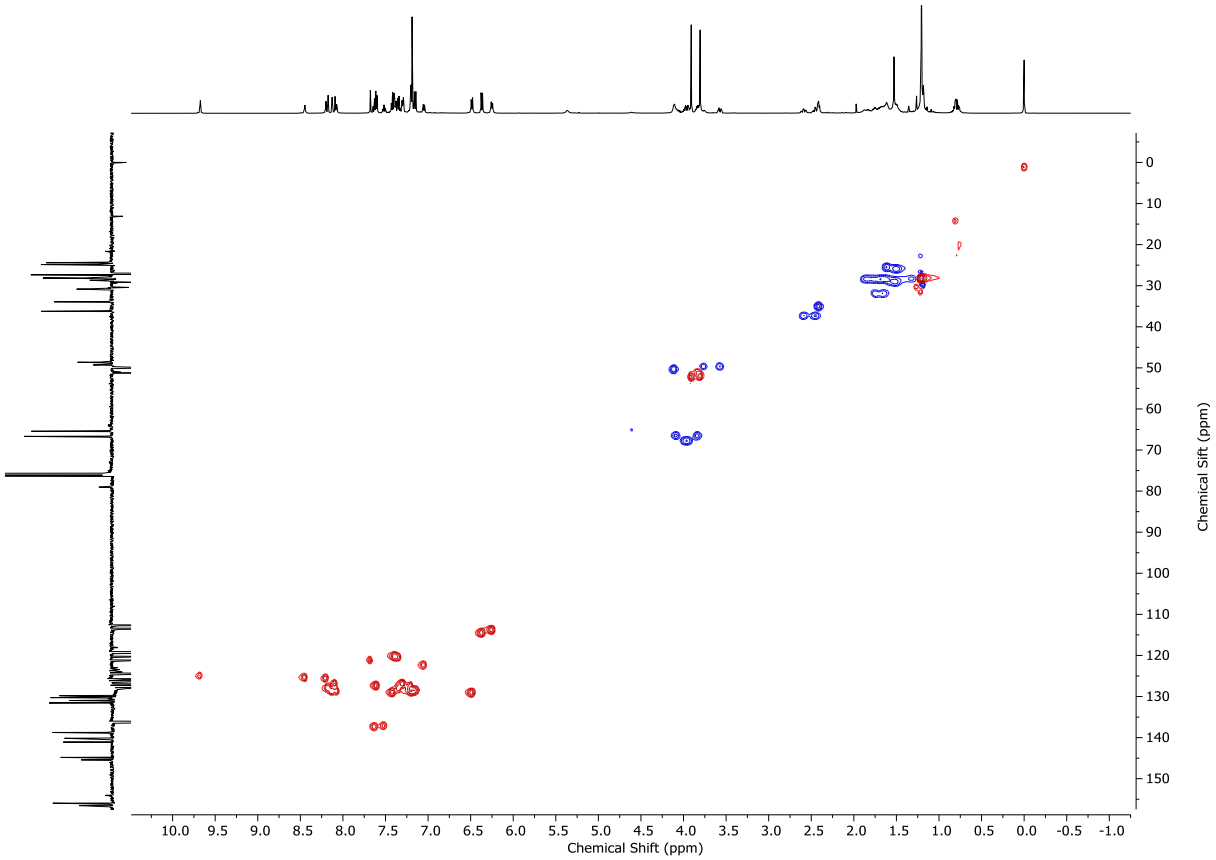

Figure 4.109 - HSQC NMR ($CDCl_3$) of (Z_m,$S_{co\text{-}c}$)-**10** (97 : 3 *dr*).

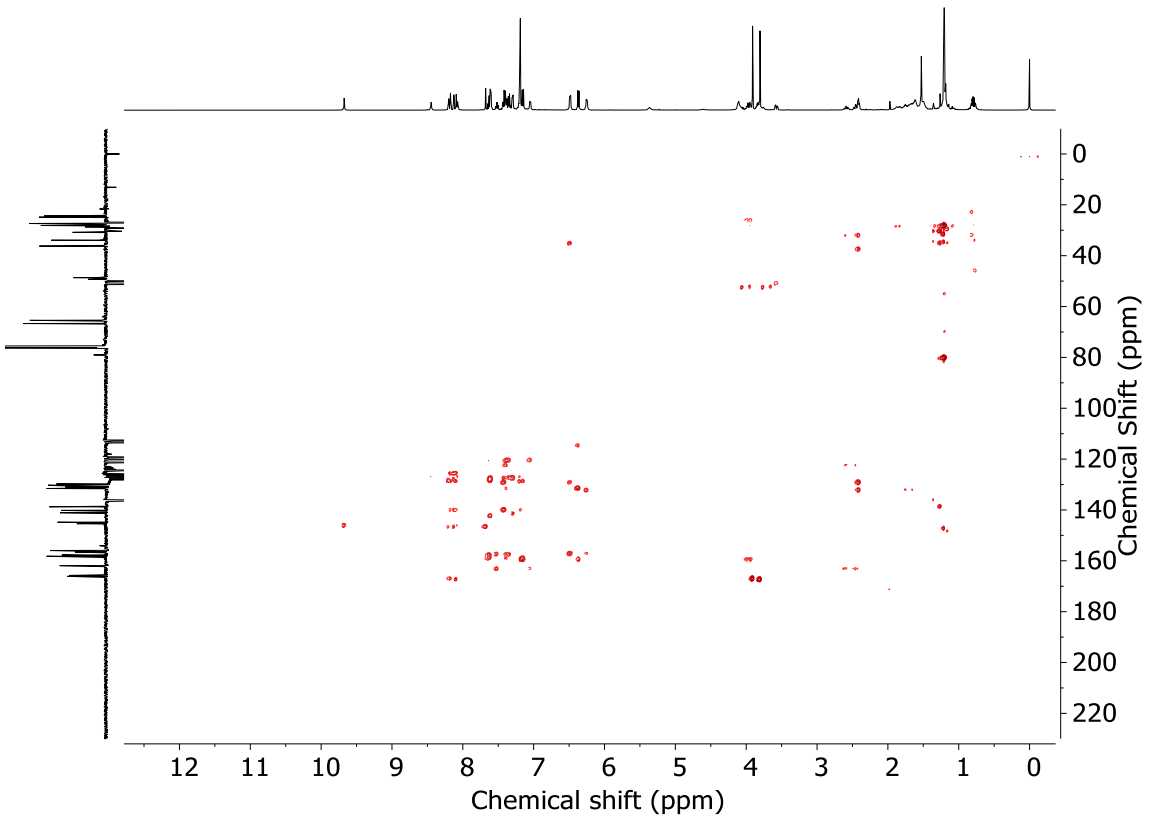

Figure 4.110 - HMBC NMR ($CDCl_3$) of (Z_m,$S_{co\text{-}c}$)-**10** (97 : 3 *dr*).

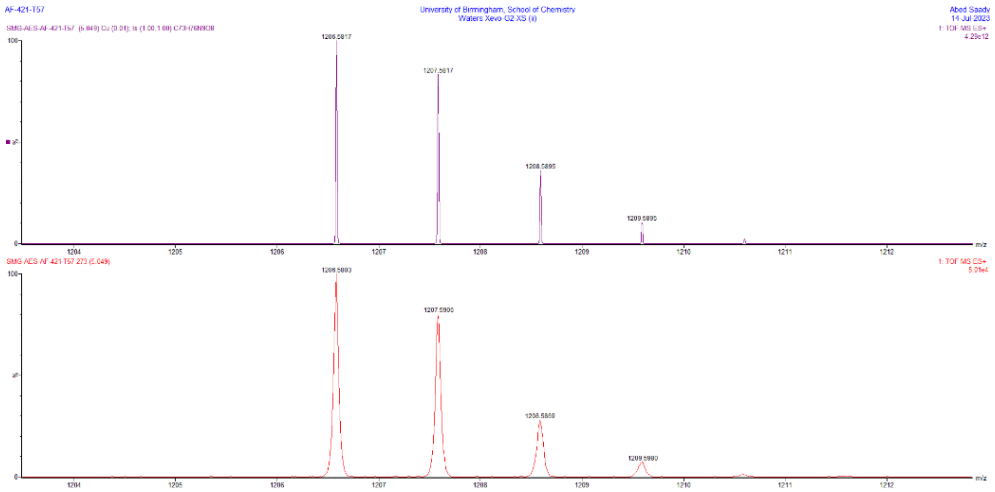

Figure 4.111 - Calculated (top) and observed (bottom) isotopic patterns for (Z_m,$S_{co\text{-}c}$)-**10**.

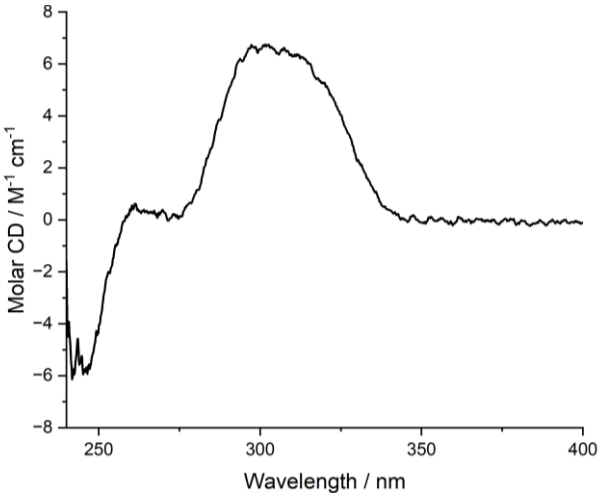

Figure 4.112 - Circular dichroism spectra of (Z_m,$S_{co\text{-}c}$)-**10**. (63.5 μM) at 293 K in $CHCl_3$

Rotaxane (Z_m)-11

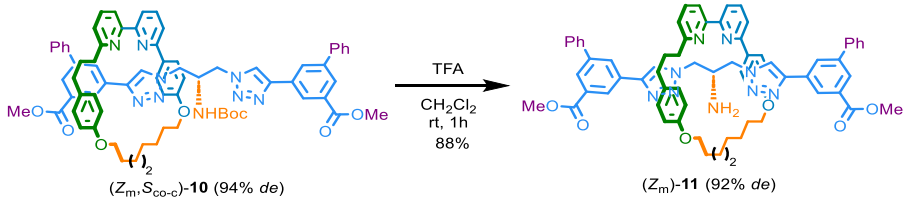

(Z_m,$S_{co\text{-}c}$)-**10** (94% *de*) (Z_m)-**11** (92% *de*)

A vessel was charged with rotaxane (Z_m,$S_{co\text{-}c}$)-**10** (15.0 mg, 0.012 mmol), TFA (21.4 μL, 0.18 mmol), and CH_2Cl_2 (1 mL). The reaction mixture was stirred at rt for 1 h. CH_2Cl_2 (10 mL) was added, washed with sat. $NaHCO_3$ solution (10 mL), brine (10 mL), and the combined organic extracts were dried ($MgSO_4$) and concentrated *in vacuo*. Chromatography (*n*-hexane-EtOAc 0→40%) gave rotaxane (Z_m)-**11** as a white foam (12.1 mg, 88%, 92% *de*).

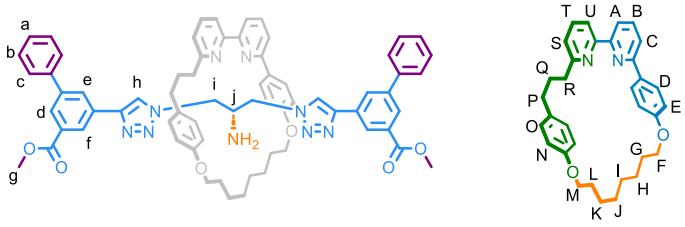

^{1}H NMR (500 MHz, $CDCl_3$) δ: 8.74 (s, 2H, H_h), 8.38 (t, J = 1.7, 2H, H_f), 8.19 (t, J = 1.7, 2H, H_d), 8.13 (t, J = 1.7, 2H, H_e), 7.60 (app t, J = 7.8, 1H, H_B),7.57-7.50 (m, 5H, H_b or H_c, H_T), 7.43-7.33 (m, 9H, H_a, H_b or H_c, H_A, H_C, H_U), 7.07 (d, J = 7.8, 1H, H_S), 7.21 (d, J = 8.6, 2H, H_E), 6.65 (d, J = 8.4, 2H, H_N), 6.56 (d, J = 8.6, 2H, H_D), 6.50 (d, J = 8.4, 2H, H_O), 4.10 (t, J = 6.1, 2H, H_F), 4.05 (t, J = 6.0, 2H, H_M), 3.93 (s, 6H, H_g), 3.77 (dd, J = 14.4, 4.2, 2H, H_i), 3.66-3.59 (m, 3H, $H_{i'}$, NH), 2.99 (app. sept. J = 3.5, 1H, H_j), 2.49 (t, J = 5.3, 2H, H_R), 2.46-2.40 (m, 2H, H_P) 1.87 (t, J = 5.4, 2H, H_L), 1.83-1.43 (m, 12H, H_G, H_H, H_I, H_J, H_K, H_Q, superimposed with H_2O)

^{13}C NMR (125 MHz, $CDCl_3$) δ: 166.9, 162.8, 159.1, 159.1, 157.7, 157.1, 157.0, 146.1, 141.8, 139.8, 137.4, 137.1, 132.4, 132.1, 131.8, 131.1, 129.4, 128.8, 128.7, 128.4, 127.8, 127.3, 127.1, 125.3, 122.8, 122.5, 120.5, 120.5, 120.3, 114.9, 114.0, 67.5, 66.4, 53.8, 52.2, 50.2, 37.1, 35.0, 32.5, 29.5, 28.7, 28.6, 28.5, 25.9, 25.6.

HR-ESI-MS (+ve) m/z = 1106.5 $[M+H]^+$, for isotopic pattern see Figure 4.118.

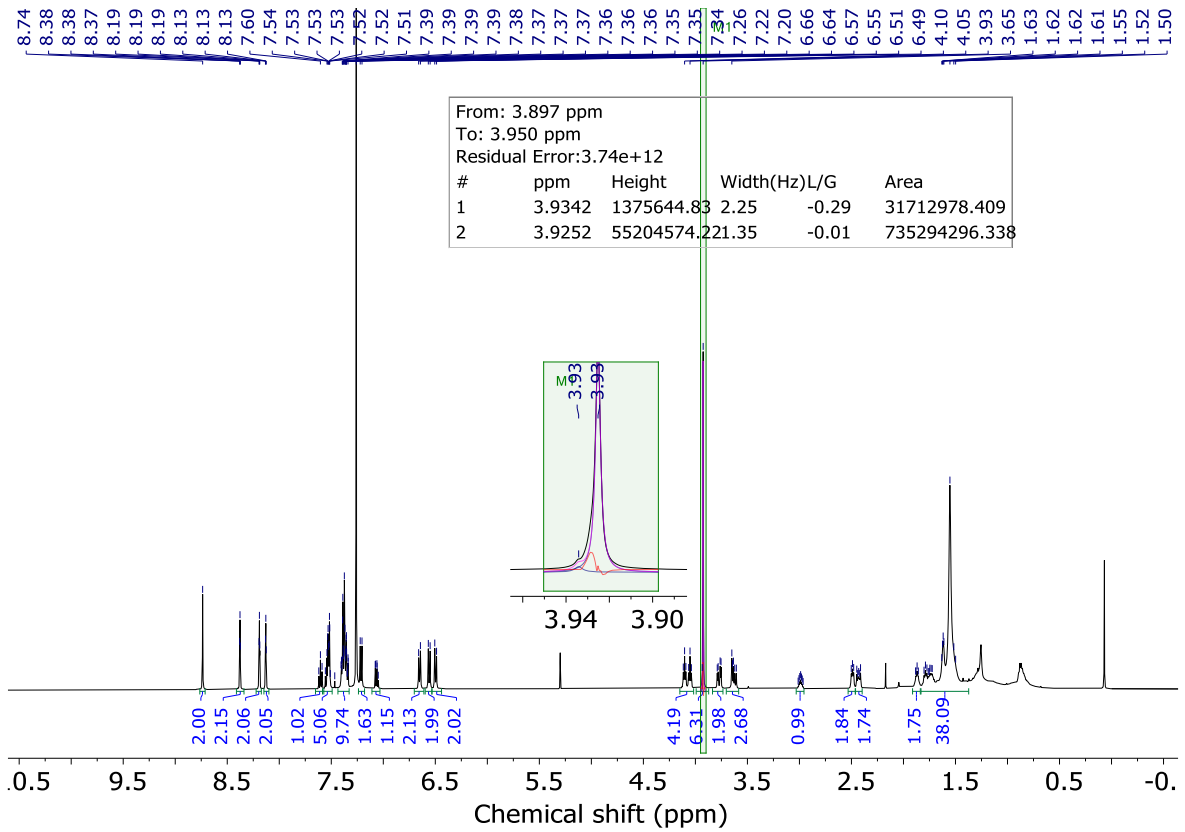

Figure 4.113 - ^{1}H NMR ($CDCl_3$, 500 MHz) of (Z_m)-**11** (96 :4 *dr*).

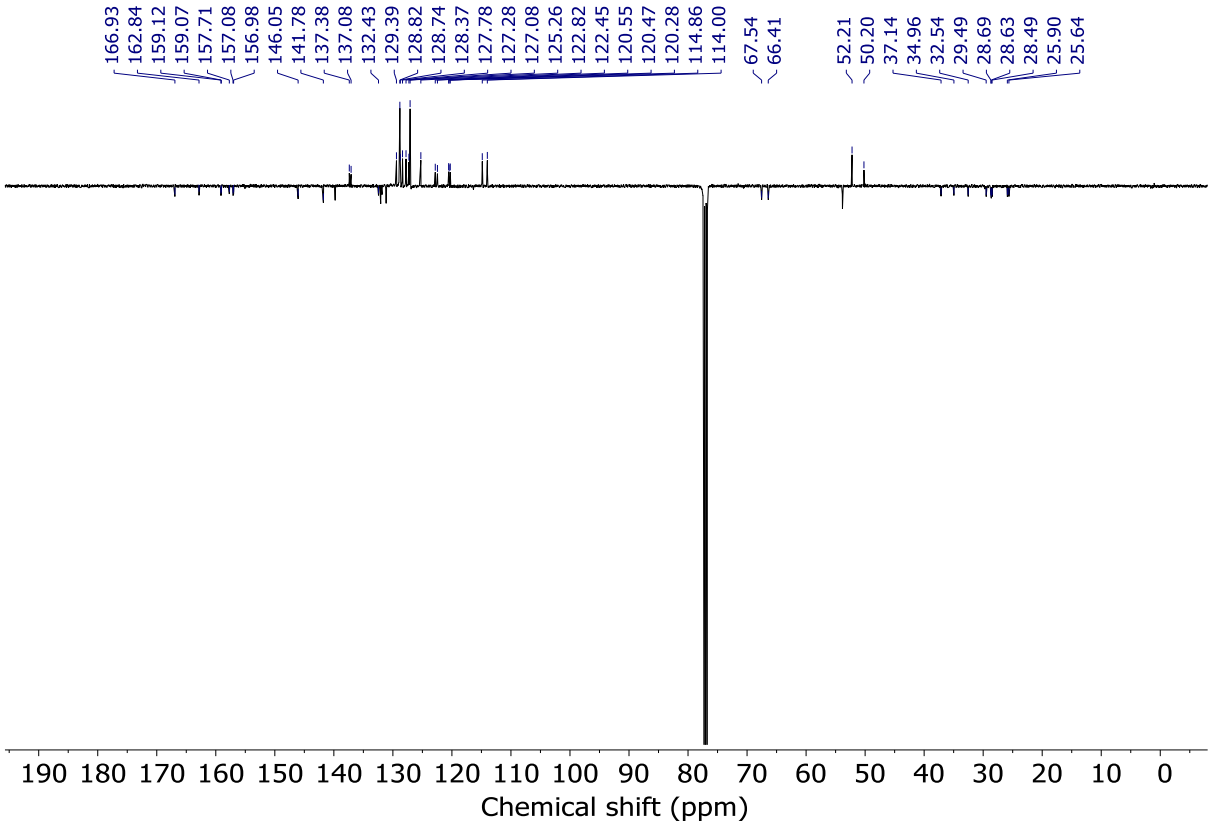

Figure 4.114 - JMOD NMR ($CDCl_3$, 126 MHz) of (Z_m)-**11**.

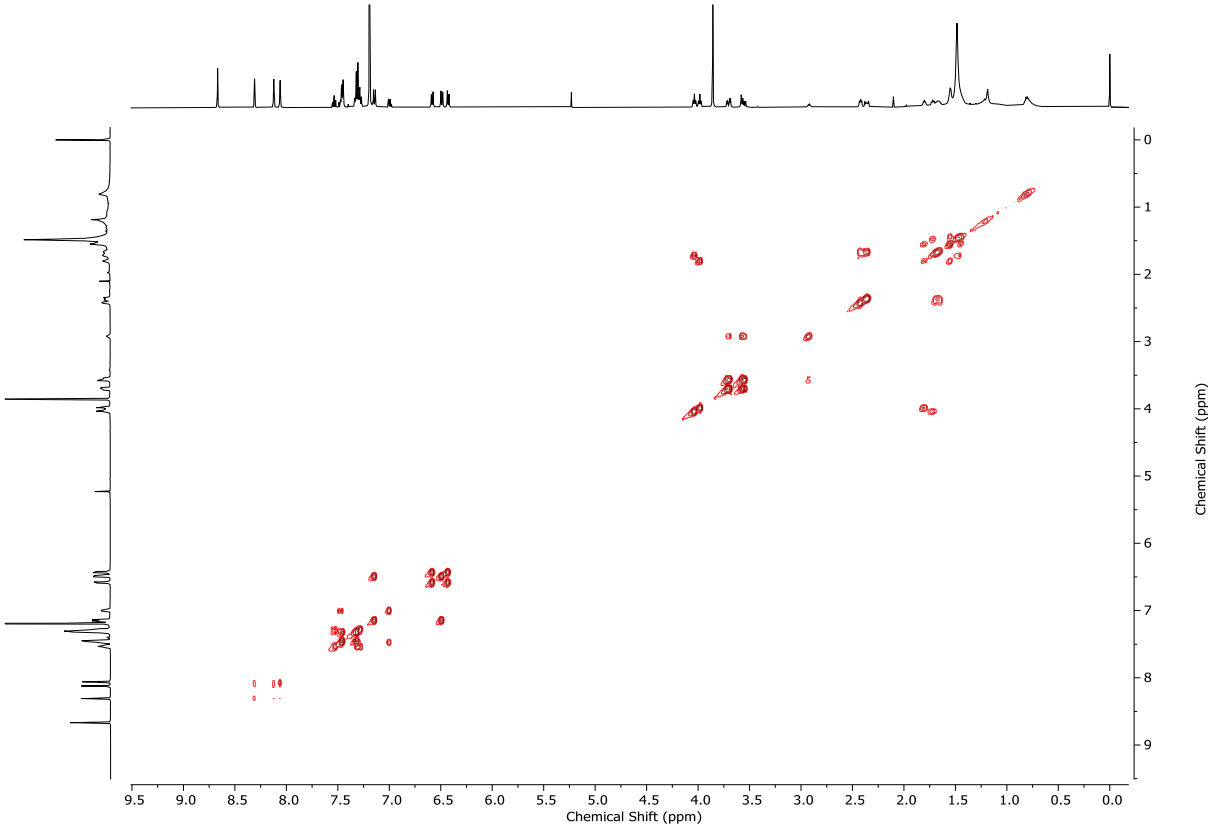

Figure 4.115 - COSY NMR ($CDCl_3$) of (Z_m)-**11**.

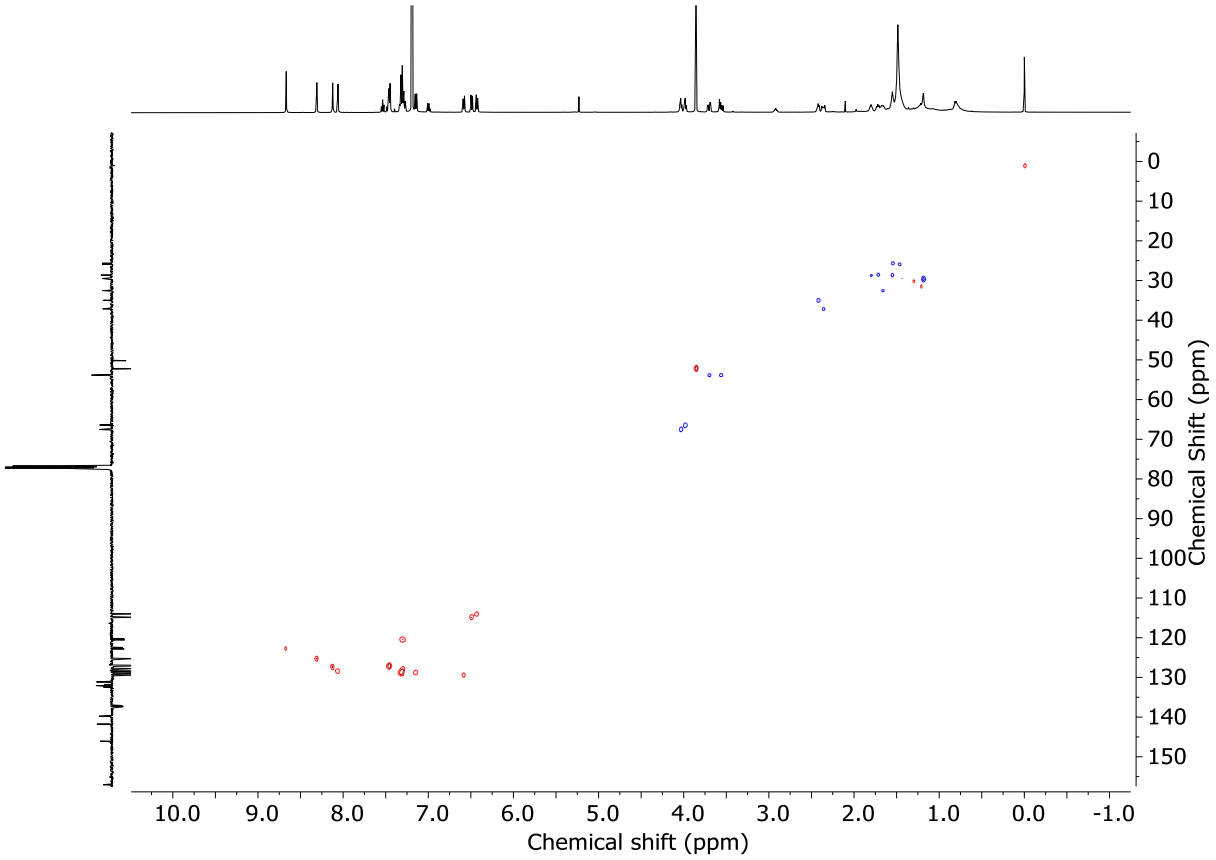

Figure 4.116 - HSQC NMR ($CDCl_3$) of (Z_m)-**11**.

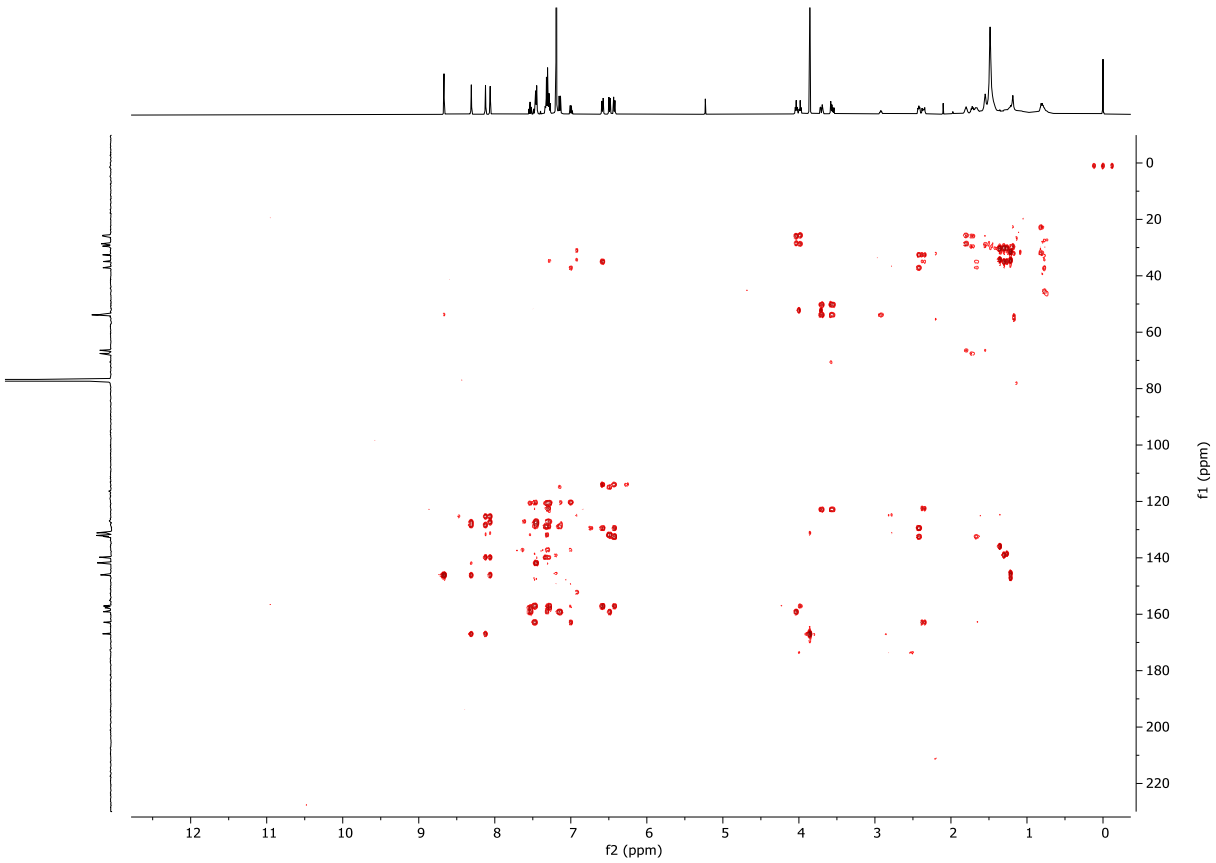

Figure 4.117 - HMBC NMR ($CDCl_3$) of (Z_m)-**11**.

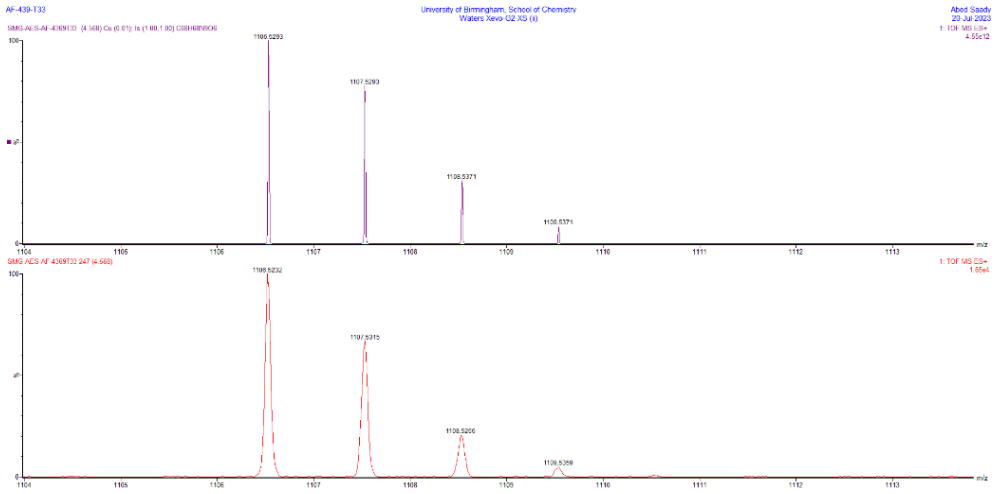

Figure 4.118 - Calculated (top) and observed (bottom) isotopic patterns for (Z_m)-**11**.

4.4.4. Absolute stereochemistry of type 2 mechanical geometric isomers

Methods to assign the absolute stereochemistry of interlocked molecules are still in development. However, we have previously proposed methods for the assignment of absolute stereochemistry in mechanically planar chiral catenanes and rotaxanes, which are based on oriented covalent sub-units[2] and mechanically axially chiral catenanes and rotaxanes, which are based on facially dissymmetric components.[5a] In all cases we make use of Cahn-Ingold-Prelog (CIP)-derived atom priorities to unambiguously assign vectors associated the bilateral dissymmetry of the covalent sub-components. Here we extend these rules to mechanical geometric isomers. In all cases, the stereochemical assignment is achieved by considering the relative orientation of the vectors associated with the individual components. Those vectors can be identified by a step-by-step approach based on the rules outlined below.

A particular challenge with assigning the absolute stereochemistry of the non-canonical type II mechanical geometric isomers of rotaxanes is that the outcome depends on the relative orientation of the axle within the cavity of the oriented macrocycle (c.f., deciding which orientation to observe a covalent stereocentre to assign the stereolabel). To ensure that the notional interconversion of type **I**, type **II** and catenane mechanical geometric isomers occurs with retention of stereolabel, we propose that the axle be oriented with the in-plane substituents of the prochiral centre pointing towards the observer. We note that this contradicts our previous proposal for the assignment of the related mechanical axial stereogenic unit of rotaxanes and for this reason we have decided to revise our guidelines on the latter.[5b] Based on this, the following rules can be used for the absolute stereochemistry of type **II** mechanically geometric isomers of rotaxanes:

4.4.4.1. Step by step approach

Step 1 Following to the Cahn-Ingold-Prelog (CIP) rules, identify the highest priority atom on one ring and label it as "**A**"

Step 2: Moving outward from A in spheres, as per the CIP method for assigning covalent stereogenic centres, determine the highest priority atom (CIP) that can be used to define an orientation of the ring (typically a ligand of **A**) and label it as "**B**". If A does not lie within the ring structure, the same method is used but atom **B** is the atom in the earliest sphere that allows direction to be defined. The orientation of the ring is defined by the vector A → B, which, where relevant, passes through the intervening atoms (*i.e.*, follows the bonds).

Step 3/4: Repeat steps (1) and (2) on the second subcomponent to identity its orientation.

Step 5: Reduce the assembly to the corresponding vectors and observe their relative orientation at the crossing point within the rings (catenanes) or from the macrocycle to the axle (rotaxanes).

Step 6: If the vectors are syn to one another, the stereogenic unit is defined as Z_m whereas anti gives rise to E_m.

If the vectors **A→B** and **C→D** are syn (point toward the same direction), the molecule will be labelled as Z_m whereas anti (point in opposite directions) gives rise to E_m.

4.4.4.2. Worked example – MGI-2 rotaxane 11

Step 1: The highest priority in the macrocycle is the phenolic ether O highlighted, labelled **A**.

Step 2: The highest priority ligand of **A** is the quaternary C of the aromatic ring. This is labelled **B.**

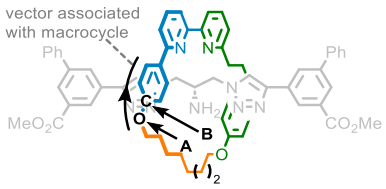

Step 3: The highest priority prochiral centre in the axle is the carbon bearing the amine unit. This is redrawn such that the in-axle substituents are oriented towards the observer.

Step 4: The highest priority exocyclic atom is the amine N. This is labelled "**A**". The proton is labelled "**B**".

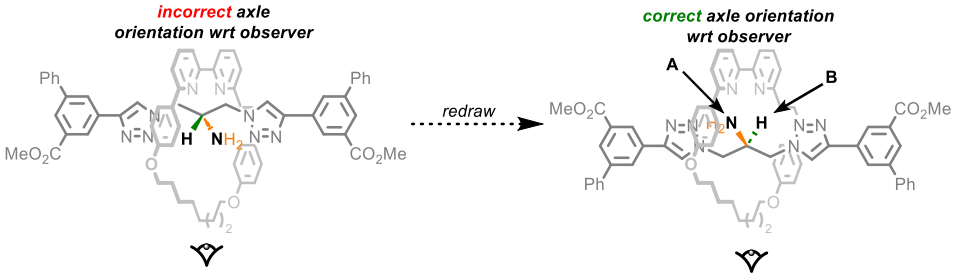

Step 5: Reduce the assembly to the respective vectors.

Step 6: View the relative orientations of the vectors. As they point in opposite directions, the stereoisomer shown is (E_m)-**65.**

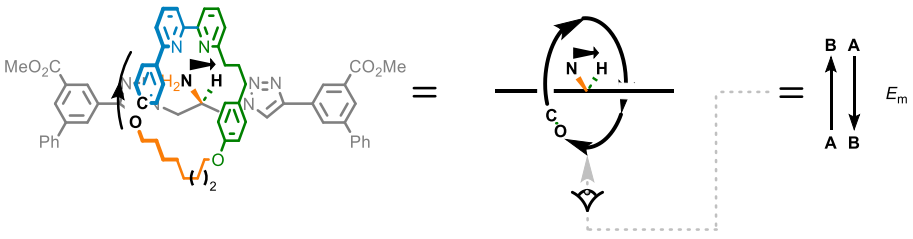

4.4.5. Rotaxanes 4, 5, 10 and 11 – three possible sets of stereodescriptors

The separable diastereomers of rotaxanes **4** and **10**, and the co-conformational diastereomers of rotaxanes **5** and **11**, can be fully described with three different sets of stereolabels. This can be readily demonstrated by considering simple structural changes to rotaxane **4** (Figure 116); i. if the prochiral stereocentre is magically flattened (**4`**) the only remaining stereochemistry is co-conformational mechanically planar chiral; ii. if the macrocycle is allowed to occupy the mirror plane associated with the prochiral unit (**4``**) the only stereochemistry arises from a type II mechanical geometric stereogenic unit; iii. if the macrocycle is symmetrized (**4```**) only a co-conformational covalent stereogenic unit remains.

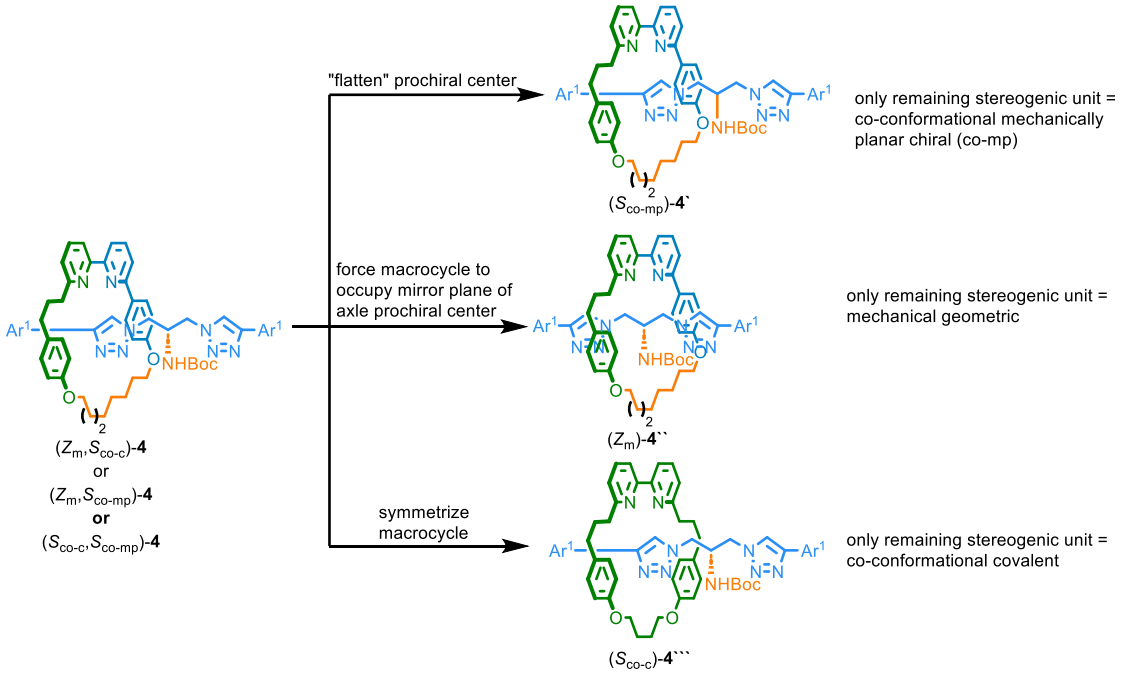

Figure 4.119 - Notional changes to the structure of rotaxane **4** that highlight the different stereogenic units present

Thus, it could be said that rotaxane **4** is simultaneously co-conformationally mechanically planar chiral, displays mechanical geometric type II isomerism and contains a co-conformational covalent stereogenic centre. However, if two of these stereogenic units are defined the third is automatically specified and thus the third label is redundant.

In such situations the choice of the two stereolabels to use is somewhat arbitrary but we prefer the geometric + co-conformational covalent description because i. it highlights the form of stereochemistry that does not depend on the co-conformation of the components (the E_m stereodecriptor is co-conformationally invariant, whereas the $S_{co\text{-}mp}$ and $S_{co\text{-}c}$ descriptors are not – the notional shuttling of the macrocycle from one of the axle to the other inverts these labels); ii. the $S_{co\text{-}c}$ stereolabel is more intuitively obvious than the $S_{co\text{-}mp}$ stereolabel and highlights the desymmetrization of the axle.

4.5. Bibliography

1 H. L. Frisch, E. Wasserman, *J. Am. Chem. Soc.* **1961**, *83*, 3789–3795.

2 (a) E. M. G. Jamieson, F. Modicom, S. M. Goldup, *Chem. Soc. Rev.* **2018**, *47*, 5266–5311. (b) N. Pairault, J. Niemeyer, *Synlett* **2018**, *29*, 689-698. (c) N. H. Evans, *Chem. Eur. J.* **2018**, *24*, 3101–3112.

3 G. Schill, *Catenanes, Rotaxanes and Knots*, Academic Press, New York, **1971**.

4 C. Gaeta, C. Talotta, S. Mirra, L. Margarucci, A. Casapullo, P. Neri, *Org. Lett.* **2013**, *15*, 116–119.

5 (a) J. R. J. Maynard, P. Gallagher, D. Lozano, P. Butler, S. M. Goldup, *Nat. Chem.* **2022**, *14*, 1038–1044. (b) P. R. Gallagher, A. Savoini, A. Saady, J. R. J. Maynard, P. V. W. Butler, G. J. Tizzard, S. M. Goldup, *J. Am. Chem. Soc.* **2024**, *146*, 9134–9141.

6 N. Pairault, F. Rizzi, D. Lozano, E. M. G. Jamieson, G. J. Tizzard, S. M. Goldup, *Nat. Chem.* **2023**, *15*, 781–786.

7 We have previously defined “conditional mechanical stereochemistry” as that which depends on the symmetry properties of the interlocked components but not their relative co-conformation. Thus, conditional mechanical stereochemistry is a permanent rather than dynamic property of the structure, akin to covalent stereogenic units such as stereogenic centres.

8 P. J. Canfield, I. M. Blake, Z. L. Cai, I. J. Luck, E. Krausz, R. Kobayashi, J. R. Reimers, M. J. Crossley, *Nat. Chem.* **2018**, *10*, 615–624.

9 S. H. Reisberg, Y. Gao, A. S. Walker, E. J. N. Helfrich, J. Clardy, P. S. Baran, *Science* **2020**, *367*, 458–463.

10 E. Eliel, S. Wilen, L. Mander, Stereochemistry of Organic Compounds; John Wiley and Sons, Inc.: New York, 1994.

11 The z-axis is defined as perpendicular to the ring plane passing through its centre. Where necessary, we define the orientation of a rotation axis or the principal axis of a point group being in the plane of the ring using the subscript “x”. Where this is not specified the rotation axis should be assumed to lie perpendicular to the ring.

12 We have previously asserted[2a] that mechanical chirality arises in catenanes when the only improper symmetry operations of the individual rings lie perpendicular or coplanar with the macrocycle plane, corresponding to C_{nv} or C_{nh} symmetry respectively. However, this cannot account for the observation that S_2 symmetric rings, for which a simple reflection plane is not a symmetry operation, can produce mechanically planar chiral or geometric isomerism in catenanes and rotaxane. The need for both components to lack a C_2 axis parallel to the ring plane/perpendicular to the axle is universal in that it can be applied to all of the mechanical stereogenic ring and axle point groups.

13 We note that these ring symmetries have previously been shown to give rise to co-conformational[14] mechanical stereochemistry. See ref. 2a and A. Rodriguez-Rubio, A. Savoini, F. Modicom, P. Butler, S. M. Goldup, *J. Am. Chem. Soc.* **2022**, *144*, 11927–11932.

14 For selected examples of co-conformational stereochemistry see - (a) M. Alvarez-Perez, S. M. Goldup, D. A. Leigh, A. M. Slawin, *J. Am. Chem. Soc.* **2008**, *130*, 1836–1838. (b) Y. Mochizuki, K. Ikeyatsu, Y. Mutoh, S. Hosoya, S. Saito, *Org. Lett.* **2017**, *19*, 4347–4350. (c) Y. Wang, J. Gong, X. Wang, W. J. Li, X. Q. Wang, X. He, W. Wang, H. B. Yang, *Angew. Chem. Int. Ed.* **2022**, e202210542. (d) S. Corra, C. de Vet, M. Baroncini, A. Credi, S. Silvi, *Chem* **2021**, *7*, 2137–2150. (d) E. Liu, S. Cherraben, L. Boulo, C. Troufflard, B. Hasenknopf, G. Vives, M. Sollogoub, *Chem* **2023**, *9*, 1147–1163.

15 We note that these point groups are more properly referred to as C_s with the orientation of the single remaining reflection plane defined. We use C_{1v} and C_{1h} here to emphasize the direct link with the general C_{nv} and C_{nh} point groups symmetries that give rise to MPC and MAC stereogenic units respectively.

16 T. Damhus, C. E. Schaeffer, *Inorg. Chem.* **2002**, *22*, 2406–2412.

17 It should be noted that the unusual symmetry of such rings means that they also express dynamic co-conformational covalent stereochemistry. See Experimental and Supplementary Information section 4.4.1 for more details.

18 The subscript highlights the mechanical origin of the geometric isomerism.

19 R. J. Bordoli, S. M. Goldup, *J. Am. Chem. Soc.* **2014**, *136*, 4817–4820.

20 For seminal examples see - (a) Y. Kaida, Y. Okamoto, J. C. Chambron, D. K. Mitchell, J. P. Sauvage, *Tetrahedron Lett.* **1993**, *34*, 1019–1022. (b) C. Yamamoto, Y. Okamoto, T.

Schmidt, R. Jager, F. Vogtle, *J. Am. Chem. Soc.* **1997**, *119*, 10547–10548. (c) Y. Makita, N. Kihara, N. Nakakoji, T. Takata, S. Inagaki, C. Yamamoto, Y. Okamoto, *Chem. Lett.* **2007**, *36*, 162–163.

21 J. R. J. Maynard, S. M. Goldup, *Chem* **2020**, *6*, 1914–1932.

22 (a) M. A. Jinks, A. de Juan, M. Denis, C. J. Fletcher, M. Galli, E. M. G. Jamieson, F. Modicom, Z. Zhang, S. M. Goldup, *Angew. Chem. Int. Ed.* **2018**, *57*, 14806–14810. (b) C. Tian, S. D. P. Fielden, B. Perez-Saavedra, I. J. Vitorica-Yrezabal, D. A. Leigh, *J. Am. Chem. Soc.* **2020**, *142*, 9803–9808. (c) A. Imayoshi, B. V. Lakshmi, Y. Ueda, T. Yoshimura, A. Matayoshi, T. Furuta, T. Kawabata, *Nat. Commun.* **2021**, *12*, 404. (d) M. F. Li, X. L. Chia, C. Tian, Y. Zhu, *Chem* **2022**, *8*, 2843–2855. (e) A. de Juan, D. Lozano, A. W. Heard, M. A. Jinks, J. M. Suarez, G. J. Tizzard, S. M. Goldup, *Nat. Chem.* **2022**, *14*, 179–187.

23 (a) M. Denis, J. E. M. Lewis, F. Modicom, S. M. Goldup, *Chem* **2019**, *5*, 1512–1520. (b) S. Zhang, A. Rodríguez-Rubio, A. Saady, G. J. Tizzard, S. M. Goldup, *Chem* **2023**, *9*, 1195–1207.

24 A. Arduini, F. Ciesa, M. Fragassi, A. Pochini, A. Secchi, *Angew. Chem. Int. Ed.* **2005**, *44*, 278–281.

25 Selected examples - (a) A. Arduini, R. Bussolati, A. Credi, G. Faimani, S. Garaudee, A. Pochini, A. Secchi, M. Semeraro, S. Silvi, M. Venturi, *Chem. Eur. J.* **2009**, *15*, 3230–3242. (b) M. Xue, Y. S. Su, C. F. Chen, *Chem. Eur. J.* **2010**, *16*, 8537–8544. (c) T. Pierro, C. Gaeta, C. Talotta, A. Casapullo, P. Neri, *Org. Lett.* **2011**, *13*, 2650–2653. (d) A. Arduini, R. Bussolati, A. Credi, A. Secchi, S. Silvi, M. Semeraro, M. Venturi, *J. Am. Chem. Soc.* **2013**, *135*, 9924–9930. (e) R. Ciao, C. Talotta, C. Gaeta, L. Margarucci, A. Casapullo, P. Neri, *Org. Lett.* **2013**, *15*, 5694–5697. (f) Y.-X. Xia, T. Xie, Y. Han, C.-F. Chen, *Org. Chem. Front.* **2014**, *1*. (g) H. X. Wang, Z. Meng, J. F. Xiang, Y. X. Xia, Y. Sun, S. Z. Hu, H. Chen, J. Yao, C. F. Chen, *Chem. Sci.* **2016**, *7*, 469–474. (h) V. Zanichelli, G. Ragazzon, A. Arduini, A. Credi, P. Franchi, G. Orlandini, M. Venturi, M. Lucarini, A. Secchi, S. Silvi, *Eur. J. Org. Chem.* **2016**, *2016*, 1033–1042. (g) P. La Manna, C. Talotta, C. Gaeta, A. Soriente, M. De Rosa, P. Neri, *J. Org. Chem.* **2017**, *82*, 8973–8983. (h) J. S. Cui, Q. K. Ba, H. Ke, A. Valkonen, K. Rissanen, W. Jiang, *Angew. Chem. Int. Ed.* **2018**, *57*, 7809–7814. (i) K. A. Li, Z. Wang, C. D. Xie, T. Chen, H. Qiang, Y. A. Liu, X. S. Jia, W. B. Hu, K. Wen, *Org. Biomol. Chem.* **2019**, *17*, 4975–4978. (j) M. Bazzoni, L. Andreoni, S. Silvi, A. Credi, G. Cera, A. Secchi, A. Arduini, *Chem. Sci.* **2021**, *12*, 6419–6428. (k) G. Cera, A. Arduini, A. Secchi, A. Credi, S. Silvi, *Chem. Rec.* **2021**, *21*, 1161–1181. (l) L. Andreoni, F. C.

Bonati, J. Groppi, D. Balestri, G. Cera, A. Credi, A. Secchi, S. Silvi, *Chem. Commun.* **2023**, *59*, 4970–4973.

26 IUPAC have noted that several definitions of prochirality are in use (IUPAC Gold Book: https://goldbook.iupac.org/terms/view/P04859, accessed 15/12/2023). Here, and throughout, we use the term prochiral to mean an achiral structure that becomes chiral if an existing atom/group is replaced by different one.

27 For a previous report in which a prochiral macrocycle was used but no selectivity reported see: F. Saito, J. W. Bode, *Chem. Sci.* **2017**, *8*, 2878–2884.

28 V. Zanichelli, L. Dallacasagrande, A. Arduini, A. Secchi, G. Ragazzon, S. Silvi, A. Credi, *Molecules* **2018**, *23*, 1156.

29 M. Denis, S. M. Goldup, *Nat. Rev. Chem.* **2017**, *1*, 0061.

30 (a) V. Aucagne, K. D. Hanni, D. A. Leigh, P. J. Lusby, D. B. Walker, *J. Am. Chem. Soc.* **2006**, *128*, 2186–2187. (b) H. Lahlali, K. Jobe, M. Watkinson, S. M. Goldup, *Angew. Chem. Int. Ed.* **2011**, *50*, 4151–4155.

31 A. Saady, S. M. Goldup, *Chem* **2023**, *9*, 2110–2127.

32 The exception to this general statement is if the axle is divided at the prochiral centre itself, such that in the forward reaction this centre is converted from sp^2 to sp^3 hybridization. In this case the half-axle that contains the sp^2 hybridized centre can also be described as prochiral but, confusingly, this is an alternative definition of the same word.[26]

33 J. E. M. Lewis, R. J. Bordoli, M. Denis, C. J. Fletcher, M. Galli, E. A. Neal, E. M. Rochette, S. M. Goldup, *Chem. Sci.* **2016**, *7*, 3154–3161.

34 All reported diastereoselectivities were determined by integration of signals identified as corresponding to the two diastereomers in the ^{1}35 The variation in *de* at different stages of the synthesis of rotaxanes **11** corresponds to a 1% variation in the ratio of these integrals and is thus within the error of the measurement.[34]

36 This is a common feature of interlocked molecules produced using the AT-CuAAC reaction of small bipyridine macrocycles: H. Lahlali, K. Jobe, M. Watkinson, S. M. Goldup, *Angew. Chem. Int. Ed.* **2011**, *50*, 4151–4155.

37 K. Hirose, M. Ukimi, S. Ueda, C. Onoda, R. Kano, K. Tsuda, Y. Hinohara, Y. Tobe, *Symmetry* **2018**, *10*, 20.

38 A. W. Heard, S. M. Goldup, *Chem* **2020**, *6*, 994–1006.

39 (a) M. Gaedke, F. Witte, J. Anhauser, H. Hupatz, H. V. Schroder, A. Valkonen, K. Rissanen, A. Lutzen, B. Paulus, C. A. Schalley, *Chem. Sci.* **2019**, *10*, 10003–10009. (b) Y. Wang, J. Gong, X. Wang, W. J. Li, X. Q. Wang, X. He, W. Wang, H. B. Yang, *Angew. Chem. Int. Ed.* **2022**, e202210542.

40 Selected examples - (a) J. F. Nierengarten, C. O. Dietrich-Buchecker, J. P. Sauvage, *J. Am. Chem. Soc.* **1994**, *116*, 375–376. (b) C. D. Pentecost, K. S. Chichak, A. J. Peters, G. W. Cave, S. J. Cantrill, J. F. Stoddart, *Angew. Chem. Int. Ed.* **2007**, *46*, 218–222. (c) C. Schouwey, J. J. Holstein, R. Scopelliti, K. O. Zhurov, K. O. Nagornov, Y. O. Tsybin, O. S. Smart, G. Bricogne, K. Severin, *Angew. Chem. Int. Ed.* **2014**, *53*, 11261–11265. (d) J. E. Beves, J. J. Danon, D. A. Leigh, J. F. Lemonnier, I. J. Vitorica-Yrezabal, *Angew. Chem. Int. Ed. Engl.* **2015**, *54*, 7555–7559. (e) Z. Cui, Y. Lu, X. Gao, H. J. Feng, G. X. Jin, *J. Am. Chem. Soc.* **2020**, *142*, 13667–13671. (f) D. P. August, J. Jaramillo-Garcia, D. A. Leigh, A. Valero, I. J. Vitorica-Yrezabal, *J. Am. Chem. Soc.* **2021**, *143*, 1154–1161. (g) H.-N. Feng, Z. Sun, S. Chen, Z.-H. Zhang, Z. Li, Z. Zhong, T. Sun, Y. Ma, L. Zhang, *Chem* **2023**, *9*, 859–868.

41 Selected examples - (a) C. Lincheneau, B. Jean-Denis, T. Gunnlaugsson, *Chem. Commun.* **2014**, *50*, 2857–2860. (b) R. Zhu, J. Lubben, B. Dittrich, G. H. Clever, *Angew. Chem. Int. Ed.* **2015**, *54*, 2796–2800. (c) C. S. Wood, T. K. Ronson, A. M. Belenguer, J. J. Holstein, J. R. Nitschke, *Nat. Chem.* **2015**, *7*, 354–358. (d) T. Sawada, M. Yamagami, K. Ohara, K. Yamaguchi, M. Fujita, *Angew. Chem. Int. Ed.* **2016**, *55*, 4519–4522. (e) T. Feng, X. Li, Y. Y. An, S. Bai, L. Y. Sun, Y. Li, Y. Y. Wang, Y. F. Han, *Angew. Chem. Int. Ed.* **2020**, *59*, 13516–13520. (f) Z. Cui, X. Gao, Y. J. Lin, G. X. Jin, *J. Am. Chem. Soc.* **2022**, *144*, 2379–2386.

42 A. Pigorsch, M. Kockerling, *Cryst.Growth Des*. **2016**, *16*, 4240–4246.

43 S. Ogi, T. Ikeda, R. Wakabayashi, S. Shinkai, M. Takeuchi, *Chemistry* **2010**, *16*, 8285–8290.

44 Y. Akae, H. Sogawa, T. Takata, European J. Org. Chem. 2019, 2019, 3605–3613.

Chapter 5: Thesis Conclusions and Outlook

This thesis marks a significant milestone in the understanding and synthesis of mechanically stereogenic molecules. **Chapter 1** introduces the concept and consequences of the mechanical bond, and the development of both language and strategies in the synthesis of mechanically interlocked molecules. Forms of stereochemistry arising from the mechanical bond are then discussed in detail, including description of work undertaken during my studies that have contributed to the knowledge of mechanical stereochemistry. These contributions are later presented in subsequent chapters. In summary, **Chapter 2** presents the analysis of the mechanically axially chiral stereogenic unit, which led us to an efficient approach towards enantiopure MAC catenanes, and to recognise and synthesise a noncanonical class of mechanically chiral rotaxanes that had previously been overlooked. **Chapter 3** presents an investigation into how facial selectivity arises in mechanical bond formation, and therefore how MAC and MGI molecules – which rely on a prochiral macrocycle – can be synthesised stereoselectively. Our findings then enabled us to demonstrate the first direct enantioselective synthesis of a MAC rotaxane. Finally, **Chapter 4** presents the identification of 'the final stereogenic unit of [2]rotaxanes' through analysis of the mechanical geometric stereogenic unit, with its subsequent stereoselective synthesis *via* a chiral-interlocking auxiliary strategy.

In **Chapter 2**, we wanted to address the fact that while the MAC stereogenic unit was known, no enantiopure examples, where the mechanical bond provided the sole source of stereochemistry had been disclosed. Towards this aim, we re-examined the mechanical axial stereogenic unit of catenanes, with attention to how the facial dissymmetry that is required in the rings arises structurally. These resulting semi-structural representations revealed that such molecules, which relied on prochiral macrocycles, could display co-conformational covalent stereochemistry by displacement of one macrocycle from its highest symmetry arrangement, thus leading to diastereomeric co-conformations. We hypothesised that if the interconversion of these diastereomeric co-conformations could be inhibited, this phenomenon could be exploited to afford mechanical epimers, that if separable by silica gel chromatography, could be converted to the enantiomeric MAC catenanes without the need for chiral resolution strategies by removal of the steric barrier. Towards this, mechanical bond formation between a facially dissymetric macrocycle containing a sulfoxide moiety and a serine-derived premacrocycle resulted in mechanical epimers in which interconversion was inhibited by methyl ester and *N*-Boc groups. The resulting mechanical epimers were formed in 42% *de* and were fortunately separable *via*

silica gel chromatography. Conversion of diastereomerically pure catenanes to structures - in which the mechanically axially chiral stereogenic unit is the only fixed source of stereochemistry - was achieved by removing the Boc group and proceeded with excellent stereopurity (>99% *ee*). We were also troubled by the fact that while the process of notional ring-opening-and-stoppering on a minimal schematic representation of a mechanical planar chiral catenane afforded the analogous MPC rotaxane, the same operation on a minimal schematic representation of a MAC catenane afforded an achiral object. However, carrying out the same operation on a semi-structural representation, in which both rings contained a single prochiral unit, the analogous chiral rotaxane became clear. This previously overlooked noncanonical class of mechanically chiral rotaxane also yielded to the same co-conformational auxiliary strategy. Mechanical bond formation between a sulfoxide macrocycle and a *N*-Boc protected serine-derived azide afforded mechanical epimers in 50% *de* that following separation by silica gel chromatography were converted to enantiomeric rotaxanes in excellent stereopurity (>99% *ee*). We also investigated another route towards the synthesis of MAC rotaxanes and catenanes *via* oxidation of a sulfide macrocycle following mechanical bond formation. Notably, we were able to achieve inversion of stereoselectivity with respect to the direct route through use of 2-iodoxybenzoic acid to oxidise both sulfide catenanes and rotaxanes in 22% and 20% *de* respectively.

We were equally pleased and intrigued that selectivity was observed in the AT-CuAAC reaction towards MAC catenanes and rotaxanes and was further investigated in **Chapter 3**. This was based on preliminary results from **Chapter 2**, which included a brief solvent screen and SCXRD data showing the presence of an intercomponent interaction. These findings led to the hypothesis that facial selectivity was arising due a hydrogen bonding interaction between amine and sulfoxide moieties of the axle and macrocycle, leading to some degree of pre-organisation prior to mechanical bond formation. To investigate this hypothesis various *N*-acyl serine-derived azides with different degrees of NH polarisation were prepared and employed in the AT-CuAAC reaction with the previously prepared sulfoxide macrocycle. In agreement with the above hypothesis, substrates with more polarised NH bonds resulted in increased facial selectivity with a high degree of diastereoselectivity (70% *de*) being obtained with a trifluoroacetamide functionalised azide at room temperature. Furthermore, removal of hydrogen bonding interactions by *N*-methylation led to almost no selectivity being observed. Facial selectivity was also found to be greater in aprotic solvents, and temperature was also identified as a factor influencing selectivity. Under optimised conditions, selectivities of up to 82% *de* were able to be achieved by reaction of trifluoroacetamide azide in dichloromethane at –40 °C. A similar trend was observed in the synthesis of *N*-Boc protected rotaxane diastereomers, with selectivities of up to 80% *de* when the

AT-CuAAC reaction as carried out at –78 °C. Conveniently, this allowed us to directly prepare enantioenriched MAC rotaxanes in a one-pot, two-step reaction without the separation of diastereomeric rotaxanes. This was achieved by the *in situ* TFA-mediated demetallation and removal of the *N*-Boc group in good selectivity (78% *ee*) and agreement with the optimised diastereoselective synthesis. More excitingly, the use of an NH polarised, *N*-formylated azide allowed the direct enantioselective synthesis of MAC rotaxanes due to the formyl group being too small to inhibit co-conformational exchange. This proceeded in remarkable enantioselectivity of up to 70% *ee* at –40 °C. To the best of our knowledge, this is the highest reported direct enantioselective synthesis of any chiral rotaxane bearing only mechanical stereochemistry. Mechanical geometric isomers based on prochiral macrocycles and their stereoselective synthesis had received very little attention in literature and fortunately, also yielded to this strategy – with a single hydrogen bonding interaction proving sufficient to impart facial selectivity in mechanical bond formation. Similarly, optimisation of substrate NH polarisation as well as reaction temperature and solvent led to the synthesis of type 1 MGI rotaxanes and MGI catenanes in up to 90% and 92% *de* respectively with the use of similar highly electron-poor acetanilide motifs.

In recently discovering the previously overlooked mechanical axial stereogenic unit in rotaxanes, we were intrigued by the question; are there any mechanical stereogenic units of [2]catenanes and [2]rotaxanes still lying undetected? To address this, in **Chapter 4** we undertook a from first principles analysis of rotaxane and catenane stereochemistry by initially examining which building blocks of 2-component catenanes and rotaxanes can give rise to conditional mechanical stereogenic units. This analysis led us to two interesting discoveries. Firstly, that S_{2n} symmetric rings are oriented and their combination – or a combination of S_{2n} and C_{nh} rings – gives rise to a mechanical planar chiral stereogenic unit. Secondly, the identification of a previously overlooked rotaxane geometric stereogenic unit. Fortunately, our analysis also demonstrated that this is not only the final stereogenic unit of [2]rotaxanes, but that all conditional mechanical stereogenic units of 2-component catenanes and rotaxanes are now known. Following our discovery of this 'type 2' rotaxane mechanical geometric stereogenic unit, we considered strategies for its selective synthesis. Despite our efforts, attempts to selectively prepare rotaxane MGI-2 isomers directly were unsurprisingly unsuccessful - likely due to the absence of weak interactions such as a hydrogen bond that we exploited previously. While performing AT-CuAAC reactions at lower temperatures increased the diastereoselectivity of the reaction, the resulting mixtures were inseparable, so another approach had to be contemplated. Considering that the minimal schematic representation of an MGI-2 rotaxane is composed of a facially dissymetric C_{1v} axle and

an oriented macrocycle, the challenge in their selective synthesis is the same that presents itself to the synthesis of MPC rotaxanes – how to thread an oriented ring onto an axle with control over their relative orientation. Fortunately, a strategy to do so – a chiral interlocking auxiliary synthesis – is known and was applicable to the stereoselective synthesis of MGI-2 rotaxanes through modification of our central serine-derived building block. Use of this strategy allowed the synthesis of both isomers in high diastereopurity (>90% *de*).

Examining these pieces of research, they present comprehensive studies of fundamental mechanical stereogenic units, with findings supported by extensive experimental evidence and underpinned by theory. Although the findings in **Chapter 2** brought much deserved attention to a relatively under-investigated form of mechanical stereochemistry, in hindsight our method used to assign the absolute stereochemistry of the mechanically axially stereogenic unit was incorrect. Fortunately, this error was rectified in later work presented in **Chapters 3** and **4** through further evaluation of the connection between catenane and rotaxane stereochemistry. Furthermore, while the findings in **Chapter 3** indicate that hydrogen bonding is a key factor in directing facial selectivity in the mechanical bond formation, little effort was made to delineate the effects of steric factors, with substrates changing both steric and electronic properties. Experiments to address this could include reaction various of *para*-substituted *N*-benzoylated serine derived azides. This would allow the electronic properties of the substrate to be finely tuned with respect to known Hammet parameters, with structural differentiation far from the amine and reactive azide. Alternatively, as they have proven effective in highly selective syntheses of MPC molecules, catalytic desymmetrisation approaches could also be further investigated towards MAC and also MGI molecules. Additionally, it should be noted that while the optimisation of the selective synthesis of MAC catenanes was not investigated in subsequent studies, we expect them to yield to similar strategies.

Collectively, the research presented in this thesis concludes that all the mechanical stereogenic units of simple 2-component catenanes and rotaxanes have now been defined, with efficient methods in hand to allow their stereoselective synthesis. This will hopefully enable the increasing interest in applications of mechanically stereogenic interlocked molecules to accelerate, with such molecules already being reported as the basis of molecular machines, and most notably the mechanical planar chiral stereogenic unit, which use is well-established in enantioselective sensors, catalysts, and chiroptical switches. It is therefore not unreasonable to expect that the remaining mechanical stereogenic units will soon be utilised for such applications. As mechanically stereogenic molecules can possess chiral, flexible but crowded environments imposed by the mechanical bond – reminiscent of an enzyme active site – I believe that their use

in enantioselective catalysis is one of the greatest areas of interest. While not an area of research that is unexplored, advances in their stereoselective synthesis will hopefully allow increased interest and reports of a wide range of mechanical stereogenic units being utilised as mechanically stereogenic catalysts. Moreover, as previously demonstrated in dynamic systems, structures that can display co-conformational stereochemistry such as mechanically axially chiral systems could serve as convenient platforms for sensing chiral molecules and as chiroptical switches.

Furthermore, while this thesis establishes clear definitions and efficient strategies to synthesise fundamental mechanical stereogenic units, there are still many challenges to tackle in mechanical stereochemistry. One such challenge is in the synthesis of structures - whose stereochemistry arises due to increased crossing points and in structures of higher order. While stereoselective syntheses of such architectures have been reported from covalent chiral components, examples where the mechanical bond provides the sole source of stereochemistry are yet to be reported and, as a result, their potential benefits and applications are poorly explored. Similarly to rotaxanes and catenanes, it would be of interest to determine the influence of mechanical stereochemistry in isolation from residual covalent stereochemistry in their potential applications, and as the removal of covalent stereochemistry post-mechanical bond formation has been well-demonstrated in the context of rotaxanes and catenanes, it is hoped that this is answered soon. To conclude, despite these challenges, we have never been in a better position to harness mechanical stereochemistry to solve chemical problems – we are finally at the end of its beginning, with the golden age of mechanical stereochemistry lying ahead!

Appendix A: Published Research Article

The following research article reproduced in Chapter 2 is shown in its published version:

J. R. J. Maynard, P. Gallagher, D. Lozano, P. Butler, S. M. Goldup, Mechanically axially chiral catenanes and noncanonical mechanically axially chiral rotaxanes. *Nat. Chem.* **2022**, *14*, 1038–1044. https://doi.org/10.1038/s41557-022-00973-6

ARTICLES
https://doi.org/10.1038/s41557-022-00973-6

nature chemistry

Mechanically axially chiral catenanes and noncanonical mechanically axially chiral rotaxanes

John R. J. Maynard[1,2], Peter Gallagher[1,2], David Lozano[1], Patrick Butler[1] and Stephen M. Goldup[1]✉

Chirality typically arises in molecules because of a rigidly chiral arrangement of covalently bonded atoms. Less generally appreciated is that chirality can arise when molecules are threaded through one another to create a mechanical bond. For example, when two macrocycles with chemically distinct faces are joined to form a catenane, the structure is chiral, although the rings themselves are not. However, enantiopure mechanically axially chiral catenanes in which the mechanical bond provides the sole source of stereochemistry have not been reported. Here we re-examine the symmetry properties of these molecules and in doing so identify a straightforward route to access them from simple chiral building blocks. Our analysis also led us to identify an analogous but previously unremarked upon rotaxane stereogenic unit, which also yielded to our co-conformational auxiliary approach. With methods to access mechanically axially chiral molecules in hand, their properties and applications can now be explored.

The term chiral was introduced by Lord Kelvin over a century ago to describe objects that are distinct from their own mirror image[1]. Chirality is relevant in many scientific areas[2–5], but particularly chemistry, because different mirror image forms of a molecule famously have different biological properties. Indeed, the shape of a molecule is a major determinant of its function[6]. Chemists have thus invested substantial effort to develop methods that produce molecules with control over their stereochemistry[7]. A major part of this effort, which has led to two Nobel prizes[8,9], has focused on methods to selectively make molecules in one mirror image form because these are hard to separate using standard techniques. Although chirality is a whole-molecule property[10], chemists often trace the appearance of molecular chirality back to one or more rigidly chiral arrangements of atoms in the structure. The most famous of these is the 'stereogenic centre' embodied by a tetrahedral carbon atom bonded to four different substituents, although stereogenic planes and axes are also found in important natural and synthetic structures. Chiral molecules containing such classical covalent stereogenic units have been studied extensively. Less explored are chiral molecules whose stereochemistry arises absent any covalent stereogenic unit, such as Möbius ladders[11], molecular knots[12] and mechanically interlocked molecules[13,14].

In 1961, Wasserman and Frisch identified that interlocked molecules called catenanes (two molecular rings joined like links in a chain) can display non-classical 'mechanical' stereochemistry[15]—when both rings are 'oriented' (C_{nh} symmetry), a catenane exists in two mirror image forms (Fig. 1a). A decade later, Schill proposed that rotaxanes composed of an oriented ring encircling an axle whose ends are distinct are also chiral (Fig. 1a)[16]. In both cases, the sub-components that make up the interlocked structure are not themselves chiral, which is readily emphasized using commonly employed schematic representations that focus on the symmetry properties of the components (Fig. 1a). These representations also make clear that such topologically chiral catenanes and mechanically planar chiral rotaxanes are related notionally through ring opening. Although such molecules were initially challenging to make as single enantiomers[17–21], recent efforts have allowed them to be accessed in good enantiopurity using standard synthetic approaches[22–27].

Wasserman and Frisch also hinted at, but did not explicitly depict, a second form of catenane stereochemistry that arises when achiral rings with distinct faces (C_{nv}) are combined (Fig. 1b)[15]. In 2002, Puddephat and colleagues reported the first synthesis of such a mechanically axially chiral catenane as a racemate[28,29]. However, no enantiopure examples in which the mechanical bond provides the sole source of stereochemistry have been disclosed so far[30]. To address this challenge, we re-examined the mechanical axial stereogenic unit of catenanes with a focus on not just the symmetry of the components, but how this arises structurally. This led us not only to an efficient approach to enantiopure mechanically axially chiral catenanes but also to recognize and synthesize a noncanonical class of mechanically chiral rotaxanes that had previously been overlooked.

Results and discussion

Insights from semi-structural schematic representations. The minimal schematic representation of a mechanically axially chiral catenane (Fig. 1b) does not specify how the facial dissymmetry of the macrocycles arises. The most obvious way this can be achieved chemically is by including a prochiral unit in both rings (Fig. 1c, **I**)[28,30]. Strikingly, whereas the minimal schematic representation of a mechanically axially chiral catenane suggests there can be no rotaxane equivalent of this stereogenic unit (Fig. 1b), the semi-structural representation reveals that the notional ring-opening process gives rise to a chiral rotaxane (Fig. 1d). Even when the ring encircles the prochiral unit of the axle (**IV**) there is no representation that is achiral. We thus see that rotaxanes can display a previously unremarked upon noncanonical mechanically axially chiral stereogenic unit.

Building on the semi-structural analysis above, we returned to the general symmetry properties of mechanically axially chiral molecules. Whereas the components of catenane **II** and rotaxane **IV** have C_{1v} point group symmetry, more generally, mechanical axial stereochemistry will arise in catenanes whose rings have C_{nv} symmetry and rotaxanes whose axle has C_{1v} symmetry (for an extended

[1]Chemistry, University of Southampton, Highfield, Southampton, UK. [2]These authors contributed equally: John R. J. Maynard, Peter Gallagher.
✉e-mail: s.goldup@soton.ac.uk

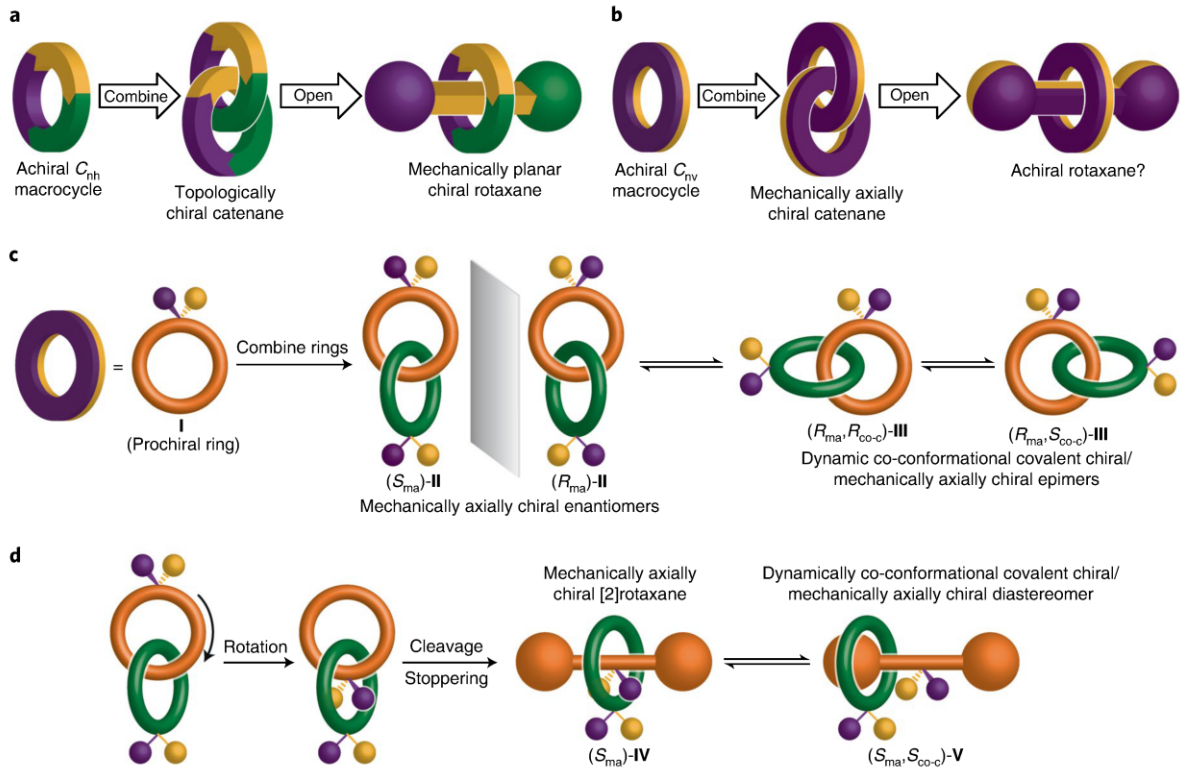

Fig. 1 | Schematic depictions of the mechanical stereogenic units of chiral catenanes and rotaxanes (stereolabels are arbitrary). a, The mechanical topological and planar chiral stereogenic units of catenanes and rotaxanes are related by a notional ring-opening process. **b**, The minimal schematic representation of a mechanically axially chiral catenane suggests that there is no analogous axially chiral rotaxane. **c**, Semi-structural representations of axially chiral catenanes reveal that such molecules can display co-conformational covalent chirality alongside the fixed mechanical stereogenic unit. **d**, The semi-structural representation reveals that rotaxanes display a related but previously unrecognized form of stereochemistry.

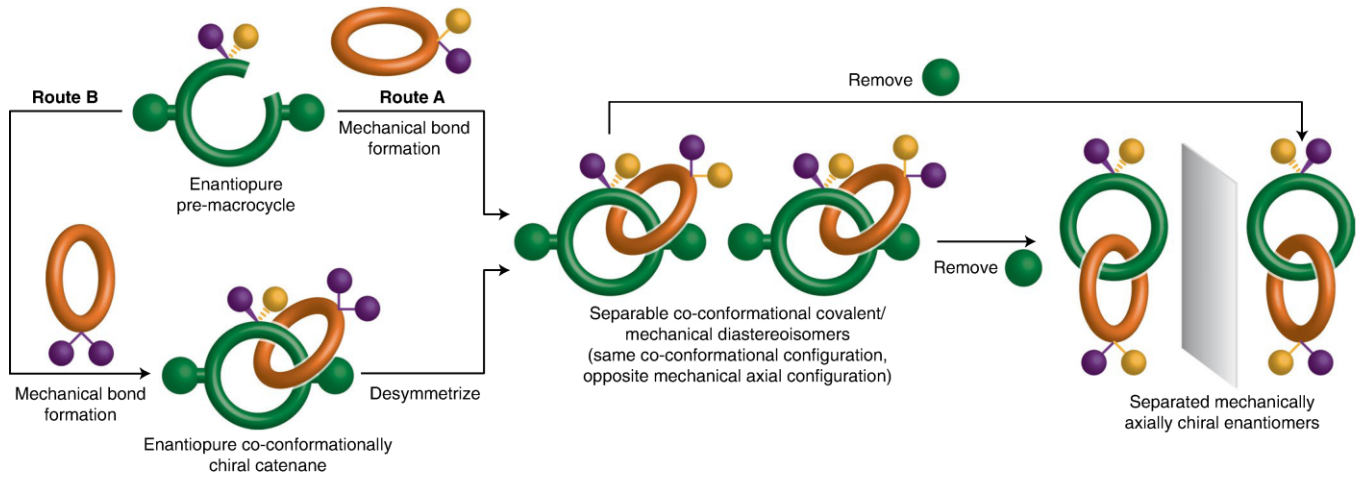

Fig. 2 | Proposed co-conformational auxiliary approach for the synthesis of axially chiral catenanes. If the prochiral substituents and blocking groups are large enough to prevent co-conformational isomerism, the diastereomers can be separated and then converted into enantiomeric axially chiral catenanes.

discussion see Supplementary Section 13.1). Such structures will tend to exhibit prochirality[31]—any single structural modification that does not lie on a symmetry plane will result in a chiral object (for an extended discussion see Supplementary Section 13.2). As a direct consequence, although mechanically axially chiral molecules can always, in theory, adopt a highly symmetrical co-conformation (for example **II** and **IV**) that only expresses mechanical axial stereochemistry, if either ring is displaced from this arrangement, the resulting structure contains both a mechanically axially chiral stereogenic unit and a co-conformational covalent stereogenic unit (for example, **III** and **V**). These lower-symmetry arrangements exist as pairs of co-conformational diastereomers and are an inherent property of mechanically axially chiral molecules (for an extended discussion see Supplementary Section 13.3).

A co-conformational auxiliary approach to axially chiral catenanes and rotaxanes. Having recognized that co-conformational diastereoisomerism is a fundamental property of mechanically

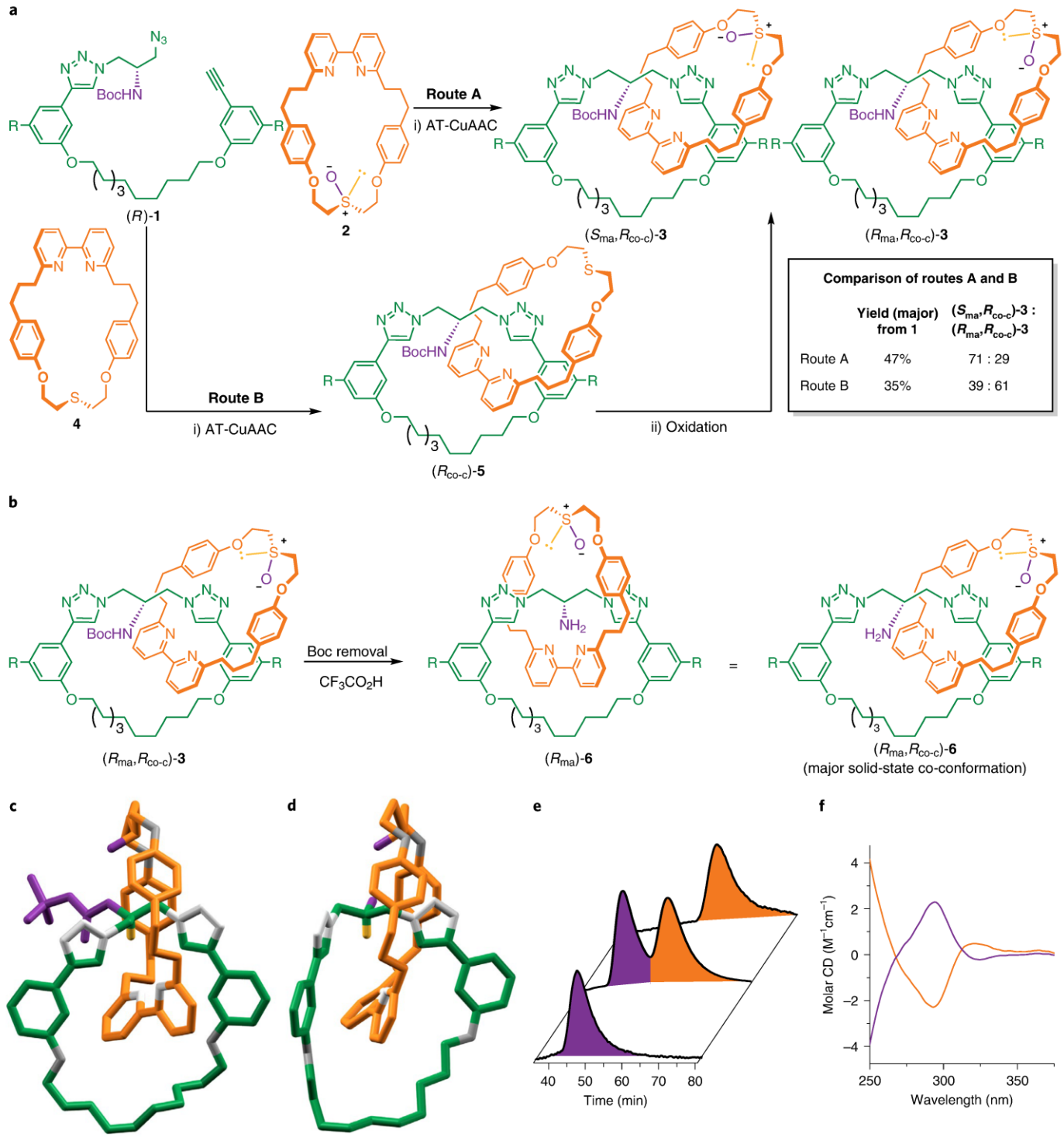

Fig. 3 | Synthesis and analysis of enantiopure axially chiral catenane 6. a, Synthesis and separation of catenane diastereomers **3** from (*R*)-**1** by route A or route B (Fig. 2) with opposite diastereoselectivity. Reagents and conditions: (i) $[Cu(MeCN)_4]PF_6$, N^iPr_2Et, CH_2Cl_2, room temperature (r.t.), 16 h; (ii) IBX, NEt_4Br, $CHCl_3$-H_2O (99:1), r.t., 16 h. **b**, Conversion of catenane **3** to enantiomeric catenanes **6**. Reagents and conditions: CF_3CO_2H, CH_2Cl_2, 0 °C, 1 h. **c**, The solid-state structure (R groups omitted for clarity) of *rac*-(S_{ma},$R_{co\text{-}c}$)-**3** allowed the major products of routes A and B to be assigned. **d**, The solid-state structure (R groups omitted for clarity) of *rac*-**6** contains *rac*-(S_{ma},$R_{co\text{-}c}$)-**6** as the major co-conformational diastereomer. **e**,**f**, Analysis of (R_{ma})-**6** (purple) and (S_{ma})-**6** (orange) by chiral stationary phase HPLC (**e**) and CD spectroscopy (**f**), respectively, confirmed their enantiopurity and their chiral nature. IBX = 2-iodoxybenzoic acid. R = CO_2Me.

axially chiral molecules, it became obvious that a co-conformational stereogenic unit could act as a temporary source of chiral information in their synthesis (Fig. 2). By forming a mechanical bond selectively on one side of a prochiral unit (route A) and designing the structure such that co-conformational exchange is initially blocked, the mechanically axially chiral catenane product would be formed as a pair of separable diastereomers with identical co-conformational covalent (co-c) configuration (e.g. $R_{co\text{-}c}$) but opposite mechanical

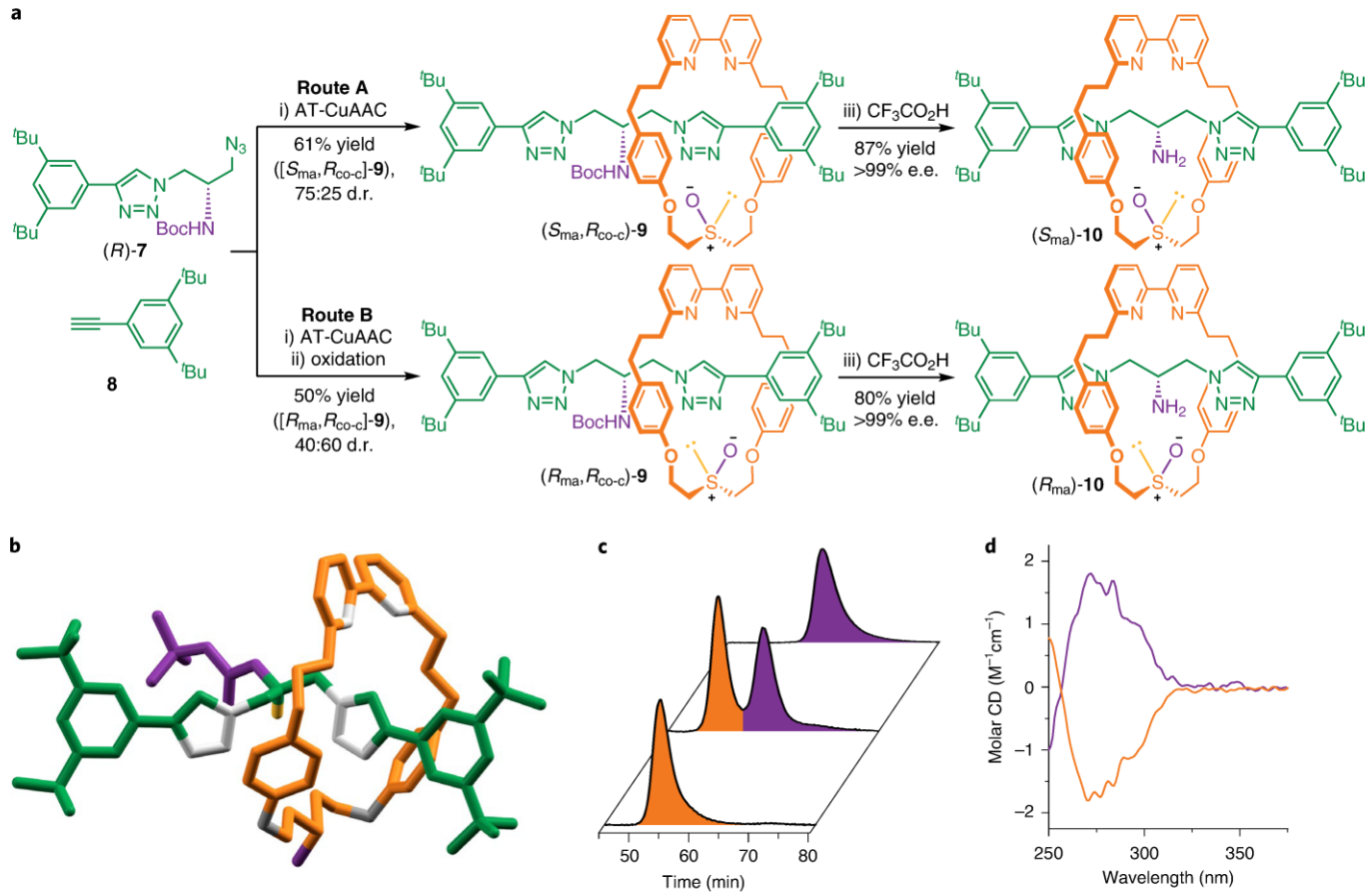

Fig. 4 | Synthesis of mechanically axially chiral rotaxane 10. a, Synthesis of diastereomeric mechanically axially chiral rotaxanes **9** by route A or B gives separable rotaxanes **9** that are converted to **10** by removal of the Boc group. Reagents and conditions: (i) macrocycle **2** (route A) or macrocycle **4** (route B), $[Cu(MeCN)_4]PF_6$, N^iPr_2Et, CH_2Cl_2, r.t., 16 h; (ii) IBX, NEt_4Br, $CHCl_3$-H_2O (99:1), r.t., 16 h; (iii) CF_3CO_2H, CH_2Cl_2, r.t., 16 h. **b**, SCXRD analysis of (R_{ma},$R_{co\text{-}c}$)-**9** allowed the major products of routes A and B to be assigned. **c**,**d**, Analysis of (R_{ma})-**10** (purple) and (S_{ma})-**10** (orange) by chiral stationary phase HPLC (**c**) and CD spectroscopy (**d**), respectively, confirmed their enantiopurity and their chiral nature.

axial (ma) configuration (R_{ma} or S_{ma}). Alternatively, installing a facially symmetrical ring on one side of a prochiral centre would give rise to a single co-conformational enantiomer (route B). Subsequent desymmetrization of the faces of the ring would give rise to the same pair of diastereomers. Removal of the groups preventing co-conformational motion would give mechanically axially chiral enantiomers in which the mechanical bond provides the sole fixed source of stereochemistry. An advantage of this co-conformational chiral auxiliary approach is that co-conformational enantiomers can be made using chiral pool starting materials by choosing where the mechanical bond is formed[17,32–34].

To demonstrate our co-conformational auxiliary approach, (*R*)-serine was elaborated to pre-macrocycle (*R*)-**1** (Supplementary Section 2 and Fig. 3a). Macrocycle **2**, which contains a prochiral sulfoxide, was readily synthesized (Supplementary Section 3) using a Ni-mediated macrocyclization protocol[35]. Catenane formation was achieved by reacting (*R*)-**1** with macrocycle **2** under active-template[36] Cu-mediated alkyne–azide cycloaddition (AT-CuAAC)[37] conditions[38] (route A, Supplementary Section 4.1); slow addition of (*R*)-**1** to a solution of **2**, $[Cu(MeCN)_4]$ and N^iPr_2Et in CH_2Cl_2 gave catenanes **3**, in which co-conformational motion is prevented by the bulky ester and *N*-Boc groups, as a separable mixture of diastereomers (d.r. = 71:29). A brief screen of the reaction solvent did not allow us to identify conditions that enhanced the stereoselectivity of the reaction (Supplementary Section 10.1). Catenanes **3** were also synthesized by reaction of (*R*)-**1** with macrocycle **4** to give ($R_{co\text{-}c}$)-**5** followed oxidation to give catenanes **3** (route B). The diastereoselectivity obtained depended strongly on the oxidant used (Supplementary Section 10.2). The maximum selectivity (39:61 d.r.) without unwelcome over-oxidation was achieved when 2-iodoxybenzoic acid[39] (IBX) was used. Thus, under our optimal conditions, routes A and B proceeded with appreciable but opposite stereoselectivity. Single-crystal X-ray diffraction (SCXRD) analysis of the major product of *rac*-**1** and **2** allowed the different major stereoisomers produced by routes A and B to be assigned (Fig. 3c and Supplementary Section 12.1).

Conversion of diastereomers **3** to structures in which the mechanically axially chiral stereogenic unit is the only fixed source of stereochemistry can be achieved by removing the Boc group (Fig. 3b and Supplementary Section 5) or reducing the esters (Supplementary Section 6). Accordingly, removal of the Boc group from (R_{ma},$R_{co\text{-}c}$)-**3** or (S_{ma},$R_{co\text{-}c}$)-**3** gave (R_{ma})-**6** (>99% e.e.) and (S_{ma})-**6** (>99% e.e.), respectively (Fig. 3e). The enantiomeric nature of these structures is supported by circular dichroism (CD) analysis (Fig. 3f). The solid-state structure of *rac*-**6** (Fig. 3d) contains both co-conformational diastereomers, with the *rac*-(S_{ma}-$R_{co\text{-}c}$) co-conformation observed to dominate (~80:20; Supplementary Section 12.2).

The same strategy was used to synthesize mechanically axially chiral rotaxane **10** (Fig. 4). Serine-derived azide (*R*)-**7** (Supplementary Section 7), alkyne **8** and macrocycle **2** were reacted under AT-CuAAC conditions[40] to give a separable mixture (75:25 d.r.) of rotaxane diastereomers **9** (route A). Rotaxanes **9** could also

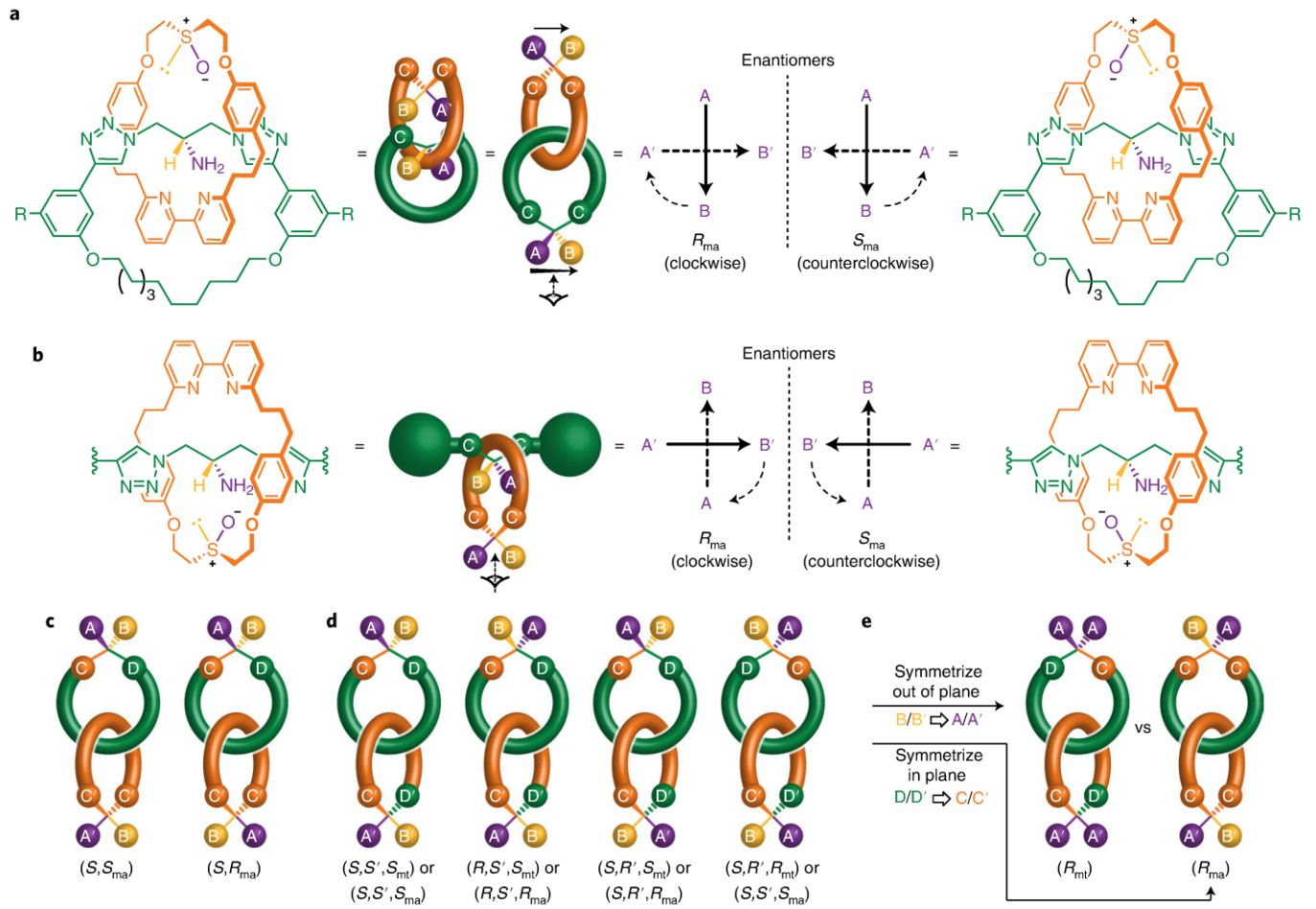

Fig. 5 | Assignment and further analysis of the mechanical axial stereogenic unit. a,**b**, Methods to assign the stereogenic units of mechanically axially chiral catenanes (**a**) and rotaxanes (**b**) by specifying the relative orientation of prochiral moieties. **c**, The two diastereomers identified in catenanes containing one prochiral and one fixed covalent stereogenic centre. **d**, The four diastereomers identified in catenanes containing a covalent stereogenic centre in both rings, whose structures can be specified using either a mechanical topological (R_{mt} or S_{mt}) or mechanical axial (R_{ma} or S_{ma}) stereodescriptor. **e**, Selective symmetrization of the in-plane or out-of-plane substituents of one diastereomer of **d** gives a topologically or axially chiral catenane, respectively. $R = CO_2Me$.

be accessed by reaction of (*R*)-**7**, **8** and macrocycle **4** followed by oxidation (route B). As with catenanes **3**, the diastereoselectivity of route B varied depending on the oxidant used (Supplementary Section 10.4), and the highest diastereoselectivity was obtained with IBX (40:60). SCXRD analysis (Supplementary Section 12.4) of the major isomer obtained using route B with (*R*)-**7** (Fig. 4b) allowed the major products of routes A and B to be assigned. Removal of the Boc group from separated samples of (R_{ma},$R_{co\text{-}c}$)-**9** and (S_{ma},$R_{co\text{-}c}$)-**9** gave (R_{ma})-**10** and (S_{ma})-**10**, respectively, in excellent enantiopurity (>99% e.e.; Fig. 4c). (R_{ma})-**10** and (S_{ma})-**10** produce mirror-image CD spectra (Fig. 4d), emphasizing the chiral nature of the new rotaxane mechanical axial stereogenic unit.

Stereochemical assignment and properties of the mechanically axially chiral stereogenic unit. The assignment of the mechanically axially chiral stereogenic unit relies on identifying the highest-priority faces of each ring, as proposed by Stoddart and Bruns[13]. However, because this rule had not been applied in a real system, we immediately encountered difficulties; to unambiguously assign the highest-priority face of each ring, the relative orientations of the prochiral units must be specified (for an extended discussion see Supplementary Section 14.1). On reflection, we suggest that, in the case of catenanes, the in-plane substituents of the prochiral moieties be positioned at the extremities of the structure and oriented so they 'point' towards one another (Fig. 5a). Conversely, in the equivalent rotaxane, we suggest they be oriented to point in the same direction (Fig. 5b). The latter, somewhat counterintuitive, proposal is designed to ensure that a mechanically axially chiral rotaxane derived from the notional ring opening of an axially chiral catenane would retain the same stereolabel. The absolute stereochemistry of both mechanically axially chiral catenanes and rotaxanes can then be assigned by viewing the ensemble along the axis connecting the prochiral units and observing the relative orientation of the vectors from the out-of-plane substituent with the highest priority to the lowest priority as shown; a clockwise direction of rotation from the head of the front vector to the tail of the rear vector is assigned as R_{ma} and a counterclockwise path assigned as S_{ma}. This approach can be readily extended to molecules where facial dissymmetry arises due to prochiral stereogenic axes or planes (Supplementary Section 14.2).

Finally, we considered the stereochemical nature of catenanes in which one or both prochiral units are replaced with covalent stereocentres. Such structures represent logical alternative precursors to axially chiral catenanes if they could be prepared diastereoselectively and the in-plane substituents subsequently symmetrized. Furthermore, there has been a suggestion that the latter class might

contain both mechanical axial and mechanical topological stereogenic units[41]. In the case of catenanes containing one stereogenic and one prochiral centre (Fig. 5c), ligand permutation analysis reveals two diastereomers (shown) and their enantiomers (that is, four stereoisomers total), consistent with one covalent centre and one mechanical axial stereogenic unit (for an extended discussion see Supplementary Section 15.1).

In the case of catenanes containing a stereogenic centre in each ring, ligand permutation reveals four diastereomers (Fig. 5d) and their enantiomers (eight stereoisomers total), consistent with two covalent and one mechanical stereogenic unit (for an extended discussion see Supplementary Section 15.2). However, the nature of the mechanical stereochemistry is ambiguous; each structure can be assigned both a mechanical axial (R_{ma} or S_{ma}) or a mechanical topological stereodescriptor (R_{mt} or S_{mt}), but only one of these is required to fully specify the structure. This analysis suggests that it would be incorrect to describe such catenanes as simultaneously topologically and mechanically axially chiral—one of the stereolabels would be redundant—but it is unclear which description should take priority. Our preference would be to apply the mechanical topological stereodescriptor, as this captures one of the interesting features of the system, that one component of its stereochemistry is topologically invariant[42]. This analysis may appear philosophical in nature, but it has implications for the synthesis of chiral catenanes. If a single diastereomer of such a catenane could be isolated, it could be converted to an axially chiral catenane by selective symmetrization of the in-plane substituents, or a topologically chiral catenane by symmetrization of the out-of-plane substituents (Fig. 5e). This analysis further highlights that how a stereogenic unit is conceptualized can guide the development of new methodologies.

Conclusions

Detailed analysis of the symmetry properties of the mechanically axially chiral stereogenic unit of catenanes, and in particular the use of semi-structural representations, allowed us to identify an efficient co-conformational auxiliary approach to mechanically axially chiral catenanes and revealed a previously overlooked noncanonical axially chiral stereogenic unit in rotaxanes. The latter is a rare example of a 'new' source of stereoisomerism, as opposed to an overlooked pathway of isomer exchange[43,44] or an overlooked opportunity for atropisomerism[45], as have recently been reported. The rotaxane mechanical axial stereogenic is so closely related to that of catenanes it is surprising that it was overlooked for so long, which may in part be due to the use of schematic structures (Fig. 1b) that focus on symmetry without reference to the underlying chemical structure; although these are useful, they can also obscure important chemical information. Indeed, given that the fixed mechanical stereogenic units of catenanes (topological and axial) now both have an equivalent in rotaxane structures (planar and axial), it appears sensible to suggest that the stereochemistry of rotaxanes and catenanes be unified rather than treated as separate, as they typically are[46].

Our analysis also led to the surprising conclusion that catenanes based on two rings each containing a single stereogenic centre can be described as either mechanically topologically or axially chiral, but that only one mechanical stereodescriptor is required to specify their structure, an observation with implications for future studies. Given the increasing interest in applications of chiral interlocked molecules[34,47–51], including examples based on mechanical and co-conformationally chiral systems[52–54], as well as other exotic or hard to access mechanical stereogenic units[55–60], we anticipate these results will spur progress in the development of functional chiral interlocked systems[61]. Finally, it should be noted that dynamic stereochemistry related to that of mechanically axially chiral catenanes and rotaxanes can also arise due to conformational and co-conformational processes[62,63], both of which have been observed but are poorly understood (for an extended discussion see Supplementary Section 16). Such systems have potential applications as stereodynamic probes.

Online content

Any methods, additional references, Nature Research reporting summaries, source data, extended data, supplementary information, acknowledgements, peer review information; details of author contributions and competing interests; and statements of data and code availability are available at https://doi.org/10.1038/s41557-022-00973-6.

Received: 18 February 2022; Accepted: 12 May 2022;
Published online: 27 June 2022

References

1. Kelvin, W. T. *Baltimore Lectures on Molecular Dynamics and the Wave Theory of Light* 619 (C. J. Clay & Sons, 1904).
2. Zschiesche, D. et al. Chiral symmetries in nuclear physics. *HNPS Adv. Nucl. Phys* **9**, 170–209 (2020).
3. Petitjean, M. Symmetry, antisymmetry and chirality: use and misuse of terminology. *Symmetry* **13**, 603 (2021).
4. Mezey, P. G. Chirality measures and graph representations. *Comput. Math. Appl.* **34**, 105–112 (1997).
5. da Motta, H. Chirality and neutrinos, a student first approach. *J. Phys. Conf. Ser.* **1558**, 012014 (2020).
6. Diaz, D. B. et al. Illuminating the dark conformational space of macrocycles using dominant rotors. *Nat. Chem.* **13**, 218–225 (2021).
7. Eliel, E. L., Wilen, S. H. & Mander, L. N. *Stereochemistry of Organic Compounds* (Wiley, 1994).
8. The Nobel Prize in Chemistry 2001; https://www.nobelprize.org
9. The Nobel Prize in Chemistry 2021; https://www.nobelprize.org
10. Mislow, K. & Siegel, J. Stereoisomerism and local chirality. *J. Am. Chem. Soc.* **106**, 3319–3328 (1984).
11. Herges, R. Topology in chemistry: designing Mobius molecules. *Chem. Rev.* **106**, 4820–4842 (2006).
12. Fielden, S. D. P., Leigh, D. A. & Woltering, S. L. Molecular knots. *Angew. Chem. Int. Ed.* **56**, 11166–11194 (2017).
13. Bruns, C. J. & Stoddart, J. F. *The Nature of the Mechanical Bond: From Molecules to Machines* (Wiley, 2016).
14. Jamieson, E. M. G., Modicom, F. & Goldup, S. M. Chirality in rotaxanes and catenanes. *Chem. Soc. Rev.* **47**, 5266–5311 (2018).
15. Frisch, H. L. & Wasserman, E. Chemical topology. *J. Am. Chem. Soc.* **83**, 3789–3795 (1961).
16. Schill, G. *Catenanes, Rotaxanes and Knots* (Academic Press, 1971).
17. Maynard, J. R. J. & Goldup, S. M. Strategies for the synthesis of enantiopure mechanically chiral molecules. *Chem* **6**, 1914–1932 (2020).
18. Chambron, J. C., Dietrich-Buchecker, C., Rapenne, G. & Sauvage, J. P. Resolution of topologically chiral molecular objects. *Chirality* **10**, 125–133 (1998).
19. Yamamoto, C., Okamoto, Y., Schmidt, T., Jager, R. & Vogtle, F. Enantiomeric resolution of cycloenantiomeric rotaxane, topologically chiral catenane, and pretzel-shaped molecules: observation of pronounced circular dichroism. *J. Am. Chem. Soc.* **119**, 10547–10548 (1997).
20. Hirose, K. et al. The asymmetry is derived from mechanical interlocking of achiral axle and achiral ring components—syntheses and properties of optically pure [2]rotaxanes. *Symmetry* **10**, 20 (2018).
21. Gaedke, M. et al. Chiroptical inversion of a planar chiral redox-switchable rotaxane. *Chem. Sci.* **10**, 10003–10009 (2019).
22. Imayoshi, A. et al. Enantioselective preparation of mechanically planar chiral rotaxanes by kinetic resolution strategy. *Nat. Commun.* **12**, 404 (2021).
23. Tian, C., Fielden, S. D. P., Perez-Saavedra, B., Vitorica-Yrezabal, I. J. & Leigh, D. A. Single-step enantioselective synthesis of mechanically planar chiral [2] rotaxanes using a chiral leaving group strategy. *J. Am. Chem. Soc.* **142**, 9803–9808 (2020).
24. Bordoli, R. J. & Goldup, S. M. An efficient approach to mechanically planar chiral rotaxanes. *J. Am. Chem. Soc.* **136**, 4817–4820 (2014).
25. Jinks, M. A. et al. Stereoselective synthesis of mechanically planar chiral rotaxanes. *Angew. Chem. Int. Ed.* **57**, 14806–14810 (2018).
26. de Juan, A. et al. A chiral interlocking auxiliary strategy for the synthesis of mechanically planar chiral rotaxanes. *Nat. Chem.* **14**, 179–187 (2022).
27. Denis, M., Lewis, J. E. M., Modicom, F. & Goldup, S. M. An auxiliary approach for the stereoselective synthesis of topologically chiral catenanes. *Chem* **5**, 1512–1520 (2019).
28. McArdle, C. P., Van, S., Jennings, M. C. & Puddephatt, R. J. Gold(I) macrocycles and topologically chiral [2]catenanes. *J. Am. Chem. Soc.* **124**, 3959–3965 (2002).

29. Habermehl, N. C., Jennings, M. C., McArdle, C. P., Mohr, F. & Puddephatt, R. J. Selectivity in the self-assembly of organometallic gold(I) rings and [2] catenanes. *Organometallics* **24**, 5004–5014 (2005).
30. Theil, A., Mauve, C., Adeline, M.-T., Marinetti, A. & Sauvage, J.-P. Phosphorus-containing [2]catenanes as an example of interlocking chiral structures. *Angew. Chem. Int. Ed.* **45**, 2104–2107 (2006).
31. IUPAC. *Compendium of Chemical Terminology* (*the* '*Gold Book*') 2nd edn (eds McNaught, A. D. and Wilkinson, A) (Blackwell Scientific Publications, 1997); https://doi.org/10.1351/goldbook
32. Alvarez-Perez, M., Goldup, S. M., Leigh, D. A. & Slawin, A. M. A chemically-driven molecular information ratchet. *J. Am. Chem. Soc.* **130**, 1836–1838 (2008).
33. Carlone, A., Goldup, S. M., Lebrasseur, N., Leigh, D. A. & Wilson, A. A three-compartment chemically-driven molecular information ratchet. *J. Am. Chem. Soc.* **134**, 8321–8323 (2012).
34. Cakmak, Y., Erbas-Cakmak, S. & Leigh, D. A. Asymmetric catalysis with a mechanically point-chiral rotaxane. *J. Am. Chem. Soc.* **138**, 1749–1751 (2016).
35. Lewis, J. E. M. et al. High yielding synthesis of 2,2′-bipyridine macrocycles, versatile intermediates in the synthesis of rotaxanes. *Chem. Sci.* **7**, 3154–3161 (2016).
36. Denis, M. & Goldup, S. M. The active template approach to interlocked molecules. *Nat. Rev. Chem.* **1**, 0061 (2017).
37. Aucagne, V., Hanni, K. D., Leigh, D. A., Lusby, P. J. & Walker, D. B. Catalytic 'click' rotaxanes: a substoichiometric metal-template pathway to mechanically interlocked architectures. *J. Am. Chem. Soc.* **128**, 2186–2187 (2006).
38. Lewis, J. E. M., Modicom, F. & Goldup, S. M. Efficient multicomponent active template synthesis of catenanes. *J. Am. Chem. Soc.* **140**, 4787–4791 (2018).
39. Shukla, V. G., Salgaonkar, P. D. & Akamanchi, K. G. A mild, chemoselective oxidation of sulfides to sulfoxides using o-iodoxybenzoic acid and tetraethylammonium bromide as catalyst. *J. Org. Chem.* **68**, 5422–5425 (2003).
40. Lahlali, H., Jobe, K., Watkinson, M. & Goldup, S. M. Macrocycle size matters: 'small' functionalized rotaxanes in excellent yield using the CuAAC active template approach. *Angew. Chem. Int. Ed.* **50**, 4151–4155 (2011).
41. Schroder, H. V., Zhang, Y. & Link, A. J. Dynamic covalent self-assembly of mechanically interlocked molecules solely made from peptides. *Nat. Chem* **13**, 850–857 (2021).
42. Walba, D. M. Topological stereochemistry. *Tetrahedron* **41**, 3161–3212 (1985).
43. Canfield, P. J. et al. A new fundamental type of conformational isomerism. *Nat. Chem.* **10**, 615–624 (2018).
44. Canfield, P. J., Govenlock, L. J., Reimers, J. & Crossley, M. J. Recent advances in stereochemistry reveal classification shortcomings. Preprint at https://doi.org/10.26434/chemrxiv.12488525.v1 (2020).
45. Reisberg, S. H. et al. Total synthesis reveals atypical atropisomerism in a small-molecule natural product, tryptorubin A. *Science* **367**, 458–463 (2020).
46. Lukin, O., Godt, A. & Vogtle, F. Residual topological isomerism of intertwined molecules. *Chem. Eur. J.* **10**, 1878–1883 (2004).
47. Martinez-Cuezva, A., Saura-Sanmartin, A., Alajarin, M. & Berna, J. Mechanically interlocked catalysts for asymmetric synthesis. *ACS Catal.* **10**, 7719–7733 (2020).
48. Pairault, N. & Niemeyer, J. Chiral mechanically interlocked molecules—applications of rotaxanes, catenanes and molecular knots in stereoselective chemosensing and catalysis. *Synlett* **29**, 689–698 (2018).
49. Mitra, R., Zhu, H., Grimme, S. & Niemeyer, J. Functional mechanically interlocked molecules: asymmetric organocatalysis with a catenated bifunctional Brønsted acid. *Angew. Chem. Int. Ed.* **56**, 11456–11459 (2017).
50. Pairault, N. et al. Heterobifunctional rotaxanes for asymmetric catalysis. *Angew. Chem. Int. Ed.* **59**, 5102–5107 (2020).
51. Dommaschk, M., Echavarren, J., Leigh, D. A., Marcos, V. & Singleton, T. A. Dynamic control of chiral space through local symmetry breaking in a rotaxane organocatalyst. *Angew. Chem. Int. Ed.* **58**, 14955–14958 (2019).
52. Heard, A. W. & Goldup, S. M. Synthesis of a mechanically planar chiral rotaxane ligand for enantioselective catalysis. *Chem* **6**, 994–1006 (2020).
53. Gaedke, M. et al. Chiroptical inversion of a planar chiral redox-switchable rotaxane. *Chem. Sci.* **10**, 10003–10009 (2019).
54. Corra, S. et al. Chemical on/off switching of mechanically planar chirality and chiral anion recognition in a [2]rotaxane molecular shuttle. *J. Am. Chem. Soc.* **141**, 9129–9133 (2019).
55. Wood, C. S., Ronson, T. K., Belenguer, A. M., Holstein, J. J. & Nitschke, J. R. Two-stage directed self-assembly of a cyclic [3]catenane. *Nat. Chem.* **7**, 354–358 (2015).
56. Caprice, K. et al. Diastereoselective amplification of a mechanically chiral [2] catenane. *J. Am. Chem. Soc.* **143**, 11957–11962 (2021).
57. Cui, Z., Lu, Y., Gao, X., Feng, H. J. & Jin, G. X. Stereoselective synthesis of a topologically chiral Solomon link. *J. Am. Chem. Soc.* **142**, 13667–13671 (2020).
58. Carpenter, J. P. et al. Controlling the shape and chirality of an eight-crossing molecular knot. *Chem* **7**, 1534–1543 (2021).
59. Leigh, D. A. et al. Tying different knots in a molecular strand. *Nature* **584**, 562–568 (2020).
60. Corra, S., de Vet, C., Baroncini, M., Credi, A. & Silvi, S. Stereodynamics of *E*/*Z* isomerization in rotaxanes through mechanical shuttling and covalent bond rotation. *Chem* **7**, 2137–2150 (2021).
61. David, A. H. G. & Stoddart, J. F. Chiroptical properties of mechanically interlocked molecules. *Isr. J. Chem.* **61**, 608–621 (2021).
62. Ashton, P. R. et al. Molecular meccano, part 23. Self-assembling cyclophanes and catenanes possessing elements of planar chirality. *Chem. A Eur. J.* **4**, 299–310 (1998).
63. Caprice, K. et al. Diastereoselective amplification of a mechanically chiral [2] catenane. *J. Am. Chem. Soc.* **143**, 11957–11962 (2021).

Data availability

All characterization data for novel compounds (NMR, MS, CD, HPLC) are available through the University of Southampton data repository (https://doi.org/10.5258/SOTON/D2185). Crystallographic data have been uploaded to the CCDC and are available under accession nos. 2109976 (*rac*-(S_{ma},$R_{co\text{-}c}$)-**3**), 2115463 (*rac*-**6**), 2109991 (*rac*-**S15**) and 2109992 ((R_{ma},$R_{co\text{-}c}$)-**9**).

Acknowledgements

S.M.G. thanks the ERC (agreement no. 724987) and the Royal Society for a Wolfson Research Fellowship (RSWF\FT\180010). P.B. thanks the University of Southampton for a Presidential Scholarship. P.G. thanks the University of Southampton for funding.

Author contributions

J.R.J.M. and P.G. contributed equally. Both have the right to place themselves as first author on their CVs. J.R.J.M. and S.M.G. developed the co-conformational auxiliary concept. J.R.J.M. synthesized **3** and **5** and collected SCXRD diffraction data for a reduced product of catenane **5**. P.G. synthesized **9** and **10**, determined the stereochemistry of rotaxanes **9**, and managed the preparation of manuscript graphics. D.L. optimized the synthesis and purification of **3** and **5**, synthesized **6** and determined the stereochemistry of catenanes **3**. P.B. collected the X-ray diffraction data of **3**, **6** and **9** and fully refined all SCXRD data. D.L. and P.G. managed the preparation of the Supplementary Information. S.M.G. directed the research. All authors contributed to the analysis of the results and the writing of the manuscript.

Competing interests

The authors declare no competing interests.

Additional information

Supplementary information The online version contains supplementary material available at https://doi.org/10.1038/s41557-022-00973-6.

Correspondence and requests for materials should be addressed to Stephen M. Goldup.

Appendix B: Published Research Article

The following research article reproduced in Chapter 3 is shown in its published version:

P. R. Gallagher, A. Savoini, A. Saady, J. R. J. Maynard, P. W. V. Butler, G. J. Tizzard, S. M. Goldup, Facial Selectivity in Mechanical Bond Formation: Axially Chiral Enantiomers and Geometric Isomers from a Simple Prochiral Macrocycle. *J. Am. Chem. Soc.* **2024**, *146*, 9134–9141. https://doi.org/10.1021/jacs.3c14329

JACS
JOURNAL OF THE AMERICAN CHEMICAL SOCIETY
pubs.acs.org/JACS

Article

Facial Selectivity in Mechanical Bond Formation: Axially Chiral Enantiomers and Geometric Isomers from a Simple Prochiral Macrocycle

Peter R. Gallagher,[§] Andrea Savoini,[§] Abed Saady, John R. J. Maynard, Patrick W. V. Butler, Graham J. Tizzard, and Stephen M. Goldup*

Cite This: *J. Am. Chem. Soc.* 2024, 146, 9134−9141

Read Online

ACCESS | Metrics & More | Article Recommendations | Supporting Information

ABSTRACT: In 1971, Schill recognized that a prochiral macrocycle encircling an oriented axle led to geometric isomerism in rotaxanes. More recently, we identified an overlooked chiral stereogenic unit in rotaxanes that arises when a prochiral macrocycle encircles a prochiral axle. Here, we show that both stereogenic units can be accessed using equivalent strategies, with a single weak stereodifferentiating interaction sufficient for moderate to excellent stereoselectivity. Using this understanding, we demonstrated the first direct enantioselective (70% *ee*) synthesis of a mechanically axially chiral rotaxane.

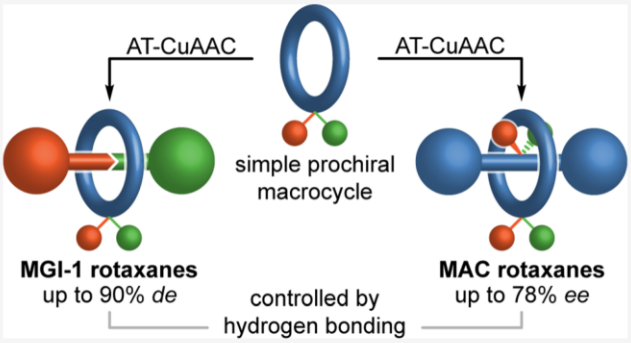

INTRODUCTION

Early in the development of the chemistry of the mechanical bond,[1] Schill recognized that when a macrocycle containing a prochiral center such that its faces are distinguishable encircles an axle with distinguishable ends, the rotaxane can exist as distinct geometric isomers even though the individual components are stereochemically trivial.[2] Although molecules that correspond to the type 1[3] mechanical geometric isomers (MGI-1) of rotaxanes have been reported, the vast majority where the mechanical bond provides the sole stereogenic unit[4] are constructed from calixarenes[5] or similar macrocycles[6] whose facial dissymmetry arises from the fixed cone-shaped conformation of the threaded ring.[7] The same is true of the corresponding catenane stereogenic unit first reported by Gaeta and Neri.[8] In these cases, facial dissymmetry is expressed over the whole macrocycle, which has been shown to lead to the stereoselective formation of the corresponding rotaxanes. However, to our knowledge, the only MGI-1 rotaxanes in which a single covalent prochiral center differentiates the faces of the ring,[9] as envisaged by Schill, were reported by Bode and Saito,[10] where no stereoselectivity was reported.

More recently,[11] we identified that when a facially dissymmetric macrocycle encircles a prochiral axle, an overlooked mechanically axially chiral (MAC)[12] stereogenic unit arises that is analogous to the MAC stereogenic unit of catenanes identified by Wasserman and Frisch over 60 years earlier.[13] Having made this observation, we demonstrated that such molecules can be synthesized using a diastereoselective co-conformational chiral auxiliary[14] active template[15] Cu-mediated alkyne−azide cycloaddition (AT-CuAAC)[16,17] approach with a ring whose facial dissymmetry arises from a single prochiral sulfoxide unit.

If we consider a schematic AT-CuAAC retrosynthesis of MGI-1 isomers (Figure 1a) and MAC enantiomers (Figure 1b), in which the axle is divided into two components that couple through the macrocycle in the forward synthesis, the common challenge involved in the stereoselective synthesis of both becomes obvious; we must control which face of the macrocycle is oriented toward which half-axle component in the mechanical bond-forming step.

Here, by re-examining our stereoselective synthesis of MAC rotaxanes, we identify that a single H-bond between the sulfoxide unit and one of the two half-axle components appears to play a key role in the reaction outcome. We use this understanding to develop a stereoselective approach to rotaxane MGI-1 isomers that can be extended directly to their catenane counterparts. Finally, we apply these principles to the direct synthesis of MAC rotaxanes without the need to produce diastereomeric intermediates.

Received: December 18, 2023
Revised: February 12, 2024
Accepted: February 14, 2024
Published: March 20, 2024

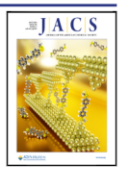

https://doi.org/10.1021/jacs.3c14329
J. Am. Chem. Soc. 2024, 146, 9134−9141

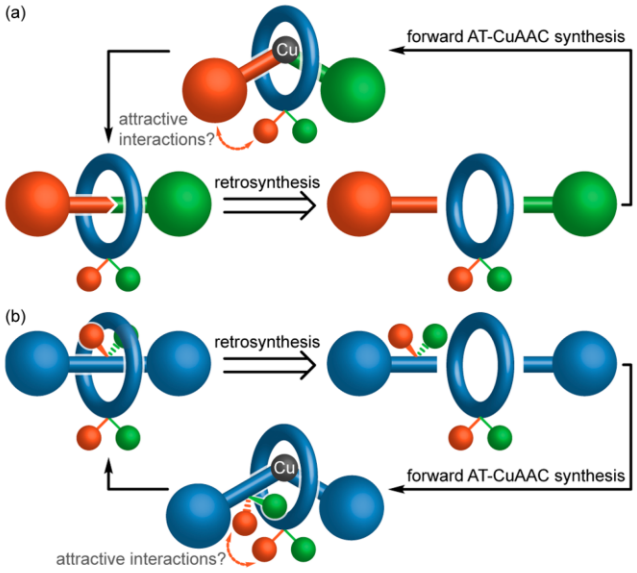

Figure 1. Schematic active template retrosyntheses of the mechanical (a) type 1 geometric isomers and (b) axially chiral enantiomers of rotaxanes, highlighting the need to control facial selectivity in the mechanical bond-forming step and the potential for attractive interactions between one face of the macrocycle and one of the half-axles to provide this control.

RESULTS AND DISCUSSION

Effect of the Conditions and Substrate Structure in the Synthesis of MAC Rotaxanes 4. Previously,[11] we found that the AT-CuAAC reaction of azide (*R*)-**1a**, macrocycle **2**, and alkyne **3** gave rotaxane diastereomers (R_{ma},R_{co-c})[18]-**4a** (major) and (S_{ma},R_{co-c})-**4a** (minor) in 50% *de* (Scheme 1 and Table 1, entry 1). These products have the same co-conformational covalent configuration[19] (set by the configuration of **1a**) but opposite mechanical axial configuration. They are separable because the steric bulk of the NHBoc group prevents the epimerization of the covalent stereocenter by shuttling of the macrocycle between triazole-containing compartments. The solid-state structure obtained by single-crystal X-ray diffraction (SCXRD) of an analogous catenane[11] contained a close contact between the polarized NH of the carbamate unit and the O atom of the sulfoxide unit, which suggested that an H-bond between these groups may play a role in the observed stereoselectivity.[20]

To test this proposal, we first compared the outcome of reactions performed in CH_2Cl_2 and EtOH, the latter being a more competitive H-bonding solvent, and found that the stereoselectivity was indeed reduced to 14% *de* (entry 2). Furthermore, the reactions of azides **1b–d** to give rotaxanes **4b–d** (entries 3–5) proceeded with selectivities that paralleled the polarization of the N–H unit; trifluoroacetamide **1d** produced rotaxane **4d** in the highest selectivity (70% *de*), followed by trichloroacetamide **1c** (48% *de*) then acetamide **1b** (36% *de*). The SCXRD structure of the major isomer of **4d** (Figure 2) revealed the same (R_{ma},R_{co-c}) configuration as that of **4a**, with an NH···O H-bond observed between the amide NH and sulfoxide units. Methylated trifluoroacetamide rotaxane **4e** was produced in 10% *de* (entry 6), which, although consistent with the key role of the NH···O H-bond, suggests that there is some inherent facial bias between the azide and alkyne half-axles in the AT-CuAAC reactions of **2**.

Scheme 1. Synthesis of Rotaxanes 4[a]

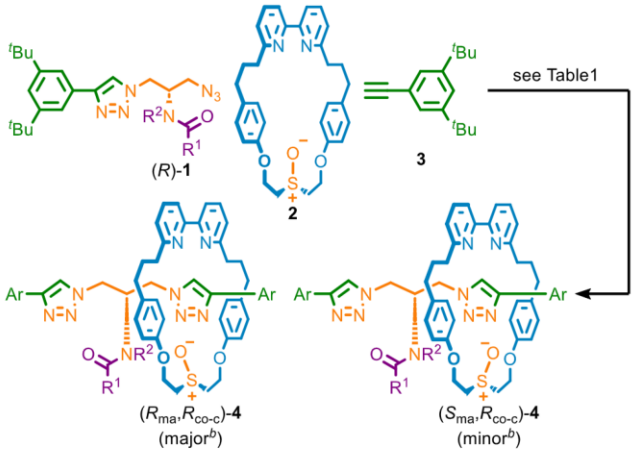

[a]Reagents and conditions (see also Table 1): (*R*)-**1** (1.1 equiv), **2** (1 equiv), **3** (1.1 equiv), $[Cu(CH_3CN)_4]PF_6$ (0.96 equiv), $^iPr_2NEt$ (2 equiv). [b]Determined by SCXRD for **1a**[11] and **1d** (Figure 1); **1b**, **c**, and **e** are presumed. Ar = 3,5-di-^{t}Bu-C_6H_3.

Table 1. Effect of the Reaction Conditions and Substrate on the AT-CuAAC Diastereoselective Synthesis of Rotaxanes 4

entry	substrate	conditions	selectivity[a]
1[11]	**1a** (R^1 = O^{t}Bu, R^2 = H)	CH_2Cl_2, rt	50% *de*
2	**1a** (R^1 = O^{t}Bu, R^2 = H)	EtOH, rt	14% *de*
3	**1b** (R^1 = Me, R^2 = H)	CH_2Cl_2, rt	36% *de*
4	**1c** (R^1 = CCl_3, R^2 = H)	CH_2Cl_2, rt	48% *de*
5	**1d** (R^1 = CF_3, R^2 = H)	CH_2Cl_2, rt	70% *de*
6	**1d** (R^1 = CF_3, R^2 = H)	EtOH, rt	16% *de*
7	**1e** (R^1 = CF_3, R^2 = Me)	CH_2Cl_2, rt	10% *de*
8	**1a** (R^1 = O^{t}Bu, R^2 = H)	CH_2Cl_2, −40 °C	72% *de*
9	**1a** (R^1 = O^{t}Bu, R^2 = H)	CH_2Cl_2, −78 °C	80% *de*
10	**1d** (R^1 = CF_3, R^2 = H)	CH_2Cl_2, −40 °C	82% *de*
11	**1d** (R^1 = CF_3, R^2 = H)	CH_2Cl_2, −78 °C	70% *de*

[a]Determined by ^{1}H NMR analysis of the crude reaction product.

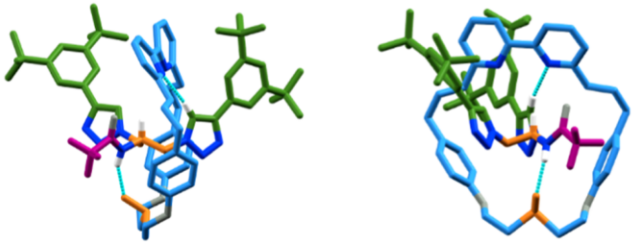

Figure 2. SCXRD structure of [(R_{ma},R_{co-c})-**4d** (major isomer), with key intercomponent interactions highlighted. Colors as in Scheme 1, including the sulfoxide (SO) moiety to highlight the differentiation of the macrocycle faces, except N [dark blue], O [gray], and H [white]. The majority of H was omitted.

The effect of the temperature on the stereoselectivity of the reactions of **1a** and **1d** was more complicated. Whereas reducing the reaction temperature in the synthesis of **4a** from rt (entry 1) to −40 °C (entry 8) and −78 °C (entry 9) increased the observed selectivity, that for **4d** was higher at −40 °C (entry 10) and then fell at −78 °C (entry 11). We suggest that this slightly counterintuitive observation can be rationalized in broad terms by considering that the AT-CuAAC reaction takes place over several steps,[21] which include an

https://doi.org/10.1021/jacs.3c14329
J. Am. Chem. Soc. 2024, 146, 9134–9141

equilibrium between diastereomeric azide/acetylide complexes **I**, followed by irreversible formation of the corresponding triazolides **II** (Scheme 2).[22] The observed stereoselectivity is thus a composite function of the pre-equilibrium step (K_{eq}) and the relative rates (k_{RR}, k_{SR}) at which intermediates **I** progress to triazolides **II**. The effect of temperature on the reaction to produce **4d** suggests the pre-equilibrium and kinetic resolution steps respond differently to changes in temperature, resulting in the observed behavior.[23]

Scheme 2. Proposed AT-CuAAC Mechanism Highlighting Pre-Equilibrium and Kinetic Resolution Steps

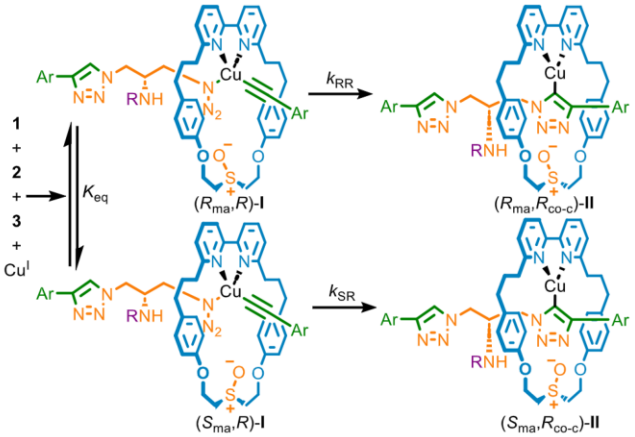

Stereoselective Synthesis of MGI-1 Rotaxanes. Having demonstrated that a single H-bond between the sulfoxide unit and one of the incoming half-axle components appears to be important in the synthesis of rotaxanes **4**, we turned our attention to the synthesis of analogous rotaxanes expressing the MGI-1 stereogenic unit.

Intrigued by the small but measurable stereoselectivity observed in the formation of **4e**, which cannot arise due to the proposed stereodifferentiating NH···O interaction, we examined the AT-CuAAC coupling between macrocycle **2**, and half-axles **3** and **5**, neither of which contain a directing group. At rt in CH_2Cl_2 (Scheme 3a, entry 1), geometric isomers (E_m)-**6** and (Z_m)-**6** were formed in low but significant stereoselectivity (24% *de*), confirming that the AT-CuAAC reactions of **2** are not only biased by the H-bond identified in the case of rotaxanes **4**.[24] Analysis of the separated isomers of **6** by SCXRD allowed their absolute stereochemistry to be determined (Figure 3a,b). Replacing the solvent with THF marginally improved the selectivity (28% *de*, entry 2), as did lowering the reaction temperature to −20 °C (40% *de*, entry 3), but, as with **4d**, reduced selectivity was observed at lower temperatures (entries 4 and 5). Using EtOH as a solvent was comparable to THF (entry 6).[25]

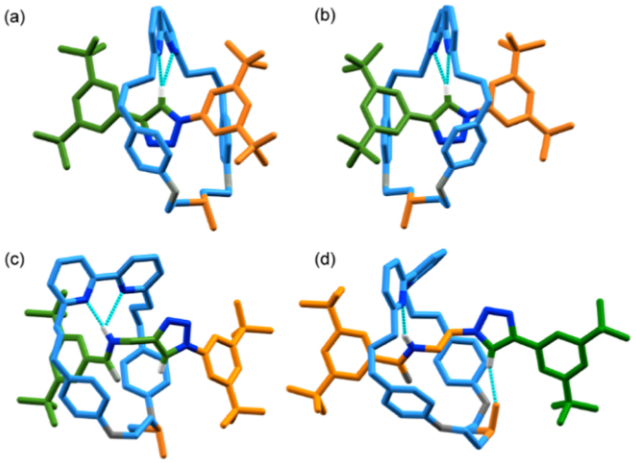

Figure 3. (a) Solid-state structures of (a) (Z_m)-**6**, (b) (E_m)-**6**, (c) (Z_m)-**9**, and (d) (E_m)-**11** with key intercomponent interactions highlighted. Colors as in Scheme 1, including the sulfoxide (SO) moiety to emphasize the macrocycle faces, except for O (gray), N (dark blue), and H (white). The majority of H was omitted for clarity.

Scheme 3. AT-CuAAC Synthesis of Rotaxane Geometric Isomers of Type 1. (a) Effect of Conditions on the Formation of Rotaxanes 6.[a] (b) Effect of the Half-Axle Structure, on the Stereoselectivity of Mechanical Bond Formation with Macrocycle 2[b,c]

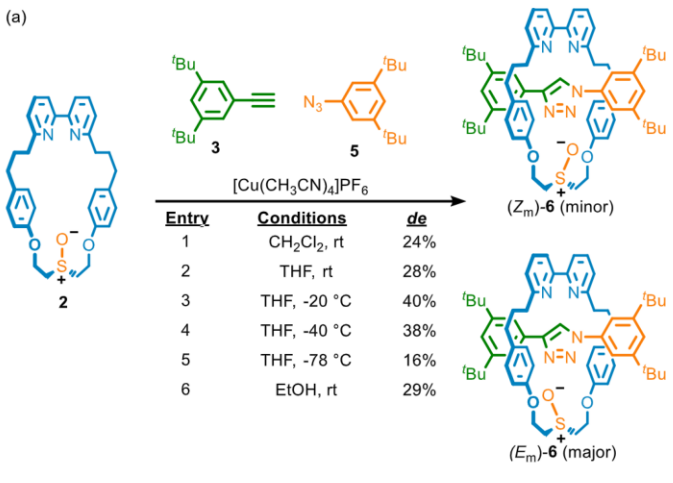

Entry	Conditions	*de*
1	CH_2Cl_2, rt	24%
2	THF, rt	28%
3	THF, -20 °C	40%
4	THF, -40 °C	38%
5	THF, -78 °C	16%
6	EtOH, rt	29%

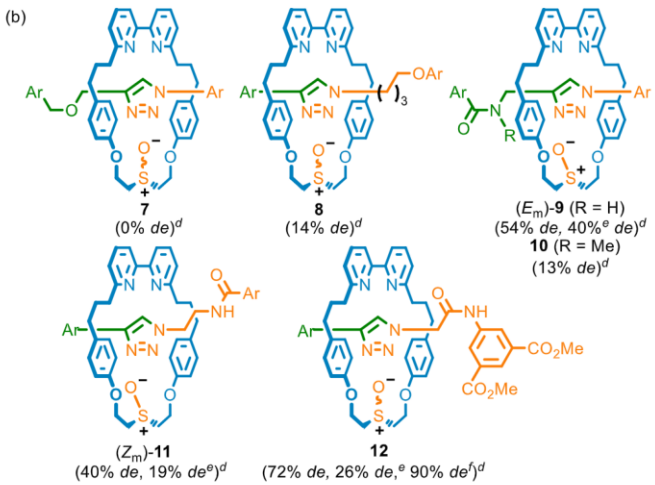

[a]Reagents and conditions: 2 (1 equiv), 3 (1.1 equiv), 5 (1.1 equiv), $[Cu(CH_3CN)_4]PF_6$ (0.96 equiv), $^iPr_2EtN$ (2 equiv). [b]Synthesized in THF at rt (Scheme 3a, entry 2) unless otherwise stated. [c]Stereochemistry of the major isomer indicated where determined. [d]Determined by ^1H NMR analysis of the crude reaction product. [e]Synthesized in EtOH. [f]Synthesized at −40 °C in THF. Ar = 3,5-di-^{t}Bu-C_6H_3.

https://doi.org/10.1021/jacs.3c14329
J. Am. Chem. Soc. 2024, 146, 9134−9141

Although the selectivities observed in the formation of **4e** and **6** are consistent with some inherent facial bias between the azide and alkyne half-axles in the mechanical bond-forming step, when a propargylic alkyne was employed with aryl azide **5** to generate rotaxane **7**, no stereoselectivity was observed (Scheme 3b). In contrast, the reaction of an alkyl azide and aryl acetylene **3** to give rotaxane **8** proceeded in an appreciable stereoselectivity (14% *de*). Thus, although it is clearly possible to achieve low selectivities in the AT-CuAAC reactions of **2** in the absence of obvious directing interactions, this is highly substrate-dependent, and its origins are unclear at this time.[26]

Returning to our H-bonding-directed approach, when a propargylic amide was reacted with **2** to give **9**, significantly improved stereoselectivity (54% *de*) was obtained, which was reduced in EtOH (40% *de*). The corresponding *N*-methyl amide gave rise to rotaxane **10** in low selectivity (13% *de*). The AT-CuAAC coupling of **3** and an alkyl azide bearing a simple amide gave rotaxane **11** in moderate stereoselectivity (40% *de*), which was reduced in EtOH (19% *de*). Thus, the amide can be placed in either coupling partner. Finally, rotaxane **12**, whose amide NH is expected to be more polarized than that of **11**, was produced in good selectivity (72% *de*) at rt, which was improved (90% *de*) when the same reaction was conducted at −40 °C. Reducing the temperature further did not improve the observed stereocontrol and led to a slow reaction. Replacing the reaction solvent with EtOH once again led to reduced selectivity (26% *de*).

As in the case of rotaxanes **4**, the high selectivity observed in the synthesis of **9**, **11**, and **12** is consistent with the key role of an NH···O interaction between the macrocycle and half-axle in controlling the facial selectivity in the AT-CuAAC reactions of macrocycle **2**. However, we previously observed[11] this interaction in the solid-state structures of both diastereomers of epimeric MAC catenanes even though, in principle, in one diastereomer, the S−O bond could be expected to project away from the NH unit, which is possible due to the flexible nature of macrocycle **2**. The major isomers of rotaxanes **9** and **11** determined by SCXRD (Figure 3c,d, respectively) highlight the importance of this flexibility; although both were formed selectively, counterintuitively, the ring is oriented in opposite directions with respect to the amide in the major diastereomer of each. Thus, although the NH···O interaction appears able to direct the synthesis of MGI-1 isomers, the major product depends on the detailed structure of the half-axles used.[27] We also note that whereas an NH···O interaction is observed in the SCXRD structure of **4d**, in the case of **9** and **11**, this is replaced by an NH···N interaction between the amide proton and one of the bipyridine N atoms, with the SO unit instead interacting with the polarized C−H of the triazole moiety in an inter- or intramolecular manner, respectively, presumably because the NH unit is geometrically accessible to the macrocycle in rotaxanes **9** and **11** whereas it is not in the case of **4d**.

Stereoselective Synthesis of an MGI Catenane. Having established that a polarized NH unit appears sufficient to control the synthesis of MGI-1 rotaxanes with macrocycle **2**, we briefly investigated whether the same approach could be applied to the related isomers of catenanes. Pre-macrocycle **13**, which contains an activated amide unit analogous to that of **12**, reacted with **2** under our AT-CuAAC catenane-forming conditions (Scheme 4)[28] to give **14** with good stereocontrol (80% *de*, entry 1). The same reaction in $CHCl_3$-EtOH gave reduced selectivity (60% *de*, entry 2), whereas performing the reaction at 0 °C in CH_2Cl_2 increased the selectivity (92% *de*, entry 3). Lowering the temperature further (−40 °C) had no significant effect (90% *de*, entry 4). Thus, unsurprisingly, given the similarity of their stereogenic units, MGI-1 rotaxanes and MGI catenanes can be made with good stereocontrol using equivalent strategies.

Scheme 4. Stereoselective Synthesis of Catenane 14[a]

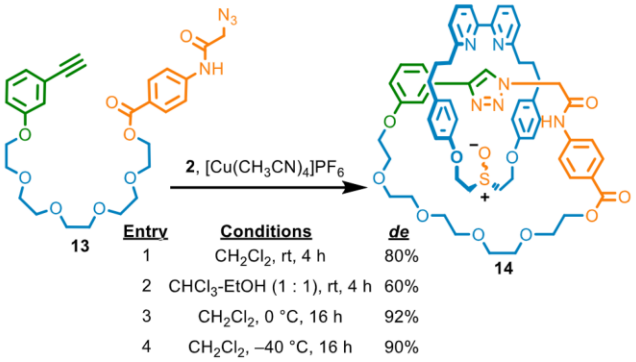

Entry	Conditions	*de*
1	CH_2Cl_2, rt, 4 h	80%
2	$CHCl_3$-EtOH (1 : 1), rt, 4 h	60%
3	CH_2Cl_2, 0 °C, 16 h	92%
4	CH_2Cl_2, −40 °C, 16 h	90%

[a]Reagents and conditions: **13** (2 equiv) was added over the time stated using a syringe pump to **2** (1 equiv), $[Cu(CH_3CN)_4]PF_6$ (0.97 equiv), $^iPr_2EtN$ (4 equiv).

Direct Enantioselective Synthesis of MAC Rotaxanes. Finally, we returned to apply our findings to the stereoselective synthesis of the enantiomers of MAC rotaxanes. In our original report,[11] we separated the diastereomers of epimeric rotaxanes **4a** before removing the Boc group to generate rotaxane **15** (Scheme 5), in which the MAC stereogenic unit is the only fixed source of stereochemistry. This was necessary as the AT-CuAAC reaction only proceeded in 50% *de*; the ultimate purpose of developing methodologies to produce stereochemically complex mechanically interlocked molecules is so that they can then be investigated in applications such as sensing[29] or catalysis,[30] for which they must be of high stereopurity.

Scheme 5. Two-Step, One-Pot Synthesis of Enantioenriched MAC Rotaxanes 15[a,b]

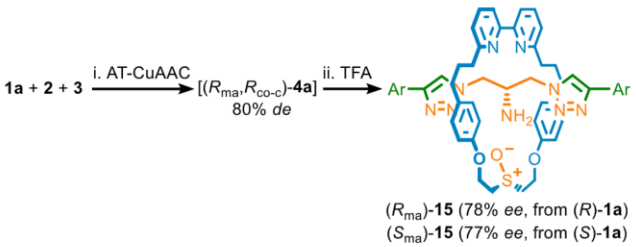

(R_{ma})-**15** (78% *ee*, from (*R*)-**1a**)
(S_{ma})-**15** (77% *ee*, from (*S*)-**1a**)

[a]Reagents and conditions: i. **1a** (1.1 equiv), **2** (1 equiv), **3** (1.1 equiv), $[Cu(CH_3CN)]PF_6$ (0.96 equiv), $^iPr_2EtN$ (2 equiv), CH_2Cl_2, 16 h; ii. TFA, CH_2Cl_2, −78 °C to rt, 6 h. [b]Determined by analytical CSP-HPLC. Ar = 3,5-di-^{t}Bu-C_6H_3.

Trivially, our optimized conditions for the diastereoselective formation of **4a** (Table 1, entry 9) removes the need for the separation of the MAC epimers and so allows the synthesis of highly enantioenriched samples of rotaxane **15** in a two-step, one-pot manner (Scheme 5); AT-CuAAC coupling of (*R*)-**1a** followed by TFA-mediated removal of the Boc group gave rotaxane (R_{ma})-**15** in good stereoselectivity (78% *ee*) in

https://doi.org/10.1021/jacs.3c14329
J. Am. Chem. Soc. 2024, 146, 9134−9141

agreement with that observed for **4a** (80% *de*). The same reaction with (*S*)-**1a** gave (S_{ma})-**5** (77% *ee*).

More excitingly, the high stereoselectivity observed in the AT-CuAAC reaction of azides **1** bearing a polarized NH presents the opportunity for the direct synthesis of MAC rotaxanes without the need for first forming separable co-conformational diastereomers; if the N substituent is too small to trap the macrocycle in one triazole-containing compartment, the only fixed stereochemistry in the product is provided by the MAC stereogenic unit. Thus, the reaction of primary amine-containing azide (*R*)-**1e** with macrocycle **2** and alkyne **3** at rt gave MAC rotaxane **15** directly but in low stereoselectivity (16% *ee*, Scheme 6, entry 1), which increased when the reaction was performed at −40 °C (28% *ee*, entry 2) and improved further still at −78 °C (42% *ee*, entry 3). CSP-HPLC analysis of a sample of rotaxane (R_{ma})-**15** produced from (*R*)-**1a** (Scheme 5) and comparison with the same product from (*R*)-**1f** confirmed that the latter also produces (R_{ma})-**15** as the major product (Figure 4a).

Scheme 6. Direct Synthesis of Enantioenriched Mechanically Axially Chiral Rotaxanes 15 and 16[a]

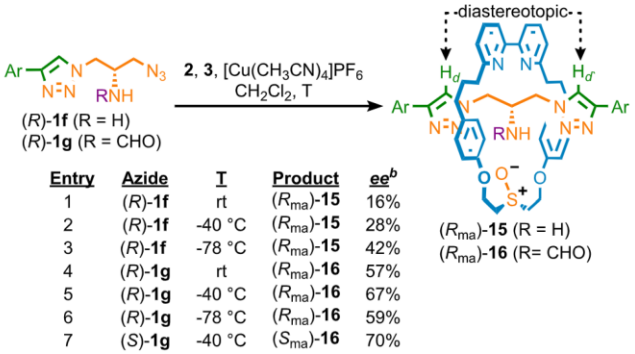

Entry	Azide	T	Product	ee[b]
1	(*R*)-**1f**	rt	(R_{ma})-**15**	16%
2	(*R*)-**1f**	-40 °C	(R_{ma})-**15**	28%
3	(*R*)-**1f**	-78 °C	(R_{ma})-**15**	42%
4	(*R*)-**1g**	rt	(R_{ma})-**16**	57%
5	(*R*)-**1g**	-40 °C	(R_{ma})-**16**	67%
6	(*R*)-**1g**	-78 °C	(R_{ma})-**16**	59%
7	(*S*)-**1g**	-40 °C	(S_{ma})-**16**	70%

[a]Reagents and conditions: i. **1** (1.1 equiv), **2** (1 equiv), **3** (1.1 equiv), [Cu(CH$_3$CN)]PF$_6$ (0.96 equiv), ^{i}Pr$_2$EtN (2 equiv), CH$_2$Cl$_2$, 16 h. [b]Determined by analytical CSP-HPLC. Ar = 3,5-di-^{t}Bu-C$_6$H$_3$.

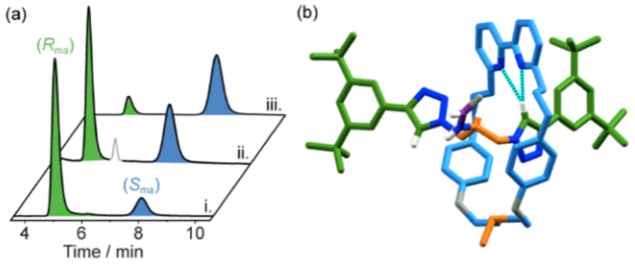

Figure 4. (a) CSP-HPLC analysis of i. (R_{ma})-**16** (67% *ee*) produced from (*R*)-**1g**; ii. (R_{ma})-**16** (21% *ee*) produced from (R_{ma})-**15** (21% ee; minor impurity highlighted in gray), and iii. (S_{ma})-**16** (70% *ee*) produced from (*S*)-**1g**. (b) Solid-state structure of *rac*-**16**, in which the N−H···O bond between the SO unit and the amide is intermolecular (colors as in Scheme 6, including the sulfoxide (SO) moiety to highlight the differentiation of the macrocycle faces, except N [dark blue], O [gray], and H [white]). The majority of H was omitted for clarity.

When instead formamide-containing azide (*R*)-**1g** was reacted with **2** and **3**, even at rt rotaxane **16**[31] was obtained in reasonable stereopurity (57% *ee*, entry 3), which was improved further at −40 °C (67% *ee*, entry 4). Conducting this reaction at −78 °C reduced the observed stereoselectivity (59% *ee*, entry 5), suggesting that, as with azide **1d**, the pre-equilibrium and kinetic resolution steps result in an unusual temperature dependence. CSP-HPLC analysis of a sample of rotaxane **16** produced by formylation of a sample of rotaxane (R_{ma})-**15** of known stereopurity and comparison with the same compound produced from (*R*)-**1g** confirmed that the latter produces (R_{ma})-**16** as the major stereoisomer. When (*S*)-**1g** was reacted instead, (S_{ma})-**16** was produced (70% *ee*, entry 6). The solid-state structure of **16** obtained by SCXRD (Figure 4b) did not display the expected intermolecular NH···O H-bond; instead, the same interaction was found to occur in an intermolecular fashion within the unit cell.

The different co-conformational behaviors of **4a**, **15**, and **16** are clear from the analysis of their respective ^{1}H NMR spectra. Diastereomers (R_{ma},R_{co-c})-**4a** and (S_{ma},R_{co-c})-**4a** are separable species; heating a mixture of diastereomers **4a** resulted in no change in their ratio (Figure S47), confirming that the macrocycle cannot shuttle between the two compartments due to the large NHBoc unit. In contrast, the diastereotopic triazole resonances H$_d$[32] of amine rotaxane **15** appear as two sharp singlets at 298 K, indicating that diastereomeric co-conformations (R_{ma},R_{co-c})-**15** and (S_{ma},R_{co-c})-**15** are in fast exchange on the ^{1}H NMR timescale through rapid shuttling of the macrocycle between the two triazole-containing compartments (Figure S190). The same resonances for formamide rotaxane **16** are broad at 298 K, although once again, only two signals are observed (Figure S200). This observation is consistent with (R_{ma},R_{co-c})-**16** and (S_{ma},R_{co-c})-**16** exchanging on the ^{1}H NMR timescale, albeit more slowly than (R_{ma},R_{co-c})-**15** and (S_{ma},R_{co-c})-**15**, in keeping with the larger steric bulk of the formamide group of **16**. Accordingly, increasing the temperature resulted in the sharpening of the two resonances corresponding to protons H$_d$ (Figure S211).

CONCLUSIONS

In conclusion, we have demonstrated that type 1 rotaxane mechanical geometric isomers and mechanically axially chiral enantiomers can be obtained by controlling facial selectivity in an AT-CuAAC synthesis. Specifically, we show that an H-bonding interaction between a prochiral macrocycle and a functional group contained in one of the two half-axles (rotaxane synthesis) or unsymmetrically disposed in the corresponding pre-macrocycle structure (catenane synthesis) appears to be sufficient to control the reaction outcome. Although the focus of our discussion has been on reaction stereoselectivities, it should be noted that, as is typically the case for AT-CuAAC reactions mediated by bipyridine macrocycles,[33] all of the interlocked structures reported were obtained in good to excellent isolated yield (50−90%, see the SI for details). The high selectivity observed with optimized substrates allowed us to design a direct enantioselective synthesis of mechanically axially chiral rotaxanes, only the second[34a] example of a direct stereoselective synthesis of a mechanically chiral molecule and the first of this recently identified stereogenic unit. To date, type 1 mechanical geometric isomers of rotaxanes based on calixarenes and similar cone-shaped macrocycles,[5,8b,6d,e] as well as structures expressing combinations of mechanical and covalent stereochemistry[4h] have been investigated as components of molecular switches and motors. Here, we have demonstrated that such isomerism can be expressed and controlled in much simpler macrocycles, opening up new motifs for study. Similarly, mechanically planar chiral molecules, for which

https://doi.org/10.1021/jacs.3c14329
J. Am. Chem. Soc. 2024, 146, 9134−9141

stereoselective methods are known,[14,26,34] have been investigated as enantioselective sensors,[29] catalysts,[30] and chiroptical switches.[35] With methodological concepts now in hand to efficiently synthesize their mechanically axially chiral cousins in high stereopurity, we eagerly anticipate the chemical applications to which molecules containing this stereogenic unit will soon be put.

■ ASSOCIATED CONTENT

Data Availability Statement

Characterization data for reported compounds is available from the University of Birmingham UBIRA eData repository at https://doi.org/10.25500/edata.bham.00001077.

Supporting Information

The Supporting Information is available free of charge at https://pubs.acs.org/doi/10.1021/jacs.3c14329.

Procedures and full characterization data (NMR, MS, CD, SCXRD, HPLC as appropriate) for all novel compounds and discussion (PDF)

Accession Codes

CCDC 2303663, 2307076, and 2307119−2307122 contain the supplementary crystallographic data for this paper. These data can be obtained free of charge via www.ccdc.cam.ac.uk/data_request/cif, by emailing data_request@ccdc.cam.ac.uk, or by contacting The Cambridge Crystallographic Data Centre, 12 Union Road, Cambridge CB2 1EZ, U.K.; fax: +44 1223 336033.

■ AUTHOR INFORMATION

Corresponding Author

Stephen M. Goldup − *Chemistry, University of Southampton, Southampton SO17 1BJ, U.K.; School of Chemistry, University of Birmingham, Birmingham B15 2TT, U.K.;* orcid.org/0000-0003-3781-0464; Email: s.m.goldup@bham.ac.uk

Authors

Peter R. Gallagher − *Chemistry, University of Southampton, Southampton SO17 1BJ, U.K.; School of Chemistry, University of Birmingham, Birmingham B15 2TT, U.K.;* orcid.org/0000-0002-5501-523X

Andrea Savoini − *Chemistry, University of Southampton, Southampton SO17 1BJ, U.K.; School of Chemistry, University of Birmingham, Birmingham B15 2TT, U.K.;* orcid.org/0000-0002-8333-406X

Abed Saady − *Chemistry, University of Southampton, Southampton SO17 1BJ, U.K.; School of Chemistry, University of Birmingham, Birmingham B15 2TT, U.K.*

John R. J. Maynard − *Chemistry, University of Southampton, Southampton SO17 1BJ, U.K.*

Patrick W. V. Butler − *Chemistry, University of Southampton, Southampton SO17 1BJ, U.K.*

Graham J. Tizzard − *Chemistry, University of Southampton, Southampton SO17 1BJ, U.K.*

Complete contact information is available at: https://pubs.acs.org/10.1021/jacs.3c14329

Author Contributions

[§]P.R.G. and A.S. contributed equally to this work.

Notes

The authors declare no competing financial interest.

■ ACKNOWLEDGMENTS

S.M.G. thanks the ERC (Agreement no. 724987) and Royal Society (IEC\R3\193163) for funding and the Royal Society for a Wolfson Research Fellowship (RSWF\FT\180010). A. Saady thanks the Council for Higher Education-Israel for a personal fellowship. A. Savoini thanks the Royal Society and the University of Birmingham for funding. P.R.G. thanks the University of Southampton and the University of Birmingham for funding. P.W.V.B. thanks the University of Southampton for a Presidential Scholarship.

■ REFERENCES

(1) Bruns, C. J.; Stoddart, J. F. *The Nature of the Mechanical Bond: From Molecules to Machines*; Wiley, 2016.

(2) Schill, G. *Catenanes, Rotaxanes and Knots*; Academic Press: New York, 1971.

(3) We have recently identified a second form of rotaxane geometric stereochemistry and so have proposed that these are disambiguated by the addition of the type 1/2 label: Savoini, A.; Gallagher, P. R.; Saady, A.; Goldup, S. M. The Final Stereogenic Unit of [2]Rotaxanes: Type 2 Geometric Isomers. *J. Am. Chem. Soc.* **2024**, DOI: 10.1021/jacs.3c14594.

(4) The stereochemistry of rotaxanes and catenanes whose macrocycle contains one or more covalent stereogenic centre in the main chain (e.g., as found in cyclodextrin rings) and whose axle/second ring respectively are oriented can be fully described by a covalent stereodescriptor and either a mechanical planar stereolabel or mechanical geometric stereolabel. We prefer the mechanically planar description as, in the case of catenanes, this typically although not always[34g] refers to a topological source of stereochemistry, one of the unusual properties of such systems. For selected examples of structures that conform to this class of molecule see: (a) Armspach, D.; Ashton, P. R.; Ballardini, R.; Balzani, V.; Godi, A.; Moore, C. P.; Prodi, L.; Spencer, N.; Stoddart, J. F.; Tolley, M. S.; Wear, T. J.; Williams, D. J.; Stoddart, J. F. Catenated Cyclodextrins. *Chem. - Eur. J.* **1995**, *1* (1), 33−55. (b) Craig, M. R.; Hutchings, M. G.; Claridge, T. D. W.; Anderson, H. L. Rotaxane-encapsulation enhances the stability of an azo dye, in solution and when bonded to cellulose. *Angew. Chem., Int. Ed.* **2001**, *40* (6), 1071−1074. (c) Wang, Q. C.; Ma, X.; Qu, D. H.; Tian, H. Unidirectional threading synthesis of isomer-free [2]rotaxanes. *Chem. - Eur. J.* **2006**, *12* (4), 1088−1096. (d) Bruns, C.J. Exploring and Exploiting the Symmetry-Breaking Effect of Cyclodextrins in Mechanomolecules. *Symmetry* **2019**, *11* (10), No. 1249. (e) Makita, Y.; Kihara, N.; Takata, T. Synthesis and kinetic resolution of directional isomers of [2]rotaxanes bearing a lariat crown ether wheel. *Supramol. Chem.* **2021**, *33* (1−2), 1−7. (f) Schröder, H. V.; Zhang, Y.; Link, A. J. Dynamic covalent self-assembly of mechanically interlocked molecules solely made from peptides. *Nat. Chem.* **2021**, *13* (9), 850−857. (g) Lopez-Leonardo, C.; Saura-Sanmartin, A.; Marin-Luna, M.; Alajarin, M.; Martinez-Cuezva, A.; Berna, J. Ring-to-Thread Chirality Transfer in [2]-Rotaxanes for the Synthesis of Enantioenriched Lactams. *Angew. Chem., Int. Ed.* **2022**, *61* (39), No. e202209904. (h) Liu, E.; Cherraben, S.; Boulo, L.; Troufflard, C.; Hasenknopf, B.; Vives, G.; Sollogoub, M. A molecular information ratchet using a cone-shaped macrocycle. *Chem* **2023**, *9* (5), 1147−1163.

(5) Selected examples: (a) Arduini, A.; Ciesa, F.; Fragassi, M.; Pochini, A.; Secchi, A. Selective synthesis of two constitutionally isomeric oriented calix[6]arene-based rotaxanes. *Angew. Chem., Int. Ed.* **2005**, *44* (2), 278−281. (b) Arduini, A.; Bussolati, R.; Credi, A.; Faimani, G.; Garaudee, S.; Pochini, A.; Secchi, A.; Semeraro, M.; Silvi, S.; Venturi, M. Towards controlling the threading direction of a calix[6]arene wheel by using nonsymmetric axles. *Chem. - Eur. J.* **2009**, *15* (13), 3230−3242. (c) Pierro, T.; Gaeta, C.; Talotta, C.; Casapullo, A.; Neri, P. Fixed or invertible calixarene-based directional shuttles. *Org. Lett.* **2011**, *13* (10), 2650−2653. (d) Arduini, A.; Bussolati, R.; Credi, A.; Secchi, A.; Silvi, S.; Semeraro, M.; Venturi, M.

Toward directionally controlled molecular motions and kinetic intra- and intermolecular self-sorting: threading processes of nonsymmetric wheel and axle components. *J. Am. Chem. Soc.* **2013**, *135* (26), 9924−9930. (e) Ciao, R.; Talotta, C.; Gaeta, C.; Margarucci, L.; Casapullo, A.; Neri, P. An oriented handcuff rotaxane. *Org. Lett.* **2013**, *15* (22), 5694−5697. (f) Zanichelli, V.; Ragazzon, G.; Arduini, A.; Credi, A.; Franchi, P.; Orlandini, G.; Venturi, M.; Lucarini, M.; Secchi, A.; Silvi, S. Synthesis and Characterization of Constitutionally Isomeric Oriented Calix[6]arene-Based Rotaxanes. *Eur. J. Org. Chem.* **2016**, *2016* (5), 1033−1042. (g) La Manna, P.; Talotta, C.; Gaeta, C.; Soriente, A.; De Rosa, M.; Neri, P. Threading of an Inherently Directional Calixarene Wheel with Oriented Ammonium Axles. *J. Org. Chem.* **2017**, *82* (17), 8973−8983. (h) Bazzoni, M.; Andreoni, L.; Silvi, S.; Credi, A.; Cera, G.; Secchi, A.; Arduini, A. Selective access to constitutionally identical, orientationally isomeric calix[6]arene-based [3]rotaxanes by an active template approach. *Chem. Sci.* **2021**, *12* (18), 6419−6428. (i) Cera, G.; Arduini, A.; Secchi, A.; Credi, A.; Silvi, S. Heteroditopic Calix[6]arene Based Intervowen and Interlocked Molecular Devices. *Chem. Rec.* **2021**, *21* (5), 1161−1181. (j) Andreoni, L.; Bonati, F. C.; Groppi, J.; Balestri, D.; Cera, G.; Credi, A.; Secchi, A.; Silvi, S. Selective enhancement of organic dye properties through encapsulation in rotaxane orientational isomers. *Chem. Commun.* **2023**, *59* (33), 4970−4973.

(6) Selected examples: (a) Xue, M.; Su, Y. S.; Chen, C. F. Isomeric squaraine-based [2]pseudorotaxanes and [2]rotaxanes: synthesis, optical properties, and their tubular structures in the solid state. *Chem. - Eur. J.* **2010**, *16* (28), 8537−8544. (b) Xia, Y.-X.; Xie, T.; Han, Y.; Chen, C.-F. Triptycene-derived calix[6]arene analogues: synthesis, structure and complexation with paraquat derivatives. *Org. Chem. Front.* **2014**, *1* (2), 140−147. (c) Wang, H. X.; Meng, Z.; Xiang, J. F.; Xia, Y. X.; Sun, Y.; Hu, S. Z.; Chen, H.; Yao, J.; Chen, C. F. Guest-dependent directional complexation based on triptycene derived oxacalixarene: formation of oriented rotaxanes. *Chem. Sci.* **2016**, *7* (1), 469−474. (d) Cui, J. S.; Ba, Q. K.; Ke, H.; Valkonen, A.; Rissanen, K.; Jiang, W. Directional Shuttling of a Stimuli-Responsive Cone-Like Macrocycle on a Single-State Symmetric Dumbbell Axle. *Angew. Chem., Int. Ed.* **2018**, *57* (26), 7809−7814. (e) Li, K. A.; Wang, Z.; Xie, C. D.; Chen, T.; Qiang, H.; Liu, Y. A.; Jia, X. S.; Hu, W. B.; Wen, K. Unidirectional complexation of pillar[4]arene[1]-benzoquinoneoxime with alkyl alcohols. *Org. Biomol. Chem.* **2019**, *17* (20), 4975−4978.

(7) (a) Li, K. A.; Wang, Z.; Xie, C. D.; Chen, T.; Qiang, H.; Liu, Y. A.; Jia, X. S.; Hu, W. B.; Wen, K. Unidirectional complexation of pillar[4]arene[1]benzoquinoneoxime with alkyl alcohols. *Org. Biomol. Chem.* **2019**, *17* (20), 4975−4978. (b) Wang, X.; Gan, Q.; Wicher, B.; Ferrand, Y.; Huc, I. Directional Threading and Sliding of a Dissymmetrical Foldamer Helix on Dissymmetrical Axles. *Angew. Chem., Int. Ed.* **2019**, *58* (13), 4205−4209.

(8) (a) Gaeta, C.; Talotta, C.; Mirra, S.; Margarucci, L.; Casapullo, A.; Neri, P. Catenation of calixarene annulus. *Org. Lett.* **2013**, *15* (1), 116−119. (b) Zanichelli, V.; Dallacasagrande, L.; Arduini, A.; Secchi, A.; Ragazzon, G.; Silvi, S.; Credi, A. Electrochemically Triggered Co-Conformational Switching in a [2]catenane Comprising a Non-Symmetric Calix[6]arene Wheel and a Two-Station Oriented Macrocycle. *Molecules* **2018**, *23* (5), No. 1156.

(9) For a detailed discussion of facial dissymmetry in interlocked structures see ref 11.

(10) Saito, F.; Bode, J. W. Synthesis and stabilities of peptide-based [1]rotaxanes: molecular grafting onto lasso peptide scaffolds. *Chem. Sci.* **2017**, *8* (4), 2878−2884.

(11) Maynard, J. R. J.; Gallagher, P.; Lozano, D.; Butler, P.; Goldup, S. M. Mechanically axially chiral catenanes and noncanonical mechanically axially chiral rotaxanes. *Nat. Chem.* **2022**, *14* (9), 1038−1044.

(12) (a) Jamieson, E. M. G.; Modicom, F.; Goldup, S. M. Chirality in rotaxanes and catenanes. *Chem. Soc. Rev.* **2018**, *47* (14), 5266−5311. (b) Pairault, N.; Niemeyer, J. Chiral Mechanically Interlocked Molecules - Applications of Rotaxanes, Catenanes and Molecular Knots in Stereoselective Chemosensing and Catalysis. *Synlett* **2018**, *29* (6), 689−698. (c) Evans, N. H. Chiral Catenanes and Rotaxanes: Fundamentals and Emerging Applications. *Chem. - Eur. J.* **2018**, *24* (13), 3101−3112.

(13) Frisch, H. L.; Wasserman, E. Chemical Topology. *J. Am. Chem. Soc.* **1961**, *83*, 3789−3795.

(14) Maynard, J. R. J.; Goldup, S. M. Strategies for the Synthesis of Enantiopure Mechanically Chiral Molecules. *Chem* **2020**, *6* (8), 1914−1932.

(15) Denis, M.; Goldup, S. M.The active template approach to interlocked molecules. *Nat. Rev. Chem.* 2017, *1* (8), 0061.

(16) Aucagne, V.; Hanni, K. D.; Leigh, D. A.; Lusby, P. J.; Walker, D. B. Catalytic ″click″ rotaxanes: a substoichiometric metal-template pathway to mechanically interlocked architectures. *J. Am. Chem. Soc.* **2006**, *128* (7), 2186−2187.

(17) Saady, A.; Goldup, S. M. Triazole formation and the click concept in the synthesis of interlocked molecules. *Chem* **2023**, *9* (8), 2110−2127.

(18) The suffix “ma” indicates that the label refers to the mechanical axial stereogenic unit. The suffix “co-c” indicates that the stereochemical label refers to the co-conformational covalent stereogenic unit.[11]

(19) We note that others have referred to such co-conformational covalent stereochemistry as “mechanical point chirality” (Cakmak, Y.; Erbas-Cakmak, S.; Leigh, D. A. Asymmetric Catalysis with a Mechanically Point-Chiral Rotaxane. *J. Am. Chem. Soc.* **2016**, *138* (6), 1749−1751.). We introduced the co-conformational covalent description[12a] as it is more precise and information rich; it highlights that that the stereogenic unit arises due to desymmetrization of a covalent pro-stereogenic unit and that these stereoisomers can in principle be converted by co-conformational movement. One of the reviewers of this manuscript suggested the term “co-configurational isomers” might be more useful and clearer for a nonexpert. We hesitate to adopt it here as changes in nomenclature should be properly discussed and put in the wider context of the field. However, we wanted to give credit to our anonymous reviewer for this intriguing suggestion and will consider its use in future.

(20) We note that the previously reported SCXRD structure of minor diastereomer (S_{ma},$R_{co\text{-}c}$)-**4a**[11] contains the same interaction but in this case it occurs intermolecularly between neighboring molecules in the unit cell, as observed for **4d** (Figure 1).

(21) (a) Neal, E. A.; Goldup, S. M. Competitive formation of homocircuit [3]rotaxanes in synthetically useful yields in the bipyridine-mediated active template CuAAC reaction. *Chem. Sci.* **2015**, *6* (4), 2398−2404. (b) Neal, E. A.; Goldup, S. M. A Kinetic Self-Sorting Approach to Heterocircuit [3]Rotaxanes. *Angew. Chem., Int. Ed.* **2016**, *55* (40), 12488−12493. (c) Modicom, F.; Jamieson, E. M. G.; Rochette, E.; Goldup, S. M. Chemical Consequences of the Mechanical Bond: A Tandem Active Template-Rearrangement Reaction. *Angew. Chem., Int. Ed.* **2019**, *58* (12), 3875−3879.

(22) Winn, J.; Pinczewska, A.; Goldup, S. M. Synthesis of a rotaxane Cu(I) triazolide under aqueous conditions. *J. Am. Chem. Soc.* **2013**, *135* (36), 13318−13321.

(23) We note that our results cannot rule out that either K_{eq} or $k_{SS}/_{SR}$ depends on a large negative entropy of reaction or activation respectively, which may also account for the unexpected temperature dependence of the AT-CuAAC reaction.

(24) The subscript is intended to indicate the mechanical origin of the stereochemistry. For a detailed discussion of how the mechanical stereogenic unit is assigned in such systems, see SI Section 8.

(25) Other combinations of solvent and temperature did not improve the reaction stereoselectivity. See SI Sction 9 for further details.

(26) (a) Jinks, M. A.; de Juan, A.; Denis, M.; Fletcher, C. J.; Galli, M.; Jamieson, E. M. G.; Modicom, F.; Zhang, Z.; Goldup, S. M. Stereoselective Synthesis of Mechanically Planar Chiral Rotaxanes. *Angew. Chem., Int. Ed.* **2018**, *57* (45), 14806−14810. (b) de Juan, A.; Lozano, D.; Heard, A. W.; Jinks, M. A.; Suarez, J. M.; Tizzard, G. J.; Goldup, S. M. A chiral interlocking auxiliary strategy for the synthesis

https://doi.org/10.1021/jacs.3c14329
J. Am. Chem. Soc. 2024, 146, 9134−9141

of mechanically planar chiral rotaxanes. *Nat. Chem.* **2022**, *14* (2), 179−187.

(27) Unfortunately, we were unable to determine the absolute stereochemistry of rotaxane **10** as crystals suitable for SCXRD analysis were not forthcoming.

(28) Lewis, J. E. M.; Modicom, F.; Goldup, S. M. Efficient Multicomponent Active Template Synthesis of Catenanes. *J. Am. Chem. Soc.* **2018**, *140* (14), 4787−4791.

(29) Hirose, K.; Ukimi, M.; Ueda, S.; Onoda, C.; Kano, R.; Tsuda, K.; Hinohara, Y.; Tobe, Y. The Asymmetry is Derived from Mechanical Interlocking of Achiral Axle and Achiral Ring Components -Syntheses and Properties of Optically Pure [2]-Rotaxanes. *Symmetry* **2018**, *10* (1), No. 20.

(30) Heard, A. W.; Goldup, S. M. Synthesis of a Mechanically Planar Chiral Rotaxane Ligand for Enantioselective. *Catalysis. Chem.* **2020**, *6* (4), 994−1006.

(31) ^{1}H NMR analysis of **16** confirmed that the ring is able to shuttle past the formamide unit. See SI Section 11.

(32) The ^{1}H spectra of rotaxanes **15** and **16** are extremely complicated because the mechanical bond renders any nuclei not related by single bond rotation (e.g., the ^{t}Bu groups of the axle unit) magnetically inequivalent; for example, all of the methylene protons flanking the amine unit in the axle are magnetically inequivalent. For this reason, when assigning the ^{1}H NMR spectra of these molecules (see the SI), we took the decision to assign different letters to carbon atoms (and the associated protons) whose equivalence is lifted by the mechanical bond and reserved prime notation to differentiate diastereotopic geminal protons. Thus, although the triazole protons of rotaxanes **15** and **16** are labelled in Scheme 6 as H_d and $H_{d'}$ in accordance with standard practice for diastereotopic signals to aid an intuitive understanding of the diagram, they are assigned as H_d and H_h in their characterization data.

(33) For recent examples of functionalized and functional molecules synthesized in good to excellent yield using the AT-CuAAC reaction mediated by bipyridine macrocycles see: (a) Zhang, Z.; Tizzard, G. J.; Williams, J. A. G.; Goldup, S. M. Rotaxane PtII-complexes: mechanical bonding for chemically robust luminophores and stimuli responsive behaviour. *Chem. Sci.* **2020**, *11* (7), 1839−1847. (b) Acevedo-Jake, A.; Ball, A. T.; Galli, M.; Kukwikila, M.; Denis, M.; Singleton, D. G.; Tavassoli, A.; Goldup, S. M. AT-CuAAC Synthesis of Mechanically Interlocked Oligonucleotides. *J. Am. Chem. Soc.* **2020**, *142* (13), 5985−5990. (c) Cirulli, M.; Salvadori, E.; Zhang, Z. H.; Dommett, M.; Tuna, F.; Bamberger, H.; Lewis, J. E. M.; Kaur, A.; Tizzard, G. J.; van Slageren, J.; Crespo-Otero, R.; Goldup, S. M.; Roessler, M. M. Rotaxane Co(II) Complexes as Field-Induced Single-Ion Magnets. *Angew. Chem., Int. Ed.* **2021**, *60* (29), 16051−16058. (d) Rajamalli, P.; Rizzi, F.; Li, W.; Jinks, M. A.; Gupta, A. K.; Laidlaw, B. A.; Samuel, I. D. W.; Penfold, T. J.; Goldup, S. M.; Zysman-Colman, E. Using the Mechanical Bond to Tune the Performance of a Thermally Activated Delayed Fluorescence Emitter. *Angew. Chem., Int. Ed.* **2021**, *60* (21), 12066−12073. (e) Maynard, J. R. J.; Galmes, B.; Stergiou, A. D.; Symes, M. D.; Frontera, A.; Goldup, S. M. Anion-pi Catalysis Enabled by the Mechanical Bond. *Angew. Chem., Int. Ed.* **2022**, *61* (12), No. e202115961. (g) Saady, A.; Malcolm, G.; Fitzpatrick, M.; Pairault, N.; Tizzard, G.; Mohammed, S.; Tavassoli, A.; Goldup, S. M. A Platform Approach to Cleavable Macrocycles for the Controlled Disassembly of Mechanically Caged Molecules. *Angew. Chem., Int. Ed.* **2024**, No. e202400344.

(34) (a) Denis, M.; Lewis, J. E. M.; Modicom, F.; Goldup, S. M. An Auxiliary Approach for the Stereoselective Synthesis of Topologically Chiral Catenanes. *Chem* **2019**, *5* (6), 1512−1520. (b) Tian, C.; Fielden, S. D. P.; Perez-Saavedra, B.; Vitorica-Yrezabal, I. J.; Leigh, D. A. Single-Step Enantioselective Synthesis of Mechanically Planar Chiral [2]Rotaxanes Using a Chiral Leaving Group Strategy. *J. Am. Chem. Soc.* **2020**, *142* (21), 9803−9808. (c) Imayoshi, A.; Lakshmi, B. V.; Ueda, Y.; Yoshimura, T.; Matayoshi, A.; Furuta, T.; Kawabata, T. Enantioselective preparation of mechanically planar chiral rotaxanes by kinetic resolution strategy. *Nat. Commun.* **2021**, *12* (1), No. 404. (d) Li, M. F.; Chia, X. L.; Tian, C.; Zhu, Y. Mechanically planar chiral rotaxanes through catalytic desymmetrization. *Chem* **2022**, *8* (10), 2843−2855. (e) Rodríguez-Rubio, A.; Savoini, A.; Modicom, F.; Butler, P.; Goldup, S. M. A Co-conformationally "Topologically" Chiral Catenane. *J. Am. Chem. Soc.* **2022**, *144* (27), 11927−11932. (f) Zhang, S.; Rodríguez-Rubio, A.; Saady, A.; Tizzard, G. J.; Goldup, S. M. A chiral macrocycle for the stereoselective synthesis of mechanically planar chiral rotaxanes and catenanes. *Chem* **2023**, *9* (5), 1195−1207. (g) Pairault, N.; Rizzi, F.; Lozano, D.; Jamieson, E. M. G.; Tizzard, G. J.; Goldup, S. M. A catenane that is topologically achiral despite being composed of oriented rings. *Nat. Chem.* **2023**, *15* (6), 781−786.

(35) (a) Gaedke, M.; Witte, F.; Anhauser, J.; Hupatz, H.; Schroder, H. V.; Valkonen, A.; Rissanen, K.; Lutzen, A.; Paulus, B.; Schalley, C. A. Chiroptical inversion of a planar chiral redox-switchable rotaxane. *Chem. Sci.* **2019**, *10* (43), 10003−10009. (b) Wang, Y.; Gong, J.; Wang, X.; Li, W. J.; Wang, X. Q.; He, X.; Wang, W.; Yang, H. B. Multistate Circularly Polarized Luminescence Switching through Stimuli-Induced Co-Conformation Regulations of Pyrene-Functionalized Topologically Chiral [2]Catenane. *Angew. Chem., Int. Ed.* **2022**, *61*, No. e202210542.

https://doi.org/10.1021/jacs.3c14329
J. Am. Chem. Soc. 2024, 146, 9134−9141

Appendix C: Published Research Article

The following research article reproduced in Chapter 4 is shown in its published version:

A. Savoini, P. R. Gallagher, A. Saady, S. M. Goldup, The Final Stereogenic Unit of [2]Rotaxanes: Type 2 Geometric Isomers. *J. Am. Chem. Soc.* **2024**, *146*, 8472–8479. https://doi.org/10.1021/jacs.3c14594

JACS
JOURNAL OF THE AMERICAN CHEMICAL SOCIETY
pubs.acs.org/JACS

Article

The Final Stereogenic Unit of [2]Rotaxanes: Type 2 Geometric Isomers

Andrea Savoini,[§] Peter R. Gallagher,[§] Abed Saady,[§] and Stephen M. Goldup*

Cite This: J. Am. Chem. Soc. 2024, 146, 8472−8479

ABSTRACT: Mechanical stereochemistry arises when the interlocking of stereochemically trivial covalent subcomponents results in a stereochemically complex object. Although this general concept was identified in 1961, the stereochemical description of these molecules is still under development to the extent that new forms of mechanical stereochemistry are still being identified. Here, we present a simple analysis of rotaxane and catenane stereochemistry that allowed us to identify the final missing simple mechanical stereogenic unit, an overlooked form of rotaxane geometric isomerism, and demonstrate its stereoselective synthesis.

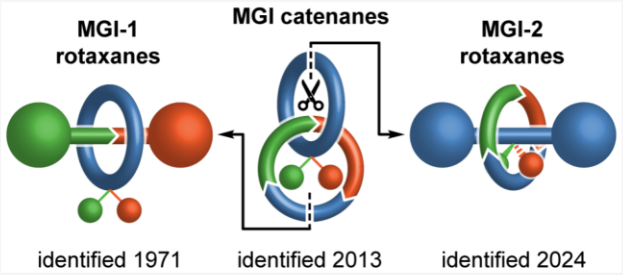

INTRODUCTION

In 1961,[1] Wasserman and Frisch recognized that interlocking two non-stereogenic rings can result in a chiral catenane where the enantiomers are related by inverting the relative orientations of the two rings.[2] A decade later,[3] Schill identified a similar phenomenon when a ring encircles an axle in a rotaxane, and that geometric isomerism is also possible in such systems. Since these first reports, the pantheon of mechanical stereogenic units in simple [2]catenanes and [2]rotaxanes has expanded beyond those envisaged by Wassermann and Frisch, and Schill; in 2013,[4] Gaeta and Neri recognized that catenanes can also express mechanical geometric isomerism and more recently, we identified a previously overlooked class of mechanically chiral rotaxanes[5a] and reanalyzed the planar chiral stereochemistry of catenanes to show that, although they were hitherto simply described as "topologically chiral", this is not an essential characteristic of this stereogenic unit.[6]

The recent discovery of new conditional[7] mechanical stereogenic units contrasts with covalent organic stereochemistry where, although new pathways of isomerization[8] and previously overlooked expressions of atropisomerism[9] have recently been reported, the archetypal stereogenic units (centers, axes, planes, helices, and multiple bonds)[10] are long-established. This raises an obvious question; are there any mechanical stereogenic units of [2]catenanes and [2]rotaxanes still lying undetected? Here, we provide a simple stereochemical analysis that shows the answer is yes. Working from first-principles we identify a previously overlooked rotaxane geometric stereogenic unit but also demonstrate that this is the final one to be found; our pantheon is now complete (Figure 2). Using concepts developed for the synthesis of chiral rotaxanes, we demonstrate the first stereoselective synthesis of these new type 2 rotaxane mechanical geometric isomers.

RESULTS AND DISCUSSION

Examining the Achiral Building Blocks of [2]-Catenanes Confirms that the Set of Known Stereogenic Units is Complete. We first recognize that the highest symmetry ring point group, $D_{\infty h}$, contains the achiral D_{nd}, C_{nh}, C_{nv}, and S_{2n} subgroups and that therefore rings of these symmetries are the complete set of building blocks of catenane mechanical stereochemistry (see Supporting Information Section 1 for further discussion). Second, we recognize that any ring that has a C_2-axis in the macrocycle plane $[C_{2(x)}]$[11] cannot give rise to a conditional mechanical stereogenic unit because this symmetry operation of the separated rings corresponds to the notional process of switching their relative orientations in the corresponding [2]catenane (Figure 1a). Although this observation appears obvious, to our knowledge, this is the first time it has been stated explicitly.[12] Thus, we can discard rings of D_{nd}, and $C_{2v(x)}$ and $C_{2h(x)}$ symmetry.[11,13,14]

The visually tractable D_{4h} point group contains the C_{4v}, C_{4h}, and S_4 subgroups, representative of C_{nv}, C_{nh}, and S_{2n}, and so we modified a D_{4h} ring to generate these structures by adding four equally spaced, equivalent vectors perpendicular and/or tangential to the ring plane in different relative orientations to highlight the key features of these achiral macrocycles (Figure 1b). Taking this approach, we find that to ensure that $C_{2(x)}$ is not a symmetry operation of the ring, it must either be oriented (C_{nh} or S_{2n}; characterized by vectors tangential to the

Received: December 22, 2023
Revised: February 12, 2024
Accepted: February 14, 2024
Published: March 18, 2024

https://doi.org/10.1021/jacs.3c14594
J. Am. Chem. Soc. 2024, 146, 8472−8479

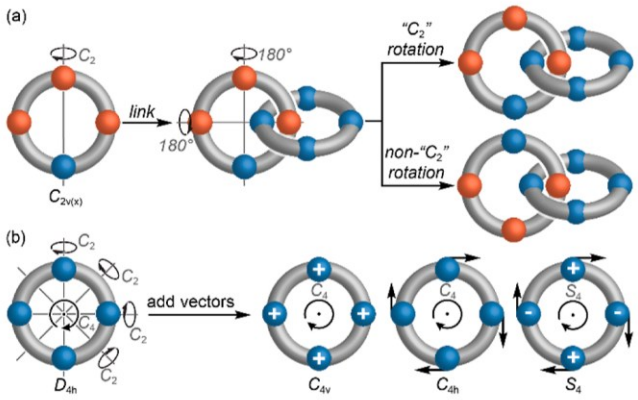

Figure 1. (a) Schematic demonstration that the $C_{2(x)}$[11] symmetry operation of a non-interlocked ring corresponds to the notional process of inverting the relative ring orientations in a [2]catenane; hence, any ring for which $C_{2(x)}$ is a symmetry operation cannot give rise to conditional mechanical stereoisomers. (b) Conversion of a D_{4h} symmetric structure to rings of C_{4v}, C_{4h}, and S_4 symmetry, which we propose to be representative of the complete set of oriented (C_{nh} and S_{2n}) and facially dissymmetric (C_{nv}) building blocks of catenane stereochemistry, by the addition of simple vectors (± refer to vectors projecting up/down, respectively, perpendicular to the plane of the ring).

ring circumference that define its direction), or facially dissymmetric (C_{nv}; characterized by vectors perpendicular to the ring plane that differentiate its faces).

The requirement for the rings of a [2]catenane to be oriented or facially dissymmetric for mechanical stereochemistry to arise is not a new observation; combining two oriented C_{nh} rings or two facially dissymmetric C_{nv} rings gives rise to the chiral catenanes originally identified by Wasserman and Frisch,[1] illustrated here using rings of C_{1h} and C_{1v} symmetry,[15] respectively (Figure 2a). The vectors associated with the orientation or facial dissymmetry of the individual rings can never become coplanar in the resultant catenanes, and thus, the stereochemistry of such structures can be defined using the resulting oriented skew lines.[16] The skew lines lie parallel to the associated ring when two oriented rings are combined but perpendicular to the rings when two facially dissymmetric rings are combined, which provides robust definitions of the canonical mechanically planar chiral (MPC) and mechanically axially chiral (MAC) stereogenic units of [2]catenanes, respectively. Thus, the only surprising result from our analysis is that S_{2n} symmetric rings are oriented and thus give rise to a mechanical stereogenic unit, which to the best of our knowledge has not previously been noted. However, we suggest that combining two S_{2n} macrocycles (or a combination of S_{2n} and C_{nh} rings) gives rise to the MPC stereogenic unit, as defined by the orientation of the skew lines associated with the rings, rather than a new form of mechanical stereochemistry.[17]

Finally, combining one facially dissymmetric C_{nv} ring and one oriented C_{nh} (or S_{2n}) ring results in an achiral structure because the associated skew lines can be made coplanar in the interlocked structure. However, two mechanical geometric isomers (MGI) are possible because the vectors can be arranged syn (Z_m) or anti (E_m) (Figure 2a).[18]

Analyzing the Achiral Building Blocks of Rotaxanes Reveals the Final Mechanical Stereogenic Unit. The same analysis can be used to identify the axle point group

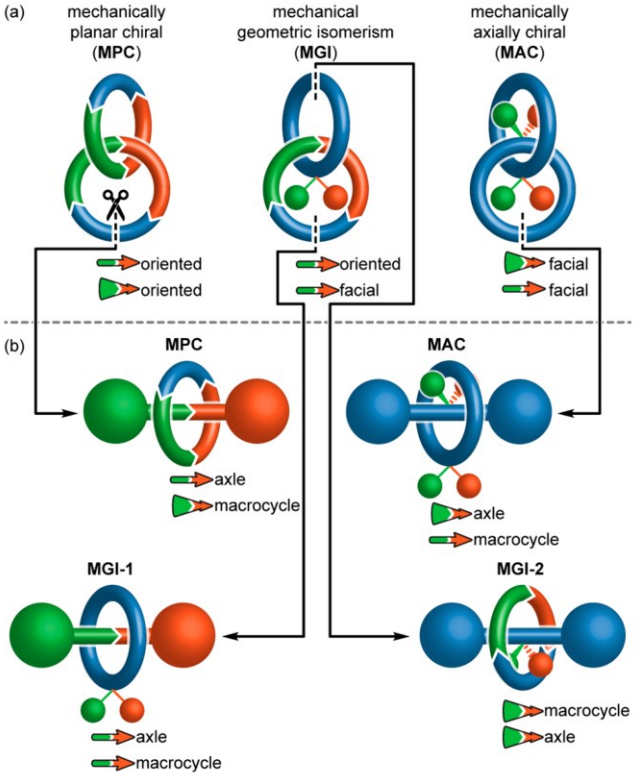

Figure 2. (a) Complete set of catenane mechanical stereogenic units that can be constructed from the archetypal rings identified (Figure 1) and their relationship with the (b) mechanical stereogenic units of rotaxanes via a notional ring-opening-and-stoppering operation, including the newly identified "type 2" rotaxane mechanical geometric unit. The vectors shown characterize their stereochemistry and their relationship to the components that gives rise to them defines the stereogenic unit.

symmetries that can give rise to mechanical stereochemistry in a rotaxane and thus the complete set of rotaxane stereogenic units (see Supporting Information Section 2). However, the same result is reached more intuitively by identifying that rotaxanes and catenanes are interconverted by a notional ring-opening-and-stoppering operation (Figure 2b), which, as previously noted, leads to the conclusion that MPC catenanes and rotaxanes are directly related,[6] as are the MAC pair.[5a] Once again, these rotaxane stereogenic units can be differentiated by considering the relative orientation of the skew lines that characterize their configuration; the MPC stereogenic unit of rotaxanes is defined as arising when the vector associated with the axle lies along its axis, whereas the MAC stereogenic unit arises when the vector associated with the axle is perpendicular to its axis. These axle vectors lie perpendicular to the vector associated with the ring when interlocked with oriented or facially dissymmetric rings, respectively.

It is when we turn to the MGI stereogenic unit of catenanes that we find a surprise. Because the two rings are distinct, there are two possible products of the opening-and-stoppering sequence, one of which is the canonical MGI rotaxane stereogenic unit identified by Schill, and the other is a previously overlooked form of rotaxane geometric isomerism. The former is characterized by the coplanar vectors associated with the two components lying parallel to the axle, whereas in the latter, these vectors lie perpendicular to the axle. We propose that the labels "type 1" and "type 2" are used to

https://doi.org/10.1021/jacs.3c14594
J. Am. Chem. Soc. 2024, 146, 8472−8479

distinguish between the canonical and noncanonical geometric isomers of rotaxanes (MGI-1 and MGI-2, respectively), with the numeral assigned by the order in which they were identified.

Catenane and Rotaxane Stereochemistry—Conclusions. Our simple, first-principles approach has allowed us to unambiguously identify and define all the possible conditional stereogenic units of rotaxanes and catenanes and confirm that, now that a previously overlooked MGI-2 rotaxane stereochemistry has been found, the pantheon of unique stereogenic units is complete. Based on this analysis, methods exist to stereoselectively synthesize all conditional mechanical stereogenic units of [2]catenanes and [2]rotaxanes apart from MGI-2 rotaxanes; although until 2014,[19] chiral stationary phase high-performance liquid chromatography (HPLC) was required to produce enantioenriched samples of mechanically chiral molecules[20] since this time, methodologies[21] for the stereoselective synthesis of MPC[6,13,22,23] and MAC[5] catenanes and rotaxanes have been disclosed. Similarly, the first stereoselective synthesis of MGI-1 rotaxanes was reported in 2005[24] using calixarene rings, and since then many examples based on cone-shaped macrocycles,[25] and more recently simple prochiral[26] rings,[5b,27] have been reported. The corresponding MGI catenanes are less well studied but yield to similar strategies to the corresponding rotaxanes.[4,5b,28]

Retrosynthetic Analysis of the "New" MGI-2 Stereogenic Unit. Having identified the MGI-2 stereogenic unit, we considered what strategies could be used for its selective synthesis. Notionally, the challenge in the synthesis of MGI-2 rotaxanes is the same as that of MPC rotaxanes—how to thread an oriented ring onto an axle with control over their relative orientation (Figure 3a). We previously achieved this for MPC rotaxanes[22a,e] using an active template[29] Cu-mediated alkyne−azide cycloaddition (AT-CuAAC[30,31]) approach, in which the intermediates leading to the different enantiomers are diastereomeric due to a covalent chiral auxiliary. This analysis suggests that a similar approach is possible in the case of MGI-2 rotaxanes (Figure 3b). Although it may seem counterintuitive to synthesize the achiral MGI-2 stereogenic unit using chiral starting materials, it should be noted that almost regardless of where the prochiral axle is subdivided,[32] a chiral starting material is produced. However, this is symmetrized during mechanical bond formation, so no additional auxiliary removal step is required. Furthermore, a racemic mixture of starting materials would lead to the same MGI-2 product mixture using this direct approach.

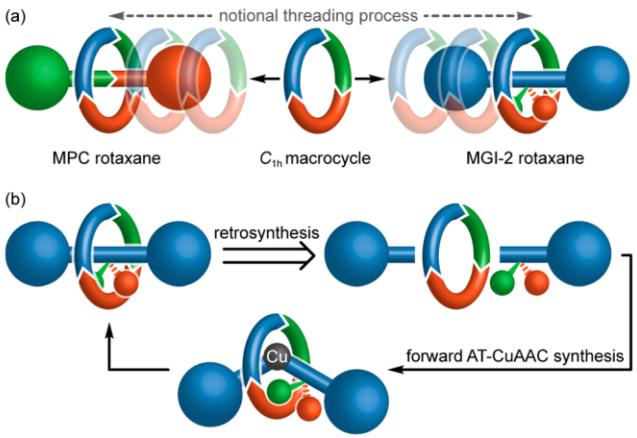

Figure 3. (a) Comparison of the MGI-2 and MPC stereogenic units highlighting the common challenge of selectively threading of an oriented ring onto an oriented or facially dissymmetric axle, respectively. (b) Retrosynthesis of the MGI-2 stereogenic unit using a direct AT-CuAAC approach. The forward reaction proceeds via two possible diastereomeric intermediates (one shown). Although one of the half-axle units is chiral, this is symmetrized in the forward reaction, and the same achiral, diastereomeric mixture is produced whether the starting material is enantiopure or racemic.

Attempted Direct Synthesis of MGI-2 Rotaxanes 5. Thus, we initially attempted the synthesis of a rotaxane expressing the MGI-2 stereogenic unit using a stepwise AT-CuAAC approach. Reaction of oriented macrocycle **1**,[33] alkyne **2**, and serine-based azide (*S*)-**3** under our AT-CuAAC conditions[22a] in CH_2Cl_2 gave rotaxane **4** as a mixture of diastereomers (17% *de*,[34] Scheme 1, entry 1) that differ in their MGI-2 configuration but have the same co-conformational covalent configuration, which is fixed due to the bulky NHBoc unit that prevents the macrocycle from shuttling between the two triazole compartments.

The same reaction in THF (entry 2) or EtOH (entry 3) gave lower selectivity (3 and 16% *de*, respectively), whereas lower temperatures (entries 4 and 5) gave increased selectivity at the expense of reduced conversion. Unfortunately, the (Z_m,$S_{co\text{-}c}$)-**4** and (E_m,$S_{co\text{-}c}$)-**4** diastereomers proved hard to separate; the best we could achieve was a 59% *de* sample starting from a 17% *de* sample after several rounds of chromatography. We were also unable to separate rotaxanes

Scheme 1. Poorly Selective Direct AT-CuAAC Synthesis of Type 2 Rotaxane Geometric Isomers 5 via Chiral Diastereomers 4[a]

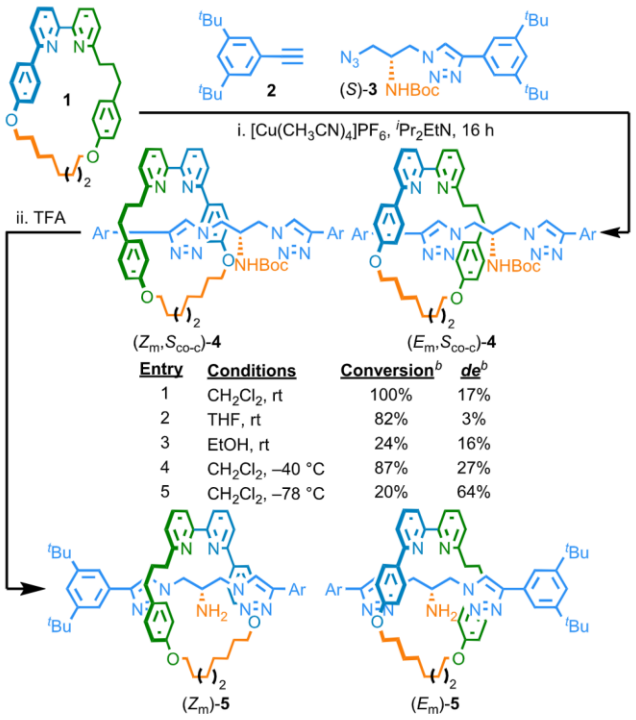

Entry	Conditions	Conversion[b]	*de*[b]
1	CH_2Cl_2, rt	100%	17%
2	THF, rt	82%	3%
3	EtOH, rt	24%	16%
4	CH_2Cl_2, −40 °C	87%	27%
5	CH_2Cl_2, −78 °C	20%	64%

[a]Reagents and conditions: (i) **1** (1 equiv), **2** (1.1 equiv), (*S*)-**3** (1.1 equiv), $[Cu(CH_3CN)_4]PF_6$ (0.97 equiv), $^iPr_2EtN$ (2 equiv). (ii) TFA, CH_2Cl_2, rt, 1 h. [b]Determined by ^1H NMR analysis of the crude reaction product. Ar = 3,5-di-^{t}Bu-C_6H_3.

https://doi.org/10.1021/jacs.3c14594
J. Am. Chem. Soc. 2024, 146, 8472−8479

5, which express only the MGI-2 stereogenic unit, obtained by removal of the Boc group from the mixture of rotaxanes **4**.

The disappointing stereoselectivity in the formation of rotaxanes **4** is perhaps unsurprising; we have previously identified that AT-CuAAC auxiliary approaches to MPC rotaxanes, which are analogous to the direct approach to the achiral MGI-2 stereogenic units presented here, only proceed efficiently when a sterically hindered α-chiral azide half-axle is used.[22a,e] This is hard to realize practically in the case of the MGI-2 stereogenic unit as it would nominally require iterative CuAAC couplings of a 1,1-bis-azide synthon. Thus, we returned to our comparison of the MPC and MGI-2 stereogenic units and recognized that our chiral interlocking auxiliary strategy,[19] which reliably loads macrocycle **1** onto the axle of almost any rotaxane in a specific orientation that is determined by the absolute stereochemistry of the amino acid-derived azide used, corresponds to the desired notional oriented threading process (Figure 3a).

Stereoselective Synthesis of MGI-2 Rotaxanes 11 Using an Interlocking Auxiliary Approach. Coupling of azide (*S*)-**6** with *o*-Me acetylene half-axle (*S*)-**7** in the presence of macrocycle **1** gave rotaxane (S,S,R_{mp})-**8** (Scheme 2), in which the macrocycle preferentially encircles the less hindered triazole unit, in excellent stereoselectivity (94% *de*). Subsequent Suzuki coupling produced rotaxane (S,S,R_{mp})-**9** as the major co-conformational isomer. Transesterification with MeOH gave rotaxane ($E_m,S_{co\text{-}c}$)-**10**, which contains an MGI-2 and a co-conformational stereogenic unit, in excellent stereopurity (92% *de*).[35] Removal of the Boc group provided rotaxane (E_m)-**11** that expresses only MGI-2 stereochemistry, again in high stereopurity (94% *de*). The same synthesis but starting from (*R*)-**6** and (*S*)-**7** gave ($Z_m,S_{co\text{-}c}$)-**10** (94% *de*), which was then converted to (Z_m)-**11** (92% *de*).

We note that the absolute MGI-2 configuration of the product of this interlocking auxiliary approach depends not on the enantiomer of chiral auxiliary **6** used but instead on the diastereomer of the axle produced in the first coupling step; the reaction of the (*S*)-**6**/(*S*)-**7** (Scheme 1) or (*R*)-**6**/(*R*)-**7** (not shown) pairs to give (S,S,R_{mp})-**8** or (R,R,S_{mp})-**8**, respectively, would both ultimately produce (E_m)-**11**. However, unlike in the case of a direct AT-CuAAC synthesis (Figure 3b and Scheme 1), a racemic mixture of starting materials would always lead to an equal mixture of MGI-2 isomers by using this approach.

Analysis of Rotaxanes 10 and 11. Rotaxanes ($E_m,S_{co\text{-}c}$)-**10** and ($Z_m,S_{co\text{-}c}$)-**10** have distinct ^{1}H NMR spectra (Figure 4b,d respectively) that each correspond to one of the inseparable isomers obtained using a direct AT-CuAAC approach to the same molecules (*c.f.*, **4**, see Supporting Information Section 4) (Figure 4c). The ^{1}H NMR spectra of the two geometric isomers of rotaxanes **11** (Figure 4a,e) are also distinct from one another, but they suggest molecules of much higher symmetry than rotaxanes **10**. This is not because the macrocycle preferentially encircles the amine unit; the high chemical shift of triazole protons H_h in rotaxanes **11** is consistent with the macrocycle exchanging between the two triazole containing compartments where it engages in a C−H···N H-bond.[36] Instead, and in contrast with MAC rotaxanes,[5] based on a similar prochiral axle, the two co-conformers of rotaxanes **11** are enantiomeric and so the H_h pair are enantiotopic and isochronous.

Interestingly, the absolute stereochemistry of the co-conformations of rotaxane **11** (Scheme 3), and that of static

Scheme 2. Chiral Interlocking Auxiliary Synthesis of MGI-2 Rotaxanes 10 and 11[a]

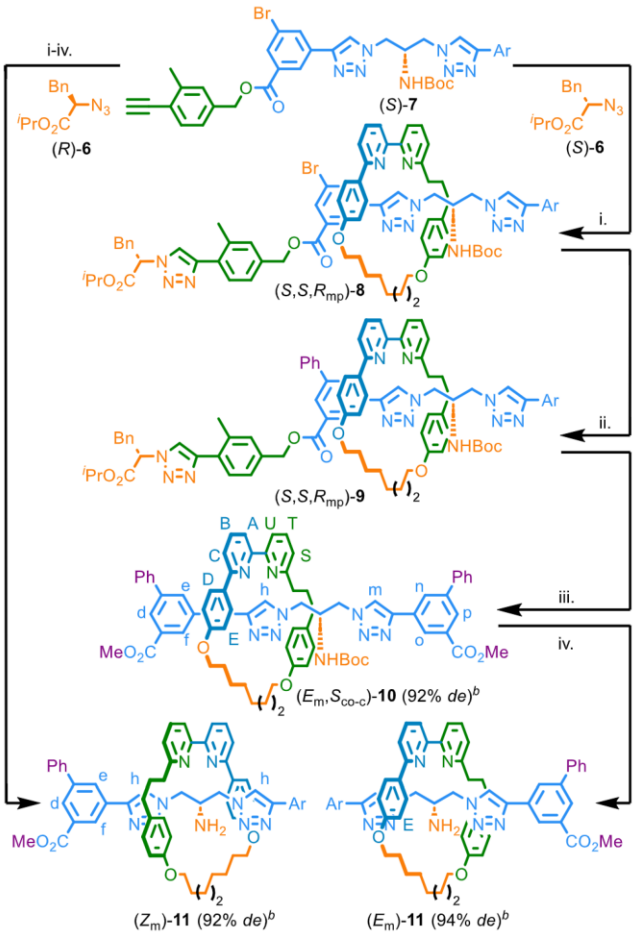

[a]Reagents and conditions: (i) **1** (1 equiv),**6** (1.1 equiv), (*S*)-**7** (1.1 equiv), $[Cu(CH_3CN)_4]PF_6$ (0.99 equiv), $^iPr_2Et$ (2 equiv), CH_2Cl_2, rt, 16 h. (ii) $PhB(OH)_2$, $Pd(PPh_3)_4$, K_2CO_3, acetone-^{i}PrOH-H_2O (2:1:1), 60 °C, 3 h. (iii) K_2CO_3, CH_2Cl_2-MeOH, rt, 3 h. (iv) TFA, CH_2Cl_2, rt, 1 h. [b]Determined by ^{1}H NMR analysis. Ar = 3-CO_2Me-5-Ph-C_6H_3.

diastereomers **4** and **10**, can be fully described using two of three possible stereolabels, of which we strongly prefer the co-conformational covalent and MGI-2 description as this captures the desymmetrization of the axle component upon shuttling and the sole fixed stereogenic unit of the molecule. The co-conformational MPC/MGI-2 description fails to capture the former, and the co-conformational covalent/co-conformational MPC description obscures the fixed MGI-2 unit, with both stereolabels inverting under co-conformational exchange (see Supporting Information Section 7 for an extended discussion).

■ CONCLUSIONS

In conclusion, we have presented a simple stereochemical analysis to identify the complete set of [2]catenane and [2]rotaxane mechanical stereoisomers and, in doing so, recognized a new form of rotaxane geometric isomerism. Furthermore, retrosynthetic analysis of the noncanonical type 2 geometric stereogenic unit allowed us to make the link to the mechanical planar chiral stereogenic unit of rotaxanes, which

https://doi.org/10.1021/jacs.3c14594
J. Am. Chem. Soc. 2024, 146, 8472−8479

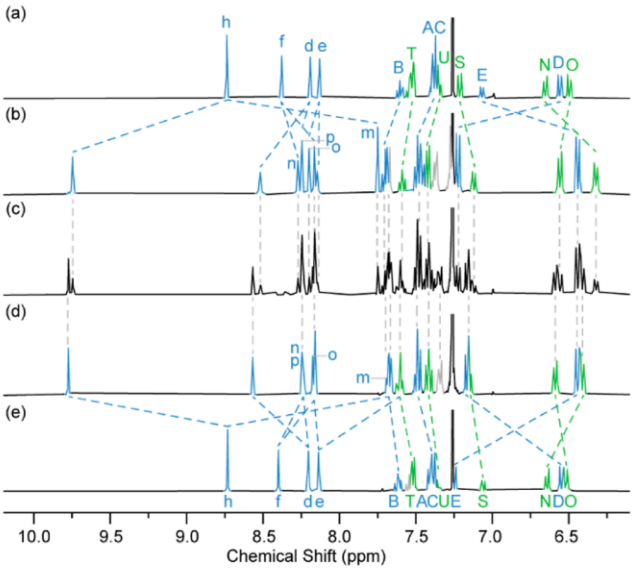

Figure 4. Partial ^{1}H NMR (400 MHz, $CDCl_3$, 298 K) spectra of (a) (Z_m)-**11** (92% *de*), (b) (Z_m,$S_{co\text{-}c}$)-**10** (94% *de*), (c) **10** (16% *de*, obtained by a direct AT-CuAAC coupling, see Supporting Information Section 4), and (d) (E_m,$S_{co\text{-}c}$)-**10** (92% *de*) (e) (E_m)-**11** (94% *de*). Peak assignment and colors are the same as shown in Scheme 2.

Scheme 3. Co-Conformational Exchange between the Enantiomeric Co-Conformations of Rotaxane (Z_m)-11 Highlighting the Different Stereochemical Labels that Can Be Applied to Fully Assign Their Absolute Stereochemistry[a]

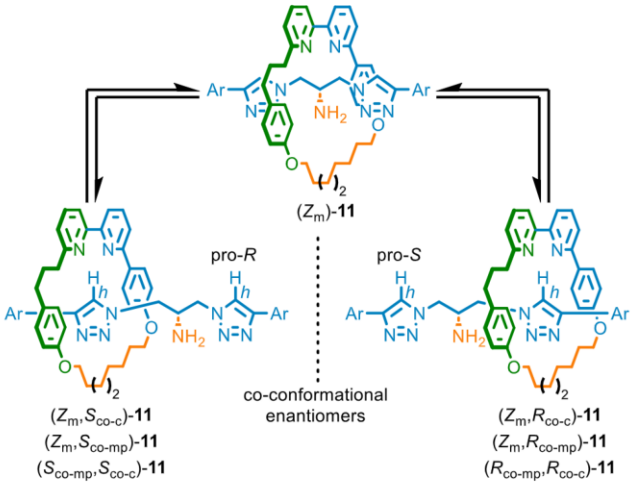

[a]Ar = 3-CO_2Me-5-Ph-C_6H_3.

led ultimately to the first stereoselective synthesis of such molecules.

Now that all of the mechanical stereogenic units of simple [2]catenanes and [2]rotaxanes have been delineated and concepts developed to allow their stereoselective synthesis,[4−6,21−25,28] it is reasonable to propose that, 62 years after such systems were first discussed,[1] we have finally reached the end of the beginning of the study of mechanical stereochemistry. Such molecules have already been used as the basis of molecular machines,[14c] enantioselective sensors[37] and catalysts,[38] and chiroptical switches,[39] work which will only accelerate as methods to synthesize them improve. Moreover, we suggest it is time now to set our sights beyond these simple structures and develop methodologies for the systematic synthesis of structures whose stereochemistry arises due to the presence of additional crossing points[40] or larger numbers of interlocked components[41] so that the potential benefits of such architectures can also be explored.

■ ASSOCIATED CONTENT

Data Availability Statement

Data (characterization data for reported compounds) is available from the University of Birmingham UBIRA eData repository at https://doi.org/10.25500/edata.bham.00001074.

Supporting Information

The Supporting Information is available free of charge at https://pubs.acs.org/doi/10.1021/jacs.3c14594.

Procedures and full characterization data (NMR, MS, CD, SCXRD, HPLC as appropriate) for all novel compounds (PDF)

■ AUTHOR INFORMATION

Corresponding Author

Stephen M. Goldup − *School of Chemistry, University of Southampton, Southampton SO17 1BJ, U.K.; School of Chemistry, University of Birmingham, Birmingham B15 2TT, U.K.;* orcid.org/0000-0003-3781-0464; Email: s.m.goldup@bham.ac.uk

Authors

Andrea Savoini − *School of Chemistry, University of Southampton, Southampton SO17 1BJ, U.K.; School of Chemistry, University of Birmingham, Birmingham B15 2TT, U.K.;* orcid.org/0000-0002-8333-406X

Peter R. Gallagher − *School of Chemistry, University of Southampton, Southampton SO17 1BJ, U.K.; School of Chemistry, University of Birmingham, Birmingham B15 2TT, U.K.;* orcid.org/0000-0002-5501-523X

Abed Saady − *School of Chemistry, University of Southampton, Southampton SO17 1BJ, U.K.; School of Chemistry, University of Birmingham, Birmingham B15 2TT, U.K.*

Complete contact information is available at: https://pubs.acs.org/10.1021/jacs.3c14594

Author Contributions

[§]A. Savoini, P.R.G., and A. Saady contributed equally.

Notes

The authors declare no competing financial interest.

■ ACKNOWLEDGMENTS

S.M.G. thanks the ERC (agreement no. 724987) for funding and the Royal Society for a Wolfson Research Fellowship (RSWF\FT\180010). A. Saady thanks the Council for Higher Education-Israel for a personal fellowship. A. Savoini thanks the Royal Society and University of Birmingham for funding. P.R.G. thanks the University of Southampton and the University of Birmingham for funding.

■ REFERENCES

(1) Frisch, H. L.; Wasserman, E. Chemical Topology. *J. Am. Chem. Soc.* **1961**, *83*, 3789−3795.

(2) (a) Jamieson, E. M. G.; Modicom, F.; Goldup, S. M. Chirality in rotaxanes and catenanes. *Chem. Soc. Rev.* **2018**, *47* (14), 5266−5311.

(b) Niemeyer, J.; Pairault, N. Chiral Mechanically Interlocked Molecules - Applications of Rotaxanes, Catenanes and Molecular Knots in Stereoselective Chemosensing and Catalysis. *Synlett* **2018**, *29* (06), 689−698. (c) Evans, N. H. Chiral Catenanes and Rotaxanes: Fundamentals and Emerging Applications. *Chem. Eur. J.* **2018**, *24* (13), 3101−3112.

(3) Schill, G. *Catenanes, Rotaxanes and Knots*; Academic Press: New York, 1971.

(4) Gaeta, C.; Talotta, C.; Mirra, S.; Margarucci, L.; Casapullo, A.; Neri, P. Catenation of calixarene annulus. *Org. Lett.* **2013**, *15* (1), 116−119.

(5) (a) Maynard, J. R. J.; Gallagher, P.; Lozano, D.; Butler, P.; Goldup, S. M. Mechanically axially chiral catenanes and noncanonical mechanically axially chiral rotaxanes. *Nat. Chem.* **2022**, *14* (9), 1038−1044. (b) Gallagher, P. R.; Savoini, A.; Saady, A.; Maynard, J. R. J.; Butler, P. V. W.; Tizzard, G. J.; Goldup, S. M. Facial Selectivity in Mechanical Bond Formation: Axially Chiral Enantiomers and Geometric Isomers from a Simple Prochiral Macrocycle. *J. Am. Chem. Soc.* **2024**, DOI: 10.1021/jacs.3c14329.

(6) Pairault, N.; Rizzi, F.; Lozano, D.; Jamieson, E. M. G.; Tizzard, G. J.; Goldup, S. M. A catenane that is topologically achiral despite being composed of oriented rings. *Nat. Chem.* **2023**, *15* (6), 781−786.

(7) We have previously defined "conditional mechanical stereochemistry" as that which depends on the symmetry properties of the interlocked components but not their relative co-conformation. Thus, conditional mechanical stereochemistry is a permanent rather than dynamic property of the structure, akin to covalent stereogenic units such as stereogenic centers.

(8) Canfield, P. J.; Blake, I. M.; Cai, Z.-L.; Luck, I. J.; Krausz, E.; Kobayashi, R.; Reimers, J. R.; Crossley, M. J. A new fundamental type of conformational isomerism. *Nat. Chem.* **2018**, *10* (6), 615−624.

(9) Reisberg, S. H.; Gao, Y.; Walker, A. S.; Helfrich, E. J. N.; Clardy, J.; Baran, P. S. Total synthesis reveals atypical atropisomerism in a small-molecule natural product, tryptorubin A. *Science* **2020**, *367* (6476), 458−463.

(10) Eliel, E.; Wilen, S.; Mander, L. *Stereochemistry of Organic Compounds*; John Wiley and Sons, Inc.: New York, 1994.

(11) The *z*-axis is defined as perpendicular to the ring plane passing through its center. Where necessary, we define the orientation of a rotation axis or the principal axis of a point group being in the plane of the ring using the subscript "*x*". Where this is not specified the rotation axis should be assumed to lie perpendicular to the ring.

(12) We have previously proposed[2a] that mechanical chirality arises in catenanes when the only improper symmetry operations of the individual rings lie perpendicular or coplanar with the macrocycle plane, corresponding to C_{nv} or C_{nh} symmetry respectively. However, this cannot account for the observation that S_2 symmetric rings, for which a simple reflection plane is not a symmetry operation, can produce mechanically planar chiral or geometric isomerism in catenanes and rotaxane. The need for both components to lack a C_2 axis parallel to the ring plane/perpendicular to the axle is universal in that it can be applied to all of the mechanically stereogenic ring and axle point groups.

(13) We note that these ring symmetries have previously been shown to give rise to co-conformational[14] mechanical stereochemistry. See Ref 2a and (a) Rodriguez-Rubio, A.; Savoini, A.; Modicom, F.; Butler, P.; Goldup, S. M. A Co-conformationally "Topologically" Chiral Catenane. *J. Am. Chem. Soc.* **2022**, *144* (27), 11927−11932.

(14) For selected examples of co-conformational stereochemistry see: (a) Alvarez-Perez, M.; Goldup, S. M.; Leigh, D. A.; Slawin, A. M. Z. A chemically-driven molecular information ratchet. *J. Am. Chem. Soc.* **2008**, *130* (6), 1836−1838. (b) Mochizuki, Y.; Ikeyatsu, K.; Mutoh, Y.; Hosoya, S.; Saito, S. Synthesis of Mechanically Planar Chiral rac-[2]Rotaxanes by Partitioning of an Achiral [2]Rotaxane: Stereoinversion Induced by Shuttling. *Org. Lett.* **2017**, *19* (16), 4347−4350. (c) Corra, S.; de Vet, C.; Baroncini, M.; Credi, A.; Silvi, S. Stereodynamics of E/Z isomerization in rotaxanes through mechanical shuttling and covalent bond rotation. *Chem* **2021**, *7* (8), 2137−2150. (d) Liu, E.; Cherraben, S.; Boulo, L.; Troufflard, C.; Hasenknopf, B.; Vives, G.; Sollogoub, M. A molecular information ratchet using a cone-shaped macrocycle. *Chem* **2023**, *9* (5), 1147−1163.

(15) We note that these point groups are more properly referred to as C_s with the orientation of the single remaining reflection plane defined. We use C_{1v} and C_{1h} here to emphasize the direct link with the general C_{nv} and C_{nh} point groups symmetries that give rise to MPC and MAC stereogenic units respectively.

(16) Damhus, T.; Schaeffer, C. E. Three reference systems for chirality specification. Application, geometric properties, and mutual relationships. *Inorg. Chem.* **1983**, *22* (17), 2406−2412.

(17) It should be noted that the unusual symmetry of such rings means that they also express dynamic co-conformational covalent stereochemistry. See Supporting Information Section 1 for more details.

(18) The subscript highlights the mechanical origin of the geometric isomerism.

(19) Bordoli, R. J.; Goldup, S. M. An efficient approach to mechanically planar chiral rotaxanes. *J. Am. Chem. Soc.* **2014**, *136* (13), 4817−4820.

(20) For seminal examples see: (a) Kaida, Y.; Okamoto, Y.; Chambron, J.-C.; Mitchell, D. K.; Sauvage, J.-P. The Separation of Optically-Active Copper (I) Catenates. *Tetrahedron Lett.* **1993**, *34* (6), 1019−1022. (b) Yamamoto, C.; Okamoto, Y.; Schmidt, T.; Jager, R.; Vogtle, F. Enantiomeric resolution of cycloenantiomeric rotaxane, topologically chiral catenane, and pretzel-shaped molecules: Observation of pronounced circular dichroism. *J. Am. Chem. Soc.* **1997**, *119* (43), 10547−10548. (c) Makita, Y.; Kihara, N.; Nakakoji, N.; Takata, T.; Inagaki, S.; Yamamoto, C.; Okamoto, Y. Catalytic Asymmetric Synthesis and Optical Resolution of Planar Chiral Rotaxane. *Chem. Lett.* **2007**, *36*, 162−163.

(21) Maynard, J. R. J.; Goldup, S. M. Strategies for the Synthesis of Enantiopure Mechanically Chiral Molecules. *Chem* **2020**, *6* (8), 1914−1932.

(22) (a) Jinks, M. A.; de Juan, A.; Denis, M.; Fletcher, C. J.; Galli, M.; Jamieson, E. M. G.; Modicom, F.; Zhang, Z.; Goldup, S. M. Stereoselective Synthesis of Mechanically Planar Chiral Rotaxanes. *Angew. Chem., Int. Ed.* **2018**, *57* (45), 14806−14810. (b) Tian, C.; Fielden, S. D. P.; Perez-Saavedra, B.; Vitorica-Yrezabal, I. J.; Leigh, D. A. Single-Step Enantioselective Synthesis of Mechanically Planar Chiral [2]Rotaxanes Using a Chiral Leaving Group Strategy. *J. Am. Chem. Soc.* **2020**, *142* (21), 9803−9808. (c) Imayoshi, A.; Lakshmi, B. V.; Ueda, Y.; Yoshimura, T.; Matayoshi, A.; Furuta, T.; Kawabata, T. Enantioselective preparation of mechanically planar chiral rotaxanes by kinetic resolution strategy. *Nat. Commun.* **2021**, *12* (1), 404. (d) Li, M.; Chia, X. L.; Tian, C.; Zhu, Y. Mechanically planar chiral rotaxanes through catalytic desymmetrization. *Chem* **2022**, *8* (10), 2843−2855. (e) de Juan, A.; Lozano, D.; Heard, A. W.; Jinks, M. A.; Suarez, J. M.; Tizzard, G. J.; Goldup, S. M. A chiral interlocking auxiliary strategy for the synthesis of mechanically planar chiral rotaxanes. *Nat. Chem.* **2022**, *14* (2), 179−187.

(23) (a) Denis, M.; Lewis, J. E. M.; Modicom, F.; Goldup, S. M. An Auxiliary Approach for the Stereoselective Synthesis of Topologically Chiral Catenanes. *Chem* **2019**, *5* (6), 1512−1520. (b) Zhang, S.; Rodríguez-Rubio, A.; Saady, A.; Tizzard, G. J.; Goldup, S. M. A chiral macrocycle for the stereoselective synthesis of mechanically planar chiral rotaxanes and catenanes. *Chem* **2023**, *9* (5), 1195−1207.

(24) Arduini, A.; Ciesa, F.; Fragassi, M.; Pochini, A.; Secchi, A. Selective synthesis of two constitutionally isomeric oriented calix[6]-arene-based rotaxanes. *Angew. Chem., Int. Ed.* **2005**, *44* (2), 278−281.

(25) Selected examples: (a) Arduini, A.; Bussolati, R.; Credi, A.; Faimani, G.; Garaudee, S.; Pochini, A.; Secchi, A.; Semeraro, M.; Silvi, S.; Venturi, M. Towards controlling the threading direction of a calix[6]arene wheel by using nonsymmetric axles. *Chem. Eur. J.* **2009**, *15* (13), 3230−3242. (b) Xue, M.; Su, Y.-S.; Chen, C.-F. Isomeric squaraine-based [2]pseudorotaxanes and [2]rotaxanes: synthesis, optical properties, and their tubular structures in the solid state. *Chem. Eur. J.* **2010**, *16* (28), 8537−8544. (c) Pierro, T.; Gaeta, C.;

Talotta, C.; Casapullo, A.; Neri, P. Fixed or invertible calixarene-based directional shuttles. *Org. Lett.* **2011**, *13* (10), 2650−2653. (d) Arduini, A.; Bussolati, R.; Credi, A.; Secchi, A.; Silvi, S.; Semeraro, M.; Venturi, M. Toward directionally controlled molecular motions and kinetic intra- and intermolecular self-sorting: threading processes of non-symmetric wheel and axle components. *J. Am. Chem. Soc.* **2013**, *135* (26), 9924−9930. (e) Ciao, R.; Talotta, C.; Gaeta, C.; Margarucci, L.; Casapullo, A.; Neri, P. An oriented handcuff rotaxane. *Org. Lett.* **2013**, *15* (22), 5694−5697. (f) Xia, Y.-X.; Xie, T.; Han, Y.; Chen, C.-F. Triptycene-derived calix[6]arene analogues: synthesis, structure and complexation with paraquat derivatives. *Org. Chem. Front.* **2014**, *1* (2), 140. (g) Wang, H.-X.; Meng, Z.; Xiang, J.-F.; Xia, Y.-X.; Sun, Y.; Hu, S.-Z.; Chen, H.; Yao, J.; Chen, C.-F. Guest-dependent directional complexation based on triptycene derived oxacalixarene: formation of oriented rotaxanes. *Chem. Sci.* **2016**, *7* (1), 469−474. (h) Zanichelli, V.; Ragazzon, G.; Arduini, A.; Credi, A.; Franchi, P.; Orlandini, G.; Venturi, M.; Lucarini, M.; Secchi, A.; Silvi, S. Synthesis and Characterization of Constitutionally Isomeric Oriented Calix[6]-arene-Based Rotaxanes. *Eur. J. Org Chem.* **2016**, *2016* (5), 1033−1042. (i) La Manna, P.; Talotta, C.; Gaeta, C.; Soriente, A.; De Rosa, M.; Neri, P. Threading of an Inherently Directional Calixarene Wheel with Oriented Ammonium Axles. *J. Org. Chem.* **2017**, *82* (17), 8973−8983. (j) Cui, J. S.; Ba, Q. K.; Ke, H.; Valkonen, A.; Rissanen, K.; Jiang, W. Directional Shuttling of a Stimuli-Responsive Cone-Like Macrocycle on a Single-State Symmetric Dumbbell Axle. *Angew. Chem., Int. Ed.* **2018**, *57* (26), 7809−7814. (k) Li, K.-A.; Wang, Z.; Xie, C.-D.; Chen, T.; Qiang, H.; Liu, Y. A.; Jia, X.-S.; Hu, W.-B.; Wen, K. Unidirectional complexation of pillar[4]arene[1]-benzoquinoneoxime with alkyl alcohols. *Org. Biomol. Chem.* **2019**, *17* (20), 4975−4978. (l) Bazzoni, M.; Andreoni, L.; Silvi, S.; Credi, A.; Cera, G.; Secchi, A.; Arduini, A. Selective access to constitutionally identical, orientationally isomeric calix[6]arene-based [3]rotaxanes by an active template approach. *Chem. Sci.* **2021**, *12* (18), 6419−6428. (m) Cera, G.; Arduini, A.; Secchi, A.; Credi, A.; Silvi, S. Heteroditopic Calix[6]arene Based Intervowen and Interlocked Molecular Devices. *Chem. Rec.* **2021**, *21* (5), 1161−1181. (n) Andreoni, L.; Cester Bonati, F.; Groppi, J.; Balestri, D.; Cera, G.; Credi, A.; Secchi, A.; Silvi, S. Selective enhancement of organic dye properties through encapsulation in rotaxane orientational isomers. *Chem. Commun.* **2023**, *59* (33), 4970−4973.

(26) IUPAC have noted that several definitions of prochirality are in use (IUPAC Gold Book: https://goldbook.iupac.org/terms/view/P04859, accessed 15/12/2023). Here, and throughout, we use the term prochiral to mean an achiral structure that becomes chiral if an existing atom/group is replaced by different one.

(27) For a previous report in which a prochiral macrocycle was used but no selectivity reported see: (a) Saito, F.; Bode, J. W. Synthesis and stabilities of peptide-based [1]rotaxanes: molecular grafting onto lasso peptide scaffolds. *Chem. Sci.* **2017**, *8* (4), 2878−2884.

(28) Zanichelli, V.; Dallacasagrande, L.; Arduini, A.; Secchi, A.; Ragazzon, G.; Silvi, S.; Credi, A. Electrochemically Triggered Co-Conformational Switching in a [2]catenane Comprising a Non-Symmetric Calix[6]arene Wheel and a Two-Station Oriented Macrocycle. *Molecules* **2018**, *23* (5), 1156.

(29) Denis, M.; Goldup, S. M. The active template approach to interlocked molecules. *Nat. Rev. Chem* **2017**, *1* (8), 0061.

(30) (a) Aucagne, V.; Hanni, K. D.; Leigh, D. A.; Lusby, P. J.; Walker, D. B. Catalytic "click" rotaxanes: a substoichiometric metal-template pathway to mechanically interlocked architectures. *J. Am. Chem. Soc.* **2006**, *128* (7), 2186−2187. (b) Lahlali, H.; Jobe, K.; Watkinson, M.; Goldup, S. M. Macrocycle size matters: "small" functionalized rotaxanes in excellent yield using the CuAAC active template approach. *Angew. Chem., Int. Ed.* **2011**, *50* (18), 4151−4155.

(31) Saady, A.; Goldup, S. M. Triazole formation and the click concept in the synthesis of interlocked molecules. *Chem* **2023**, *9* (8), 2110−2127.

(32) The exception to this general statement is if the axle is divided at the prochiral center itself, such that in the forward reaction this centre is converted from sp^2 to sp^3 hybridization. In this case the half-axle that contains the sp^2 hybridized centre can also be described as prochiral but, confusingly, this is an alternative definition of the same word.[26]

(33) Lewis, J. E. M.; Bordoli, R. J.; Denis, M.; Fletcher, C. J.; Galli, M.; Neal, E. A.; Rochette, E. M.; Goldup, S. M. High yielding synthesis of 2,2′-bipyridine macrocycles, versatile intermediates in the synthesis of rotaxanes. *Chem. Sci.* **2016**, *7*, 3154−3161.

(34) All reported diastereoselectivities were determined by integration of signals identified as corresponding to the two diastereomers in the ^{1}H NMR spectra of the mixture. See Supporting Information Section 3 for a brief discussion of the ^{1}H NMR methods used.

(35) The variation in *de* at different stages of the synthesis of rotaxanes **11** corresponds to a 1% variation in the ratio of these integrals and is thus within the error of the measurement.[34]

(36) This is a common feature of interlocked molecules produced using the AT-CuAAC reaction of small bipyridine macrocycles. See ref 30b.

(37) Hirose, K.; Ukimi, M.; Ueda, S.; Onoda, C.; Kano, R.; Tsuda, K.; Hinohara, Y.; Tobe, Y. The Asymmetry is Derived from Mechanical Interlocking of Achiral Axle and Achiral Ring Components Syntheses and Properties of Optically Pure [2]-Rotaxanes. *Symmetry* **2018**, *10* (1), 20.

(38) Heard, A. W.; Goldup, S. M. Synthesis of a Mechanically Planar Chiral Rotaxane Ligand for Enantioselective Catalysis. *Chem* **2020**, *6* (4), 994−1006.

(39) (a) Gaedke, M.; Witte, F.; Anhauser, J.; Hupatz, H.; Schroder, H. V.; Valkonen, A.; Rissanen, K.; Lutzen, A.; Paulus, B.; Schalley, C. A. Chiroptical inversion of a planar chiral redox-switchable rotaxane. *Chem. Sci.* **2019**, *10* (43), 10003−10009. (b) Wang, Y.; Gong, J.; Wang, X.; Li, W.-J.; Wang, X.-Q.; He, X.; Wang, W.; Yang, H.-B. Multistate Circularly Polarized Luminescence Switching through Stimuli-Induced Co-Conformation Regulations of Pyrene-Functionalized Topologically Chiral [2]Catenane. *Angew. Chem.* **2022**, *134*, No. e202210542.

(40) Selected examples: (a) Nierengarten, J. F.; Dietrich-Buchecker, C. O.; Sauvage, J. P. Synthesis of a doubly interlocked [2]-catenane. *J. Am. Chem. Soc.* **1994**, *116* (1), 375−376. (b) Pentecost, C. D.; Chichak, K. S.; Peters, A. J.; Cave, G. W. V.; Cantrill, S. J.; Stoddart, J. F. A molecular solomon link. *Angew. Chem., Int. Ed.* **2007**, *46* (1−2), 218−222. (c) Schouwey, C.; Holstein, J. J.; Scopelliti, R.; Zhurov, K. O.; Nagornov, K. O.; Tsybin, Y. O.; Smart, O. S.; Bricogne, G.; Severin, K. Self-assembly of a giant molecular Solomon link from 30 subcomponents. *Angew. Chem., Int. Ed.* **2014**, *53* (42), 11261−11265. (d) Beves, J. E.; Danon, J. J.; Leigh, D. A.; Lemonnier, J.-F.; Vitorica-Yrezabal, I. J. A Solomon link through an interwoven molecular grid. *Angew. Chem., Int. Ed.* **2015**, *54* (26), 7555−7559. (e) Cui, Z.; Lu, Y.; Gao, X.; Feng, H.-J.; Jin, G.-X. Stereoselective Synthesis of a Topologically Chiral Solomon Link. *J. Am. Chem. Soc.* **2020**, *142* (32), 13667−13671. (f) August, D. P.; Jaramillo-Garcia, J.; Leigh, D. A.; Valero, A.; Vitorica-Yrezabal, I. J. A Chiral Cyclometalated Iridium Star of David [2]Catenane. *J. Am. Chem. Soc.* **2021**, *143* (2), 1154−1161. (g) Feng, H.-N.; Sun, Z.; Chen, S.; Zhang, Z.-H.; Li, Z.; Zhong, Z.; Sun, T.; Ma, Y.; Zhang, L. A Star of David [2]catenane of single handedness. *Chem* **2023**, *9* (4), 859−868.

(41) Selected examples: (a) Lincheneau, C.; Jean-Denis, B.; Gunnlaugsson, T. Self-assembly formation of mechanically interlocked [2]- and [3]catenanes using lanthanide ion [Eu(III)] templation and ring closing metathesis reactions. *Chem. Commun.* **2014**, *50* (22), 2857. (b) Zhu, R.; Lubben, J.; Dittrich, B.; Clever, G. H. Stepwise halide-triggered double and triple catenation of self-assembled coordination cages. *Angew. Chem., Int. Ed.* **2015**, *54* (9), 2796−2800. (c) Wood, C. S.; Ronson, T. K.; Belenguer, A. M.; Holstein, J. J.; Nitschke, J. R. Two-stage directed self-assembly of a cyclic [3]catenane. *Nat. Chem.* **2015**, *7* (4), 354−358. (d) Sawada, T.; Yamagami, M.; Ohara, K.; Yamaguchi, K.; Fujita, M. Peptide [4]Catenane by Folding and Assembly. *Angew. Chem., Int. Ed.* **2016**, *55* (14), 4519−4522. (e) Feng, T.; Li, X.; An, Y.-Y.; Bai, S.; Sun, L.-Y.; Li, Y.; Wang, Y.-Y.; Han, Y.-F. Backbone-Directed Self-

https://doi.org/10.1021/jacs.3c14594
J. Am. Chem. Soc. 2024, 146, 8472−8479

Assembly of Interlocked Molecular Cyclic Metalla[3]Catenanes. *Angew. Chem., Int. Ed.* **2020**, *59* (32), 13516−13520. (f) Cui, Z.; Gao, X.; Lin, Y.-J.; Jin, G.-X. Stereoselective Self-Assembly of Complex Chiral Radial [5]Catenanes Using Half-Sandwich Rhodium/Iridium Building Blocks. *J. Am. Chem. Soc.* **2022**, *144* (5), 2379−2386.

https://doi.org/10.1021/jacs.3c14594
J. Am. Chem. Soc. 2024, 146, 8472−8479